

Reestablishing Neural Plasticity in Regenerated Spiral Ganglion Neurons and Sensory Hair Cells for Hearing Loss 2020

Lead Guest Editor: Renjie Chai

Guest Editors: Geng-lin Li, Jian Wang, Jing Zou, and Hai Huang





**Reestablishing Neural Plasticity in Regenerated
Spiral Ganglion Neurons and Sensory Hair
Cells for Hearing Loss 2020**

Neural Plasticity

**Reestablishing Neural Plasticity in
Regenerated Spiral Ganglion Neurons
and Sensory Hair Cells for Hearing Loss
2020**

Lead Guest Editor: Renjie Chai

Guest Editors: Geng-lin Li, Jian Wang, Jing Zou,
and Hai Huang



Copyright © 2021 Hindawi Limited. All rights reserved.

This is a special issue published in "Neural Plasticity" All articles are open access articles distributed under the Creative Commons Attribution License, which permits unrestricted use, distribution, and reproduction in any medium, provided the original work is properly cited.

Chief Editor

Michel Baudry, USA

Editorial Board

Eckart Altenmüller, Germany
Victor Anggono, Australia
Sergio Bagnato, Italy
Laura Baroncelli, Italy
Michel Baudry, USA
Michael S. Beattie, USA
Nicoletta Berardi, Italy
Michael Borich, USA
Davide Bottari, Italy
Clive R. Bramham, Norway
Kalina Burnat, Poland
Gaston Calfa, Argentina
Martin Cammarota, Brazil
Carlo Cavaliere, Italy
Rajnish Kumar Chaturvedi, India
Guy Cheron, Belgium
Gabriela Delevati Colpo, USA
Michele Fornaro, USA
Francesca Foti, Italy
Zygmunt Galdzicki, USA
Preston E. Garraghty, USA
Paolo Girlanda, Italy
Massimo Grilli, Italy
Wenbin Guo, China
Takashi Hanakawa, Japan
Anthony J. Hannan, Australia
Grzegorz Hess, Poland
Malgorzata Kossut, Poland
Feng Liu, China
Volker Mall, Germany
Stuart C. Mangel, USA
Diano Marrone, Canada
Aage R. Møller, USA
Jean-Pierre Mothet, France
Xavier Navarro, Spain
Martin Oudega, USA
Fernando Peña-Ortega, Mexico
Maurizio Popoli, Italy
Mojgan Rastegar, Canada
Emiliano Ricciardi, Italy
Gernot Riedel, United Kingdom
Simone Rossi, USA
Alessandro Sale, Italy
Marco Sandrini, United Kingdom

Gabriele Sansevero, Italy
Roland Schaette, United Kingdom
Menahem Segal, Israel
Jerry Silver, USA
Josef Syka, Czech Republic
Yasuo Terao, Japan
Daniela Tropea, Ireland
Tara Walker, Australia
Xueqiang Wang, China
Chun-Fang Wu, USA
Long-Jun Wu, USA
J. Michael Wyss, USA
Lin Xu, China

Contents

Hearing Loss: Reestablish the Neural Plasticity in Regenerated Spiral Ganglion Neurons and Sensory Hair Cells 2020

Renjie Chai , Geng-lin Li, Jian Wang , Jing Zou, and Hai Huang
Editorial (4 pages), Article ID 9897461, Volume 2021 (2021)

Hair Cell Protection from Ototoxic Drugs

Peng Wu , Xianmin Wu , Chunhong Zhang , Xiaoyun Chen , Yideng Huang , and He Li 
Review Article (9 pages), Article ID 4909237, Volume 2021 (2021)

Low-Intensity Ultrasound Causes Direct Excitation of Auditory Cortical Neurons

Xiaofei Qi , Kexin Lyu , Long Meng , Cuixian Li , Hongzheng Zhang , Lili Niu , Zhengrong Lin , Hairong Zheng , and Jie Tang 
Research Article (10 pages), Article ID 8855055, Volume 2021 (2021)

Developmental and Functional Hair Cell-Like Cells Induced by Atoh1 Overexpression in the Adult Mammalian Cochlea In Vitro

Lingyi Kong , Yuan Xin , Fanglu Chi , Jie Chen , and Juanmei Yang 
Research Article (10 pages), Article ID 8885813, Volume 2020 (2020)

Distinct Expression Patterns of Apoptosis and Autophagy-Associated Proteins and Genes during Postnatal Development of Spiral Ganglion Neurons in Rat

Shule Hou , Penghui Chen, Jiarui Chen , Junmin Chen , Lianhua Sun , Jianyong Chen , Baihui He , Yue Li , Huan Qin , Yuren Hong , Shuna Li , Jingchun He , Dekun Gao , Fabio Mammano , and Jun Yang 
Research Article (9 pages), Article ID 9387560, Volume 2020 (2020)

Research Progress of Hair Cell Protection Mechanism

Yurong Mu, Hongguo Su, Fan Wu, Jianming Yang , and Dan Li 
Review Article (6 pages), Article ID 8850447, Volume 2020 (2020)

Hsp70/Bmi1-FoxO1-SOD Signaling Pathway Contributes to the Protective Effect of Sound Conditioning against Acute Acoustic Trauma in a Rat Model

Guoxia Zhu, Yongxiang Wu, Yang Qiu, Keyong Tian , Wenjuan Mi, Xinqin Liu, Yuanyuan Chen, Jinwen Jia, Jiasheng Luo , Lianjun Lu , and Jianhua Qiu 
Research Article (22 pages), Article ID 8823785, Volume 2020 (2020)

Altered Brain Activity and Functional Connectivity in Unilateral Sudden Sensorineural Hearing Loss

Jiawei Chen, Bo Hu, Peng Qin, Wei Gao, Chengcheng Liu, Dingjing Zi, Xuerui Ding, Ying Yu, Guangbin Cui , and Lianjun Lu 
Research Article (11 pages), Article ID 9460364, Volume 2020 (2020)

Cisplatin-Induced Stria Vascularis Damage Is Associated with Inflammation and Fibrosis

Na Zhang, Jing Cai, Lei Xu , Haibo Wang , and Wenwen Liu 
Research Article (13 pages), Article ID 8851525, Volume 2020 (2020)

Effects of SoundBite Bone Conduction Hearing Aids on Speech Recognition and Quality of Life in Patients with Single-Sided Deafness

Qiong Luo , Ying Shen , Ting Chen , Zhong Zheng , Haibo Shi , Yanmei Feng , and Zhengnong Chen 

Research Article (8 pages), Article ID 4106949, Volume 2020 (2020)

The Influence of Cochlear Implant-Based Electric Stimulation on the Electrophysiological Characteristics of Cultured Spiral Ganglion Neurons

Na Shen, Lei Zhou, Bin Lai , and Shufeng Li 

Research Article (8 pages), Article ID 3108490, Volume 2020 (2020)

Cochlear Implantation in a Patient with a Novel POU3F4 Mutation and Incomplete Partition Type-III Malformation

Xiuhua Chao, Yun Xiao, Fengguo Zhang, Jianfen Luo, Ruijie Wang, Wenwen Liu, Haibo Wang, and Lei Xu 

Research Article (9 pages), Article ID 8829587, Volume 2020 (2020)

Mitochondrial Dysfunction and Therapeutic Targets in Auditory Neuropathy

Baoyi Feng, Chenxi Jin, Zhenzhe Cheng, Xingle Zhao, Zhuoer Sun, Xiaofei Zheng, Xiang Li, Tingting Dong, Yong Tao , and Hao Wu 

Review Article (10 pages), Article ID 8843485, Volume 2020 (2020)

Atrial Natriuretic Peptide Improves Neurite Outgrowth from Spiral Ganglion Neurons In Vitro through a cGMP-Dependent Manner

Fei Sun , Ke Zhou , Ke-yong Tian , Jie Wang, Jian-hua Qiu , and Ding-jun Zha 

Research Article (12 pages), Article ID 8831735, Volume 2020 (2020)

A Novel Spontaneous Mutation of the SOX10 Gene Associated with Waardenburg Syndrome Type II

Sen Chen , Yuan Jin , Le Xie, Wen Xie , Kai Xu , Yue Qiu , Xue Bai , Hui-Min Zhang , Xiao-Zhou Liu, Xiao-Hui Wang, Wei-Jia Kong , and Yu Sun 

Research Article (8 pages), Article ID 9260807, Volume 2020 (2020)

Targeted Next-Generation Sequencing Identifies Separate Causes of Hearing Loss in One Deaf Family and Variable Clinical Manifestations for the p.R161C Mutation in SOX10

Xiaoyu Yu , Yun Lin , and Hao Wu 

Research Article (8 pages), Article ID 8860837, Volume 2020 (2020)

Transcript Profiles of Stria Vascularis in Models of Waardenburg Syndrome

Linjun Chen, Lin Wang, Lei Chen, Fangyuan Wang, Fei Ji, Wei Sun, Hui Zhao , Weiju Han , and Shiming Yang 

Research Article (9 pages), Article ID 2908182, Volume 2020 (2020)

The Regenerative Potential of Facial Nerve Motoneurons following Chronic Axotomy in Rats

Yusu Ni , Diyan Chen, Yi Jiang, Danhong Qiu, Wen Li, and Huawei Li 

Research Article (9 pages), Article ID 8884511, Volume 2020 (2020)

Contents

Compound Heterozygous Mutations in TMC1 and MYO15A Are Associated with Autosomal Recessive Nonsyndromic Hearing Loss in Two Chinese Han Families

Pengcheng Xu, Jun Xu , Hu Peng, and Tao Yang 

Research Article (7 pages), Article ID 8872185, Volume 2020 (2020)

Hearing Phenotypes of Patients with Hearing Loss Homozygous for the GJB2 c.235delc Mutation

Chang Guo, Sha-Sha Huang, Yong-Yi Yuan , Ying Zhou, Ning Wang, Dong-Yang Kang, Su-Yan Yang, Xin Zhang, Xue Gao , and Pu Dai 

Research Article (11 pages), Article ID 8841522, Volume 2020 (2020)

Stem Cell-Based Therapeutic Approaches to Restore Sensorineural Hearing Loss in Mammals

Muhammad Waqas , Iram Us-Salam, Zainab Bibi, Yunfeng Wang , He Li , Zhongshou Zhu , and Shuangba He 

Review Article (10 pages), Article ID 8829660, Volume 2020 (2020)

Differences in Clinical Characteristics and Brain Activity between Patients with Low- and High-Frequency Tinnitus

Jiajia Zhang, Zhen Zhang, Shujian Huang, Huiqun Zhou, Yanmei Feng, Haibo Shi, Dan Wang , Wenya Nan , Hui Wang , and Shankai Yin

Research Article (12 pages), Article ID 5285362, Volume 2020 (2020)

Loss of Cochlear Ribbon Synapse Is a Critical Contributor to Chronic Salicylate Sodium Treatment-Induced Tinnitus without Change Hearing Threshold

Wei Zhang, Zhe Peng, ShuKui Yu, Qing-Ling Song, Teng-Fei Qu, Lu He, Ke Liu , and Shu-Sheng Gong 

Research Article (9 pages), Article ID 3949161, Volume 2020 (2020)

Alternative Splicing of Cdh23 Exon 68 Is Regulated by RBM24, RBM38, and PTBP1

Nana Li, Haibo Du, Rui Ren, Yanfei Wang, and Zhigang Xu 

Research Article (11 pages), Article ID 8898811, Volume 2020 (2020)

A Neurophysiological Study of Musical Pitch Identification in Mandarin-Speaking Cochlear Implant Users

Jieqing Cai, Yimeng Liu, Minyun Yao, Muqing Xu, and Hongzheng Zhang 

Research Article (11 pages), Article ID 4576729, Volume 2020 (2020)

Toxic Effects of 3,3-Iminodipropionitrile on Vestibular System in Adult C57BL/6J Mice In Vivo

Shan Zeng, Wenli Ni, Hui Jiang, Dan You, Jinghan Wang, Xiaoling Lu, Liman Liu, Huiqian Yu, Jingfang Wu, Fangyi Chen, Huawei Li, Yunfeng Wang , Yan Chen , and Wenyan Li 

Research Article (11 pages), Article ID 1823454, Volume 2020 (2020)

An In Vitro Study on Prestin Analog Gene in the Bullfrog Hearing Organs

Zhongying Wang, Minfei Qian, Qixuan Wang, Huihui Liu, Hao Wu , and Zhiwu Huang 

Research Article (9 pages), Article ID 3570732, Volume 2020 (2020)

High Frequency of AIFM1 Variants and Phenotype Progression of Auditory Neuropathy in a Chinese Population

Hongyang Wang, Dan Bing, Jin Li, Linyi Xie, Fen Xiong, Lan Lan, Dayong Wang, Jing Guan, and Qiuju Wang 

Research Article (12 pages), Article ID 5625768, Volume 2020 (2020)

Auditory Neural Plasticity in Tinnitus Mechanisms and Management

Kunkun Wang, Dongmei Tang, Jiaoyao Ma, and Shan Sun 

Review Article (17 pages), Article ID 7438461, Volume 2020 (2020)

Four Novel Variants in POU4F3 Cause Autosomal Dominant Nonsyndromic Hearing Loss

Tian-Yi Cui, Xue Gao, Sha-Sha Huang, Yan-Yan Sun, Si-Qi Zhang, Xin-Xia Jiang, Yan-Zhong Yang, Dong-Yang Kang, Qing-Wen Zhu , and Yong-Yi Yuan 

Research Article (12 pages), Article ID 6137083, Volume 2020 (2020)

Targeted Next-Generation Sequencing Identified Compound Heterozygous Mutations in MYO15A as the Probable Cause of Nonsyndromic Deafness in a Chinese Han Family

Longhao Wang, Lin Zhao, Hu Peng, Jun Xu, Yun Lin, Tao Yang , and Hao Wu 

Research Article (6 pages), Article ID 6350479, Volume 2020 (2020)

Involvement of Cholesterol Metabolic Pathways in Recovery from Noise-Induced Hearing Loss

Na Sai , Xi Shi, Yan Zhang, Qing-qing Jiang, Fei Ji, Shuo-long Yuan, Wei Sun, Wei-Wei Guo , Shi-Ming Yang , and Wei-Ju Han 

Research Article (17 pages), Article ID 6235948, Volume 2020 (2020)

An Age-Related Hearing Protection Locus on Chromosome 16 of BXD Strain Mice

Qing Yin Zheng , Lihong Kui, Fuyi Xu , Tihua Zheng, Bo Li, Melinda McCarty, Zehua Sun, Aizheng Zhang, Luying Liu, Athena Starlard-Davenport, Ruben Stepanyan, Bo Hua Hu, and Lu Lu 

Research Article (11 pages), Article ID 8889264, Volume 2020 (2020)

Jervell and Lange-Nielsen Syndrome due to a Novel Compound Heterozygous KCNQ1 Mutation in a Chinese Family

Yue Qiu, Sen Chen, Xia Wu, Wen-Juan Zhang, Wen Xie, Yuan Jin, Le Xie, Kai Xu, Xue Bai, Hui-Min Zhang, Xiao-Zhou Liu, Xiao-Hui Wang, Yu Sun , and Wei-Jia Kong 

Research Article (8 pages), Article ID 3569359, Volume 2020 (2020)

Editorial

Hearing Loss: Reestablish the Neural Plasticity in Regenerated Spiral Ganglion Neurons and Sensory Hair Cells 2020

Renjie Chai ^{1,2}, Geng-lin Li,³ Jian Wang ⁴, Jing Zou,⁵ and Hai Huang⁶

¹State Key Laboratory of Bioelectronics, School of Life Sciences and Technology, Jiangsu Province High-Tech Key Laboratory for Bio-Medical Research, Southeast University, Nanjing 210096, China

²Co-Innovation Center of Neuroregeneration, Nantong University, Nantong 226001, China

³Biology Department, University of Massachusetts Amherst, Amherst, MA 01003, USA

⁴School of Communication Science & Disorders, Dalhousie University, 5850 College Street, Halifax, NS, Canada B3J1Y6

⁵Hearing and Balance Research Unit, Field of Otolaryngology, School of Medicine, University of Tampere, Tampere, Finland

⁶Department of Cell and Molecular Biology, Tulane University, New Orleans, LA 70118, USA

Correspondence should be addressed to Renjie Chai; renjiec@seu.edu.cn

Received 13 October 2021; Accepted 13 October 2021; Published 19 October 2021

Copyright © 2021 Renjie Chai et al. This is an open access article distributed under the Creative Commons Attribution License, which permits unrestricted use, distribution, and reproduction in any medium, provided the original work is properly cited.

Hearing loss in one of the most common sensory disorders among people around the world, and it has often been referred to as an “invisible disability.” Globally, over 1.5 billion people are currently experiencing hearing loss to some degree in 2021, accounting for 20% of the world’s population, of which, an estimated 430 million have hearing loss of moderate or higher severity in the better hearing ear, and this number could increase to 2.5 billion by 2050 according to WHO report. Multiple risk factors could contribute to one’s hearing capacity during his/her lifetime course, including genetic factors, ototoxic chemicals, noise exposure, trauma to the ear or head, and age-related degeneration. Among all cases of hearing disorders, 85% of them are under the category of sensorineural hearing loss (SNHL). Although SNHL is induced by various factors through different approaches and mechanisms, the major cause for SNHL is irreversible loss of either inner ear hair cells (HCs) or degeneration of spiral ganglion neurons (SGNs). At present, there is no effective treatments for SNHL available, thus, it is not curable yet. In recent years, many studies are dedicated to working on the regenerative capacity of developing and functional HCs and SGNs, and promising results on animal models present us with the potential of regenerating HCs and SGNs by gene therapy, stem cell induction, and signaling pathway manipulation. This raises the possibility of curing SNHL in the foreseeable future. In

2017 and 2018, we have published two special issues of “Hearing Loss: Reestablish the Neural Plasticity in Regenerated Spiral Ganglion Neurons and Sensory Hair Cells.” This year, we are delighted to present a new series of articles and reviews covering the up-to-date progress on HC development, HC damage and protection, HC regeneration, SGN development and protection, and inherited hearing loss.

1. Hair Cell Development

(Z) Wang et al. (An *in vitro* study on prestin analog gene in the bullfrog hearing organs) for the first time identify the prestin analog gene in the bullfrog hearing organ functioning as a motor protein by nonlinear capacitance, and this might lead to reveal of possible roles of prestin in the active hearing processes found in many nonmammalian species. N. Li et al. (Alternative splicing of *Cdh23* exon 68 is regulated by RBM24, RBM38, and PTBP1) explore the mechanism of alternative underlying the production of cadherin 23, a key part in forming tip links in the hair cells and elucidate that RBM24, RBM38, and PTBP1 are involved in splicing of *Cdh23* exon 68.

2. Hair Cell Damage and Protection

- (N) Sai et al. (Involvement of cholesterol metabolic pathways in recovery from noise-induced hearing loss) explore the molecular mechanisms of acute noise-induced hearing loss in miniature pigs and identify the possible participation of activation of metabolic, inflammatory, and innate immunity pathways in acute noise-induced hearing loss and also report the importance of cholesterol metabolic pathway in recovery of hearing ability following noise-induced hearing loss. K. Wang et al. (Auditory neural plasticity in tinnitus mechanisms and management) provide a comprehensive review on the epidemiology and classification of tinnitus and discuss the currently available treatments based on valid evidence for their mechanisms and efficacy, which leads to the conclusion of no specific medication for tinnitus treatment at present. J. Cai et al. (A neurophysiological study of musical pitch identification in Mandarin-speaking cochlear implant users) investigate the neurophysiological mechanisms accounting for the musical pitch identification abilities of Mandarin-speaking cochlear implant (CI) users and confirm mismatch negativity is a viable marker of cortical pitch perception in Mandarin-speaking CI users. J. Zhang et al. (Differences in clinical characteristics and brain activity between patients with low- and high-frequency tinnitus) compare the differences in clinical characteristics and brain activity between patients with low- and high-frequency tinnitus (LFT and HFT, respectively) by high-density electroencephalography and report significant changes related to increased gamma in the LFT group and decreased alpha1 in the HFT group. Q. Luo et al. (Effects of soundbite bone conduction hearing aids on speech recognition and quality of life in patients with single-sided deafness) demonstrate the effectiveness of SoundBite bone conduction hearing aids for patients with single-sided deafness by using different measurements both in a quiet and noisy environment. N. Zhang et al. (Cisplatin-induced stria vascularis damage is associated with inflammation and fibrosis) for the first time demonstrate that cisplatin induce fibrosis, inflammation, and the complex expression change of cell junctions in the stria vascularis (SV) and report after cisplatin treatment, tight junction, and gap junction proteins are down-regulated. J. Chen et al. (Altered brain activity and functional connectivity in unilateral sudden sensorineural hearing loss) report functional alterations in brain regions in patients with sudden sensorineural hearing loss within the acute period of hearing loss, especially in the striatum, auditory cortex, visual cortex, MTG, AG, precuneus, and limbic lobes. G. Zhu et al. (Hsp70-Bmi1-FoxO1-SOD signaling pathway contributes to the protective effect of sound conditioning against acute acoustic trauma in a rat model) investigate the exact mechanisms involved in the pro-

protective effect of sound conditioning (SG) in mammals and report the improvement of SGN survival of SG after noise-induced stress response via controlling mitochondrial function and ROS levels, the involvement of Hsp70/Bmi1-FoxO1-SOD signaling pathway in the protection of SC against acute acoustic trauma (AAT) and the underlying mechanisms of decreased sensitivity to AAT following treatment with SC in rats. Y. Mu et al. (Research progress of hair cell protection mechanism) provide a brief review on the latest research progress about hair cell (HC) protection and regeneration mechanism, including HC development, apoptosis, protection, and regeneration, providing evidence to prevent and treat hearing-related diseases in the future.

3. Hair Cell Regeneration

- (S) Zeng et al. (Toxic effects of 3,3'-iminodipropionitrile on vestibular system in adult C57BL-6J mice *in vivo*) report the activation of Notch and Wnt signaling during the limited hair cell self-regeneration ability in the adult mouse utricle after vestibular sensory epithelium damage caused by a single injection of 3,3'-iminodipropionitrile. M. Waqas et al. (Stem cell-based therapeutic approaches to restore sensorineural hearing loss in mammals) provide a brief review to discuss the potential of various stem cells to restore sensorineural hearing loss in mammals and explain the current therapeutic applications of stem cells to regenerate or replace the lost hair cells and spiral ganglion neurons in both human and mouse inner ear. L. Kong et al. (Development and functional hair cell-like cells induced by Atoh1 overexpression in the adult mammalian cochlea *in vitro*) demonstrate that hair cell-like cell (HCLCs) formation is induced in the adult mouse cochlea by using a three-dimensional cochlear culture system and an adenoviral-mediated delivery vector to overexpress Atoh1 and report these HCLCs share similar functions and developmental process to that of normal hair cells.

4. Spiral Ganglion Neuron Development and Protection

- (T) Sun et al. (Atrial natriuretic peptide improves neurite outgrowth from spiral ganglion neurons *in vitro* through a cGMP-dependent manner) demonstrate that atrial natriuretic peptide (ANP), a cardiac-derived hormone presented in mammalian inner ear, and its receptors are expressed in neurons within the cochlear spiral ganglion of postnatal rat and report the influence of ANP on neurite outgrowth of SGNs via the NPR-A/cGMP/PKG pathway *in vitro* in a dose-dependent manner. B. Feng et al. (Mitochondrial dysfunction and therapeutic targets in auditory neuropathy) present a brief

review on mitochondrial biological functions associated with spiral ganglion neurons and to discuss the interaction between mitochondrial dysfunction and auditory neuropathies (AN), together with current mitochondrion treatment for sensorineural hearing loss. The authors also suggest to explore pharmaceutical therapeutics to protect mitochondrion dysfunction as a feasible and effective treatments for patients with AN. N. Shen et al. (The influence of cochlear implant-based electric stimulation on the electrophysiological characteristics of cultured spiral ganglion neurons) discover that cochlear implant-based electrical stimulation with 50 μ A or 100 μ A significantly inhibit the voltage depended calcium current of spiral ganglion neurons in vitro while the firing of action potential remains unchanged. S. Hou et al. (Distinct expression patterns of apoptosis and autophagy-associated proteins and genes during postnatal development of spiral ganglion neurons in rat) for the first time demonstrate the distinct roles of autophagy and apoptosis in spiral ganglion cells during specific developmental phases in rats in a time-dependent manner identified with morphological changes, specific marks of autophagy and apoptosis, apoptotic bodies and autophagosomes and autolysosomes, and apoptotic activity. Y. Ni et al. (The regenerative potential of facial nerve motoneurons following chronic axotomy in rats) demonstrate that the greatest regeneration potential of the facial nerve of rats exists within 5 months after chronic axotomy identified by growth-associated protein 43 and Shh signaling pathway may involve in the regeneration.

5. Inherited Hearing Loss

(Y) Qiu et al. (Jervell and Lange-Nielsen Syndrome due to a novel compound heterozygous KCNQ1 mutation in a Chinese family) identify the possible pathogenic cause of Jervell and Lange-Nielsen syndrome by a compound heterozygosity for two mutations c.1741A>T and c.477+5G>A in KCNQ1 gene in a Chinese family using next-generation sequencing. Q. Zheng et al. (An age-related hearing protection locus on chromosome 16 of BXD strain mice) report an age-related hearing protection locus on chromosome 16 at 57~76 Mb with a maximum LOD of 5.7 in BXD strain mice by hearing screening of 54 BXD strains at age between 12 and 32 months. L. Wang et al. (Targeted next-generation sequencing identified compound heterozygous mutations in MYO15A as the probable cause of nonsyndromic deafness in a Chinese Han family) demonstrate compound heterozygous mutations c.3658_3662del (p. E1221Wfs*23) and c.6177+1G>T are two genetic candidates of congenital hearing loss by targeted next-generation sequencing in a Chinese Han family. T. Cui et al. (Four novel variants in POU4F3 cause autosomal dominant nonsyndromic hearing

loss) report four novel variants in POU4F3, i.e., c.696G>T, c.325C>T, c.635T>C, and c.183delG, as cause of autosomal dominant nonsyndromic hearing loss in four different Chinese families using targeted next-generation sequencing and Sanger sequencing. H. Wang et al. (High frequency of AIFM1 variants and phenotype progression of auditory neuropathy in a Chinese population) investigate 50 patients with auditory neuropathy (AN) by Sanger sequencing or next-generation sequencing and confirm among late-onset AN cases, AIFM1 is the primary related gene, and p.Leu344Phe is the most common recurrent variant. P. Xu et al. (Compound heterozygous mutations in TMC1 and MYO15A are associated with autosomal recessive nonsyndromic hearing loss in two Chinese Han families) report two novel compound heterozygous mutations, i.e., p.R34X/p.M413T in TMC1 and p.S3417del/p.R1407T in MYO15A, in two recessive Chinese Han deaf families by targeted next-generation sequencing and Sanger sequencing confirms the intrafamilial cosegregation of the mutations with hearing phenotype in both families. L. Chen et al. (Transcript profiles of stria vascularis in models of waardenburg syndrome) compare the transcript profiles of stria vascularis of Waardenburg syndrome in Mitf-M mutant pig and mouse models using GO analysis and report significant gene changes in tyrosine metabolism, melanin formation, and ion transportation in both models, as well as a huge difference on the gene expression patterns and function. C. Guo et al. (Hearing phenotypes of patients with hearing loss homozygous for the GJB2 c.235delc mutation) investigate the hearing phenotypes of 244 Chinese patients with hearing loss associated with the homozygous c.235delC mutation of GJB2 and report a significant variation in their binaural hearing loss phenotypes, including severity of hearing loss, and audiogram shapes. S. Chen et al. (A novel spontaneous mutation of the SOX10 gene associated with waardenburg syndrome type II) report a novel heterozygous spontaneous c.246delC mutation in SOX10 in a Chinese family with Waardenburg syndrome (WS) type II, which may produce a truncated protein causing failure activation of MITF gene expression, a key regulator of melanocyte development in WS. X. Yu et al. (Targeted next-generation sequencing identifies separate causes of hearing loss in one deaf family and variable clinical manifestations for the p.R161C mutation in SOX10) demonstrate the heterozygous c.481C>T mutation in SOX10 and the homozygous c.235delC mutation in GJB2 as separate pathogenic mutations in distinct affected family members in a Chinese Han family with hearing loss. X. Chao et al. (Cochlear implantation in a patient with a novel POU3F4 mutation and incomplete partition type-III malformation) report a novel a novel frame shift variant c.400_401insACTC of the POU3F4

gene in a Chinese family with X-linked inheritance hearing loss and the patient carrying this mutation and diagnosed with partition type-III malfunction benefit from cochlear implantation (CI) but the effectiveness of CI declines with the age of patient.

In this special issue of “Hearing Loss: Reestablish the Neural Plasticity in Regenerated Sprial Ganglion Neurons and Sensory Hair Cells,” we have articles covering from development, protection, and regeneration of hair cells and spiral ganglion neurons, to genetic information of inherited hearing loss. All studies included present us with not only significant perspectives on the physiology and pathology of cochlea but also the latest advances in revealing the underlying molecular/neural mechanisms of hearing loss and the potential of regeneration of functional HCs and SGNs. We believe this special issue will provide vital innovations for future research in hearing area and contribute to medical interventions and treatments of cochlear damage in SNHL.

Conflicts of Interest

The editors declare that they have no conflicts of interest regarding the publication of this special issue.

Renjie Chai
Geng-lin Li
Jian Wang
Jing Zou
Hai Huang

Review Article

Hair Cell Protection from Ototoxic Drugs

Peng Wu , Xianmin Wu , Chunhong Zhang , Xiaoyun Chen , Yideng Huang ,
and He Li 

Department of Otolaryngology, First Affiliated Hospital of Wenzhou Medical University, Wenzhou City,
325000 Zhejiang Province, China

Correspondence should be addressed to Yideng Huang; huangyidengwz@yeah.net and He Li; lihewuyao@163.com

Received 29 March 2020; Accepted 28 June 2021; Published 12 July 2021

Academic Editor: Geng lin Li

Copyright © 2021 Peng Wu et al. This is an open access article distributed under the Creative Commons Attribution License, which permits unrestricted use, distribution, and reproduction in any medium, provided the original work is properly cited.

Hearing loss is often caused by death of sensory hair cells (HCs) in the inner ear. HCs are vulnerable to some ototoxic drugs, such as aminoglycosides (AGs) and the cisplatin. The most predominant form of drug-induced cell death is apoptosis. Many efforts have been made to protect HCs from cell death after ototoxic drug exposure. These mechanisms and potential targets of HCs protection will be discussed in this review. And we also propose further investigation in the field of HCs necrosis and regeneration, as well as future clinical utilization.

1. Introduction

Hearing loss is the most common sensory impairment in humans. It is estimated that there were 466 million people living with hearing loss in 2018 [1]. Hearing loss is often caused by death of sensory hair cells (HCs) in the inner ear, which function in transducing the sound waves into electric signals [2–6]. HCs are vulnerable to a variety of different stresses, such as aging, acoustic trauma, genetic disorders, infection, and exposure to some ototoxic drugs [7–13]. Unfortunately, the mammals only have very limited HC regeneration ability, and the death of HCs in mammals is irreversible, thus leading to permanent hearing deficit [13–18]. Although hearing loss is not a life-threatening disease, it can affect the patient's quality of life, especially in children, which will cause delays in language acquisition and dumb. That will cause significant burden on families and society.

Currently, the most effective and convenient protection is avoiding exposure to known ototoxic drugs. Although there are several drugs that can injure HCs, the most commonly encountered ototoxic drugs are the aminoglycosides (AGs) and the antineoplastic agent cisplatin. AGs are the most commonly prescribed antibiotics, such as gentamicin, amikacin,

kanamycin, and neomycin, which are usually used in the treatment of infections caused by aerobic gram-negative bacteria. Cisplatin is a platinum-based chemotherapeutic drug, which is often used for the chemotherapy of malignant tumors. But the ototoxicity limits the clinical application of these two kinds of drugs. Both AGs and cisplatin can induce apoptotic cell death in HCs, especially the outer HCs of the basal turn [9, 19–23].

HCs can undergo cell death through apoptosis and necrosis. But the most predominant form of drug-induced cell death is apoptosis. In order to protect HCs from ototoxic insult, a better understanding of the mechanisms of aminoglycoside- and cisplatin-induced hair cell death is required. Current studies of these apoptotic cell death mechanisms and potential targets of HC protection are discussed in this review.

2. Mechanism and Protection

2.1. Route of Ototoxic Drugs into Hair Cells. After systemic administration, ototoxic drugs can pass the blood-labyrinth barrier (BLB) and enter the endolymph via the Reissner's membrane, especially via the stria vascularis [24]. After that, they enter into HCs and cause cell death.

Multiple pathways for entry of AGs and cisplatin into HCs exist. One pathway is endocytosis at the apical and synaptic poles of HCs, although direct evidence for its involvement in cytotoxicity has not been found [25, 26]. Transport through ion channels, especially mechanoelectrical transducer (MET) channel, is supposed to play an important role in AGs uptake into HCs [25–28]. Some researchers suggest AGs and cisplatin can enter the HCs through MET channel [25, 29, 30] or Copper Transporter 1 (CTR1) [31], respectively, which are located at the top of hair cell stereocilia. Other studies suggest that MET channel is also a major contributor to the entry of cisplatin into HCs, at least in the zebrafish [32, 33]. But a direct interaction between cisplatin and mammalian MET channels has not been reported. Some researchers reveal that cisplatin entry into cochlear and HCs is also mediated by organic cation transporter (OCT), and the expression of OCT2, an isoforms of OCT, has been detected in HCs, as well as in stria vascularis [31, 34]. There is also evidence for the participation of transient receptor potential (TRP) channels, a family of polymodal ion channels activated by a variety of physical and chemical stimulation, such as oxidative stress, tissue damage, and inflammation [28]. TRP channels, such as TRPA1, TRPV1, and TRPV4, are additional candidate aminoglycoside-permeant channels, and all of them are found expressed in the HCs [35–37]. Exposure to immunostimulatory lipopolysaccharides, to simulate of bacterial infections, increased the cochlear expression of TRPV1 and hair cell uptake of gentamicin, thus, exacerbate ototoxicity of AGs [38]. In murine cochlear cultures, when the MET channels were disabled, the activated TRPA1 channels will facilitate the uptake of gentamicin [37].

2.2. Efforts in Inhibiting the Uptake of Drugs. Avoiding ototoxic drugs entry into HCs is the primary step. On the level of the MET channel, there are two possibilities exist. The first one is steric modification of the chemical structure of drugs. The MET channel pore, which has a diameter at its narrowest part of at least 1.25–1.5 nm, is large enough to allow AGs to enter the hair cell cytosol [39]. Therefore, widening the AG diameter by binding of certain molecules appears a promising strategy to inhibit AGs passing through the MET channel. But this binding must be irrelevant for antimicrobial activity [40]. The second way is blocking the MET channel to prevent ototoxic drugs entering HCs, especially for AGs. MET channel blocker, such as ORC-13661, can protect HCs against both AGs and cisplatin [41]. Because blocking of the MET channel would prevent hair cell depolarization and affect hearing function, therefore, the blockage must be temporary [42, 43].

Myosin7a is supposed to mediate AG endocytosis, and the uptake of AGs was decreased in Myosin7a mutant mice. This indicate a promising target for HC protection [44].

Intratympanic administration of copper sulfate, a CTR1 inhibitor, or knockdown of CTR1 with small interfering RNA can decrease the uptake and cytotoxicity of cisplatin and prevent hearing loss caused by cisplatin, both in vitro and in vivo [31]. OCT knockout or inhibition of

OCT with cimetidine protects HCs against cisplatin-induced ototoxicity [34].

3. The Involvement of Mitochondrial Dysfunction and DNA Damage

The entry of AGs into HCs can lead to mtDNA mutations and thus affect the RNA translation and protein synthesis within mitochondria [45] and therefore leading to a decrease in ATP synthesis. With the decrease of energy production, the mitochondrial membrane integrity is compromised and thus leading to the leakage of cytochrome c, the generation of reactive oxygen species (ROS), and activation of stress kinases [46, 47]. The accumulation of ROS and cytochrome c will lead to the activation of the upstream caspases and subsequent apoptotic cell death. On the other hand, both ROS and stress kinases can cause cell death directly, as well as by amplifying insults targeting the mitochondria. And ROS can also cause mtDNA defects.

As for cisplatin, the ototoxic mechanism has been shown to be associated with several factors, such as oxidative stress, DNA damage, and inflammatory cytokines. Several studies have implicated the mitochondrial pathways in the apoptosis of HCs after cisplatin administration [48]. Exposure to cisplatin can also cause excessive generation of ROS via the NADPH-oxidase (NOX) pathway [49, 50], which will activate the mitochondrial apoptosis pathway that mentioned above. The signal transducers and activators of transcription 1 (STAT1) is an important mediator of cell death, and the STAT1 phosphorylation was found in HCs after exposure to cisplatin. STAT1 is involved in the response to the release of ROS, inflammatory cytokines, and DNA damage [51].

All these mechanisms of drug-induced hair cell death and protection will be discussed below.

3.1. Reactive Oxygen Species. ROS are mainly generated by the mitochondria in mammalian cells. AGs can combine with iron salts, and the iron-AG complexes catalyze free radical reactions and lead to ROS generation [52]. As mentioned above, AGs decrease the ATP synthesis, which will increase the permeability of mitochondrial transmembrane and the leakage of cyt-c and ROS. The ROS can also generate via the NOX3 pathway after cisplatin exposure. The ROS overload leads to the depletion of the cochlear antioxidant enzyme system (e.g., superoxide dismutase, catalase, glutathione peroxidase, and glutathione reductase), which scavenges and neutralizes the generated superoxide and hydrogen peroxide [53]. The release of ROS causes further damage to mitochondrial components, such as mtDNA, mitochondrial membranes, and respiratory chain proteins, as well as nuclear DNA associated with mitochondrial function [54]. The ultimate effect of increased ROS generation is to promote apoptotic cell death, as described above.

3.2. Neutralization of Reactive Oxygen Species. Some studies have reported that antioxidants can promote HC survival in drug-induced ototoxicity, including coenzyme Q10 [55]; α -lipoic acid [56]; D-methionine [57]; thiourea [58]; vitamins

B, C, and E [59]; N-acetylcysteine (NAC) [60]; and hormone melatonin [61]. Knockdown of NOX3 by intratympanic delivery of short interfering RNA (siRNA) protects against cisplatin-induced HC death [62]. Reducing the expression of TRPV1 or NOX3 can inhibit the ROS generation and the transcription factor STAT1 activation. And STAT1 activation will promote proapoptotic actions of cisplatin [63]. This indicates the inhibition of TRPV1 or NOX3 as promising approaches for reducing cisplatin ototoxicity. Another candidate strategy is the use of iron chelators, 2,3-dihydroxybenzoate [64], and acetylsalicylate (ASA) [65], which can compete with AGs for iron binding.

However, effects of these long-term treatments remain to be studied.

3.3. Caspase-Mediated Apoptosis. It has generally been accepted that the ototoxic drug-induced hair cell death shares a common pathway: caspase activation.

Caspases are divided into upstream and downstream members, which are normally inactive by binding with inhibitor of apoptosis proteins (IAP) [66, 67]. The upstream caspases are activated by proapoptotic signals, such as cytochrome c [68, 69], p53 [49], antiapoptotic Bcl-2 proteins [70, 71], tumor necrosis factor (TNF) family [72], and nuclear factor kappa B (NF- κ B) [73]. And the downstream caspases are activated by upstream caspases.

Caspase-8 is an upstream member, which is linked to membrane-associated death receptors. Caspase-8 can activate by ligands such as Fas or TNF- α and subsequently activate downstream caspases such as caspases-3, -6, and -7 [72, 74]. Although caspase-8 is activated in HCs after AG administration [75], inhibition of this pathway does not prevent HC death or prevent caspase-3 activation [76]. Thus, it does not play a key role in HC death.

Caspase-9 is also an upstream member, which is triggered by nonreceptor stimulation, such as cytokine c releasing from mitochondrial [69]. After activation, caspase-9 can cleave and activate downstream caspases-3, which eventually leading to apoptotic HC death [75]. Caspase-3 is a downstream member, which mediates apoptotic program by cleaving proteins necessary for cell survival, such as cytoskeletal proteins [77]. The cisplatin-induced activation of caspase-9 and caspase-3 was seen in HEI/OC1 cells [78] and UB/OC1 cells [79].

3.4. Inhibition of Caspase Members. Studies have shown that intracochlear administration with specific inhibitors of caspase-9 or caspase-3 can prevent AG-induced or cisplatin-induced HC death and hearing loss [48, 80]. Caspase inhibitors, such as z-VAD-FMK and z-LEHD-FMK, can protect HCs against AG-induced cell death [81, 82]. Intracochlear perfusions with caspase-3 inhibitor (z-DEVD-fmk) and caspase-9 inhibitor (z-LEHD-fmk) prevent hearing loss and loss of HCs in cisplatin treated guinea pigs [48]. Several other efforts targeting the different steps in caspase activation are also promising. For example, NF- κ B inhibitors, such as Bay 11-7085 or SN-50, can inhibit cisplatin-induced caspase-3 activation and apoptosis in HEI/OC1 cells [78].

3.5. BCL-2 Family. The Bcl-2 family can be categorized as antiapoptotic (e.g., Bcl-2 and Bcl-XL) or proapoptotic (e.g., Bax, Bak, Bcl-Xs, Bid, Bad, and Bim) members [83, 84]. Antiapoptotic Bcl-2 members can bind to proapoptotic Bcl-2 members, which will neutralize the proapoptotic signal [85]. The balance between the antiapoptotic and proapoptotic members is crucial for the living of the cell. When the balance tilts to proapoptosis, the proapoptotic Bcl-2 members, such as Bax and Bid, will translocate from the cytoplasm to the mitochondria, which will increase the permeability of mitochondrial transmembrane and lead to the generation of ROS and leakage of cytochrome c into the cytoplasm, thus eventually activate caspase-9 and caspase-3 and lead to apoptotic cell death as mentioned above [86, 87]. Recently, the increased expression of Bax and the decreased expression of Bcl-XL were observed in UB/OC-1 cells after cisplatin treatment [79]. The overexpression of Bcl-2 can inhibit the release of cytochrome c, thereby inhibiting the apoptosis cascade. This has been confirmed by some researchers in cochlear cell line or mouse utricles following AGs or cisplatin exposure [48, 70, 88].

3.6. Efforts on Targeting the Bcl-2 Family. Targeting the Bcl-2 family as the upstream mediator of apoptosis can prevent AG-induced hair cell death. Some studies reveal that overexpression of the antiapoptotic Bcl-2 members can inhibit apoptotic hair cell death following AG exposure *in vitro* and *in vivo* [70, 87, 89], while epigallocatechin gallate (EGCG), a known inhibitor of STAT1, can reverse the balance of Bax and Bcl-XL to antiapoptotic, which will protect HCs against apoptosis after cisplatin administration [79].

3.7. The c-jun NH2-Terminal Kinases (JNKs). The c-jun NH2-terminal kinases (JNKs) are key modulators of apoptosis, which are activated in response to cellular insults, such as generation of ROS, in HCs treated with neomycin and cisplatin [90, 91]. JNK activation acts as upstream of cytochrome c redistribution and caspase activation [92, 93]. When activated, JNKs can activate the transcription factors c-Jun, c-FOS, ELK-1, and Bcl-2. After AG administration, the increased JNKs, c-Jun, c-FOS, and Bcl-2 have been observed in HCs [94–96].

3.8. Inhibitors of the JNK Pathway. JNK inhibitors such as CEP-1347 [97] and CEP 11004 [91] can attenuate hair cell loss following AG administration. But, JNK inhibitor does not protect HCs against cisplatin-induced cell death, nor does it prevent redistribution of cytochrome c [48].

The mechanisms of AG-induced and cisplatin-induced HCs death are summarized in Figure 1.

3.9. Other Promising Targets. There are some other mechanisms underlying the ototoxic of AGs and cisplatin, such as heat shock proteins (HSP), p53, and NF- κ B as well as calcium-dependent proteases, and so on. Researchers have achieved promising outcomes. For example, overexpression of HSP-70 in transgenic mice can protect HCs against both aminoglycoside- and cisplatin-induced hair cell death [98, 99]. It is indicated that p53 acts upstream of mitochondrial

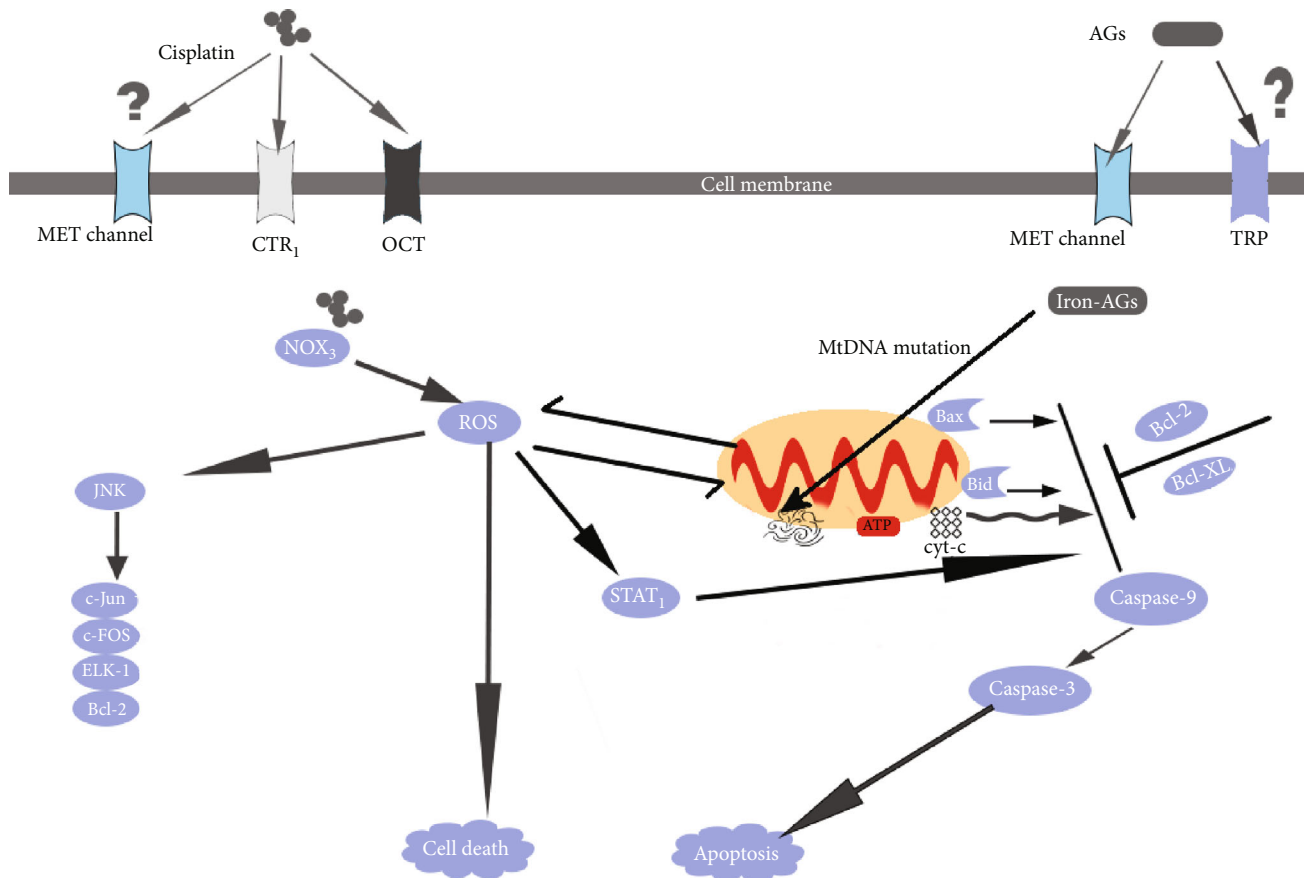


FIGURE 1: AGs and cisplatin enter the HCs through MET channel or CTR₁. The iron-AG complexes cause mtDNA mutations and affect the protein synthesis. The decrease of ATP synthesis, as well as the translocation of proapoptotic Bcl-2 members (Bax and Bid) will increase the permeability of mitochondrial transmembrane. Thus, leading to the leakage of cyt-c and ROS. The cyt-c will lead to the caspase activation and apoptosis. ROS can cause cell death or amplify insults targeting mitochondria. The iron-AG complexes can catalyze free radical reactions and lead to ROS generation. ROS can also generate via the NOX₃ pathway. When JNK was activated by ROS, it will activate some key modulators of apoptosis (c-Jun, c-FOS, ELK-1, and Bcl-2). ROS can also activate STAT₁, which will promote proapoptotic actions of cisplatin. AG: aminoglycoside; MET: mechano-electrical transducer; CTR₁: Copper Transporter 1; OCT: organic cation transporter; TRP: transient receptor potential; NOX₃: NADPH-oxidase 3; ROS: reactive oxygen species; cyt-c: cytochrome c; STAT₁: transcription factor; JNK: c-jun NH₂-terminal kinase.

apoptotic pathway and downregulation of the p53 gene protects HCs from cisplatin-induced Bax translocation, caspase-3 activation, cytochrome c translocation, and cell death [100]. Although p53 inhibitor protects against cisplatin-induced ototoxicity, the systemic application will interfere with the anticancer efficacy of cisplatin, while it is revealed that the intratympanic application of p53 inhibitor, such as pifithrin-a, protects auditory function without compromising the anticancer efficacy of cisplatin [100]. It has been revealed that Wnt/ β -catenin signaling has an important role in protecting HCs against neomycin-induced HC loss. The overexpression of β -catenin can reduce forkhead box O3 transcription factor (Foxo3) and Bim expression and ROS levels after neomycin exposure [11]. This might be a new therapeutic target. Some researchers used rapamycin, an autophagy activator, to increase the autophagy activity and found that the ROS levels, apoptosis, and cell death were significantly decreased after neomycin or gentamicin exposure,

suggesting that autophagy might be correlated with AG-induced HC death [101]. It is also revealed that meflofenamic acid can attenuate cisplatin-induced oxidative stress and apoptosis in HEI-OC1 cells, by inhibiting cisplatin-induced upregulation of autophagy [12].

3.10. Potential Drug Targets. With increased understanding of ototoxic cell death, a numerous of therapeutic efforts have been made to target different steps of in HC death. The HEI-OC1 and UB/OC-1 cell lines, organ explants, larval zebrafish lateral-line neuromasts, and some animal model (e.g., chicken, rat, mouse, and guinea pig) are the most commonly used research strategies. The delivery of test compounds can be performed by intratympanic, intraperitoneal, intramuscular, subcutaneous, intracochlear, and oral administration. Potential drug targets for treatment of AG and cisplatin ototoxicity are summarized in Table 1.

TABLE 1: Potential drug targets for treatment of AG and cisplatin ototoxicity.

Compound	Ototoxic drug	Mechanism	Materials and methods	References
ORC-13661	AG and cisplatin	Block MET channel	Mouse cochlear cultures, <i>in vitro</i> zebrafish, <i>in vitro</i>	[41]
Copper sulfate	Cisplatin	CTR1 inhibitor, inhibit uptake	HEI-OC1 cells, <i>in vitro</i> Mice, <i>in vivo</i> , i.t.	[31]
Cimetidine	Cisplatin	OCT blocker, inhibit uptake	Mice, <i>in vivo</i> , i.p.	[34]
Coenzyme Q10	Cisplatin	Antioxidant	Rat, <i>in vivo</i> , oral administrations	[55]
α -Lipoic acid	AG	Antioxidant	Guinea pigs, <i>in vivo</i> , i.m.	[56]
D-Methionine	AG	Antioxidant	Guinea pigs, <i>in vivo</i> , i.p.	[57]
Thiourea	Cisplatin	Antioxidant	Guinea pigs, <i>in vivo</i> , intracochlear perfusion by osmotic pump	[58]
Vitamins B, C, and E	Cisplatin	Antioxidant	Rat, <i>in vivo</i> , i.p.	[59]
N-Acetylcysteine	AG	Antioxidant	Rat, <i>in vivo</i> , i.p.	[60]
Hormone melatonin	Cisplatin	Antioxidant	Rat, <i>in vivo</i> , i.p.	[61]
siRNA	Cisplatin	Inhibit TRPV1 or NOX3 Inhibit ROS generation and STAT1 activation	UB/OC-1 cells, <i>in vitro</i> Rat, <i>in vivo</i> , i.t.	[62]
2,3-Dihydroxybenzoate	AG	Iron chelators Compete with AG for iron binding	Guinea pigs, <i>in vivo</i> , i.p.	[64]
Acetylsalicylate	AG	Iron chelators, compete with AG for iron binding Antioxidant	Guinea pigs, <i>in vivo</i> , oral administration	[65]
EGCG	Cisplatin	STAT1 inhibitor Antiapoptotic	Rat, <i>in vivo</i> , oral administrations	[79]
Bay 11-7085	Cisplatin	NF- κ B inhibitors Inhibit caspase-3 activation	HEI/OC1 cells, <i>in vivo</i>	[78]
SN-50	Cisplatin	NF- κ B inhibitors Inhibit caspase-3 activation	HEI/OC1 cells, <i>in vivo</i>	[78]
z-VAD-FMK	AG	General caspase inhibitor	Guinea pigs, <i>in vivo</i> , intracochlear perfusion by osmotic pump	[81]
z-LEHD-FMK	AG	Caspase-9 inhibitor	Guinea pigs, <i>in vivo</i> , intracochlear perfusion by osmotic pump	[81]
z-DEVD-fmk	Cisplatin	Caspase-3 inhibitor	Guinea pigs, <i>in vivo</i> , intracochlear perfusion by minipump	[48]
z-LEHD-fmk	Cisplatin	Caspase-9 inhibitor	Guinea pigs, <i>in vivo</i> , intracochlear perfusion by minipump	[48]
CEP-1347	AG	JNK inhibitor	Guinea pigs, <i>in vivo</i> , s.c.	[97]
CEP 11004	AG	JNK inhibitor	Chicken vestibular hair cell culture, <i>in vitro</i>	[91]
Pifithrin-a	Cisplatin	p53 inhibitor Inhibit mitochondrial apoptotic pathway	Mouse cochlear culture, <i>in vitro</i>	[100]

AG: aminoglycoside; MET: mechanoelectrical transducer; CTR1: Copper Transporter 1; OCT: organic cation transporter; siRNA: short interfering RNA; TRP: transient receptor potential; NOX3: NADPH-oxidase 3; ROS: reactive oxygen species; STAT1: transcription factor; EGCG: epigallocatechin gallate; JNK: c-jun NH2-terminal kinase; i.t.: intratympanic; i.p.: intraperitoneal; i.m.: intramuscular; s.c.: subcutaneous.

4. Conclusion

As discussed above, many efforts have been made to protect HCs from cell death after ototoxic drug exposure. The outcomes are promising, but risks also arise. For example, endotoxemia-mediated inflammation can enhance aminoglycoside trafficking across the BLB and potentiate AG-induced ototoxicity. This indicates that patients with severe infections are at greater risk of AG-induced hearing loss than previously recognized. Systemic interference with cell signal-

ing pathways may also have unknown physiological consequences. So, it is extremely difficult to apply clinically. For example, as an iron chelator, ASA itself is ototoxic and can cause tinnitus, vertigo, and hearing loss. On the other side, long-term treatment with antiapoptotic drugs bears a potential carcinogenic risk, as apoptosis is crucial in preventing uncontrolled cell proliferation. Although antioxidants are well established as otoprotectants, some studies show that administered of a single antioxidant in high oxidative environment would be rapidly oxidized and produce only

transient benefit in preventing hearing loss [102]. As for AGs can remain in HCs for months, thus, use of a single antioxidant in high-risk human populations has not produced expected benefits; the outcomes of long-term and mixture administration with other drugs are also need to be well studied.

A variety kind of insults to the inner ear can cause HC death and hearing loss. Although the most predominant form of drug-induced cell death is apoptosis, necrotic features are also seen in HCs following AG exposure [19]. This suggests that the apoptotic and necrotic cell death that occurs in HCs may share among many ototoxic events, while the necrosis and associated pathways are still unclear in HCs after ototoxic drug exposure. Research in the mechanisms of regulated necrosis in HCs may improve our understanding of the complex communications between different signaling cascades. On the other side, great progresses have been made in the field of HC regeneration. For example, it has been reported that *Lgr5*-expressing cells can differentiate into HCs [17], and several genes have been identified that regulate the regeneration of HCs [13, 18]. These are also promising strategies.

Thus, a full understanding of the mechanisms in ototoxic drug-induced hearing loss still remains urgent, and the possibility of future clinical utilization is also need to be well evaluated.

Conflicts of Interest

The authors declare that there is no conflict of interest regarding the publication of this article.

Acknowledgments

This research was jointly supported by the Zhejiang Provincial Natural Science Foundation of China and the Wenzhou basic scientific research project under Grant Nos. LY19H130003, LY19H130004, Y20H130015, and Y20180091.

References

- [1] J. Guo, R. Chai, H. Li, and S. Sun, "Protection of hair cells from ototoxic drug-induced hearing loss," *Advances in Experimental Medicine and Biology*, vol. 1130, pp. 17–36, 2019.
- [2] Y. Liu, J. Qi, X. Chen et al., "Critical role of spectrin in hearing development and deafness," *Science advances*, vol. 5, no. 4, article eaav7803, 2019.
- [3] Y. Wang, J. Li, X. Yao et al., "Loss of CIB2 causes profound hearing loss and abolishes mechanoelectrical transduction in mice," *Frontiers in Molecular Neuroscience*, vol. 10, p. 401, 2017.
- [4] C. Zhu, C. Cheng, Y. Wang et al., "Loss of ARHGEF6 causes hair cell stereocilia deficits and hearing loss in mice," *Frontiers in Molecular Neuroscience*, vol. 11, p. 362, 2018.
- [5] J. Qi, Y. Liu, C. Chu et al., "A cytoskeleton structure revealed by super-resolution fluorescence imaging in inner ear hair cells," *Cell Discovery*, vol. 5, no. 1, p. 12, 2019.
- [6] J. Qi, L. Zhang, F. Tan et al., "Espn distribution as revealed by super-resolution microscopy of stereocilia," *American Journal of Translational Research*, vol. 12, no. 1, pp. 130–141, 2020.
- [7] Z. H. He, S. Y. Zou, M. Li et al., "The nuclear transcription factor FoxG1 affects the sensitivity of mimetic aging hair cells to inflammation by regulating autophagy pathways," *Redox Biology*, vol. 28, article 101364, 2020.
- [8] S. Gao, C. Cheng, M. Wang et al., "Blebbistatin inhibits neomycin-induced apoptosis in hair cell-like HEI-OC-1 cells and in cochlear hair cells," *Frontiers in Cellular Neuroscience*, vol. 13, p. 590, 2019.
- [9] Y. Zhang, W. Li, Z. He et al., "Pre-treatment with fasudil prevents neomycin-induced hair cell damage by reducing the accumulation of reactive oxygen species," *Frontiers in Molecular Neuroscience*, vol. 12, p. 264, 2019.
- [10] W. Liu, X. Xu, Z. Fan et al., "Wnt signaling activates TP53-induced glycolysis and apoptosis regulator and protects against cisplatin-induced spiral ganglion neuron damage in the mouse cochlea," *Antioxidants & Redox Signaling*, vol. 30, no. 11, pp. 1389–1410, 2019.
- [11] L. Liu, Y. Chen, J. Qi et al., "Wnt activation protects against neomycin-induced hair cell damage in the mouse cochlea," *Cell Death & Disease*, vol. 7, no. 3, article e2136, 2016.
- [12] H. Li, Y. Song, Z. He et al., "Meclofenamic acid reduces reactive oxygen species accumulation and apoptosis, inhibits excessive autophagy, and protects hair cell-like HEI-OC1 cells from cisplatin-induced damage," *Frontiers in Cellular Neuroscience*, vol. 12, p. 139, 2018.
- [13] S. Zhang, Y. Zhang, Y. Dong et al., "Knockdown of *Foxg1* in supporting cells increases the trans-differentiation of supporting cells into hair cells in the neonatal mouse cochlea," *Cellular and Molecular Life Sciences*, vol. 77, no. 7, pp. 1401–1419, 2020.
- [14] F. Tan, C. Chu, J. Qi et al., "AAV-*ie* enables safe and efficient gene transfer to inner ear cells," *Nature Communications*, vol. 10, no. 1, p. 3733, 2019.
- [15] C. Cheng, Y. Wang, L. Guo et al., "Age-related transcriptome changes in Sox2+ supporting cells in the mouse cochlea," *Stem Cell Research & Therapy*, vol. 10, no. 1, p. 365, 2019.
- [16] X. Lu, S. Sun, J. Qi et al., "Bmi1 regulates the proliferation of cochlear supporting cells via the canonical Wnt signaling pathway," *Molecular Neurobiology*, vol. 54, no. 2, pp. 1326–1339, 2017.
- [17] T. Wang, R. Chai, G. S. Kim et al., "Lgr5+ cells regenerate hair cells via proliferation and direct transdifferentiation in damaged neonatal mouse utricle," *Nature Communications*, vol. 6, no. 1, p. 6613, 2015.
- [18] B. C. Cox, R. Chai, A. Lenoir et al., "Spontaneous hair cell regeneration in the neonatal mouse cochlea in vivo," *Development*, vol. 141, no. 4, pp. 816–829, 2014.
- [19] C. T. Dinh, S. Goncalves, E. Bas, T. R. Van De Water, and A. Zine, "Molecular regulation of auditory hair cell death and approaches to protect sensory receptor cells and/or stimulate repair following acoustic trauma," *Frontiers in Cellular Neuroscience*, vol. 9, p. 96, 2015.
- [20] A. Li, D. You, W. Li et al., "Novel compounds protect auditory hair cells against gentamycin-induced apoptosis by maintaining the expression level of H3K4me2," *Drug Delivery*, vol. 25, no. 1, pp. 1033–1043, 2018.
- [21] S. Sun, M. Sun, Y. Zhang et al., "In vivo overexpression of X-linked inhibitor of apoptosis protein protects against neomycin-induced hair cell loss in the apical turn of the cochlea during the ototoxic-sensitive period," *Frontiers in Cellular Neuroscience*, vol. 8, p. 248, 2014.

- [22] Z. He, S. Sun, M. Waqas et al., "Reduced TRMU expression increases the sensitivity of hair-cell-like HEI-OC-1 cells to neomycin damage in vitro," *Scientific Reports*, vol. 6, no. 1, article 29621, 2016.
- [23] X. Yu, W. Liu, Z. Fan et al., "c-Myb knockdown increases the neomycin-induced damage to hair-cell-like HEI-OC1 cells in vitro," *Scientific Reports*, vol. 7, article 41094, no. 1, 2017.
- [24] Q. Wang and P. S. Steyger, "Trafficking of systemic fluorescent gentamicin into the cochlea and hair cells," *Journal of the Association for Research in Otolaryngology*, vol. 10, no. 2, pp. 205–219, 2009.
- [25] A. Alharazneh, L. Luk, M. Huth et al., "Functional hair cell mechanotransducer channels are required for aminoglycoside ototoxicity," *PLoS One*, vol. 6, no. 7, article e22347, 2011.
- [26] A. A. Vu, G. S. Nadaraja, M. E. Huth et al., "Integrity and regeneration of mechanotransduction machinery regulate aminoglycoside entry and sensory cell death," *PLoS One*, vol. 8, no. 1, article e54794, 2013.
- [27] E. Hashino and M. Shero, "Endocytosis of aminoglycoside antibiotics in sensory hair cells," *Brain Research*, vol. 704, no. 1, pp. 135–140, 1995.
- [28] B. Nilius and A. Szallasi, "Transient receptor potential channels as drug targets: from the science of basic research to the art of medicine," *Pharmacological Reviews*, vol. 66, no. 3, pp. 676–814, 2014.
- [29] W. Marcotti, S. M. van Netten, and C. J. Kros, "The aminoglycoside antibiotic dihydrostreptomycin rapidly enters mouse outer hair cells through the mechano-electrical transducer channels," *The Journal of Physiology*, vol. 567, no. 2, pp. 505–521, 2005.
- [30] J. E. Gale, W. Marcotti, H. J. Kennedy, C. J. Kros, and G. P. Richardson, "FM1-43 dye behaves as a permeant blocker of the hair-cell mechanotransducer channel," *The Journal of Neuroscience*, vol. 21, no. 18, pp. 7013–7025, 2001.
- [31] S. S. More, O. Akil, A. G. Ianculescu, E. G. Geier, L. R. Lustig, and K. M. Giacomini, "Role of the copper transporter, CTR1, in platinum-induced ototoxicity," *The Journal of Neuroscience*, vol. 30, no. 28, pp. 9500–9509, 2010.
- [32] A. J. Thomas, D. W. Hailey, T. M. Stawicki et al., "Functional mechanotransduction is required for cisplatin-induced hair cell death in the zebrafish lateral line," *The Journal of Neuroscience*, vol. 33, no. 10, pp. 4405–4414, 2013.
- [33] S. Sheth, D. Mukherjee, L. P. Rybak, and V. Ramkumar, "Mechanisms of cisplatin-induced ototoxicity and otoprotection," *Frontiers in Cellular Neuroscience*, vol. 11, p. 338, 2017.
- [34] G. Ciarimboli, D. Deuster, A. Knief et al., "Organic cation transporter 2 mediates cisplatin-induced oto- and nephrotoxicity and is a target for protective interventions," *The American Journal of Pathology*, vol. 176, no. 3, pp. 1169–1180, 2010.
- [35] J. Zheng, C. Dai, P. S. Steyger et al., "Vanilloid receptors in hearing: altered cochlear sensitivity by vanilloids and expression of TRPV1 in the organ of corti," *Journal of Neurophysiology*, vol. 90, no. 1, pp. 444–455, 2003.
- [36] S. E. Myrdal and P. S. Steyger, "TRPV1 regulators mediate gentamicin penetration of cultured kidney cells," *Hearing Research*, vol. 204, no. 1-2, pp. 170–182, 2005.
- [37] R. S. Stepanyan, A. A. Indzhykulian, A. C. Vélez-Ortega et al., "TRPA1-mediated accumulation of aminoglycosides in mouse cochlear outer hair cells," *Journal of the Association for Research in Otolaryngology*, vol. 12, no. 6, pp. 729–740, 2011.
- [38] M. Jiang, H. Li, A. Johnson et al., "Inflammation up-regulates cochlear expression of TRPV1 to potentiate drug-induced hearing loss," *Science advances*, vol. 5, no. 7, article eaaw1836, 2019.
- [39] H. E. Farris, C. L. LeBlanc, J. Goswami, and A. J. Ricci, "Probing the pore of the auditory hair cell mechanotransducer channel in turtle," *The Journal of Physiology*, vol. 558, no. 3, pp. 769–792, 2004.
- [40] M. E. Huth, A. J. Ricci, and A. G. Cheng, "Mechanisms of aminoglycoside ototoxicity and targets of hair cell protection," *International journal of otolaryngology*, vol. 2011, Article ID 937861, 19 pages, 2011.
- [41] S. R. Kitcher, N. K. Kirkwood, E. D. Camci et al., "ORC-13661 protects sensory hair cells from aminoglycoside and cisplatin ototoxicity," *JCI Insight*, vol. 4, no. 15, 2019.
- [42] A. Ricci, "Differences in mechano-transducer channel kinetics underlie tonotopic distribution of fast adaptation in auditory hair cells," *Journal of Neurophysiology*, vol. 87, no. 4, pp. 1738–1748, 2002.
- [43] A. J. Hudspeth, Y. Choe, A. D. Mehta, and P. Martin, "Putting ion channels to work: mechano-electrical transduction, adaptation, and amplification by hair cells," *Proceedings of the National Academy of Sciences of the United States of America*, vol. 97, no. 22, pp. 11765–11772, 2000.
- [44] T. Hasson, P. G. Gillespie, J. A. Garcia et al., "Unconventional myosins in inner-ear sensory epithelia," *The Journal of Cell Biology*, vol. 137, no. 6, pp. 1287–1307, 1997.
- [45] S. N. Hobbie, S. Akshay, S. K. Kalapala, C. M. Bruell, D. Shcherbakov, and E. C. Böttger, "Genetic analysis of interactions with eukaryotic rRNA identify the mitoribosome as target in aminoglycoside ototoxicity," *Proceedings of the National Academy of Sciences of the United States of America*, vol. 105, no. 52, pp. 20888–20893, 2008.
- [46] H. Li, A. Kachelmeier, D. N. Furness, and P. S. Steyger, "Local mechanisms for loud sound-enhanced aminoglycoside entry into outer hair cells," *Frontiers in Cellular Neuroscience*, vol. 9, p. 130, 2015.
- [47] M. X. Guan, "Mitochondrial 12S rRNA mutations associated with aminoglycoside ototoxicity," *Mitochondrion*, vol. 11, no. 2, pp. 237–245, 2011.
- [48] J. Wang, S. Ladrech, R. Pujol, P. Brabet, T. R. Van De Water, and J. L. Puel, "Caspase inhibitors, but not c-Jun NH2-terminal kinase inhibitor treatment, prevent cisplatin-induced hearing loss," *Cancer Research*, vol. 64, no. 24, pp. 9217–9224, 2004.
- [49] J. R. García-Berrocal, J. Nevado, R. Ramírez-Camacho et al., "The anticancer drug cisplatin induces an intrinsic apoptotic pathway inside the inner ear," *British Journal of Pharmacology*, vol. 152, no. 7, pp. 1012–1020, 2007.
- [50] C. Casares, R. Ramírez-Camacho, A. Trinidad, A. Roldán, E. Jorge, and J. R. García-Berrocal, "Reactive oxygen species in apoptosis induced by cisplatin: review of physiopathological mechanisms in animal models," *European Archives of Oto-Rhino-Laryngology*, vol. 269, no. 12, pp. 2455–2459, 2012.
- [51] N. C. Schmitt, E. W. Rubel, and N. M. Nathanson, "Cisplatin-induced hair cell death requires STAT1 and is attenuated by epigallocatechin gallate," *The Journal of Neuroscience*, vol. 29, no. 12, pp. 3843–3851, 2009.
- [52] S. Denamur, D. Tyteca, J. Marchand-Brynaert et al., "Role of oxidative stress in lysosomal membrane permeabilization

- and apoptosis induced by gentamicin, an aminoglycoside antibiotic," *Free Radical Biology & Medicine*, vol. 51, no. 9, pp. 1656–1665, 2011.
- [53] D. Mukherjea, S. Ghosh, P. Bhatta et al., "Early investigational drugs for hearing loss," *Expert Opinion on Investigational Drugs*, vol. 24, no. 2, pp. 201–217, 2015.
- [54] N. D. Bonawitz, M. S. Rodeheffer, and G. S. Shadel, "Defective mitochondrial gene expression results in reactive oxygen species-mediated inhibition of respiration and reduction of yeast life span," *Molecular and Cellular Biology*, vol. 26, no. 13, pp. 4818–4829, 2006.
- [55] L. Astolfi, E. Simoni, F. Valente et al., "Correction: coenzyme Q10 plus multivitamin treatment prevents cisplatin ototoxicity in rats," *PLoS One*, vol. 12, no. 9, article e0185525, 2017.
- [56] B. J. Conlon, J. M. Aran, J. P. Erre, and D. W. Smith, "Attenuation of aminoglycoside-induced cochlear damage with the metabolic antioxidant alpha-lipoic acid," *Hearing Research*, vol. 128, no. 1-2, pp. 40–44, 1999.
- [57] D. J. Fox, M. D. Cooper, C. A. Speil et al., "d-Methionine reduces tobramycin-induced ototoxicity without antimicrobial interference in animal models," *Journal of Cystic Fibrosis*, vol. 15, no. 4, pp. 518–530, 2016.
- [58] A. Ekborn, G. Laurell, H. Ehrsson, and J. Miller, "Intracochlear administration of thiourea protects against cisplatin-induced outer hair cell loss in the guinea pig," *Hearing Research*, vol. 181, no. 1-2, pp. 109–115, 2003.
- [59] S. A. Tokgöz, E. Vuralkan, N. D. Sonbay et al., "Protective effects of vitamins E, B and C and L-carnitine in the prevention of cisplatin-induced ototoxicity in rats," *The Journal of Laryngology and Otology*, vol. 126, no. 5, pp. 464–469, 2012.
- [60] I. Aladag, M. Guven, and M. Songu, "Prevention of gentamicin ototoxicity with N-acetylcysteine and vitamin A," *The Journal of Laryngology and Otology*, vol. 130, no. 5, pp. 440–446, 2016.
- [61] J. de Araujo, L. S. M. Serra, L. Lauand, S. A. S. Kückelhaus, and A. L. L. Sampaio, "Protective effect of melatonin on cisplatin-induced ototoxicity in rats," *Anticancer Research*, vol. 39, no. 5, pp. 2453–2458, 2019.
- [62] D. Mukherjea, S. Jajoo, C. Whitworth et al., "Short interfering RNA against transient receptor potential vanilloid 1 attenuates cisplatin-induced hearing loss in the rat," *The Journal of Neuroscience*, vol. 28, no. 49, pp. 13056–13065, 2008.
- [63] T. Kaur, D. Mukherjea, K. Sheehan, S. Jajoo, L. P. Rybak, and V. Ramkumar, "Short interfering RNA against STAT1 attenuates cisplatin-induced ototoxicity in the rat by suppressing inflammation," *Cell Death & Disease*, vol. 2, no. 7, article e180, 2011.
- [64] P. Sinswat, W. J. Wu, S. H. Sha, and J. Schacht, "Protection from ototoxicity of intraperitoneal gentamicin in guinea pig," *Kidney International*, vol. 58, no. 6, pp. 2525–2532, 2000.
- [65] S. H. Sha and J. Schacht, "Salicylate attenuates gentamicin-induced ototoxicity," *Laboratory Investigation*, vol. 79, no. 7, pp. 807–813, 1999.
- [66] A. G. Cheng, L. L. Cunningham, and E. W. Rubel, "Mechanisms of hair cell death and protection," *Current Opinion in Otolaryngology & Head and Neck Surgery*, vol. 13, no. 6, pp. 343–348, 2005.
- [67] D. Brenner and T. W. Mak, "Mitochondrial cell death effectors," *Current Opinion in Cell Biology*, vol. 21, no. 6, pp. 871–877, 2009.
- [68] L. M. Leoni, Q. Chao, H. B. Cottam et al., "Induction of an apoptotic program in cell-free extracts by 2-chloro-2'-deoxyadenosine 5'-triphosphate and cytochrome c," *Proceedings of the National Academy of Sciences of the United States of America*, vol. 95, no. 16, pp. 9567–9571, 1998.
- [69] H. R. Stennicke and G. S. Salvesen, "Caspases - controlling intracellular signals by protease zymogen activation," *Biochimica et Biophysica Acta*, vol. 1477, no. 1-2, pp. 299–306, 2000.
- [70] L. L. Cunningham, J. I. Matsui, M. E. Warchol, and E. W. Rubel, "Overexpression of Bcl-2 prevents neomycin-induced hair cell death and caspase-9 activation in the adult mouse utricle in vitro," *Journal of Neurobiology*, vol. 60, no. 1, pp. 89–100, 2004.
- [71] A. B. Coffin, E. W. Rubel, and D. W. Raible, "Bax, Bcl2, and p53 differentially regulate neomycin- and gentamicin-induced hair cell death in the zebrafish lateral line," *Journal of the Association for Research in Otolaryngology*, vol. 14, no. 5, pp. 645–659, 2013.
- [72] M. Muzio, B. R. Stockwell, H. R. Stennicke, G. S. Salvesen, and V. M. Dixit, "An induced proximity model for caspase-8 activation," *The Journal of Biological Chemistry*, vol. 273, no. 5, pp. 2926–2930, 1998.
- [73] H. So, H. Kim, Y. Kim et al., "Evidence that cisplatin-induced auditory damage is attenuated by downregulation of pro-inflammatory cytokines via Nrf2/HO-1," *Journal of the Association for Research in Otolaryngology*, vol. 9, no. 3, pp. 290–306, 2008.
- [74] M. E. Peter and P. H. Krammer, "The CD95(APO-1/Fas) DISC and beyond," *Cell Death and Differentiation*, vol. 10, no. 1, pp. 26–35, 2003.
- [75] L. L. Cunningham, A. G. Cheng, and E. W. Rubel, "Caspase activation in hair cells of the mouse utricle exposed to neomycin," *The Journal of Neuroscience*, vol. 22, no. 19, pp. 8532–8540, 2002.
- [76] D. Bodmer, D. Brors, K. Pak, M. Bodmer, and A. F. Ryan, "Gentamicin-induced hair cell death is not dependent on the apoptosis receptor Fas," *The Laryngoscope*, vol. 113, no. 3, pp. 452–455, 2003.
- [77] S. Kothakota, T. Azuma, C. Reinhard et al., "Caspase-3-generated fragment of gelsolin: effector of morphological change in apoptosis," *Science*, vol. 278, no. 5336, pp. 294–298, 1997.
- [78] W. H. Chung, S. H. Boo, M. K. Chung, H. S. Lee, Y. S. Cho, and S. H. Hong, "Proapoptotic effects of NF-kappaB on cisplatin-induced cell death in auditory cell line," *Acta Otolaryngologica*, vol. 128, no. 10, pp. 1063–1070, 2008.
- [79] V. Borse, R. F. H. al Aameri, K. Sheehan et al., "Epigallocatechin-3-gallate, a prototypic chemopreventative agent for protection against cisplatin-based ototoxicity," *Cell Death & Disease*, vol. 8, no. 7, article e2921, 2017.
- [80] W. Liu, H. Staecker, H. Stupak, B. Malgrange, P. Lefebvre, and T. R. Van De Water, "Caspase inhibitors prevent cisplatin-induced apoptosis of auditory sensory cells," *Neuroreport*, vol. 9, no. 11, pp. 2609–2614, 1998.
- [81] T. Okuda, K. Sugahara, T. Takemoto, H. Shimogori, and H. Yamashita, "Inhibition of caspases alleviates gentamicin-induced cochlear damage in guinea pigs," *Auris, Nasus, Larynx*, vol. 32, no. 1, pp. 33–37, 2005.
- [82] J. I. Matsui, A. Haque, D. Huss et al., "Caspase inhibitors promote vestibular hair cell survival and function after aminoglycoside treatment in vivo," *The Journal of Neuroscience*, vol. 23, no. 14, pp. 6111–6122, 2003.

- [83] C. Borner, "The Bcl-2 protein family: sensors and checkpoints for life-or-death decisions," *Molecular Immunology*, vol. 39, no. 11, pp. 615–647, 2003.
- [84] T. Lindsten, W. X. Zong, and C. B. Thompson, "Defining the role of the Bcl-2 family of proteins in the nervous system," *The Neuroscientist*, vol. 11, no. 1, pp. 10–15, 2005.
- [85] H. Xiang, Y. Kinoshita, C. M. Knudson, S. J. Korsmeyer, P. A. Schwartzkroin, and R. S. Morrison, "Bax involvement in p53-mediated neuronal cell death," *The Journal of Neuroscience*, vol. 18, no. 4, pp. 1363–1373, 1998.
- [86] S. Shimizu, Y. Eguchi, W. Kamiike et al., "Bcl-2 prevents apoptotic mitochondrial dysfunction by regulating proton flux," *Proceedings of the National Academy of Sciences of the United States of America*, vol. 95, no. 4, pp. 1455–1459, 1998.
- [87] S. C. Pfannenstiel, M. Praetorius, P. K. Plinkert, D. E. Brough, and H. Staecker, "Bcl-2 gene therapy prevents aminoglycoside-induced degeneration of auditory and vestibular hair cells," *Audiology & Neuro-Otology*, vol. 14, no. 4, pp. 254–266, 2009.
- [88] P. Devarajan, M. Savoca, M. P. Castaneda et al., "Cisplatin-induced apoptosis in auditory cells: role of death receptor and mitochondrial pathways," *Hearing Research*, vol. 174, no. 1-2, pp. 45–54, 2002.
- [89] Y. H. Liu, X. M. Ke, Y. Qin, Z. P. Gu, and S. F. Xiao, "Adeno-associated virus-mediated Bcl-xL prevents aminoglycoside-induced hearing loss in mice," *Chinese Medical Journal*, vol. 120, no. 14, pp. 1236–1240, 2007.
- [90] H. M. Shen and Z. G. Liu, "JNK signaling pathway is a key modulator in cell death mediated by reactive oxygen and nitrogen species," *Free Radical Biology & Medicine*, vol. 40, no. 6, pp. 928–939, 2006.
- [91] J. I. Matsui, J. E. Gale, and M. E. Warchol, "Critical signaling events during the aminoglycoside-induced death of sensory hair cells in vitro," *Journal of Neurobiology*, vol. 61, no. 2, pp. 250–266, 2004.
- [92] K. Sugahara, E. W. Rubel, and L. L. Cunningham, "JNK signaling in neomycin-induced vestibular hair cell death," *Hearing Research*, vol. 221, no. 1-2, pp. 128–135, 2006.
- [93] J. E. Lee, T. Nakagawa, T. S. Kim et al., "Signaling pathway for apoptosis of vestibular hair cells of mice due to aminoglycosides," *Acta Oto-Laryngologica. Supplementum*, vol. 124, pp. 69–74, 2004.
- [94] L. P. Rybak and C. A. Whitworth, "Ototoxicity: therapeutic opportunities," *Drug Discovery Today*, vol. 10, no. 19, pp. 1313–1321, 2005.
- [95] U. Pirvola, L. Xing-Qun, J. Virkkala et al., "Rescue of hearing, auditory hair cells, and neurons by CEP-1347/KT7515, an inhibitor of c-Jun N-terminal kinase activation," *The Journal of Neuroscience*, vol. 20, no. 1, pp. 43–50, 2000.
- [96] J. Wang, T. R. Van De Water, C. Bonny, F. de Ribaupierre, J. L. Puel, and A. Zine, "A peptide inhibitor of c-Jun N-terminal kinase protects against both aminoglycoside and acoustic trauma-induced auditory hair cell death and hearing loss," *The Journal of Neuroscience*, vol. 23, no. 24, pp. 8596–8607, 2003.
- [97] A. A. Eshraghi, J. Wang, E. Adil et al., "Blocking c-Jun-N-terminal kinase signaling can prevent hearing loss induced by both electrode insertion trauma and neomycin ototoxicity," *Hearing Research*, vol. 226, no. 1-2, pp. 168–177, 2007.
- [98] T. G. Baker, S. Roy, C. S. Brandon et al., "Heat shock protein-mediated protection against cisplatin-induced hair cell death," *Journal of the Association for Research in Otolaryngology*, vol. 16, no. 1, pp. 67–80, 2015.
- [99] M. Taleb, C. S. Brandon, F. S. Lee, K. C. Harris, W. H. Dillmann, and L. L. Cunningham, "Hsp70 inhibits aminoglycoside-induced hearing loss and cochlear hair cell death," *Cell Stress & Chaperones*, vol. 14, no. 4, pp. 427–437, 2009.
- [100] N. Benkafadar, J. Menardo, J. Bourien et al., "Reversible p53 inhibition prevents cisplatin ototoxicity without blocking chemotherapeutic efficacy," *EMBO Molecular Medicine*, vol. 9, no. 1, pp. 7–26, 2017.
- [101] Z. He, L. Guo, Y. Shu et al., "Autophagy protects auditory hair cells against neomycin-induced damage," *Autophagy*, vol. 13, no. 11, pp. 1884–1904, 2017.
- [102] K. N. Prasad and S. C. Bondy, "Increased oxidative stress, inflammation, and glutamate: potential preventive and therapeutic targets for hearing disorders," *Mechanisms of Ageing and Development*, vol. 185, article 111191, 2020.

Research Article

Low-Intensity Ultrasound Causes Direct Excitation of Auditory Cortical Neurons

Xiaofei Qi ^{1,2,3,4} Kexin Lyu ^{5,6} Long Meng ⁷ Cuixian Li ^{1,2,4,6,8}
Hongzheng Zhang ^{5,6} Lili Niu ⁷ Zhengrong Lin ⁷ Hairong Zheng ⁷
and Jie Tang ^{1,2,4,6,8}

¹Department of Physiology, School of Basic Medical Sciences, Southern Medical University, Guangzhou, China

²Key Laboratory of Mental Health of the Ministry of Education, Southern Medical University, Guangzhou, China

³Department of Anesthesiology, Shenzhen Maternity and Child Healthcare Hospital, Southern Medical University, Shenzhen, China

⁴Guangdong-Hong Kong-Macao Greater Bay Area Center for Brain Science and Brain-Inspired Intelligence, Southern Medical University, Guangzhou, China

⁵Department of Otolaryngology Head & Neck Surgery, Zhujiang Hospital, Southern Medical University, Guangzhou, China

⁶Hearing Research Center, Southern Medical University, Guangzhou, China

⁷Paul C. Lauterbur Research Center for Biomedical Imaging, Institute of Biomedical and Health Engineering, Shenzhen Institutes of Advanced Technology, Chinese Academy of Sciences, Shenzhen, China

⁸Institute of Mental Health, Southern Medical University, Guangzhou, China

Correspondence should be addressed to Hairong Zheng; hr.zheng@siat.ac.cn and Jie Tang; jietang@smu.edu.cn

Received 14 April 2020; Revised 2 May 2020; Accepted 19 March 2021; Published 5 April 2021

Academic Editor: Renjie Chai

Copyright © 2021 Xiaofei Qi et al. This is an open access article distributed under the Creative Commons Attribution License, which permits unrestricted use, distribution, and reproduction in any medium, provided the original work is properly cited.

Cochlear implantation is the first-line treatment for severe and profound hearing loss in children and adults. However, deaf patients with cochlear malformations or with cochlear nerve deficiencies are ineligible for cochlear implants. Meanwhile, the limited spatial selectivity and high risk of invasive craniotomy restrict the wide application of auditory brainstem implants. A noninvasive alternative strategy for safe and effective neuronal stimulation is urgently needed to address this issue. Because of its advantage in neural modulation over electrical stimulation, low-intensity ultrasound (US) is considered a safe modality for eliciting neural activity in the central auditory system. Although the neural modulation ability of low-intensity US has been demonstrated in the human primary somatosensory cortex and primary visual cortex, whether low-intensity US can directly activate auditory cortical neurons is still a topic of debate. To clarify the direct effects on auditory neurons, in the present study, we employed low-intensity US to stimulate auditory cortical neurons *in vitro*. Our data show that both low-frequency (0.8 MHz) and high-frequency (>27 MHz) US stimulation can elicit the inward current and action potentials in cultured neurons. *c-Fos* staining results indicate that low-intensity US is efficient for stimulating most neurons. Our study suggests that low-intensity US can excite auditory cortical neurons directly, implying that US-induced neural modulation can be a potential approach for activating the auditory cortex of deaf patients.

1. Introduction

In mammals, the cochlear hair cells transduce the sound mechanical stimulation into electrical neural signals [1–3], which then be transferred by spiral ganglion neurons (SGNs) into the auditory cortex to have hearing ability. Previous studies have already shown that hair cells are very easy to be injured in response of various stresses, including ototoxic

drugs, aging, noise, and inflammation [4–7]. The cochlear implant (CI) is a common treatment for hearing loss in children and adults, which can partially replace the function of hair cells. The multielectrode array converts acoustic signals into electrical signals which stimulate SGNs directly, activating auditory nervous system to generate hearing. This treatment requires anatomically intact cochlear nerves and normal function of SGNs for better outcomes [8]. Poor

outcomes can be seen frequently in profound hearing loss patients with cochlear malformations or with cochlear nerve deficiencies due to the lack of accurate stimuli on SGNs by electrode. For example, deaf patients with neurofibromatosis type 2 (NF2), complete cochlear ossification, or cochlear nerve avulsion are not amenable to cochlear implant.

Auditory brainstem implant (ABI) or cranial nerve implants have been developed to restore auditory perception in these patients. The multielectrode array embedded within the brainstem stimulates the cochlear nucleus or higher stages of auditory nucleus directly, conferring the response of the central auditory system [9, 10]. However, because of the small number of electrodes and the broad region of neurons activated by each channel, the spatial selectivity of ABI is limited, restricting the outcomes of ABI [11]. Moreover, invasive surgery is required for ABI in the deep brain, increasing the complexity of surgery and the risk of complications [12]. Presently, only approximately 1,000 ABI procedures have been performed worldwide [11]. This number is far less than the population of deaf patients who are ineligible for CI. A noninvasive method stimulating the auditory nervous system is urgently needed.

Since the first observation of activation effects of ultrasound (US) on frog muscles in 1940, the effects of US stimulation on nerve system have been of great interests for neuroscientists [13, 14]. In the past decade, US has been demonstrated to modulate the neural activity in the thalamus, cortex, and hippocampus of different species, including humans [15–19]. Considering the penetrating and focusable characteristics of US stimulation, these findings suggest that US could be used as a noninvasive approach to modulating neural activity precisely [20, 21]. Based on these advantages, the concept of sonogenetics has been proposed as an alternative to optogenetics to advance the investigation and application of neuroscience [13, 14].

An obvious question that can be raised is whether US could replace electrical neural stimulation in ABI or cranial nerve implants. If central auditory neurons could be activated noninvasively by US, it is possible that the auditory response could be restored while avoiding the risk of craniotomy for many patients. Low-intensity US can result in the neural modulation in the human primary somatosensory cortex [22–24] and primary visual cortex [25], but whether US stimulation can directly activate the auditory cortex is not clear. In the present study, we examined the effects of low-intensity US stimulation on cultured auditory cortical neurons. Our data shows that low-intensity US is sufficient to elicit the excitation of single neurons. US stimulations with different frequencies are effective in activating most auditory cortical neurons. Our finding suggests that US is a potential approach to stimulating the auditory cortex safely and effectively, and further investigation of US stimulation as a method to restore hearing of patients suffering from hearing loss is meaningful.

2. Materials and Methods

2.1. Low-Intensity Ultrasound Stimulation. In the present study, a homemade ultrasound stimulation system was

designed and used to stimulate single cultured cortical neurons or HEK293T cells. The pulsed ultrasound waves were generated by a computer-gated signal generator (RIGOL, DG4162) and amplified by a power amplifier (ZHL-5W-1, Mini-Circuits, Brooklyn, NY, USA). The ultrasound waves were then applied to the ultrasound transducer with a tip diameter of ~ 3 mm (Figure 1(a)). Each US stimulation contains 500 tone burst pulses at a center frequency of 0.8 MHz and a repetition frequency of 1 kHz with a duty cycle of 50% (Figure 1(b)). The interval between stimulus was 1 second. The peak-to-peak pressure was measured, and the output intensity was limited at 0.3 MPa. During the experiment, the transducer was tilted at 45° to the culture dish, and the tip of the transducer was submerged in the extracellular solution where the cells were located. Under a microscopy, the transducer was moved to the cell closely to stimulate the cell.

In some experiments, a custom-made ultrasound neuro-modulation chip was used to generate surface acoustic waves. This chip consists of miniaturized interdigital transducers (IDTs) and an agar plate. The surface acoustic waves were generated from IDTs, and its wavelength was $160 \mu\text{m}$ at the resonant frequency of 27.42 MHz. The recording chamber where cells were located consisted of polydimethylsiloxane material with a diameter of 0.8 cm and a depth of 3 mm. The tone bursts of sinus ultrasound waves were generated by a computer-gated signal generator (RIGOL, DG4162), amplified by a power amplifier (ZHL-5 W-1, Mini-Circuits, Brooklyn, NY, USA) and applied to the IDTs. The ultrasound frequency, RPF, and voltage amplitude were controlled. The cells cultured on slips were placed in the chamber and received US stimulation for 1 s with a 9 s interval. The acoustic pressure generated by IDTs in the experiments was approximately 0.13 MPa measured by laser Doppler velocimetry (UHF-120 Ultra High-Frequency Vibrometer, Polytec, Germany).

2.2. Primary Cortical Neuron and HEK293T Cell Culture.

Animal experiments were approved by the Animal Ethics Committee of Southern Medical University. For the primary culture of cortical neurons, fetal C57 mice were obtained at embryonic days 16–18. The whole brain was collected from fetal mice, and the auditory cortex was dissected and digested with 0.25% trypsin at 37°C for 10 min. The neurons were centrifuged and suspended in Dulbecco's modified Eagle's medium (DMEM, Gibco, Life Technologies, USA) with 10% FBS and plated at a density of $6 \sim 7 \times 10^4$ cells/cm² on poly-L-lysine (Sigma-Aldrich, St. Louis, MO, USA)-coated coverslips and cultured in a humidified 5% CO₂ atmosphere at 37°C . After the neurons were adhered, the medium was changed to neurobasal medium (Gibco, life, USA) containing 2% B27 supplement (Gibco, life, USA). Afterwards, half of the medium was changed twice a week. At 14–18 days, the cells were removed for the experiments. HEK293T cells were cultured in DMEM (Gibco, Life Technologies, USA) supplemented with 10% fetal bovine serum (Gibco, Life Technologies, USA), as described previously [26, 27].

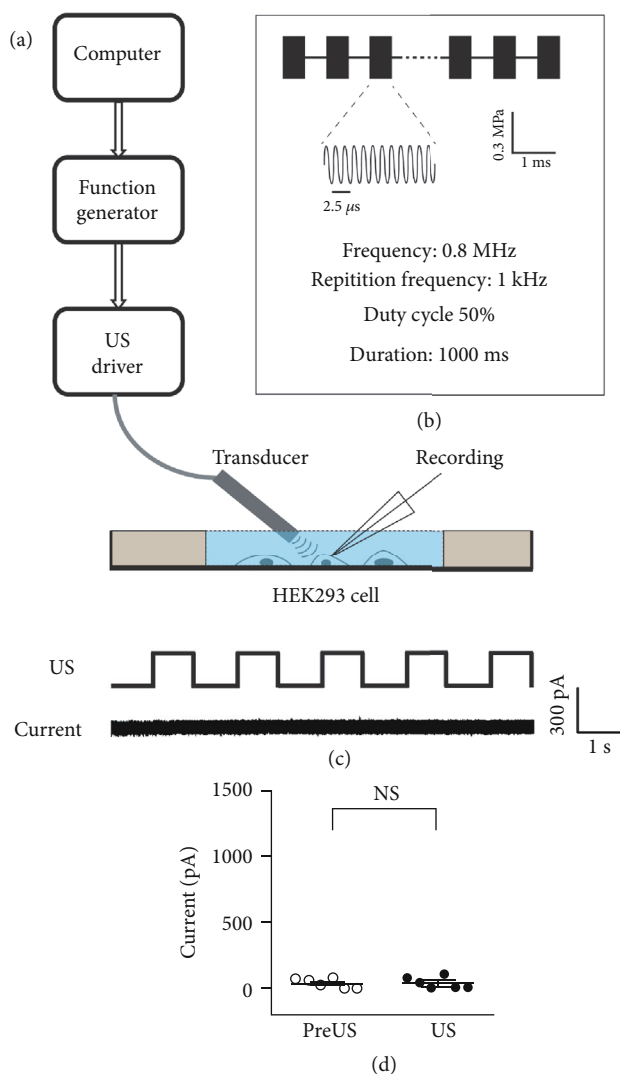


FIGURE 1: The ultrasound stimulation system and the patch clamp recording of cultured cells. (a) A schematic illustration of our combined recording and ultrasound system. The response to ultrasound stimulation of a single HEK293 cell was measured. (b) A schematic illustration of the pulsed waves of ultrasound stimulation, with an acoustic pressure of 0.3 MPa, 1 kHz repetition frequency, and 50% duty cycle. (c) US stimulation did not elicit changes in the membrane current of a representative HEK293 cell. (d) The mean current amplitude before and during US stimulation. Data are presented as the mean \pm SE. NS: no statistic difference, $p > 0.05$, $n = 7$, paired t -test.

2.3. Electrophysiological Recording. The membrane current was recorded under whole-cell patch clamp recording mode as described in our previous study for different cell types [28–31]. In brief, under the whole-cell patch configuration, the membrane potential of neuron or HEK293T cell was held at -70 mV with a patch clamp amplifier (700B, Axon Instruments, USA). The membrane current before or during US stimulation was amplified, digitalized, and recorded by a patch clamp amplifier (700B) and a processor (1440A, Axon Instruments, USA). The extracellular solution contained (in mmol/L) 150 NaCl, 1 MgCl₂, 2.5 CaCl₂, 10 HEPES, and 10 glucose, with a pH of 7.4 and osmotic pressure of

305 mmol/L. The intracellular solution of glass pipettes (resistance in the range of 2–5 M Ω) contained (in mmol/L) 140CsCl, 2MgCl₂, 2Mg-ATP, 1EGTA, 5HEPES, and 10 glucose with a pH of 7.35 and an osmotic pressure of 305 mmol/L.

The action potential of neurons was recorded under whole-cell patch clamp mode. After the configuration of the whole-cell patch, the cell was held at $I = 0$ under current clamp mode. The membrane potential before or during US stimulation was amplified, digitalized, and recorded by a patch clamp amplifier (700B) and a processor (1440A, Axon Instruments, USA). The extracellular solution contained (in mmol/L) 136 NaCl, 2.5 KCl, 1.3 MgSO₄, 10 HEPES, 10 glucose, and 2.5 CaCl₂ with a pH of 7.2–7.4 and an osmotic pressure of 290–310 mmol/L. The intracellular solution of glass pipettes (resistance in the range of 2–5 M Ω) contained (in mmol/L) KCl 130, Na-HEPES 10, EGTA 0.2, MgCl₂ 2, with a pH 7.2, and osmotic pressure at 290–300 mmol/L.

For spike recording, the potential was recorded with the cell-attach (or loose patch) method using the same setup. When the tip of the recording electrode was attached to the membrane of the neurons, the neurons were held at $I = 0$ under the current clamp. The potential before or during US stimulation was amplified, digitalized, and recorded by a patch clamp amplifier (700B) and a processor (1440A, Axon Instruments, USA).

2.4. Immunocytochemical Fluorescent Staining. For MAP2 staining, after culturing for 14 days, the cortical neurons were fixed with 4% paraformaldehyde for 20–30 min at room temperature. After washing with PBS, the neurons were treated with 3% Triton X-100 for permeabilization. Then, the cells were blocked with 10% goat serum for 2 h. The neurons were then incubated with MAP2 primary antibody (1 : 1000, Proteintech, Chicago, IL, USA) in blocking buffer at 4°C overnight. After washing out the primary antibody with PBS, the neurons were incubated with a secondary antibody conjugated with Alexa Fluor568 (1 : 1000; goat-anti-rabbit, Life Tech, USA) in dark for 2 h at room temperature. Then, the cells were washed and mounted with ProLong Gold antifade mounting reagent (Invitrogen, Carlsbad, CA) on a glass slide. The fluorescence images were acquired using a confocal microscope (A1+, Nikon, Japan).

Detection of c-Fos expression was performed in neuron cultures with or without US stimulation. The neurons on the coverslip were fixed and treated with 3% Triton X-100. For neurons receiving US stimulation, this step should be performed within 30 min after stimulation. Then, the neurons were incubated with c-Fos primary antibody (BS1130, Bioworld Tech) at 4°C overnight. After washing out the primary antibody with PBS, the neurons were incubated with a secondary antibody conjugated with Alexa Fluor568 (1 : 1000; goat-anti-rabbit, Life Tech, USA) in dark for 2 h at room temperature. The fluorescence images were acquired, and the fluorescence intensity was calculated using a confocal microscope (A1+, Nikon, Japan).

2.5. Data Analysis and Statistics. The data analysis was performed using SPSS 22.0 (IBM, USA). A paired t -test was

performed between the pre- and post-US stimulation groups; a two-sample *t*-test was performed between two groups. A repeated-measures ANOVA was applied when comparing two groups at different time points. Significance was defined as $p < 0.05$. GraphPad Prism 7 (GraphPad Software, San Diego, CA) was used for plotting.

3. Results

A customized ultrasound (US) stimulation system was used to stimulate the cultured cells. As shown in Figure 1(a), the US waves were delivered through a US transducer, which was submerged in the extracellular solution at a 45-degree angle to the bottom of the recording dish. This system results in a direct US stimulation to the recording cells and minimized acoustic reverberation. Each US stimulus comprised 500 tone burst pulses as shown in Figure 1(b). The center frequency of US stimulus was set at 800 kHz with a duty cycle of 50% at a repetition frequency of 1 kHz. The acoustic pressure was set at 0.3 MPa to minimize any possible thermal effects. By using a micromanipulator, the tip of the US transducer and the recording electrode were placed in the same view under the microscope such that the responses of the US-stimulated cell could be recorded by the patch-clamp recording system.

First, the possible effects of US stimulation were examined in the HEK293T cells. After the achieving whole-cell configuration, US stimulation was delivered to the recorded cell every other second for 20 s. Figure 1(c) shows a 10 s membrane current trail of a representative HEK293T cell. No detectable transmembrane current was found during the whole measurement during either US stimulation or the non-US period. Comparing the average membrane current during US stimulation (US, 38.33 ± 18.3 pA, mean \pm SE) and the intervals of US stimuli (pre-US, 40.00 ± 14.4 pA, mean \pm SE), no difference made by US was found for the seven HEK293T cells recorded (Figure 1(d), $p = 0.96$, the paired *t*-test). We thus confirmed that the low power US stimuli elicited no significant effect on HEK293T cells, including any possible changes to whole-cell patch configuration or thermal effects.

The effects of US stimulation on auditory cortical neurons were examined in primary neuron cultures. Cultures of primary cortical neurons were prepared from the mouse auditory cortex on embryonic day (E) 17 [32, 33]. Dissected cells were cultured in neurobasal medium for at least 14 days to remove the neuroglial cells. We verified the composition of the cell culture by examining the immunofluorescence of MAP2, a marker of mature neurons. As shown in Figure 2(a), after culturing for 14 days in vitro (DIV), most cells were MAP2 positive, indicating that the culture was almost purely neural and the astrocytes and oligodendrocytes were negligible.

The responses of cultured neurons to US stimuli were examined by a whole-cell patch clamp at DIV 14 to 18. Figure 2(b) shows the representative membrane current of a neuron in response to 0.3 MPa US stimuli. We observed no current change without US stimulation, whereas the neuron showed robust and large inward currents upon US stim-

uli. For six neurons measured, the mean frequency of the inward current (US+, 0.12 ± 0.04 Hz, mean \pm SE) and their mean amplitude (US+, 694.5 ± 73.3 pA, mean \pm SE) were significantly higher than those when US was absent (US-, $p = 0.04$ for frequency and $p = 0.003$ for amplitude, one-way ANOVA) (Figures 2(c) and 2(d)). Compared with the current changes recorded from HEK293T cells, the cortical neurons showed a significant response to US stimuli ($p = 0.035$ for frequency and $p = 0.001$ for amplitude, one-way ANOVA). Thus, these data confirmed that the cultured auditory cortical neurons could be activated by our US stimulation setup.

In the central auditory system, action potentials are critical for the information flow between neurons [34]. Therefore, we further measured the membrane potential to determine whether US stimulation could elicit action potentials of the culture neurons. Using the same US stimulation at the holding potential at -70 mV, we found that the representative neuron showed more action potentials during the period of delivered US stimulus (Figure 3(a)). Comparing with the spontaneous response, the number of action potentials for all nine neurons recorded increased significantly in response to US stimuli (Figure 3(b) 1.74 ± 0.33 , mean \pm SE, $p < 0.001$, paired *t*-test).

Together with the inward current data, these results suggest that low-power and low-frequency US is sufficient to activate cortical neurons in vitro. Our finding is consistent with the reported results by measuring the low-frequency US-induced Ca^{2+} influx in brain slices [18]. However, several investigations have indicated that US stimuli with much higher frequency also produce remarkable biological effects on *elegans* and rat hippocampal neurons [35–37]. To determine whether high-frequency US can activate auditory cortical neurons as well, we employed the same ultrasound chip to deliver US to the neurons as described in previous research [35, 37]. This ultrasound chip generated surface acoustic waves such that the neurons attached on a region of the bottom of slice were stimulated by US with a resonant frequency of 27.42 MHz (Figure 4(a)). The spikes of stimulated neurons were recorded by the cell attached recording method, by which the long-term neural responses to US could be monitored. Figure 4(b) shows the spikes of a representative neuron before and during US stimulation. Before US was delivered, the neuron showed some spontaneous spikes with a low firing rate (pre-US in Figure 4(b)). We found that its firing rate was increased by several rounds of US stimulation (US in Figure 4(b)). For all nine neurons examined, the mean firing rate after 15 rounds of US stimuli was 4.91 ± 1.54 Hz (mean \pm SE), which was significantly higher than the spontaneous firing rate (0.39 ± 0.17 Hz, mean \pm SE) before US stimulation (Figure 4(c), $p = 0.015$, the paired *t*-test). We also noticed that their firing rates were gradually increased with the rounds of US stimuli, implying the changes in excitation of the stimulated neurons (Figure 4(d)).

To further determine the effects of US on the overall neurons, the *c-Fos* expression was examined for all neurons in the stimulation region on the slice. As an immediate early gene, *c-Fos* sensitizes to neural activity, resulting in the accumulation of *c-Fos* protein in the activated neurons [38]. As

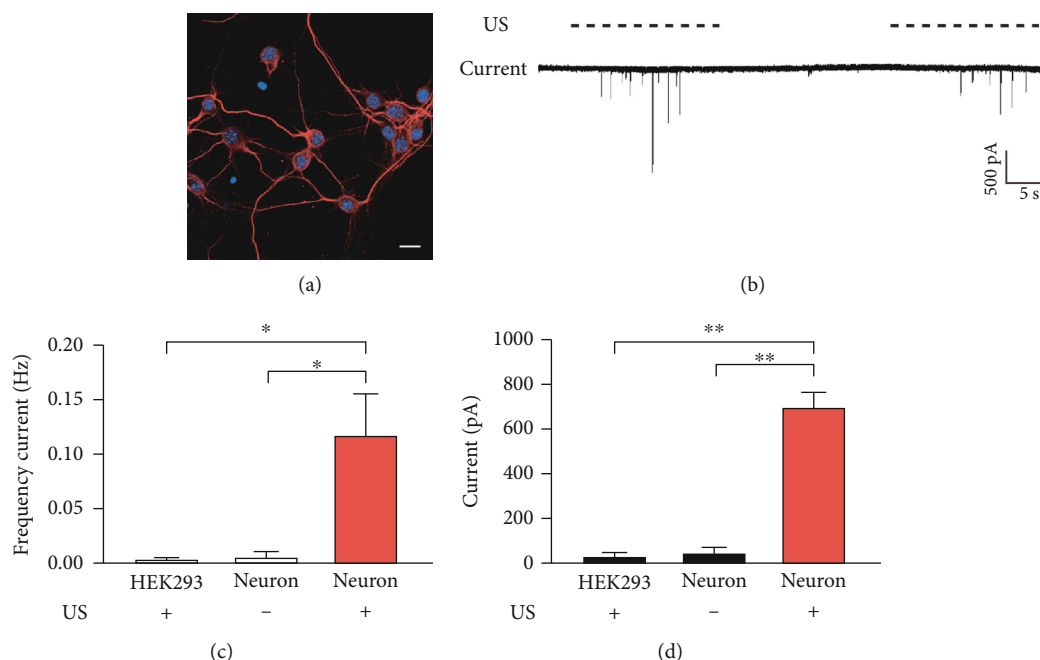


FIGURE 2: Ultrasound stimulation induces inward current in cultured cortical neurons. (a) A representative confocal image shows the immunofluorescence of MAP2 (red), a marker of mature neurons, of the cultured neurons after 14 days *in vitro*. The nuclei were labeled by DAPI (blue). Bar = 20 μm . (b) The membrane current recording of a representative neuron in response to US stimuli. The dashed lines show the stimulation of US pulses. (c, d) The mean frequency (c) and amplitude (d) of inward current of neurons with or without US stimulation. The response of HEK293 cells is compared as the control. Data are presented as the mean \pm SE. * $p < 0.05$; ** $p < 0.01$; $n = 6$ for each group, one-way ANOVA.

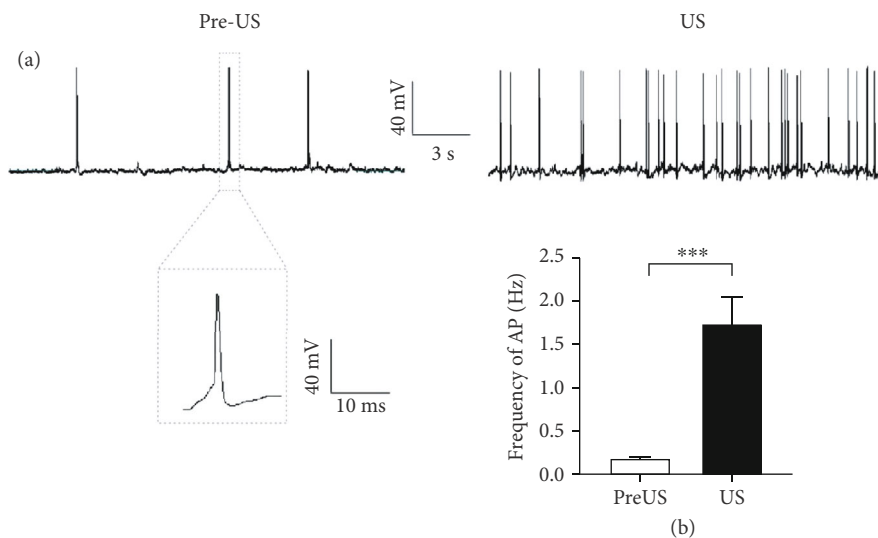


FIGURE 3: Ultrasound stimulation elicits action potentials in cultured cortical neurons. (a) Representative traces show the action potentials of a cultured cortical neuron before (pre-US) and during (US) US stimulation. Inset shows the shape of the action potential. (b) The mean frequencies of the action potentials of spontaneous firing (pre-US) and during (US) US stimulation. Data are presented as the mean \pm SE. *** $p < 0.001$, $n = 9$, paired *t*-test.

shown in the confocal images of c-Fos immunofluorescence (Figure 5(a)), after 5 min of US stimulation, the increased fluorescence of c-Fos was observed in most neurons with very few exceptions (white arrows in Figure 5(a)). We calculated the intensity of c-Fos immunofluorescence for all neu-

rons. Compared with the controls without US stimulation, the curve of cumulative fluorescence intensity was shifted to the right by US (Figure 5(b), $p < 0.001$, two-way ANOVA). The mean fluorescence intensity was increased from 742.7 ± 81.1 (mean \pm SE) to 1462.5 ± 147.7 (mean \pm SE) after US

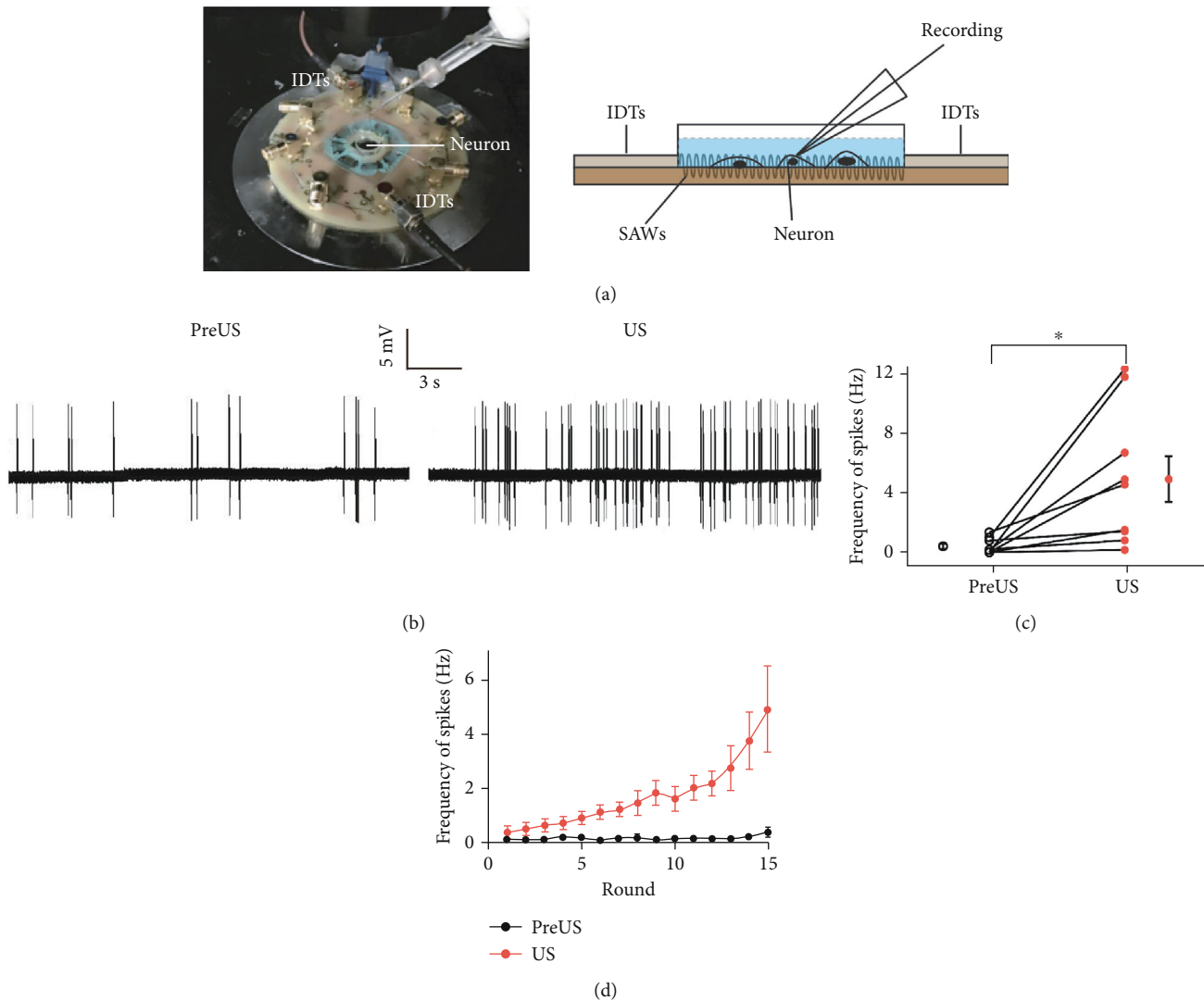


FIGURE 4: High-frequency ultrasound activates cultured auditory cortical neurons. (a) The ultrasound neural stimulation chip. Left, the photograph of the ultrasound neural stimulation chip used in the experiment. Right, a schematic illustration of the chip. The ultrasound neural stimulation chip consists of miniaturized interdigital transducers (IDTs) and an agar plate. The responses of neurons to surface acoustic waves (SAWs) were recorded. (b) The representative traces show the action potentials of a cultured cortical neuron before (pre-US) and during (US) US stimulation. (c) The changes of frequencies of action potential before (pre-US, open circles) and during (US, red circles) US stimulation for nine neurons. The mean values are also shown. Data are presented as the mean \pm SE. * $p < 0.05$, $n = 9$, paired t -test. (d) The frequency of action potentials increased with the repeated US stimulation. Data are presented as the mean \pm SE, $n = 9$.

stimulation, indicating that high-frequency US activated neurons significantly (Figure 5(c), $p < 0.0027$, Student's t -test).

4. Discussion

US stimulation provides a theoretical advantage over electrical stimulation for neuronal stimulation because of its noninvasive nature. In the past 20 years, scientists have found that low-intensity ultrasound can result in transient modulation of neural activity as a safe brain stimulation modality [13, 14]. In many mammalian species, in vivo and in vitro US stimulation have been demonstrated to modulate the activity of thalamic [15, 19], cortical [16, 17], and hippocampal [17, 18] circuits. There is also evidence that low-intensity US

can result in the same neuromodulation in the human primary somatosensory cortex [22–24] and primary visual cortex [25]. In the present study, for the first time, we demonstrated that US stimulation modulates single-neuron discharge in the cultured neurons from mouse auditory cortex (Figures 2, 3, and 4). Both focused US (Figures 2 and 3) and surface US waves (Figures 4 and 5) are efficient at activating auditory cortical neurons. We also found that high-frequency US stimulation is as efficient as low-frequency US. These results consistent with the reported findings in different brain regions and in genetically modified neurons [16, 37, 39]. Although our results were observed in mice, we expect that low-intensity US can be applied to modulate the neural activity in human auditory cortex.

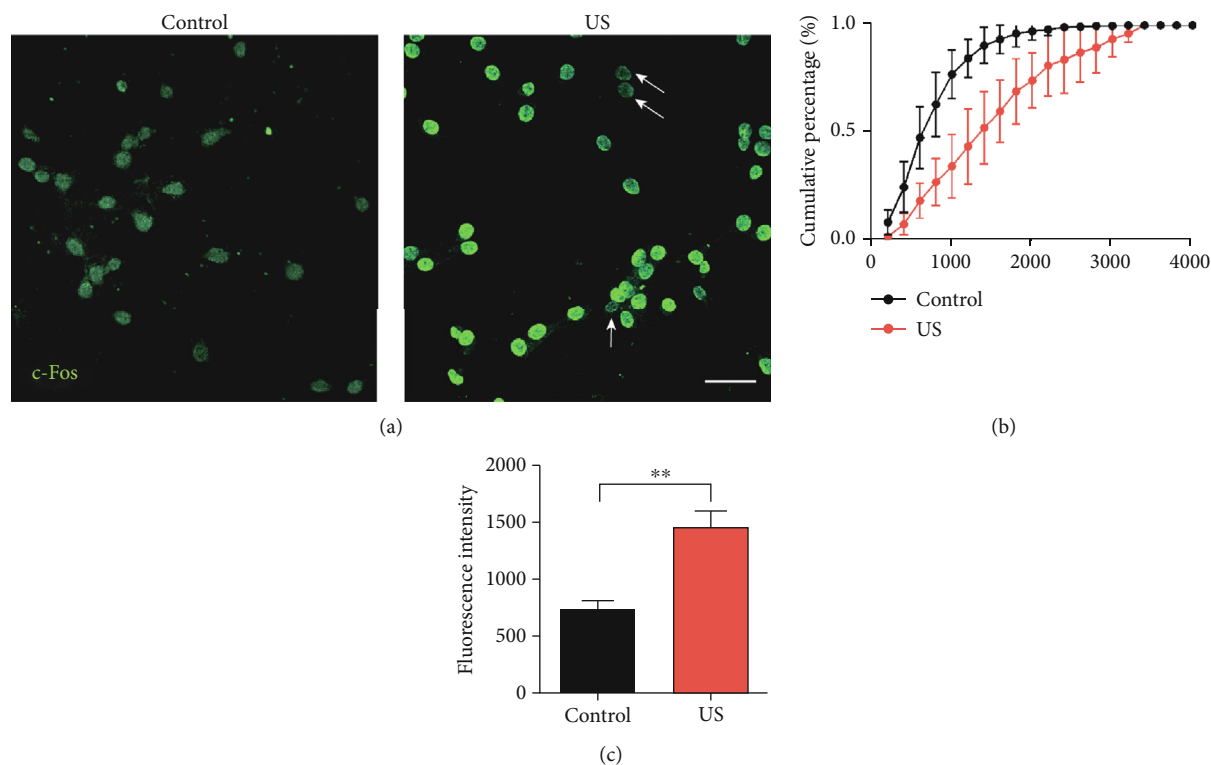


FIGURE 5: US stimulation increased c-Fos expression in auditory cortical neurons. (a) The representative confocal images show the immunofluorescence of c-Fos (green) of the cultured neurons with (right, US) or without (left, control) US stimulation. Arrows indicate the neurons without obvious increasing of c-Fos expression. Bar = 50 μm . (b) Cumulative percentage of c-Fos fluorescence intensity with (red line) or without (black line) US stimulation. Data are presented as the mean \pm SE, $n = 5$ cultures. (c) The mean intensity of c-Fos fluorescence of neurons with (red, US) or without (black, control) US stimulation. Data are presented as the mean \pm SE. $**p < 0.01$, $n = 5$, Student's t -test.

The cause of hearing loss is extremely heterogeneous and mainly caused by hair cell malfunction [40–42], and CI can partially have the hair cells function to compensate the hair cell loss. Thus, for children and adults suffering from severe and profound hearing loss, CI is the first-line treatment for hearing rehabilitation. Through a multielectrode array implanted in the cochlea, CI treatment stimulates the peripheral auditory system directly, conferring the restoration of hearing. However, the outcomes of CI rely on the normal anatomy and function of cochlear nerves [8]. This requirement excludes a population of patients with malfunction or malformation of cochlear nerves from CI candidates. ABI or cranial nerve implants have been developed for these deaf patients [9, 10]. By placing a multielectrode surface array within the brainstem, the cochlear nucleus or higher stages of auditory nucleus are directly stimulated by the ABI device. Similar with the situation for CI, the number of electrodes in an ABI device is usually small (21 electrodes in ABI541, the latest ABI device of Cochlear Corporation, Sydney, Australia). Because a broad region of neurons is activated by each channel, the poor spatial selectivity restricts the outcomes of ABI. This may explain the highly variable results of over 1,000 ABI procedures performed worldwide to date [11]. Meanwhile, implant migration and the risk of postoperative complications of craniotomy, including CSF leak, cerebellar contusion, meningitis, and hydrocephalus, also limit ABI

surgery from becoming a wide spread procedure such as the CI [11, 12]. Considering the population of deaf patients with a nonfunctional and/or unimplantable cochlea, alternative strategies for safe and effective neuronal stimulation are urgently needed.

With the physical advantages, US can be focused across the human body and skull bone to deep-brain regions with millimeter spatial resolutions as a nonsurgical approach [20, 21]. US stimulation overcomes some limitations of other brain stimulation techniques. Compared with electric-based stimulations, US stimulation does not require the implant of electrodes while providing improved spatial selectivity versus transcranial electric stimulation [43] and transcranial magnetic stimulation [44]. US stimulation does not need genetic modification of neurons, which is required by optogenetic neural stimulation. Therefore, US stimulation offers an alternative strategy for patients who are ineligible for CI and ABI surgery.

For the central auditory system, it appears that the auditory cortex may be the appropriate region for receiving US stimulation. The functional structure of the auditory cortex offers many advantages for safe and region-specific US neuromodulation. Unlike the subcortical nuclei (i.e., cochlear nucleus, inferior colliculus, and auditory thalamus) [33, 45, 46], the auditory cortex is located on the surface of brain, which can be more easily and precisely stimulated by US

stimulation. Meanwhile, the frequency presentation and other functional maps are arranged along the surface of the auditory cortex [32, 34, 47]. Through geometry of the transducers and phased arrays of ultrasound, it is instrumental in modulating the auditory cortex in a region-specific way with a high spatial resolution. Certainly, the spatial configuration and miniaturization of the US device should be modified to suit the application in the future.

However, several recent studies have questioned whether US stimulation can directly stimulate action potentials of cortical neurons. When ultrasound was focused on the mouse brain, Sato et al. found that the auditory startle reflex was elicited rather than the direct activation of motor circuits [48]. Guo et al. observed auditory and somatosensory cortical activity when ultrasound was applied to the brain, but these brain activations were abolished when the cochlear pathway was eliminated [49]. They postulated that the skull resonances caused by ultrasound radiation pressure result in the responses of the cochlear hair cells, leading to the activation of the whole auditory pathway including the auditory cortex. The activity of other nonauditory cortical areas could be elicited by the cross-modal projections from the auditory system. Their findings are a big challenge to the idea that US stimulation can be used as an alternative strategy for ABI. If US stimulation cannot activate auditory neurons directly, US is invalid for patients lacking normal cochlear functions. Our data indicate that low-intensity US stimulation can activate auditory cortical neurons directly regardless of the frequency and other parameters of US stimuli (Figures 3 and 4). Our finding is supported by a study demonstrating that transcranial focused ultrasound can evoke the same motor responses in deaf knockout mice as in normal hearing mice [50]. Therefore, we propose that US stimulation is efficient at activating the auditory cortex, and the application of US neural stimulation is worthy of further investigation for deaf patients.

5. Conclusions

Both low-frequency (0.8 MHz) and high-frequency (>27 MHz) ultrasound stimulation can activate auditory cortical neurons in vitro. Low-intensity US-induced neural stimulation is efficient for most cultured neurons. Our study suggests that low-intensity US can directly excite auditory cortical neurons.

Data Availability

Data will be made available on request to corresponding author.

Conflicts of Interest

The authors declare that there is no conflict of interest regarding the publication of this paper.

Acknowledgments

This work was supported by the Key-Area Research and Development Program of Guangdong Province

(2018B030331001), National Natural Science Foundation of China (11534013, 81901397, and 81670922), the Program for Changjiang Scholars and Innovative Research Team in the University (IRT_16R37), and Shenzhen Science and Technology Innovation Committee (JCYJ20180306173115719).

References

- [1] J. Qi, X. Chen, M. Tang et al., "Critical role of spectrin in hearing development and deafness," *Science Advances*, vol. 5, no. 4, article eaav7803, 2019.
- [2] C. Zhu, C. Cheng, Y. Wang et al., "Loss of ARHGEF6 causes hair cell stereocilia deficits and hearing loss in mice," *Frontiers in Molecular Neuroscience*, vol. 11, p. 362, 2018.
- [3] Y. Wang, J. Li, X. Yao et al., "Loss of CIB2 causes profound hearing loss and abolishes mechano-electrical transduction in mice," *Frontiers in Molecular Neuroscience*, vol. 10, p. 401, 2017.
- [4] Z. H. He, S. Y. Zou, M. Li et al., "The nuclear transcription factor FoxG1 affects the sensitivity of mimetic aging hair cells to inflammation by regulating autophagy pathways," *Redox Biology*, vol. 28, article 101364, 2020.
- [5] W. Liu, X. Xu, Z. Fan et al., "Wnt signaling activates TP53-induced glycolysis and apoptosis regulator and protects against cisplatin-induced spiral ganglion neuron damage in the mouse cochlea," *Antioxidants & Redox Signaling*, vol. 30, no. 11, pp. 1389–1410, 2019.
- [6] Z. He, L. Guo, Y. Shu et al., "Autophagy protects auditory hair cells against neomycin-induced damage," *Autophagy*, vol. 13, no. 11, pp. 1884–1904, 2017.
- [7] L. Liu, Y. Chen, J. Qi et al., "Wnt activation protects against neomycin-induced hair cell damage in the mouse cochlea," *Cell Death & Disease*, vol. 7, no. 3, article e2136, 2016.
- [8] N. L. Deep, E. M. Dowling, D. Jethanamest, and M. L. Carlson, "Cochlear implantation: an overview," *Journal of Neurological Surgery Part B: Skull Base*, vol. 80, no. 2, pp. 169–177, 2019.
- [9] V. Colletti, M. Carner, V. Miorelli, M. Guida, L. Colletti, and F. Fiorino, "Auditory brainstem implant (ABI): new frontiers in adults and children," *Otolaryngology and Head and Neck Surgery*, vol. 133, no. 1, pp. 126–138, 2005.
- [10] M. S. Schwartz and E. P. Wilkinson, "Auditory brainstem implant development," *Laryngoscope*, vol. 127, no. 8, pp. 1909–1915, 2017.
- [11] N. L. Deep, B. Choudhury, and J. J. Roland, "Auditory brainstem implantation: an overview," *Journal of Neurological Surgery Part B: Skull Base*, vol. 80, no. 2, pp. 203–208, 2019.
- [12] V. Colletti, R. V. Shannon, M. Carner, S. Veronese, and L. Colletti, "Complications in auditory brainstem implant surgery in adults and children," *Otology & Neurotology*, vol. 31, no. 4, pp. 558–564, 2010.
- [13] W. J. Tyler, S. W. Lani, and G. M. Hwang, "Ultrasonic modulation of neural circuit activity," *Current Opinion in Neurobiology*, vol. 50, pp. 222–231, 2018.
- [14] O. Naor, S. Krupa, and S. Shoham, "Ultrasonic neuromodulation," *Journal of Neural Engineering*, vol. 13, no. 3, article 031003, 2016.
- [15] R. F. Dallapiazza, K. F. Timbie, S. Holmberg, J. Gatesman, and M. B. Lopes, "Noninvasive neuromodulation and thalamic mapping with low-intensity focused ultrasound," *Journal of Neurosurgery*, vol. 128, no. 3, pp. 875–884, 2018.

- [16] R. L. King, J. R. Brown, W. T. Newsome, and K. B. Pauly, "Effective parameters for ultrasound-induced *in vivo* neurostimulation," *Ultrasound in Medicine & Biology*, vol. 39, no. 2, pp. 312–331, 2013.
- [17] Y. Tufail, A. Matyushov, N. Baldwin et al., "Transcranial pulsed ultrasound stimulates intact brain circuits," *Neuron*, vol. 66, no. 5, pp. 681–694, 2010.
- [18] W. J. Tyler, Y. Tufail, M. Finsterwald, M. L. Tauchmann, E. J. Olson, and C. Majestic, "Remote excitation of neuronal circuits using low-intensity, low-frequency ultrasound," *PLoS One*, vol. 3, no. 10, article e3511, 2008.
- [19] P. S. Yang, H. Kim, W. Lee et al., "Transcranial focused ultrasound to the thalamus is associated with reduced extracellular GABA levels in rats," *Neuropsychobiology*, vol. 65, no. 3, pp. 153–160, 2012.
- [20] J. Blackmore, S. Shrivastava, J. Sallet, C. R. Butler, and R. O. Cleveland, "Ultrasound neuromodulation: a review of results, mechanisms and safety," *Ultrasound in Medicine & Biology*, vol. 45, no. 7, pp. 1509–1536, 2019.
- [21] A. Fomenko, C. Neudorfer, R. F. Dallapiazza, S. K. Kalia, and A. M. Lozano, "Low-intensity ultrasound neuromodulation: an overview of mechanisms and emerging human applications," *Brain Stimulation*, vol. 11, no. 6, pp. 1209–1217, 2018.
- [22] W. Legon, P. Bansal, R. Tyshynsky, L. Ai, and J. K. Mueller, "Transcranial focused ultrasound neuromodulation of the human primary motor cortex," *Scientific Reports*, vol. 8, no. 1, article 10007, 2018.
- [23] W. Legon, T. F. Sato, A. Opitz et al., "Transcranial focused ultrasound modulates the activity of primary somatosensory cortex in humans," *Nature Neuroscience*, vol. 17, no. 2, pp. 322–329, 2014.
- [24] W. Lee, H. Kim, Y. Jung, I. U. Song, Y. A. Chung, and S. S. Yoo, "Image-guided transcranial focused ultrasound stimulates human primary somatosensory cortex," *Scientific Reports*, vol. 5, no. 1, article 8743, 2015.
- [25] W. Lee, H. C. Kim, Y. Jung et al., "Transcranial focused ultrasound stimulation of human primary visual cortex," *Scientific Reports*, vol. 6, no. 1, article 34026, 2016.
- [26] J. Tang, J. L. Pecka, B. Fritzsche, K. W. Beisel, and D. Z. He, "Lizard and frog prestin: evolutionary insight into functional changes," *PLoS One*, vol. 8, no. 1, article e54388, 2013.
- [27] X. Tan, J. L. Pecka, J. Tang, S. Lovas, K. W. Beisel, and D. Z. Z. He, "A motif of eleven amino acids is a structural adaptation that facilitates motor capability of eutherian prestin," *Journal of Cell Science*, vol. 125, no. 4, pp. 1039–1047, 2012.
- [28] J. Hang, W. Pan, A. Chang et al., "Synchronized progression of prestin expression and auditory brainstem response during postnatal development in rats," *Neural Plasticity*, vol. 2016, Article ID 4545826, 10 pages, 2016.
- [29] M. Fu, M. Chen, X. Yan, X. Yang, J. Xiao, and J. Tang, "The effects of urethane on rat outer hair cells," *Neural Plasticity*, vol. 2016, Article ID 3512098, 11 pages, 2016.
- [30] J. Tang, J. L. Pecka, X. Tan, K. W. Beisel, and D. Z. He, "Engineered pendrin protein, an anion transporter and molecular motor," *The Journal of Biological Chemistry*, vol. 286, no. 35, pp. 31014–31021, 2011.
- [31] A. Chang, P. Chen, S. Guo et al., "Specific influences of early acoustic environments on cochlear hair cells in postnatal mice," *Neural Plasticity*, vol. 2018, Article ID 5616930, 13 pages, 2018.
- [32] J. Tang and N. Suga, "Corticocortical interactions between and within three cortical auditory areas specialized for time-domain signal processing," *The Journal of Neuroscience*, vol. 29, no. 22, pp. 7230–7237, 2009.
- [33] J. Tang, Z. J. Xiao, and J. X. Shen, "Delayed inhibition creates amplitude tuning of mouse inferior collicular neurons," *Neuroreport*, vol. 19, no. 15, pp. 1445–1449, 2008.
- [34] J. Tang and N. Suga, "Modulation of auditory processing by cortico-cortical feed-forward and feedback projections," *Proceedings of the National Academy of Sciences of the United States of America*, vol. 105, no. 21, pp. 7600–7605, 2008.
- [35] W. Zhou, J. Wang, K. Wang et al., "Ultrasound neuro-modulation chip: activation of sensory neurons in *Caenorhabditis elegans* by surface acoustic waves," *Lab on a Chip*, vol. 17, no. 10, pp. 1725–1731, 2017.
- [36] S. Ibsen, A. Tong, C. Schutt, S. Esener, and S. H. Chalasani, "Sonogenetics is a non-invasive approach to activating neurons in *Caenorhabditis elegans*," *Nature Communications*, vol. 6, no. 1, article 8264, 2015.
- [37] J. Ye, S. Tang, L. Meng et al., "Ultrasonic control of neural activity through activation of the mechanosensitive channel MscL," *Nano Letters*, vol. 18, no. 7, pp. 4148–4155, 2018.
- [38] M. Sheng and M. E. Greenberg, "The regulation and function of *c-fos* and other immediate early genes in the nervous system," *Neuron*, vol. 4, no. 4, pp. 477–485, 1990.
- [39] P. P. Ye, J. R. Brown, and K. B. Pauly, "Frequency dependence of ultrasound neurostimulation in the mouse brain," *Ultrasound in Medicine & Biology*, vol. 42, no. 7, pp. 1512–1530, 2016.
- [40] F. Tan, C. Chu, J. Qi et al., "AAV-*ie* enables safe and efficient gene transfer to inner ear cells," *Nature Communications*, vol. 10, no. 1, article 3733, 2019.
- [41] Z. He, Q. Fang, H. Li et al., "The role of FOXP1 in the postnatal development and survival of mouse cochlear hair cells," *Neuropharmacology*, vol. 144, pp. 43–57, 2019.
- [42] S. Sun, M. Sun, Y. Zhang et al., "In vivo overexpression of X-linked inhibitor of apoptosis protein protects against neomycin-induced hair cell loss in the apical turn of the cochlea during the ototoxic-sensitive period," *Frontiers in Cellular Neuroscience*, vol. 8, p. 248, 2014.
- [43] M. A. Nitsche, L. G. Cohen, E. M. Wassermann et al., "Transcranial direct current stimulation: state of the art 2008," *Brain Stimulation*, vol. 1, no. 3, pp. 206–223, 2008.
- [44] V. Walsh and A. Cowey, "Transcranial magnetic stimulation and cognitive neuroscience," *Nature Reviews. Neuroscience*, vol. 1, no. 1, pp. 73–80, 2000.
- [45] J. Tang, W. Yang, and N. Suga, "Modulation of thalamic auditory neurons by the primary auditory cortex," *Journal of Neurophysiology*, vol. 108, no. 3, pp. 935–942, 2012.
- [46] Q. Qiu, J. Tang, Z. Yu et al., "Latency represents sound frequency in mouse IC," *Science in China. Series C, Life Sciences*, vol. 50, no. 2, pp. 258–264, 2007.
- [47] J. Tang, Z. Xiao, and N. Suga, "Bilateral cortical interaction: modulation of delay-tuned neurons in the contralateral auditory cortex," *The Journal of Neuroscience*, vol. 27, no. 31, pp. 8405–8413, 2007.
- [48] T. Sato, M. G. Shapiro, and D. Y. Tsao, "Ultrasonic neuromodulation causes widespread cortical activation via an indirect auditory mechanism," *Neuron*, vol. 98, no. 5, pp. 1031–1041.e5, 2018.

- [49] H. Guo, M. Hamilton, S. Offutt et al., "Ultrasound produces extensive brain activation via a cochlear pathway," *Neuron*, vol. 98, no. 5, pp. 1020–1030.e4, 2018.
- [50] M. Mohammadjavadi, P. P. Ye, A. Xia, J. Brown, G. Popelka, and K. B. Pauly, "Elimination of peripheral auditory pathway activation does not affect motor responses from ultrasound neuromodulation," *Brain Stimulation*, vol. 12, no. 4, pp. 901–910, 2019.

Research Article

Developmental and Functional Hair Cell-Like Cells Induced by Atoh1 Overexpression in the Adult Mammalian Cochlea *In Vitro*

Lingyi Kong ¹, Yuan Xin ¹, Fanglu Chi ^{2,3,4,5}, Jie Chen ¹ and Juanmei Yang ^{2,3,4,5}

¹Department of Otolaryngology, Shanghai Children's Medical Center, Shanghai JiaoTong University School of Medicine, Shanghai, China

²Department of Otolaryngology and Skull Base Surgery, Eye Ear Nose and Throat Hospital, Fudan University, Shanghai, China

³Shanghai Clinical Medical Center of Hearing Medicine, Shanghai, China

⁴Key Laboratory of Hearing Medicine of National Health Commission of the People's Republic of China, Shanghai, China

⁵Research Institute of Otolaryngology, Fudan University, Shanghai, China

Correspondence should be addressed to Jie Chen; 13611715123@163.com and Juanmei Yang; yangjuanmei1982@126.com

Lingyi Kong and Yuan Xin contributed equally to this work.

Received 24 April 2020; Revised 17 September 2020; Accepted 21 October 2020; Published 5 November 2020

Academic Editor: Renjie Chai

Copyright © 2020 Lingyi Kong et al. This is an open access article distributed under the Creative Commons Attribution License, which permits unrestricted use, distribution, and reproduction in any medium, provided the original work is properly cited.

Hair cells (HCs) in the mammalian cochlea cannot spontaneously regenerate once damaged, resulting in permanent hearing loss. It has been shown that Atoh1 overexpression induces hair cell-like cells (HCLCs) in the cochlea of newborn rodents, but this is hard to achieve in adult mammals. In this study, we used a three-dimensional cochlear culture system and an adenoviral-mediated delivery vector to overexpress Atoh1 in adult mouse cochlea. HCLCs were successfully induced from 3 days after virus infection (3 DVI) *in vitro*, and the number increased with time. HCLCs were myosin7a positive and distinguishable from remnant HCs in a culture environment. Meanwhile, patch-clamp results showed that noninward outward potassium currents (sustained outward potassium currents) could be recorded in HCLCs and that their magnitude increased with time, similar to normal HCs. Furthermore, transient HCN currents were recorded in some HCLCs, indicating that the HCLCs experienced a developmental stage similar to normal HCs. We also compared the electrophysiological features of HCLCs from adult mice with native HCs and found the HCLCs gradually matured, similar to the normal HCs. Meanwhile, HCLCs from adult mice possessed the same bundles as developmental HCs. However, these HCLCs did not express prestin, which is a special marker for outer hair cells (OHCs), even at 13 DVI. These results demonstrate that Atoh1 overexpression induces HCLC formation in the adult mammalian cochlea and that these HCLCs were functional and experienced a developmental process similar to that of normal HCs.

1. Introduction

Hair cells (HCs), which serve as inner ear sensory cells, are essential for the transduction of mechanical stimulation into hearing and balance signals in the inner ear. In lower vertebrates, such as birds and zebrafish, lost HCs can be replaced by spontaneous HC regeneration [1–4]. However, unlike these vertebrates, following acoustic overstimulation, ototoxic drug, trauma, or aging, HC loss in the mammalian inner ear is irreversible and is the primary reason for permanent sensorineural hearing loss [5–8].

HC reproduction in mammals has made great progress in recent years, including the intervention of stem cells, supporting cell (SC) reprogramming, and the direct conversion of nonsensory epithelial cells of the cochlea [9–16]. Atoh1 is a basic helix-loop-helix transcription factor that is both necessary and sufficient for the development and genesis of HCs [17]. Atoh1 is gradually upregulated before HC formation and is downregulated during the HC maturation process [17–19]. The absence of Atoh1 in embryonic mice induces complete loss of both HCs and associated SCs [17, 19, 20]. In contrast, Atoh1 overexpression induces the formation of

HCLCs both *in vitro* and *in vivo* [10, 21–23]. Meanwhile, it appears that HCLCs induced by different approaches remain in the developmental stage, which is a limiting factor for functional recovery [10, 22]. A recent study has shown that Atoh1 overexpression significantly enhanced HC regeneration and sustained functional recovery in the adult vestibule [11]. Meanwhile, another recent study also showed that multiple reprogramming, including Atoh1 overexpression, induces HCLCs in the adult cochlea *in vitro* and *in vivo* [24]. However, whether HCLCs induced by Atoh1 possess similar electrical physiological function as normal HCs is still unknown.

To address these questions, a human adenovirus serotype 5 (*Ad5*) vector encoding Atoh1 (*Atoh1*) and/or RFP (*RFP-Atoh1-*) or RFP-Atoh1 (*RFP-Atoh1+*) was used to overexpress Atoh1 in cultured mouse cochlea *in vitro*, and we assessed the morphological and functional features of HCLCs at different days after viral infection (DVI). Patch-clamp results showed the similarities and differences with respect to electrophysiological features between HCLCs and native HCs at different time points.

2. Material and Methods

2.1. Ethics Statement. This study was performed in accordance with the guidelines of the appropriate Institutional Animal Care and Use Committee of the Eye & ENT Hospital of Fudan University, Shanghai, China, and the Shanghai Children's Medical Center of Shanghai JiaoTong University School of Medicine, Shanghai, China.

2.2. Cochlear Explant Cultures and Viral Infection. Adult C57BL/6 mice (JSJ Company, Shanghai, China), ranging from 8 to 10 weeks of age, were used in this study. Mice were decapitated, and the cochleae were carefully dissected out. Then, under a dissecting microscope (Zeiss), a hole was perforated at the apex of the cochlea, and the round window was opened and expanded by gently rotating the tip using a syringe needle. Using a fine-tipped pipette, phosphate buffer solution (PBS, HyClone) was gently flushed through the oval and round windows (as inlets) and the hole at the apex (as an outlet) (Figure 1(a)). Finally, the whole cochlea with the sensory epithelium was cultured in this experiment in Dulbecco's modified Eagle medium as follows: nutrient mixture F-12 (DMEM/F12, Invitrogen) medium containing 10% fetal bovine serum (FBS, Invitrogen) was used on the first day of culture.

The human adenovirus serotype 5 (*Ad5*) vector (with a final concentration of 1.0×10^8 pfu/ml) encoding RFP and/or Atoh1 (*RFP-Atoh1+/-*) was used in this study. On the next day of culture, the virus diluted in the serum-free culture medium supplemented with B27 (Invitrogen) was added for a 12-hour infection and then replaced with serum-free medium every two days until the end of the culture. Petri dishes were kept in an incubator at 37°C with 5% CO₂ during culture. The moment of adenovirus addition was recorded as day 0, then 1 day after viral infection (1 DVI), and so on.

2.3. Tissue Preparation and Immunofluorescence Staining. After 3 and 7 DVI, specimens were fixed in 4% paraformaldehyde (in PBS) at room temperature (RT) for 30 min followed by 10% ethylenediaminetetraacetic acid (EDTA) at RT for 8 hours to decalcify the bones. The bony capsule of the cochlea was dissected under the microscope. Then, the basilar membrane and associated organ of the Corti were carefully stripped from the modiolus. Next, the tectorial membrane and stria vascularis were torn off. The apical turn of the basilar membrane was prepared for immunofluorescence staining.

All specimens were blocked in 5% goat serum for 30 minutes at RT. Primary antibodies against myosin7a (1:200, mouse, DSHB, MYO7A 138-1) and/or prestin (1:200, Rabbit, Santa Cruz, sc-293212) diluted in 5% goat serum/0.1% Triton X-100/PBS were added overnight at 4°C. The next day, appropriate secondary antibodies, complementary to the primary antibodies, were used at RT for 2-3 hours in darkness. Secondary antibodies included donkey anti-rabbit Alexa Fluor 488 IgG (1:1000, Jackson, 112-546-143) and/or donkey anti-mouse Alexa Fluor 555 IgG (1:1000, Jackson, 715-165-151). Bundles were detected by Alexa Fluor 488-labeled phalloidin (1:1000, Thermo Fisher, A12379). 4',6-diamidino-2-phenylindole (DAPI; 1:1000, Sigma, D9542), stained for 10 min, was used to visualize nuclei. Slides were mounted and placed in a slide box at 4°C overnight to dry. Subsequently, slides were visualized under a Zeiss LSM 510 confocal laser-scanning microscope (Carl Zeiss, Germany).

2.4. Electrophysiological Recordings. Whole-cell patch-clamp recordings (HEKA, Germany) were used to detect electrophysiological properties of specimens (the apical turn of the basilar membrane) on 3, 5, and 7-9 DVI. Extracellular solutions (mM) are summarized as follows: 144 NaCl, 5.8 KCl, 0.9 MgCl₂, 1.3 CaCl₂, 10 HEPES, 5.6 glucose, pH 7.2-7.3, and osmotic pressure: 300-310 mOsm. Patch pipette filling solutions contained (mM) 1 EGTA, 135 KCl, 2 MgCl₂, 0.1 CaCl₂, 5 Mg₂ATP, 0.5 NaGTP, 10 HEPES, 10 Na₂ phosphocreatine, pH 7.2-7.3, and osmotic pressure: 290-300 mOsm. Borosilicate glass capillaries (OD 1.5 mm, ID 1.0 mm) were used to prepare patch pipettes on a horizontal multistep puller (Sutter con. USA). In the bath, pipettes had a resistance of 6-8 MΩ. Seal resistances higher than 1 MΩ were considered for recording. Currents were amplified using an Axopatch 200B amplifier (Molecular Devices, Union City, CA, USA), and data were digitized using an analog-to-digital converter (Digidata 1322; Molecular Devices, USA). Currents with a leak current less than 100 pA were accepted for statistical analysis.

2.5. Statistical Analysis. Statistical analyses were performed using GraphPad Prism (v8.0c software, GraphPad, San Diego, CA, USA). Statistical significance was determined using Student's *t*-tests and two-way ANOVA followed by Bonferroni's multiple comparisons test. Electrophysiological data were analyzed using Igor (HEKA Instruments, USA) and Origin Pro 8.0 (Microcal Software, USA). Nonlinear regression analysis was performed to quantify the

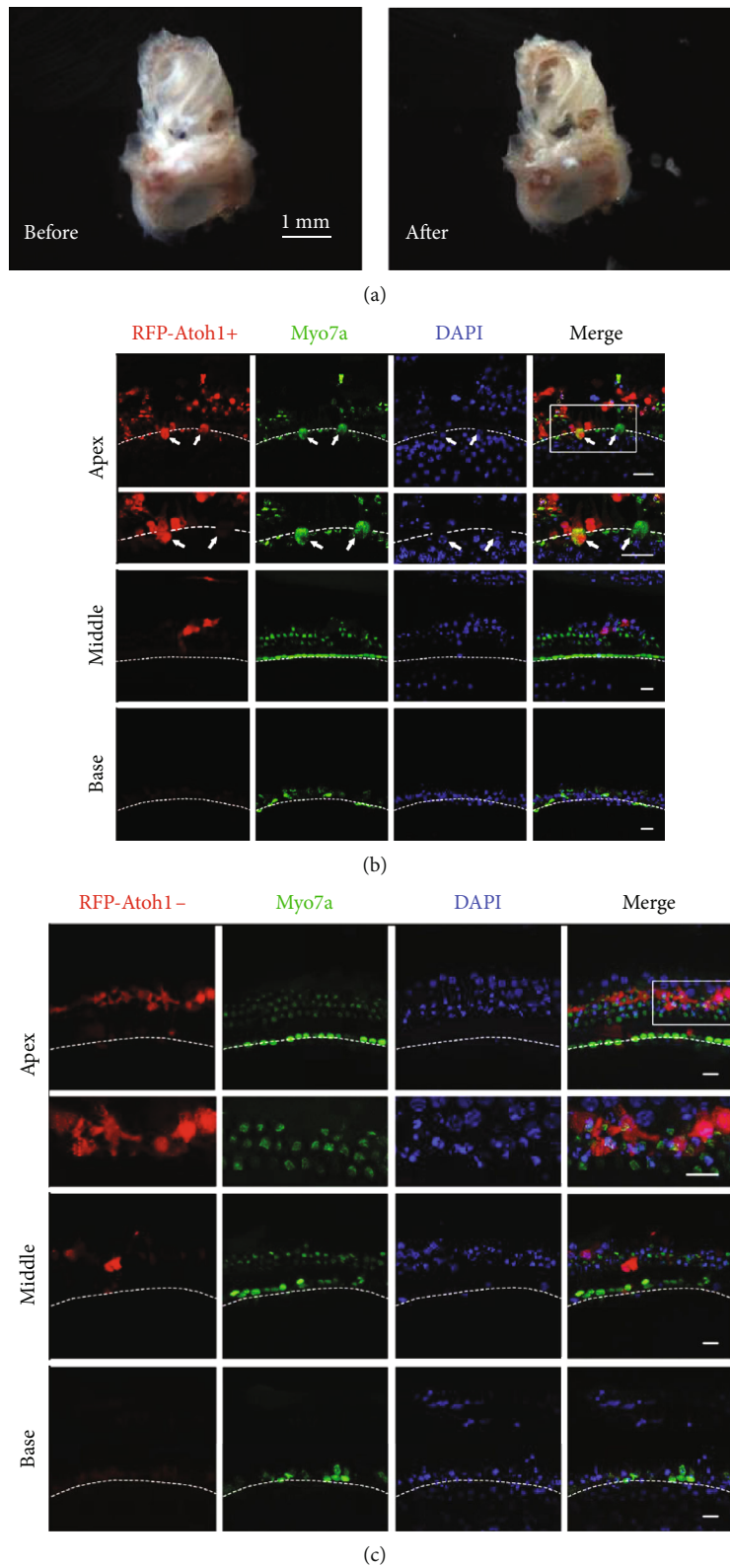


FIGURE 1: *Atoh1* overexpression induces HCLC formation in the apical turn of adult mouse cochleae. (a) Establishment of adult cochlea explant cultures. A freshly dissected adult mouse cochlea with the intact bone (before) and with the holes perforated (after) before culture. (b, c) Infection status of *RFP-Atoh1+* in apical (apex), middle (middle), and basal (base) turns of mouse cochleae at 3 DVI. HCLCs (arrows) were found in the IHC region of apical turn. Remnant myosin7a+ HCs appear shrunken and in a dying state. *RFP-Atoh1-* were used as controls. Scale bars: 1 mm in (a), 15 μ m in (b) and (c). Rectangular boxes show areas from which high magnification and dashed lines mark the IHC region.

goodness-of-fit via computation of the Boltzmann equation. In this study, n values represent the number of biologically independent samples. Data are shown as the mean \pm s.d., and p values less than 0.05 were considered significant: * $p < 0.05$, ** $p < 0.01$, and *** $p < 0.001$.

3. Results

3.1. *Atoh1* Overexpression Induces HCLC Formation in the Sensory Epithelial Region in the Apical Turn of Adult Mouse Cochleae. As shown in Figures 1(a)–1(c), myosin7a+ HCLCs were detected in the sensory region in the *Atoh1* overexpression group (*RFP-Atoh1+*) from 3 DVI at the apical turn. HCLCs were distinguishable from the remnant native HCs. In the control group, myosin7a+ native HCs were shrunken and relatively well arranged at 3 DVI (Figure 1(c)). In the *Atoh1* overexpression group, myosin7a+ HCLCs (arrows) were much larger and rounder than the remnant native HCs (Figure 1(b)). At the middle and basal turns, the viral infection rate was low, and only a small amount of SCs was RFP positive with no HCLCs detected (Figures 1(b) and 1(c)).

At 5 and 7 DVI, myosin7a+ native HCs were also shrunken and scattered in the control group (Figure 2(b)). In the *Atoh1* overexpression group, myosin7a+ HCLCs (arrowheads) were round or oval in shape and much larger than the native HC debris (Figure 2(a)). The number of HCLCs increased from 3.00 ± 1.41 at 3 DVI to 9.60 ± 2.70 at 5 DVI per $150 \mu\text{m}$ along the long axis of the cochlea ($n = 5$), which is significantly higher than respective control levels. However, 7 DVI (10.60 ± 3.05 ; $n = 5$) was not significantly different from 5 DVI (Figure 2(c)).

3.2. *Atoh1*-Induced HCLCs Possess Bundles Similar to Developmental HCs but Do Not Express Prestin in Mature Cochleae. Phalloidin was stained to detect whether HCLCs possess similar bundles as developmental HCs. According to our results, HC bundles were observed at the apical side of HCLCs (Figures 3(b) and 3(c)). Moreover, we used prestin, a specific motor protein expressed in the OHCs, to identify HCLCs at 7 and 11 DVI. As shown in Figure 3(a), although some shrunken OHC debris still expressed prestin with pyknotic nuclei, HCLCs were prestin negative both at 7 ($n = 5$) and 11 DVI ($n = 3$). In the control group, there were no HCLCs and only some scattered HC debris was prestin positive ($n = 5$) (Figure 3(a)).

3.3. Outward K^+ and HCN Currents of *Atoh1*-Induced HCLCs in Mature Cochleae. A whole-cell patch-clamp recording technique was used to assess electrophysiological properties of HCLCs. Distinguishable among the HCLCs were remnant native HCs and nonsensory epithelial cells in the HC region. For native IHCs, we could see V-shaped bundles in a relative orderly arrangement. However, in native OHCs, the condition was too deteriorated to patch successfully (data not shown). For native IHCs, the condition was better than in native OHCs. For HCLCs, which were round and large, shown in red fluorescence and in better condition, they exhibited more durability in extracellular solutions dur-

ing the patch time. Nonsensory epithelial cells in the sensory epithelium are finger shaped.

Sustained outward potassium (K^+) currents in HCLCs were recorded in the *RFP-Atoh1+* group at 3, 5, and 7–9 DVI, which were $3.23 \pm 1.42 \text{ nA}$ ($n = 9$), $3.46 \pm 0.14 \text{ nA}$ ($n = 5$), and $3.89 \pm 1.50 \text{ nA}$ ($n = 9$), respectively (Figure 4(a)). In the *RFP-Atoh1-* (control) group, RFP+ cells in the sensory epithelial region merely expressed small sustained K^+ currents, which were $400 \pm 29.37 \text{ pA}$ ($n = 5$). The remnant IHCs also expressed small sustained K^+ currents, which were $390 \pm 18.37 \text{ pA}$ ($n = 5$) (Figure 4(b)). For HCLCs, the size of current-density relationships made no difference among the three *Atoh1+* groups, including 3, 5, and 7–9 DVI; however, all three groups were significantly larger than the control group ($p < 0.01$) (Figure 4(d)). Activation curves were obtained by analyzing tail currents at a fixed membrane potential (-30 mV), and voltage-dependent activation curves at 3, 5, and 7–9 DVI were independently fitted with the Boltzmann equation. The results showed significant differences ($p < 0.01$) (Figure 4(c)).

Figure 5(a) shows 7HCN currents, as time-dependent inward rectifier K^+ / Na^+ permeable conductance, recorded at different time points, which were $1.59 \pm 0.96 \text{ nA}$ ($n = 3$), $1.11 \pm 0.55 \text{ nA}$ ($n = 4$), and $0.84 \pm 0.36 \text{ nA}$ ($n = 3$). The amplitude of current density gradually decreased and then disappeared in sequence from 3 to 9 DVI, and differences were statistically significant ($p < 0.01$). Meanwhile, the proportion of recorded HCN currents primitively increased from 33.3% (3/9) at 3 DVI to 80% at 5 DVI (4/5), whereas it decreased to 37.5% on 7 DVI (3/8), suggesting that the appearance of HCN currents was a transient change (Figure 5(b)). By 9 DVI, HCN currents could no longer be recorded (0/5).

3.4. Comparison of Electrophysiological Properties of HCLCs from Adult Mice with Normal HCs. To compare electrophysiological properties of HCLCs and normal HCs, outward K^+ currents of HCLCs and OHCs in the developmental stage were measured. Although recorded currents from these cells seemed similar to HCLCs, the mean membrane capacitance (C_m) was different, as shown in Figures 5(c) and 5(d). First, the sustained outward K^+ currents of the inner and outer HCs of wild-type P9 mice were recorded, which were $2.09 \pm 0.57 \text{ nA}$ ($n = 5$) and $1.84 \pm 0.21 \text{ nA}$ ($n = 5$), respectively (Figure 5(c)). On 3 DVI, the mean amplitude of the current density of HCLCs showed no statistical difference from the inner and outer HCs. Another two groups (5 and 7–9 DVI) were higher than IHCs in P9 mice ($p < 0.05$); however, they still showed no statistical significant compared to OHCs. Second, the K^+ currents of the inner and outer HCs in adult (P60) cochleae were also recorded, which were $2.73 \pm 0.64 \text{ nA}$ ($n = 5$) and $2.24 \pm 0.28 \text{ nA}$ ($n = 5$), respectively (Figure 5(d)). The mean amplitude of current density in the three groups (3, 5, and 7–9 DVI) was higher than the HCs in the adult cochlea ($p < 0.01$).

4. Discussion

In recent years, great progress has been made in HC regeneration in neonatal and adult cochleae [10, 11, 16, 24–27]. Recent studies have shown that sustained *Atoh1*

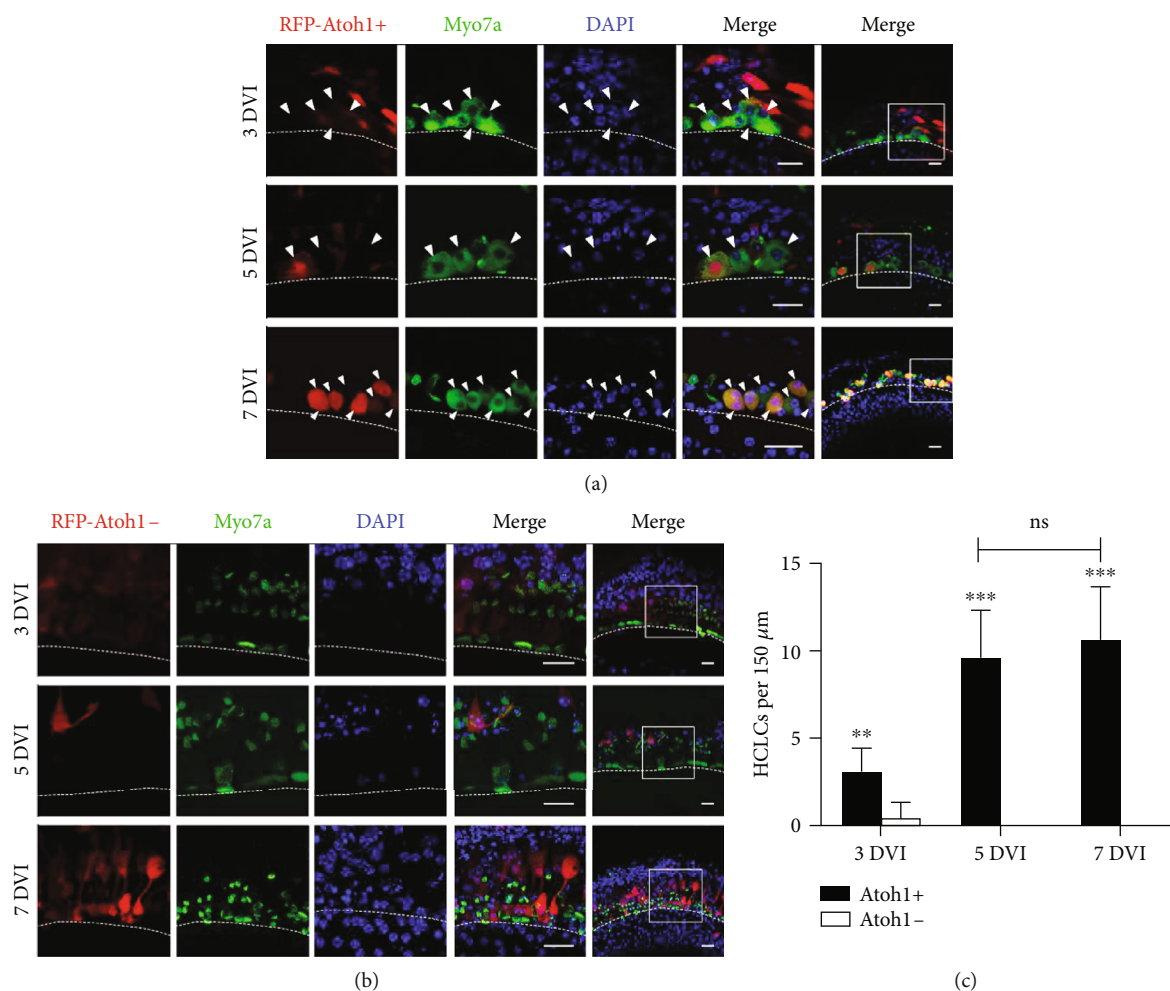


FIGURE 2: HCLCs were successfully induced from 3 DVI *in vitro*, and their numbers increased with time. (a, b) HCLCs (arrowheads) at 3, 5, and 7 DVI. *RFP-Atoh1-* was used as controls. (c) Quantification of HCLCs per 150 μm cochlea length at 3, 5, and 7 DVI in both *Atoh1+* and *Atoh1-* groups ($n = 5$). Scale bars: 15 μm in (a) and (b). Rectangular boxes show areas from which high magnification and dashed lines mark the IHC region.

overexpression enhances the maturation of regenerated HCs in the damaged vestibular system [11, 12, 28]. HCs induced by *Atoh1* in neonatal mammals are reminiscent of “ancestral” HCs that have commonalities with vestibular HCs [11, 29]. However, initial *Atoh1* overexpression levels are correlative with mature levels and arrangement of HCLCs [30]. Higher initial *Atoh1* overexpression levels induce more mature HCLCs according to electrophysiological results [30].

In this study, *Atoh1* overexpression induced HCLCs in adult mice *in vitro*. On 3 DVI, several HCLCs were myosin7a positive in the sensory region, especially in the IHC region. Some HCLCs overlapped with RFP fluorescence, and some did not, consistent with previous studies [30, 31], due to *Atoh1* expression level decreasing once HCLCs become mature. Meanwhile, HCLCs were distinguishable from remnant HCs. HCLCs exhibited a much rounder, bigger, and fresher appearance. Remnant HCs seemed to shrink and be in a dying state. The number of HCLCs increased from 3 DVI to 7 DVI. HCLCs at 7 DVI still failed to express prestin, a marker of mature OHCs. This is likely because the HCLCs were not mature enough, or perhaps the HCLCs were IHC-

like cells. The HCLCs possessed bundles at the apical aspect similar to the developmental HCs, indicating incomplete maturity.

Compared to ectopic HCLCs induced from the neonatal inner ear, HCLCs from adult mice were primarily in the sensory region, especially the IHC region. Ectopic HCLCs induced from the neonatal inner ear are primarily from the nonsensory region, including the LER (lesser epithelial region) and GER (greater epithelial region) [29, 31–33]. This is mostly due to the LER and GER cells being stretched in the culture environment, which facilitates viral infection. For the adult cochlear culture, we reserved the cochlear bone, and the sensory region was the infection area. The IHC region in adult sensory epithelium presents a relatively loose structure, facilitating adenovirus infection. In the control group, no HCLCs were detected. Remnant HCs died in the culture environment, and cell debris was also myosin7a positive and even prestin positive. HCLCs *in situ* may directly build connections with the tectorial membrane and associated neurons, which may lead to eliciting mechanical transduction for hearing restoration.

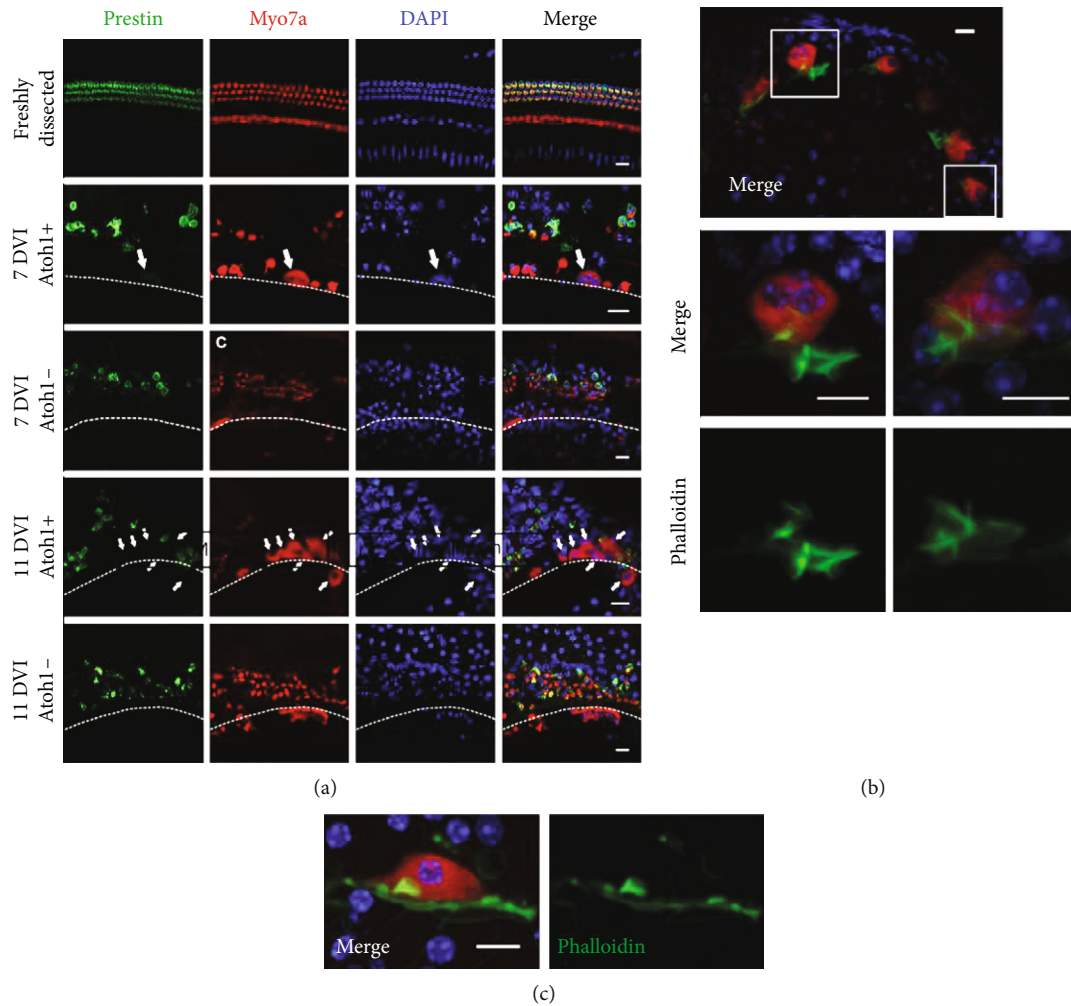


FIGURE 3: *Atoh1*-induced HCLCs possessed bundles similar to developmental HCs but did not express prestin in mature cochleae. (a) Distribution of prestin in a freshly dissected cochlea of an adult mouse. HCLCs (arrows) and remnant IHCs were prestin negative, and remnant OHCs were prestin positive at 7 and 11 DVI after *Atoh1* infection. (b) Hair cell bundles were observed at the apical side of HCLCs. (c) Several HCLC bundles were relatively well organized with V-shaped structures. Scale bar = 15 μm in (a), 10 μm in (b) and (c). Rectangular boxes show areas from which high magnification and dashed lines mark the IHC region.

In the cochlea, *Atoh1*-induced HCLC formation occurs primarily through direct transdifferentiation due to the limitations of the proliferation of SCs [34]. In our study, there were no HCLCs detected in the control group, indicating HCLC formation depends on *Atoh1* overexpression, and there was no HC regeneration in the adult cochlea, distinct from the adult vestibule.

From embryonic development to maturation, HCs undergo an extremely complicated maturation process [7, 29, 35–38]. In addition to a series of related protein expression, the expression of outward K^+ and HCN currents in HCs also goes through developmental changes. In the developmental stage, cochlear HCs express nondeactivated outward K^+ current (sustained outward K^+ current) and do not express fast deactivated outward K^+ current (transient outward K^+ current), and the amplitude increases with the time as HCs mature [35, 37, 39, 40]. Meanwhile, cochlear OHCs and IHCs transiently express HCN currents [36, 39].

A previous study reported that after *Atoh1* overexpression, a fast deactivated outward potassium rectifier (I_{K}) first

appeared in most of the ectopic HCs, followed by sustained outward K^+ current appearing later, and the proportion of cells with the sustained current increased over time as the HCLCs matured [29]. This means that HCLCs with no deactivated outward K^+ current are more mature than HCLCs with fast-deactivated outward potassium. Similarly, HCN current first appeared in most of the ectopic HCs, then disappeared, and the proportion of cells with HCN current decreased over time as the HCLCs matured [29], indicating that HCLCs with HCN current are more immature. Thus, these ectopic HCLCs seem primordial. Another study reported that initial *Atoh1* overexpression levels define the maturity level and arrangement of HCLCs, with higher initial *Atoh1* overexpression levels inducing more mature HCLCs according to electrophysiological results, which process the higher proportion of sustained outward K^+ current and lower proportion of HCN current [25].

For HCLCs induced by *Atoh1* in adult cochlea, no transient outward current was recorded, and all of the HCLCs expressed sustained outward K^+ current, distinct from

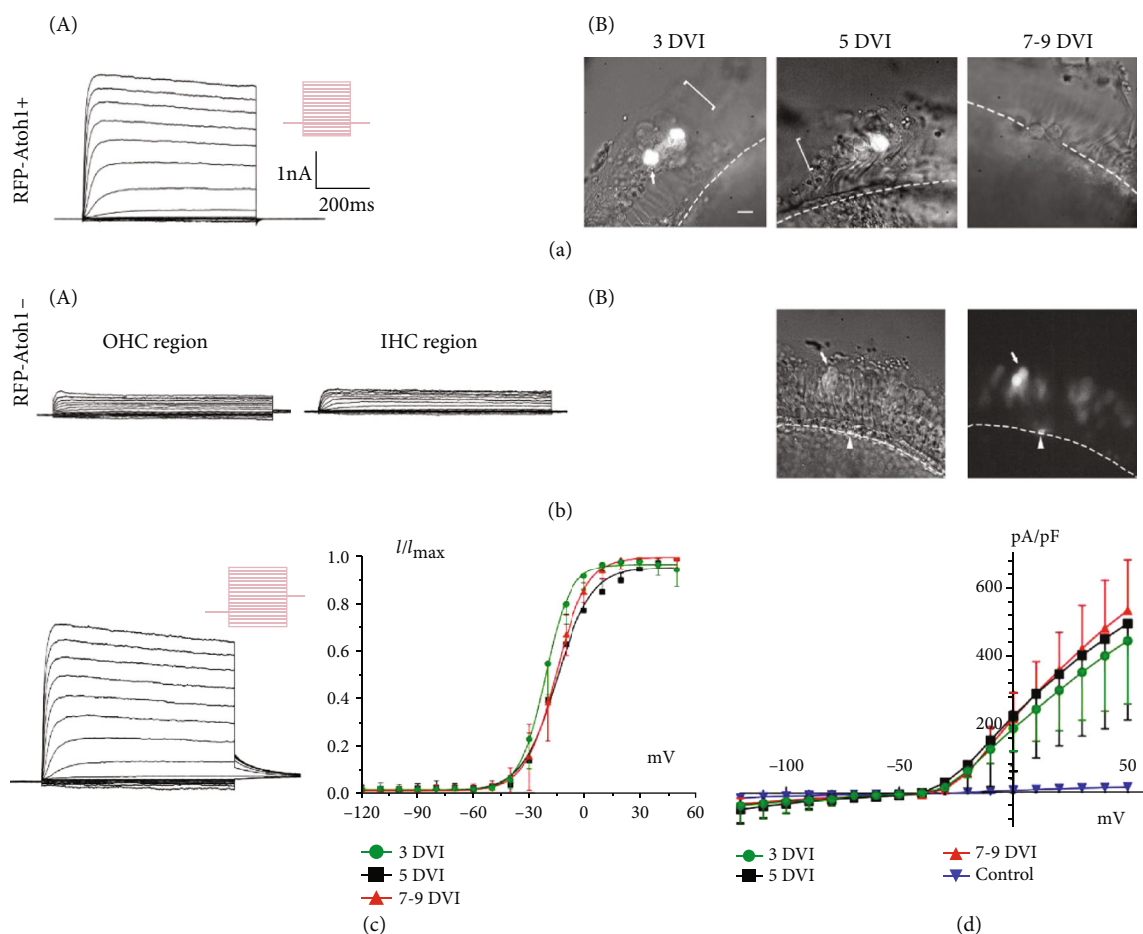


FIGURE 4: Sustained outward potassium currents of Atoh1-induced HCLCs in adult cochleae. (a) Representative samples of recorded sustained outward K⁺ currents (A) and micrographs of patched HCLCs (B) obtained from the 3, 5, and 7-9 DVI in the *Atoh1*⁺ group. HCLCs are shown in RFP fluorescence and appear fresher. The voltage protocol is shown beside the traces. The cell clamp was held at a holding potential of -80 mV, and the voltage steps ranged from -120 to 50 mV in 10 mV increments to evoke voltage-dependent currents. (b) Representative outward K⁺ currents (A) and micrographs (B) of RFP⁺ cells (nonsensory epithelial cells) from the OHC and IHC regions in the control group. (c) Sustained outward K⁺ currents with tail currents and voltage-dependent activation curves of HCLCs. (d) I-V curves summarizing the magnitude of outward K⁺ currents in HCLCs from 3, 5, and 7-9 DVI and the control group, respectively. Scale bar = 20 μ m.

ectopic HCLCs harvested from neonatal cochlea. These results may suggest that HCLCs from adult cochlea induced by *Atoh1* exhibit faster development. HCLCs from adult cochlea also transiently expressed HCN currents, indicating that HCLCs from adult cochlea also experienced a developmental process.

We also compared HCLCs from adult cochleae at different time points with normal inner and outer HCs at P9 and P60. For mouse IHCs, a very small outward K⁺ current debuts at E14.5. Later, spontaneous action potentials (SAPs) occur at E17.5, and the magnitude of outward K⁺ currents increases steadily until the onset of hearing (about P12-14) [35, 37, 41]. Therefore, the magnitude of outward K⁺ currents in IHCs of P9 cochlea is on the rise. Judging from our research results, the maturity of HCLCs on 3 DVI was similar to IHCs in P9 cochlea. However, at 5 and 7-9 DVI, the HCLCs from adult cochlea were more mature than IHCs in the P9 cochlea (Figure 5(c)). Maturation of OHCs is achieved at about P8, a little earlier than in IHCs. In our study, the

magnitudes of outward K⁺ currents in HCLCs at all time points were similar to normal OHCs in P9 cochlea. Furthermore, HCLCs from adult cochlea expressed sustained outward K⁺ current without the transient outward currents observed in native HCs. In general, these results demonstrated that outward K⁺ currents in HCLCs process a developmental regularity and synchrony, the same as normal HCs.

HCN currents, also known as inward rectifier (*I_h*) currents, have been largely recorded in immature HCs and regenerated ectopic HCs [36, 38, 41]. Similar to *IK1* current in developing HCs, the function of the HCN current is setting the resting potential and regulating potential repolarization [36]. The inwardly transient currents will disappear abruptly when the HCs reach maturity, between approximately P12 and P14 in IHCs and earlier in OHCs [35, 36]. In our study, transient expression of HCN currents from 3 to 9 DVI mimicked the developmental process as that found in normal HCs. Additionally, the time point that HCN currents disappeared was on 9 DVI, about one week earlier than normal

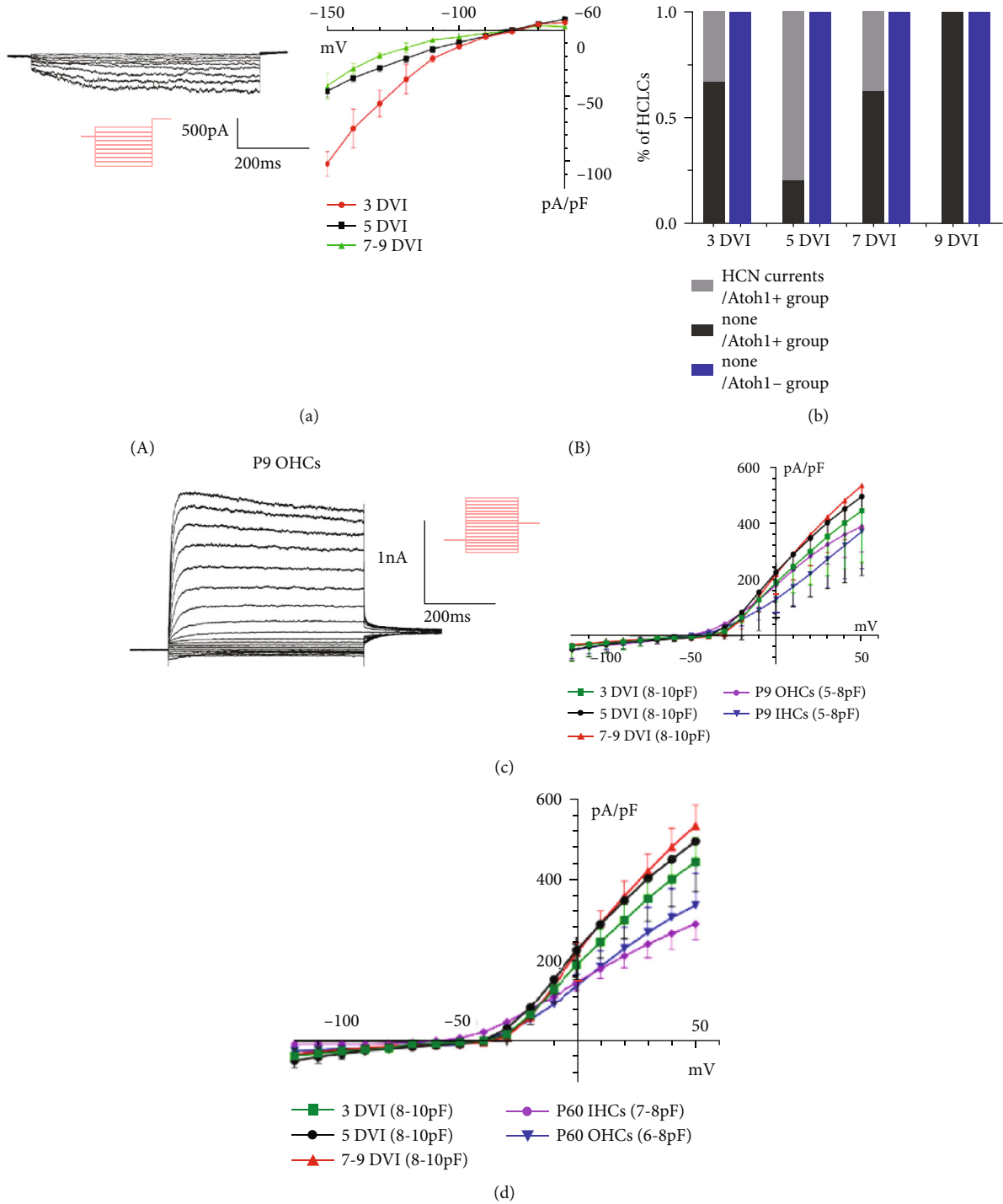


FIGURE 5: HCN currents of Atoh1-induced HCLCs and comparison of outward potassium currents of HCLCs from adult mice to normal HCs. (a) Representative HCN currents and I-V curves of HCLCs. The cell clamp was held at a holding potential of -70 mV, and the voltage steps ranged from -150 to -60 mV in 10 mV increments to evoke voltage-dependent currents. (b) Bar graph demonstrating the proportion of recorded HCN currents. (c) Representative outward K⁺ currents (A) recorded from P9 OHC. The I-V curves (B) show amplitudes of current density of OHCs and IHCs in P9 cochlea and HCLCs induced by Atoh1 in adult cochlea. (d) The I-V curves of OHCs and IHCs in P60 cochlea and Atoh1-induced HCLCs in adult cochlea.

HCs and ectopic HCLCs induced from the neonatal inner ear, strongly indicating that functional development of the HCLCs was occurring relatively faster.

The cell state of remnant IHCs and OHCs degenerated in the culture environment. For remnant IHCs in the culture, only small sustained outward current could be recorded. For the OHC remnants in the culture environment, we were unable to even patch the cells.

5. Conclusions

In this study, HCLCs were induced in adult mouse cochleae by *Atoh1* overexpression, and they were distinguishable in the sensory region. HCLCs expressed sustained outward K^+ currents, and the magnitude increased with time similar to the developmental HCs. They also transiently expressed HCN channel currents similar to HCs, mimicking the developing stage. Meanwhile, HC bundles were detected in HCLCs in a developmental process, but they did not express prestin. These findings indicate that HCLCs from adult mice induced by *Atoh1* overexpression undergo a similar developmental process as that of normal HCs, thereby providing guideline for future research into hearing restoration.

Data Availability

All data used to support the findings of this study are available from the corresponding author upon request.

Conflicts of Interest

The authors declare that they have no competing interests.

Authors' Contributions

Lingyi Kong and Yuan Xi contributed equally to this study.

Acknowledgments

This work was supported by the Natural Science Foundation of Shanghai (grant number 19ZR1408700) to J.Y. and the National Natural Science Foundation of China (grant number 81700907) to Y.X. and (grant number 81970889) to F.C.

References

- [1] J. T. Corwin and D. A. Cotanche, "Regeneration of sensory hair cells after acoustic trauma," *Science (New York, N.Y.)*, vol. 240, no. 4860, pp. 1772–1774, 1988.
- [2] H. R. Brignull, D. W. Raible, and J. S. Stone, "Feathers and fins: non-mammalian models for hair cell regeneration," *Brain Research*, vol. 1277, pp. 12–23, 2009.
- [3] B. M. Ryals and E. W. Rubel, "Hair cell regeneration after acoustic trauma in adult Coturnix quail," *Science (New York, N.Y.)*, vol. 240, no. 4860, pp. 1774–1776, 1988.
- [4] J. S. Kniss, L. Jiang, and T. Piotrowski, "Insights into sensory hair cell regeneration from the zebrafish lateral line," *Current Opinion in Genetics & Development*, vol. 40, pp. 32–40, 2016.
- [5] O. Bermingham-McDonogh and T. A. Reh, "Regulated reprogramming in the regeneration of sensory receptor cells," *Neuron*, vol. 71, no. 3, pp. 389–405, 2011.
- [6] K. Kawamoto, M. Izumikawa, L. A. Beyer, G. M. Atkin, and Y. Raphael, "Spontaneous hair cell regeneration in the mouse utricle following gentamicin ototoxicity," *Hearing Research*, vol. 247, no. 1, pp. 17–26, 2009.
- [7] M. E. Warchol, P. R. Lambert, B. J. Goldstein, A. Forge, and J. T. Corwin, "Regenerative proliferation in inner ear sensory epithelia from adult guinea pigs and humans," *Science (New York, N.Y.)*, vol. 259, no. 5101, pp. 1619–1622, 1993.
- [8] A. Forge, L. Li, J. T. Corwin, and G. Nevill, "Ultrastructural evidence for hair cell regeneration in the mammalian inner ear," *Science (New York, N.Y.)*, vol. 259, no. 5101, pp. 1616–1619, 1993.
- [9] J. Shou, J. L. Zheng, and W. Q. Gao, "Robust generation of new hair cells in the mature mammalian inner ear by adenoviral expression of *Hath1*," *Molecular and Cellular Neuroscience*, vol. 23, no. 2, pp. 169–179, 2003.
- [10] T. Yamashita, F. Zheng, D. Finkelstein et al., "High-resolution transcriptional dissection of in vivo *Atoh1*-mediated hair cell conversion in mature cochleae identifies *Isl1* as a co-reprogramming factor," *PLoS Genetics*, vol. 14, no. 7, article e1007552, 2018.
- [11] Z. N. Sayyid, T. Wang, L. Chen, S. M. Jones, and A. G. Cheng, "*Atoh1* directs regeneration and functional recovery of the mature mouse vestibular system," *Cell Reports*, vol. 28, no. 2, pp. 312–324.e4, 2019.
- [12] T. Weber, U. Zimmermann, H. Winter et al., "Thyroid hormone is a critical determinant for the regulation of the cochlear motor protein prestin," *Proceedings of the National Academy of Sciences of the United States of America*, vol. 99, no. 5, pp. 2901–2906, 2002.
- [13] S. Zhang, Y. Zhang, Y. Dong et al., "Knockdown of *Foxg1* in supporting cells increases the trans-differentiation of supporting cells into hair cells in the neonatal mouse cochlea," *Cellular and Molecular Life Sciences : CMLS*, vol. 77, no. 7, pp. 1401–1419, 2020.
- [14] J. Wu, W. Li, C. Lin et al., "Co-regulation of the Notch and Wnt signaling pathways promotes supporting cell proliferation and hair cell regeneration in mouse utricles," *Scientific Reports*, vol. 6, no. 1, p. 29418, 2016.
- [15] M. Waqas, S. Zhang, Z. He, M. Tang, and R. Chai, "Role of Wnt and Notch signaling in regulating hair cell regeneration in the cochlea," *Frontiers of Medicine*, vol. 10, no. 3, pp. 237–249, 2016.
- [16] W. Li, D. You, Y. Chen, R. Chai, and H. Li, "Regeneration of hair cells in the mammalian vestibular system," *Frontiers of Medicine*, vol. 10, no. 2, pp. 143–151, 2016.
- [17] N. A. Bermingham, B. A. Hassan, S. D. Price et al., "*Math1*: an essential gene for the generation of inner ear hair cells," *Science (New York, N.Y.)*, vol. 284, no. 5421, pp. 1837–1841, 1999.
- [18] P. J. Lanford, R. Shailam, C. R. Norton, T. Gridley, and M. W. Kelley, "Expression of *Math1* and *HES5* in the cochleae of wildtype and *Jag2* mutant mice," *Journal of the Association for Research in Otolaryngology : JARO*, vol. 1, no. 2, pp. 161–171, 2000.
- [19] P. Chen, J. E. Johnson, H. Y. Zoghbi, and N. Segil, "The role of *Math1* in inner ear development: uncoupling the establishment of the sensory primordium from hair cell fate determination," *Development (Cambridge, England)*, vol. 129, no. 10, pp. 2495–2505, 2002.

- [20] C. Woods, M. Montcouquiol, and M. W. Kelley, "Math1 regulates development of the sensory epithelium in the mammalian cochlea," *Nature Neuroscience*, vol. 7, no. 12, pp. 1310–1318, 2004.
- [21] M. C. Kelly, Q. Chang, A. Pan, X. Lin, and P. Chen, "Atoh1 directs the formation of sensory mosaics and induces cell proliferation in the postnatal mammalian cochlea in vivo," *The Journal of neuroscience : the official journal of the Society for Neuroscience*, vol. 32, no. 19, pp. 6699–6710, 2012.
- [22] Z. Liu, J. A. Dearman, B. C. Cox et al., "Age-dependent in vivo conversion of mouse cochlear pillar and Deiters' cells to immature hair cells by Atoh1 ectopic expression," *The Journal of neuroscience : the official journal of the Society for Neuroscience*, vol. 32, no. 19, pp. 6600–6610, 2012.
- [23] Z. Gao, M. C. Kelly, D. Yu et al., "Spatial and age-dependent hair cell generation in the postnatal mammalian utricle," *Molecular Neurobiology*, vol. 53, no. 3, pp. 1601–1612, 2016.
- [24] Y. Shu, W. Li, M. Huang et al., "Renewed proliferation in adult mouse cochlea and regeneration of hair cells," *Nature Communications*, vol. 10, no. 1, p. 5530, 2019.
- [25] Y. Chen, S. Zhang, R. Chai, and H. Li, "Hair cell regeneration," *Advances in Experimental Medicine and Biology*, vol. 1130, pp. 1–16, 2019.
- [26] B. C. Cox, R. Chai, A. Lenoir et al., "Spontaneous hair cell regeneration in the neonatal mouse cochlea in vivo," *Development (Cambridge, England)*, vol. 141, no. 4, pp. 816–829, 2014.
- [27] S. Zhang, D. Liu, Y. Dong et al., "Frizzled-9+ supporting cells are progenitors for the generation of hair cells in the postnatal mouse cochlea," *Frontiers in Molecular Neuroscience*, vol. 12, p. 184, 2019.
- [28] S.-M. Yang, W. Chen, W.-W. Guo et al., "Regeneration of stereocilia of hair cells by forced Atoh1 expression in the adult mammalian cochlea," *PloS One*, vol. 7, no. 9, article e46355, 2012.
- [29] J. Yang, S. Bouvron, P. Lv, F. Chi, and E. N. Yamoah, "Functional features of trans-differentiated hair cells mediated by Atoh1 reveals a primordial mechanism," *The Journal of Neuroscience : The Official Journal of the Society for Neuroscience*, vol. 32, no. 11, pp. 3712–3725, 2012.
- [30] Y. Zheng, W. Luo, R. Ma et al., "The Atoh1 expression levels are correlated with the arrangement, ciliary morphology, and electrophysiological characteristics of ectopic hair cell-like cells," *Neuroscience Letters*, vol. 720, article 134758, 2020.
- [31] J. Yang, N. Cong, Z. Han, Y. Huang, and F. Chi, "Ectopic hair cell-like cell induction by Math1 mainly involves direct trans-differentiation in neonatal mammalian cochlea," *Neuroscience Letters*, vol. 549, pp. 7–11, 2013.
- [32] J. L. Zheng and W. Q. Gao, "Overexpression of Math1 induces robust production of extra hair cells in postnatal rat inner ears," *Nature Neuroscience*, vol. 3, no. 6, pp. 580–586, 2000.
- [33] W.-W. Luo, J.-M. Yang, Z. Han et al., "Atoh1 expression levels define the fate of rat cochlear nonsensory epithelial cells in vitro," *Molecular Medicine Reports*, vol. 10, no. 1, pp. 15–20, 2014.
- [34] J. Cafaro, G. S. Lee, and J. S. Stone, "Atoh1 expression defines activated progenitors and differentiating hair cells during avian hair cell regeneration," *Developmental Dynamics*, vol. 236, no. 1, pp. 156–170, 2007.
- [35] C. J. Kros, J. P. Ruppertsberg, and A. Rusch, "Expression of a potassium current in inner hair cells during development of hearing in mice," *Nature*, vol. 394, no. 6690, pp. 281–284, 1998.
- [36] W. Marcotti, G. S. Geleoc, G. W. Lennan, and C. J. Kros, "Transient expression of an inwardly rectifying potassium conductance in developing inner and outer hair cells along the mouse cochlea," *Pflugers Archiv : European Journal of Physiology*, vol. 439, no. 1-2, pp. 113–122, 1999.
- [37] W. Marcotti, S. L. Johnson, M. C. Holley, and C. J. Kros, "Developmental changes in the expression of potassium currents of embryonic, neonatal and mature mouse inner hair cells," *The Journal of Physiology*, vol. 548, no. 2, pp. 383–400, 2003.
- [38] G. S. Geleoc, J. R. Risner, and J. R. Holt, "Developmental acquisition of voltage-dependent conductances and sensory signaling in hair cells of the embryonic mouse inner ear," *The Journal of Neuroscience : The Official Journal of the Society for Neuroscience*, vol. 24, no. 49, pp. 11148–11159, 2004.
- [39] G. D. Housley, W. Marcotti, D. Navaratnam, and E. N. Yamoah, "Hair cells—beyond the transducer," *The Journal of Membrane Biology*, vol. 209, no. 2-3, pp. 89–118, 2006.
- [40] A. Hafidi, M. Beurg, and D. Dulon, "Localization and developmental expression of BK channels in mammalian cochlear hair cells," *Neuroscience*, vol. 130, no. 2, pp. 475–484, 2005.
- [41] H. Ohmori, "Studies of ionic currents in the isolated vestibular hair cell of the chick," *The Journal of Physiology*, vol. 350, no. 1, pp. 561–581, 1984.

Research Article

Distinct Expression Patterns of Apoptosis and Autophagy-Associated Proteins and Genes during Postnatal Development of Spiral Ganglion Neurons in Rat

Shule Hou ^{1,2,3} Penghui Chen,^{1,2,3} Jiarui Chen ⁴ Junmin Chen ^{1,2,3} Lianhua Sun ^{1,2,3}
Jiayong Chen ^{1,2,3} Baihui He ^{1,2,3} Yue Li ^{1,2,3} Huan Qin ^{1,2,3} Yuren Hong ⁵
Shuna Li ^{1,2,3} Jingchun He ^{1,2,3} Dekun Gao ^{1,2,3} Fabio Mammano ^{6,7}
and Jun Yang ^{1,2,3}

¹Department of Otorhinolaryngology-Head & Neck Surgery, Xinhua Hospital, Shanghai Jiaotong University School of Medicine, Shanghai, China

²Shanghai Jiaotong University School of Medicine Ear Institute, Shanghai, China

³Shanghai Key Laboratory of Translational Medicine on Ear and Nose diseases, Shanghai, China

⁴Department of Otorhinolaryngology-Head & Neck Surgery, Shanghai Children's Hospital, Shanghai Jiaotong University, Shanghai, China

⁵Laboratory of Electron Microscope Center, Shanghai Medical College, Fudan University, Shanghai, China

⁶Department of Physics and Astronomy "G. Galilei", University of Padua, Padova, Italy

⁷Department of Biomedical Sciences, Institute of Cell Biology and Neurobiology, Italian National Research Council, Monterotondo, Italy

Correspondence should be addressed to Fabio Mammano; fabio.mammano@unipd.it and Jun Yang; yangjun@xinhuamed.com.cn

Received 12 February 2020; Revised 18 June 2020; Accepted 6 October 2020; Published 17 October 2020

Academic Editor: Renjie Chai

Copyright © 2020 Shule Hou et al. This is an open access article distributed under the Creative Commons Attribution License, which permits unrestricted use, distribution, and reproduction in any medium, provided the original work is properly cited.

Autophagy and apoptosis have a complex interplay in the early embryo development. The development of spiral ganglion neurons (SGNs) in addition to Corti's organ in the mammalian cochlea remains crucial in the first two-week postnatal period. To investigate the roles of apoptosis and autophagy in the development of SGNs, light microscopy was used to observe the morphological changes of SGNs. The number of SGNs was decreased from P1 to P7 and plateaued from P10 to P14. Immunohistochemistry results revealed positive expression of cleaved-caspase3, bcl-2, microtubule-associated protein light chain 3-II (LC3-II), Beclin1, and sequestosome 1 (SQSTM1/P62) in SGNs. The apoptotic bodies and autophagosomes and autolysosomes were also identified by transmission electron microscopy at P1 and P7. Real-time PCR and western blotting results revealed that the apoptotic activity peaked at P7 and the autophagy activity was gradually upregulated along with the development. Taken together, our results for the first time showed that autophagy and apoptosis in SGNs play distinct roles during specific developmental phases in a time-dependent manner.

1. Introduction

The auditory function in neonatal rats remains immature, and the cochlear structure and function gradually attain maturity by the second postnatal week. The dendrites of immature spiral ganglion neurons (SGNs) develop innerva-

tions to both outer hair cells (OHCs) and inner hair cells (IHCs) simultaneously by the end of pregnancy [1]. During postnatal days 1-7, the immature SGNs are differentiated into type I SGNs and type II SGNs [2]. In addition, the neurites then go through crucial refinement and retraction steps, establishing a specific connection between type I SGNs and

IHCs and between type II SGNs and OHCs [1, 3]. Subsequently, the calyx of Held gradually matures in the cochlear nucleus, thereby establishing the function of cochlear output [4]. These bipolar SGNs develop long processes that connect the hair cells (HCs) in the cochlea with the neurons in the cochlear nucleus in order to process accuracy and speed required for auditory information. The specific and appropriate connection between the periphery and central auditory systems is eventually completed at postnatal days 10–12 [5]. The number of SGNs during this period was shown to be reduced [6]. However, the underlying mechanism of transient degeneration and differentiation of SGNs still remains elusive.

Apoptosis (“self-killing”) and autophagy (“self-eating”) are two self-destruction processes that play an important role in the development of inner ear. Also, they are considered important for the maturation of both HCs and SGNs [7, 8], and both apoptosis and autophagy are critical for the survival of HCs and SGNs under varied destruction conditions. Apoptosis is type I programmed cell death that plays a vital role in the development and differentiation of the cochlea [8]. In 2000, Nikolic et al. have used the TdT-mediated dUTP Nick-End Labeling (TUNEL) technique and the results revealed that apoptosis substantially occurs in the cochlear ganglion between E16 and P1 but occasionally occurs between P1 and P14 [9]. However, Ehteler and Nofsinger have reported about 27% reduction in the number of SGNs from P3 to P7 [6]. On the other hand, previous reports have shown that autophagy involves a complex connection with apoptosis in the inner ear HCs and SGNs. In the majority of cases, autophagy inhibits cell apoptosis by strengthening cell antistress capacity. Strikingly, autophagy carries out cell death through other pathways and is known as type II or autophagic cell death [10]. Some common and similar stimulus molecules can induce either autophagy or apoptosis or both [11]. However, time-dependent autophagic activities in cochlear SGNs after two weeks of birth have not yet been reported. Therefore, the autophagic and apoptotic characteristic changes during two weeks after birth were evaluated using light and electron microscopy. Furthermore, the autophagic machinery genes such as microtubule-associated protein light chain 3-II (LC3-II), Beclin1, and sequestosome 1 (SQSTM1/P62) and apoptosis-related factors including *bcl-2*, *cleaved-caspase-3*, and *caspase-3* were detected to investigate differential expression patterns of autophagy and apoptotic-associated proteins and genes and their putative correlation during the development of SGNs in rats in the present study.

2. Materials and Methods

2.1. Animals. Rats (Sprague–Dawley) were purchased from Shanghai SIPPR-BK Laboratory Animals Co. Ltd. All animal operations were in accordance with the guidelines approved by the experimental animal care institution of Xinhua Hospital, Medical College of Shanghai Jiaotong University. In the current experiment, the first postnatal day (P1) was the birthday. P1, P3, P5, P7, P10, and P14 are considered the postnatal time points after the birthday.

2.2. Hematoxylin-Eosin (HE) Staining. Cochleas of rats ($n = 3$) (P1–P14) were removed as described previously [12]. The cochleas were 4% PFA fixed, 10% EDTA decalcified, dehydrated by a graded ethanol series, and embedded in paraffin. Then, 3 μm sections were cut and deparaffinized, followed by staining with 75% alum hematoxylin and 0.15% eosin and rehydration with xylene and graded ethanol series.

2.3. Transmission Electron Microscope (TEM). After anesthesia, rats at P1 and P7 underwent cardiac perfusion with ice-cold 2.5% glutaraldehyde (no. G5882, Sigma, USA). The cochleas were dissected and fixed with 2.5% glutaraldehyde for 24 h and decalcified in 10% EDTA. Subsequently, the cochleas were fixed with 1% osmic acid for 2 h at room temperature, rinsed with 0.1 M PBS for 3 times, and dehydrated with ethanol and acetone. The cochleas were immersed in Epon 812. Ultrathin sections (60–70 nm) of cochleas were prepared. Then, the sections were stained with alkaline lead citrate and uranyl acetate and observed under a Philips CM-120 transmission electron microscope (Amsterdam, Philips, The Netherlands).

2.4. Immunohistochemical Staining. The paraffin-embedded tissue sections of P7 rat cochlea were blocked in a 1x PBS buffer containing 5% BSA (Sangon Biotech, C500626, China) and 0.3% Triton X-100 (Sigma, no. 30-5140, USA) at room temperature for 1 h, then incubated with the following primary antibodies at 4°C overnight: anti-MAP LC3II mouse monoclonal antibody (1:300; Santa Cruz, sc-271625, USA), anti-SQSTM1/P62 recombinant rabbit monoclonal antibody (1:200; Abcam, ab109012, USA), anti-Beclin1 rabbit polyclonal antibody (1:200; Abcam, ab62557, USA), anti-Bcl2 mouse monoclonal antibody (1:200; Servicebio, GB12318, China), anti-cleaved caspase3 rabbit polyclonal antibody (1:500; Servicebio, GB11009, China), and anti-caspase3 rabbit polyclonal antibody (1:500; Servicebio, GB11009-1, China). After three washes with 0.01 M PBS for 10 mins, the sample sections were incubated with the HRP-conjugated goat anti-rabbit/mouse IgG for IHC (ready to use) (1:300; Sangon Biotech, D110073, China) at room temperature for 40 min. After being incubated for 5 mins using a DAB Substrate kit (Sangon Biotech, E670033, China), the specimens were observed under a microscope (Olympus BX43, Tokyo, Japan) and images processed using Adobe Photoshop software.

2.5. Quantitative Real-Time PCR. The total RNA of SGNs was extracted by Trizol chloroform isopropanol method, and then, the concentration was determined. cDNA was obtained by using TaqMan® Reverse Transcription Reagents (no. N8080234, ThermoFisher Scientific), and the reaction was carried out in triplicate using SYBR™ Green PCR Master Mix (no. 4344463, ThermoFisher Scientific). β -Actin was used as the endogenous reference, and autophagy-related genes *LC3-II*, *P62*, and *Beclin1* and apoptosis-related genes *Bcl2* and *Caspase3* were used as target genes. The primers used for amplification are provided in a list in Table 1. The coefficient of variation about target genes and endogenous

TABLE 1: Primers for real-time-PCR.

Gene	Forward (5'-3')	Reverse (5'-3')
<i>LC3 II</i>	ATCAACATTCTGACGGAGCGG	ATCTGCCTGCTTGTCCCTGGTT
<i>P62</i>	TGTCTTGGGGAAGGGTTCGAT	GCATAAGCTTCACATGGGGGT
<i>Beclin1</i>	CCTCTGAAACTGGACACGAGC	GCTGGGGGGATGAATCTTCGA
<i>Bcl2</i>	TCTTTGAGTTCGGTGGGGTCA	AGTTCACAAAAGGCATCCAG
<i>Caspase3</i>	GAAAGCCGAAACTCTTCATCAT	ATGCCATATCATCGTCAGTTCC
<i>β-Actin</i>	TGCTATGTTGCCCTAGACTTCG	GTTGGCATAGAGGTCTTTACGG

reference gene was calculated. The relative expression level of mRNAs was calculated by the $2^{-\Delta\Delta CT}$ method.

2.6. Western Blotting Analysis. Samples were extracted from the isolated P1-P14 cochlear SGNs. The sample proteins were resolved by SDS-PAGE on 12% polyacrylamide gels and transferred to polyvinylidene fluoride (PVDF) membranes (Millipore, USA). The membranes were blocked (Beyotime, China) under ambient temperature for 1 h and probed with the following primary antibodies at 4°C overnight: anti-MAP LC3II mouse monoclonal antibody (1:1000; Santa Cruz, sc-271625), anti-SQSTM1/P62 recombinant rabbit monoclonal antibody (1:1000; Abcam, ab109012, USA), anti-Beclin1 rabbit polyclonal antibody (1:1000; Abcam, ab62557, USA), anti-caspase3 rabbit polyclonal antibody (1:1000; Cell Signaling Technology, no. 9662, USA), anti-cleave-caspase3 rabbit monoclonal antibody (Cell Signaling Technology, no. 9664, 1:1000, USA), anti-Bcl2 rabbit monoclonal antibody (1:2000; Wanleibio, WL01556, China), and GAPDH (1:2000; Proteintech, 60004-1-Ig, USA). After three washes, the membranes were incubated with a secondary antibody, HRP-labeled goat anti-rabbit IgG or anti-mouse IgG (1:1000; Beyotime, A0208/A0216, China), at 37°C for 1 h. Subsequently, the chemiluminescence reagent (Millipore, A : B = 1 : 1, USA) was utilized to develop the immunoreactive bands, and the images were analyzed using the Bio-Rad ChemiDoc XRS+ (Bio-Rad Company, USA). At least three independent experiments were carried out.

2.7. Statistical Analysis. Data are expressed as mean \pm SEM, and all experiments were repeated at least three times. Statistical analyses were conducted using GraphPad prism 6 software. Student's *t*-test was used to judge the significant effects between different groups. $P < 0.05$ were considered significantly. Image J software was used to measure the cross-sectional area and to count SGNs to calculate the density of SGNs (the number of SGNs in the cochlea divided by the cross-sectional area).

3. Result

3.1. Morphological and Quantitative Changes in SGNs during Postnatal Development. The HE staining of SGNs in rats at P1-P14 showed morphological transition at the middle turn (Figure 1). The size of the individual SGN was shown to be significantly increased, and the ratio of the nucleus to the

cytoplasm gradually declined from P1 to P14 (Figure 1). The growth rate in the first postnatal week was more than that recorded in the second postnatal week. The density of SGNs was decreased by about 33% during the first week and then plateaued from P10 to P14. The ossification of the bone wall around SGNs started at P7. However, before P7, a distinct boundary between immature SGNs and undifferentiated mesenchymal cells was shown to be absent. The Schwann cells were gradually matured, encompassing the SGN cell body as well as the neurites upon development.

3.2. Apoptosis and Autophagy in SGNs under TEM. At P1, several apoptotic bodies were shown as cytoplasmic membrane blebbing, chromatin condensation along the nuclear envelope, chromatin margination, and cell shrinkage (Figure 2(a)), while the nuclear membrane, plasma membrane, and organelles were well preserved. Consecutively, the glial cells and SGNs could not be distinguished (Figure 2(a), A1). However, the apoptotic body is rarely identified at other time points. At P7, the ratio of the nucleus to the cytoplasm in the neurons became evident (Figure 2(b), B1). Also, several autophagic vacuoles and autolysosomes were identified in SGNs at P7 (Figure 2(b), B2-B6).

3.3. Immunohistochemical Staining for Apoptosis and Autophagy. Immunohistochemical staining results of LC3-II, P62, cleaved-caspase3, and Bcl-2 showed positive expression of autophagy- and apoptosis-associated proteins in SGNs (Figure 3) at P7.

3.4. Real-Time PCR Quantitative Analysis of Apoptosis-Associated Genes and Autophagy Machinery Genes in SGNs during the Postnatal Development. The results of real-time PCR quantitative analysis revealed dynamic changes in autophagy machinery genes and apoptosis-associated genes at a transcription level. The expression of *LC3-II* demonstrated an upward trend from P1 to P14, except that it was higher at P5 than at P7 (Figure 4(a)). The expression of *P62* showed gradual declination during these postnatal two weeks (Figure 4(b)), while the expression of *Beclin1* showed an increasing trend (Figure 4(c)). *Bcl2* and *Caspase3* showed similar expression trend during postnatal development. *Bcl2* exhibited maximal expression at P1, which was decreased by 76.3% at P3. The expression of *Bcl2* at P7 was increased by about 1.42-fold when compared to that at P5, followed by a sharp declination by 37.3% at P10 (Figure 4(d)). The expression of *Caspase3* was shown to be

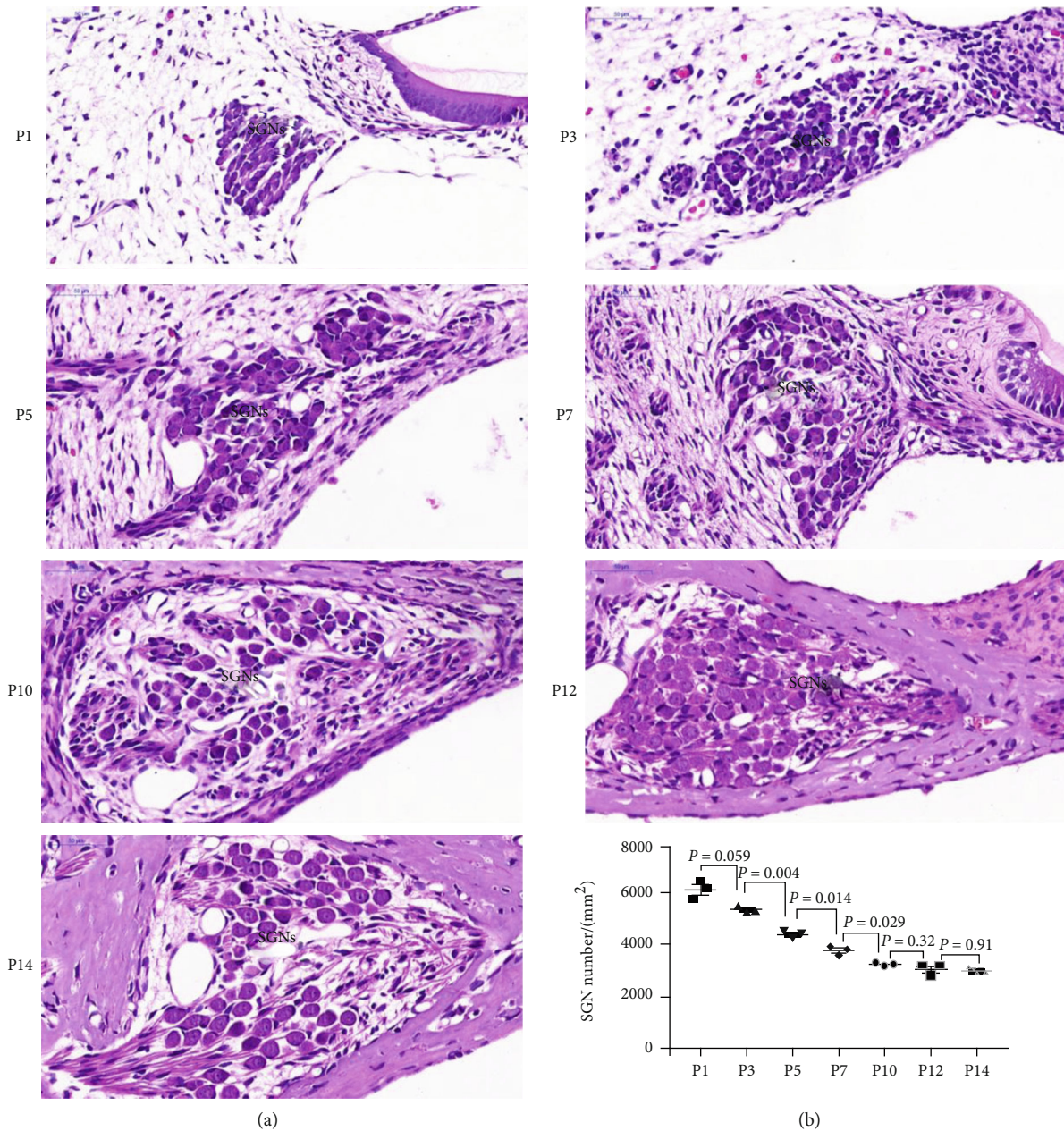


FIGURE 1: HE staining of SGNs during postnatal weeks from P1 to P14. The SGNs are obtained from the middle turn of the rat cochlea. The immature neurons and glial cells were basophilic and are indicated by blue staining from P1 to P5. The Schwann cells at P12 and P14 were adhered and surrounded by neurons. In the first postnatal week, the density of SGNs was decreased by about 33% and was stabilized in the second week. Scale bars = 50 μm . The number/mm² of SGNs was counted and is shown at the lower part of (b).

decreased at P5, which showed a peak at P7, showing a 2.2-fold decrease when compared to that at P5, and then declined from P7 to P14 (Figure 4(e)). During the postnatal two weeks, the overall expression trend of apoptosis was initially increased and then declined, and autophagy was gradually increased in rat cochlea SGNs (Figure 4(f)).

3.5. Western Blot Analysis of Apoptosis-Associated Proteins and Autophagy Machinery Proteins in SGN during the Postnatal Development. Western blot analysis showed dynamic alteration in apoptosis-associated proteins and

autophagy machinery proteins at a protein level. The expression of Bcl-2 was maximized at P7 and sharply declined at P10 and P14 (Figure 5(c)). Caspase3 demonstrated a relatively low expression at P1 and declined further at P3, followed by an increase at P5 and P7 and a sharp decrease at P10 and P14 (Figure 5(b)). Caspase3 and cleaved-caspase3 showed a strong expression at P5 and P7 (Figure 5(c)). The apoptosis-associated proteins expressed maximal apoptotic activity at P7. On the other hand, the expression of LC3-II showed an upward trend from P1 to P10 and declined at P14 (Figure 6(b)). P62 demonstrated

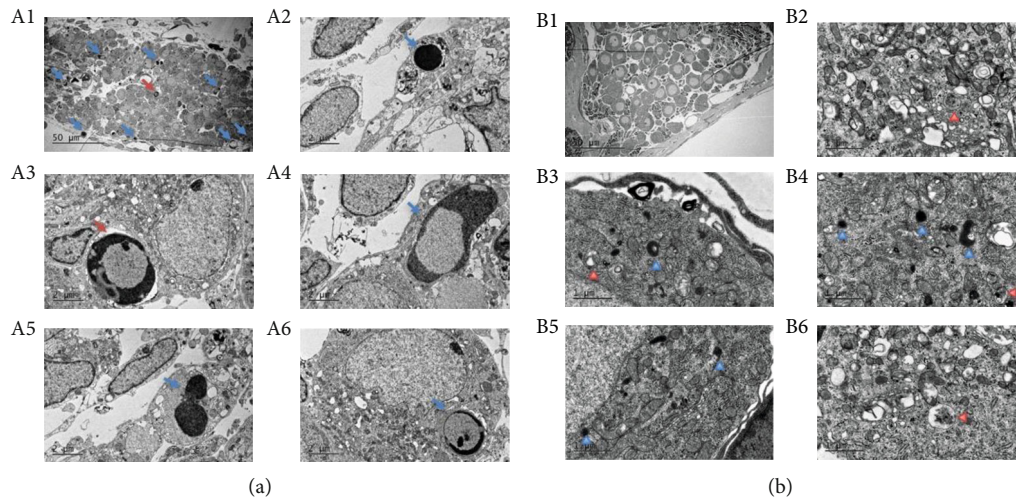


FIGURE 2: TEM observation of apoptosis and autophagy in SGNs during postnatal development. (A1) The overview of SGNs at P1 showing many apoptotic bodies (blue and red arrow). Scale bars = 50 μ m. The morphological differences among various apoptotic cells and nuclear chromatin condensation: (A4) some condensed chromatin moves under the nuclear membrane or (A3) assumes a crescent shape; (A2) some condensed chromatin occupies the whole nuclear area. Scale bars = 2 μ m. (A5) The arrow indicates the cell body of secondary necrosis. Scale bars = 2 μ m. (B1) The overview of SGNs at P7, scale bars = 50 μ m. (B2, B3, B4, and B6) Red arrows indicate autophagosomes, which are presented as double membrane structures and contain a cytoplasm or organelles. (B3–B5) Blue arrows represent autolysosomes. Scale bars = 1 μ m.

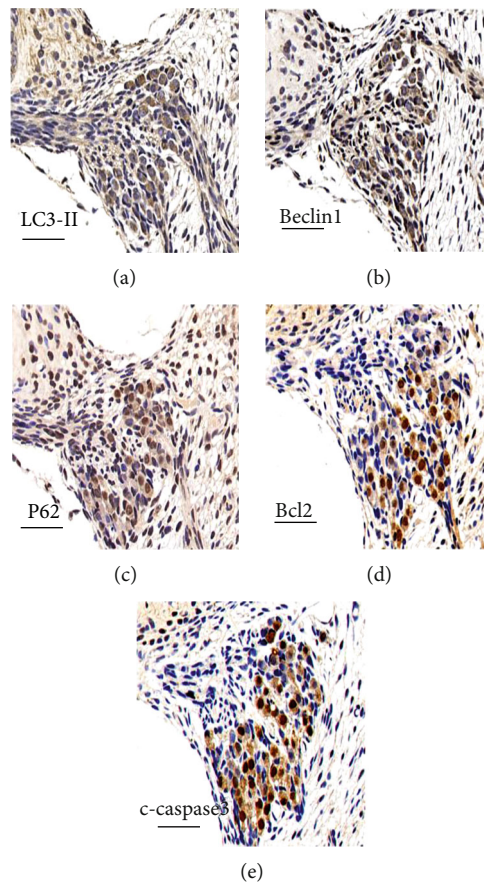


FIGURE 3: Immunohistochemical staining for autophagy and apoptosis-associated genes at P7. (a), (b) (c), (d), and (e) represent immunohistochemical staining for LC3-II, Beclin1, P62, Bcl-2, and cleaved-caspase3, respectively. The images were obtained from the middle turn of rat cochlea. In the area of SGNs, a positive brown staining was observed in the cytoplasm or nucleus. Scale bars = 50 μ m.

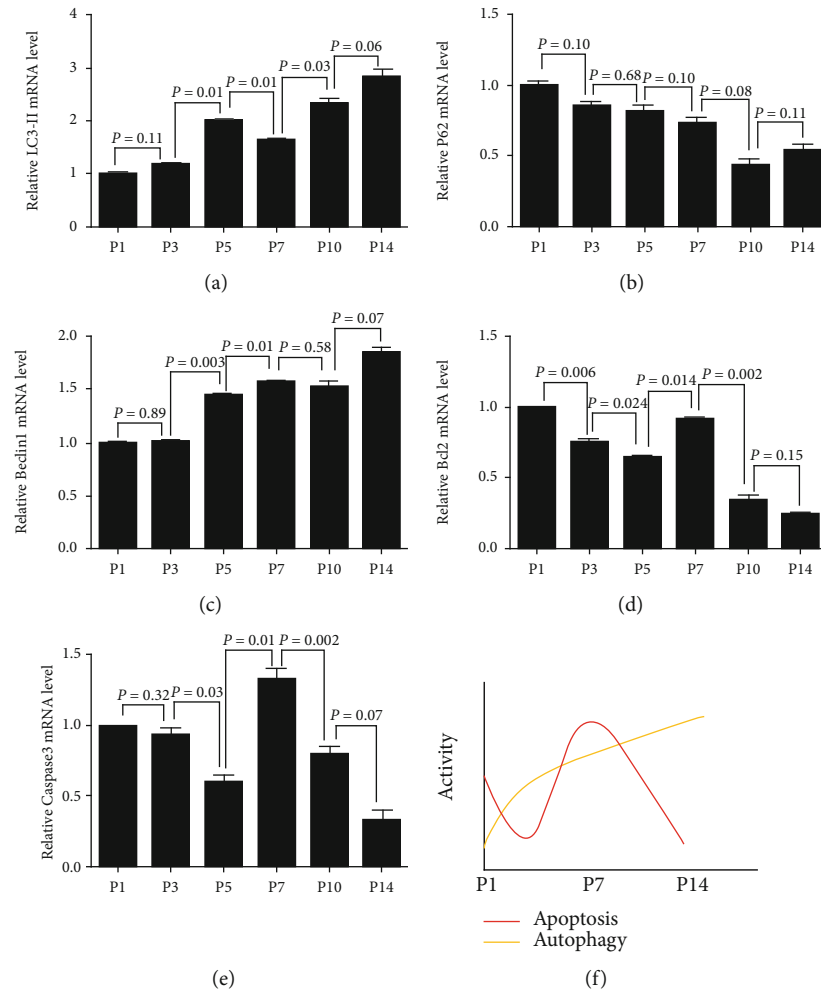


FIGURE 4: Real-time PCR quantitative analysis of autophagy machinery genes and apoptosis-associated genes in SGNs during the postnatal development. (a–c) The transcription expression of *LC3-II*, *P62*, and *Beclin1* showed that the autophagy activity was upregulated with the development of SGNs. (d, e) The transcription expression of *Bcl2* and *Caspase3* showed maximal apoptotic activity at P7. (f) The overall expression trend of apoptosis and autophagy. Data from triplicate samples were normalized to those at P1. Significant differences were evaluated using repeated measures ANOVA.

low expression at P1, elevated by about 1.5-fold at P3, and gradually decreased from P3 to P14 (Figure 6(c)). The maximal expression of *Beclin1* was observed at P7 (Figure 6(d)), which was much earlier than that observed for *LC3-II*.

4. Discussion

HCs in the cochlea play a critical role in the conversion of mechanical sound waves into neural signals, and SGNs transmit these signals to the auditory cortex for hearing. Therefore, HCs and SGNs are considered critical for auditory function. In the mammal's inner ear, HCs and SGNs are vulnerable to multiple damages, but the regenerative ability of HCs and SGNs is limited in mammals, and so most of the damaged HCs and SGNs cannot spontaneously regenerate. Thus, hearing loss in most of the patients is induced by gene mutations, noise, different ototoxic drugs, inflammation, or aging, causing malfunctioning of HCs or SGNs [13]. In the inner ear, apoptosis is genetically aroused in response to var-

ious damages, including noise, different ototoxic drugs, inflammation, or aging in HCs and SGNs [13]. The expression of *Bcl2*, *caspase3*, and cleaved-*caspase3* represents the level of apoptotic activity. Our results showed that the activity of apoptosis peaked at P7 and declined sharply at P10 and P14. Therefore, P7 might be considered a crucial developmental time point. Firstly, Schwartz et al. have found a 27% reduction in the number of SGNs between P3 and P7 [14], which was consistent with that of the apoptotic bodies detected by TEM. Secondly, it has been reported that the neurites underneath the HCs completed refinement and retraction by P8 [3]. Finally, the SGNs begin to differentiate into type I and type II SGNs after P7 [2]. This quantitative alteration of *caspase3* suggests that the reduced number of cells between P3 and P7 might be generated by apoptosis due to lack of trophic factors and stimulation from sensory HCs [15]. Although it remains difficult to distinguish whether type I or type II SGNs undergo apoptotic cell death based on the present results, the immature type II SGNs are

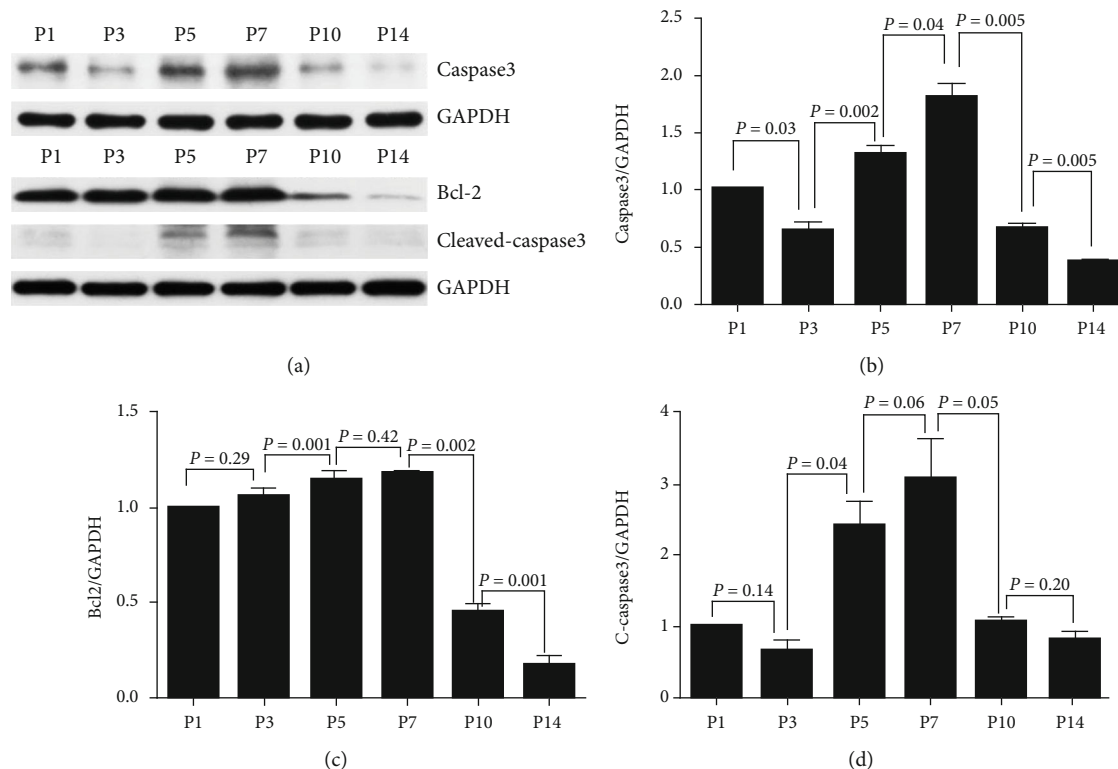


FIGURE 5: Western blot quantitative analysis for dynamic changes in apoptosis-associated proteins in SGN. (a) The protein expression levels of Bcl2, caspase3, cleaved-caspase3, and GAPDH were measured by western blotting at different developmental time points. (b), (c), and (d) show the half quantitative analysis of Bcl2, caspase3, and cleaved-caspase3 expressions, respectively; and it was normalized to that of GAPDH expression levels. Significant differences were evaluated using repeated measures ANOVA.

shown to be in maximum number as they lose afferent innervation from OHCs between P3 and P7 [16].

Autophagy is a critical mechanism of cell death and involves differentiation and development [7, 17]. It is characterized by double-membrane vacuole structures known as autophagosomes. de Iriarte Rodriguez et al. have demonstrated a twofold *Beclin1* and *Atg9a* mRNA expression at P30 when compared to that at P0 [18], suggesting the upregulation of autophagic activity with growth during postnatal development. However, the expression trend of these genes during P0–P14, which is a key phase of development, remains unclear. In this study, the real-time PCR results showed that the expression of *LC3-II* and *Beclin1* was upregulated, while that of *P62* was downregulated in cochlear SGNs from P1 to P14. Western blotting analysis results revealed that the maximal expression of *LC3-II* and *Beclin1* proteins in cochlear SGNs was at P10 and P7, respectively.

A previous study conducted in chicken showed that the inhibition of *LC3-II* resulted in the accumulation of apoptotic cells in otic vesicles [19]. These results supported that autophagy provided energy for removing the damaged organelles or apoptotic cells and is regarded essential for the migration of neural precursors. Additionally, Kuma et al. have found decreased levels of amino acids in the plasma and adipose tissues of *Atg5*-, *Atg7*-, *Atg9*-, and *Atg16*-mutant mice, and these mice died shortly after birth,

suggesting that autophagy serves as an energy source during the perinatal period [15]. Generally, the upregulated autophagic activity during the first postnatal week induces energy for undergoing apoptosis, and this peaks at P7. Moreover, with the increasing cell size and the ratio of the cytoplasm to the nucleus along with the development, a large number of proteins and organelles are required for generating high-level autophagy. In terms of differentiation, active autophagy facilitates the turnover of specific receptors and factors in order to promote different cell fates [7]. In addition, the maturely differentiated neurons might face various external injuries, and therefore, autophagy plays a homeostatic role in refreshing intracellular components and resistance to external stress [16].

More importantly, the correlation between apoptosis and autophagy might be more complicated than speculated [20]. Autophagy and apoptosis are triggered by common upstream signals that occasionally combine with the processes [21]. In other patients, the cell switches between the two responses in a mutually exclusive manner [22]. Thus, the purpose of distinct expression patterns of autophagy- and apoptosis-associated proteins and genes during the two postnatal weeks is to satisfy the requirement for the development of SGNs. However, the molecular machinery underlying the change in apoptosis and autophagy still remains unclear.

In summary, the present morphological experiment revealed reduction in the number of SGNs and increment

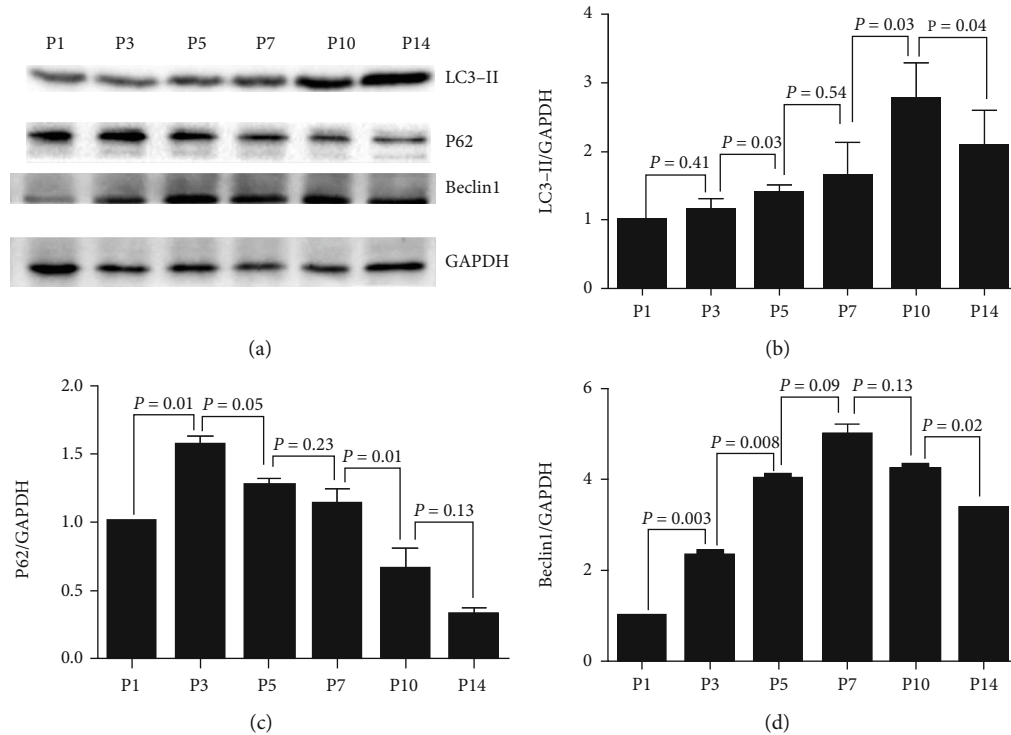


FIGURE 6: Western blot quantitative analysis for the dynamic change in autophagy machinery proteins. (a) The protein expression levels of LC3-II, P62, Beclin1, and GAPDH were measured by western blotting at different developmental time points. (b), (c), and (d) show the half quantitative analysis of LC3-II, P62, and Beclin1 expressions, respectively, and it was normalized to that of the GAPDH. Significant differences were evaluated using repeated measures ANOVA.

in cell size during postnatal development. For the first time, the time-dependent dynamic alteration of apoptosis and autophagy from P1 to P14 in rat cochlear SGNs was examined. The results of apoptosis reached the peak at P7, and autophagy reached the peak at P10 or in the later stages. This suggested that both apoptosis and autophagy play distinct roles during different developmental time points, although the significance of inconsistencies at these time points that show peak in the expressions remained unclear. Therefore, additional studies are warranted to clarify the correlation between apoptosis and autophagy as well as the underlying mechanisms during cochlear development.

Data Availability

All data used during the study are available from the corresponding author by request.

Conflicts of Interest

The authors declare no competing financial interests.

Authors' Contributions

Shule Hou was responsible for the study conception, and data quality control and wrote the manuscript. Penghui Chen was responsible for data quality control and wrote the manuscript. Jiarui Chen was responsible for the study conception, immunohistochemical staining, and statistical

data analysis. Lianhua Sun was responsible for the real-time PCR experiments. Jianyong Chen was responsible for data quality control. Yue Li was responsible for the collection of cochlear samples for H&E experiments. Junmin Chen was responsible for the collection of cochlear samples for TEM experiments. Baihui He was responsible for the collection of cochlear SGN samples for western blot. Yuren Hong was responsible for the TEM experiments. Huan Qin and Dekun Gao analyzed the data. Shuna Li was responsible for the collection of cochlear SGN samples for real-time PCR. Jingchun He was responsible for data quality control. Fabio Mammano was responsible for the study conception. Jun Yang was responsible for data quality control and wrote the manuscript. Shule Hou, Penghui Chen, and Jiarui Chen contributed equally to this work.

Acknowledgments

This work was supported by the National Natural Science Foundation of China (81873698 and 81600799).

References

- [1] S. M. Echteler, "Developmental segregation in the afferent projections to mammalian auditory hair cells," *Proceedings of the National Academy of Sciences of the United States of America*, vol. 89, no. 14, pp. 6324–6327, 1992.
- [2] M. Barclay, A. F. Ryan, and G. D. Housley, "Type I vs type II spiral ganglion neurons exhibit differential survival and

- neuritogenesis during cochlear development,” *Neural Development*, vol. 6, no. 1, p. 33, 2011.
- [3] L. C. Huang, M. Barclay, K. Lee et al., “Synaptic profiles during neurite extension, refinement and retraction in the developing cochlea,” *Neural Development*, vol. 7, no. 1, p. 38, 2012.
- [4] R. L. Snyder and P. A. Leake, “Topography of spiral ganglion projections to cochlear nucleus during postnatal development in cats,” *The Journal of Comparative Neurology*, vol. 384, no. 2, pp. 293–311, 1997.
- [5] L. Delacroix and B. Malgrange, “Cochlear afferent innervation development,” *Hearing Research*, vol. 330, Part B, pp. 157–169, 2015.
- [6] S. M. Echterler and Y. C. Nofsinger, “Development of ganglion cell topography in the postnatal cochlea,” *The Journal of Comparative Neurology*, vol. 425, no. 3, pp. 436–446, 2000.
- [7] N. Mizushima and B. Levine, “Autophagy in mammalian development and differentiation,” *Nature Cell Biology*, vol. 12, no. 9, pp. 823–830, 2010.
- [8] Y. Leon, S. Sanchez-Galiano, and I. Gorospe, “Programmed cell death in the development of the vertebrate inner ear,” *Apoptosis*, vol. 9, no. 3, pp. 255–264, 2004.
- [9] P. Nikolic, L. E. Jarlebark, T. E. Billett, and P. R. Thorne, “Apoptosis in the developing rat cochlea and its related structures,” *Developmental Brain Research*, vol. 119, no. 1, pp. 75–83, 2000.
- [10] E. H. Baehrecke, “Autophagy: dual roles in life and death?,” *Nature Reviews Molecular Cell Biology*, vol. 6, no. 6, pp. 505–510, 2005.
- [11] F. Demarchi, C. Bertoli, T. Copetti et al., “Calpain is required for macroautophagy in mammalian cells,” *The Journal of Cell Biology*, vol. 175, no. 4, pp. 595–605, 2006.
- [12] J. Liu, L. Cai, Y. He, and J. Yang, “Apoptosis pattern and alterations of expression of apoptosis-related factors of supporting cells in Kölliker’s organ in vivo in early stage after birth in rats,” *European Journal of Histochemistry*, vol. 61, no. 3, article 2706, 2017.
- [13] W. Yan, W. Liu, J. Qi et al., “A three-dimensional culture system with Matrigel promotes purified spiral ganglion neuron survival and function in vitro,” *Molecular Neurobiology*, vol. 55, no. 3, pp. 2070–2084, 2018.
- [14] A. M. Schwartz, M. Parakkal, and R. L. Gulley, “Postnatal development of spiral ganglion cells in the rat,” *The American Journal of Anatomy*, vol. 167, no. 1, pp. 33–41, 1983.
- [15] A. Kuma, M. Hatano, M. Matsui et al., “The role of autophagy during the early neonatal starvation period,” *Nature*, vol. 432, no. 7020, pp. 1032–1036, 2004.
- [16] M. P. Taylor and K. Kirkegaard, “Potential subversion of autophagosomal pathway by picornaviruses,” *Autophagy*, vol. 4, no. 3, pp. 286–289, 2014.
- [17] F. Cecconi and B. Levine, “The role of autophagy in mammalian development: cell makeover rather than cell death,” *Developmental Cell*, vol. 15, no. 3, pp. 344–357, 2008.
- [18] R. de Iriarte Rodriguez, S. Pulido, L. Rodriguez-de la Rosa, M. Magarinos, and I. Varela-Nieto, “Age-regulated function of autophagy in the mouse inner ear,” *Hearing Research*, vol. 330, Part A, pp. 39–50, 2015.
- [19] M. R. Aburto, H. Sanchez-Calderon, J. M. Hurle, I. Varela-Nieto, and M. Magarinos, “Early otic development depends on autophagy for apoptotic cell clearance and neural differentiation,” *Cell Death & Disease*, vol. 3, no. 10, article e394, 2012.
- [20] M. C. Maiuri, E. Zalckvar, A. Kimchi, and G. Kroemer, “Self-eating and self-killing: crosstalk between autophagy and apoptosis,” *Nature Reviews Molecular Cell Biology*, vol. 8, no. 9, pp. 741–752, 2007.
- [21] S. Yousefi, R. Perozzo, I. Schmid et al., “Calpain-mediated cleavage of Atg5 switches autophagy to apoptosis,” *Nature Cell Biology*, vol. 8, no. 10, pp. 1124–1132, 2006.
- [22] X. Qu, Z. Zou, Q. Sun et al., “Autophagy gene-dependent clearance of apoptotic cells during embryonic development,” *Cell*, vol. 128, no. 5, pp. 931–946, 2007.

Review Article

Research Progress of Hair Cell Protection Mechanism

Yurong Mu,¹ Hongguo Su,² Fan Wu,³ Jianming Yang^{1,4} ,⁴ and Dan Li¹ 

¹Department of Otorhinolaryngology, Union Hospital, Tongji Medical College, Huazhong University of Science and Technology, Wuhan 430022, China

²Department of Otorhinolaryngology, Head and Neck Surgery, Zhongnan Hospital of Wuhan University, Wuhan 430071, China

³Otorhinolaryngology Department, Sun Yat-sen Memorial Hospital, Sun Yat-sen University, 107 West Yan Jiang Road, Guangzhou 510120, China

⁴Department of Otorhinolaryngology, The Second Affiliated Hospital of Anhui Medical University, Hefei 230601, China

Correspondence should be addressed to Jianming Yang; jmyang88@163.com and Dan Li; danli@hust.edu.cn

Received 20 April 2020; Revised 16 May 2020; Accepted 30 September 2020; Published 9 October 2020

Academic Editor: Renjie Chai

Copyright © 2020 Yurong Mu et al. This is an open access article distributed under the Creative Commons Attribution License, which permits unrestricted use, distribution, and reproduction in any medium, provided the original work is properly cited.

How to prevent and treat hearing-related diseases through the protection of hair cells (HCs) is the focus in the field of hearing in recent years. Hearing loss caused by dysfunction or loss of HCs is the main cause of hearing diseases. Therefore, clarifying the related mechanisms of HC development, apoptosis, protection, and regeneration is the main goal of current hearing research. This review introduces the latest research on mechanism of HC protection and regeneration.

1. Introduction

Hearing loss has become one of the common health problems in the world, and more and more people suffer from deafness. In recent years, with the exploration and understanding of the mechanism of deafness, many researchers hope to improve or restore hearing through promoting HC survival or regeneration. We will introduce the research progress and new findings of the mechanism of protecting and regenerating in HCs in this manuscript.

2. The Development of HCs

The inner ear of the mammal originates from the ectoderm of the embryo, and the ectoderm is locally thickened to form the auditory placode, and then the auditory placode is recessed to form an otic cup. When the otic cup closes off, a sac-like otic vesicle is formed [1, 2]. At E10.5-11, the cochlea duct is derived from the ventral side of the otic vesicle, and the bottom layer of the cochlea forms the proneurosensory domain. At E14.5, the differentiation of sensory precursor cells was initially from the central domain in the basal of the cochlea, which progressively extends toward the apex and basal, and finally differentiates into inner ear cells such as HCs and sup-

porting cells (SCs) [3]. In this process, the differentiation of sensory precursor cells into HCs and SCs mainly depends on the expression of the transcription factor Math1 (also known as Atoh1, [4]). The development of the inner and outer HCs progressed gradually from the basal turn to the apex turn, and the inner HCs (IHCs) develop earlier than the outer HCs (OHCs) [5–8].

HCs are located on the organ of Corti, which includes a row of IHCs and three rows of OHCs and SCs. The OHCs mechanically amplify and detect low-level sound, thereby enhancing the responsiveness of the sensory epithelium to different sound frequencies. The IHCs transmit the sound stimulation to the nerve; thereby, the sound stimulation is transformed into nerve excitement electrical signals, which is then transmitted along the auditory nerve to the auditory center to generate hearing [9]. SCs provide structural and nutritional support for the long-term survival of HCs.

3. The Apoptosis of HCs

HC apoptosis is a process that occurs programmatically under the control of genes and involves multiple triggering factors and signaling pathways. As we all know, ototoxic drugs, noise, aging, and other factors can cause apoptosis of

HCs, and the main mechanisms of apoptosis can be roughly divided into the following two.

3.1. Exogenous Pathway of HCs Apoptosis. Exogenous pathways can be triggered by a variety of factors, such as cell surface death receptor (FasL), which can cause the recruitment of specific adaptor proteins and the activation of caspases-8 and caspases-10. Other exogenous receptors include tumor necrosis factor alpha (TNF- α), tumor necrosis factor-related apoptosis-inducing ligand (TRAIL), and death receptor (DR), each of which can affect specific intracellular medium and eventually activate caspase (a protease family that plays an important role in programmed cell death and inflammation). In addition, TNF- α can also activate JNK, inhibit the antiapoptotic factor Bcl-2 through phosphorylation, and eventually cause apoptosis [10].

3.2. Endogenous Pathway of HC Apoptosis. The endogenous apoptosis pathway of HCs can be activated by intracellular stressors, such as reactive oxygen species (ROS). Previous studies have reported that HC loss caused by ototoxic drugs is usually associated with ROS accumulation, which can induce mitochondrial depolarization and trigger apoptosis [11]. Mitochondria are the main place for cells to produce ROS. Normally, the production level of ROS is low, which plays an important role in signal transduction, immune response, and gene expression regulation. But when the accumulation of reactive oxygen species is excessive, it will have a toxic effect on the cells and eventually lead to apoptosis [12]. The appropriate level of reactive oxygen species can promote autophagy and renew damaged cell components, thereby maintaining the stability of the intracellular environment. Autophagy is a physiologically conservative multistep process for recycling endogenous or exogenous cytoplasmic materials, such as misfolded proteins, lipids, organelles (mitochondria and ribosomes), cellular components, and peroxide enzyme and virus or bacteria, and finally degraded after fusion with lysosome [13]. Previous studies have reported that induced autophagy can inhibit the accumulation of ROS after aminoglycoside damage, thereby playing a role in promoting HC survival [14]. In addition, endogenous apoptosis pathways can be activated not only by intracellular stressors (such as ROS), but also by activated exogenous pathways, which shows that the two pathways are not completely independent.

4. The Regeneration of HCs

Most inner ear HCs of mammals are formed in the embryonic stage. After birth, due to congenital infections, noise, and improper use of ototoxic drugs such as aminoglycoside antibiotics, the HCs are irreversibly damaged and eventually lead to permanent hearing impairment [15]. Unlike mammals, the inner ear HCs of vertebrates such as fish and birds can be restored to normal levels after HC regeneration, mainly through the following two ways: the mitotic regeneration, the SCs proliferate and divide first and then a part of the SCs differentiate into HCs. In the direct transdifferentia-

tion, the SCs directly differentiate into HCs without undergoing proliferation and division [16].

Adult mammalian cannot spontaneously generate new HCs, but in recent years, studies have found that HCs, SCs, and pluripotent stem cells near the damaged area of the inner ear may be the source of HC regeneration under certain conditions. HC regeneration involves coordinated regulation of multiple factors and signaling pathways. In SC transdifferentiation-related research, it was found that the transcription factor Hes/Hey in the Notch signaling pathway can affect cell fate during development by combining the *Atoh1* promoter region. In addition, the regulation of multiple cell fate-related genes such as *p27*, *Atoh1*, and *Pou4f3* can enable the functional regeneration of HCs in adult animals. The role of epigenetics in HC regeneration has also been proven. For example, histone demethylase LSD1 affects the expression of genes related to HC development and transdifferentiation by regulating the level of H3K4 methylation modification [17]. miRNAs have been shown to participate in the regulation of the expression of many important genes during cochlea development, thereby affecting the processes of cochlea cell proliferation, migration, development, and apoptosis [18]. For example, miR-183 and miR-210 were found to play an important role in the transdifferentiation of SCs to HCs [19, 20]. In addition, the control of the number of regenerated HCs, the reconstruction of cell structure, the effective arrangement of cilia, the fine docking of nerve synapses, etc. are all important basis for evaluating the success of HC regeneration [21]. Through continuous exploration of the mechanism of sensory HC regeneration, it will help to solve the problem of mammalian sensory HC regeneration in the future.

5. HC Regeneration-Related Signaling Pathways

During the development of cochlea HCs, a variety of signaling pathways and signaling molecules are involved in regulating their differentiation and development, including Notch, Wnt, BMP, FGF, Shh, and JNK [22]. Inhibition or activation of related signaling pathways can increase the number of transdifferentiated or proliferated HCs after damage [23].

5.1. The Role of Notch Signaling Pathway in HC Regeneration. Notch signaling molecules and their receptors are membrane integrins. Cells can directly receive signals from neighboring cells through the receptors on their surface and transmit them to the nucleus, thereby activating the expression of related transcription factors in the nucleus [24, 25]. The Notch signaling pathway plays a variety of roles in the development of the inner ear, from the formation of the ear in the embryo to the generation of SCs, HCs, and neurons [26]. Notch signaling can inhibit the differentiation of sensory precursor cells into HCs in adult rats, but after inner ear injury, the activation of Notch signaling pathway has the potential to promote HC regeneration [27–29].

5.2. The Role of Wnt Signaling Pathway in HC Regeneration. The Wnt signaling pathway is a highly conserved signaling

pathway in the early stages of biological development and participates in regulating physiological processes such as embryonic development and differentiation, cell proliferation and growth, and cell polarity formation. The canonical Wnt/ β -catenin signaling pathway regulates the specialization of the auditory placode and the differentiation of the otic vesicle in the early stages of inner ear development [30]. During the early development of the cochlea, the canonical Wnt signaling pathway is upregulated in cochlea precursor sensory cells, and the inhibition of Wnt/ β -catenin signaling reduces HC formation in the differentiating organ of Corti [31]. In addition, the Wnt/PCP signaling pathway plays an important role in the arrangement of the stereocilia of HCs and the extension of the cochlea duct [32]. *Lgr5*⁺ cells in the cochlea of newborn mice have been shown to be an HC progenitor cell, which can regenerate HCs by direct differentiation or mitosis. Studies have found that inhibition of Notch can reactivate the inhibited Wnt signal, thereby promoting mitosis of *Lgr5*⁺ progenitor cells and generating new HCs [33].

5.3. The Role of BMP Signaling Pathway in HC Regeneration. Bone morphogenetic protein (BMP) belongs to the transforming growth factor beta (TGF- β) superfamily, and its ligands are expressed in the ear development of many animal species, including precursor sensory regions and sensory cells [34]. BMP signaling pathway plays an important role in gastrulation, mesoderm formation, and bone and nervous system development [35, 36]. Related studies of the inner ear have found that the BMP signaling pathway plays a regulatory role in the process of inner ear morphogenesis, formation and development of nerve fibers, HC development, etc. [37, 38]. When BMP signaling pathway is blocked, HCs and SCs decrease, and when exogenous BMP is added, HCs will increase [39].

5.4. The Role of FGF Signaling Pathway in HC Regeneration. Fibroblast growth factor (FGF) is an important intercellular signaling molecule. FGF plays a regulatory role in various physiological or pathological processes by binding to specific receptors on the cell membrane, such as embryonic development and organ formation, cell growth, tissue repair, tumorigenesis, and inflammation [40]. The FGF signaling pathway plays an important role in multiple stages of inner ear development, such as the formation of auditory placode and otic vesicle, the proliferation, and differentiation of sensory epithelial cells [41–43]. Studies have shown that inhibiting FGF can lead to the differentiation of precursor cells or SCs into HCs [44]. In the process of culturing inner ear sensory progenitor cells in vitro, ectopic activation of FGF receptor (FGFR) in mesenchyme is sufficient to increase sensory progenitor cell proliferation and cochlea length [45].

5.5. The Role of Shh Signaling Pathway in HC Regeneration. Shh is a class of Hedgehog (Hh) protein family, which regulates the gene expression of neighboring or distant cells in the form of extracellular secreted proteins and participates in regulating the development of multiple tissues and organs, affecting the occurrence of tumors and inducing tissue polarity [46, 47]. Shh is an important regulator of inner ear

development and plays an important role in regulating inner ear morphogenesis, formation of spiral neurons, and differentiation of HCs [48]. Shh gene deletion can cause severe inner ear developmental disorders, such as malformation or loss of ventral structures (cochlea duct and saccule) and dorsal structure (semicircular canal, utricle, and endolymphatic ductus), and developmental disorders of Corti organs and ganglion nerve cells [49, 50]. However, there are still few reports on Shh signaling pathway in HC regeneration, so its regulatory mechanism remains to be elucidated.

6. HC Protection-Related Drug Applications

Currently known drugs that have protective effects on HCs mainly include JNK kinase inhibitors and antioxidant drugs. In mouse and guinea pig experiments, JNK kinase inhibitors can prevent hearing loss caused by noise exposure, ototoxic drug treatment, trauma, and other factors [51, 52]. The JNK kinase inhibitor AM-111 has now completed the phase III clinical trial. For severe sensorineural hearing loss, AM-111 has a good hearing protection effect [53]. Antioxidant drugs including N-acetylcysteine, ebselen (glutathione peroxidase mimic), D-methionine, vitamin E, and flunarizine all show hearing protection [54–56]. The hearing protection effect of antioxidant drugs may be related to the removal of free radicals and the synergistic effect on other antioxidant enzymes to maintain the integrity of the cell membrane and reduce the oxidative stress response of cells.

7. Application of Gene Therapy in HC Protection

Gene therapy refers to the treatment or prevention of diseases through the addition and expression of genes. These gene fragments can reconstruct or correct those missing or abnormal gene functions and can interfere with the pathogenic process. Adeno-associated virus (AAV) vector is a vector that transfers genes into cochlea cells. It has a highly efficient transduction effect and is safe and stable in terms of long-term expression. The vector constructed based on AAV1 can effectively transduce IHCs and spiral ganglion cells and introduce secreted proteins into the cochlea, thereby protecting inner ear sensory cells from drug-induced damage [57]. Although the AAV vector can transduce mouse cochlea IHCs, the OHCs are still difficult to transduce. There is also an AAV-*ie* viral vector that can efficiently transduce cochlea SCs and induce the SCs to transdifferentiate into HCs. With the continuous optimization of the AAV virus, Isgrig et al. have proved that AAV2.7m8 can efficiently infect cochlea IHCs and OHCs. In addition, AAV2.7m8 can also efficiently infect inner pillar cells and inner phalangeal cells [58]. These studies prove that the AAV virus as an excellent vector for inner ear gene therapy has a good application prospect.

8. Application of Exosomes in HC Protection

Exosomes are membrane-bound nanovesicles that contain a variety of biomolecules such as lipids, proteins, and nucleic

acids. Exosomes are produced by cells through exocytosis and then taken up by target cells, which can transmit biological signals between local or distant cells [59]. Exosomes promote the interaction between HSP70 and TLR4 through intercellular communication, thereby activating non-cell-autonomous protective signaling in the inner ear and protecting HCs from aminoglycoside-induced damage [60]. Studies have found that exosome-associated AAV vectors have a higher efficiency of transducing cochlea and vestibular HCs than traditional AAV vectors [61].

9. Application of Biomaterials in HC Protection

Biomaterials are a type of artificial or natural materials that can be made alone or together with drugs for the treatment and replacement of tissues and organs and ultimately replace or repair human organs and tissues to achieve the remodeling of their physiological functions, without adversely affecting the body. The selection of biomaterials is particularly important for nerve regeneration, which requires a high biocompatibility with host tissues [62]. Researchers use the three-dimensional culture system and the regulation of various signaling pathways to cultivate pluripotent stem cells into inner ear organs containing functional HCs [63]. Compared with 2D, the 3D matrix gel culture system significantly promotes the growth of spiral ganglion explants and preserves the fine structure of spiral ganglion explants, so it can be used to simulate the three-dimensional structure of spiral ganglia under physiological conditions [64]. When therapeutic biomaterials enter the inner ear, they are restricted by the existence of biological structures and blood-brain barriers. Therefore, the construction of liposome nanoparticles or multifunctional nanoparticle-based drug delivery systems will help treat a variety of inner ear diseases [65].

10. Application of Stem Cell Therapy in Hearing Protection

Stem cell transplantation therapy uses stem cell pluripotency to restore or replace the function of spiral ganglion cells and HCs. Studies have found that bone marrow mesenchymal stem cells, embryonic stem cells (ESCs), adult inner ear stem cells, and neural stem cells can all become inner ear HC-like cells after inducing proliferation and differentiation [66]. When human pluripotent stem cell- (hPSC-) derived neurons are cocultured with rat HCs and cochlea nucleus neurons, hPSC-derived neurons are induced by inner ear HCs and cochlea nucleus neurons to form many new synapses [67]. It is known that $Lgr5^+$ and $Lgr6^+$ progenitor cells are a large number of progenitor cell groups present in the inner ear, both of which can be induced to generate HCs [68]. Although the research on inner ear stem cells has made great breakthroughs, there are still many problems waiting to be solved, such as the survival time of stem cells differentiated into cochlea sensory epithelial cells in the body and whether their physiological functions can function normally, how to deliver stem cells to the correct position, and how to avoid the body's immune rejection reaction.

11. Conclusion

The development and regeneration of HCs involve multiple factors and signaling pathways. At this stage, researchers have made many important discoveries about the protection and regeneration of HCs. With a more comprehensive understanding of the mechanism of HC regeneration, gene therapy and stem cell therapy will become important treatment options for the treatment of ear diseases in the future.

Abbreviations

HCs:	Hair cells
SCs:	Supporting cells
IHCs:	Inner HCs
OHCs:	Outer HCs
FasL:	Fas and Fas ligand
TNF- α :	Tumor necrosis factor alpha
TRAIL:	Tumor necrosis factor-related apoptosis-inducing ligand
DR:	Death receptor
JNK:	C-Jun N-terminal kinase
ROS:	Reactive oxygen species
BMP:	Bone morphogenetic protein
TGF- β :	Transforming growth factor beta
FGF:	Fibroblast growth factor
FGFR:	FGF receptor
AAV:	Adeno-associated virus
TLR4:	Toll-like receptor 4
HSP70:	Heat shock protein 70
ESCs:	Embryonic stem cells
hPSCs:	Human pluripotent stem cells.

Conflicts of Interest

The authors declare no competing financial interests.

Authors' Contributions

Yurong Mu and Hongguo Su contributed equally to this work.

References

- [1] K. F. Barald and M. W. Kelley, "From placode to polarization: new tunes in inner ear development," *Development*, vol. 131, no. 17, pp. 4119–4130, 2004.
- [2] B. Fritzsche, N. Pan, I. Jahan, and K. L. Elliott, "Inner ear development: building a spiral ganglion and an organ of Corti out of unspecified ectoderm," *Cell and Tissue Research*, vol. 361, no. 1, pp. 7–24, 2015.
- [3] M. W. Kelley, "Regulation of cell fate in the sensory epithelia of the inner ear," *Nature Reviews Neuroscience*, vol. 7, no. 11, pp. 837–849, 2006.
- [4] J. Mulvaney and A. Dabdoub, "Atoh 1, an essential transcription factor in neurogenesis and intestinal and inner ear development: function, regulation, and context dependency," *Journal of the Association for Research in Otolaryngology*, vol. 13, no. 3, pp. 281–293, 2012.

- [5] M. L. Basch, R. M. Brown II, H.-I. Jen, and A. K. Groves, "Where hearing starts: the development of the mammalian cochlea," *Journal of Anatomy*, vol. 228, no. 2, pp. 233–254, 2016.
- [6] T. Cai, M. L. Seymour, H. Zhang, F. A. Pereira, and A. K. Groves, "Conditional deletion of *Atoh1* reveals distinct critical periods for survival and function of hair cells in the organ of Corti," *The Journal of Neuroscience*, vol. 33, no. 24, pp. 10110–10122, 2013.
- [7] P. Chen, J. E. Johnson, H. Y. Zoghbi, and N. Segil, "The role of *Math 1* in inner ear development: uncoupling the establishment of the sensory primordium from hair cell fate determination," *Development*, vol. 129, no. 10, pp. 2495–2505, 2002.
- [8] M. Lavigne-Rebillard and R. Pujol, "Auditory hair cells in human fetuses: synaptogenesis and ciliogenesis," *Journal of Electron Microscopy Technique*, vol. 15, no. 2, pp. 115–122, 1990.
- [9] B. A. Nayagam, M. A. Muniak, and D. K. Ryugo, "The spiral ganglion: connecting the peripheral and central auditory systems," *Hearing Research*, vol. 278, no. 1-2, pp. 2–20, 2011.
- [10] I. N. Lavrik, "Systems biology of death receptor networks: live and let die," *Cell Death & Disease*, vol. 5, no. 5, p. e1259, 2014.
- [11] H. Li, Y. Song, Z. He et al., "Meclofenamic acid reduces reactive oxygen species accumulation and apoptosis, inhibits excessive autophagy, and protects hair cell-like HEI-OC1 cells from cisplatin-induced damage," *Frontiers in Cellular Neuroscience*, vol. 12, no. 139, 2018.
- [12] Z.-H. He, S.-Y. Zou, M. Li et al., "The nuclear transcription factor *FoxG1* affects the sensitivity of mimetic aging hair cells to inflammation by regulating autophagy pathways," *Redox Biology*, vol. 28, pp. 101364–101364, 2020.
- [13] D. Verzella, A. Pescatore, D. Capece et al., "Life, death, and autophagy in cancer: NF- κ B turns up everywhere," *Cell Death & Disease*, vol. 11, no. 3, p. 210, 2020.
- [14] Z. He, L. Guo, Y. Shu et al., "Autophagy protects auditory hair cells against neomycin-induced damage," *Autophagy*, vol. 13, no. 11, pp. 1884–1904, 2017.
- [15] D. N. Furness, "Molecular basis of hair cell loss," *Cell and Tissue Research*, vol. 361, no. 1, pp. 387–399, 2015.
- [16] L. Jansson, G. S. Kim, and A. G. Cheng, "Making sense of Wnt signaling—linking hair cell regeneration to development," *Frontiers in Cellular Neuroscience*, vol. 9, no. 66, 2015.
- [17] Y. He, D. Tang, C. Cai, R. Chai, and H. Li, "LSD1 is required for hair cell regeneration in Zebrafish," *Molecular Neurobiology*, vol. 53, no. 4, pp. 2421–2434, 2016.
- [18] C. M. Croce and G. A. Calin, "miRNAs, cancer, and stem cell division," *Cell*, vol. 122, no. 1, pp. 6–7, 2005.
- [19] S. Riccardi, S. Bergling, F. Sigoillot et al., "MiR-210 promotes sensory hair cell formation in the organ of corti," *BMC Genomics*, vol. 17, no. 1, p. 309, 2016.
- [20] M. Ebeid, P. Sripal, J. Pecka, K. W. Beisel, K. Kwan, and G. A. Soukup, "Transcriptome-wide comparison of the impact of *Atoh1* and miR-183 family on pluripotent stem cells and multipotent otic progenitor cells," *PLoS One*, vol. 12, no. 7, article e0180855, 2017.
- [21] X. Lu, Y. Shu, M. Tang, and H. Li, "Mammalian cochlear hair cell regeneration and ribbon synapse reformation," *Neural Plasticity*, vol. 2016, Article ID 2523458, 9 pages, 2016.
- [22] A. Samarajeewa, B. E. Jacques, and A. Dabdoub, "Therapeutic potential of Wnt and Notch signaling and epigenetic regulation in mammalian sensory hair cell regeneration," *Molecular Therapy*, vol. 27, no. 5, pp. 904–911, 2019.
- [23] H. Bai, L. Jiang, X. Wang et al., "Transcriptomic analysis of mouse cochleae suffering from gentamicin damage reveals the signalling pathways involved in hair cell regeneration," *Scientific Reports*, vol. 9, no. 1, article 10494, 2019.
- [24] M. Waqas, S. Zhang, Z. He, M. Tang, and R. Chai, "Role of Wnt and Notch signaling in regulating hair cell regeneration in the cochlea," *Frontiers of Medicine*, vol. 10, no. 3, pp. 237–249, 2016.
- [25] E. Savary, J. C. Sabourin, J. Santo et al., "Cochlear stem/progenitor cells from a postnatal cochlea respond to *Jagged1* and demonstrate that Notch signaling promotes sphere formation and sensory potential," *Mechanisms of Development*, vol. 125, no. 8, pp. 674–686, 2008.
- [26] R. Brown and A. K. Groves, "Hear, hear for Notch: control of cell fates in the inner ear by Notch signaling," *Biomolecules*, vol. 10, no. 3, p. 370, 2020.
- [27] R. Brooker, K. Hozumi, and J. Lewis, "Notch ligands with contrasting functions: *Jagged1* and *Delta1* in the mouse inner ear," *Development*, vol. 133, no. 7, pp. 1277–1286, 2006.
- [28] Z. Liu, T. Owen, J. Fang, and J. Zuo, "Overactivation of Notch1 signaling induces ectopic hair cells in the mouse inner ear in an age-dependent manner," *PLoS One*, vol. 7, no. 3, article e34123, 2012.
- [29] K. Mizutari, M. Fujioka, M. Hosoya et al., "Notch inhibition induces cochlear hair cell regeneration and recovery of hearing after acoustic trauma," *Neuron*, vol. 77, no. 1, pp. 58–69, 2013.
- [30] C. S. Jayasena, T. Ohyama, N. Segil, and A. K. Groves, "Notch signaling augments the canonical Wnt pathway to specify the size of the otic placode," *Development*, vol. 135, no. 13, pp. 2251–2261, 2008.
- [31] B. E. Jacques, C. Puligilla, R. M. Weichert et al., "A dual function for canonical Wnt/ β -catenin signaling in the developing mammalian cochlea," *Development*, vol. 139, no. 23, pp. 4395–4404, 2012.
- [32] E. Gómez-Orte, B. Sáenz-Narciso, S. Moreno, and J. Cabello, "Multiple functions of the noncanonical Wnt pathway," *Trends in Genetics*, vol. 29, no. 9, pp. 545–553, 2013.
- [33] W. Li, J. Wu, J. Yang et al., "Notch inhibition induces mitotically generated hair cells in mammalian cochleae via activating the Wnt pathway," *Proceedings of the National Academy of Sciences*, vol. 112, no. 1, pp. 166–171, 2015.
- [34] S.-H. Oh, R. Johnson, and D. K. Wu, "Differential expression of bone morphogenetic proteins in the developing vestibular and auditory sensory organs," *The Journal of Neuroscience*, vol. 16, no. 20, pp. 6463–6475, 1996.
- [35] J. M. Granjeiro, R. C. Oliveira, J. C. Bustos-Valenzuela, M. C. Sogayar, and R. Taga, "Bone morphogenetic proteins: from structure to clinical use," *Brazilian Journal of Medical and Biological Research*, vol. 38, no. 10, pp. 1463–1473, 2005.
- [36] G.-Q. Zhao, "Consequences of knocking out BMP signaling in the mouse," *Genesis*, vol. 35, no. 1, pp. 43–56, 2003.
- [37] M. N. Blauwkamp, L. A. Beyer, L. Kabara et al., "The role of bone morphogenetic protein 4 in inner ear development and function," *Hearing Research*, vol. 225, no. 1-2, pp. 71–79, 2007.
- [38] X. Yang, L. H. Castilla, X. Xu et al., "Angiogenesis defects and mesenchymal apoptosis in mice lacking SMAD5," *Development*, vol. 126, no. 8, pp. 1571–1580, 1999.
- [39] S. Liu, W. Li, Y. Chen, Q. Lin, Z. Wang, and H. Li, "Mouse auditory organ development required bone morphogenetic

- protein signaling," *Neuroreport*, vol. 22, no. 8, pp. 396–401, 2011.
- [40] M. Klagsbrun, "The fibroblast growth factor family: structural and biological properties," *Progress in Growth Factor Research*, vol. 1, no. 4, pp. 207–235, 1989.
- [41] R. K. Ladher, T. J. Wright, A. M. Moon, S. L. Mansour, and G. C. Schoenwolf, "FGF8 initiates inner ear induction in chick and mouse," *Genes & Development*, vol. 19, no. 5, pp. 603–613, 2005.
- [42] T. Schimmang, "Expression and functions of FGF ligands during early otic development," *The International Journal of Developmental Biology*, vol. 51, no. 6-7, pp. 473–481, 2007.
- [43] T. Hayashi, C. A. Ray, and O. Bermingham-McDonogh, "Fgf20 is required for sensory epithelial specification in the developing cochlea," *The Journal of neuroscience : the official journal of the Society for Neuroscience*, vol. 28, no. 23, pp. 5991–5999, 2008.
- [44] B. E. Jacques, A. Dabdoub, and M. W. Kelley, "Fgf signaling regulates development and transdifferentiation of hair cells and supporting cells in the basilar papilla," *Hearing Research*, vol. 289, no. 1-2, pp. 27–39, 2012.
- [45] S.-H. Huh, M. E. Warchol, and D. M. Ornitz, "Cochlear progenitor number is controlled through mesenchymal FGF receptor signaling," *eLife*, vol. 4, 2015.
- [46] M. T. Cobourne, G. M. Xavier, M. Depew et al., "Sonic hedgehog signalling inhibits palatogenesis and arrests tooth development in a mouse model of the nevoid basal cell carcinoma syndrome," *Developmental Biology*, vol. 331, no. 1, pp. 38–49, 2009.
- [47] S. Watson, C. Serrate, and S. Vignot, "Sonic Hedgehog signaling pathway: from embryology to molecular targeted therapies," *Bulletin du Cancer*, vol. 97, no. 12, pp. 1477–1483, 2010.
- [48] X. Hu, J. Huang, L. Feng, S. Fukudome, Y. Hamajima, and J. Lin, "Sonic hedgehog (SHH) promotes the differentiation of mouse cochlear neural progenitors via the Math1-Brn3.1 signaling pathway in vitro," *Journal of Neuroscience Research*, vol. 88, no. 5, pp. 927–935, 2010.
- [49] A. S. Brown and D. J. Epstein, "Otic ablation of smoothed reveals direct and indirect requirements for Hedgehog signaling in inner ear development," *Development (Cambridge, England)*, vol. 138, no. 18, pp. 3967–3976, 2011.
- [50] E. H. Waldman, A. Castillo, and A. Collazo, "Ablation studies on the developing inner ear reveal a propensity for mirror duplications," *Developmental Dynamics*, vol. 236, no. 5, pp. 1237–1248, 2007.
- [51] A. A. Eshraghi, J. Wang, E. Adil et al., "Blocking c-Jun-N-terminal kinase signaling can prevent hearing loss induced by both electrode insertion trauma and neomycin ototoxicity," *Hearing Research*, vol. 226, no. 1-2, pp. 168–177, 2007.
- [52] A. A. Eshraghi, J. He, C. H. Mou et al., "D-JNK1-1 treatment prevents the progression of hearing loss in a model of cochlear implantation trauma," *Otology & Neurotology*, vol. 27, no. 4, pp. 504–511, 2006.
- [53] H. Staecker, G. Jokovic, S. Karpishchenko et al., "Efficacy and safety of AM-111 in the treatment of acute unilateral sudden deafness-a double-blind, randomized, placebo-controlled phase 3 study," *Otology & Neurotology*, vol. 40, no. 5, pp. 584–594, 2019.
- [54] G. Lorito, S. Hatzopoulos, G. Laurell et al., "Dose-dependent protection on cisplatin-induced ototoxicity - an electrophysiological study on the effect of three antioxidants in the Sprague-Dawley rat animal model," *Medical Science Monitor*, vol. 17, no. 8, pp. BR179–BR186, 2011.
- [55] V. Villani, C. Zucchella, G. Cristalli et al., "Vitamin E neuroprotection against cisplatin ototoxicity: preliminary results from a randomized, placebo-controlled trial," *Head & Neck*, vol. 38, Supplement 1, pp. E2118–E2121, 2016.
- [56] H. So, H. Kim, Y. Kim et al., "Evidence that cisplatin-induced auditory damage is attenuated by downregulation of pro-inflammatory cytokines via Nrf2/HO-1," *Journal of the Association for Research in Otolaryngology : JARO*, vol. 9, no. 3, pp. 290–306, 2008.
- [57] Y. Liu, T. Okada, K. Shimazaki et al., "Protection against aminoglycoside-induced ototoxicity by regulated AAV vector-mediated GDNF gene transfer into the cochlea," *Molecular Therapy*, vol. 16, no. 3, pp. 474–480, 2008.
- [58] K. Isgrig, D. S. McDougald, J. Zhu, H. J. Wang, J. Bennett, and W. W. Chien, "AAV2.7m8 is a powerful viral vector for inner ear gene therapy," *Nature Communications*, vol. 10, no. 1, p. 427, 2019.
- [59] C. He, S. Zheng, Y. Luo, and B. Wang, "Exosome Theranostics: biology and translational medicine," *Theranostics*, vol. 8, no. 1, pp. 237–255, 2018.
- [60] A. M. Breglio, L. A. May, M. Barzik et al., "Exosomes mediate sensory hair cell protection in the inner ear," *The Journal of Clinical Investigation*, vol. 130, no. 5, pp. 2657–2672, 2020.
- [61] B. György, C. Sage, A. A. Indzhukulian et al., "Rescue of hearing by gene delivery to inner-ear hair cells using exosome-associated AAV," *Molecular Therapy*, vol. 25, no. 2, pp. 379–391, 2017.
- [62] G. Li, K. Chen, D. You et al., "Laminin-coated electrospun regenerated silk fibroin Mats promote neural progenitor cell proliferation, differentiation, and survival in vitro," *Frontiers in Bioengineering and Biotechnology*, vol. 7, p. 190, 2019.
- [63] K. R. Koehler, J. Nie, E. Longworth-Mills et al., "Generation of inner ear organoids containing functional hair cells from human pluripotent stem cells," *Nature Biotechnology*, vol. 35, no. 6, pp. 583–589, 2017.
- [64] G. Sun, W. Liu, Z. Fan et al., "The three-dimensional culture system with matrigel and neurotrophic factors preserves the structure and function of spiral ganglion neuron in vitro," *Neural Plasticity*, vol. 2016, Article ID 4280407, 15 pages, 2016.
- [65] M. N. Kayyali, J. R. A. Woollorton, A. J. Ramsey et al., "A novel nanoparticle delivery system for targeted therapy of noise-induced hearing loss," *Journal of Controlled Release*, vol. 279, pp. 243–250, 2018.
- [66] M. Y. Lee and Y.-H. Park, "Potential of gene and cell therapy for inner ear hair cells," *BioMed Research International*, vol. 2018, Article ID 8137614, 11 pages, 2018.
- [67] T. Hyakumura, S. McDougall, S. Finch, K. Needham, M. Dottori, and B. A. Nayagam, "Organotypic cocultures of human pluripotent stem cell derived-neurons with mammalian inner ear hair cells and cochlear nucleus slices," *Stem Cells International*, vol. 2019, Article ID 8419493, 14 pages, 2019.
- [68] Y. Zhang, L. Guo, X. Lu et al., "Characterization of Lgr6+ cells as an enriched population of hair cell progenitors compared to Lgr5+ cells for hair cell generation in the neonatal mouse cochlea," *Frontiers in Molecular Neuroscience*, vol. 11, p. 147, 2018.

Research Article

Hsp70/Bmi1-FoxO1-SOD Signaling Pathway Contributes to the Protective Effect of Sound Conditioning against Acute Acoustic Trauma in a Rat Model

Guoxia Zhu,^{1,2} Yongxiang Wu,^{1,3,4} Yang Qiu,¹ Keyong Tian ¹, Wenjuan Mi,¹ Xinqin Liu,⁵ Yuanyuan Chen,⁴ Jinwen Jia,⁶ Jiasheng Luo ², Lianjun Lu ⁷, and Jianhua Qiu ¹

¹Department of Otolaryngology-Head and Neck Surgery, Xijing Hospital, Fourth Military Medical University, Xi'an, Shaanxi, China 710032

²Department of Otolaryngology, Head and Neck Surgery, Xi'an People's Hospital/Xi'an Fourth Hospital, Xi'an, Shaanxi, China 710043

³Department of Otolaryngology-Head and Neck Surgery, Chinese PLA General Hospital, Beijing, China 100853

⁴Department of Otolaryngology-Head and Neck Surgery, General Hospital of Xinjiang Military Region, Urumchi, Xinjiang, China 830011

⁵Department of Occupational and Environmental Health, Ministry of Education Key Lab of Hazard Assessment and Control in Special Operational Environment and Shaanxi Key Laboratory of Free Radical Biology and Medicine, Fourth Military Medical University, Xi'an, Shaanxi, China 710032

⁶Department of Otolaryngology, Head and Neck Surgery, The Fifth Affiliated Hospital of Xinjing Medical University, Urumchi, Xinjiang, China 830011

⁷Department of Otolaryngology-Head and Neck Surgery, Tangdu Hospital, Fourth Military Medical University, Xi'an, China 710038

Correspondence should be addressed to Jiasheng Luo; l-js@163.com, Lianjun Lu; lujianj@fmmu.edu.cn, and Jianhua Qiu; qiujh@fmmu.edu.cn

Guoxia Zhu, Yongxiang Wu, and Yang Qiu contributed equally to this work.

Received 15 April 2020; Revised 27 July 2020; Accepted 5 August 2020; Published 5 October 2020

Academic Editor: Renjie Chai

Copyright © 2020 Guoxia Zhu et al. This is an open access article distributed under the Creative Commons Attribution License, which permits unrestricted use, distribution, and reproduction in any medium, provided the original work is properly cited.

Sound conditioning (SC) is defined as “toughening” to lower levels of sound over time, which reduces a subsequent noise-induced threshold shift. Although the protective effect of SC in mammals is generally understood, the exact mechanisms involved have not yet been elucidated. To confirm the protective effect of SC against noise exposure (NE) and the stress-related signaling pathway of its rescue, we observed target molecule changes caused by SC of low frequency prior to NE as well as histology analysis *in vivo* and verified the suggested mechanisms in SGNs *in vitro*. Further, we investigated the potential role of Hsp70 and Bmi1 in SC by targeting SOD1 and SOD2 which are regulated by the FoxO1 signaling pathway based on mitochondrial function and reactive oxygen species (ROS) levels. Finally, we sought to identify the possible molecular mechanisms associated with the beneficial effects of SC against noise-induced trauma. Data from the rat model were evaluated by western blot, immunofluorescence, and RT-PCR. The results revealed that SC upregulated Hsp70, Bmi1, FoxO1, SOD1, and SOD2 expression in spiral ganglion neurons (SGNs). Moreover, the auditory brainstem responses (ABRs) and electron microscopy revealed that SC could protect against acute acoustic trauma (AAT) based on a significant reduction of hearing impairment and visible reduction in outer hair cell loss as well as ultrastructural changes in OHCs and SGNs. Collectively, these results suggested that the contribution of Bmi1 toward decreased sensitivity to noise-induced trauma following SC was triggered by Hsp70 induction and associated with enhancement of the antioxidant system and decreased mitochondrial superoxide accumulation. This contribution of Bmi1 was achieved by direct targeting of SOD1 and SOD2, which was regulated by FoxO1. Therefore, the Hsp70/Bmi1-FoxO1-SOD signaling pathway might contribute to the protective effect of SC against AAT in a rat model.

1. Introduction

Sound conditioning (SC), known as noise-induced “toughening,” is widely defined as acoustic stimulation at a low intensity for an extended period of time prior to an elevated noise exposure (NE), which reduces the permanent threshold shift caused by a high-intensity sound. Clinically, SC has the greatest potential for treating acute acoustic trauma (AAT), as there is currently no other effective therapy. While SC has been shown to have a protective effect in most mammals, the specific mechanisms involved have not yet been explained. Currently, there are several hypotheses regarding this mechanism: (1) functional reconstruction of OHCs, (2) upregulation of heat shock proteins (Hsp), (3) upregulation of antioxidative enzymes, (4) increases in stress-dependent metabolic activity, (5) alteration of intracellular calcium concentration, (6) increases in blood flow in the cochlea, and (7) changes in lateral efferent functional activity [1, 2]. A previous study suggested that prior to a loud noise, SC (a pure tone of 500 Hz) could enhance the removal of stress-induced free radicals to protect hearing [3]. Then, another study confirmed that SC of the low frequency (a pure tone of 1 kHz) prior to a loud noise upregulated tyrosine hydroxylase in the lateral efferent to protect against acoustic trauma [4]. Furthermore, another work showed that the protective mechanism of hair cells during SC of low frequency (sound conditioning prior to a loud noise) was carried out through an increase in cellular cytoskeleton proteins and through the relief of intracellular calcium overloading caused by NE [5]. Moreover, recent research suggested that the beneficial mechanisms of SC which was prior to a loud noise initiate in the cochlea and eventually reach the central auditory system. This phenomenon might be in part related to an interplay between the calcitonin and nitric oxide signaling pathways and increases in the cytosolic calcium buffering capacity induced by SC [6]. In addition, the research by Roy et al. indicated that SC was also protective against two classes of ototoxic drugs (aminoglycosides and cisplatin) [7]. Therefore, it has been widely accepted that preconditioning to sound, especially sound conditioning of low frequency prior to a loud noise (but not sound conditioning after acoustic trauma), is a well-documented strategy to provide protection against AAT and the underlying mechanisms behind the protective effect of SC largely might refer to cochlear tissue.

Interestingly, these data lend further support to the growing body of evidence that specific gene polymorphisms may influence the susceptibility of noise-induced hearing loss, such as Rs3735715 polymorphisms in the GRHL2 gene [8], as well as Rs208679 and rs769217 polymorphisms in the Catalase (CAT) gene [9]. Furthermore, animal research has revealed that homologous animals have different threshold shifts following exposure to noise of the same intensity levels [10]. Pouyatos et al. found that OHCs in a high-frequency area were heavily injured in guinea pigs after the octave band noise (4 kHz, 110 dB, and 8 or 16 kHz at 97 dB) exposure and intervention with an antioxidant inhibitor, while the OHCs from a low-frequency area and the inner hair cells exhibited almost normal [11]. Moreover, exogenous hydrogen peroxide induced a more severe impairment to the OHCs in the

high-frequency area than in the other locations [12, 13]. However, antioxidants rescued OHCs in high-frequency areas with a small amount of glutathione, which increased their survival rate, which was generally lower than that of normal guinea pigs [14]. All of the above findings provide evidence that OHCs in high-frequency areas are vulnerable to ROS due to insufficient antioxidation [15]. Thus far, an imbalance in the redox state caused by oxidative stress has been confirmed to play a crucial role in the progress of acoustic trauma [16–18]. Conversely, it is technically and theoretically feasible to enhance the antioxidant system and increase endogenous antioxidant by sound conditioning of low frequency prior to a loud noise, while higher frequencies or even noise might result in hearing loss.

Moreover, regardless of the tissue or cell type, they have their own means of protection against stress-induced acoustic trauma. In most stress incidents such as hypoxia, oxidative stress, temperature shock, and heavy metal poisoning, Hsp70 plays a key role in maintaining protein homeostasis and the correction of protein folding to promote cell survival by directly unfolding misfolded proteins in an ATP-dependent fashion [19]. Conversely, it has been demonstrated that Bmi1, a member of the polycomb group transcription factors, has a significant role in hair cell survival by regulating the redox balance and ROS levels [20, 21]. However, it is still unknown whether both Hsp70 and Bmi1 are genuinely involved in the protective effect of SC against AAT or not.

Therefore, based on the ROS-induced acoustic trauma caused by NE and SC of low frequency prior to a loud noise, the purpose of our study was to investigate the protective effect of SC against AAT and to confirm the stress-related signaling pathway of its rescue. Given the integrity of auditory pathways and the importance of afferent nerves, we specifically focused on both the organ of Corti and the SGNs. Here, we found that SC of low frequency not only protected against AAT based on significant improvements in hearing threshold and an apparent reduction in OHC loss but also improved SGN survival following noise-induced stress response via the increasing amount of mitochondria, regulating mitochondrial function and decreasing ROS levels in rat SGNs, and we first have demonstrated a new theory on the protection of SC against AAT in which upregulation of Hsp70, Bmi1, FoxO1, SOD is involved. Lastly, we suggested that the Hsp70/Bmi1-FoxO1-SOD signaling pathway might contribute to the enhancement of the antioxidant system and a reduction in ROS accumulation for the decreased sensitivity to noise-induced trauma after treatment with SC. Our study was exploratory, and these results from our work could help us easily understand how to protect against AAT by SC and its underlying mechanisms; clinically, these issues will provide a better preventive strategy for AAT.

2. Materials and Methods

2.1. Animals and Exposure. In this study, 108 healthy adult male Sprague-Dawley rats weighing 200–300 g with a normal Preyer’s reflex were provided by the Laboratory Animal Center of the Fourth Military Medical University. The inclusion and exclusion criteria were predetermined that all the

animals in this study should have a good hearing without hearing loss caused by tympanitis, drug, noise, genetic problem, and so on. All rats had been raised with sufficient food and water in a tranquil animal cage (the plastic box with railing cover) for 5 days prior to the test (the sound levels were 20-30 dB in each cage in which every four rats were housed).

They were randomly divided into the control group (Ctrl), sound conditioning group (SC), noise exposure group (NE), and sound conditioning plus noise exposure group (SC+NE) by the simple randomization, and the initial number of animals used per group was twenty-seven (Table of random number was used in our study. Each rat had its own number based on its weight which ranged from 1 to 108. Then, every rat was given a random three-digit sequence generated by the random number generator (table of random number) in sequence. Next, these random three-digit sequences which had been assigned to rats were arranged in descending order. Finally, the top 27 rats were matched with Ctrl, the next 27 rats were matched with SC, the last 27 rats were matched with SC+NE, and the rest were matched with NE.). Six animals were excluded based on the exclusion criteria (tympanitis) or died during experiments. One rat in Ctrl, two rats in NE, and three rats in SC+NE were replaced before killing of animals. To minimize animal suffering, an intraperitoneal (i.p.) injection of pentobarbital sodium (30 mg/kg) was used during experiments. The NE group was exposed to white noise at 115 dB SPL for 6 hours per day over two consecutive days with anesthesia to lower stress hormones which might affect the results of the study; in the SC group, all of the animals were exposed to a pure tone of 1 kHz at 85 dB SPL for 24 hours based on Niu and Canlon's study protocol [4]; the Ctrl group was given a sham exposure; the animals in the SC+NE group were exposed to SC before NE and were allowed to rest for 3 hours between SC and NE with anesthesia. The exposure protocol has been described in previous publications from our department [22, 23] (Figure 1(a)). Briefly, exposure was conducted in a ventilated soundproof cabinet where the animals had ad libitum access to food and water except for the rats anesthetized for the noise exposure. A Radio Shack Super Tweeter (Tandy Corp, FT Worth, USA), which was located above the cages, generated a noise (white noise, 115 dB SPL) and a pure tone (1 kHz at 85 dB SPL) that was then amplified by a power amplifier (Yamaha, Japan) and delivered to a loudspeaker. The homogeneity of the sound field was confirmed by a sound level meter (Bruel and Kjaer, China) that was secured within the cabinet.

2.2. Auditory Brainstem Response (ABR) Measurement. ABRs to both the click stimuli and the pure tone frequencies in the soundproof chamber on the day before exposure and at approximately 24 hours after the last exposure were available to evaluate hearing alterations in the SD rats in the Ctrl, SC, NE, and SC+NE groups. The ABR experimenter was unaware of the animal's group during ABR measurement. Each animal was gently anesthetized with an intraperitoneal (i.p.) injection of pentobarbital sodium (30 mg/kg) and then was placed on an electric heating plate (37.1–37.5°C) to maintain body temperature. The reference electrode was

placed beneath the pinna of the test ear, with the ground electrode placed beneath the apex of the nose, and the active electrode was placed beneath the skin on the top of the head. All of the electrodes were subcutaneously placed at each site within 5 min of the administration of anesthesia. The ABR test started immediately after the needle electrode implantation. Each test ear received the stimulus signal at a repeating rate of 10/s generated through Intelligent Hearing Systems (Bio-Logic Systems, USA), and the stimulus signal was delivered through earphones with a 10 min interval between left and right ears. The signal intensity was decreased gradually by a 5 dB step until the visually discernible ABR waveform disappeared. The lowest sound level that caused this waveform was defined as the "threshold." Five repetitions of each threshold were presented. The waves were amplified ten times by Intelligent Hearing Systems. The highest sound level was less than 90 dB to avoid drastic acoustic trauma [23, 24].

2.3. Scanning Electron Microscopy (SEM) and Transmission Electron Microscopy (TEM). Cochlear sensory epithelia surface preparation and OHC count in animals from the Ctrl, SC, NE, and SC+NE groups (each group: $n=6$ from 3 animals) were carried out as described in a previous study from our department. Briefly, following ABR measurement, deeply anesthetized animals from each group were decapitated on the first day after exposure. The cochleae were removed immediately and gently perfused with 2.5% phosphate-buffered glutaraldehyde (pH 7.4) through the open round window and the cochlear apex. The cochleae remained in the same solution overnight. The bony capsule was removed after washing with 0.1 M phosphate-buffered saline (PBS). The spiral ligament and stria vascularis were removed under a dissecting microscope, and the Reissner's membrane was separated. The dissected specimens were rinsed with 0.1 M PBS, then postfixed in 1% osmium tetroxide for 2 hours, and incubated in 2% tannic acid twice for 30 min. The cochleae were dehydrated in a series of graded ethanol solutions and dried in a critical point dryer (Hitachi, Japan). The specimens were fixed on a metal stage, gold-coated in a sputter coater (Ion Sputter, Hitachi, Japan), and observed under SEM (Hitachi, Japan). The experimenter was unaware of the animal's group during the experimentation of OHC count. OHCs were counted by hand using five consecutive images from each slide. The principle of counting is such that if an OHC is not completely contained within the image, the cell was counted only if found at the top or left edge of the image. The missing hair cells and stereocilia were quantified along the entire basilar membrane. The percentage of missing OHCs in each row was calculated and compared among the four groups [22, 23]. In addition, the apex turn of the basilar membrane was considered as the low-frequency area of 0 to 30 percent distance from the apex for the cochlea; the middle turn was the middle-frequency area of 30 to 60 percent distance from the apex, and the base turn was the high-frequency area of 60 to 100 percent distance from the apex. Scale in Figure 2(c) showed frequency and percent distance from the apex for rat cochlea according to Muller's study [25].

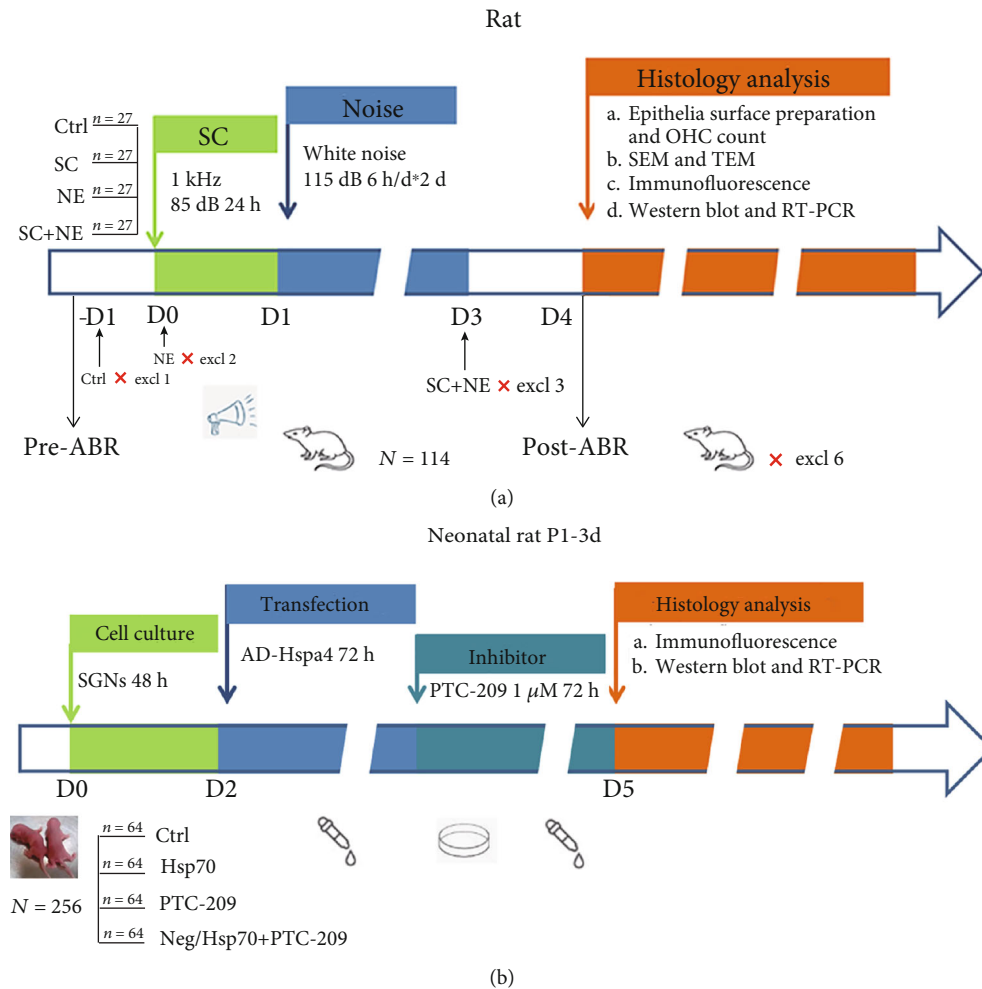


FIGURE 1: Chronogram of the experiment in vivo (a) and in vitro (b). (a) 114 rats were available in the experiment in vivo, but there were six animals that were excluded based on the exclusion criteria (tympatitis) or died during experiments. Rats were exposed to a pure tone of 1 kHz at 85 dB SPL (SC) for 24 hours; then, some of them and others were exposed to white noise at 115 dB SPL (NE) for 6 hours per day over two consecutive days with anesthesia; they were allowed to rest for 3 hours between SC and NE with anesthesia. Hearing was evaluated with auditory brainstem responses (ABRs) before 1 day prior to exposure and 1 day after exposure. At the end of the study in vivo, cochleae were dissected and processed for histology analysis. (b) The spiral ganglion neuron cells (SGNs) from 256 neonatal rats were harvested and then cultured on culture dishes for 48 h; next, AD-Hspa4 (Hsp70-overexpressing adenovirus) and 1 μM PTC-209 (a small-molecule inhibitor of Bmi1) were, respectively, added to the appropriate cells and incubated for 72 hours at 37°C. At the end of the study in vitro, SGNs were processed for histology analysis.

Deeply anesthetized animals from each group were perfused transcardially with 0.9% saline followed by a fixative solution of 2.5% glutaraldehyde and 4% paraformaldehyde in 0.1 M PBS (pH 7.4) immediately after the ABR measurements. The cochleae were removed immediately, maintained in the same solution at 4°C for at least 24 hours, and decalcified with 10% EDTA at 23°C for two weeks. Following washing with 0.1 M PBS, the cochleae were divided into small blocks of approximately 1 mm³ in size under a dissecting microscope (Olympus, Japan), then fixed with 1% osmic acid for 2 hours, gradually dehydrated in gradient acetone, and embedded in Epon812 for polymerization. Next, the sample blocks were sectioned at a 10 μm thickness and stained with Evans blue to visualize the spiral ganglion. Following visualization, ultrathin 70 nm thick sections were prepared and stained with uranyl acetate and lead citrate following a conventional protocol.

Finally, the ultrathin sections were observed under TEM (JEM, Japan) to reveal the ultrastructure of SGNs in the cochlea. The experimenter of electron microscopy was unaware of the animal's group during the experimentation of observation.

2.4. Western Blot. Twelve deeply anesthetized rats from each group were sacrificed immediately after the last ABR measurement by decapitation on ice, and the modiolus tissues (or SGN cells *in vitro*) from the same group were harvested, pooled, and stored at -80°C until use. The pooled tissues were lysed in sample buffer containing 1x Tris-EDTA, NaCl (100 mM), 1% Triton X-100, and 1x protease inhibitors. Following mechanical lysis and protein extraction, protein concentration was determined by using a BCA assay kit (Millipore, catalog number BCA1-1KT). Equal amounts

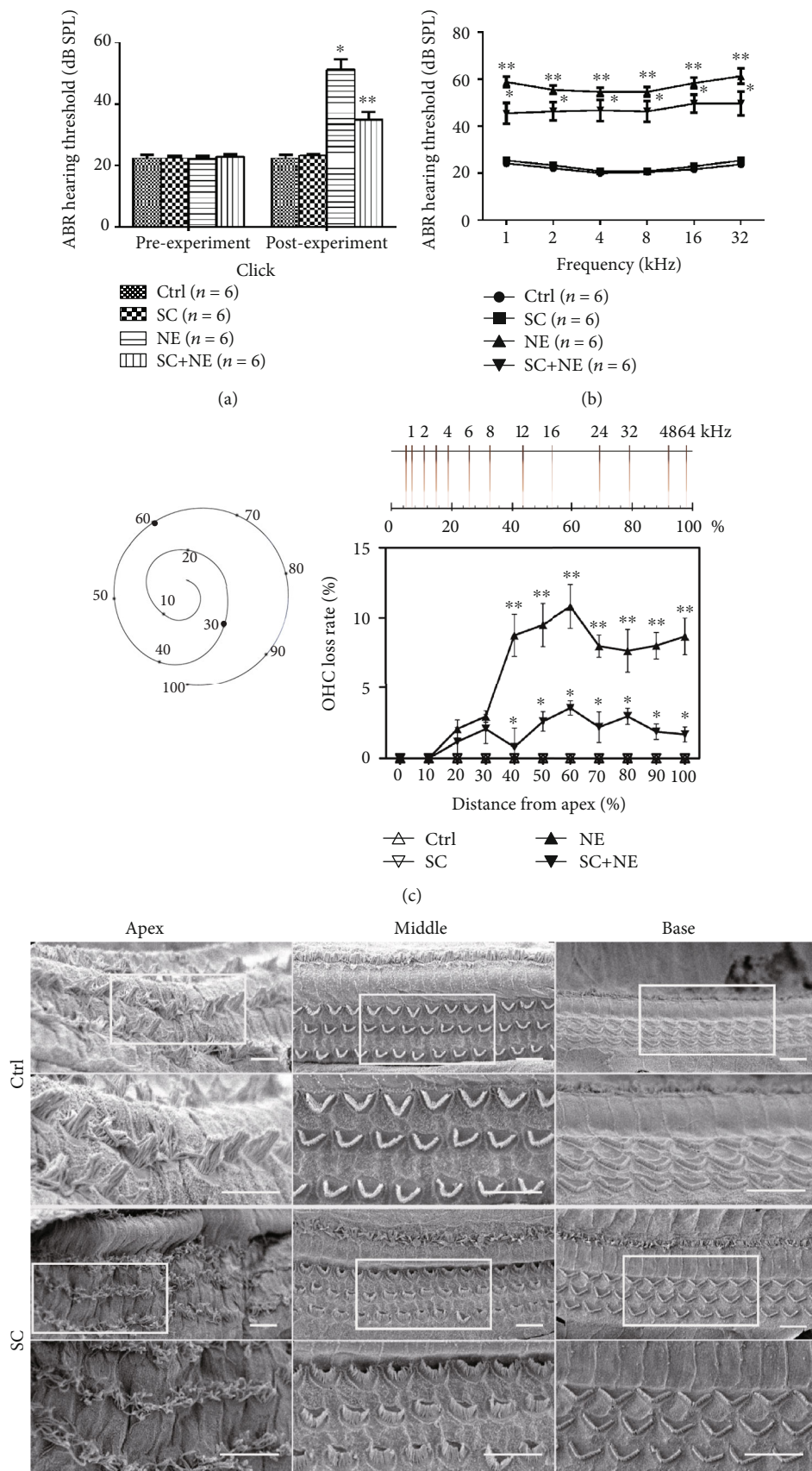


FIGURE 2: Continued.

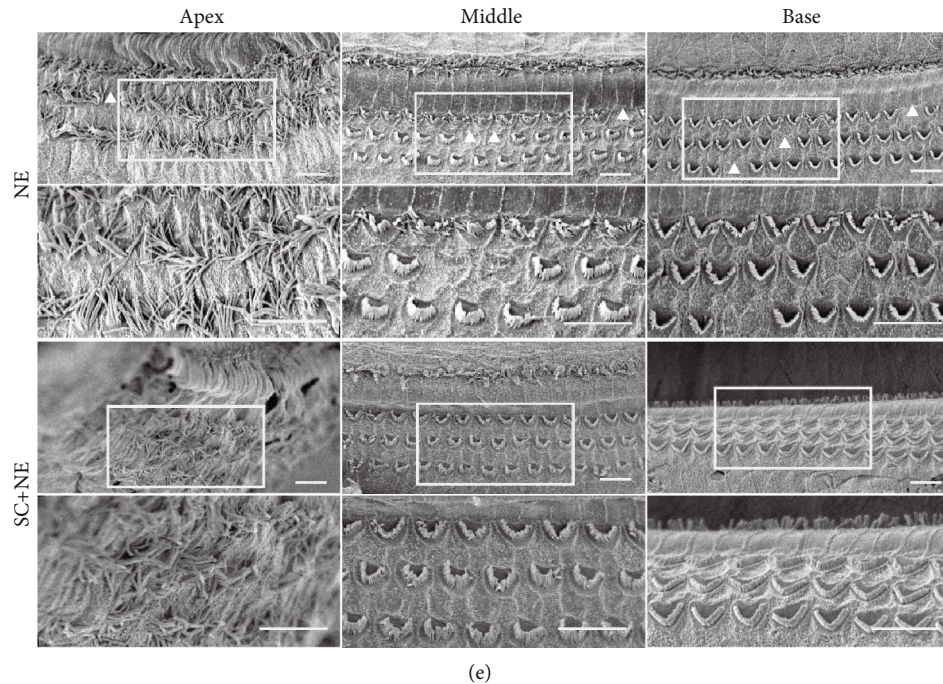


FIGURE 2: ABR click and tone and basilar membrane and OHC loss. (a) Hearing thresholds of click sound from four groups before and after noise exposure (NE vs. Ctrl: $*P < 0.01$, SC+NE vs. NE: $**P < 0.01$; mean \pm SEM, $n = 6$ animals/group). (b) Hearing thresholds of pure tone from four groups after noise exposure (NE vs. Ctrl: $*P < 0.05$, SC+NE vs. NE: $**P < 0.01$; mean \pm SEM, $n = 6$ animals/group). Ctrl: control group; SC: sound conditioning group which was exposed to a pure tone of 1 kHz at 85 dB SPL for 24 hours; NE: noise exposure group which was exposed to white noise at 115 dB SPL for 6 hours per day over 2 consecutive days; SC+NE: sound conditioning and noise exposure group which was exposed to a pure tone of 1 kHz at 85 dB SPL for 24 hours, and then 3 hours later, followed by white noise at 115 dB SPL for 6 hours per day over 2 consecutive days. Scanning electron micrographs for OHCs in different turns of basilar membrane from the Ctrl and SC groups (d) as well as the NE and SC+NE groups (e). The lower row pictures are the upper row ones at high magnification. White frames show the enlarged areas; triangular arrows indicate OHC loss. Scale bars represent $10 \mu\text{m}$. Percentage of OHC loss in different turns from four groups presented in (c) was analyzed with Tukey's multiple comparisons test (Base_{NE} vs. SC+NE: $*P < 0.05$, Middle_{NE} vs. SC+NE: $**P < 0.05$; mean \pm SD, $n = 6$ pictures from 3 animals/group). Scale is showing frequency and percent distance from the apex for rat cochlea according to Muller (1991). The apex turn of the basilar membrane was considered as the low-frequency area of 0 to 30 percent distance from the apex for the cochlea; the middle turn was the middle-frequency area of 30 to 60 percent distance from the apex, and the base turn was the high-frequency area of 60 to 100 percent distance from the apex.

(approximately 100 ng/lane) of protein were loaded on 12% sodium dodecyl sulfate-polyacrylamide gels (SDS-PAGE) (Bio-Rad, catalog number 1610173) (120 V for 80 min at room temperature), electrophoresed, and transferred to PVDF membranes (Sigma-Aldrich, catalog number GE10600122) by electroblotting (200 mA for 40 min at 4°C) in 1x transfer buffer (Sigma-Aldrich, catalog number PCG3011). After being blocked in 5% nonfat dry milk and 0.1% Tween-20 in PBS (pH 7.4, 0.01 M) (Sigma-Aldrich, catalog number 9005-64-5) for 1 hour at 25°C , the membranes were incubated overnight at 4°C with different primary antibodies (rabbit anti-FoxO1 polyclonal antibody, 1:1000, Cell Signal, catalog number 2880; rabbit anti-Hsp70 polyclonal antibody, 1:1000, Abcam, catalog number ab79852; rabbit anti-Bmi1 polyclonal antibody, 1:1000, Abcam, catalog number ab38295; rabbit anti-SOD1 polyclonal antibody, 1:1000, Proteintech, catalog number 10269-1-AP; or rabbit anti-SOD2 polyclonal antibody, 1:1000, GeneTex, catalog number GTX116093). The membranes were then incubated with an HRP-conjugated secondary antibody (goat anti-rabbit antibody, Bioworld, catalog number BS13278) for 1 hour at room temperature. Equal protein loading was confirmed by stripping the blots

and reprobng them with a polyclonal rabbit anti- β -actin antibody (1:1000, GeneTex, catalog number GTX109639) followed by incubation with the same HRP-conjugated secondary antibody. The protein bands were detected by using a chemiluminescence detection technique (FluorChem, Alpha Innotech, USA), and the gray density of the detected bands was analyzed with NIH ImageJ software. The experimenter of western blot was unaware of the animal's group during the experimentation.

2.5. Reverse Transcription and Quantitative Real-Time PCR (Quantitative RT-PCR). This assay was used to detect mRNA expression levels of Hsp70, Bmi1, SOD1, and SOD2 in the rat spiral ganglion cells from the four groups. Total RNA was isolated by TRIzol reagent (Life Technologies Corporation, catalog number 15596026) according to the manufacturer's instructions. Reverse transcription was performed with a First Strand cDNA Synthesis Kit (GeneCopoeia, catalog number AORT-0020) according to the manufacturer's instructions. Quantitative RT-PCR was performed with an All-in-One qPCR Mix (GeneCopoeia, catalog number QP001). Quantitative RT-PCR primers for Hsp70 (RQP051424), Bmi1

TABLE 1: Primers used for quantitative RT-PCR.

Gene	Lot No.	Primer ID	Amplicon size	GenBank accession number	Annealing temperature
Hsp70	RQP051424	Rn-QRP-10166	133	NM_031971.2	60°C
Bmi1	RQP083017	Rn-QRP-10984	119	NM_001107368.2	60°C
SOD1	RQP049577	Rn-QRP-10681	128	NM_017050.1	60°C
SOD2	RQP049578	Rn-QRP-10168	91	NM_017051.2	60°C
β -Actin	RQP051050	Rn-QRP-10046	98	NM_031144.2	60°C

(RQP083017), SOD1 (RQP049577), SOD2 (RQP049578), and β -actin (RQP051050) were purchased from GeneCopoeia (GeneCopoeia, China). The forward and reverse primers of each PCR set, the sizes of PCR products, GenBank accession numbers, primer IDs, and annealing temperatures are presented in Table 1. RT-PCR was performed for forty cycles with the following parameters: 10 min at 95°C for predenaturation, and in each cycle, 10 s at 95°C for denaturing, 30 s at 60°C for annealing, and 15 s at 72°C for extending (Bio-Rad, USA). All quantitative RT-PCR analyses were conducted with the CFX Manager 3.0 (Bio-Rad, USA). Expression levels of Hsp70 and other genes were normalized to that of β -actin by the delta Ct value. The experimenter of PCR was unaware of the animal's group during the experimentation.

2.6. Immunofluorescence. Rats from each group were perfused transcardially with freshly prepared 4% paraformaldehyde in 0.1 M PBS (pH 7.4) under deep anesthesia with pentobarbital sodium (60 mg/kg) after ABR measurements. The cochleae were postfixed with the same fixative at 4°C for at least 24 hours, decalcified with 10% EDTA at 23°C for 1 week, dehydrated in 30% sucrose for 24 hours, embedded in OCT glue (SAKURA, catalog number 4583), and sectioned at a 10 μ m thickness in the midmodiolus plane on a cryostat (Leica, Germany). The sections were soaked with 0.3% hydrogen peroxide in methanol for 10 min to inactivate endogenous peroxidase and blocked with goat serum (Abcam, catalog number ab7481) at 37°C for 30 min. Then, they were incubated with rabbit anti-Hsp70 polyclonal antibody (1:100, Abcam), rabbit anti-Bmi1 polyclonal antibody (1:100, Abcam), rabbit anti-FoxO1 monoclonal antibody (1:100, Cell Signal), rabbit anti-SOD1 polyclonal antibody (1:100, Proteintech) or rabbit anti-SOD2 polyclonal antibody (1:100, GeneTex), MitoSOX™ Red mitochondrial superoxide indicator for live-cell imaging (5 μ M, Invitrogen, catalog number M36008), and mouse anti-tubulin monoclonal antibody (1:100, Abcam, catalog number ab7751) at 4°C overnight. Primary antibodies were omitted from the negative controls for these antibodies. Then, sections were incubated with Alexa Fluor 488 Donkey anti-Mouse IgG Highly Cross-Adsorbed Secondary Antibody (1:200, Life Technologies, catalog number A-21202) or Alexa Fluor 647 Donkey anti-Mouse IgG Highly Cross-Adsorbed Secondary Antibody (1:200, Life Technologies, catalog number A-31571) and Alexa Fluor 594 goat anti-rabbit IgG Highly Cross-Adsorbed Secondary Antibody (1:200, Life Technologies, catalog number A-11012) at 37°C for 30 min, followed by staining with DAPI or Hoechst 33258 (1:1000, Boster, catalog number

AR1176 or catalog number AR1169) at 37°C for 10 min. Three washes in 0.01 M PBS were carried out in the intervals of each step above. Next, the sections were mounted on collagen-coated glass slides and visualized under a fluorescence microscope (Olympus, Japan), while the quantity of target protein expression was analyzed by fluorescence intensity. The experimenter of the fluorescence microscope was unaware of the animal's group during the experimentation of observation.

2.7. Cell Culture and Transfection. In this study, 256 healthy neonatal Sprague-Dawley rats (P1-3d) were used for cell culture. Before the experiment starts, cell culture preparation including sterilization and disinfection of cell culture room and operations area and disinfection of work clothes, aseptic mask, sterile gloves, and operating instruments should be strictly implemented, and animals should also be disinfected in time before they are killed quickly. The disinfected animals were sacrificed immediately by decapitation on ice with anesthesia in the disinfected operation room. Then, the modiolus tissues (SGNs) from the killed animals' cochleae were dissected, harvested, and pooled on ice under the stereomicroscope (Leica, Germany) in a super clean bench. After treatment with 0.125% collagenase IV (Thermo Fisher Scientific, catalog number 17104019) and 0.25% trypsinase (Thermo Fisher Scientific, catalog number 25200-056), the spiral ganglion neuron cells (SGNs) from 20 newborn rats per time were cultured on culture dishes in SGN culture medium Dulbecco's modified Eagle's medium with 2% B27 (Thermo Fisher Scientific, catalog number 17504-044), 10 μ g/ml brain-derived neurotrophic factor (BDNF, PeproTech, catalog number 450-02), and 1% penicillin-streptomycin solution (100,000 U/l, HyClone, catalog number SV30010) [26, 27]. Then, the SGNs were cultured at 37°C in a humidified incubator (Thermo Scientific, USA) with 5% CO₂ for 5 days, and the medium was refreshed every 2-3 days. Following a 48-hour incubation, the culture dish of SGNs was divided into four dishes for different interventions, to which 1 μ M PTC-209 (a specific inhibitor of Bmi1 with an IC50 value of 0.5 μ M, Selleckchem, CAS No. 315704-66-6, catalog number S7372), AD-Hspa4 (2E + 10 PFU/ml, 17999-1, GeneChem, China), AD-CON177 (3E + 10 PFU/ml, CMV-MCS-3FLAG-SV40-EGFP, GeneChem, China), and enhanced infection solution (GeneChem, China) were added to the appropriate cells and incubated for 72 hours at 37°C. Finally, we observed and disposed of the SGNs from the different procedures [28] (Figure 1(b)). The experimenter of cell culture was unaware of the animal's group during the experimentation of observation.

2.8. Statistical Analysis. Experiments were replicated a minimum of three times. The group size (n) in vivo was determined by the variability of measurements and the magnitude of the differences between groups. Based on our previous as well as current preliminary studies and sample size calculation (Type I error probability α , type II error probability β , permissible error δ , and standard deviation S were used to estimate effect size, when the formula of the sample size required for comparison of means of two samples was performed ($n_1 = n_2 = 2[\sigma(u_\alpha + u_\beta)/u]^2 + u_\alpha^2/4$), we determined that six animals per group provide sufficient statistical power (While double-tailed α was 0.05 and single-tailed β was 0.1 in our study, $u_{\alpha/2}$ was 1.96 and u_β was 1.282. According to our protocol, standard deviation S equaled to σ was 2.4 and permissible error δ was 5. Finally, the number of animals per group was 5.80 based on the formula of sample size calculation.). Data are presented as means \pm SD (standard deviations) or means \pm SEM (standard error of mean). The assessment (Q-Q plot) of the normality of data was carried out by SPSS version 17.0 software package (SPSS Inc., Chicago, Ill.). The test (linear regression model) for outliers was conducted on the data by SPSS Data Validation, and no data point was excluded. Two-way analysis of variance was used for comparisons among the different groups that were impacted by two factors, and comparisons with more than two groups were performed with one-way analysis of variance (ANOVA). Further tests included the Student-Newman-Keuls- (SNK-) q test for post hoc comparisons or Tukey's multiple comparisons test using GraphPad Prism 5. Statistical analysis of the comparisons between the two groups was accomplished by Student's t -test. All tests were two-tailed, and differences were considered to be statistically significant at $P < 0.05$. The experimenters were unaware of the animal's group during experimentation and statistical analysis. Furthermore, the analysis or experimental group assignment was performed by a different person than the experimenter, while all rats were randomly divided into the groups by a simple randomization protocol described in the following. Thus, blinding was achieved in our study.

2.9. Compliance with Ethical Standards. All procedures concerning animals in this study were approved by the Institutional Animal Care and Use Committee of the Fourth Military Medical University (Permit number, SYXK 2008-005) and were in compliance with the Guide for the Care and Use of Laboratory Animals.

3. Results

3.1. SC Protection against Hearing Loss Caused by Acute Noise Exposure. ABR click and tone burst profiles were successfully obtained from rats in each group one day before and after exposure. One-way ANOVA can detect significant changes in hearing function (Figure 2(a)). There was a significant group difference found in postthreshold ($F = 38.96$, $P < 0.0001$) among the four groups. In particular, SNK- q tests revealed that there was a significant difference found in the postthreshold between the NE and Ctrl groups ($q = 13.37$, $*P < 0.01$) and between the NE and SC+NE groups ($q = 7.56$,

$**P < 0.01$). However, no significant difference was found between the SC and Ctrl groups ($q = 0.39$, $P > 0.01$).

The ABR hearing threshold for pure tone frequencies was calculated via two-way ANOVA to detect significant changes in the hearing function (Figure 2(b)). Notably, there was a significant group difference ($F = 302.20$, $P < 0.0001$) found among three of the groups (the NE, SC+NE, and Ctrl groups). SNK- q tests also showed that there was a significant difference found in the postthreshold between the NE and Ctrl groups ($q = 76.28$, $**P < 0.001$) and between the NE and SC+NE groups ($q = 15.88$, $*P < 0.001$). However, no significant difference was found between the SC and Ctrl groups ($q = 8.944$, $P > 0.001$). All of these data supported our concept that SC protected against AAT but did not result in hearing impairment on fully mature rats.

3.2. Effects of SC and Acute Noise Exposure on Hair Cell Structure. Scanning electron microscopy (SEM) revealed different effects of SC and acute noise exposure on the basilar membrane structure. The results showed that the stereocilia were well organized in "V" or "W" shapes in the Ctrl group. Furthermore, SC resulted in the functional reconstruction of OHCs which included shortening and thickening of the cilia except for misalignment and loosening of the outer hairs in the apex turn of the basilar membrane, while acute noise exposure leads to OHC loss, lodging, fusion, and disappearance of cilia (Figures 2(d) and 2(e)).

Moreover, we analyzed the proportion of OHC loss among the different groups from the base to the apex turns (Figure 2(c)). Tukey's multiple comparisons test revealed that there was a noticeable hair cell loss in both the base and middle turns of the basilar membrane in the NE group compared with the Ctrl group ($F = 235.5$ (column factor: treatment), $P < 0.0001$; $q_B = 23.92$, $*P < 0.05$; $q_M = 28.68$, $*P < 0.05$), while no significant differences were found between these two groups in the apex turn of the basilar membrane ($q_A = 3.70$, $P > 0.05$). This finding suggested that acute noise exposure could clearly result in OHC loss in both the base and middle turns but not the apex turn of the basilar membrane. Furthermore, compared with the NE group, less hair cell loss in both the base and middle turns of the basilar membrane was found in the SC+NE group along with shortening and thickening of the cilia, while misalignment and loosening of the outer hairs in the apex turn of the basilar membrane were not improved ($q_{B'} = 17.40$, $**P < 0.05$; $q_{M'} = 21.82$, $**P < 0.05$). However, this group exhibited no obvious hair cell loss in the apex turn of the basilar membrane with the same reconstruction of OHCs ($q_{A'} = 1.31$, $P > 0.05$). This result suggested that SC could protect against OHC loss caused by NE in both the base and middle turns of the basilar membrane on fully mature rats.

3.3. Ultrastructural Changes in SGNs Caused by SC and Acute Noise Exposure. Transmission electron microscopy (TEM) revealed ultrastructural changes in SGNs caused by SC and acute noise exposure on fully mature rats. SC increased the number of mitochondria in the SGNs, enhanced the electron density of the mitochondria in SGNs, and narrowed the interspace of the mitochondrial matrix. Conversely, NE

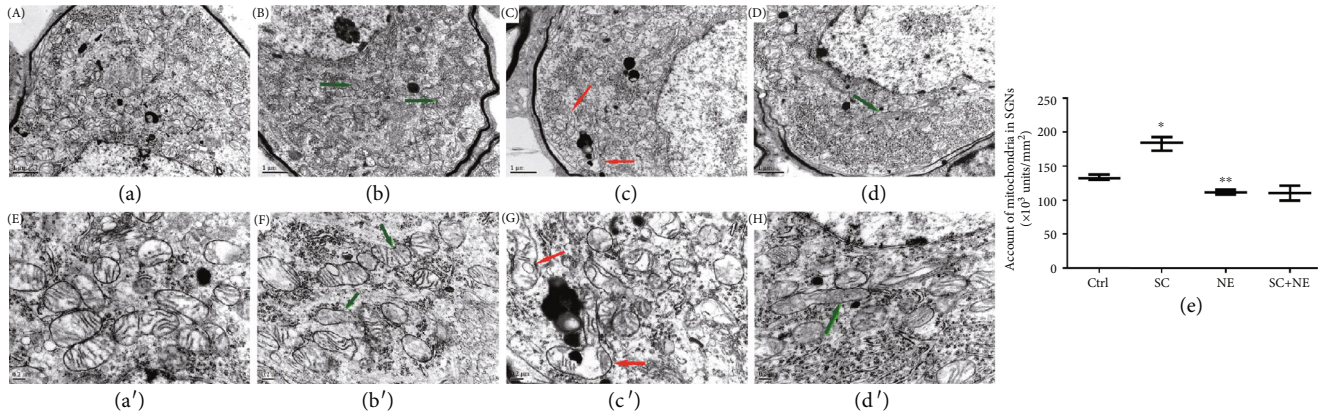


FIGURE 3: Ultrastructural changes of spiral ganglion neuron. Electron transmission micrographs for SGNs in the control group (a/a'), sound conditioning group (b/b'), noise exposure group (c/c'), and sound conditioning and noise exposure group (d/d'). Green arrows showed that sound conditioning could enhance the electron density in the mitochondrion of spiral ganglion neuron cells and narrow the interspace of the mitochondrion. Red arrows indicated that noise exposure could result in the destruction of the mitochondrion in SGNs, the lower electron density, larger interspace, and the formation of the vacuole in the mitochondrion. Scale bars represent $1 \mu\text{m}$ and $0.2 \mu\text{m}$. The account of a mitochondrion in spiral ganglion neuron cell of SD rat presented in (e) was analyzed with one-way ANOVA ($F = 55.17$; $P < 0.0001$), followed by Newman-Keuls' post hoc test ($\times 10^3$ units/ mm^2 , $n = 6$ pictures from 3 animals/group, mean \pm SD; Ctrl vs. NE: ** $P < 0.05$, SC vs. Ctrl: * $P < 0.05$).

resulted in the shrinkage of SGNs, decreased the numbers of mitochondria in the SGNs, lowered electron density, and enlarged the interspace between the mitochondrial matrix and the formation of vacuoles in the mitochondria (Figure 3).

We calculated the number of mitochondria in the SGNs of fully mature rats and analyzed their density by the SNK- q test. It showed that the densities of mitochondria were significantly different between the NE and Ctrl groups ($q = 4.78$, ** $P < 0.05$) and between the SC and Ctrl groups ($q = 10.86$, * $P < 0.05$) (Figure 3(e)). This result indicated that SC increased the quantity of mitochondria while NE reduced it. But there was no difference between the account of mitochondria in the SC+NE and NE groups shown in Figure 3(e) ($q = 0.23$, $P > 0.05$). It means that NE nullified the protection of mitochondria by SC and SC could largely enhance the density of mitochondria to protect against NE-induced trauma instead of increasing the quantity of mitochondria.

3.4. Effects of SC and Acute Noise Exposure on Hsp70, Bmi1, SOD1, SOD2, and FoxO1 Expression Levels in the Rat Spiral Ganglion Cells. The IF results revealed that NE lowered Hsp70, Bmi1, FoxO1, SOD1, and SOD2 fluorescence levels in SGNs of a fully mature rat, while SC increased Hsp70, Bmi1, FoxO1, SOD1, and SOD2 fluorescence levels in SGNs (Supplementary Table 1). The WB results of decline at the protein level of Hsp70, Bmi1, SOD1, and SOD2 expressions were found in the NE group, while increased expression of Hsp70, Bmi1, SOD1, and SOD2 expression was found in the SC group (Figures 4(a), 5, and 6 and Supplementary Table 2). In addition, the IF results also revealed that NE lowered Hsp70, Bmi1, SOD1, and SOD2 fluorescence levels in both hair cells and cochlear lateral wall of a fully mature rat, while SC increased Hsp70, Bmi1, SOD1, and SOD2 fluorescence levels in these two regions (Supplementary Figure 3 and 4 and Supplementary Table 1).

Furthermore, the results indicated that SC reversed the downregulation of Hsp70, Bmi1, FoxO1, SOD1, and SOD2 expression caused by NE in SGNs of a fully mature rat. Moreover, RT-PCR exhibited that Hsp70, Bmi1, SOD1, and SOD2 mRNA expression was increased in the SGNs of the SC group compared with that of the Ctrl group (* $P < 0.05$; $n = 6$) (Figure 4(b)).

3.5. Overexpression of Hsp70 Significantly Enhanced Bmi1, SOD1, SOD2, and FoxO1 Expression in Rat SGNs and Decreased ROS Accumulation In Vitro. Analysis of the neuronal cells on neonatal cultures expressing a green fluorescent protein (GFP) coded in the same vector as the Hsp70-overexpressing vector was coupled to the GFP sequence, which indicated that $66.7\% \pm 7.8\%$ ($n = 4$ independent cell culture preparations) of the neuronal cells present in the cultures were transfected with Hsp70. After the transfection of SGNs with Hsp70-overexpressing adenovirus *in vitro*, IF results (Figures 7(a)–7(d)/7(a')–7(d') and Supplementary Table 1) revealed that ratios of Bmi1, SOD1, SOD2, and FoxO1 fluorescence levels were all increased in the SGNs of neonatal culture compared with the negative control.

Following transfection of the SGNs with Hsp70 overexpressing the adenovirus on neonatal cultures *in vitro*, WB results (Figure 7(e)/7(e') and Supplementary Table 2) also revealed that similar results were found at the protein level of Hsp70, Bmi1, FoxO1, SOD1, and SOD2 expression. There were clearly significant differences between the Hsp70-overexpressing adenovirus and negative control groups ($F = 3400.31$, ** $P < 0.05$). Moreover, RT-PCR revealed that Hsp70, SOD1, and SOD2 mRNA expression increases in the SGNs of neonatal culture except for Bmi1 mRNA expression (Figure 8(f) and Supplementary Figure 2).

In addition, there was a significant difference between the Hsp70-overexpressing adenovirus and negative control groups in ROS accumulation labeled by MitoSOX Red (a

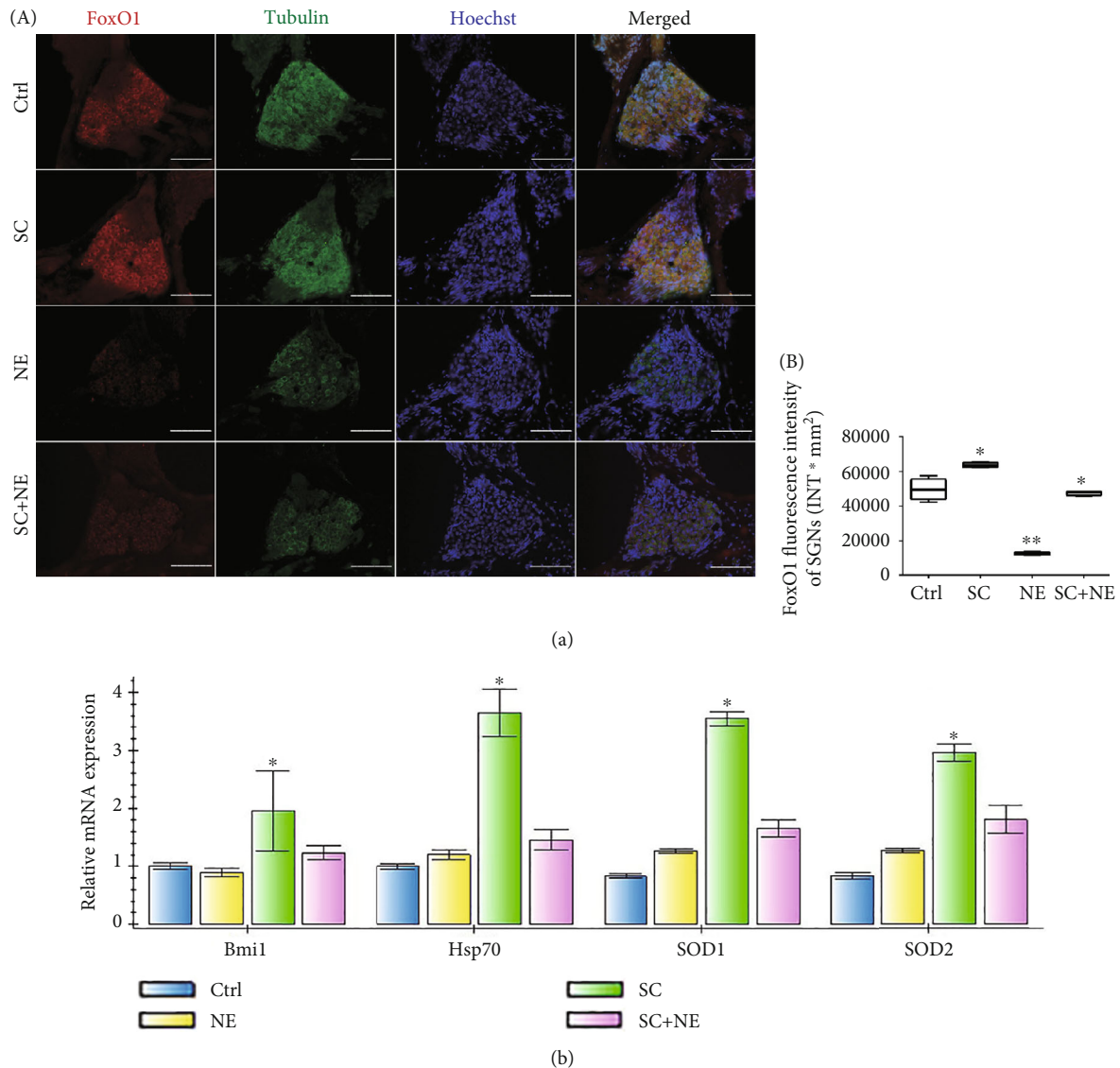


FIGURE 4: FoxO1 protein and Hsp70, Bmi1, SOD1, and SOD2 mRNA expressions of SGNs after sound conditioning and acute noise exposure. Distributions and expressions of FoxO1 (a) protein were detected with the immune-fluorescence assay in the Ctrl and SC groups as well as the NE and SC+NE groups (A), while the quantity of these protein expressions was analyzed by fluorescence intensity (B). FoxO1 (red) and tubulin (green) as SGN marker were, respectively, labeled with fluorescent secondary antibody, and nuclei (blue) were labeled with Hoechst. Scale bars represent 100 μm (a). Statistical analysis of the results presented in (B) was performed with one-way ANOVA (FoxO1: $F = 155.3$, $P < 0.0001$), followed by Newman-Keuls' post hoc test (* $P < 0.05$, ** $P < 0.01$; $n = 6$ pictures from 3 animals/group). Furthermore, values are means \pm SD. Relative mRNA expressions of Bmi1, Hsp70, SOD1, and SOD2 were determined by quantitative RT-PCR (b). β -Actin RNA level was used as an endogenous control. Values are means \pm SD ($n = 6$ animals/group). * $P < 0.05$ vs. control group.

mitochondrial superoxide indicator for live cells), and the Hsp70-overexpressing adenovirus group ($q = 31.64$, ** $P < 0.05$) showed an apparent decrease in ROS accumulation of neonatal culture *in vitro* (Figure 8(a)/8(c)/8(e)).

3.6. PTC-209 Decreased the Expression of Bmi1, SOD1, and SOD2 in Rat SGNs and Significantly Increased ROS Accumulation in Rat SGNs *In Vitro*. Following treatment with PTC-209 on neonatal cultures *in vitro*, IF results (Figures 9(a)/9(a'), 9(c)/9(c'), and 9(d)/9(d') and Supplementary Table 1) revealed that Bmi1, SOD1, and SOD2

fluorescence levels were all decreased in SGNs compared with those in the control group. There were clearly significant differences between the PTC-209 and control groups except for the Hsp70 fluorescence levels ($t = 0.8032$, $P > 0.05$) (Supplementary Figure 1). WB results (Figure 9(e)/9(e') and Supplementary Table 2) also revealed similar results at the protein level of Bmi1, SOD1, and SOD2 expression with the exception of Hsp70 expression after treatment with PTC-209. There were significant and marked differences between the PTC-209 and the control groups ($F = 7931.17$, * $P < 0.05$). Moreover, RT-PCR showed that Bmi1, SOD1, and SOD2

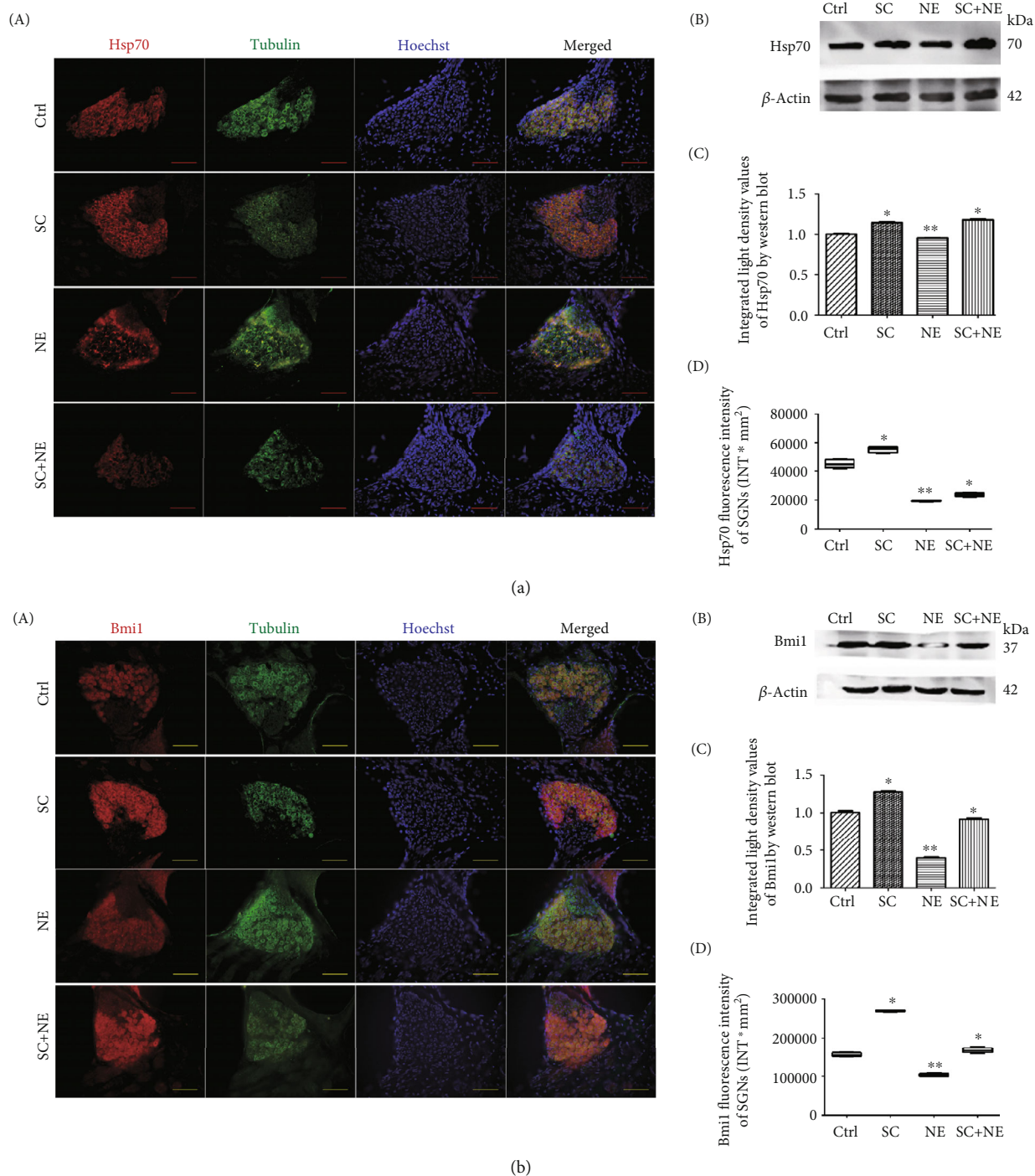


FIGURE 5: Hsp70 and Bmi1 protein expressions of SGNs after sound conditioning and acute noise exposure. Distributions and expressions of Hsp70 (a) and Bmi1 (b) protein were detected with the immune-fluorescence assay in the Ctrl and SC groups as well as the NE and SC+NE groups (A), while the quantity of these protein expressions was analyzed by fluorescence intensity (D). Hsp70/Bmi1 (red) and tubulin (green) as SGN marker were, respectively, labeled with fluorescent secondary antibody, and nuclei (blue) were labeled with Hoechst. Scale bars represent 100 μ m. Protein expressions of these were also assessed with western blot (B), while the quantity of these protein expressions was analyzed by integrated light density (C). β -Actin protein was available as an endogenous control. Furthermore, values are means \pm SD ($n = 12$ animals/group). * $P < 0.05$ vs. control group; ** $P < 0.05$ vs. control group. Statistical analysis of the results presented in (C) was performed with one-way ANOVA (Hsp70: $F = 126.5$, $P < 0.0001$; Bmi1: $F = 478.8$, $P < 0.0001$), followed by Newman-Keuls' post hoc test (* $P < 0.05$, ** $P < 0.05$; $n = 12$ animals/group). Statistical analysis of the results presented in (D) was performed with one-way ANOVA (Hsp70: $F = 303.4$, $P < 0.0001$; Bmi1: $F = 940.7$, $P < 0.0001$), followed by Newman-Keuls' post hoc test (* $P < 0.05$, ** $P < 0.05$; $n = 6$ pictures from 3 animals/group). Furthermore, values are means \pm SD.

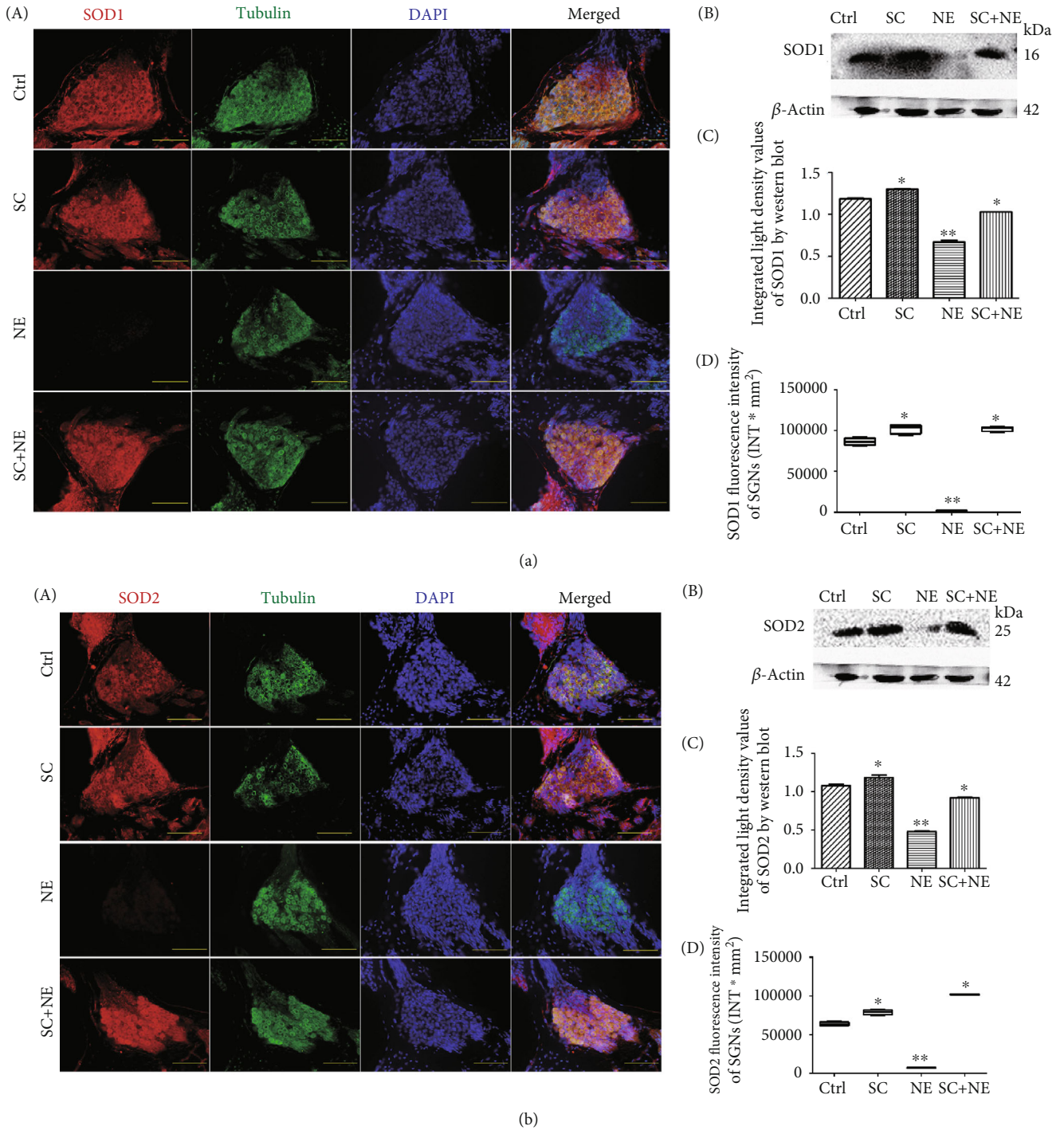


FIGURE 6: SOD1 and SOD2 protein expressions of SGNs after sound conditioning and acute noise exposure. Distributions and expressions of SOD1 (a) and SOD2 (b) protein were detected with the immune-fluorescence assay in the Ctrl and SC groups as well as the NE and SC+NE groups (A), while the quantity of these protein expressions was analyzed by fluorescence intensity (D). SOD1/SOD2 (red) and tubulin (green) as SGN marker were, respectively, labeled with fluorescent secondary antibody, and nuclei (blue) were labeled with DAPI. Scale bars represent 100 μ m. Protein expressions of these were also assessed with western blot (B), while the quantity of these protein expressions was analyzed by integrated light density (C). β -Actin protein was available as an endogenous control. Furthermore, values are means \pm SD ($n = 12$ animals/group). * $P < 0.05$ vs. control group; ** $P < 0.05$ vs. control group. Statistical analysis of the results presented in (C) was performed with one-way ANOVA (SOD1: $F = 579.5$, $P < 0.0001$; SOD2: $F = 271.3$, $P < 0.0001$), followed by Newman-Keuls' post hoc test (* $P < 0.05$, ** $P < 0.05$; $n = 12$ animals/group). Statistical analysis of the results presented in (D) was performed with one-way ANOVA (SOD1: $F = 1335.0$, $P < 0.0001$; SOD2: $F = 1521$, $P < 0.0001$), followed by Newman-Keuls' post hoc test (* $P < 0.05$, ** $P < 0.05$; $n = 6$ pictures from 3 animals/group). Furthermore, values are means \pm SD.

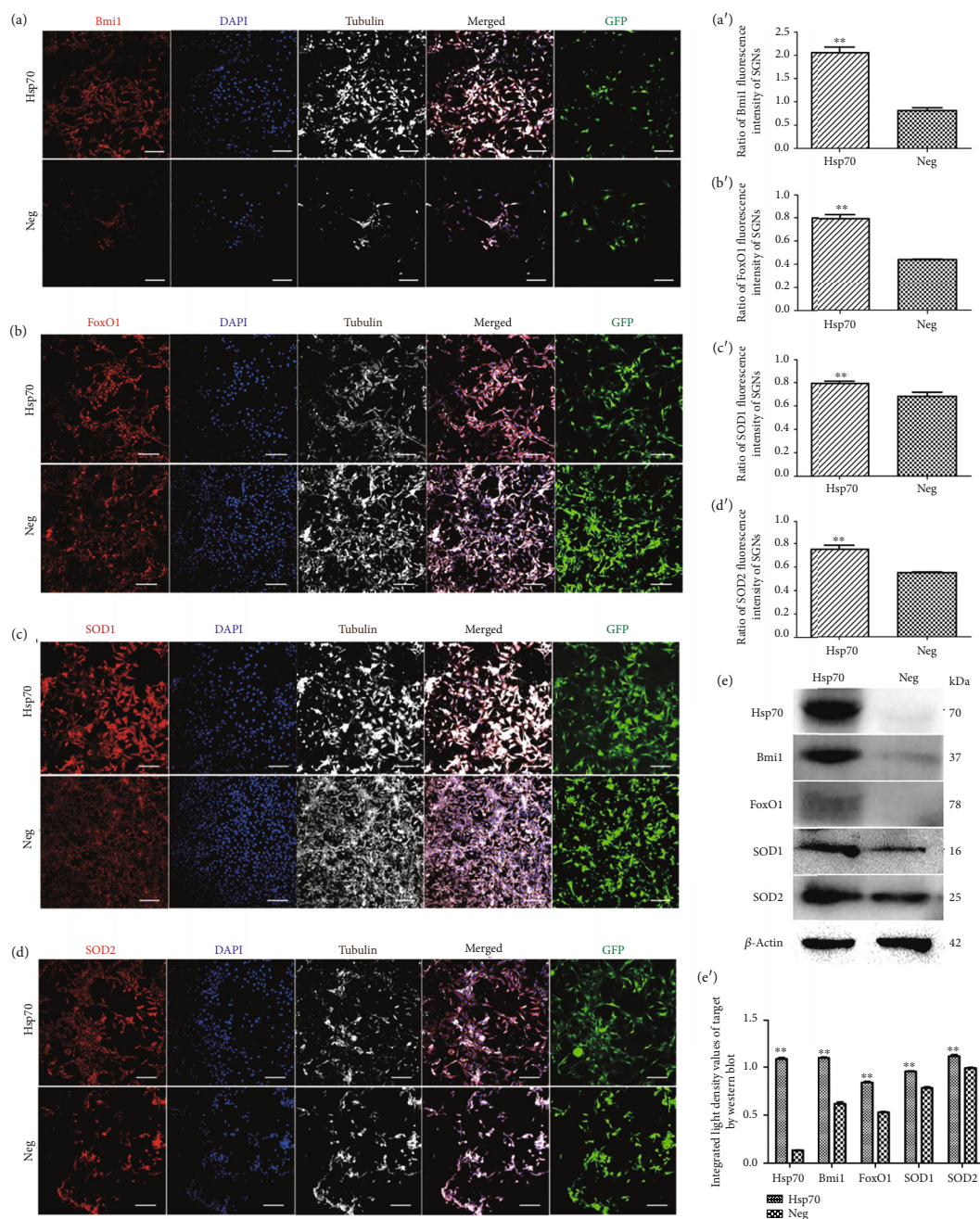


FIGURE 7: Bmi1, FoxO1, SOD1, and SOD2 expressions of overexpressed HSP70 SGNs. Distributions and expressions of Bmi1, FoxO1, SOD1, and SOD2 protein in SGNs were detected with the immune-fluorescence assay in the Hsp70-overexpressing adenovirus and negative control groups (a–d), while the quantity of these protein expressions was analyzed by the ratio of fluorescence intensity (a'–d'). After successful transfection by Hsp70-overexpressing adenovirus or empty vector adenovirus as GFP (green) shown, Bmi1/FoxO1/SOD1/SOD2 (red) and tubulin (white) as SGN marker were, respectively, labeled with fluorescent secondary antibody and nuclei (blue) were labeled with DAPI. Scale bars represent 100 μ m. SGNs expressing a green fluorescent protein (GFP) coded in the same vector as the Hsp70-overexpressing vector was coupled to the GFP sequence, indicating that 66.7% \pm 7.8% ($n = 4$ independent cell culture preparations) of the neuronal cells present in the cultures were transfected with Hsp70. Therefore, ratios of Bmi1, FoxO1, SOD1, and SOD2 fluorescence intensity to GFP were calculated. Furthermore, values are means \pm SD ($N = 40$ animals from 2 groups). ** $P < 0.05$ vs. negative group. Statistical analysis of the results presented in (a'–d') was performed with Student's t -test (** $P < 0.05$; $N = 40$ animals from 2 groups). After successful transfection by Hsp70-overexpressing adenovirus or empty vector adenovirus, protein expressions of Hsp70, Bmi1, FoxO1, SOD1, and SOD2 were assessed with western blot (e), while the quantity of these protein expressions was analyzed by integrated light density (e'). β -Actin protein was available as an endogenous control. Furthermore, values are means \pm SD. ** $P < 0.05$ vs. negative group. Statistical analysis of the results was performed with two-way ANOVA (interaction: $F(4, 20) = 459.8$; $P < 0.0001$; row factor: $F(4, 20) = 493.74$; $P < 0.0001$; column factor: $F(1, 20) = 3400.31$; $P < 0.0001$), followed by Student's t -test (** $P < 0.05$; $n = 12$ animals/group).

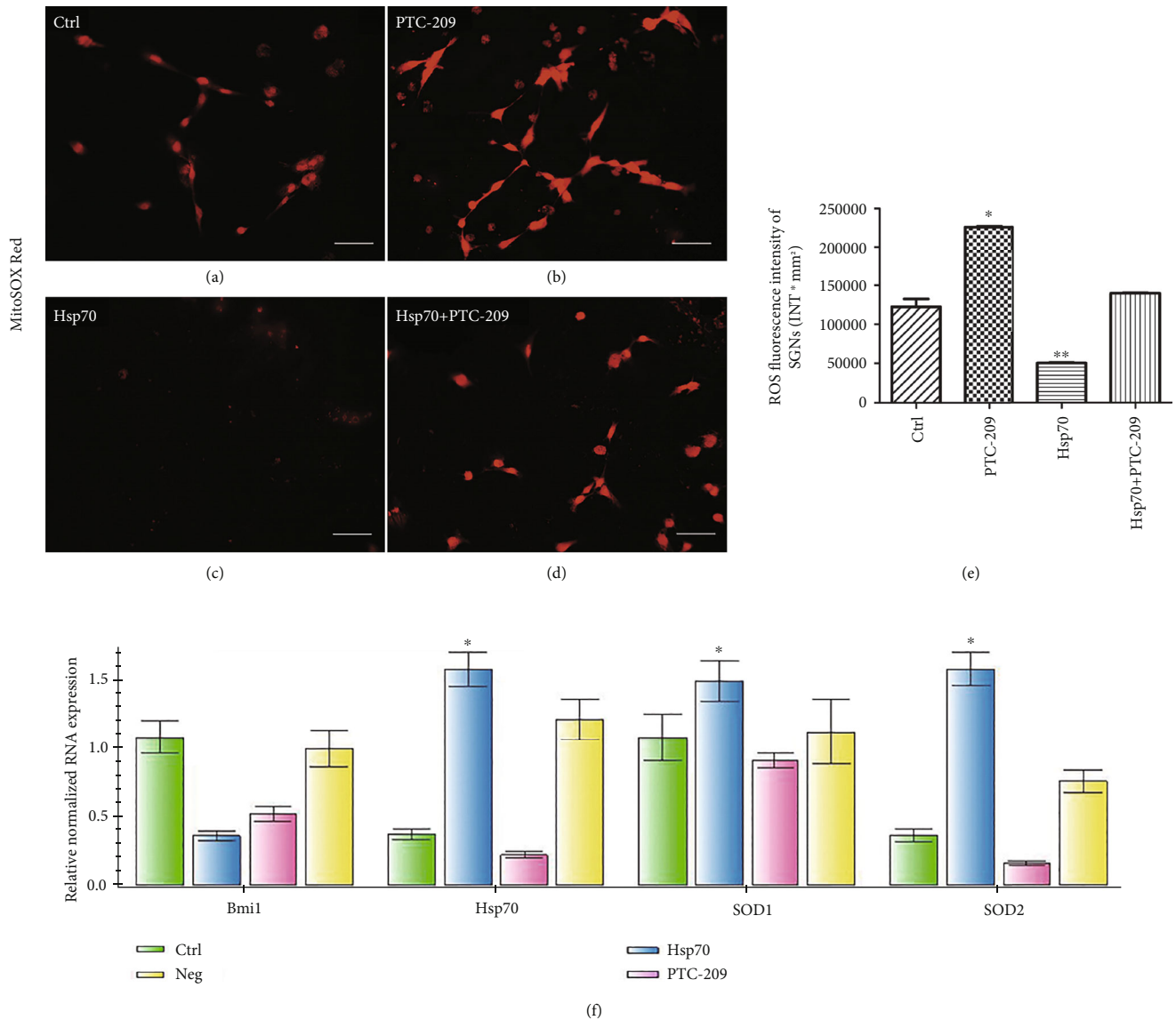


FIGURE 8: ROS accumulation of different treatments in SGNs and Bmi1, Hsp70, SOD1, and SOD2 mRNA expression of SGNs *in vitro*. ROS accumulation in SGNs was showed by MitoSOX Red and was detected with the immune-fluorescence assay in the control group (a), PTC-209 treated group (b), Hsp70-overexpressing adenovirus group (c), and Hsp70-overexpressing adenovirus followed the PTC-209-treated group (d), while the quantity of ROS accumulation was analyzed by fluorescence intensity (e). Scale bars represent 50 μ m. Furthermore, values are means \pm SD ($N = 80$). * $P < 0.05$ vs. control group; ** $P < 0.05$ vs. control group. Statistical analysis of the results presented in (e) was performed with one-way ANOVA ($F = 634.9$; $P < 0.0001$), followed by Newman-Keuls' post hoc test (* $P < 0.05$, ** $P < 0.05$; $N = 80$ animals from 4 groups). Relative mRNA expressions of Bmi1, Hsp70, SOD1, and SOD2 were determined by quantitative RT-PCR (f). β -Actin RNA level was used as an endogenous control. Values are means \pm SD ($n = 12$ animals/group). * $P < 0.05$ vs. control group.

mRNA expressions were also clearly decreased in the SGNs on neonatal cultures of the PTC-209 group compared with that of the control group except for Hsp70 mRNA expression (Figure 8(f)).

In addition, there was a significant difference between the PTC-209 and control groups in ROS accumulation of neonatal culture labeled by MitoSOX Red. In the PTC-209 group, ROS accumulation ($q = 36.17$, * $P < 0.05$) was significantly increased *in vitro*, while a decrease in ROS accumulation of neonatal culture by the Hsp70-overexpressing adenovirus is offset by PTC-209 (Figures 8(a)–8(e)).

3.7. FoxO1 Was a Direct Target of Bmi1 in Rat SGNs. After treatment with PTC-209 on neonatal cultures *in vitro*, IF results (Figure 9(b)/9(b')) revealed that FoxO1 (a transcription factor responsible for the stress response and redox balance) fluorescence levels ($t = 13.02$, * $P < 0.05$) are lower in the SGNs. WB analysis (Figure 9(e)/9(e')) also showed that FoxO1 expression ($t = 50.89$, * $P < 0.05$) is decreased in SGNs on neonatal cultures of the PTC-209 group. There was a significant difference found between the PTC-209 and control groups in FoxO1 expression ($F = 7931.17$, * $P < 0.05$), which was directly decreased by PTC-209.

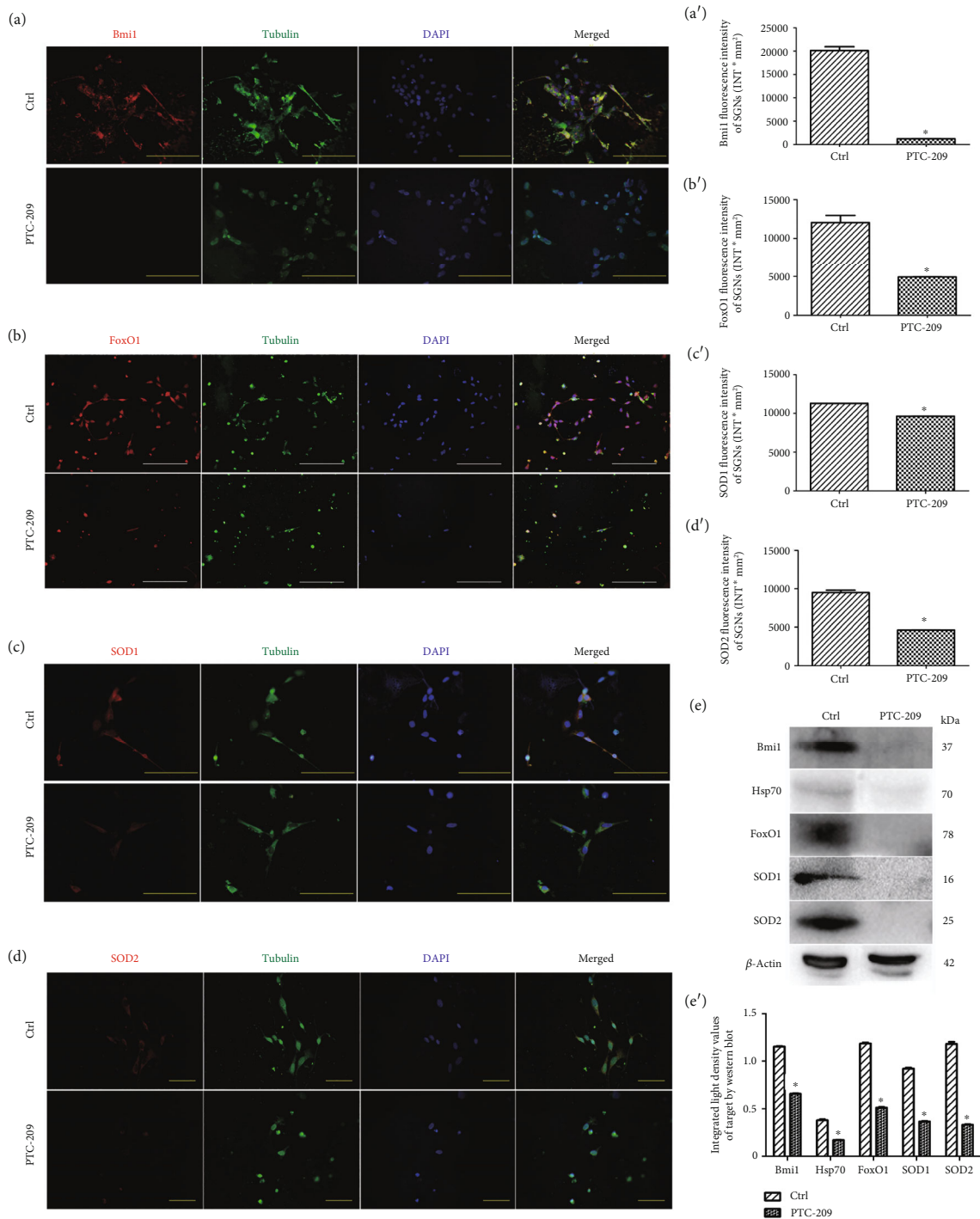


FIGURE 9: Bmi1, FoxO1, SOD1, and SOD2 expressions in SGNs after PTC-209 treatment. Distributions and expressions of Bmi1, FoxO1, SOD1, and SOD2 protein in SGNs were detected with the immune-fluorescence assay in the control group and the PTC-209 treated groups (a–d), while the quantity of these protein expressions was analyzed by fluorescence intensity (a'–d'). After PTC-209 treatment, Bmi1/FoxO1/SOD1/SOD2 (red) and tubulin (green) as SGN marker were, respectively, labeled with fluorescent secondary antibody and nuclei (blue) were labeled with DAPI. Scale bars represent 100 μm and 50 μm . Furthermore, values are means \pm SD ($N = 40$ animals from 2 groups). * $P < 0.05$ vs. control group. Statistical analysis of the results presented in (a'–d') was performed with Student's t -test (* $P < 0.05$; $N = 40$ animals from 2 groups). After PTC-209 treatment, protein expressions of Hsp70, Bmi1, FoxO1, SOD1, and SOD2 were assessed with western blot (e), while the quantity of these protein expressions was analyzed by integrated light density (e'). β -Actin protein was available as an endogenous control. Furthermore, values are means \pm SD. * $P < 0.05$ vs. control group. Statistical analysis of the results was performed with two-way ANOVA (interaction: $F(4, 20) = 283.78$; $P < 0.0001$; row factor: $F(4, 20) = 1276.15$; $P < 0.0001$; column factor: $F(1, 20) = 7931.17$; $P < 0.0001$), followed by Student's t -test (* $P < 0.05$; $n = 12$ animals/group).

4. Discussion

Hearing loss is a common sensory disorder all over the world; by far, there are around 466 million patients with hearing disability worldwide. In order to have hearing, HCs are needed for transducing sound vibrations into electrical signaling, and SGNs transmit these electrical signals into the auditory cortex [29–32]. Thus, the majority of the hearing loss is caused by the malfunction or damage of HCs or SGNs. Both HCs or SGNs are vulnerable to be injured by noise, ototoxic drugs, inflammation, biological aging, and genetic defects [16, 33–37]. In recent years, many previous reports used transcription regulation to promote the inner ear stem cells to regenerate the HCs [38–42] and used biomaterials, electrical stimulation, and magnetic regulation to promote the neural stem cells to regenerate the SGNs [43–46] and to promote the maturation of SGNs [47–49]. However, the mammals only have very limited HC and SGN regeneration ability [50–55]; thus, hearing loss is irreversible by far. Thus, to fully understand the detailed protective mechanism of SC in mammals and to effectively protect the HCs and SGNs against various damages are very important. The primary goals of this study were to identify the involvement of Hsp70 and Bmi1 in the protective effect of SC against AAT by targeting SOD1 and SOD2, regulated by the FoxO1 signaling pathway, and to verify the effects of free oxygen radical alteration related to the underlying mechanisms *in vitro* and *in vivo*. In this study, we confirmed that SC prior to a loud noise protected against AAT based on significant improvements in hearing impairment and an apparent reduction in OHC loss (Figure 2) as well as ultrastructural changes in OHCs and SGNs of a fully mature rat (Figure 3). Next, we reported that these functional and ultrastructural changes in rat SGNs were accompanied by significant upregulation of Hsp70, Bmi1, FoxO1, SOD1, and SOD2 protein expression (Figures 5, 6, and 4(a)), which indicated that these proteins were involved in the protective effect of SC against AAT in rats. Furthermore, we used transfection with Hsp70-overexpressing adenovirus and coculture with PTC-209 to verify the Hsp70/Bmi1-FoxO1-SOD signaling pathway and its effect on ROS (mitochondrial superoxide) accumulation of neonatal culture *in vitro* (Figures 7–10). To our knowledge, this is the first report that upregulation of Hsp70 and Bmi1 expression was involved in the protective effect of SC against AAT by targeting SOD1 and SOD2 in rat SGNs, regulated by the FoxO1 signaling pathway.

Previous research lends progressive support to the evidence that oxidative stress, generated in part by glutamate excitotoxicity, impaired mitochondrial function, and GSH depletion resulted in cochlear injury induced by AAT. Therefore, enhancing the cellular oxidative stress defense pathways in the cochlea alleviated noise-induced cochlear injury [56]. Previous studies have further confirmed that AAT is closely related to the degeneration of the antioxidant system in the organs [11–14]. Thus, SC could protect hearing by enhancement of the antioxidant system [1–5, 7, 57–59]. Our results *in vivo* also indicated that SC protected against AAT as it did not result in hearing loss in the studied rats. Furthermore, hair cell loss caused by NE was reduced by SC in both the

base and middle turns of the basilar membrane, while the apex is less vulnerable to AAT and SC is of no advantage in that area. Interestingly, SC also increased the quantity of mitochondria, enhanced their function in the SGN cells, and reversed the injury and dysfunction of mitochondria in the SGNs caused by NE. The changes in mitochondria of SGNs were direct proof that the antioxidant system in the organs was enhanced, which contributed to less sensitivity in AAT. Therefore, the findings above in our study fully supported the suggestion that SC could protect against AAT by enhancement of the antioxidant system in the SGNs. Moreover, SC was also reported to be capable of improving the removal of oxidation products by enhancement of the antioxidant system, which protected against AAT [3]. Furthermore, we found that Hsp70, Bmi1, FoxO1, SOD1, and SOD2 were all involved in the SC-induced enhancement of the antioxidant system and reduced ROS accumulation in the SGNs.

It is widely known that the Hsp70 family of heat shock proteins composed of molecular chaperones of approximately 70 kDa in size played a critical role in protein homeostasis. The Hsp70 proteins possess a highly conserved domain structure that is comprised of the following main domains: an ~44 kDa N-terminal nucleotide-binding domain (NBD) which exhibited ATPase activity and was highly conserved; a middle flexible linker region; an ~15 kDa substrate-binding domain (SBD), which interacts with the stretches of the hydrophobic amino acids in the peptides; and an ~10 kDa α -helical C-terminal domain that is believed to form a “lid” that closes over the substrate and mediated cochaperone binding [60–63]. Hsp70 proteins played a crucial role in the mediation of correct protein folding and, consequently, in the maintenance of protein homeostasis. Hsp70 directly unfolded misfolded proteins, in adenosine triphosphate- (ATP-) dependent fashion. These proteins also enhanced cell survival following a multitude of stressors, including elevated temperature, hypoxia, oxidative stress, and others. This survival role was reflected in the ability of Hsp70 to buffer the toxicity of denatured and misfolded proteins that accumulated during stress [19]. Many previous studies demonstrated that Hsp induction was a critical stress response in the inner ear that could promote the survival of hair cells exposed to both classes of ototoxic drugs [64–68] and lowered the risks of AAT in mice [69]. In addition, the expression of Hsp70 was increased in the inner ear of mice by exposure to low-frequency noise (LFN), which suggested that Hsp70 played an important part in protecting the inner ears from LFN [70]. Furthermore, strong evidence from recent studies has also shown that SC triggered Hsp70 induction and enhanced its expression *in vivo* [5, 7, 59, 71–73]. According to our study, the RT-PCR, WB, and IF results showed that increased expression of Hsp70 was also involved in the protective effects of SC against AAT in rats. Therefore, we suggested that SC increased Hsp70 expression in the SGNs to enhance cell survival following a noise-induced stress response.

Conversely, evidence from previous studies suggested that Bmi1 improved cell survival by regulating mitochondrial function and ROS levels in the thymocytes and neurons,

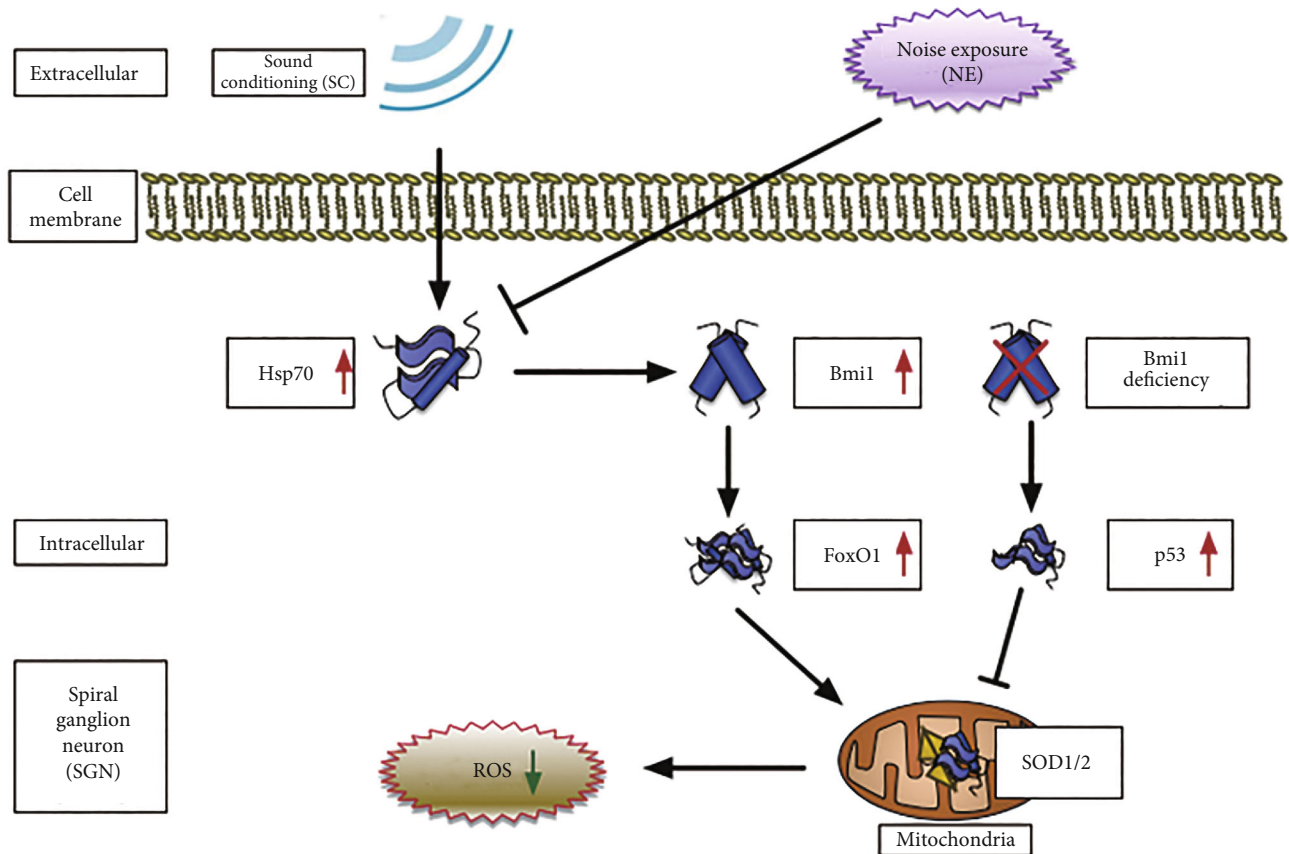


FIGURE 10: A model for the mechanism of Hsp70-induced Bmi1 upregulation in the protection of sound conditioning against acute acoustic trauma by directly targeting SOD1 and SOD2 regulated by the FoxO1 signaling pathway. Hsp70/Bmi1-FoxO1-SOD1/SOD2 signaling pathway decreases sensitivity in noise-induced trauma following sound conditioning by controlling mitochondrial function and ROS level in rat's SGN. Meanwhile, based on previous studies, other pathway is also involved in Bmi1 deficiency-induced ROS accumulation, such as the following: Bmi1 deficiency directly leads to p53-mediated repression of antioxidant genes, resulting in increased ROS.

which had a close bearing on the antioxidants and the removal of oxidation products [3]. Bmi1, a member of the polycomb protein family, could bind to the Runx1/CBF β transcription factor complex to silence target genes in a PRC2-independent manner [74]. Abdouh et al. confirmed that other than in stem cells and rapidly dividing cells, Bmi1 was expressed in terminally differentiated cells such as neurons and increased in Bmi1 expression in cortical neurons which activated antioxidant genes to regulate ROS generation and protected against DNA damage-induced cell apoptosis as well as mitochondrial injury [75]. In neurons, Bmi1 also suppressed p53-induced cell apoptosis by regulating antioxidation [76]. Furthermore, a previous report also showed that Bmi1-deficient thymocytes impaired mitochondrial function, which led to a marked increase in intracellular ROS levels and a subsequent engagement of the DDR pathway [77]. Rizo et al. found that a reduced ability of self-renewal was associated with enhanced apoptosis in Bmi1- CD34(+) stem cells, which coincided with increased levels of intracellular ROS [78]. Furthermore, overexpression of Bmi1 in vivo protected human embryonic stem cells (HSCs) from ROS damage and extended the lifespan of HSCs [79], whereas Bmi1 transduction in vitro reduced irradiation-induced ROS levels by suppressing the oxidase

genes and increased repair of the DNA damage in human keratinocytes [80]. Furthermore, in a recent study by Chen et al., Bmi1 was demonstrated to have an important role in hair cell survival via controlling the redox balance and ROS levels [20]. Our study in vivo and in vitro produced similar results to Chen et al. However, the current study also found that these functional and ultrastructural changes of mitochondria were accompanied by significant upregulation of Hsp70 and Bmi1 expression induced by SC and that overexpression of Hsp70 significantly enhanced Bmi1 expression in rat SGNs (Hsp70 might stabilize Bmi1 at the protein level rather than increase it at the transcriptional level) and clearly decreased mitochondrial superoxide accumulation, while Bmi1 inhibitor attenuated the effect of Hsp70 transfection. This finding suggested that SC induce increased Bmi1 expression in the SGNs, which was triggered by Hsp70 induction to improve cell survival by regulating mitochondrial function and mitochondrial superoxide levels.

It is widely accepted that several pathways are involved in Bmi1 deficiency-induced ROS accumulation, including the following: (1) Bmi1 deficiency leads to mitochondrial dysfunction resulting in a rise of intracellular ROS and subsequent engagement of the DDR pathway, in which Chk2 and

p53 were activated [77]; (2) Bmi1 deficiency directly leads to p53-mediated repression of the antioxidant genes, resulting in increased ROS levels [75]. However, how to control mitochondrial function and ROS level in SGNs by Bmi1 upregulation and the mechanism by which SC exerted a protective effect against AAT have remained unknown. To fix this problem, we further investigated FoxO1 (a transcription factor responsible for the stress response and redox balance) [81], SOD1 (an antioxidant gene whose protein is found in the cytoplasm), and SOD2 (an antioxidant gene whose protein is found in the mitochondrial ridge) expressions in SGNs *in vivo* and *in vitro* by transfection with Hsp70-overexpressing adenovirus and coculture with PTC-209. Ultimately, we found that functional and ultrastructural changes in the mitochondria were still associated with a significant upregulation of FoxO1, SOD1, and SOD2 expression induced by SC and we also confirmed that PTC-209 significantly decreased FoxO1, SOD1, and SOD2 expressions in the rat SGNs and increased mitochondrial superoxide accumulation, while overexpression of Hsp70 significantly reversed these expressions in the rat SGNs. We suggested that changes in SOD1/SOD2 expression could be involved in the protective effects of SC and a consequence of cell protection. Therefore, our results indicated that the Hsp70/Bmi1-FoxO1-SOD signaling pathway was involved in the protective effect of SC against AAT and regulated mitochondrial function and the mitochondrial superoxide levels in rat SGNs (Figure 10), which coincided with the regulation of oxidative stress and mitochondrial dysfunction by FoxO1 in human QBC939 cells from a recent study [82]. Meanwhile, the involvement of the Hsp70/Bmi1-FoxO1-SOD signaling pathway in other regions of cochlear tissue (such as hair cells and cochlear lateral wall) behind the protective effect of SC has also been conformed further by our immunolabeling data. However, in view of the complexity of regulating Bim1 expression in SGNs, we still believe that there might be additional signaling pathways that regulate mitochondrial function and ROS levels in rat SGNs. Therefore, more research on this issue should be performed. In addition, the overexpression experiments on cultured SGN were performed on neonatal cultures whereas our noise exposure/preconditioning experiments were performed on fully mature rats. Although immature SGNs differ in many ways from mature ones (expression of ion channels, etc.) [83], there is no significant difference between the changes of a target molecule *in vivo* and *in vitro* based on our current research data.

Thus, we found that SC of low frequency prior to a loud noise not only protected against AAT based on significant improvements in hearing impairment and an apparent reduction in OHC loss but also improved SGN survival following a noise-induced stress response via controlling mitochondrial function and ROS levels in rat SGNs, and we are the first to have demonstrated a new theory on the protection of SC against AAT in which the Hsp70/Bmi1-FoxO1-SOD signaling pathway was involved. Lastly, we suggested that the enhancement of the antioxidant system and a reduction in ROS accumulation might be the main reasons for decreased sensitivity to noise-induced trauma

following treatment with SC. The results from our work help us to understand the protective capacity of SC against AAT and the underlying mechanisms involved.

5. Conclusions and Future Directions

In summary, the *in vitro* and *in vivo* data presented here provide evidence that (i) SC improved SGN survival following noise-induced stress response via controlling mitochondrial function and ROS levels, (ii) Hsp70/Bmi1-FoxO1-SOD signaling pathway was involved in the protection of SC against AAT, and (iii) enhancement of the antioxidant system and a reduction in ROS accumulation might be the main reasons for the decreased sensitivity to AAT following treatment with SC in the rats. Clinically, these issues could provide a better preventive strategy for AAT.

5.1. Limitations of Our Work. Due to technical issues, the harvested tissues in western blot included other supporting cells in addition to SGN so that the data of western blot does not coincide with that of immunofluorescence *in vivo* (especially for Hsp70). This issue might be resolved by tissue purification technology. The roles of Hsp70 and Bmi1 have been demonstrated *in vitro* but not fully *in vivo*. The role of FoxO1 in the upregulation of SOD should be demonstrated further. Furthermore, so far, it is still unclear how the FoxO1 signaling pathway activates antioxidant genes to control mitochondrial function and ROS levels. Finally, whether the SC stimulus of other higher frequencies or even noise might protect against hearing loss more effectively or not should be considered to study further. Therefore, more research on these issues should be performed in our next study.

Data Availability

The data used to support the findings of this study were supplied by Jianhua Qiu under license and so cannot be made freely available. Requests for access to these data should be made to Jianhua Qiu (qiujh@fmmu.edu.cn).

Conflicts of Interest

The authors declare no competing interests.

Authors' Contributions

ZGX, WYX, and QY proposed the idea, did the research, analyzed data, and wrote the paper; TKY, MWJ, LXQ, CYY, and JJW provided support and participated in discussions on the research; QJH, LLJ, and LJS gave us valuable advice and revised the manuscript. All authors have read and approved the final manuscript. Guoxia Zhu, Yongxiang Wu, and Yang Qiu contributed equally to this work.

Acknowledgments

The authors wish to thank Zhenzhen Liu for excellent technical assistance. We thank American Journal Experts for editing service. This study was supported by grants from the International Cooperation and Communication Project of the

Natural Scientific Foundation of China (NSFC, No. 81110097), the Natural Scientific Foundation of China (NSFC, Nos. 81400459, 81172635, and 81803187), the Youth Development Project of Military Medical Science and Technology (MMST, Nos. 14QNP023), and the Scientific Incubation Foundation of Xi'an People's Hospital/Xi'an Fourth Hospital (Nos. ZD-3).

Supplementary Materials

Supplementary 1. Supplementary Figure 1: Hsp70 expression in SGNs after PTC-209 treatment distribution and expression of Hsp70 protein in SGNs was detected with immunofluorescence assay in the control group and PTC-209 treated groups (A), while the quantity of Hsp70 protein expression was analyzed by fluorescence intensity (B). After PTC-209 treatment, Hsp70 (red) and tubulin (green) as SGN marker were, respectively, labeled with fluorescent secondary antibody and nuclei (blue) were labeled with DAPI. Scale bars represent 50 μm . Furthermore, values are means \pm SD ($N = 40$ animals from 2 groups). $P > 0.05$ vs. control group. Statistical analysis of the results presented in (B) was performed with Student's t -test ($P > 0.05$; $N = 40$ animals from 2 groups). Supplementary 2. Supplementary Figure 2: Hsp70, SOD1, SOD2, and Bmi1 mRNA expression of SGNs *in vitro*. Relative mRNA expressions of Hsp70, SOD1, SOD2, and Bmi1 were determined by quantitative RT-PCR. β -Actin RNA level was used as an endogenous control. Values are means \pm SD ($n = 12$ animals/group). $*P < 0.05$ Hsp70 vs. control group. Supplementary 3. Supplementary Figure 3: Hsp70 and Bmi1 protein expressions in hair cells and cochlear lateral wall after sound conditioning and acute noise exposure. Distributions and expressions of Hsp70 (A) and Bmi1 (B) protein were detected with immunofluorescence assay in the Ctrl and SC groups as well as the NE and SC+NE groups (a), while the quantity of these protein expressions in both hair cells (b) and cochlear lateral wall (c) was analyzed by fluorescence intensity. Hsp70/Bmi1 (red) was labeled with fluorescent secondary antibody, and nuclei (blue) were labeled with Hoechst. Scale bars represent 100 μm . Furthermore, values are means \pm SD. Statistical analysis of the results presented in (b) (Hsp70: $F = 80.74$, $P < 0.0001$; Bmi1: $F = 86.64$, $P < 0.0001$) and (c) (Hsp70: $F = 684.6$, $P < 0.0001$; Bmi1: $F = 338.2$, $P < 0.0001$) was performed with one-way ANOVA, followed by Newman-Keuls' post hoc test ($*P < 0.05$, $**P < 0.05$; $n = 6$ pictures from 3 animals/group). Supplementary 4. Supplementary Figure 4: SOD1 and SOD2 protein expressions in hair cells and cochlear lateral wall after sound conditioning and acute noise exposure. Distributions and expressions of SOD1 (A) and SOD2 (B) protein were detected with immunofluorescence assay in the Ctrl and SC groups as well as the NE and SC+NE groups (a), while the quantity of these protein expressions in both hair cells (b) and cochlear lateral wall (c) was analyzed by fluorescence intensity. SOD1/SOD2 (red) was labeled with fluorescent secondary antibody, and nuclei (blue) were labeled with Hoechst. Scale bars represent 100 μm . Furthermore, values are means

\pm SD. Statistical analysis of the results presented in (b) (SOD1: $F = 233.0$, $P < 0.0001$; SOD2: $F = 79.93$, $P < 0.0001$) and (c) (SOD1: $F = 143.0$, $P < 0.0001$; SOD2: $F = 199.8$, $P < 0.0001$) was performed with one-way ANOVA, followed by Newman-Keuls' post hoc test ($*P < 0.05$, $**P < 0.05$; $n = 6$ pictures from 3 animals/group). Supplementary 5. Supplementary Table 1: statistical results of immunofluorescence of target protein expression *in vivo* and *in vitro* (Student-Newman-Keuls- (SNK-) q test for post hoc comparisons (NE or SC vs. Ctrl) $**P < 0.05$, $*P < 0.05$; Student's t -test for the comparisons between the two groups (Hsp70 vs. Neg or PTC-209 vs. Ctrl) $**P < 0.05$, $*P < 0.05$). Supplementary 6. Supplementary Table 2: statistical results of western blot of target protein expression *in vivo* and *in vitro* (Student-Newman-Keuls- (SNK-) q test for post hoc comparisons (NE or SC vs. Ctrl) $**P < 0.05$, $*P < 0.05$; Student's t -test for the comparisons between the two groups (Hsp70 vs. Neg or PTC-209 vs. Ctrl) $**P < 0.05$, $*P < 0.05$). (Supplementary Materials)

References

- [1] T. Miyakita, P. A. Hellstrom, E. Frimanson, and A. Axelsson, "Effect of low level acoustic stimulation on temporary threshold shift in young humans," *Hearing Research*, vol. 60, no. 2, pp. 149–155, 1992.
- [2] M. Pukkila, S. Zhai, J. Virkkala, U. Pirvola, and J. Ylikoski, "The "toughening" phenomenon in rat's auditory organ," *Acta Oto-Laryngologica. Supplementum*, vol. 529, pp. 59–62, 1997.
- [3] A. A. Jacono, B. Hu, R. D. Kopke, D. Henderson, T. R. Van De Water, and H. M. Steinman, "Changes in cochlear antioxidant enzyme activity after sound conditioning and noise exposure in the chinchilla," *Hearing Research*, vol. 117, no. 1-2, pp. 31–38, 1998.
- [4] X. Niu and B. Canlon, "Activation of tyrosine hydroxylase in the lateral efferent terminals by sound conditioning," *Hearing Research*, vol. 174, no. 1-2, pp. 124–132, 2002.
- [5] H. Zuo, B. Cui, X. She, and M. Wu, "Changes in guinea pig cochlear hair cells after sound conditioning and noise exposure," *Journal of Occupational Health*, vol. 50, no. 5, pp. 373–379, 2008.
- [6] J. C. Alvarado, V. Fuentes-Santamaria, M. C. Gabaldon-Ull, T. Jareno-Flores, J. M. Miller, and J. M. Juiz, "Noise-induced "toughening" effect in Wistar rats: enhanced auditory brainstem responses are related to calretinin and nitric oxide synthase upregulation," *Frontiers in Neuroanatomy*, vol. 10, p. 19, 2016.
- [7] S. Roy, M. M. Ryals, A. B. Van den Bruele, T. S. Fitzgerald, and L. L. Cunningham, "Sound preconditioning therapy inhibits ototoxic hearing loss in mice," *The Journal of Clinical Investigation*, vol. 123, no. 11, pp. 4945–4949, 2013.
- [8] X. Li, Z. Zhu, W. Li, L. Wei, B. Zhao, and Z. Hao, "Polymorphism in GRHL2 gene may contribute to noise-induced hearing loss susceptibility: a meta-analysis," *Brazilian Journal of Otorhinolaryngology*, vol. 86, no. 3, pp. 370–375, 2020.
- [9] J. Yang, J. Zhang, X. Wang et al., "Identification of functional tag single nucleotide polymorphisms within the entire CAT gene and their clinical relevance in patients with noise-induced hearing loss," *International Journal of Clinical and Experimental Pathology*, vol. 8, no. 3, pp. 2852–2863, 2015.

- [10] H. Liu, G. Li, J. Lu et al., "Cellular differences in the cochlea of CBA and B6 mice may underlie their difference in susceptibility to hearing loss," *Frontiers in Cellular Neuroscience*, vol. 13, p. 60, 2019.
- [11] B. Pouyatos, C. A. Gearhart, A. Nelson-Miller, S. Fulton, and L. D. Fechter, "Selective vulnerability of the cochlear basal turn to acrylonitrile and noise," *Journal of Toxicology*, vol. 2009, Article ID 908596, 2009.
- [12] W. J. Clerici and L. Yang, "Direct effects of intraperilymphatic reactive oxygen species generation on cochlear function," *Hearing Research*, vol. 101, no. 1-2, pp. 14–22, 1996.
- [13] N. Dehne, J. Lautermann, W. J. F. ten Cate, U. Rauhen, and H. de Groot, "In vitro effects of hydrogen peroxide on the cochlear neurosensory epithelium of the guinea pig," *Hearing Research*, vol. 143, no. 1-2, pp. 162–170, 2000.
- [14] S. H. Sha, R. Taylor, A. Forge, and J. Schacht, "Differential vulnerability of basal and apical hair cells is based on intrinsic susceptibility to free radicals," *Hearing Research*, vol. 155, no. 1-2, pp. 1–8, 2001.
- [15] M. Qi, Y. Qiu, X. Zhou et al., "Regional up-regulation of NOX2 contributes to the differential vulnerability of outer hair cells to neomycin," *Biochemical and Biophysical Research Communications*, vol. 500, no. 2, pp. 110–116, 2018.
- [16] Z. H. He, S. Y. Zou, M. Li et al., "The nuclear transcription factor FoxG1 affects the sensitivity of mimetic aging hair cells to inflammation by regulating autophagy pathways," *Redox Biology*, vol. 28, p. 101364, 2020.
- [17] W. Liu, X. Xu, Z. Fan et al., "Wnt signaling activates TP53-induced glycolysis and apoptosis regulator and protects against cisplatin-induced spiral ganglion neuron damage in the mouse cochlea," *Antioxidants & Redox Signaling*, vol. 30, no. 11, pp. 1389–1410, 2019.
- [18] L. Liu, Y. Chen, J. Qi et al., "Wnt activation protects against neomycin-induced hair cell damage in the mouse cochlea," *Cell death & disease*, vol. 7, no. 3, p. e2136, 2016.
- [19] M. E. Murphy, "The HSP70 family and cancer," *Carcinogenesis*, vol. 34, no. 6, pp. 1181–1188, 2013.
- [20] Y. Chen, L. Li, W. Ni et al., "Bmi1 regulates auditory hair cell survival by maintaining redox balance," *Cell death & disease*, vol. 6, no. 1, p. e1605, 2015.
- [21] X. Lu, S. Sun, J. Qi et al., "Bmi1 regulates the proliferation of cochlear supporting cells via the canonical Wnt signaling pathway," *Molecular Neurobiology*, vol. 54, no. 2, pp. 1326–1339, 2017.
- [22] X. Li, X. B. Mao, R. Y. Hei et al., "Protective role of hydrogen sulfide against noise-induced cochlear damage: a chronic intracochlear infusion model," *PLoS one*, vol. 6, no. 10, p. e26728, 2011.
- [23] Y. X. Wu, G. X. Zhu, X. Q. Liu et al., "Noise alters guinea pig's blood-labyrinth barrier ultrastructure and permeability along with a decrease of cochlear claudin-5 and occludin," *BMC Neuroscience*, vol. 15, no. 1, p. 136, 2014.
- [24] X. Liu, G. Zheng, Y. Wu et al., "Lead exposure results in hearing loss and disruption of the cochlear blood-labyrinth barrier and the protective role of iron supplement," *Neurotoxicology*, vol. 39, pp. 173–181, 2013.
- [25] M. Muller, "Frequency representation in the rat cochlea," *Hearing Research*, vol. 51, no. 2, pp. 247–254, 1991.
- [26] Z. J. Ding, X. Chen, X. X. Tang et al., "Calpain inhibitor PD150606 attenuates glutamate induced spiral ganglion neuron apoptosis through apoptosis inducing factor pathway in vitro," *PLoS one*, vol. 10, no. 4, p. e0123130, 2015.
- [27] W. Liu, Z. Fan, Y. Han, D. Zhang, J. Li, and H. Wang, "Intranuclear localization of apoptosis-inducing factor and endonuclease G involves in peroxynitrite-induced apoptosis of spiral ganglion neurons," *Neurological Research*, vol. 34, no. 10, pp. 915–922, 2012.
- [28] Z.-J. Ding, X. Chen, X.-X. Tang et al., "Apoptosis-inducing factor and calpain upregulation in glutamate-induced injury of rat spiral ganglion neurons," *Molecular Medicine Reports*, vol. 12, no. 2, pp. 1685–1692, 2015.
- [29] C. Zhu, C. Cheng, Y. Wang et al., "Loss of ARHGGEF6 causes hair cell stereocilia deficits and hearing loss in mice," *Frontiers in Molecular Neuroscience*, vol. 11, p. 362, 2018.
- [30] Y. Wang, J. Li, X. Yao et al., "Loss of CIB2 causes profound hearing loss and abolishes mechano-electrical transduction in mice," *Frontiers in Molecular Neuroscience*, vol. 10, p. 401, 2017.
- [31] J. Qi, L. Zhang, F. Tan et al., "Espn distribution as revealed by super-resolution microscopy of stereocilia," *American Journal of Translational Research*, vol. 12, no. 1, pp. 130–141, 2020.
- [32] J. Qi, Y. Liu, C. Chu et al., "A cytoskeleton structure revealed by super-resolution fluorescence imaging in inner ear hair cells," *Cell Discovery*, vol. 5, no. 1, p. 12, 2019.
- [33] S. Gao, C. Cheng, M. Wang et al., "Blebbistatin inhibits neomycin-induced apoptosis in hair cell-like HEI-OC-1 cells and in cochlear hair cells," *Frontiers in Cellular Neuroscience*, vol. 13, p. 590, 2020.
- [34] Y. Zhang, W. Li, Z. He et al., "Pre-treatment with fasudil prevents neomycin-induced hair cell damage by reducing the accumulation of reactive oxygen species," *Frontiers in Molecular Neuroscience*, vol. 12, p. 264, 2019.
- [35] H. Li, Y. Song, Z. He et al., "Meclofenamic acid reduces reactive oxygen species accumulation and apoptosis, inhibits excessive autophagy, and protects hair cell-like HEI-OC1 cells from cisplatin-induced damage," *Frontiers in Cellular Neuroscience*, vol. 12, p. 139, 2018.
- [36] Z. He, L. Guo, Y. Shu et al., "Autophagy protects auditory hair cells against neomycin-induced damage," *Autophagy*, vol. 13, no. 11, pp. 1884–1904, 2017.
- [37] Z. He, Q. Fang, H. Li et al., "The role of FOXG1 in the postnatal development and survival of mouse cochlear hair cells," *Neuropharmacology*, vol. 144, pp. 43–57, 2019.
- [38] S. Zhang, Y. Zhang, Y. Dong et al., "Knockdown of Foxg1 in supporting cells increases the trans-differentiation of supporting cells into hair cells in the neonatal mouse cochlea," *Cellular and Molecular Life Sciences*, vol. 77, no. 7, pp. 1401–1419, 2020.
- [39] C. Cheng, Y. Wang, L. Guo et al., "Age-related transcriptome changes in Sox2+ supporting cells in the mouse cochlea," *Stem cell research & therapy*, vol. 10, no. 1, p. 365, 2019.
- [40] D. You, L. Guo, W. Li et al., "Characterization of Wnt and Notch-responsive Lgr5+ hair cell progenitors in the striolar region of the neonatal mouse utricle," *Frontiers in Molecular Neuroscience*, vol. 11, p. 137, 2018.
- [41] Y. Chen, X. Lu, L. Guo et al., "Hedgehog signaling promotes the proliferation and subsequent hair cell formation of progenitor cells in the neonatal mouse cochlea," *Frontiers in Molecular Neuroscience*, vol. 10, p. 426, 2017.
- [42] Y. He, X. Lu, F. Qian, D. Liu, R. Chai, and H. Li, "Insm1a is required for zebrafish posterior lateral line development," *Frontiers in Molecular Neuroscience*, vol. 10, p. 241, 2017.

- [43] M. Tang, J. Li, L. He et al., "Transcriptomic profiling of neural stem cell differentiation on graphene substrates," *Colloids and surfaces. B, Biointerfaces*, vol. 182, p. 110324, 2019.
- [44] G. Li, K. Chen, D. You et al., "Laminin-coated electrospun regenerated silk fibroin mats promote neural progenitor cell proliferation, differentiation, and survival in vitro," *Frontiers in Bioengineering and Biotechnology*, vol. 7, p. 190, 2019.
- [45] Q. Fang, Y. Zhang, X. Chen et al., "Three-dimensional graphene enhances neural stem cell proliferation through metabolic regulation," *Frontiers in Bioengineering and Biotechnology*, vol. 7, p. 436, 2020.
- [46] S. Han, J. Sun, S. He, M. Tang, and R. Chai, "The application of graphene-based biomaterials in biomedicine," *American Journal of Translational Research*, vol. 11, no. 6, pp. 3246–3260, 2019.
- [47] W. Yan, W. Liu, J. Qi et al., "A three-dimensional culture system with Matrigel promotes purified spiral ganglion neuron survival and function in vitro," *Molecular Neurobiology*, vol. 55, no. 3, pp. 2070–2084, 2018.
- [48] G. Sun, W. Liu, Z. Fan et al., "The three-dimensional culture system with Matrigel and neurotrophic factors preserves the structure and function of spiral ganglion neuron in vitro," *Neural Plasticity*, vol. 2016, Article ID 4280407, 15 pages, 2016.
- [49] S. Han, Y. Xu, J. Sun et al., "Isolation and analysis of extracellular vesicles in a morpho butterfly wing-integrated microvortex biochip," *Biosensors & Bioelectronics*, vol. 154, p. 112073, 2020.
- [50] B. C. Cox, R. Chai, A. Lenoir et al., "Spontaneous hair cell regeneration in the neonatal mouse cochlea in vivo," *Development*, vol. 141, no. 4, pp. 816–829, 2014.
- [51] Y. Zhang, L. Guo, X. Lu et al., "Characterization of Lgr6+ cells as an enriched population of hair cell progenitors compared to Lgr5+ cells for hair cell generation in the neonatal mouse cochlea," *Frontiers in Molecular Neuroscience*, vol. 11, p. 147, 2018.
- [52] S. Zhang, Y. Zhang, P. Yu et al., "Characterization of Lgr5+ progenitor cell transcriptomes after neomycin injury in the neonatal mouse cochlea," *Frontiers in Molecular Neuroscience*, vol. 10, p. 213, 2017.
- [53] C. Cheng, L. Guo, L. Lu et al., "Characterization of the transcriptomes of Lgr5+ hair cell progenitors and Lgr5- supporting cells in the mouse cochlea," *Frontiers in Molecular Neuroscience*, vol. 10, p. 122, 2017.
- [54] J. Wu, W. Li, C. Lin et al., "Co-regulation of the Notch and Wnt signaling pathways promotes supporting cell proliferation and hair cell regeneration in mouse utricles," *Scientific Reports*, vol. 6, no. 1, p. 29418, 2016.
- [55] T. Wang, R. Chai, G. S. Kim et al., "Lgr5+ cells regenerate hair cells via proliferation and direct transdifferentiation in damaged neonatal mouse utricle," *Nature Communications*, vol. 6, no. 1, p. 6613, 2015.
- [56] R. D. Kopke, J. K. M. Coleman, J. Liu, K. C. M. Campbell, and R. H. Riffenburgh, "Candidate's thesis: enhancing intrinsic cochlear stress defenses to reduce noise-induced hearing loss," *The Laryngoscope*, vol. 112, no. 9, pp. 1515–1532, 2002.
- [57] B. Canlon and A. Fransson, "Morphological and functional preservation of the outer hair cells from noise trauma by sound conditioning," *Hearing Research*, vol. 84, no. 1-2, pp. 112–124, 1995.
- [58] L. W. Henselman, D. Henderson, M. Subramaniam, and V. Sallustio, "The effect of 'conditioning' exposures on hearing loss from impulse noise," *Hearing Research*, vol. 78, no. 1, pp. 1–10, 1994.
- [59] N. Yoshida and M. C. Liberman, "Sound conditioning reduces noise-induced permanent threshold shift in mice," *Hearing Research*, vol. 148, no. 1-2, pp. 213–219, 2000.
- [60] E. B. Bertelsen, L. Chang, J. E. Gestwicki, and E. R. P. Zuiderweg, "Solution conformation of wild-type E. coli Hsp70 (DnaK) chaperone complexed with ADP and substrate," *Proceedings of the National Academy of Sciences of the United States of America*, vol. 106, no. 21, pp. 8471–8476, 2009.
- [61] P. Bork, C. Sander, and A. Valencia, "An ATPase domain common to prokaryotic cell cycle proteins, sugar kinases, actin, and hsp70 heat shock proteins," *Proceedings of the National Academy of Sciences of the United States of America*, vol. 89, no. 16, pp. 7290–7294, 1992.
- [62] K. M. Flaherty, C. DeLuca-Flaherty, and D. B. McKay, "Three-dimensional structure of the ATPase fragment of a 70K heat-shock cognate protein," *Nature*, vol. 346, no. 6285, pp. 623–628, 1990.
- [63] X. Zhu, X. Zhao, W. F. Burkholder et al., "Structural analysis of substrate binding by the molecular chaperone DnaK," *Science*, vol. 272, no. 5268, pp. 1606–1614, 1996.
- [64] L. L. Cunningham and C. S. Brandon, "Heat shock inhibits both aminoglycoside- and cisplatin-induced sensory hair cell death," *Journal of the Association for Research in Otolaryngology*, vol. 7, no. 3, pp. 299–307, 2006.
- [65] S. P. Francis, I. I. Kramarenko, C. S. Brandon, F. S. Lee, T. G. Baker, and L. L. Cunningham, "Celastrol inhibits aminoglycoside-induced ototoxicity via heat shock protein 32," *Cell death & disease*, vol. 2, no. 8, p. e195, 2011.
- [66] L. A. May, I. I. Kramarenko, C. S. Brandon et al., "Inner ear supporting cells protect hair cells by secreting HSP70," *The Journal of Clinical Investigation*, vol. 123, no. 8, pp. 3577–3587, 2013.
- [67] M. Taleb, C. S. Brandon, F. S. Lee, M. I. Lomax, W. H. Dillmann, and L. L. Cunningham, "Hsp70 inhibits aminoglycoside-induced hair cell death and is necessary for the protective effect of heat shock," *Journal of the Association for Research in Otolaryngology : JARO*, vol. 9, no. 3, pp. 277–289, 2008.
- [68] M. Taleb, C. S. Brandon, F. S. Lee, K. C. Harris, W. H. Dillmann, and L. L. Cunningham, "Hsp70 inhibits aminoglycoside-induced hearing loss and cochlear hair cell death," *Cell Stress & Chaperones*, vol. 14, no. 4, pp. 427–437, 2009.
- [69] M. A. Gratton, A. Eleftheriadou, J. Garcia et al., "Noise-induced changes in gene expression in the cochleae of mice differing in their susceptibility to noise damage," *Hearing Research*, vol. 277, no. 1-2, pp. 211–226, 2011.
- [70] H. Ninomiya, N. Ohgami, R. Oshino et al., "Increased expression level of Hsp70 in the inner ears of mice by exposure to low frequency noise," *Hearing Research*, vol. 363, pp. 49–54, 2018.
- [71] I. Meltser and B. Canlon, "Protecting the auditory system with glucocorticoids," *Hearing Research*, vol. 281, no. 1-2, pp. 47–55, 2011.
- [72] Y. Tahera, I. Meltser, P. Johansson, H. Salman, and B. Canlon, "Sound conditioning protects hearing by activating the hypothalamic-pituitary-adrenal axis," *Neurobiology of Disease*, vol. 25, no. 1, pp. 189–197, 2007.
- [73] N. Yoshida, A. Kristiansen, and M. C. Liberman, "Heat stress and protection from permanent acoustic injury in mice," *The Journal of Neuroscience*, vol. 19, no. 22, pp. 10116–10124, 1999.

- [74] M. Yu, T. Mazor, H. Huang et al., "Direct recruitment of polycomb repressive complex 1 to chromatin by core binding transcription factors," *Molecular Cell*, vol. 45, no. 3, pp. 330–343, 2012.
- [75] M. Abdouh, W. Chato, J. El Hajjar, J. David, J. Ferreira, and G. Bernier, "Bmi1 is down-regulated in the aging brain and displays antioxidant and protective activities in neurons," *PLoS one*, vol. 7, no. 2, p. e31870, 2012.
- [76] W. Chato, M. Abdouh, J. David et al., "The polycomb group gene Bmi1 regulates antioxidant defenses in neurons by repressing p53 pro-oxidant activity," *The Journal of Neuroscience*, vol. 29, no. 2, pp. 529–542, 2009.
- [77] J. Liu, L. Cao, J. Chen et al., "Bmi1 regulates mitochondrial function and the DNA damage response pathway," *Nature*, vol. 459, no. 7245, pp. 387–392, 2009.
- [78] A. Rizo, S. Olthof, L. Han, E. Vellenga, G. de Haan, and J. J. Schuringa, "Repression of BMI1 in normal and leukemic human CD34(+) cells impairs self-renewal and induces apoptosis," *Blood*, vol. 114, no. 8, pp. 1498–1505, 2009.
- [79] S. Nakamura, M. Oshima, J. Yuan et al., "Bmi1 confers resistance to oxidative stress on hematopoietic stem cells," *PLoS one*, vol. 7, no. 5, p. e36209, 2012.
- [80] Q. Dong, J. E. Oh, W. Chen et al., "Radioprotective effects of Bmi-1 involve epigenetic silencing of oxidase genes and enhanced DNA repair in normal human keratinocytes," *The Journal of Investigative Dermatology*, vol. 131, no. 6, pp. 1216–1225, 2011.
- [81] L. O. Klotz, C. Sanchez-Ramos, I. Prieto-Arroyo, P. Urbanek, H. Steinbrenner, and M. Monsalve, "Redox regulation of FoxO transcription factors," *Redox Biology*, vol. 6, pp. 51–72, 2015.
- [82] W. He, A. Zhang, L. Qi et al., "FOXO1, a potential therapeutic target, regulates autophagic flux, oxidative stress, mitochondrial dysfunction, and apoptosis in human cholangiocarcinoma QBC939 cells," *Cellular Physiology and Biochemistry*, vol. 45, no. 4, pp. 1506–1514, 2018.
- [83] F. Stephani, V. Scheuer, T. Eckrich et al., "Deletion of the Ca²⁺ channel subunit $\alpha 2\delta 3$ differentially affects Cav2.1 and Cav2.2 currents in cultured spiral ganglion neurons before and after the onset of hearing," *Frontiers in Cellular Neuroscience*, vol. 13, p. 278, 2019.

Research Article

Altered Brain Activity and Functional Connectivity in Unilateral Sudden Sensorineural Hearing Loss

Jiawei Chen,¹ Bo Hu,² Peng Qin,³ Wei Gao,¹ Chengcheng Liu,¹ Dingjing Zi,¹ Xuerui Ding,¹ Ying Yu,² Guangbin Cui^{ID},² and Lianjun Lu^{ID}¹

¹Department of Otolaryngology Head and Neck Surgery, Tangdu Hospital, Fourth Military Medical University, Xi'an 710038, China

²Department of Radiology & Functional and Molecular Imaging Key Lab of Shaanxi Province, Tangdu Hospital, Fourth Military Medical University, Xi'an 710038, China

³Student Brigade, Fourth Military Medical University, Xi'an 710032, China

Correspondence should be addressed to Guangbin Cui; cuibtd@fmmu.edu.cn and Lianjun Lu; lulianj@fmmu.edu.cn

Jiawei Chen, Bo Hu, and Peng Qin contributed equally to this work.

Received 24 March 2020; Revised 4 August 2020; Accepted 18 August 2020; Published 22 September 2020

Academic Editor: Jian Wang

Copyright © 2020 Jiawei Chen et al. This is an open access article distributed under the Creative Commons Attribution License, which permits unrestricted use, distribution, and reproduction in any medium, provided the original work is properly cited.

Background. Sudden sensorineural hearing loss (SSNHL) is an otologic emergency and could lead to social difficulties and mental disorders in some patients. Although many studies have analyzed altered brain function in populations with hearing loss, little information is available about patients with idiopathic SSNHL. This study is aimed at investigating brain functional changes in SSNHL via functional magnetic resonance imaging (fMRI). **Methods.** Thirty-six patients with SSNHL and thirty well-matched normal hearing individuals underwent resting-state fMRI. Amplitude of low-frequency fluctuation (ALFF), fractional ALFF (fALFF), and functional connectivity (FC) values were calculated. **Results.** In the SSNHL patients, ALFF and fALFF were significantly increased in the bilateral putamen but decreased in the right calcarine cortex, right middle temporal gyrus (MTG), and right precentral gyrus. Widespread increases in FC were observed between brain regions, mainly including the bilateral auditory cortex, bilateral visual cortex, left striatum, left angular gyrus (AG), bilateral precuneus, and bilateral limbic lobes in patients with SSNHL. No decreased FC was observed. **Conclusion.** SSNHL causes functional alterations in brain regions, mainly in the striatum, auditory cortex, visual cortex, MTG, AG, precuneus, and limbic lobes within the acute period of hearing loss.

1. Introduction

Hearing loss is one of the most common sensory disorders in the world. According to the World Health Organization, there are approximately 470 million patients with disabling hearing loss worldwide [1]. Sudden sensorineural hearing loss (SSNHL) is an otologic emergency that is defined as a sensorineural hearing decline of ≥ 30 dB in at least three consecutive frequencies in the pure-tone audiogram within 72 hours [2]. SSNHL is usually unilateral, with bilateral involvement accounting for less than 5% of the cases [3]. Recent population-based studies reported that the incidence of

SSNHL ranges from 5 to 27 per 100,000 with a rapidly increasing annual incidence [4, 5]. The inner ear hair cells are mainly responsible for transducing sound vibrations into electrical impulses, and then these electrical signals are transmitted by spiral ganglion neurons (SGNs) into the brainstem to have the hearing function [6–10]. Thus, most cases of hearing loss are due to the damage or malfunction of hair cells or SGNs, both of which are sensitive and vulnerable to noise, aminoglycosides, chemotherapy regimens, inflammation, biological aging, and genetic defects [11–17]. Although some pathophysiological hypotheses have been proposed, the exact mechanisms of SSNHL remain unclear. Moreover,

most of the studies on SSNHL focused on the hair cells and SGNs, while the alterations in the intensity and synchronization of brain activity after SSNHL have rarely been investigated. Auditory deprivation may impose a substantial socioeconomic burden on patients. Those who do not recover normal hearing have difficulties in sound localization and social communication, which may cause potentially mental disorders such as anxiety and depression [18, 19]. Therefore, studies that are aimed at elucidating the changes and underlying mechanisms of higher-order brain functions in deaf individuals are necessary.

Previous studies have reported alterations in the activity and functional organization of the cerebral cortex in subjects with unilateral hearing loss (UHL). Patients with long-term unilateral hearing impairment exhibited altered connectivity with other sensory and higher-order networks within and beyond the auditory network, reflecting a cross-modal functional reorganization in UHL [20]. Plasticity of the cortical tonotopic map within the primary auditory cortex has also been observed in patients with unilateral sensorineural hearing loss and tinnitus [21]. Another connectome analysis showed altered connections and nodal centrality in several brain functional networks in patients with UHL caused by acoustic neuromas [22]. These studies showed evidence of cortical functional reorganization following UHL. However, there have been limited studies [23, 24] available on the differences in brain function between unilateral SSNHL patients and normal hearing people. The changes in cortical activity and functional organization following SSNHL remain largely unknown.

Functional magnetic resonance imaging (fMRI) is a non-invasive technique for investigating the changes in brain function in many disorders, which could provide valuable information for elucidating the pathogenesis and guiding clinical practice. Based on the blood-oxygenation-level-dependent (BOLD) signals, fMRI has been reported to reflect underlying neuronal activity [25]. Analyses of the amplitude of low-frequency fluctuations (ALFF) and functional connectivity (FC) are two important methods used in fMRI studies. ALFF is defined as the amplitude of brain BOLD signal fluctuations in the low-frequency range (0.01-0.08 Hz), which could reflect the spontaneous neuronal activity of the cerebral cortex [26]. The analysis of FC calculates the temporal correlation of BOLD signal fluctuations between spatially remote brain regions. Positive FC indicates activity synchronization and functional correlation between two voxels or brain areas [27]. These two methods have been widely applied to explore alterations in the activity and organization of the brain in hearing loss and other diseases, including depressive disorder, Alzheimer's disease, and schizophrenia [28–32]. Analyses of ALFF and FC simultaneously allow researchers to explore the synchronization between brain regions and the activation of each brain region. Although a large number of fMRI studies have been performed in individuals with UHL, the changes in cortical function during the acute period of SSNHL have rarely been investigated.

To address these questions, we conducted ALFF, fractional ALFF (fALFF), and FC analyses with resting-state fMRI in patients with SSNHL and normal hearing people.

We hypothesized that SSNHL would change the intensity and synchronization of cerebral activity.

2. Materials and Methods

2.1. Participants. Thirty-six patients with mild to profound unilateral SSNHL were recruited from the Department of Otolaryngology Head and Neck Surgery of Tangdu Hospital. Patients with UHL ≥ 30 dB in at least three consecutive frequencies within 72 hours were diagnosed with unilateral SSNHL according to the 2019 Sudden Hearing Loss Clinical Practice Guideline of the American Academy of Otolaryngology-Head and Neck Surgery Foundation (AAO-HNSF) [2]. Pure-tone audiometry was performed to calculate the pure-tone average (PTA) and assess hearing thresholds. Thirty sex- and age-matched normal hearing participants were recruited from the local community. The exclusion criteria included conductive hearing loss, Ménière's disease, acute or chronic otitis media, and central nervous system disorders such as brain trauma, tumors, and cerebrovascular disease. The data from scans of six SSNHL participants were excluded for excessive head movement. Finally, 30 unilateral SSNHL and 30 healthy control (HC) participants were recruited in our study. All the SSNHL and HC participants were right-handed. All the participants provided written informed consent, and the study protocol was approved by the ethics committee of Tangdu Hospital of the Air Force Medical University. Intergroup comparisons of age and body mass index (BMI) were conducted using two-tailed, two-sample Student's *t*-tests with SPSS 23 software (IBM, Armonk, NY, USA). In SSNHL patients, the differences in PTA before and after treatment were compared using two-tailed, paired-sample Student's *t*-tests. The significance level was set at $p < 0.05$.

2.2. MRI Data Acquisition. The MRI data were acquired before patients received any treatment. MRI scans were performed at the Radiology Department of Tangdu Hospital using a GE Discovery MR750 3.0T scanner (General Electric Healthcare Systems, Boston, MA, USA) with an eight-channel phased-array head coil. Foam paddings were used to restrict head motion, and ear plugs were used to reduce scanner noise. During the data acquisition period, the participants were told to stay awake with their eyes closed in the scanner. Structural images including high-resolution T1-weighted images were acquired by using a three-dimensional brain volume (3D-BRAVO) sequence with the following parameters: echo time (TE) = 3.2 ms, inversion time (TI) = 450 ms, repetition time (TR) = 8.2 ms, flip angle (FA) = 12°, field of view (FOV) = 256 × 256 mm², acquisition matrix = 256 × 256, slice thickness = 1.0 mm, and slice number = 188.

BOLD images were acquired by using a gradient-recalled echo-echo-planar imaging (GRE-EPI) sequence with the following parameters: TE = 30 ms, TR = 2000 ms, time points = 185, FA = 90°, FOV = 220 × 220 mm², acquisition matrix = 64 × 64, slice thickness = 3 mm, slice number = 36, interslice gaps = 4 mm, and in-plane spatial resolution = 3.4375 × 3.4375 mm².

TABLE 1: Demographic and clinical information of the SSNHL patients and HC individuals.

	SSNHL	HC	<i>p</i> value
Number (<i>n</i>)	30	30	—
Sex (male/female)	16/14	16/14	—
Age (year)	43.43 ± 14.62	42.57 ± 11.47	0.799
BMI (kg/m ²)	24.15 ± 3.89	23.96 ± 2.70	0.827
Side of hearing loss (left/right)	13/17	—	—
Hearing loss duration (day)	11.60 ± 9.64	—	—
PTA of affected ear (dB HL)			
Before treatment	87.80 ± 29.32*	—	—
After treatment	72.80 ± 36.01*	—	<0.001
PTA of unaffected ear (dB HL)			
Before treatment	18.70 ± 11.51*	—	—
After treatment	15.17 ± 6.28*	—	0.043

All data are presented as the mean ± SD. Data with asterisks were compared with paired-sample Student's *t*-test methods. BMI: body mass index; PTA: pure-tone average.

2.3. MRI Data Preprocessing. Functional MRI data were preprocessed using Data Processing and Analysis for Brain Imaging (DPABI) [33] and Statistical Parametric Mapping (SPM12) software (<https://www.fil.ion.ucl.ac.uk/spm/software/spm12/>) in the MATLAB R2014a platform (MATLAB 2014a, Mathworks, Inc, Natick, MA). The first 10 time points were discarded. The remaining images underwent a preprocessing procedure including slice timing and head motion correction, normalization to the Montreal Neurological Institute (MNI) space, linear trend removal, nuisance covariate regression, bandpass filtering (0.01-0.08 Hz), and smoothing with a 6 mm full width at half maximum (FWHM) isotropic Gaussian kernel. Any image with head motion > 3 mm translation or 3° rotation in any direction was excluded.

2.4. ALFF and fALFF Analysis. ALFF and fALFF were analyzed using the Data Processing Assistant for Resting-State fMRI (DPARSF) software [34]. The time series were converted into the frequency domain to obtain the power spectrum. ALFF was obtained by calculating the mean square root of the power spectrum of the signal with a frequency window of 0.01-0.08 Hz. To obtain the fALFF, the ratio of the power spectrum across 0.01-0.08 Hz to that across the entire frequency range was calculated. The ALFF and fALFF values were compared between the SSNHL and HC groups using two-tailed, two-sample Student's *t*-test with SPM12 software after regressing out nuisance covariates including sex, age, and BMI. Gaussian random field (GRF) correction for multiple comparisons was used, because it corrects the false positive rate at both the voxel and cluster levels. The significance levels were set at voxel < 0.005 and cluster < 0.025, as one recent study showed that this level effectively reduced the false positive rate below 0.05 [35].

2.5. Voxel-Wise FC Analysis. FC analysis was performed using SPM12 and RESTing-state fMRI data analysis Toolkit (REST 1.6) [36]. Forty-four of the 112 brain regions in the

Harvard-Oxford Atlas were selected as regions of interest (ROIs). The mean time series signal of each brain region was calculated. Correlation coefficients were calculated between the mean time series signal of each ROI and that of voxels across the whole brain. The correlation coefficients of each voxel were Z-scored to improve normality. Then, the resulting values of all voxels were compared between the SSNHL and HC groups to identify the brain areas with significant differences in FC. GRF was used for multiple comparison corrections. The results were visualized based on the Ch2 brain template using DPABI software.

2.6. ROI-Wise FC Analysis. Correlation coefficients between 44 selected ROIs and all 112 brain regions in the Harvard-Oxford Atlas for each participant were transformed with the Fisher's *r* to *z* method. Using SPSS 23 software, intergroup comparisons were performed with one-way ANOVA and the post hoc Dunnett's *t*-test. Multiple comparisons were corrected with both false discovery rate (FDR) and network-based statistic (NBS) methods [37]. The significance level was set at *p* < 0.05. FC with intergroup significant differences was visualized using BrainNet Viewer software [38].

3. Results

3.1. Demographic and Clinical Information. The demographic and clinical information of both groups are presented in Table 1. There were no significant differences in age or BMI between the SSNHL and HC groups. In patients with SSNHL, an average of 15 dB HL improvement was observed in the PTA of the affected ear after treatment. The difference in the PTA of the affected ear before and after treatment was significant (*p* < 0.001). The significant difference (*p* = 0.043) in the PTA of the unaffected ear before and after treatment may come from the measurement deviation of the pure-tone audiometry test.

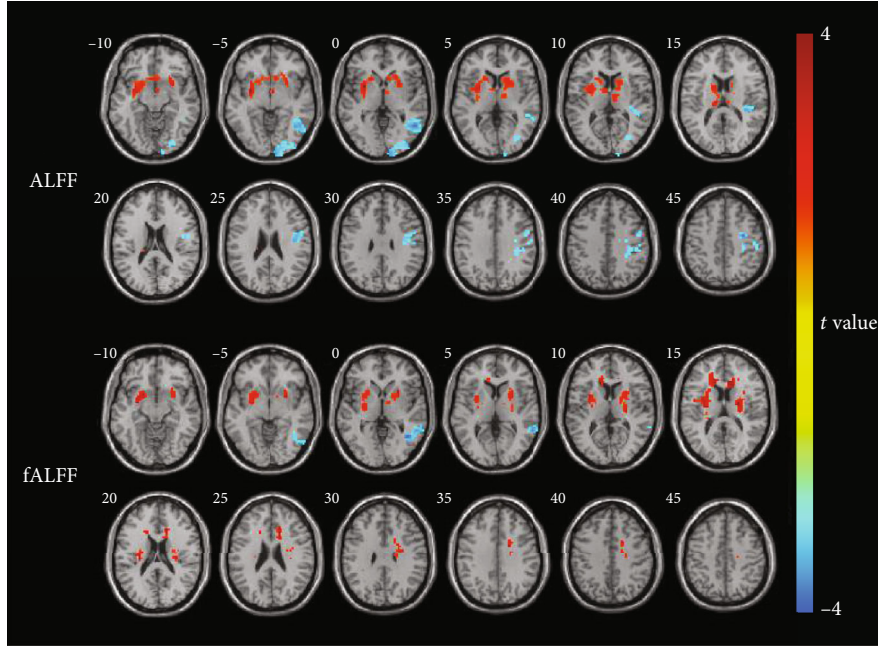


FIGURE 1: Intergroup comparison of ALFF and fALFF between the SSNHL and HC groups. The ALFF value of the SSNHL group was significantly increased in a cluster located in the left putamen but was decreased in three clusters located in the right calcarine cortex, right MTG, and right precentral gyrus compared with the HC group. The fALFF value in the SSNHL group was significantly increased in two clusters located in the right and left putamen but was decreased in a cluster located in the right MTG. Significantly increased ALFF or fALFF values are indicated in red, while significantly decreased ALFF or fALFF values are indicated in blue.

TABLE 2: The peak MNI coordinates and intensity of brain clusters with significant intergroup differences in ALFF and fALFF.

	Brain region	MNI coordinates $x, y,$ and z			Number of voxels	Peak intensity
Increased ALFF	L putamen	-30	6	0	707	4.953
	R calcarine cortex	12	-99	-3	194	-3.830
Decreased ALFF	R middle temporal gyrus	51	-57	-3	205	-4.452
	R precentral gyrus	30	-9	42	209	-4.392
Increased fALFF	R putamen	27	-12	18	372	4.528
	L putamen	-30	0	12	362	4.586
Decreased fALFF	R middle temporal gyrus	42	-57	-3	119	-4.131

L: left; R: right.

3.2. Voxel-Wise ALFF and fALFF Analysis. Intergroup comparisons showed differences in ALFF and fALFF between the SSNHL and HC groups (Figure 1). The ALFF value in the SSNHL group, compared with that in the HC group, was significantly increased in a cluster located in the left putamen. The ALFF value was significantly decreased in three clusters located in the right calcarine cortex, right middle temporal gyrus (MTG), and right precentral gyrus. fALFF values were significantly increased in two clusters located in the right and left putamen. The fALFF value was significantly decreased in a cluster located in the right MTG. The peak MNI coordinates and peak intensities of these clusters are presented in Table 2.

3.3. Voxel-Wise FC Analysis. Among the intergroup comparisons, we found 9 ROIs with significantly increased FC with other brain clusters in the SSNHL group (Figure 2). No

decreased FC was observed. Compared with the HC group, the SSNHL group showed increased FC mainly between the bilateral auditory cortices and left striatum, the left visual cortex and left striatum, the right MTG and bilateral visual cortices, and the bilateral lingual gyri (LG) and left middle frontal gyrus (MFG). The peak intensity and MNI coordinates of these clusters are presented in Table 3.

3.4. ROI-Wise FC Analysis. Compared with the HC group, significantly increased FCs were observed in the SSNHL group between the left angular gyrus (LAG) and the left supracalcarine cortex (ISCLC) (Figures 3(a) and 3(c)), as well as between the posterior division of the left parahippocampal gyrus (IPHG.p) and ROIs mainly located in the bilateral temporal lobes and the left frontal lobe (Figures 3(b) and 3(c)).

To further investigate the brain functional alterations after hearing loss on different sides, the SSNHL patients were then

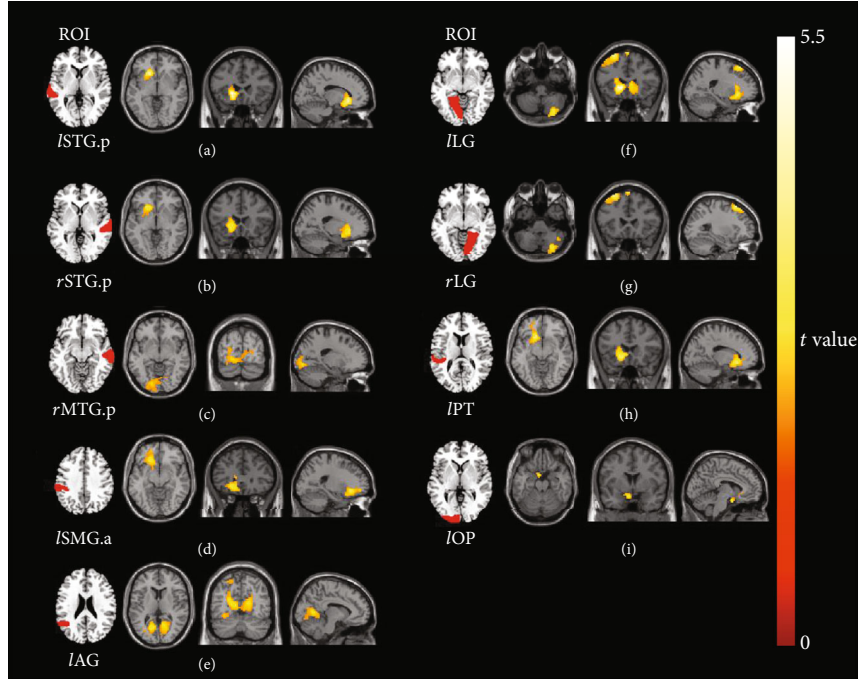


FIGURE 2: Intergroup comparisons of voxel-wise FC between the SSNHL and HC groups. Compared with the HC group, the SSNHL group showed significantly increased voxel-wise FC values in nine ROIs, including (a) the *lSTG.p* and a cluster located in the left putamen and left caudate nucleus, (b) the *rSTG.p* and a cluster located in the left putamen and left caudate nucleus, (c) the *rMTG.p* and a cluster located in the bilateral lingual gyri and the right calcarine cortex, (d) the *lSMG.a* and a cluster located in the left inferior frontal gyrus, (e) the *lAG* and a cluster located in the bilateral calcarine cortex and left posterior cingulate cortex, (f) the *lLG* and three clusters located in the right cerebellum posterior lobe, left caudate nucleus, and left MFG, (g) the *rLG* and two clusters located in the right cerebellum posterior lobe and left MFG, (h) the *lPT* and a cluster located in the left caudate nucleus and left putamen, and (i) the *lOP* and a cluster located in the left caudate nucleus and left putamen. The color bar indicates the *t*-value of voxels with significant intergroup differences. STG: superior temporal gyrus; MTG: middle temporal gyrus; SMG: supramarginal gyrus; AG: angular gyrus; LG: lingual gyrus; PT: planum temporale; OP: occipital pole; *l*: left; *r*: right; *a*: anterior division; *p*: posterior division.

TABLE 3: The peak MNI coordinates and intensity of brain clusters with significant intergroup differences in voxel-wise FC values.

ROI	Brain region	MNI coordinates <i>x</i> , <i>y</i> , and <i>z</i>			Number of voxels	Peak intensity
<i>lSTG.p</i>	L putamen/L caudate nucleus	-18	24	-3	397	5.174
<i>rSTG.p</i>	L putamen/L caudate nucleus	-15	21	-3	328	4.147
<i>rMTG.p</i>	Bl lingual gyri/R calcarine	-18	-84	-6	700	3.486
<i>lSMG.a</i>	L inferior frontal gyrus	-21	30	-9	535	4.210
<i>lAG</i>	Bl calcarine cortices/L posterior cingulate cortex	-9	-66	9	1042	3.861
<i>lLG</i>	R cerebellum posterior lobe	30	-78	-45	592	4.021
	L caudate nucleus	-12	24	-3	647	5.312
	L middle frontal gyrus	-27	24	60	512	4.634
<i>rLG</i>	R cerebellum posterior lobe	30	-75	-42	590	4.068
	L middle frontal gyrus	-27	24	60	381	4.705
<i>lPT</i>	L caudate nucleus/L putamen	-15	21	-9	364	4.480
<i>lOP</i>	L caudate nucleus/L putamen	-6	3	-21	321	4.147

STG: superior temporal gyrus; MTG: middle temporal gyrus; SMG: supramarginal gyrus; AG: angular gyrus; LG: lingual gyrus; PT: planum temporale; OP: occipital pole; L or *l*: left; R or *r*: right; Bl: bilateral; *a*: anterior division; *p*: posterior division.

divided into the left (L-SSNHL, $n = 13$) and right (R-SSNHL, $n = 17$) hearing loss subgroups for ROI-wise FC analyses. One-way ANOVA and post hoc analyses showed that the L-SSNHL subgroup displayed significantly increased FC

between the *lMTG.to* and bilateral subcallosal cortex (SCC) compared to the HC group (Figure S1).

Moreover, to better match the patients and healthy population, the HC group was also divided into two subgroups

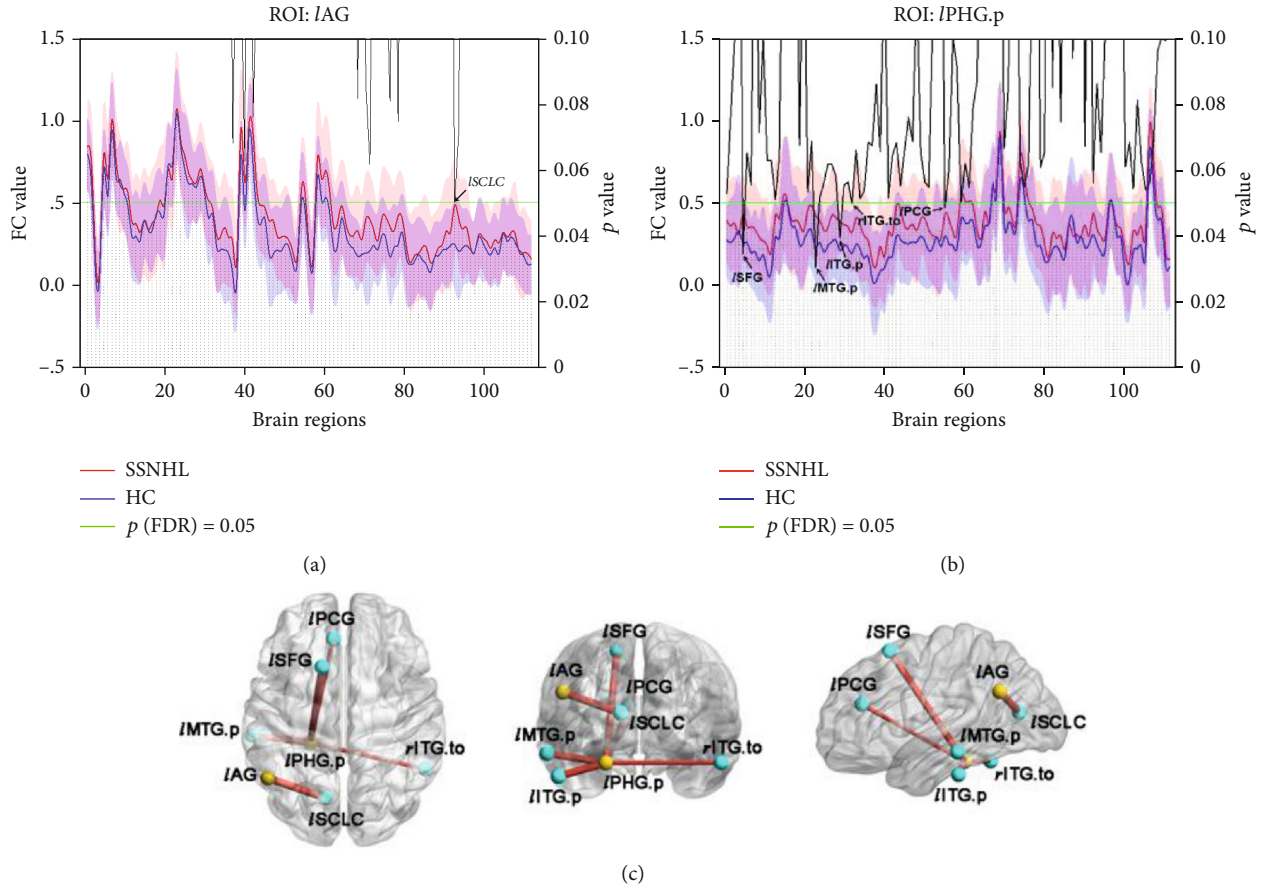


FIGURE 3: Intergroup comparison of ROI-wise FC between the SSNHL and HC groups. FC between the *IAG* and *ISCLC* was significantly increased (a). FCs between the */PHG.p* and ROIs mainly located in the bilateral temporal lobes and left frontal lobe were significantly increased (b). The x-axis coordinates correspond to the numbers of the brain regions in the Harvard-Oxford Atlas. The y-axis coordinates on the left indicate the FC value, while those on the right indicate the p value. The red and blue curves indicate the mean FC values of the pair of ROIs in each group, and the shadow reflects the standard deviations. The black line indicates intergroup differences between each pair of ROIs, with a p value less than 0.05 where the black line is below the green horizontal line. ROI-wise FCs with significant difference between the SSNHL and HC groups are presented in a node and edge graph (c). The yellow balls indicate the seed ROI, while the cyan balls indicate the ROIs with significantly different FC values. The size of the sticks corresponds to the t -values from the two-sample t -tests. SCLC: supracalcarine cortex; PHG: parahippocampal gyrus; SFG: superior frontal gyrus; ITG: inferior temporal gyrus; PCG: paracingulate gyrus; *l*: left; *p*: posterior division; *to*: temporooccipital part.

corresponding to the L-SSNHL and R-SSNHL subgroups, namely HC-1 ($n = 13$) and HC-2 ($n = 17$). Intergroup comparisons were performed between the L-SSNHL and HC-1 subgroups, as well as between the R-SSNHL and HC-2 subgroups using the two-sample t -test. Compared with the HC-1 subgroup, the L-SSNHL subgroup showed significantly increased FCs between the bilateral MTG and ROIs mainly located in the bilateral occipital lobes and the right limbic lobe (Figures 4(a)–4(d) and 5(a)). In addition, increased FCs were observed between the posterior division of the left supramarginal gyrus (*ISMG.p*) and ROIs located in the left parietal lobe (Figures 4(e) and 5(a)). Increased FCs were also observed between the *IAG* and ROIs mainly located in the bilateral frontal lobes, occipital lobes, and limbic lobes (Figures 4(f) and 5(b)).

We noticed that there were some inconsistencies in results derived from one-way ANOVA and two-sample t -test. We further compared the p values before and after FDR correction and found that these inconsistencies were

mainly caused by the setting of the statistical threshold (Tables S1 and S2).

When using the NBS method for the correction of multiple comparisons, FCs were significantly increased between ROIs mainly located in the bilateral temporal lobes (*lMTG.a*, *lMTG.p*, *rMTG.p*, and *lMTG.to*) and occipital lobes (*lLG*, *rLG*, and *rOP*) in the L-SSNHL subgroup compared to the HC-1 subgroup (Figure S2). These results were also similar to those derived from FDR correction. However, SSNHL did not result in decreased FC in the SSNHL group or in the L-SSNHL subgroup. No significant differences were observed between the R-SSNHL and HC-2 subgroups.

4. Discussion

In this study, the patients with SSNHL showed changes in spontaneous neuronal activity and FC in multiple brain regions during the acute period of hearing loss. In the patients with SSNHL, ALFF and fALFF were increased in

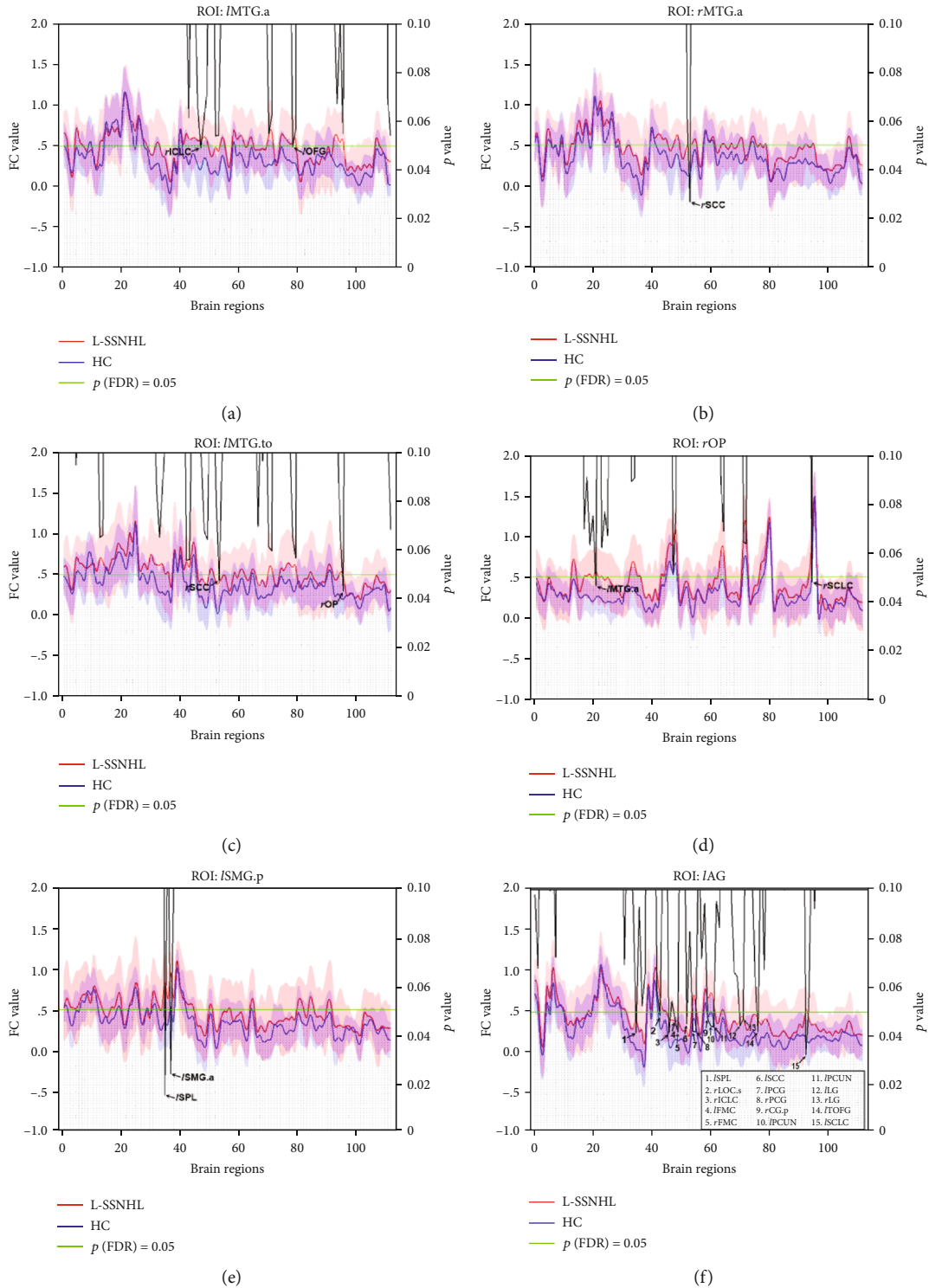


FIGURE 4: Intergroup comparisons of ROI-wise FC between the L-SSNHL and HC-1 subgroups. Compared with the HC-1 subgroup, the L-SSNHL subgroup showed significantly increased FCs between (a) the *l*MTG.a and the *r*ICLC and *l*OFG, (b) the *r*MTG.a and the *r*SCC, (c) the *l*MTG.to and the *r*SCLC and *r*OP, (d) the *r*OP and the *l*MTG.a and *r*SCLC, (e) the *l*SMG.p and the *l*SPL and *l*SMG.a, and (f) the *l*AG and 15 ROIs indicated in the legend. MTG: middle temporal gyrus; OP: occipital pole; SMG: supramarginal gyrus; AG: angular gyrus; ICLC: intracalcarine cortex; OFG: occipital fusiform gyrus; SCC: subcallosal cortex; SCLC: supracalcarine cortex; SPL: superior parietal lobule; LOC: lateral occipital cortex; FMC: frontal medial cortex; PCG: paracingulate gyrus; CG: cingulate gyrus; PCUN: precuneus; LG: lingual gyrus; TOFG: temporal occipital fusiform cortex; *l*: left; *r*: right; a: anterior division; p: posterior division; s: superior division; to: temporooccipital part.

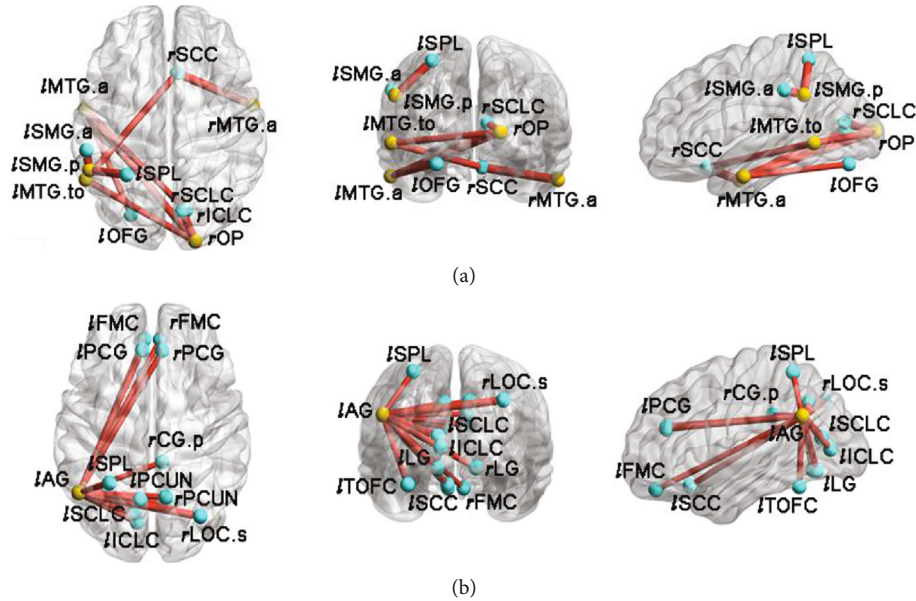


FIGURE 5: ROI-wise FC patterns with significant alterations between the L-SSNHL and HC-1 subgroups. Compared with the HC-1 subgroup, the L-SSNHL subgroup showed significantly increased FCs between the bilateral MTG and ROIs mainly located in the bilateral occipital lobes and the right limbic lobe, and between the *lSMG.p* and the left parietal cortex (a). Increased FCs were observed between the *lAG* and ROIs, mainly located in the bilateral frontal lobes, occipital lobes, and limbic lobes (b). The yellow balls indicate the seed ROI while the cyan balls indicate the ROIs with significantly different FC values. MTG: middle temporal gyrus; OP: occipital pole; SMG: supramarginal gyrus; AG: angular gyrus; ICLC: intracalcarine cortex; OFG: occipital fusiform gyrus; SCC: subcallosal cortex; SCLC: supracalcarine cortex; SPL: superior parietal lobule; LOC: lateral occipital cortex; FMC: frontal medial cortex; PCG: paracingulate gyrus; CG: cingulate gyrus; PCUN: precuneus; LG: lingual gyrus; TOFC: temporal occipital fusiform cortex; *l*: left; *r*: right; *a*: anterior division; *p*: posterior division; *to*: temporooccipital part.

the bilateral putamen but decreased in the right MTG. FC was widely increased between brain regions including the auditory cortex, visual cortex, striatum, AG, PCUN, and limbic lobes.

Although the precise etiology of SSNHL has not been identified, several pathophysiological mechanisms have been postulated in previous studies. The potential causes included viral infections, vascular occlusion, endolymphatic hydrops, autoimmunity, neoplastic disease, ototoxic drugs, and head injury [3, 39]. The present study focused on spontaneous neuronal activity and FC in patients with SSNHL, which may contribute to improving the understanding of some clinical issues, such as speech comprehension impairments and the occurrence of emotional disorders in patients with SSNHL. A previous study reported a restoration of maximum speech discrimination scores (SDS) without an improvement in PTA in patients with SSNHL [40]. This phenomenon may be mediated by the remodeling of the cortex associated with speech comprehension and processing, which was consistent with the results of our FC analysis results. We hope that our discoveries will complement previous studies and help to explain the pathophysiological mechanisms of SSNHL.

In the SSNHL group, ALFF and *fALFF* values were increased in the bilateral putamen. This result suggested that SSNHL might lead to enhanced neuronal activity in the putamen, which is associated with the regulation of body movement and language processing [41–43]. A previous study

showed that the activation of the putamen and caudate nucleus was increased in congenitally deaf adults when they were watching sign language [44]. As hearing loss causes difficulties in the perception and localization of sound, the brain may compensate for the function of language processing by increasing the activity of the putamen. Moreover, previous studies have shown that the STG had direct anatomical connections with the putamen and caudate nucleus [45]. This corticostriatal connection is related to spatial awareness and the encoding of the spatial locations of sounds [46, 47]. In the current study, patients with SSNHL showed increased FC values between the bilateral STG and left striatum, which may indicate alterations in the ability of sound localization and speech processing.

The MTG is associated with complicated sound processing, language comprehension, semantic memory, and integration of different types of information both within and across modalities (visual, auditory, or sensorimotor) [48–50]. In the present study, decreased ALFF and *fALFF* values in the right MTG suggested that the function of sound recognition and language processing was weakened due to insufficient acoustic stimulation in patients with SSNHL. In the SSNHL groups, the *rMTG.p* displayed increased FC with the bilateral LG and the right calcarine cortex, both of which are associated with visual function. Moreover, in the L-SSNHL subgroup, significantly increased FC values were also observed between the left MTG and visual cortical areas. These results indicated that cross-modal cortical

reorganization occurred in patients with SSNHL, i.e., reduced acoustic stimulus input may have led to the transformation of cortical function from the auditory sense toward the visual sense in the MTG via cross-modal neuroplasticity. This finding was consistent with previous studies [51, 52]. In addition, our findings also indicated that cross-modal reorganization can occur within the acute period of SSNHL, which is consistent with a previous report [24].

The AG is located at the junction between the temporal, parietal, and occipital lobes. Given its rich anatomical connections to other brain structures, the AG is considered an essential hub for information integration of different modalities [53]. In the present study, the FC values in the L-SSNHL subgroup were increased between the *l*AG and 15 other brain regions, which are mainly located in visual cortical areas, limbic lobes, and the bilateral PCUN. Thus, hearing loss might lead to enhanced integration and processing of visual information, potentially representing a compensatory neural mechanism in which reduced auditory information inputs are compensated with an enhanced visual sense. In the limbic lobe, the SCC has been identified as an important brain area in emotional information processing [54]. The paracingulate gyrus (PCG) is involved in manipulating information concerning social interactions [55]. Previous studies reported an association between SSNHL and an increased incidence of affective disorders, including anxiety and depression [18, 19]. Based on the findings of our study and other researchers, we proposed that the increased FC between the *l*AG and limbic lobes is associated with cognitive alternations and emotional modulation after the occurrence of SSNHL. This finding suggested that some proportion of patients with SSNHL may require psychotherapy.

As one of the key nodes of the default mode network (DMN), the PCUN exhibited increased activation at rest [56]. The PCUN plays a critical role in the mental representation of sounds and the construction of multimodal sensory imagery [57]. In the present study, increased FC between the *l*AG and bilateral PCUN may have represented a compensatory enhancement of multimodal sensory perception in the absence of hearing.

This study has several limitations. First, the background noise produced by the fMRI scanner reached more than 100 dB SPL. Although earplugs were used during scanning, the noise inevitably stimulated the auditory system to some extent. Due to the hearing discrepancy between the patients and HC individuals, the activation of the brain by the scanner noise may differ. In future studies, we will attempt to more effectively reduce and shield the background noise. Second, since the sample size of the present study was relatively small, it was difficult to perform analyses of ALFF and voxel-wise FC in the L-SSNHL and R-SSNHL subgroups. Combining these two subgroups of patients may have obscured some findings. More studies with larger sample sizes are needed to further clarify the alterations in brain function in SSNHL. Third, mental assessment of the SSNHL patients was not performed in this study. Considering that some affective disorders have been associated with SSNHL, future studies are needed to provide more information about the underlying mechanisms.

5. Conclusion

Based on the results of our study, SSNHL caused alterations in the neuronal activity and FC of brain regions mainly including the striatum, auditory cortex, visual cortex, MTG, AG, precuneus, and limbic lobes within the acute period of hearing loss.

Data Availability

The data used to support the findings of this study are available from the corresponding authors upon request.

Conflicts of Interest

The authors declare that there is no competing financial interest associated with this paper.

Authors' Contributions

Jiawei Chen, Bo Hu, and Peng Qin contributed equally to this work. Guangbin Cui and Lianjun Lu are co-senior authors of the study.

Acknowledgments

The authors would like to thank Prof. Wen Wang for helpful advice on the experimental methods.

Supplementary Materials

Figure S1: intergroup comparison of ROI-wise FC between the L-SSNHL, R-SSNHL, and HC groups. One-way ANOVA and post hoc analyses showed that FCs between *l*MTG.to and *l*SCC and *r*SCC were significantly increased between the L-SSNHL and HC groups. In the upper panel, the *x*-axis coordinates correspond to the numbers of the brain region in the Harvard-Oxford Atlas. The *y*-axis coordinates on the left indicate the FC value, while the ones on the right indicate the *p* value. The red and blue curves indicate mean FC values of the pair of ROIs in each group, with the shadow refers to the standard deviations. The black line indicates intergroup differences of each pair of ROIs, where the black line below the green horizontal line indicates *ap* value less than 0.05. The lower panel shows ROI-wise FC patterns with significant differences. The yellow ball indicates the seed ROI, while the cyan balls indicates the ROIs with significantly different FC values. The size of the sticks corresponds to the *F* values of one-way ANOVA analysis. MTG: middle temporal gyrus; SCC: subcallosal cortex; *l*: left; *r*: right; to, temporooccipital part. Table S1: the one-way ANOVA results of intergroup comparison between the L-SSNHL, R-SSNHL, and HC groups. Table S2: the two-sample two-tailed *t*-test results of intergroup comparison between the L-SSNHL and HC-1 subgroups. Figure S2: intergroup comparison of ROI-wise FC between the L-SSNHL and HC-1 subgroups by network-based statistics (NBS) analysis. FCs were significantly increased between ROIs mainly located at the bilateral temporal lobes (*l*MTG.a, *l*MTG.p, *r*MTG.p, and *l*MTG.to) and occipital lobes (*l*LG, *r*LG, and *r*OP) between the L-SSNHL and HC-1 subgroups. (*Supplementary Materials*)

References

- [1] World Health Organization, *Addressing the Rising Prevalence of Hearing Loss*, World Health Organization, Geneva, 2018.
- [2] S. S. Chandrasekhar, B. S. Tsai Do, S. R. Schwartz et al., "Clinical practice guideline: sudden hearing loss (update)," *Otolaryngology-Head and Neck Surgery*, vol. 161, 1_Supplement, pp. S1-S45, 2019.
- [3] B. E. Schreiber, C. Agrup, D. O. Haskard, and L. M. Luxon, "Sudden sensorineural hearing loss," *Lancet*, vol. 375, no. 9721, pp. 1203-1211, 2010.
- [4] S. H. Kim, S. J. Kim, H. Im, T. H. Kim, J. J. Song, and S. W. Chae, "A trend in sudden sensorineural hearing loss: data from a population-based study," *Audiology and Neurotology*, vol. 22, no. 6, pp. 311-316, 2018.
- [5] T. H. Alexander and J. P. Harris, "Incidence of sudden sensorineural hearing loss," *Otology & Neurotology*, vol. 34, no. 9, pp. 1586-1589, 2013.
- [6] Y. Liu, J. Qi, X. Chen et al., "Critical role of spectrin in hearing development and deafness," *Science Advances*, vol. 5, no. 4, article eaav7803, 2019.
- [7] Y. Wang, J. Li, X. Yao et al., "Loss of CIB2 causes profound hearing loss and abolishes mechano-electrical transduction in mice," *Frontiers in Molecular Neuroscience*, vol. 10, p. 401, 2017.
- [8] C. Zhu, C. Cheng, Y. Wang et al., "Loss of ARHGEF6 causes hair cell stereocilia deficits and hearing loss in mice," *Frontiers in Molecular Neuroscience*, vol. 11, p. 362, 2018.
- [9] J. Qi, Y. Liu, C. Chu et al., "A cytoskeleton structure revealed by super-resolution fluorescence imaging in inner ear hair cells," *Cell Discovery*, vol. 5, no. 1, p. 12, 2019.
- [10] J. Qi, L. Zhang, F. Tan et al., "Espin distribution as revealed by super-resolution microscopy of stereocilia," *American Journal of Translational Research*, vol. 12, no. 1, pp. 130-141, 2020.
- [11] Z. H. He, S. Y. Zou, M. Li et al., "The nuclear transcription factor FoxG1 affects the sensitivity of mimetic aging hair cells to inflammation by regulating autophagy pathways," *Redox Biol*, vol. 28, article 101364, 2020.
- [12] S. Gao, C. Cheng, M. Wang et al., "Blebbistatin inhibits neomycin-induced apoptosis in hair cell-like HEI-OC-1 cells and in cochlear hair cells," *Frontiers in Cellular Neuroscience*, vol. 13, p. 590, 2020.
- [13] Y. Zhang, W. Li, Z. He et al., "Pre-treatment with Fasudil prevents neomycin-induced hair cell damage by reducing the accumulation of reactive oxygen species," *Frontiers in Molecular Neuroscience*, vol. 12, p. 264, 2019.
- [14] W. Liu, X. Xu, Z. Fan et al., "Wnt signaling activates TP53-induced glycolysis and apoptosis regulator and protects against cisplatin-induced spiral ganglion neuron damage in the mouse cochlea," *Antioxidants & Redox Signaling*, vol. 30, no. 11, pp. 1389-1410, 2019.
- [15] L. Liu, Y. Chen, J. Qi et al., "Wnt activation protects against neomycin-induced hair cell damage in the mouse cochlea," *Cell Death & Disease*, vol. 7, no. 3, article e2136, 2016.
- [16] H. Li, Y. Song, Z. He et al., "Meclofenamic acid reduces reactive oxygen species accumulation and apoptosis, inhibits excessive autophagy, and protects hair cell-like HEI-OC1 cells from cisplatin-induced damage," *Frontiers in Cellular Neuroscience*, vol. 12, p. 139, 2018.
- [17] S. Zhang, Y. Zhang, Y. Dong et al., "Knockdown of Foxg1 in supporting cells increases the trans-differentiation of supporting cells into hair cells in the neonatal mouse cochlea," *Cellular and Molecular Life Sciences*, vol. 77, no. 7, pp. 1401-1419, 2020.
- [18] J. Y. Kim, J. W. Lee, M. Kim, M. J. Kim, and D. K. Kim, "Association of idiopathic sudden sensorineural hearing loss with affective disorders," *JAMA Otolaryngology-Head & Neck Surgery*, vol. 144, no. 7, pp. 614-621, 2018.
- [19] F. Arslan, E. Aydemir, Y. S. Kaya, H. Arslan, and A. Durmaz, "Anxiety and depression in patients with sudden one-sided hearing loss," *Ear, Nose, & Throat Journal*, vol. 97, no. 10-11, pp. E7-E9, 2018.
- [20] Y. Zhang, Z. Mao, S. Feng, X. Liu, J. Zhang, and X. Yu, "Monaural-driven functional changes within and beyond the auditory cortical network: evidence from long-term unilateral hearing impairment," *Neuroscience*, vol. 371, pp. 296-308, 2018.
- [21] N. Ghazaleh, W. V. D. Zwaag, S. Clarke, D. V. D. Ville, R. Maire, and M. Saenz, "High-resolution fMRI of auditory cortical map changes in unilateral hearing loss and tinnitus," *Brain Topography*, vol. 30, no. 5, pp. 685-697, 2017.
- [22] Y. Zhang, Z. Mao, S. Feng et al., "Altered functional networks in long-term unilateral hearing loss: a connectome analysis," *Brain and Behavior*, vol. 8, no. 2, article e00912, 2018.
- [23] Y. Cai, J. Li, Y. Chen et al., "Inhibition of brain area and functional connectivity in idiopathic sudden sensorineural hearing loss with tinnitus, based on resting-state EEG," *Frontiers in Neuroscience*, vol. 13, 2019.
- [24] H. Xu, W. Fan, X. Zhao et al., "Disrupted functional brain connectome in unilateral sudden sensorineural hearing loss," *Hearing Research*, vol. 335, pp. 138-148, 2016.
- [25] J. R. Hennig, O. Speck, M. A. Koch, and C. Weiller, "Functional magnetic resonance imaging: a review of methodological aspects and clinical applications," *Journal of Magnetic Resonance Imaging*, vol. 18, no. 1, pp. 1-15, 2003.
- [26] Z. Yu-Feng, H. Yong, Z. Chao-Zhe et al., "Altered baseline brain activity in children with ADHD revealed by resting-state functional MRI," *Brain and Development*, vol. 29, no. 2, pp. 83-91, 2007.
- [27] B. Biswal, F. Zerrin Yetkin, V. M. Haughton, and J. S. Hyde, "Functional connectivity in the motor cortex of resting human brain using echo-planar MRI," *Magnetic Resonance in Medicine*, vol. 34, no. 4, pp. 537-541, 1995.
- [28] S. Xia, T. B. Song, J. Che et al., "Altered brain functional activity in infants with congenital bilateral severe sensorineural hearing loss: a resting-state functional MRI study under sedation," *Neural Plasticity*, vol. 2017, Article ID 8986362, 8 pages, 2017.
- [29] S. Puschmann and C. M. Thiel, "Changed crossmodal functional connectivity in older adults with hearing loss," *Cortex*, vol. 86, pp. 109-122, 2017.
- [30] F. de Vos, M. Koini, T. M. Schouten et al., "A comprehensive analysis of resting state fMRI measures to classify individual patients with Alzheimer's disease," *NeuroImage*, vol. 167, pp. 62-72, 2018.
- [31] P. C. Mulders, P. F. van Eijndhoven, A. H. Schene, C. F. Beckmann, and I. Tendolcar, "Resting-state functional connectivity in major depressive disorder: a review," *Neuroscience & Biobehavioral Reviews*, vol. 56, pp. 330-344, 2015.
- [32] Y. Tang, Q. Zhou, M. Chang et al., "Altered functional connectivity and low-frequency signal fluctuations in early psychosis and genetic high risk," *Schizophrenia Research*, vol. 210, pp. 172-179, 2019.

- [33] C. G. Yan, X. D. Wang, X. N. Zuo, and Y. F. Zang, "DPABI: data processing & analysis for (resting-state) brain imaging," *Neuroinformatics*, vol. 14, no. 3, pp. 339–351, 2016.
- [34] Y. Chao-Gan and Z. Yu-Feng, "DPARSF: a MATLAB toolbox for "pipeline" data analysis of resting-state fMRI," *Frontiers in Systems Neuroscience*, vol. 4, p. 13, 2010.
- [35] X. Chen, B. Lu, and C. G. Yan, "Reproducibility of R-fMRI metrics on the impact of different strategies for multiple comparison correction and sample sizes," *Human Brain Mapping*, vol. 39, no. 1, pp. 300–318, 2018.
- [36] X. W. Song, Z. Y. Dong, X. Y. Long et al., "REST: a toolkit for resting-state functional magnetic resonance imaging data processing," *PLoS One*, vol. 6, no. 9, article e25031, 2011.
- [37] A. Zalesky, A. Fornito, and E. T. Bullmore, "Network-based statistic: identifying differences in brain networks," *NeuroImage*, vol. 53, no. 4, pp. 1197–1207, 2010.
- [38] M. Xia, J. Wang, and Y. He, "BrainNet Viewer: a network visualization tool for human brain connectomics," *PLoS One*, vol. 8, no. 7, article e68910, 2013.
- [39] G. Li, D. You, J. Ma, W. Li, H. Li, and S. Sun, "The role of autoimmunity in the pathogenesis of sudden sensorineural hearing loss," *Neural Plasticity*, vol. 2018, Article ID 7691473, 9 pages, 2018.
- [40] Y. Noguchi, M. Takahashi, T. Ito, T. Fujikawa, Y. Kawashima, and K. Kitamura, "Delayed restoration of maximum speech discrimination scores in patients with idiopathic sudden sensorineural hearing loss," *Auris Nasus Larynx*, vol. 43, no. 5, pp. 495–500, 2016.
- [41] Y. Aramaki, M. Haruno, R. Osu, and N. Sadato, "Movement initiation-locked activity of the anterior putamen predicts future movement instability in periodic bimanual movement," *Journal of Neuroscience*, vol. 31, no. 27, pp. 9819–9823, 2011.
- [42] K. M. Tagarelli, K. F. Shattuck, P. E. Turkeltaub, and M. T. Ullman, "Language learning in the adult brain: a neuroanatomical meta-analysis of lexical and grammatical learning," *NeuroImage*, vol. 193, pp. 178–200, 2019.
- [43] N. Viñas-Guasch and Y. J. Wu, "The role of the putamen in language: a meta-analytic connectivity modeling study," *Brain Structure and Function*, vol. 222, no. 9, pp. 3991–4004, 2017.
- [44] A. Moreno, F. Limousin, S. Dehaene, and C. Pallier, "Brain correlates of constituent structure in sign language comprehension," *NeuroImage*, vol. 167, pp. 151–161, 2018.
- [45] E. H. Yeterian and D. N. Pandya, "Corticostriatal connections of the superior temporal region in rhesus monkeys," *The Journal of Comparative Neurology*, vol. 399, no. 3, pp. 384–402, 1998.
- [46] L. Leinonen, J. Hyvärinen, and A. R. A. Sovijärvi, "Functional properties of neurons in the temporo-parietal association cortex of awake monkey," *Experimental Brain Research*, vol. 39, no. 2, p. 203, 1980.
- [47] H. O. Karnath, "New insights into the functions of the superior temporal cortex," *Nature Reviews Neuroscience*, vol. 2, no. 8, pp. 568–576, 2001.
- [48] K. Tibbetts, B. Ead, A. Umansky et al., "Interregional brain interactions in children with unilateral hearing loss," *Otolaryngology-Head and Neck Surgery*, vol. 144, no. 4, pp. 602–611, 2011.
- [49] J. Xu, J. Wang, L. Fan et al., "Tractography-based parcellation of the human middle temporal gyrus," *Scientific Reports*, vol. 5, no. 1, 2016.
- [50] M. S. Beauchamp, K. E. Lee, B. D. Argall, and A. Martin, "Integration of auditory and visual information about objects in superior temporal sulcus," *Neuron*, vol. 41, no. 5, pp. 809–823, 2004.
- [51] H. Glick and A. Sharma, "Cross-modal plasticity in developmental and age-related hearing loss: clinical implications," *Hearing Research*, vol. 343, pp. 191–201, 2017.
- [52] M. Stropahl, K. Plotz, R. Schönfeld et al., "Cross-modal reorganization in cochlear implant users: auditory cortex contributes to visual face processing," *NeuroImage*, vol. 121, pp. 159–170, 2015.
- [53] M. L. Seghier, "The angular gyrus: multiple functions and multiple subdivisions," *The Neuroscientist*, vol. 19, no. 1, pp. 43–61, 2012.
- [54] A. W. Laxton, J. S. Neimat, K. D. Davis et al., "Neuronal coding of implicit emotion categories in the subcallosal cortex in patients with depression," *Biological Psychiatry*, vol. 74, no. 10, pp. 714–719, 2013.
- [55] H. Walter, M. Adenzato, A. Ciaramidaro, I. Enrici, L. Pia, and B. G. Bara, "Understanding intentions in social interaction: the role of the anterior paracingulate cortex," *Journal of Cognitive Neuroscience*, vol. 16, no. 10, pp. 1854–1863, 2004.
- [56] M. E. Raichle, "The brain's default mode network," *Annual Review of Neuroscience*, vol. 38, no. 1, pp. 433–447, 2015.
- [57] D. Spada, L. Verga, A. Iadanza, M. Tettamanti, and D. Perani, "The auditory scene: an fMRI study on melody and accompaniment in professional pianists," *NeuroImage*, vol. 102, pp. 764–775, 2014.

Research Article

Cisplatin-Induced Stria Vascularis Damage Is Associated with Inflammation and Fibrosis

Na Zhang, Jing Cai, Lei Xu , Haibo Wang , and Wenwen Liu 

Department of Otolaryngology-Head and Neck Surgery, Shandong Provincial ENT Hospital, Cheeloo College of Medicine, Shandong University, Jinan 250022, China

Correspondence should be addressed to Haibo Wang; whbot11@163.com and Wenwen Liu; wenwenliu_1@yahoo.com

Received 19 April 2020; Revised 5 August 2020; Accepted 3 September 2020; Published 22 September 2020

Academic Editor: Jian Wang

Copyright © 2020 Na Zhang et al. This is an open access article distributed under the Creative Commons Attribution License, which permits unrestricted use, distribution, and reproduction in any medium, provided the original work is properly cited.

The stria vascularis (SV) generates the endocochlear potential (EP) in the inner ear and is necessary for proper hair cell (HC) mechanotransduction and hearing. Cell junctions are indispensable for the establishment of compositionally distinct fluid compartments in the inner ear. Ototoxic drug cisplatin can damage SV and cause sensorineural hearing loss; however, the underlying mechanisms behind such injury are unclear. In this study, after the intraperitoneal injection of cisplatin (3 mg/kg/day for 7 days) in mice, we determined the auditory function by EP recording and auditory brainstem response (ABR) analysis, observed the ultrastructure of SV by transmission electron microscopy (TEM), and examined the expression and distribution of cell junction proteins by western blot, PCR, and immunofluorescence staining. We discovered that the EP was significantly reduced while ABR thresholds were significantly elevated in cisplatin-treated mice; cisplatin induced ultrastructural changes in marginal cells (MCs), endothelial cells (ECs), pericytes, etc. We found that cisplatin insulted auditory function not only by reducing the expression of zonula occludens protein-1 (ZO-1) in MCs of the SV but also by decreasing the expression of connexin 26 (Cx26) and connexin 43 (Cx43) in MCs and basal cells (BCs). More importantly, cisplatin induced activations of perivascular-resident macrophage-like melanocytes (PVM/Ms) and interleukin-1beta (IL-1 β) as well as increased expressions of profibrotic proteins such as laminin and collagen IV in SV. Thus, our results firstly showed that cisplatin induced fibrosis, inflammation, and the complex expression change of cell junctions in SV.

1. Introduction

The endolymph is the atypical potassium-rich extracellular fluid which results in a 80-millivolt positive potential known as the endocochlear potential (EP), an essential driving force for hearing function [1]. Stria vascularis (SV), a heterogenous and nonsensory epithelial tissue in the lateral wall of the cochlea, generates and maintains the high concentration of potassium in the endolymph. The intrastrial fluid-blood barrier separates the SV from peripheral circulation, and the integrity of the barrier is critical for maintaining inner ear homeostasis, especially for sustaining the EP [2]. Disruption of the barrier is closely associated with hearing disorders including autoimmune inner ear disease, noise-induced hearing loss, and age-related hearing loss [3, 4]. Studies have reported that particular cell types in SV were identified as critical to prevent the leakage of solutes and generate EP, thus

far including marginal cells (MCs), intermediate cells (ICs), and basal cells (BCs) [5–7]. MCs face the endolymph and extend basolateral projections that interdigitate with ICs which have projections that run in both directions toward MCs apically and BCs at the basolateral end. BCs play a role in barrier formation by connecting to each other by gap junctions (GJs) to prevent leakage of ions. In addition, other cell types in the SV include perivascular-resident macrophage-like melanocytes (PVM/Ms), pericytes, and endothelial cells (ECs) [8, 9].

Cisplatin is a widely used chemotherapeutic drug effectively against a variety of tumor types. Unfortunately, cisplatin can cause serious ototoxic side effects by directly damaging the hair cells (HCs) and spiral ganglion neurons [10, 11], and it has been reported that cisplatin interfered with SV function, resulting in depression of the EP [12] and inhibition of membrane-bound enzyme systems [13].

Histologically, cisplatin-induced damages to the SV consist of PVM/M atrophy, swelling and blebbing of the MCs, and vacuolation of the latter's cytoplasm [14]. Alam et al. have revealed that a significantly increased number of Bax-positive cells and decreased number of Bcl-2-positive cells were found in SV following cisplatin treatment [15]. Nevertheless, the underlying mechanisms of cisplatin ototoxicity are complex, and it is not clear if all the components constituting the SV (i.e., MCs, PVM/Ms, and capillary) are equally sensitive to cisplatin ototoxicity. In addition, the effect of cisplatin on cell junctions in SV, such as tight junctions (TJs) and GJs which are important in maintaining ion concentration gradient between the endolymph and the perilymph, is unknown yet.

In view of the above, we hypothesized that the ototoxic effects of cisplatin could be induced by an alteration of cell junctions of the endothelial layer. Here, the mice were injected intraperitoneally (i.p.) with 3 mg/kg cisplatin for 7 consecutive days, and we found that cisplatin damaged the SV via changing expressions of cell junction proteins zonula occludens protein-1 (ZO-1), connexin 26 (Cx26), and connexin 43 (Cx43). More importantly, we identified that cisplatin induced interleukin-1 β (IL-1 β) activation and increased the expression of profibrotic proteins such as laminin and collagen IV, as well as led to structural morphologic alterations of the cell junction component in SV. This work establishes a basis for exploring the underlying mechanisms of cisplatin-induced SV injury and might offer novel therapeutic targets for the prevention of hearing loss resulting from SV dysfunction.

2. Materials and Methods

2.1. Animals and Cisplatin Administration. C57BL/6 mice were obtained from the Animal Center of Shandong University (Jinan, China). The mice were housed in a temperature-controlled (20–22°C) room and a 12/12 h light/dark cycle and had free access to food and drinking water. Experiments were performed on age- and sex-matched 6- to 8-week-old mice weighing 17–23 g. After acclimation for a week, the mice were randomly divided into two groups ($n = 18$ per group) depending on the administered cisplatin (Jiangsu Haosen Pharmaceutical Co. Ltd., Jiangsu, China) dose as follows: control group, the mice were intraperitoneally (i.p.) injected with 0.9% physiological saline (the vehicle of cisplatin, 0.6 ml/100 g) once a day for 7 days; cisplatin group, the mice were i.p. injected with 3 mg/kg cisplatin in 0.9% physiological saline once a day for 7 days.

All study protocols were approved by the Animal Care Committee of Shandong University and conformed with the Guideline for the Care and Use of Laboratory Animal of the National Institutes of Health.

2.2. Auditory Function Evaluation. The auditory function of mice was evaluated by auditory brainstem response (ABR) analysis. ABR responses were measured with a tone burst stimulus at 4, 8, 12, 16, 24, and 32 kHz using the TDT system 3 (Tucker-Davis Technologies, Alachua, FL, USA) with 1024 stimulus repetitions per record in a sound isolation booth.

Briefly, a total of 36 mice ($n = 18$ per group) were anesthetized with a mixture of xylazine (10 mg/kg) and ketamine (100 mg/kg) by i.p. injection and placed on a warm heating pad during ABR recordings. The sound delivery tube of an inserted earphone was tightly fitted into the external auditory canal; needle electrodes were inserted into subcutaneous tissue at the vertex (record electrode), ipsilateral ear (reference electrode), and back (ground electrode). The sound level started from a 90 dB sound pressure level (SPL) and decreased in 5 dB increments to the acoustic threshold. At each frequency, the ABR threshold was determined, which refers to the minimal SPL resulting in a reliable ABR recording with one or more distinguishable waves that can be clearly identified by visual inspection. It is necessary to repeat the process for low SPLs around the threshold to ensure the consistency of the waveforms. Following the ABR hearing measurements, tissues from the same mice were used to conduct histological, biochemical, or molecular analyses.

2.3. Endocochlear Potential Recording. Mice were anesthetized as described above, and body temperature was maintained at 37°C using a heating pad. Then, the cochlea was exposed by a ventral approach and the bone over the spiral ligament of the basal turn was gently picked to form a small hole (~30 μ m). A glass pipette as the record electrode filled with 3 M KCl with the resistance of 12–20 M Ω was installed on a motorized manipulator (IVM Single, Scientifica Limited, UK). An Axopatch 200B amplifier (Molecular Devices, LLC., USA) with an Axon Digidata 1550B interfaced by software pCLAMP (version 10.6, Molecular Devices, LLC., USA) was used for the current-clamp recording of EP. When the microelectrode advanced through the round window membrane into the scala tympani, the potential was set to zero as the baseline. Then, the microelectrode was advanced into the scala media through the basilar membrane to record EP. The reference electrode was inserted in the neck muscles of the mice.

2.4. Sample Collection. Following the ABR measurements, the mice were sacrificed by cervical dislocation and the temporal bones were excised from the head. After removal of stapes from the oval window and piercing of the round window and the cochlear top, the cochleae were fixed in 4% paraformaldehyde (PFA) (Sigma-Aldrich, St. Louis, MO) overnight at 4°C and then rinsed in 37°C phosphate-buffered saline (PBS, pH 7.4) to remove any residual PFA. The right cochleae were decalcified in PBS containing 10% ethylenediaminetetraacetic acid (EDTA) for 30 hours at 4°C, dehydrated by successive incubation in 10%, 20%, and 30% sucrose in PBS, and embedded with O.C.T compound (Tissue-Tek, Sakura Finetek, USA) for frozen sections. Frozen sections were cut into 7 μ m sections using a cryostat (Leica CM1850, Leica, Nussloch, Germany). The lateral wall of the left cochlea was microdissected from the bony wall of the cochlea. Localizing the pigmented strip in the cochlear lateral wall, the SV was gently microdissected from the spiral ligament using fine forceps and adhered on a small slide precoated with celltack for immunofluorescence staining.

2.5. Immunofluorescence Staining. The SV tissues and frozen sections were permeabilized in 0.5% Triton X-100 (Sigma-Aldrich) for 1 hour and immunoblocked with 1% fish gelatin solution (G7765, Sigma) for another 1 hour. The specimens were incubated with different primary antibodies: ZO-1 (1:1000; 61-7300, Thermo Fisher), Cx26 (1:200; LS-B6429-50, Life Technologies), Cx43 (1:400; Ab135763, Abcam), laminin (1:200; Ab30320, Abcam), collagen IV (1:200; Ab6586, Abcam), alpha-smooth muscle actin (α -SMA, 1:200; Ab5694, Abcam), and CD68 (1:100; Ab53444, Abcam), diluted in 1% bovine serum albumin-(BSA-) PBS, respectively, at 4°C overnight. The next day, cells were incubated with secondary antibodies (Invitrogen, A21202, A21206, A31571, A31573, and A10040) along with DAPI (D9542, Sigma-Aldrich, USA) at room temperature for 1 h. Coverslips were then mounted, and the samples were observed under a laser scanning confocal microscope (Leica SP8; Leica, Germany).

2.6. TEM. Animals were decapitated under deep anesthesia, and the cochlear tissue was collected, washed fast with PBS, and immediately placed in 3% glutaraldehyde fixative solution (pH 7.4). The sample block was trimmed 1 mm \times 1 mm \times 3 mm, according to the conventional TEM sample preparation method followed by rinsing, as well as 1% osmic acid (OsO_4) fixed, dehydrated, soaked, and epon 812 embedded; semi- and ultrathin radial sections were cut from the basal turn with lead citrate and uranyl acetate electron staining. Finally, the strial sections were observed using a transmission electron microscope (JEOL 1200EX, Japan) in Jinan WeiYa Bio-Technology Co., Ltd. (Jinan, China).

2.7. mRNA Extraction and Real-Time Polymerase Chain Reaction (PCR). The total RNA of the SV was extracted with the RNA extraction kit (RNeasy Mini QIAcube Kit, Qiagen, Valencia, CA). The relative expression levels of target gene mRNA were measured by real-time PCR using an Eppendorf AG 22331 PCR machine (Hamburg, Germany). The 20 μ l real-time PCR reaction system included 2x SYBR Green Premix EX Taq 10 μ l (RR42LR, Takara Biotech), 1 μ g cDNA template, 1 μ l forward primer, and 1 μ l reverse primer, with deionized water complementing for the rest of the volume. The real-time PCR parameters were pregenerated at 95°C for 3 min, then 40 cycles of degeneration at 95°C for 50 s, annealing at 60°C for 45 s, and elongation at 72°C for 50 s. The specificity of each PCR reaction was confirmed by melting curve analysis. The sequences of primers used in this experiment were listed below: *zo-1*, forward primer: 5' CTCCAGTCAGCCCGCAAAG 3', reverse primer: 5' CAAGACAACATCCCCTTCTTGA 3'; *cx26*, forward primer: 5' TCGGGGGTGTCAACAAACAC 3', reverse primer: 5' CGTAGCATAATTCTTGCAGCC 3'; *cx43*, forward primer: 5' TGGCTGTCGGTGCTCTTCATT 3', reverse primer: 5' GTGGGCACAGACACGAATATGAT 3'; *collagen IV*, forward primer: 5' AATCCCAGGAGGAC GAGGTGT 3', reverse primer: 5' GGATTACCCACTTG CCCCAG 3'; *laminin*, forward primer: 5' GACCTCCCA CTTACAGAGCAG 3', reverse primer: 5' TGTACCGTG

CTGAGGTGAAT 3'; *IL-1 β* , forward primer: 5' GATGAA GGGCTGCTTCCAAACC 3', reverse primer: 5' GGTGCT CATGTCTCATCCTGG 3'; and *β -actin*, forward primer: 5' GTCCCTCACCCCTCCCAAAAG 3', reverse primer: 5' GCTGCCTCAACACCTCAACCC3'.

2.8. Protein Extraction and Western Blotting. The total protein of SV was extracted with cold RIPA lysis buffer (P0013B; Beyotime Institute of Biotechnology, Shanghai, China) plus protease inhibitor cocktail (P8340; Sigma, USA) for 30 minutes at 4°C and then centrifuged at 12000 g for 20 minutes at 4°C. Protein concentrations were detected by the BCA Protein Assay Kit (Shenergy Biocolor Bioscience & Technology Company, Shanghai, China). The same amount of protein samples was denatured in 99°C for 10 min and separated by 10% SDS-PAGE gel electrophoresis. Then, the proteins were transferred to polyvinylidene difluoride membranes. The membranes were blocked in 5% skim milk for 1 hour at room temperature and then were incubated with different primary antibodies: ZO-1 (1:200; 61-7300, Thermo Fisher), connexin 26 (Cx26, 1:200; LS-B6429-50, Life Technologies), connexin 43 (Cx43, 1:200; Ab135763), laminin (1:200; Ab30320, Abcam), collagen IV (1:200; Ab6586, Abcam), and anti- β -actin antibody (1:2000 dilution; ZSGB-BIO, Beijing, China) in 3% BSA at 4°C overnight. The next day, the membranes were incubated with HRP-conjugated goat anti-mouse or goat anti-rabbit IgG antibodies (1:2000 dilution; ZSGB-BIO, Beijing, China) at room temperature for 1 hour. Finally, the protein signals were detected using an ECL kit (Millipore, Billerica, MA, USA) and analyzed by ImageJ software. All blocking, incubation, and washing were performed in TBST solution (Tris-buffered saline and 0.05% Tween 20).

2.9. Cell Counting. As for cell quantification, we imaged the entire cochlea using a 400 \times 2.5 objective and used ImageJ software to quantify the immunostaining-positive cells. In detail, we measured the relative length of the scale bar (20 μ m) in the figure and set scale to 20 μ m in the ImageJ software. Then, we used the "point selections" tool in the ImageJ to count the immunostaining-positive cell number.

2.10. Statistical Analysis. All statistical analysis was performed with SPSS 13.0 software (SPSS Inc., USA). Results were expressed as mean \pm standard deviation (SD). Statistical comparisons were performed by independent-samples *t*-tests. Differences with a *p* value < 0.05 were considered to be statistically significant.

3. Results

3.1. Cisplatin Induces Insult to Auditory Function. To investigate the effect of cisplatin on auditory function, C57BL/6 mice at 6-8 weeks were given i.p. injections of cisplatin for 7 days (Figure 1(a)), and we found that the EP in cisplatin-treated mice was significantly reduced compared to the control group (Figure 1(b), *p* < 0.001), as EP in the control and cisplatin-treated mice was 91.3 \pm 1.53 mV and 44.8 \pm 5.62 mV, respectively. The auditory functions of mice were

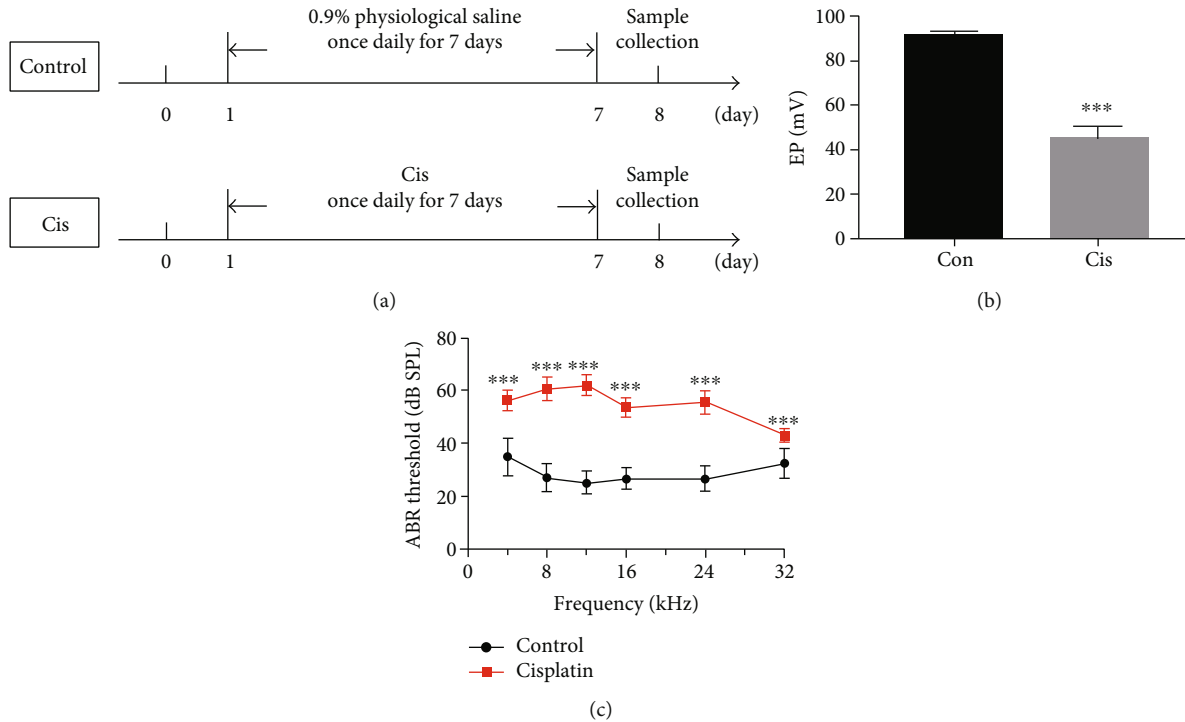


FIGURE 1: Cisplatin induced insult to auditory function. (a) C57BL/6 mice were divided into 2 groups and given i.p. injection of drugs as illustrated. (b) Endocochlear potentials were measured 7 days after cisplatin administration (3 mg/day/kg, i.p.). The EP in cisplatin-treated mice was significantly reduced compared to the control group ($n = 3$). (c) ABR thresholds were measured at 4, 8, 12, 16, 24, and 48 kHz in the control and cisplatin groups, and the ABR thresholds were elevated in the cisplatin group compared to the control group at all frequencies measured ($n = 18$). Data are shown as mean \pm SD. Cis: cisplatin; *** $p < 0.001$.

evaluated using the ABR test. The ABR thresholds were elevated in the cisplatin group compared to the control group at all frequencies measured (Figure 1(c), $p < 0.001$), suggesting that cisplatin effectively impaired auditory function in mice in our study.

3.2. Cisplatin Changes the Ultrastructure of SV Cells. The ultrastructure of SV was observed by TEM after cisplatin administration. In the control tissues, the SV was in a normal morphology, as indicated by the characteristic differences in electron density between the darker MCs with their finger-like processes and the lighter PVM/Ms and BCs (Figure 2(a)). Both the size and shape of cell nuclei appeared normal, with nucleoli and proportional amounts of euchromatin and denser heterochromatin (Figure 2(a)). However, a thicker SV and more blood vessels were observed in the cisplatin-treated mice compared to the control group. It should be noted here that most of the nuclei, which were very light, were abnormal in shape. Especially in the MCs, the nuclei were large and round rather than oval and often with indistinguishable and disorganized nucleolus; moreover, the MCs were atrophied and the cell-cell connections were interrupted (Figure 2(a)). Moreover, our analyses revealed that the number of mitochondria was much lower in SV of cisplatin-treated mice compared with the control ones, in which mitochondria were prevalent and occurred in a highly organized manner (Figure 2(a)). Besides, analysis of ultrathin sections showed that cisplatin treatment led to reduced endo-

thelial cells, a swollen endoplasmic reticulum, and a thinner vascular wall compared to control mice (Figure 2(b)). We also observed changes in pericytes migrating away from blood vessels (Figure 2(b)).

3.3. Cisplatin Alters the Expression Pattern and Decreases the Expression of ZO-1 in SV. Immunofluorescence staining was used to assess the effect of cisplatin on the typical localization pattern of tight junction protein ZO-1 after 7 days of administration. In control mice, the ZO-1 signal appeared at the cell surface and localized to the cell-cell junction of MCs, with a more prominent and clear immunostaining at the intercellular border (Figure 3(a)), which clearly suggested the presence of physiological tightness of the barrier. However, the exposure of MCs to cisplatin resulted in protein delocalization, leading to a “zipper-like” staining pattern and holes that became visible between cells (Figure 3(a)). In addition, western blotting and qPCR results revealed significant decreases of ZO-1 expression in cisplatin-treated mice compared to the control group (Figures 3(b)–3(d)), indicating that the TJ between MCs was damaged after cisplatin treatment.

Furthermore, the TEM analyses also showed that the number of cell projections interdigitated and TJs coexisting with the MCs or located in their vicinity were distinctly reduced in cisplatin-treated mice compared with the controls (Figure 3(e)). In the classic view, the intrastrial fluid-blood barrier is composed of the basement membrane and endothelial cells that connect to each other with TJs [16] to form

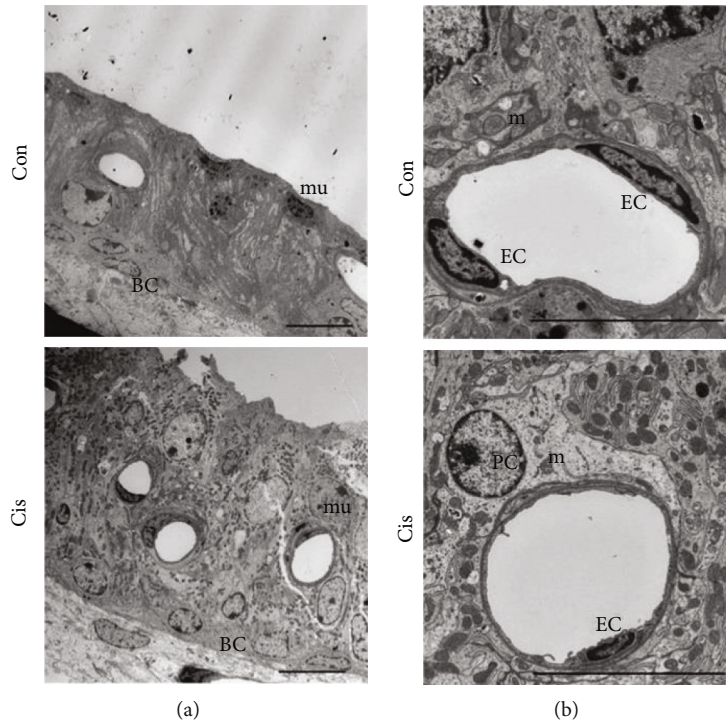


FIGURE 2: Cisplatin changes the ultrastructure of SV cells. (a, b) The ultrastructure of SV was observed by TEM. Both the size and the shape of cell nuclei appeared normal, and mitochondria were prevalent and occurred in a highly organized manner in the control mice. A thicker SV and more blood vessels were observed in the cisplatin-treated mice; the numbers of mitochondria and endothelial cells were reduced; and most of the cells were in an abnormal shapes with large and round nuclei, a swollen endoplasmic reticulum, and a thinner vascular wall in cisplatin-treated mice. Con: 0.9% physiological saline; Cis: cisplatin; EC: endothelial cell; m: mitochondrion; PC: pericyte; mu: marginal cell nucleus. Scale bars, 10 μm .

a diffusion barrier that prevents most blood-borne substances from entering the ear [17]. Observations revealed the presence of endothelial cell nuclei with irregular morphology, intact organelles in the cytoplasm, and intact TJ structure between endothelial cells (Figures 3(e) and 3(f)). After cisplatin exposure for 7 days, the TJs were open and intermittently widened between adjacent ECs (Figures 3(e) and 3(f)), indicating that the cisplatin ototoxicity was associated with an altered TJ organization.

3.4. Cisplatin Reduces Expressions of Cx26 and Cx43 in SV. To assess the effect of cisplatin on GJ protein expression, immunofluorescence staining and TEM were used after the mice were treated with cisplatin injection. As revealed by immunofluorescence, Cx26 was mainly flocculently expressed in the basal layer and Cx43 was expressed in the MCs and BCs, and they were both localized in the cytoplasm of cells (Figures 4(a)–4(c)). Cisplatin treatment resulted in frequently dispersed staining of Cx26 in the cell cytoplasm of BCs (Figure 4(a)), as well as the reduction of Cx43 signal intensity (Figures 4(b) and 4(c)). Within some MCs, however, a very strong linear Cx43 signal on the plasma membrane of MCs was found as the prevalent staining pattern compared with the control (Figure 4(b)). Further quantitative evaluation of the Cx26 and Cx43 protein and mRNA expression by western blotting and qPCR also reflected the qualitative results (Figures 4(d)–4(f)).

The results of TEM showed that the number of anchoring connections at the basal layer was reduced (Figure 4(g)), and the number of GJs coexisting with the BCs or located in their vicinity was reduced in cisplatin-treated mice compared with the controls. Similar reduction was also observed in the case of the spiral ligament that, as a rule, contained only single or few TJs (Figure 4(g)). After cisplatin treatment, the expression and number of GJs were reduced significantly, indicating that the GJs were damaged in SV.

3.5. Cisplatin Promotes Translocation of α -SMA-Positive Cells into SV and Increases the Expression of Collagen IV and Laminin. Myofibroblasts are a subset of activated fibroblasts, characterized by expression of α -SMA, which is the principal cell type responsible for excessive extracellular matrix (ECM) deposition [18]. We found that cisplatin increased the translocation of α -SMA-positive cells into SV compared to the control mice (Figure 5(a)). These data suggested that cisplatin exerted a promotive effect on transformation of fibroblasts into myofibroblasts during the fibrogenesis process.

We next investigated whether markers of ECM were increased in SV after cisplatin administration so as to determine the effects of cisplatin on fibrogenesis in mice. Collagen IV was mainly expressed in the cytoplasm of MCs (Figure 5(b)), and the increased protein and mRNA levels of collagen IV were found remarkably after cisplatin

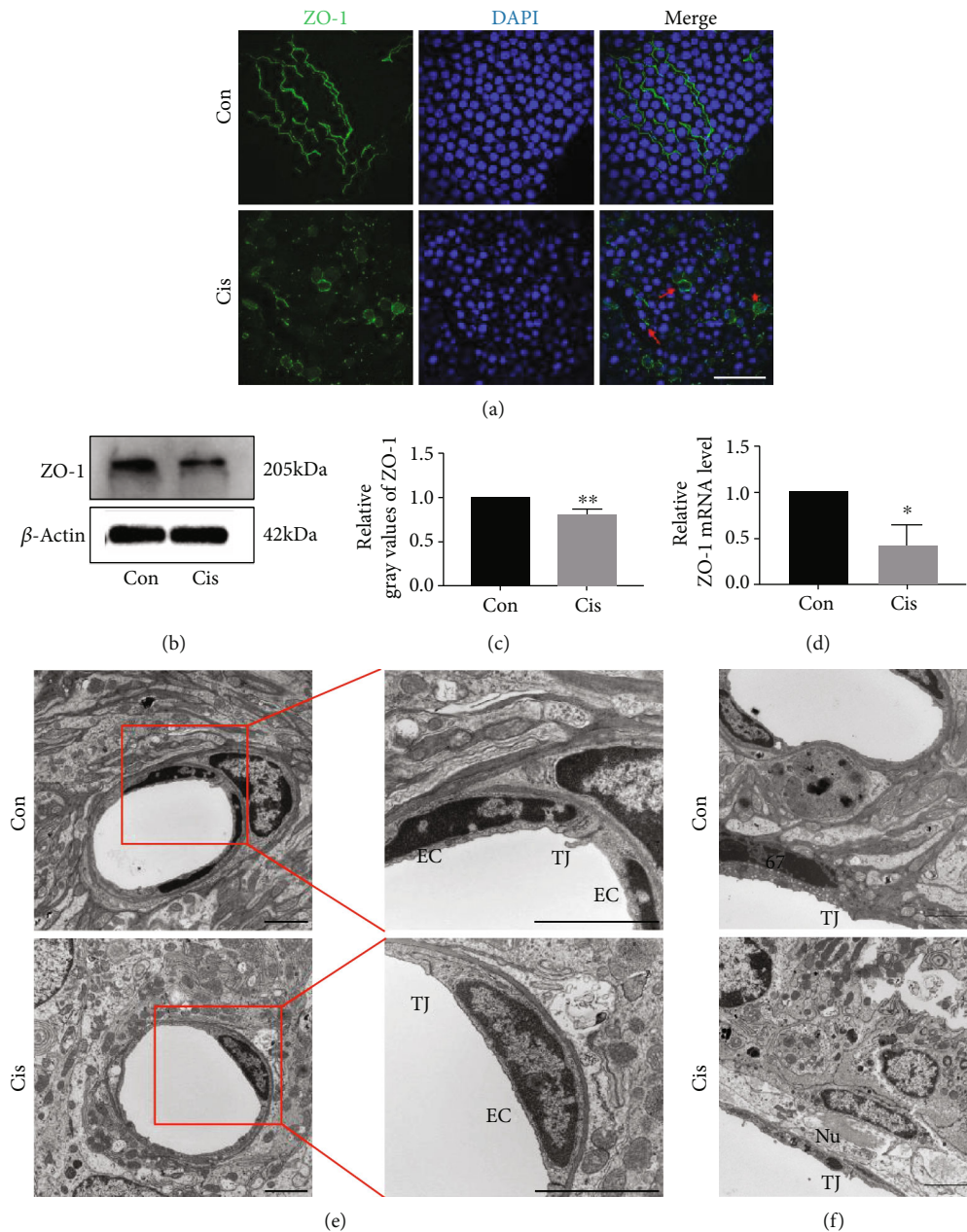


FIGURE 3: Cisplatin alters the expression pattern and decreases the expression of ZO-1 in SV. (a) The distribution of ZO-1 (green) in MCs by immunofluorescence staining. The moderate-to-strong ZO-1 signal is visible as a continuous wavy line between adjacent MCs in control mice, while the weak-to-moderate ZO-1 signal is seen mainly in the cell cytoplasm in cisplatin-treated mice. Asterisks show holes formed between marginal cells. Arrows point to morphological alterations in intercellular junctions. Nuclei were stained with DAPI (blue). Scale bars, 100 μm . (b) Western blot analysis of the cell lysates of SV treated with cisplatin. β -Actin was used as a loading control. (c) Densitometric quantification of the mean (SD) ratio of ZO-1 expressed as mean \pm SD ($n = 3$). (d) qRT-PCR shows mRNA for ZO-1 in the SV ($n = 3$). (e) The ultrastructure of SV was analyzed by TEM. TJs between adjacent ECs were extremely tight in control mice; the right window (zoomed inset) displays a higher magnification of the TJs between ECs; TJs were open and intermittently widened between adjacent ECs in cisplatin-treated mice. Scale bars, 2 μm . (f) TJs between adjacent MCs were extremely tight in the control mice; TJs were open between adjacent MCs in cisplatin-treated mice. Scale bars, 2 μm . Con: 0.9% physiological saline; Cis: cisplatin; TJ: tight junction; EC: endothelial cell; m: mitochondrion; Nu: marginal cell nucleus. $*p < 0.05$, $**p < 0.01$, and $***p < 0.001$.

treatment (Figures 5(e)–5(g)). We also observed a significant increased expression of laminin (Figures 5(d)–5(g)), an analyzed marker of vascular lesions. In accordance with the TEM result in Figure 2(d), the blood vessel cavity became rounder, and pericytes migrated away from blood vessels (Figure 5(c)).

In brief, our data indicated that fibrosis in SV was induced after cisplatin treatment.

3.6. Cisplatin Activates PVM/Ms in SV. Studies have shown that PVM/Ms control barrier integrity by affecting the

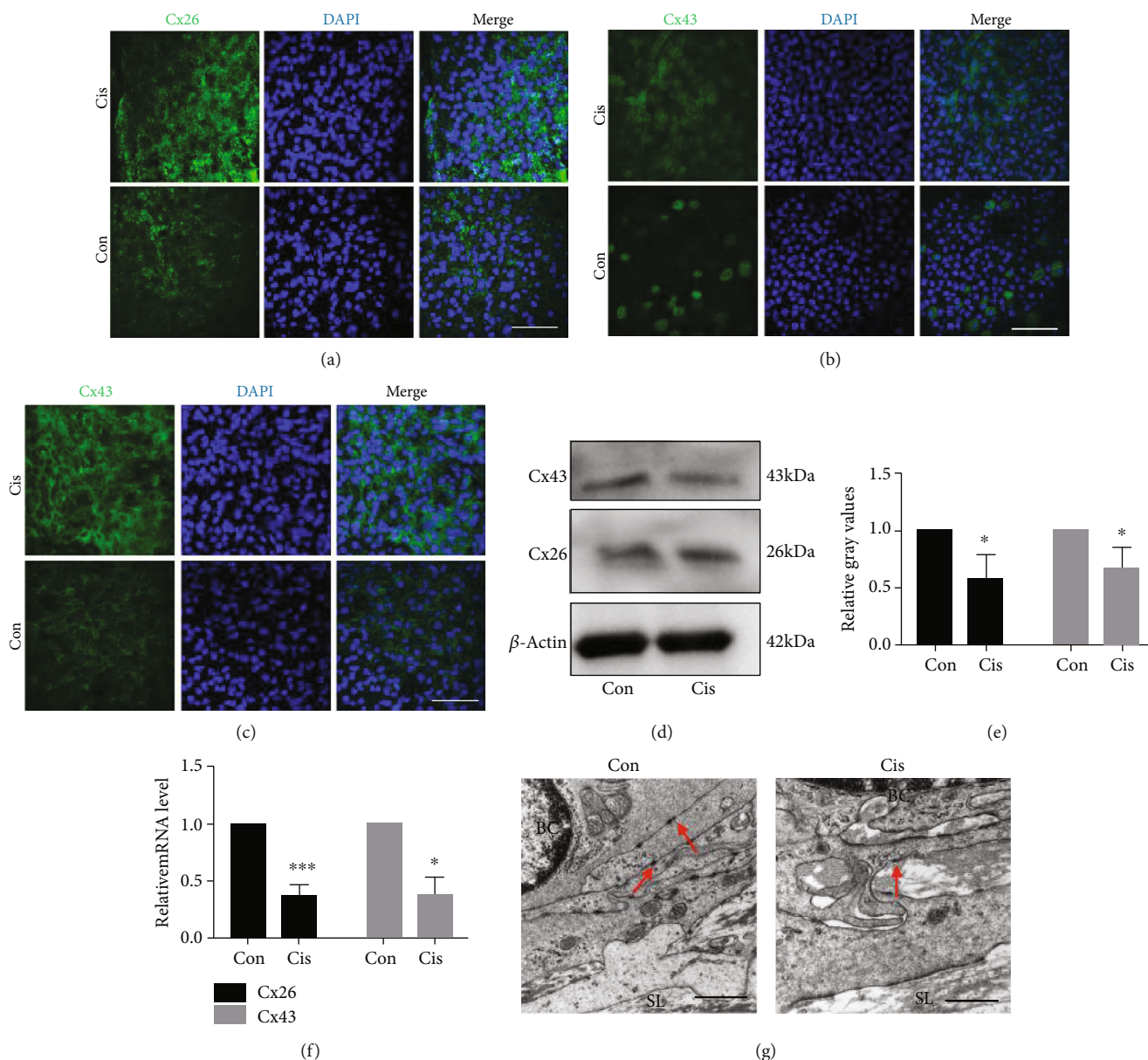


FIGURE 4: Cisplatin reduces expressions of Cx26 and Cx43 in SV. (a) The distribution of Cx26 (green) in BCs by immunofluorescence staining. The moderate-to-strong Cx26 signal is visible in the cell cytoplasm of BCs in the control, while the weak-to-moderate Cx26 signal is seen in cisplatin-treated mice. Nuclei were stained with DAPI (blue). Scale bars, 100 μ m. (b, c). The distribution of Cx43 (green) in the MCs (b) and BCs (c) by immunofluorescence staining. After the treatment of cisplatin, the weak-to-moderate Cx43 signal was found in the SV. A strong signal for Cx43 was found in some MCs in cisplatin-treated mice. Nuclei were stained with DAPI (blue). Scale bars, 100 μ m. (d) Western blot analysis of the cell lysates of SV treated with cisplatin. β -Actin was used as a loading control. (e) Densitometric quantification of the mean (SD) ratio of Cx43 and Cx26 expressed as mean \pm SD ($n = 3$). (f) qRT-PCR shows mRNA for Cx43 and Cx26 in the SV ($n = 3$). (g) The ultrastructure of SV analyzed by TEM. The number of anchoring connections at the basal layer is reduced in cisplatin-treated mice. Arrows point to anchoring connections. Scale bars, 10 μ m. BC: basal cells; SL: spiral ligament; Con: 0.9% physiological saline; Cis: cisplatin. * $p < 0.05$, ** $p < 0.01$, and *** $p < 0.001$.

expression of tight junction-associated proteins [19]. PVM/Ms were marked with a special antibody against CD68 and strial capillaries with Griffonia simplicifolia IB4 (GS-IB4; Figure 6(a)). We found that the PVM/Ms were highly invested on the abluminal surface of capillaries (Figure 6(a)). The number of PVM/Ms in the SV decreased statistically after cisplatin treatment in mice compared with

the control group (Figure 6(c)). Immunofluorescence results showed that the morphology of PVM/Ms was changed, the volume of PVM/Ms was enlarged, and the number of PVM/Ms branches was increased, as well as some of the branches became flat and amoeboid shaped (Figure 6(b)). The relative mRNA level of proinflammatory cytokine IL-1 β secreted by PVM/Ms was also significantly increased

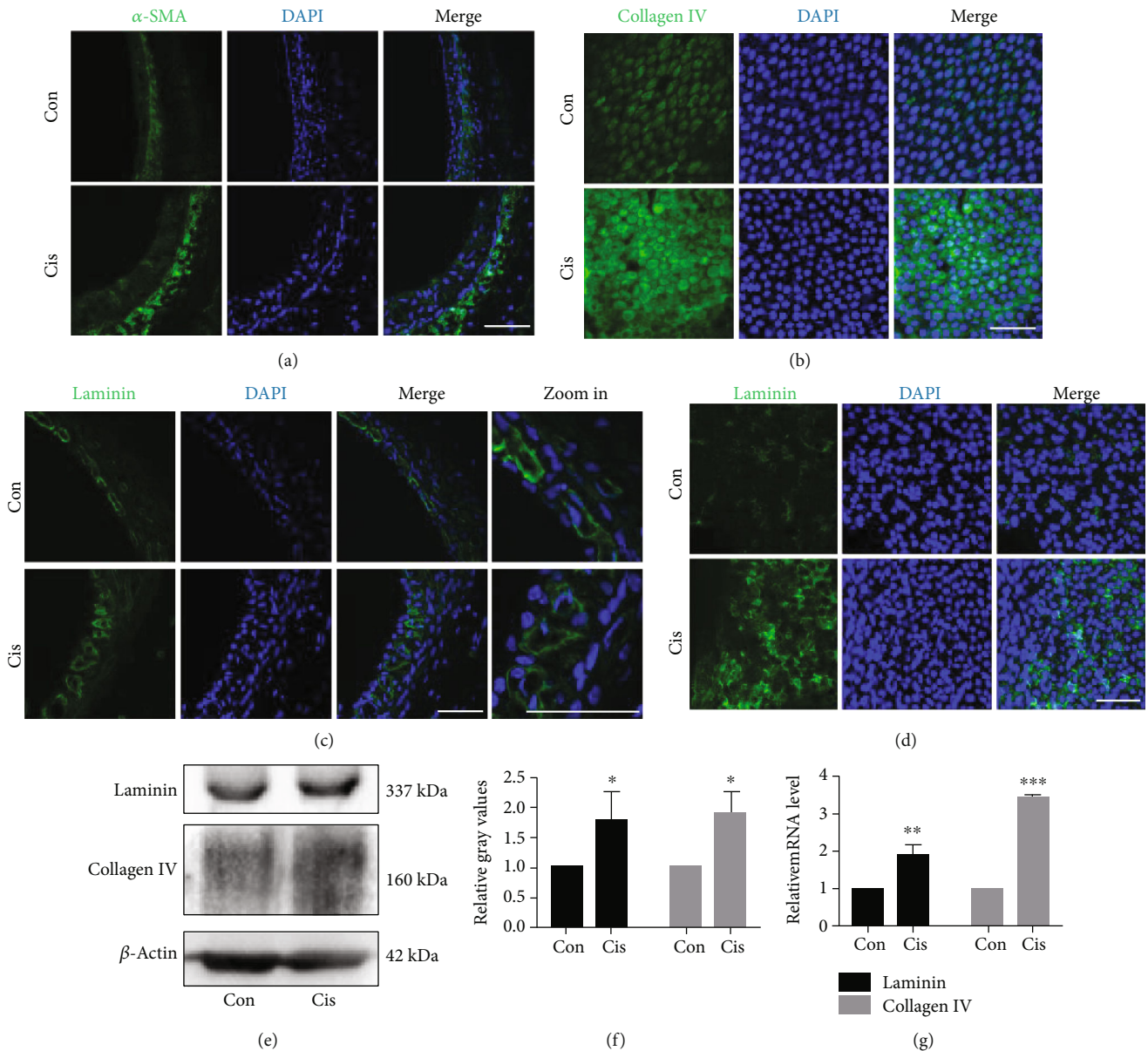


FIGURE 5: Cisplatin promotes translocation of α -SMA-positive cells into SV and increases the expression of collagen IV and laminin. (a) Confocal immunofluorescence for α -SMA in lateral tissue. Nuclei were stained with DAPI (blue). Scale bars, 100 μ m. (b) The distribution of collagen IV (green) in the MCs by immunofluorescence staining. After the treatment of cisplatin, the weak-to-moderate collagen IV signal was found in the SV. Nuclei were stained with DAPI (blue). Scale bars, 100 μ m. (c, d) The distribution of laminin (green) in frozen sections (c) and surface preparation (d) by immunofluorescence staining. After the treatment of cisplatin, the expression of laminin increased after cisplatin treatment, blood vessel cavity became rounder, and pericytes migrated away from blood vessels. Scale bars, 100 μ m. (e) Western blot of cell lysates of SV treated with cisplatin. β -Actin was used as a loading control. (g) qRT-PCR shows mRNA for laminin and collagen IV in the SV ($n = 3$). Con: 0.9% physiological saline; Cis: cisplatin. * $p < 0.05$, ** $p < 0.01$, and *** $p < 0.001$.

(Figure 6(d)). Together, these data suggested that PVM/Ms and their secreted IL-1 β may be involved in the damage of cell junction in SV induced by cisplatin.

4. Discussion

Hearing loss is one of the most common sensory disorder in human population, which affects 466 million people all over the world. Hearing loss can be caused by a variety of different stresses and injuries, such as genetic disorders,

aging, noise acoustic trauma, inflammation, infection, and exposure to different ototoxic drugs, including cisplatin [20–28]. Unfortunately, once the inner ear cochlea was damaged, the mammals only have very limited regeneration ability, which makes hearing loss irreversible in mammals [29–35]. Hearing loss significantly decreases the patient's life quality; and for the children, hearing loss will delay the language acquisition and affect the learning ability. Thus, to protect the cochlea and the hearing ability is very important.

Cisplatin-induced reduction of EP, which is generated and maintained by SV processes, has been observed after application of single high-dose cisplatin injection [36], following repeated systemic administration [37] and during perilymphatic administration [38]. In our previous study, we observed that 3 mg/kg/day i.p. injection of cisplatin for 7 consecutive days could cause obvious damages to the spiral ganglion neurons, vestibular HCs, and impairments to the cochlea [11, 39, 40]. Although studies in rodents have established cisplatin-dependent inner ear dysfunction and there are now evidences suggesting that cisplatin exerts cytotoxic effect on the SV, whether cisplatin alters the cell-cell junctions in the SV remains elusive. In this study, for the first time, we found that the treatment of cisplatin caused SV lesions in mice, which suggested that the cisplatin-induced SV damage might be associated with inflammation and the fibrosis process.

In general, cisplatin depletes cytoplasmic organelles, damages the mitochondria, and causes formation of lipid bodies and vacuoles [41]. The mainly impacted targets of cisplatin in SV are the MCs and the ICs [42, 43]. In our study, we found that the EP in cisplatin-treated mice was significantly reduced compared to that in the control group, suggesting that cisplatin damaged the SV and thus impaired the auditory function in mice. Consistently, our TEM results showed that the subnuclear processes, endoplasmic reticulum, nuclei, and mitochondria of the SV were extensively damaged by cisplatin. It has been reported that after 30 min i.p. infusion of 16 mg/kg cisplatin, SV edema can be present [44]. We found that cisplatin treatment (3 mg/kg/day for 7 days) causes SV edema in basal regions. Unlike the extracellular edema that is generally observed secondary to loop diuretics [45], the edema secondary to cisplatin appears to be intracellular which could account for the bulging and rupturing of MCs [42]. Strial capillaries have a minor role in blood flow regulation but a crucial role in maintaining the EP, ion transport, and endolymphatic fluid balance [1, 2]. We found that cisplatin treatment led to a reduced number of endothelial cells and thinner vascular wall. Three-dimensional FLAIR imaging detected that the blood-labyrinth barrier (BLB) breaks down with the enhancement of the endolabyrinthic fluid signal in patients with sudden hearing loss [46]. Thus, the edema of SV induced by cisplatin might also result in BLB breakdown and increase vascular permeability. Moreover, we found an increase in vessel density after cisplatin treatment. A study has reported that in temporal lobe epilepsy patients, the vessel density was associated with hypoxia and inflammation [47]. But there has been hardly any evidence on the vascular remodeling affected by cisplatin, and the role of angiogenesis is instead unclear, which needs to be further studied.

TJs are located on the lateral side of epithelial cells, forming the structural basis of selective cellular permeability. Like in other barrier systems, the intrastrial fluid-blood barrier is a highly specialized vascular epithelium composed of the basement membrane and ECs formed a diffusion barrier that prevents transport of most blood-borne substances into the inner ear [17]. TJs in the SV are also important in maintaining the ion concentration gradient between the endolymph

and the perilymph [5]. ZO-1 is a recognition protein for TJ placement, and loss of ZO-1 results in disorganization of TJs [48]. In this study, we found that the ZO-1 signal appeared at the cell surfaces and localized to the cell-cell junction of MCs, which suggested the presence of the physiological tightness of the barrier. After cisplatin exposure, ZO-1 expression was reduced with impaired functionality of SV. This idea is strengthened by the TEM results. Therefore, these results suggest that cisplatin could destroy the TJ organization between MCs and vascular endothelial cells and increase the permeability of the SV.

GJ proteins are specific connexins in the membrane of neighboring cells, responsible for exchanging of electric and chemical signals between cells. Cx26 is seen in GJs of all cells in the cochlea which participates in the circulation of potassium ions from HCs to MCs of the SV and the maintenance of cellular homeostasis [49]. A major portion (>50%) of non-syndromic hereditary deafness is caused by Cx26 gene mutations. Loss of Cx26 results in congenital hearing loss and cochlear development failure, as well as dysplasia of HCs [50]. Cx43 gene is expressed in the mouse inner ear and plays a role in the vascular system [51]. In our study, cisplatin treatment resulted in frequently dispersed staining of Cx26 and Cx43 in the cell cytoplasm. The number of anchoring connections at the basal layer of SV and spiral ligament was reduced, indicating that the GJs were damaged in the SV and spiral ligament. We suggest that the reduction of the cell junction protein is a consequence of internalization into the cytoplasm. Indeed, the reduction of the ZO-1 signal and its translocation from the membrane to the cytoplasmic compartment was reported to be physically associated with degradation of the GJ organization in the Sertoli cell line [3]. Thus, the diminished expression of Cx43 of cisplatin-treated mice may result, at least in part, from the decreased ZO-1 expression. Our results allow us to propose a working model: the cell junction of SV is damaged by cisplatin, thus leading to an increased permeability, allowing uncontrolled passage of ions and proteins, which together allow more cisplatin to enter into the inner ear and, in turn, provoke severe ototoxicity and impairment in auditory function.

It was important to give an answer whether and how the expression of TJs is related to the changes of the GJ expression observed in cisplatin-treated mice, and the question aroused whether diminished TJ and GJ protein expression in SV may be related to structural changes seen at the ultrastructural level, which are currently under study in this laboratory.

PVM/Ms are regulatory cells in the intrastrial fluid-blood barrier which are in close contact with vessels and critical for barrier function. Studies have shown that PVM/Ms affect barrier integrity by affecting the expression of TJ-associated proteins, and loss of PVM/Ms is associated with tissue edema [19]. In this study, we observed that the number of CD68-positive cells was decreased in SV after cisplatin treatment, but the remaining cells became bigger and longer in size, suggesting cisplatin could activate and damage PVM/Ms at the same time. Some studies suggested that cisplatin promoted excessive production of reactive oxygen species and proapoptotic factors in cochlear cells, leading to cell apoptosis

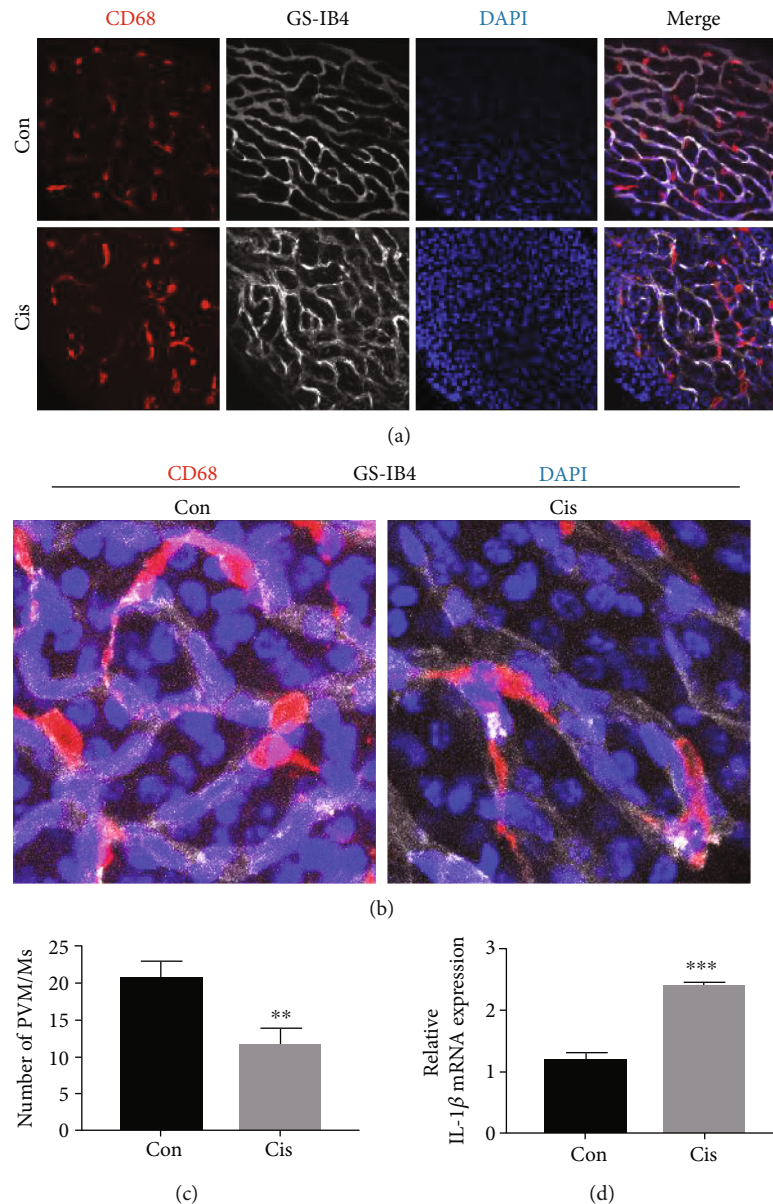


FIGURE 6: Cisplatin activates PVM/Ms in SV. (a) The distribution of PVM/Ms by immunofluorescence staining. PVM/Ms were marked with a special antibody against CD68 (red) and strial capillaries with Griffonia Simplicifolia IB4 (gray). Nuclei were stained with DAPI (blue). The PVM/Ms were highly invested on the abluminal surface of capillaries. Scale bars, 100 μm . (b) Zoom in of immunofluorescence staining. (c) Quantification of CD68-positive infiltration per SV area ($n = 5$). (d) qRT-PCR shows mRNA for IL-1 β in the SV. $n = 6$. ** $p < 0.01$ and *** $p < 0.001$.

through caspase activation [11, 15, 52]. We speculate that cisplatin-triggered activation of PVM/Ms, by its effect on extending cytokine production, could also extend cisplatin-induced inner ear inflammation. The specific signals underlying PVM/M activation are still not fully clear. IL-1 β is a major proinflammatory cytokine which is produced by activated macrophages and is widely regarded as a hallmark of inflammatory gene cascades [53]. A recent study also revealed that PVM/Ms in the mouse cochlea could activate the NLRP3 inflammasome in response to stimulation with lipopolysaccharide plus adenosine triphosphate, which results in IL-1 β secretion [54]. We found that the IL-1 β was also significantly increased after cisplatin treatment in

SV. In our preliminary experiments, cytokines such as IL-2, IL-4, and IL-10 in SV were also detected in mice after cisplatin treatment; however, the results showed that there were no significant differences of these cytokines in SV between the control group and the cisplatin-treated group (data not shown). We speculate that excessive expression and/or aberrant activation of IL-1 β and PVM/Ms in the cochlea might contribute to the deterioration of hearing function, which needs to be investigated in further experiments.

Increased levels of laminin immunoreactivity have been reported in blood vessel basal lamina, following cerebral ischemia [55] and quinolinic acid [56] treatments. Notably, a similar upregulation in laminin and collagen IV levels is

found in mice injected with cisplatin. The laminin overexpression is explained by an improved accessibility of laminin epitope disconnection of the gliovascular junctions in damaged blood vessels [57]. According to these authors, gliovascular junctions could limit the accessibility of the basal lamina of blood vessels to antibodies, thus “hiding” the laminin epitopes. Therefore, upregulation of laminin and collagen IV expression is one of the consequences from BLB modification and cisplatin promotes the progression of SV fibrosis by increasing the expression of ECM components. The presence of α -SMA-positive myofibroblast-like cells is considered a hallmark for the development of kidney fibrosis [18]. In our study, we found increased localization of α -SMA-positive cells in the SV. These results are in agreement with *in vitro* and *in vivo* studies that have shown areas of fibrosis-activated macrophages generating soluble mediators that modulate activation and proliferation of myofibroblasts [58, 59]. Therefore, our findings suggest that cisplatin might promote the progression of SV fibrosis through the regulation of macrophage infiltration, secretion of IL-1 β , and accumulation of laminin and collagen IV.

In summary, the present investigation showed that there were structural morphologic alterations of the cell junction component in the mice SV; TJ and GJ proteins were down-regulated substantially after cisplatin treatment. Our findings suggested that the changes induced by cisplatin may be associated with PVM/Ms activation, IL-1 β secretion, and ECM overexpression. The results reported herein provide evidence that the interaction of cisplatin with the BLB in SV results in a translocation of the cell junction apparatus that, in turn, could result in secondary injuries to the inner ear. Further investigation on the molecular mechanism underlying cisplatin-induced SV damage could bring new targets to develop specific therapies against cisplatin ototoxicity.

Data Availability

The datasets used and analyzed during the current study are available from the corresponding authors on reasonable request.

Conflicts of Interest

The authors declare that there are no conflicts of interest regarding the publication of this paper.

Authors' Contributions

Na Zhang and Jing Cai contributed equally to this work.

Acknowledgments

This work was supported by the Taishan Scholars Program of Shandong Province (Nos. tsqn201909189 and ts20130913), National Natural Science Foundation of China (Nos. 81700918 and 81670932), and Key Project of Shandong Provincial Programs for Research and Development (2017CXGC1213).

References

- [1] P. Wangemann, “K⁺ cycling and the endocochlear potential,” *Hearing Research*, vol. 165, no. 1-2, pp. 1–9, 2002.
- [2] S. K. Juhn, B. A. Hunter, and R. M. Odland, “Blood-labyrinth barrier and fluid dynamics of the inner ear,” *The International Tinnitus Journal*, vol. 7, no. 2, pp. 72–83, 2001.
- [3] J. Gilleron, D. Carette, P. Durand, G. Pointis, and D. Segretain, “Connexin 43 a potential regulator of cell proliferation and apoptosis within the seminiferous epithelium,” *The International Journal of Biochemistry & Cell Biology*, vol. 41, no. 6, pp. 1381–1390, 2009.
- [4] X. Shi, “Cochlear pericyte responses to acoustic trauma and the involvement of hypoxia-inducible factor-1 α and vascular endothelial growth factor,” *The American Journal of Pathology*, vol. 174, no. 5, pp. 1692–1704, 2009.
- [5] S.-i. Kitajiri, M. Furuse, K. Morita et al., “Expression patterns of claudins, tight junction adhesion molecules, in the inner ear,” *Hearing Research*, vol. 187, no. 1-2, pp. 25–34, 2004.
- [6] F. Nin, H. Hibino, K. Doi, T. Suzuki, Y. Hisa, and Y. Kurachi, “The endocochlear potential depends on two K⁺ diffusion potentials and an electrical barrier in the stria vascularis of the inner ear,” *Proc Natl Acad Sci USA*, vol. 105, no. 5, pp. 1751–1756, 2008.
- [7] Y. Mori, M. Watanabe, T. Inui et al., “Ca²⁺ regulation of endocochlear potential in marginal cells,” *The Journal of Physiological Sciences*, vol. 59, no. 5, pp. 355–365, 2009.
- [8] L. Neng, F. Zhang, A. Kachelmeier, and X. Shi, “Endothelial cell, pericyte, and perivascular resident macrophage-type melanocyte interactions regulate cochlear intrastrial fluid-blood barrier permeability,” *Journal of the Association for Research in Otolaryngology : JARO*, vol. 14, no. 2, pp. 175–185, 2013.
- [9] X. Shi, “Pathophysiology of the cochlear intrastrial fluid-blood barrier (review),” *Hearing Research*, vol. 338, pp. 52–63, 2016.
- [10] H. Li, Y. Song, Z. He et al., “Meclofenamic acid reduces reactive oxygen species accumulation and apoptosis, inhibits excessive autophagy, and protects hair cell-like HEI-OC1 cells from cisplatin-induced damage,” *Frontiers in Cellular Neuroscience*, vol. 12, p. 139, 2018.
- [11] W. Liu, X. Xu, Z. Fan et al., “Wnt signaling activates TP53-induced glycolysis and apoptosis regulator and protects against cisplatin-induced spiral ganglion neuron damage in the mouse cochlea,” *Antioxidants & Redox Signaling*, vol. 30, no. 11, pp. 1389–1410, 2019.
- [12] N. Tsukasaki, C. A. Whitworth, and L. P. Rybak, “Acute changes in cochlear potentials due to cisplatin,” *Hearing Research*, vol. 149, no. 1-2, pp. 189–198, 2000.
- [13] T. Koch and B. Gloddek, “Inhibition of adenylate-cyclase-coupled G protein complex by ototoxic diuretics and cisplatin in the inner ear of the guinea pig,” *European archives of oto-rhino-laryngology*, vol. 248, no. 8, pp. 459–464, 1991.
- [14] S. Sluyter, S. F. L. Klis, J. C. M. J. de Groot, and G. F. Smoorenburg, “Alterations in the stria vascularis in relation to cisplatin ototoxicity and recovery,” *Hearing Research*, vol. 185, no. 1-2, pp. 49–56, 2003.
- [15] S. A. Alam, K. Ikeda, T. Oshima et al., “Cisplatin-induced apoptotic cell death in Mongolian gerbil cochlea,” *Hearing Research*, vol. 141, no. 1-2, pp. 28–38, 2000.
- [16] M. Sakagami, T. Matsunaga, and P. H. Hashimoto, “Fine structure and permeability of capillaries in the stria vascularis

- and spiral ligament of the inner ear of the guinea pig," *Cell and Tissue Research*, vol. 226, no. 3, pp. 511–522, 1982.
- [17] S. K. Juhn, L. P. Rybak, and S. Prado, "Nature of blood-labyrinth barrier in experimental conditions," *The Annals of Otology, Rhinology, and Laryngology*, vol. 90, pp. 135–141, 2016.
- [18] L. L. Falke, S. Gholizadeh, R. Goldschmeding, R. J. Kok, and T. Q. Nguyen, "Diverse origins of the myofibroblast—implications for kidney fibrosis," *Nature Reviews. Nephrology*, vol. 11, no. 4, pp. 233–244, 2015.
- [19] W. Zhang, M. Dai, A. Fridberger et al., "Perivascular-resident macrophage-like melanocytes in the inner ear are essential for the integrity of the intrastrial fluid-blood barrier," *Proc Natl Acad Sci USA*, vol. 109, no. 26, pp. 10388–10393, 2012.
- [20] Z.-H. He, S.-Y. Zou, M. Li et al., "The nuclear transcription factor FoxG1 affects the sensitivity of mimetic aging hair cells to inflammation by regulating autophagy pathways," *Redox Biology*, vol. 28, p. 101364, 2020.
- [21] S. Gao, C. Cheng, M. Wang et al., "Blebbistatin inhibits neomycin-induced apoptosis in hair cell-like HEI-OC-1 cells and in cochlear hair cells," *Frontiers in Cellular Neuroscience*, vol. 13, p. 590, 2019.
- [22] Y. Zhang, W. Li, Z. He et al., "Pre-treatment with fasudil prevents neomycin-induced hair cell damage by reducing the accumulation of reactive oxygen species," *Frontiers in Molecular Neuroscience*, vol. 12, p. 264, 2019.
- [23] Y. Liu, J. Qi, X. Chen et al., "Critical role of spectrin in hearing development and deafness," *Science advances*, vol. 5, 2019.
- [24] L. Liu, Y. Chen, J. Qi et al., "Wnt activation protects against neomycin-induced hair cell damage in the mouse cochlea," *Cell Death & Disease*, vol. 7, no. 3, p. e2136, 2016.
- [25] Y. Wang, J. Li, X. Yao et al., "Loss of CIB2 causes profound hearing loss and abolishes mechano-electrical transduction in mice," *Frontiers in Molecular Neuroscience*, vol. 10, p. 401, 2017.
- [26] Z. He, Q. Fang, H. Li et al., "The role of FOXG1 in the postnatal development and survival of mouse cochlear hair cells," *Neuropharmacology*, vol. 144, pp. 43–57, 2019.
- [27] Z. He, L. Guo, Y. Shu et al., "Autophagy protects auditory hair cells against neomycin-induced damage," *Autophagy*, vol. 13, no. 11, pp. 1884–1904, 2017.
- [28] C. Zhu, C. Cheng, Y. Wang et al., "Loss of ARHGEF6 causes hair cell stereocilia deficits and hearing loss in mice," *Frontiers in Molecular Neuroscience*, vol. 11, p. 362, 2018.
- [29] S. Zhang, Y. Zhang, Y. Dong et al., "Knockdown of Foxg1 in supporting cells increases the trans-differentiation of supporting cells into hair cells in the neonatal mouse cochlea," *Cellular and Molecular Life Sciences*, vol. 77, no. 7, pp. 1401–1419, 2020.
- [30] F. Tan, C. Chu, J. Qi et al., "AAV-ie enables safe and efficient gene transfer to inner ear cells," *Nature Communications*, vol. 10, no. 1, p. 3733, 2019.
- [31] C. Cheng, Y. Wang, L. Guo et al., "Age-related transcriptome changes in Sox2+ supporting cells in the mouse cochlea," *Stem Cell Research & Therapy*, vol. 10, no. 1, p. 365, 2019.
- [32] S. Zhang, D. Liu, Y. Dong et al., "Frizzled-9+ supporting cells are progenitors for the generation of hair cells in the postnatal mouse cochlea," *Frontiers in Molecular Neuroscience*, vol. 12, p. 184, 2019.
- [33] X. Lu, S. Sun, J. Qi et al., "Bmi1 regulates the proliferation of cochlear supporting cells via the canonical Wnt signaling pathway," *Molecular Neurobiology*, vol. 54, no. 2, pp. 1326–1339, 2017.
- [34] T. Wang, R. Chai, G. S. Kim et al., "Lgr5+ cells regenerate hair cells via proliferation and direct transdifferentiation in damaged neonatal mouse utricle," *Nature Communications*, vol. 6, no. 1, 2015.
- [35] B. C. Cox, R. Chai, A. Lenoir et al., "Spontaneous hair cell regeneration in the neonatal mouse cochlea in vivo," *Development*, vol. 141, no. 4, pp. 816–829, 2014.
- [36] R. Ravi, S. M. Somani, and L. P. Rybak, "Mechanism of cisplatin ototoxicity: antioxidant system," *Pharmacology & Toxicology*, vol. 76, no. 6, pp. 386–394, 1995.
- [37] J. Wang, R. V. Lloyd Faulconbridge, A. Fetoni, M. J. Guitton, R. Pujol, and J. L. Puel, "Local application of sodium thiosulfate prevents cisplatin-induced hearing loss in the guinea pig," *Neuropharmacology*, vol. 45, no. 3, pp. 380–393, 2003.
- [38] S. J. O'Leary, S. F. L. Klis, J. C. M. J. de Groot, F. P. T. Hamers, and G. F. Smoorenburg, "Perilymphatic application of cisplatin over several days in albino guinea pigs: dose-dependency of electrophysiological and morphological effects," *Hearing Research*, vol. 154, no. 1-2, pp. 135–145, 2001.
- [39] X. Wu, J. Cai, X. Li et al., "Allicin protects against cisplatin-induced vestibular dysfunction by inhibiting the apoptotic pathway," *European Journal of Pharmacology*, vol. 805, pp. 108–117, 2017.
- [40] X. Wu, X. Li, Y. Song et al., "Allicin protects auditory hair cells and spiral ganglion neurons from cisplatin-induced apoptosis," *Neuropharmacology*, vol. 116, pp. 429–440, 2017.
- [41] L. P. Rybak, D. Mukherjee, and V. Ramkumar, "Mechanisms of cisplatin-induced ototoxicity and prevention," *Seminars in Hearing*, vol. 40, no. 2, pp. 197–204, 2019.
- [42] R. P. Meech, K. C. M. Campbell, L. P. Hughes, and L. P. Rybak, "A semiquantitative analysis of the effects of cisplatin on the rat stria vascularis," *Hearing Research*, vol. 124, no. 1-2, pp. 44–59, 1998.
- [43] J. E. Lee, T. Nakagawa, T. Kita et al., "Mechanisms of apoptosis induced by cisplatin in marginal cells in mouse stria vascularis," *ORL; journal for oto-rhino-laryngology and its related specialties*, vol. 66, no. 3, pp. 111–118, 2004.
- [44] K. C. Campbell, R. P. Meech, L. P. Rybak, and L. F. Hughes, "D-Methionine protects against cisplatin damage to the stria vascularis," *Hearing Research*, vol. 138, no. 1-2, pp. 13–28, 1999.
- [45] L. P. Rybak, C. Whitworth, A. Weberg, and V. Scott, "Effects of organic acids on the edema of the stria vascularis induced by furosemide," *Hearing Research*, vol. 59, no. 1, pp. 75–84, 1992.
- [46] H. Y. Lee, S. Y. Jung, M. S. Park, S. G. Yeo, S. Y. Lee, and S. K. Lee, "Feasibility of three-dimensional fluid-attenuated inversion recovery magnetic resonance imaging as a prognostic factor in patients with sudden hearing loss," *European archives of oto-rhino-laryngology*, vol. 269, no. 8, pp. 1885–1891, 2012.
- [47] V. Rigau, M. Morin, M.-C. Rousset et al., "Angiogenesis is associated with blood-brain barrier permeability in temporal lobe epilepsy," *Brain: a journal of neurology*, vol. 130, no. 7, pp. 1942–1956, 2007.
- [48] X. Yi, Y. Wang, and F. S. Yu, "Corneal epithelial tight junctions and their response to lipopolysaccharide challenge," *Investigative Ophthalmology & Visual Science*, vol. 41, no. 13, pp. 4093–4100, 2000.
- [49] T. Kikuchi, R. S. Kimura, D. L. Paul, T. Takasaka, and J. C. Adams, "Gap junction systems in the mammalian cochlea,"

- Brain Research. Brain Research Reviews*, vol. 32, no. 1, pp. 163–166, 2000.
- [50] J. Chen, J. Chen, Y. Zhu, C. Liang, and H.-B. Zhao, “Deafness induced by connexin 26 (GJB2) deficiency is not determined by endocochlear potential (EP) reduction but is associated with cochlear developmental disorders,” *Biochemical and Biophysical Research Communications*, vol. 448, no. 1, pp. 28–32, 2014.
- [51] M. Cohen-Salmon, S. Maxeiner, O. Krüger, M. Theis, K. Willecke, and C. Petit, “Expression of the connexin43- and connexin45-encoding genes in the developing and mature mouse inner ear,” *Cell and Tissue Research*, vol. 316, no. 1, pp. 15–22, 2004.
- [52] J. R. García-Berrocal, J. Nevado, R. Ramírez-Camacho et al., “The anticancer drug cisplatin induces an intrinsic apoptotic pathway inside the inner ear,” *British Journal of Pharmacology*, vol. 152, no. 7, pp. 1012–1020, 2007.
- [53] A. Weber, P. Wasiliew, and M. Kracht, “Interleukin-1 (IL-1) pathway,” *Science signaling*, vol. 3, no. 105, 2010.
- [54] H. Nakanishi, Y. Kawashima, K. Kurima et al., “NLRP3 mutation and cochlear autoinflammation cause syndromic and nonsyndromic hearing loss DFNA34 responsive to anakinra therapy,” *Proceedings of the National Academy of Sciences*, vol. 114, no. 37, pp. E7766–E7775, 2017.
- [55] Q. Han, B. Li, H. Feng et al., “The promotion of cerebral ischemia recovery in rats by laminin-binding BDNF,” *Biomaterials*, vol. 32, no. 22, pp. 5077–5085, 2011.
- [56] J. K. Ryu, N. Jantarotnotai, and J. G. McLarnon, “Thalidomide inhibition of vascular remodeling and inflammatory reactivity in the quinolinic acid-injected rat striatum,” *Neuroscience*, vol. 163, no. 2, pp. 601–608, 2009.
- [57] M. Kálmán, J. Mahalek, A. Adorján et al., “Alterations of the perivascular dystrophin-dystroglycan complex following brain lesions: an immunohistochemical study in rats,” *Histology and Histopathology*, vol. 26, no. 11, pp. 1435–1452, 2011.
- [58] Y. Li, X. Wang, L. Zhang et al., “Upregulation of allograft inflammatory factor-1 expression and secretion by macrophages stimulated with aldosterone promotes renal fibroblasts to a profibrotic phenotype,” *International Journal of Molecular Medicine*, vol. 42, no. 2, pp. 861–872, 2018.
- [59] Y.-Y. Wang, H. Jiang, J. Pan et al., “Macrophage-to-myofibroblast transition contributes to interstitial fibrosis in chronic renal allograft injury,” *Journal of the American Society of Nephrology*, vol. 28, no. 7, pp. 2053–2067, 2017.

Research Article

Effects of SoundBite Bone Conduction Hearing Aids on Speech Recognition and Quality of Life in Patients with Single-Sided Deafness

Qiong Luo ¹, Ying Shen ¹, Ting Chen ², Zhong Zheng ¹, Haibo Shi ¹, Yanmei Feng ¹
and Zhengnong Chen ¹

¹Department of Otolaryngology Head and Neck Surgery, Shanghai Jiaotong University Affiliated Sixth People's Hospital, Shanghai Key Laboratory of Sleep Disordered Breathing, Shanghai, China

²Department of Stomatology, Shanghai Jiaotong University Affiliated Sixth People's Hospital, China

Correspondence should be addressed to Yanmei Feng; feng.yanmei@126.com and Zhengnong Chen; jasley@126.com

Received 13 March 2020; Revised 5 August 2020; Accepted 18 August 2020; Published 8 September 2020

Academic Editor: Geng lin Li

Copyright © 2020 Qiong Luo et al. This is an open access article distributed under the Creative Commons Attribution License, which permits unrestricted use, distribution, and reproduction in any medium, provided the original work is properly cited.

Objectives. To analyze the clinical application of SoundBite bone conduction hearing aids by assessing the improvement of speech recognition and the scores of the benefit scale questionnaire for patients with single-sided deafness (SSD). **Design.** Nine patients aged 24 to 61 years with SSD for more than 3 months were enrolled in this study. The patients could understand and repeat Mandarin and have good compliance with the study. The measurements were evaluated before and after one month of wearing hearing aids using the pure tone audiometry threshold, speech recognition in quiet and in noise, and the Glasgow Benefit Inventory (GBI) benefit scale score. **Results.** Pure tone audiometry results showed that the average hearing threshold of good ears and bad ears was 11.4 ± 2.6 dB HL and 89.9 ± 6.4 dB HL, respectively. The average hearing threshold of bad ears after wearing hearing aids was 23.5 ± 9.0 dB HL. Statistical analysis showed that the hearing improvement for the bad ears after wearing hearing aids was significant. The speech audiometry results showed that the disyllable word recognition score of the bad ears in quiet increased significantly at 50 dB SPL by 40 ± 12 percentage points and at 65 dB SPL by 71 ± 15 percentage points. As for the speech recognition in noise, when the signal sound came from the bad ear side and the noise from the good ear side ($S_{SSD}N_{AH}$), the speech recognition score (SRS) significantly increased by 17 ± 6 and 9 ± 4 at a signal-to-noise ratio (SNR) of -2 dB and -5 dB, respectively, after wearing the hearing aids. When the signal sound came from the front of the patient and the noise from the bad ear side (S_0N_{SSD}), the SRS scores were reduced by 5 ± 5 and 7 ± 5 percentage points at SNR equal to -2 dB and -5 dB, which was significantly different from that before wearing the hearing aids. When the signal and noise both came from the front of the patients (S_0N_0), the SRS was not significantly increased by 5 ± 4 percentage points at SNR equal to -2 dB compared to before wearing hearing aids. However, the SRS was significantly increased by 5 ± 2 percentage points at SNR equal to -5 dB compared to before wearing hearing aids. The average total GBI score was 31 ± 12 for the nine patients, with an average score of 32 ± 10 , 31 ± 8 , and 30 ± 7 for general conditions, social support, and physical health, respectively. The results of the questionnaires showed that patients' quality of life was improved after wearing SoundBite bone conduction hearing aids. **Conclusions.** SoundBite bone conduction hearing aids are a good choice for patients with SSD, as it could improve the speech recognition ability of patients both in a quiet and noisy environment and improves the quality of life after wearing hearing aids.

1. Introduction

Single-sided deafness (SSD) refers to severe to profound sensorineural hearing loss on one side (>70 dB HL) and an average hearing threshold of 0.5 to 4 kHz ≤ 25 dB HL on the good ear [1]. People with SSD generally do not wear hearing

aids because they can depend on the good ear in daily life. Slattery tested the ability of human listeners to localize broadband noise bursts in the absence of binaural localization cues. The patients demonstrate that monaural cues can provide useful localization information in the horizontal as well as in the vertical dimension [2]. However, they often face

barriers for speech communication in a noisy environment, especially when the sound source is on the bad ear side [3]. Patients with SSD often need to turn their head when communicating with others in order to use their good ears, with some patients feeling embarrassed or inconvenienced [4]. Moreover, the SSD patients are not able to distinguish the source of the sound.

Current intervention options for SSD include cochlear implants and hearing aids. Previous studies have shown that cochlear implants in SSD patients can improve speech recognition and sound source localization [5, 6]. However, studies have shown that SSD patients have different benefits after cochlear implantation, and cochlear implants are expensive, which makes patients unwilling to choose cochlear implants. As for hearing aids for SSD intervention, air conduction hearing aids and bone conduction hearing aids can be used. Air conduction hearing aids can be implemented on the bad side or on the healthy side by means of signal transmission. Contralateral routing of the signal system is a choice. Both ears need to be equipped with hearing aids. The auxiliary hearing device is worn on the bad ear to receive signals and transmit them to the contralateral ear. The main hearing device is worn on the good ear to receive and amplify the contralateral signals. Bone conduction hearing aid is another treatment method for SSD, which includes surgically implanted hearing aids and nonsurgically implanted hearing aids. However, implantable bone conduction hearing aids fix the sound processor onto the skull, which generates a large amount of pressure on the skull and can stimulate skin hyperplasia and cause pain in the patient. In addition, the transmission of sound is weakened due to the barrier of soft tissue. Nowadays, BAHA (Cochlear in Australia) is the most commonly used bone conduction hearing aid, which requires surgical implantation. Many patients have concerns about the impact of surgery and the infection on the wound. Studies have shown that 29% of surgical patients will experience infections near the implanted device, soft tissue proliferation, skin irritation, and displacement of implant [7]. In addition, bone conduction hearing aids offer no obvious hearing improvement at frequencies above 4 kHz [8]. Some studies [9–11] have shown that the average air conduction hearing threshold of 0.25 to 4 kHz after the subject wears BAHA was improved by 30.2 to 39.1 dB. Xia et al. tested [12] 12 cases wearing soft-band bone conduction hearing aids; the SRT was improved to 5.91 dB, which was better than naked ears with 13.64 dB. BAHA also has defects in the localization of the sound source in patients with extremely severe SSD. Currently, some controversies about hearing aid gain, sound source localization ability, and speech recognition under noise in implanted patients exist [13, 14]. Therefore, some patients with SSD are reluctant to use implantable bone conduction hearing aids [15, 16].

The advantage of nonimplantable bone conduction hearing aids is that they do not require complicated surgical procedures. A nonimplantable bone conduction device on the skull [17] requires placing a behind-the-ear (BTE) microphone in a hearing-impaired ear to simulate the acoustic characteristics of normal auricles. SoundBite bone conduction hearing aid is such a hearing device. The microphone

receives the sound, and then, the sound is processed by BTE digital audio equipment. A removable in-the-mouth (ITM) device is fixed onto the teeth and directly coupled to the skull. The ITM device generates vibration that passes through the skull to the cochlea. The ITM device is directly fixed onto the dental bones, and the sound transmission will not be hindered by soft tissues. The sound transmission efficiency is higher than that achieved by adhesion or clamping.

A previous study compared eight bone conduction hearing aids' maximum output and gain; the researchers found that within the frequency range of 4 to 8 kHz, the maximum output and gain for each bone conduction device were different, with SoundBite demonstrating better performance [17]. In another study, the researchers measured the speech recognition threshold (SRT) with the noise from different directions while wearing SoundBite for SSD patients. The results showed that the SRT was an average of 2.5 dB lower than that without wearing SoundBite with the signal coming from the front and the noise from the good ear side. The SRT did not change when the noise came from the front. The SRT was reduced by 2.3 dB when the noise came from the bad ear side [18]. Also, studies have shown that SoundBite is comparable to, or even better than, BAHA in English speakers.

To date, however, there is no research investigating SoundBite bone conduction hearing aids in Chinese SSD patients. In this study, Chinese speech recognition in quiet and in noisy environments was evaluated before and after wearing the hearing aids. The GBI scale is designed for use only once postintervention, as a measure of change related to a specific surgical or medical intervention. The questionnaire consists of 18 questions answered using a five-point Likert scale, addressing change in health status post any intervention. The responses are then scaled and averaged to give a score with a range -100 (poorest outcome) through 0 (no change) to +100 (best outcome). A positive value indicates that the patient has benefited to a certain degree in quality of life after medical intervention, a zero score indicates no change, and a negative value indicates that the health level has deteriorated after the intervention. It is widely used in otolaryngology to report change in the quality of life post-intervention [19]. The GBI scale was used to assess the impact of patients' general conditions, social support, and physical health benefit of hearing aids and to explore the clinical application of SoundBite bone conduction hearing aids in Chinese patients with SSD.

2. Materials and Methods

2.1. Ethics Statement. The study and the informed consent procedures were approved by the local ethics committee (Ethics Committee of the Shanghai Sixth People's Hospital, approval number: 2018-092), and written informed consent was obtained before participation.

2.2. Enrollment Indications. SSD patients who were 18 years or older were enrolled in this study. All the enrolled patients should have SSD history longer than 3 months. Before fitting

TABLE 1: Characteristics of the single-side deafness patients in this study.

Subject no.	Gender	Age	Deafness ear	Duration of deafness	Causes of deafness
01	Male	61	Right	20 years	Sudden deafness
02	Male	35	Right	20 years	Postoperative acoustic neuroma
03	Female	41	Left	2 years	Postoperative acoustic neuroma
04	Male	40	Right	2 years	Sudden deafness
05	Female	24	Right	3 years	Sudden deafness
06	Female	30	Right	2 years	Sudden deafness
07	Male	46	Left	6 months	Sudden deafness
08	Female	35	Left	More than 30 years	Congenital deafness
09	Female	44	Right	7 years	Postoperative acoustic neuroma

a SoundBite appliance (Sonitus Medical Technology Company, Shanghai), the teeth of the patients were examined completely by a dentist to make sure that the teeth are healthy; there can be no active caries or periodontal or endodontic conditions affecting the abutment teeth [4].

Subjects were excluded if they met any of the following criteria: (1) currently using other hearing aids, such as BAHA, contralateral routing of signals, and TransEar; (2) speech recognition score (SRS) is disproportionately lower than what would be predicted with the pure tone audiometry (PTA); and (3) patients have psychological or mental conditions that may interfere with understanding, informed consent, compliance, and cooperation.

2.3. Basic Characteristics of Patients. Altogether, 9 patients with SSD for more than 3 months were enrolled in this study. The patients aged between 24 and 61 years with an average age of 39.3 ± 10.8 years, including 4 males and 5 females (see Table 1). The patients could understand and repeat Mandarin and demonstrated good compliance to wearing the hearing aid and to the evaluation of the hearing aid. The subjects had an average hearing threshold on the good ear ≤ 25 dB HL across 0.5, 1, 2, and 4 kHz. The etiology for SSD includes 5 cases of sudden deafness, 3 cases of postoperative acoustic neuroma, and 1 case of congenital unilateral sensorineural hearing loss.

2.4. Hearing Aid Fitting. During the whole study, the devices were fitted using the open SoundBite fitting software. The gain was adjusted to the most comfortable level for the patient. PTA was tested after adjustment. The fitted PTA must meet the criteria that the difference between the average air conduction hearing threshold (averaged across 0.5, 1, 2, and 4 kHz) after fitting and that in the healthy ear is within 15 dB. Feedback noise cancellation was turned on if there was howling.

2.5. Testing Procedure. The patients completed the PTA and tympanogram test before wearing a hearing aid. The Middle Ear Analyzer (Flute Basic, Italy) was used for the tympanogram. PTA tests were performed in a sound-proofed room with noise less than 30 dB (A) and a calibrated GSI-61™ audiometer (The United States) coupled with TDH 39 headphones.

The speech audiometry test was performed in a standard sound-proofed room with noise less than 30 dB (A) calibrated sound field. Before the test, the subjects were familiarized with the test process. The subjects were required to repeat what they heard; then, the audiologist judged whether the restatement was correct. After the test, the system will automatically calculate the SRS and display the results.

The materials named XinAiFeiYang issued by the People's Liberation Army General Hospital of Chinese were used for disyllable word recognition in quiet. The material includes 5 test lists, each list contains 40 words, which are enough to make the consonants and tones present in each list representative of those in the language used in daily life [20]. It has been clinically verified by many centers that it can meet the clinical requirements for test reliability, validity, and practicality [21]. Disyllable word recognition test was performed with a calibrated audiometer (Astera Conera, Denmark). TDH39 headphones were used to test the disyllable word SRS at 50 and 65 dB sound pressure level (SPL) which represents low and medium sound levels for communication.

The Mandarin HINT materials were used for SRS under noise. The Mandarin HINT test materials were donated by the House Ear Research Institute. It includes an exercise list, 12 test lists, and 20 sentences each list. Two calibrated loudspeakers (System 600, Tannoy) were used to present the sound. Both loudspeakers were placed at 1 m distance from the subject's head. The SRS under noise was evaluated under the following sound field conditions: (1) the signal sound came from the bad ear side and the noise from the good ear side ($S_{SSD}N_{AH}$), (2) the signal sound came from the front of the patient and the noise from the bad ear side (S_0N_{SSD}), and (3) the signal and noise both came from the front of the patients (S_0N_0). The noise for SRS is steady-state noise, which is spectrally matched to the average spectrum of the sentences. The sentence recognition score was measured at a noise intensity of 65 dB SPL and SNR of -2 and -5 dB.

The subjects underwent PTA, the abovementioned speech audiometry test before and after one month of wearing hearing aids, and the GBI questionnaire test one month after wearing a hearing aid. The impacts of SoundBite bone conduction hearing aids on hearing and speech audiometry results were analyzed before and after wearing the hearing aids, and the GBI questionnaire score result was analyzed after wearing the hearing aids.

All tests and the GBI questionnaire evaluation were performed by an experienced and professionally trained audiologist.

2.6. Statistical Analysis. Statistical analysis was carried out using the Statistical Package for Social Sciences (SPSS) version 19.0 (Chicago, IL, USA). The hearing thresholds, SRS under quiet and noisy environment between before and after wearing hearing aids, were compared with paired-sample *t*-tests.

3. Results

3.1. Pure Tone Audiometry. The average hearing threshold of good and bad ears before wearing the hearing aids was 11.4 ± 2.6 dB HL and 89.9 ± 6.4 dB HL, respectively. The average hearing threshold of bad ears after fitting the hearing aid was 23.5 ± 9.0 dB HL (see Figure 1), representing a significantly improved hearing of 66.4 ± 14.9 dB compared to that before wearing the hearing aid ($p < 0.001$).

3.2. Speech Audiometry in Quiet. The disyllable word SRS under quiet condition at 50 and 65 dB SPL for the good ears was $70 \pm 20\%$ and $89 \pm 16\%$. The SRS in quiet at the two intensities was both 0% for the bad ears before wearing the hearing aids. After wearing the hearing aid, the SRS for the bad ears, obtained at 50 and 65 dB SPL, was increased by 40 ± 12 and 71 ± 15 percentage points (see Figure 2), respectively. The differences of SRS between before and after wearing the hearing aid were significant for both speech intensities ($p < 0.001$).

3.3. Speech Audiometry in Noisy. The speech recognition in noise was evaluated with sentence materials. When the signal came from the bad ear side and the noise came from the good ear side ($S_{SSD}N_{AH}$), the SRS scores were $28 \pm 17\%$ and $9 \pm 10\%$ without a hearing aid with the SNR at -2 dB and -5 dB, respectively. After wearing the hearing aid, the SRS scores were $45 \pm 16\%$ and $18 \pm 9\%$, which significantly increased by 17 ± 6 and 9 ± 4 percentage points compared to that before wearing the hearing aid ($p < 0.001$).

When the signal came from the front of the patient and the noise came from the bad ear side (S_0N_{SSD}), the SRS scores were $95 \pm 3\%$ and $84 \pm 7\%$ without a hearing aid with the SNR at -2 dB and -5 dB, respectively. After wearing the hearing aid, the SRS scores were $90 \pm 5\%$ and $77 \pm 8\%$. The SRS scores were reduced by 5 ± 5 and 7 ± 5 percentage points with the two SNRs, respectively. The differences between the two SRSs before and after fitting the hearing aid were statistically significant ($p < 0.05$).

When the signal and noise both came from the front of the patients (S_0N_0), the SRS scores were $75 \pm 9\%$ and $43 \pm 11\%$ without a hearing aid with the SNR at -2 and -5 dB, respectively. After wearing the hearing aid, the SRS scores were $80 \pm 10\%$ and $48 \pm 11\%$ with the two SNRs, respectively. The SRS was not significantly increased by 5 ± 4 percentage points with the SNR at -2 dB compared with that before wearing hearing aids ($p > 0.05$); however, the SRS was significantly increased by 5 ± 2 percentage points with the SNR at

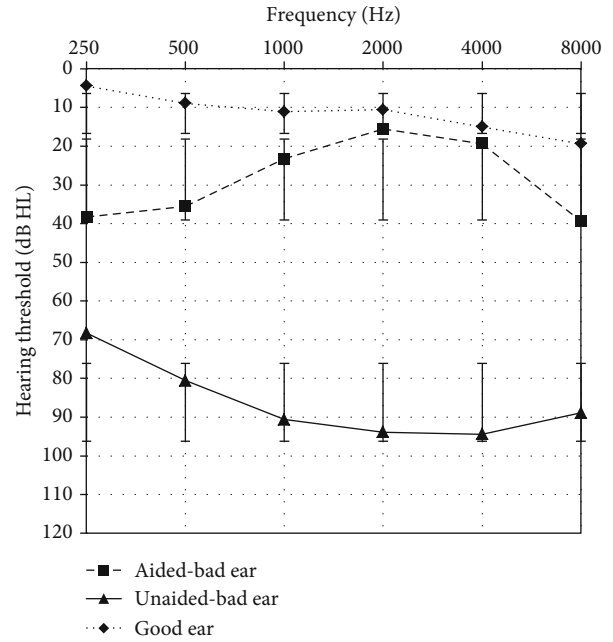


FIGURE 1: Average pure tone thresholds of SSD patients at frequencies of 250 to 8000 Hz before and after wearing a SoundBite bone conduction hearing aid. The lines represent the threshold of the good ear, the bad ear without the hearing aid, and the bad ear with the hearing aid. The bars represent one standard deviation.

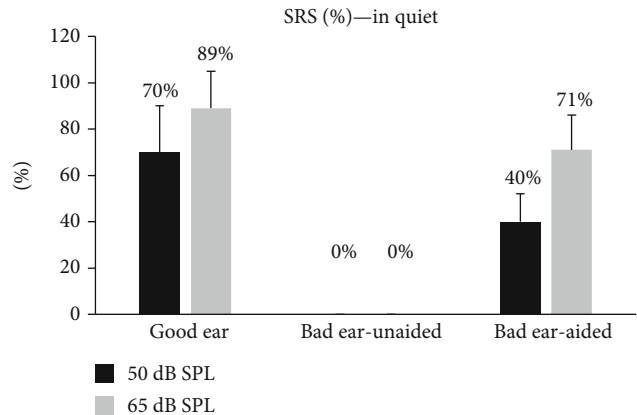


FIGURE 2: Disyllable word SRS under quiet environment of the good ear and the bad ear before and after wearing SoundBite bone conduction hearing aids for SSD patients at sound intensity 50 and 65 dB SPL. The bars represent one standard deviation.

-5 dB compared with that before wearing hearing aids ($p < 0.05$) (see Figure 3).

3.4. GBI Score. The average GBI total score from the nine patients was 31 ± 12 , with the average scores for the three subscales of general, social support, and physical health of 32 ± 10 , 31 ± 8 , and 30 ± 7 , respectively. The results of the questionnaires showed that patients' quality of life improved significantly after wearing SoundBite bone conduction hearing aids (see Figure 4).

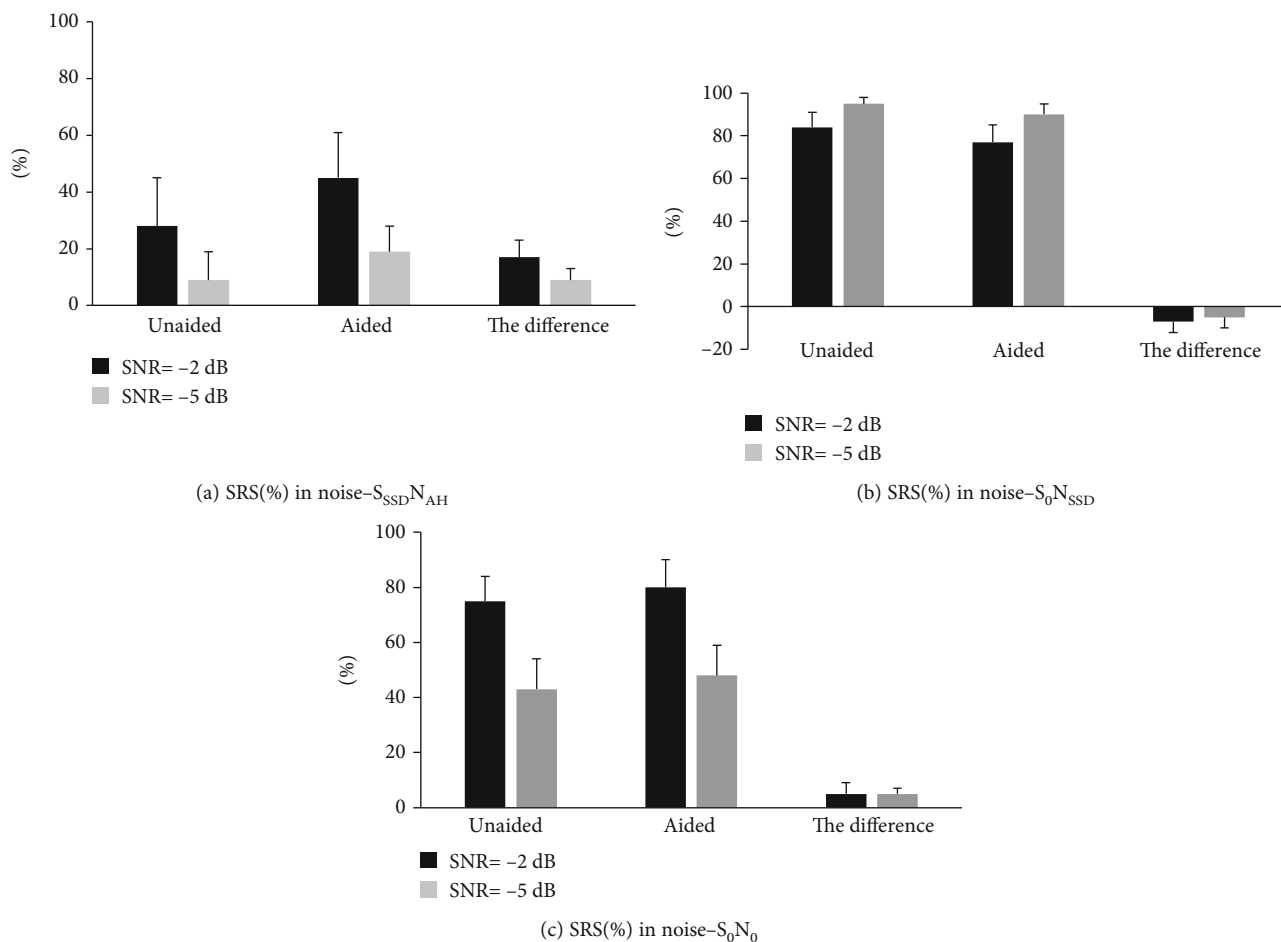


FIGURE 3: SRS under noisy environment before and after wearing SoundBite bone conduction hearing aids for SSD patients. The noise was at 65 dB SPL, and the SNR was equal to -2 and -5 dB. (a) $S_{SSD}N_{AH}$: the signal sound came from the bad ear side and the noise came from the good ear side. (b) S_0N_{SSD} : the signal sound came from the front of the patient and the noise came from the bad ear side. (c) S_0N_0 : the signal and noise both came from the front of the patients. The bars represent one standard deviation.

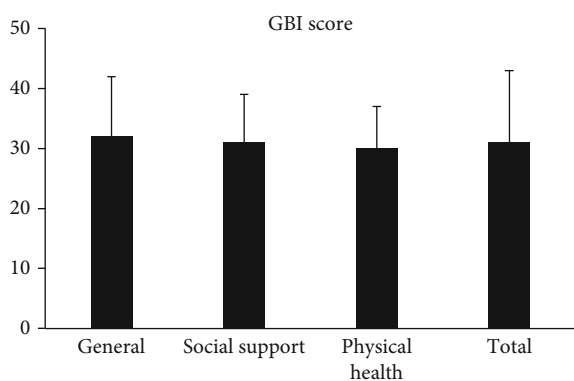


FIGURE 4: Glasgow Benefit Inventory (GBI) scores after wearing SoundBite bone conduction hearing aids for SSD patients. The total score and three subscale scores of general, social support, and physical health are shown separately. The bars represent one standard deviation.

4. Discussion

In this study, 9 patients with SSD wore SoundBite bone conduction hearing aids for one month. Their hearing, speech

recognition, and life benefits were evaluated before and after one month of wearing. This study was first performed in Mandarin Chinese speakers with speech tests using Chinese materials. The results showed that after wearing the hearing aid, the air conduction hearing threshold (across 0.5-4 kHz) decreased by 66.4 ± 14.9 dB for the bad ear. Under a quiet environment, the disyllable word SRS in the bad ear was improved by 40 ± 12 and 71 ± 15 percentage points after wearing the hearing aid with the speech signal at 50 and 65 dB SPL, respectively. Under a noisy environment, the SRS was increased by 17 ± 6 and 9 ± 4 percentage points with $S_{SSD}N_{AH}$ at SNR -2 and -5 dB, respectively. The SRS scores were reduced by 5 ± 5 and 7 ± 5 percentage points with S_0N_{SSD} at SNR -2 and -5 dB, respectively. The SRS scores were improved by 5 ± 4 and 5 ± 2 percentage points with S_0N_0 at SNR -2 and -5 dB, respectively. The GBI benefit scale showed that the general conditions, social support, and physical health were improved after wearing the hearing aid.

Our study showed that the average aided hearing threshold for frequencies across 0.5, 1, 2, and 4 kHz was 23.5 dB HL. These results are consistent with previous studies, which showed the aided threshold of 21.3 dB for frequencies across 1, 2, 3, 4, and 6 kHz after wearing SoundBite for one month

[22]. A previous study showed that BAHA is less effective at a frequency compensation of 4 kHz and above. This may be related to the attenuation of high-frequency sound vibration through subcutaneous tissues; thus, the acoustic signal could be weakened by 10-15 dB [23]. Our study showed that the average hearing threshold for frequencies across 4 and 8 kHz after wearing SoundBite was 29.4 dB HL. Therefore, SoundBite hearing aids are better than BAHA in the improvement of hearing at medium and high frequencies, which is critical for speech clearance and helps to improve speech intelligibility and speech recognition [14].

Disyllable word has an important value in auditory speech evaluation [24]. The results of this study showed that in patients with SSD, the SRS for disyllable word under quiet is increased with the signal at the bad ear side, especially at a moderate sound level. The SRS at the soft sound level of 50 dB SPL increased by 40 percentage points, and the SRS at a moderate sound level of 65 dB SPL increased by 71 percentage points after wearing the hearing aid, representing significant differences compared to that before wearing the hearing aid ($p < 0.001$). After wearing SoundBite, the improvement at moderate sound intensity was better than that at soft sound intensity, suggesting that the speech recognition of patients in a quiet environment was greatly improved at the everyday life sound level.

Spatial hearing and binaural hearing play an important role in the localization of sound sources, especially in a noisy environment. The main reason for speech recognition disturbance in a noisy environment for patients with SSD is the head shadow effect [25]. This is a physical phenomenon caused by the blocking of the sound by the head. When the sound reaches the opposite ear, it is attenuated and results in the SNR of the side closer to the signal higher than that in the other ear. Therefore, people are able to benefit from the head shadow effect regardless of the direction of the noise [26]. The results of this study showed that speech recognition improved significantly in both SNRs of -2 and -5 dB. In a previous study of 28 patients who wore SoundBite for 6 months, the speech recognition threshold decreased by 2.5 dB [18], which is equivalent to 25 percentage points increase in SRS, as 1 dB decrease in speech recognition threshold is equivalent to 10 percentage points increase in SRS [27]. The difference between these two studies could be explained by the difference in the configuration of speech and noise. Although the noise in both studies was on the good ear side, the voice in this study came from the bad ear side while the speech in Murray's study came from the front. The head shadow effect in this study increased the difficulty of speech recognition. Therefore, the SRS in noise seems to be a little lower than that in Murray's study. Moreover, the small sample size of this study and the short wearing time may also explain the difference between these two studies. A previous study comparing the SRT after wearing SoundBite one day and one month showed that the increase by 0.8 dB between one day and one month was statistically significant [18]. Therefore, the speech improvement could be more significant with the extension time of wearing the hearing aids. The speech audiometry was evaluated after one month of wearing in this study, while it was evaluated after 6 months of wearing in

Murray's study. It may be expected that the effect on SRS will gradually increase with the longtime use of the hearing aid by the patients. The improved head shadow effect in SSD patients wearing SoundBite could be explained by the output of the device. Mark found that the maximum output frequency of SoundBite is above 2 kHz, which help the patients overcome the head shadow effect, so the SRS under noise was improved significantly by SoundBite bone conduction hearing aids [17].

When the signal and noise both came from the front of the patients (S_0N_0), both ears receive the signal and noise, which is different from listening with one ear, the subject hears louder. The subjects rely on the redundant information provided at the two ears, enhanced detection of smaller differences in signals, and improved speech recognition [28]. The auditory system is able to adjust the signals arriving at both ears by using the distinct time, level, and spectral cues occurring between the two ears. This permits a better separation of target and masker and improves intelligibility of the desired signal [29]. Gantz studied 10 patients with bilateral cochlear implants at condition S_0N_0 and found the SRS increased by 10.6 percentage points [30]. Our result obtained from the condition S_0N_0 showed that the SRS under noise environment increased significantly after wearing the hearing aid, which is consistent with the results obtained from bilateral cochlear implants.

While for the condition S_0N_{SSD} , the signal came from the front of the patient and the noise from the bad ear side, the noise and the signals are spatially separated. Our results show that the SRS deteriorates after wearing aid. The main reason is that when the noise is located at the bad ear side, the noise is amplified by the SoundBite and also be transmitted to the good ear side. As a result, the SNR of the good ear decreases and the noise interference results in a decrease in speech recognition.

SSD patients cannot accurately determine the sound source and need to turn their heads to find the sound. Moreover, speech recognition is not ideal in a noisy environment, which greatly affects the quality of life of patients [31, 32]. The abbreviated profile of hearing aid benefit (APHAB) hearing aid gain scale is usually used to evaluate the benefit of SoundBite. Studies have shown that the average APHAB score with SoundBite was 23.2, which was higher than the BAHA score -7 to 17 [33-36]. In this study, the GBI benefit scale was used to evaluate the general conditions, social support, and physical health of patients with SSD after wearing SoundBite. The average score after wearing SoundBite was 31 ± 12 . A previous study using GBI to evaluate the life quality showed that GBI questionnaire total score with the Sophono Alpha 2 transcutaneous bone-anchored sound processor was 14 ± 11.0 , with subscale general situation score 18 ± 18.3 , social support score 18 ± 22.7 , and physical health score -4 ± 11.1 [37]. The scores in all aspects were worse than those of the SoundBite in this study, especially for the impact of hearing aids on physical health. The main reason for significant improvement is that the SoundBite does not require surgery, which reduces the patient's fear and the chance of postoperative infection. Also, the device without surgery can gain more support from family members and

friends. The easy procedure to remove the device also makes the subjects feel convenient. All these factors result in higher GBI score compared with that of implanted bone conduction hearing aids.

5. Conclusions

SoundBite bone conduction hearing aids are beneficial for SSD patients. It could improve the speech recognition ability of patients in a quiet and noisy environment and quality of life after wearing it for one month. However, the sample size in this experiment is small, and the long-term effects of this device on the speech recognition and quality of life under various listening environment should be explored in further clinical research.

Data Availability

The form data used to support the findings of this study are available on request to the corresponding author: Dr. Yanmei Feng, email: feng.yanmei@126.com.

Additional Points

Research direction is audiology and vestibular function evaluation.

Conflicts of Interest

The authors have no conflicts of interest to disclose.

Authors' Contributions

Qiong Luo and Ying Shen contribute equally to the paper.

Acknowledgments

The authors thank all the people who participated in the study. Thanks are due to Sonitus Medical Technology company for donating SoundBite bone conduction hearing aids. Thanks are due to Professor Xin Xi and the House Ear Research Institute for providing the speech audiometry materials. The study was supported by the National Natural Science Foundation of China (Grant No. 81771015) through Yanmei Feng. In addition, this study was also supported by grants-in-aid from Shanghai Municipal Commission of Science and Technology (Grant No.18DZ2260200).

References

- [1] C. Vincent, S. Arndt, J. B. Firszt et al., "Identification and evaluation of cochlear implant candidates with asymmetrical hearing loss," *Audiology & Neuro-Otology*, vol. 20, no. 1, pp. 87–89, 2015.
- [2] W. H. Slaterry 3rd. and J. C. Middlebrooks, "Monaural sound localization: acute versus chronic unilateral impairment," *Hearing Research*, vol. 75, no. 1-2, pp. 38–46, 1994.
- [3] E. W. Sargent, B. Herrmann, C. S. Hollenbeak, and A. E. Bankaitis, "The minimum speech test battery in profound unilateral hearing loss," *Otology & Neurotology*, vol. 22, no. 4, pp. 480–486, 2001.
- [4] R. J. Miller, "It's time we listened to our teeth: the SoundBite hearing system," *American Journal of Orthodontics & Dentofacial Orthopedics*, vol. 138, no. 5, pp. 666–669, 2010.
- [5] J. B. Firszt, L. K. Holden, R. M. Reeder, S. B. Waltzman, and S. Arndt, "Auditory abilities after cochlear implantation in adults with unilateral deafness: a pilot study," *Otology & Neurotology*, vol. 33, no. 8, pp. 1339–1346, 2012.
- [6] D. Tavora-Vieira, G. De Ceulaer, P. J. Govaerts, and G. P. Rajan, "Cochlear implantation improves localization ability in patients with unilateral deafness," *Ear and Hearing*, vol. 36, no. 3, pp. e93–e98, 2015.
- [7] J. C. Hobson, A. J. Roper, R. Andrew, M. P. Rothera, P. Hill, and K. M. Green, "Complications of bone-anchored hearing aid implantation," *The Journal of Laryngology and Otology*, vol. 124, no. 2, pp. 132–136, 2010.
- [8] A. J. Bosman, F. M. Snik, E. A. Mylanus, and W. R. J. Cremers, "Fitting range of the BAHA Intenso," *International Journal of Audiology*, vol. 48, no. 6, pp. 346–352, 2009.
- [9] F. R. Su, J. H. Ding, L. Bo, and X. G. Liu, "BAHA implanted in patients with congenital microtia," *Chinese Journal of Otology*, vol. 12, pp. 563–565, 2014.
- [10] Y. H. Zou and S. M. Yang, "BAHA softband in patients with congenital malformation of middle and outer ears," *Chinese Journal of Otology*, vol. 10, p. 23, 2012.
- [11] Y. H. Zou, Q. S. Jiao, and S. M. Yang, "Preliminary report on clinical application of implantable BAHA," *Chinese Journal of Otology*, vol. 10, p. 278, 2012.
- [12] J. Y. Xia, Q. N. Yu, X. Xi, and B. Yang, "Speech recognition in noise of the unilateral conductive or mixed hearing impaired patients using sophonotron bone conduction hearing aid with softband," *Journal of Audiology and Speech Pathology*, vol. 2, pp. 181–184, 2018.
- [13] A. Hagr, "BAHA: bone-anchored hearing aid," *Int J Health Sci (Qassim)*, vol. 1, no. 2, pp. 265–276, 2007.
- [14] B. C. Moore and G. R. Popelka, "Preliminary comparison of bone-anchored hearing instruments and a dental device as treatments for unilateral hearing loss," *International Journal of Audiology*, vol. 52, no. 10, pp. 678–686, 2013.
- [15] R. A. Battista, K. Mullins, R. M. Wiet, A. Sabin, J. Kim, and V. Rauch, "Sound localization in unilateral deafness with the Baha or TransEar device," *JAMA Otolaryngology. Head & Neck Surgery*, vol. 139, no. 1, pp. 64–70, 2013.
- [16] D. Siau, B. Dhillon, R. Andrews, and K. M. J. Green, "Bone-anchored hearing aids and un-ilateral sensorineural hearing loss: why do patients reject them," *Journal of Laryngology & Otology*, vol. 129, no. 4, pp. 321–325, 2015.
- [17] M. J. Syms and K. E. Hernandez, "Bone conduction hearing: device auditory capability to aid in device selection," *Otolaryngology and Head and Neck Surgery*, vol. 150, no. 5, pp. 866–871, 2014.
- [18] M. Murray, G. R. Popelka, and R. Miller, "Efficacy and safety of an in-the-mouth bone conduction device for single-sided deafness," *Otology & Neurotology*, vol. 32, no. 3, pp. 437–443, 2011.
- [19] J. Hendry, A. Chin, I. R. C. Swan, M. A. Akeroyd, and G. G. Browning, "The Glasgow Benefit Inventory: a systematic review of the use and value of an otorhinolaryngological generic patient-recorded outcome measure," *Clinical Otolaryngology*, vol. 41, pp. 259–275, 2015.
- [20] S. Wang, R. Mannell, P. Newall, H. Zhang, and D. Han, "Development and evaluation of Mandarin disyllabic materials

- for speech audiometry in China,” *International Journal of Audiology*, vol. 46, pp. 719–731, 2009.
- [21] X. Xi, G. Y. Huang, F. Ji et al., “The establishment of computer-assisted Chinese speech audiometry platform,” *Chinese Scientific Journal of Hearing and Speech Rehabilitation*, vol. 8, pp. 31–34, 2010.
- [22] R. K. Gurgel and C. Shelton, “The SoundBite hearing system: patient-assessed safety and benefit study,” *Laryngoscope*, vol. 123, no. 11, pp. 2807–2812, 2013.
- [23] B. Hakansson, A. Tjellstrom, U. Rosenhall, and P. Carlsson, “The bone-anchored hearing aid. Principal design and a psychoacoustical evaluation,” *Acta Oto-Laryngologica*, vol. 100, pp. 229–239, 2009.
- [24] J. Katz, R. F. Burkard, and L. Medwetsky, *Handbook of Clinical Audiology*, Lippincott Williams & Wilkins, Philadelphia, 5th edition, 2002.
- [25] G. Kim, H. M. Ju, S. H. Lee, H. S. Kim, J. A. Kwon, and Y. J. Seo, “Efficacy of bone-anchored hearing aids in single-sided deafness,” *Otology & Neurotology*, vol. 38, no. 4, pp. 473–483, 2017.
- [26] R. Laszig, A. Aschendorff, M. Stecker et al., “Benefits of bilateral electrical stimulation with the nucleus cochlear implant in adults: 6-month postoperative results,” *Otology and Neurotology*, vol. 25, no. 6, pp. 958–968, 2004.
- [27] S. D. Soli and L. L. Wong, “Assessment of speech intelligibility in noise with the Hearing in Noise Test,” *International Journal of Audiology*, vol. 47, pp. 356–361, 2009.
- [28] E. C. Schafer, A. M. Amlani, D. Paiva, L. Nozari, and S. Verret, “A meta-analysis to compare speech recognition in noise with bilateral cochlear implants and bimodal stimulation,” *International Journal of Audiology*, vol. 50, no. 12, pp. 871–880, 2011.
- [29] R. Carhart, “Problems in the measurement of speech discrimination,” *Archives of Otolaryngology*, vol. 82, no. 3, pp. 253–260, 1965.
- [30] B. J. Gantz, R. S. Tyler, J. T. Rubinstein et al., “Binaural cochlear implants placed during the same operation,” *Otology & Neurotology*, vol. 23, no. 2, pp. 169–180, 2002.
- [31] C. K. Giardina, E. J. Formeister, and O. F. Adunka, “Cochlear implants in single-sided deafness,” *Current Surgery Reports*, vol. 2, pp. 1–11, 2014.
- [32] M. Valente and K. Oeding, “Transcranial contralateral routing of the signal as a fitting option for patients with single-sided deafness,” *Seminars in Hearing*, vol. 31, no. 4, pp. 366–377, 2010.
- [33] M. K. Hol, S. J. Kunst, A. F. Snik, and C. W. R. J. Cremers, “Pilot study on the effectiveness of the conventional CROS, the transcranial CROS and the BAHA transcranial CROS in adults with unilateral inner ear deafness,” *European Archives of Oto-Rhino-Laryngology*, vol. 267, no. 6, pp. 889–896, 2010.
- [34] J. W. House, J. W. Kutz Jr., J. Chung, and L. M. Fisher, “Bone-anchored hearing aid subjective benefit for unilateral deafness,” *Laryngoscope*, vol. 120, no. 3, pp. 601–607, 2010.
- [35] K. Oeding, M. Valente, and J. Kerckhoff, “Effectiveness of the directional microphone in the Baha® Divino™,” *Journal of the American Academy of Audiology*, vol. 21, no. 8, pp. 546–557, 2010.
- [36] H. W. Yuen, D. Bodmer, K. Smilsky, J. M. Nedzelski, and J. M. Chen, “Management of single-sided deafness with the bone-anchored hearing aid,” *Otolaryngology and Head and Neck Surgery*, vol. 141, no. 1, pp. 16–23, 2009.
- [37] D. Bernardeschi, F. Y. Russo, Y. Nguyen et al., “Audiological results and quality of life of Sophono Alpha 2 transcutaneous bone-anchored implant users in single-sided deafness,” *Audiology & Neuro-Otology*, vol. 21, no. 3, pp. 158–164, 2016.

Research Article

The Influence of Cochlear Implant-Based Electric Stimulation on the Electrophysiological Characteristics of Cultured Spiral Ganglion Neurons

Na Shen,^{1,2} Lei Zhou,¹ Bin Lai¹ ,³ and Shufeng Li^{2,4} 

¹Department of Otolaryngology, Zhongshan Hospital, Fudan University, Shanghai, China

²ENT Institute and Department of Otolaryngology, Eye & ENT Hospital, Fudan University, Shanghai, China

³State Key Laboratory of Medical Neurobiology, Institutes of Brain Science, Fudan University, Shanghai 200032, China

⁴NHC Key Laboratory of Hearing Medicine (Fudan University), Shanghai, China

Correspondence should be addressed to Bin Lai; laibin@fudan.edu.cn and Shufeng Li; lisf@fudan.edu.cn

Received 24 March 2020; Revised 22 July 2020; Accepted 17 August 2020; Published 6 September 2020

Academic Editor: Jian Wang

Copyright © 2020 Na Shen et al. This is an open access article distributed under the Creative Commons Attribution License, which permits unrestricted use, distribution, and reproduction in any medium, provided the original work is properly cited.

Background. Cochlear implant-based electrical stimulation may be an important reason to induce the residual hearing loss after cochlear implantation. In our previous study, we found that charge-balanced biphasic electrical stimulation inhibited the neurite growth of spiral ganglion neurons (SGNs) and decreased Schwann cell density in vitro. In this study, we want to know whether cochlear implant-based electrical stimulation can induce the change of electrical activity in cultured SGNs. **Methods.** Spiral ganglion neuron electrical stimulation in vitro model is established using the devices delivering cochlear implant-based electrical stimulation. After 48 h treatment by 50 μ A or 100 μ A electrical stimulation, the action potential (AP) and voltage depended calcium current (I_{Ca}) of SGNs are recorded using whole-cell electrophysiological method. **Results.** The results show that the I_{Ca} of SGNs is decreased significantly in 50 μ A and 100 μ A electrical stimulation groups. The reversal potential of I_{Ca} is nearly +80 mV in control SGN, but the reversal potential decreases to +50 mV in 50 μ A and 100 μ A electrical stimulation groups. Interestingly, the AP amplitude, the AP latency, and the AP duration of SGNs have no statistically significant differences in all three groups. **Conclusion.** Our study suggests cochlear implant-based electrical stimulation only significantly inhibit the I_{Ca} of cultured SGNs but has no effect on the firing of AP, and the relation of I_{Ca} inhibition and SGN damage induced by electrical stimulation and its mechanism needs to be further studied.

1. Introduction

Acoustic signal is transferred by cochlear hair cells from mechanical vibration, and then the signal is transmitted to the auditory cortex via SGNs. Cochlear hair cells in the cochlea are critical for hearing ability [1, 2], and most of the hearing loss is due to irreversible hair cell loss. Cochlear implants can partially replace the function of cochlear hair cells and is the most efficient clinical treatment currently for hearing loss patients. Hybrid cochlear implants, known as the electroacoustic stimulation developed to be used for the patients with high-frequency sensorineural hearing loss and low-frequency residual hearing, has a better clinical effect than the traditional full insertion cochlear implant

[3–7]. The use of a shorter, thinner cochlear implant electrode array makes it possible to reduce implantation trauma in the low-frequency region of the cochlea, since the array is only inserted into the basal to the middle part of the cochlea, leaving the apical cochlea intact. When “soft” surgery techniques are used, low-frequency residual hearing can be preserved [8]. It can afford better speech and musical melody recognition than full insertion cochlear implant [6, 9–11].

However, the key point of such benefits in the hybrid cochlear implant depends on the preservation of residual hearing within the implanted inner ear. Unfortunately, more and more clinical researches showed that residual hearing would appear tardive and progressive loss after the hybrid cochlear implant [12–14]. But the mechanism of it was still

not clear. Surgical trauma [15], inflammatory, or immune response can be the reasons leading to hair cell death [16]. The formation of fibrosis or new bone growth after implantation can also theoretically cause hair loss by attenuating the traveling wave [17]. But the hearing loss caused by the trauma can be reduced through the optimum-designed implanted electrodes and the enhancement of operate skills [18, 19]. Therefore, the simple trauma cannot explain the mechanism of the tardive and progressive hearing loss.

Electrical stimulation may be an important reason to the residual hearing loss after implantation. Electrical stimulation can promote the neural stem cell's differentiation into neurons and can promote the maturation of newly generated neuron [20, 21], and also can directly excite the SGNs and their peripheral processes, and the residual hair cells in the low-frequency area [22]. Thus, we suppose that during the electrical-acoustic stimulation, the electrical stimulation may spread to the low-frequency area, then excite the cochlear hair cells and SGNs. This excitation can overlap with the acoustic stimulation and induce the excitatory toxicity. Like the noise-induced deafness, the main mechanisms of the noise-induced deafness are the glutamate excite-toxicity, calcium overload, and oxidative stress [23–25]. Electrical stimulation can both induce voltage-gating calcium channels (VDCCs) opening, and the calcium influx and multiple types of VDCCs are involved in the neurite growth inhibition of SGNs [26] induced by the electrical stimulation. The continuous electrical stimulation may cause excessive Ca^{2+} influx and lead to toxic effect which induces SGN death [27]. This was verified by our previous study [26] that charge-balanced biphasic electrical stimulation inhibited the neurite growth of SGNs and decreased Schwann cell density in vitro. But the effect of cochlear implant-based electrical stimulation on the electrophysiological characteristics, the base of neuronal signal transmission, of spiral ganglion neurons is unclear.

In this study, we use the electrophysiological method to study whether cochlear implant-based electrical stimulation can induce the change of the voltage-dependent calcium currents (I_{Ca}) and the AP firing characteristics of SGNs.

2. Materials and Methods

2.1. Spiral Ganglion Cultures. Postnatal day 4 (P4) to P6 rat pups of both sexes were provided and bred by the Laboratory Animal Center of the Eye, Ear, Nose and Throat Hospital (Shanghai, China) under routine conditions according to the institute's ethical and environmental guidelines. Dissociated spiral ganglion cultures were prepared as follows. Ganglia were dissected from the rat pups after being sacrificed by decapitation, dissociated with trypsin and collagenase, plated on polyornithine/laminin-coated 4-well or 8-well culture chambers (Nalge Nunc International, Naperville, IL), and maintained in high glucose Dulbecco's Modified Eagle's Medium (DMEM) (Gibco, Grand Island, US) with N2 supplement (Invitrogen, Carlsbad, CA) with 10% fetal bovine serum and fresh insulin (10 $\mu\text{g}/\text{ml}$, Sigma-Aldrich, St. Louis, MO) in a humidified incubator

with 37°C, 5.0% CO_2 . The cultures were placed in the incubator for twenty-four hours, and then maintained for another 48 hr with electrical stimulation to fix for current-clamp experiments.

2.2. Electrical Stimulation. Two platinum wires were placed into one well which we wanted to give the electrical stimulation. And then, it should be connected to the artificial cochlea device (Reseat Medical Tech. Co., Ltd, Shanghai, CN) when we gave the electrical stimulation (Figure 1(a)). The parameters for the electrical stimulation were as follows: the pulse width was 65 ms, the frequency was 200 ms (Figure 1(b)), and the current intensity was 50 μA or 100 μA .

2.3. Electrophysiology Experiments. Action potential (AP) and voltage-activated Ca^{2+} current (I_{Ca}) were performed using an Axopatch 200B amplifier (Molecular Devices). Electrodes (4–5 $\text{M}\Omega$) were pulled from borosilicate glass with P-97 (Sutter, USA). Extracellular solution for APs contained the following (in mM): 145 NaCl, 6 KCl, 2 CaCl_2 , 1 MgCl_2 , 10 Glucose, and 1 HEPES, at pH 7.3. The tips of the pipettes were filled with the internal solution containing the following (in mM): 133 K-gluconate, 8 NaCl, 0.6 EGTA, 2 $\text{Mg}\cdot\text{ATP}$, 0.3 $\text{Na}_3\text{-GTP}$, and 10 HEPES, at pH 7.3. Extracellular solution for I_{Ca} contained the following (in mM): 120 Choline chloride, 20 TEACl, 5 4-AP, 0.02 linopirdine, 2 CsCl, 1.8–5 CaCl_2 , 0.5 MgCl_2 , 10 HEPES, and 5 D-glucose, at pH 7.4 with NaOH. The tips of the pipettes were filled with the internal solution containing the following (in mM): 70 CsCl, 70 N-methyl-D-glucamine (NMDG), 1 MgCl_2 , 10 HEPES, 2–5 EGTA, 1 CaCl_2 , and 4Cs2ATP, at pH 7.2 with CsOH. Recordings were made from neuronal somata at room temperature. Because the cultures contain neuronal and non-neuronal cells, neurons were confirmed by the presence of a large, transient inward sodium current in whole-cell voltage-clamp mode. A holding potential of -70 mV was chosen to assess responses at a level in which there is minimal voltage-dependent ion channel activation. For AP recording, the APs were induced by injecting the current (100 pA, 2000 ms duration) under current clamp mode. I_{Ca} current traces were generated with depolarizing voltage steps from a holding potential of -70 mV to 80 mV and stepped to varying positive potentials ($\Delta = -10$ mV). Whole-cell Ca^{2+} current amplitudes at varying test potentials were measured at the peak and steady-state levels using a peak and steady-state detection routine; the current magnitude was divided by the cell capacitance (pF) to generate the current density–voltage relationship. Voltage traces and currents were amplified, filtered (bandpass 2–10 kHz), and digitized at 5–500 kHz using an analog-to-digital convertor Digidata 1200 (Molecular Devices); Data were analyzed using clamp-fit 10.0 software. Data are presented as Mean \pm SEM.

2.4. Statistical Analysis. Graphs were prepared and statistical analysis was done using GraphPad Prism 5.01 (GraphPad Software, Inc.; CA, USA). The significance of differences among all conditions was compared by unpaired *t*-test and One-way ANOVA Kruskal-Wallis test ($p < 0.05$).

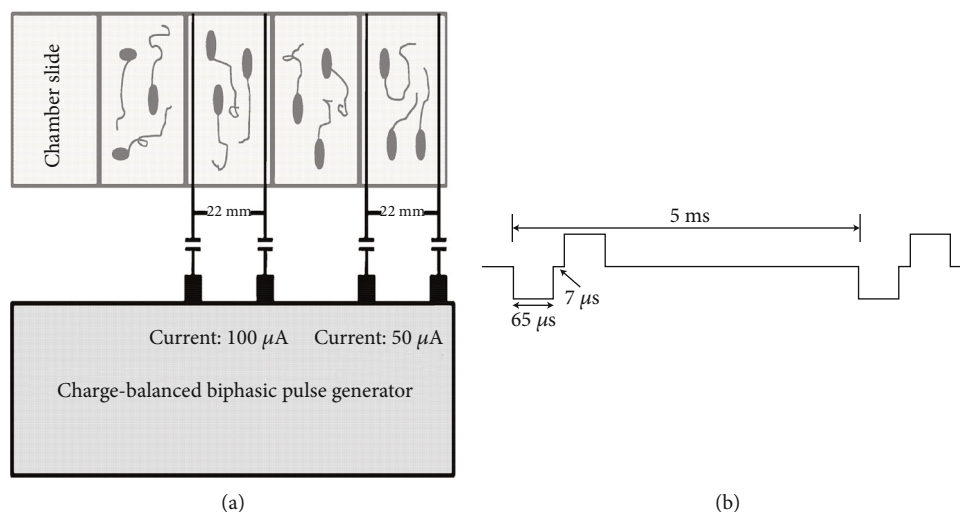


FIGURE 1: The cultured spiral ganglion neurons (SGNs) are treated with charge-balanced biphasic electrical stimulation. (a) Four-well chamber slides were used in this culture system. Four holes adjacent to the floor were made on two opposite walls of each chamber to introduce two platinum-iridium wires at the two opposite borders. The wires were connected to charge-balanced biphasic pulse generators. (b) The biphasic pluses used for the electrical stimulation were 50 μ A or 100 μ A amplitude, 65 μ s pulse width, 8 μ s open-circuit interphase gap, 4862 μ s short-circuit phase, and 200 Hz frequency.

3. Results

3.1. The Electrical Stimulation Inhibits the Voltage-Dependent Calcium Currents (I_{Ca}) of SGNs. The I_{Ca} was recorded on the cultured SGNs after different electrical stimulation (Figures 2(a) and 2(b)), and the current-voltage curves of I_{Ca} were analyzed. The result showed that the inhibited effect of electrical stimulation on the I_{Ca} was obvious when the membrane potential was depolarized from the range between 0 mV and +80 mV. The I_{Ca} was activated at -60 mV and reached a peak at 20 mV. From -20 mV to +80 mV, the I_{Ca} was significantly decreased in 50 μ A and 100 μ A groups compared with the control group. The I_{Ca} has no difference between 50 μ A and 100 μ A groups. The reversal potential of I_{Ca} was nearly $+75.8 \pm 4.325$ mV in the control group, but after electrical stimulation, the reversal potentials were $+47.5 \pm 3.497$ mV and $+46.3 \pm 4.369$ mV in 50 μ A and 100 μ A groups correspondingly (Figures 2(c) and 2(d)).

3.2. The Influence of Electrical Stimulation on the AP Firing Characteristics of SGNs. A total of 34 SGNs were recorded (control group: $n = 10$; 50 μ A group: $n = 12$ and 100 μ A group: $n = 12$). Three type action potentials release modes could be found under a depolarized current (100 pA; 2000 ms during) in all neurons; Type I neuron had only one AP after depolarized current stimulation, type II had 2~6 AP and type III could continue firing during the test pulse (Figure 3(a)). The firing characteristics of the first AP were analyzed including AP amplitude, AP decay time, AP half width, and AP rise time. The AP amplitude had no statistically significant difference in all three groups (control group: 69.52 ± 5.880 mV; 50 μ A group: 80.48 ± 3.629 mV and 100 μ A group: 64.82 ± 3.156 mV). The AP latency (control group: 7.150 ± 0.937 ms; 50 μ A group: 8.967 ± 1.292 ms and 100 μ A group: 8.054 ± 1.716 ms) and AP duration (con-

trol group: 4.142 ± 0.912 ms; 50 μ A group: 3.967 ± 0.683 ms and 100 μ A group: 3.647 ± 0.677 ms) also had no statistically significant difference in all three groups (Figures 3(b)–3(e)).

4. Discussion

In mammal's inner ear, cochlear hair cells and SGNs are two key cell types for hearing ability, Cochlear hair cells convert the mechanical sound vibrations into electronic neural signals, and SGNs transmit these electronic signals to the auditory cortex. In mammal's inner ear, cochlear hair cells and SGNs are sensitive for multiple stress and injuries, including noise, gene mutation, ototoxic drugs, inflammation, and aging [28–31]. On the other hand, the mammal's cochlea only has very limited hair cell and SGN regeneration ability, most of the hair cell loss and SGN loss are permanent and cannot be reversed [32, 33]. Thus, most of the hearing loss is irreversible, and there is no clinical treatment to perfectly cure hearing loss in the clinic by far. Cochlear implant (CI) is an artificial instrument, which is the most widely used neural prosthetic by delivering electrical signals converted from sound information to spiral ganglion neurons and can partially replace the function of cochlear hair cells, and thus is the most efficient clinical treatment currently for hearing loss patients. In the last decade, electric-acoustic stimulation (EAS) technology was newly developed for patients with severe or profound high-frequency hearing loss and residual low-frequency hearing. EAS technology significantly improves music appreciation and speech recognition in background noise through the preservation of residual low-frequency [3, 34]. Unfortunately, clinical trials showed that 30–75% of EAS recipients experienced delayed progressive loss of residual low-frequency hearing over time after the activation of EAS [12–14]. However, the mechanism of this delayed hearing impairment is still not clear by far. In this

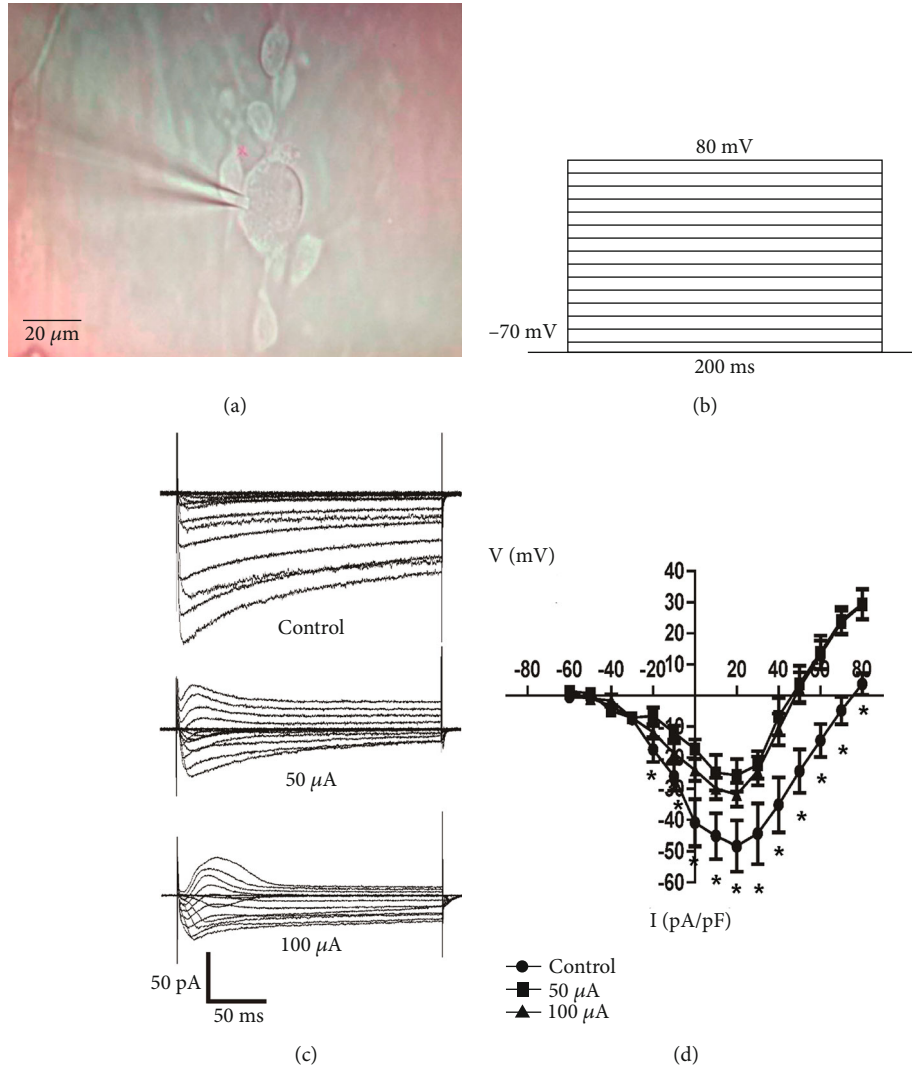


FIGURE 2: Electrical stimulation decreases voltage-dependent calcium currents (I_{Ca}) of SGNs. (a) One SGN was patched with the tip of the microelectrode. (b) The stimulation parameters of voltage-dependent calcium current. (c, d) The inhibitory effect of electrical stimulation was obvious when the membrane potential was depolarized with the step ranging between 0 mV and +80 mV. The I_{Ca} was activated at -60 mV and reached the peak at 20 mV, the reversal potential of I_{Ca} was nearly +75.8 mV \pm 4.325 in control neuron, but electrical stimulation could change the reversal potential to +47.5 mV \pm 3.497 and +46.3 mV \pm 4.369 in 50 μ A and 100 μ A groups ($p < 0.05$).

study, we explored the influence of cochlear implant-based electric stimulation on the electrophysiological characteristics of cultured spiral ganglion neurons.

Calcium overload and oxidative stress are the main causes for SGNs death [27] and the important mechanisms of delayed neuronal death [35]. Our previous study found that charge-balanced biphasic electrical stimulation inhibited the neurite growth of SGNs and decreased Schwann cell density in vitro, and calcium influx through multiple types of VDCCs was involved in the electrical stimulation-induced neurites growth inhibition in SGNs [26]. In this study, we found that I_{Ca} was significantly reduced after 48 h electrical stimulation in both 50 μ A and 100 μ A group. There may be two reasons for the inhibition of I_{Ca} caused by electrical stimulation. Firstly, electrical stimulation can decrease voltage-dependent calcium channel expression on the membrane of SGNs, which may be a self-protection mechanism of neurons

to reduce the increase of intracellular calcium. Secondly, I_{Ca} is directly proportional to the difference of calcium ion concentration inside and outside of the neuron. Electrical stimulation can lead to the release of calcium ions from the intracellular calcium storage; the increase of intracellular calcium concentration can decrease the difference of calcium ion concentration inside and outside of the neuron and leads to the decrease of I_{Ca} . Although calcium overload and calcium deficiency are the opposite, they can all be caused by the same stimulus, but only in different stage [36, 37]. There are several evidences for calcium deficiency inducing the apoptosis of neuron. Nakamura et al. found that there was no calcium overload of the neurons in the late stage of apoptosis [38] and even the resting calcium level is lower than normal, and the voltage-dependent calcium influx is significantly reduced [39]. Decreasing extracellular calcium concentration or blocking voltage-gated calcium channels

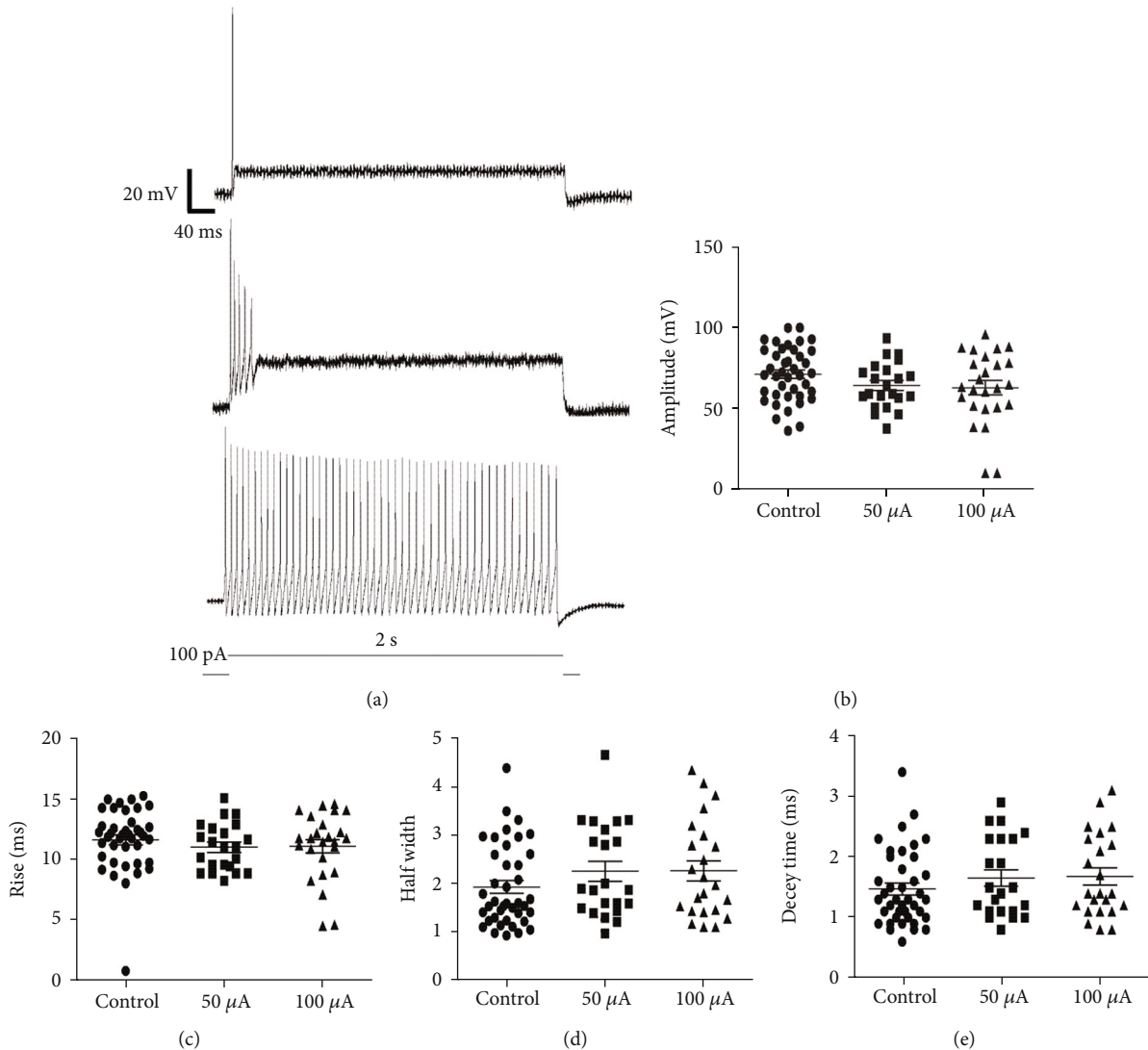


FIGURE 3: Influence of electrical stimulation on the firing characteristics of SGNs. (a) Type I neuron had only one action potential after electrical stimulation, type II had 2–6 action potentials, and type III could continue firing APs during the test pulse. (b–e) AP amplitude, latency, and duration had no statistically significant differences in all three groups ($p > 0.05$).

can both trigger neuronal apoptosis [40]. Therefore, neuronal survival may depend on appropriate intracellular calcium set points [41]. Excessively high or low calcium is not conducive to the survival of neurons [42, 43]. In conclusion, the change in voltage-dependent calcium current induced by electrical stimulation reflects an imbalance in intracellular calcium homeostasis, which may be a major cause of neuronal death and apoptosis in the later period, although there is no significant abnormality in AP firing in SGNs.

Electrical stimulation generated by CI itself may also be one of the important factors to affect the survival of residual SGNs. Previous studies have reported that the electric conductive biomaterials and the electrical stimulation have very obvious effects on regulating the proliferation and differentiation of neural stem cells [44, 45], as well as on regulating the survival and maturation of neurons, including SGNs [46]. In this study, we found that electrical stimulation could decrease the I_{Ca} but had no effect on the action potential firing in cul-

tured SGNs. This result suggests that, although CI can simulate sound stimulation and activate the SGNs, but long-term stimulation of CI will break the calcium balance of SGNs and affect the long-term survival of SGNs negatively.

In addition, Schwann cells, as the main glial cells of the peripheral nervous system, have been shown to secrete a variety of nerve growth factors and axon protection factors, such as glial cell line-derived neurotrophic factor (GDNF) and brain Brain-derived neurotrophic factor (BDNF), can promote the growth of nerve cells [47]. Therefore, electrical stimulation may also affect the surrounding Schwann cells, causing them to degenerate and further aggravate the inhibitory effect of electrical stimulation on the growth and function of spiral neurons.

The SGNs are the first-class neurons of the auditory system [48]. Two types of SGNs were found to compose the first neural elements in the auditory pathway [49]. Type I SGNs exhibit input from only one inner hair cell, whereas type II

SGNs extend long projections and receive input from dozens of outer hair cell [50]. Reid et al. proved that there were two types of SGNs with different electrophysiological firing pattern. Type I SGNs could be consistently classified as rapidly accommodating at stimulation and firing only one action potential, while type II SGNs fired significantly more action potentials in response to stimulation [49]. In this study, we also found SGNs with one action potential and 2~6 action potential after electrical stimulation. According to the previous reports, these two types of SGNs can be defined. But one type of SGNs that could continue firing was found in this study. Can it be the third type of SGNs? We will confirm this in the further study.

The firing characteristics of the first AP were analyzed including AP amplitude, AP decay time, AP half width, and AP rise time. There were no statistical significance in all the three groups. This may prompt that electrical stimulation can affect the axon length of SGNs [26] by changing the status of calcium ion channel, but it could not change the AP firing of SGNs by affecting the voltage-dependent sodium channel and potassium channel. The axon retraction may damage the intact between SGNs and cochlear hair cells and cause hearing loss.

5. Conclusion

Our study suggests cochlear implant-based electrical stimulation only significantly inhibit the I_{Ca} of cultured SGNs but has no effect on the release of AP, and the relation of I_{Ca} inhibition and SGN damage induced by electrical stimulation and its mechanism needs to be further studied.

Data Availability

The data used to support the findings of this study are available from the corresponding author upon request.

Conflicts of Interest

The authors declare that they have no conflicts of interest.

Authors' Contributions

NS and LZ contributed to the experiments of this paper as well as related statistical analysis. BL and SL contributed to the design of all the experiments, the writing of the manuscript, and the preparation of figures. Na Shen and Lei Zhou contributed equally to this paper.

Acknowledgments

We thank Changjian Xu and Zengjun Sun from Shanghai Cochlear Engineering Technology Research Center, for their technique support of adjust of multichannel charge-balanced biphasic pulse generator. This study was supported by the National Natural Science Foundation of China (NSFC, 31970956, 81171482 and 81670927), the Research Special Fund for Public Welfare Industry of Health (201202001), the Fund of the Science and Technology Commission of

Shanghai Municipality (12DZ2251700), and the Shanghai Pujiang Program (18PJD004).

References

- [1] Y. Liu, J. Qi, X. Chen et al., "Critical role of spectrin in hearing development and deafness," *Science advances*, vol. 5, no. 4, 2019.
- [2] J. Qi, Y. Liu, C. Chu et al., "A cytoskeleton structure revealed by super-resolution fluorescence imaging in inner ear hair cells," *Cell discovery*, vol. 5, no. 1, 2019.
- [3] B. J. Gantz and C. W. Turner, "Combining acoustic and electrical hearing," *Laryngoscope*, vol. 113, no. 10, pp. 1726–1730, 2003.
- [4] J. Mueller, R. Behr, C. Knaus, C. Milewski, F. Schoen, and J. Helms, "Electrical stimulation of the auditory pathway in deaf patients following acoustic neurinoma surgery and initial results with a new auditory brainstem implant system," *Advances in Oto-Rhino-Laryngology*, vol. 57, pp. 229–235, 2000.
- [5] J. Kiefer, M. Pok, O. Adunka et al., "Combined electric and acoustic stimulation of the auditory system: results of a clinical study," *Audiology and Neurotology*, vol. 10, no. 3, pp. 134–144, 2005.
- [6] C. W. Turner, L. A. J. Reiss, and B. J. Gantz, "Combined acoustic and electric hearing: preserving residual acoustic hearing," *Hearing Research*, vol. 242, no. 1-2, pp. 164–171, 2008.
- [7] S. Irving, L. Gillespie, R. Richardson, D. Rowe, J. B. Fallon, and A. K. Wise, "Electroacoustic stimulation: now and into the future," *BioMed Research International*, vol. 2014, Article ID 350504, 17 pages, 2014.
- [8] C. Tanaka, A. Nguyen-Huynh, K. Loera, G. Stark, and L. Reiss, "Factors associated with hearing loss in a normal-hearing guinea pig model of hybrid cochlear implants," *Hearing Research*, vol. 316, pp. 82–93, 2014.
- [9] B. S. Wilson, D. T. Lawson, J. M. Müller, R. S. Tyler, and J. Kiefer, "Cochlear implants: some likely next steps," *Annual Review of Biomedical Engineering*, vol. 5, no. 1, pp. 207–249, 2003.
- [10] C. W. Turner, B. J. Gantz, C. Vidal, A. Behrens, and B. A. Henry, "Speech recognition in noise for cochlear implant listeners: benefits of residual acoustic hearing," *The Journal of the Acoustical Society of America*, vol. 115, no. 4, pp. 1729–1735, 2004.
- [11] K. E. Gfeller, C. Olszewski, C. Turner, B. Gantz, and J. Oleson, "Music perception with cochlear implants and residual hearing," *Audiology and Neurotology*, vol. 11, no. 1, pp. 12–15, 2006.
- [12] B. J. Gantz, M. R. Hansen, C. W. Turner, J. J. Oleson, L. A. Reiss, and A. J. Parkinson, "Hybrid 10 clinical trial," *Audiology & Neuro-Otology*, vol. 14, no. 1, pp. 32–38, 2009.
- [13] W. Gstoettner, S. Helbig, C. Settevendemie, U. Baumann, J. Wagenblast, and C. Arnoldner, "A new electrode for residual hearing preservation in cochlear implantation: first clinical results," *Acta Oto-Laryngologica*, vol. 129, no. 4, pp. 372–379, 2009.
- [14] P. L. Santa Maria, C. Domville-Lewis, C. M. Sucher, R. Chester-Browne, and M. D. Atlas, "Hearing preservation surgery for cochlear implantation—hearing and quality of life after 2 years," *Otology & Neurotology*, vol. 34, no. 3, pp. 526–531, 2013.

- [15] P. S. Roland and C. G. Wright, "Surgical aspects of cochlear implantation: mechanisms of insertional trauma," in *Cochlear and Brainstem Implants*, vol. 64, pp. 11–30, 2006.
- [16] A. A. Eshraghi, C. Gupta, T. R. van de Water et al., "Molecular mechanisms involved in cochlear implantation trauma and the protection of hearing and auditory sensory cells by inhibition of c-Jun-N-terminal kinase signaling," *Laryngoscope*, vol. 123, Supplement 1, pp. S1–14, 2013.
- [17] C. H. Choi and J. S. Oghalai, "Predicting the effect of post-implant cochlear fibrosis on residual hearing," *Hearing Research*, vol. 205, no. 1–2, pp. 193–200, 2005.
- [18] O. Adunka, J. Kiefer, M. H. Unkelbach, T. Lehnert, and W. Gstoettner, "Development and evaluation of an improved cochlear implant electrode design for electric acoustic stimulation," *Laryngoscope*, vol. 114, no. 7, pp. 1237–1241, 2004.
- [19] S. Berrettini, F. Forli, and S. Passetti, "Preservation of residual hearing following cochlear implantation: comparison between three surgical techniques," *The Journal of Laryngology & Otolaryngology*, vol. 122, no. 3, pp. 246–252, 2008.
- [20] R. Guo, S. Zhang, M. Xiao et al., "Accelerating bioelectric functional development of neural stem cells by graphene coupling: implications for neural interfacing with conductive materials," *Biomaterials*, vol. 106, pp. 193–204, 2016.
- [21] Z. He, S. Zhang, Q. Song et al., "The structural development of primary cultured hippocampal neurons on a graphene substrate," *Biointerfaces*, vol. 146, pp. 442–451, 2016.
- [22] S. Y. Kang, D. J. Colesa, D. L. Swiderski, G. L. Su, Y. Raphael, and B. E. Pflugst, "Effects of hearing preservation on psychophysical responses to cochlear implant stimulation," *Journal of the Association for Research in Otolaryngology*, vol. 11, no. 2, pp. 245–265, 2010.
- [23] H. W. Lin, A. C. Furman, S. G. Kujawa, and M. C. Liberman, "Primary neural degeneration in the Guinea pig cochlea after reversible noise-induced threshold shift," *Journal of the Association for Research in Otolaryngology*, vol. 12, no. 5, pp. 605–616, 2011.
- [24] Q. Wang and S. H. Green, "Functional role of neurotrophin-3 in synapse regeneration by spiral ganglion neurons in inner hair cells after excitotoxic trauma in vitro," *Journal of Neuroscience*, vol. 31, no. 21, pp. 7938–7949, 2011.
- [25] J. L. Puel, J. Ruel, C. G. d'Aldin, and R. Pujol, "Excitotoxicity and repair of cochlear synapses after noise-trauma induced hearing loss," *Neuroreport*, vol. 9, no. 9, pp. 2109–2114, 1998.
- [26] N. Shen, Q. Liang, Y. Liu et al., "Charge-balanced biphasic electrical stimulation inhibits neurite extension of spiral ganglion neurons," *Neuroscience Letters*, vol. 624, pp. 92–99, 2016.
- [27] J. L. Hegarty, A. R. Kay, and S. H. Green, "Trophic support of cultured spiral ganglion neurons by depolarization exceeds and is additive with that by neurotrophins or cAMP and requires elevation of [Ca²⁺]_i within a set range," *The Journal of Neuroscience*, vol. 17, no. 6, pp. 1959–1970, 1997.
- [28] L. Liu, Y. Chen, J. Qi et al., "Wnt activation protects against neomycin-induced hair cell damage in the mouse cochlea," *Cell Death & Disease*, vol. 7, no. 3, 2016.
- [29] C. Zhu, C. Cheng, Y. Wang et al., "Loss of ARHGEF6 causes hair cell stereocilia deficits and hearing loss in mice," *Frontiers in Molecular Neuroscience*, vol. 11, p. 362, 2018.
- [30] W. Liu, X. Xu, Z. Fan et al., "Wnt signaling activates TP53-induced glycolysis and apoptosis regulator and protects against cisplatin-induced spiral ganglion neuron damage in the mouse cochlea," *Antioxidants & Redox Signaling*, vol. 30, no. 11, pp. 1389–1410, 2019.
- [31] Z. H. He, S. Y. Zou, M. Li et al., "The nuclear transcription factor FoxG1 affects the sensitivity of mimetic aging hair cells to inflammation by regulating autophagy pathways," *Redox Biology*, vol. 28, p. 101364, 2020.
- [32] C. Cheng, Y. Wang, L. Guo et al., "Age-related transcriptome changes in Sox2+ supporting cells in the mouse cochlea," *Stem Cell Research & Therapy*, vol. 10, no. 1, p. 365, 2019.
- [33] F. Tan, C. Chu, J. Qi et al., "AAV-ie enables safe and efficient gene transfer to inner ear cells," *Nature Communications*, vol. 10, no. 1, p. 3733, 2019.
- [34] C. Vonilberg, J. Kiefer, J. Tillein et al., "Electric-acoustic stimulation of the auditory system," *ORL*, vol. 61, no. 6, pp. 334–340, 1999.
- [35] D. W. Choi and S. M. Rothman, "The role of glutamate neurotoxicity in hypoxic-ischemic neuronal death," *Annual Review of Neuroscience*, vol. 13, no. 1, pp. 171–182, 1990.
- [36] J. M. Lee, G. J. Zipfel, and D. W. Choi, "The changing landscape of ischaemic brain injury mechanisms," *Nature*, vol. 399, no. 6738, pp. A7–14, 1999.
- [37] S. P. Yu, L. M. Canzoniero, and D. W. Choi, "Ion homeostasis and apoptosis," *Current Opinion in Cell Biology*, vol. 13, no. 4, pp. 405–411, 2001.
- [38] T. Nakamura, H. Minamisawa, Y. Katayama et al., "Increased intracellular Ca²⁺ concentration in the hippocampal CA1 area during global ischemia and reperfusion in the rat: a possible cause of delayed neuronal death," *Neuroscience*, vol. 88, no. 1, pp. 57–67, 1999.
- [39] J. A. Connor, S. Razani-Boroujerdi, A. C. Greenwood, R. J. Cormier, J. J. Petrozzino, and R. C. S. Lin, "Reduced voltage-dependent Ca²⁺ signaling in CA1 neurons after brief ischemia in gerbils," *Journal of Neurophysiology*, vol. 81, no. 1, pp. 299–306, 1999.
- [40] J. Y. Koh and C. W. Cotman, "Programmed cell death: its possible contribution to neurotoxicity mediated by calcium channel antagonists," *Brain Research*, vol. 587, no. 2, pp. 233–240, 1992.
- [41] W. He, J. F. Sun, R. Y. Jiang, Z. J. Zhang, Q. Chen, and Y. H. Huang, "Effect of calcium-sensing receptor on the apoptosis of rat spinal cord neurons in anoxia/reoxygenation injury and its significance," *Zhongguo yi xue ke xue Yuan xue bao. Acta Academiae Medicinae Sinicae*, vol. 39, no. 5, pp. 623–628, 2017.
- [42] T. Koike and S. Tanaka, "Evidence that nerve growth factor dependence of sympathetic neurons for survival in vitro may be determined by levels of cytoplasmic free Ca²⁺," *Proceedings of the National Academy of Sciences of the United States of America*, vol. 88, no. 9, pp. 3892–3896, 1991.
- [43] L. Jiang, J. Zhong, X. Dou, C. Cheng, Z. Huang, and X. Sun, "Effects of ApoE on intracellular calcium levels and apoptosis of neurons after mechanical injury," *Neuroscience*, vol. 301, pp. 375–383, 2015.
- [44] Q. Fang, Y. Zhang, X. Chen et al., "Three-dimensional graphene enhances neural stem cell proliferation through metabolic regulation," *Frontiers in Bioengineering and Biotechnology*, vol. 7, 2020.
- [45] J. Zhao, M. Tang, J. Cao et al., "Structurally tunable reduced graphene oxide substrate maintains mouse embryonic stem cell pluripotency," *Advanced Science*, vol. 6, no. 12, p. 1802136, 2019.

- [46] R. Guo, X. Ma, M. Liao et al., “Development and application of cochlear implant-based electric-acoustic stimulation of spiral ganglion neurons,” *ACS Biomaterials Science & Engineering*, vol. 5, no. 12, pp. 6735–6741, 2019.
- [47] P. C. Roehm and M. R. Hansen, “Strategies to preserve or regenerate spiral ganglion neurons,” *Current Opinion in Otolaryngology & Head and Neck Surgery*, vol. 13, no. 5, pp. 294–300, 2005.
- [48] D. J. Zha, Y. Lin, D. J. Zha et al., “Infrared video patch-clamp technique for spiral ganglion neurons in rat cochlear slices,” *Acta Otolaryngol*, vol. 129, no. 5, pp. 527–532, 2009.
- [49] M. A. Reid, J. Flores-Otero, and R. L. Davis, “Firing patterns of type II spiral ganglion neurons in vitro,” *Journal of Neuroscience*, vol. 24, no. 3, pp. 733–742, 2004.
- [50] S. Sun, T. Babola, G. Pregonig et al., “Hair cell mechanotransduction regulates spontaneous activity and spiral ganglion subtype specification in the auditory system,” *Cell*, vol. 174, no. 5, pp. 1247–1263.e15, 2018.

Research Article

Cochlear Implantation in a Patient with a Novel *POU3F4* Mutation and Incomplete Partition Type-III Malformation

Xiuhua Chao, Yun Xiao, Fengguo Zhang, Jianfen Luo, Ruijie Wang, Wenwen Liu, Haibo Wang, and Lei Xu 

Department of Otolaryngology-Head and Neck Surgery, Shandong Provincial ENT Hospital, Cheeloo College of medicine, Shandong University, Jinan 250022, China

Correspondence should be addressed to Lei Xu; sdphxl@126.com

Received 17 April 2020; Revised 5 August 2020; Accepted 24 August 2020; Published 1 September 2020

Academic Editor: Jian Wang

Copyright © 2020 Xiuhua Chao et al. This is an open access article distributed under the Creative Commons Attribution License, which permits unrestricted use, distribution, and reproduction in any medium, provided the original work is properly cited.

Aims. This study is aimed at (1) analyzing the clinical manifestations and genetic features of a novel *POU3F4* mutation in a nonsyndromic X-linked recessive hearing loss family and (2) reporting the outcomes of cochlear implantation in a patient with this mutation. **Methods.** A patient who was diagnosed as the IP-III malformation underwent cochlear implantation in our hospital. The genetic analysis was conducted in his family, including the whole-exome sequencing combined with Sanger sequencing and bioinformatic analysis. Clinical features, preoperative auditory and speech performances, and postoperative outcomes of cochlear implant (CI) were assessed on the proband and his family. **Results.** A novel variant c.400_401insACTC (p.Q136LfsX58) in the *POU3F4* gene was detected in the family, which was cosegregated with the hearing loss. This variant was absent in 200 normal-hearing persons. The phylogenetic analysis and structure modeling of Pou3f4 protein further confirmed that the novel mutation was pathogenic. The proband underwent cochlear implantation on the right ear at four years old and gained greatly auditory and speech improvement. However, the benefits of the CI declined about three and a half years postoperation. Though the right ear had been reimplemented, the outcomes were still worse than before. **Conclusion.** A novel frame shift variant c.400_401insACTC (p.Q136LfsX58) in the *POU3F4* gene was identified in a Chinese family with X-linked inheritance hearing loss. A patient with this mutation and IP-III malformation could get good benefits from CI. However, the outcomes of the cochlear implantation might decline as the patient grows old.

1. Introduction

Congenital deafness affects approximately 1 in 1,000 newborns. It is estimated that 20% of congenital hearing loss was caused by inner ear malformations (IEM) [1]. The etiology of IEM remains unknown. In mammals' inner ear, the cochlear hair cells transform the mechanical vibration of sound waves into the acoustic electrical information [2–5], while spiral ganglion neurons (SGNs) further deliver the acoustic electrical information all the way to the auditory cortex to establish the hearing ability. Many previous studies have reported that hair cell malformation caused by genetic factors, ototoxic drugs, aging, noise, and inflammation leads to IEM and hearing loss [6–9]. Incompletely partition type III (IP-III) is a relatively rare IEM that accounts for approximately 2% of all cochlear malformations [10]. The diagnosis

of IP-III cochlear malformation is mainly based on its unique imaging features. The characters of temporal bone high-resolution CT (HRCT) in patients with IP-III malformation include the enlargement of the lateral end of the internal auditory canal (IAC), absence of the cochlear modulus, partial hypoplasia of the cochlea, abnormally communication between the IAC and cochlea, and stapes fixation. This malformation was first described by Nance et al. in 1971 [11], then Sennaroglu and Saatci classified it as a type of cochlear abnormality with incomplete partition and named it as IP-III [12].

A previous study found that IP-III malformation was a disease associated with X-linked hereditary deafness caused by *POU3F4* gene mutation [13]. *POU3F4* gene mutation is the most common cause related to X-linked nonsyndromic deafness, which accounts for about 50% of all X-linked

deafness patients [14]. Human *POU3F4* gene locates on chromosome Xq21.1. This gene encodes the protein with bipartite DNA-binding domains, which belong to a superfamily of POU domain transcription factors [15]. The transcription factor *POU3F4* binds DNA using a specific DNA-binding domain, which is divided into two subdomains, a POU-specific (POUs) and a POU homeodomain (POU_{HD}). POU superfamily genes play an important role in organ formation and cell differentiation. In the mice, *POU3F4* is expressed in the mesenchyme cells surrounding the developing inner ear epithelium with limited or no expression in the hair cells or SGNs [16, 17]. It is critical for the development of the spiral limbus, the scala tympani, and the temporal bone [18, 19]. Studies in the *POU3F4* knockout mice suggested that *POU3F4* deficiency caused defects in otic fibrocytes and stria vascularis, both of which were essential for the sound transduction [20].

In the clinic, patients with *POU3F4* mutation present with IP-III malformation, mixed or severe to profound sensorineural hearing loss (SNHL). For patients with severe to profound SNHL, cochlear implantation is still a unique effective treatment. It has been reported that the outcomes of cochlear implant (CI) in patients with IP-III malformation were worse than those who have normal cochlea and varied greatly among individuals [16, 21, 22]. To date, it is still hard to predict the cochlear implantation outcomes in patients with severe cochlea malformations preoperatively. Furthermore, because of the absence of the cochlear modulus and the abnormally communication between the IAC and cochlea, the electrode array was easily inserted into the IAC and severe cerebrospinal fluid (CSF) gusher often occurred during the surgery [21]. Thus, it is still a challenge to do cochlear implantation in this kind of patient.

In this paper, we reported the cochlear implantation in a patient with IP-III malformation. The clinical characteristics and genetic analysis in his family were also displayed. This is the first study to identify a c.400_401insACTC(p.Q136LfsX58) in the *POU3F4* gene associated with X-linked hereditary deafness in Asians. By molecular testing, we provided definitive diagnosis and genetic counseling for this family and further enriched the pathogenic mutation spectrum of the *POU3F4* gene. Our results also shed light on the potential use of IP-III malformation genotypes as meaningful biological markers of the outcome of CI.

2. Materials and Methods

2.1. Subjects. This study was approved by the Shandong University ethical committee (number 014). All participants involved in the project signed written informed consent. A Chinese family affected by X-linked inheritance hearing loss was recruited. The proband came to our hospital when he was four years old due to hearing loss and no speech. Besides, 200 persons with normal hearing were collected. All audiometric tests and physical examinations were evaluated at Shandong Provincial ENT Hospital.

2.2. Clinical Evaluations. The medical history of the proband was obtained, including health condition at birth, newborn

hearing screening, onset and progress of hearing loss, otitis media and ototoxic drug using history, hearing aid using history, maternal health during pregnancy, and other relevant clinical manifestations to exclude any history of other diseases and environmental factors. He underwent a series of clinical tests including physical examinations, distortion product otoacoustic emission, tympanometry, pure tone audiometry, auditory brainstem response (ABR), and temporal bone MRI and CT scans.

2.3. Genetic Analyses. Genomic DNA of each member in the family and 200 normal-hearing controls were extracted from the peripheral blood using a DNA extraction kit (AXYGEN). The common mutations of *GJB2*, *SLC26A4*, and mtDNA 12S rRNA genes were excluded by the “SNPscan assay” (Genesky Biotechnologies Inc., Shanghai, China). Whole-exome sequencing (WES) was used to investigate genetic variations underlying the hearing loss in the family. Genomic DNA was fragmented to 180~280 bp, and the DNA library was created following established Illumina paired-end protocols. The Agilent SureSelect Human All ExonV6 Kit (Agilent Technologies, Santa Clara, CA, USA) was employed for exome capture according to the manufacturer’s instructions. The Illumina NovaSeq 6000 platform (Illumina Inc., San Diego, CA, USA) was used for genomic DNA sequencing by Yinfeng Gene Technology Co., Ltd. (Beijing, China) to generate 150 bp paired-end reads with a minimum coverage of 10× for ~97% of the target sequence (mean coverage of 100×). The resulting fastq data were analysed by in-house quality control software to remove low-quality reads and were then aligned to the reference human genome (hs37d5) using the Burrows-Wheeler Aligner [23], and duplicate reads were marked using Sambamba tools [24]. Annotation was performed using ANNOVAR [25]. After whole-exome sequencing, we identified one candidate mutation. The PCR and Sanger sequencing were performed to determine whether the variant was cosegregated with hearing loss in the family. The following primers were synthesized: 5′-GCCTAATTTGGAAAGCGAGC-3′ and 5′-AAATCCGCGCTGCTCCAGT-3′ (BGI Inc., China). The PCR and amplification were performed according to a previous protocol [26]. The sequence of *POU3F4* fragment was performed using the DNASTAR software.

2.4. Phylogenetic and Structural Analyses. Phylogenetic analysis of Pou3f4 was performed with multiple sequence alignment using BioEdit software. The sequences included NP_000298.3 (Homo sapiens), NP_032927.1 (Mus musculus), NP_058948.1 (Rattus norvegicus), NP_001181188.1 (Macaca mulatta), XP_003317585.1 (Pan troglodytes), XP_010820097.1 (Bos taurus). Three-dimensional (3D) modeling of the human wild-type and mutant *POU3F4* protein was carried out using I-TASSER (<http://zhanglab.ccmb.med.umich.edu/>). The wild-type domain includes 361 amino acids (NP_000298.3), and the mutant domain includes 192 amino acids. Predicted wild-type and mutant protein structures were observed and analyzed using PyMOL visualization software.

2.5. Cochlear Implantation. A standard transmastoid facial recess approach was used for cochlear implantation. The 1 J electrode array (Advanced Bionics Corp., Sylmar, CA) was implanted in the proband on the right ear when he was four years old. The electrode array was fully inserted. Four years post the first implantation, the right ear had been reimplanted with a new 1 J electrode array due to the deterioration of the cochlear implant benefits. He underwent the third cochlear implantation on the left ear when he was nine and a half years old because his parents were not satisfied with the outcomes of the reimplantation. The left ear was also implanted with the 1 J electrode array. The electrode arrays were fully inserted in both ears.

During the operation, CSF gusher occurred upon opening the round window. After the insertion of the electrodes, the cochleostomy was blocked using prepared muscle tissue. No CSF leakage was observed after surgery. Intraoperative CT scan was utilized to ensure the electrode array at the correct position and did not insert into the IAC. No complications were observed postoperatively. He came back regularly for programming and evaluation. Aided hearing thresholds and speech perception were tested to evaluate the outcomes of cochlear implants. Besides, the auditory and speech ability were accessed using categories of auditory performance (CAP) and speech intelligibility rating (SIR).

3. Results

3.1. Clinical Features. The proband (II-2) and three unaffected members in his consanguineous family were enrolled in this study (Figure 1(a)). The proband failed to pass the newborn hearing screening. He began to use hearing aids on both ears since one year old. The otoacoustic emissions were bilaterally absent. The ABR thresholds with clicks were 70 dB nHL in the left ear and 95 dB nHL in the right ear when he was one year old. No ABR response could be found on both ears at 100 dB nHL before the operation. Pure tone audiometry showed bilateral profound SNHL (Figure 1(d)). He has normal external ear and tympanic membrane. Acoustic immittance showed type A tympanograms in both ears. High-resolution temporal bone CT scan revealed the absence of the bony modiolus, hypoplasia of cochlea, enlarged internal acoustic canal, abnormal communication between the internal acoustic canal and the cochlear, and vestibular abnormalities (Figure 2(a)). MRI showed a normal internal auditory canal; the facial nerve and vestibule cochlear nerve could be seen clearly on both sides (Figure 2(b)). Pure tone audiometry of the proband's mother and brother were shown in Figures 1(b) and 1(c). All the proband's parents and brother have normal hearing, denying a family history of hearing loss.

3.2. Identification of the Novel Mutation c.400_401insACTC in POU4F3. After the whole-exome sequencing in family members, an insertion mutation c.400_401insACTC (p.Q136LfsX58) in the *POU3F4* gene was detected in the proband suggesting a potential disease-causing factor in his family. In order to verify that the mutation was cosegregated with the hearing loss, the direct sequencing of the mutation site of

the *POU3F4* gene in all family members was conducted. As shown in Figure 3(a), the identified novel mutation c.400_401insACTC in *POU4F3* mutation cosegregates with hearing loss in this family. The mother of the proband (I-2) with this heterozygous mutation presented normal hearing. The variant was not present in two hundred normal hearing controls. The mutation leads to a reading frame shift at amino acid position 136 and results in a premature termination in *POU3F4* (Figure 3(c)). As shown in Figure 3(b), the protein sequences were highly evolutionarily conserved and implicated to have a significant functional consequence. The dysfunction of the truncated protein without the DNA-binding domains of POU_s and POU_{HD} might contribute to the observed phenotype in the affected member of the Chinese family.

A molecular model of *POU3F4* was constructed based on the crystal structure of paired box domain (PDB ID: 2XSD). The predicted structures of wild-type and mutant proteins were observed and analyzed using PyMOL. As shown in Figure 4, the protein Pou3f4 bound to the DNA elements with POU_s and POU_{HD} domains. Compared with the wild-type structure of the Pou3f4, the truncated protein showed elimination of the specific DNA-binding domain, leading to lose the DNA-binding ability.

3.3. Outcomes of Cochlear Implantation. The proband gained great improvement on the auditory and speech ability after the first implantation. The audiometric thresholds improved to approximately 30 dB HL across all speech frequencies except the 4 kHz (Figure 5(a)). The CAP scale improved from 1 to 6, and the SIR scale improved from 1 to 4 at three years post the first implantation. The speech recognition tested three years postoperatively showed monosyllable words score was 61%, and bisyllable words score was 55%. He studied in an ordinary school, and the main mode of communication was verbal language. Approximately three and a half years post the first implantation, the benefits of the cochlear implant began to decline. His parents noticed that he began to have slurred speech. The hearing threshold at the 1 kHz increased greatly, and there was no response at 4 kHz (Figure 5(b)). He began to use lip reading to assist communication. The temporal bone CT scan showed that the electrode array was at the correct position in the cochlea (Figure 2(c)). The impedance of the electrodes was stable and in normal range. The speech processor was in good condition. Though the cochlear implant had been programmed several times, the outcomes were still worse than before.

The hearing threshold with the cochlear implantation on the right ear at two years post the reimplantation was displayed in Figure 5(c). The patient got little benefit at the frequency of 500 Hz and still has no response at 4 kHz. The speech recognition tested two years postoperatively showed monosyllable words score was 20%, and the bisyllable words score was 13%. The hearing threshold with the cochlear implantation on the left ear six months postoperatively was displayed in Figure 5(d). Similar hearing threshold frequency shape was seen on the left ear as it is shown on the right ear. The speech recognition tested on the left ear showed monosyllable words score was 48%, and the bisyllable words score

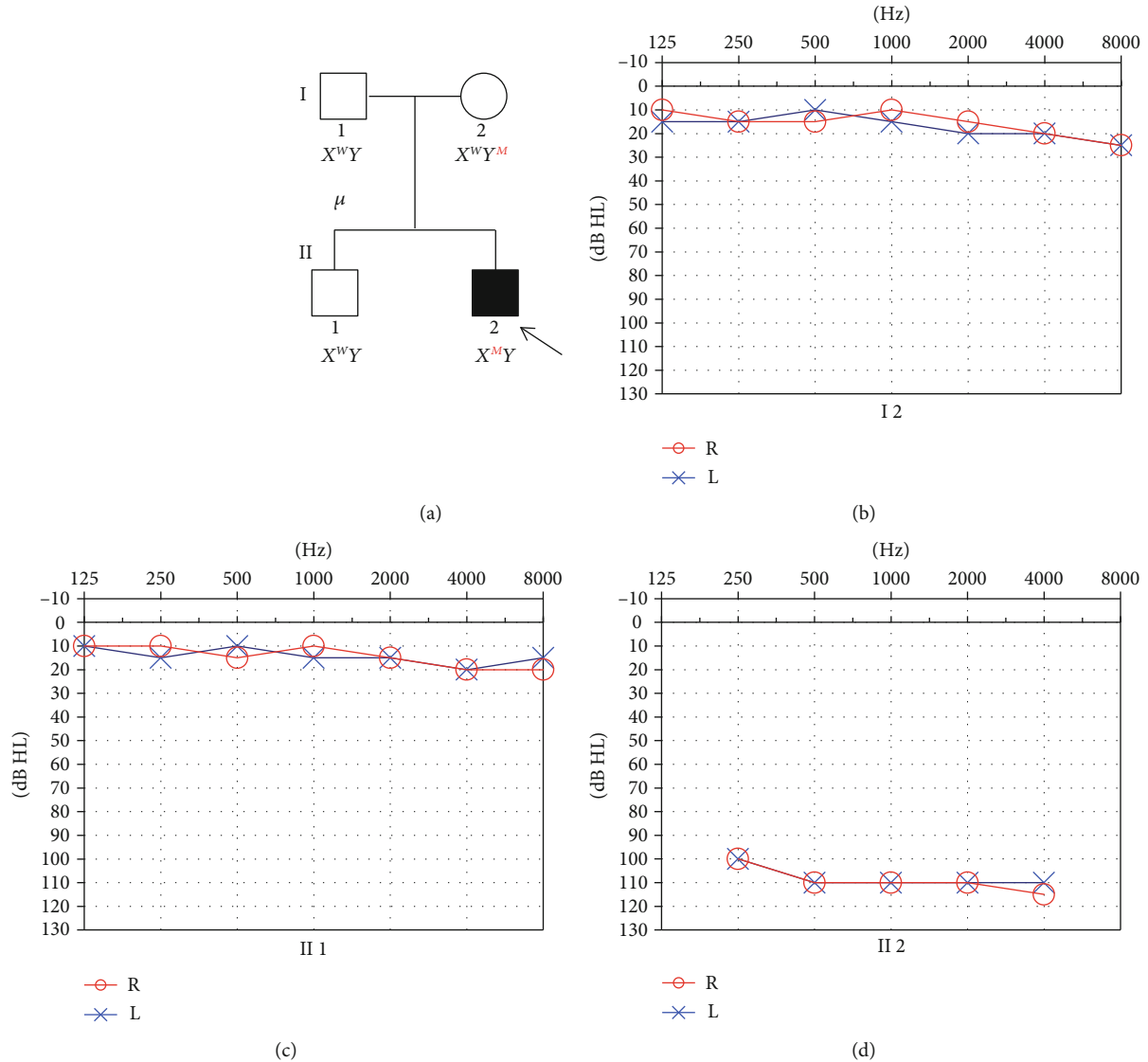


FIGURE 1: Clinical phenotype presentations of the pedigree. (a) Pedigree of a Chinese family displaying X-linked inheritance hearing loss (arrow indicates the proband; mutation c.400_401insACTC in *POU3F4* gene denoted as M); (b–d) Pure-tone audiograms of the family. Frequency in hertz (Hz) is plotted on the x -axis and the hearing level in decibels (dB HL) on the y -axis.

was 27%. Better speech perception was obtained with bilateral cochlear implants: monosyllable words score was 56%, and the bisyllable words score was 47%. Facial nerve stimulation by cochlear implantation was seen in the right ear.

4. Discussion

In this study, we identified a novel mutation c.400_401insACTC in the *POU3F4* gene causing SNHL loss in a X-linked recessive Chinese family combined WES and Sanger sequencing. The c.400_401insACTC mutation resulted in frame shift at amino acid position 136 located in upstream of the POU structure (p.Q136LfsX58). This frame shift caused a premature termination resulting in a protein lacking the entire POU homeodomain and specific homeodomain. Compared with the wild-type structure of the Pou3f4, the truncated protein caused by c.400_401insACTC

mutation severely disrupts the DNA binding ability of *POU3F4*. Thus, the transcriptional activity of this truncated Pou3f4 protein has been completely abolished. Previous studies indicated that the hearing loss in patients with *POU3F4* mutation was caused by the functional deficit of the Pou3f4 protein [27, 28]. In this study, the proband showed specific IP-III malformation and progressive hearing loss. To date, more than 70 pathogenic variants of the *POU3F4* gene have been reported in the Human Gene Mutation Database, including intragenic mutations, complete or partial deletions, duplications, insertions, and other chromosomal deletions. Most of the pathologic mutations are deletion or intragenic mutations, and only a few are inversion mutations. Moteki et al. also reported an insertion mutation (c.727_728insA) in *POU3F4* which also caused progressive hearing loss and IP-III malformation [29]. The severity of hearing loss among patients with different types of *POU3F4*

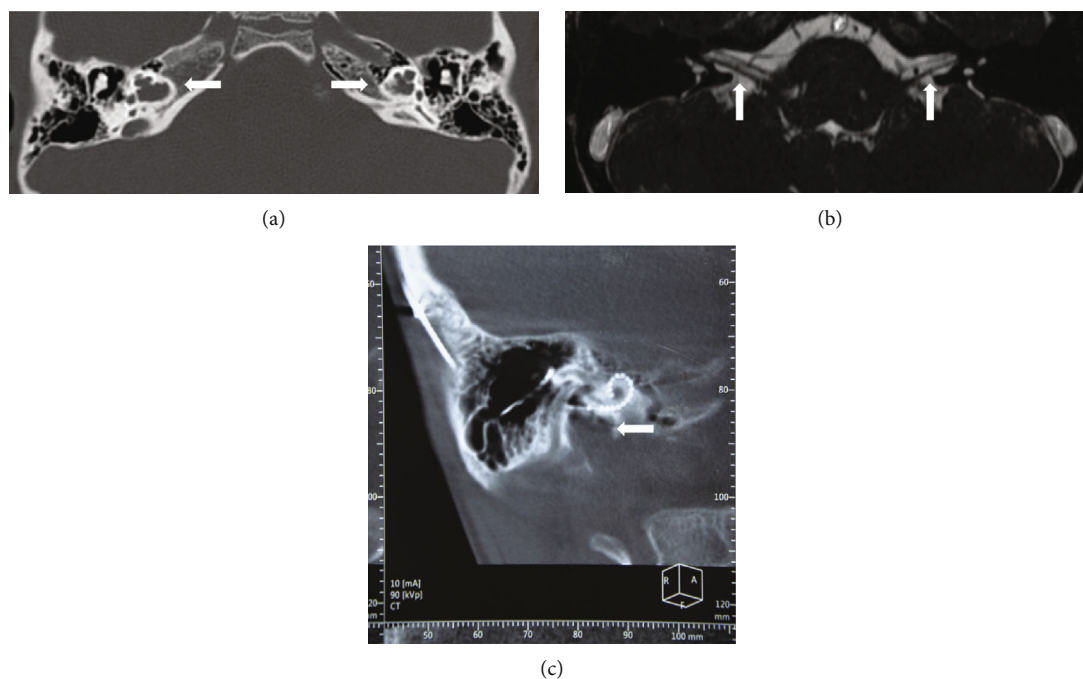


FIGURE 2: (a) Temporal bone CT images of the proband demonstrating dilation of the bottom of the internal auditory canal (IAC), bony plate deficiency between the basal turn of the cochlea and the IAC, absence of the modiolus, but the interscalar septa of the cochlea are present (arrow); (b) Axial MRI through the IAC displaying the vestibulocochlear nerve and the facial nerve; (c) Three-dimensional reconstruction of the cochlea showed that the electrode array was in the correct position.

mutations varied greatly. To date, no correlation was found between certain genotypes and initial auditory phenotype [28, 30].

The proband underwent sequentially cochlear implantation on both ears. The auditory and speech ability improved greatly after the first cochlear implantation. Three years post-operatively, the CAP score was 6, which meant that the patient can communicate with others without lip reading. Besides, the SIR score improved to 4 which meant that his pronunciation was clearly enough that could be understood by an acquaintance. However, the speech recognition scores with CI on both ears were lower than previously reported patients who have normal cochlea [31, 32]. It has been reported that the outcomes of cochlear implantation in patients with IP-III malformation were generally poorer than patients with normal cochlea [22, 27, 33]. Electrical stimuli delivered by the CI are first encoded by the SGNs, and subsequently transmitted to, and processed by, higher-level neural structures. Thus, the ability of the SGNs to faithfully encode and process electrical information is critical for CI outcomes. It has been demonstrated that the number and capability of the SNGs is an important factor for CI outcomes [34–36]. Animal studies showed that the radial bundle fasciculation and hair cell innervation of the SGNs were impaired after *Pou3f4* is deleted from otic mesenchyme [34]. Presumably, the responsiveness of SGNs to electric stimuli was impaired in patients with *POU3F4* mutation. Furthermore, the benefits of CI varied greatly among individual patients with IP-III malformation. Stankovic et al. reported that CI had limited benefits on the auditory and speech perception in patients with IP-III malformation [22]. In contrast, Kim et al. reported that patients with

IP-III malformation acquired good speech after cochlear implantation [33]. Factors accounting for these variations are still not well understood. Choi et al. reported that the *POU3F4* genotype might be an important factor for the outcomes of cochlear implantation [27]. In that study, patients with the *POU3F4* truncation or deletion mutations had poorer speech performance than patients with other types of mutations [27]. In our study, the insertion mutation c.400_401insACTC in the *POU3F4* gene resulted in the loss of the conserved domains of *Pou3f4* protein. However, the patient presented good outcomes with a cochlear implant. Many factors might contribute to the contradictory results, such as the type of electrode array, implantation age, and follow-up time were different in these two studies. Besides, only few patients were included in these two studies, and more data were needed to investigate the relationship of the *POU3F4* genotype and the outcomes of cochlear implantation.

In this study, we firstly reported that the outcomes of the cochlear implantation in patients with IP-III malformation would decline. Since the position of the electrode array, the device and processor were in good condition, we speculated that deterioration of the benefits was caused by the changes of the function of the SGNs in the cochlea. It has been reported that the SGNs density begins to decline by the end of the first postnatal week in *POU3F4* knock out mouse [37]. To date, there were no direct evidences that showed that the function of the SGNs would decline in patients with *POU3F4* mutation. However, it has been reported that patients with *POU3F4* mutation often presented with progressive hearing loss [38], which might indicate that the function of the SGNs would decline with age.

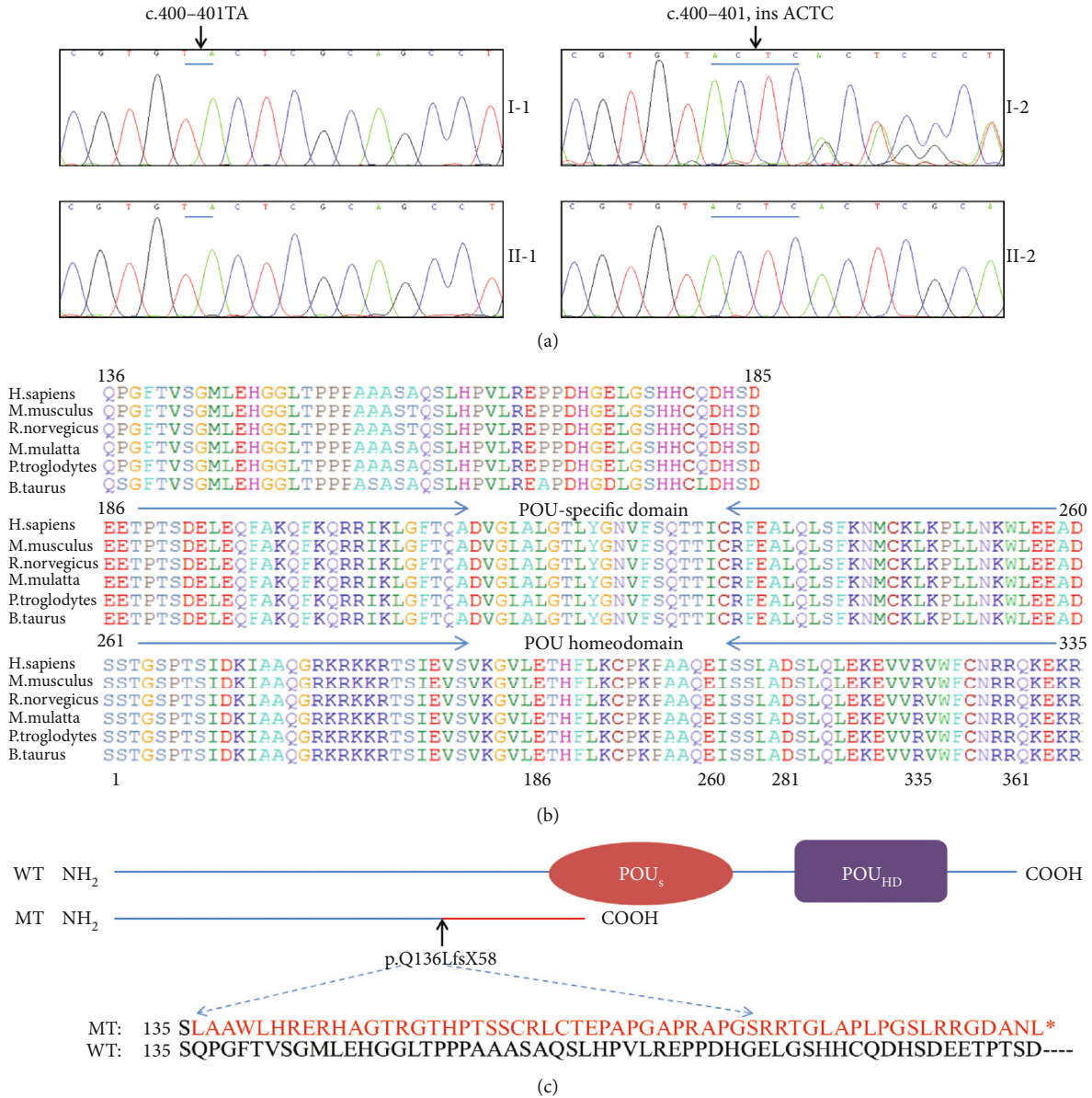


FIGURE 3: Partial sequence chromatograms, conservation analysis, and schematic illustration of Pou3f4. (a) DNA sequencing profile showing the c.400_401insACTC mutation in *POU3F4*. The sequence chromatograms were analyzed from PCR products of four family members. The arrow indicates the location of the nucleotide changes. (b) Protein alignment showing conservation of part residues of Pou3f4 across six species. (c) Schematic illustration of Pou3f4 protein labeled with the mutation identified in this study. The mutation introduces frame shift and a premature stop codon at amino acid 194, resulting in the nonfunctional protein without the POU_s and POU_{HD} domains.

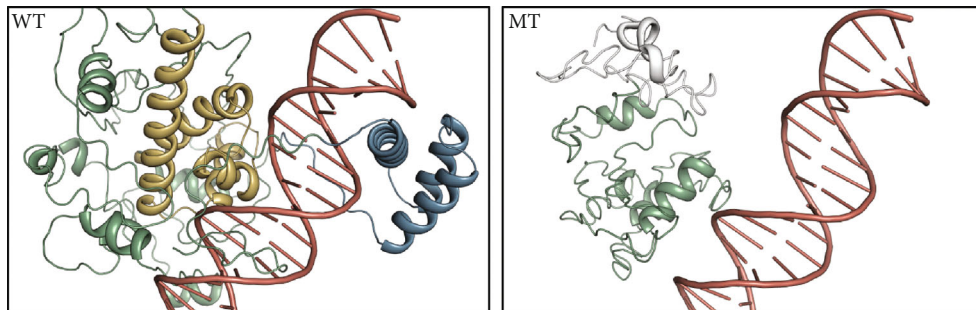


FIGURE 4: Structural simulation of Pou3f4. Compared with the wild-type (WT) protein, the structure of the mutant protein is incomplete, leading to lose the DNA-binding ability. The POU_s (yellow) and POU_{HD} (blue) domains are shown in different colors.

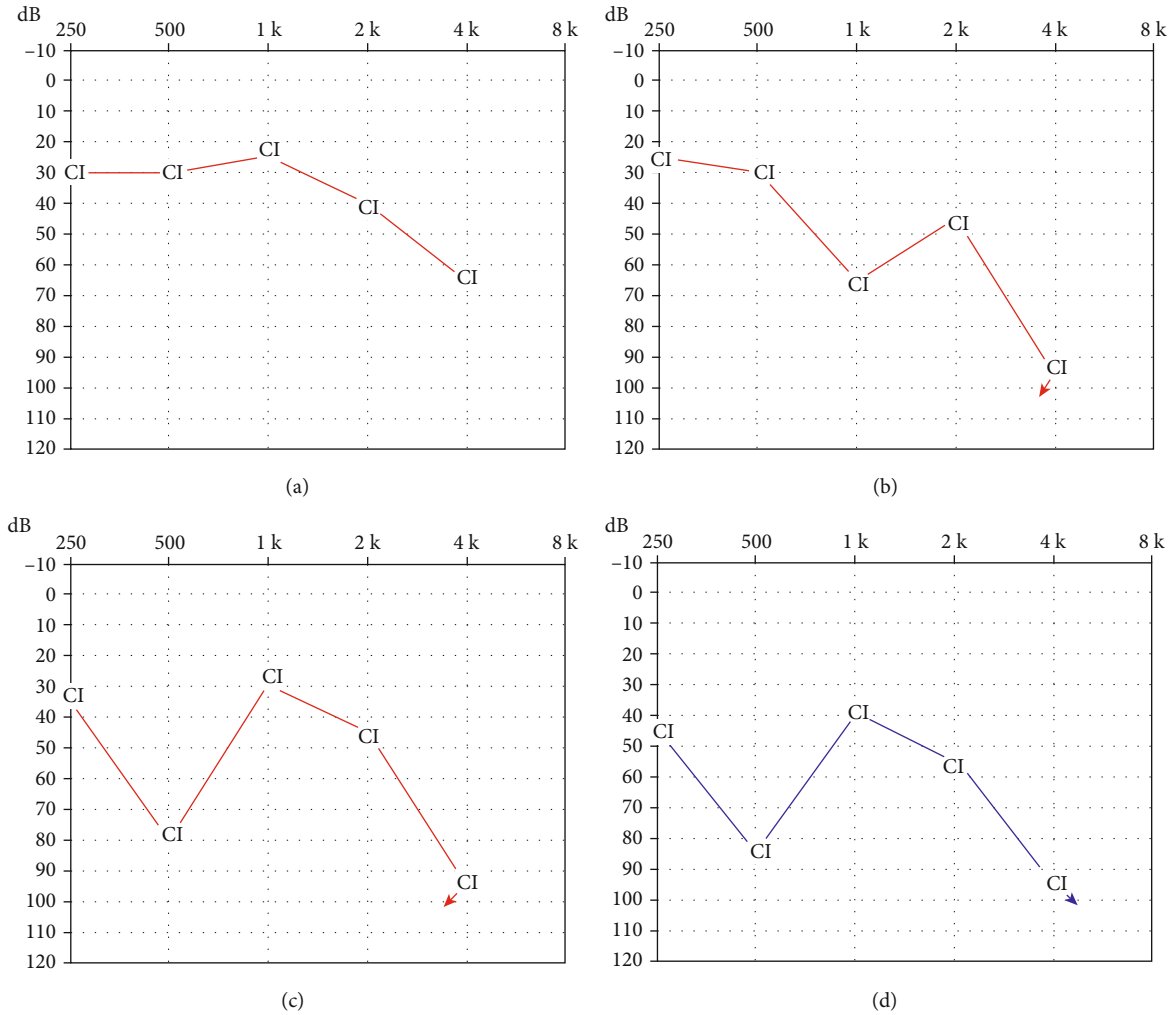


FIGURE 5: Audiometric thresholds with cochlear implants at different time points in different ears. (a) and (b) were hearing threshold on the right ear tested three and four years post the first implantation; (c) Hearing threshold on the right ear tested two years post the reimplantation; (d) Hearing threshold on the left ear tested half a year post the implantation. CI means hearing threshold with cochlear implant; arrow means no response.

After the deterioration of the CI benefits, the hearing thresholds were only increased in some specific frequencies. This indicated that the number and responsiveness of the SGNs might vary along the cochlea. Because of the absence of the modulus in patient with IP-III malformation, the distribution and function of residual SGNs in the cochlea are still unclear. In this study, the patient had no response on 4kHz on both ears, which indicated that the function of the SGNs around the basal electrodes might be worse than others. This was consistent with previously reported results. Stankovic et al. has reported the outcomes of cochlear implantation in four patients with *POU3F4* mutation; none of them could perceive sound from the basal electrodes [22]. Before the reimplantation, the proband showed bad response on 1kHz and 4kHz. However, he showed high threshold on 500Hz and 4kHz after the reimplantation. This might be due to the insertion depths of the electrode array in those two operations that were different. Thus, the stimulating frequencies to the SGNs had been reshaped.

5. Study Limitations

This study has several potential limitations. One potential limitation is that the neurophysiological mechanisms underlying the deterioration of the CI outcomes had not been assessed. Currently, the electrically evoked compound action potential (eCAP), a near-field neural response generated by the SGNs, has been widely used to evaluate the functional status of the SGNs [36]. The slope of eCAP input/output (I/O) function and neural refractoriness are associated with the density and function of the surviving neural population [32]. Besides, the maximum eCAP amplitude and eCAP threshold are also determined by the number of CN fibers activated by electrical stimuli [39]. In this study, the proband only did the introoperation neural response imaging (NRI). However, it has been reported that the NRI thresholds post the first half-year of implantation cannot faithfully reflect the response of the SGNs. In addition, none eCAP input/output (I/O) function data were collected before the reimplantation. Therefore, we failed to compare the function of SGNs

before and post the deterioration of the CI benefits. More comprehensive eCAP responses would be assessed to follow-up on the functional changes of the SGNs in the future.

6. Conclusion

In this study, a novel mutation c.400_401insACTC (p.Q136LfsX58) in the *POU3F4* gene was identified in a Chinese family with X-linked recessive hearing loss. The molecular genetic research showed the association between X-linked hearing loss and mutations in *POU3F4*, providing the definitive diagnosis and genetic counseling for this family and further enriched pathogenic mutation spectrum of the *POU3F4* gene. The patient with this variant showed specific IP-III malformation and progressive hearing loss. Patients with this mutation could get benefits from cochlear implantation. However, the outcomes of the cochlear implantation might decline as the patient grows old. The mechanism of the effect of the *POU3F4* genotype on the distribution and function of SGNs in IP-III malformation deserves further investigation.

Data Availability

All the data in this study were collected in Shandong Provincial ENT Hospital. The processed data are available within the article.

Conflicts of Interest

The authors declare that they have no conflicts of interest.

Authors' Contributions

Xiuhua Chao and Yun Xiao contributed equally to this work.

Acknowledgments

This work was supported by grants from the National Natural Science Foundation of China (No. 81800905 and No. 81670932), the Key Project of Shandong Provincial Programs for Research and Development (2017CXGC1213), and the Taishan Scholars Program of Shandong Province (No. ts20130913 and No. tsqn201909189).

References

- [1] L. Sennaroglu and M. D. Bajin, "Classification and current management of inner ear malformations," *Balkan Medical Journal*, vol. 34, no. 5, pp. 397–411, 2017.
- [2] Y. Liu, J. Qi, X. Chen et al., "Critical role of spectrin in hearing development and deafness," *Science Advances*, vol. 5, no. 4, p. eaav7803, 2019.
- [3] J. Qi, Y. Liu, C. Chu et al., "A cytoskeleton structure revealed by super-resolution fluorescence imaging in inner ear hair cells," *Cell Discovery*, vol. 5, no. 1, 2019.
- [4] Y. Wang, J. Li, X. Yao et al., "Loss of CIB2 causes profound hearing loss and abolishes mechano-electrical transduction in mice," *Frontiers in Molecular Neuroscience*, vol. 10, 2017.
- [5] C. Zhu, C. Cheng, Y. Wang et al., "Loss of ARHGEF6 causes hair cell stereocilia deficits and hearing loss in mice," *Frontiers in Molecular Neuroscience*, vol. 11, 2018.
- [6] Z. He, L. Guo, Y. Shu et al., "Autophagy protects auditory hair cells against neomycin-induced damage," *Autophagy*, vol. 13, no. 11, pp. 1884–1904, 2017.
- [7] Z.-h. He, S.-y. Zou, M. Li et al., "The nuclear transcription factor FoxG1 affects the sensitivity of mimetic aging hair cells to inflammation by regulating autophagy pathways," *Redox Biology*, vol. 28, p. 101364, 2020.
- [8] L. Liu, Y. Chen, J. Qi et al., "Wnt activation protects against neomycin-induced hair cell damage in the mouse cochlea," *Cell Death & Disease*, vol. 7, no. 3, pp. e2136–e2136, 2016.
- [9] W. Liu, X. Xu, Z. Fan et al., "Wnt signaling activates TP53-induced glycolysis and apoptosis regulator and protects against cisplatin-induced spiral ganglion neuron damage in the mouse cochlea," *Antioxidants & Redox Signaling*, vol. 30, no. 11, pp. 1389–1410, 2019.
- [10] L. Sennaroglu and M. D. Bajin, "Incomplete partition type III: a rare and difficult cochlear implant surgical indication," *Auris Nasus Larynx*, vol. 45, no. 1, pp. 26–32, 2018.
- [11] W. E. Nance, R. Settleff, A. McLeod et al., "X-linked mixed deafness with congenital fixation of the stapedial footplate and perilymphatic gusher," *Birth Defects Original Article Series*, vol. 7, no. 4, pp. 64–69, 1971.
- [12] L. Sennaroglu and I. Saatci, "A new classification for cochleovestibular malformations," *Laryngoscope*, vol. 112, no. 12, pp. 2230–2241, 2002.
- [13] Y. de Kok, S. van der Maarel, M. Bitner-Glindzicz et al., "Association between X-linked mixed deafness and mutations in the POU domain gene *POU3F4*," *Science*, vol. 267, no. 5198, pp. 685–688, 1995.
- [14] M. B. Petersen, Q. Wang, and P. J. Willems, "Sex-linked deafness," *Clinical Genetics*, vol. 73, no. 1, pp. 14–23, 2008.
- [15] J. M. Mathis, D. M. Simmons, X. He, L. W. Swanson, and M. G. Rosenfeld, "Brain 4: a novel mammalian POU domain transcription factor exhibiting restricted brain-specific expression," *The EMBO Journal*, vol. 11, no. 7, pp. 2551–2561, 1992.
- [16] D. Phippard, L. Lu, D. Lee, J. C. Saunders, and E. B. Crenshaw, "Targeted mutagenesis of the POU-domain gene *Brn4/Pou3f4* causes developmental defects in the inner ear," *The Journal of Neuroscience*, vol. 19, no. 14, pp. 5980–5989, 1999.
- [17] M. O. Trowe, H. Maier, M. Schweizer, and A. Kispert, "Deafness in mice lacking the T-box transcription factor *Tbx18* in otic fibrocytes," *Development*, vol. 135, no. 9, pp. 1725–1734, 2008.
- [18] D. S. Samadi, J. C. Saunders, and E. B. Crenshaw, "Mutation of the POU-domain gene *Brn4/Pou3f4* affects middle-ear sound conduction in the mouse," *Hearing Research*, vol. 199, no. 1–2, pp. 11–21, 2005.
- [19] A.-P. Xia, T. Kikuchi, O. Minowa et al., "Late-onset hearing loss in a mouse model of DFN3 non-syndromic deafness: morphologic and immunohistochemical analyses," *Hearing Research*, vol. 166, no. 1–2, pp. 150–158, 2002.
- [20] M. H. Song, S.-Y. Choi, L. Wu et al., "Pou3f4 deficiency causes defects in otic fibrocytes and stria vascularis by different mechanisms," *Biochemical and Biophysical Research Communications*, vol. 404, no. 1, pp. 528–533, 2011.
- [21] H. Smeds, J. Wales, F. Asp et al., "X-linked malformation and cochlear implantation," *Otology & Neurotology*, vol. 38, no. 1, pp. 38–46, 2017.

- [22] K. M. Stankovic, A. M. Hennessey, B. Herrmann, and L. A. Mankariou, "Cochlear implantation in children with congenital X-linked deafness due to novel mutations in POU3F4-Gene," *The Annals of Otolaryngology, Rhinology, and Laryngology*, vol. 119, no. 12, pp. 815–822, 2010.
- [23] H. Li and R. Durbin, "Fast and accurate short read alignment with Burrows-Wheeler transform," *Bioinformatics*, vol. 25, no. 14, pp. 1754–1760, 2009.
- [24] A. Tarasov, A. J. Vilella, E. Cuppen, I. J. Nijman, and P. Prins, "Sambamba: fast processing of NGS alignment formats," *Bioinformatics*, vol. 31, no. 12, pp. 2032–2034, 2015.
- [25] K. Wang, M. Li, and H. Hakonarson, "ANNOVAR: functional annotation of genetic variants from high-throughput sequencing data," *Nucleic Acids Research*, vol. 38, no. 16, p. e164, 2010.
- [26] F. Zhang, X. Bai, Y. Xiao et al., "Identification of a novel mutation in SLC26A4 gene in a Chinese family with enlarged vestibular aqueduct syndrome," *International Journal of Pediatric Otorhinolaryngology*, vol. 85, pp. 75–79, 2016.
- [27] B. Y. Choi, Y. H. An, J. J. Song et al., "Clinical observations and molecular variables of patients with hearing loss and incomplete partition type III," *Laryngoscope*, vol. 126, no. 3, pp. E123–E128, 2016.
- [28] H. K. Lee, M. H. Song, M. Kang et al., "Clinical and molecular characterizations of novel POU3F4 mutations reveal that DFN3 is due to null function of POU3F4 protein," *Physiological Genomics*, vol. 39, no. 3, pp. 195–201, 2009.
- [29] H. Moteki, A. E. Shearer, S. Izumi et al., "De novo mutation in X-linked hearing loss-associated POU3F4 in a sporadic case of congenital hearing loss," *Annals of Otolaryngology & Laryngology*, vol. 124, 1_suppl, pp. 169S–176S, 2015.
- [30] A. Kanno, H. Mutai, K. Namba et al., "Frequency and specific characteristics of the incomplete partition type III anomaly in children," *Laryngoscope*, vol. 127, no. 7, pp. 1663–1669, 2017.
- [31] M. Davcheva-Chakar, E. Sukarova-Stefanovska, V. Ivanovska, V. Lazarevska, I. Filipche, and B. Zafirovska, "Speech perception outcomes after cochlear implantation in children with GJB2/DFNB1 associated deafness," *Balkan Medical Journal*, vol. 31, no. 1, pp. 60–63, 2014.
- [32] J. R. Kim, P. J. Abbas, C. J. Brown, C. P. Etlar, S. O'Brien, and L. S. Kim, "The relationship between electrically evoked compound action potential and speech perception: a study in cochlear implant users with short electrode array," *Otolaryngology & Neurotology*, vol. 31, no. 7, pp. 1041–1048, 2010.
- [33] L. Kim, C. E. Wisely, S. Lucius, J. Weingarten, and E. E. Dodson, "Positive outcomes and surgical strategies for bilateral cochlear implantation in a child with X-linked deafness," *Annals of Otolaryngology, Rhinology, and Laryngology*, vol. 125, no. 2, pp. 173–176, 2015.
- [34] T. M. Coate, S. Raft, X. Zhao, A. K. Ryan, E. B. Crenshaw III, and M. W. Kelley, "Otic mesenchyme cells regulate spiral ganglion axon fasciculation through a Pou3f4/EphA4 signaling pathway," *Neuron*, vol. 73, no. 1, pp. 49–63, 2012.
- [35] S. He, B. S. Shahsavarani, T. C. McFayden et al., "Responsiveness of the electrically stimulated cochlear nerve in children with cochlear nerve deficiency," *Ear and Hearing*, vol. 39, no. 2, pp. 238–250, 2018.
- [36] B. E. Pflingst, A. P. Hughes, D. J. Colesa, M. M. Watts, S. B. Strahl, and Y. Raphael, "Insertion trauma and recovery of function after cochlear implantation: evidence from objective functional measures," *Hearing Research*, vol. 330, pp. 98–105, 2015.
- [37] P. M. Brooks, K. P. Rose, M. L. MacRae et al., "Pou3f4-expressing otic mesenchyme cells promote spiral ganglion neuron survival in the postnatal mouse cochlea," *The Journal of Comparative Neurology*, vol. 528, no. 12, pp. 1967–1985, 2020.
- [38] V. Corvino, P. Apisa, R. Malesci, C. Laria, G. Auletta, and A. Franze, "X-linked sensorineural hearing loss: a literature review," *Current Genomics*, vol. 19, no. 5, pp. 327–338, 2018.
- [39] L. Xu, J. Skidmore, J. Luo et al., "The effect of pulse polarity on neural response of the electrically stimulated cochlear nerve in children with cochlear nerve deficiency and children with normal-sized cochlear nerves," *Ear and Hearing*, vol. 41, no. 5, pp. 1306–1319, 2020.

Review Article

Mitochondrial Dysfunction and Therapeutic Targets in Auditory Neuropathy

Baoyi Feng,^{1,2,3} Chenxi Jin,^{1,2,3} Zhenzhe Cheng,^{1,2,3} Xingle Zhao,^{1,2,3} Zhuoer Sun,^{1,2,3} Xiaofei Zheng,^{1,2,3} Xiang Li,^{1,2,3} Tingting Dong,⁴ Yong Tao ^{1,2,3} and Hao Wu ^{1,2,3}

¹Department of Otolaryngology-Head and Neck Surgery, Shanghai Ninth People's Hospital, Shanghai Jiaotong University School of Medicine, No. 639, Zhizaoju Road, Shanghai 200011, China

²Ear Institute, Shanghai Jiaotong University School of Medicine, No. 115, Jinzun Road, Shanghai 200011, China

³Shanghai Key Laboratory of Translation Medicine on Ear and Nose Disease, No. 115, Jinzun Road, Shanghai 200011, China

⁴Biobank of Ninth People's Hospital, Shanghai Jiao Tong University School of Medicine, No. 115, Jinzun Road, Shanghai 200011, China

Correspondence should be addressed to Yong Tao; taoyent@foxmail.com and Hao Wu; wuhao622@sina.cn

Received 24 April 2020; Revised 27 May 2020; Accepted 11 July 2020; Published 28 August 2020

Academic Editor: Renjie Chai

Copyright © 2020 Baoyi Feng et al. This is an open access article distributed under the Creative Commons Attribution License, which permits unrestricted use, distribution, and reproduction in any medium, provided the original work is properly cited.

Sensorineural hearing loss (SNHL) becomes an inevitable worldwide public health issue, and deafness treatment is urgently imperative; yet their current curative therapy is limited. Auditory neuropathies (AN) were proved to play a substantial role in SNHL recently, and spiral ganglion neuron (SGN) dysfunction is a dominant pathogenesis of AN. Auditory pathway is a high energy consumption system, and SGNs required sufficient mitochondria. Mitochondria are known treatment target of SNHL, but mitochondrion mechanism and pathology in SGNs are not valued. Mitochondrial dysfunction and pharmacological therapy were studied in neurodegeneration, providing new insights in mitochondrion-targeted treatment of AN. In this review, we summarized mitochondrial biological functions related to SGNs and discussed interaction between mitochondrial dysfunction and AN, as well as existing mitochondrion treatment for SNHL. Pharmaceutical exploration to protect mitochondrion dysfunction is a feasible and effective therapeutics for AN.

1. Introduction

Hearing loss is one of the most crucial public health issues. According to the 70th World Health Assembly (WHA), 360 million people are suffering from auditory dysfunction in the world, accounting for 5% of the world's population. Besides, more than 1000 million juveniles are risky to hearing disorder [1]. Auditory dysfunction causes speech communication barrier, cognitive disorder, psychological isolation, and inferiority but also brings a heavy burden on family and society. SNHL is the major type of deafness, representing damage in the inner ear or auditory nerves that travel from the ear to the brain [2]. The etiology of deafness is complex, and SGNs draw more and more attention recently [3].

AN or auditory disease was first proposed by Kaga et al. [4] and Starr et al. [5] in 1996, referring to an

acquired disorder characteristic of slight hearing impairment with wave I-III absence of auditory brainstem response (ABR) and speech recognition disorder, while distortion product otoacoustic emission (DPOAEs) and cochlear microphonic potential (CMs) did not change. AN may present as a sole clinical phenotype or just be one of the symptoms in systematic diseases like hereditary sensorimotor neuropathies (HSMN) or other demyelinating diseases. Pathology evidence demonstrated auditory nerve damage and loss of inner hair cells (IHCs) and ribbon synapses in AN. AN could be aroused by hereditary defects; for instance, mutation of genes encoding otoferlin or vesicular glutamate transporter 3 was found to induce IHC presynaptic and postsynaptic dysfunctions, respectively. And exogenous damage is another key contributor to be reckoned with, including noise exposure, ototoxic

drugs, hyperbilirubinemia or thiamin deficiency in infant, or presbycusis [6].

Mitochondrion dysfunction is a major reason for neuropathy. Mitochondria, serving as the engines of eukaryotic cells, participate in cellular energy metabolism, ROS generation, calcium homeostasis, and apoptosis. Mitochondria exhibit special dynamic nature, with feature of pluralistic morphology and great interconnectivity, which determine their function and network structure. Mitochondrion dysfunction is a key reason in aging and neurodegeneration like Alzheimer's disease (AD), amyotrophic lateral sclerosis (ALS), Charcot-Marie-Tooth disease (CMT), and optic atrophy [7]. Additionally, association between mitochondrial biology and optic neuropathies were also detailedly illustrated by pathology and relevant molecular and therapeutic targets. Patients with neuropathy including myoclonic epilepsy with ragged-red fibers (MERRF); mitochondrial encephalomyopathy, lactic acidosis, and stroke-like episodes (MELAS); Charcot-Marie-Tooth disease type 2A (CMT2A); and HSMN caused by mitochondrial dysfunction [8] were also observed suffering from sensorineural hearing loss [9, 10]. The mutation of optic atrophy 1 (OPA1), a key protein related to mitochondrial fusion, was proved to cause syndromic autosomal dominant optic atrophy (DOA+) with auditory dysfunction [11], which reveals to the potential association between auditory nerves and mitochondria in the development of hearing disorders.

Thus, it is of great significance to explore mitochondrial mechanism of auditory neuropathy and may identify the therapeutic target of auditory neuropathy. In this review, we supply a brief introduction in the mitochondrial structure and function which is correlative to auditory neuropathy and illustrate the potential mechanism between mitochondrial dysfunction and auditory neuropathy. Ultimately, we enumerate the effective therapies targeting mitochondrion dysfunction in AN.

2. Mitochondrial Genome and Function

2.1. Mitochondrial Genome. Mitochondrial DNA (mtDNA), which is a mitochondrion-specific genetic system, exists as double-stranded circular molecule with a length of 16569 bp in human. Composed of a heavy strand and a light strand, mtDNA encodes 2 rRNAs, 22 tRNAs, and 13 subunits of the proteins and complexes in respiratory chain including COX I, II, and III and ATP synthase [12], illustrating its crucial role in oxidative phosphorylation (OXPHOS). Plenty of mutations in mtDNA are associated with anomalous OXPHOS. The diversity of mtDNA mutation was observed in neurodegeneration due to the neurons vulnerable to energy supply, especially during aging [13]. The deletion of mtDNA aggravated age-related hearing loss at 12 months of Fischer 344 male rats [14], while D257A and T7511C mutation in mtDNA accelerated the progression of age-related hearing loss and degeneration of HCs and SGNs [15, 16]. Moreover, mitochondria are sensitive to ROS since excessive ROS impedes unfolding of protein; therefore, ROS induce mtDNA mutation [17].

MtDNA is of maternal inheritance, and the copy number of mtDNA reaches nearly 1000 in majority of cells, hundreds of times as nuclear DNA genomes. Additionally, mitochondrial biogenesis or heteroplasmy occurs independently in cell division, allowing mutated mtDNA distributed unevenly in subcultured cells without efficient repairment, which was observed in most of the mitochondrial disease [18].

2.2. Mitochondrial Homeostasis. Mitochondrion is an organelle with high interconnection and constant movement, forming cellular networks through a dynamic process. Mitochondrial homeostasis refers to the steady status of the mitochondrial network structure between mitochondrial biogenesis and degradation, including mitochondrial fusion and fission, mitophagy, and trafficking. Disorders of mitochondrial homeostasis have been found in aging and plenty of age-related diseases like neurodegeneration and cardiovascular disease.

Mitochondrial biogenesis is a renewed process of mitochondria by growth and division, associated with protein synthesis, import, and assembly under the guidance of nuclear DNA and mtDNA [19]. Fusion acts on mitochondrial remodelling, modulated by proteolytic processing and PINK1-dependent ubiquitination. Fission allows the extraction of damage segment and quality control of mitochondria, which depends on several critical proteins owning highly conserved dynamic GTPase domain. Mitofusins 1 and 2 (Mfn1 and Mfn2) are located in the outer mitochondrial membrane, and Opa1 was anchored in the inner mitochondrial membrane. Fusion and fission are also involved in the process of mitophagy with the help of dynamic-related protein 1 (Drp1), a crucial mediator of mitochondrial fission assembled with Fis1 after posttranslational modifications, which could accelerate mitochondrial division [10, 20]. Apoptosis could be activated by means of regulating proapoptotic factors delivered and expressed in the cytoplasm, such as cyto-c and Bcl-2 [21–24].

Mitophagy is a vital process for mitochondrial quality control that could eliminate impaired mitochondria in time. When mitochondrial membrane potential vanished, PINK1 aggregated on the mitochondrial outer membrane with phosphorylation of Mfn2 and Parkin, inducing ubiquitination of multiple downstream proteins. Finally, impaired mitochondria were separated [10]. Besides, mitochondrial renewal and long-distance energy supply rely on mitochondrial trafficking orthodromic and antidromic. It is essential to neuron that their survival leans more heavily on mitochondrial trafficking than other cells for its high energy consumption and unique cellular morphology. Studies demonstrated fundamental significance to mitochondrial trafficking of motor/adaptor complex composed of kinesin, dynein, Milton, and Miro [25]. Mitochondrial trafficking mechanism in neurodegeneration has been widely studied in AD, Parkinson's disease, Huntington's disease, and amyotrophic lateral sclerosis (ALS) [26].

2.3. Mitochondrial Energetic Metabolism. As a cellular energy organ in eukaryote, mitochondria play vital roles in energy metabolism and ATP production through two essential

process, the citric acid cycle (TCA) and OXPHOS. The TCA cycle is a critical task in aerobic respiration of eukaryotes as well as an ultimate metabolic step of carbohydrates, fats, and proteins. The cycle starts with citrate production as acetyl-coenzyme A enters the TCA cycle and ends as fumarate is converted into oxaloacetate, in which electron carriers NADH and FADH₂ are manufactured and further participating in electron transfer to electron transport chain (ETC) [27]. The OXPHOS system operates as the launch of ETC. ETC is situated in the inner membrane of mitochondria (IMM), performing functions in conveying electrons through complex I-III, cyto-c, and complex IV successively to convert oxygen to water and driving proton gradient production. Coenzyme Q (CoQ) is the key intermediate electron transporter of this process. With the actuation of proton gradient, ATP is released via ADP phosphorylation through complex V (ATP synthase). Nonetheless, there is still a bit of energy that remained besides the portion consumed by ATP synthesis, as the protons are able to leak across IMM and induce ROS generation to mitochondrial matrix via complexes I and III to a great extent [28]. ROS is an indispensable regulator for normal cellular activities covering intercellular communication as the secondary messenger, proliferation, differentiation, and apoptosis, while excessive accumulation of ROS might lead to oxidative damage, cell death, and diseases like cancer as well as neurodegeneration [29].

Besides, mitochondria also impact apoptosis and regulate calcium flux through mitochondrion-associated ER membranes, which not only act as the second messenger but also are essential to neurotransmitter release like glutamine [30]. As there is a high consumption of energy, normal activities of neuron are bound up with functional mitochondria, including auditory nerves.

3. Mitochondrial Dysfunction in Auditory Neuropathy

3.1. Auditory Neuropathy and the Role of SGNs in Auditory Pathway. Neuropathy is a common pathology in SNHL, related to age-related hearing loss and noise-induced hearing loss. Significant SGN degeneration followed by age is observed in apical and basal turns of both human and other mammals' cochlea, while inner or outer hair cells (OHCs) remain existing [31–34]. In Alzheimer's disease (AD), a study found significant loss of SGNs, rather than HC death, which could be found in the cochlea of both 9- and 12-month-old 3xTg-AD model mice [35]. Meanwhile, it was demonstrated that swollen cochlear nerve dendrites were seen in the first 24 h after noise exposure which could lead to temporary threshold shifts (TTS), without HC loss [36]. DPOAE threshold shifts were mild, suggesting that neuropathy and loss of ribbon synapse also contributed to the hearing loss prior to OHC damage. OHCs recovered 2 weeks after exposure, but delayed neurodegeneration was still observed for a long time [37]. In addition to aggravation of ABR threshold and aberrant compound potential of spiral ganglion, impaired SGNs also conducted

to degraded precision of acoustic signal encoding and abnormal speech recognition [6].

Most of SGNs are bipolar cells located in Rosenthal's canal around the modiolus, serving as the primary afferent nerves with innervation of the sensory HCs and cochlear nucleus [38, 39]. About 95% of SGNs embedded in myelin formed by satellite glial cells are connected to IHCs, named type I SGNs [40]. The rest of the neurons are type II SGNs and act as postsynaptic sites of OHCs. When action potentials of HCs were initiated by acoustic signal, glutamine, the neurotransmitters were released at ribbon synapses, which was highly specific with precise and speedy information transmission, inducing action potential of SGNs through AMPA receptors [41, 42]. Consequently, SGNs gathered sound signals from dendrites and communicated to an auditory nucleus through axon. The average length of fiber between SGN and HCs in human was nearly 32 mm [43], which required high energetic consumption and protein synthesis to complete long distance transportation [44]. Imperative requirement of energy support by mitochondria in SGNs indicated the contribution of mitochondrial dysfunction may induce auditory neuropathy (Figure 1).

3.2. Mitochondrial Homeostasis in Auditory Neuropathy. Deregulation of mitochondrial homeostatic mechanism might probably contribute to auditory neuropathy, with dysfunctional mitochondrion biogenesis or impaired dynamics. PGC1- α , a key regulator of mitochondrial biogenesis, was also found increased in HCs and auditory cortex, which might improve the sensitivity of age-related hearing loss [45–47]. Additionally, it was found that mutation of tRNA 5-methylaminomethyl-2-thiouridylate methyltransferase (TRMU), the tRNA-modified protein, was related to incidence of SNHL [48, 49]. Dysfunction on mitochondrial protein synthesis plays a fundamental role in SNHL development, when tryptophanyl-tRNA synthetase 2 (Wars2) and mitochondrial ribosomal protein S2 (MRPS2), which are critical to the process, were proved to lead to severe SNHL and SGN loss during mutation [50, 51]. Mitochondrial protein transport dysfunction also drives the development of SNHL, such as GFER, mitochondrial disulfide relay system protein [52], and DDP [53]. Performing as the critical protein of mitochondrial fission, OPA1 R455H missense mutations were also discovered linking to auditory neuropathy. The absence of ABR, serious speech perception impairment with preserved activity of OHCs, points to the damage of IHCs, ribbon synapse, or auditory nerves [54]. PINK1 is widely expressed in mouse cochlea and able to protect SGNs from cisplatin-induced ototoxicity [55]. Conversely, mitophagy deficiency due to Drp-1 inhibition might give rise to age-related hearing loss with impaired mitochondrial membrane potential HC damage [56].

3.3. Redox Homeostasis and Energetic Metabolism in Auditory Neuropathy. Due to abundant antioxidant enzyme and low transfer potential energy, mitochondria with integrated structure and function can defend against the formation of ROS [57]. ROS homeostasis was associated with

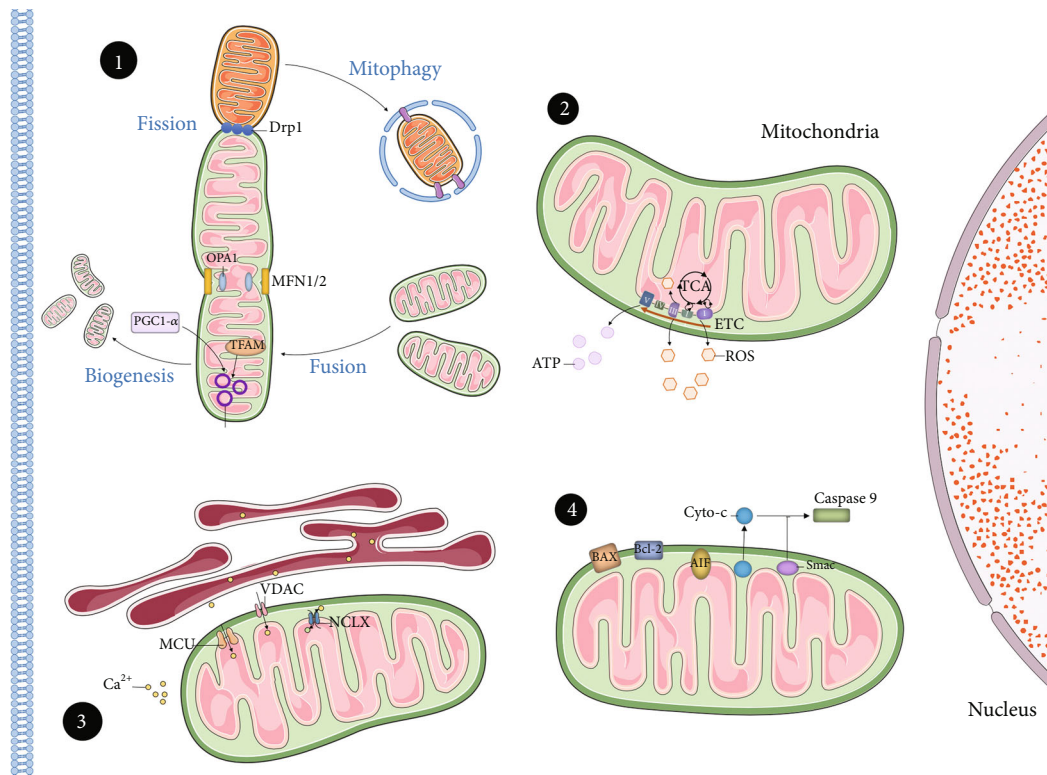


FIGURE 1: Mitochondrial dysfunction mechanism of spiral ganglion neurons in auditory neuropathy. Although mechanisms of mitochondrial dysfunction have not been illustrated distinctly, damages in following targets have been mentioned: (1) mitochondrial homeostasis including biogenesis, dynamics, and mitophagy; (2) redox homeostasis and energetic metabolism; (3) mitochondrial calcium homeostasis; and (4) proapoptotic signal in mitochondria. Drp1: dynamin-related protein 1; MFN1/2: mitofusin 1/2; OPA1: optic atrophy 1; PGC1- α : peroxisome proliferator-activated receptor γ coactivator-1 α ; TFAM: mitochondrial transcription factor A; TCA: tricarboxylic acid; ETC: electron transport chain; MCU: mitochondrial calcium uniporter; VDAC: voltage-dependent anion channel; NCLX: Na⁺/Ca²⁺/Li⁺ exchanger; Bcl-2: B cell lymphoma-2; BAX: Bcl-2 associated protein X; AIF: apoptosis inducing factor.

neurodegeneration and auditory neuropathy [58]. Three-week-old mice infected with murine congenital cytomegalovirus (MCMV) in neonatal were found to be suffering from hearing loss, and MCMV-infected cultured SGNs in vitro displayed elevated ROS levels and activated NLRP3 inflammasome, which can be suppressed by ROS inhibitor NAC [59]. Additionally, ROS is related to cochlear neuropathy in presbycusis. Evaluated mtDNA oxidative damage and mitochondrial ultrastructural damage in SGNs and auditory cortex were described in aging C57/B6j mice [60]. To mimic human's presbycusis, a senescence-accelerated mouse prone 8 (SAMP8) mouse model was chosen to study the mechanism of ARHL. SGNs of SAMP8 mice own disorganized mitochondria with missing cristae at 12 months, and MDA (a lipid peroxidation) increased and antioxidant enzyme decreased in 1 month, compared to wild-type mice [61]. Disrupted CMP-Neu5Ac hydroxylase (Cmah) is also involved in ARHL. Cmah-null mice showed significant downregulation of ROS gene degradation such as Gpxs and Sod; meanwhile, SGNs lost dramatically. KEGG pathway analysis demonstrated downregulation of mitochondrial molecular transport regulator gene, including Crumbs homolog 1 (Crb1), mitochondrial fission process 1 (Mtfp1), Ras homolog family member T2 (RhoT2), soluble oxidase component (Soc2), and ATP synthase F1 (Atp5f1),

indicating mitochondrial dysfunction [62]. The mutation of the protein that can affect ROS production and degradation such as superoxide dismutase (SOD) [63], glutathione S-transferases (GST) [64], mitochondrial uncoupling proteins (UCPs) [65] were found be associated with ARHL.

Now, we have consensus that excessive ROS production aroused cochlear injury in NIHL [66, 67]. Noise exposure induced ROS damage, and raised mitochondrial calcium leads to endoplasmic reticulum (ER) and extracellular fluid, which damage abnormal mitochondrial membrane potential [68–70]. The stria vascularis also contributed to neuropathy: lipid peroxide formation and swollen blood vessels in stria vascularis reduced cochlear blood flow [71, 72], resulting in cochlea ischemia reperfusion and secondary injury by ROS. Noise exposure also caused glutamate excitotoxic neural swelling [67, 73]. A previous study of excessive ROS production after noise exposure focus on the HCs rather than SGN. Although it was still unknown whether ROS was associated with synapse and SGNs damage in NIHL, SGN was susceptible to hypoxia demonstrated by patients who experienced perinatal and postnatal hypoxia [74].

TCA cycle is a key process for energy-intensive auditory nerves. Isocitrate dehydrogenase 2 (IDH2) is one of the isozymes of IDH and can convert NADP⁺ to NADPH, involved in TCA cycle. IDH2 dysfunction accelerated apoptosis and

caused cardiac impairment due to oxidative stress [75, 76]. Severe oxidative damage and more fragmented nuclear DNA in SGNs were seen in *Idh2^{-/-}* mice at 24 months compared to WT, indicating IDH2 deficiency promotes age-related hearing loss [77]. Calorie restriction protected HC and SGN degeneration by the promotion of mitochondrial antioxidant defense with sirtuin 3 (Sirt3), which boosted longevity and hearing maintenance [78]. Besides, Sirt3 and Sirt1 help inhibit p53 and restrain apoptosis [79].

3.4. Calcium Homeostasis in Auditory Neuropathy. Calcium ions (Ca^{2+}) are secondary messengers in many crucial cellular activities, for instance, cell death and organ development. To maintain proper Ca^{2+} signaling, a mitochondrion is a vital mediator of calcium in ER, the major intracellular Ca^{2+} pool. Mitochondrion-associated ER membranes (MAMs), referring to ER-mitochondrion connection, possess calcium transport proteins and channels [80]. MAMs permit fast calcium flux between ER and mitochondrial matrix, which is essential for neural excitation. After being released by ER, calcium ions traverse voltage-dependent anion-selective channel (VDAC) and mitochondrial calcium uniporter (MCU) located in the bilayer of mitochondria and can be extruded to the cytoplasm by sodium calcium exchanger (NCLX) [81]. MCU regulates the activity of enzymes in the TCA cycle [82] and sensitivity of synapses in cochlea after noise exposure. MCU was found to be increased in HCs after noise. Treatment with MCU siRNA or specific MCU inhibitor Ru360 alleviated HCs and ribbon synapse degeneration after noise into CBA/J mice. MCU inhibition reduced ABR wave I amplitude damage, suggesting that MCU was correlated to cochlear synaptopathy [83]. Moreover, superfluous calcium uptake results in swollen mitochondria and abnormal mitochondrial membrane potential, inducing mitochondrial apoptotic factors released to the cytoplasm [84].

3.5. Apoptosis in Neuropathy. Mitochondria are of great importance to induce apoptosis under intrinsic and extrinsic stimulations by means of proapoptotic signal like activation of BH3-only protein or calcium influx and releasing apoptotic protein including cyto-c, caspases, AIF, and Smac [85, 86]. Abnormal mitochondrial might cause apoptosis in cochlear nerves. Apoptosis-inducing factor (AIF), a flavoprotein and redox enzyme located in mitochondrial intermembrane which can condense chromatin and fracture DNA, was found to be activated by glutamate, which resulted in SGN apoptosis. Calpain was proved to promote mature AIF [87]. Pyridoxine damaged nerve fiber by inducing overload of mitochondrial calcium and activation of apoptosis signal from Bcl-2 family ROS generation and mitochondrial potential transition (MPT) were also aroused after pyridoxine treatment [88]. Although overexpression of bcl-2 might inhibit SGN apoptosis, growth of SGN neurite was suppressed in vitro [89].

4. Therapy in Auditory Neuropathy

With the intensive study of mechanism between mitochondrial dysfunction and auditory neuropathy, novel perspec-

tives of mitochondrion-targeted therapies were explored. There were several therapies targeting mitochondrial, which will rescue auditory neuropathy fundamentally (Figure 2).

4.1. Antioxidants. Antioxidants were elucidated to protect SNHL by eliminating excessive ROS products, including an intrinsic system such as SODs and GSH and extrinsic system such as inhibitors of calcium, HSP, or salicylate [90].

CoQ10, a common redox in mitochondria and cofactor of respiratory chain, has the capacity of permitting electron and proton transport through ETC and debriding ROS as the antioxidant [91]. Supplementation of water-soluble coenzyme Q10 analog (Qter) alleviated damage of SGNs after noise exposure [92] as well as prevented presbycusis in murine [93].

Methylene blue (MB), distinguished as histological dye, was first applied to clinical practice for the treatment of malaria. Besides, MB could also prevent mitochondria from overproduction of ROS by rerouting electron from NADH to cyto-c and was proved beneficial to neurodegeneration covering NIHL, AD, and PD [94]. Pretreatment with MB diminished ROS and evaluated neurotrophin-3 (NT-3) level, protecting nerve terminals between HCs and SGNs from NIHL [95].

The limitation of the antioxidants was distinct that they could not sweep up ROS in mitochondria precisely and effectively. Recently, studies have shown mitochondrion-targeted antioxidant could not aggregate precedingly [96]. MitoQ comprises CoQ10 and lipophilic triphenyl phosphonium (TPP), endowing CoQ10 with the ability to go through a phospholipid bilayer and gather inside mitochondria rapidly, which could stabilize mitochondrial function by enhancing mitochondrial fusion via activation of PGC1- α and upregulation of Mfn2 in the PD model [97]. Besides, other mitochondrion-targeted antioxidants like Mito VitE, and SkQ1 were developed, while the therapeutic effect to auditory neuropathy required verification [98].

4.2. Sirtuin Mediators. Sirtuins are from NAD⁺-dependent deacylase family which is of great importance to aging and nervous system. SIRT1 participates in the regulation of cellular ROS, synaptic plasticity, and extending lifespan in collaboration with SIRT3, the modulator of mitochondrial metabolism [99]. Sirtuin mediators like resveratrol and NAD⁺ supplement are also popular in antiaging [100], which were also found efficient in NIHL [101, 102]. Resveratrol, an activator of SIRT1, is a natural antioxidant relevant to mitochondrial biogenesis and modification of mitochondrial function. Mitigatory SGN degeneration and enhance expression of PINK and Parkin were observed in the mice with long-term replenishment, revealing intensive mitophagy but improved mitochondrial function [100]. Additionally, resveratrol was able to eliminate toxicity protein SGNs from injury caused by noise exposure [101].

NAD, as key coenzyme in several cellular events, took part in the crucial process in mitochondrial metabolism and was associated with axonal degenerations and neurodegeneration. Supplementation of NAD could protect damage

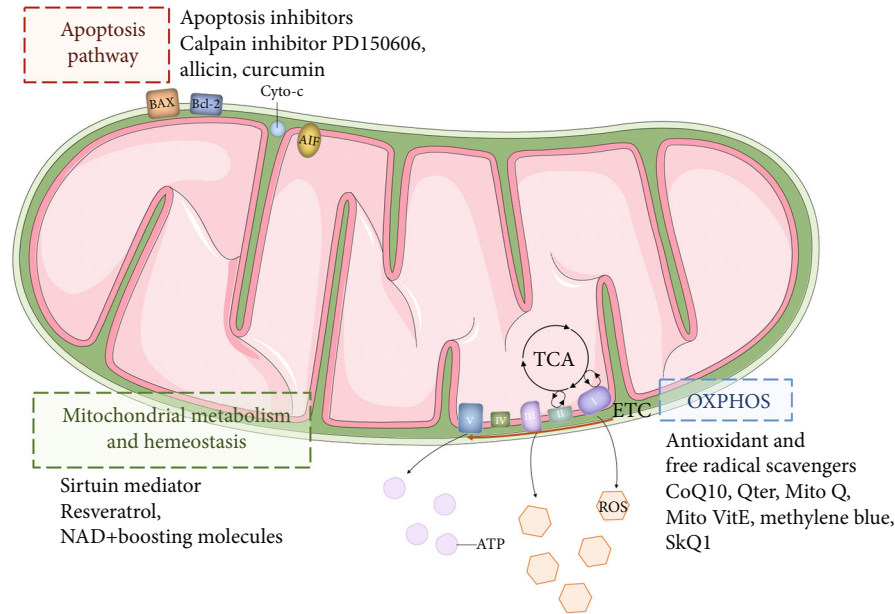


FIGURE 2: Pharmacological targets of mitochondria in auditory neuropathy. Pharmacological therapeutics of mitochondrial dysfunction to rescue auditory neuropathies are still limited. Proven therapeutic strategy targets are comprised of apoptosis inhibition, sirtuin mediators maintaining mitochondrial homeostasis and capability of metabolism, and antioxidants and free radical scavengers that are helpful to alleviate oxidative stress.

neurons and delay neurodegeneration [103]. In hearing loss induced by Mn, NAD was suggested to prevent auditory nerve fibers and SGNs from axonal degeneration and cell apoptosis [102].

4.3. Apoptosis Inhibitors. Due to apoptosis induced by mitochondrial dysfunction, inhibitors of apoptosis targeting mitochondria were developed and found efficient to SNHL. A calpain inhibitor PD150606 could suppress calpain by mediating AIF induced by glutamine and caspase-12 activation, restraining apoptosis processing and SGNs in vitro [87]. Meanwhile, allicin [104] and curcumin [105] were found to protect SGNs from ototoxic drugs, when paeoniflorin and neurotrophin might exert as protective effect through the PINK1/BAD pathway [89, 106].

Others such as gene therapy [107] and stem cell therapy [108] still have been studied. But auditory neuropathy treatment is still limited, requiring more exploration.

5. Conclusion

Mitochondrial dysfunction was demonstrated to involve in both hereditary and acquired hearing loss, and the mechanism of ROS damage and mutation of mtDNA in HC were studied intensively. Mitochondrion function as the energy manufacturer and regulator of apoptosis and calcium homeostasis, which is able to induce SGN damage. The function of mitochondria and the association to neurodegeneration have been excavated, extending perspective on the relationship between mitochondrial dysfunction and auditory neuropathy. Here, we summarized the associ-

ation between auditory neuropathy and mitochondrial dysfunction of SGNs, as well as therapeutics targeting mitochondria in AN. Treatments of optic neuropathy including drugs, gene, and stem cell therapies [109] inspired us to explore effective therapeutics for AN.

Conflicts of Interest

The authors declare that they have no competing interests.

Acknowledgments

This review was supported by the following foundations: Hao Wu was supported by the Key Project of the National Natural Science Foundation of China (NSFC 81330023), the National Key Technology Research and Development Program of the Ministry of Science and Technology of China (SQ2017YFSF080012), Shanghai Key Laboratory of Translational Medicine on Ear and Nose Diseases (14DZ2260300), Shanghai Municipal Science and Technology Major Project (2018SHZDZX05), and Innovative Research Team of High-Level Local Universities in Shanghai; Yong Tao was supported by the National Natural Science Foundation of China (NSFC 81800900), Shanghai Science and Technology Committee (18411953600, 18ZR1422100, and 18PJ1406900), the Program for Professor of Special Appointment (Eastern Scholar) at Shanghai Institutions of Higher Learning, Shanghai Municipal Health Commission (2018YQ59), Two Hundred Talent of Shanghai Jiaotong University School of Medicine (2019821), and Shanghai Ninth People's Hospital (QC201804).

References

- [1] World Health Organization, *Prevention of deafness and hearing loss*, Seventieth World Health Assembly, Geneva, 2017.
- [2] Y. Liu, J. Qi, X. Chen et al., "Critical role of spectrin in hearing development and deafness," *Science Advances*, vol. 5, no. 4, article eaav7803, 2019.
- [3] S. Zhang, Y. Zhang, Y. Dong et al., "Knockdown of Foxg1 in supporting cells increases the trans-differentiation of supporting cells into hair cells in the neonatal mouse cochlea," *Cellular and Molecular Life Sciences*, vol. 77, no. 7, pp. 1401–1419, 2020.
- [4] K. Kaga, M. Nakamura, M. Shinogami, T. Tsuzuku, K. Yamada, and M. Shindo, "Auditory nerve disease of both ears revealed by auditory brainstem responses, electrocochleography and otoacoustic emissions," *Scandinavian Audiology*, vol. 25, no. 4, pp. 233–238, 2009.
- [5] A. Starr, T. W. Picton, Y. Sininger, L. J. Hood, and C. I. Berlin, "Auditory neuropathy," *Brain*, vol. 119, no. 3, pp. 741–753, 1996.
- [6] T. Moser and A. Starr, "Auditory neuropathy—neural and synaptic mechanisms," *Nature Reviews Neurology*, vol. 12, no. 3, pp. 135–149, 2016.
- [7] E. A. Schon and S. Przedborski, "Mitochondria: the next (neurode)generation," *Neuron*, vol. 70, no. 6, pp. 1033–1053, 2011.
- [8] K. W. Chung, S. B. Kim, K. D. Park et al., "Early onset severe and late-onset mild Charcot-Marie-Tooth disease with mitofusin 2 (MFN2) mutations," *Brain*, vol. 129, no. 8, pp. 2103–2118, 2006.
- [9] S. DiMauro and E. A. Schon, "Mitochondrial disorders in the nervous system," *Annual Review of Neuroscience*, vol. 31, no. 1, pp. 91–123, 2008.
- [10] F. Burté, V. Carelli, P. F. Chinnery, and P. Yu-Wai-Man, "Disturbed mitochondrial dynamics and neurodegenerative disorders," *Nature Reviews Neurology*, vol. 11, no. 1, pp. 11–24, 2015.
- [11] A. Starr and G. Rance, "Auditory neuropathy," *Handbook of Clinical Neurology*, vol. 129, pp. 495–508, 2015.
- [12] T. Yasukawa and D. Kang, "An overview of mammalian mitochondrial DNA replication mechanisms," *Journal of Biochemistry*, vol. 164, no. 3, pp. 183–193, 2018.
- [13] N. Nissanka and C. T. Moraes, "Mitochondrial DNA damage and reactive oxygen species in neurodegenerative disease," *FEBS Letters*, vol. 592, no. 5, pp. 728–742, 2018.
- [14] S. Yin, Z. Yu, R. Sockalingam, M. Bance, G. Sun, and J. Wang, "The role of mitochondrial DNA large deletion for the development of presbycusis in Fischer 344 rats," *Neurobiology of Disease*, vol. 27, no. 3, pp. 370–377, 2007.
- [15] B. K. Crawley and E. M. Keithley, "Effects of mitochondrial mutations on hearing and cochlear pathology with age," *Hearing Research*, vol. 280, no. 1–2, pp. 201–208, 2011.
- [16] K. Ishikawa, Y. Tamagawa, K. Takahashi et al., "Temporal bone histopathologic abnormalities associated with mitochondrial mutation T7511C," *The Laryngoscope*, vol. 116, no. 11, pp. 1982–1986, 2006.
- [17] S. Pickles, P. Vigie, and R. J. Youle, "Mitophagy and quality control mechanisms in mitochondrial maintenance," *Current Biology*, vol. 28, no. 4, pp. R170–R185, 2018.
- [18] M. J. Young and W. C. Copeland, "Human mitochondrial DNA replication machinery and disease," *Current Opinion in Genetics & Development*, vol. 38, pp. 52–62, 2016.
- [19] F. R. Jornayvaz and G. I. Shulman, "Regulation of mitochondrial biogenesis," *Essays in Biochemistry*, vol. 47, pp. 69–84, 2010.
- [20] A. R. Anzell, R. Maizy, K. Przyklenk, and T. H. Sanderson, "Mitochondrial quality control and disease: insights into ischemia-reperfusion injury," *Molecular Neurobiology*, vol. 55, no. 3, pp. 2547–2564, 2018.
- [21] L. L. Xie, F. Shi, Z. Tan, Y. Li, A. M. Bode, and Y. Cao, "Mitochondrial network structure homeostasis and cell death," *Cancer Science*, vol. 109, no. 12, pp. 3686–3694, 2018.
- [22] X. Yu, W. Liu, Z. Fan et al., "c-Myb knockdown increases the neomycin-induced damage to hair-cell-like HEI-OC1 cells in vitro," *Scientific Reports*, vol. 7, no. 1, article 41094, 2017.
- [23] Z. He, L. Guo, Y. Shu et al., "Autophagy protects auditory hair cells against neomycin-induced damage," *Autophagy*, vol. 13, no. 11, pp. 1884–1904, 2017.
- [24] H. Li, Y. Song, Z. He et al., "Meclofenamic acid reduces reactive oxygen species accumulation and apoptosis, inhibits excessive autophagy, and protects hair cell-like HEI-OC1 cells from cisplatin-induced damage," *Frontiers in Cellular Neuroscience*, vol. 12, p. 139, 2018.
- [25] T. L. Schwarz, "Mitochondrial trafficking in neurons," *Cold Spring Harbor Perspectives in Biology*, vol. 5, no. 6, 2013.
- [26] J. Gao, L. Wang, J. Liu, F. Xie, B. Su, and X. Wang, "Abnormalities of mitochondrial dynamics in neurodegenerative diseases," *Antioxidants*, vol. 6, no. 2, p. 25, 2017.
- [27] I. Martinez-Reyes and N. S. Chandel, "Mitochondrial TCA cycle metabolites control physiology and disease," *Nature Communications*, vol. 11, no. 1, p. 102, 2020.
- [28] J. A. Stuart, S. Cadenas, M. B. Jekabsons, D. Roussel, and M. D. Brand, "Mitochondrial proton leak and the uncoupling protein 1 homologues," *Biochimica et Biophysica Acta*, vol. 1504, no. 1, pp. 144–158, 2001.
- [29] L. Milkovic, A. Cipak Gasparovic, M. Cindric, P. A. Mouthuy, and N. Zarkovic, "Short overview of ROS as cell function regulators and their implications in therapy concepts," *Cells*, vol. 8, no. 8, p. 793, 2019.
- [30] J. Nunnari and A. Suomalainen, "Mitochondria: in sickness and in health," *Cell*, vol. 148, no. 6, pp. 1145–1159, 2012.
- [31] E. M. Keithley and M. L. Feldman, "Spiral ganglion cell counts in an age-graded series of rat cochleas," *The Journal of Comparative Neurology*, vol. 188, no. 3, pp. 429–441, 1979.
- [32] E. M. Keithley, "Pathology and mechanisms of cochlear aging," *Journal of Neuroscience Research*, pp. 1–11, 2019.
- [33] C. A. Makary, J. Shin, S. G. Kujawa, M. C. Liberman, and S. N. Merchant, "Age-related primary cochlear neuronal degeneration in human temporal bones," *Journal of the Association for Research in Otolaryngology*, vol. 12, no. 6, pp. 711–717, 2011.
- [34] L. M. Viana, J. T. O'Malley, B. J. Burgess et al., "Cochlear neuropathy in human presbycusis: confocal analysis of hidden hearing loss in post-mortem tissue," *Hearing Research*, vol. 327, pp. 78–88, 2015.
- [35] S. E. Wang and C. H. Wu, "Physiological and histological evaluations of the cochlea between 3xTg-AD mouse model of Alzheimer's diseases and R6/2 mouse model of Huntington's diseases," *The Chinese Journal of Physiology*, vol. 58, no. 6, pp. 359–366, 2015.

- [36] D. Robertson, "Functional significance of dendritic swelling after loud sounds in the guinea pig cochlea," *Hearing Research*, vol. 9, no. 3, pp. 263–278, 1983.
- [37] S. G. Kujawa and M. C. Liberman, "Adding insult to injury: cochlear nerve degeneration after "temporary" noise-induced hearing loss," *The Journal of Neuroscience*, vol. 29, no. 45, pp. 14077–14085, 2009.
- [38] Z. Ruzsnaik and G. Szucs, "Spiral ganglion neurones: an overview of morphology, firing behaviour, ionic channels and function," *Pflügers Archiv*, vol. 457, no. 6, pp. 1303–1325, 2009.
- [39] A. M. Berglund and D. K. Ryugo, "Hair cell innervation by spiral ganglion neurons in the mouse," *The Journal of Comparative Neurology*, vol. 255, no. 4, pp. 560–570, 1987.
- [40] W. Liu, M. Boström, A. Kinnefors, F. Linthicum, and H. Rask-Andersen, "Expression of myelin basic protein in the human auditory nerve—an immunohistochemical and comparative study," *Auris Nasus Larynx*, vol. 39, no. 1, pp. 18–24, 2012.
- [41] E. Glowatzki and P. A. Fuchs, "Transmitter release at the hair cell ribbon synapse," *Nature Neuroscience*, vol. 5, no. 2, pp. 147–154, 2002.
- [42] C. Wichmann and T. Moser, "Relating structure and function of inner hair cell ribbon synapses," *Cell and Tissue Research*, vol. 361, no. 1, pp. 95–114, 2015.
- [43] F. Rattay, T. Potrusil, C. Wenger, A. K. Wise, R. Glueckert, and A. Schrott-Fischer, "Impact of morphometry, myelination and synaptic current strength on spike conduction in human and cat spiral ganglion neurons," *PLoS One*, vol. 8, no. 11, article e79256, 2013.
- [44] Y. Takihara, M. Inatani, K. Eto et al., "In vivo imaging of axonal transport of mitochondria in the diseased and aged mammalian CNS," *Proceedings of the National Academy of Sciences of the United States of America*, vol. 112, no. 33, pp. 10515–10520, 2015.
- [45] S. Hao, L. Wang, K. Zhao, X. Zhu, and F. Ye, "Rs1894720 polymorphism in MIAT increased susceptibility to age-related hearing loss by modulating the activation of miR-29b/SIRT1/PGC-1 α signaling," *Journal of Cellular Biochemistry*, vol. 120, no. 4, pp. 4975–4986, 2019.
- [46] X. Y. Zhao, J. L. Sun, Y. J. Hu et al., "The effect of overexpression of PGC-1 α on the mtDNA4834 common deletion in a rat cochlear marginal cell senescence model," *Hearing Research*, vol. 296, pp. 13–24, 2013.
- [47] Y. Zhong, Y. Hu, W. Peng et al., "Age-related decline of the cytochrome c oxidase subunit expression in the auditory cortex of the mimetic aging rat model associated with the common deletion," *Hearing Research*, vol. 294, no. 1-2, pp. 40–48, 2012.
- [48] Z. He, S. Sun, M. Waqas et al., "Reduced TRMU expression increases the sensitivity of hair-cell-like HEI-OC-1 cells to neomycin damage in vitro," *Scientific Reports*, vol. 6, no. 1, article 29621, 2016.
- [49] Q. Zhang, L. Zhang, D. Chen et al., "Deletion of Mtu1 (Trmu) in zebrafish revealed the essential role of tRNA modification in mitochondrial biogenesis and hearing function," *Nucleic Acids Research*, vol. 46, no. 20, pp. 10930–10945, 2018.
- [50] T. Gardeitchik, M. Mohamed, B. Ruzzenente et al., "Bi-allelic mutations in the mitochondrial ribosomal protein MRPS2 cause sensorineural hearing loss, hypoglycemia, and multiple OXPHOS complex deficiencies," *American Journal of Human Genetics*, vol. 102, no. 4, pp. 685–695, 2018.
- [51] T. Agnew, M. Goldsworthy, C. Aguilar et al., "A Wars2 mutant mouse model displays OXPHOS deficiencies and activation of tissue-specific stress response pathways," *Cell Reports*, vol. 25, no. 12, pp. 3315–3328.e6, 2018.
- [52] A. Di Fonzo, D. Ronchi, T. Lodi et al., "The mitochondrial disulfide relay system protein GFER is mutated in autosomal-recessive myopathy with cataract and combined respiratory-chain deficiency," *American Journal of Human Genetics*, vol. 84, no. 5, pp. 594–604, 2009.
- [53] F. Bahmad, S. N. Merchant, J. B. Nadol, and L. Tranebjærg, "Otopathology in Mohr-Tranebjærg syndrome," *Laryngoscope*, vol. 117, no. 7, pp. 1202–1208, 2007.
- [54] R. Santarelli, R. Rossi, P. Scimemi et al., "OPA1-related auditory neuropathy: site of lesion and outcome of cochlear implantation," *Brain*, vol. 138, no. 3, pp. 563–576, 2015.
- [55] Q. Yang, G. Sun, H. Yin et al., "PINK1 protects auditory hair cells and spiral ganglion neurons from cisplatin-induced ototoxicity via inducing autophagy and inhibiting JNK signaling pathway," *Free Radical Biology & Medicine*, vol. 120, pp. 342–355, 2018.
- [56] H. Lin, H. Xiong, Z. Su et al., "Inhibition of DRP-1-dependent mitophagy promotes cochlea hair cell senescence and exacerbates age-related hearing loss," *Frontiers in Cellular Neuroscience*, vol. 13, 2019.
- [57] M. T. Lin and M. F. Beal, "Mitochondrial dysfunction and oxidative stress in neurodegenerative diseases," *Nature*, vol. 443, no. 7113, pp. 787–795, 2006.
- [58] W. Liu, X. Xu, Z. Fan et al., "Wnt signaling activates TP53-induced glycolysis and apoptosis regulator and protects against cisplatin-induced spiral ganglion neuron damage in the mouse cochlea," *Antioxidants & Redox Signaling*, vol. 30, no. 11, pp. 1389–1410, 2019.
- [59] W. Zhuang, C. Wang, X. Shi et al., "MCMV triggers ROS/NLRP3-associated inflammasome activation in the inner ear of mice and cultured spiral ganglion neurons, contributing to sensorineural hearing loss," *International Journal of Molecular Medicine*, vol. 41, no. 6, pp. 3448–3456, 2018.
- [60] Z.-D. du, L. He, C. Tu et al., "Mitochondrial DNA 3,860-bp deletion increases with aging in the auditory nervous system of C57BL/6J mice," *ORL-Journal for Oto-Rhino-Laryngology Head and Neck Surgery*, vol. 81, no. 2-3, pp. 92–100, 2019.
- [61] J. Menardo, Y. Tang, S. Ladrech et al., "Oxidative stress, inflammation, and autophagic stress as the key mechanisms of premature age-related hearing loss in SAMP8 mouse cochlea," *Antioxidants & Redox Signaling*, vol. 16, no. 3, pp. 263–274, 2012.
- [62] D. N. Kwon, W. J. Park, Y. J. Choi, S. Gurunathan, and J. H. Kim, "Oxidative stress and ROS metabolism via down-regulation of sirtuin 3 expression in Cmah-null mice affect hearing loss," *Aging*, vol. 7, no. 8, pp. 579–594, 2015.
- [63] L. S. Nolan, B. A. Cadge, M. Gomez-Dorado, and S. J. Dawson, "A functional and genetic analysis of SOD2 promoter variants and their contribution to age-related hearing loss," *Mechanisms of Ageing and Development*, vol. 134, no. 7-8, pp. 298–306, 2013.
- [64] E. van Eyken, G. van Camp, E. Franssen et al., "Contribution of the N-acetyltransferase 2 polymorphism NAT2*6A to age-related hearing impairment," *Journal of Medical Genetics*, vol. 44, no. 9, pp. 570–578, 2007.

- [65] S. Sugiura, Y. Uchida, T. Nakashima, F. Ando, and H. Shimokata, "The association between gene polymorphisms in uncoupling proteins and hearing impairment in Japanese elderly," *Acta Oto-Laryngologica*, vol. 130, no. 4, pp. 487–492, 2009.
- [66] E. C. Bottger and J. Schacht, "The mitochondrion: a perpetrator of acquired hearing loss," *Hearing Research*, vol. 303, pp. 12–19, 2013.
- [67] D. Henderson, E. C. Bielefeld, K. C. Harris, and B. H. Hu, "The role of oxidative stress in noise-induced hearing loss," *Ear and Hearing*, vol. 27, no. 1, pp. 1–19, 2006.
- [68] P. H. G. M. Willems, R. Rossignol, C. E. J. Dieteren, M. P. Murphy, and W. J. H. Koopman, "Redox homeostasis and mitochondrial dynamics," *Cell Metabolism*, vol. 22, no. 2, pp. 207–218, 2015.
- [69] C. Batandier, X. Lerverve, and E. Fontaine, "Opening of the mitochondrial permeability transition pore induces reactive oxygen species production at the level of the respiratory chain complex I," *The Journal of Biological Chemistry*, vol. 279, no. 17, pp. 17197–17204, 2004.
- [70] A. Kurabi, E. M. Keithley, G. D. Housley, A. F. Ryan, and A. C. Y. Wong, "Cellular mechanisms of noise-induced hearing loss," *Hearing Research*, vol. 349, pp. 129–137, 2017.
- [71] P. R. Thorne, A. L. Nuttall, F. Scheibe, and J. M. Miller, "Sound-induced artifact in cochlear blood flow measurements using the laser Doppler flowmeter," *Hearing Research*, vol. 31, no. 3, pp. 229–234, 1987.
- [72] Y. Wang, K. Hirose, and M. C. Liberman, "Dynamics of noise-induced cellular injury and repair in the mouse cochlea," *Journal of the Association for Research in Otolaryngology*, vol. 3, no. 3, pp. 248–268, 2002.
- [73] J. L. Puel, J. Ruel, C. G. d'Aldin, and R. Pujol, "Excitotoxicity and repair of cochlear synapses after noise-trauma induced hearing loss," *Neuroreport*, vol. 9, no. 9, pp. 2109–2114, 1998.
- [74] Y. Orita, I. Sando, M. Miura, S. I. Haginomori, and B. E. Hirsch, "Cochleosaccular pathology after perinatal and postnatal asphyxia: histopathologic findings," *Otology & Neurotology*, vol. 23, no. 1, pp. 34–38, 2002.
- [75] Z. J. Reitman and H. Yan, "Isocitrate dehydrogenase 1 and 2 mutations in cancer: alterations at a crossroads of cellular metabolism," *JNCI-Journal of the National Cancer Institute*, vol. 102, no. 13, pp. 932–941, 2010.
- [76] H. J. Ku and J. W. Park, "IDH2 deficiency promotes mitochondrial dysfunction and cardiac hypertrophy in mice," *European Journal of Clinical Investigation*, vol. 45, pp. 13–13, 2015.
- [77] K. White, M. J. Kim, C. Han et al., "Loss of IDH2 accelerates age-related hearing loss in male mice," *Scientific Reports*, vol. 8, no. 1, p. 5039, 2018.
- [78] C. Han and S. Someya, "Maintaining good hearing: calorie restriction, Sirt3, and glutathione," *Experimental Gerontology*, vol. 48, no. 10, pp. 1091–1095, 2013.
- [79] L. Bordone and L. Guarente, "Calorie restriction, SIRT1 and metabolism: understanding longevity," *Nature Reviews Molecular Cell Biology*, vol. 6, no. 4, pp. 298–305, 2005.
- [80] S. Marchi, M. Bittremieux, S. Missiroli et al., "Endoplasmic reticulum-mitochondria communication through Ca^{2+} signaling: the importance of mitochondria-associated membranes (MAMs)," in *Organelle Contact Sites. Advances in Experimental Medicine and Biology*, vol. 997, M. Tagaya and T. Simmen, Eds., pp. 49–67, Springer, Singapore, 2017.
- [81] C. Giorgi, S. Marchi, and P. Pinton, "Publisher Correction: The machineries, regulation and cellular functions of mitochondrial calcium," *Nature Reviews Molecular Cell Biology*, vol. 19, no. 11, pp. 746–746, 2018.
- [82] G. S. B. Williams, L. Boyman, and W. J. Lederer, "Mitochondrial calcium and the regulation of metabolism in the heart," *Journal of Molecular and Cellular Cardiology*, vol. 78, pp. 35–45, 2015.
- [83] X. Wang, Y. Zhu, H. Long et al., "Mitochondrial calcium transporters mediate sensitivity to noise-induced losses of hair cells and cochlear synapses," *Frontiers in Molecular Neuroscience*, vol. 11, p. 469, 2019.
- [84] C. Giorgi, F. Baldassari, A. Bononi et al., "Mitochondrial Ca^{2+} and apoptosis," *Cell Calcium*, vol. 52, no. 1, pp. 36–43, 2012.
- [85] S. Y. Jeong and D. W. Seol, "The role of mitochondria in apoptosis," *BMB Reports*, vol. 41, no. 1, pp. 11–22, 2008.
- [86] S. Matsuyama and J. C. Reed, "Mitochondria-dependent apoptosis and cellular pH regulation," *Cell Death and Differentiation*, vol. 7, no. 12, pp. 1155–1165, 2000.
- [87] Z. J. Ding, X. Chen, X. X. Tang et al., "Calpain inhibitor PD150606 attenuates glutamate induced spiral ganglion neuron apoptosis through apoptosis inducing factor pathway in vitro," *PLoS One*, vol. 10, no. 4, 2015.
- [88] C. Park, H. Lim, S. K. Moon, and R. Park, "Pyridoxine preferentially induces auditory neuropathy through mitochondrial dysfunction and endoplasmic reticulum stress-mediated apoptosis," *Annals of Otology Rhinology and Laryngology*, vol. 128, Supplement 6, pp. 117s–124s, 2019.
- [89] J. P. Renton, N. Xu, J. J. Clark, and M. R. Hansen, "Interaction of neurotrophin signaling with Bcl-2 localized to the mitochondria and endoplasmic reticulum on spiral ganglion neuron survival and neurite growth," *Journal of Neuroscience Research*, vol. 88, no. 10, pp. 2239–2251, 2010.
- [90] E. Tavanai and G. Mohammadkhani, "Role of antioxidants in prevention of age-related hearing loss: a review of literature," *European Archives of Oto-Rhino-Laryngology*, vol. 274, no. 4, pp. 1821–1834, 2017.
- [91] H. N. Bhagavan and R. K. Chopra, "Coenzyme Q10: absorption, tissue uptake, metabolism and pharmacokinetics," *Free Radical Research*, vol. 40, no. 5, pp. 445–453, 2009.
- [92] A. R. Fetoni, P. de Bartolo, S. L. M. Eramo et al., "Noise-induced hearing loss (NIHL) as a target of oxidative stress-mediated damage: cochlear and cortical responses after an increase in antioxidant defense," *Journal of Neuroscience*, vol. 33, no. 9, pp. 4011–4023, 2013.
- [93] L. Guastini, R. Mora, M. Dellepiane, V. Santomauro, M. Giorgio, and A. Salami, "Water-soluble coenzyme Q10 formulation in presbycusis: long-term effects," *Acta Oto-Laryngologica*, vol. 131, no. 5, pp. 512–517, 2010.
- [94] D. Tucker, Y. Lu, and Q. Zhang, "From mitochondrial function to neuroprotection—an emerging role for methylene blue," *Molecular Neurobiology*, vol. 55, no. 6, pp. 5137–5153, 2018.
- [95] J. S. Park, I. Jou, and S. M. Park, "Attenuation of noise-induced hearing loss using methylene blue," *Cell Death & Disease*, vol. 5, no. 4, article e1200, 2014.
- [96] Y. R. Kim, J. I. Baek, S. H. Kim et al., "Therapeutic potential of the mitochondria-targeted antioxidant MitoQ in mitochondrial-ROS induced sensorineural hearing loss caused by *Idh2* deficiency," *Redox Biology*, vol. 20, pp. 544–555, 2019.

- [97] Y. Xi, D. Feng, K. Tao et al., "MitoQ protects dopaminergic neurons in a 6-OHDA induced PD model by enhancing Mfn2-dependent mitochondrial fusion via activation of PGC-1 α ," *Biochimica et Biophysica Acta (BBA) - Molecular Basis of Disease*, vol. 1864, no. 9, pp. 2859–2870, 2018.
- [98] C. Fujimoto and T. Yamasoba, "Mitochondria-targeted antioxidants for treatment of hearing loss: a systematic review," *Antioxidants*, vol. 8, no. 4, p. 109, 2019.
- [99] C. K. Singh, G. Chhabra, M. A. Ndiaye, L. M. Garcia-Peterson, N. J. Mack, and N. Ahmad, "The role of sirtuins in antioxidant and redox signaling," *Antioxidants & Redox Signaling*, vol. 28, no. 8, pp. 643–661, 2018.
- [100] H. Xiong, S. Chen, L. Lai et al., "Modulation of miR-34a/SIRT1 signaling protects cochlear hair cells against oxidative stress and delays age-related hearing loss through coordinated regulation of mitophagy and mitochondrial biogenesis," *Neurobiology of Aging*, vol. 79, pp. 30–42, 2019.
- [101] H. Xiong, Y. Ou, Y. Xu et al., "Resveratrol promotes recovery of hearing following intense noise exposure by enhancing cochlear SIRT1 activity," *Audiology and Neurotology*, vol. 22, no. 3-5, pp. 303–310, 2018.
- [102] L. Wang, D. Ding, R. Salvi, and J. A. Roth, "Nicotinamide adenine dinucleotide prevents neuroaxonal degeneration induced by manganese in cochlear organotypic cultures," *Neurotoxicology*, vol. 40, pp. 65–74, 2014.
- [103] L. Rajman, K. Chwalek, and D. A. Sinclair, "Therapeutic potential of NAD-boosting molecules: the in vivo evidence," *Cell Metabolism*, vol. 27, no. 3, pp. 529–547, 2018.
- [104] X. Wu, X. Li, Y. Song et al., "Allicin protects auditory hair cells and spiral ganglion neurons from cisplatin - induced apoptosis," *Neuropharmacology*, vol. 116, pp. 429–440, 2017.
- [105] W. Liu, Z. Fan, Y. Han et al., "Curcumin attenuates peroxynitrite-induced neurotoxicity in spiral ganglion neurons," *Neurotoxicology*, vol. 32, no. 1, pp. 150–157, 2011.
- [106] X. Yu, R. Man, Y. Li et al., "Paeoniflorin protects spiral ganglion neurons from cisplatin-induced ototoxicity: possible relation to PINK1/BAD pathway," *Journal of Cellular and Molecular Medicine*, vol. 23, no. 8, pp. 5098–5107, 2019.
- [107] H. Staecker, W. Liu, B. Malgrange, P. P. Lefebvre, and T. R. van de Water, "Vector-mediated delivery of bcl-2 prevents degeneration of auditory hair cells and neurons after injury," *ORL-Journal for Oto-Rhino-Laryngology and Its Related Specialties*, vol. 69, no. 1, pp. 43–50, 2006.
- [108] Y. H. Hsu, Y. T. Wu, C. Y. Huang et al., "Generation of an induced pluripotent stem cell line from a 39-year-old female patient with severe-to-profound non-syndromic sensorineural hearing loss and a A1555G mutation in the mitochondrial MTRNR1 gene," *Stem Cell Research*, vol. 25, pp. 245–249, 2017.
- [109] M. I. G. Lopez Sanchez, J. G. Crowston, D. A. Mackey, and I. A. Troncone, "Emerging mitochondrial therapeutic targets in optic neuropathies," *Pharmacology & Therapeutics*, vol. 165, pp. 132–152, 2016.

Research Article

Atrial Natriuretic Peptide Improves Neurite Outgrowth from Spiral Ganglion Neurons *In Vitro* through a cGMP-Dependent Manner

Fei Sun ¹, Ke Zhou ², Ke-yong Tian ¹, Jie Wang,³ Jian-hua Qiu ¹ and Ding-jun Zha ¹

¹Department of Otolaryngology-Head and Neck Surgery, Xijing Hospital, Fourth Military Medical University, Xi'an, Shaanxi 710032, China

²Center of Clinical Laboratory Medicine of PLA, Department of Laboratory Medicine, Xijing Hospital, Fourth Military Medical University, Xi'an, Shaanxi 710032, China

³Department of Otolaryngology-Head and Neck Surgery, The Affiliated Children Hospital of Xi'an Jiaotong University, Xi'an, Shaanxi 710003, China

Correspondence should be addressed to Jian-hua Qiu; qiujh@fmmu.edu.cn and Ding-jun Zha; zhadjun@fmmu.edu.cn

Received 23 April 2020; Revised 7 July 2020; Accepted 9 July 2020; Published 28 August 2020

Academic Editor: Renjie Chai

Copyright © 2020 Fei Sun et al. This is an open access article distributed under the Creative Commons Attribution License, which permits unrestricted use, distribution, and reproduction in any medium, provided the original work is properly cited.

The spiral ganglion neurons (SGNs) are the primary afferent neurons in the spiral ganglion (SG), while their degeneration or loss would cause sensorineural hearing loss. As a cardiac-derived hormone, atrial natriuretic peptide (ANP) plays a critical role in cardiovascular homeostasis through binding to its functional receptors (NPR-A and NPR-C). ANP and its receptors are widely expressed in the mammalian nervous system where they could be implicated in the regulation of multiple neural functions. Although previous studies have provided direct evidence for the presence of ANP and its functional receptors in the inner ear, their presence within the cochlear SG and their regulatory roles during auditory neurotransmission and development remain largely unknown. Based on our previous findings, we investigated the expression patterns of ANP and its receptors in the cochlear SG and dissociated SGNs and determined the influence of ANP on neurite outgrowth *in vitro* by using organotypic SG explants and dissociated SGN cultures from postnatal rats. We have demonstrated that ANP and its receptors are expressed in neurons within the cochlear SG of postnatal rat, while ANP may promote neurite outgrowth of SGNs via the NPR-A/cGMP/PKG pathway in a dose-dependent manner. These results indicate that ANP would play a role in normal neurogenesis of SGN during cochlear development and represents a potential therapeutic candidate to enhance regeneration and regrowth of SGN neurites.

1. Introduction

Sensorineural hearing loss (SNHL) is a major health problem which affects millions of individuals worldwide. SNHL is associated with irreversible degeneration of the cochlear sensory cells within the auditory portion of the inner ear, including hair cells (HCs) and spiral ganglion neurons (SGNs). In the mammalian inner ear, the HCs in the organ of Corti function in transducing the sound mechanical stimulation into the primary acoustic signals [1–3], while the SGNs are the primary afferent neurons in the spiral ganglion (SG)

and play a critical role in hearing, transmitting primary acoustic information from HCs to the higher auditory centers of the central nervous system (CNS) [4–6]. Loss of HCs, primarily resulting from noise trauma, ototoxic drugs, infections, aging, and genetic mutations, with sequential degeneration of SGNs, ultimately leads to permanent SNHL [7–15]. The current preferred treatment of SNHL for patients with profound HC loss and mostly intact SGNs includes cochlear implants, which uses electrode arrays to substitute for mechanosensory HCs in generating electrical impulses to the auditory nerve [16]. In order to promote regeneration

and guiding of neurites from residual auditory neurons, many potential guidance cues are under research, due to their influence on neurite outgrowth behavior and subsequent performance of cochlear implants [6, 17–23].

SG is a peripheral cluster of both neurons and glial cells located in Rosenthal's canal, which coils around the cochlear modiolus and forms the auditory nerve. SGNs are divided into two subpopulations, type I and type II, according to their different morphologies, synaptic connections, and functions. Approximately 95% of SGNs are larger, bipolar, and myelinated type I neurons, which can be further subdivided into three subtypes (Type IA, Type IB, and Type IC), innervating the inner HCs with their peripheral dendrites to principally encode the auditory signals [24–26]. The remaining 5% of SGNs are smaller, pseudomonopolar, and nonmyelinated type II neurons, which innervate the outer HCs and some of the supporting cells to provide sensory feedback, controlling the sensitivity of the auditory epithelium to specific sound stimuli. Additionally, the perikaryons of all types of SGNs are enveloped by satellite glial cells, forming loose myelin around the type I neuronal somata. Both peripheral dendrites and intracochlear axons of type I SGNs are myelinated by Schwann cells, whereas their central axons from the peripheral-central glial transition zone (glia limitans) to the terminal synapses in the cochlear nucleus are myelinated by oligodendrocytes and astrocytes [27, 28]. It is necessary to understand the expression, function, and signaling interactions of the regulatory substances which affect axonal development and neuronal plasticity of primary auditory neurons, to offer optimal strategies of manipulating connections between sensory epithelium or implanted electrodes and neurites of SGNs, and eventually provide promising pharmacological targets that facilitate new and effective therapies for hearing impairment.

Atrial natriuretic peptide (ANP) is a 28 amino acid peptide predominantly synthesized and secreted by the cardiac atria and is the first member of the natriuretic peptide family [29], which also includes brain natriuretic peptide (BNP) and C-type natriuretic peptide (CNP). ANP interacts with two specific, high affinity natriuretic peptide receptors, NPR-A and NPR-C, on the plasma membrane of target cells to mediate its physiological effects [30–32]. The natriuretic peptide receptor-A (NPR-A, also known as NPR1 or GC-A) is a transmembrane receptor coupled to the particulate guanylyl cyclase (GC) which catalyzes the synthesis of the second messenger cyclic guanosine-3',5'-monophosphate (cGMP). cGMP modulates the activity of specific effector molecules including cGMP-regulated isoforms of phosphodiesterases, cyclic-nucleotide-gated ion channels, and cGMP-dependent protein kinases G (PKG), which in turn regulate diverse biological responses associated with blood vessel tone, transepithelial ion transportation, neuronal excitability, neuronal development, and neurite pathfinding, and the sensory transduction pathways underlying olfaction and vision [31, 32]. The natriuretic peptide receptor-C (NPR-C), which lacks the GC domain, contributes to the clearance of ANP and other natriuretic peptides from the circulation through receptor-mediated internalization and degradation. In addition, evidence has shown that NPR-C can also affect other

second messenger signaling by activating phospholipase C and inhibiting adenylyl cyclase [33].

In addition to the cardiovascular system, the tissue-specific distribution and function of ANP, NPR-A, and NPR-C have been established in several tissues including the kidney, adrenal, lung, adipose tissue, and retina. Furthermore, ANP and its receptors have been found in the CNS, leading us to speculate that ANP may function as a neuromodulator or neuropeptide involved in neuronal and glial functions [34–36]. Importantly, their presence in the secretory and sensory compartments of the rodent inner ear is well documented, suggesting ANP may act as a local hormone regulating the fluid and electrolyte balance in the inner ear [37–51]. Previous reports revealed that ANP receptors have been localized to the cochlear modiolus of the guinea pig [42] and rat SG [51]. However, little is known regarding the localization and functional roles of ANP and its receptors in the inner ear, and here, we have focused our attention on them.

In our previous study, we have already investigated the expression patterns of ANP and its receptors, which provided direct evidence for the presence and synthesis of ANP as well as its receptors in the cochlear SG [52, 53]. In our current study, we reassessed the distribution of ANP and its receptors in the cochlear SG as well as in dissociated SGNs, and determined the influence of ANP on neurite outgrowth *in vitro* by using organotypic SG explants and dissociated SGN cultures from postnatal rats. We have demonstrated that ANP and its receptors are expressed in neurons within the cochlear SG of postnatal rat, while ANP may promote neurite outgrowth of SGNs via the NPR-A/cGMP/PKG pathway in a dose-dependent manner.

2. Materials and Methods

2.1. Animals and Tissue Preparation. All experiments were approved by the Animal Care Committee of Fourth Military Medical University, China, on the care and use of Laboratory Animal for Research Purposes. All cochleae used in this investigation were obtained from postnatal day 3 (P3) or day 14 (P14) Sprague-Dawley rats provided by the Laboratory Animal Center of the Fourth Military Medical University. All rat pups were sacrificed by decapitation, and the skulls were opened midsagittally. With the aid of a dissecting microscope (SZX16; Olympus, Japan), the rat cochleae were removed from the temporal bone, washed in ice-cold Hank's Balanced Salt Solution (HBSS; Thermo Fisher Scientific, USA), and collected for further use.

2.2. Preparation of Cochlear Sections and Spiral Ganglion Neurons Culture. For cochlear cryosections, the cochleae from P14 rats were fixed with 4% paraformaldehyde (PFA) in phosphate buffer (PB; 0.1 M, pH 7.2) by perfusion via the round and oval windows and then incubated with the same fixative overnight at 4°C. The cochleae were decalcified in a 5% EDTA solution for 2 days, followed by cryoprotection in 30% sucrose solution overnight at 4°C. The samples were then embedded in Tissue-Tek OCT compound (Sakura Finetek, USA) at -20°C, sectioned into 12 µm thick midmodiolar

cross-sections using a cryostat microtome (CM1850; Leica, Germany) and mounted on poly-L-lysine-coated slides.

Dissociated cultures of SGNs were prepared from P3 rat pups and maintained as described previously [54–56]. Briefly, each SG was isolated from the cochlea in ice-cold HBSS by sequential removal of the bony cochlear capsule, the spiral ligament, and the organ of the Corti, leaving the SGNs within the modiolus. The modiolus tissues were transferred into $\text{Ca}^{2+}/\text{Mg}^{2+}$ free HBSS with 0.25% trypsin and 0.1% collagenase type IV (all Thermo Fisher Scientific) at 37°C for 20 min to enzymatically dissociate the cells. The enzymatic reaction was quenched by the addition of 10% fetal bovine serum (FBS; Thermo Fisher Scientific). After three washes with culture medium, the tissues were mechanically dissociated by trituration with a flame-polished Pasteur pipette. The dissociated cells were resuspended in a neural maintenance medium consisting of Dulbecco's modified Eagle medium/Ham's F12 medium (DMEM/F12) supplemented with 1x B27, 1x N2, and 1% penicillin-streptomycin (all Thermo Fisher Scientific) and plated at a density of 1.0×10^6 cells/glass bottom dish previously coated with poly-L-lysine (0.1 mg/mL in 10 mM borate buffer, pH 8.4; Thermo Fisher Scientific) to adhere for 4 h at 37°C, 5% CO_2 , and 95% humidity. After attachment was confirmed under an inverted microscope (Eclipse TE2000-U; Nikon, Japan), 1 mL of neural maintenance medium was added in each neuronal cell culture and incubated for 48 h prior to fixation with 4% PFA for 20 min at room temperature (RT).

2.3. Expression Pattern Analysis of ANP and Its Receptors by Immunofluorescence. For immunohistochemistry, the cochlear sections and fixed SGNs cultures were washed with phosphate-buffered saline (PBS; 0.01 M, pH 7.4), blocked with 5% bovine serum albumin (BSA; Sigma-Aldrich, USA) and 0.1% Triton X-100 in PBS for 40 min at 37°C, and incubated overnight at 4°C with the following primary antibodies diluted in antibody solution (1% BSA and 0.1% Triton X-100 in PBS): polyclonal rabbit anti-ANP antibody (1:500; Cat# PA5-29559, Thermo Fisher Scientific), polyclonal rabbit anti-NPR-A antibody (1:500; Cat# PA5-29049, Thermo Fisher Scientific), polyclonal rabbit anti-NPR-C antibody (1:500; Cat# PA5-96947, Thermo Fisher Scientific), and monoclonal mouse anti-Tubulin β -III (TUJ1) antibody (1:500; Cat# ab78078, Abcam, UK). After washing, samples were treated with the appropriate secondary antibodies diluted in antibody solution for 2 h at RT: Alexa Fluor 488-conjugated donkey anti-mouse IgG (1:500; Cat# A-21202, Thermo Fisher Scientific) and Alexa Fluor 594-conjugated donkey anti-rabbit IgG (1:500; Cat# A-21207, Thermo Fisher Scientific). Each experiment also included a negative control where the primary antibody was omitted. After rinsing, specimens were treated with the nuclear stain, 4',6-diamidino-2-phenylindole (DAPI; diluted 1:1000; Thermo Fisher Scientific) for 15 min at RT, mounted with Prolong Gold anti-fading mounting medium (Thermo Fisher Scientific), and subsequently examined under a spectral scanning laser confocal microscope (FV1000; Olympus, Japan). All images were saved as TIFF files using Olympus confocal soft-

ware (FV10-ASW 4.2; Olympus) and processed with Adobe Photoshop CS6 (Adobe Systems, USA) for adjustments of brightness and/or contrast.

2.4. Spiral Ganglion Explants and Spiral Ganglion Neuron Cultures. The cochlea dissection procedures were performed as described in previous studies with slight modifications [56–59]. The cochleae from P3 rats were immersed in ice-cold HBSS; then, the cochlear capsule was opened by fine forceps and the membranous labyrinth was removed from the modiolus under a dissecting microscope. The spiral lamina containing the SG was carefully separated from the modiolus and cut into equal portions of 300–500 μm before being transferred to the culture dish. The Cell-Tak Cell and Tissue Adhesive (Corning, USA) precoated 15 mm glass bottom culture dishes (Advance BioScience, USA) were loaded with 100 μL primary attachment medium consisting of DMEM, 10% FBS, 25 mM HEPES buffer, and 1% penicillin-streptomycin (all Thermo Fisher Scientific). Then, each dissected explant was plated onto single-glass bottom dish, and the culture medium was carefully aspirated from dishes containing SG explants, leaving only 10 μL to allow the tissue to settle for 3–5 min. For three-dimensional culture, 100 μL of a 20% Matrigel (Corning) mixture diluted in the primary attachment medium was dropped on to the tissue explants directly and left the tissues adhering overnight at 37°C, 5% CO_2 , and 95% humidity. After attachment was confirmed, SG explants incubated in neural maintenance medium with or without 20 ng/mL recombinant brain-derived neurotrophic factor (BDNF; PeproTech, USA) were served as control cultures. Experimental cultures were incubated in neural maintenance medium supplemented with 100 nM or 1 μM of ANP (Caymanchem, USA), 1 μM of the membrane-permeable cGMP analogue 8-(4-chlorophenylthio) guanosine-3',5'-cyclic monophosphate (8-pCPT-cGMP; Sigma-Aldrich), or 1 μM ANP plus 1 μM of the PKG inhibitor KT5823 (Sigma-Aldrich), respectively. For each condition, three cochlear neural explants were cultured for 7 days in a 37°C humidified incubator containing 5% CO_2 prior to fixation for neurite outgrowth study, and culture medium was changed every other day.

The dissociated SGNs prepared as described above, were resuspended in neural maintenance medium and plated at a density of 2.0×10^5 cells/coated glass bottom dish. After attachment, cells from different experimental cultures were incubated in neural maintenance medium in the absence or in the presence of pharmacological reagents identical to those in SG explant cultures: 20 ng/mL BDNF, 100 nM ANP, 1 μM ANP, 1 μM 8-pCPT-cGMP, or 1 μM ANP plus 1 μM KT5823. For each condition, three culture dishes seeded with dissociated SGNs were fed with fresh medium every other day and cultured for 5 days prior to fixation.

2.5. Immunofluorescent Analysis of Neurite Outgrowth Spiral Ganglion Explants and Neurons. After the culture period, SG explants or SGN cells were fixed in 4% PFA for 20 min at RT. Both explants and cells were blocked with 5% BSA and 0.1% Triton X-100 in PBS, followed by incubation with anti-Tubulin β -III primary antibody (diluted 1:500) and Alexa

Fluor 488-conjugated donkey anti-mouse IgG (diluted 1:500) to selectively stain the neural components of the explants or cells, then counterstained with DAPI (diluted 1:1000) to visualize the nuclei. All specimens in the glass bottom dish were mounted with Prolong Gold medium and examined under the confocal microscope.

In vitro Images of the immunostained cultures were analyzed by using ImageJ software (version 1.46r; NIH, USA) according to a previous study [60]. Neurite tracing was performed by using the “Analyze-Set Scale” function, the pixel unit of neurite length measurement was set in micrometers. Images were rendered with segmentation function, and neurite tracer function was applied choosing the starting point at the SGN cell bodies, resulting in a compiled skeleton render of all measured neurites. Only those neurites contained entirely within the image were analyzed. Neurite outgrowth from the SG explants was evaluated by measuring the number and lengths of the processes. Total number and the neurite length of the dissociated SGNs were also analyzed. Statistical analysis was performed using a one-way analysis of variance (ANOVA) followed by Bonferroni’s post hoc test. Data presented in the text and figures are means and standard error of the mean (means \pm SEM). Analysis was performed using the Statistical Program for Social Science software (SPSS, version 22.0; IBM Inc., USA). *P* values less than 0.05 ($P < 0.05$) were considered statistically significant.

3. Results

3.1. Distribution of ANP and Its Receptors in Spiral Ganglion and Spiral Ganglion Neurons of Postnatal Rats. To investigate the localizations of ANP and its receptors within the SG, we coimmunostained cochlear sections from P14 rats with antibodies against a neuronal marker, class III β -tubulin. No noticeable apical-to-basal gradients of ANP and its receptors immunoreactivities were observed in the SG regions along the length of the cochlear tonotopic axis. Hence, the midcochlear turn was taken as a representative of the entire length of the cochlea for analysis of the cellular localizations of ANP and its receptors. As shown in Figure 1, the immunoreactivity of ANP, NPR-A, or NPR-C was colocalized with β -III tubulin-positive somata of SGNs, respectively. ANP was predominantly immunoreactive in the neuronal perikarya, including the plasma membrane and cytoplasm of SGNs (Figure 1(a)). The distribution of NPR-A (Figure 1(b)) and NPR-C (Figure 1(c)) in SGNs was rather similar, and they were predominantly immunoreactive in the plasma membrane and cytoplasm of SGNs and appeared more pronounced in the cellular membrane. Some heterogeneity in the levels of immunoreactivities of ANP, NPR-A, and NPR-C were also observed, with less colocalization in a subpopulation of SGNs. No immunoreactivity was observed in the negative controls where the primary antibody was omitted (data not shown).

To confirm the distribution pattern of ANP and its receptors in SGNs, we also performed immunohistochemistry on SG cell cultures using the same neuronal marker. As shown in Figure 2, the immunoreactivity of ANP, NPR-A, or NPR-C was colocalized with β -III tubulin-positive SGNs,

respectively. In detail, the distribution of ANP and its receptors were immunoreactive all over each neuron including soma and neurites. No immunoreactivity was also observed in the negative controls where the primary antibody was omitted (data not shown).

3.2. Influence of ANP on Neurite Number and Neurite Length in Spiral Ganglion Explants. To determine the possible role of ANP in affecting neurite outgrowth of SGNs, we firstly quantified the number and length of neurites from SG explants from P3 rats maintained in culture medium supplemented with different reagents *in vitro* for 7 d. Representative images from different experimental cultures were shown in Figure 3. The SG explants incubated in culture medium without any supplement were used as a negative/baseline control, while explants incubated in culture medium supplemented with BDNF for trophic support of neurite outgrowth of SGNs were served as a positive control. Immunofluorescence and quantitative analysis of neuron-specific β -III tubulin-positive neurites revealed the number of neurites per explant was 46.0 ± 3.8 , and the average neurite length was $1002.8 \pm 155.5 \mu\text{m}$ for negative control samples (Figure 3(a)). As expected, abundant neurite sprouting and elongating were seen in explants treated with 20 ng/mL BDNF, and the average number and length of neurites from positive control samples were 191.7 ± 5.8 and $1645.8 \pm 58.1 \mu\text{m}$, respectively (Figure 3(b)). Strikingly, robust neurite extension from SG explants was seen after treatment with different dosage of ANP. The number and length of neurites were 92.0 ± 1.7 and $1438.3 \pm 141.0 \mu\text{m}$ for 100 nM ANP-treated samples (Figure 3(c)) and were 151.0 ± 2.3 and $1551.2 \pm 109.1 \mu\text{m}$ for 1 μM ANP-treated samples (Figure 3(d)), respectively. At any dosage of ANP (100 nM and 1 μM), a statistically significant increase in neurite outgrowth compared to the negative control was observed, while a significant difference was also found when compared to the positive control. To gain insight into the mechanism of ANP in promoting neurite outgrowth, we investigated whether this peptide acts through the GC-coupled receptors, NPR-A, which could elicit cGMP production. Results indicated that number (133.0 ± 3.79) and length ($1374.8 \pm 102.5 \mu\text{m}$) of elongating neurites from SG explants treated with 1 μM 8-pCPT-cGMP, a cGMP analogue, were also significantly different from the negative and positive controls (Figure 3(e)). Treatment with 1 μM KT5823, a selective inhibitor of PKG, appeared to abrogate SGN neurite sprouting and outgrowth (47.3 ± 5.2 and $955.2 \pm 109.2 \mu\text{m}$) in the presence of 1 μM ANP (Figure 3(f)), and the resulting neurite outgrowth did not significantly differ from the negative control. Taken together, these results indicated that ANP could promote SG neurite outgrowth via the NPR-A/cGMP/PKG pathway in a dose-dependent manner.

3.3. Influence of ANP on Cell Number and Neurite Length of Dissociated Spiral Ganglion Neurons. To validate the influence of ANP on the survival and neurite outgrowth of SGNs, we subsequently quantified the cell number and neurite length of dissociated SGNs from P3 rats maintained in culture medium with additives identical to those in explant

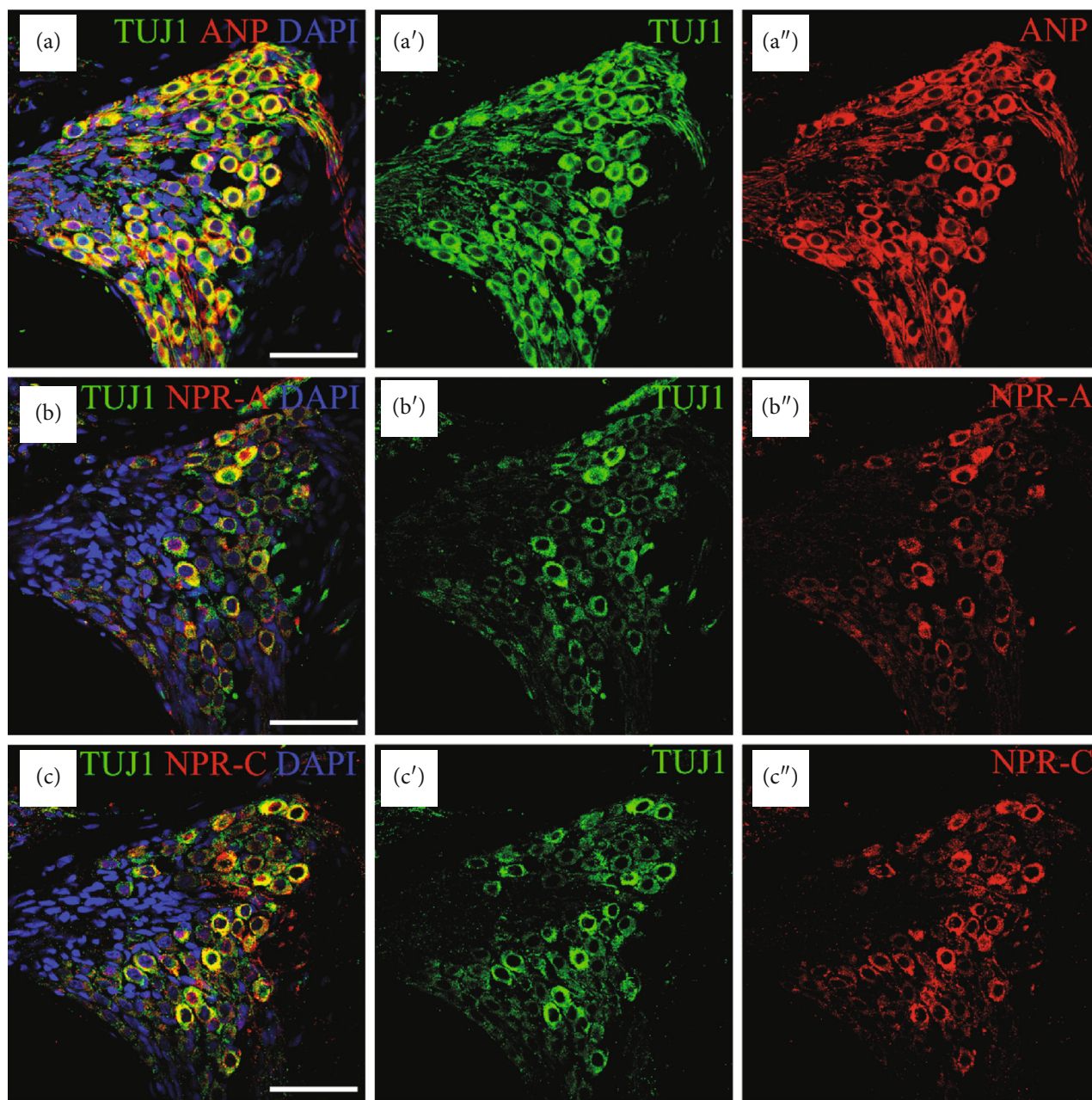


FIGURE 1: Immunolocalization of ANP, NPR-A, and NPR-C in SGNs within the SG of P14 rats. Merge and single-channel images of cochlear sections triple labeled with antibodies against neural marker TUJ1 (green), ANP/NPR-A/NPR-C (red), and DAPI (blue). (a) ANP was predominantly immunoreactive in the perikarya of SGNs. NPR-A (b) and NPR-C (c) were predominantly immunoreactive in the plasma membrane and cytoplasm of SGNs and appeared more pronounced in the cellular membrane. Scale bars = 50 μm .

cultures *in vitro* for 5 d. The dissociated neurons incubated in culture medium supplemented with or without 20 ng/mL BDNF were used as a positive or negative control, respectively. Representative images from different experimental cultures were shown in Figure 4. The average number of neurons per culture dish was 54.0 ± 1.5 , and the average neurite length per neuron was $209.5 \pm 19.5 \mu\text{m}$ in negative control samples (Figure 4(a)). Significantly increased number of neurons (78.3 ± 2.0) and elongating neurite outgrowth ($763.2 \pm 84.4 \mu\text{m}$) were seen in cell cultures treated with 20 ng/mL BDNF (Figure 4(b)). The number of neurons

and length of neurite were 69.0 ± 1.2 and $410.4 \pm 29.5 \mu\text{m}$ for 100 nM ANP-treated neurons (Figure 4(c)), 70.0 ± 1.3 and $543.5 \pm 31.5 \mu\text{m}$ for 1 μM ANP-treated neurons (Figure 4(d)), and 65.7 ± 2.9 and $475.2 \pm 33.4 \mu\text{m}$ for 1 μM 8-pCPT-cGMP-treated neurons (Figure 4(e)), respectively. These observations were all significantly different from either negative or positive control samples. As expected, 1 μM ANP failed to either increase neuronal number or induce neurite outgrowth of SGNs (53.6 ± 1.2 and $255.5 \pm 18.7 \mu\text{m}$) in the presence of 1 μM KT5823 (Figure 4(f)). Collectively, these results indicated that the

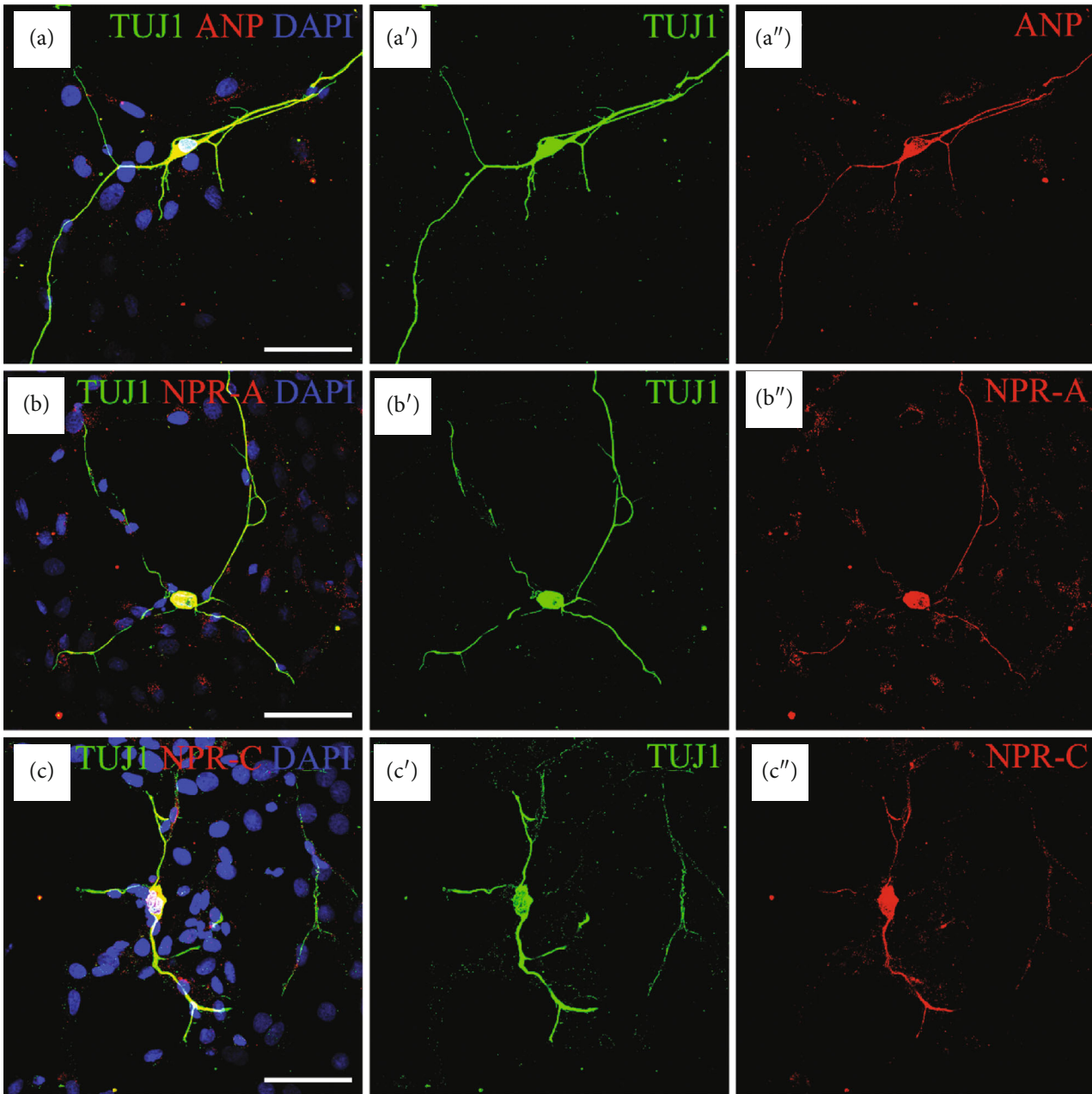


FIGURE 2: Immunolocalization of ANP, NPR-A, and NPR-C in dissociated SGNs from P3 rats. Merge and single-channel images of SG cells triple labeled with antibodies against TUJ1 (green), ANP/NPR-A/NPR-C (red), and DAPI (blue). The immunoreactivity of ANP (a), NPR-A (b), or NPR-C (c) was colocalized with β -III tubulin-positive SGNs, respectively, distributed in the neuronal soma and neurites. Scale bars = 50 μ m.

ANP/NPR-A/cGMP/PKG pathway may promote neuronal survival to some extent and would enhance neurite outgrowth of SGNs in a dose-dependent manner.

Interestingly, when treated with ANP, a number of dissociated SGNs made more than one branches from a single neurite. This effect could be apparently seen in BDNF, ANP, and cGMP analogue 8-pCPT-cGMP-treated neurons, indicating that neurotrophins and ANP signaling could exert a trophic support for neurite outgrowth and axon branching (Figures 4(b)–4(e)). Thus, the effect of axonal branching or pathfinding mediated by the ANP/NPR-A/cGMP/PKG path-

way still need more comprehensive evaluation during cochlear development for better understanding the exquisite mechanisms underlying the assembly of auditory circuits.

4. Discussion

To promote the regeneration of SGN and to guide the neurite outgrowth of SGN is a critical scientific question in the hearing research fields. In recent years, many previous reports used transcription regulation, biomaterials, electrical stimulation, and magnetic regulation to promote the regeneration

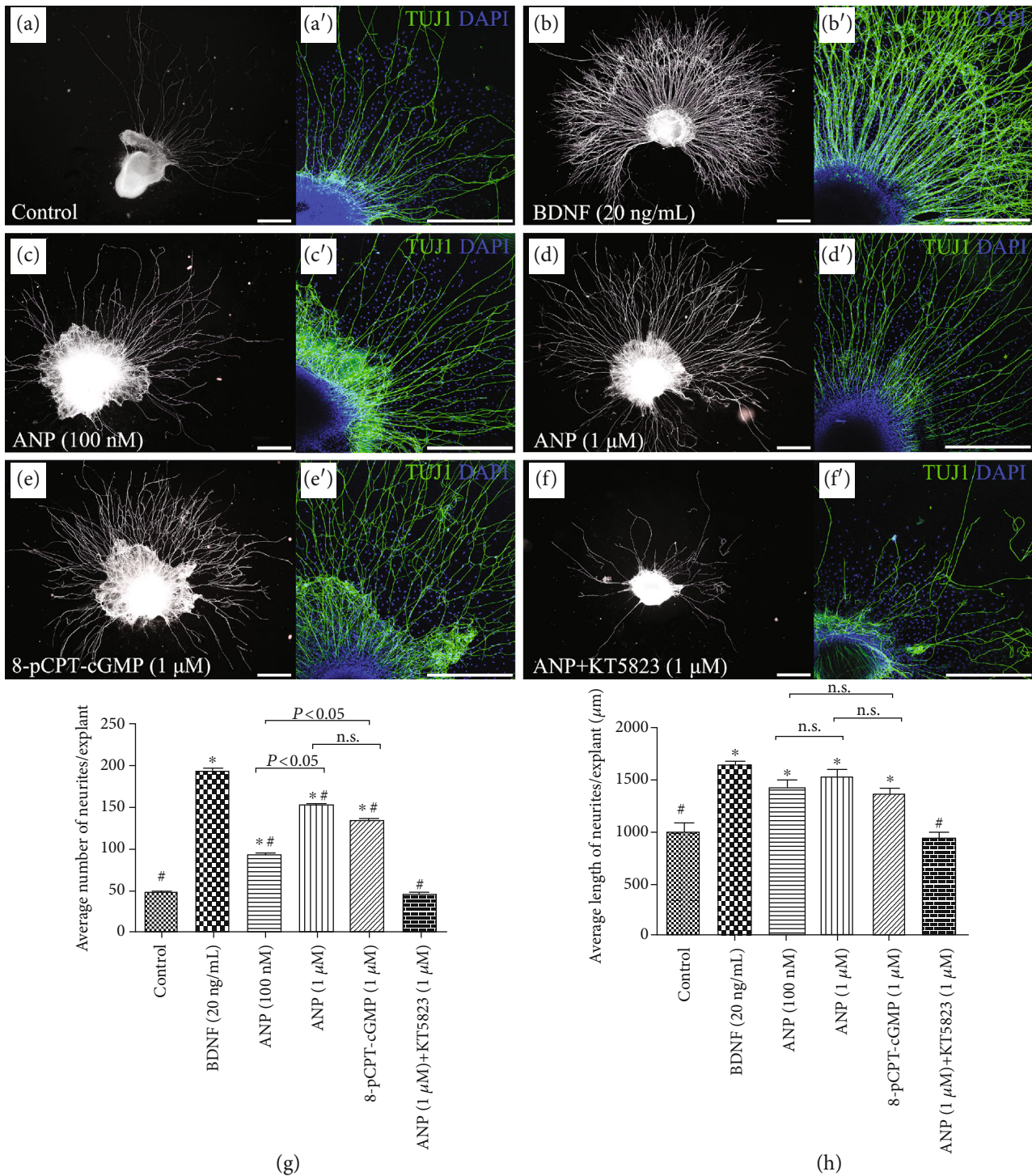


FIGURE 3: ANP promotes neurite outgrowth of SG explants *in vitro*. Immunohistochemical analysis of cochlear SG explants maintained in culture medium alone as a control (a), or treated with 20 ng/mL BDNF (b), 100 nM ANP (c), 1 μM ANP (d), 1 μM 8-pCPT-cGMP (e), or 1 μM ANP plus 1 μM KT5823 (f) for 7 d. Neurons were labeled with TuJ1 (green), while nuclei were stained with DAPI (blue). Scale bars = 500 μm. In each experimental culture, three cochlear neural explants were studied for neurite outgrowth, and the number of neurite outgrowth (g) and average neurite outgrowth length (h) of explants were calculated. Results are expressed as mean ± SEM (**P* < 0.05, versus negative control samples; #*P* < 0.05, versus positive control samples/BDNF; n.s., *P* > 0.05).

and maturation of SGNs and other nervous tissues [23, 57, 60–67]. In our previous researches, we have already studied the expression patterns of ANP and its receptors by immunohistochemical and molecular biological analyses, with the

aim of identifying their cellular localizations, expression levels, and the potential functions within the SG of postnatal rat. The immunoreactivity of ANP and its receptors distributed in SGNs and perineuronal glial cells, with differential

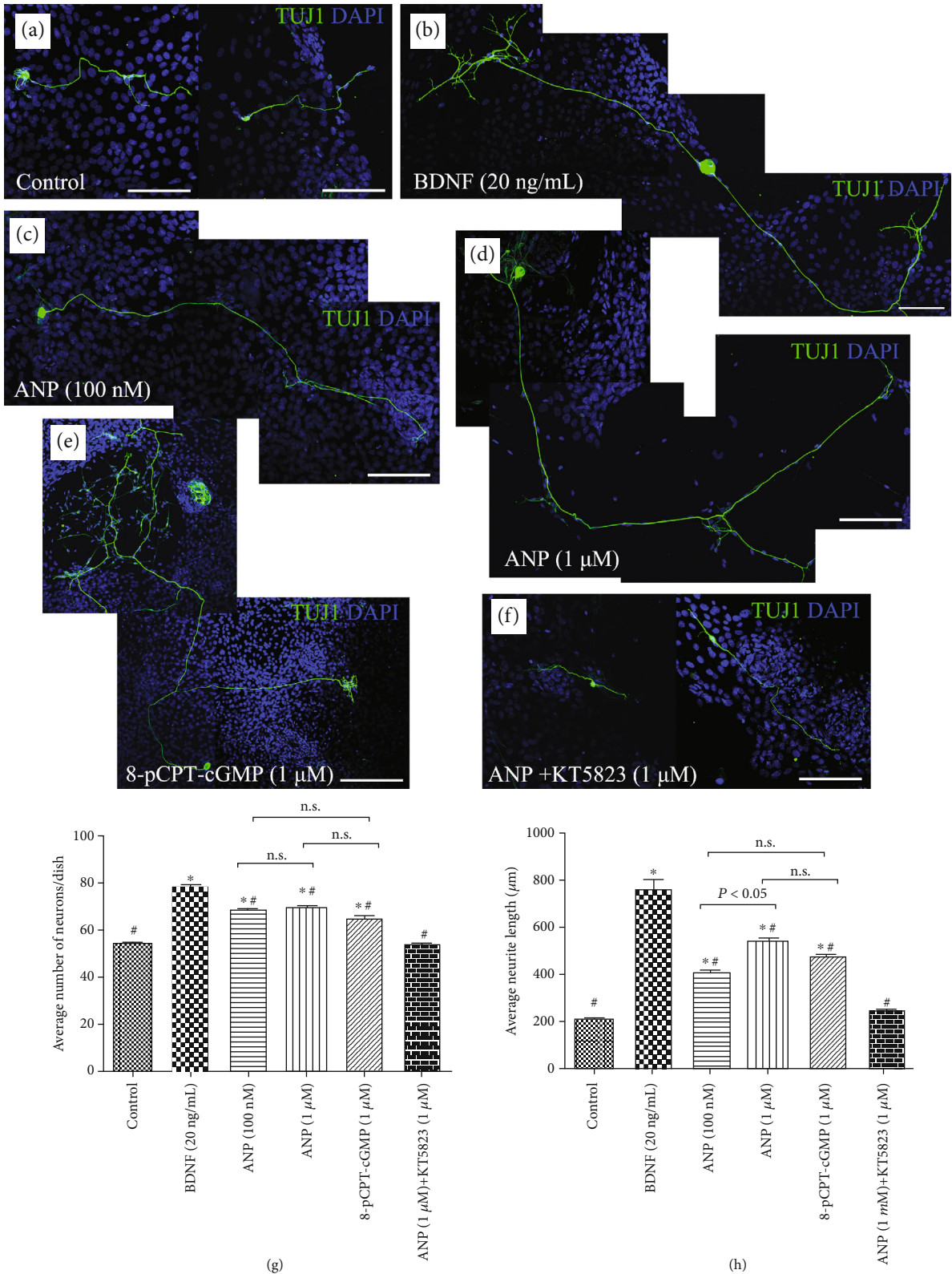


FIGURE 4: ANP promotes neurite outgrowth of dissociated SGNs *in vitro*. Immunohistochemical analysis of dissociated SGNs maintained in culture medium alone (a), or treated with 20 ng/mL BDNF (b), 100 nM ANP (c), 1 μM ANP (d), 1 μM 8-pCPT-cGMP (e), or 1 μM ANP plus 1 μM KT5823 (f) for 5 d. Neurons were labeled with TuJ1 (green), while nuclei were stained with DAPI (blue). Scale bars = 100 μm. In each experimental culture, three SGNs seeded-culture dishes were studied for neurite outgrowth, and the cell number (g) and average neurite outgrowth length (h) of dissociated SGNs were calculated. Results are expressed as mean ± SEM (**P* < 0.05, versus negative control samples; #*P* < 0.05, versus positive control samples/BDNF; n.s., *P* > 0.05).

expression levels of both mRNA and protein in the rat SG during postnatal development. All these data provided a general idea about the temporal and spatial expression profiles of ANP and its receptors within the cochlear SG, suggesting possible roles for ANP in modulating neuronal and glial functions within the SG during auditory neurotransmission and development [52, 53].

In our current study, we performed immunofluorescent analysis on cochlear cryosections as well as dissociated SGNs to validate the distribution of ANP and its receptors in SGNs. Additionally, the influence of ANP on neurite outgrowth was also determined by using organotypic SG explants and dissociated SGN cultures from postnatal rats *in vitro*. We have demonstrated that ANP and its receptors localize in SGNs within cochlear sections and dissociated cultures. ANP, NPR-A, and NPR-C were predominantly immunoreactive in the neuronal perikarya of SGNs, which was consistent with our previous results [52, 53].

ANP, as well as the other two major components of the natriuretic peptide family, BNP and CNP, together with their receptors (NPRs), are widely expressed in the neuronal and glial elements within rodent and mammalian CNS. Additionally, circumstantial evidences indicate that natriuretic peptides and receptors are also distributed in the neural region of peripheral sensory organs, particularly in the sensory ganglia including the dorsal root ganglion (DRG), as well as the ganglia in the retina and inner ear [42, 51, 68–73]. All they could potentially be involved in the regulation of several aspects of neuronal functions such as synaptic transmission and information processing, neural development, neuroprotection, neuroinflammation, neurovascular and blood-brain barrier integrity, and brain fluid homeostasis [34–36]. Especially, many recent researches have shown the significance of the cGMP signaling pathway for neuronal development and neurite pathfinding both in the central and peripheral nervous system, thus providing some hints on the possible functions of natriuretic peptides in axonal development. cGMP signaling elicited by activation of the transmembrane GC-coupled natriuretic peptide receptor NPR-B (also known as NPR2 or GC-B) by the ligand CNP control sensory axon bifurcation of DRG neurons entering the spinal cord [74–83]. Interestingly, the same phenomenon was also found in the cranial sensory ganglion neurons entering the hindbrain including cochlear SGNs [84–88]. Likewise, the mouse lacking cGMP-dependent protein kinase 1 (PKG1) or NPR-B has a defect in the central axonal projection of the DRG sensory neurons [74–78, 81–83] or SGNs [84–88], respectively. Consequently, all these results emphasize a strong significance of the CNP/NPR-B/cGMP/PKG1 pathway regulating neurite outgrowth or pathfinding during neuronal development.

Taking together the results of previous studies and our current work demonstrating colocalization of ANP and its receptors in cochlear SGNs, we hypothesize that ANP may be involved in the regulation of axonal development in the auditory circuits, since ANP also activates a cGMP-dependent signaling cascade upon binding to NPR-A. To test this hypothesis, the influence of ANP on neurite outgrowth was determined in organotypic SG explants and dissociated

SGN cultures from postnatal rats *in vitro*. Since neurotrophins play a critical role in SGN development and maintenance and have been shown to promote SGN survival and enhance neurite elongation [89, 90], SG explants and dissociated SGN cultures incubated with BDNF additive were used as a positive control. Without any additional trophic support, neurite outgrowth from SGNs from explants or dissociated cultures in negative control samples is very limited. The observed neurite outgrowth induced by ANP is dose dependent and significantly different from that of negative control cultures. Furthermore, additional experiments using cell permeable cGMP analogue or a PKG inhibitor further confirmed the role of the ANP/NPRA/cGMP/PKG pathway in neurite elongation, since this activity can be replicated by using 8-pCPT-cGMP and abolished by KT-5823. Taken together, all our data indicated that ANP could enhance neurite outgrowth of SGNs via the NPR-A/cGMP/PKG pathway in a dose-dependent manner and may promote neuronal survival to some extent.

In conclusion, we have demonstrated that ANP and its receptors are expressed in neurons within the cochlear SG of postnatal rat, while ANP may promote neurite outgrowth of SGNs via the NPR-A/cGMP/PKG pathway in a dose-dependent manner. These results indicate that ANP would play a role in normal neuritogenesis of SGN during cochlear development and represents a potential therapeutic candidate to enhance regeneration and regrowth of SGN neurites. Our data offer a good starting point to identify these potential elements and generate new hypotheses; functional experiments must be performed for any gene of interest in such signaling pathway, as we have for NPR1 (NPR-A), which inspire us to investigate the modulatory effects of ANP on several types of neuronal functions within the SG may be involved in through its cell surface receptors. The role of ANP in the regulation of neural development may support it as a key regulator for auditory development and regeneration within the cochlear SG. Manipulation of cGMP levels and activation of PKG by activating ANP and receptor signals represent a potential therapeutic approach to support SGN survival as well as enhance regeneration and regrowth of SGN neurites, which promise to be a fruitful area for developing new and effective therapies for hearing impairment.

Data Availability

The data used to support the findings of this study are available from the corresponding author upon request.

Conflicts of Interest

The authors declare that there are no conflicts of interest regarding the publication of this article.

Authors' Contributions

Fei Sun, Ke Zhou, Ke-yong Tian, and Jie Wang contributed equally to this work.

Acknowledgments

This research was supported by grants from the National Basic Research Program of China (973 Project, 2014CB541700), National Natural Science Foundation of China (81870732 and 81803187), Key Research and Development Program of Shaanxi Province (2018PT-01), Innovation Capability Support Program of Shaanxi Province (2017ZDXM-SF-061), Natural Science Foundation of Shaanxi Province (2019JQ-434), and Disciplinary Research Startup Program of Xijing Hospital in Fourth Military Medical University (XJZT19ML23 and XJZT18ML54).

References

- [1] Y. Liu, J. Qi, X. Chen et al., “Critical role of spectrin in hearing development and deafness,” *Science Advances*, vol. 5, no. 4, article eaav7803, 2019.
- [2] Y. Wang, J. Li, X. Yao et al., “Loss of CIB2 causes profound hearing loss and abolishes mechano-electrical transduction in mice,” *Frontiers in Molecular Neuroscience*, vol. 10, p. 401, 2017.
- [3] C. Zhu, C. Cheng, Y. Wang et al., “Loss of ARHGEF6 causes hair cell stereocilia deficits and hearing loss in mice,” *Frontiers in Molecular Neuroscience*, vol. 11, p. 362, 2018.
- [4] B. A. Nayagam, M. A. Muniak, and D. K. Ryugo, “The spiral ganglion: connecting the peripheral and central auditory systems,” *Hearing Research*, vol. 278, no. 1-2, pp. 2–20, 2011.
- [5] Z. Ruzsnák and G. Szucs, “Spiral ganglion neurones: an overview of morphology, firing behaviour, ionic channels and function,” *Pflügers Archiv*, vol. 457, no. 6, pp. 1303–1325, 2009.
- [6] K. D. Zhang and T. M. Coate, “Recent advances in the development and function of type II spiral ganglion neurons in the mammalian inner ear,” *Seminars in Cell & Developmental Biology*, vol. 65, pp. 80–87, 2017.
- [7] R. K. Shepherd and N. A. Hardie, “Deafness-induced changes in the auditory pathway: implications for cochlear implants,” *Audiology & Neuro-Otology*, vol. 6, no. 6, pp. 305–318, 2001.
- [8] Z. H. He, S. Y. Zou, M. Li et al., “The nuclear transcription factor FoxG1 affects the sensitivity of mimetic aging hair cells to inflammation by regulating autophagy pathways,” *Redox Biology*, vol. 28, article 101364, 2020.
- [9] S. Gao, C. Cheng, M. Wang et al., “Blebbistatin inhibits neomycin-induced apoptosis in hair cell-like HEI-OC-1 cells and in cochlear hair cells,” *Frontiers in Cellular Neuroscience*, vol. 13, p. 590, 2020.
- [10] Y. Zhang, W. Li, Z. He et al., “Pre-treatment with fasudil prevents neomycin-induced hair cell damage by reducing the accumulation of reactive oxygen species,” *Frontiers in Molecular Neuroscience*, vol. 12, p. 264, 2019.
- [11] W. Liu, X. Xu, Z. Fan et al., “Wnt signaling activates TP53-induced glycolysis and apoptosis regulator and protects against cisplatin-induced spiral ganglion neuron damage in the mouse cochlea,” *Antioxidants & Redox Signaling*, vol. 30, no. 11, pp. 1389–1410, 2019.
- [12] L. Liu, Y. Chen, J. Qi et al., “Wnt activation protects against neomycin-induced hair cell damage in the mouse cochlea,” *Cell Death & Disease*, vol. 7, no. 3, article e2136, 2016.
- [13] H. Li, Y. Song, Z. He et al., “Meclofenamic acid reduces reactive oxygen species accumulation and apoptosis, inhibits excessive autophagy, and protects hair cell-like HEI-OC1 cells from cisplatin-induced damage,” *Frontiers in Cellular Neuroscience*, vol. 12, p. 139, 2018.
- [14] S. Zhang, Y. Zhang, Y. Dong et al., “Knockdown of Foxg1 in supporting cells increases the trans-differentiation of supporting cells into hair cells in the neonatal mouse cochlea,” *Cellular and Molecular Life Sciences*, vol. 77, no. 7, pp. 1401–1419, 2020.
- [15] Z. He, L. Guo, Y. Shu et al., “Autophagy protects auditory hair cells against neomycin-induced damage,” *Autophagy*, vol. 13, no. 11, pp. 1884–1904, 2017.
- [16] R. Guo, X. Ma, M. Liao et al., “Development and application of cochlear implant-based electric-acoustic stimulation of spiral ganglion neurons,” *ACS Biomaterials Science & Engineering*, vol. 5, no. 12, pp. 6735–6741, 2019.
- [17] G. Li, K. Chen, D. You et al., “Laminin-coated electrospun regenerated silk fibroin mats promote neural progenitor cell proliferation, differentiation, and survival in vitro,” *Frontiers in Bioengineering and Biotechnology*, vol. 7, p. 190, 2019.
- [18] K. Q. Fan, Y. Y. Li, H. L. Wang et al., “Stress-induced metabolic disorder in peripheral CD4+ T cells leads to anxiety-like behavior,” *Cell*, vol. 179, no. 4, pp. 864–879.e19, 2019.
- [19] Q. Fang, Y. Zhang, X. Chen et al., “Three-dimensional graphene enhances neural stem cell proliferation through metabolic regulation,” *Frontiers in Bioengineering and Biotechnology*, vol. 7, p. 436, 2020.
- [20] J. Zhao, M. Tang, J. Cao et al., “Structurally tunable reduced graphene oxide substrate maintains mouse embryonic stem cell pluripotency,” *Advanced Science*, vol. 6, no. 12, article 1802136, 2019.
- [21] D. Li, X. Yan, Y. Hu et al., “Two-photon image tracking of neural stem cells via iridium complexes encapsulated in polymeric nanospheres,” *ACS Biomaterials Science & Engineering*, vol. 5, no. 3, pp. 1561–1568, 2019.
- [22] S. Han, Y. Xu, J. Sun et al., “Isolation and analysis of extracellular vesicles in a Morpho butterfly wing- integrated microvortex biochip,” *Biosensors and Bioelectronics*, vol. 154, article 112073, 2020.
- [23] M. Tang, J. Li, L. He et al., “Transcriptomic profiling of neural stem cell differentiation on graphene substrates,” *Colloids and Surfaces B: Biointerfaces*, vol. 182, p. 110324, 2019.
- [24] S. Sun, T. Babola, G. Pregernig et al., “Hair cell mechanotransduction regulates spontaneous activity and spiral ganglion subtype specification in the auditory system,” *Cell*, vol. 174, no. 5, pp. 1247–1263.e15, 2018.
- [25] B. R. Shrestha, C. Chia, L. Wu, S. G. Kujawa, M. C. Liberman, and L. V. Goodrich, “Sensory neuron diversity in the inner ear is shaped by activity,” *Cell*, vol. 174, no. 5, pp. 1229–1246.e17, 2018.
- [26] C. Petitpré, H. Wu, A. Sharma et al., “Neuronal heterogeneity and stereotyped connectivity in the auditory afferent system,” *Nature Communications*, vol. 9, no. 1, article 3691, 2018.
- [27] A. Toesca, “Central and peripheral myelin in the rat cochlear and vestibular nerves,” *Neuroscience Letters*, vol. 221, no. 1, pp. 21–24, 1996.
- [28] E. J. Jeon, N. Xu, L. Xu, and M. R. Hansen, “Influence of central glia on spiral ganglion neuron neurite growth,” *Neuroscience*, vol. 177, pp. 321–334, 2011.
- [29] A. J. de Bold, H. B. Borenstein, A. T. Veress, and H. Sonnenberg, “A rapid and potent natriuretic response to intravenous injection of atrial myocardial extract in rats,” *Life Sciences*, vol. 28, no. 1, pp. 89–94, 1981.

- [30] E. R. Levin, D. G. Gardner, and W. K. Samson, "Natriuretic peptides," *The New England Journal of Medicine*, vol. 339, no. 5, pp. 321–328, 1998.
- [31] L. R. Potter, S. Abbey-Hosch, and D. M. Dickey, "Natriuretic peptides, their receptors, and cyclic guanosine monophosphate-dependent signaling functions," *Endocrine Reviews*, vol. 27, no. 1, pp. 47–72, 2006.
- [32] L. R. Potter, A. R. Yoder, D. R. Flora, L. K. Antos, and D. M. Dickey, "Natriuretic peptides: their structures, receptors, physiologic functions and therapeutic applications," in *cGMP: Generators, Effectors and Therapeutic Implications. Handbook of Experimental Pharmacology*, vol. 191 Springer, Berlin, Heidelberg.
- [33] R. A. Rose and W. R. Giles, "Natriuretic peptide C receptor signalling in the heart and vasculature," *The Journal of Physiology*, vol. 586, no. 2, pp. 353–366, 2008.
- [34] L.-H. Cao and X.-L. Yang, "Natriuretic peptides and their receptors in the central nervous system," *Progress in Neurobiology*, vol. 84, no. 3, pp. 234–248, 2008.
- [35] J. Prado, M. A. Baltrons, P. Pifarré, and A. García, "Glial cells as sources and targets of natriuretic peptides," *Neurochemistry International*, vol. 57, no. 4, pp. 367–374, 2010.
- [36] S. Mahinrad, A. J. M. de Craen, S. Yasar, D. van Heemst, and B. Sabayan, "Natriuretic peptides in the central nervous system: novel targets for cognitive impairment," *Neuroscience & Biobehavioral Reviews*, vol. 68, pp. 148–156, 2016.
- [37] Y. J. Yoon, E. J. Lee, and S. H. Kim, "Synthesis of atrial natriuretic peptide in the rabbit inner ear," *The Laryngoscope*, vol. 122, no. 7, pp. 1605–1608, 2012.
- [38] T. Koch, B. Gloddek, and S. Gutzke, "Binding sites of atrial natriuretic peptide (ANP) in the mammalian cochlea and stimulation of cyclic GMP synthesis," *Hearing Research*, vol. 63, no. 1-2, pp. 197–202, 1992.
- [39] G. Krause, A. M. Meyer zum Gottesberge, G. Wolfram, and R. Gerzer, "Transcripts encoding three types of guanylyl-cyclase-coupled trans-membrane receptors in inner ear tissues of guinea pigs," *Hearing Research*, vol. 110, no. 1-2, pp. 95–106, 1997.
- [40] A. Meyer zum Gottesberge and J. Lamprecht, "Localization of the atrial natriuretic peptide binding sites in the inner ear tissue—possibly an additional regulating system," *Acta Oto-Laryngologica. Supplementum*, vol. 468, pp. 53–57, 1989.
- [41] A. M. Meyer zum Gottesberge, M. Gagelmann, and W. G. Forssmann, "Atrial natriuretic peptide-like immunoreactive cells in the guinea pig inner ear," *Hearing Research*, vol. 56, no. 1-2, pp. 86–92, 1991.
- [42] J. Lamprecht and A. M. Meyer zum Gottesberge, "The presence and localization of receptors for atrial natriuretic peptide in the inner ear of the guinea pig," *Archives of Oto-Rhino-Laryngology*, vol. 245, no. 5, pp. 300–301, 1988.
- [43] A. Meyer zum Gottesberge, A. Schleicher, C. Drummer, and R. Gerzer, "The volume protective natriuretic peptide system in the inner ear comparison between vestibular and cochlear compartments," *Acta Oto-Laryngologica. Supplementum*, vol. 520, Part 1, pp. 170–173, 1995.
- [44] L. Qiao, Y. Han, P. Zhang, Z. Cao, and J. Qiu, "Detection of atrial natriuretic peptide and its receptor in marginal cells and cochlea tissues from the developing rats," *Neuro Endocrinology Letters*, vol. 32, no. 2, pp. 187–192, 2011.
- [45] T. Seebacher, E. Beitz, H. Kumagami, K. Wild, J. P. Ruppertsberg, and J. E. Schultz, "Expression of membrane-bound and cytosolic guanylyl cyclases in the rat inner ear," *Hearing Research*, vol. 127, no. 1-2, pp. 95–102, 1999.
- [46] M. Suzuki, H. Kitano, T. Kitanishi et al., "RT-PCR analysis of mRNA expression of natriuretic peptide family and their receptors in rat inner ear," *Molecular Brain Research*, vol. 55, no. 1, pp. 165–168, 1998.
- [47] Y.-J. Yoon and S. Hellström, "Immunohistochemical localization of α -atrial natriuretic polypeptide in the rat cochlea," *Acta Oto-Laryngologica*, vol. 112, no. 4, pp. 604–610, 2009.
- [48] Y. J. Yoon and M. Anniko, "Distribution of alpha-ANP in the cochlea and the vestibular organs," *ORL*, vol. 56, no. 2, pp. 73–77, 1994.
- [49] Y. J. Yoon, E. J. Lee, S. Hellstrom, and J. S. Kim, "Atrial natriuretic peptide modulates auditory brainstem response of rat," *Acta Oto-Laryngologica*, vol. 135, no. 12, pp. 1293–1297, 2015.
- [50] H. X. Chen, J. L. Wang, Q. C. Liu, and J. H. Qiu, "Distribution and location of immunoreactive atrial natriuretic peptides in cochlear stria vascularis of guinea pig," *Chinese Medical Journal*, vol. 107, no. 1, pp. 53–56, 1994.
- [51] H. Furuta, N. Mori, L. Luo, and A. F. Ryan, "Detection of mRNA encoding guanylate cyclase A/atrial natriuretic peptide receptor in the rat cochlea by competitive polymerase chain reaction and in situ hybridization," *Hearing Research*, vol. 92, no. 1-2, pp. 78–84, 1995.
- [52] F. Sun, K. Zhou, S. Wang et al., "Expression and localization of atrial natriuretic peptide and its receptors in rat spiral ganglion neurons," *Brain Research Bulletin*, vol. 95, pp. 28–32, 2013.
- [53] F. Sun, K. Zhou, S. Wang, P. Liang, M. Zhu, and J. Qiu, "Expression patterns of atrial natriuretic peptide and its receptors within the cochlear spiral ganglion of the postnatal rat," *Hearing Research*, vol. 309, pp. 103–112, 2014.
- [54] N. Xu, J. Engbers, S. Khaja, L. Xu, J. J. Clark, and M. R. Hansen, "Influence of cAMP and protein kinase A on neurite length from spiral ganglion neurons," *Hearing Research*, vol. 283, no. 1-2, pp. 33–44, 2012.
- [55] P. J. Atkinson, C. H. Cho, M. R. Hansen, and S. H. Green, "Activity of all JNK isoforms contributes to neurite growth in spiral ganglion neurons," *Hearing Research*, vol. 278, no. 1-2, pp. 77–85, 2011.
- [56] G. Sun, W. Liu, Z. Fan et al., "The three-dimensional culture system with Matrigel and neurotrophic factors preserves the structure and function of spiral ganglion neuron in vitro," *Neural Plasticity*, vol. 2016, Article ID 4280407, 15 pages, 2016.
- [57] M. Waqas, S. Sun, C. Xuan et al., "Bone morphogenetic protein 4 promotes the survival and preserves the structure of flow-sorted Bhlhb5+ cochlear spiral ganglion neurons in vitro," *Scientific Reports*, vol. 7, no. 1, article 3506, 2017.
- [58] S. J. Meas, K. Nishimura, M. Scheibinger, and A. Dabdoub, "In vitro methods to cultivate spiral ganglion cells, and purification of cellular subtypes for induced neuronal reprogramming," *Frontiers in Neuroscience*, vol. 12, p. 822, 2018.
- [59] K. Leitmeyer, A. Glutz, C. Setz et al., "Simvastatin results in a dose-dependent toxic effect on spiral ganglion neurons in an in vitro organotypic culture assay," *BioMed Research International*, vol. 2016, Article ID 3580359, 7 pages, 2016.
- [60] J. S. Kempfle, K. Nguyen, C. Hamadani et al., "Bisphosphonate-linked TrkB agonist: cochlea-targeted delivery of a neurotrophic agent as a strategy for the treatment of hearing loss," *Bioconjugate Chemistry*, vol. 29, no. 4, pp. 1240–1250, 2018.
- [61] S. Han, J. Sun, S. He, M. Tang, and R. Chai, "The application of graphene-based biomaterials in biomedicine," *American*

- Journal of Translational Research*, vol. 11, no. 6, pp. 3246–3260, 2019.
- [62] W. Yan, W. Liu, J. Qi et al., “A three-dimensional culture system with Matrigel promotes purified spiral ganglion neuron survival and function in vitro,” *Molecular Neurobiology*, vol. 55, no. 3, pp. 2070–2084, 2018.
- [63] Y. Yang, Y. Zhang, R. Chai, and Z. Gu, “Designs of biomaterials and microenvironments for neuroengineering,” *Neural Plasticity*, vol. 2018, Article ID 1021969, 10 pages, 2018.
- [64] Z. Liu, M. Tang, J. Zhao, R. Chai, and J. Kang, “Looking into the future: toward advanced 3D biomaterials for stem-cell-based regenerative medicine,” *Advanced Materials*, vol. 30, no. 17, article e1705388, 2018.
- [65] L. Xia, W. Zhu, Y. Wang, S. He, and R. Chai, “Regulation of neural stem cell proliferation and differentiation by graphene-based biomaterials,” *Neural Plasticity*, vol. 2019, Article ID 3608386, 11 pages, 2019.
- [66] R. Guo, S. Zhang, M. Xiao et al., “Accelerating bioelectric functional development of neural stem cells by graphene coupling: implications for neural interfacing with conductive materials,” *Biomaterials*, vol. 106, pp. 193–204, 2016.
- [67] L. Shang, Y. Yu, W. Gao et al., “Bio-inspired anisotropic wettability surfaces from dynamic ferrofluid assembled templates,” *Advanced Functional Materials*, vol. 28, no. 7, article 1705802, 2018.
- [68] E. M. Abdelalim, C. Masuda, and I. Tooyama, “Expression of natriuretic peptide-activated guanylate cyclases by cholinergic and dopaminergic amacrine cells of the rat retina,” *Peptides*, vol. 29, no. 4, pp. 622–628, 2008.
- [69] E. M. Abdelalim, J. P. Bellier, and I. Tooyama, “Expression of NPR-B in neurons of the dorsal root ganglia of the rat,” *Peptides*, vol. 43, pp. 56–61, 2013.
- [70] Z. W. Li, B. Wu, P. Ye, Z. Y. Tan, and Y. H. Ji, “Brain natriuretic peptide suppresses pain induced by BmK I, a sodium channel-specific modulator, in rats,” *The Journal of Headache and Pain*, vol. 17, no. 1, p. 90, 2016.
- [71] A. Marchenkova, S. Vilotti, E. Fabbretti, and A. Nistri, “Brain natriuretic peptide constitutively downregulates P2X3 receptors by controlling their phosphorylation state and membrane localization,” *Molecular Pain*, vol. 11, p. s12990-015-0074, 2015.
- [72] G. Z. Xu, J. Tian, Y. M. Zhong, and X. L. Yang, “Natriuretic peptide receptors are expressed in rat retinal ganglion cells,” *Brain Research Bulletin*, vol. 82, no. 3-4, pp. 188–192, 2010.
- [73] E. M. Abdelalim and I. Tooyama, “NPR-C is expressed in the cholinergic and dopaminergic amacrine cells in the rat retina,” *Peptides*, vol. 31, no. 1, pp. 180–183, 2010.
- [74] A. Dumoulin, G. Ter-Avetisyan, H. Schmidt, and F. G. Rathjen, “Molecular analysis of sensory axon branching unraveled a cGMP-dependent signaling cascade,” *International Journal of Molecular Sciences*, vol. 19, no. 5, article 1266, 2018.
- [75] H. Schmidt, M. Werner, P. A. Heppenstall et al., “cGMP-mediated signaling via cGK1 α is required for the guidance and connectivity of sensory axons,” *The Journal of Cell Biology*, vol. 159, no. 3, pp. 489–498, 2002.
- [76] H. Schmidt, D. M. Dickey, A. Dumoulin et al., “Regulation of the natriuretic peptide receptor 2 (Npr 2) by phosphorylation of juxtamembrane serine and threonine residues is essential for bifurcation of sensory axons,” *The Journal of Neuroscience*, vol. 38, no. 45, pp. 9768–9780, 2018.
- [77] H. Schmidt, A. Stonkute, R. Jüttner, D. Koesling, A. Friebe, and F. G. Rathjen, “C-type natriuretic peptide (CNP) is a bifurcation factor for sensory neurons,” *Proceedings of the National Academy of Sciences of the United States of America*, vol. 106, no. 39, pp. 16847–16852, 2009.
- [78] H. Schmidt, A. Stonkute, R. Jüttner et al., “The receptor guanylyl cyclase Npr 2 is essential for sensory axon bifurcation within the spinal cord,” *The Journal of Cell Biology*, vol. 179, no. 2, pp. 331–340, 2007.
- [79] I. Kishimoto, T. Tokudome, T. Horio et al., “C-type natriuretic peptide is a Schwann cell-derived factor for development and function of sensory neurones,” *Journal of Neuroendocrinology*, vol. 20, no. 11, pp. 1213–1223, 2008.
- [80] C. Xia, M. Nguyen, A. K. Garrison et al., “CNP/cGMP signaling regulates axon branching and growth by modulating microtubule polymerization,” *Developmental Neurobiology*, vol. 73, no. 9, pp. 673–687, 2013.
- [81] Z. Zhao and L. Ma, “Regulation of axonal development by natriuretic peptide hormones,” *Proceedings of the National Academy of Sciences of the United States of America*, vol. 106, no. 42, pp. 18016–18021, 2009.
- [82] Z. Zhao, Z. Wang, Y. Gu, R. Feil, F. Hofmann, and L. Ma, “Regulate axon branching by the cyclic GMP pathway via inhibition of glycogen synthase kinase 3 in dorsal root ganglion sensory neurons,” *The Journal of Neuroscience*, vol. 29, no. 5, pp. 1350–1360, 2009.
- [83] H. Schmidt, S. Peters, K. Frank, L. Wen, R. Feil, and F. G. Rathjen, “Dorsal root ganglion axon bifurcation tolerates increased cyclic GMP levels: the role of phosphodiesterase 2A and scavenger receptor Npr 3,” *The European Journal of Neuroscience*, vol. 44, no. 12, pp. 2991–3000, 2016.
- [84] C. C. Lu, J. M. Appler, E. A. Houseman, and L. V. Goodrich, “Developmental profiling of spiral ganglion neurons reveals insights into auditory circuit assembly,” *The Journal of Neuroscience*, vol. 31, no. 30, pp. 10903–10918, 2011.
- [85] G. Ter-Avetisyan, F. G. Rathjen, and H. Schmidt, “Bifurcation of axons from cranial sensory neurons is disabled in the absence of Npr2-induced cGMP signaling,” *The Journal of Neuroscience*, vol. 34, no. 3, pp. 737–747, 2014.
- [86] C. C. Lu, X. J. Cao, S. Wright, L. Ma, D. Oertel, and L. V. Goodrich, “Mutation of Npr2 leads to blurred tonotopic organization of central auditory circuits in mice,” *PLoS Genetics*, vol. 10, no. 12, article e1004823, 2014.
- [87] S. Wolter, D. Möhrle, H. Schmidt et al., “GC-B deficient mice with axon bifurcation loss exhibit compromised auditory processing,” *Frontiers in Neural Circuits*, vol. 12, p. 65, 2018.
- [88] H. Schmidt and B. Fritsch, “Npr2 null mutants show initial overshooting followed by reduction of spiral ganglion axon projections combined with near-normal cochleotopic projection,” *Cell and Tissue Research*, vol. 378, no. 1, pp. 15–32, 2019.
- [89] A. J. Evans, B. C. Thompson, G. G. Wallace et al., “Promoting neurite outgrowth from spiral ganglion neuron explants using polypyrrole/BDNF-coated electrodes,” *Journal of Biomedical Materials Research. Part A*, vol. 91, no. 1, pp. 241–250, 2009.
- [90] K. Stankovic, C. Rio, A. Xia et al., “Survival of adult spiral ganglion neurons requires erbB receptor signaling in the inner ear,” *The Journal of Neuroscience*, vol. 24, no. 40, pp. 8651–8661, 2004.

Research Article

A Novel Spontaneous Mutation of the *SOX10* Gene Associated with Waardenburg Syndrome Type II

Sen Chen ¹, Yuan Jin ¹, Le Xie,¹ Wen Xie ¹, Kai Xu ¹, Yue Qiu ¹, Xue Bai ¹, Hui-Min Zhang ¹, Xiao-Zhou Liu,¹ Xiao-Hui Wang,¹ Wei-Jia Kong ^{1,2} and Yu Sun ¹

¹Department of Otorhinolaryngology, Union Hospital, Tongji Medical College, Huazhong University of Science and Technology, Wuhan 430022, China

²Institute of Otorhinolaryngology, Tongji Medical College, Huazhong University of Science and Technology, 430022 Wuhan, China

Correspondence should be addressed to Wei-Jia Kong; entwjkong@hust.edu.cn and Yu Sun; sunyu@hust.edu.cn

Received 6 February 2020; Revised 19 March 2020; Accepted 30 March 2020; Published 28 August 2020

Guest Editor: Geng-lin Li

Copyright © 2020 Sen Chen et al. This is an open access article distributed under the Creative Commons Attribution License, which permits unrestricted use, distribution, and reproduction in any medium, provided the original work is properly cited.

Waardenburg syndrome (WS), also known as auditory-pigmentary syndrome, is the most common cause of syndromic hearing loss. It is responsible for 2–5% of congenital deafness. WS is classified into four types depending on the clinical phenotypes. Currently, pathogenic mutation of *PAX3*, *MITF*, *EDNRB*, *EDN3*, *SNAI2*, or *SOX10* can cause corresponding types of WS. Among them, *SOX10* mutation is responsible for approximately 15% of type II WS or 50% of type IV WS. We report the case of a proband in a Chinese family who was diagnosed with WS type II. Whole exome sequencing (WES) of the proband detected a novel heterozygous spontaneous mutation: *SOX10* c.246delC. According to analysis based on nucleic acid and amino acid sequences, this mutation may produce a truncated protein, with loss of the HMG structure domain. Therefore, this truncated protein may fail to activate the expression of the *MITF* gene, which regulates melanocytic development and plays a key role in WS. Our finding expands the database of *SOX10* mutations associated with WS and provides more information regarding the molecular mechanism of WS.

1. Introduction

Waardenburg syndrome (WS), also known as auditory-pigmentary syndrome, is one of the most common causes of syndromic deafness, associated with 2–5% of congenital deafness cases [1]. According to correlational research, sporadic cases of WS have been reported worldwide; the highest reported incidence is among Kenyan Africans, who have an incidence of 1 in 20,000 [2]. WS accounts for approximately 1% of the deaf population in China. Basic clinical symptoms of WS include dystopia of the canthus; abnormal pigmentation of the skin, hair, and eyes; different degrees of unilateral or bilateral sensorineural deafness; and a high and wide nasal base. The disease is divided into four types; type I exhibits only these basic symptoms. The clinical manifestations of type II are basically the same as type I, but without dystopia of the canthus. The clinical manifestations of type III are the same as type I, but combined with upper limb deformity,

while type IV exhibits basically the same symptoms as type II, but combined with Hirschsprung disease (gastrointestinal malformation) [3–6]. Mutations of the *PAX3*, *SOX10*, *MITF*, *SNAI2*, *EDNRB*, and *EDN3* genes have been found in cases of the different types of WS [7, 8]. According to previous reports, *SOX10* mutations cause approximately 15% of type II WS and 45–55% of type IV WS [9, 10]. To date, the total number of reported *SOX10* pathogenic mutations related to WS is 82, according to the Leiden Open Variation Database (LOVD) (<https://grenada.lumc.nl/LOVD2/WS/home>).

The *SOX10* gene (SRY- (sex-determining region Y-) box 10) is located on chromosome 22q13.1. It contains five exons and encodes a protein which consists of 466 amino acids, with a relative molecular weight of approximately 51,000 [11]. *SOX10* belongs to the SOX (SRY-related HMG-box) family, and it is first expressed in the dorsal neural tube at the early stage of neural crest cell (NCC) migration. With differentiation of the NCC, *SOX10* begins to be widely

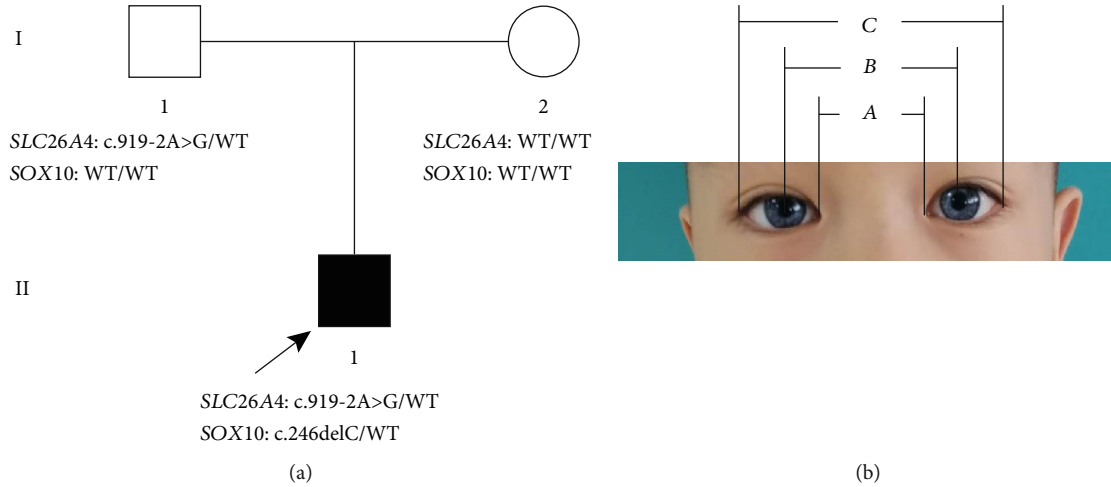


FIGURE 1: Family pedigree and clinical features of the proband. The (a) pedigree indicates that Family II-1 had a spontaneous heterozygous mutation (*SOX10* c.246delC), which is marked black. Family I-1 only carried the mutation of the *SLC26A4* gene. (b) The iris heterochromia in both eyes of the proband, which are blue. *a*, *b*, and *c* indicate the distance between the inner canthi, pupils, and outer canthi. WT: wild type.

TABLE 1: Genetic variants found in this family.

Gene	Variant	Protein level	Type	Father	Mother	Proband
<i>SOX10</i>	c.246delC	p.Gly82GlyfsX27	Heterozygous	Normal	Normal	Heterozygous
<i>SLC26A4</i>	c.919-2A>G	Splicing	Heterozygous	Heterozygous	Normal	Heterozygous

expressed throughout the adult body, such as in the hair follicles, inner ear, iris, and gastrointestinal tract. *SOX10* acts as a transcription factor of the microphthalmia-associated transcription factor (*MITF*) gene, and *MITF* plays a key role in the development of melanocytes [12]. Currently, it is believed that the aetiology of WS is caused by the abnormal development of NCC [7, 13, 14]. Additionally, the hearing loss of WS may relate to the abnormal proliferation, survival, differentiation, or migration of NCC-derived melanocytes (a type of intermedia cells of the stria vascularis) [15]. In the mouse inner ear, the *SOX10* gene starts to express in the otic vesicle of the cochlea at embryonic day 9.5-12.5 (E9.5-E12.5), and the expression is restricted to supporting cells (SCs) of the cochlear epithelium, glial cells, and marginal and intermedia layers of the stria vascularis after birth [16–18]. Knockout of the *SOX10* gene leads to the death of NCC-derived Schwann cells in a mouse model [19]. However, the role that it played in supporting cells is still unknown.

As WS has a lot of genetic heterogeneity, the molecular mechanism of WS needs better understanding, and more cases of gene mutation associated with WS need to be collected. Here, we report a novel heterozygous *SOX10* mutation in a Chinese family, which provides more information about the molecular diagnosis of WS.

2. Materials and Methods

2.1. Family Description. Family member II-1: a seven-year-old boy, who failed to pass hearing screening and who had white hair at the front of his forehead and bilateral blue irises,

was diagnosed with type II WS. Neither parent of the boy exhibited similar symptoms (Figure 1(a) and Table 1).

2.2. Clinical Examination. The proband underwent audiological examination including otoscopic examination, pure tone audiometry, auditory brainstem response (ABR), distortion product otoacoustic emissions (DPOAE), and auditory immittance and auditory steady-state evoked responses (ASSR). A computed tomography (CT) scan of the proband was also performed. The distance between the inner canthi (*a*) of the proband was measured at 29 mm, the distance between the pupils (*b*) was 54 mm, and the distance between the outer canthi (*c*) was 89 mm. The *W* exponent was obtained according to the formulae $X = (2a - 0.2119c - 3.909)/c$; $Y = (2a - 0.2479b - 3.909)/b$; and $W = X + Y + a/b$ (Figure 1(b)) [20].

2.3. Mutation Detection and Analysis. Targeted sequencing and Sanger sequencing were performed by BGI Genomics (Wuhan, China). After obtaining informed consent, we collected 3–5 mL of venous peripheral blood from the proband and his parents to prepare DNA. Genomic DNA from all the family members was extracted according to the manufacturer's standard procedure using the QIAamp DNA Blood Midi Kit (Qiagen Inc., Hilden, Germany). The genomic DNA of the family was fragmented using a Covaris LE220 ultrasonicator (Covaris Inc., Woburn, Massachusetts, USA) to generate a paired-end library (200–250 bp). Following array hybridization, elution, and postcapture amplification, the library was enriched. An Agilent 2100 Bioanalyzer and ABI StepOne were used to estimate the magnitude

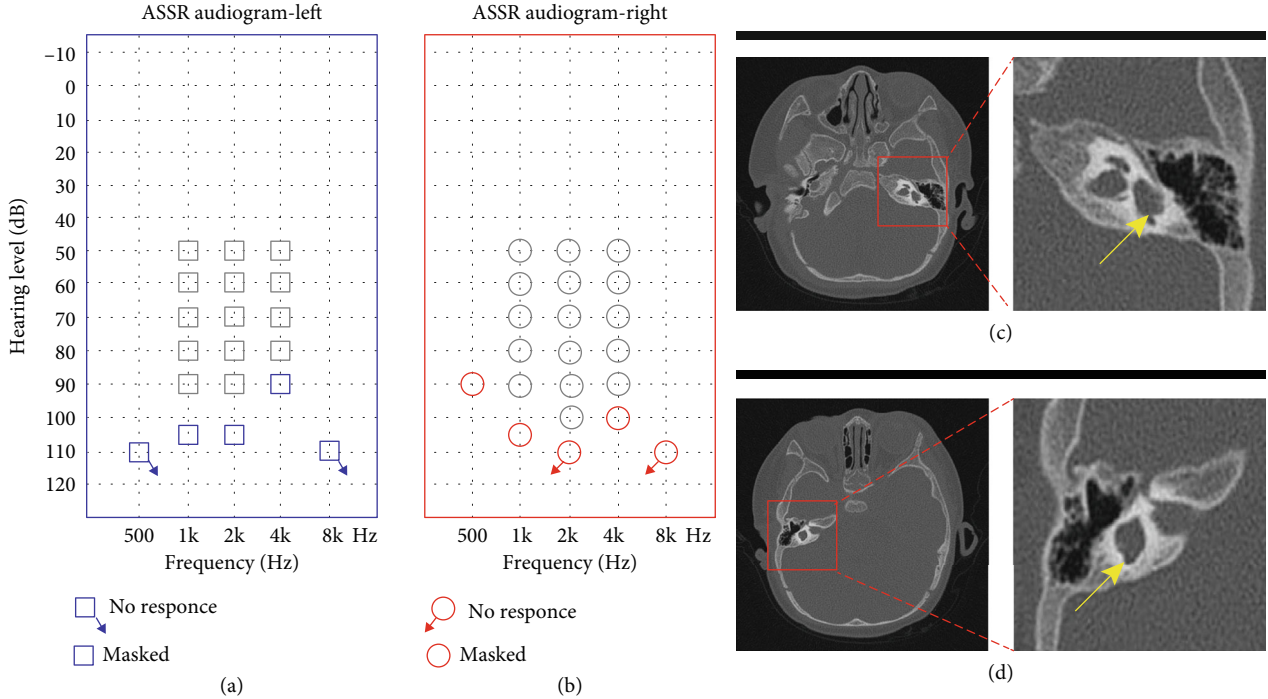


FIGURE 2: Clinical audiology examination and temporal bone CT scan of the proband. (a) ASSR (auditory steady-state responses) of the left ear: 105 dB, 105 dB, and 90 dB at 1, 2, and 4 kHz, respectively; the remaining frequencies showed no response. (b) ASSR of the right ear: 90 dB, 105 dB, and 100 dB at 500 Hz, 1, and 4 kHz; the remaining frequencies showed no response. (c) Semicircular canal abnormalities shown on high-resolution axial CT in the red square (left ear). (d) Semicircular canal abnormalities shown on high-resolution axial CT in the red square (right ear).

enrichment of the products. Subsequently, the amplified libraries were used for circularization and sequencing on the BGISEQ-500 platform. For circularization, PCR products with different barcodes were pooled together at equimolar concentrations to yield a final amount of 80 ng. Each pool was subsequently heat-denatured, and the single-strand DNA was mixed with an MGIEasy™ DNA Library Prep Kit V1 (PN: 85-05533-00, BGI, Shenzhen, China) to form a 60 μ L reaction system, which was subsequently incubated at 37°C for 30 minutes. Finally, 20 μ L of each single-circle-library pool was used as input to prepare the DNB. Each pool was then sequenced on one lane, using 100SR chemistry with a BGISEQ-500RS high-throughput sequencing kit (PN: 85-05238-01, BGI). After sequencing, the data were automatically demultiplexed by index. The “clean reads” (with a length of 90 bp) derived from targeted sequencing and filtering were then aligned to the human genome reference (hg19) using the BWA (Burrows Wheeler Aligner) Multi-Vision software package. After alignment, the output files were used to perform sequencing coverage and depth analysis of the target region, single-nucleotide variants (SNVs), and INDEL calling. We detected SNVs and indels using GATK software. All SNVs and indels were referenced and compared with multiple databases, including the National Center for Biotechnology Information (NCBI) GenBank database (<https://www.ncbi.nlm.nih.gov/nucleotide/>), the Database of Single Nucleotide Polymorphisms (dbSNP) (<http://www.ncbi.nlm.nih.gov/projects/SNP/>), and the 1000 Genomes Database (<https://www.internationalgenome.org>). According to the

high-throughput sequencing results, Sanger sequencing was performed to confirm whether his parents had the same mutations.

3. Results

3.1. Clinical Data. The proband had white hair at the front of his forehead and bilateral blue irises. His parents had no pigmentary abnormalities in the skin, the hair, and the eye or any other WS-associated phenotypes. The audiology examination of the proband showed failed bilateral otoacoustic emissions; all bilateral ABR thresholds were over 105 dB nHL; ASSR showed the thresholds of the left ear were 105 dB nHL at 1 kHz, 105 dB nHL at 2 kHz, and 90 dB nHL at 4 kHz, while the thresholds of the right ear were 90 dB nHL at 500 Hz, 105 dB nHL at 1 kHz, and 100 dB nHL at 4 kHz (Figures 2(a) and 2(b)). The temporal bone CT scan suggested that the shape and size of the bilateral cochleae were not obviously abnormal; however, the middle and top circles of the cochleae were obscurely decomposed, the vestibule was slightly enlarged on both sides, all the right semicircular canals were fused with the vestibule, the left posterior and superior semicircular canals were short, and the horizontal semicircular canal was fused with the vestibule (Figures 2(c) and 2(d)). We substituted the measured distances of inner canthi (a), pupil (b), and outer canthi (c) into the W exponent formula (as introduced in Section 2.2) and obtained that the W exponent was 1.687, less than 1.95 (Figure 1(b)).

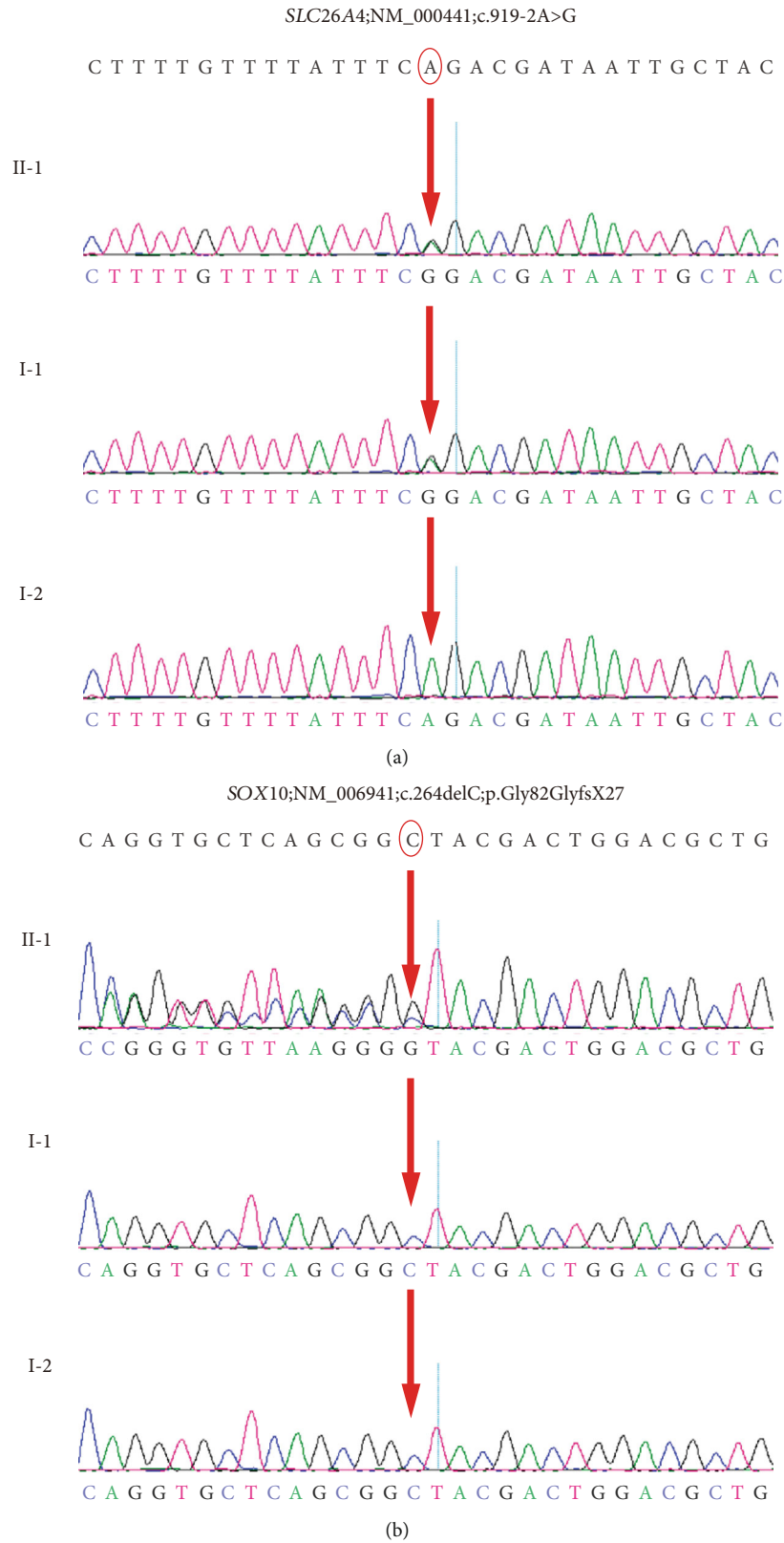


FIGURE 3: Genetic sequencing results of the proband and his parents. The red arrow indicates the site of the base deletion or substitution.

3.2. *Mutation Identification Data.* The NGS results were compared with the human reference genome (GRCh37/hg19). The proband carried two heterozygous mutations: the *SOX10*

c.246delC and the *SLC26A4* c.919-2A>G; the c.246delC mutation was a truncation with deletion of the no. 246 nucleotide cytosine, occurring in EX2/CDS1 of *SOX10*. No report related

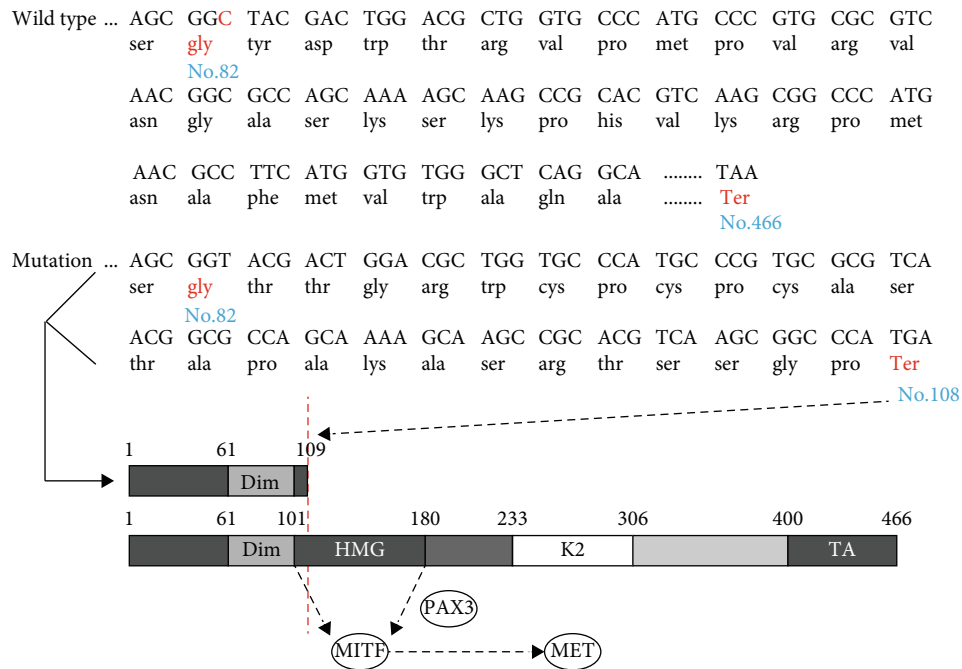


FIGURE 4: Amino acid coding diagram for the proband and schematic diagram of the *SOX10* gene domain. The red letters indicate the changed amino acids and the site of the stop codon. The mutation caused early termination of the coding sequence. If a deletion mutation occurs in front of the HMG domain, the HMG domain cannot combine with the promoter of the target gene (*MITF*).

to the c.246delC mutation in *SOX10* was found in the HGMD (Figure 3(b)). The c.919-2A>G mutation was a splice mutation of no. 919-2 nucleotide from adenine to guanine, occurring in intron7 of *SLC26A4* (Figure 3(a)). The father of the proband only carried the mutation of the *SLC26A4* gene, at the same mutation site as that of the proband, while the mother of the proband had the wild-type *SOX10* and *SLC26A4* genes.

3.3. Functional Analysis of the Mutant Protein. The *SOX10* gene contains three main functional domains: a SOX Group E domain which is highly conserved, the carboxy terminal (C-terminal) transactivation (TA) domain, and a highly conserved and highly active component domain: the highly mobility group (HMG) (102–181 amino acids). The mutation identified in the proband occurred in amino acid no. 82, with deletion of nucleotide C in position no. 246 causing a frameshift mutation. Consequently, the original glycine encoded by GGC at nucleotide nos. 244–246 was changed into glycine encoded by GGG. Following the change at no. 82 glycine, the no. 108 amino acid was converted into a termination codon (Figure 4).

4. Discussion

A diagnosis of type II WS was established in the proband. In terms of clinical diagnosis, audiology testing showed that the proband suffered from profound bilateral congenital sensorineural deafness; we calculated a *W* index of 1.687, less than 1.95, indicating that the proband had no dystopia of the canthus; the proband had white hair on his head and had bilateral blue irises at birth, but no digestive tract abnormalities

[21]. In terms of the genetic test results, we found two genetic mutations in the proband; the *SLC26A4* gene related to the syndrome type deafness with vestibular pipe expansion showed autosomal recessive inheritance. According to a previous report, in the appropriate clinical context, bilateral agenesis or hypoplasia of the semicircular canals or both, associated with an enlarged vestibule and cochlear deformity, strongly suggests a diagnosis of WS linked to a *SOX10* mutation, so we speculate that the spontaneous *SOX10* c.246delC mutation may be the cause of the type II WS of the proband [9]. Previous studies have suggested that type II WS patients with *SOX10* mutations have a very high spontaneous mutant rate [22].

Sensorineural hearing loss is a common clinical phenotype in WS patients with *SOX10* mutations. In the inner ear, most of the hearing loss induced by gene mutations, ototoxic drugs, and aging is caused by the hair cell malfunction [23–27]. A previous study showed that *SOX10* mutation will cause both hair cell and SC loss in a heterozygous Dom mouse model [15]. In pigs, shorter cochlear conduct was induced by *SOX10* p.Arg109Trp missense mutation [28]. There are complex regulatory networks between SCs and hair cells [29, 30]. Although *SOX10* is only expressed in SCs, it may affect the survival of hair cells by regulating the function of SCs. Therefore, more detailed observations should be made to explore the effect of the *SOX10* gene on SC function. Moreover, SC-targeted gene therapy can be tried in a murine model [31]. *SOX10* is a key transcription factor in the migration and differentiation of NCC, and its mutations lead to abnormal differentiation of NCC-derived melanocytes, which results in abnormal pigment distribution and deafness and is the main cause of WS [32]. *SOX10* can exert its

TABLE 2: The mutation of *SOX10* in WS4 probands in the literature.

Gene	Nucleotide changes	Amino acid changes	Exon	WS subtype	Reference
<i>SOX10</i>	c.1333delT	p.Ser445Glnfs*57	5	WS4	6
<i>SOX10</i>	c.1107ins19	p.Thr370Serfs*38	5	WS4	40
<i>SOX10</i>	c.752_753ins7	p.Gly252Alafs*31	5	WS4	41
<i>SOX10</i>	c.895delC	p.Gln299Serfs*12	5	WS4	5

function by binding to the promoter or enhancer of the target gene alone or together with other transcription factors. *MITF*, *TYR*, *TYRP1*, *DCT*, *MPZ*, *GJB1*, *RET*, *DCT*, and *EDNRB* are the downstream target genes directly regulated by *SOX10*. These target genes are directly or indirectly involved in melanin synthesis, among which *MITF* is a key regulatory gene for melanocyte development and melanin synthesis. *SOX10* can act alone or directly with *PAX3* to generate a coeffect to stimulate and upregulate the expression of *MITF* [12, 33]. The *SOX10* c.246delC mutation resulted in early termination of the coding protein sequence at amino acid position 108, and consequently, the mutant protein did not contain the HMG domain and the TA domain. The main function of the HMG domain is to identify and bind the promoter of the target gene [34] (Figure 4), so the heterozygous *SOX10* c.246delC mutant protein could not effectively activate the *MITF* promoter, causing a decrease in effective *MITF* protein expression, leading to an insufficient dose effect, and resulting in disordered melanocyte development and abnormal melanin synthesis. The main function of melanocytes is to produce melanin to ensure the pigmentation of hair and skin. Melanocytes developed from NCC are widely expressed in the dermis, epidermis, vascular striae of the inner ear, and choroid of the eye, and their developmental disorder will lead to WS characterized by hearing loss and abnormal distribution of pigment in the skin and hair [12, 35]. The mutation *SOX10* c.246delC (exon 2 in NM_006941) has not been reported according to the Human Gene Mutation Database (HGMD) (<http://www.hgmd.cf.ac.uk/ac/index.php>) [7].

In addition, through analysis of the reported cases and the literature, we found that when the *SOX10* mutation site occurred behind the 180th amino acid, or you could say after the HMG domain, it caused more severe symptoms of type IV WS [5, 6, 36–39] (Table 2). We speculate that the reason may be due to the truncated mutation which means that the HMG domain loses the normal function of the protein, but can combine with the target gene promoter. It then competes with the normal protein for binding sites and restrains the influence of the normal protein, leading to more serious consequences. The exact molecular mechanism remains to be confirmed.

5. Conclusion

We identified a new mutation site in the *SOX10* gene, explored the possible pathological mechanism of the clinical phenotype caused by this mutation, expanded the database of WS pathogenic gene mutations, and deepened the association between the mutation site and the clinical phenotype,

so as to further explore the molecular pathogenic mechanism of WS.

Data Availability

The data used to support the findings of this study are included within the article.

Ethical Approval

This study was reviewed and approved by the responsible committee on human experimentation (Tongji Medical College, Huazhong University of Science and Technology). No animals were used for the studies. All human procedures were conducted in accordance with the Declaration of Helsinki (1964).

Consent

Written informed consent was obtained from all participants or their guardians.

Conflicts of Interest

The authors declare that they have no competing interests.

Authors' Contributions

Sen Chen and Yuan Jin contributed equally to this work.

Acknowledgments

This work was supported by a grant from the National Nature Science Foundation of China (81771003, 81570923, 81470696, and 81500793). The authors thank the family for their participation in this study.

References

- [1] A. P. Read and V. E. Newton, "Waardenburg syndrome," *Journal of Medical Genetics*, vol. 34, no. 8, pp. 656–665, 1997.
- [2] C. S. Nayak and G. Isaacson, "Worldwide distribution of Waardenburg syndrome," *Annals of Otolaryngology, Rhinology & Laryngology*, vol. 112, no. 9, pp. 817–820, 2016.
- [3] V. Pingault, N. Bondurand, K. Kuhlbrodt et al., "SOX10 mutations in patients with Waardenburg-Hirschsprung disease," *Nature Genetics*, vol. 18, no. 2, pp. 171–173, 1998.
- [4] J. Ma, K. Lin, H. C. Jiang et al., "A novel mutation of the PAX3 gene in a Chinese family with Waardenburg syndrome type I," *Molecular Genetics & Genomic Medicine*, vol. 7, no. 7, article e00798, 2019.

- [5] A. R. Hogan, K. A. Rao, W. L. Thorson, H. L. Neville, J. E. Sola, and E. A. Perez, "Waardenburg syndrome type IV de novo SOX10 variant causing chronic intestinal pseudo-obstruction," *Pediatr Gastroenterol Hepatol Nutr*, vol. 22, no. 5, pp. 487–492, 2019.
- [6] X. Wang, Y. Zhu, N. Shen et al., "A de novo deletion mutation in SOX10 in a Chinese family with Waardenburg syndrome type 4," *Scientific Reports*, vol. 7, no. 1, 2017.
- [7] V. Pingault, D. Ente, F. Dastot-Le Moal, M. Goossens, S. Marlin, and N. Bondurand, "Review and update of mutations causing Waardenburg syndrome," *Human Mutation*, vol. 31, no. 4, pp. 391–406, 2010.
- [8] S. Issa, N. Bondurand, E. Faubert et al., "EDNRB mutations cause Waardenburg syndrome type II in the heterozygous state," *Human Mutation*, vol. 38, no. 5, pp. 581–593, 2017.
- [9] M. Elmaleh-Berges, C. Baumann, N. Noel-Petroff et al., "Spectrum of temporal bone abnormalities in patients with Waardenburg syndrome and SOX10 mutations," *AJNR. American Journal of Neuroradiology*, vol. 34, no. 6, pp. 1257–1263, 2013.
- [10] N. Suzuki, H. Mutai, F. Miya et al., "A case report of reversible generalized seizures in a patient with Waardenburg syndrome associated with a novel nonsense mutation in the penultimate exon of SOX10," *BMC Pediatrics*, vol. 18, no. 1, p. 171, 2018.
- [11] X. P. Wang, Z. Q. Hao, Y. L. Liu et al., "Functional analysis of a SOX10 gene mutation associated with Waardenburg syndrome II," *Biochemical and Biophysical Research Communications*, vol. 493, no. 1, pp. 258–262, 2017.
- [12] M. D. Saleem, "Biology of human melanocyte development, Piebaldism, and Waardenburg syndrome," *Pediatric Dermatology*, vol. 36, no. 1, pp. 72–84, 2019.
- [13] R. Mollaaghababa and W. J. Pavan, "The importance of having your SOX on: role of SOX10? in the development of neural crest-derived melanocytes and glia," *Oncogene*, vol. 22, no. 20, pp. 3024–3034, 2003.
- [14] R. A. Spritz, P. W. Chiang, N. Oiso, and A. Alkhateeb, "Human and mouse disorders of pigmentation," *Current Opinion in Genetics & Development*, vol. 13, no. 3, pp. 284–289, 2003.
- [15] M. Tachibana, Y. Kobayashi, and Y. Matsushima, "Mouse models for four types of Waardenburg syndrome," *Pigment Cell Research*, vol. 16, no. 5, pp. 448–454, 2003.
- [16] K.-i. Watanabe, K. Takeda, Y. Katori et al., "Expression of the Sox10 gene during mouse inner ear development," *Molecular Brain Research*, vol. 84, no. 1-2, pp. 141–145, 2000.
- [17] T. Wakaoka, T. Motohashi, H. Hayashi et al., "Tracing Sox10-expressing cells elucidates the dynamic development of the mouse inner ear," *Hearing Research*, vol. 302, pp. 17–25, 2013.
- [18] X. Hao, Y. Xing, M. W. Moore et al., "Sox10 expressing cells in the lateral wall of the aged mouse and human cochlea," *Plos One*, vol. 9, no. 6, article e97389, 2014.
- [19] Y. Y. Mao, S. Reiprich, M. Wegner, and B. Fritzsche, "Targeted deletion of Sox10 by Wnt1-cre defects neuronal migration and projection in the mouse inner ear," *Plos One*, vol. 9, no. 4, article e94580, 2014.
- [20] J. E. Reynolds, M. L. Marazita, J. M. Meyer et al., "Major-locus contributions to variability of the craniofacial feature dystopia canthorum in Waardenburg syndrome," *American Journal of Human Genetics*, vol. 58, no. 2, pp. 384–392, 1996.
- [21] M. Rosa Junior, L. M. Santana, B. F. Ramos, and H. F. Ramos, "Teaching NeuroImages: Waardenburg syndrome type 2," *Neurology*, vol. 92, no. 16, pp. e1935–e1936, 2019.
- [22] L. Sun, X. Li, J. Shi et al., "Molecular etiology and genotype-phenotype correlation of Chinese Han deaf patients with type I and type II Waardenburg syndrome," *Scientific Reports*, vol. 6, no. 1, 2016.
- [23] Z. H. He, S. Y. Zou, M. Li et al., "The nuclear transcription factor FoxG1 affects the sensitivity of mimetic aging hair cells to inflammation by regulating autophagy pathways," *Redox Biology*, vol. 28, p. 101364, 2020.
- [24] W. Liu, X. Xu, Z. Fan et al., "Wnt signaling activates TIGAR and protects against cisplatin-induced spiral ganglion neuron damage in the mouse cochlea," *Antioxidants & Redox Signaling*, vol. 30, no. 11, pp. 1389–1410, 2019.
- [25] Z. He, L. Guo, Y. Shu et al., "Autophagy protects auditory hair cells against neomycin-induced damage," *Autophagy*, vol. 13, no. 11, pp. 1884–1904, 2017.
- [26] Y. Chen, L. Liu, Y. Zhang, R. Chai, and H. Li, "Wnt activation protects against neomycin-induced hair cell damage in the mouse cochlea," *Cell Death & Disease*, vol. 130, no. S3, p. S105, 2016.
- [27] Y. Liu, J. Qi, X. Chen et al., "Critical role of spectrin in hearing development and deafness," *Science Advances*, vol. 5, no. 4, p. eaav7803, 2019.
- [28] Q. Q. Hao, L. Li, W. Chen et al., "Key genes and pathways associated with inner ear malformation in SOX10:p.R109W mutation pigs," *Frontiers in Molecular Neuroscience*, vol. 11, p. 181, 2018.
- [29] G. Wan, G. Corfas, and J. S. Stone, "Inner ear supporting cells: rethinking the silent majority," *Seminars in Cell & Developmental Biology*, vol. 24, no. 5, pp. 448–459, 2013.
- [30] S. Zhang, Y. Zhang, Y. Dong et al., "Knockdown of Foxg1 in supporting cells increases the trans-differentiation of supporting cells into hair cells in the neonatal mouse cochlea," *Cellular and Molecular Life Sciences*, vol. 77, no. 7, pp. 1401–1419, 2020.
- [31] F. Tan, C. Chu, J. Qi et al., "AAV-ie enables safe and efficient gene transfer to inner ear cells," *Nature Communications*, vol. 10, no. 1, p. 3733, 2019.
- [32] N. Bondurand and M. H. Sham, "The role of SOX10 during enteric nervous system development," *Developmental Biology*, vol. 382, no. 1, pp. 330–343, 2013.
- [33] H. Zhang, H. Chen, H. Luo et al., "Functional analysis of Waardenburg syndrome-associated PAX3 and SOX10 mutations: report of a dominant-negative SOX10 mutation in Waardenburg syndrome type II," *Human Genetics*, vol. 131, no. 3, pp. 491–503, 2012.
- [34] S. Wissmuller, T. Kosian, M. Wolf, M. Finzsch, and M. Wegner, "The high-mobility-group domain of Sox proteins interacts with DNA-binding domains of many transcription factors," *Nucleic Acids Research*, vol. 34, no. 6, pp. 1735–1744, 2006.
- [35] J. Ma, Z. Zhang, H. C. Jiang et al., "A novel dominant mutation in the SOX10 gene in a Chinese family with Waardenburg syndrome type II," *Molecular Medicine Reports*, vol. 19, no. 3, pp. 1775–1780, 2019.
- [36] J. Ma, T. S. Zhang, K. Lin et al., "Waardenburg syndrome type II in a Chinese patient caused by a novel nonsense mutation in the SOX10 gene," *International Journal of Pediatric Otorhinolaryngology*, vol. 85, pp. 56–61, 2016.
- [37] K. Chen, L. Zong, M. Liu et al., "De novo dominant mutation of SOX10 gene in a Chinese family with Waardenburg syndrome type II," *International Journal of Pediatric Otorhinolaryngology*, vol. 78, no. 6, pp. 926–929, 2014.

- [38] R. M. Fernandez, R. Nunez-Ramos, M. V. Enguix-Riego et al., "Waardenburg syndrome type 4: report of two new cases caused by SOX10 mutations in Spain," *American Journal of Medical Genetics. Part A*, vol. 164A, no. 2, pp. 542–547, 2014.
- [39] F. Liang, M. Zhao, L. Fan et al., "Identification of a de novo mutation of SOX10 in a Chinese patient with Waardenburg syndrome type IV," *International Journal of Pediatric Otorhinolaryngology*, vol. 91, pp. 67–71, 2016.

Research Article

Targeted Next-Generation Sequencing Identifies Separate Causes of Hearing Loss in One Deaf Family and Variable Clinical Manifestations for the p.R161C Mutation in *SOX10*

Xiaoyu Yu ^{1,2,3}, Yun Lin ^{1,2,3} and Hao Wu ^{1,2,3}

¹Department of Otorhinolaryngology-Head and Neck Surgery, Shanghai Ninth People's Hospital, Shanghai Jiao Tong University School of Medicine, Shanghai, China

²Ear Institute, Shanghai Jiao Tong University School of Medicine, Shanghai, China

³Shanghai Key Laboratory of Translational Medicine on Ear and Nose Diseases, Shanghai, China

Correspondence should be addressed to Hao Wu; haowu@sh-jei.org

Received 22 April 2020; Revised 6 July 2020; Accepted 13 July 2020; Published 28 August 2020

Academic Editor: Renjie Chai

Copyright © 2020 Xiaoyu Yu et al. This is an open access article distributed under the Creative Commons Attribution License, which permits unrestricted use, distribution, and reproduction in any medium, provided the original work is properly cited.

Hearing loss is the most common sensory deficit in humans. Identifying the genetic cause and genotype-phenotype correlation of hearing loss is sometimes challenging due to extensive clinical and genetic heterogeneity. In this study, we applied targeted next-generation sequencing (NGS) to resolve the genetic etiology of hearing loss in a Chinese Han family with multiple affected family members. Targeted sequencing of 415 deafness-related genes identified the heterozygous c.481C>T (p.R161C) mutation in *SOX10* and the homozygous c.235delC (p.L79Cfs*3) mutation in *GJB2* as separate pathogenic mutations in distinct affected family members. The *SOX10* c.481C>T (p.R161C) mutation has been previously reported in a Caucasian patient with Kallmann syndrome that features congenital hypogonadotropic hypogonadism with anosmia. In contrast, family members carrying the same p.R161C mutation in this study had variable Waardenburg syndrome-associated phenotypes (hearing loss and/or hair hypopigmentation) without olfactory or reproductive anomalies. Our results highlight the importance of applying comprehensive diagnostic approaches such as NGS in molecular diagnosis of hearing loss and show that the p.R161C mutation in *SOX10* may be associated with a wide range of variable clinical manifestations.

1. Introduction

Hearing loss is the most prevalent neurosensory impairment in humans, affecting over half a billion people worldwide [1, 2]. In a mammals' inner ear, cochlear hair cells (HCs) take responsibility to convert the mechanical sound waves into electrical signals [3–5], which make the HCs very important for hearing function. Many previous reports have already shown that HCs can be injured due to genetic factors, noise, ototoxic drugs, aging, or inflammation [6–13]; and it is estimated that 50%–60% of early-onset hearing loss is due to genetic factors [14, 15]. Based on the association with other clinical features, approximately 70% of genetic hearing loss is nonsyndromic and 30% is syndromic. Currently, more than 100 genes for nonsyndromic hearing loss have been identified, and over 700 different forms of syndromic hearing

impairment have been described [16, 17]. The extremely high genetic and phenotypic heterogeneity sometimes makes the diagnosis of genetic hearing loss challenging.

Mutations in *SOX10* have been associated with various forms of syndromic hearing loss. *SOX10* is a transcription factor involved in cell fate determination and cell lineage development, especially in the forming and differentiation of the neural crest [18]. A variety of mutations in *SOX10* may result in various developmental defects including type II (WS2, OMIM 611584) and type IV (WS4, OMIM 613266) Waardenburg syndrome (WS) featuring auditory and pigmentary abnormalities, with the latter also exhibiting short-segment Hirschsprung disease (HD, OMIM 142623) [19–22]. Recently, mutations in *SOX10* have been identified in a few patients with Kallmann syndrome (KS, OMIM 308700) with deafness, which is characterized by

hypogonadotropic hypogonadism, anosmia and hearing loss [23–26]. However, it remains unknown if there is a specific genotype-phenotype correlation between certain *SOX10* mutations and Kallmann syndrome.

In the present study, we applied targeted NGS to identify the genetic etiology of hearing loss in a moderate-sized Chinese Han family with apparently complex inheritance. In different affected family members, we identified separate genetic causes in recessive mutation in the *GJB2* gene and dominant mutation in the *SOX10* gene. Despite the fact that *SOX10* c.481C>T (p.R161C) mutation was previously associated with Kallmann syndrome, family members with this mutation in our study had either normal or only WS2 (hearing loss and hair hypopigmentation) phenotype, indicating a rather variable clinical manifestation.

2. Subjects and Methods

2.1. Subjects and Clinical Assessments. The proband (Figure 1(a), IV-1) with bilateral profound sensorineural hearing loss was enrolled through the Department of Otorhinolaryngology at Shanghai Ninth People's Hospital. Four other subjects (III-1, II-2, II-1, and II-2) from the four-generation family and 100 Chinese Han normal hearing controls were also included in this study. The clinical evaluation included a detailed medical history questionnaire and a thorough physical examination. Auditory evaluations were performed in all participants, including otoscopic examination, otoacoustic emissions (OAEs), auditory evoked potentials (AEPs), or pure-tone audiometry. High-resolution computerized tomography (CT) scan of the temporal bone was performed in proband IV-1. Sense of smell was evaluated by self-report, questioning, or olfactory tests. Blood sample was collected from the proband and her family members, and total DNA was extracted from peripheral blood leukocytes using standard protocols.

2.2. Ethics Statement. Written informed consent was obtained from all study participants or their guardians. All experimental procedures in this study were approved by the Ethics Committee of Shanghai Ninth People's Hospital, Shanghai Jiao Tong University School of Medicine.

2.3. Targeted Genomic Enrichment and Massively Parallel Sequencing. The quality and quantity of genomic DNA were assessed by gel electrophoresis and spectrophotometry. Libraries were prepared using the Illumina standard protocol. Targeted enrichment of all exons and flanking splicing sites of 415 genes implicated in sensorineural hearing loss (for the list of genes, see Supplementary Table S1) was completed using MyGenostics Gencap™ capture kit (MyGenostics, Baltimore, MD, USA) following the manufacturer's protocol. The enrichment libraries were sequenced on Illumina NextSeq 500 sequencer.

2.4. Bioinformatics Analysis. The high-quality reads were mapped to the human genome sequence (hg19) with a Burrows-Wheeler-Alignment Tool, and GATK Haplotype-Caller was used to detect small insertions or deletions (InDels) and Single Nucleotide Variants (SNVs) [27, 28]. The identified

SNVs and InDels were then annotated using the ANNOVAR software [29]. The missense, frameshift, nonsense, and splicing variants with a minor allele frequency < 1% were further interrogated as candidate pathogenic mutations. For allele frequencies, we used 1000 Genomes (<http://www.1000genomes.org/>), ESP6500 (<http://evs.gs.washington.edu/EVS/>), and ExAC (<http://exac.broadinstitute.org/>) databases. An ensemble tool REVEL (rare exome variant ensemble learner) was used to predict the pathogenicity of missense variants [30]. The ClinVar database and Human Gene Mutation Database (HGMD) were used to further annotate known pathogenic variants. Pathogenicity of the candidate variants was interpreted following American College of Medical Genetics and Genomics (ACMG) standards and guidelines 2015 [31].

2.5. Sanger Sequencing. The candidate variants in *SOX10* and *GJB2* gene were amplified by polymerase chain reaction (PCR) and analyzed by Sanger sequencing. The primer sequences for PCR amplification are provided in Supplementary Table S3.

3. Results

3.1. Clinical Findings. The female proband VI-1 was born from nonconsanguineous parents (Figure 1(a)). She failed the neonatal hearing screening, and further examination revealed bilateral profound sensorineural hearing loss (>95 dB, Figure 1(b)). Her computed tomography scan of the temporal bone revealed slight dilation of the posterior semicircular canals in both ears. When examined at 7 years of age, she had normal dark irides, normal fundus oculi, and no pigmentary alterations in the skin or hair. Dystopia canthorum, limb anomaly, and Hirschsprung disease were absent. Neurological examination was normal.

The proband's mother III-2 had prelingual, bilateral, profound hearing loss. Interview and visual inspection of III-2 did not find pigmentation defects and musculoskeletal anomalies. The father III-1 had normal hearing but reported to develop a white forelock at approximately 8 years of age and prematurely gray hair at 20 years of age. The paternal grandmother II-1 had severe congenital bilateral hearing loss and reported a frontal white forelock and premature graying of hair since approximately 15 years of age. All family members reported normal sense of smell, which was confirmed by olfactory tests. Both III-2 and II-1 had normal puberty and spontaneous pregnancy.

3.2. Genetic Analysis Results. Targeted next-generation sequencing of 415 deafness-related genes identified a homozygous c.235delC (p.L79Cfs*3) variant in *GJB2* as the pathogenic cause of hearing loss for the mother III-2 (Figure 2(a)). In the proband IV-1 and her father III-1, we detected 10 and 12 rare (MAF < 0.01 in public databases) heterogeneous nonsynonymous variants, respectively (Supplementary Table S2). Of these, the c.481C>T (p.R161C) variant in *SOX10* has been previously reported resulting in Kallmann syndrome in a Caucasian patient [32]. It substitutes a well-conserved arginine by cystine in the high-mobility group (HMG) domain of *SOX10* (Figure 2(b)). This variant was

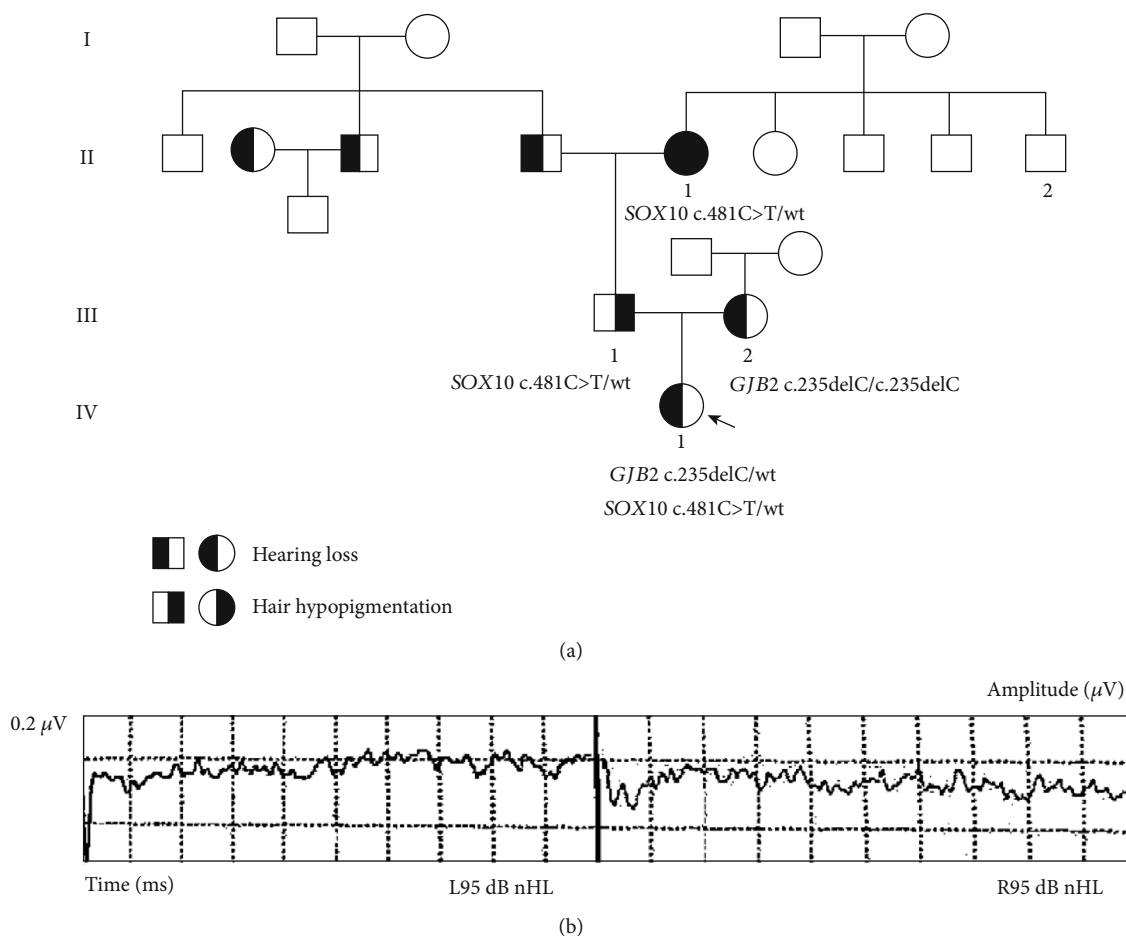


FIGURE 1: Pedigree of the family and clinical findings of the proband IV-1: (a) pedigree and genotype showing the c.481C>T (p.R161C) mutation in *SOX10* and the c.235delC (p.L79Cfs*3) mutation in *GJB2*; (b) auditory evoked potentials showing bilateral profound sensorineural hearing loss.

not observed in genotyping of 100 Chinese Han normal controls and was predicted as damaging by in silico assessment with REVEL [30]. According to the 2015 ACMG guideline, c.481C>T (p.R161C) in *SOX10* was classified as likely pathogenic (PS1+PM2). Sanger sequencing validated the presence of this variant in IV-1, III-1, and II-1, three individuals with WS-associated phenotypes (Figure 2(a)).

4. Discussion

The cause of hearing loss is extremely heterogeneous, and in many regions of the world, deaf people tend to marry with each other to form rather complex deaf families [33–40]. In one such family, we identified two separate genetic causes of hearing loss in distinct affected members, including the recessive c.235delC (p.L79Cfs*3) mutation in *GJB2* (III-2) and the dominant c.481C>T (p.R161C) mutation in *SOX10* (II-1, III-1, and IV-1). While the c.235delC (p.L79Cfs*3) mutation in *GJB2* is quite common and well characterized in East Asians, the c.481C>T (p.R161C) mutation in *SOX10*

was far less frequent and its clinical manifestations were not consistent in different reports [32, 41].

In this study, the clinical manifestations of the family members carrying the c.481C>T (p.R161C) mutation in *SOX10* are distinct along three different generations: typical WS2 phenotype (hearing loss and hair hypopigmentation) in the paternal grandmother, hair hypopigmentation only in the father, and hearing loss only in the proband. The c.481C>T (p.R161C) mutation affected the HMG domain of *SOX10*, which is the sequence-specific DNA-binding domain, and was predicted to be damaging by in silico assessment.

The same *SOX10* c.481C>T (p.R161C) mutation has previously been reported in a Caucasian patient with Kallmann syndrome, in whom the presence or absence of hearing loss and pigmentation defect was not described (Table 1) [32]. Kallmann syndrome is a developmental disease that combines congenital hypogonadotropic hypogonadism with anosmia [42]. Our patients manifested hearing loss and hair hypopigmentation, but no anosmia or delayed puberty. This phenotypic difference suggests that other factors, such as modifier gene or epigenetic events, might contribute to the

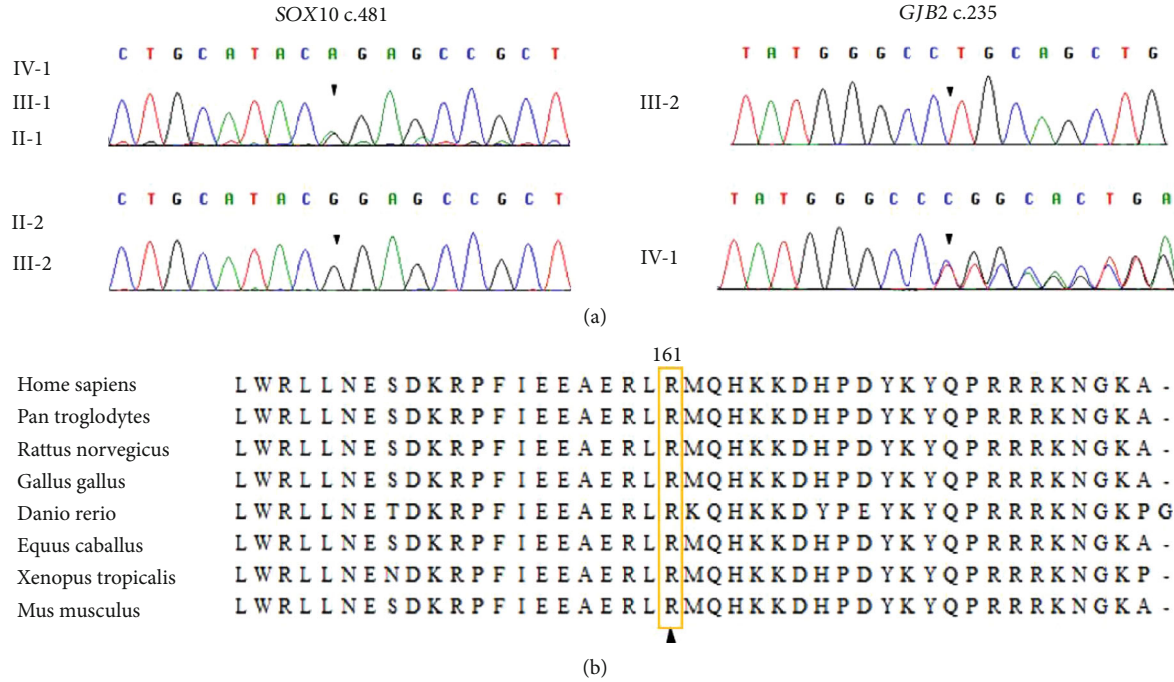


FIGURE 2: The *GJB2* c.235delC (p.L79Cfs*3) and the *SOX10* c.481C>T (p.R161C) mutations identified in the family. (a) Sequence chromatogram showing the genotyping results of the family members. The proband IV-1, her father III-1, and the grandmother II-1 had heterogeneous *SOX10* c.481C>T (p.R161C, arrow) mutation. The mother III-2 carried a homozygous *GJB2* c.235delC (p.L79Cfs*3) mutation. (b) Alignment of *SOX10* sequences from various species showing conservation of the arginine residue at position 161.

TABLE 1: Summary of clinical findings in patients with *SOX10* c.481C>T (p.R161C) mutation.

Patient	IV-1	III-1	II-1	Marcos et al.[32]	Bademci et al.[41]
Age	7 y	34 y	60 y	n.d.	9 y; 11 y
Gender	F	M	F	n.d.	F; M
Hearing loss/inner ear imaging					
Hearing loss	Profound	—	Profound	n.d.	Profound
Abnormal semicircular canal	Post. SCC dilatation	NA	NA	n.d.	n.d.
Pigmentation defects					
Pigmentary disturbances of iris	—	—	—	n.d.	n.d.
Iris heterochromia	—	—	—	n.d.	n.d.
Skin depigmentation	—	—	—	n.d.	n.d.
White forelock	—	+	+	n.d.	n.d.
Premature graying	—	+	+	n.d.	n.d.
Eye anomalies					
Telecanthus	—	—	—	n.d.	n.d.
Retinal pigmentation defect	—	—	—	n.d.	n.d.
Gastrointestine					
Constipation	—	—	—	n.d.	n.d.
Hirschsprung disease	—	—	—	n.d.	n.d.
Hypogonadotropic hypogonadism					
Delayed puberty	NA	—	—	+	n.d.
Anosmia or severe hyposmia	—	—	—	+	n.d.
Genetic					
<i>SOX10</i> mutation	c.481C>T	c.481C>T	c.481C>T	c.481C>T	c.481C>T

n.d.: not described; NA: not applicable; y: year.

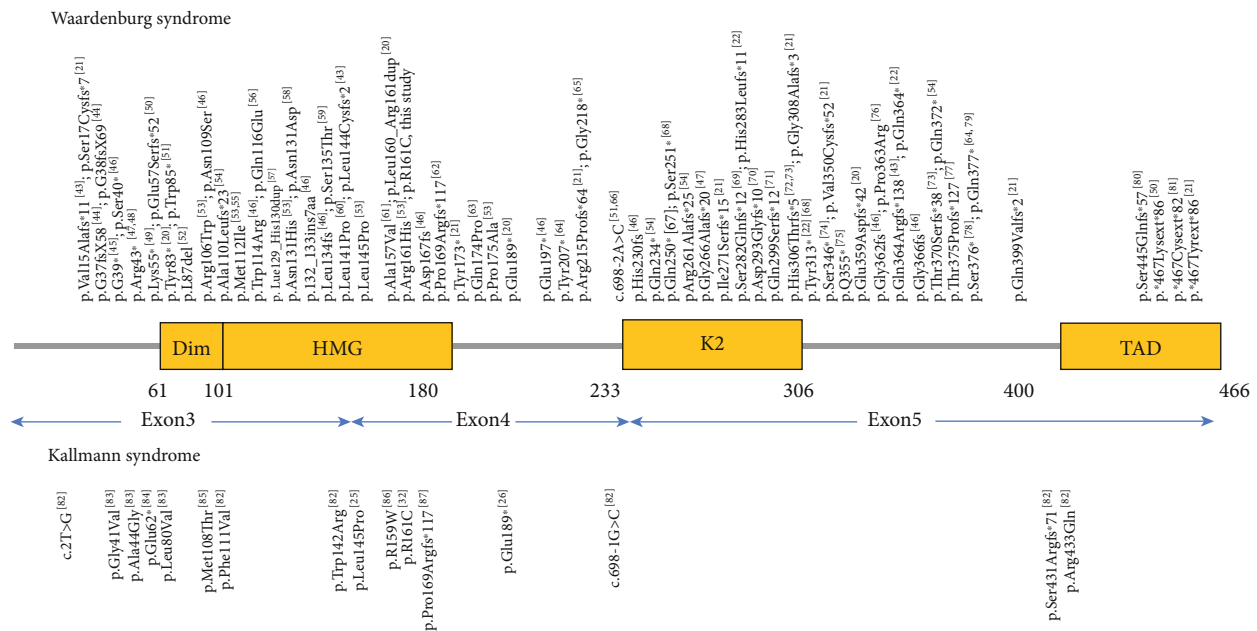


FIGURE 3: Schematic representation of the SOX10 domains and overview of SOX10 mutations and their associated phenotypes.

expression of the KS phenotypes. To date, the SOX10 c.481C>T (p.R161C) mutation has been identified in six patients from three families (Table 1) [32, 41]. Hearing loss was observed in four of the six patients and seems to be a consistent feature in mutation carriers, while hypogonadism and anosmia symptoms were described only in one patient.

Most of SOX10 mutations are private and were identified in sporadic cases, making it difficult to correlate the genotypes with the distinct disease phenotypes. Herein, we identified a KS-associated SOX10 mutation in a family with WS2, indicating that the same SOX10 mutation can underlie both WS and KS. Among over 80 published SOX10 mutations, three (p.Leu145Pro, p.Pro169Argfs*117 and p.Glu189*) were also found to lead to different phenotypes (Figure 3) [43–87]. Further investigation is needed to clarify the underlying mechanisms of incomplete penetrance and high phenotypic variability caused by SOX10 mutations.

Our study also demonstrates that targeted NGS is a powerful strategy to discover causative genes in rare, heterogeneous disorders such as hearing loss. WS caused by SOX10 mutations can resemble nonsyndromic hearing loss in young children who do not present with pigmentary abnormality. Targeted NGS has the potential to identify such mutations which would improve the management of hearing loss by genetic counseling for the children and risk assessment of the relatives.

Data Availability

The data supporting the findings of this study are available within the article and the supplementary files.

Conflicts of Interest

The authors declare that they have no competing interests.

Authors' Contributions

Hao Wu was responsible for the conceptualization, funding acquisition, project administration, supervision, writing, review, and editing. Xiaoyu Yu and Yun Lin were responsible for the formal analysis and investigation. Xiaoyu Yu was responsible for the writing of the original draft.

Acknowledgments

This research was supported by grants from the National Natural Science Foundation of China (81730028 to HW) and Shanghai Municipal Science and Technology Commission (14DZ2260300 to HW).

Supplementary Materials

Supplementary Table S1: a list of 415 deafness-related genes included in the targeted gene panel. Supplementary Table S2: candidate variants identified by targeted NGS in the proband VI-1 and her parents III-1 and III-2. Supplementary Table S3: primers used in this study. (*Supplementary Materials*)

References

- [1] A. M. Sheffield and R. J. H. Smith, "The epidemiology of deafness," *Cold Spring Harbor Perspectives in Medicine*, vol. 9, no. 9, 2019.
- [2] B. S. Wilson, D. L. Tucci, M. H. Merson, and G. M. O'Donoghue, "Global hearing health care: new findings and perspectives," *Lancet*, vol. 390, no. 10111, pp. 2503–2515, 2017.
- [3] Y. Liu, J. Qi, X. Chen et al., "Critical role of spectrin in hearing development and deafness," *Science Advances*, vol. 5, no. 4, p. eaav7803, 2019.

- [4] Y. Wang, J. Li, X. Yao et al., “Loss of CIB2 causes profound hearing loss and abolishes mechano-electrical transduction in mice,” *Frontiers in Molecular Neuroscience*, vol. 10, p. 401, 2017.
- [5] C. Zhu, C. Cheng, Y. Wang et al., “Loss of ARHGEF6 causes hair cell stereocilia deficits and hearing loss in mice,” *Frontiers in Molecular Neuroscience*, vol. 11, p. 362, 2018.
- [6] Z.-h. He, S.-y. Zou, M. Li et al., “The nuclear transcription factor FoxG1 affects the sensitivity of mimetic aging hair cells to inflammation by regulating autophagy pathways,” *Redox Biology*, vol. 28, p. 101364, 2020.
- [7] S. Gao, C. Cheng, M. Wang et al., “Blebbistatin inhibits neomycin-induced apoptosis in hair cell-like HEI-OC-1 cells and in cochlear hair cells,” *Frontiers in Cellular Neuroscience*, vol. 13, 2020.
- [8] Y. Zhang, W. Li, Z. He et al., “Pre-treatment with fasudil prevents neomycin-induced hair cell damage by reducing the accumulation of reactive oxygen species,” *Frontiers in Molecular Neuroscience*, vol. 12, p. 264, 2019.
- [9] W. Liu, X. Xu, Z. Fan et al., “Wnt signaling activates TP53-induced glycolysis and apoptosis regulator and protects against cisplatin-induced spiral ganglion neuron damage in the mouse cochlea,” *Antioxidants & Redox Signaling*, vol. 30, no. 11, pp. 1389–1410, 2019.
- [10] L. Liu, Y. Chen, J. Qi et al., “Wnt activation protects against neomycin-induced hair cell damage in the mouse cochlea,” *Cell Death & Disease*, vol. 7, no. 3, article e2136, 2016.
- [11] H. Li, Y. Song, Z. He et al., “Meclofenamic acid reduces reactive oxygen species accumulation and apoptosis, inhibits excessive autophagy, and protects hair cell-like HEI-OC1 cells from cisplatin-induced damage,” *Frontiers in Cellular Neuroscience*, vol. 12, p. 139, 2018.
- [12] S. Zhang, Y. Zhang, Y. Dong et al., “Knockdown of Foxg1 in supporting cells increases the trans-differentiation of supporting cells into hair cells in the neonatal mouse cochlea,” *Cellular and Molecular Life Sciences : CMLS*, vol. 77, no. 7, pp. 1401–1419, 2020.
- [13] Z. He, L. Guo, Y. Shu et al., “Autophagy protects auditory hair cells against neomycin-induced damage,” *Autophagy*, vol. 13, no. 11, pp. 1884–1904, 2017.
- [14] W. E. Nance, “The genetics of deafness,” *Mental Retardation and Developmental Disabilities Research Reviews*, vol. 9, no. 2, pp. 109–119, 2003.
- [15] K. W. Chang, “Genetics of hearing loss—nonsyndromic,” *Otolaryngologic Clinics of North America*, vol. 48, no. 6, pp. 1063–1072, 2015.
- [16] R. J. Gorlin, R. J. Gorlin, H. V. Toriello, and M. M. Cohen, *Hereditary Hearing Loss and Its Syndromes*, Oxford University Press, 1995.
- [17] T. Koffler, K. Ushakov, and K. B. Avraham, “Genetics of hearing loss: syndromic,” *Otolaryngologic Clinics of North America*, vol. 48, no. 6, pp. 1041–1061, 2015.
- [18] K. Kuhlbrodt, B. Herbarth, E. Sock, I. Hermans-Borgmeyer, and M. Wegner, “Sox10, a novel transcriptional modulator in glial cells,” *The Journal of neuroscience : the official journal of the Society for Neuroscience*, vol. 18, no. 1, pp. 237–250, 1998.
- [19] N. Bondurand, F. Dastot-le Moal, L. Stanchina et al., “Deletions at the SOX10 gene locus cause Waardenburg syndrome types 2 and 4,” *American Journal of Human Genetics*, vol. 81, no. 6, pp. 1169–1185, 2007.
- [20] V. Pingault, N. Bondurand, K. Kuhlbrodt et al., “SOX10 mutations in patients with Waardenburg-Hirschsprung disease,” *Nature Genetics*, vol. 18, no. 2, pp. 171–173, 1998.
- [21] V. Pingault, D. Ente, F. Dastot-Le Moal, M. Goossens, S. Marlin, and N. Bondurand, “Review and update of mutations causing Waardenburg syndrome,” *Human Mutation*, vol. 31, no. 4, pp. 391–406, 2010.
- [22] K. Inoue, M. Khajavi, T. Ohyama et al., “Molecular mechanism for distinct neurological phenotypes conveyed by allelic truncating mutations,” *Nature Genetics*, vol. 36, no. 4, pp. 361–369, 2004.
- [23] A. K. Topaloglu and L. D. Kotan, “Genetics of hypogonadotropic hypogonadism,” *Endocrine development*, vol. 29, pp. 36–49, 2016.
- [24] P. Barraud, J. A. St John, C. C. Stolt, M. Wegner, and C. V. Baker, “Olfactory ensheathing glia are required for embryonic olfactory axon targeting and the migration of gonadotropin-releasing hormone neurons,” *Biology open*, vol. 2, no. 7, pp. 750–759, 2013.
- [25] E. Suzuki, Y. Izumi, Y. Chiba et al., “Loss-of-function SOX10 mutation in a patient with Kallmann syndrome, hearing loss, and iris hypopigmentation,” *Hormone Research in Paediatrics*, vol. 84, no. 3, pp. 212–216, 2015.
- [26] F. Wang, S. Zhao, Y. Xie, W. Yang, and Z. Mo, “De novo SOX10 nonsense mutation in a patient with Kallmann syndrome, deafness, iris hypopigmentation, and hyperthyroidism,” *Annals of Clinical and Laboratory Science*, vol. 48, no. 2, pp. 248–252, 2018.
- [27] H. Li and R. Durbin, “Fast and accurate short read alignment with Burrows–Wheeler transform,” *Bioinformatics*, vol. 25, no. 14, pp. 1754–1760, 2009.
- [28] A. McKenna, M. Hanna, E. Banks et al., “The Genome Analysis Toolkit: a MapReduce framework for analyzing next-generation DNA sequencing data,” *Genome Research*, vol. 20, no. 9, pp. 1297–1303, 2010.
- [29] K. Wang, M. Li, and H. Hakonarson, “ANNOVAR: functional annotation of genetic variants from high-throughput sequencing data,” *Nucleic Acids Research*, vol. 38, no. 16, article e164, 2010.
- [30] N. M. Ioannidis, J. H. Rothstein, V. Pejaver et al., “REVEL: an ensemble method for predicting the pathogenicity of rare missense variants,” *American Journal of Human Genetics*, vol. 99, no. 4, pp. 877–885, 2016.
- [31] S. Richards, on behalf of the ACMG Laboratory Quality Assurance Committee, N. Aziz et al., “Standards and guidelines for the interpretation of sequence variants: a joint consensus recommendation of the American College of Medical Genetics and Genomics and the Association for Molecular Pathology,” *Genetics in Medicine*, vol. 17, no. 5, pp. 405–423, 2015.
- [32] S. Marcos, J. Sarfati, C. Leroy et al., “The prevalence of CHD7 missense versus truncating mutations is higher in patients with Kallmann syndrome than in typical CHARGE patients,” *The Journal of Clinical Endocrinology and Metabolism*, vol. 99, no. 10, pp. E2138–E2143, 2014.
- [33] S. Sun, M. Sun, Y. Zhang et al., “In vivo overexpression of X-linked inhibitor of apoptosis protein protects against neomycin-induced hair cell loss in the apical turn of the cochlea during the ototoxic-sensitive period,” *Frontiers in Cellular Neuroscience*, vol. 8, 2014.
- [34] T. Wang, R. Chai, G. S. Kim et al., “Lgr5+ cells regenerate hair cells via proliferation and direct transdifferentiation in

- damaged neonatal mouse utricle,” *Nature Communications*, vol. 6, no. 1, 2015.
- [35] F. Tan, C. Chu, J. Qi et al., “AAV-ie enables safe and efficient gene transfer to inner ear cells,” *Nature Communications*, vol. 10, no. 1, p. 3733, 2019.
- [36] Z. He, et al. S. Sun, M. Waqas et al., “Reduced TRMU expression increases the sensitivity of hair-cell-like HEI-OC-1 cells to neomycin damage in vitro,” *Scientific Reports*, vol. 6, no. 1, 2016.
- [37] X. Yu, W. Liu, Z. Fan et al., “c-Myb knockdown increases the neomycin-induced damage to hair-cell-like HEI-OC1 cells in vitro,” *Scientific Reports*, vol. 7, no. 1, 2017.
- [38] Z. He, Q. Fang, H. Li et al., “The role of FOXP1 in the postnatal development and survival of mouse cochlear hair cells,” *Neuropharmacology*, vol. 144, pp. 43–57, 2019.
- [39] J. Qi, Y. Liu, C. Chu et al., “A cytoskeleton structure revealed by super-resolution fluorescence imaging in inner ear hair cells,” *Cell Discovery*, vol. 5, no. 1, 2019.
- [40] J. Qi, L. Zhang, F. Tan et al., “Espin distribution as revealed by super-resolution microscopy of stereocilia,” *American Journal of Translational Research*, vol. 12, no. 1, pp. 130–141, 2020.
- [41] G. Bademci, F. B. Cengiz, J. Foster II et al., “Variations in multiple syndromic deafness genes mimic non-syndromic hearing loss,” *Scientific Reports*, vol. 6, no. 1, 2016.
- [42] C. Dodé and J.-P. Hardelin, “Kallmann syndrome,” *European Journal of Human Genetics*, vol. 17, no. 2, pp. 139–146, 2009.
- [43] M. A. P. Bocángel, U. S. Melo, L. U. Alves et al., “Waardenburg syndrome: novel mutations in a large Brazilian sample,” *European Journal of Medical Genetics*, vol. 61, no. 6, pp. 348–354, 2018.
- [44] H. Chen, L. Jiang, Z. Xie et al., “Novel mutations of PAX3, MITF, and SOX10 genes in Chinese patients with type I or type II Waardenburg syndrome,” *Biochemical and Biophysical Research Communications*, vol. 397, no. 1, pp. 70–74, 2010.
- [45] Y. Arimoto, K. Namba, A. Nakano, and T. Matsunaga, “Chronic constipation recognized as a sign of a SOX10 mutation in a patient with Waardenburg syndrome,” *Gene*, vol. 540, no. 2, pp. 258–262, 2014.
- [46] L. Sun, X. Li, J. Shi et al., “Molecular etiology and genotype-phenotype correlation of Chinese Han deaf patients with type I and type II Waardenburg syndrome,” *Scientific Reports*, vol. 6, no. 1, 2016.
- [47] V. Pingault, A. Guiochon-Mantel, N. Bondurand et al., “Peripheral neuropathy with hypomyelination, chronic intestinal pseudo-obstruction and deafness: a developmental “neural crest syndrome” related to a SOX10 mutation,” *Annals of Neurology*, vol. 48, no. 4, pp. 671–676, 2000.
- [48] J. Ma, Z. Zhang, H. C. Jiang et al., “A novel dominant mutation in the SOX10 gene in a Chinese family with Waardenburg syndrome type II,” *Molecular Medicine Reports*, vol. 19, no. 3, pp. 1775–1780, 2019.
- [49] J. Ma, T. S. Zhang, K. Lin et al., “Waardenburg syndrome type II in a Chinese patient caused by a novel nonsense mutation in the SOX10 gene,” *International Journal of Pediatric Otorhinolaryngology*, vol. 85, pp. 56–61, 2016.
- [50] M. H. Sham, V. C. Lui, B. L. Chen, M. Fu, and P. K. Tam, “Novel mutations of SOX10 suggest a dominant negative role in Waardenburg-Shah syndrome,” *Journal of Medical Genetics*, vol. 38, no. 9, article E30, pp. 30e–330, 2001.
- [51] L. Jiang, H. Chen, W. Jiang et al., “Novel mutations in the SOX10 gene in the first two Chinese cases of type IV Waardenburg syndrome,” *Biochemical and Biophysical Research Communications*, vol. 408, no. 4, pp. 620–624, 2011.
- [52] K. Chen, L. Zong, M. Liu et al., “De novo dominant mutation of SOX10 gene in a Chinese family with Waardenburg syndrome type II,” *International Journal of Pediatric Otorhinolaryngology*, vol. 78, no. 6, pp. 926–929, 2014.
- [53] A. Chaoui, Y. Watanabe, R. Touraine et al., “Identification and functional analysis of SOX10 missense mutations in different subtypes of Waardenburg syndrome,” *Human Mutation*, vol. 32, no. 12, pp. 1436–1449, 2011.
- [54] V. Pingault, M. Girard, N. Bondurand et al., “SOX10 mutations in chronic intestinal pseudo-obstruction suggest a complex physiopathological mechanism,” *Human Genetics*, vol. 111, no. 2, pp. 198–206, 2002.
- [55] V. Pingault, L. Pierre-Louis, A. Chaoui et al., “Phenotypic similarities and differences in patients with a p.Met112Ile mutation in SOX10,” *American Journal of Medical Genetics Part A*, vol. 164a, no. 9, pp. 2344–2350, 2014.
- [56] P. Bogdanova-Mihaylova, M. D. Alexander, R. P. J. Murphy, and S. M. Murphy, “Waardenburg syndrome: a rare cause of inherited neuropathy due to SOX10 mutation,” *Journal of the Peripheral Nervous System : JPNS*, vol. 22, no. 3, pp. 219–223, 2017.
- [57] A. Hemmi, K. Okamura, R. Tazawa et al., “Waardenburg syndrome type IIE in a Japanese patient caused by a novel non-frame-shift duplication mutation in the SOX10 gene,” *The Journal of Dermatology*, vol. 45, no. 5, pp. e110–e111, 2018.
- [58] K. Okamura, N. Oiso, G. Tamiya et al., “Waardenburg syndrome type IIE in a Japanese patient caused by a novel missense mutation in the SOX10 gene,” *The Journal of Dermatology*, vol. 42, no. 12, pp. 1211–1212, 2015.
- [59] N. Bondurand, K. Kuhlbrodt, V. Pingault et al., “A molecular analysis of the Yemenite deaf-blind hypopigmentation syndrome: SOX10 dysfunction causes different neurocristopathies,” *Human Molecular Genetics*, vol. 8, no. 9, pp. 1785–1789, 1999.
- [60] N. Jalilian, M. A. Tabatabaiefar, H. Alimadadi, and M. R. Noori-Dalooi, “SOX10 mutation causes Waardenburg syndrome associated with distinctive phenotypic features in an Iranian family: a clue for phenotype-directed genetic analysis,” *International Journal of Pediatric Otorhinolaryngology*, vol. 96, pp. 122–126, 2017.
- [61] M. Morín, A. Viñuela, T. Rivera et al., “A de novo missense mutation in the gene encoding the SOX10 transcription factor in a Spanish sporadic case of Waardenburg syndrome type IV,” *American Journal of Medical Genetics Part A*, vol. 146a, no. 8, pp. 1032–1037, 2008.
- [62] M. Iso, M. Fukami, R. Horikawa, N. Azuma, N. Kawashiro, and T. Ogata, “SOX10 mutation in Waardenburg syndrome type II,” *American Journal of Medical Genetics Part A*, vol. 146a, no. 16, pp. 2162–2163, 2008.
- [63] C. P. Barnett, R. Mendoza-Londono, S. Blaser et al., “Aplasia of cochlear nerves and olfactory bulbs in association with SOX10 mutation,” *American Journal of Medical Genetics Part A*, vol. 149a, no. 3, pp. 431–436, 2009.
- [64] E. M. Southard-Smith, M. Angrist, J. S. Ellison et al., “The Sox10(Dom) mouse: modeling the genetic variation of Waardenburg-Shah (WS4) syndrome,” *Genome Research*, vol. 9, no. 3, pp. 215–225, 1999.
- [65] N. Suzuki, H. Mutai, F. Miya et al., “A case report of reversible generalized seizures in a patient with Waardenburg syndrome

- associated with a novel nonsense mutation in the penultimate exon of SOX10," *BMC Pediatrics*, vol. 18, no. 1, p. 171, 2018.
- [66] Y. Sznajder, C. Coldéa, F. Meire, I. Delpierre, T. Sekhara, and R. L. Touraine, "A de novo SOX10 mutation causing severe type 4 Waardenburg syndrome without Hirschsprung disease," *American Journal of Medical Genetics Part A*, vol. 146a, no. 8, pp. 1038–1041, 2008.
- [67] K. Inoue, K. Shilo, C. F. Boerkoel et al., "Congenital hypomyelinating neuropathy, central dysmyelination, and Waardenburg-Hirschsprung disease: phenotypes linked by SOX10 mutation," *Annals of Neurology*, vol. 52, no. 6, pp. 836–842, 2002.
- [68] R. L. Touraine, T. Attié-Bitach, E. Manceau et al., "Neurological phenotype in Waardenburg syndrome type 4 correlates with novel SOX10 truncating mutations and expression in developing brain," *American Journal of Human Genetics*, vol. 66, no. 5, pp. 1496–1503, 2000.
- [69] Y. Akutsu, K. Shirai, A. Takei et al., "A patient with peripheral demyelinating neuropathy, central dysmyelinating leukodystrophy, Waardenburg syndrome, and severe hypoganglionosis associated with a novel SOX10 mutation," *American Journal of Medical Genetics Part A*, vol. 176, no. 5, pp. 1195–1199, 2018.
- [70] A. Unzicker, V. Pingault, T. Meyer, S. Rauthe, A. Schütz, and S. Kunzmann, "A novel SOX10 mutation in a patient with PCWH who developed hypoxic-ischemic encephalopathy after *E. coli* sepsis," *European Journal of Pediatrics*, vol. 170, no. 11, pp. 1475–1480, 2011.
- [71] A. R. Hogan, K. A. Rao, W. L. Thorson, H. L. Neville, J. E. Sola, and E. A. Perez, "Waardenburg syndrome type IV de novo SOX10 variant causing chronic intestinal pseudo-obstruction," *Pediatric Gastroenterology, Hepatology & Nutrition*, vol. 22, no. 5, pp. 487–492, 2019.
- [72] A. Viñuela, M. Morín, M. Villamar et al., "Genetic and phenotypic heterogeneity in two novel cases of Waardenburg syndrome type IV," *American Journal of Medical Genetics Part A*, vol. 149a, no. 10, pp. 2296–2302, 2009.
- [73] R. M. Fernández, R. Núñez-Ramos, M. V. Enguix-Riego et al., "Waardenburg syndrome type 4: report of two new cases caused by SOX10 mutations in Spain," *American Journal of Medical Genetics Part A*, vol. 164a, no. 2, pp. 542–547, 2014.
- [74] J. B. G. M. Verheij, D. A. Sival, J. H. van der Hoeven et al., "Shah-Waardenburg syndrome and PCWH associated with SOX10 mutations: a case report and review of the literature," *European Journal of Paediatric Neurology*, vol. 10, no. 1, pp. 11–17, 2006.
- [75] H. H. Wang, H. S. Chen, H. B. Li et al., "Identification and functional analysis of a novel mutation in the SOX10 gene associated with Waardenburg syndrome type IV," *Gene*, vol. 538, no. 1, pp. 36–41, 2014.
- [76] H. J. Jung, S. A. Jin, S. J. N. Choi, S. C. Lee, and S. J. Yun, "A de novo SOX10 mutation in a patient with Waardenburg syndrome type IV," *Journal of the American Academy of Dermatology*, vol. 68, no. 6, pp. e177–e178, 2013.
- [77] S. B. Minami, K. Nara, H. Mutai et al., "A clinical and genetic study of 16 Japanese families with Waardenburg syndrome," *Gene*, vol. 704, pp. 86–90, 2019.
- [78] F. Toki, N. Suzuki, K. Inoue et al., "Intestinal aganglionosis associated with the Waardenburg syndrome: report of two cases and review of the literature," *Pediatric Surgery International*, vol. 19, no. 11, pp. 725–728, 2003.
- [79] T. Oshimo, K. Fukai, Y. Abe et al., "Pediatric case report: clinical profile of a patient with PCWH with p.Q377X nonsense mutation in the SOX10 gene," *The Journal of Dermatology*, vol. 39, no. 12, pp. 1022–1025, 2012.
- [80] X. Wang, Y. Zhu, N. Shen et al., "A de novo deletion mutation in SOX10 in a Chinese family with Waardenburg syndrome type 4," *Scientific Reports*, vol. 7, no. 1, 2017.
- [81] K. Inoue, Y. Tanabe, and J. R. Lupski, "Myelin deficiencies in both the central and the peripheral nervous systems associated with a SOX10 mutation," *Annals of Neurology*, vol. 46, no. 3, pp. 313–318, 1999.
- [82] V. Pingault, V. Bodereau, V. Baral et al., "Loss-of-function mutations in SOX10 cause Kallmann syndrome with deafness," *American Journal of Human Genetics*, vol. 92, no. 5, pp. 707–724, 2013.
- [83] W. Dai, J. Wu, Y. Zhao et al., "Functional analysis of SOX10 mutations identified in Chinese patients with Kallmann syndrome," *Gene*, vol. 702, pp. 99–106, 2019.
- [84] K. Vaaralahti, J. Tommiska, V. Tillmann et al., "De novo SOX10 nonsense mutation in a patient with Kallmann syndrome and hearing loss," *Pediatric Research*, vol. 76, no. 1, pp. 115–116, 2014.
- [85] L. Maione, S. Brailly-Tabard, J. Nevoux, J. Bouligand, and J. Young, "Reversal of congenital hypogonadotropic hypogonadism in a man with Kallmann syndrome due to SOX10 mutation," *Clinical Endocrinology*, vol. 85, no. 6, pp. 988–989, 2016.
- [86] Q. Zhang, H. H. He, M. U. Janjua et al., "Identification of two novel mutations in three Chinese families with Kallmann syndrome using whole exome sequencing," *Andrologia*, vol. 52, no. 7, article e13594, 2020.
- [87] Y. Izumi, I. Musha, E. Suzuki et al., "Hypogonadotropic hypogonadism in a female patient previously diagnosed as having Waardenburg syndrome due to a sox10 mutation," *Endocrine*, vol. 49, no. 2, pp. 553–556, 2015.

Research Article

Transcript Profiles of Stria Vascularis in Models of Waardenburg Syndrome

Linjun Chen,¹ Lin Wang,² Lei Chen,³ Fangyuan Wang,^{1,4,5,6} Fei Ji,^{1,4,5,6} Wei Sun,⁷
Hui Zhao ^{1,4,5,6} Weiju Han ^{1,4,5,6} and Shiming Yang ^{1,4,5,6}

¹College of Otolaryngology Head and Neck Surgery, Chinese PLA General Hospital, Beijing, China

²Nursing Department, Hainan Hospital of Chinese PLA General Hospital, Sanya 572013, China

³Chongqing Academy of Animal Science, Chongqing 402460, China

⁴National Clinical Research Center for Otolaryngologic Diseases, Beijing, China

⁵Key Lab of Hearing Science, Ministry of Education, China

⁶Beijing Key Lab of Hearing Impairment for Prevention and Treatment, Beijing, China

⁷Department of Communicative Disorders and Sciences, Center for Hearing and Deafness, The State University of New York at Buffalo, Buffalo, New York, USA

Correspondence should be addressed to Hui Zhao; huizhao301ent@163.com, Weiju Han; hanweiju@aliyun.com, and Shiming Yang; shm_yang@163.com

Received 24 February 2020; Revised 18 May 2020; Accepted 26 June 2020; Published 1 August 2020

Academic Editor: Geng lin Li

Copyright © 2020 Linjun Chen et al. This is an open access article distributed under the Creative Commons Attribution License, which permits unrestricted use, distribution, and reproduction in any medium, provided the original work is properly cited.

Background. Waardenburg syndrome is an uncommon genetic condition characterized by at least some degree of congenital hearing loss and pigmentation deficiencies. However, the genetic pathway affecting the development of stria vascularis is not fully illustrated. **Methods.** The transcript profile of stria vascularis of Waardenburg syndrome was studied using Mitf-M mutant pig and mice models. Therefore, GO analysis was performed to identify the differential gene expression caused by Mitf-M mutation. **Results.** There were 113 genes in tyrosine metabolism, melanin formation, and ion transportations showed significant changes in pig models and 191 genes in mice models. In addition, there were some species-specific gene changes in the stria vascularis in the mouse and porcine models. The expression of tight junction-associated genes, including *Cadm1*, *Cldn11*, *Pcdh1*, *Pcdh19*, and *Cdh24* genes, were significantly higher in porcine models compared to mouse models. Vascular-related and ion channel-related genes in the stria vascularis were also shown significant difference between the two species. The expression of *Col2a1*, *Col3a1*, *Col11a1*, and *Col11a2* genes were higher, and the expression of *Col8a2*, *Cd34*, and *Ncam* genes were lower in the porcine models compared to mouse models. **Conclusions.** Our data suggests that there is a significant difference on the gene expression and function between these two models.

1. Background

Waardenburg syndrome (WS) is a rare genetic condition characterized by at least some degree of congenital hearing loss and pigmentation deficiencies [1]. WS has more than 20 mutations in the *Mitf* allele [2, 3], including *Mitf*^{mi-vga9}, *Mitf*^{mi-bw}, and *Mitf*^{mi-ce}, which have been identified to cause hearing loss and changes in pigmentation. Although the mouse model is widely used in disease phenotypes and pathogenic mechanisms of deafness-related research [4–8], many shortcomings have also been found in studying human

genetic diseases. As there is a tremendous evolutionary difference between mouse and human, it may cause a huge biological difference in anatomy, energy metabolism, and auditory perception [9, 10]. For example, the developmental patterns of auditory organs are different in mice and humans: human's hearing developed before birth while mouse's hearing did not fully develop until two weeks after birth [11]. Some studies [4, 12] found that human embryonic developmental diseases are difficult to be replicated in some of the mouse models. Therefore, different animal models, such as cattle [13], horses [14], dogs [15, 16], and pigs [17] were also

necessary to be used to study genetic diseases. Pigs are precocial species with fully developed auditory system at birth. Recent studies also found the cochlear anatomy is very similar to human [18–21]. As pigs are large-scale animals with high reproductive efficiency and economical convenience, it is a good model for study auditory genetic diseases [22–24].

The stria vascularis plays an important role in maintaining the cochlear endolymphatic potentials (EP) which is essential for the mechanical electrical conduction of the hair cells [25–29]. The stria vascularis is composed with the macrophage-like melanocytes, which also called the intermediate cells [28, 30, 31]. The potassium ions in the Scala media are produced by the intermediate cells and several potassium channels and transporters in the lateral wall, such as KCNQ1/KCNE1, KCNQ4, KCNN2, KCNJ10, and SLC12A2, are also involved in maintaining the endolymphatic potentials [26, 32–34]. When malfunction of stria vascularis will result in hearing loss [35]. For example, Marcus [36] reported that *Kcnj10* knockout can decrease EP value from +80 mV to 1 mV, and the K⁺ concentration decrease from 110 mM to 60 mM in their mouse models. In our previous studies, we found that *Mitf-M* knockout can decrease the EP to 18 mV in the mouse model [37]. In the *Mitf* knockout pig model, we found that the *Mitf* mutation caused the value of EP dropped from +78 mV to +3 mV, which was lower than the mouse model [18]. In the wild type pig, the potassium concentration in the endolymph was 142 mM higher than those in the perilymph. Our previous study found the potassium concentration dropped to 0 mM in the *Mitf* mutant pigs [18]. We expect that there may be different genes in maintaining the EP in mice and pigs, and the mutation of *Mitf* gene may cause a different change in potassium channels. To answer these questions, this study attempted to detect changes in the genetic profiles of these two species caused by *Mitf-M* gene mutation in RNA transcriptome level. As most of the current researches only use mouse models, this paper will further detect the RNA transcriptome difference in the stria vascularis between the large animals and mouse models.

2. Results

2.1. Gene Expression Changes Caused by *Mitf-M* Mutation.

The activation of different genes in the stria vascularis of pigs and mice caused by the *Mitf-M* mutation compared to their W/T controls were screened using the DESeq package software. The conditions for screening differential genes were corrected *p* value <0.05. The intersections of the differential genes in the pigs and mice were obtained using the Venn diagrams. The results were shown in Table 1. There were 14 common differential genes between the *Mitf* mutant animals and the controls. There were 177 specific differential genes in mouse model and 99 specific differential genes in pig models (Figure 1).

The GO analysis and the KEGG pathway analysis were performed on the David Database (adjusted *p* value <0.05). The results were shown in Figure 2. The main pathway caused by *Mitf* mutation was the KEGG pathway, enriched in the tyrosine metabolism (mmu00350) and the melanogen-

TABLE 1: The common DEGs in pigs/mice with/without *Mitf-M* mutation.

Gene_Name	hom_pig	het_pig	MM_mouse	WW_mouse
<i>Tyr</i>	0.014667	9.40833	0.00233	37.4824
<i>Emilin2</i>	65.6574	36.3192	52.3576	20.7289
<i>Gsn</i>	199.663	289.825	64.9488	223.727
<i>Dct</i>	1.09829	135.912	0.00277	774.431
<i>GpnmB</i>	2.22801	47.8019	1.14682	86.5487
<i>Ednrb</i>	1.19691	12.2565	1.66075	26.9099
<i>Ucma</i>	198.465	285.077	256.207	523.427
<i>Slc45a2</i>	0.793729	24.5716	3.9E-07	45.1788
<i>Tspan10</i>	3.93361	18.2708	0.036796	14.1373
<i>Clca2</i>	68.3216	50.1806	1.59181	0.120315
<i>Kcnj10</i>	4.4472	14.4644	16.594	111.93
<i>Trpm1</i>	0.009755	14.7644	0.035483	6.75993
<i>Plp1</i>	0.215656	4.79304	7.71325	34.9961
<i>Kcnj13</i>	0.149383	14.6624	1.753	14.403

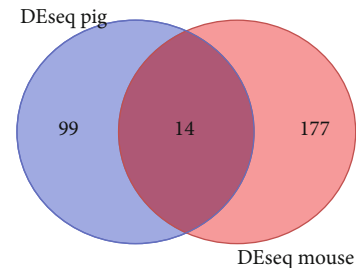


FIGURE 1: Venn diagram of DEGs in *Mitf-M* mutant and normal pigs/mice. The left circle represents the DEGs in the *Mitf-M* mutant and normal pigs; the right circle represents the DEGs in the *Mitf-M* mutant and normal mice. The middle part represents the DEGs in the *Mitf-M* mutant and normal pigs/mice.

esis pathway (Melanogenesis, mmu04916). The GO analysis was mainly enriched in the biological process of ion transport (ion transport, GO: 0006811) and the integral component of plasma membrane (GO: 0005887) (Figure 2).

2.2. Stria Vascularis Specific Ion Transport-Related Gene Analysis.

Ion transport-related genes were extracted from RNA transcriptome data from the normal and *Mitf-m* mutant pigs and mice samples for cluster analysis. The results showed many ion transport-related genes were highly expressed in both species through MeV cluster analysis (Figure 3). The *Mitf* mutation was coaffected with *Trpm1*, *Kcnj13*, and *Slc45a2* genes in both species. There were significant differences in ion channel regulation between pigs and mice. The expression of *Kcnn1*, *Clcn2*, and *Trpm4* genes was higher in pigs than those genes in the mice, whereas the expression of *Trpm7*, *Kcnq1*, and *Kcnj8* genes was found higher in mice compared to the pigs.

2.3. The Specific Tight Junction-Associated Genes in the Stria Vascularis.

The tight junction-associated genes were extracted from the RNA transcriptome data from the *Mitf* mutant and

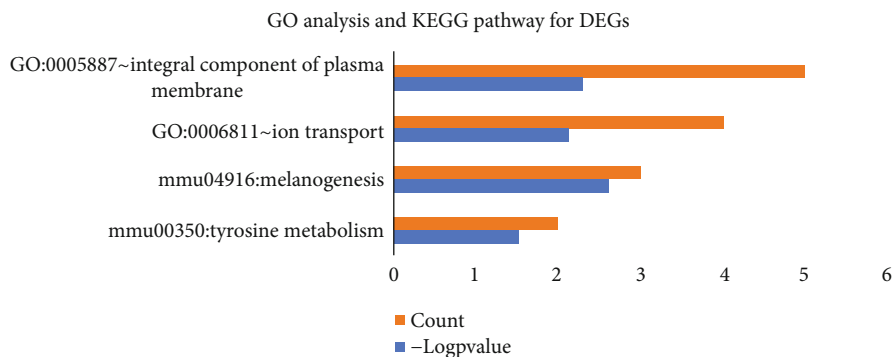


FIGURE 2: List of GO-terms with significant enrichment of DEGs. From top to bottom, the enrichment value decreases. The red X-axis indicates the number of unigenes in a category; the blue X-axis indicates the value of $\log_2(p)$ value in corresponding category. The Y-axis indicates the specific category.

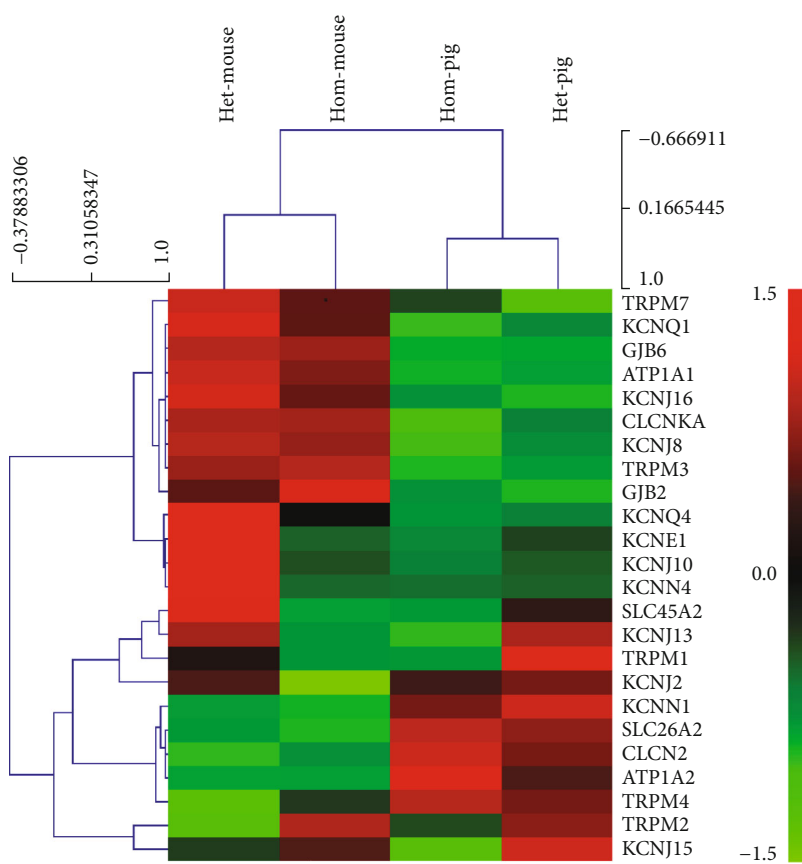


FIGURE 3: Ion channel relevant genes for cluster analysis heat map. Each column represents an experimental sample. Hom-mouse and het-mouse represent *Mitf*-M knockout mice and normal control mice. Hom-pig and het-pig represent *Mitf*-M mutant pigs and normal control pigs. Each row represents a gene. Different expressions are shown in different colors: red represents more expression and green represents less expression.

normal pigs/mice for cluster analysis. The expression of tight junctions in the stria vascularis of the two species was different (Figure 4). The *Cadm1*, *Cldn11*, *Pcdh1*, *Pcdh19*, and *Cdh24* genes expressed higher in pigs compared to those genes in mice, whereas *Ncam*, *Cldn6*, *Cldn9*, and *Cldn14* genes expressed higher in mice compared to pigs. And it was found that both the structures of the stria vascularis in two groups were intact. As the marginal nuclei

and the cell connections were intact. The three layers of cells were obvious, and the basal cells were closely connected (Figure 5).

2.4. *Stria Vascularis Specific Vascular Development-Related Genes*. Extracted vascular development-related genes from the RNA transcriptome data of the *Mitf* mutant and normal pigs/mice were used for cluster analysis. There was a

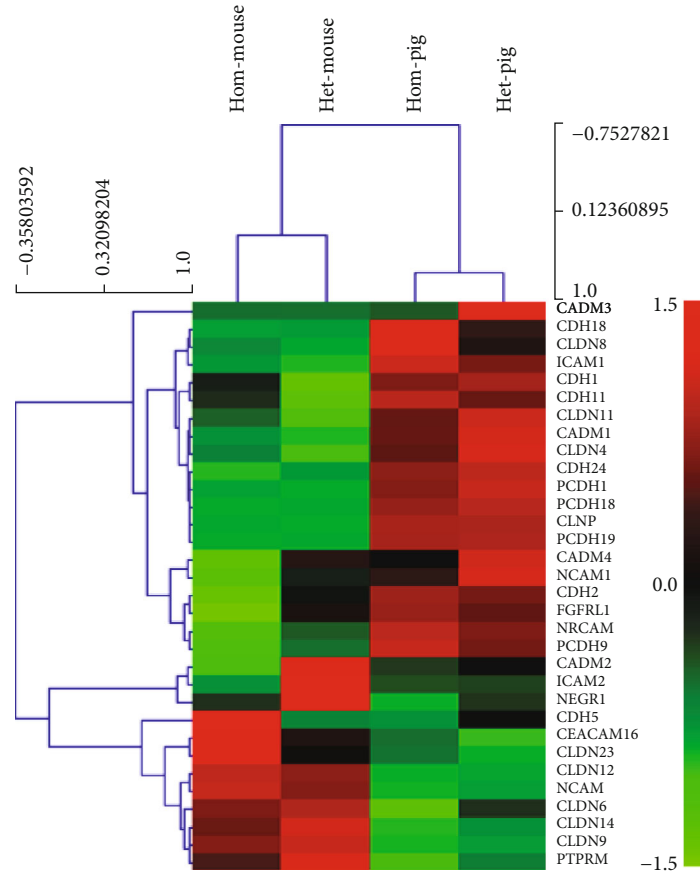


FIGURE 4: Tight junction relevant genes for cluster analysis heat map. Hom-mouse and het-mouse represent *Mitf*-M knockout mice and normal control mice. Hom-pig and het-pig represent *Mitf*-M mutant pigs and normal control pigs.

significant difference in the vascular developmental genes in the stria vascularis between these two species (Figure 6). The *Col2a1*, *Col3a1*, *Col11a1*, and *Col11a2* genes expressed higher in the pigs than the mice, whereas the *Col8a2*, *Cd34*, and *Ncam* genes expressed higher in the mice compared to the pigs.

3. Discussion

This study reviewed the changes of *Mitf*-M mutation on gene expression in the cochlea. *Mitf* has many subtypes [38], in which type M is specifically expressed in melanocytes [39], by direct association with related pigmentases such as tyrosinase (*Tyr*), dopachrome tautomerase (*Dct*), endothelin receptor type B (*Ednrb*), and solute carrier family 45 member 2 (*Slc45a2*), regulating the survival, migration, and differentiation of melanocytes [40]. Among them, *Mitf*-M gene [38, 39] plays a key role in regulating tyrosine metabolic pathway and melanin production, mainly regulating downstream pigment-related enzymes such as *Tyr*, *Dct*, and *Tyrp1*. *Mitf*-M also controls cytoskeleton and intercellular tight protein to regulate morphology and migration of melanocytes. In this study, we found the main gene pathway caused by the *Mitf*-M mutation is on ion transport pathway, including the tyrosine, acid metabolism, and melanin forma-

tion pathways, in the cochlear stria vascularis of both mice and pigs. Our data are consistent with previous reports [39].

Our previous studies reported that the *Mitf*-M gene mutation in the Waardenburg 2A pigs and mice through a deletion of the *Mitf*-M genes, which caused melanocytes failed to migrate to the cochlear stria vascularis. It can cause drops of EP and damages of cochlear hair cells. In this study, we also identified a significant decrease of the K^+ channel-associated genes, i.e., *Trpm1*, *Kcnj13*, *Slc45a2*, and *Kcnj10*. From our RNA-seq sequencing analysis, *Clcnka* and *Kcnj15* genes showed a significant difference in pig models, whereas the *Kcnq4*, *Kcnn4*, *Kcne1*, and *Kcnj2* genes are affected mainly in the mouse models. KCNJ13 (KIR7.1) and KCNJ10 (KIR4.1) belong to the inward rectifier potassium channel category. KCNJ10 is known as the key channel of potassium transport. It has been deeply studied in deafness-related diseases, and its deletion can lead to the reduction of EP and potassium ion concentration [36, 41–45]. However, *Kcnj13*, *Trpm1*, and *Slc45a2* were rarely reported in auditory researches. In addition, TRPM1 is a nonselective voltage-gated cation channel in the transient receptor potential (TRP) family, and the *Mitf* mutation can lead to the deletion of *Trpm1* [46]. SLC45A2 is a cross-mediated melanin synthesis in membrane transporter [47], which is regulated by *Mitf* via the cAMP pathway through *Tyr* and *Dct* genes, the major pigment-related genes [48, 49].

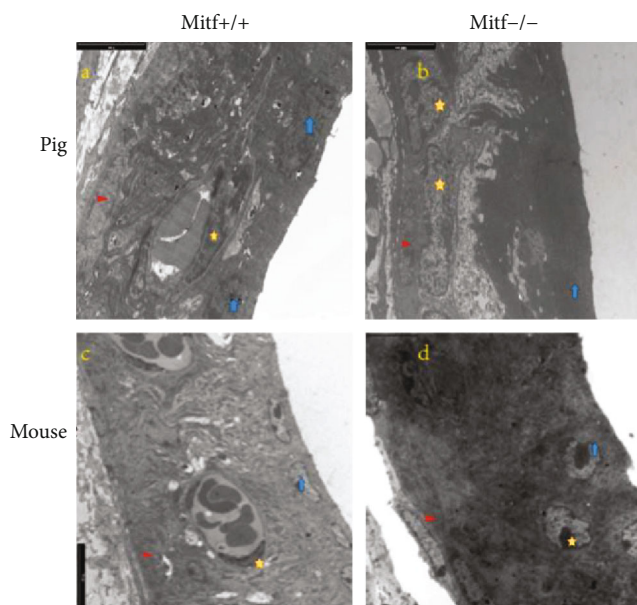


FIGURE 5: The SEM shows the cochlear stria vascularis of *Mitf* mutant and normal pigs/mice. (a) A normal pig's stria vascularis. (b) The stria vascularis from a mutant pig. (c) The stria vascularis from a normal mouse. (d) The stria vascularis from a mutant mouse. The red triangle marks the basal cells, the yellow pentagon marks the middle cells, and the blue arrow marks the marginal cells. The scale bar is 5 μm .

The stria vascularis transcriptome data of the two species indicated that *Mitf*-M played an important role in regulating the expression of the *Trpm1*, *Kcnj13*, *Slc45a2*, and *Kcnj10* genes in the stria vascularis. In both species, *Mitf*-M may play an important role in the auditory development and maintain the EP in the cochlea. Although there were huge biological differences between pigs and mice, we found that common gene changes in both species caused by *Mitf*-M. *Mitf*-M mutation induced a significant change in *Cln2*, *Kcnn1*, and *Trpm4* genes in the both models. CLCN2 [34] is an important component of chloride channel, which coordinates potassium and chloride exchanges. The function of KCNN1 has not been reported in the inner ears. KCNN1 belongs to the calcium ion-mediated potassium channels and plays an important role in the regulation of neural inflammation and nerve aging by microglia [50]. In mice, *Kcnq1*, *Trpm7*, and *Kcnj8* were significantly affected. KCNQ1 is a calcium ion-dependent potassium channel [45]. When *Kcnq1* is deleted, it will cause degeneration of the outer hair cells, which is clinically characterized as Jervell and Lange-Nielsen syndrome, one condition that causes profound hearing loss from birth and a disruption of the heart's normal rhythm. KCNE1 and KCNQ1 are important potassium-secreting channels in the stria vascularis marginal cells [26, 45, 51]. KCNE1 regulates KCNQ1 expression and increases ion transport [52].

The tight junctions and vascular endothelial cells are important components of the blood labyrinth barrier as well as ion channels [30, 53–57]. Our cluster analysis of the RNA transcriptome data from both pigs and mice showed that the

tight junctions were significantly different in the stria vascularis of these two species. The expression of *Cadm1*, *Cldn11*, *Pcdh1*, *Pcdh19*, and *Cdh24* was found higher in pigs compared to mice, whereas the expression of *Ncam*, *Cldn6*, *Cldn9*, and *Cldn14* genes were higher in mice compared to pigs. Cluster analysis of vascular-related genes revealed that it was significantly different in the stria vascularis of the two species. The higher expression in pigs is *Col2a1*, *Col3a1*, *Col11a1*, and *Col11a2*, whereas the expression of *Col8a2*, *Cd34*, and *Ncam* genes was higher in mice compared to pigs. These results may reveal that the two animals may invoke different genes to regulate the tight junction, just as the ion channels. The differences between the two species' evolutionary relationship, living habits, and anatomy may result in significant differences in these gene expressions [56, 58, 59]. It is more suitable to choose animal model closer to humans to study auditory related diseases.

In summary, we show that by leveraging RNA-seq for the analysis of the stria vascularis of the WS models, it helps to understand the regulatory mechanisms related to the loss of EP and deafness. These data provide insight into ion channel-defining genes and illustrate the possible genes associated with the WS hearing loss. These results may make a fundamental effect on the gene therapy, which used to rescue the elapse of the endocochlear potential in the stria vascularis.

4. Conclusion

Our research reveals that there exists a huge difference on the gene expression and function between these two models. According to the different expression in the genetic profiles of these two species caused by *Mitf*-M gene mutation in RNA transcriptome level, there may be different genes transcript pathway caused by *mitf* mutation in regulating the potassium channels in mice and pigs. And this transcriptome data may provide a basis for the gene therapy in treating the Waardenburg syndrome.

5. Material and Methods

5.1. Animals. Both *Mitf* mutant and normal pigs and mice have been used in this experiment. The generation of the *Mitf* mutant pigs and mice have been described in our previous publications [17, 37]. The experimental protocols were approved by the ethics committee of the Chinese PLA Medical School.

5.2. RNA Isolation from Stria Vascularis Tissue. Tissues of the stria vascularis of pigs were obtained from four normal pigs and four *Mitf* mutant pigs at E85 of embryonic stage as previous study described [17]. The tissues of stria vascularis of mice were obtained from ten normal mice and ten *Mitf* mutant mice at postnatal 30 days as previous studies described [7, 37]. The total RNA of these tissues was extracted separately using Trizol reagent (Invitrogen, CA, USA) following the manufacturer's protocol. The quantity, purity, and integrity of the collected total RNA were analyzed with NanoPhotometer® spectrophotometer (IMPLEN, CA,

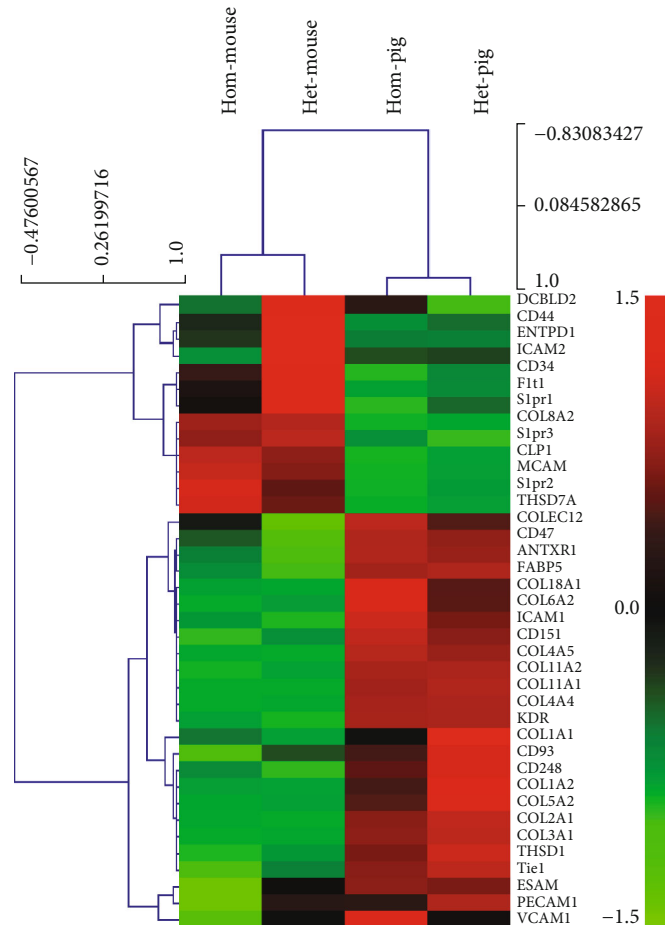


FIGURE 6: Heat analysis of clustering analysis of genes associated with specific vascular endothelial cell in normal and *Mitf* mutant pigs/mice (hom-mouse and het-mouse represent *Mitf*-M knockout mice and normal mice, hom-pig and het-pig represent *Mitf*-M mutant pigs and normal pigs).

USA), a Bioanalyzer 2100, and RNA Nano 6000 Assay Kit (Agilent, CA, USA). Approximately, 4 μ g of total RNA was used for the RNA sample preparations as previous studies described [60, 61].

5.3. Library Construction and Sequencing. The NEBNext® Ultra TM RNA Library Prep Kit for Illumina® (NEB, USA) was used for the sequencing library preparation, which was conducted with an Illumina HiSeq TM 2000 system following the manufacturer's recommended protocol (Illumina Company Ltd, San Diego, CA, USA) as previous studies described [61, 62].

5.4. RNA-Seq Reads Mapping. The reference genome and gene model annotation files were obtained from Genome Web (<http://asia.ensembl.org/index.html>). The index of the reference genome was built using Hisat2 software (v2.0.5), and the paired-end clean reads were aligned to the reference genome. A database of potential splice junctions was built and confirmed by comparing the previously unmapped reads against the database of putative junctions. The aligned read files were processed by Cufflinks software, which used the normalized RNA-seq fragment counts to measure the relative abundances of the transcriptome. The unit of measure-

ment was fragmented per kilobase of exons per million fragments mapped (FPKM). Reads were mapped into the mouse NCBI38 (ensembl release 68) and the *Sus scrofa* 11.1 (*sus scrofa* ensembl release 94) using default options.

5.5. Gene Ontology (GO) and Pathway Enrichment Analysis of DEGs. Differential expression analysis of *Mitf*-M mutant and normal pigs/mice were performed using the DESeq R package [63]. Using the adjusted p values 0.05 and setting the absolute fold change of 2 as the threshold for significantly differential expression. Using Gene Ontology (GO) and KEGG to analyze high-throughput genome and transcriptome data in the DAVID database [64–68], which is an important online tool for these analyses. The DEGs list was uploaded to the DAVID [64] analysis tool, and $p < 0.05$ was considered statistically significant. The DEGs was uploaded to the MeV software (<https://sourceforge.net/projects/mev-tm4/>) to get the relevant heat map.

5.6. Selecting Deafness Gene of SV Transcriptomes from RNA-Seq Data. In obtaining our data for known deafness genes, we used a database of known deafness genes from these sources: (1) Hereditary Hearing Loss homepage [69] and (2) Hereditary hearing loss and deafness overview [27, 45].

5.7. *The Transmission Electron Microscopy (TEM)*. To prepare samples for TEM examination, the stria vascularis were washed with 0.1 M PBS and then postfixed in 1% osmium tetroxide and then dehydrated by a series of ethanol before embedded in plastic Agar 100 resin. After polymerization, the stria vascularis was cut into ultrathin sections (3 μm), stained with toluidine blue, were mounted on 0.7% formvar coated copper grids, contrasted by 0.5% uranyl acetate and lead citrate, then examined under a transmission electron microscopy (Philips Tecnai10) [70].

Data Availability

Readers can access additional experimental data in optional supplementary materials.

Conflicts of Interest

The authors declare no competing financial interests.

Authors' Contributions

Linjun Chen and Yi Wang contributed equally to this work.

Acknowledgments

This research was supported by grants from the National Science Foundation of China (81470683, 81770992 to Weiju Han and 81670940 to Shiming Yang). Neither the entire paper nor any part of its contents has been published or has been accepted elsewhere.

Supplementary Materials

Deseq GO Analysis. Pig and mouse DEG. (*Supplementary materials*)

References

- [1] J. Song, Y. Feng, F. R. Acke, P. Coucke, K. Vleminckx, and I. J. Dhooge, "Hearing loss in Waardenburg syndrome: a systematic review," *Clinical Genetics*, vol. 89, no. 4, pp. 416–425, 2016.
- [2] T. Hai, W. Guo, J. Yao et al., "Creation of miniature pig model of human Waardenburg syndrome type 2A by ENU mutagenesis," *Human Genetics*, vol. 136, no. 11–12, pp. 1463–1475, 2017.
- [3] A. Watanabe, K. Takeda, B. Ploplis, and M. Tachibana, "Epistatic relationship between Waardenburg Syndrome genes MITF and PAX3," *Nature Genetics*, vol. 18, no. 3, pp. 283–286, 1998.
- [4] K. K. Ohlemiller, S. M. Jones, and K. R. Johnson, "Application of mouse models to research in hearing and balance," *Journal of the Association for Research in Otolaryngology*, vol. 17, no. 6, pp. 493–523, 2016.
- [5] R. Omichi, S. B. Shibata, C. C. Morton, and R. J. H. Smith, "Gene therapy for hearing loss," *Human molecular genetics*, vol. 28, no. R1, pp. R65–R79, 2019.
- [6] X. Gao, Y. Tao, V. Lamas et al., "Treatment of autosomal dominant hearing loss by *in vivo* delivery of genome editing agents," *Nature*, vol. 553, no. 7687, pp. 217–221, 2018.
- [7] F. Tan, C. Chu, J. Qi et al., "AAV-*ie* enables safe and efficient gene transfer to inner ear cells," *Nature Communications*, vol. 10, no. 1, p. 3733, 2019.
- [8] B. Pan, C. Askew, A. Galvin et al., "Gene therapy restores auditory and vestibular function in a mouse model of Usher syndrome type 1c," *Nature Biotechnology*, vol. 35, no. 3, pp. 264–272, 2017.
- [9] D. Wang, "Evolution and Restoration of Structures and Functions of the Human Central Nervous System—A Review," *Journal of Neurorestoration*, vol. 1, no. 1, pp. 60–70, 2015.
- [10] U. Müller and P. G. Barr-Gillespie, "New treatment options for hearing loss," *Nature Reviews Drug Discovery*, vol. 14, no. 5, pp. 346–365, 2015.
- [11] N. X. Tritsch and D. E. Bergles, "Developmental regulation of spontaneous activity in the mammalian cochlea," *The Journal of Neuroscience*, vol. 30, no. 4, pp. 1539–1550, 2010.
- [12] K. Bommakanti, J. S. Iyer, and K. M. Stankovic, "Cochlear histopathology in human genetic hearing loss: State of the science and future prospects," *Hearing Research*, vol. 382, p. 107785, 2019.
- [13] U. Philipp, B. Lupp, S. Mömke et al., "A MITF mutation associated with a dominant white phenotype and bilateral deafness in German Fleckvieh cattle," in *PLoS ONE*, vol. 6, no. 12, p. e28857, e28857, 2011.
- [14] R. Hauswirth, B. Haase, M. Blatter et al., "Mutations in MITF and PAX3 cause "splashed white" and other white spotting phenotypes in horses," *PLoS Genetics*, vol. 8, no. 4, p. e1002653, 2012.
- [15] S. Tsuchida, T. Takizawa, K. Abe, M. Okamoto, and M. Tagawa, "Identification of microphthalmia-associated transcription factor isoforms in dogs," *Veterinary Journal*, vol. 182, no. 2, pp. 283–293, 2009.
- [16] I. B. Körberg, E. Sundström, J. R. S. Meadows et al., "A simple repeat polymorphism in the MITF-M promoter is a key regulator of white spotting in dogs," *PLoS ONE*, vol. 9, no. 8, p. e104363, 2014.
- [17] L. Chen, W. Guo, L. Ren et al., "A de novo silencer causes elimination of MITF-M expression and profound hearing loss in pigs," *BMC Biology*, vol. 14, no. 1, 2016.
- [18] W. Guo, H. Yi, L. Ren et al., "The Morphology and Electrophysiology of the Cochlea of the Miniature Pig," *The Anatomical Record*, vol. 298, no. 3, pp. 494–500, 2015.
- [19] Y. Du, L.-l. Ren, Q.-q. Jiang et al., "Degeneration of saccular hair cells caused by MITF gene mutation," *Neural Development*, vol. 14, no. 1, p. 1, 2019.
- [20] Q.-Q. Hao, L. Li, W. Chen et al., "Key Genes and Pathways Associated With Inner Ear Malformation in SOX10 p.R109W Mutation Pigs," *Frontiers in Molecular Neuroscience*, vol. 11, 2018.
- [21] H. Yi, W. Guo, W. Chen, L. Chen, J. Ye, and S. Yang, "Miniature pigs: a large animal model of cochlear implantation," *American Journal of Translational Research*, vol. 8, no. 12, pp. 5494–5502, 2016.
- [22] X.-J. Ji, W. Chen, X. Wang et al., "Canalostomy is an ideal surgery route for inner ear gene delivery in big animal model," *Acta Oto-Laryngologica*, vol. 139, no. 11, pp. 939–947, 2019.
- [23] F.-. W. An, H. Yuan, W. Guo et al., "Establishment of a Large Animal Model for Eustachian Tube Functional Study in Miniature Pigs," *The Anatomical Record*, vol. 302, no. 6, pp. 1024–1038, 2018.

- [24] J. M. Lovell and G. M. Harper, "The morphology of the inner ear from the domestic pig *Sus scrofa*," *Journal of Microscopy*, vol. 228, no. 3, pp. 345–357, 2007.
- [25] A. A. Dror and K. B. Avraham, "Hearing Impairment: A Panoply of Genes and Functions," *Neuron*, vol. 68, no. 2, pp. 293–308, 2010.
- [26] S. Korrapati, I. Taukulis, R. Olszewski et al., "Single Cell and Single Nucleus RNA-Seq Reveal Cellular Heterogeneity and Homeostatic Regulatory Networks in Adult Mouse Stria Vascularis," *Frontiers in molecular neuroscience*, vol. 12, p. 316, 2019.
- [27] S. Uetsuka, G. Ogata, S. Nagamori et al., "Molecular architecture of the stria vascularis membrane transport system, which is essential for physiological functions of the mammalian cochlea," *The European Journal of Neuroscience*, vol. 42, no. 3, pp. 1984–2002, 2015.
- [28] S. Nyberg, N. J. Abbott, X. Shi, P. S. Steyger, and A. Dabdoub, "Delivery of therapeutics to the inner ear: The challenge of the blood-labyrinth barrier," *Science Translational Medicine*, vol. 11, no. 482, p. eaao0935, 2019.
- [29] H. Liu, L. Chen, K. P. Giffen et al., "Cell-Specific Transcriptome Analysis Shows That Adult Pillar and Deiters' Cells Express Genes Encoding Machinery for Specializations of Cochlear Hair Cells," *Frontiers in Molecular Neuroscience*, vol. 11, 2018.
- [30] X. Shi, "Pathophysiology of the cochlear intrastrial fluid-blood barrier (review)," *Hearing Research*, vol. 338, pp. 52–63, 2016.
- [31] P. Chen, Y. Chai, H. Liu et al., "Postnatal Development of Microglia-Like Cells in Mouse Cochlea," *Neural Plasticity*, vol. 2018, Article ID 1970150, 5 pages, 2018.
- [32] A. A. Zdebik, P. Wangemann, and T. J. Jentsch, "Potassium ion movement in the inner ear: insights from genetic disease and mouse models," *Physiology*, vol. 24, no. 5, pp. 307–316, 2009.
- [33] Z. Jin, I. Uhlen, K. Wei-Jia, and D. Mao-li, "Cochlear homeostasis and its role in genetic deafness," *Journal of Otology*, vol. 4, no. 1, pp. 15–22, 2009.
- [34] F. Lang, V. Vallon, M. Knipper, and P. Wangemann, "Functional significance of channels and transporters expressed in the inner ear and kidney," *American Journal of Physiology-Cell Physiology*, vol. 293, no. 4, pp. C1187–C1208, 2007.
- [35] O. K. Egilmez and M. T. Kalciglu, "Genetics of Nonsyndromic Congenital Hearing Loss," *Scientifica*, vol. 2016, Article ID 7576064, 9 pages, 2016.
- [36] D. C. Marcus, T. Wu, P. Wangemann, and P. Kofuji, "KCNJ10 (Kir4.1) potassium channel knockout abolishes endocochlear potential," *American Journal of Physiology-Cell Physiology*, vol. 282, no. 2, pp. C403–C407, 2002.
- [37] H. Liu, Y. Li, L. Chen et al., "Organ of Corti and Stria Vascularis: Is there an Interdependence for Survival?," *PLoS One*, vol. 11, no. 12, p. e0168953, 2016.
- [38] C. R. Goding and H. Arnheiter, "MITF—the first 25 years," *Genes & Development*, vol. 33, no. 15–16, pp. 983–1007, 2019.
- [39] T. Chen, B. Zhao, Y. Liu et al., "MITF-M regulates melanogenesis in mouse melanocytes," *Journal of Dermatological Science*, vol. 90, no. 3, pp. 253–262, 2018.
- [40] H. T. Michael, C. Graff-Cherry, S. Chin et al., "Partial Rescue of Ocular Pigment Cells and Structure by Inducible Ectopic Expression of Mitf-M in MITF-Deficient Mice," *Investigative Ophthalmology & Visual Science*, vol. 59, no. 15, pp. 6067–6073, 2018.
- [41] H. Locher, J. C. M. J. de Groot, L. van Iperen, M. A. Huisman, J. H. M. Frijns, and S. M. Chuva de Sousa Lopes, "Development of the stria vascularis and potassium regulation in the human fetal cochlea: Insights into hereditary sensorineural hearing loss," *Developmental Neurobiology*, vol. 75, no. 11, pp. 1219–1240, 2015.
- [42] J. Chen and H. B. Zhao, "The role of an inwardly rectifying K⁺ channel (Kir4.1) in the inner ear and hearing loss," *Neuroscience*, vol. 265, pp. 137–146, 2014.
- [43] H. Yang, H. Xiong, Q. Huang et al., "Compromised potassium recycling in the cochlea contributes to conservation of endocochlear potential in a mouse model of age-related hearing loss," *Neuroscience Letters*, vol. 555, pp. 97–101, 2013.
- [44] P. Wangemann, E. M. Itza, B. Albrecht et al., "Loss of KCNJ10 protein expression abolishes endocochlear potential and causes deafness in Pendred syndrome mouse model," *BMC Medicine*, vol. 2, no. 1, 2004.
- [45] R. Mittal, M. Aranke, L. H. Debs et al., "Indispensable role of ion channels and transporters in the auditory system," *Journal of Cellular Physiology*, vol. 232, no. 4, pp. 743–758, 2017.
- [46] A. J. Miller, J. Du, S. Rowan, C. L. Hershey, H. R. Widlund, and D. E. Fisher, "Transcriptional regulation of the melanoma prognostic marker melastatin (TRPM1) by MITF in melanocytes and melanoma," *Cancer Research*, vol. 64, no. 2, pp. 509–516, 2004.
- [47] K. Inagaki, T. Suzuki, S. Ito et al., "Oculocutaneous albinism type 4: six novel mutations in the membrane-associated transporter protein gene and their phenotypes," *Pigment Cell Research*, vol. 19, no. 5, pp. 451–453, 2006.
- [48] K. S. Hoek, N. C. Schlegel, O. M. Eichhoff et al., "Novel MITF targets identified using a two-step DNA microarray strategy," *Pigment Cell & Melanoma Research*, vol. 21, no. 6, pp. 665–676, 2008.
- [49] J. Du and D. E. Fisher, "Identification of Aim-1 as the underwhite mouse mutant and its transcriptional regulation by MITF," *Journal of Biological Chemistry*, vol. 277, no. 1, pp. 402–406, 2001.
- [50] A. M. Dolga and C. Culmsee, "Protective roles for potassium SK/KCa2 channels in microglia and neurons," *Frontiers in Pharmacology*, vol. 3, 2012.
- [51] V. Wilms, C. Köppl, C. Söffgen, A.-M. Hartmann, and H. G. Nothwang, "Molecular bases of K⁺ secretory cells in the inner ear: shared and distinct features between birds and mammals," *Scientific Reports*, vol. 6, no. 1, 2016.
- [52] N. Strutz-Seebohm, G. Seebohm, O. Fedorenko et al., "Functional Coassembly of KCNQ4 with KCNE- β -Subunits in *Xenopus* Oocytes," *Cellular Physiology and Biochemistry*, vol. 18, no. 1–3, pp. 57–66, 2006.
- [53] E. I. Bartle, T. C. Rao, T. M. Urner, and A. L. Mattheyses, "Bridging the gap: Super-resolution microscopy of epithelial cell junctions," *Tissue Barriers*, vol. 6, no. 1, p. e1404189, 2017.
- [54] W. Liu, A. Schrott-Fischer, R. Glueckert, H. Benav, and H. Rask-Andersen, "The Human 'Cochlear Battery' - Claudin-11 Barrier and Ion Transport Proteins in the Lateral Wall of the Cochlea," *Frontiers in Molecular Neuroscience*, vol. 10, 2017.
- [55] S. Kitajiri, T. Katsuno, H. Sasaki, J. Ito, M. Furuse, and S. Tsukita, "Deafness in occludin-deficient mice with dislocation of tricellulin and progressive apoptosis of the hair cells," *Biology Open*, vol. 3, no. 8, pp. 759–766, 2014.

- [56] Y. Wallez and P. Huber, "Endothelial adherens and tight junctions in vascular homeostasis, inflammation and angiogenesis," *Biochimica et Biophysica Acta (BBA) - Biomembranes*, vol. 1778, no. 3, pp. 794–809, 2008.
- [57] Y. Liu, J. Qi, X. Chen et al., "Critical role of spectrin in hearing development and deafness," *Science Advances*, vol. 5, no. 4, 2019.
- [58] N. V. Goncharov, A. D. Nadeev, R. O. Jenkins, and P. V. Avdonin, "Markers and biomarkers of endothelium: when something is rotten in the state," *Oxidative Medicine and Cellular Longevity*, vol. 2017, Article ID 9759735, 27 pages, 2017.
- [59] D. R. Trune, "Ion homeostasis in the ear: mechanisms, maladies, and management," *Current Opinion in Otolaryngology & Head and Neck Surgery*, vol. 18, no. 5, pp. 413–419, 2010.
- [60] Y. Zhang, L. Guo, X. Lu et al., "Characterization of Lgr6+ Cells as an Enriched Population of Hair Cell Progenitors Compared to Lgr5+ Cells for Hair Cell Generation in the Neonatal Mouse Cochlea," *Frontiers in Molecular Neuroscience*, vol. 11, 2018.
- [61] S. Zhang, Y. Zhang, P. Yu et al., "Characterization of Lgr5+ progenitor cell transcriptomes after neomycin injury in the neonatal mouse cochlea," *Frontiers in Molecular Neuroscience*, vol. 10, p. 213, 2017.
- [62] C. Cheng, L. Guo, L. Lu et al., "Characterization of the transcriptomes of Lgr5+ hair cell progenitors and Lgr5- supporting cells in the mouse cochlea," *Frontiers in Molecular Neuroscience*, vol. 10, 2017.
- [63] R. Gupta, I. Dewan, R. Bharti, and A. Bhattacharya, "Differential expression analysis for RNA-Seq data," *ISRN Bioinformatics*, vol. 2012, Article ID 817508, 8 pages, 2012.
- [64] D. W. Huang, B. T. Sherman, and R. A. Lempicki, "Systematic and integrative analysis of large gene lists using DAVID bioinformatics resources," *Nature Protocols*, vol. 4, no. 1, pp. 44–57, 2009.
- [65] G. Dennis, B. T. Sherman, D. A. Hosack et al., "DAVID: Database for Annotation, Visualization, and Integrated Discovery," *Genome Biology*, vol. 4, no. 9, 2003.
- [66] S. Zhang, Y. Zhang, Y. Dong et al., "Knockdown of Foxg1 in supporting cells increases the trans-differentiation of supporting cells into hair cells in the neonatal mouse cochlea," *Cellular and Molecular Life Sciences*, vol. 77, no. 7, pp. 1401–1419, 2020.
- [67] M. Tang, J. Li, L. He et al., "Transcriptomic profiling of neural stem cell differentiation on graphene substrates," *Colloids and Surfaces B: Biointerfaces*, vol. 182, p. 110324, 2019.
- [68] C. Cheng, Y. Wang, L. Guo et al., "Age-related transcriptome changes in Sox2+ supporting cells in the mouse cochlea," *Stem Cell Research & Therapy*, vol. 10, no. 1, p. 365, 2019.
- [69] G. Van Camp and R. Smith, vol. 18, 2015 Hereditary Hearing Loss Home Page Available at: <http://hereditaryhearingloss.org>.
- [70] Z. He, L. Guo, Y. Shu et al., "Autophagy protects auditory hair cells against neomycin-induced damage," *Autophagy*, vol. 13, no. 11, pp. 1884–1904, 2017.

Research Article

The Regenerative Potential of Facial Nerve Motoneurons following Chronic Axotomy in Rats

Yusu Ni ¹, Diyan Chen,¹ Yi Jiang,² Danhong Qiu,³ Wen Li,⁴ and Huawei Li ^{1,5,6,7,8}

¹Otology and Skull Base Surgery Department, Eye and ENT Hospital of Shanghai Medical School, Fudan University, China

²Department of Ophthalmology, Shanghai Xin Shi Jie Eye Hospital, Shanghai, China

³Otolaryngology Department, Pudong Hospital, Shanghai, China

⁴Central Laboratory, Eye and ENT Hospital of Shanghai Medical School, Fudan University, China

⁵ENT Institute and Otorhinolaryngology Department of Eye & ENT Hospital, State Key Laboratory of Medical Neurobiology and MOE Frontiers Center for Brain Science, Fudan University, Shanghai 200031, China

⁶Institutes of Biomedical Sciences, Fudan University, Shanghai 200032, China

⁷NHC Key Laboratory of Hearing Medicine (Fudan University), Shanghai 200031, China

⁸The Institutes of Brain Science and the Collaborative Innovation Center for Brain Science, Fudan University, Shanghai 200032, China

Correspondence should be addressed to Yusu Ni; niyusu@aliyun.com and Huawei Li; hwli@shmu.edu.cn

Received 11 April 2020; Revised 9 June 2020; Accepted 16 June 2020; Published 1 August 2020

Academic Editor: Hai Huang

Copyright © 2020 Yusu Ni et al. This is an open access article distributed under the Creative Commons Attribution License, which permits unrestricted use, distribution, and reproduction in any medium, provided the original work is properly cited.

Background. The precise mechanisms of nerve regeneration remain unclear. The potential of facial nerve regeneration and probable mechanisms involved following chronic facial nerve injury should be further studied. **Methods.** Adult male Wistar rats were used to model either (i) facial nerve injury (axotomy) or (ii) reinjury (chronic axotomy followed by a second axotomy within 5 months). The rats were housed in the animal facility of the Eye and ENT Hospital of Shanghai Medical School, Fudan University (Shanghai, China). Expression of Shh (sonic hedgehog) and growth-associated protein 43 (GAP43, a neuronal marker) was detected in bilateral facial nuclei using reverse transcriptase PCR, western blotting analysis, and immunohistochemistry. The number of surviving motoneurons was quantified, and facial nerve regeneration was examined using transmission electron microscopy. **Results.** Reinjury of the facial nerve 12 weeks after the first axotomy resulted in upregulation of GAP43 mRNA and protein expression in neurons ipsilateral to the axotomy; immunohistochemistry revealed that Shh expression was higher compared with control side facial nuclei at the same time point. GAP43 expression subsequently decreased. **Conclusion.** The greatest regeneration potential of the facial nerve occurred within 5 months following chronic axotomy in rats, and regeneration may involve the Shh signaling pathway.

1. Introduction

Peripheral facial paralysis was characterized by paralysis of all facial expression muscles in the affected side, and facial muscle movement disorder was the main characteristic, which caused great psychological stress, mental trauma to the patients. No matter what cause of peripheral facial paralysis, if the drug treatment was ineffective, they should consider early surgical treatment [1–4].

Although, some scholars believed the facial nerve had a greater capacity for regeneration than any other neuron in the central nervous system; in this regard, the facial nerve was very similar to peripheral motor nerves [5–8]. For those patients with facial paralysis for a long time, the curative effects after operation were often not ideal [1–4]; the most important reason was the loss of the most facial nerve motor neurons, which led to the ability decline of facial nerve regeneration [9].

For years, researchers have never stopped looking for effective treatments to promote facial nerve regeneration [10–13].

Previous studies have shown that nerve injuries induce a variety of molecular responses that may be involved in the regeneration of injured neurons [11, 13–16]. In the neurons, the efficacy and the specificity of neurotrophic factors to support regeneration depend on the presence of their respective receptors and their number. The receptors for NGF, FGF-2, BDNF, GDNF, and IGF-I are synthesized by neurons and are upregulated following axotomy. Seitz et al. research and analysis showed that recovery of motor function after peripheral nerve injury is related with a complex regulation of lesion-associated neurotrophic factors and cytokines, which include BDNF, FGF2, IGF2, IGF1, and NGF protein [17].

Some scholars have also made some progress in promoting the recovery of injured facial nerve function by using degradable neural catheters and dedifferentiated fat cells [18], either by local administration of nerve catheters (e.g., neurotrophic factors) [19] or by injecting stem cells into nerve ducts [20–23].

No matter which way to promote the regeneration of facial nerve after injury, how to protect or reduce the nonapoptosis of motor neurons of facial nerve after injury is indeed the most critical step to improve the repair of facial nerve regeneration [9]. Although many molecules involved in facial nerve repair have been characterized, the precise mechanisms of nerve regeneration remain unclear. Interestingly, some studies have demonstrated that electrical stimulation could promote peripheral nerve regeneration or the functional recovery of paralyzed facial nerves and nerve reinnervation of paralyzed muscles [24–26]. However, the mechanism by which electrical stimulation promotes nerve regeneration is unclear, and we speculate that it may be related to the electrical stimulation of the peripheral nerve, which activated the regenerative or functionally protective neural signaling pathway.

Mammals have three genes with homology to the Hh gene (sonic hedgehog (Shh), Indian hedgehog (Ihh), and desert hedgehog (Dhh)). Shh signaling played important roles for patterning and cell fate specification in the central nervous system, and Shh shows low expression in the neural stem/progenitor cells in the dorsal telencephalon. Shh signaling in neocortex development has been shown to regulate intermediate progenitor cells, thereby maintaining the proliferation, survival, and differentiation of neurons in the neocortex [27–30].

In adult rats, sonic hedgehog (Shh) expression is upregulated 24 hours after facial nerve axotomy and then starts to decline 4 weeks later [31]. Although the precise molecular circuitry of regeneration is unclear, this expression pattern implies a function for Shh in mature motoneurons [32].

In this study, we investigated the potential of facial nerve regeneration and whether it was affected by activation of the Shh signaling pathways.

2. Methods and Materials

2.1. Animals. Adult male Wistar rats (weighing 200–250 g) were housed in the animal facility of the Eye and ENT

Hospital of Shanghai Medical School, Fudan University (Shanghai, China). All animal experiments and care protocols were performed under the approval of the institution's ethical committee for care and use of laboratory animals.

2.2. Axotomy Models. Animal experiments were performed under general anesthesia using an intraperitoneal injection of a mixture of ketamine hydrochloride (135 mg/kg) and xylazine hydrochloride (6.5 mg/kg). Animals were divided into two experimental groups. In Group I (axotomy), the right facial nerve stem (including the posterior auricular branch) was transected approximately 3 mm distal from the stylomastoid foramen, a 2 mm segment of the distal portion of the nerve was removed, the distal stump was ligated with 3-0 silk thread to prevent the regeneration of axons from their targets, and 5-0 silk thread was used to label the proximal nerve stump. In Group II (reinjury involving chronic axotomy followed by second axotomy), at 12, 20, 28, and 36 weeks (w) after the initial facial nerve axotomy, the proximal 1 mm nerve stump (including the posterior auricular branch) was reaxotomized and the distal stump was ligated with 3-0 silk thread. Intact contralateral sides served as controls. There were 10 rats in each experimental group at each observation time.

2.3. Tissue Collection. At 13, 21, 29, and 37 w after the initial facial nerve axotomy in Group I, and 1 w after the facial nerve was reaxotomized in Group II, ten rats were randomly selected. Five were transcardially perfused with normal saline (0.9% NaCl) followed by 4% paraformaldehyde (PFA). The brainstems of these rats were removed, postfixed in 4% PFA for 24 h, and dehydrated in phosphate-buffered saline (PBS) containing 15% sucrose followed by 30% sucrose/PBS solution. Tissues were then snap frozen and stored at -80°C . Coronal brainstem sections were cut at a thickness of $20\ \mu\text{m}$ with a cryostat and used for immunohistochemistry. Each treatment group was randomly examined to eliminate any systematic handling biases. The remaining five rats were rapidly decapitated under general anesthesia. The brains were removed quickly and stored in liquid nitrogen until required for reverse transcriptase PCR (RT-PCR) and western blotting analysis.

2.4. Immunohistochemistry. Cellular morphology was examined by staining slides with 1% toluidine blue (Sigma, St. Louis, MO). Briefly, slides were placed in distilled water for 2 min followed by 1% toluidine blue for 20 min at 40°C . Slides were then rinsed in water followed by 95% ethanol, and covered with a coverslip.

Immunohistochemistry was performed to identify cellular expression of growth-associated protein-43 (GAP43), Shh, and glial fibrillary acidic protein (GFAP). Double fluorescence labeling was performed to identify cellular expression of Shh in GAP43- or GFAP-positive cells using a mouse monoclonal anti-Shh antibody (Sigma, 1:1000 dilution) and polyclonal anti-GAP43 (rabbit anti-rat GAP43, 1:500 dilution; Abcam, Cambridge, UK) and anti-GFAP antibodies (rabbit anti-rat GFAP, 1:100 dilution; Sigma). Cryosections were fixed in 4% PFA containing 0.5% Triton

X-100 before incubation with primary antibodies overnight at 4°C. Sections were then washed and incubated with a secondary fluorescein isothiocyanate- (FITC-) labeled antibody (goat anti-rabbit, 1:200 dilution; Jackson ImmunoResearch, West Grove, PA) or tetramethylrhodamine isothiocyanate- (TRITC-) labeled antibody (goat anti-mouse, 1:200 dilution; Jackson ImmunoResearch). Fluorescence images were captured using a confocal microscope (Leica, Wetzlar, Germany) and analyzed with Image Pro Plus software version 6.0 (Media Cybernetics, Rockville, MD).

2.5. Reverse Transcription Polymerase Chain Reaction (RT-PCR). Frozen brain stems were quickly sectioned in a coronal orientation at a thickness of 100 μm using a cryostat. Two sections of the experimental and control side facial nuclei at the same location (based on location within the brain stem) of each rat were homogenized in TRIzol reagent (Invitrogen, Carlsbad, CA). Total RNA was extracted and reverse transcribed using a SuperScript™ III First-Strand Synthesis System RT-PCR kit (Invitrogen). The PCR reaction contained 3 μL of cDNA, 5 μL of 10 \times PCR buffer, 1.5 μL of 50 mM MgCl_2 , 1 μL of 10 mM dNTP mixture (0.2 μM each), 1 μL of sense primer (0.2 $\mu\text{M}/\text{L}$), 1 μL of antisense primer (0.2 $\mu\text{M}/\text{L}$), 0.2 μL (1 unit) of Platinum Taq DNA Polymerase (Invitrogen), and H_2O to generate a total volume of 50 μL . GAP43 PCR reactions were performed using 5'-ATGCTG TGCTGTATGAGAAGAACC-3' (sense) and 5'-GGCAAC GTGGAAAGCCGTTTCTTAAAGT-3' (antisense) primers [32] under the following conditions: 94°C for 2 min; 30 cycles of 94°C for 30 sec, 57°C for 30 sec, and 72°C for 45 sec; and final extension at 72°C for 10 min. GAPDH-specific primers [31] were 5'-TCGTGGAGTCTACTGGCGTCTT-3' (sense) and 5'-CCTCTCTCTTGCTCTCAGTATC-3' (antisense). GAPDH was used as an internal control. All primers were synthesized by Sangon Bio-Engineering Co. Ltd. (Shanghai, China). Amplification products and a 100 bp DNA ladder (Takara Bio, Kusatsu, Japan) were separated by 3% agarose gel electrophoresis and then visualized using ethidium bromide staining and ultraviolet light.

2.6. Western Blotting Analysis. Proteins were extracted using TRIzol reagent according to the manufacturer's instructions. Protein concentrations were measured using BCA Protein Assay Kit (Bipeic Biopharma Corporation, USA) with bovine serum albumin standards and then equalized. Samples were denatured at 100°C for 5 min, separated by 12% sodium dodecyl sulfate polyacrylamide gel electrophoresis, and transferred to a 0.45 μm polyvinylidene difluoride membrane (Immobilon-P; EMD Millipore, Burlington, MA). The membrane was blocked in a solution of 50 mM Tris HCl, 100 mM NaCl, and 0.1% Tween-20, pH 7.4 (TBST) containing 5% nonfat dry milk, followed by incubation with a 1:500 dilution of polyclonal rabbit anti-rat GAP43 antibody (Abcam) in 5% nonfat dry milk (in TBST) at 4°C overnight. Membranes were washed three times with TBST buffer for 5 min each and further incubated with a 1:2000 dilution of horseradish peroxidase- (HRP-) conjugated goat anti-rabbit IgG at room temperature for 2 h. After washing the membrane, HRP activ-

ity was detected using an enhanced chemiluminescence kit (Roche Diagnostics, Mannheim, Germany). GAPDH (1:5000, mouse anti-GAPDH; Kangcheng, Shanghai, China) was used as an internal control. X-ray autoradiography was performed using Kodak X-Omat BT film (Rochester, NY).

2.7. Facial Nerve Stem Toluidine Blue Staining and Transmission Electron Microscopy (TEM). The regeneration axons were detected through facial nerve stem semithin section toluidine blue staining and facial nerve stem ultrathin section transmission electron microscopy analyses.

2.8. Data Collection and Statistical Analysis. Optical densities of GAP43 were measured using Quantity One software version 4.4.0 (Bio-Rad, Hercules, CA). For each rat, the number of surviving motoneurons was quantified by counting the number of neurons containing a visible nucleus-nucleolus in every second 20 μm section throughout the length of the facial nucleus. Motoneuron counts were recorded as the percentage of motoneurons contralateral to the axotomy and graphed as the mean and standard error of the mean. One-way ANOVA was performed using Stata 8.0 software (Stata, College Station, TX) and $P < 0.05$ was considered significant.

3. Results

3.1. Following Reinjury, GAP43 mRNA and Protein in Facial Motoneurons Were Initially Upregulated, but Then Gradually Decreased. Fluorescence labeling was used to identify cellular expression of GAP43 after facial nerve axotomy and reaxotomy. In facial nerve motoneurons of Group I animals (axotomy only), GAP43 was expressed at a low level on both the control side (Figure 1(a)) and the chronically axotomized side (Figure 1(b)). However, GAP43 expression gradually decreased on the reinjured side. Animals with reaxotomy at 12 w exhibited higher GAP43 expression in the ipsilateral facial nucleus (Figure 1(d)) compared with the control side (Figure 1(c)). At 28 w after the initial axotomy, GAP43 expression in the reinjured side was not higher than the control side and may have been weaker.

GAP43 mRNA transcripts were semiquantified by RT-PCR analysis of total RNA purified from facial nuclei from five independent experiments. In Group I animals (axotomy only), GAP43 transcripts in the axotomized side were present at a lower level compared with control sides at 12, 20, 28, and 36 w after axotomy (Figure 2(a)). However, as observed by microscopy, GAP43 mRNA expression was upregulated in injured sides compared with control sides of Group II animals reaxotomized 12 w after the initial facial nerve axotomy. However, GAP43 mRNA was present at a similar level to that of control sides when reinjury was performed at 20 w or 28 w. At 36 w, GAP43 transcript levels were lower in injured sides compared with control sides (Figure 2(b)).

Western blot analysis was used to semiquantify the expression of GAP43 protein, which was visualized as a 36 kDa band. At all experimental time points in Group I (axotomy alone), GAP43 protein was lower in the injured side compared with the control side (Figure 2(c)). In Group II (reaxotomy), GAP43 protein expression was increased

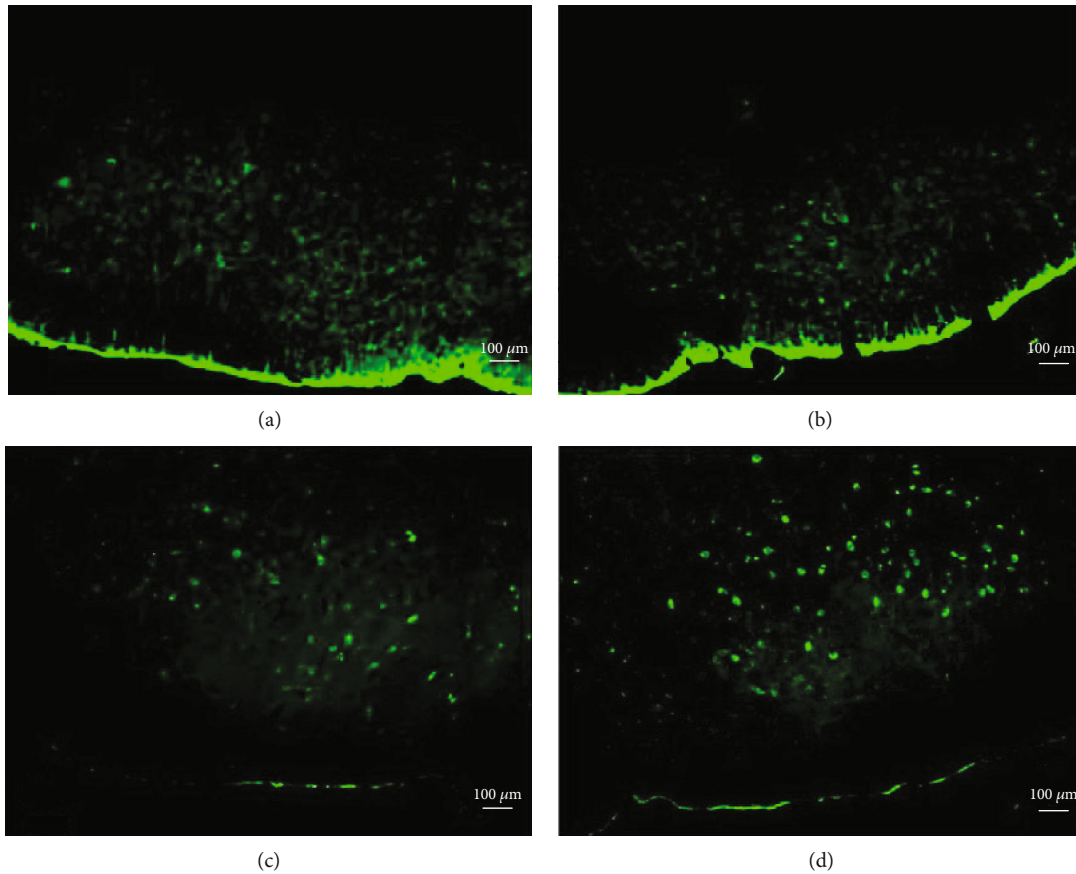


FIGURE 1: In Group I, GAP43 was expressed at a low level on the normal control side (a) and chronically axotomized side (b), but was higher in the facial nucleus at 12 w reaxotomy (d) compared with the control side (c).

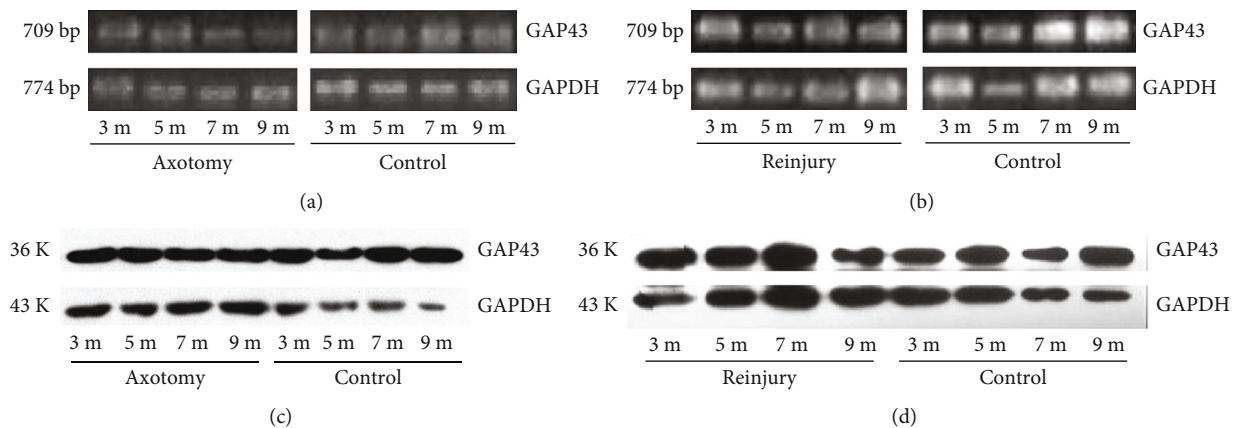


FIGURE 2: RT-PCR and western blot analysis of total RNA. GAP43 transcripts and GAP43 protein expression at 3, 5, 7, and 9 months after axotomy.

when reaxotomy was performed 12 w or 20 w after the initial facial nerve axotomy. Expression of GAP43 protein was similar to that of its control side at 28 w, but was decreased at 36 w (Figure 2(d)).

3.2. Facial Nerve Axons Initially Regenerated and Then Gradually Decreased in the Reinjured Side. When reaxotomy

was performed at 12 w or 20 w, toluidine blue staining and transmission electron microscopy revealed regeneration of facial nerve axons on the reinjured side. At 28 w, there was a significantly reduced number of regenerating axons (data not shown).

Using transmission electron microscopy, regenerating axons and a small number of Schwann cells could be

visualized. Most of the region was filled with collagen fibers, and perineuria appeared normal. However, hardly any surviving axons were observed and perineuria appeared collapsed at 28 w (Figure 3).

3.3. The Relationship between Changes in Facial Nerve Regeneration Potential and Shh

3.3.1. Shh Is Expressed in GAP43-Positive Neurons and Not Glial Cells. Double fluorescence labeling of the brain stem containing bilateral facial nuclei and subsequent laser scanning confocal fluorescence microscopy showed that although GFAP-positive glial cells did not express Shh, most GFAP-positive cells were located close to or wrapped around Shh-positive cells (Figure 4). GAP43 is a marker of neurons, and GAP43-positive cells in the facial nerve indicate motoneurons. These motoneurons expressed Shh at a higher level than GFAP-positive cells (Figure 5). Moreover, our results suggest that glial cells are activated after reinjury of the facial nerve, whereby they mainly locate around Shh-positive motoneuron cells.

3.3.2. Following Facial Nerve Reinjury, Shh Protein Expression Decreased Over Time. In Group I single axotomy animals, double fluorescence labeling of the facial nucleus revealed weaker expression of GAP43 and Shh in the axotomized side compared with the control side (data not shown). In Group II reinjured animals, expression of GAP43 and Shh in the reinjured side was higher at 12 w compared with the control facial nucleus side (Figure 6). Reinjury at 36 w after the initial axotomy resulted in GAP43 and Shh expression levels that were no higher than observed in their respective control sides. After 36 w, the expression of GAP43 and Shh had decreased even more.

4. Discussion

Facial nerve axotomy in adult rats results in the degeneration of a third of facial motoneurons [33]. The loss of neurons takes several weeks and it is not understood how and why the remaining two-thirds of facial motoneurons survive. However, it is known that neurons have the potential to regenerate for a certain period following facial nerve axotomy [34, 35].

Factors that affect axonal fate after facial nerve axotomy include slow retrograde transport of large molecules such as cytokines and trophic factors, as well as the loss of target-derived trophic factors [34, 36, 37]. Genetic factors may also be associated with the potential to regenerate.

Very often, facial paralysis patients cannot be operated on immediately, which means that surgical procedures to repair the facial nerve can occur long after the initial paralysis. The time frame during which reparative surgery is still effective is unclear. Facial nerve false neuroma near the brain stump needs to be removed prior to facial paralysis transplant surgery. After this initial removal, nerve transplantation is carried out. Whether and the extent to which the facial nerve regenerates is dependent on its regeneration potential after facial nerve stump removal. If the capacity

for facial nerve regeneration is extremely low, repair is difficult, even after the nerve graft has been performed.

The results of this study suggest that facial nerve regeneration mainly occurs after early reinjury of the chronically axotomized facial nerve. Therefore, the regeneration potential of the facial nerve is related to the timing of the second axotomy. Interestingly, only early reinjury (occurring less than 5 months after the initial injury) induced upregulation of Shh and Smo, whereas later reaxotomy had no effect.

Strong Shh immunoreactivity was observed in the cell bodies of facial motoneurons (GAP43-positive cells), but not detected in the cell bodies of astrocytes (GFAP-positive cells). This selective upregulation of Shh in reaxotomized motoneurons may play an important role in altering its functions. The regeneration of motoneurons may be dependent on Shh, which may influence regeneration through (as yet) unidentified molecules. Additional studies of Shh signaling are required to clarify precisely how the cellular network is preserved in nerve regeneration.

Our study also showed that Shh was upregulated in a time-dependent manner. Three months after facial nerve axotomy, Shh in the facial nucleus on the experimental side was significantly lower compared with the control side. Following facial nerve axotomy, motoneurons of the facial nucleus do not have a target; therefore, we hypothesize that the observed decrease in Shh results from the loss of a target. However, as nearly a third of facial motoneurons were lost and lower expression of Shh could simply be caused by the absence of neurons.

Our experiments show that the later the time point of reinjury, the weaker the Shh expression and at the same time the weaker the GAP43 expression. We speculate that maybe because of the decrease in Shh activation capacity may lead to a reduction in facial nerve regeneration. It is well known that astrocyte responses occur around neurons after facial nerve injury; astrocytes were closely related to neuronal cells and regulate the development and repair of the central nervous system. A variety of cytokines secreted by astrocytes also play an important role in regulating the signal transmission and synaptic transmission [5], as further confirmed in this study.

We propose that after facial nerve axotomy, the function of residual motoneurons is different. The surviving motoneurons are in a substate, and although parts of the motoneurons are still viable, they have very poor ability to regenerate nerve fibers. We speculate that as Shh signaling is activated, downstream regulatory transcription factors play an important role in the reversal of these substate neurons and can subsequently stimulate nerve regeneration.

We also found that at 4 months after facial nerve axotomy, facial nerve perineuria had disaggregated and a few myelin sheaths could be detected. However, 5–7 months after the initial axotomy, the perineurium of the nerves had disappeared and the remaining spaces had been replaced by fibrous connective tissue. This is another reason why axotomized facial nerve surgery should be carried out as early as possible.

Clinically, for some patients who cannot undergo surgery soon after facial nerve injury, surgical treatment in the later

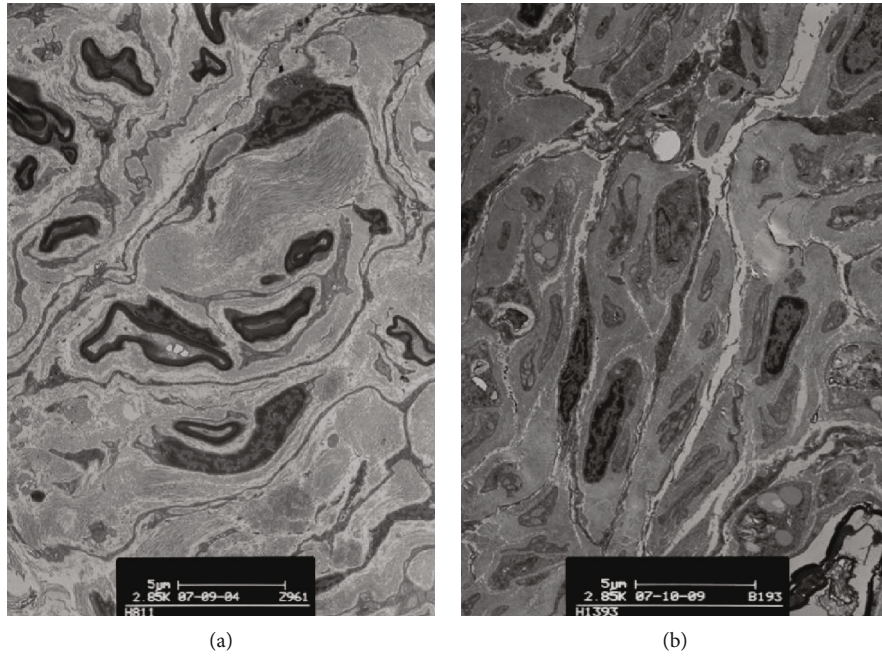


FIGURE 3: Most of the region was filled with collagen fibers and perineuria appeared normal at 12 w (a). Transmission electron microscopy showed hardly any surviving axons were observed and perineuria appeared collapsed at 28 w (b).

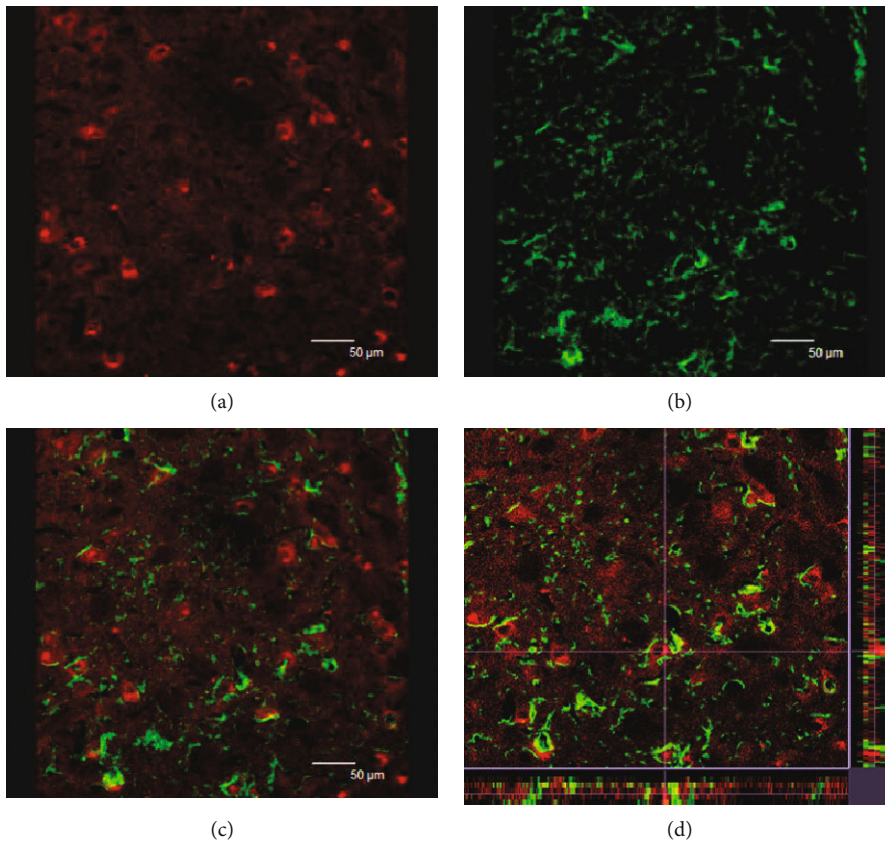


FIGURE 4: Facial nucleus double fluorescent-labeling laser scanning confocal fluorescence microscopy: red indicates sonic hedgehog-positive cells (a); green indicates GFAP-positive cells (b). GFAP-positive cells did not express sonic hedgehog. Panel (c) was the merger of panel (a) and panel (b). Panel (d) is the 3D image of confocal imaging (c).

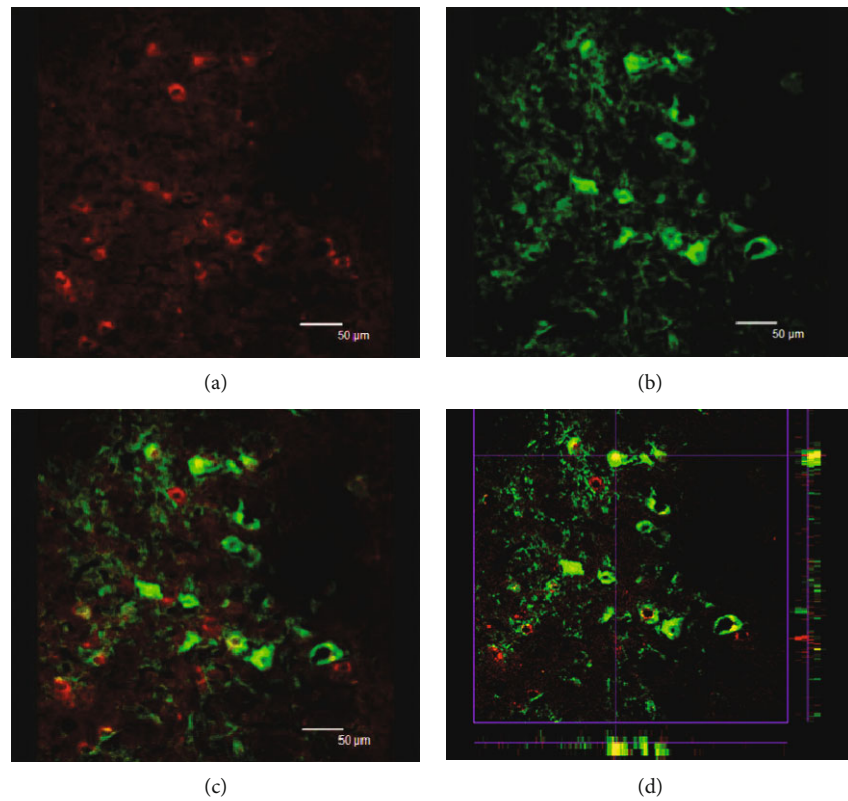


FIGURE 5: Facial nucleus double fluorescent-labeling laser scanning confocal fluorescence microscopy: green indicates GAP43-positive neurons (b); red indicates sonic hedgehog-positive cells (a). The GAP43-positive neurons were stronger expressing sonic hedgehog. Panel (c) was the merger of panel (a) and panel (b). Panel (d) is the 3D image of confocal imaging (c).

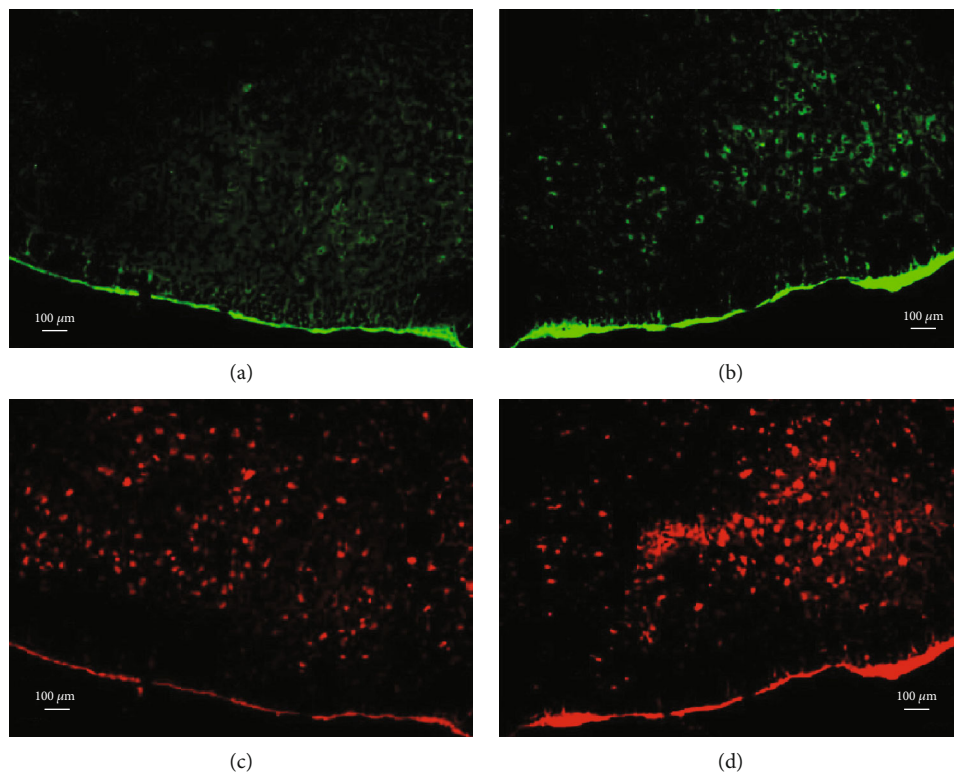


FIGURE 6: Double fluorescent labeling. In the reinjury group (16 w), expression of GAP43 (b) and sonic hedgehog (d) was apparently higher in the reinjured side compared with the control side of the facial nucleus (a) and (c).

stage, including facial nerve decompression, could be regarded as facial nerve reinjury. Our results have a therapeutic implication for clinical treatment of facial nerve after injury and imply that regeneration can be promoted through transgenes. We have shown that after initial axotomy, there is a critical time period that determines the potential of facial nerve regeneration after initial axotomy, and that activation of the Shh signaling pathway is closely related to facial nerve regeneration after reinjury.

5. Conclusion

The purpose of this study was to investigate the nature of facial nerve regeneration to better understand the critical time points and mechanisms involved in regeneration. After facial nerve chronic axotomy in rats, the regeneration potential of the facial nerve peaked within 5 months and maybe was potentially dependent on activation of the Shh signaling pathway.

Data Availability

The data used to support the findings of this study are included within the article.

Ethical Approval

All protocols involving animal experiments were approved by the Animal Care and Use Committee of Fudan University.

Conflicts of Interest

The authors declare that they have no known competing financial interests or personal relationships that could have appeared to influence the work reported in this paper.

Authors' Contributions

Yusu Ni and Huawei Li designed this experimental study. Yusu Ni, Diyan Chen, Yi Jiang, Danhong Qiu, and Wen Li performed the experimental animal procedures and the assessments of all outcome parameters and the tissue analyses. Yusu Ni wrote the manuscript, and Huawei Li revised the manuscript to its final draft. All authors read and approved the final version of this manuscript. Drs. Yusu Ni, Diyan Chen, and Yi Jiang contributed equally to this article.

Acknowledgments

We thank the technicians of the Electron Microscopy Laboratory of Shanghai Medical College of Fudan University for the transmission electron microscopy of our samples. This work was supported by the grant from the National Nature Science Foundation of China (No. 81230019) and from the Nature Science Foundation of Shanghai Science and Technology Committee (17ZR1404600).

References

- [1] W. Zhengmin, *Ear Microscopic Surgery*, Shanghai Science and Technology Education Press, Shanghai, 2004.
- [2] H. Dongyi, *Neurology and Lateral Skull Base Surgery*, Science Press, Beijing, 2008.
- [3] K. Weijia and Z. Liang, *Otolaryngology, Head and Neck Surgery*, People's Health Publishing House, Beijing, 3rd edition, 2015.
- [4] S. Hong and Z. Luo, *Otolaryngology, Head and Neck Surgery*, People's Health Publishing House, Beijing, 9th edition, 2018.
- [5] M. May and B. M. Schaitkin, *The Facial Nerve: May's Second Edition*, Thieme Medical Publishers, New York, NY, 2000.
- [6] E. Euler de Souza Lucena, F. P. Guzen, J. R. Lopes de Paiva Cavalcanti, C. A. Galvão Barboza, E. Silva do Nascimento Júnior, and J. S. Cavalcante, "Experimental considerations concerning the use of stem cells and tissue engineering for facial nerve regeneration: a systematic review," *Journal of Oral and Maxillofacial Surgery*, vol. 72, no. 5, pp. 1001–1012, 2014.
- [7] T. Gordon, S. You, S. L. Cassar, and W. Tetzlaff, "Reduced expression of regeneration associated genes in chronically axotomized facial motoneurons," *Experimental Neurology*, vol. 264, pp. 26–32, 2015.
- [8] D. N. Olmstead, N. A. Mesnard-Hoaglin, R. J. Batka, M. M. Haulcomb, W. M. Miller, and K. J. Jones, "Facial nerve axotomy in mice: a model to study motoneuron response to injury," *Journal of Visualized Experiments*, vol. 23, no. 96, 2015.
- [9] S. Rink, H. Bendella, S. M. Akkin, M. Manthou, M. Grosheva, and D. N. Angelov, "Experimental studies on facial nerve regeneration," *The Anatomical Record*, vol. 302, no. 8, pp. 1287–1303, 2019.
- [10] O. Guntinas-Lichius and D. N. Angelov, "Experimental studies for the improvement of facial nerve regeneration," *HNO*, vol. 56, no. 2, pp. 122–130, 2008.
- [11] T. Takeda, S. Takeda, T. Okada, A. Kakigi, and T. Yamasoba, "Experimental studies on the recovery processes from severe facial palsy and the development of its sequelae," *Otology & Neurotology*, vol. 36, no. 5, pp. 896–903, 2015.
- [12] R. B. Ahuja, P. Chatterjee, R. Gupta, P. Shrivastava, and G. K. Gupta, "A new paradigm in facial reanimation for long-standing palsies?," *Indian Journal of Plastic Surgery*, vol. 48, no. 1, pp. 30–37, 2015.
- [13] K. Hashimoto, H. Matsumine, H. Osaki et al., "Prevention of denervated muscle atrophy with accelerated nerve-regeneration by babysitter procedure in rat facial nerve paralysis model," *Microsurgery*, pp. 1–9, 2020.
- [14] A. Golzadeh and R. Mohammadi, "Effect of local administration of platelet-derived growth factor B on functional recovery of peripheral nerve regeneration: a sciatic nerve transection model," *Dental Research Journal*, vol. 13, no. 3, pp. 225–232, 2016.
- [15] Y. Wang, X. Zhao, M. Huojia, H. Xu, and Y. Zhuang, "Transforming growth factor- β 3 promotes facial nerve injury repair in rabbits," *Experimental and Therapeutic Medicine*, vol. 11, no. 3, pp. 703–708, 2016.
- [16] M. Grosheva, K. Nohroudi, A. Schwarz et al., "Comparison of trophic factors' expression between paralyzed and recovering muscles after facial nerve injury. A quantitative analysis in time course," *Experimental Neurology*, vol. 279, pp. 137–148, 2016.
- [17] M. Seitz, M. Grosheva, E. Skouras et al., "Poor functional recovery and muscle polyinnervation after facial nerve injury

- in fibroblast growth factor-2^{-/-} mice can be improved by manual stimulation of denervated vibrissal muscles,” *Neuroscience*, vol. 182, pp. 241–247, 2011.
- [18] H. Fujimaki, H. Matsumine, H. Osaki et al., “Dedifferentiated fat cells in polyglycolic acid-collagen nerve conduits promote rat facial nerve regeneration,” *Regenerative Therapy*, vol. 11, pp. 240–248, 2019.
- [19] Z. Zhang, X. Li, Z. Li et al., “Collagen/nano-sized β -tricalcium phosphate conduits combined with collagen filaments and nerve growth factor promote facial nerve regeneration in miniature swine: an in vivo study,” *Oral Surgery, Oral Medicine, Oral Pathology, Oral Radiology*, vol. 128, no. 5, pp. 472–478, 2019.
- [20] M. Shimizu, H. Matsumine, H. Osaki et al., “Adipose-derived stem cells and the stromal vascular fraction in polyglycolic acid-collagen nerve conduits promote rat facial nerve regeneration,” *Wound Repair and Regeneration*, vol. 26, no. 6, pp. 446–455, 2018.
- [21] W. Kamei, H. Matsumine, H. Osaki et al., “Axonal supercharged interpositional jump-graft with a hybrid artificial nerve conduit containing adipose-derived stem cells in facial nerve paresis rat model,” *Microsurgery*, vol. 38, no. 8, pp. 889–898, 2018.
- [22] D. M. Saez, R. T. Sasaki, D. de Oliveira Martins, M. Chacur, I. Kerkis, and M. C. P. da Silva, “Rat facial nerve regeneration with human immature dental pulp stem cells,” *Cell Transplantation*, vol. 28, no. 12, pp. 1573–1584, 2019.
- [23] R. de Carvalho Raimundo, F. S. Landim, A. C. A. Gomes, C. B. M. M. Castro, V. A. Silva Junior, and B. C. do Egito Vasconcelos, “Morphofunctional effect of stem cells on the regeneration of the facial nerve in a rat model,” *Journal of Oral and Maxillofacial Surgery*, vol. 77, no. 10, pp. 2168.e1–2168.e12, 2019.
- [24] M. P. Willand, M. A. Nguyen, G. H. Borschel, and T. Gordon, “Electrical stimulation to promote peripheral nerve regeneration,” *Neurorehabilitation and Neural Repair*, vol. 30, no. 5, pp. 490–496, 2015.
- [25] A. Raslan, M. A. M. Salem, A. Al-Hussaini, O. Guntinas-Lichius, and A. Irintchev, “Brief electrical stimulation improves functional recovery after femoral but not after facial nerve injury in rats,” *The Anatomical Record*, vol. 302, no. 8, pp. 1304–1313, 2019.
- [26] E. Mäkelä, H. Venesvirta, M. Ilves et al., “Facial muscle reanimation by transcutaneous electrical stimulation for peripheral facial nerve palsy,” *Journal of Medical Engineering & Technology*, vol. 43, no. 3, pp. 155–164, 2019.
- [27] H. Roelink, J. A. Porter, C. Chiang et al., “Floor plate and motor neuron induction by different concentrations of the amino-terminal cleavage product of sonic hedgehog autoproteolysis,” *Cell*, vol. 81, no. 3, pp. 445–455, 1995.
- [28] A. R. I. Altaba, T. M. Jessell, and H. Roelink, “Restrictions to Floor Plate Induction by *hedgehog* and Winged-Helix Genes in the Neural Tube of Frog Embryos,” *Molecular and Cellular Neuroscience*, vol. 6, no. 2, pp. 106–121, 1995.
- [29] S. Agarwala, T. A. Sanders, and C. W. Ragsdale, “Sonic hedgehog control of size and shape in midbrain pattern formation,” *Science*, vol. 291, no. 5511, pp. 2147–2150, 2001.
- [30] M. Komada, “Sonic hedgehog signaling coordinates the proliferation and differentiation of neural stem/progenitor cells by regulating cell cycle kinetics during development of the neocortex,” *Congenital Anomalies*, vol. 52, no. 2, pp. 72–77, 2012.
- [31] C. Akazawa, H. Tsuzuki, Y. Nakamura et al., “The upregulated expression of sonic hedgehog in motor neurons after rat facial nerve axotomy,” *The Journal of Neuroscience*, vol. 24, no. 36, pp. 7923–7930, 2004.
- [32] C. Akazawa and S. Kohsaka, “In vivo characterization of sonic hedgehog in the peripheral nerve regeneration,” *Brain and Nerve*, vol. 59, no. 12, pp. 1341–1346, 2007.
- [33] V. Krishnan, Y. L. Ma, J. M. Moseley, A. G. Geiser, S. Friant, and C. A. Frolik, “Bone anabolic effects of sonic/Indian hedgehog are mediated by BMP-2/4-dependent pathways in the neonatal rat metatarsal model,” *Endocrinology*, vol. 142, no. 2, pp. 940–947, 2001.
- [34] M. P. LT, K. J. Fernandes, C. C. Chan, J. L. Vanderluit, and W. Tetzlaff, “Axonal reinjury reveals the survival and re-expression of regeneration-associated genes in chronically axotomized adult mouse motoneurons,” *Experimental Neurology*, vol. 188, no. 2, pp. 331–340, 2004.
- [35] A. F. Hottinger, M. Azzouz, N. Deglon, P. Aebischer, and A. D. Zurn, “Complete and long-term rescue of lesioned adult motoneurons by lentiviral-mediated expression of glial cell line-derived neurotrophic factor in the facial nucleus,” *The Journal of Neuroscience*, vol. 20, no. 15, pp. 5587–5593, 2000.
- [36] C. J. Serpe, A. P. Kohm, C. B. Huppenbauer, V. M. Sanders, and K. J. Jones, “Exacerbation of facial motoneuron loss after facial nerve transection in severe combined immunodeficient (scid) mice,” *The Journal of Neuroscience*, vol. 19, no. 11, p. RC7, 1999.
- [37] C. J. Serpe, V. M. Sanders, and K. J. Jones, “Kinetics of facial motoneuron loss following facial nerve transection in severe combined immunodeficient mice,” *Journal of Neuroscience Research*, vol. 62, no. 2, pp. 273–278, 2000.

Research Article

Compound Heterozygous Mutations in *TMC1* and *MYO15A* Are Associated with Autosomal Recessive Nonsyndromic Hearing Loss in Two Chinese Han Families

Pengcheng Xu,^{1,2,3} Jun Xu ,^{1,2,3} Hu Peng,⁴ and Tao Yang ^{1,2,3}

¹Department of Otorhinolaryngology-Head and Neck Surgery, Shanghai Ninth People's Hospital, Shanghai Jiao Tong University School of Medicine, Shanghai, China

²Ear Institute, Shanghai Jiao Tong University School of Medicine, Shanghai, China

³Shanghai Key Laboratory of Translational Medicine on Ear and Nose Diseases, Shanghai, China

⁴Department of Otolaryngology-Head and Neck Surgery, Changzheng Hospital, Second Military Medical University, Shanghai, China

Correspondence should be addressed to Tao Yang; taoyang@sh-jei.org

Received 22 April 2020; Revised 12 June 2020; Accepted 6 July 2020; Published 1 August 2020

Academic Editor: Renjie Chai

Copyright © 2020 Pengcheng Xu et al. This is an open access article distributed under the Creative Commons Attribution License, which permits unrestricted use, distribution, and reproduction in any medium, provided the original work is properly cited.

Genetic hearing loss is a common sensory disorder, and its cause is highly heterogeneous. In this study, by targeted next-generation sequencing of 414 known deafness genes, we identified compound heterozygous mutations p.R34X/p.M413T in *TMC1* and p.S3417del/p.R1407T in *MYO15A* in two recessive Chinese Han deaf families. Intrafamilial cosegregation of the mutations with the hearing phenotype was confirmed in both families by the Sanger sequencing. Auditory features of the affected individuals are consistent with that previously reported for recessive mutations in *TMC1* and *MYO15A*. The two novel mutations identified in this study, p.M413T in *TMC1* and p.R1407T in *MYO15A*, are classified as likely pathogenic according to the guidelines of ACMG. Our study expanded the mutation spectrums of *TMC1* and *MYO15A* and illustrated that genotype-phenotype correlation in combination with next-generation sequencing may improve the accuracy for genetic diagnosis of deafness.

1. Introduction

Congenital hearing impairment is a common birth defect worldwide, occurring in approximately 1-2 per 1000 infants. With increasing age, the prevalence continues to rise to 2.7 per 1000 before age five and 3.5 per 1000 through adolescence [1]. To date, more than 100 genes have been reported to be associated with nonsyndromic hearing loss (NSHL), including 76 autosomal recessive nonsyndromic hearing loss (ARNSHL) genes, 48 autosomal dominant nonsyndromic hearing loss (ADNSHL) genes, and 5 X-linked nonsyndromic hearing loss genes (Hereditary Hearing Loss Homepage; <https://hereditaryhearingloss.org/>, updated in January 2020). Hair cells (HCs) in the cochlea mainly function in converting the sound mechanical waves into the electric neural signals [2-4] which make it extremely critical for the hearing ability. Many previous studies have shown that HCs can be damaged due to genetic factors, ototoxic drugs, noise,

inflammation, or aging, among which genetic account for 50% of the HC malfunction [5-11].

The *TMC1* gene is located on chromosome 9q21 and contains 24 exons that encodes a 760 amino acid membrane protein TMC1 with six transmembrane domains [12, 13]. TMC1 is a pore-forming subunit of the mechanotransduction complex that is predicted to have transmembrane domains with intracellular N and C termini and one conserved TMC domain [14]. TMC1 is expressed in the mouse inner ear and has been suggested to involve in the functional maturation and survival of cochlear HCs [12]. It has been reported that mutations in *TMC1* may cause both prelingual profound autosomal recessive deafness DFNB7/11 and postlingual progressive autosomal dominant deafness DFNA36 [13]. To date, more than 60 mutations in *TMC1* are reported worldwide [15], with the recessive mutations predominantly associated with prelingual severe-to-profound hearing loss [15, 16].

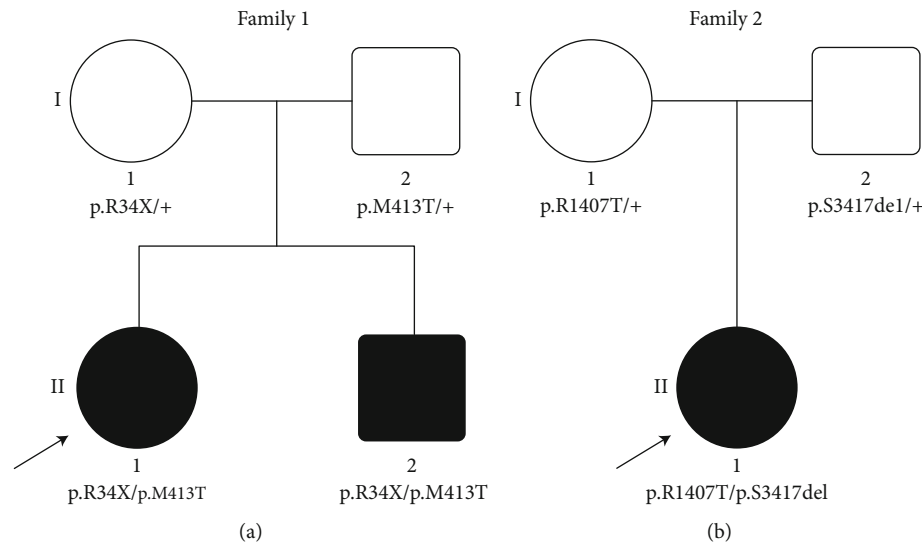


FIGURE 1: Pedigrees and genotypes of Family 1 (a) and Family 2 (b).

The HC stereocilia is critical to maintain the function of HC [17, 18]. The *MYO15A* gene is located at chromosome 17p11.2 and contains 66 coding exons, which encodes an unconventional myosin protein Myosin XVA [19]. Myosin XVA is a large actin-based motor protein. In cochlear hair cells, it is critical for elongation and differentiation of the stereocilia [20]. Myosin XVA displays an important role in the mechanotransduction of cochlear hair cells. Myosin XVA through its carboxy-terminal PDZ-ligand interacts with the third PDZ domain of whirlin, and then delivers whirlin to the tips of stereocilia [21]. *MYO15A* mutations are responsible for congenital deafness DFNB3 in human and cochleovestibular dysfunction in shaker 2 mice which shows abnormally short stereocilia bundles and diminished staircase [20, 21]. It is one of the most common causes of ADNSHL in Mideast countries due to prevalent consanguineous marriage [22, 23], with majority associated with prelingual severe-to-profound hearing loss and mutations in exon 2 leading to a milder auditory phenotype [23].

In this study, we presented the clinical characterization and genetic analysis of two Chinese Han families affected by ARNSHL. Using targeted next-generation sequencing of 414 known deafness genes, we identified compound heterozygous mutations in *TMC1* and *MYO15A* as the genetic causes of the hearing loss in those families.

2. Materials and Methods

2.1. Subjects and Clinical Evaluations. This study included two nuclear Chinese Han recessive deaf families: Family 1 (Figure 1(a)) and Family 2 (Figure 1(b)). All affected family members underwent clinical evaluation in the Department of Otolaryngology-Head and Neck Surgery, Shanghai Ninth People's Hospital, Shanghai Jiao Tong University School of Medicine, Shanghai, China. The evaluation included a complete medical history interview and a comprehensive physical examination including otoscopic examination to exclude hearing loss due to infections, trauma, or other environmen-

tal factories. Middle ear function was evaluated through tympanometry, and the function of the outer hair cells of the cochlea was evaluated by distortion production otoacoustic emissions (DPOAE). Pure-tone audiometry (PTA) was calculated as the average of the hearing threshold of patients at 500, 1,000, 2,000, and 4,000 Hz. The degree of hearing loss was defined as mild (26–40 dB HL), moderate (41–55 dB HL), moderately severe (56–70 dB HL), severe (71–90 dB HL), and profound (>90 dB HL). Hearing thresholds reported in this study were averaged air-conducted pure-tone thresholds of each side. Tandem gait and the Romberg testing were performed for vestibular function examination. Computerized tomography (CT) scan of the temporal bone was carried out to assess the development of the anatomical structures of the middle and inner ear for the available subjects. This study was approved by the ethnic committee of Shanghai Ninth People's Hospital. Written informed consents were obtained from each participant or from parents of the young subject.

2.2. Mutation Identification. The genomic DNA of peripheral blood was extracted from all subjects using a Blood DNA kit according to the standard protocol (QIAamp DNA Blood Mini Kit, QIAGEN, Shanghai). Targeted next-generation sequencing was performed as previously reported [24, 25]. The exons, splicing sites, and flanking intronic region of 414 known deafness-related genes (Table S1) were captured by a customized capture assay (MyGenostics, Beijing, China). Candidate pathogenic mutations were defined as nonsynonymous (including nonsense, missense, splice-site, and indels) variants that had allele frequencies under 0.01 in the 1000 Genomes database, the dbSNP database, the Exome Aggregation Consortium database (ExAC), and data from 200 Chinese Han normal-hearing control individuals. The potential pathogenic effects of candidate mutations were evaluated by *in silico* tools Mutation Taster, SIFT, and PolyPhen2. Cosegregation of the disease phenotype and the causative mutation was confirmed in all family members by

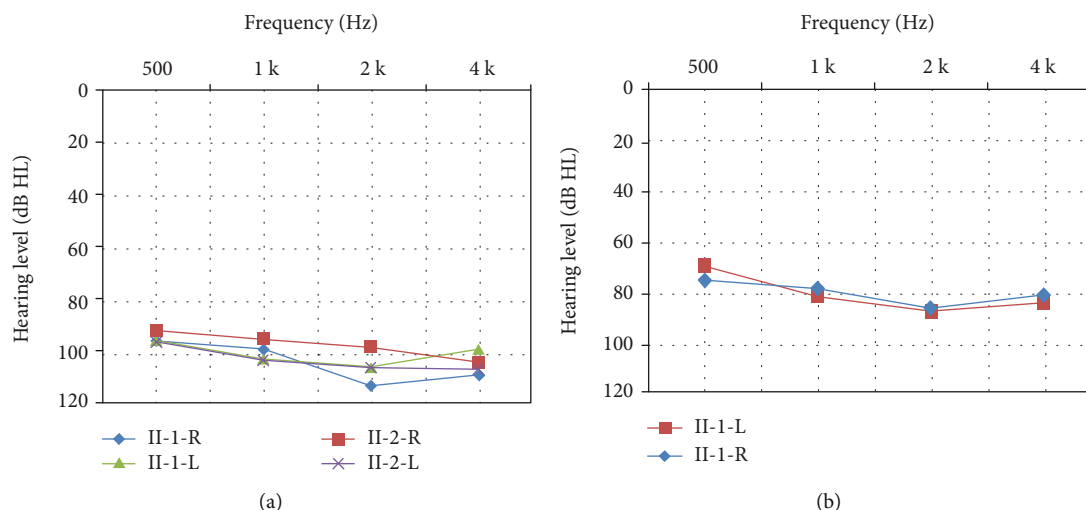


FIGURE 2: Audiograms of the affected members of Family 1 (a) and Family 2 (b).

PCR amplification and the Sanger sequencing. Pathogenicity of the mutations were classified following the guidelines of ACMG 2015 [26].

3. Results

3.1. Clinical Characterization

3.1.1. Family 1. Family 1 has two affected siblings born to two normal-hearing parents (Figure 1(a)). The proband II-1 was a 26-year-old female with congenital sensorineural hearing loss. Tympanogram indicated normal function of the middle ear. Bilateral DPOAE were absent. Both II-1 and her younger brother II-2 suffered from bilateral, profound hearing impairment with PTA thresholds above 90 dB HL (Figure 2(a)). Tandem gait and the Romberg testing displayed no symptoms of vestibular dysfunction. Temporal bone CT scans showed no obvious abnormalities. No apparent additional syndromic features were found.

3.1.2. Family 2. The proband II-1 of Family 2 (Figure 1(b)) was a 10-year-old girl, who suffered from prelingual bilateral hearing impairment. Auditory examination and PTA showed the sensorineural hearing loss is severe (Figure 2(b)). Tympanogram displayed a type A curve, indicating normal function of the middle ear. Bilateral DPOAE were absent, and no vestibular dysfunction was recorded for the proband. No other abnormality was discovered by the medical history and physical examination.

3.2. Mutation Analysis. Targeted next-generation sequencing of 414 known deafness genes was performed for the probands Family1-II-1 and Family2-II-1. A total of 9 and 13 candidate variants were identified, respectively (Table S2). In Family 1, compound heterozygous mutations c.100C>T (p.R34X) and c.1238T>C (p.M413T) in *TMC1* (NM_138691) were identified as the only candidate mutations consistent with the recessive inheritance. The Sanger sequencing revealed that the mutations cosegregated with the hearing phenotype in Family 1, as the unaffected parents, were heterozygous carriers of single mutations p.R34X (mother

I-1) and p.M413T (father I-2), while the affected siblings both had compound heterozygous mutations (Figure 3(a)). These two mutations were not detected in 200 Chinese Han normal-hearing controls and are not present in 1000 Genomes and ExAC databases. The p.R34X mutation with minor allele frequency (MAF) of 0.0002 in ExAC has been previously detected in many patients from Pakistan, Iran, Turkey, and Tunisia but is relatively rare in China [16, 27–29]. On the other hand, while the p.M413T mutation is novel. Based on the ACMG guidelines, the p.R34X and p.M413T mutations in *TMC1* were classified as pathogenic (PVS1+PS1+PM2+BS2) and likely pathogenic (PM2+PM3+PP3), respectively.

In Family 2, compound heterozygous variants c.10245_10247delCTC (p.S3417del) and c.4220G>C (p.R1407T) in *MYO15A* (NM_016239) were considered the only candidate pathogenic variants consistent with the recessive inheritance. The Sanger sequencing confirmed that the mutations cosegregated with the hearing phenotype in Family 2, as the unaffected parents were heterozygous carriers of single mutations p.R1407T (mother I-1) and p.S3417del (father I-2) (Figure 4(a)). These two mutations were not detected in 200 Chinese Han normal-hearing controls and are not present in 1000 Genomes and ExAC databases. The p.S3417del mutation with MAF of 0.000016 in ExAC has been previously reported to cause autosomal recessive hearing loss in Japanese and Korean patients, but not in the Chinese population [30, 31]. The p.R1407T mutation is novel. Based on the ACMG guidelines, the p.S3417del and p.R1407T mutations in *MYO15A* were classified as pathogenic (PS1+PM2+PM3+PM4) and likely pathogenic (PM2+PM3+PP3), respectively.

4. Discussion

Recessive hearing loss accounts for the majority (80%) of genetic hearing loss [32]. Among many genes responsible for ARSNHL, mutations in *GJB2* are the most frequent causes [33, 34], followed by that in *SLC26A4*, *TMC1*, and *MYO15A* especially in Middle East countries where

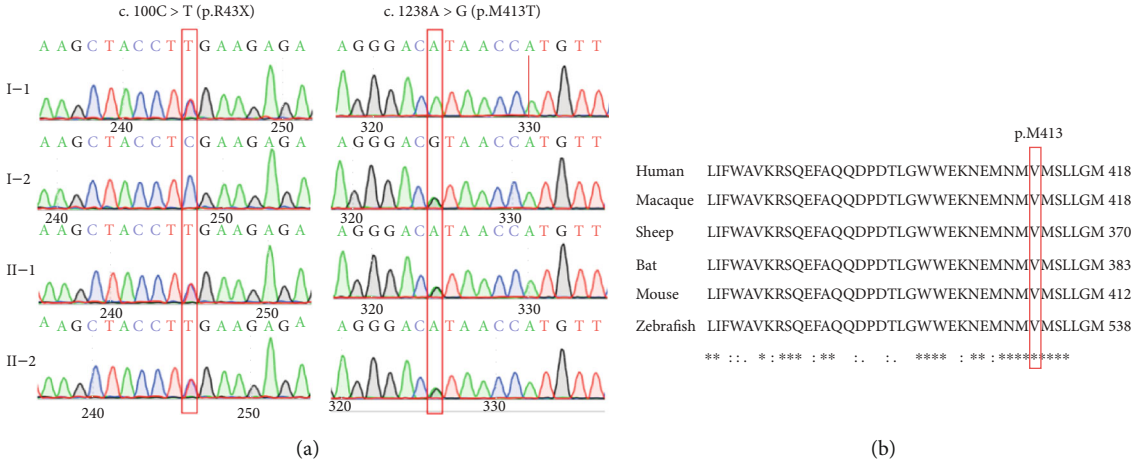


FIGURE 3: (a) The Sanger sequencing results of the p.R34X and p.M413T mutations in *TMC1* in Family 1. (b) Multispecies sequence alignment of the M413 residue.

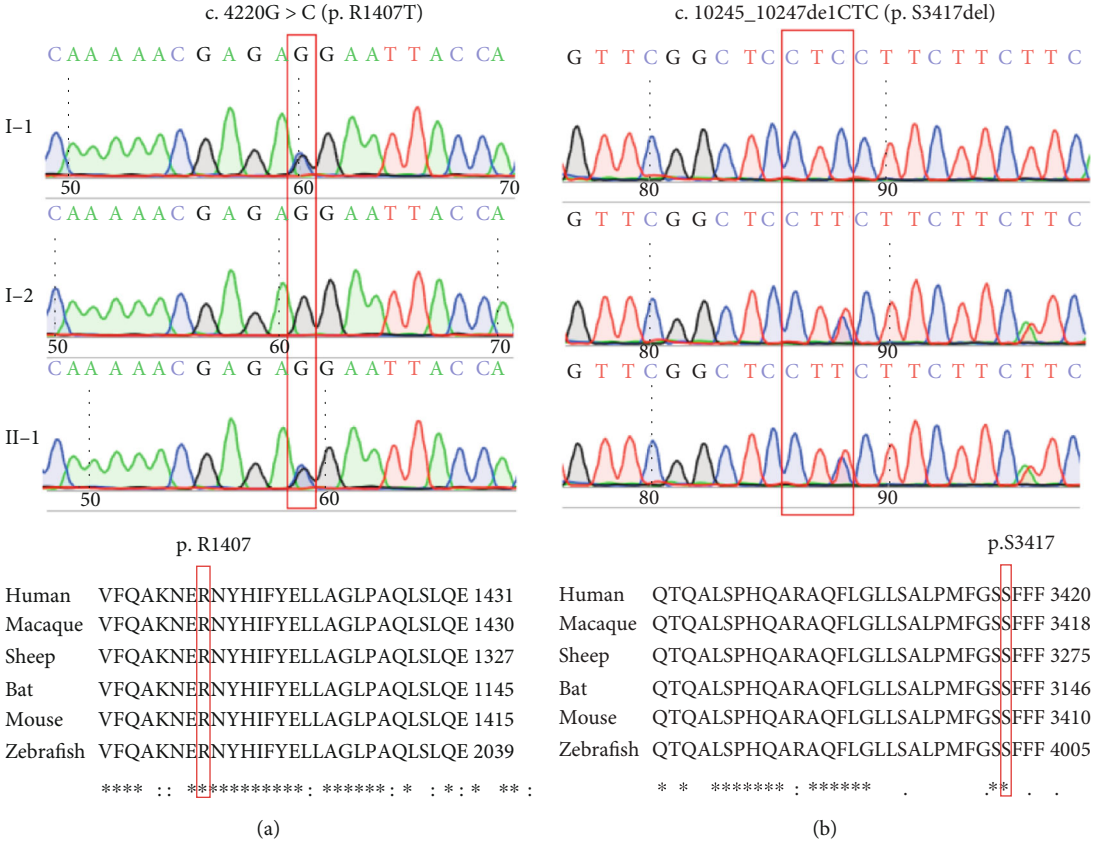


FIGURE 4: (a) The Sanger sequencing results of the p.S3417del and p.R1407T mutations in *MYO15A* in Family 2. (b) Multispecies sequence alignment of the S3417 and R1407 residues.

consanguineous marriage is common [15, 22, 35]. On the contrary, in China where consanguineous marriage is far less frequent, recessive mutations in *TMC1* and *MYO15A* were not as extensively reported in the literature.

In Family 1, we identified compound heterozygous mutations p.R34X and p.M413T in *TMC1*. The p.R34X mutation is the most common *TMC1* mutation in Pakistan [36]. Using polymorphic markers, Ben Said et al. showed that this non-

sense mutation is an old founder mutation emerged between the years 1075 and 1900 along with the third Hadhramaut population movements [27]. This nonsense mutation is predicted to produce a prematurely truncated protein and is associated with congenital, severe-to-profound deafness [13, 27]. The p.M413T mutation identified in this study has not been previously reported. It is predicted as deleterious by computational tools PolyPhen2 and SIFT. The p.M413T

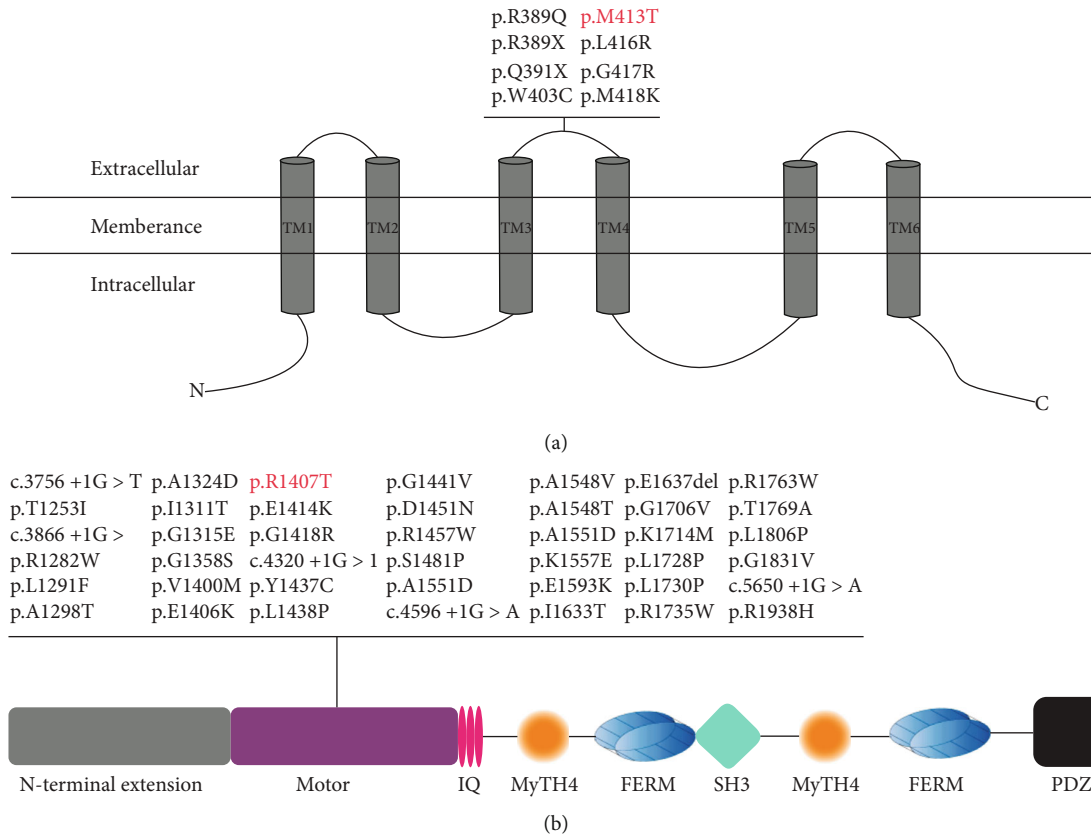


FIGURE 5: (a) Transmembrane domain structure of TMC1 and mutations in the second extracellular loop of TMC1. The novel p.M413T mutation identified in this study is in red. (b) Protein structure of Myosin XVA and missense mutations in the motor domain. The novel p.R1407T mutation identified in this study is in red.

mutation is located in the second extracellular loop between the third and fourth transmembrane domains of TMC1, and the methionine 413 residue is well conserved among different species (Figure 3(b)). At least seven mutations in the second extracellular loop, including five missense mutations, have already been associated with ARNSHL and ADNSHL (Figure 5(a)), suggesting an important role of this particular region in the inner ear function of TMC1.

In Family 2, we identified compound heterozygous mutations p.S3417del and p.R1407T in *MYO15A*. The p.S3417del mutation deletes a serine3417 residue at the second FERM domain of Myosin XVA. The FERM domain is a protein-binding domain important in cargo transport and cytoplasmic protein connection to the membrane [37, 38]. This mutation has been previously reported in Japanese and Korean deaf patients but not in the Chinese population [30, 31]. The novel p.R1407T mutation identified in this study is predicted as deleterious by computational tools PolyPhen2 and SIFT. This mutation is located in the motor domain of Myosin XVA, which is next to the long N-terminal extension and is highly conserved among different species (Figure 4(b)). To date, more than 40 missense mutations in the motor domain of *MYO15A* have been associated with ARSNHL (Figure 5(b)). The motor domain is essential for ATP activity and possesses two binding sites for actin and ATP, which can produce force to move the actin filaments. In the mouse model, *MYO15A* mutation in the motor

domain results shorter stereocilia with an abnormal staircase structure [39].

Considering the high degree of genetic heterogeneity, the next-generation sequencing (NGS) technology has been proven an effective method for genetic testing of hearing loss in recent years. However, previous studies have showed that NGS in deaf patients, especially the sporadic cases, may detect a significant amount of rare, nonsynonymous variants with unknown functional significance and sometimes even results in false-positive diagnosis [25]. In this study, we obtained a detailed hearing phenotype for all patients, which is consistent with those from previous reports for ARSNHL patients with recessive *TMC1* and *MYO15A* mutations. Our data suggested that the genotype-phenotype correlation may facilitate more accurate genetic diagnosis of deafness in such cases.

5. Conclusions

Compound heterozygous mutations p.R34X/p.M413T in *TMC1* and p.S3417del/p.R1407T in *MYO15A* were identified as the pathogenic causes of ARSNHL in two Chinese Han families. Our results expanded the mutation spectrum of those two genes and showed that NGS in combination with genotype-phenotype correlation may provide a more accurate diagnosis for genetic deafness.

Data Availability

The data used to support the findings of this study are available from the corresponding authors upon request.

Conflicts of Interest

The authors declare no conflicts of interests.

Authors' Contributions

Pengcheng Xu, Jun Xu, and Hu Peng contributed equally to this work.

Acknowledgments

This research was supported by grants from the Shanghai Municipal Education Commission–Gaofeng Clinical Medicine Grant (20152519 to TY), Science Project of Shanghai Municipal Commission of Health and Family Planning (201540173 to HP), and National Natural Science Foundation of China (81702643 to HP).

Supplementary Materials

Table S1: the 414 deafness-related genes sequenced by targeted NGS. Table S2: candidate mutations identified in probands F1-II-1 and F2-II-1 by targeted NGS. (*Supplementary Materials*)

References

- [1] C. C. Morton and W. E. Nance, "Newborn hearing screening—a silent revolution," *The New England Journal of Medicine*, vol. 354, no. 20, pp. 2151–2164, 2006.
- [2] Y. Liu, J. Qi, X. Chen et al., "Critical role of spectrin in hearing development and deafness," *Science Advances*, vol. 5, no. 4, 2019.
- [3] Y. Wang, J. Li, X. Yao et al., "Loss of CIB2 causes profound hearing loss and abolishes mechano-electrical transduction in mice," *Frontiers in molecular neuroscience*, vol. 10, 2017.
- [4] C. Zhu, C. Cheng, Y. Wang et al., "Loss of ARHGEF6 causes hair cell stereocilia deficits and hearing loss in mice," *Frontiers in molecular neuroscience*, vol. 11, 2018.
- [5] Z. H. He, S. Y. Zou, M. Li et al., "The nuclear transcription factor FoxG1 affects the sensitivity of mimetic aging hair cells to inflammation by regulating autophagy pathways," *Redox biology*, vol. 28, p. 101364, 2020.
- [6] Y. Zhang, W. Li, Z. He et al., "Pre-treatment with fasudil prevents neomycin-induced hair cell damage by reducing the accumulation of reactive oxygen species," *Frontiers in Molecular Neuroscience*, vol. 12, 2019.
- [7] R. Chai, S. Gao, C. Cheng et al., "Blebbistatin inhibits neomycin-induced apoptosis in hair cell-like HEI-OC-1 cells and in cochlear hair cells," *Frontiers in Cellular Neuroscience*, vol. 13, 2019.
- [8] L. Liu, Y. Chen, J. Qi et al., "Wnt activation protects against neomycin-induced hair cell damage in the mouse cochlea," *Cell death & disease*, vol. 7, no. 3, 2016.
- [9] W. Liu, X. Xu, Z. Fan et al., "Wnt signaling activates TP53-induced glycolysis and apoptosis regulator and protects against cisplatin-induced spiral ganglion neuron damage in the mouse cochlea," *Antioxidants & redox signaling*, vol. 30, no. 11, pp. 1389–1410, 2019.
- [10] H. Li, Y. Song, Z. He et al., "Meclofenamic acid reduces reactive oxygen species accumulation and apoptosis, inhibits excessive autophagy, and protects hair cell-like HEI-OC1 cells from cisplatin-induced damage," *Frontiers in cellular neuroscience*, vol. 12, 2018.
- [11] S. Zhang, Y. Zhang, Y. Dong et al., "Knockdown of Foxg1 in supporting cells increases the trans-differentiation of supporting cells into hair cells in the neonatal mouse cochlea," *Cellular and Molecular Life Sciences*, vol. 77, no. 7, pp. 1401–1419, 2020.
- [12] Y. Kawashima, G. S. G. Géléoc, K. Kurima et al., "Mechanotransduction in mouse inner ear hair cells requires transmembrane channel-like genes," *The Journal of Clinical Investigation*, vol. 121, no. 12, pp. 4796–4809, 2011.
- [13] K. Kurima, L. M. Peters, Y. Yang et al., "Dominant and recessive deafness caused by mutations of a novel gene, TMC1, required for cochlear hair-cell function," *Nature Genetics*, vol. 30, no. 3, pp. 277–284, 2002.
- [14] Y. Jia, Y. Zhao, T. Kusakizako et al., "TMC1 and TMC2 proteins are pore-forming subunits of mechanosensitive ion channels," *Neuron*, vol. 105, no. 2, pp. 310–321.e3, 2020.
- [15] K. Ramzan, M. Al-Owain, N. S. Al-Numair et al., "Identification of TMC1 as a relatively common cause for nonsyndromic hearing loss in the Saudi population," *American Journal of Medical Genetics. Part B, Neuropsychiatric Genetics*, vol. 183, pp. 172–180, 2019.
- [16] H. Wang, K. Wu, J. Guan et al., "Identification of four TMC1 variations in different Chinese families with hereditary hearing loss," *Molecular Genetics & Genomic Medicine*, vol. 6, no. 4, pp. 504–513, 2018.
- [17] J. Qi, L. Zhang, F. Tan et al., "Espn distribution as revealed by super-resolution microscopy of stereocilia," *American journal of Translational Research*, vol. 12, no. 1, pp. 130–141, 2020.
- [18] J. Qi, Y. Liu, C. Chu et al., "A cytoskeleton structure revealed by super-resolution fluorescence imaging in inner ear hair cells," *Cell discovery*, vol. 5, no. 1, 2019.
- [19] Y. Liang, A. Wang, I. A. Belyantseva et al., "Characterization of the human and mouse unconventional myosin XV genes responsible for hereditary deafness DFNB3 and shaker 2," *Genomics*, vol. 61, no. 3, pp. 243–258, 1999.
- [20] I. A. Belyantseva, E. T. Boger, and T. B. Friedman, "Myosin XVa localizes to the tips of inner ear sensory cell stereocilia and is essential for staircase formation of the hair bundle," *Proceedings of the National Academy of Sciences of the United States of America*, vol. 100, pp. 13958–13963, 2003.
- [21] I. A. Belyantseva, E. T. Boger, S. Naz et al., "Myosin-XVa is required for tip localization of whirlin and differential elongation of hair-cell stereocilia," *Nature Cell Biology*, vol. 7, no. 2, pp. 148–156, 2005.
- [22] Z. Fattahi, A. E. Shearer, M. Babanejad et al., "Screening for MYO15A gene mutations in autosomal recessive nonsyndromic, GJB2 negative Iranian deaf population," *American Journal of Medical Genetics. Part A*, vol. 158A, no. 8, pp. 1857–1864, 2012.
- [23] J. Zhang, J. Guan, H. Wang et al., "Genotype-phenotype correlation analysis of MYO15A variants in autosomal recessive

- non-syndromic hearing loss,” *BMC Medical Genetics*, vol. 20, no. 1, p. 60, 2019.
- [24] X. Wang, L. Wang, H. Peng, T. Yang, and H. Wu, “A novel p.G141R mutation in ILDR1 leads to recessive nonsyndromic deafness DFNB42 in two Chinese Han families,” *Neural plasticity*, vol. 2018, Article ID 7272308, 6 pages, 2018.
- [25] L. He, X. Pang, H. Liu, Y. Chai, H. Wu, and T. Yang, “Targeted next-generation sequencing and parental genotyping in sporadic Chinese Han deaf patients,” *Clinical Genetics*, vol. 93, no. 4, pp. 899–904, 2018.
- [26] S. Richards, on behalf of the ACMG Laboratory Quality Assurance Committee, N. Aziz et al., “Standards and guidelines for the interpretation of sequence variants: a joint consensus recommendation of the American College of Medical Genetics and Genomics and the Association for Molecular Pathology,” *Genetics in Medicine*, vol. 17, no. 5, pp. 405–423, 2015.
- [27] M. B. Saïd, M. Hmani-Aifa, I. Amar et al., “High frequency of the p.R34X mutation in the TMC1 gene associated with non-syndromic hearing loss is due to founder effects,” *Genetic Testing and Molecular Biomarkers*, vol. 14, no. 3, pp. 307–311, 2010.
- [28] A. Tlili, I. B. Rebeh, M. Aifa-Hmani et al., “TMC1 but not TMC2 is responsible for autosomal recessive nonsyndromic hearing impairment in Tunisian families,” *Audiology & Neuro-Otology*, vol. 13, no. 4, pp. 213–218, 2008.
- [29] M. Alobathani, A. Al Mutery, W. K. E. A. Mohamed, and A. Tlili, “Identification of nonsense mutation in TMC1 gene inducing hearing loss by clinical exome sequencing,” *Journal of Biological Sciences and Medicine*, vol. 4, pp. 1–6, 2018.
- [30] M. Y. Chang, C. Lee, J. H. Han et al., “Expansion of phenotypic spectrum of MYO15A pathogenic variants to include postlingual onset of progressive partial deafness,” *BMC Medical Genetics*, vol. 19, no. 1, p. 29, 2018.
- [31] M. Miyagawa, S. Y. Nishio, M. Hattori et al., “Mutations in the MYO15A Gene are a significant cause of nonsyndromic hearing loss,” *Annals of Otology, Rhinology & Laryngology*, vol. 124, 1_supplement, pp. 158S–168S, 2015.
- [32] O. K. Egilmez and M. T. Kalcioğlu, “Genetics of nonsyndromic congenital hearing loss,” *Scientifica*, vol. 2016, Article ID 7576064, 9 pages, 2016.
- [33] X. Yu, Y. Lin, J. Xu et al., “Molecular epidemiology of Chinese Han deaf patients with bi-allelic and mono-allelic GJB2 mutations,” *Orphanet Journal of Rare Diseases*, vol. 15, no. 1, p. 29, 2020.
- [34] M. B. Petersen and P. J. Willems, “Non-syndromic, autosomal-recessive deafness,” *Clinical Genetics*, vol. 69, no. 5, pp. 371–392, 2006.
- [35] S. Sang, J. Ling, X. Liu et al., “Proband whole-exome sequencing identified genes responsible for autosomal recessive non-syndromic hearing loss in 33 Chinese nuclear families,” *Frontiers in Genetics*, vol. 10, p. 639, 2019.
- [36] S. I. Kitajiri, R. McNamara, T. Makishima et al., “Identities, frequencies and origins of TMC1 mutations causing DFNB7/B11 deafness in Pakistan,” *Clinical Genetics*, vol. 72, no. 6, pp. 546–550, 2007.
- [37] A. H. Chishti, A. C. Kim, S. M. Marfatia et al., “The FERM domain: a unique module involved in the linkage of cytoplasmic proteins to the membrane,” *Trends in Biochemical Sciences*, vol. 23, no. 8, pp. 281–282, 1998.
- [38] J. Li, Y. He, M. L. Weck, Q. Lu, M. J. Tyska, and M. Zhang, “Structure of Myo7b/USH1C complex suggests a general PDZ domain binding mode by MyTH4-FERM myosins,” *Proceedings of the National Academy of Sciences of the United States of America*, vol. 114, no. 19, pp. E3776–E3785, 2017.
- [39] D. W. Anderson, F. J. Probst, I. A. Belyantseva et al., “The motor and tail regions of myosin XV are critical for normal structure and function of auditory and vestibular hair cells,” *Human Molecular Genetics*, vol. 9, no. 12, pp. 1729–1738, 2000.

Research Article

Hearing Phenotypes of Patients with Hearing Loss Homozygous for the *GJB2* c.235delc Mutation

Chang Guo,^{1,2,3} Sha-Sha Huang,^{1,2,3} Yong-Yi Yuan ^{1,2,3} Ying Zhou,^{1,2,3} Ning Wang,⁴ Dong-Yang Kang,^{1,2,3} Su-Yan Yang,^{1,2,3} Xin Zhang,^{1,2,3} Xue Gao ^{1,2,3,5} and Pu Dai ^{1,2,3}

¹College of Otolaryngology Head and Neck Surgery, Chinese PLA General Hospital, Chinese PLA Medical School, 28 Fuxing Road, Beijing 100853, China

²National Clinical Research Center for Otolaryngologic Diseases, State Key Lab of Hearing Science, Ministry of Education, China

³Beijing Key Lab of Hearing Impairment Prevention and Treatment, Beijing, China

⁴Department of Pediatric Surgery, Chinese PLA General Hospital, Chinese PLA Medical School, 28 Fuxing Road, Beijing 100853, China

⁵Department of Otolaryngology, PLA Rocket Force Characteristic Medical Center, 16# XinWai Da Jie, Beijing 100088, China

Correspondence should be addressed to Xue Gao; mixueer01110@126.com and Pu Dai; daipu301@vip.sina.com

Received 12 April 2020; Revised 18 June 2020; Accepted 30 June 2020; Published 1 August 2020

Academic Editor: Renjie Chai

Copyright © 2020 Chang Guo et al. This is an open access article distributed under the Creative Commons Attribution License, which permits unrestricted use, distribution, and reproduction in any medium, provided the original work is properly cited.

Hereditary hearing loss is characterized by remarkable phenotypic heterogeneity. Patients with the same pathogenic mutations may exhibit various hearing loss phenotypes. In the Chinese population, the c.235delC mutation is the most common pathogenic mutation of *GJB2* and is closely related to hereditary recessive hearing loss. Here, we investigated the hearing phenotypes of patients with hearing loss associated with the homozygous c.235delC mutation, paying special attention to asymmetric interaural hearing loss. A total of 244 patients with the *GJB2* c.235delC homozygous mutation encountered from 2007 to 2015 were enrolled. The severity of hearing loss was scaled with the American Speech-Language-Hearing Association (ASHA). Auditory phenotypes were analyzed, and three types of interaural asymmetry were defined based on audiograms: Type A (asymmetry of hearing loss severity), Type B (asymmetry of audiogram shape), and Type C (Type A plus Type B). Of the 488 ears (244 cases) examined, 71.93% (351) presented with profound hearing loss, 14.34% (70) with severe hearing loss, and 9.43% (46) with moderate to severe hearing loss. The most common audiogram shapes were descending (31.15%) and flat (24.18%). A total of 156 (63.93%) of the 244 patients exhibited asymmetric interaural hearing loss in terms of severity and/or audiogram shape. Type A was evident in 14 of these cases, Type B in 106, and Type C in 36. In addition, 211 of 312 ears (67.63%) in the interaural hearing asymmetry group showed profound hearing loss, and 59 (18.91%) exhibited severe hearing loss, with the most common audiogram shapes being flat (27.88%) and descending (22.12%). By contrast, in the interaural hearing symmetry group, profound hearing loss was observed in 140 ears (79.55%), and the most common audiograms were descending (46.59%) and residual (21.59%). Hearing loss associated with the *GJB2* c.235delC homozygous mutation shows diverse phenotypes, and a considerable proportion of patients show bilateral hearing loss asymmetry.

1. Introduction

Hearing loss (HL) is one of the most common neurosensory impairments in humans [1]. The World Health Organization estimated in 2020 that over 5% of the world's population (approximately 466 million people) suffer from HL [2].

Sensorineural HL (SNHL) is the most common form of HL and typically is caused by a loss of functional sensory hair cells (HCs) and supporting cells (SCs) within the cochlea [3, 4]. HCs and SCs develop from common progenitor cells within the prosensory domain of the developing cochlea [5]. HCs transfer mechanical vibration into an acoustic

electrical signal, which is then transmitted to the auditory cortex via spiral ganglion neurons (SGNs). SCs are important cells that support HCs and hold the potential to regenerate HCs once damaged [6–8]. HCs and SCs are very sensitive and vulnerable to stress and damage, classified mainly as genetic factors, environmental factors, ototoxic drugs, aging, inflammation, and other unknown etiologies [9–11]. Among these, genetic factors are responsible for approximately 50–60% of cases of HL [12]. Whereas 70% of genetic HL cases are nonsyndromic HL (NSHL), 30% are syndromic. Approximately 80% of NSHL cases are inherited via an autosomal recessive mode, whereas other cases are inherited in an autosomal dominant, X-linked, or mitochondrial mode [13, 14]. To date, more than 100 genes have been shown to cause NSHL [15]. Despite this, the most common cause of NSHL is mutations in *GJB2* [16, 17].

The *GJB2* gene encodes a 26 kDa gap junction protein known as connexin 26 (Cx26) [18]. Cx26 consists of an N-terminal helix, four transmembrane helices (TM1–4), two extracellular loops (E1 and E2), a cytoplasmic loop (CL), and a C-terminus [19]. Cx26 is expressed in the inner ear, which contains SCs, stria vascularis, spiral ligament, and spiral limbus [20]. Cx26 is associated with proteins that form a transmembrane hexameric gap junction channel known as a connexon. These channels are believed to play a role in the recycling of potassium ions from HCs to the endolymph [21, 22]. *GJB2* is involved in a series of physiological hearing processes including cochlear development, endocochlear potential generation, active cochlear amplification, and second messenger transduction [23, 24].

The *GJB2* mutation is one of the most common pathogenic factors related to genetic HL, and *GJB2* usually is the first deafness gene to be evaluated during clinical diagnosis due to the observations that *GJB2* is the most common human deafness gene in almost all populations studied so far. Currently, more than 300 mutations in *GJB2* have been reported (the Human Gene Mutation Database) [25]. Notably, several alleles have been found to be particularly enriched in certain populations: c.35delG in Europe, America, North Africa, and the Middle East; c.71G>A in India and Pakistan; c.167delT in Ashkenazi Jews; and c.109G>A in East and Southeast Asia [16, 26–28]. The contribution of *GJB2* mutations to genetic HL varies by ethnicity, but such mutations are the primary cause of congenital severe-to-profound autosomal recessive NSHL (up to 50% worldwide) [29, 30]. In addition, mild and moderate HL are associated with *GJB2* common mutations such as c.35delG and c.109G>A, showing diverse hearing phenotypes [31, 32]. In the Chinese population, the most common *GJB2* mutation is c.235delC (68.9%) [33]. Base deletion creates a frameshift mutation, and early termination of translation yields a non-functional protein [34]. Although severe-to-profound HL is the most common clinical presentation of patients with *GJB2* c.235delC, various hearing phenotypes have been reported, and the HL caused by the mutation exhibits clinical heterogeneity [35, 36].

Understanding genotype-phenotype relationships will provide novel insights into molecular diagnosis, genetic counseling, and genetic therapy. Many approaches, such as

cochlear implant surgery, gene therapy, and cell therapy, have been used to treat *GJB2*-related HL [37–39]. Since 2009, preimplantation genetic diagnosis (PGD), an effective method to prevent the recurrence of genetic HL, has been successfully applied to protect babies against *GJB2*-related HL [40, 41]. We believe that more treatment options will be available for these patients in the future. Here, we analyzed audiological data of 244 patients with *GJB2* c.235delC homozygous mutation-induced HL and explored the phenotypic diversity of HL in patients with *GJB2* c.235delC with a focus on the symmetry (or lack thereof) of binaural hearing.

2. Materials and Methods

2.1. Clinical Data. Patients for whom complete audiological data were available and who visited the molecular diagnostic center of the Chinese PLA General Hospital from 2007 to 2015 were included. The inclusion criteria were (1) binaural SNHL with a complete hearing history, data from physical examination and a detailed ENT examination, and audiological test results; (2) DNA sequence of patients were confirmed to have *GJB2* c.235delC homozygous mutation; and (3) no syndromic HL or ear-related diseases (e.g., acute or chronic otitis media, advanced Meniere's disease, acoustic neuroma, meningoencephalitis, or trauma). A total of 244 subjects (130 males and 114 females) were included.

2.2. Research Methods

2.2.1. Genomic DNA Extraction. Peripheral blood samples were collected from arm veins, and the genomic DNA of leukocytes was extracted [42].

2.2.2. Detection of Mutations in the Coding Region of *GJB2*. We performed primer design, PCR amplification, and direct sequencing using the methods described by Dai et al. [43]. We compared the results to the wild-type sequence (*GJB2*: NM_004004) using GeneTool Lite ver. 1.0.

2.2.3. Audiologic Evaluation. Audiological tests were performed in the hearing center of the Chinese PLA General Hospital. Tests included pure-tone audiometry (or behavioral audiometry) for patients > 4 years old and multiple-frequency auditory steady-state evoked response (ASSR) tests for patients ≤ 4 years old.

(1) HL Severity. We derived the average air conduction (AC) pure-tone hearing thresholds or ASSR response thresholds at 0.5, 1, 2, and 4 kHz for both ears. If data could not be obtained at any frequency using the maximal output, that output was taken to be the hearing or response threshold. Using the American Speech-Language-Hearing Association (ASHA) [44], we scaled hearing as normal (threshold: ≤25 dB), mild HL (threshold: 25.1–40 dB), moderate HL (threshold: 40.1–55 dB), moderately severe HL (threshold: 55.1–70 dB), severe HL (threshold: 70.1–90 dB), and profound HL (threshold: >90 dB, including total deafness). According to WHO criteria [45], disabling HL referred to HL greater than 40 dB in the better hearing ear in adults and HL greater than

30 dB in the better hearing ear in children (age ≤ 15 years old). HL progression was defined as an elevation of the average hearing or response thresholds by >15 dB in one or both ears between audiograms. Only patients with multiple audiograms and at least a 4-month gap between audiograms were included in the analysis of progressive HL [46].

(2) *Audiogram Shapes*. We recognized seven shapes of pure-tone threshold audiograms: descending (≥ 15 dB HL difference between the [better] average thresholds at 250 and 500 Hz and those at 4,000 and 8,000 Hz), flat (≤ 15 dB HL difference between all thresholds from 125 to 8,000 Hz), valley like (≥ 10 dB HL difference between the poorest midfrequency [1,000–2,000 Hz] threshold and those at higher and lower frequencies), ascending (≥ 15 dB HL difference between the average thresholds at 250 and 500 Hz and the [better] average thresholds at 4,000 and 8,000 Hz), residual (residual hearing at only one or two frequencies), total deafness (no hearing at any frequency when outputs are maximal), and unclassified (none of the above). We defined descending, flat, valley like, ascending, residual, and total deafness shapes as “regular” audiograms.

We recognized seven shapes of ASSR audiograms: descending (≥ 15 dB HL difference between the [better] mean thresholds at 500 and 1,000 Hz and those at 2,000 and 4,000 Hz), flat (≤ 15 dB HL difference between all thresholds from 500 to 4,000 Hz), valley like (≥ 10 dB HL difference between the poorest midfrequency [1,000–2,000 Hz] threshold and those at higher and lower frequencies), ascending (≥ 15 dB HL difference between the mean thresholds at 500 and 1,000 Hz and the [better] mean thresholds at 2,000 and 4,000 Hz), residual (residual hearing at only one or two frequencies), total deafness (no hearing at any frequency when outputs are maximal), and unclassified (none of the above). Similarly, we defined the first six shapes of audiograms as “regular” audiograms.

(3) *Asymmetric Hearing Phenotypes*. (1) *Asymmetry of HL severity (Type A asymmetry)*: binaural audiograms were shaped similarly, but hearing thresholds differed, with an HL difference ≥ 10 dB at a minimum of four frequencies, an HL difference ≥ 15 dB at two frequencies, or an HL difference ≥ 25 dB at one frequency (Figure 1(a)).

(2) *Asymmetry of audiogram shape (Type B asymmetry)*: HL on either side was similar (average hearing threshold difference ≤ 15 dB) but audiogram shapes differed, and at least one ear exhibited a regular audiogram (e.g., a descending type in one ear but a flat type in the other; Figure 1(b)).

(3) *Asymmetry of HL severity and audiogram shape (Type C asymmetry)*: the average hearing threshold difference was >15 dB. In addition, if the audiogram shapes were different, at least one ear exhibited a regular audiogram. If the two audiograms were irregular, the binaural hearing threshold difference was considered asymmetric. Alternatively, if the hearing threshold difference was ≥ 15 dB at two frequencies from 0.125–8 kHz, or ≥ 10 dB at three frequencies, there was likely Type C asymmetry (Figure 1(c)).

3. Results

3.1. *Patient Demographics*. The patients ranged in age from 3 months to 45 years: 138 patients were 0–4 years, 60 were 5–71 years, and 46 were 18–45 years. Definite ages of onset were identified in 166 patients and ranged from birth to 24 years (average: 1.9 years). Note that six patients were siblings from three families (two per family); the remaining patients were sporadic cases.

3.2. *HL Severity*. The HL severity (both ears) for all 244 patients is shown in Table 1. Profound HL was most common (71.93%, 351/488), followed by severe HL (14.34%, 70/488) and moderately severe HL (9.43%, 46/488). Fewer patients exhibited moderate HL (4.10%, 20/488) or mild HL (0.2%, 1/488). All patients showed disabling HL. Only five patients met the criteria for inclusion in the progressive HL analysis, but none of them had progressive HL.

3.3. *Audiograms*. Among the 244 cases (488 ears), descending (30.94%, 151/488) and flat (24.39%, 119/488) were the most common audiogram shapes, followed by residual (15.57%, 76/488), total deafness (5.53%, 27/488), valley like (5.33%, 26/488), and ascending (2.05%, 10/488). The unclassified shape constituted 16.19% (79/488) of all audiograms. Table 2 shows that 40.16% (98/244) of cases exhibited the same (regular) audiogram shape in both ears.

3.4. *Interaural Hearing Asymmetry*. A total of 88 of the 244 cases were symmetric in terms of both HL severity and audiogram shape. By contrast, 156 (63.93%) cases were asymmetric in terms of audiogram shape and/or HL severity (14 Type A, 106 Type B, and 36 Type C). In the latter group, 211 ears (67.63%) exhibited profound HL and 59 (18.91% of all ears) exhibited severe HL. In patients with symmetric HL, 140 ears (79.55%) exhibited profound HL (Table 3).

Of the 156 patients with asymmetric interaural HL, 87 ears (27.88%) exhibited flat, 69 (22.12%) descending, and 37 (11.86%) residual audiograms. Of the 88 cases with symmetric interaural HL, 82 ears (46.59%) exhibited descending, 38 (21.59%) residual, and 32 (18.18%) flat audiograms (Table 4).

3.5. *HL Severity and Audiograms in Different Age Groups*. We categorized age into four groups: group 1 (≤ 6 years old), group 2 (6.1–12 years old), group 3 (12.1–18 years old), and group 4 (≥ 18 years old). There were 156, 29, 17, and 42 patients in groups 1, 2, 3, and 4, respectively.

HL severity (both ears) in the different age groups is shown in Table 5. Among all groups, profound HL was the most common type of HL. In groups 1 and 4, severe HL was the second most common type of HL, followed by moderately severe and moderate HL. By contrast, in group 2, moderately severe and moderate HL were the second most common types of HL, followed by severe HL. Similarly, in group 3, moderately severe HL was the second most common type of HL, and a smaller proportion of patients showed moderate and severe HL. However, only one patient in group 1 exhibited mild HL.

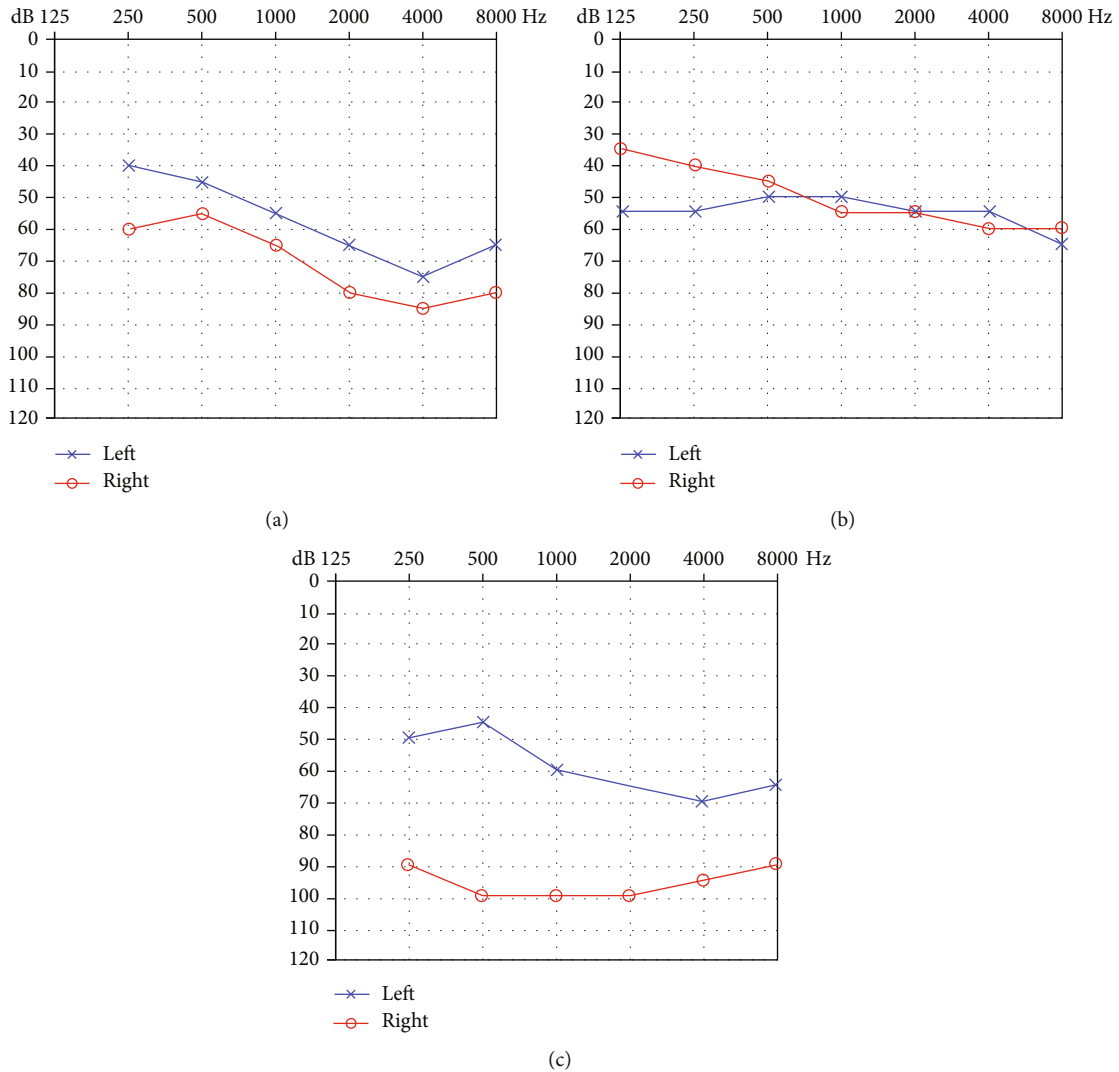


FIGURE 1: (a) Audiogram of asymmetry of HL severity (Type A asymmetry). (b) Audiogram of asymmetry of audiogram shape (Type B asymmetry). (c) Audiogram of asymmetry of hearing loss severity and audiogram shape (Type C asymmetry). In all audiograms, the frequency in hertz (Hz) is plotted on the x -axis and the hearing level in decibels (dB HL) on the y -axis.

TABLE 1: HL severity (both ears).

HL severity	Worse ear					Cases	
	Mild	Moderate	Moderate to severe	Severe	Profound		
	Mild	0	0	0	1	0	1
	Moderate		5	7	3	0	15
Better ear	Moderate to severe			11	10	7	28
	Severe				15	26	41
	Profound					159	159

Italics indicate patients with the same HL severity in both ears.

The audiograms (both ears) in the different age groups are shown in Table 6. In group 1, the most common audiogram shape was flat (28.53%). In groups 2-4, descending was the most common audiogram shape (50%–61.76%). Among all groups, total deafness was relatively rare.

The interaural hearing asymmetry in the different age groups is shown in Table 7. Whereas Type B asymmetry

(50.64%) was the most common type in group 1, symmetry was the most common in groups 2-4 (~41-53%). In groups 1-3, Type A asymmetry was the least common, whereas in group 4, Type C asymmetry was the least common.

3.6. *HL in Three Sets of Siblings.* Set 1 was composed of two sisters (Figure 2(a)). Their normal-hearing parents were

TABLE 2: Audiogram shapes of both ears.

Audiogram shape	Descending	Flat	Residual	The other ear		Total deafness	Other	
				Valley like	Ascending			
One ear	Descending	<i>50</i>	21	8	6	1	2	13
	Flat		<i>21</i>	12	8	4	3	29
	Residual			<i>19</i>	1	0	5	12
	Valley like				<i>1</i>	1	1	7
	Ascending					<i>1</i>	0	2
	Total deafness						6	4
	Other							6

Italics indicate patients with the same audiogram shape in both ears.

TABLE 3: HL severity in patients with asymmetric and symmetric interaural HL.

HL severity	Mild	Moderate	Worse ear			Cases
			Moderate to severe	Severe	Profound	
Better ear	Mild	<i>0 (0)</i>	0 (0)	0 (0)	0 (1)	0 (1)
	Moderate		<i>4 (1)</i>	4 (3)	0 (3)	8 (7)
	Moderate to severe			<i>4 (7)</i>	1 (9)	5 (23)
	Severe				<i>4 (11)</i>	6 (35)
	Profound					<i>69 (90)</i>

(1) The value outside/inside each pair of parentheses represents the number of patients with symmetric/asymmetric interaural HL. (2) Italics indicate patients with the same HL severity in both ears.

TABLE 4: Audiogram shapes in patients with asymmetric and symmetric interaural HL.

Audiogram shape	Descending	Flat	Residual	The other ear		Total deafness	Other
				Valley like	Ascending		
One ear	Descending	<i>41 (9)</i>	0 (21)	0 (8)	0 (6)	0 (1)	0 (13)
	Flat		<i>16 (5)</i>	0 (12)	0 (8)	0 (4)	0 (29)
	Residual			<i>19 (0)</i>	0 (1)	0 (0)	0 (12)
	Valley like				<i>1 (0)</i>	0 (1)	0 (7)
	Ascending					<i>0 (1)</i>	0 (2)
	Total deafness						<i>6 (0)</i>
	Other						<i>5 (1)</i>

(1) The value outside/inside each pair of parentheses represents the number of patients with symmetric/asymmetric interaural HL. (2) Italics indicate patients with the same audiogram shape for both ears.

TABLE 5: Degree of hearing loss in patients (both ears) according to age group.

Age	Degree of hearing loss				
	Mild	Moderate	Moderate to severe	Severe	Profound
Group 1	1 (0.32%)	2 (0.64%)	19 (6.09%)	42 (13.46%)	248 (79.49%)
Group 2	0	12 (20.69%)	12 (20.69%)	9 (15.52%)	25 (43.10%)
Group 3	0	4 (11.76%)	8 (23.53%)	4 (11.76%)	18 (52.94%)
Group 4	0	2 (2.38%)	7 (8.33%)	15 (17.86%)	60 (71.43%)

Group 1 (≤ 6 years old), group 2 (6.1–12 years old), group 3 (12.1–18 years old), and group 4 (≥ 18 years old). The value outside each pair of parentheses represents the number of ears with this degree of hearing loss; the value inside each pair of parentheses represents the percentage of ears with this degree of hearing loss relative to the total number of ears in each group.

heterozygous carriers of c.235delC. The older sister (II-1) suffered from moderate and severe HL in the left and right ears. The younger sister (II-2) suffered from binaural moderate HL. The audiograms of the older sister were descending

and unclassified (one ear each). The audiograms of the younger sister were flat in both ears. The older sister exhibited Type C asymmetric HL, and the younger sister exhibited symmetric HL. Set 2 was composed of two brothers

TABLE 6: Types of audiograms in patients (both ears) with different age groups.

Age	Types of audiograms						
	Descending	Flat	Residual	Valley like	Ascending	Total deafness	Other
Group 1	56 (17.95%)	89 (28.53%)	53 (16.99%)	20 (6.41%)	7 (2.24%)	23 (7.37%)	64 (20.51%)
Group 2	32 (55.17%)	11 (18.97%)	2 (3.45%)	5 (8.62%)	2 (3.45%)	0	6 (10.34%)
Group 3	21 (61.76%)	5 (14.71%)	3 (8.82%)	0	0	1 (2.94%)	4 (11.76%)
Group 4	42 (50.00%)	14 (16.67%)	17 (20.24%)	1 (11.90%)	1 (11.90%)	3 (3.57%)	6 (7.14%)

Group 1 (≤ 6 years old), group 2 (6.1–12 years old), group 3 (12.1–18 years old), and group 4 (≥ 18 years old). The value outside each pair of parentheses represents the number of ears with this type of audiogram; the value inside each pair of parentheses represents the percentage of ears with this type of audiogram relative to the total number of ears in each group.

TABLE 7: Interaural hearing symmetry or asymmetry in patients according to age group.

Age	Interaural hearing symmetry or asymmetry			
	Symmetry	Type A	Type B	Type C
Group 1	47 (30.13%)	7 (4.49%)	79 (50.64%)	23 (14.74%)
Group 2	12 (41.38%)	1 (3.45%)	10 (34.48%)	6 (20.69%)
Group 3	9 (52.94%)	0	6 (35.29%)	2 (11.76%)
Group 4	20 (47.62%)	6 (14.29%)	11 (26.19%)	5 (11.90%)

Group 1 (≤ 6 years old), group 2 (6.1–12 years old), group 3 (12.1–18 years old), and group 4 (≥ 18 years old). The value outside each pair of parentheses represents the number of patients with interaural hearing symmetry or asymmetry; the value inside each pair of parentheses represents the percentage of patients with interaural hearing symmetry or asymmetry relative to the total number of patients in each group.

(Figure 2(b)). Their normal-hearing parents were heterozygous carriers of c.235delC. Both brothers (II-1 and II-2) presented with binaural profound HL. The audiograms of the elder brother were descending in both ears. The audiograms of the younger brother were descending and flat (one ear each). The elder brother exhibited symmetric HL, and the younger brother exhibited Type B asymmetric HL. Set 3 was composed of an older sister and a younger brother (Figure 2(c)). Their parents and sister were all heterozygous carriers of c.235delC and had no hearing problems. Both siblings (II-1 and II-3) exhibited similar binaural moderate to severe HL with descending and flat audiograms (one of each). Both exhibited Type B asymmetric HL (Figure 3 and Table 8).

4. Discussion

HL has become a global public health problem. In addition to impaired communication, HL is associated with language delays, social adaptation problems, and even dementia [47]. Hereditary SNHL is genetically heterogeneous, and pathogenic mutations have been identified in approximately 50–60% of cases [48]. *GJB2* mutation is a major cause of hereditary NSHL, and most mutations are located in the coding region [49]. Up to 50% of cases of autosomal recessive NSHL are attributable to *GJB2* mutation in many populations worldwide [29, 30]. Therefore, genetic testing for *GJB2* mutations is a primary screening process for the molecular diagnosis of HL. As we mentioned previously, the *GJB2*

mutation spectrum varies ethnically and geographically. In the Chinese population, the c.235delC homozygous mutation is the most common mutation in *GJB2* [33]. This gene encodes the connexin 26 (Cx26) protein. The gap junction proteins of adjacent cells allow for the exchange of information and materials; electrolytes, second messengers, and metabolites move through these channels, underlying both intercellular communication and homeostasis of the cochlear fluids, endolymph, and perilymph [50, 51]. Mutations in the *GJB2* coding region can cause frameshifts affecting protein translation and gap junction protein structure, resulting in a defective protein [52]. The *GJB2* c.235delC mutation causes early termination of translation and produces a nonfunctional Cx26 protein. The null Cx26 can induce apoptosis and oxidative damage in the cochlear duct, reduce the release of glutathione from connexin hemichannels, and decrease nutrient delivery to the sensory epithelium via cochlear gap junctions, thereby leading to HL. Cx26-deficient mouse models showed congenital HL and cochlear developmental disorders [53–55]. *GJB2*-related HL is usually binaural [42, 56], as in all 244 patients in this study. Profound HL was the most common (71.93%, 351/488) HL in our patients, followed by severe (14.34%, 70/488), moderately severe (9.43%, 46/488), and moderate (4.10%, 20/488) HL. Mild HL was seen in only 0.2% (1/488) of cases. Zhao et al. [35] retrospectively analyzed the hearing phenotypes of a large group of Chinese patients with HL caused by *GJB2* c.235delC biallelic mutations and found that most patients exhibited severe or profound HL, with only a few showing moderate HL. We also found that profound HL was most common; however, a considerable proportion of our cases exhibited moderate (4.10%) or moderately severe (9.43%) HL. HL phenotypes thus differ. All patients in our study showed disabling HL, indicating that *GJB2*-related HL usually has a negative impact on quality of life, ability to listen in noisy environments, communication with others, and comprehension ability, regardless of whether hearing in the two ears is symmetric. In the analysis of progressive HL, all five patients who met the criteria showed stabilization of HL. Our results were consistent with those of Chorath et al. [46], who concluded that progression of *GJB2*-related HL was rare. Unfortunately, the number of patients included was limited, and more follow-up data are required in future studies. Some researchers use the following definitions to classify audiograms [57, 58]: descending (>15 dB HL difference between the [better] average thresholds at 500 and 1,000 Hz and those

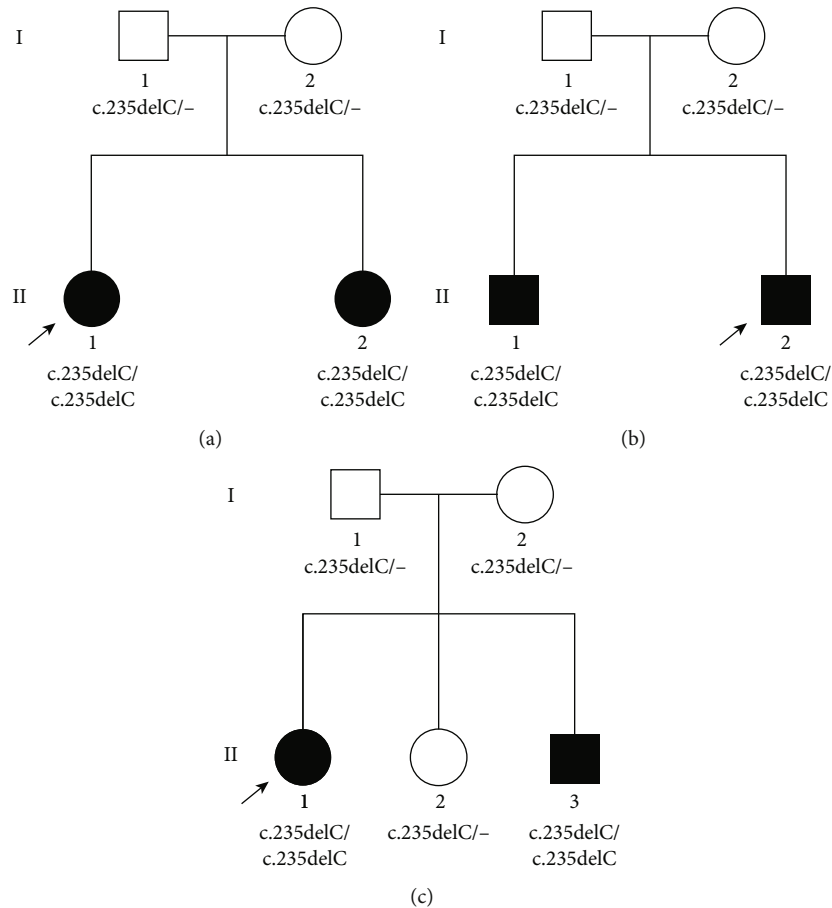


FIGURE 2: (a–c) are genotypes of the pedigrees for sets 1, 2, and 3, respectively.

at 4,000 and 8,000 Hz), flat (<15 dB HL difference between all thresholds from 250 to 8,000 Hz), midfrequency U-shaped (>15 dB HL difference between the poorest midfrequency [1,000–2,000 Hz] thresholds and those of higher and lower frequencies), and ascending (>15 dB HL difference between the average thresholds at 500 and 1,000 Hz and the [better] thresholds at 4,000 and 8,000 Hz). However, in our clinic, we found that the results yielded using these definitions sometimes do not agree with the characteristics of the audiograms. Thus, we amended the definitions. First, we changed the difference in dB HL from >15 dB to ≥ 15 dB for both the descending and ascending types, from <15 dB to ≤ 15 dB for the flat type, and from >15 dB to ≥ 10 dB for the valley-like type. Second, we used 250 and 500 Hz (not 500 and 1,000 Hz) as the low frequencies for the descending and ascending types and 2,000 and 4,000 Hz (not 4,000 and 8,000 Hz) as the high frequencies when evaluating ASSR data. In addition, when defining the flat type of ASSR, we use frequencies from 500 to 4,000 Hz. Third, we consider the residual and total deafness types to be “regular” types. We found that the descending (30.94%) and flat (24.39%) types were the most common, followed by the residual (15.57%), total deafness (5.53%), valley-like (5.33%), and ascending (2.05%) types. Our findings are similar to those of King et al. [57] in that most audiograms were descending, flat, or residual.

The phenotypes of genetic HL remain poorly understood. We analyzed the audiograms of 244 cases with homozygous *GJB2* c.235delC-associated HL. No consensus definition of “asymmetry” in the context of binaural HL has emerged. Early studies [59–61] proposed that an interaural difference(s) in pure-tone thresholds ≥ 10 dB at two frequencies or ≥ 15 dB at one frequency constitutes asymmetric HL. In a 2007 audiogram classification system (AMCLASS) [62, 63], audiograms were considered asymmetric if at least three frequencies differed by ≥ 10 dB, two by ≥ 15 dB, or one by ≥ 20 dB over the range of 0.25–8 kHz. In 2009, Mazzoli et al. [64] defined asymmetric HL as differences > 10 dB for at least two frequencies. These criteria concern only the severity of HL, not the audiogram shape; the picture is thus incomplete. To better characterize asymmetry, we divided it into three types with reference to both audiogram shape and HL severity. A substantial proportion of our cases with binaural HL exhibited interaural asymmetry in terms of audiogram shape and/or HL severity. A total of 156 (63.93%) patients exhibited asymmetric HL: 14 in terms of HL severity (Type A), 106 in terms of audiogram shape (Type B), and 36 with both Type A and B features (Type C). Our figures differ significantly from those of Wang et al. [36], who found a rate of asymmetric HL of 37.37% in children with biallelic protein-truncating mutations. This difference is probably attributable to variation in the definitions of binaural asymmetric HL. It is clear,

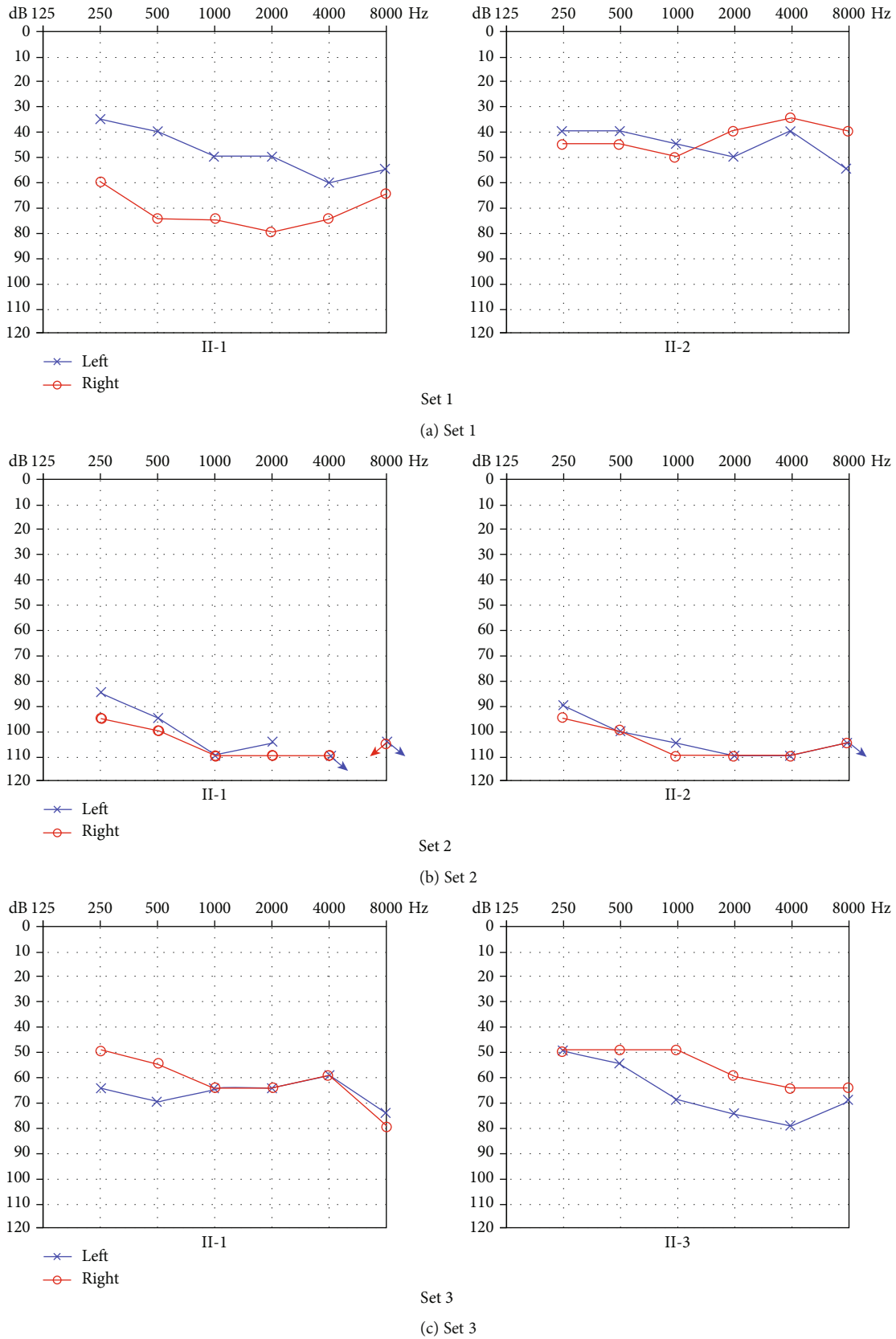


FIGURE 3: (a) Audiograms of two sisters (II-1 and II-2) in set 1. (b) Audiograms of two brothers (II-1 and II-2) in set 2. (c) Audiograms of the older sister (II-1) and younger brother (II-3) in set 3.

TABLE 8: HL severity and audiogram shapes in three pairs of siblings.

		HL severity		Audiogram shape	
		Left ear	Right ear	Left ear	Right ear
Set 1	Older sister	Moderate	Severe	Descending	Other
	Younger sister	Moderate	Moderate	Flat	Flat
Set 2	Older brother	Profound	Profound	Descending	Descending
	Younger brother	Profound	Profound	Descending	Flat
Set 3	Older sister	Moderate to severe	Moderate to severe	Flat	Descending
	Younger brother	Moderate to severe	Moderate to severe	Descending	Flat

however, that the *GJB2* c.235delC mutation is associated with significant variation in the binaural HL phenotype, evidencing a high level of genetic heterogeneity.

Among our 156 patients exhibiting interaural HL asymmetry, 211 ears (67.63%) suffered profound HL and 59 (18.91%) suffered severe HL. By contrast, in the 88 cases evidencing symmetric interaural HL, 140 ears (79.55%) showed profound HL. Thus, HL in such patients is likely to be profound or severe regardless of symmetry or asymmetry. It is worth noting that in patients with symmetric interaural HL, daily communication with others will be challenging since most suffered from bilateral profound HL. Among patients with asymmetric HL, audiograms were (in order) flat (27.88%), descending (22.12%), and residual (11.86%). By contrast, among patients with symmetric HL, audiograms were (in order) descending (46.59%), residual (21.59%), and flat (18.18%). Such subtle differences may be attributable to variation in HL severity. In all groups of different ages, profound HL was most common. HL severity tended to be more serious in group 1 (≤ 6 years old) and group 4 (≥ 18 years old). Among the patients < 18 years old, the most common audiogram shapes were descending and flat, whereas among the adult patients, the most common audiogram shapes were descending and residual. The differences may also be attributable to variation in HL severity. Among patients ≤ 6 years old, Type B asymmetry was the most common. However, among patients > 6 years old, symmetry was the most common. In three sibling pairs, HL severity was similar but audiogram shapes differed. Asymmetry may be attributable to one or more of heredity, epigenetics, and/or the environment. However, the mechanism of *GJB2*-related HL remains unclear. More clinical data, combined with full-exome and whole-genome sequencing, are needed.

5. Conclusion

A considerable proportion of patients homozygous for the *GJB2* c.235delC mutation exhibit significant variation in their binaural HL phenotypes, reflecting a high degree of bilateral HL asymmetry.

Data Availability

The data used to support the findings of this study are available from the corresponding authors upon request.

Ethical Approval

This study was approved by the Ethics Committee of the Chinese People's Liberation Army General Hospital (reference number S2016-120-02).

Disclosure

The funders had no role in study design, data collection and analysis, decision to publish, or preparation of the manuscript.

Conflicts of Interest

The authors have no conflicts of interest to declare.

Authors' Contributions

Chang Guo and Sha-Sha Huang contributed equally to this work.

Acknowledgments

We sincerely thank all the family members for their participation and cooperation in this study. This study was supported by grants from the National Key R&D Project (2016YFC1000700, 2016YFC1000704), National Natural Science Foundation of China (81730029, 61827805), and Beijing Natural Science Foundation (7191011) to Pu Dai; grants from the Beijing Natural Science Foundation (7192234) and National Natural Science Foundation of China (81570929) to Xue Gao; a grant from the National Natural Science Foundation of China (81870731) to Sha-Sha Huang; and grants from the National Key R&D Project (2016YFC1000706), National Natural Science Foundation of China (81873704), and Fostering Funds of Chinese PLA General Hospital for National Distinguished Young Scholar Science Fund (2017-JQPY-001) to Yong-Yi Yuan.

References

- [1] S. Ahmadmehrabi, J. Brant, D. J. Epstein, M. J. Ruckenstein, and D. J. Rader, "Genetics of postlingual sensorineural hearing loss," *The Laryngoscope*, pp. 1–9, 2020.
- [2] "Deafness and hearing loss," March 2020, <https://www.who.int/newsroom/fact-sheets/detail/deafness-and-hearing-loss>.

- [3] Y. Liu, J. Qi, X. Chen et al., “Critical role of spectrin in hearing development and deafness,” *Science Advances*, vol. 5, no. 4, 2019.
- [4] J. Qi, Y. Liu, C. Chu et al., “A cytoskeleton structure revealed by super-resolution fluorescence imaging in inner ear hair cells,” *Cell Discovery*, vol. 5, no. 1, 2019.
- [5] R. Beach, J. M. Abitbol, B. L. Allman, J. L. Esseltine, Q. Shao, and D. W. Laird, “GJB2 mutations linked to hearing loss exhibit differential trafficking and functional defects as revealed in cochlear-relevant cells,” *Frontiers in Cell and Developmental Biology*, vol. 8, 2020.
- [6] S. Zhang, Y. Zhang, Y. Dong et al., “Knockdown of Foxg1 in supporting cells increases the trans-differentiation of supporting cells into hair cells in the neonatal mouse cochlea,” *Cellular and Molecular Life Sciences*, vol. 77, no. 7, pp. 1401–1419, 2020.
- [7] C. Cheng, Y. Wang, L. Guo et al., “Age-related transcriptome changes in Sox2+ supporting cells in the mouse cochlea,” *Stem Cell Research & Therapy*, vol. 10, no. 1, p. 365, 2019.
- [8] S. Zhang, D. Liu, Y. Dong et al., “Frizzled-9+ supporting cells are progenitors for the generation of hair cells in the postnatal mouse cochlea,” *Frontiers in Molecular Neuroscience*, vol. 12, p. 184, 2019.
- [9] Z. He, L. Guo, Y. Shu et al., “Autophagy protects auditory hair cells against neomycin-induced damage,” *Autophagy*, vol. 13, no. 11, pp. 1884–1904, 2017.
- [10] W. Liu, X. Xu, Z. Fan, G. Sun, Y. Han, and D. Zhang, “Wnt signaling activates TIGAR and protects against cisplatin-induced spiral ganglion neuron damage in the mouse cochlea,” *Antioxidants & Redox Signaling*, vol. 30, no. 11, pp. 1389–1410, 2019.
- [11] Z.-h. He, S.-y. Zou, M. Li et al., “The nuclear transcription factor Foxg1 affects the sensitivity of mimetic aging hair cells to inflammation by regulating autophagy pathways,” *Redox Biology*, vol. 28, article 101364, 2020.
- [12] K. W. Chang, “Genetics of Hearing Loss–Nonsyndromic,” *Otolaryngologic Clinics of North America*, vol. 48, no. 6, pp. 1063–1072, 2015.
- [13] H. K. Kurtulgan, E. E. Altuntaş, M. E. Yıldırım, Ö. Özdemir, B. Bağcı, and İ. Sezgin, “The analysis of GJB2, GJB3, and GJB6 gene mutations in patients with hereditary nonsyndromic hearing loss living in Sivas,” *The Journal of International Advanced Otolaryngology*, vol. 15, no. 3, pp. 373–378, 2019.
- [14] M. Koohiyan, A. Ahmadi, F. Koohian, S. Aghaei, B. Amiri, and M. Hashemzadeh-Chaleshtorica, “An update of spectrum and frequency of GJB2 mutations causing hearing loss in the south of Iran: A literature review,” *International Journal of Pediatric Otorhinolaryngology*, vol. 119, pp. 136–140, 2019.
- [15] X. Yu, Y. Lin, J. Xu et al., “Molecular epidemiology of Chinese Han deaf patients with bi-allelic and mono-allelic GJB2 mutations,” *Orphanet Journal of Rare Diseases*, vol. 15, no. 1, p. 29, 2020.
- [16] M. Koohiyan, F. Azadegan-Dehkordi, F. Koohian, and M. Hashemzadeh-Chaleshtori, “Genetics of hearing loss in North Iran population: an update of spectrum and frequency of GJB2 mutations,” *Journal of Audiology & Otolaryngology*, vol. 23, no. 4, pp. 175–180, 2019.
- [17] J. Shinagawa, H. Moteki, S.-y. Nishio, Y. Noguchi, and S.-i. Usami, “Haplotype analysis of GJB2 mutations: founder effect or mutational hot spot?,” *Genes*, vol. 11, no. 3, p. 250, 2020.
- [18] M. Kabra, P. K. Singh, S. Sharma, M. Ghosh, S. S. Shastri, and N. Gupta, “Spectrum of GJB2 gene variants in Indian children with non-syndromic hearing loss,” *The Indian Journal of Medical Research*, vol. 147, no. 6, pp. 615–618, 2018.
- [19] S. Maeda, S. Nakagawa, M. Suga et al., “Structure of the connexin 26 gap junction channel at 3.5 Å resolution,” *Nature*, vol. 458, no. 7238, pp. 597–602, 2009.
- [20] H. Xia, X. Huang, H. Xu et al., “GJB2 c.235delC variant associated with autosomal recessive nonsyndromic hearing loss and auditory neuropathy spectrum disorder,” *Genetics and Molecular Biology*, vol. 42, no. 1, pp. 48–51, 2019.
- [21] H. Jiang, Y. Niu, L. Qu, X. Huang, X. Zhu, and G. Tang, “A novel compound heterozygous mutation in the GJB2 gene is associated with non-syndromic hearing loss in a Chinese family,” *Bioscience Trends*, vol. 12, no. 5, pp. 470–475, 2018.
- [22] F. Mammamo, “Inner ear connexin channels: roles in development and maintenance of cochlear function,” *Cold Spring Harbor Perspectives in Medicine*, vol. 9, no. 7, 2019.
- [23] L. Mei, J. Chen, L. Zong et al., “A deafness mechanism of digenic Cx26 (GJB2) and Cx30 (GJB6) mutations: Reduction of endocochlear potential by impairment of heterogeneous gap junctional function in the cochlear lateral wall,” *Neurobiology of Disease*, vol. 108, pp. 195–203, 2017.
- [24] X. Lin, X. Lin, G. Li et al., “Hearing consequences in GJB2 knock-in mice: implications for human p.V37I mutation,” *Aging*, vol. 11, no. 18, pp. 7416–7441, 2019.
- [25] <http://www.hgmd.cf.ac.uk/>.
- [26] H. Kaheel, A. Breß, M. A. Hassan et al., “Frequency of c.35delG mutation in GJB2 gene (connexin 26) in Syrian patients with nonsyndromic hearing impairment,” *Genetics Research International*, vol. 2017, 3 pages, 2017.
- [27] H. Shaikh, A. M. Waryah, A. K. Narsani et al., “Genetic testing of non-familial deaf patients for CIB2 and GJB2 mutations: phenotype and genetic counselling,” *Biochemical Genetics*, vol. 55, no. 5-6, pp. 410–420, 2017.
- [28] M. H. Bouzaher, C. P. Worden, and A. Jeyakumar, “Systematic review of pathogenic GJB2 variants in the Latino population,” *Otology & Neurotology*, vol. 41, p. 2, 2019.
- [29] N. Kecskeméti, M. Szönyi, A. Gáborján et al., “Analysis of GJB2 mutations and the clinical manifestation in a large Hungarian cohort,” *European Archives of Oto-Rhino-Laryngology*, vol. 275, no. 10, pp. 2441–2448, 2018.
- [30] A. M. Sheffield and R. J. H. Smith, “The epidemiology of deafness,” *Cold Spring Harbor Perspectives in Medicine*, vol. 9, no. 9, 2019.
- [31] J.-C. Leclère, M.-S. Le Gac, C. Le Maréchal, C. Ferec, and R. Marianowski, “GJB2 mutations: Genotypic and phenotypic correlation in a cohort of 690 hearing-impaired patients, toward a new mutation?,” *International Journal of Pediatric Otorhinolaryngology*, vol. 102, pp. 80–85, 2017.
- [32] Y. Chai, D. Chen, L. Sun et al., “The homozygous p.V37I variant of GJB2 is associated with diverse hearing phenotypes,” *Clinical Genetics*, vol. 87, no. 4, pp. 350–355, 2015.
- [33] P. Dai, F. Yu, B. Han et al., “GJB2 mutation spectrum in 2063 Chinese patients with nonsyndromic hearing impairment,” *Journal of Translational Medicine*, vol. 7, no. 1, p. 26, 2009.
- [34] F. Yu, P. Dai, and D. Y. Han, “GJB2 gene mutation and prelingual hereditary non-syndromic deafness,” *Otolaryngology Foreign Medical Sciences*, vol. 29, no. 6, pp. 359–361, 2005.
- [35] F.-F. Zhao, Y.-B. Ji, D.-Y. Wang et al., “Phenotype-genotype correlation in 295 Chinese deaf subjects with biallelic causative mutations in the GJB2 Gene,” *Genetic Testing & Molecular Biomarkers*, vol. 15, no. 9, pp. 619–625, 2011.

- [36] X. Wang, L. Huang, X. Zhao et al., "Children with GJB2 gene mutations have various audiological phenotypes," *Bioscience Trends*, vol. 12, no. 4, pp. 419–425, 2018.
- [37] B. György, C. Sage, A. A. Indzhukulian et al., "Rescue of Hearing by Gene Delivery to Inner-Ear Hair Cells Using Exosome-Associated AAV," *Molecular Therapy*, vol. 25, no. 2, pp. 379–391, 2017.
- [38] R. Mittal, D. Nguyen, A. P. Patel et al., "Recent advancements in the regeneration of auditory hair cells and hearing restoration," *Frontiers in Molecular Neuroence*, vol. 10, 2017.
- [39] X. Gao, Y. Tao, V. Lamas et al., "Treatment of autosomal dominant hearing loss by in vivo delivery of genome editing agents," *Nature*, vol. 553, no. 7687, pp. 217–221, 2018.
- [40] G. Altarescu, T. Eldar-Geva, B. Brooks et al., "Preimplantation genetic diagnosis (PGD) for nonsyndromic deafness by polar body and blastomere biopsy," *Journal of Assisted Reproduction and Genetics*, vol. 26, no. 7, pp. 391–397, 2009.
- [41] W. P. Xiong, D. Y. Wang, Y. Gao et al., "Reproductive management through integration of PGD and MPS-based noninvasive prenatal screening/diagnosis for a family with GJB2-associated hearing impairment," *Science China Life Sciences*, vol. 58, no. 9, pp. 829–838, 2015.
- [42] Z. Y. Dai, B. C. Sun, S. S. Huang et al., "Audiological features/genotype correlations in GJB2 mutation," *Chinese Journal of Otolaryngology*, vol. 1, pp. 34–36, 2014.
- [43] P. Dai, F. Yu, D.-y. Kang et al., "Diagnostic methods and clinic application for mtDNA A1555G and GJB2 and SLC26A4 genes in deaf patients," *Chinese Journal of Otorhinolaryngology Head and Neck Surgery*, vol. 40, no. 10, pp. 769–773, 2005.
- [44] T. Koffler, K. Ushakov, and K. B. Avraham, "Genetics of Hearing Loss: Syndromic," *Otolaryngologic Clinics of North America*, vol. 48, no. 6, pp. 1041–1061, 2015.
- [45] <https://www.who.int/news-room/fact-sheets/detail/deafness-and-hearing-loss>.
- [46] K. H. Lee, D. A. Larson, G. Shott et al., "Audiologic and temporal bone imaging findings in patients with sensorineural hearing loss and GJB2 mutations," *Laryngoscope*, vol. 119, no. 3, pp. 554–558, 2009.
- [47] K. T. Chorath, M. J. Willis, N. Morton-Gonzaba, W. J. Humann, and A. Moreira, "Mesenchymal stem cells for sensorineural hearing loss: protocol for a systematic review of pre-clinical studies," *Systematic Reviews*, vol. 8, no. 1, p. 126, 2019.
- [48] M. M. Cohen and R. J. Gorlin, "Epidemiology, etiology and genetic patterns," in *Hereditary Hearing Loss and its Syndromes*, R. J. Gorlin, H. V. Toriello, and M. M. Cohen, Eds., pp. 9–21, Oxford University Press, Oxford, 1995.
- [49] G. Lucotte and F. Diéterlen, "The 35delG mutation in the connexin 26 gene (GJB2) associated with congenital deafness: European carrier frequencies and evidence for its origin in ancient Greece," *Genetic Testing*, vol. 9, no. 1, pp. 20–25, 2005.
- [50] I. Todt, H. C. Hennies, D. Basta, and A. Ernst, "Vestibular dysfunction of patients with mutations of connexin 26," *Neuroreport*, vol. 16, no. 11, pp. 1179–1181, 2005.
- [51] S. L. Johnson, F. Ceriani, O. Houston et al., "Connexin-mediated signaling in nonsensory cells is crucial for the development of sensory inner hair cells in the mouse cochlea," *The Journal of Neuroscience*, vol. 37, no. 2, pp. 258–268, 2017.
- [52] M. Blanchard, B. Thierry, S. Marlin, and F. Denoyelle, "Genetic aspects of congenital sensorineural hearing loss," *Archives de Pédiatrie*, vol. 19, no. 8, pp. 886–889, 2012.
- [53] J. Chen, J. Chen, Y. Zhu, C. Liang, and H.-B. Zhao, "Deafness induced by Connexin 26 (GJB2) deficiency is not determined by endocochlear potential (EP) reduction but is associated with cochlear developmental disorders," *Biochemical and Biophysical Research Communications*, vol. 448, no. 1, pp. 28–32, 2014.
- [54] H. B. Zhao, "Hypothesis of K⁺-recycling defect is not a primary deafness mechanism for Cx26 (GJB2) deficiency," *Frontiers in Molecular Neuroence*, vol. 10, no. 126, 2017.
- [55] A. R. Fetoni, V. Zorzi, F. Paciello et al., "Cx26 partial loss causes accelerated presbycusis by redox imbalance and dysregulation of Nfr2 pathway," *Redox Biology*, vol. 19, pp. 301–317, 2018.
- [56] F. Denoyelle, S. Marlin, D. Weil et al., "Clinical features of the prevalent form of childhood deafness, DFNB1, due to a connexin-26 gene defect: implications for genetic counselling," *Lancet*, vol. 353, no. 9161, pp. 1298–1303, 1999.
- [57] X. Z. Liu, A. Pandya, S. Angeli et al., "Audiological features of GJB2 (connexin 26) deafness," *Ear and Hearing*, vol. 26, no. 3, pp. 361–369, 2005.
- [58] K. A. King, T. Makishima, C. K. Zalewski et al., "Analysis of auditory phenotype and karyotype in 200 females with turner syndrome," *Ear and Hearing*, vol. 28, no. 6, pp. 831–841, 2007.
- [59] N. Y. Bu-Saba, E. E. Rebeiz, S. D. Salman, A. R. Thornton, and C. West, "Significance of false-positive auditory brainstem response: a clinical study," *The American Journal of Otolaryngology*, vol. 15, no. 2, pp. 233–236, 1994.
- [60] R. A. Hendrix, R. M. Dedio, and A. P. Sclafani, "The use of diagnostic testing in asymmetric sensorineural hearing loss," *Otolaryngology–Head and Neck Surgery*, vol. 103, no. 4, pp. 593–598, 2016.
- [61] S. L. Urben, M. S. Benninger, and N. D. Gibbens, "Asymmetric sensorineural hearing loss in a community-based population," *Otolaryngology–Head and Neck Surgery*, vol. 120, no. 6, pp. 809–814, 2016.
- [62] R. H. Margolis and G. L. Saly, "Toward a standard description of hearing loss," *International Journal of Audiology*, vol. 46, no. 12, pp. 746–758, 2009.
- [63] R. H. Margolis and G. L. Saly, "Asymmetric hearing loss," *Otolaryngology & Neurotology*, vol. 29, no. 4, pp. 422–431, 2008.
- [64] M. G. V. C. Mazzoli, G. Van Camp, V. Newton, N. Giarbini, F. Declau, and A. Parving, "Recommendations for the description of genetic and audiological data for families with nonsyndromic hereditary hearing impairment," *Audiological Medicine*, vol. 1, no. 2, pp. 148–150, 2009.

Review Article

Stem Cell-Based Therapeutic Approaches to Restore Sensorineural Hearing Loss in Mammals

Muhammad Waqas ^{1,2}, Iram Us-Salam,¹ Zainab Bibi,¹ Yunfeng Wang ^{3,4}, He Li ⁵,
Zhongshou Zhu ⁶, and Shuangba He ²

¹Department of Biotechnology, Federal Urdu University of Arts, Science and Technology, Gulshan-e-Iqbal Campus, Karachi, Pakistan

²Department of Otolaryngology Head and Neck, Nanjing Tongren Hospital, School of Medicine, Southeast University, Nanjing 211102, China

³ENT Institute and Otorhinolaryngology Department of Eye & ENT Hospital, Fudan University, Shanghai 200031, China

⁴NHC Key Laboratory of Hearing Medicine (Fudan University), Shanghai 200031, China

⁵Department of Otolaryngology, First Affiliated Hospital of Wenzhou Medical University, Wenzhou City, 325000 Zhejiang Province, China

⁶Department of Otolaryngology, Ningde Municipal Hospital Affiliated of Fujian Medical University (Ningde Institute of Otolaryngology), Ningde, Fujian 352100, China

Correspondence should be addressed to Yunfeng Wang; yunfengwang@fudan.edu.cn, He Li; lihewuyao@163.com, Zhongshou Zhu; zhzhsh102@163.com, and Shuangba He; hesb@njtrh.org

Received 10 April 2020; Revised 1 June 2020; Accepted 3 July 2020; Published 1 August 2020

Academic Editor: Geng lin Li

Copyright © 2020 Muhammad Waqas et al. This is an open access article distributed under the Creative Commons Attribution License, which permits unrestricted use, distribution, and reproduction in any medium, provided the original work is properly cited.

The hair cells that reside in the cochlear sensory epithelium are the fundamental sensory structures responsible for understanding the mechanical sound waves evoked in the environment. The intense damage to these sensory structures may result in permanent hearing loss. The present strategies to rehabilitate the hearing function include either hearing aids or cochlear implants that may recover the hearing capability of deaf patients to a limited extent. Therefore, much attention has been paid on developing regenerative therapies to regenerate/replace the lost hair cells to treat the damaged cochlear sensory epithelium. The stem cell therapy is a promising approach to develop the functional hair cells and neuronal cells from endogenous and exogenous stem cell pool to recover hearing loss. In this review, we specifically discuss the potential of different kinds of stem cells that hold the potential to restore sensorineural hearing loss in mammals and comprehensively explain the current therapeutic applications of stem cells in both the human and mouse inner ear to regenerate/replace the lost hair cells and spiral ganglion neurons.

1. Introduction

The inner ear is a sophisticated and sensitive sensory organ of the body. It contains three well-known functional structures: the cochlea for sound perception, the vestibule, and the semi-circular canals for maintaining body equilibrium. The cochlea is responsible for understanding mechanical voices by transducing incoming sound vibrations into electrical impulses using hair cells (HCs) and then transmits these electrical impulses to the brainstem via spiral ganglion neuron cells (SGNs) [1–5]. The cochlear sensory epithelium has one row of inner hair cells (IHCs) and three rows of outer

hair cells (OHCs) interdigitated with multiple layers of supporting cells (SCs) (Figure 1). The OHCs are responsible to amplify the sound vibrations while the IHCs manage to convert mechanical sound into neural signals that further transmit through SGN to the auditory circuit [6–10]. Due to the exquisite transducer in nature, sensitivity and the delicate structure of these cells make them a key target for the ototoxic damage. The three rows of OHCs that externally reside are more sensitive to HC damage as compared to the IHCs. Most of the hearing loss patients have the same pathological features in common such as the HC loss and the decreased number of SGNs

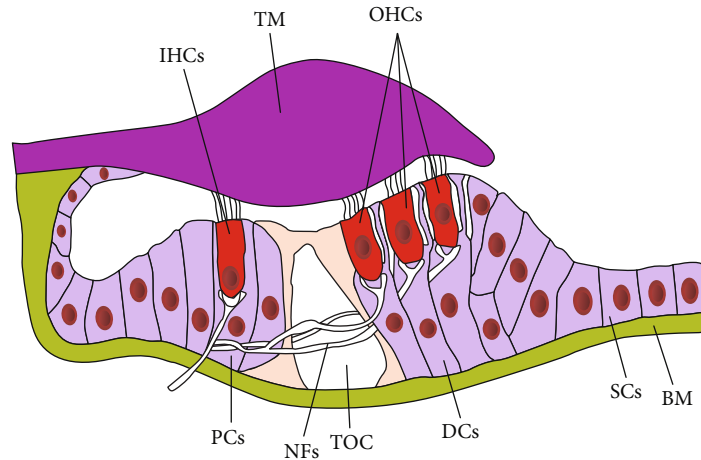


FIGURE 1: Schematic of the adult mammalian organ of Corti showing the normal arrangements of sensory and nonsensory cells on the basilar membrane. IHCs: inner hair cells; TM: tectorial membrane; OHCs: outer hair cells; PCs: pillar cells; NFs: nerve fibres; TOC: tunnel of Corti; DCs: Deiters' cells; SCs: supporting cells; BM: basilar membrane.

[11, 12]. Ototoxic insult to the sensory HCs causes hair cell death, which is mainly due to the exposure to loud noise, use of aminoglycosides or chemotherapy regimens, viral infections, biological aging, and genetically inherited disorders [13–20]. The drug-induced damage also promotes the reduction of specialized synaptic structures between IHCs and SGNs followed by the later degeneration of SGN [21–23]. In order to regenerate the SGN, many different biomaterials have been applied to promote the neural stem cells to regenerate the SGNs [24–30]. Moreover, in recent years, many previous reports used transcription regulation, electrical stimulation, and magnetic regulation to promote the regeneration and maturation of SGNs [31–36].

One way to restore hearing loss is to produce new functional HCs to replace the lost HCs in the cochlea. Regeneration of HCs and SGNs after damage could possibly yield a treatment for sensorineural hearing loss [37, 38]. Stem cells have the potential to self-renew and the ability to differentiate into multiple cell types [39]. It is now well understood that a specific population of resident SCs marked with the stem cell markers *Lgr5*, *Lgr6*, *Sox2*, *Sox9*, *Frizzled-9*, *EPCAM*, and *ABCG2* in the organ of Corti, commonly known as cochlear stem/progenitor cells, holds the stem cell-like potential to proliferate and differentiate to form both HCs and SCs [40–45]. However, the mammals only have very limited HC regeneration ability [42, 46–51]; thus, how to promote the HC regeneration ability and to promote the maturation of new regenerated HCs is the key scientific question in the hearing research field. Several research studies unravel the potential of different kinds of stem cells to generate HCs and SGNs, such as stem/progenitor cells, spiral ganglion-derived neural stem cells (endogenous stem cells), embryonic stem cells, and induced pluripotent stem cells (exogenous stem cells) [52–54]. In this review, we focus on the recent progress in the therapeutic use of different types of stem cells (endogenous and exogenous stem cells) to recover hearing function in the human and mouse inner ear.

2. Hearing Restoration Approaches

Hearing research science is primarily focused on formulating the best therapeutic strategies to renew the hearing cells (HCs and SGNs), thus restoring the natural hearing function and producing comfort to the millions of patients affected by this widely growing disorder [55]. Also, the damage to the HCs in the inner ear subsequently increases the risk of degeneration in the residual SGN. Therefore, it is essential to protect both the HCs and existing SGNs in the cochlea. More recently, stem cell therapy and gene therapy are the most promising therapeutic strategies to regenerate/replace HCs and SGNs in the cochlea after damage. Here, in this review, we will discuss the stem cell-based therapeutic strategies in the mammalian inner ear.

3. Characteristics of Stem Cells

Stem cells are better called the principal cells of the body that maintain their undifferentiated and unspecialized state in order to either directly transform into specialized cells or pursue the mitotic division to form new stem cells. Stem cells are used to restore cellular damage and recover the cell loss. Adult stem/progenitor cells, spiral ganglion-derived neural stem cells (SGN-NSCs), embryonic stem cells (ESCs), and inducible pluripotent stem cells (iPSCs) are kind of stem cells that are commonly used in therapeutics [56]. Adult stem/progenitor cells are inhabitants in the organ of Corti. There are various proteins like *Lgr5*, *Lgr6*, *Sox2*, *Sox9*, *EPCAM*, and *ABCG2* that have been recognized as reliable cochlear stem/progenitor cell markers in the mouse and human inner ear [40, 57–61]. The molecular characterization and mechanism behind the higher proliferation and regeneration ability of *Lgr5+*, *Lgr6+*, and *Sox2+* cochlear stem/progenitor cells have been thoroughly studied in mouse models using microarrays and RNA-Seq profiling, and a large dataset of genes has been identified that showed that multiple genes might regulate the proliferation and HC regeneration ability of

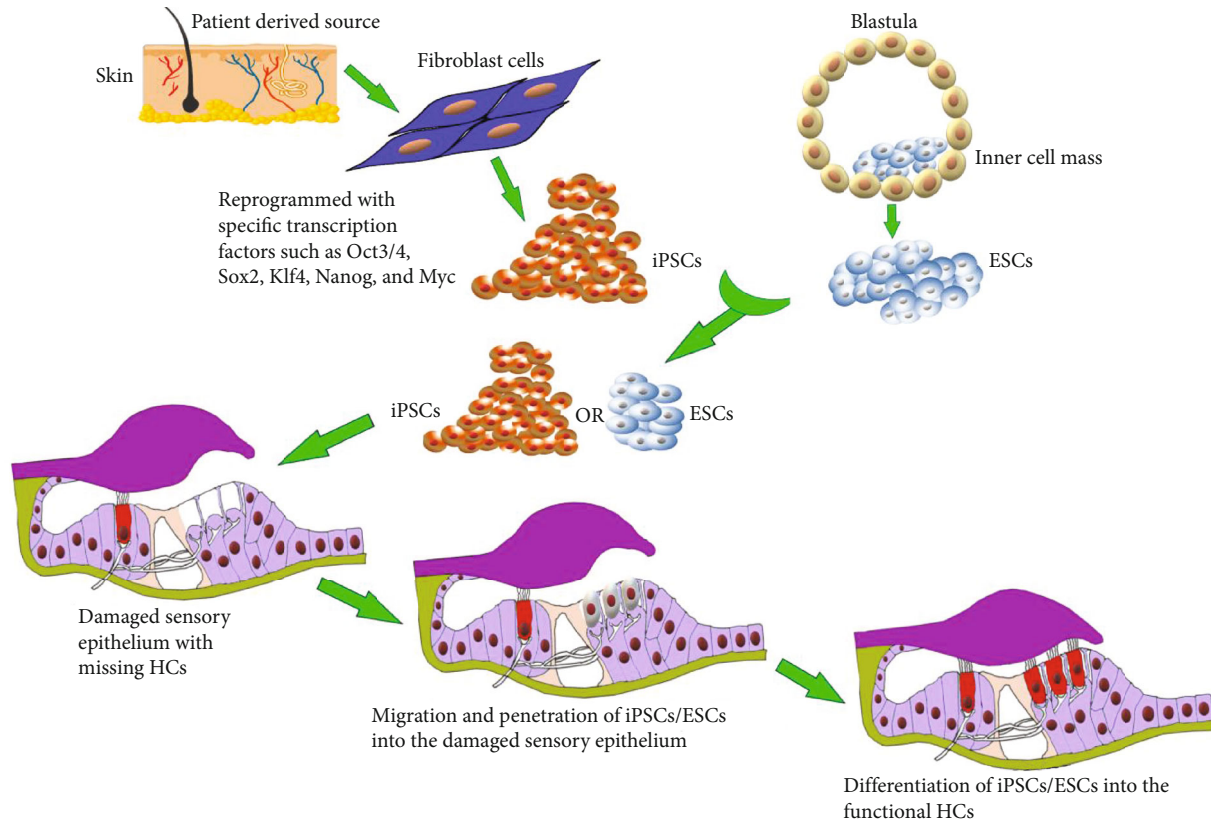


FIGURE 2: Schematic of the exogenous stem cell therapy showing the migration, penetration, and differentiation of embryonic stem cells (ESCs) or inducible pluripotent stem cells (iPSCs) to generate functional HCs in the damaged sensory epithelium.

stem/progenitor cells in the inner ear [48, 62–65]. Similarly, there is a proof for the existence of SGN stem cells that are commonly known as SGN-NSCs. These cells resided in the region of the SGN and are able to differentiate to form functional neurons [66, 67].

ESCs are pluripotent stem cells, obtained from the inner cell mass and hold the limitless potential to proliferate as well as to differentiate to form all three germ layers: ectoderm, mesoderm, and endoderm. Yet, the mouse ESCs have been more deeply investigated as compared with the human ESCs. ESCs have been widely used for in vitro culture system to deliberately induce the formation of different cell types such as liver cells, neuronal cells, cardiac cells, and pancreatic cells [68–73]. Thus, ESCs provide a significant resource of cells for replacement therapy in order to regenerate different tissues/organs.

The iPSCs are the adult differentiated cells that are genetically reprogrammed to form pluripotent stem cells. They hold a novel therapeutic ability to replace and repair the hearing cells (HCs and SGNs) in the inner ear. The mature skin fibroblast cells were the first reprogrammed iPSC generated by deliberately introducing the four crucial transcription factors including Klf4, Sox2, c-Myc, and Oct3/4 [74]. In therapeutics, the primary reason of iPSC generation from adult cells is to avoid the immunorejection in patients as the adult cells isolated, manipulated, and reintroduced as iPSCs in the same patient. Also, the use of iPSCs sufficiently decreased the ethical concerns about the use of stem cells as therapeutics.

4. Stem Cell Therapy in the Inner Ear

The use of stem cell therapy in the inner ear is a promising approach to rescue the HC damage and to reestablish the hearing function. There are two possible stem cell-based approaches to treat deafness. The first is the restoration of existing stem cells in the inner ear by stimulating the resident stem cells within the organ of Corti, therefore allowing stem cells to replace the damaged HCs and rehabilitate the normal hearing mechanism. However, the basic difficulty with this approach is the insufficient number of resident stem cells in the inner ear that are not capable to restore hearing. The second is the exogenous supply of stem cells (stem cell transplantation) into the inner ear (Figure 2). This approach is implemented by either supplying stem cells into the scala tympani through the round window and triggering these cells to migrate into the cochlear sensory epithelium [75] or directly transplanting the stem cells into the scala media. However, the high concentration of potassium and the tight junction barriers make the endolymph environment very hostile for the survival of foreign stem cells [76]. Therefore, it is important to adopt the methods that create a more hospitable environment in the cochlea. There are few strategies to do so, such as replacing the scala media fluid with the more hostile media to stem cells, systemic administration of loop diuretic drug to lower the potassium concentration, and the use of sodium caprate that disrupts the tight junctions in the cochlea [77, 78].

4.1. Stem Cell-Based Therapeutic Approaches in the Human Inner Ear. The presence of endogenous stem/progenitor cells in the adult human sensory epithelium was evident, when the pure population of cells was marked with the stem cell marker ABCG2+ve isolated from dissociated human cochlear cells via flow cytometry. These dissociated human cochlear cells also form spheres in the in vitro culture system. However, the number of spheres generated in the experiments was inadequate to further characterize these spheres for the ability to regenerate functional HCs [61]. More recently, two prosensory markers EPCAM and CD271 have been used to separate the human fetal postmitotic HC progenitors. The 3D culture of EPCAM and CD271 marked cells in Matrigel allows the formation of cell colonies that displayed the expression of stem cell markers (Sox2, Sox9, and Fbxo2). These cells regain their proliferative capability and ultimately differentiate to form HC-like cells in vitro. However, the expression of Lgr5 was not observed in the cell colonies [60].

Multiple studies have attempted the transplantation of embryonic stem cells in the inner ear in order to regenerate HCs in vitro. There were few studies that reported on the use of human embryonic stem cells (hESCs) to differentiate to form HC-like cells. In one of the studies, the hESCs were triggered to differentiate under particular signals mandatory for the specification of the early otic placode and obtain otic progenitors that differentiate into HC-like cells displaying HC-specific marker, immature stereociliary bundles. These HC-like cells also showed the electrophysiological characteristics suggesting that they are functional HCs. Some other otic progenitors differentiate to form neuronal cells exhibiting specific neuronal markers and having electrophysiological properties, suggesting that these cells are also able to generate functional auditory neuronal cell fate [79]. The generation of human otic progenitors was relied on the fibroblast growth factor signaling, and the newly regenerated HC-like cells showed the specific HC markers and immature stereociliary bundles. However, these HCs are unable to build the fully matured HC cytoarchitecture, which is necessary to restore hearing function [80].

To overcome this nonfunctionality of matured HC-like cells, the three-dimensional culture system has been successfully used to generate the inner ear organoid from hESCs. The inner ear organoid has the genuine cytoarchitecture of HCs, SCs, and neuronal cells as expressive of the native inner ear sensory epithelium [81]. In vitro organoid culture system promotes the study of human inner ear development and presents a disease model for therapeutic research. The other researchers also followed this 3D culture system in their hESC experiments [82]. Although the exogenous ESC implantation is a promising strategy, one problem with the survival of implanted cells in the inner ear is the high concentration of potassium in the scala media. Lee et al. address this issue by preconditioning the scala media to reduce the potassium concentration before implanting the hESCs in the deaf guinea pig cochlea. Their results showed the increased survival of hESCs in the cochlea; however, some stem cells lose their pluripotency and differentiation ability as noted by the lower expression of the Oct3/4 marker [78]. The primary

objective of this study is to figure out whether the hESCs survived after implantation in the animal model. The implanted hESCs showed attachment to the sensory epithelium even without full integration. Although there is a lack of clear evidence of integration, the application of sodium caprate strengthens the survival and encourages the differentiation of hESCs after implantation.

The capability to generate SGNs from stem cells is a compulsory requirement to develop stem cell therapy for SNHL. A group of researchers developed a protocol that allows the differentiation of hESCs into a pure population of otic neuronal progenitors (ONP) and SGN-like cells. Interestingly, the newly differentiated SGN-like cells express the specific SGN genotypic and phenotypic markers as well as extend their neurites towards the cochlear nucleus suggesting that the hESC-derived SGNs can closely replicate the features of functional human SGN [83]. Moreover, Hyakumura et al. recently described the use of human pluripotent stem cells (hPSCs) to derive sensory neuronal cells. They observed that the differentiated hPSC-derived neuronal cells formed synaptic connections with both the inner ear HCs and cochlear nucleus neurons in organotypic coculture. The contacts between hPSC-derived neuron cells and inner ear HCs and cochlear nucleus neurons are significantly positive for specific synaptic markers such as synapsin I and VGLUT1. This new auditory coculture model provides a clue for the use of stem cells in the bidirectional growth towards the target cells and tissue in the inner ear and brainstem [84]. However, the drawback is that the in vitro model does not provide enough clues to mimic in vivo physiological conditions. To address this issue, a new study demonstrated the use of nanofibrillar cellulose (NFC) hydrogel, which is a kind of artificial extracellular matrix (ECM). The use of NFC hydrogel together with the delivery of neurotrophic factor artificially creates a stem cell niche in in vitro and in vivo models. NFC hydrogel promotes the in vitro and in vivo survival and differentiation of hESC-derived ONP spheroids. The transplanted ONP spheroids have been shown to survive and neuronally differentiate into otic neuronal lineages both in vivo and in vitro. Interestingly, they also displayed protracted neurites towards the bony wall of the cochlea following the ninety days of transplantation [85].

There are some ethical concerns on the experimental utilization of human embryonic stem cells, and since then, much attention has been paid on the experimental generation of iPSCs from somatic cells to further transform to generate HC-like cells. Multiple strategies have been formulated successfully to first generate human iPSCs (hiPSCs) and then stepwise induce the differentiation of hiPSCs into the human inner ear HC-like cells [86]. There are different factors and signals that drive hiPSCs into otic sensory progenitor cells (OSPCs) to reestablish lost HCs. The rapid and efficient generation of OSPCs can be achieved by manipulating the cell signaling pathways such as modulation of Notch, Wnt, FGF, and TGF- β through the use of the differentiated monolayer culture system [87, 88]. These efficiently generated OSPCs could be established and used for disease modeling and cell-based therapies.

The correction of gene mutation in iPSCs stimulated from somatic cells of diseased persons is a promising way to treat hereditary SNHL. In two different studies, researchers begin iPSC formation from a deaf patient carrying *Myo7a* and *Myo15* mutations that are mainly responsible for deafness. CRISPR/CAS 9 gene-editing tool is used to genetically rectify the *Myo7a* and *Myo15* mutations and observe that the HC-like cells derived from the corrected iPSCs exhibited the recovered organization of the stereociliary-like structures and complete morphological and functional restoration of HCs [89, 90]. Moreover, in another study, the iPSCs were generated from the fibroblast cells of a MERRF syndrome patient with A8344G mutation of mitochondrial DNA. The iPSCs were driven by a set of transcription factors *Atoh1/Rfx1/Rfx3* that significantly increased the differentiation ability of iPSCs into *Myo7a*+ve cells. These newly differentiated HC-like cells displayed the expression of HC-related genes and facilitated the HC-like cells with more mature stereociliary bundles [91]. Also, a recent study reported that the reprogramming of urinary cells isolated from the healthy human individual turns them into iPSC. These iPSCs were further differentiated to form otic epithelial and HC-like cells. There were two different observations recorded in vivo and in vitro. In vitro conditions displayed that the newly reprogrammed HC-like cells appear to be completely mimicked in morphological and electrophysiological characteristics as with the normal HCs. However, in vivo conditions showed that a very limited number of transplanted HC-like cells moved and integrated into the resident site of original HC and fewer cells formed neuronal connections with SGNs [92].

One main concern regarding the use of iPSCs is their genetic integrity, as the use of viral vectors during reprogramming of these cells might cause the insertional mutagenesis. To address this query, Boddy et al. proposed a nonintegrating mRNA-based reprogramming of human-induced pluripotent stem cell (hiPSC) lines. The integration-free hiPSC lines were allowed to culture in the presence of FGF3 and FGF10 that trigger the process of hiPSC line differentiation into otic progenitors as confirmed by the detection of otic markers *Pax2*, *Pax8*, *Sox2*, and *Foxg1*. Subsequently, the purified otic epithelial and neuroprogenitors were differentiated to generate HC-like cells and neurons [93].

In addition, the iPSCs also served as a resource for the replacement therapy of neurons in the damaged cochlea. A study demonstrated that the hiPSC-derived neurons innervate with the developing HCs and form presynaptic connections in the in vitro coculture system. Those hiPSC-derived neural progenitors cocultured with HCs at an earlier stage of differentiation displayed a higher innervation potential as compared to the other neural progenitors [94]. However, the transplantation of these neural progenitors in the damaged cochlea remains a challenge. A recent work explained the specific stepwise neural induction method for hiPSCs to eliminate the undifferentiated cells from neurons. The hiPSC-derived neural progenitors were first established on Matrigel. Then, these neural progenitors differentiated into neurons on a 3D collagen matrix. Lastly, the hiPSC-derived neurons cultured on a 3D collagen matrix were transplanted

into the guinea pig cochlea [95]. The results showed that hiPSC-derived neuronal cells expressed specific neuronal markers and the survival of transplant-derived neurons can be achieved by controlling the inflammatory response.

4.2. Stem Cell-Based Therapeutic Approaches in the Mouse Inner Ear. The embryonic stem cells derived from mice were first used in an experiment to produce HC-like cells in vitro by formulating a proper stepwise differentiation strategy. These differentiated HC-like cells showed the full expression of HC-specific markers observed via gene expression profiling and immunostaining [96]. The *Barhl1* is a deafness gene expressed in the developing hair cells. It plays an important role in the differentiation of mouse embryonic stem cells (mESCs) into HC-like cells. The targeted disruption of *Barhl1* hindered the differentiation of mESC-derived HC-like cells in vitro [97]. Moreover, the use of mouse pluripotent stem cells displayed the successful in vitro differentiation of both embryonic stem cells and iPSCs into the HC-like cells. These newly differentiated HC-like cells were generated by applying the scheme to mimic the basic concepts of early embryonic and normal otic development. In the in vitro feeder layer of the chicken utricle, stromal cells were used for differentiation and maturation of these embryonic and iPSCs into the HC-like cells. The newly formed cells showed that the mechanosensing stereociliary structures on their surfaces resemble the mouse vestibular HCs and were responsive to the mechanical stimulation [52]. On account of the earlier detailed report, the multiple strategies are formulated based on the use of the feeder cell layers. One study on this aspect reported that the application of the feeder cell layer (ST2 stromal cell-conditioned medium) together with the transfection of the *Atoh1* transcription factor in mouse embryonic stem cells efficiently induces the formation of HC-like cells in vitro [98].

Despite the use of the feeder cell layer, some other strategies such as three-dimensional (3D) cultural systems have also been used to transform mESCs into HC-like cells, SCs, and neuronal cells. The advantage of the 3D cultural system is that the neuronal cells established synaptic connectivity with the HCs. Furthermore, the aggregate of mESCs in the 3D culture system has been guided to mimic the normal development by sequentially generating the nonneural ectoderm expressing multiple marker genes (including *FOXI3*, *GATA3*, *DLX5*, *SIX1*, and *EYA1*), preplacodal ectoderm, and otic placode (expressing *PAX2* and *PAX8* genes) [99–101]. Also, the Wnt activation enhances the inner ear organoid development from mESCs in the 3D culture system [102]. Moreover, a recent study defines the new protocol to derive inner ear organoids from mutant mESCs under chemically defined conditions. In this protocol, they developed the 3D culture method to generate the inner ear organoid from mESCs, which differentiate to form the functional HCs and innervated by the sensory-like neuronal cells. In this approach, firstly, the mESCs were derived from the blastocyst stage of a *Pax2* fluorescent reporter mouse line. Then, these *Pax2*^{EGFP/+} cells were used for inner ear organoid formation to understand the otic induction. The results displayed the higher expression of *Pax2* and active

stimulation of ERK downstream of the FGF signaling pathway in inner ear organoid development. The expression of Pax2 was persistent throughout the formation of sensory HCs, and the cochlear neurons established synaptic connections with HCs in the organoids [103, 104].

In addition, there is a novel exploration of transcriptional machinery that controls the HC fate and differentiation of mESCs. The simultaneous overexpression of three transcription factors, *Gfi1*, *POU4f3*, and *Atoh1*, directly stimulates the genetic programming in mESCs that leads to the sensory HC generation in vitro. The newly generated HCs express various HC-specific markers and revealed the polarized membrane protrusions on the HC surfaces similar to the stereociliary bundles [105]. The differentiation of mESCs by deliberate induction in culture leads to the migration of progenitor cells derived from mESCs into the cochlea. These cells also expressed the specific HC markers after transplantation into the inner ear [106, 107]. Also, it is a prerequisite condition to integrate the mESC-derived neurons into the central nervous system (CNS) for functional synaptic connectivity. An in vitro coculture system has been developed in which the mESCs were first induced to form mESC-derived SGN-like cells, and then, these SGN-like cells were allowed to coculture with CN neurons for 4–6 days in the presence of thrombospondin-1. The results showed the development of neural connections between mESC-derived SGN-like cells and CNS as confirmed by the expression of pre- and postsynaptic markers on the newly formed synaptic structures [108]. In contrast to mESCs, the use of mouse iPSCs to generate HCs and SGNs is not promising at all yet. Multiple studies reported that the mouse iPSCs could differentiate to form HC-like cells and SGNs after transplantation into the mouse cochlea; however, there is no significant improvement observed in the threshold of auditory brain response (ABR) [109–111].

Until now, in vitro studies regarding both human and mouse ESCs and iPSCs demonstrated that the specific culture conditions allow the stem cells to differentiate and achieve the desired cell fate such as HC-like cells and SGNs [112, 113]. The introduction of stem cell-derived progenitors at the spot of injury in the inner ear permits the transplanted cells to integrate and express the HC markers in the cochlear and vestibular sensory epithelium in vivo [96]. However, a very limited number of studies examined the assimilation of newly differentiated HCs into the mammalian inner ear. In multiple studies, the results regarding the implantation of stem cells to generate the functional HCs at the location of the damaged mammalian inner ear are uncertain [114, 115]. There is a limited number of transplanted cells that converted to form the required cell fate such as HCs, SCs, and neuronal and glial cells while a large number of cells were unable to achieve relevant cell types even after several weeks of transplant. The possible reason for this uncertainty is the change in the in vivo microenvironment in the mammalian cochlea, which is absolutely different from the in vitro culture conditions where HCs were generated. Another complexity is correctly targeting the damaged cochlear regions where the HCs are actually required and generation of adequate functional HCs at those sites. Also,

another considerable challenge with the stem cell therapy for HC regeneration is the appropriate HC, SC, and SGN integration and orientation within the specific sites in the cochlea.

5. Conclusion

Hearing research is mainly focused on developing different strategies to design therapeutics that help to initiate the HC regeneration/replacement process in the inner ear to ultimately recover hearing loss. Multiple studies on the animal model have been successfully conducted that allow the clinical applications of endogenous and exogenous stem cells in order to regenerate/replace HCs in the mammalian inner ear. However, there are numerous challenging questions that need to be dealt with before executing these therapeutic strategies in humans. Some of them include the risk of tumorigenesis after implanting the stem cells, possible detrimental effects to the patients, and appropriate and controlled growth of stem cells at the site of cell transplantation in the cochlea. Also, the high cost of stem cell therapy makes it unreachable for a large number of hearing loss patients. In addition, the success rate of stem cell therapy is not high enough yet. Regardless of these limitations, stem cell therapy is still a promising future strategy to start HC regeneration/replacement in the adult mammalian cochlea to recover sensorineural hearing loss.

Data Availability

This is a review article, and the data supporting this review article are from previously reported studies and datasets, which have been cited in the text.

Conflicts of Interest

The authors declare that they have no competing interests.

Acknowledgments

The authors appreciate the Higher Education Commission (HEC) of Pakistan for their support and valuable assistance to the institute.

References

- [1] Y. Liu, J. Qi, X. Chen et al., “Critical role of spectrin in hearing development and deafness,” *Science Advances*, vol. 5, no. 4, article eaav7803, 2019.
- [2] Y. Wang, J. Li, X. Yao et al., “Loss of CIB2 Causes Profound Hearing Loss and Abolishes Mechano-electrical Transduction in Mice,” *Frontiers in Molecular Neuroscience*, vol. 10, p. 401, 2017.
- [3] C. Zhu, C. Cheng, Y. Wang et al., “Loss of ARHGEF6 Causes Hair Cell Stereocilia Deficits and Hearing Loss in Mice,” *Frontiers in Molecular Neuroscience*, vol. 11, p. 362, 2018.
- [4] J. Qi, Y. Liu, C. Chu et al., “A cytoskeleton structure revealed by super-resolution fluorescence imaging in inner ear hair cells,” *Cell Discovery*, vol. 5, no. 1, 2019.

- [5] J. Qi, L. Zhang, F. Tan et al., “Espn distribution as revealed by super-resolution microscopy of stereocilia,” *American Journal of Translational Research*, vol. 12, no. 1, pp. 130–141, 2020.
- [6] A. J. Hudspeth, “Integrating the active process of hair cells with cochlear function,” *Nature Reviews Neuroscience*, vol. 15, no. 9, pp. 600–614, 2014.
- [7] R. Fettiplace and C. M. Hackney, “The sensory and motor roles of auditory hair cells,” *Nature Reviews Neuroscience*, vol. 7, no. 1, pp. 19–29, 2006.
- [8] D. Z. He, S. Jia, and P. Dallos, “Mechano-electrical transduction of adult outer hair cells studied in a gerbil hemicochlea,” *Nature*, vol. 429, no. 6993, pp. 766–770, 2004.
- [9] P. Avan, B. Büki, and C. Petit, “Auditory distortions: origins and functions,” *Physiological Reviews*, vol. 93, no. 4, pp. 1563–1619, 2013.
- [10] T. Moser and A. Starr, “Auditory neuropathy—neural and synaptic mechanisms,” *Nature Reviews. Neurology*, vol. 12, no. 3, pp. 135–149, 2016.
- [11] T. J. McGill and H. F. Schuknecht, “Human cochlear changes in noise induced hearing loss,” *The Laryngoscope*, vol. 86, no. 9, pp. 1293–1302, 1976.
- [12] J. B. Nadol, B. J. Burgess, B. J. Gantz et al., “Histopathology of Cochlear Implants in Humans,” *Annals of Otolaryngology, Rhinology & Laryngology*, vol. 110, no. 9, pp. 883–891, 2001.
- [13] V. A. McHaney, G. Thibadoux, F. A. Hayes, and A. A. Green, “Hearing loss in children receiving cisplatin chemotherapy,” *The Journal of Pediatrics*, vol. 102, no. 2, pp. 314–317, 1983.
- [14] L. P. Rybak, “Drug ototoxicity,” *Annual Review of Pharmacology and Toxicology*, vol. 26, no. 1, pp. 79–99, 1986.
- [15] M. Waqas, S. Gao, Iram-us-Salam, M. K. Ali, Y. Ma, and W. Li, “Inner Ear Hair Cell Protection in Mammals against the Noise-Induced Cochlear Damage,” *Neural Plasticity*, vol. 2018, Article ID 3170801, 9 pages, 2018.
- [16] Z. H. He, S. Y. Zou, M. Li et al., “The nuclear transcription factor FoxG1 affects the sensitivity of mimetic aging hair cells to inflammation by regulating autophagy pathways,” *Redox Biology*, vol. 28, article 101364, 2020.
- [17] S. Gao, C. Cheng, M. Wang et al., “Blebbistatin Inhibits Neomycin-Induced Apoptosis in Hair Cell-Like HEI-OC-1 Cells and in Cochlear Hair Cells,” *Frontiers in Cellular Neuroscience*, vol. 13, 2020.
- [18] Y. Zhang, W. Li, Z. He et al., “Pre-treatment With Fasudil Prevents Neomycin-Induced Hair Cell Damage by Reducing the Accumulation of Reactive Oxygen Species,” *Frontiers in Molecular Neuroscience*, vol. 12, p. 264, 2019.
- [19] W. Liu, X. Xu, Z. Fan et al., “Wnt Signaling Activates TP53-Induced Glycolysis and Apoptosis Regulator and Protects Against Cisplatin-Induced Spiral Ganglion Neuron Damage in the Mouse Cochlea,” *Antioxidants & Redox Signaling*, vol. 30, no. 11, pp. 1389–1410, 2019.
- [20] L. Liu, Y. Chen, J. Qi et al., “Wnt activation protects against neomycin-induced hair cell damage in the mouse cochlea,” *Cell Death & Disease*, vol. 7, no. 3, article e2136, 2016.
- [21] S. G. Kujawa and M. C. Liberman, “Adding Insult to Injury: Cochlear Nerve Degeneration after “Temporary” Noise-Induced Hearing Loss,” *Journal of Neuroscience*, vol. 29, no. 45, pp. 14077–14085, 2009.
- [22] S. G. Kujawa and M. C. Liberman, “Synaptopathy in the noise-exposed and aging cochlea: Primary neural degeneration in acquired sensorineural hearing loss,” *Hearing Research*, vol. 330 Part B, pp. 191–199, 2015.
- [23] R. Guo, X. Ma, M. Liao et al., “Development and Application of Cochlear Implant-Based Electric-Acoustic Stimulation of Spiral Ganglion Neurons,” *ACS Biomaterials Science & Engineering*, vol. 5, no. 12, pp. 6735–6741, 2019.
- [24] G. Li, K. Chen, D. You et al., “Laminin-Coated Electrospun Regenerated Silk Fibroin Mats Promote Neural Progenitor Cell Proliferation, Differentiation, and Survival in vitro,” *Frontiers in Bioengineering and Biotechnology*, vol. 7, p. 190, 2019.
- [25] K.-Q. Fan, Y. Y. Li, H. L. Wang et al., “Stress-induced metabolic disorder in peripheral CD4⁺ T cells leads to anxiety-like behavior,” *Cell*, vol. 179, no. 4, pp. 864–879.e19, 2019.
- [26] Q. Fang, Y. Zhang, X. Chen et al., “Three-Dimensional Graphene Enhances Neural Stem Cell Proliferation Through Metabolic Regulation,” *Frontiers in Bioengineering and Biotechnology*, vol. 7, 2020.
- [27] J. Zhao, M. Tang, J. Cao et al., “Structurally Tunable Reduced Graphene Oxide Substrate Maintains Mouse Embryonic Stem Cell Pluripotency,” *Advanced Science*, vol. 6, no. 12, article 1802136, 2019.
- [28] D. Li, X. Yan, Y. Hu et al., “Two-photon image tracking of neural stem cells via iridium complexes encapsulated in polymeric nanospheres,” *ACS Biomaterials Science & Engineering*, vol. 5, no. 3, pp. 1561–1568, 2019.
- [29] S. Han, Y. Xu, J. Sun et al., “Isolation and analysis of extracellular vesicles in a Morpho butterfly wing-integrated microvortex biochip,” *Biosensors and Bioelectronics*, vol. 154, article 112073, 2020.
- [30] R. Guo, S. Zhang, M. Xiao et al., “Accelerating bioelectric functional development of neural stem cells by graphene coupling: implications for neural interfacing with conductive materials,” *Biomaterials*, vol. 106, pp. 193–204, 2016.
- [31] M. Tang, J. Li, L. He et al., “Transcriptomic profiling of neural stem cell differentiation on graphene substrates,” *Colloids and Surfaces B: Biointerfaces*, vol. 182, article 110324, 2019.
- [32] S. Han, J. Sun, S. He, M. Tang, and R. Chai, “The application of graphene-based biomaterials in biomedicine,” *American Journal of Translational Research*, vol. 11, no. 6, pp. 3246–3260, 2019.
- [33] L. Xia, W. Zhu, Y. Wang, S. He, and R. Chai, “Regulation of Neural Stem Cell Proliferation and Differentiation by Graphene-Based Biomaterials,” *Neural Plasticity*, vol. 2019, Article ID 3608386, 11 pages, 2019.
- [34] Y. Yang, Y. Zhang, R. Chai, and Z. Gu, “Designs of biomaterials and microenvironments for neuroengineering,” *Neural Plasticity*, vol. 2018, Article ID 1021969, 10 pages, 2018.
- [35] L. Shang, Y. Yu, W. Gao et al., “Bio-Inspired Anisotropic Wettability Surfaces from Dynamic Ferrofluid Assembled Templates,” *Advanced Functional Materials*, vol. 28, no. 7, article 1705802, 2018.
- [36] Z. Liu, M. Tang, J. Zhao, R. Chai, and J. Kang, “Looking into the Future: Toward Advanced 3D Biomaterials for Stem-Cell-Based Regenerative Medicine,” *Advanced Materials*, vol. 30, no. 17, article 1705388, 2018.
- [37] G. Nacher-Soler, J. M. Garrido, and F. Rodriguez-Serrano, “Hearing regeneration and regenerative medicine: present and future approaches,” *Archives of Medical Science*, vol. 15, no. 4, pp. 957–967, 2019.

- [38] G. Liu, B. T. David, M. Trawczynski, and R. G. Fessler, "Advances in Pluripotent Stem Cells: History, Mechanisms, Technologies, and Applications," *Stem Cell Reviews and Reports*, vol. 16, no. 1, pp. 3–32, 2020.
- [39] M. Xia, J. Ma, S. Sun, W. Li, and H. Li, "The biological strategies for hearing re-establishment based on the stem/progenitor cells," *Neuroscience Letters*, vol. 711, article 134406, 2019.
- [40] F. Shi, J. S. Kempfle, and A. S. B. Edge, "Wnt-Responsive Lgr5-Expressing Stem Cells Are Hair Cell Progenitors in the Cochlea," *The Journal of Neuroscience*, vol. 32, no. 28, pp. 9639–9648, 2012.
- [41] R. Chai, B. Kuo, T. Wang et al., "Wnt signaling induces proliferation of sensory precursors in the postnatal mouse cochlea," *Proceedings of the National Academy of Sciences of the United States of America*, vol. 109, no. 21, pp. 8167–8172, 2012.
- [42] B. C. Cox, R. Chai, A. Lenoir et al., "Spontaneous hair cell regeneration in the neonatal mouse cochlea in vivo," *Development*, vol. 141, no. 4, pp. 816–829, 2014.
- [43] M. Waqas, S. Zhang, Z. He, M. Tang, and R. Chai, "Role of Wnt and Notch signaling in regulating hair cell regeneration in the cochlea," *Frontiers of Medicine*, vol. 10, no. 3, pp. 237–249, 2016.
- [44] N. F. Bramhall, F. Shi, K. Arnold, K. Hochedlinger, and A. S. B. Edge, "Lgr5-Positive Supporting Cells Generate New Hair Cells in the Postnatal Cochlea," *Stem Cell Reports*, vol. 2, no. 3, pp. 311–322, 2014.
- [45] K. Oshima, C. M. Grimm, C. E. Corrales et al., "Differential Distribution of Stem Cells in the Auditory And Vestibular Organs of the Inner Ear," *Journal of the Association for Research in Otolaryngology*, vol. 8, no. 1, pp. 18–31, 2007.
- [46] S. Zhang, Y. Zhang, Y. Dong et al., "Knockdown of Foxg1 in supporting cells increases the trans-differentiation of supporting cells into hair cells in the neonatal mouse cochlea," *Cellular and Molecular Life Sciences*, vol. 77, no. 7, pp. 1401–1419, 2020.
- [47] F. Tan, C. Chu, J. Qi et al., "AAV-ie enables safe and efficient gene transfer to inner ear cells," *Nature Communications*, vol. 10, no. 1, p. 3733, 2019.
- [48] C. Cheng, Y. Wang, L. Guo et al., "Age-related transcriptome changes in Sox2+ supporting cells in the mouse cochlea," *Stem Cell Research & Therapy*, vol. 10, no. 1, p. 365, 2019.
- [49] S. Zhang, D. Liu, Y. Dong et al., "Frizzled-9+ Supporting Cells Are Progenitors for the Generation of Hair Cells in the Postnatal Mouse Cochlea," *Frontiers in Molecular Neuroscience*, vol. 12, p. 184, 2019.
- [50] X. Lu, S. Sun, J. Qi et al., "Bmi1 Regulates the Proliferation of Cochlear Supporting Cells Via the Canonical Wnt Signaling Pathway," *Molecular Neurobiology*, vol. 54, no. 2, pp. 1326–1339, 2017.
- [51] T. Wang, R. Chai, G. S. Kim et al., "Lgr5+ cells regenerate hair cells via proliferation and direct transdifferentiation in damaged neonatal mouse utricle," *Nature Communications*, vol. 6, no. 1, 2015.
- [52] K. Oshima, K. Shin, M. Diensthuber, A. W. Peng, A. J. Ricci, and S. Heller, "Mechanosensitive hair cell-like cells from embryonic and induced pluripotent stem cells," *Cell*, vol. 141, no. 4, pp. 704–716, 2010.
- [53] M. Perny, C. C. Ting, S. Kleinlogel, P. Senn, and M. Roccio, "Generation of Otic Sensory Neurons from Mouse Embryonic Stem Cells in 3D Culture," *Frontiers in Cellular Neuroscience*, vol. 11, p. 409, 2017.
- [54] L. G. Dufner-Almeida, D. B. Cruz, R. C. Mingroni Netto, A. C. Batissoco, J. Oiticica, and R. Salazar-Silva, "Terapia com células-tronco para perda auditiva: já chegamos lá?," *Brazilian Journal of Otorhinolaryngology*, vol. 85, no. 4, pp. 520–529, 2019.
- [55] M. Y. Lee and Y. H. Park, "Potential of Gene and Cell Therapy for Inner Ear Hair Cells," *BioMed Research International*, vol. 2018, Article ID 8137614, 11 pages, 2018.
- [56] M. A. Parker, "Biotechnology in the treatment of sensorineural hearing loss: foundations and future of hair cell regeneration," *Journal of Speech, Language, and Hearing Research*, vol. 54, no. 6, pp. 1709–1731, 2011.
- [57] Y. Zhang, Y. Chen, W. Ni et al., "Dynamic expression of Lgr6 in the developing and mature mouse cochlea," *Frontiers in Cellular Neuroscience*, vol. 9, 2015.
- [58] A. E. Kiernan, A. L. Pelling, K. K. H. Leung et al., "Sox2 is required for sensory organ development in the mammalian inner ear," *Nature*, vol. 434, no. 7036, pp. 1031–1035, 2005.
- [59] F. Barrionuevo, A. Naumann, S. Bagheri-Fam et al., "Sox9 is required for invagination of the otic placode in mice," *Developmental Biology*, vol. 317, no. 1, pp. 213–224, 2008.
- [60] M. Roccio, M. Perny, M. Ealy, H. R. Widmer, S. Heller, and P. Senn, "Molecular characterization and prospective isolation of human fetal cochlear hair cell progenitors," *Nature Communications*, vol. 9, no. 1, p. 4027, 2018.
- [61] M. Massucci-Bissoli, K. Lezirovitz, J. Oiticica, and R. F. Bento, "Evidence of progenitor cells in the adult human cochlea: sphere formation and identification of ABCG2," *Clinics*, vol. 72, no. 11, pp. 714–717, 2017.
- [62] M. Waqas, L. Guo, S. Zhang et al., "Characterization of Lgr5+ progenitor cell transcriptomes in the apical and basal turns of the mouse cochlea," *Oncotarget*, vol. 7, no. 27, pp. 41123–41141, 2016.
- [63] C. Cheng, L. Guo, L. Lu et al., "Characterization of the Transcriptomes of Lgr5+ Hair Cell Progenitors and Lgr5-Supporting Cells in the Mouse Cochlea," *Frontiers in Molecular Neuroscience*, vol. 10, 2017.
- [64] Y. Zhang, L. Guo, X. Lu et al., "Characterization of Lgr6+ Cells as an Enriched Population of Hair Cell Progenitors Compared to Lgr5+ Cells for Hair Cell Generation in the Neonatal Mouse Cochlea," *Frontiers in Molecular Neuroscience*, vol. 11, 2018.
- [65] S. Zhang, Y. Zhang, P. Yu et al., "Characterization of Lgr5+ Progenitor Cell Transcriptomes after Neomycin Injury in the Neonatal Mouse Cochlea," *Frontiers in Molecular Neuroscience*, vol. 10, 2017.
- [66] X. Li, A. Aleardi, J. Wang, Y. Zhou, R. Andrade, and Z. Hu, "Differentiation of Spiral Ganglion-Derived Neural Stem Cells into Functional Synaptogenetic Neurons," *Stem Cells and Development*, vol. 25, no. 10, pp. 803–813, 2016.
- [67] S. Di Santo, A. Mina, A. Ducray, H. R. Widmer, and P. Senn, "Creatine supports propagation and promotes neuronal differentiation of inner ear progenitor cells," *Neuroreport*, vol. 25, no. 7, pp. 1–451, 2014.
- [68] X. L. Kuai, X. Q. Cong, X. L. Li, and S. D. Xiao, "Generation of hepatocytes from cultured mouse embryonic stem cells," *Liver Transplantation*, vol. 9, no. 10, pp. 1094–1099, 2003.
- [69] H. Basma, A. Soto-Gutiérrez, G. R. Yannam et al., "Differentiation and transplantation of human embryonic stem cell-

- derived hepatocytes,” *Gastroenterology*, vol. 136, no. 3, pp. 990–999.e4, 2009.
- [70] S. Kriks, J. W. Shim, J. Piao et al., “Dopamine neurons derived from human ES cells efficiently engraft in animal models of Parkinson’s disease,” *Nature*, vol. 480, no. 7378, pp. 547–551, 2011.
- [71] L. Yang, M. H. Soonpaa, E. D. Adler et al., “Human cardiovascular progenitor cells develop from a KDR⁺ embryonic-stem-cell-derived population,” *Nature*, vol. 453, no. 7194, pp. 524–528, 2008.
- [72] N. Lavon, O. Yanuka, and N. Benvenisty, “The effect of over-expression of Pdx1 and Foxa2 on the differentiation of human embryonic stem cells into pancreatic cells,” *Stem Cells*, vol. 24, no. 8, pp. 1923–1930, 2006.
- [73] E. Kroon, L. A. Martinson, K. Kadoya et al., “Pancreatic endoderm derived from human embryonic stem cells generates glucose-responsive insulin-secreting cells in vivo,” *Nature Biotechnology*, vol. 26, no. 4, pp. 443–452, 2008.
- [74] K. Takahashi and S. Yamanaka, “Induction of pluripotent stem cells from mouse embryonic and adult fibroblast cultures by defined factors,” *Cell*, vol. 126, no. 4, pp. 663–676, 2006.
- [75] K. R. Johnson, L. H. Gagnon, C. Tian et al., “Deletion of a Long-Range Dlx5 Enhancer Disrupts Inner Ear Development in Mice,” *Genetics*, vol. 208, no. 3, pp. 1165–1179, 2018.
- [76] M. Anniko and R. Wróblewski, “Ionic environment of cochlear hair cells,” *Hearing Research*, vol. 22, no. 1-3, pp. 279–293, 1986.
- [77] Y. H. Park, K. F. Wilson, Y. Ueda et al., “Conditioning the Cochlea to Facilitate Survival and Integration of Exogenous Cells into the Auditory Epithelium,” *Molecular Therapy*, vol. 22, no. 4, pp. 873–880, 2014.
- [78] M. Y. Lee, S. Hackelberg, K. L. Green et al., “Survival of human embryonic stem cells implanted in the guinea pig auditory epithelium,” *Scientific Reports*, vol. 7, no. 1, article 46058, 2017.
- [79] W. Chen, N. Jongkamonwiwat, L. Abbas et al., “Restoration of auditory evoked responses by human ES-cell-derived otic progenitors,” *Nature*, vol. 490, no. 7419, pp. 278–282, 2012.
- [80] M. Ronaghi, M. Nasr, M. Ealy et al., “Inner ear hair cell-like cells from human embryonic stem cells,” *Stem Cells and Development*, vol. 23, no. 11, pp. 1275–1284, 2014.
- [81] K. R. Koehler, J. Nie, E. Longworth-Mills et al., “Generation of inner ear organoids containing functional hair cells from human pluripotent stem cells,” *Nature Biotechnology*, vol. 35, no. 6, pp. 583–589, 2017.
- [82] M. Jeong, M. O’Reilly, N. K. Kirkwood et al., “Generating inner ear organoids containing putative cochlear hair cells from human pluripotent stem cells,” *Cell Death & Disease*, vol. 9, no. 9, p. 922, 2018.
- [83] A. J. Matsuoka, Z. D. Morrissey, C. Zhang et al., “Directed Differentiation of Human Embryonic Stem Cells Toward Placode-Derived Spiral Ganglion-Like Sensory Neurons,” *Stem Cells Translational Medicine*, vol. 6, no. 3, pp. 923–936, 2017.
- [84] T. Hyakumura, S. McDougall, S. Finch, K. Needham, M. Dottori, and B. A. Nayagam, “Organotypic Cocultures of Human Pluripotent Stem Cell Derived-Neurons with Mammalian Inner Ear Hair Cells and Cochlear Nucleus Slices,” *Stem Cells International*, vol. 2019, Article ID 8419493, 14 pages, 2019.
- [85] H. T. Chang, R. A. Heuer, A. M. Oleksijew et al., “An engineered three-dimensional stem cell niche in the inner ear by applying a nanofibrillar cellulose hydrogel with a sustained-release neurotrophic factor delivery system,” *Acta Biomaterialia*, vol. 108, pp. 111–127, 2020.
- [86] H. Ohnishi, D. Skerleva, S. I. Kitajiri et al., “Limited hair cell induction from human induced pluripotent stem cells using a simple stepwise method,” *Neuroscience Letters*, vol. 599, pp. 49–54, 2015.
- [87] H. Lahlou, A. Lopez-Juarez, A. Fontbonne, E. Nivet, and A. Zine, “Modeling human early otic sensory cell development with induced pluripotent stem cells,” *PLoS One*, vol. 13, no. 6, article e0198954, 2018.
- [88] H. Lahlou, E. Nivet, A. Lopez-Juarez, A. Fontbonne, S. Assou, and A. Zine, “Enriched Differentiation of Human Otic Sensory Progenitor Cells Derived From Induced Pluripotent Stem Cells,” *Frontiers in Molecular Neuroscience*, vol. 11, p. 452, 2018.
- [89] J. R. Chen, Z. H. Tang, J. Zheng et al., “Effects of genetic correction on the differentiation of hair cell-like cells from iPSCs with MYO15A mutation,” *Cell Death and Differentiation*, vol. 23, no. 8, pp. 1347–1357, 2016.
- [90] Z. H. Tang, J. R. Chen, J. Zheng et al., “Genetic Correction of Induced Pluripotent Stem Cells From a Deaf Patient With-MYO7A Mutation Results in Morphologic and Functional Recovery of the Derived Hair Cell-Like Cells,” *Stem Cells Translational Medicine*, vol. 5, no. 5, pp. 561–571, 2016.
- [91] Y.-C. Chen, C.-L. Tsai, Y.-H. Wei et al., “ATOH1/RFX1/RFX3 transcription factors facilitate the differentiation and characterisation of inner ear hair cell-like cells from patient-specific induced pluripotent stem cells harbouring A8344G mutation of mitochondrial DNA,” *Cell Death & Disease*, vol. 9, no. 4, p. 437, 2018.
- [92] J. Chen, F. Hong, C. Zhang et al., “Differentiation and transplantation of human induced pluripotent stem cell-derived otic epithelial progenitors in mouse cochlea,” *Stem Cell Research & Therapy*, vol. 9, no. 1, p. 230, 2018.
- [93] S. L. Boddy, R. Romero-Guevara, A. R. Ji et al., “Generation of Otic Lineages from Integration-Free Human-Induced Pluripotent Stem Cells Reprogrammed by mRNAs,” *Stem Cells International*, vol. 2020, Article ID 3692937, 10 pages, 2020.
- [94] N. Gunewardene, D. Crombie, M. Dottori, and B. A. Nayagam, “Innervation of cochlear hair cells by human induced pluripotent stem cell-derived neurons in vitro,” *Stem Cells International*, vol. 2016, Article ID 1781202, 10 pages, 2016.
- [95] M. Ishikawa, H. Ohnishi, D. Skerleva et al., “Transplantation of neurons derived from human iPSC cells cultured on collagen matrix into guinea-pig cochleae,” *Journal of Tissue Engineering and Regenerative Medicine*, vol. 11, no. 6, pp. 1766–1778, 2017.
- [96] H. Li, G. Roblin, H. Liu, and S. Heller, “Generation of hair cells by stepwise differentiation of embryonic stem cells,” *Proceedings of the National Academy of Sciences of the United States of America*, vol. 100, no. 23, pp. 13495–13500, 2011.
- [97] C. Zhong, Z. Chen, X. Luo et al., “Barhl1 is required for the differentiation of inner ear hair cell-like cells from mouse embryonic stem cells,” *The International Journal of Biochemistry & Cell Biology*, vol. 96, pp. 79–89, 2018.
- [98] Y. O uji, M. Sakagami, H. Omori et al., “Efficient induction of inner ear hair cell-like cells from mouse ES cells using combination of Math1 transfection and conditioned medium from

- ST2 stromal cells,” *Stem Cell Research*, vol. 23, pp. 50–56, 2017.
- [99] K. R. Koehler, A. M. Mikosz, A. I. Molosh, D. Patel, and E. Hashino, “Generation of inner ear sensory epithelia from pluripotent stem cells in 3D culture,” *Nature*, vol. 500, no. 7461, pp. 217–221, 2013.
- [100] E. Longworth-Mills, K. R. Koehler, and E. Hashino, “Generating Inner Ear Organoids from Mouse Embryonic Stem Cells,” *Methods in Molecular Biology*, vol. 1341, pp. 391–406, 2015.
- [101] J. Nie, K. R. Koehler, and E. Hashino, “Directed Differentiation of Mouse Embryonic Stem Cells Into Inner Ear Sensory Epithelia in 3D Culture,” *Methods in Molecular Biology*, vol. 1597, pp. 67–83, 2017.
- [102] R. E. DeJonge, X. P. Liu, C. R. Deig, S. Heller, K. R. Koehler, and E. Hashino, “Modulation of Wnt Signaling Enhances Inner Ear Organoid Development in 3D Culture,” *PLoS One*, vol. 11, no. 9, article e0162508, 2016.
- [103] S. A. Schaefer, A. Y. Higashi, B. Loomis et al., “From Otic Induction to Hair Cell Production: Pax2EGFP Cell Line Illuminates Key Stages of Development in Mouse Inner Ear Organoid Model,” *Stem Cells and Development*, vol. 27, no. 4, pp. 237–251, 2018.
- [104] K. R. Koehler and E. Hashino, “3D mouse embryonic stem cell culture for generating inner ear organoids,” *Nature Protocols*, vol. 9, no. 6, pp. 1229–1244, 2014.
- [105] A. Costa, L. Sanchez-Guardado, S. Juniat, J. E. Gale, N. Daudet, and D. Henrique, “Generation of sensory hair cells by genetic programming with a combination of transcription factors,” *Development*, vol. 142, no. 11, pp. 1948–1959, 2015.
- [106] N. Abboud, A. Fontbonne, I. Watabe et al., “Culture conditions have an impact on the maturation of traceable, transplantable mouse embryonic stem cell-derived otic progenitor cells,” *Journal of Tissue Engineering and Regenerative Medicine*, vol. 11, no. 9, pp. 2629–2642, 2017.
- [107] L.-D. Zhao, L. Li, N. Wu et al., “Migration and differentiation of mouse embryonic stem cells transplanted into mature cochlea of rats with aminoglycoside-induced hearing loss,” *Acta Oto-Laryngologica*, vol. 133, no. 2, pp. 136–143, 2012.
- [108] Z. Liu, Y. Jiang, X. Li, and Z. Hu, “Embryonic Stem Cell-Derived Peripheral Auditory Neurons Form Neural Connections with Mouse Central Auditory Neurons In Vitro via the $\alpha 2\delta 1$ Receptor,” *Stem Cell Reports*, vol. 11, no. 1, pp. 157–170, 2018.
- [109] M. K. Gökcan, S. Mülazimoğlu, E. Ocak et al., “Study of mouse induced pluripotent stem cell transplantation into Wistar albino rat cochleae after hair cell damage,” *Turkish Journal of Medical Sciences*, vol. 46, no. 5, pp. 1603–1610, 2016.
- [110] J. Chen, L. Guan, H. Zhu, S. Xiong, L. Zeng, and H. Jiang, “Transplantation of mouse-induced pluripotent stem cells into the cochlea for the treatment of sensorineural hearing loss,” *Acta Oto-Laryngologica*, vol. 137, no. 11, pp. 1136–1142, 2017.
- [111] H. Zhu, J. Chen, L. Guan, S. Xiong, and H. Jiang, “The transplantation of induced pluripotent stem cells into the cochleae of mature mice,” *International Journal of Clinical and Experimental Pathology*, vol. 11, no. 9, pp. 4423–4430, 2018.
- [112] A. Czajkowski, A. Mounier, L. Delacroix, and B. Malgrange, “Pluripotent stem cell-derived cochlear cells: a challenge in constant progress,” *Cellular and Molecular Life Sciences*, vol. 76, no. 4, pp. 627–635, 2019.
- [113] H. Takeda, A. Dondzillo, J. A. Randall, and S. P. Gubbels, “Challenges in Cell-Based Therapies for the Treatment of Hearing Loss,” *Trends in Neurosciences*, vol. 41, no. 11, pp. 823–837, 2018.
- [114] M. S. Hildebrand, H. H. M. Dahl, J. Hardman, B. Coleman, R. K. Shepherd, and M. G. de Silva, “Survival of partially differentiated mouse embryonic stem cells in the scala media of the guinea pig cochlea,” *Journal of the Association for Research in Otolaryngology*, vol. 6, no. 4, pp. 341–354, 2005.
- [115] M. A. Parker, D. A. Corliss, B. Gray et al., “Neural stem cells injected into the sound-damaged cochlea migrate throughout the cochlea and express markers of hair cells, supporting cells, and spiral ganglion cells,” *Hearing Research*, vol. 232, no. 1-2, pp. 29–43, 2007.

Research Article

Differences in Clinical Characteristics and Brain Activity between Patients with Low- and High-Frequency Tinnitus

Jiajia Zhang,^{1,2,3} Zhen Zhang,^{1,2,3} Shujian Huang,^{1,2,3} Huiqun Zhou,^{1,2,3} Yanmei Feng,^{1,2,3}
Haibo Shi,^{1,2,3} Dan Wang^{ID},⁴ Wenya Nan^{ID},⁵ Hui Wang^{ID},^{1,2,3} and Shankai Yin^{1,2,3}

¹Department of Otolaryngology-Head and Neck Surgery, Shanghai Jiao Tong University Affiliated Sixth People's Hospital, 600 Yishan Road, Shanghai 200233, China

²Otolaryngology Institute of Shanghai Jiao Tong University, Shanghai 200233, China

³Shanghai Key Laboratory of Sleep Disordered Breathing, Shanghai 200233, China

⁴Department of Radiology, Shanghai Jiao Tong University Affiliated Sixth People's Hospital, Shanghai 200233, China

⁵Department of Psychology, Shanghai Normal University, Shanghai 200233, China

Correspondence should be addressed to Dan Wang; joshuastonecn@hotmail.com, Wenya Nan; wynan1985@126.com, and Hui Wang; wangh2014@163.com

Received 26 February 2020; Accepted 23 June 2020; Published 26 July 2020

Academic Editor: Geng lin Li

Copyright © 2020 Jiajia Zhang et al. This is an open access article distributed under the Creative Commons Attribution License, which permits unrestricted use, distribution, and reproduction in any medium, provided the original work is properly cited.

This study was aimed at delineating and comparing differences in clinical characteristics and brain activity between patients with low- and high-frequency tinnitus (LFT and HFT, respectively) using high-density electroencephalography (EEG). This study enrolled 3217 patients with subjective tinnitus who were divided into LFT (frequency < 4000 Hz) and HFT (≥ 4000 Hz) groups. Data regarding medical history, Tinnitus Handicap Inventory, tinnitus matching, and hearing threshold were collected from all patients. Twenty tinnitus patients and 20 volunteers were subjected to 256-channel EEG, and neurophysiological differences were evaluated using standardized low-resolution brain electromagnetic tomography (sLORETA) source-localized EEG recordings. Significant differences in sex ($p < 0.001$), age ($p = 0.022$), laterality ($p < 0.001$), intensity ($p < 0.001$), tinnitus type ($p < 0.001$), persistent tinnitus ($p = 0.04$), average threshold ($p < 0.001$), and hearing loss ($p = 0.028$) were observed between LFT and HFT groups. The tinnitus pitch only appeared to be correlated with the threshold of the worst hearing loss in the HFT group. Compared with the controls, the LFT group exhibited increased gamma power ($p < 0.05$), predominantly in the posterior cingulate cortex (PCC, BA31), whereas the HFT group had significantly decreased alpha1 power ($p < 0.05$) in the angular gyrus (BA39) and auditory association cortex (BA22). Higher gamma linear connectivity between right BA39 and right BA41 was observed in the HFT group relative to controls ($t = 3.637$, $p = 0.027$). Significant changes associated with increased gamma in the LFT group and decreased alpha1 in the HFT group indicate that tinnitus pitch is crucial for matching between the tinnitus and control groups. Differences of band frequency energy in brain activity levels may contribute to the clinical characteristics and internal tinnitus “spectrum” differences.

1. Introduction

Tinnitus is characterized by the perception of an auditory phantom, such that patients perceive auditory sensations in the absence of any external sound source [1]. This condition is increasingly prevalent in both young (16.0–20.5%) and elderly populations (30%) [2, 3]. Tinnitus is commonly described as a ringing, buzzing, cricket-like, hissing, whistling, or humming sound or as a combination of these sounds [4].

The perceived sound may be soft or loud, a low- or high-pitched tone or noise, and intermittent or constant. Although most patients manage their tinnitus well, severe cases are always accompanied by other symptoms such as annoyance, anxiety, depression, insomnia, and cognitive dysfunction [5–7].

Currently, the severity of this condition is evaluated by a series of psychoacoustic tests and evaluation scales, including pitch matching (PM), loudness matching (LM), minimal masking levels (MMLS), gap detection (GAP), residual

suppression (RI), and the Tinnitus Handicap Inventory (THI) [8–11]. However, patients with tinnitus show significant heterogeneity, which mainly presents as different characteristics of sound and varying degrees of accompanying symptoms. Approximately 80% of the individuals with tinnitus have accompanying hearing loss [12]. The correspondence between the frequency of tinnitus and the frequency range of hearing loss seems to indicate the correlation between the deprivation of auditory input and tinnitus generation [13]. Nevertheless, this correspondence was mainly validated in the patients with high-frequency tinnitus, and the definite rates of correspondence at different frequency tinnitus subgroups were not clearly investigated in a large sample [12].

Indeed, tinnitus is always accompanied by a cortical reorganization due to the hearing loss [14]. Previous studies suggested a strong positive association between the subjective strength of tinnitus and the magnitude of the shift in the tinnitus frequency in the auditory cortex [15]. Other studies indicated that tinnitus results from changes in the firing patterns of neurons in the central auditory system and from changes in burst firing and neural synchrony [16]. These results suggest a potential correlation between spontaneous neural activity and tinnitus, as well as a causal link between the characteristic frequency that dominates the reorganized neural map and the tinnitus pitch [17].

High-density electroencephalography (HD-EEG), which yields data with a high temporal resolution and reasonable spatial resolution, has been identified recently as a powerful tool for studies of dynamic brain activity [16, 18, 19]. EEG enables the noninvasive reconstruction of a region of interest (ROI) via the application of source analysis methods to scalp-recorded neuronal activities [20–22]. A previous EEG-based study identified differences in the delta, beta, and gamma-frequency brain activity bands between patients with narrowband noise tinnitus and pure-tone tinnitus [23]. This type of tinnitus pitch assessment is significant not only in terms of the systematic documentation of patients' symptoms but also for monitoring the impacts of interventions and treatment planning strategies involving acoustic stimulation, such as tinnitus maskers or transcranial magnetic stimulation [16, 24, 25].

Therefore, we aimed herein to determine the internal tinnitus "spectrum" by identifying the various pitch components that contribute to the overall tinnitus sensation. Moreover, we used source-localized resting-state EEG recordings to explore potential relationships between the detailed aspects of this spectrum (high frequency versus low frequency) and neurophysiological differences between tinnitus patients and control subjects.

2. Methods

2.1. Participants. The clinical data were collected from outpatients with subjective tinnitus who visited our tinnitus clinic at the Otolaryngology-Head and Neck Surgery Department of the Sixth People's Hospital affiliated with Shanghai Jiao Tong University between May 2016 and December 2018. Patients with subjective tinnitus who were symptomatic at

the time of evaluation were included in this study. To increase the sample homogeneity, the following individuals were excluded from the study: patients with significant mental health problems, tinnitus with pulsatile tinnitus due to aberrant vascular malformation, Meniere's disease, otosclerosis, chronic headache, neurological disorders (e.g., brain tumors), and traumatic brain injury or stroke and those receiving treatment for mental disorders. Patients whose pitch of tinnitus could not be matched were also excluded. Patients with tinnitus frequency lower than 4 kHz were included in the low-frequency tinnitus (LFT) group; patients with tinnitus frequency higher than or equal to 4 kHz were included in the high-frequency tinnitus (HFT) group.

Subsequently, HD-EEG was performed on 40 participants, including 20 healthy volunteers (mean age: 38.28 ± 15.9 years; 40% men, 60% women) and 20 patients with tinnitus (mean age: 36.3 ± 11.64 years; 40% men, 60% women) who were also divided into LFT and HFT groups. Based on previous studies, EEG results of patients with tinnitus can be affected by many factors such as sex [26], the laterality of tinnitus [20], the duration of tinnitus [27], tinnitus type [23], or pure-tone threshold [13]. Consequently, those factors were matched in our study, and there were no statistically significant differences between the LFT and HFT groups regarding these parameters (Table 1). Twenty healthy volunteers were included as the control group and were matched for age, sex, and hearing threshold.

This study was approved by the Institutional Ethics Review Board of Shanghai, the Sixth People's Hospital affiliated with Shanghai Jiao Tong University, and was registered with the Chinese Clinical Trial Registry (Registration number: ChiCTR-INR-16008092). Potential consequences and benefits of the study were explained, and written informed consent was obtained from all participants before inclusion in the study.

2.2. Auditory Testing and Tinnitus Matching. All baseline evaluations and tests were performed by qualified medical assistants in a soundproof room. Audiograms were measured in 1-octave steps at frequencies ranging from 0.25 to 8 kHz using a manual audiometer (GSI-61, Grason-Stadler Inc., Eden Prairie, MN, USA) coupled with TDH-39 headphones. Tympanograms were obtained over a pressure range of 200 to -400 daPa at 226 Hz using a GSI tympanometer (TympanStar, Grason-Stadler Inc.). The passing criteria were a type A peak in the range of -100 to $+50$ daPa and a static admittance of 0.3–1.6 mho.

The loudness and pitch of tinnitus were matched using a Tinnilogic™ BT02 audiometer (Betterlife Medical Co., Ltd., Jiangsu, China) in a soundproof room. Matching was performed in a closed field. The participants were asked to concentrate on the dominant pitch of the tinnitus, and the external sound was adjusted by the tester to match the tinnitus in terms of loudness, frequency, and affected side.

2.3. Measurement of Tinnitus Severity. The 25-item beta version of the THI was used as a subjective measure of the handicap experienced due to tinnitus [28]. The participants were instructed to respond with yes (4 points), sometimes

TABLE 1: Electroencephalogram characteristics of patients with low- and high-frequency tinnitus.

Tinnitus patients	Age (yrs)	Sex	Tinnitus laterality	THI	Tinnitus pitch	Loudness	Duration (months)	PTA (≤ 2 kHz)	PTA (> 2 kHz)	
	1	36	M	L	4	350	40	7	5	6.25
	2	52	F	R	40	200	30	120	13.75	13.75
	3	29	M	R	78	150	40	3	6.25	5
	4	48	F	L	30	150	42	3	10	10
LFT	5	41	F	R	0	500	60	96	13.75	13.75
	6	38	M	L	10	125	25	12	7.5	8.75
	7	31	F	L	12	200	45	36	11.25	11.25
	8	30	F	R	26	120	48	36	6.25	7.5
	9	24	M	L	38	120	45	3	16.25	17.5
	10	33	F	R	36	100	36	3	8.75	8.75
Mean \pm SD	36.2 \pm 8.8	4 M/6F	5 L/5R	27.4 \pm 22.9	—	41.1 \pm 9.7	31.9 \pm 42.5	9.8 \pm 3.7	10.25 \pm 3.85	
	11	60	F	R	20	8000	35	6	21.25	22.5
	12	27	M	R	22	8000	5	12	6.25	7.5
	13	31	M	L	8	8000	28	6	3.75	3.75
	14	24	F	R	20	4000	55	6	0	-1.25
HFT	15	22	F	L	6	8000	48	96	3.75	3.75
	16	55	F	R	55	8000	41	36	5	7.5
	17	26	M	L	22	8000	25	6	-2.5	-2.5
	18	53	F	L	18	4000	30	12	15	16.25
	19	40	F	R	38	8200	31	6	6.25	8.75
	20	26	M	L	34	6000	33	12	16.25	17.5
Mean \pm SD	36.4 \pm 14.5	4 M/6F	5 L/5R	24.3 \pm 14.6	—	33.1 \pm 13.6	19.8 \pm 28.3	7.5 \pm 7.5	8.4 \pm 8.1	
<i>p</i> value	0.932	0.714	0.653	0.902	—	0.134	0.306	0.387	0.492	

L: left; R: right; F: female; M: male; PTA: pure-tone threshold audiometry; HFT: high-frequency tinnitus; LFT: low-frequency tinnitus; SD: standard deviation.

(2 points), or no (0 point) for each item on the inventory. These responses were added, with the total score ranging from 0 to 100 points. Depending on the total score, the handicap caused by tinnitus could be classified as slight, mild, moderate, severe, or catastrophic.

2.4. EEG Recording and Data Preprocessing. Spontaneous EEG signals were collected in a soundproof room. All participants were asked to sit upright on a chair in a comfortable position after abstaining from alcohol and caffeinated beverage consumption for 24 h prior to the recording. The EEG was recorded of each participant for 5 min with the eyes closed. EEG data were recorded with 256 channels on EGI's HydroCel Geodesic Sensor Net, and Cz was used as the reference channel. The electrode-skin impedance was controlled at < 50 k Ω for each channel. The participants were asked to remain awake and keep their eyes closed. The following settings were used: sampling rate of 1000 Hz, amplification of 20 times, and band-pass filtering between 0.15 and 200 Hz.

The offline EEG analysis was conducted using custom scripts and the EEGLAB toolbox [29] on the MATLAB platform (MathWorks, Natick, MA, USA). First, the EEG signals on the scalp were band-pass filtered between 0.5 and 70 Hz

while using a 50 Hz notch filter. The signals were then resampled at 500 Hz and segmented into 3 s epochs for EEG recording. Subsequently, the electrooculogram and electromyogram artifacts were corrected automatically using the blind source separation-based electrooculogram correction procedure [30] and canonical correlation analysis correction method, respectively, [31] available in the automatic artifact removal plug-in [30].

2.5. Scalp EEG Power Calculation. For each participant, the power spectrum density, expressed as $10 * \log_{10} (\mu V^2/Hz)$, was computed by the spectopo function provided by EEGLAB, using Welch's method with the Hamming window, and then transformed to power spectrum density units in $\mu V^2/Hz$. Based on previous research on tinnitus [32–34], this study focused on the frequency bands including delta (2–3.5 Hz), theta (4–7.5 Hz), alpha1 (8–10 Hz), alpha2 (10–12 Hz), beta1 (13–18 Hz), beta2 (18.5–21 Hz), beta3 (21.5–30 Hz), and gamma (30.5–44 Hz). Since anatomical and neurophysiological properties of the brain, cranial bone structure, and electrode impedances [35] can influence the absolute EEG power, the relative power of each frequency band was computed by the mean power of each band divided

by the mean power of 2-45 Hz. Finally, the relative power in each frequency band was averaged across all electrodes for further statistical analysis.

2.6. Source Localization. Standardized low-resolution brain electromagnetic tomography (sLORETA) is a genuine inverse solution that enables exact localization with zero error in the presence of a measurement and structured biological noise [36]. We used the method recommended by the developers of KEY-LORETA software (publicly available free at <http://www.uzh.ch/keyinst/loreta.htm>) to estimate the locations of the sources of the electrical potentials recorded on scalp EEG. Here, the artifact-free EEG epochs were exported in the ASCII format from MATLAB to LORETA software. The sLORETA analysis included the following steps: (1) computation of the sLORETA transformation matrix, (2) calculation of EEG crossspectra in the eight abovementioned frequency bands, and (3) computation of the three-dimensional (3D) cortical distribution of the electric neuronal generators for each frequency band.

2.7. Functional Connectivity. In general, functional connectivity can be expressed by the coherence and phase synchronization between time series corresponding to different spatial locations. However, any measure of dependence is highly contaminated with an instantaneous, nonphysiological contribution because of the volume conduction and low spatial resolution [37]. To solve this problem, Pascual-Marqui proposed a new technique that considerably abrogated this confounding factor [38]. Furthermore, this measure of dependence can be applied jointly to any number of brain areas (i.e., distributed cortical networks) for which the activity can be estimated using sLORETA. Consequently, nonnegative measures of linear dependence (i.e., coherence) between the multivariate time series are defined. These measures yield a zero value only in the presence of independence of the pertinent type.

Based on this principle, the lagged linear connectivity was calculated. Five bilateral ROIs were defined based on the present findings and source analysis and previous brain research related to tinnitus: (1) the secondary auditory cortex (BA21, BA22), (2) posterior cingulate cortex (BA23, BA31), (3) angular gyrus (BA39), (4) intraparietal sulcus (BA40), and (5) primary auditory cortex (BA41, BA42) [22, 32].

2.8. Statistics. The chi-squared test and *t*-test were used to determine intergroup differences (Tables 1 and 2) depending on the data type. These calculations were performed using SPSS version 24 (SPSS/PC, Chicago, IL, USA). The power spectra of groups were compared using two-way repeated-measurement ANOVAs, followed by post hoc tests (Holm-Sidak) for each frequency point (Figure 1) in SPSS. sLORETA was used to perform between-condition voxel-by-voxel comparisons of the current density distributions, which were then used to identify potential differences in brain electrical activity among the three groups. Nonparametric statistical analyses of functional sLORETA images (i.e., statistical nonparametric mapping (SnPM))

were performed for each contrast; here, a *t*-statistic corrected for multiple comparisons was used for unpaired groups ($p < 0.05$). As explained by Nichols and Holmes, the SnPM methodology does not require any assumption of Gaussianity and corrects for all multiple comparisons [39]. We performed a voxel-by-voxel test (comprising 6239 voxels each) for each different frequency band. For all analyses, a *p* value < 0.05 was considered to indicate statistical significance.

3. Results

3.1. Patient and Demographic Characteristics. The tinnitus pitches reported by patients ranged from 0.25 to 12 kHz, and 55.4% and 44.6% of subjects were classified into the LFT and HFT groups, respectively. The characteristics of the LFT and HFT groups are displayed in Table 2. Notably, these groups differed significantly with respect to sex ($p < 0.001$), with a significantly higher proportion of women in the LFT group. A significantly higher tinnitus intensity was also observed in the LFT group ($p < 0.001$). Significant intergroup differences were also observed with respect to age ($p = 0.046$), laterality ($p < 0.001$), tinnitus type ($p < 0.001$), tinnitus persistence ($p = 0.04$), average threshold ($p < 0.001$), and hearing loss ($p = 0.028$). However, THI scores did not differ significantly for the two groups ($p = 0.062$). Patients with hearing loss had a higher THI score than those with normal hearing, and this was especially notable among LFT patients who reported tinnitus frequencies of 125 Hz ($p < 0.001$) and 250 Hz ($p = 0.03$). However, we did not observe a significant difference in the THI scores between patients with and without hearing loss in the HFT group (Figure 2(a)). The tinnitus pitch was most commonly matched to high frequencies, at which the hearing threshold indicated the depth of hearing loss among the 3217 patients. However, no correlation was observed between tinnitus pitch and worst threshold in the LFT group (Figure 2(b)).

3.2. EEG Results. Figure 1 shows the EEG results of the tinnitus and control groups. The power spectrum densities recorded across all scalp electrodes in each group were averaged to show the distribution of brain activities along the frequency ranging from delta (2–3.5 Hz) to gamma (30.5–44 Hz) (Figure 1(a)). Significant power differences were observed at alpha1 ($t = 3.15$, $p < 0.01$), beta1 ($t = 2.55$, $p < 0.05$), beta3 ($t = 2.62$, $p < 0.01$), and gamma ($t = 3.92$, $p < 0.001$) bands when we compared the total tinnitus group (including the LFT and HFT groups) with the control group (Figure 1(b)). However, when we compared the subgroup with the control group, only the alpha1 and gamma band showed significant changes in the LFT and HFT groups, respectively. (Figure 1(c)). More specifically, pairwise comparisons showed that (1) the LFT group demonstrated a significantly higher level of gamma power ($t = 3.63$, $p < 0.001$) (Figure 1(d)), (2) and the HFT group had a significant decrease in alpha1 frequency band ($t = 3.71$, $p < 0.001$) (Figure 1(e)), (3) but no significant difference was found between the LFT and HFT groups across the entire frequency bands ($t = 0.58$, $p = 0.563$).

TABLE 2: Characteristics of patients with low- and high-frequency tinnitus.

Characteristics	Total (N = 3217)	Frequency of tinnitus		p value
		Low frequency (N = 1783)	High frequency (N = 1434)	
		Sex (%) (n)		
Male	43.1 (1386)	35.5 (633)	52.5 (753)	<0.001
Female	56.9 (1831)	64.5 (1150)	47.5 (681)	
		Age (year)		
Mean ± SD	50.45 ± 16.9	50.99 ± 16.9	49.79 ± 16.7	0.046
		Laterality (%) (n)		
Left	32.3 (1039)	35.6 (634)	28.2 (405)	<0.001
Right	27.6 (888)	31.2 (556)	23.2 (332)	
Bilateral	38.4 (1236)	32.1 (573)	46.2 (663)	
In head	1.7 (54)	1.1 (20)	2.4 (34)	
		THI		
Mean ± SD	30.88 ± 23.6	31.57 ± 24.1	30.02 ± 22.8	0.062
		Intensity (dB)		
Mean ± SD	15.56 ± 6.4	16.31 ± 6.2	14.63 ± 6.6	<0.001
		Duration (day)		
Mean ± SD	836.74 ± 1442.5	797.29 ± 1409.4	885.78 ± 1481.7	0.084
		Tinnitus type (%) (n)		
Pure tone	90.4 (2908)	87.4 (1559)	94.1 (1349)	<0.001
Otherwise	9.6 (309)	12.6 (224)	5.9 (85)	
		Persistent tinnitus (%) (n)		
Yes	82.2 (2645)	61.5 (1096)	66.4 (952)	0.004
No	17.8 (572)	38.5 (687)	33.6 (482)	
		Average threshold		
Mean ± SD	30.75 ± 23.8	32.449 ± 25.2	28.64 ± 21.8	<0.001
		Hearing (%) (n)		
Normal	34.4 (1107)	36.1 (643)	32.4 (464)	0.028
SNHL	65.6 (2110)	63.9 (1140)	67.6 (970)	
		Accompanying symptoms (%) (n)		
Yes	42.6 (1372)	42 (748)	43.5 (624)	0.373
No	57.4 (1845)	58 (1035)	56.5 (810)	

3.3. Source Localization Results. The sLORETA analysis revealed no significant differences between the LFT and HFT groups. In the LFT group, we observed greater gamma activity in the posterior cingulate cortex (PCC, BA31) relative to the levels in the control group (Figure 3). A synchronized decreased alpha1 activity was observed predominantly in the angular gyrus (BA39) and secondary auditory cortex (BA 22) in the HFT group in comparison to that in the control group (Figure 4).

3.4. Functional Connectivity. Increased gamma linear connectivity between the right BA39 and right BA41 was observed in the HFT group relative to that in the control group ($p = 0.027$). No statistical differences between the default mode functions and networks were observed between the LFT group and the control group. Similarly, there were no statistically significant differences in these parameters between the HFT and LFT groups (Figure 5).

4. Discussion

In the mammal's inner ear, hair cells and spiral ganglion neurons are critical for hearing ability; hair cells convert the mechanical sound waves into neural signals, and spiral ganglion neuron transmits these signals to the auditory cortex for hearing [40–42]. In the mammal's inner ear, hair cells and spiral ganglion neurons are vulnerable for multiple damages, including gene mutation, noise, different ototoxic drugs, inflammation, or aging [43–47] while the mammals only have very limited hair cell and spiral ganglion neuron regeneration ability; most of the damaged hair cells and spiral ganglion neurons cannot be spontaneously regenerate [48–55]. Thus, most of the hearing loss is irreversible; and usually, tinnitus is always accompanied with hearing loss. Tinnitus is characterized by an auditory phantom perception in the absence of any physical sound source, and by far pathophysiological mechanisms is still not clear. In this study, we explored and compared the characteristics of the neural

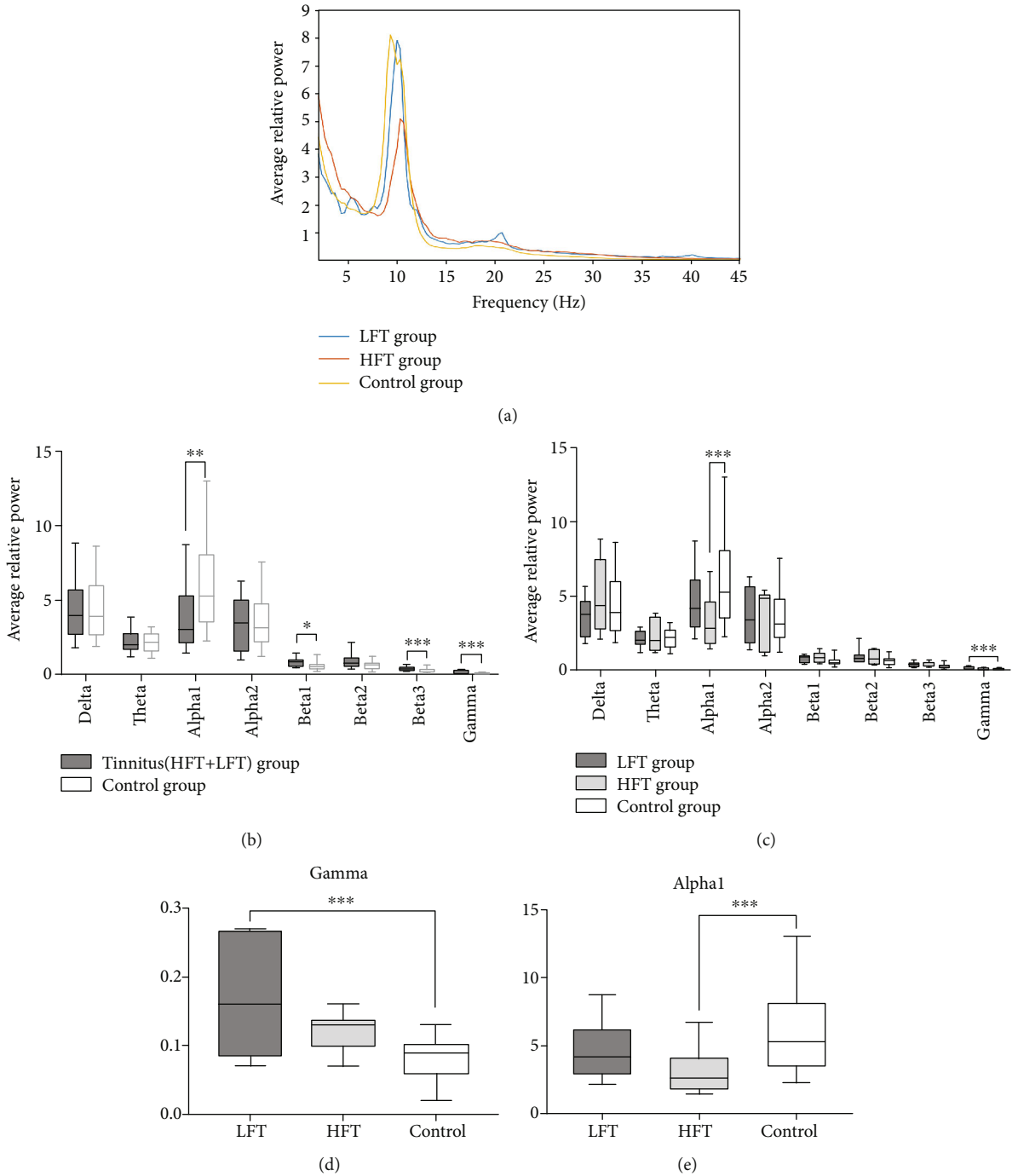


FIGURE 1: EEG results of the tinnitus and control groups: (a) the distribution of averaged brain activities along the band frequency in each group; (b) comparisons of average EEG power at eight frequency bands between the total tinnitus group and control groups; (c) intergroup comparisons of averaged brain activities; (d, e) the magnified view at gamma (30.5–44 Hz) and alpha1 (8–10 Hz) frequency bands in (c). * $p < 0.05$, ** $p < 0.01$, and *** $p < 0.001$ against the control group.

activities associated with LFT and HFT. We used an sLORETA-based source analysis of resting-state EEG data to further investigate the pathophysiology of phantom sound perception in patients with tinnitus. Notably, the comparison of patients with LFT and HFT demonstrated several significant differences with respect to sex, age, laterality, intensity, tinnitus type, persistent tinnitus, hearing loss, and comorbid diseases. Moreover, patients with hearing loss had higher

THI scores than those with normal hearing in the LFT group, whereas no such difference was observed in the HFT group. Moreover, the tinnitus pitch was correlated with high frequencies associated with the greatest hearing losses in patients with HFT, but not in those with LFT. Our EEG results revealed no significant differences in EEG power between the tinnitus groups. However, significant differences were observed between the control group and each tinnitus group. Compared

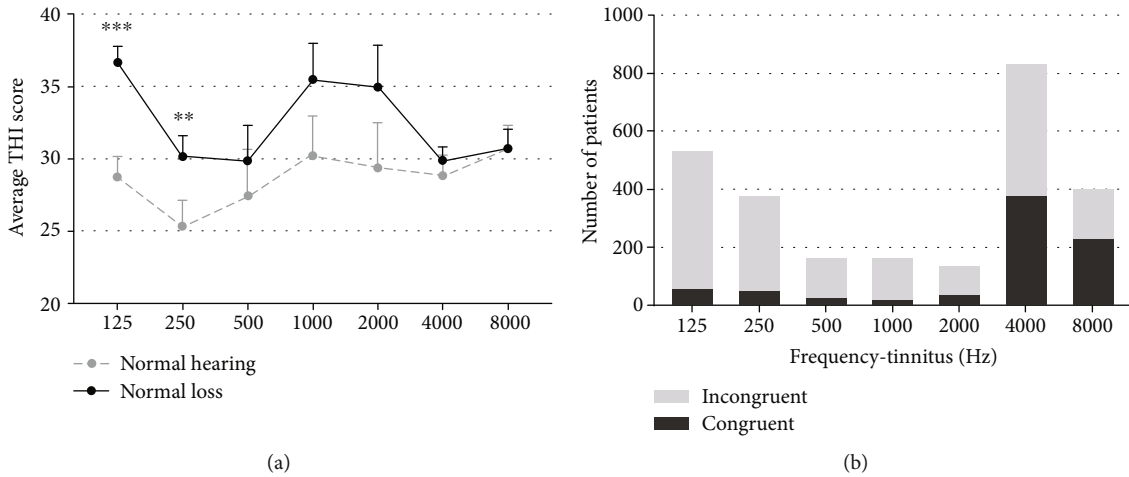


FIGURE 2: (a) Comparison of the THI scores of tinnitus patients with normal and abnormal hearing. $**p < 0.01$ and $***p < 0.001$ for differences between the labeled group at each frequency versus the normal hearing group. Error bars represent the standard errors of the means. (b) The number of patients with or without coincidence (tinnitus pitch vs. hearing threshold showed the deepness of hearing loss) in various frequency tinnitus subgroups with hearing loss.

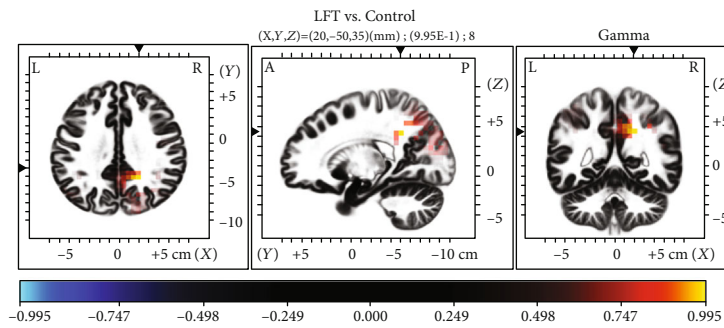


FIGURE 3: Comparison of sLORETA results between the low-frequency tinnitus (LTF) and control groups. Note the relative increase in gamma activity in the posterior cingulate cortex in patients with LTF.

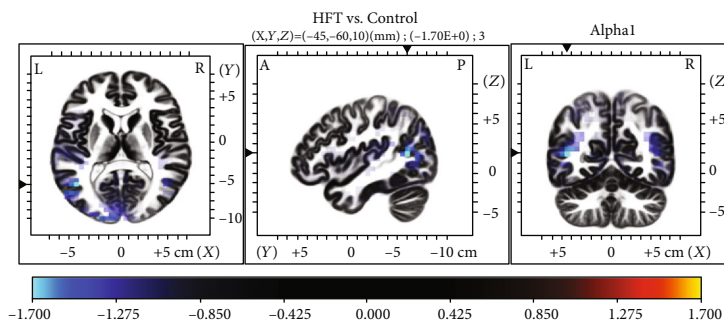


FIGURE 4: Comparison of sLORETA results between the HFT and control groups. Note the relative decreases in alpha1 activity in the angular gyrus and second auditory cortex in patients with HFT.

with the control group, the HFT group demonstrated a significant decrease in alpha1 power, and the LFT group exhibited a significant increase in gamma power. We further used sLORETA to identify the dominant brain areas associated with these differences in EEG power. Our findings suggest that differences in brain activity levels may contribute to the observed intergroup differences in characteristics.

Tinnitus is a highly heterogeneous condition with respect to the characteristics of the perceived sound, and it is associated with various degrees of associated awareness and distress, duration, and comorbidities [56, 57]. This variability would be expected in clinical presentation to be reflected by a similar variability in the structures and functions of neuronal correlates. Therefore, it is extremely challenging to identify the

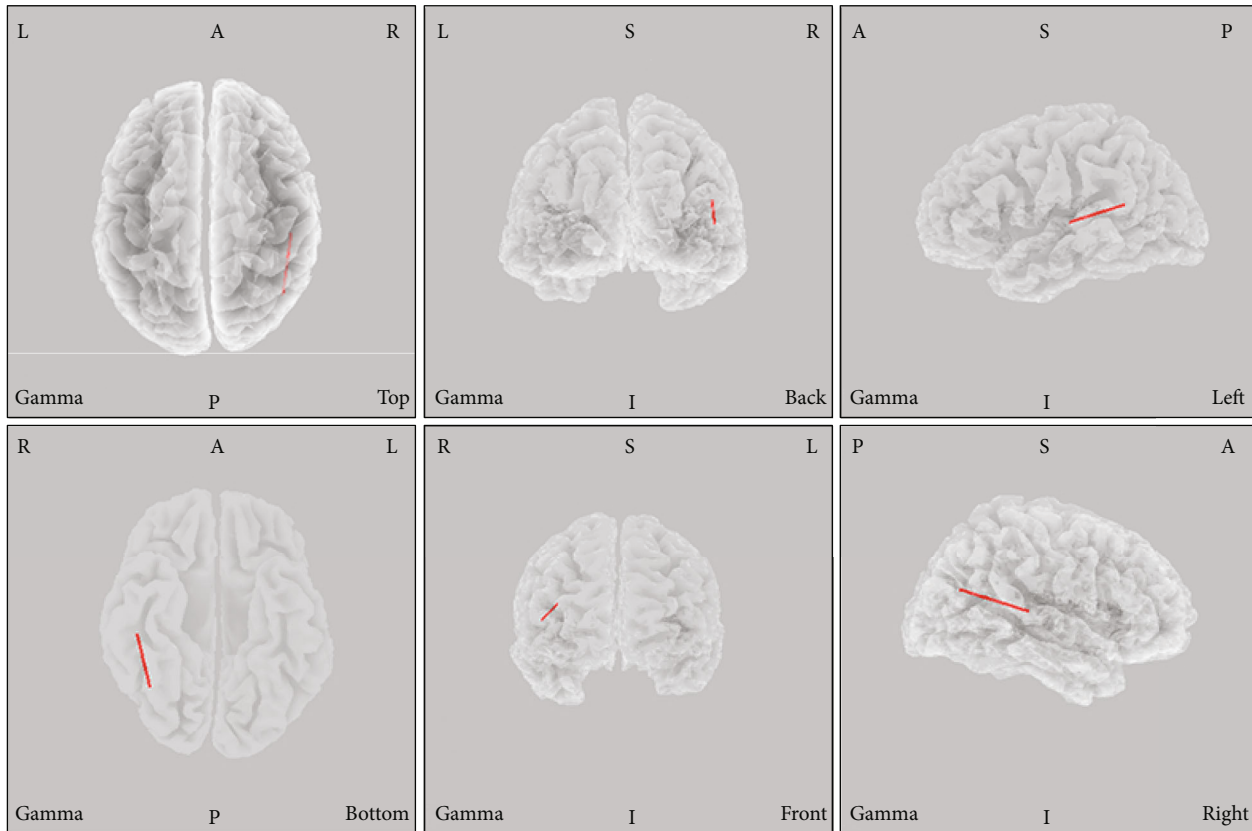


FIGURE 5: Comparison of functional connectivity between the high-frequency tinnitus (HFT) and control groups in sLORETA source space. Higher gamma linear connectivity between the right angular gyrus (BA39) and right primary auditory cortex (BA41) was observed in the HFT group relative to the control group.

underlying neuronal mechanisms of tinnitus, particularly given the high level of inconsistency among previous studies. For example, the variables that must be matched between the tinnitus and control groups remain unclear [14, 58, 59]. In this study, we matched patients in the LFT and HFT groups with respect to several demographic and clinical characteristics before exploring the underlying neurophysiological mechanisms, based on the findings of our study (Table 2). The assessment of tinnitus pitch is significant not only for the systematic documentation of patients' symptoms but also for monitoring the impacts of interventions and for treatment planning involving acoustic stimulation. In previous studies, the suppressive effect of repetitive transcranial magnetic stimulation was moderated by tinnitus type and laterality, tinnitus-related distress, and tinnitus duration, such that patients presenting with unilateral pure-tone tinnitus had significantly worse outcomes than those with noise-like tinnitus [60, 61]. Currently, no sound theory has been proposed to explain the differential effect of burst transcranial magnetic stimulation on pure-tone and noise-like tinnitus. Moreover, studies are increasingly providing strong evidence supporting the efficacy of sound therapy, during which appropriate external sounds matching the tinnitus frequency can diminish or even render tinnitus inaudible [62]. These findings suggest potential differences in the neurophysiological mechanisms underlying different tinnitus pitch types. The mechanism that may cause increasing annoyance in a patient with LFT and

hearing loss remains unclear (Figure 2). However, different auditory modalities are thought to be coded by different mechanisms and spatially separate brain networks [63]. Thus, it can be assumed that different perceptual characteristics of tinnitus (e.g., pitch and loudness) might also be coded by spatially and functionally parallel and overlapping brain networks.

The alpha rhythm may indicate cortical inhibition in an EEG, as it inhibits cell assemblies from entraining to visual stimuli and is correlated with reduced metabolic activity [64–66]. Most [67–70] resting-state MEG and EEG measurements from the temporal cortex of individuals with tinnitus reveal a reduction in alpha power (8–12 Hz) and increase in slow-wave power (delta and theta, 1–6 Hz) and gamma power (>30 Hz), which is consistent with our results [70, 71]. Notably, the HFT group demonstrated a significant decrease in alpha1 band power, and the LFT group demonstrated a significantly higher level of gamma power when compared with that of the control group, respectively. Therefore, a framework was proposed, which postulates that the reduction in ongoing inhibitory alpha activity in patients with tinnitus favors the synchronization of neurons in the gamma frequency range in the resting state. Consistent with this framework, tinnitus pitch is an important variable that must be matched between the tinnitus and control groups [72]. Moreover, these alterations in oscillatory power are proposed to be generated by thalamocortical dysrhythmia [69, 73]. Thalamocortical dysrhythmia is the consequence

of hyperpolarization of the thalamus, which has lost input due to deafferentation, resulting in a decreased external input. In response, brain plasticity attempts to obtain missing information from the auditory cortex neighborhood due to the decrease in surrounding inhibition. Mechanistically, this attempt is mediated by deinactivation of T-type Ca^{2+} channels and the generation of low-threshold bursting, which normally occurs only during sleep [73]. On an EEG, this change is represented by a slowing of theta activity to alpha activity, which is always accompanied by crossfrequency coupling with increased beta/gamma activity [22, 74]. Although cross-sectional and longitudinal studies have consistently demonstrated abnormal spectrum activities [62, 75], the results were less focused on tinnitus pitch and oscillatory power. Notably, we observed a significant correlation between tinnitus pitch and the gamma and alpha-band activity levels in our study.

Resting-state network measurements revealed an association of tinnitus with alterations in a wide range of brain areas [76–79]. In our study, HFT was associated with increased alpha1 activity in the second auditory cortex (BA22) and angular gyrus (BA39) regions relative to that in the control group (Figure 3). BA22 is involved in auditory processing and language reception. The angular gyrus has been associated with recollection-related activity, semantic processing [80], and auditory stimulus integration. LFT was associated with decreased gamma activity in the PCC relative to that in the control group (Figure 4). Previous research has demonstrated a role for the PCC in cognitive evaluation and sensory input memorization [81]. Moreover, increased connectivity within the gamma band in the right BA39 and right BA41 was observed in the HFT group relative to the control group. In a previous study of unilateral tinnitus patients, increased synchronized activity was observed in the angular gyrus [21]. In our study, all 20 tinnitus patients who underwent EEG also had unilateral tinnitus. The angular gyrus forms strong reciprocal connections with the parahippocampal area [82] and acts as a key node in the dorsal auditory pathway, the main function of which is the transformation of auditory representations into premotor responses [83]. In addition, coactivation of the angular area with the superior premotor cortex is important in spatial localization of auditory input [84]. Gamma-band activity in the auditory cortex is necessary for conscious auditory perception [74, 85] and thus may also contribute to the perception of a phantom sound. As summarized by a previous EEG study, activation of the auditory cortex may reflect the loudness of tinnitus, while conscious perception of tinnitus, its salience, and the associated distress are associated with the coactivation of different resting-state networks, such as the frontoparietal control system, PCC, auditory associated cortex, and salience network [20, 32, 59, 75, 86]. Tinnitus shares many common features with phantom pain, particularly the involvement of a vast network of brain regions, instead of the sensory cortex alone. While such networks are incompletely understood, the general idea that phantom perceptual experiences are network phenomena has gained consensus [87]. The perception of sound itself might generate tinnitus via increased activity in the auditory pathways mediated by

the interactions of auditory brain areas with nonauditory brain networks, instead of tonotopic reorganization [59].

Our study had some limitations. Tinnitus is a heterogeneous disease, and it is difficult to eliminate the various factors contributing to this heterogeneity. We note that stricter inclusion and exclusion criteria and a critical analysis of the clinical data could be applied. The results obtained from the EEG data require careful explanation because the sample sizes of our subgroups may not have been sufficiently large. Moreover, selection bias should be considered. Future studies with larger sample sizes and additional subgroup comparisons (e.g., tinnitus with or without hearing loss) are needed to investigate the characteristics and compare the differences between LFT and HFT. Such studies should focus on the definite changes in neural activities after treatment for tinnitus involving different frequencies.

5. Conclusions

In conclusion, we observed several significant differences in the clinical characteristics of patients in the LFT and HFT groups. Patients with LFT appeared to be more disadvantaged by hearing loss than those with HFT, as indicated by the THI scores. Moreover, the tinnitus pitch only appeared to be correlated with the threshold of the worst hearing loss in the HFT group. Our findings suggest significant differences in the power levels of the gamma and alpha1 bands between patients with tinnitus and controls, but not between patients with different tinnitus frequency levels. Differences in brain activity levels may contribute to the observed intergroup differences in characteristics.

Data Availability

The form data used to support the findings of this study are available on request to the corresponding author: Dr. Hui Wang, Email: wangh2014@163.com.

Conflicts of Interest

The authors declare that they have no conflicts of interest.

Authors' Contributions

Jiajia Zhang, Zhen Zhang, and Shujian Huang contributed equally to this work.

Acknowledgments

We would like to thank all the patients and their families for supporting our work. The study was supported by funding from the International Cooperation and Exchange of the National Natural Science Foundation of China (Grant No. 81720108010), the State Key Program of National Natural Science of China (Grant No. 81530029), the Shanghai Shen-Kang Hospital Management Center Project of Shanghai (Grant No. SHDC12015101), the Humanity and Social Science Youth Foundation of the Ministry of Education in China (Grant No. 19YJC190018), and the National Natural Science Foundation of China (Grant No. 81901830).

References

- [1] D. D. Walker, A. S. Cifu, and M. B. Gluth, "Tinnitus," *JAMA*, vol. 315, no. 20, pp. 2221-2222, 2016.
- [2] H. J. Kim, H. J. Lee, S. Y. An et al., "Analysis of the prevalence and associated risk factors of tinnitus in adults," *PLoS One*, vol. 10, no. 5, article e0127578, 2015.
- [3] D. Sindhusake, P. Mitchell, P. Newall, M. Golding, E. Rochtchina, and G. Rubin, "Prevalence and characteristics of tinnitus in older adults: the Blue Mountains Hearing Study," *International Journal of Audiology*, vol. 42, no. 5, pp. 289-294, 2003.
- [4] S. Vanneste, J. J. Song, and D. De Ridder, "Tinnitus and musical hallucinosis: the same but more," *NeuroImage*, vol. 82, pp. 373-383, 2013.
- [5] R. J. Park and J. D. Moon, "Prevalence and risk factors of tinnitus: the Korean National Health and Nutrition Examination Survey 2010-2011, a cross-sectional study," *Clinical Otolaryngology*, vol. 39, no. 2, pp. 89-94, 2014.
- [6] H. Hesser, E. Bankestad, and G. Andersson, "Acceptance of tinnitus as an independent correlate of tinnitus severity," *Ear and Hearing*, vol. 36, no. 4, pp. e176-e182, 2015.
- [7] E. Wallhäusser-Franke, W. Delb, T. Balkenhol, W. Hiller, and K. Hörmann, "Tinnitus-related distress and the personality characteristic resilience," *Neural Plasticity*, vol. 2014, Article ID 370307, 6 pages, 2014.
- [8] D. Golm, C. Schmidt-Samoa, P. Dechent, and B. Kröner-Herwig, "Neural correlates of tinnitus related distress: an fMRI study," *Hearing Research*, vol. 295, pp. 87-99, 2013.
- [9] D. De Ridder, S. Vanneste, N. D. Engineer, and M. P. Kilgard, "Safety and efficacy of vagus nerve stimulation paired with tones for the treatment of tinnitus: a case series," *Neuromodulation*, vol. 17, no. 2, pp. 170-179, 2014.
- [10] S. E. Shore, L. E. Roberts, and B. Langguth, "Maladaptive plasticity in tinnitus—triggers, mechanisms and treatment," *Nature Reviews Neurology*, vol. 12, no. 3, pp. 150-160, 2016.
- [11] L. E. Roberts, G. Moffat, M. Baumann, L. M. Ward, and D. J. Bosnyak, "Residual inhibition functions overlap tinnitus spectra and the region of auditory threshold shift," *Journal of the Association for Research in Otolaryngology*, vol. 9, no. 4, pp. 417-435, 2008.
- [12] A. Norena, C. Micheyl, S. Chéry-Croze, and L. Collet, "Psychoacoustic characterization of the tinnitus spectrum: implications for the underlying mechanisms of tinnitus," *Audiology & Neuro-Otology*, vol. 7, no. 6, pp. 358-369, 2002.
- [13] S. Vanneste and D. De Ridder, "Deafferentation-based pathophysiological differences in phantom sound: tinnitus with and without hearing loss," *NeuroImage*, vol. 129, pp. 80-94, 2016.
- [14] F. T. Husain, "Neuroanatomical changes due to hearing loss and chronic tinnitus: a combined VBM and DTI study," *Brain Research*, vol. 1369, pp. 74-88, 2011.
- [15] W. Muhlnickel, T. Elbert, E. Taub, and H. Flor, "Reorganization of auditory cortex in tinnitus," *Proceedings of the National Academy of Sciences of the United States of America*, vol. 95, no. 17, pp. 10340-10343, 1998.
- [16] H. Wang, B. Li, Y. Feng et al., "A pilot study of EEG source analysis based repetitive transcranial magnetic stimulation for the treatment of tinnitus," *PLoS One*, vol. 10, no. 10, article e0139622, 2015.
- [17] J. J. Eggermont and L. E. Roberts, "The neuroscience of tinnitus," *Trends in Neurosciences*, vol. 27, no. 11, pp. 676-682, 2004.
- [18] M. Seeber, L. M. Cantonas, M. Hoevels, T. Sesia, V. Visser-Vandewalle, and C. M. Michel, "Subcortical electrophysiological activity is detectable with high-density EEG source imaging," *Nature Communications*, vol. 10, no. 1, p. 753, 2019.
- [19] O. R. M. Ryyänen, J. A. K. Hyttinen, and J. A. Malmivuo, "Effect of measurement noise and electrode density on the spatial resolution of cortical potential distribution with different resistivity values for the skull," *IEEE Transactions on Biomedical Engineering*, vol. 53, no. 9, pp. 1851-1858, 2006.
- [20] S. Vanneste, P. V. Heyning, and D. D. Ridder, "Contralateral parahippocampal gamma-band activity determines noise-like tinnitus laterality: a region of interest analysis," *Neuroscience*, vol. 199, pp. 481-490, 2011.
- [21] S. Vanneste, M. Plazier, E. van der Loo, P. van de Heyning, and D. de Ridder, "The difference between uni- and bilateral auditory phantom percept," *Clinical Neurophysiology*, vol. 122, no. 3, pp. 578-587, 2011.
- [22] S. Vanneste, W. T. To, and D. De Ridder, "Tinnitus and neuropathic pain share a common neural substrate in the form of specific brain connectivity and microstate profiles," *Progress in Neuro-Psychopharmacology & Biological Psychiatry*, vol. 88, pp. 388-400, 2019.
- [23] S. Vanneste, M. Plazier, E. van der Loo, P. van de Heyning, and D. de Ridder, "The differences in brain activity between narrow band noise and pure tone tinnitus," *PLoS One*, vol. 5, no. 10, article e13618, 2010.
- [24] D. J. Hoare, R. H. Pierzycki, H. Thomas, D. McAlpine, and D. A. Hall, "Evaluation of the acoustic coordinated reset (CR[®]) neuromodulation therapy for tinnitus: study protocol for a double-blind randomized placebo-controlled trial," *Trials*, vol. 14, no. 1, p. 207, 2013.
- [25] Y. Cai, Q. Zhou, H. Yang et al., "Logistic regression analysis of factors influencing the effectiveness of intensive sound masking therapy in patients with tinnitus," *BMJ Open*, vol. 7, no. 11, article e018050, 2017.
- [26] S. Vanneste, K. Joos, and D. De Ridder, "Prefrontal cortex based sex differences in tinnitus perception: same tinnitus intensity, same tinnitus distress, different mood," *PLoS One*, vol. 7, no. 2, article e31182, 2012.
- [27] S. Vanneste, P. V. de Heyning, and D. De Ridder, "The neural network of phantom sound changes over time: a comparison between recent-onset and chronic tinnitus patients," *European Journal of Neuroscience*, vol. 34, no. 5, pp. 718-731, 2011.
- [28] C. W. Newman, S. A. Sandridge, and G. P. Jacobson, "Psychometric adequacy of the Tinnitus Handicap Inventory (THI) for evaluating treatment outcome," *Journal of the American Academy of Audiology*, vol. 9, no. 2, pp. 153-160, 1998.
- [29] A. Delorme and S. Makeig, "EEGLAB: an open source toolbox for analysis of single-trial EEG dynamics including independent component analysis," *Journal of Neuroscience Methods*, vol. 134, no. 1, pp. 9-21, 2004.
- [30] G. Gomez-Herrero, W. De Clercq, H. Anwar et al., "Automatic removal of ocular artifacts in the EEG without an EOG reference channel," in *Proceedings of the 7th Nordic Signal Processing Symposium - NORSIG 2006*, Reykjavik, Iceland, 2006.
- [31] W. D. Clercq, A. Vergult, B. Vanrumste, W. Van Paesschen, and S. Van Huffel, "Canonical correlation analysis applied to remove muscle artifacts from the electroencephalogram," *IEEE Transactions on Biomedical Engineering*, vol. 53, no. 12, pp. 2583-2587, 2006.

- [32] D. De Ridder and S. Vanneste, "Targeting the parahippocampal area by auditory cortex stimulation in tinnitus," *Brain Stimulation*, vol. 7, no. 5, pp. 709–717, 2014.
- [33] S. Vanneste and D. De Ridder, "The auditory and non-auditory brain areas involved in tinnitus. An emergent property of multiple parallel overlapping subnetworks," *Frontiers in Systems Neuroscience*, vol. 6, p. 31, 2012.
- [34] S. Vanneste and D. De Ridder, "Brain areas controlling heart rate variability in tinnitus and tinnitus-related distress," *PLoS One*, vol. 8, no. 3, article e59728, 2013.
- [35] J. D. Kropotov, *Quantitative EEG, event-related potentials and neurotherapy*, Academic Press, 2010.
- [36] R. D. Pascual-Marqui, "Standardized low-resolution brain electromagnetic tomography (sLORETA): technical details," *Methods and Findings in Experimental and Clinical Pharmacology*, vol. 24, pp. 5–12, 2002.
- [37] R. D. Pascual-Marqui, "Instantaneous and lagged measurements of linear and nonlinear dependence between groups of multivariate time series: frequency decomposition," 2007, <https://arxiv.org/abs/0711.1455>.
- [38] R. D. Pascual-Marqui, "Discrete, 3D distributed, linear imaging methods of electric neuronal activity. Part 1: exact, zero error localization," 2007, <https://arxiv.org/abs/0710.3341>.
- [39] T. E. Nichols and A. P. Holmes, "Nonparametric permutation tests for functional neuroimaging: a primer with examples," *Human Brain Mapping*, vol. 15, no. 1, pp. 1–25, 2002.
- [40] J. Qi, L. Zhang, F. Tan et al., "Espn distribution as revealed by super-resolution microscopy of stereocilia," *American Journal of Translational Research*, vol. 12, no. 1, pp. 130–141, 2020.
- [41] J. Qi, Y. Liu, C. Chu et al., "A cytoskeleton structure revealed by super-resolution fluorescence imaging in inner ear hair cells," *Cell Discovery*, vol. 5, no. 1, p. 12, 2019.
- [42] Y. Liu, J. Qi, X. Chen et al., "Critical role of spectrin in hearing development and deafness," *Science Advances*, vol. 5, no. 4, article eaav7803, 2019.
- [43] L. Liu, Y. Chen, J. Qi et al., "Wnt activation protects against neomycin-induced hair cell damage in the mouse cochlea," *Cell Death & Disease*, vol. 7, no. 3, article e2136, 2016.
- [44] Z. He, L. Guo, Y. Shu et al., "Autophagy protects auditory hair cells against neomycin-induced damage," *Autophagy*, vol. 13, no. 11, pp. 1884–1904, 2017.
- [45] Z.-h. He, S.-y. Zou, M. Li et al., "The nuclear transcription factor FoxG1 affects the sensitivity of mimetic aging hair cells to inflammation by regulating autophagy pathways," *Redox Biology*, vol. 28, article 101364, 2020.
- [46] W. Liu, X. Xu, Z. Fan et al., "Wnt signaling activates TP53-induced glycolysis and apoptosis regulator and protects against cisplatin-induced spiral ganglion neuron damage in the mouse cochlea," *Antioxidants & Redox Signaling*, vol. 30, no. 11, pp. 1389–1410, 2019.
- [47] C. Zhu, C. Cheng, Y. Wang et al., "Loss of ARHGEF6 causes hair cell stereocilia deficits and hearing loss in mice," *Frontiers in Molecular Neuroscience*, vol. 11, p. 362, 2018.
- [48] B. C. Cox, R. Chai, A. Lenoir et al., "Spontaneous hair cell regeneration in the neonatal mouse cochlea *in vivo*," *Development*, vol. 141, no. 7, pp. 816–829, 2014.
- [49] T. Wang, R. Chai, G. S. Kim et al., "Lgr5+ cells regenerate hair cells via proliferation and direct transdifferentiation in damaged neonatal mouse utricle," *Nature Communications*, vol. 6, no. 1, article 6613, 2015.
- [50] X. Lu, S. Sun, J. Qi et al., "Bmi1 regulates the proliferation of cochlear supporting cells via the canonical Wnt signaling pathway," *Molecular Neurobiology*, vol. 54, no. 2, pp. 1326–1339, 2017.
- [51] W. Yan, W. Liu, J. Qi et al., "A three-dimensional culture system with Matrigel promotes purified spiral ganglion neuron survival and function *in vitro*," *Molecular Neurobiology*, vol. 55, no. 3, pp. 2070–2084, 2018.
- [52] S. Zhang, D. Liu, Y. Dong et al., "Frizzled-9+ supporting cells are progenitors for the generation of hair cells in the postnatal mouse cochlea," *Frontiers in Molecular Neuroscience*, vol. 12, p. 184, 2019.
- [53] C. Cheng, Y. Wang, L. Guo et al., "Age-related transcriptome changes in Sox2+ supporting cells in the mouse cochlea," *Stem Cell Research & Therapy*, vol. 10, no. 1, p. 365, 2019.
- [54] F. Tan, C. Chu, J. Qi et al., "AAV-*ie* enables safe and efficient gene transfer to inner ear cells," *Nature Communications*, vol. 10, no. 1, p. 3733, 2019.
- [55] S. Zhang, Y. Zhang, Y. Dong et al., "Knockdown of Foxg1 in supporting cells increases the trans-differentiation of supporting cells into hair cells in the neonatal mouse cochlea," *Cellular and Molecular Life Sciences*, vol. 77, no. 7, pp. 1401–1419, 2020.
- [56] J. N. Al-Swiahb, E. S. Hwang, J. S. Kong, W. J. Kim, S. W. Yeo, and S. N. Park, "Clinical and audiologic characteristics of patients with sensorineural tinnitus and its association with psychological aspects: an analytic retrospective study," *European Archives of Oto-Rhino-Laryngology*, vol. 273, no. 12, p. 4161–4165, 2016.
- [57] M. Landgrebe, "Methodological aspects of clinical trials in tinnitus: a proposal for an international standard," *Journal of Psychosomatic Research*, vol. 73, no. 2, pp. 112–121, 2012.
- [58] J. R. Melcher, I. M. Knudson, and R. A. Levine, "Subcallosal brain structure: correlation with hearing threshold at supra-clinical frequencies (>8 kHz), but not with tinnitus," *Hearing Research*, vol. 295, pp. 79–86, 2013.
- [59] A. B. Elgoyhen, B. Langguth, D. de Ridder, and S. Vanneste, "Tinnitus: perspectives from human neuroimaging," *Nature Reviews Neuroscience*, vol. 16, no. 10, pp. 632–642, 2015.
- [60] B. Langguth, "Neuroimaging and neuromodulation: complementary approaches for identifying the neuronal correlates of tinnitus," *Frontiers in Systems Neuroscience*, vol. 6, p. 15, 2012.
- [61] T.-S. Noh, J.-S. Kyong, M. K. Park et al., "Treatment outcome of auditory and frontal dual-site rTMS in tinnitus patients and changes in magnetoencephalographic functional connectivity after rTMS: double-blind randomized controlled trial," *Audiology & Neurotology*, vol. 24, no. 6, pp. 293–298, 2020.
- [62] D. Baguley, D. McFerran, and D. Hall, "Tinnitus," *The Lancet*, vol. 382, no. 9904, pp. 1600–1607, 2013.
- [63] I. Adamchic, C. Hauptmann, and P. A. Tass, "Changes of oscillatory activity in pitch processing network and related tinnitus relief induced by acoustic CR neuromodulation," *Frontiers in Systems Neuroscience*, vol. 6, p. 18, 2012.
- [64] W. Klimesch, " α -band oscillations, attention, and controlled access to stored information," *Trends in Cognitive Sciences*, vol. 16, no. 12, pp. 606–617, 2012.
- [65] K. E. Mathewson, A. Lleras, D. M. Beck, M. Fabiani, T. Ro, and G. Gratton, "Pulsed out of awareness: EEG alpha oscillations represent a pulsed-inhibition of ongoing cortical processing," *Frontiers in Psychology*, vol. 2, p. 99, 2011.
- [66] T. R. Oakes, D. A. Pizzagalli, A. M. Hendrick et al., "Functional coupling of simultaneous electrical and metabolic activity in

- the human brain,” *Human Brain Mapping*, vol. 21, no. 4, pp. 257–270, 2004.
- [67] I. Adamchic, T. Toth, C. Hauptmann, and P. A. Tass, “Reversing pathologically increased EEG power by acoustic coordinated reset neuromodulation,” *Human Brain Mapping*, vol. 35, no. 5, pp. 2099–2118, 2014.
- [68] E. van der Loo, S. Gais, M. Congedo et al., “Tinnitus intensity dependent gamma oscillations of the contralateral auditory cortex,” *PLoS One*, vol. 4, no. 10, article e7396, 2009.
- [69] R. R. Llinas, U. Ribary, D. Jeanmonod, E. Kronberg, and P. P. Mitra, “Thalamocortical dysrhythmia: a neurological and neuropsychiatric syndrome characterized by magnetoencephalography,” *Proceedings of the National Academy of Sciences of the United States of America*, vol. 96, no. 26, pp. 15222–15227, 1999.
- [70] N. Weisz, “The neural code of auditory phantom perception,” *The Journal of Neuroscience*, vol. 27, no. 6, pp. 1479–1484, 2007.
- [71] N. Weisz, K. Dohrmann, and T. Elbert, “The relevance of spontaneous activity for the coding of the tinnitus sensation,” *Progress in Brain Research*, vol. 166, pp. 61–70, 2007.
- [72] I. Lorenz, N. Müller, W. Schlee, T. Hartmann, and N. Weisz, “Loss of alpha power is related to increased gamma synchronization—A marker of reduced inhibition in tinnitus?,” *Neuroscience Letters*, vol. 453, no. 3, pp. 225–228, 2009.
- [73] D. De Ridder, S. Vanneste, B. Langguth, and R. Llinas, “Thalamocortical dysrhythmia: a theoretical update in tinnitus,” *Frontiers in Neurology*, vol. 6, p. 124, 2015.
- [74] C. Potes, P. Brunner, A. Gunduz, R. T. Knight, and G. Schalk, “Spatial and temporal relationships of electrocorticographic alpha and gamma activity during auditory processing,” *NeuroImage*, vol. 97, pp. 188–195, 2014.
- [75] E. Houdayer, R. Teggi, S. Velikova et al., “Involvement of cortico-subcortical circuits in normoacoustic chronic tinnitus: a source localization EEG study,” *Clinical Neurophysiology*, vol. 126, no. 12, pp. 2356–2365, 2015.
- [76] G. Shou, M. W. Mosconi, J. Wang, L. E. Ethridge, J. A. Sweeney, and L. Ding, “Electrophysiological signatures of atypical intrinsic brain connectivity networks in autism,” *Journal of Neural Engineering*, vol. 14, no. 4, article 046010, 2017.
- [77] W. Schlee, T. Hartmann, B. Langguth, and N. Weisz, “Abnormal resting-state cortical coupling in chronic tinnitus,” *BMC Neuroscience*, vol. 10, no. 1, p. 11, 2009.
- [78] J. Y. Kim, “Alteration of functional connectivity in tinnitus brain revealed by resting-state fMRI? A pilot study,” *International Journal of Audiology*, vol. 51, no. 5, pp. 413–417, 2012.
- [79] P. Neff, C. Hemsley, F. Kraxner, S. Weidt, T. Kleinjung, and M. Meyer, “Active listening to tinnitus and its relation to resting state EEG activity,” *Neuroscience Letters*, vol. 694, pp. 176–183, 2019.
- [80] S. M. Daselaar, M. S. Fleck, and R. Cabeza, “Triple dissociation in the medial temporal lobes: recollection, familiarity, and novelty,” *Journal of Neurophysiology*, vol. 96, no. 4, pp. 1902–1911, 2006.
- [81] B. A. Vogt, D. M. Finch, and C. R. Olson, “Functional heterogeneity in cingulate cortex: the anterior executive and posterior evaluative regions,” *Cerebral Cortex*, vol. 2, no. 6, pp. 435–443, 1992.
- [82] D. M. Clower, R. A. West, J. C. Lynch, and P. L. Strick, “The inferior parietal lobule is the target of output from the superior colliculus, hippocampus, and cerebellum,” *The Journal of Neuroscience*, vol. 21, no. 16, pp. 6283–6291, 2001.
- [83] A. Karabanov, O. Blom, L. Forsman, and F. Ullen, “The dorsal auditory pathway is involved in performance of both visual and auditory rhythms,” *NeuroImage*, vol. 44, no. 2, pp. 480–488, 2009.
- [84] R. I. Schubotz, D. Y. von Cramon, and G. Lohmann, “Auditory what, where, and when: a sensory somatotopy in lateral premotor cortex,” *NeuroImage*, vol. 20, no. 1, pp. 173–185, 2003.
- [85] J. Kaiser and W. Lutzenberger, “Human gamma-band activity: a window to cognitive processing,” *NeuroReport*, vol. 16, no. 3, pp. 207–211, 2005.
- [86] N. Weisz, S. Voss, P. Berg, and T. Elbert, “Abnormal auditory mismatch response in tinnitus sufferers with high-frequency hearing loss is associated with subjective distress level,” *BMC Neuroscience*, vol. 5, no. 1, p. 8, 2004.
- [87] J. Hullfish, I. Abenes, H. B. Yoo, D. De Ridder, and S. Vanneste, “Frontostriatal network dysfunction as a domain-general mechanism underlying phantom perception,” *Human Brain Mapping*, vol. 40, no. 7, pp. 2241–2251, 2019.

Research Article

Loss of Cochlear Ribbon Synapse Is a Critical Contributor to Chronic Salicylate Sodium Treatment-Induced Tinnitus without Change Hearing Threshold

Wei Zhang,^{1,2} Zhe Peng,¹ ShuKui Yu,¹ Qing-Ling Song,¹ Teng-Fei Qu,¹ Lu He,¹ Ke Liu ¹,
and Shu-Sheng Gong ¹

¹Department of Otolaryngology-Head and Neck Surgery, Beijing Friendship Hospital, Capital Medical University, Beijing City Xi Cheng District Road 95 Yong an, Beijing 100050, China

²Department of Otolaryngology-Head and Neck Surgery, Eye Hospital China Academy of Chinese Medical Science, Beijing City Shi Jingshan District Lugu Road 33, Beijing 100040, China

Correspondence should be addressed to Ke Liu; liuke@ccmu.edu.cn and Shu-Sheng Gong; gongss1962@163.com

Received 23 February 2020; Revised 23 May 2020; Accepted 12 June 2020; Published 25 July 2020

Academic Editor: Renjie Chai

Copyright © 2020 Wei Zhang et al. This is an open access article distributed under the Creative Commons Attribution License, which permits unrestricted use, distribution, and reproduction in any medium, provided the original work is properly cited.

Tinnitus is a common auditory disease worldwide; it is estimated that more than 10% of all individuals experience this hearing disorder during their lifetime. Tinnitus is sometimes accompanied by hearing loss. However, hearing loss is not acquired in some other tinnitus generations. In this study, we injected adult rats with salicylate sodium (SS) (200 mg/kg/day for 10 days) and found no significant hearing threshold changes at 2, 4, 8, 12, 14, 16, 20, or 24 kHz (all $p > 0.05$). Tinnitus was confirmed in the treated rats via Behaviour Testing of Acoustic Startle Response (ASR) and Gap Prepulse Inhibition Test of Acoustic Startle Reflex (GPIAS). A immunostaining study showed that there is significant loss of anti-CtBP2 puncta (a marker of cochlear inner hair cell (HC) ribbon synapses) in treated animals in apical, middle, and basal turns (all $p < 0.05$). The ABR wave I amplitudes were significantly reduced at 4, 8, 12, 14, 16, and 20 kHz (all $p < 0.05$). No significant losses of outer HCs, inner HCs, or HC cilia were observed (all $p > 0.05$). Thus, our study suggests that loss of cochlear inner HC ribbon synapse after SS exposure is a contributor to the development of tinnitus without changing hearing threshold.

1. Introduction

Tinnitus is becoming a serious health problem worldwide [1–3]. It was proposed that tinnitus is probably induced by an imbalance between neuronal excitability and inhibition in the auditory circuit [4, 5]. The occurrence of tinnitus is associated with hearing loss, cochlear damage, and multiple types of the stress [6]. However, patients with normal audiogram may also exhibit tinnitus [7–10]. Clinical studies provided evidence that patients with both tinnitus and normal audiograms exhibit significant reduction in wave I amplitudes of auditory brainstem response (ABR) [11–13]. An alternative animal study showed that the mice exposed to noise develop temporary threshold shift (TTS) [14] and irreversible loss of cochlear ribbon synapses that connect cochlear inner HCs and spiral ganglion cells (SGCs) [13, 15]. However, it is

unclear whether loss of cochlear ribbon synapses contributes to tinnitus generation in patients with normal audiogram. Bauer et al. found behavioural evidence indicating that loss of auditory nerve (AN) fibers in rats may associate with tinnitus [16]; however, there is significant loss of hearing and HCs in rats after noise exposure. Thus, this model may be unsuitable for exploring the etiology of tinnitus with normal audiogram. It is necessary to find an appropriate model to identify the correlations between tinnitus with normal audiogram and loss of cochlear ribbon synapses.

SS, an active component of the nonsteroidal anti-inflammatory drug aspirin, has been commonly used to generate tinnitus in animals [17]. SS is an anti-inflammation drug used to manage rheumatoid arthritis at therapeutic dose; SS inhibits cyclooxygenase activity and prostaglandin synthesis. High-dose SS could induce tinnitus characterized

by TTS [11, 18]. However, it remains unknown whether such tinnitus features loss of cochlear ribbon synapses and/or cochlear HCs. Notably, the losses responsible for tinnitus accompanied by normal audiogram have not yet been identified.

Here, we present the evidence that an appropriate dose of SS exposure can cause tinnitus with normal audiogram and cochlear HCs, but loss of cochlear ribbon synapse suggesting loss of cochlear inner HC ribbon synapse may largely contribute to SS-induced tinnitus.

2. Materials and Methods

2.1. Animal. All studies were approved according to the Institutional Animal Care and Use Committee at the Capital Medical University of China. Wistar rats (adult, male, weighted 250 g~280 g) were obtained from the animal experimental ministry of Capital Medical University. Animals were divided into two groups according to intraperitoneal injection contents for ten days: (i) control group with injection of saline and (ii) SS-treated group with an injection of 5% (200 mg/kg) SS.

2.2. Behaviour Testing of ASR and GPIAS. ASR and GPIAS were used to measure tinnitus generation. Animals were placed in a permeable sound box resting on a sensitive piezoelectric capable of generating a voltage proportional to the magnitude of the startle responses, evoked by sound stimuli generated by a digital signal processor. The test apparatus was located in a soundproof chamber equipped with a tweeter on the chamber's ceiling about 10 cm above the rat's head. Animals were placed in the box for ten minutes prior to testing for adaptation. Test sessions include gap and no gap trial pair-arranged. The background sound is a pure tone of 12 k-16 k Hz, 70 dB, and the startle stimulus is 120 dB broad-banded noise (20 ms) in each trial. The gap lasting 75 ms was embedded in the background tone 100 ms prior to the startle stimulus. The maximum startle reflex within 250 ms after startle stimulus was recorded. Intertrial time was settled 12 sec to 21 sec randomly. ASR amplitude was recorded as the voltage generated by startle reflex of the tested animals (millivolt, mV). GPIAS was calculated as a ratio using the formula: $1 - (\text{gap}/\text{no gap})$. Animals with tinnitus have been speculated to demonstrate poorer gap detection ability, which can be measured as a lack of suppression of the startle response in gap trial. Tinnitus rats present a lower GPIAS ratio. We compared the ASR amplitude and GPIAS inhibition rates of the SS-treated and control groups.

2.3. ABR Recordings. The evoked response signal-processing System 3 hardware (Tucker Davis Technologies, Alachua, FL, USA) and SigGen/BioSig software (Tucker Davis Technologies) were used for ABR measurement. Animals were anesthetized with Xylazine (10 mg/kg) and Ketamine (90 mg/kg) and placed in a soundproof chamber. Three needle electrodes were inserted at vertex (active) and beneath of each pinna (reference and ground), subcutaneously. The ABR threshold is the lowest stimulus intensity that produced reliable and reproducible ABR waves. We evaluated the rats

hearing status before and at the end of this study and recorded ABR threshold at pure tone frequency of 2, 4, 8, 12, 16, 20, and 24 kHz. Wave I amplitude was measured peak to baseline, and latency was measured within a specified time window at 90 dB level at each frequency.

2.4. Immunostaining. Animals were decapitated after anaesthesia, and the temporal bones were removed and fixed for 2 h in 10% formaldehyde in phosphate-buffered saline (PBS). After the samples were rinsed in PBS, the basilar membranes of the cochlea were dissected out for immunostaining. Permeabilized with 0.3% TritonX-100 (Sigma-Aldrich) for 30 min and blocked with 10% normal goat serum (Jackson) for 1 h; the tissues were incubated overnight at 4°C with the following primary antibodies: rabbit anti-myosin 7a (1:300, Proteus Biosciences); phalloidin 594 (1:500, Thermo Fisher); mouse anti-CtBP2 (1:300, BD); and chicken anti-NF200 (1:200, CHEMICON). After rinsing with PBS, the samples were incubated in fluorescently labelled secondary antibodies (Alexa Fluor 488 and 568, Invitrogen/Molecular/Thermo Fisher) for 1 h at room temperature. Nuclei were visualized with 4',6-diamidino-2-phenylindole (DAPI) (AppliChem).

2.5. Confocal Microscopy Imaging. Laser scanning confocal microscopy was conducted with a 63 X oil immersion objective lens (LEICA TCS SP8). Excitation wave lengths were 488, 568, and 594 nm, and local images were digitally magnified by twofold. Sequence scanning was performed from the apex and obtained at an interval of 0.5 μm. Cross-sectioned cochleae were imaged covering the entire inner HC nucleus and areas beyond it in an image stack along the z-axis (z-stack).

2.6. Counting the Number of Ribbon Synapses, Outer HCs, and Inner HCs. Quantification of ribbon synapses, outer HCs, and inner HCs was performed in the cochlear apex turn, middle turn, and basal turn. Quantification was performed from the top of the cochlea to the bottom. In each basilar turn, we choose three visual fields containing approximately 9-11 inner HCs and 27-33 outer HCs. We selected five samples in each group to calculate the average number of ribbon synapses and HCs. The images were identified inner HC ribbon synapses by red fluorescence spot (indicating a pre synaptic ribbon) that appeared in each image. The total number of red fluorescence marks was obtained using Photoshop software. The number of marks in single inner HC was calculated. In the same way, the numbers of outer HCs and inner HCs in single image were calculated (green fluorescence staining).

2.7. Statistical Analysis. All data are presented as the mean ± SE. Statistical analysis was performed using GraphPad Prism 7 software (GraphPad Software Inc., La Jolla, CA, USA). Statistical differences between groups in ABR threshold shifts, HC counts, and synaptic counts were analyzed using one-way analysis of variance (ANOVA), followed by Bonferroni's multiple comparison test. *p* values < 0.05 were considered statistically significant.

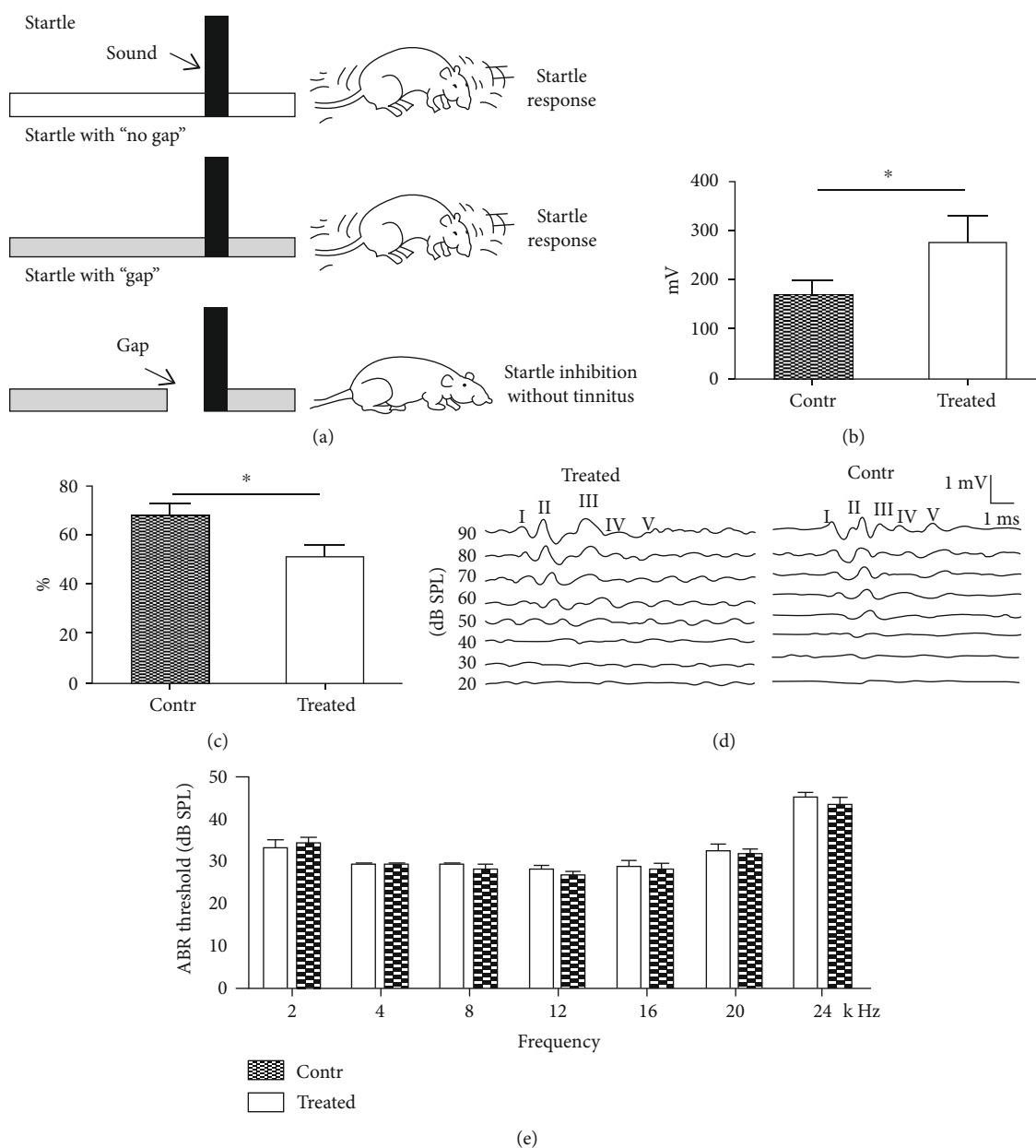


FIGURE 1: ASR and GPIAS procedures used to measure tinnitus and hearing threshold shifts before and after SS exposure. (a) Sketch map of behavior detection of tinnitus. The rat is startled in the presence of a sudden noise burst (startle stimulus). In normal animals, a silent gap in pure tone background prior to delivery of startle stimulus inhibits the startle response. The rats with putative tinnitus (sound condition is similar to the background tone) exhibit defective behavior. They do not identify the silent gap because of tinnitus. Thus, the startle response is not inhibited in rats with tinnitus, compared to controls without tinnitus. (b) ASR amplitudes of the control (dashed columns, $n = 7$) and SS-treated (blank columns, $n = 7$) groups. Average acoustic startle reflex amplitude was significantly higher in the treated group than in the control group ($*p < 0.05$). (c) GPIAS values of the control (dashed columns, $n = 10$) and SS-treated (blank columns, $n = 11$) groups; between-group differences were significant ($*p < 0.05$). (d) Representative ABR waveforms evoked by pure tone in the SS-treated (upper left) and control (upper right) rats; acoustic intensities are graded from high (90 dB SPL) to low (20 dB SPL). Waveforms are labeled by I, II, III, IV, and V. (e) Statistical analysis of hearing threshold shifts between the SS and control groups across all frequencies tested (2, 4, 8, 12, 16, 20, and 24 kHz); no significant between-group differences were found at any frequency (all $p > 0.05$). $n = 8$ for the treated group and $n = 6$ for the control group.

3. Results

3.1. Behaviour Examination of Tinnitus Induced by SS. Rats were intraperitoneally injected with SS (200 mg/kg/day) for 10 days. Tinnitus was evaluated via behaviour detections

(Figure 1(a)). First, the ASR was evaluated in both groups. The mean amplitudes of startle reflex in the treated and control group animals were 274.91 ± 53.36 and 170.08 ± 28.61 (millivolt) (Figure 1(b)). The amplitude was significantly higher in the treated group than in the control group

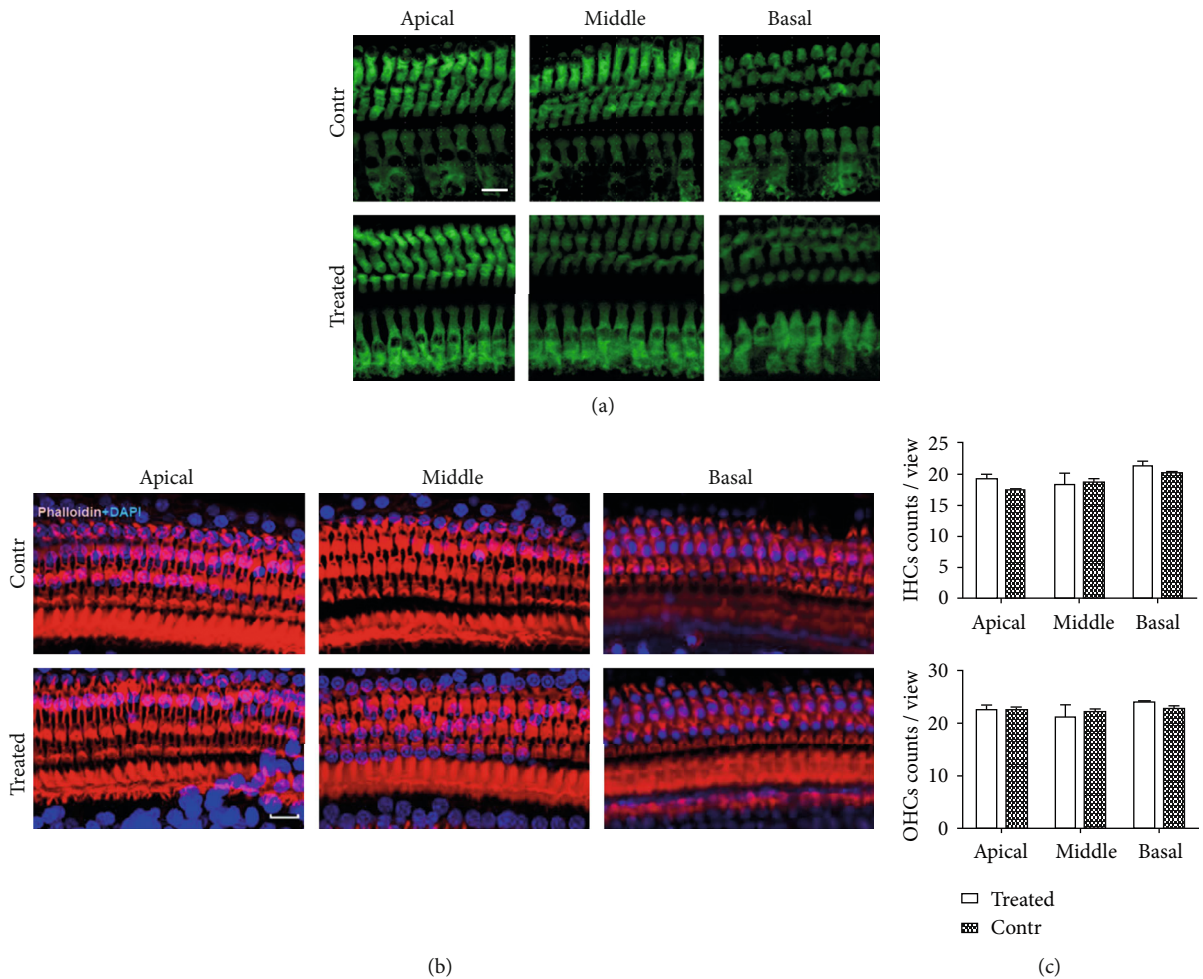


FIGURE 2: Cochlear outer and inner HC counts in the SS-treated and control rats. (a) Whole mounts of apical, middle, and basal turns were stained using myosin 7a (in green) to observe outer and inner HCs of the treated and control groups. Three rows of outer HCs and one row of inner HCs are evident; no obvious cell loss is apparent. Bar = 10 μ m. (b) Whole mounts of apical, middle, and basal turns were subjected to phalloidin staining (red) to trace HC hair bundles. No significant ciliary abnormality was apparent. Bar = 15 μ m. (c) Inner and outer HC counts of apical, middle, and basal turns of the SS-treated and control groups, respectively. Averages did not significantly differ between groups (all $p > 0.05$).

($p < 0.05$). Next, GPIAS was measured in both groups. The mean ratios in the treated and control groups were 0.5145 ± 0.045 and 0.68 ± 0.0466 (ratio) (Figure 1(c)). The mean ratio was significantly lower in the treated group than in the control group ($p < 0.05$), consistent with the previous studies. These results indicate that SS-induced tinnitus.

3.2. SS Treatment Did Not Cause Elevations of ABR Threshold. To examine whether SS exposure in this study induced hearing loss, ABR thresholds of both groups were measured. Pure tone ABR testing was performed at 2, 4, 8, 12, 16, 20, and 24 kHz 2 h after the last SS injection. For the SS-treated group, the respective results were 33.13 ± 2.10 , 29.38 ± 0.62 , 29.38 ± 0.62 , 28.13 ± 0.91 , 28.75 ± 1.56 , 32.50 ± 1.33 , and 45.00 ± 1.33 dB SPL; for the control group, the respective results were 34.17 ± 1.53 , 29.17 ± 0.83 , 28.33 ± 1.05 , 26.67 ± 1.05 , 28.33 ± 1.05 , 31.67 ± 1.05 , and 43.33 ± 1.66 dB SPL (at 2, 4, 8, 12, 16, 20, and 24 kHz). These findings were not significantly different (Figures 1(d)

and 1(e), all $p > 0.05$), indicating that SS did not cause hearing loss.

3.3. SS Exposure Did Not Induce Cochlear HC Loss. To explore whether SS exposure in the study caused the loss of cochlear HCs, we observed myosin 7a and phalloidin immunostaining to count the number of outer and inner HCs. This immunostaining revealed no differences in cell numbers among apical, middle, and basal turns in the SS group and control animals (Figures 2(a) and 2(c)); thus, SS did not induce the loss of cochlear HCs. No significant cilium loss was found from either outer or inner HCs after SS injection.

3.4. SS Exposure Caused Loss of Cochlear Inner HC Ribbon Synapses. To explore whether SS exposure triggered the loss of cochlear ribbon synapse, we applied RIBEYE/CtBP2 staining (specific for preribbon synapses). This staining was dramatically reduced in all three turns in the SS group (Figures 3(a) and 3(b)). The reductions of cochlear

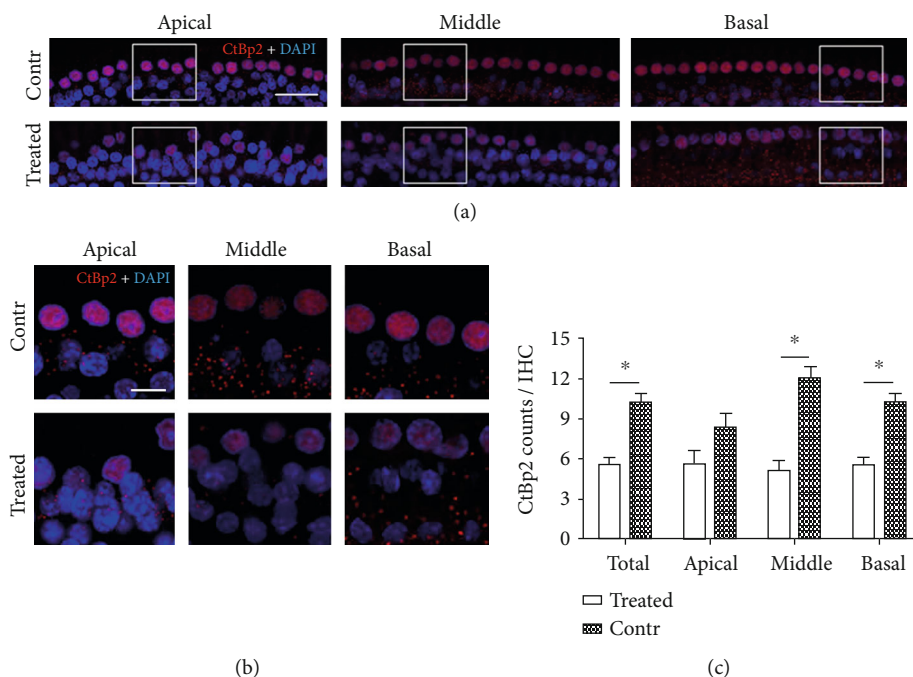


FIGURE 3: Quantitative analysis of cochlear ribbon synapses in the SS-treated and control groups. (a) Overview image of the whole mounts staining included apical, middle, and basal turns. Cochlear ribbon synapses were labeled using anti-CtBP2 staining (red, below inner HCs); cell nuclei were stained with DAPI (blue). CtBP2 was also present in the nucleus. Bar = 30 μm . (b) Enlarged images of apical, middle, and basal turns in panels of (a) (white frames); CtBP2 staining puncta were counted in randomly chosen regions containing four inner HCs. SS significantly reduced CtBP2 puncta numbers. Bar = 10 μm . (c) Quantitative analysis of cochlear ribbon synapses in the SS and control groups. The average number of CtBP2 staining puncta in apical, middle, and basal turns was analyzed, respectively. Total numbers of CtBP2 staining puncta in the two groups were also analyzed. There was a significant loss of CtBP2 staining puncta in SS-exposed rats compared to the control group (all $p < 0.05$).

inner HCs ribbon synapses were statistically significant (Figure 3(c)).

3.5. SS Exposure Disrupted Cochlear Ribbon Synapse Function. ABR wave I amplitudes were measured at 2, 4, 8, 12, 16, and 20 kHz; respective amplitudes were 462.6 ± 108.0 , 433.0 ± 81.2 , 320.8 ± 54.2 , 362.7 ± 81.4 , 217.3 ± 38.1 , and 133.2 ± 17.2 nV in SS-treated animals, whereas they were 663.6 ± 90.5 , 645.3 ± 90.18 , 511.2 ± 71.3 , 381.4 ± 48.3 , 410.6 ± 54.0 , and 254.2 ± 33.0 nV in control animals. These differences were statistically significant (Figure 4(b)), all $p < 0.05$, indicating that ABR wave I amplitude decreased significantly in the rats after SS treatment. But no significant difference was found in ABR wave I latency between the two groups.

3.6. SS Exposure Affected Morphological Properties at or near the Cochlear Ribbon Synapses. This study explored whether SS exposure affected morphological properties at or near the synaptic connections between inner HCs and AN fibers. NF-200 staining (specific for nerve fibers) identified changes in auditory innervations. We found swelling fibers of ANs and overlapped puncta (as revealed by CtBP2 and NF200 costaining) after SS exposure (Figure 4(a)). SS induced abnormalities of both presynaptic elements and postsynaptic nerve fibers, thereby disrupting ribbon synapse function.

4. Discussions

HCs in the cochlea play a critical role in converting mechanical sound waves into neural signals for hearing [19–21]. Most hearing loss induced by noise, different ototoxic drugs, inflammation, or aging is caused by the HC damage [22–29]. Ribbon synapses are vital structures between inner HC and SGNs, which are the primary synaptic structures in the sound conduction pathway and play an important role in sound signal transmission [30–32]. Previous studies have shown that ribbon synapses are highly sensitive to noise in the cochlea [33–35]. Here, we found that SS-induced tinnitus did not cause the elevations of hearing threshold or cause loss of cochlear HCs. However, the cochlear ribbon synapses were lost, and the ends of afferent AN fibers near the sites of ribbon synapses were morphologically abnormal. Thus, SS-induced tinnitus with a normal audiogram may be associated with loss of cochlear ribbon synapses.

Kujawa and Liberman found that, after noise exposure, mice exhibited significant reductions in ABR wave I amplitudes, TTS, and loss of cochlear ribbon synapses [15]. However, they did not explore other auditory disorders such as tinnitus. Clinically, Schaette and McAlpine found that ABR wave I amplitudes were reduced in patients with tinnitus who exhibited normal audiograms [18]. But they did not explore damage to cochlear ribbon synapses. Here, it might

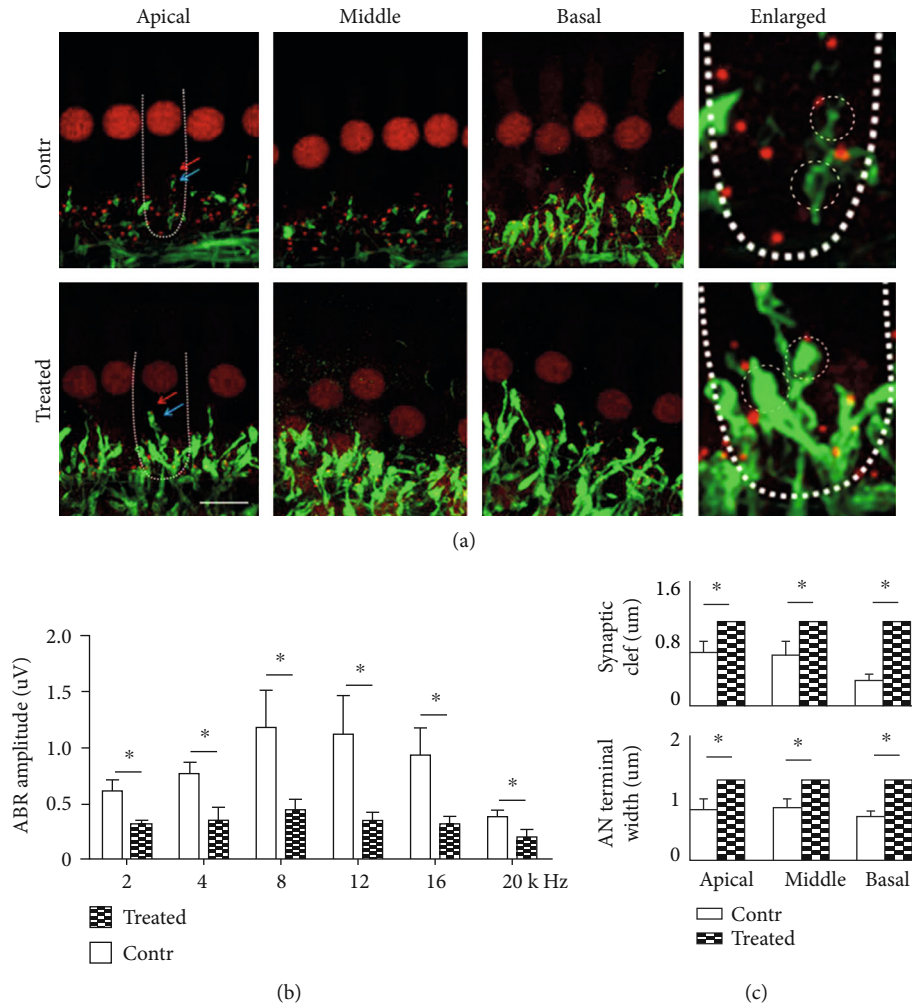


FIGURE 4: SS exposure causes swelling of fiber endings of postsynaptic ANs and amplitude changes in ABR wave I. (a) AN fibers were identified using anti-NF200 (green), and cochlear ribbon synapses were identified using anti-CtBP2 (red, blow inner HCs). Massively swollen AN fiber ends with reduced numbers of CtBP2-expressing puncta were evident in the SS group (compared to control group), as shown by white dashed lines (apical turns, left panel) and in enlargements (white circles, right panel). Bar = 10 μm . (b) ABR wave I amplitudes at 2, 4, 8, 12, 16, and 20 kHz. Amplitudes of ABR wave I were found reduced across all the frequencies above ($p > 0.05$); there were significant differences across frequencies ($p < 0.05$); $n = 8$ in the treated group and $n = 6$ in the control group. (c) Cochlear ribbon synapse morphological properties. Synaptic clef was enlarged after SS treatment; there were significant differences in apical, middle, and basal turns ($p < 0.05$, top). Swelling at the AN terminals was found after SS treatment; there were significant differences in apical, middle, and basal turns ($p < 0.05$, bottom).

be the first time that our study demonstrated the SS-induced tinnitus accompanied by a normal audiogram-featured loss of cochlear ribbon synapse.

Previous studies reported that different dosages of SS exposure can trigger tinnitus [17, 36]. SS-induced hearing threshold shifts are largely dose-dependent. For example, high-level SS exposure (>200 mg/kg) caused hearing impairment in both rats and mice [37, 38] and led to prolonged inner ear damage [39]. On the other hand, lower therapeutic doses of aspirin cause tinnitus but do not disrupt hearing threshold [40], consistent with our finding that a moderate SS dose (200 mg/kg/day) did not cause elevations of ABR thresholds.

Loss or damage of cochlear ribbon synapses will result in auditory disorder, regardless of whether hearing thresholds are affected. Cochlear ribbon synapses encode audi-

tory information via fusion of massive neurotransmitter vesicles to achieve fast and tonic releasing [41, 42]. Synaptic dysfunction may underlie certain neuropsychiatric diseases, including Huntington's disease and autism spectrum disorders [41, 42]. Excessive glutamate release and consequent excitotoxic synaptic disruption contribute to the hearing loss after noise exposure [43]. TTS was found to have permanent loss of ribbon synapses, especially in the high-frequency cochlear region, accompanied by permanent reductions in ABR wave I amplitudes [44]. In this study, we found that ribbon synapse loss and ABR wave I amplitude reduction were both associated with tinnitus. Cochlear ribbon synapse loss is indicated by this type of wave reduction. However, there are other factors affecting ABR wave amplitudes besides cochlear ribbon synapse loss.

Noise exposure causes excessive neurotransmitter release and sodium influx into the postsynaptic terminal of the SGNs, leading SGN nerve (AN nerve) endings to swell. The resulting loss of synaptic connections is irreversible [45]. We found that SS treatment induced considerable loss of inner HC ribbon synapses, similar to that caused by noise exposure [45]. We also deduce that moderate SS exposure induced loss of both cochlear presynapses and postsynapses due to reported researches [31, 46, 47]. Further, we found that AN nerve endings were grossly swollen and no longer communicated with pre-synaptic structures, suggesting that SS exposure may also cause excitotoxicity to synaptic contacts between inner HCs and SGNs, triggering tinnitus. These findings are consistent with those of Zheng, who studied ototoxins that damaged auditory neurons and HCs. SS reduced the number of peripheral SGN neurons in vitro, but did not affect HC numbers. These findings suggest that the initial SS-induced hearing disorder may indicate neuronal dysfunction (e.g., involving afferent synapses) [48]. We infer that morphological changes evident at the ends of AN fibers may also contribute to reduction of ABR wave I amplitudes, which indicate lower cochlear outputs [49]. Tinnitus is presumed to involve both peripheral and central auditory systems. In this study, it may have been caused by damage to cochlear ribbon synapses and AN at an early stage of the peripheral auditory system.

Our study showed that moderate SS doses did not significantly change the numbers of outer or inner HCs, explaining the normal audiogram. It has been shown that moderate doses of SS do not affect auditory sensitivity, but steadily induce tinnitus [40, 50]. Here, we found that damage of cochlear ribbon synapse and AN triggered early-stage tinnitus, combined with a normal audiogram. In previous studies, SS treatment reduced the amplitudes of ABR wave I, consistent with functional loss of cochlear ribbon synapse [32, 50], although if cochlear ribbon synapse number is a time-dependent pattern during tinnitus induction or not was not observed. In summary, we found that loss of cochlear inner HCs ribbon synapses may play important role in the generation of tinnitus following moderate doses of SS. Notably, other factors may contribute. Future studies will focus on SGNs and other elements of auditory processing, as tinnitus is a complicated condition.

Conflicts of Interest

The authors declare no conflict interests.

Authors' Contributions

Wei Zhang and Zhe Peng contributed equally as first authors to this work.

Acknowledgments

This study was supported by the Beijing Science and Technology Commission-Education Commission Joint Fund Project (Grant number KZ201810025040) and the National

Natural Science Foundation of China (Grant Nos. 81500789, 81700917, 81830030, 81770997, and 81771016).

References

- [1] D. Baguley, D. McFerran, and D. Hall, "Tinnitus," *The Lancet*, vol. 382, no. 9904, pp. 1600–1607, 2013.
- [2] K. Ziai, O. Moshtaghi, H. Mahboubi, and H. R. Djalilian, "Tinnitus patients suffering from anxiety and depression: a review," *The International Tinnitus Journal*, vol. 21, no. 1, pp. 68–73, 2017.
- [3] C. A. Bauer, "Tinnitus," *The New England Journal of Medicine*, vol. 378, no. 13, pp. 1224–1231, 2018.
- [4] A. C. Lee and D. A. Godfrey, "Cochlear damage affects neurotransmitter chemistry in the central auditory system," *Frontiers in Neurology*, vol. 5, p. 227, 2014.
- [5] J. Campbell, C. Bean, and A. LaBrec, "Normal hearing young adults with mild tinnitus: reduced inhibition as measured through sensory gating," *Audiology Research*, vol. 8, no. 2, p. 214, 2018.
- [6] M. Jay, H. W. L. Bhatt, and N. Bhattacharyya, "Tinnitus epidemiology: prevalence, severity, exposures and treatment patterns in the United States," *JAMA Otolaryngology Head & Neck Surgery*, vol. 142, p. 7, 2016.
- [7] G. Barnea, J. Attias, S. Gold, and A. Shahar, "Tinnitus with normal hearing sensitivity: extended high-frequency audiometry and auditory-nerve brain-stem-evoked responses," *Audiology*, vol. 29, no. 1, pp. 36–45, 1990.
- [8] T. Qu, Y. Qi, S. Yu et al., "Dynamic changes of functional neuronal activities between the auditory pathway and limbic systems contribute to noise-induced tinnitus with a normal audiogram," *Neuroscience*, vol. 408, pp. 31–45, 2019.
- [9] H. Guest, K. J. Munro, and C. J. Plack, "Tinnitus with a normal audiogram: role of high-frequency sensitivity and reanalysis of brainstem-response measures to avoid audiometric over-matching," *Hearing Research*, vol. 356, pp. 116–117, 2017.
- [10] S. Degeest, H. Keppler, and P. Corthals, "The effect of tinnitus on listening effort in normal-hearing young adults: a preliminary study," *Journal of Speech, Language, and Hearing Research*, vol. 60, no. 4, pp. 1036–1045, 2017.
- [11] J. W. Gu, B. S. Herrmann, R. A. Levine, and J. R. Melcher, "Brainstem auditory evoked potentials suggest a role for the ventral cochlear nucleus in tinnitus," *Journal of the Association for Research in Otolaryngology*, vol. 13, no. 6, pp. 819–833, 2012.
- [12] F. Naomi, G. P. M. Bramhall, F. J. Gallun, and D. Konrad-Martin, "Auditory brainstem response demonstrates that reduced peripheral auditory input is associated with self-report of tinnitus," *The Journal of the Acoustical Society of America*, vol. 146, p. 14, 2019.
- [13] N. F. Bramhall, D. Konrad-Martin, and G. P. McMillan, "Tinnitus and auditory perception after a history of noise exposure: relationship to auditory brainstem response measures," *Ear and Hearing*, vol. 39, no. 5, pp. 881–894, 2018.
- [14] L. Shi, K. Liu, H. Wang et al., "Noise induced reversible changes of cochlear ribbon synapses contribute to temporary hearing loss in mice," *Acta Oto-Laryngologica*, vol. 135, no. 11, pp. 1093–1102, 2015.
- [15] S. G. Kujawa and M. C. Liberman, "Adding insult to injury: cochlear nerve degeneration after "temporary" noise-induced

- hearing loss," *The Journal of Neuroscience*, vol. 29, no. 45, pp. 14077–14085, 2009.
- [16] C. A. Bauer, T. J. Brozoski, and K. Myers, "Primary afferent dendrite degeneration as a cause of tinnitus," *Journal of Neuroscience Research*, vol. 85, no. 7, pp. 1489–1498, 2007.
- [17] L. F. Guanyin Chen, Z. Liu, Y. Sun, H. Chang, and P. Cui, "Both central and peripheral auditory systems are involved in salicylate-induced tinnitus in rats: a behavioral study," *PLoS One*, vol. 9, no. 9, article e108659, 2014.
- [18] R. Schaette and D. McAlpine, "Tinnitus with a normal audiogram: physiological evidence for hidden hearing loss and computational model," *The Journal of Neuroscience*, vol. 31, no. 38, pp. 13452–13457, 2011.
- [19] J. Q. Yan Liu, X. Chen, M. Tang et al., "Critical role of spectrin in hearing development and deafness," *Science Advances*, vol. 5, article eaav7803, 2019.
- [20] J. Qi, Y. Liu, C. Chu et al., "A cytoskeleton structure revealed by super-resolution fluorescence imaging in inner ear hair cells," *Cell Discovery*, vol. 5, no. 1, p. 12, 2019.
- [21] J. Qi, L. Zhang, F. Tan et al., "Espin distribution as revealed by super-resolution microscopy of stereocilia," *American Journal of Translational Research*, vol. 12, pp. 130–141, 2020.
- [22] Z. H. He, S. Y. Zou, M. Li et al., "The nuclear transcription factor FoxG1 affects the sensitivity of mimetic aging hair cells to inflammation by regulating autophagy pathways," *Redox Biology*, vol. 28, article 101364, 2020.
- [23] S. Gao, C. Cheng, M. Wang et al., "Blebbistatin inhibits neomycin-induced apoptosis in hair cell-like HEI-OC-1 cells and in cochlear hair cells," *Frontiers in Cellular Neuroscience*, vol. 13, p. 590, 2020.
- [24] Y. Zhang, W. Li, Z. He et al., "Pre-treatment with fasudil prevents neomycin-induced hair cell damage by reducing the accumulation of reactive oxygen species," *Frontiers in Molecular Neuroscience*, vol. 12, p. 264, 2019.
- [25] W. Liu, X. Xu, Z. Fan et al., "Wnt signaling activates TP53-induced glycolysis and apoptosis regulator and protects against cisplatin-induced spiral ganglion neuron damage in the mouse cochlea," *Antioxidants & Redox Signaling*, vol. 30, no. 11, pp. 1389–1410, 2019.
- [26] S. Zhang, Y. Zhang, Y. Dong et al., "Knockdown of Foxg1 in supporting cells increases the trans-differentiation of supporting cells into hair cells in the neonatal mouse cochlea," *Cellular and Molecular Life Sciences*, vol. 77, no. 7, pp. 1401–1419, 2020.
- [27] F. Tan, C. Chu, J. Qi et al., "AAV-ie enables safe and efficient gene transfer to inner ear cells," *Nature Communications*, vol. 10, no. 1, p. 3733, 2019.
- [28] Z. He, L. Guo, Y. Shu et al., "Autophagy protects auditory hair cells against neomycin-induced damage," *Autophagy*, vol. 13, no. 11, pp. 1884–1904, 2017.
- [29] Z. He, Q. Fang, H. Li et al., "The role of FOXG1 in the postnatal development and survival of mouse cochlear hair cells," *Neuropharmacology*, vol. 144, pp. 43–57, 2019.
- [30] G. Matthews and P. Fuchs, "The diverse roles of ribbon synapses in sensory neurotransmission," *Nature Reviews Neuroscience*, vol. 11, no. 12, pp. 812–822, 2010.
- [31] T. M. Coate, M. K. Scott, and M. Gurjar, "Current concepts in cochlear ribbon synapse formation," *Synapse*, vol. 73, no. 5, article e22087, 2019.
- [32] J. D. Goutman, "Mechanisms of synaptic depression at the hair cell ribbon synapse that support auditory nerve function," *Proceedings of the National Academy of Sciences of the United States of America*, vol. 114, no. 36, pp. 9719–9724, 2017.
- [33] J. Wang, S. Yin, H. Chen, and L. Shi, "Noise-induced cochlear synaptopathy and ribbon synapse regeneration: repair process and therapeutic target," *Advances in Experimental Medicine and Biology*, vol. 1130, pp. 37–57, 2019.
- [34] Y. Luo, T. Qu, Q. Song et al., "Repeated moderate sound exposure causes accumulated trauma to cochlear ribbon synapses in mice," *Neuroscience*, vol. 429, pp. 173–184, 2020.
- [35] K. A. Fernandez, D. Guo, S. Micucci, V. de Gruttola, M. C. Liberman, and S. G. Kujawa, "Noise-induced cochlear synaptopathy with and without sensory cell loss," *Neuroscience*, vol. 427, pp. 43–57, 2020.
- [36] A. Sheppard ShH, G.-d. Chen, M. Ralli, and R. Salvi, "Review of salicylate induced hearing loss neurotoxicity tinnitus and neuropathophysiology," *Acta Otorhinolaryngologica Italica*, vol. 34, pp. 79–93, 2014.
- [37] C. Jiang, B. Luo, S. Manohar, G. D. Chen, and R. Salvi, "Plastic changes along auditory pathway during salicylate-induced ototoxicity: hyperactivity and CF shifts," *Hearing Research*, vol. 347, pp. 28–40, 2017.
- [38] H. Yu, K. Vikhe Patil, C. Han et al., "GLAST deficiency in mice exacerbates gap detection deficits in a model of salicylate-induced tinnitus," *Frontiers in Behavioral Neuroscience*, vol. 10, p. 158, 2016.
- [39] G. D. Chen, D. Stolzberg, E. Lobarinas, W. Sun, D. Ding, and R. Salvi, "Salicylate-induced cochlear impairments, cortical hyperactivity and re-tuning, and tinnitus," *Hearing Research*, vol. 295, pp. 100–113, 2013.
- [40] J. J. Eggermont, "Tinnitus: neurobiological substrates," *Drug Discovery Today*, vol. 10, no. 19, pp. 1283–1290, 2005.
- [41] R. Toro, M. Konyukh, R. Delorme et al., "Key role for gene dosage and synaptic homeostasis in autism spectrum disorders," *Trends in Genetics*, vol. 26, no. 8, pp. 363–372, 2010.
- [42] T. Bourgeron, "A synaptic trek to autism," *Current Opinion in Neurobiology*, vol. 19, no. 2, pp. 231–234, 2009.
- [43] R. William and M. J. M. Henry, "Afferent synaptic changes in auditory hair cells during noise-induced temporary threshold shift," *Hearing Research*, vol. 84, no. 1-2, pp. 81–90, 1995.
- [44] L. Rüttiger, W. Singer, R. Panford-Walsh et al., "The reduced cochlear output and the failure to adapt the central auditory response causes tinnitus in noise exposed rats," *PLoS One*, vol. 8, no. 3, article e57247, 2013.
- [45] D. Y. Wang, Y. C. Wang, D. Weil et al., "Screening mutations of OTOFgene in Chinese patients with auditory neuropathy, including a familial case of temperature-sensitive auditory neuropathy," *BMC Medical Genetics*, vol. 11, no. 1, p. 79, 2010.
- [46] W. Xiong, W. Wei, Y. Qi et al., "Autophagy is required for remodeling in postnatal developing ribbon synapses of cochlear inner hair cells," *Neuroscience*, vol. 431, pp. 1–16, 2020.
- [47] L. Yang, D. S. Chen, T. F. Qu et al., "Maximal number of pre-synaptic ribbons are formed in cochlear region corresponding to middle frequency in mice," *Acta Oto-Laryngologica*, vol. 138, pp. 25–30, 2018.
- [48] J. L. Zheng and W.-Q. Gao, "Differential damage to auditory neurons and hair cells by ototoxins and neuroprotection by specific neurotrophins in rat cochlear organotypic cultures," *European Journal of Neuroscience*, vol. 8, pp. 1897–1905, 1996.

- [49] S. Konadath and P. Manjula, "Auditory brainstem response and late latency response in individuals with tinnitus having normal hearing," *Intractable & Rare Diseases Research*, vol. 5, no. 4, pp. 262–268, 2016.
- [50] G.-D. Chen, M. H. Kermany, A. D'Elia et al., "Too much of a good thing: long-term treatment with salicylate strengthens outer hair cell function but impairs auditory neural activity," *Hearing Research*, vol. 265, no. 1-2, pp. 63–69, 2010.

Research Article

Alternative Splicing of *Cdh23* Exon 68 Is Regulated by RBM24, RBM38, and PTBP1

Nana Li,¹ Haibo Du,¹ Rui Ren,¹ Yanfei Wang,¹ and Zhigang Xu^{1,2} 

¹Shandong Provincial Key Laboratory of Animal Cell and Developmental Biology, School of Life Sciences, Shandong University, Qingdao, Shandong Province, China

²Shandong Provincial Collaborative Innovation Center of Cell Biology, Shandong Normal University, Jinan, Shandong Province, China

Correspondence should be addressed to Zhigang Xu; xuzg@sdu.edu.cn

Received 7 April 2020; Revised 19 June 2020; Accepted 1 July 2020; Published 25 July 2020

Academic Editor: Jian Wang

Copyright © 2020 Nana Li et al. This is an open access article distributed under the Creative Commons Attribution License, which permits unrestricted use, distribution, and reproduction in any medium, provided the original work is properly cited.

Alternative splicing plays a pivotal role in modulating the function of eukaryotic proteins. In the inner ear, many genes undergo alternative splicing, and errors in this process lead to hearing loss. Cadherin 23 (CDH23) forms part of the so-called tip links, which are indispensable for mechano-electrical transduction (MET) in the hair cells. *Cdh23* gene contains 69 exons, and exon 68 is subjected to alternative splicing. Exon 68 of the *Cdh23* gene is spliced into its mRNA only in a few cell types including hair cells. The mechanism responsible for the alternative splicing of *Cdh23* exon 68 remains elusive. In the present work, we performed a cell-based screening to look for splicing factors that regulate the splicing of *Cdh23* exon 68. RBM24 and RBM38 were identified to enhance the inclusion of *Cdh23* exon 68. The splicing of *Cdh23* exon 68 is affected in *Rbm24* knockdown or knockout cells. Moreover, we also found that PTBP1 inhibits the inclusion of *Cdh23* exon 68. Taken together, we show here that alternative splicing of *Cdh23* exon 68 is regulated by RBM24, RBM38, and PTBP1.

1. Introduction

In eukaryotic cells, the exons of precursor mRNAs (pre-mRNAs) are spliced together by a large protein complex named spliceosome to give rise to mature mRNAs [1]. Many genes undergo alternative splicing, which results in distinct mature mRNAs through splicing different exons together [2]. In this way, alternative splicing helps to produce structurally and functionally similar but not identical protein isoforms, hence contributing to proteomic diversity [3]. Tissue-specific alternative splicing also contributes to tissue specificity. Alternative splicing is regulated by specific RNA sequences and related RNA-binding proteins [2]. The RNA sequences that regulate alternative splicing are divided into different classes according to their position and function, namely, exonic splicing enhancers (ESEs), exonic splicing silencers (ESSs), intronic splicing enhancers (ISEs), and intronic splicing silencers (ISSs), which are bound by different splicing regulators [2]. Tissue-specific alternative splicing

is thought to be regulated mainly by differentially expressed splicing regulators [4, 5].

In the inner ear, many important genes have been shown to undergo alternative splicing, and dysregulation of this process causes syndromic or nonsyndromic hearing loss [6]. Cadherin 23 (CDH23) is an atypical cadherin, forming part of the so-called tip links that play a pivotal role in mechano-electrical transduction (MET) in the hair cells [7–10]. Mouse *Cdh23* gene contains 69 exons, and exon 68 is subjected to alternative splicing [11]. Interestingly, the inclusion of *Cdh23* exon 68 is only detected in the inner ear so far [8, 12, 13]. *Cdh23* exon 68 is 105 base pair (bp) long, which encodes 35 amino acids (aa) in the cytoplasmic domain of CDH23. The exon 68-encoded peptide shows no homology to any known proteins and might affect the conformation as well as protein-protein interactions of CDH23 [12–16]. At present, the mechanism responsible for the inner ear-specific alternative splicing of *Cdh23* exon 68 is still unknown.

In the present work, we performed a cell-based screening in order to identify the splicing factors that regulate the alternative splicing of *Cdh23* exon 68. The screening identified RBM24 and RBM38 that enhance the inclusion of *Cdh23* exon 68. Moreover, we also identified PTBP1 that inhibits the inclusion of *Cdh23* exon 68 through bioinformatics analysis. Our data suggest that RBM24, RBM38, and PTBP1 together regulate the alternative splicing of *Cdh23* exon 68.

2. Materials and Methods

2.1. Reverse Transcription-Polymerase Chain Reaction (RT-PCR). Total RNA from different mouse tissues or cultured cells was extracted using TRIzol reagent (Invitrogen) according to the manufacturer's protocol. Briefly, 1 μ g RNA was used for reverse transcription (RT) using PrimeScript RT Reagent Kit with gDNA Eraser (Takara, RR047A). Polymerase chain reaction (PCR) was then performed using the cDNA as template with the following primers: mouse *Esrp1* forward 5'-CAATATTGCCAAGGGTGGCG-3', reverse 5'-CTCATGCGCAGCATGACTTG-3'; mouse *Rbm24* forward 5'-GAGACATCGAGGAAGCGGTG-3', reverse 5'-TCTGGATAAGGCTGGGTGA-3'; mouse *Rbm38* forward 5'-ATGGCAGATCGGGCAGC-3', reverse 5'-AGCCCGTCTGTAAGCTCCTA-3'; mouse *Ptbp1* forward 5'-AGTGCGCATTACACTGTCCA-3', reverse 5'-CTTGAGGTCGTCTCTGACA-3'; mouse *Ptbp2* forward 5'-GCAGAAGAGGATCTGCGAAC-3', reverse 5'-CATCTTCATCTCCCGTGCTT-3'; mouse β -actin forward 5'-CGTTGACATCCGTAAGACC-3', reverse 5'-AACAGTCCGCTAGAAGCAC-3'; mouse *Cdh23* forward 5'-GACAACATCGCCAAGCTG-3', reverse (for minigene) 5'-GGCCAGCAGTGTGCC-3'; reverse (for endogenous *Cdh23*) 5'-GCAAGCTGTTGAGATCAGTGG-3'; and rat *Cdh23* forward 5'-TGGAACCTTTGGACGTGAGC-3', reverse 5'-GCTTGTGTCGAAACGGAGG-3'. For different PCR reactions, 23–40 cycles were used and the annealing temperatures were adjusted between 56 and 64°C to obtain the optimal sensitivity and specificity.

2.2. DNA Constructs. The genomic DNA ranging from exon 67 to exon 69 of mouse *Cdh23* gene was PCR amplified and inserted into pmCherry-N1 vector to construct *Cdh23* minigene reporter. Mutation or deletion was introduced into the minigene through overlapping PCR-mediated site-directed mutagenesis. The cDNAs encoding various mouse splicing factors were inserted into pEGFP-C2 or pEGFP-N2 to express GFP-fusion proteins.

2.3. Splicing Factor Screening. COS7 cells were transfected with the *Cdh23* minigene reporter and vectors expressing different splicing factors using LipoMax (Sudgen) in 24-well plates. Forty-eight hours after transfection, cells were washed with PBS and fixed with 4% paraformaldehyde (PFA) in PBS for 15 minutes. Fluorescence was detected using a confocal microscope (LSM 700, Zeiss). ImageJ software was used to quantify the intensity of fluorescence.

2.4. RNA Interference and Quantitative Real-Time PCR (qPCR). Chemically synthesized siRNAs were obtained from Sigma-Aldrich, and their sequences are as follows: siRNA-1, 5'-GCAAUAUGUAGCUUGAAUUDtT-3'; siRNA-2, 5'-CUUAAGGCCUAUAGAACUUDtT-3'; siRNA-3, 5'-CCCAAAGAGCCUGAGUAAAdTt-3'; and control siRNA, 5'-UUCUCCGAACGUGUCACGUTT-3'. COS7 cells were transfected with siRNAs using jetPRIME transfection reagent (Polyplus) in 12-well plates. Twenty-four hours after transfection, the *Cdh23* minigene reporter was transfected into the same cells using LipoMax transfection reagents. Cells were cultured for another twenty-four hours, and RNA was extracted and reversed transcribed as described above. qPCR was then performed with SYBR Premix Ex Taq (Takara, RR420A) and the QuantGene 9600 real-time system (Bioer). Sequences of primers used in the qPCR reactions are as follows: monkey *Rbm24* forward 5'-AGATCGAGGAGGCGGTGGTC-3', reverse 5'-TCTTTGTATAAGGGCTGGATGAAG-3'; mouse *Cdh23(+68)* forward 5'-AACTCTTTCACAACGGATG-3', reverse 5'-ATGGGTGGCTTGTGTCCG-3'; and monkey β -actin forward 5'-CGTGGACATCCGCAAAGACC-3', reverse 5'-CACAGTCCGCTAGAAGCA-3'.

2.5. RNA Immunoprecipitation (RIP). RIP analysis was carried out according to the standard procedure with modifications [17]. Briefly, COS7 cells were transfected with expression vectors of Myc-tagged splicing factors as well as the *Cdh23* minigene. Forty-eight hours after transfection, cells were lysed in lysis buffer containing 100 mM KCl, 5 mM MgCl₂, 10 mM HEPES-NaOH, 0.5% NP-40, 1 mM DTT, 200 units/ml RNase inhibitor (Takara, 2313A), and EDTA-free protease inhibitor cocktail (Sigma, S8830). After centrifugation at 4°C, the supernatant was collected and incubated with immobilized anti-Myc antibody (Sigma-Aldrich, Cat. No. E6654) at 4°C for 3 hours. The immunoprecipitated RNA was then used as template for RT-PCR and qPCR analysis. Primers used are as follows: mouse *Cdh23* pre-mRNA forward 5'-CAGCAGCCTAAGTGGGAAG-3' and reverse 5'-AGTCCCGAGGCTACCTC-3'.

2.6. Western Blot. COS7 cells were transfected with expression vectors in 6-well plates. Forty-eight hours after transfection, cells were washed with PBS and lysed in ice-cold lysis buffer containing 150 mM NaCl, 50 mM Tris at pH 7.5, 1% Triton X-100, and 1 mM PMSF. After centrifugation at 4°C, the supernatant was collected and separated by 10% polyacrylamide gel electrophoresis (PAGE), then transferred to PVDF membrane. The membrane was blocked in 5% nonfat milk for an hour at room temperature, then incubated with anti-GFP antibody (ABclonal, AE012) at 4°C overnight, followed by incubation with HRP-conjugated secondary antibody (Bio-Rad, 170-6516) for an hour at room temperature. The signals were detected with the ECL system (Cell Signaling Technology).

2.7. Animals. All animal experiments were approved by the Ethics Committee of Shandong University School of Life

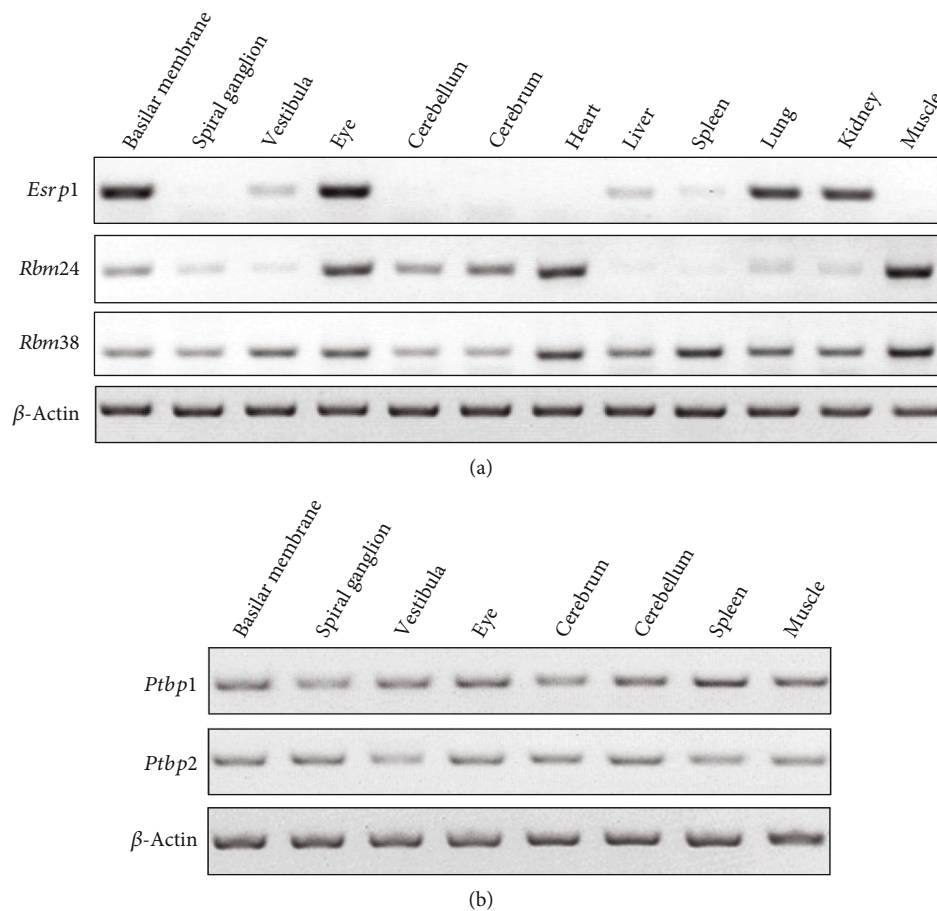


FIGURE 1: Expression of various splicing regulators in different mouse tissues. RT-PCR analysis was performed to examine the expression of splicing regulators in different tissues of P10 C57BL/6 mice. (a) Expression of *Esrp1*, *Rbm24*, and *Rbm38* was examined by RT-PCR. (b) Expression of *Ptbp1* and *Ptbp2* was examined by RT-PCR. β -Actin was used as internal control.

Sciences and conducted accordingly. Construction of *Atoh1-cre*; *Rbm24^{fllox/fllox}* mice is described elsewhere.

2.8. Statistical Analysis. Each experiment was repeated at least three times. Student's *t*-test was used to determine the statistical significance, and $p < 0.05$ was considered statistically significant. For alternative splicing events, data were shown as means \pm SEM.

3. Results

3.1. Screening Splicing Factors That Regulate the Alternative Splicing of *Cdh23* Exon 68. To identify splicing factors that regulate the inner ear-specific alternative splicing of *Cdh23* exon 68, we started with testing the known splicing factors that are expressed in the inner ear. Splicing factors SRRM4, SFSWAP, and ESRP1 play important roles in the inner ear, albeit none of them has been shown to regulate the alternative splicing of *Cdh23* exon 68 [18–20]. We previously showed that deafness-related protein ILDR1 and its homolog ILDR2 regulate alternative splicing through binding to splicing factors TRA2A, TRA2B, and SRSF1 [21]. We also found that RNA-binding protein RBM24 is specifically expressed in the hair cells [22]. The expression of these splicing factors in

the inner ear is confirmed by performing RT-PCR (Figure 1(a), data not shown). These splicing factors are used as the candidates for the following screening.

A *Cdh23* minigene reporter was constructed by fusing mouse *Cdh23* genomic sequence ranging from exon 67 to exon 69 in frame with a mCherry-encoding sequence whose expression is driven by a CMV promoter (Figure 2(a)). To facilitate the screening, we introduced a single base pair insertion in exon 68 and a single base pair deletion in exon 69. When exon 68 is included in the mature mRNA, the insertion and deletion cancel each other out and a mCherry fusion protein is expressed. However, when exon 68 is not included in the mature mRNA, the single base pair deletion in exon 69 will cause a frameshift and mCherry fusion protein will not be expressed (Figure 2(a)). This minigene was then used as the reporter to screen splicing factors that regulate the alternative splicing of *Cdh23* exon 68.

COS7 cells were transfected with the *Cdh23* minigene reporter and vectors that express different candidate splicing factors fused with GFP. Among all the splicing factors tested, RBM24 and its homolog RBM38 result in robust mCherry fluorescence (Figure 2(b)). Quantification of the red fluorescence using ImageJ shows significant increases in RBM24- or RBM38-expressing cells, but not in cells expressing other

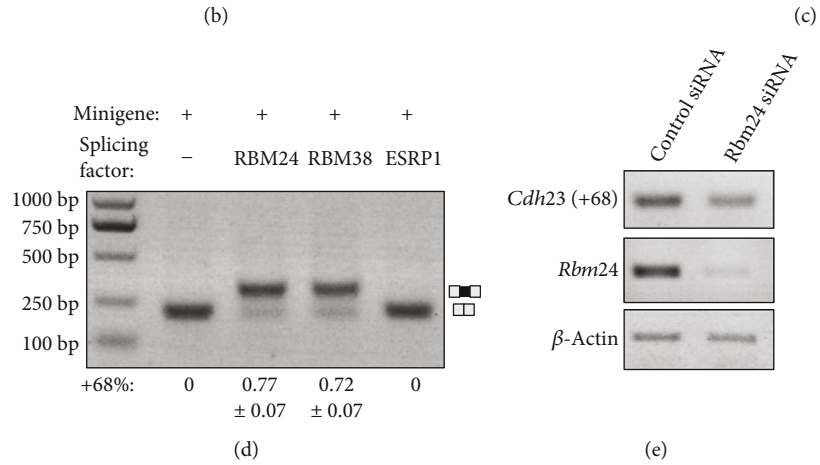
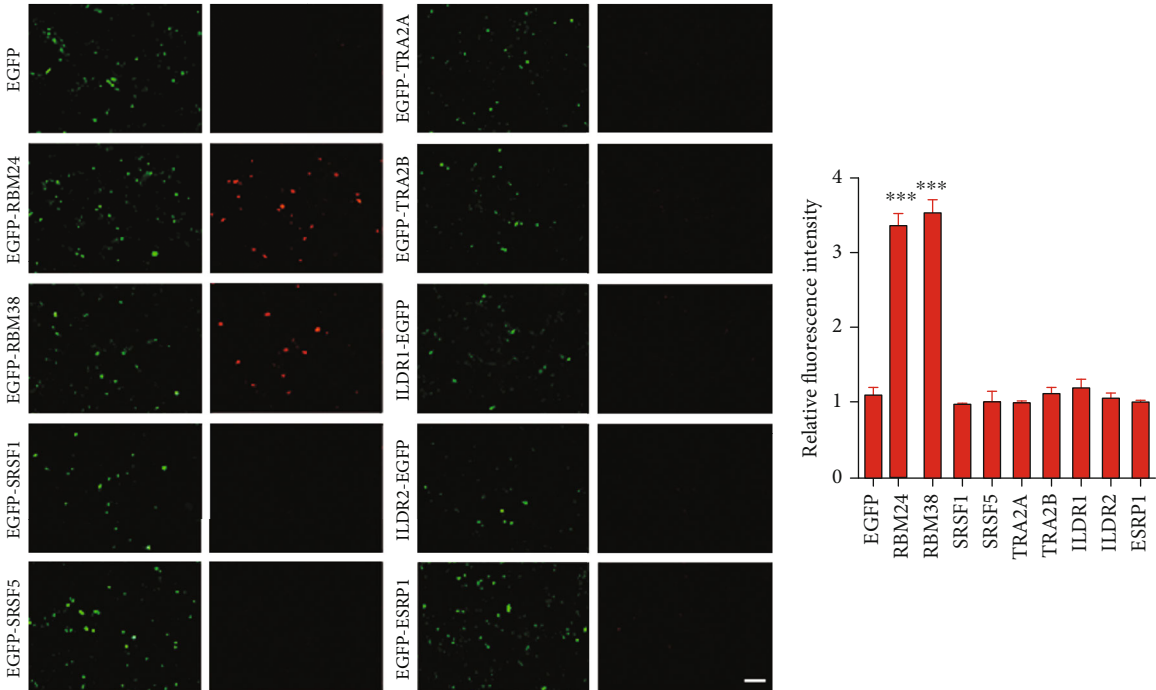
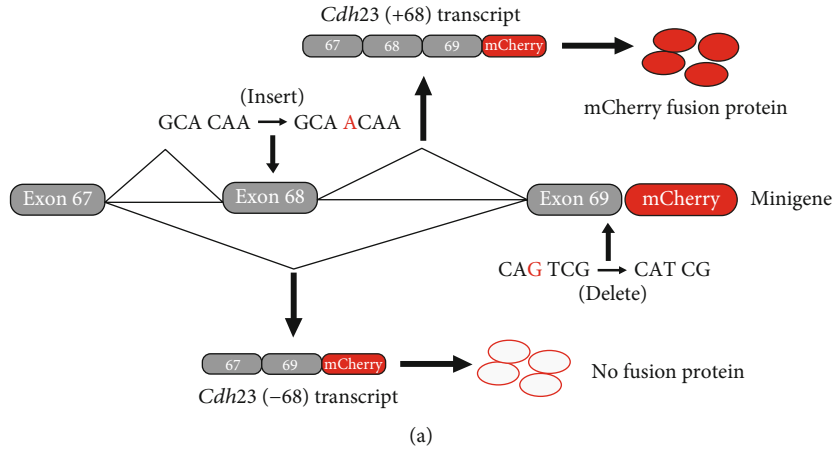


FIGURE 2: Continued.

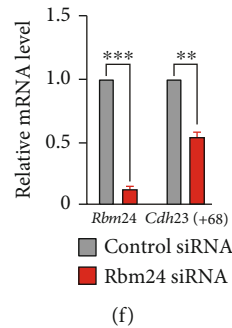


FIGURE 2: Screening splicing factors that regulate *Cdh23* exon68 inclusion. (a) Schematic drawing of the screening strategy. The *Cdh23* minigene reporter was constructed by fusing mouse *Cdh23* genomic sequence ranging from exon 67 to exon 69 in frame with a mCherry-encoding sequence. A single base pair insertion in exon 68 and a single base pair deletion in exon 69 introduced in the minigene are indicated in red. When exon 68 is included in the mature mRNA, a mCherry fusion protein is expressed. In contrast, when exon 68 is not included in the mature mRNA, the single base pair deletion in exon 69 will cause a frameshift and mCherry fusion protein will not be expressed. (b) The *Cdh23* minigene and various splicing factors were overexpressed in COS7 cells, and the resultant fluorescence was examined using a confocal microscope. Scale bar, 200 μm . (c) The relative mCherry fluorescence intensity from (b) was analyzed using ImageJ software. (d) The *Cdh23* minigene and various splicing factors were overexpressed in COS7 cells, and RT-PCR was performed to examine the inclusion of exon 68. (e, f) The *Cdh23* minigene and either *Rbm24* or control siRNAs were transfected into COS7 cells, and the expression level of *Rbm24* and *Cdh23(+68)* was examined by performing RT-PCR (e) and qPCR (f). β -Actin was used as internal control. * $p < 0.05$, ** $p < 0.01$, and *** $p < 0.001$.

splicing factors (Figure 2(c)). This result suggests that RBM24 and RBM38 are able to promote *Cdh23* exon 68 inclusion.

3.2. RBM24 and RBM38 Enhance the Inclusion of *Cdh23* Exon 68. RT-PCR was then performed to confirm the screening result. The *Cdh23* minigene was expressed in COS7 cells together with RBM24, RBM38, ESRP1, or an empty vector. RT-PCR reveals that exon 68 inclusion is not detectable in mature *Cdh23* mRNA in control cells transfected with an empty vector or ESRP1. However, exon 68 inclusion is significantly enhanced by either RBM24 or RBM38 overexpression (Figure 2(d)).

Small interfering RNAs (siRNAs) were then used to knock down the expression of endogenous *Rbm24* in COS7 cells. All three siRNAs tested inhibit *Rbm24* expression efficiently (Figures 2(e) and 2(f), data not shown). Without overexpressing the splicing enhancers, exon 68 inclusion from *Cdh23* minigene is too weak to be detected with regular RT-PCR (Figure 2(d)), possibly because of the relatively low expression level of endogenous splicing enhancers in COS7 cells. We then used primers specific for *Cdh23(+68)* isoform to examine the inclusion of exon 68. RT-PCR and qPCR results show that *Cdh23(+68)* expression level is significantly decreased by *Rbm24* knockdown (Figures 2(e) and 2(f)). Taken together, both overexpression and knockdown experiments confirm that RBM24/RBM38 could regulate the alternative splicing of *Cdh23* exon 68.

RBM24 and RBM38 have been shown to regulate alternative splicing through binding to a GUGUG motif in the ISEs [23, 24]. There are two potential GTGTG motifs located in intron 68 of the *Cdh23* gene. Motif 1 (TGTGTG) is located 30 bp downstream of *Cdh23* exon 68, while motif 2 (GTGTGGT) is located 630 bp downstream of exon 68 (Figure 3(a)). We examined whether these motifs are involved in the alternative splicing of *Cdh23* exon 68 through deleting either of them in the minigene. Both fluorescence

assay and RT-PCR results show that exon 68 inclusion enhancement by RBM24/RBM38 is completely abolished by the deletion of motif 1 but not motif 2 (Figures 3(b) and 3(c)), indicating that motif 1 is required for RBM24/RBM38-regulated inclusion of *Cdh23* exon 68.

RNA immunoprecipitation (RIP) was then performed to examine the physical interaction of RBM24/RBM38 with *Cdh23* pre-mRNA. RT-PCR results show that *Cdh23* pre-mRNA is readily coimmunoprecipitated with RBM24 or RBM38, which is significantly reduced by deletion of motif 1 but not motif 2 (Figures 3(d) and 3(f)). Similar results were obtained by performing qPCR (Figures 3(e) and 3(g)). Taken together, our present data suggest that RNA-binding proteins RBM24 and RBM38 enhance the inclusion of *Cdh23* exon 68 through binding to an ISE motif (UGUGUG).

3.3. PTBP1 Inhibits the Inclusion of *Cdh23* Exon 68. Next, we want to know how ubiquitously expressed RBM24/RBM38 drives tissue-specific alternative splicing of *Cdh23* exon 68. It has been suggested that most alternative-spliced exons are under combinatorial regulation by both splicing enhancers and repressors [25]. Therefore, RBM24-/RBM38-mediated inclusion of exon 68 in some tissues might be counteracted by yet unknown splicing repressor(s). Bioinformatics analysis suggests a potential ESS motif TCTT in *Cdh23* exon 68, which might be recognized by splicing suppressor PTBP1 (Figure 4(a)) [26]. Consistently, when overexpressed in COS7 cells, PTBP1 inhibits RBM24- or RBM38-mediated inclusion of exon 68, albeit the inhibitory effect is not very robust (Figure 4(b)). We then mutated the weak splice donor site located at the exon 68/intron 68 boundary into an artificial strong donor site, which leads to constitutive exon 68 inclusion (Figure 4(c)). When *Cdh23* minigene with this donor site mutation is used, more robust inhibition of exon 68 inclusion by PTBP1 is observed (Figure 4(c)). PTBP2 is a homolog of PTBP1 that recognizes similar binding motifs

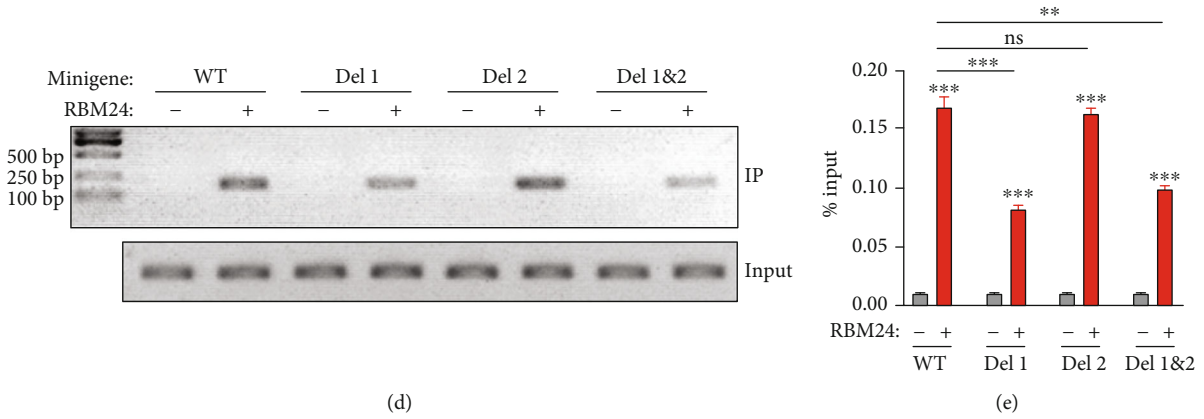
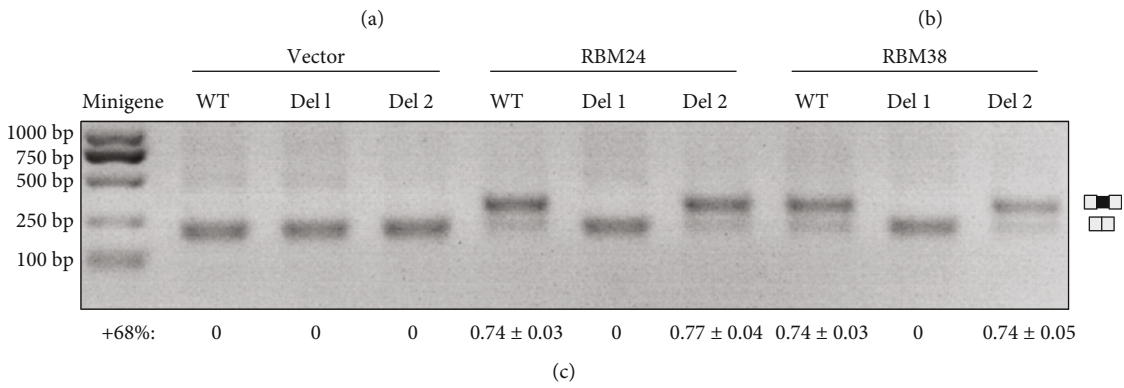
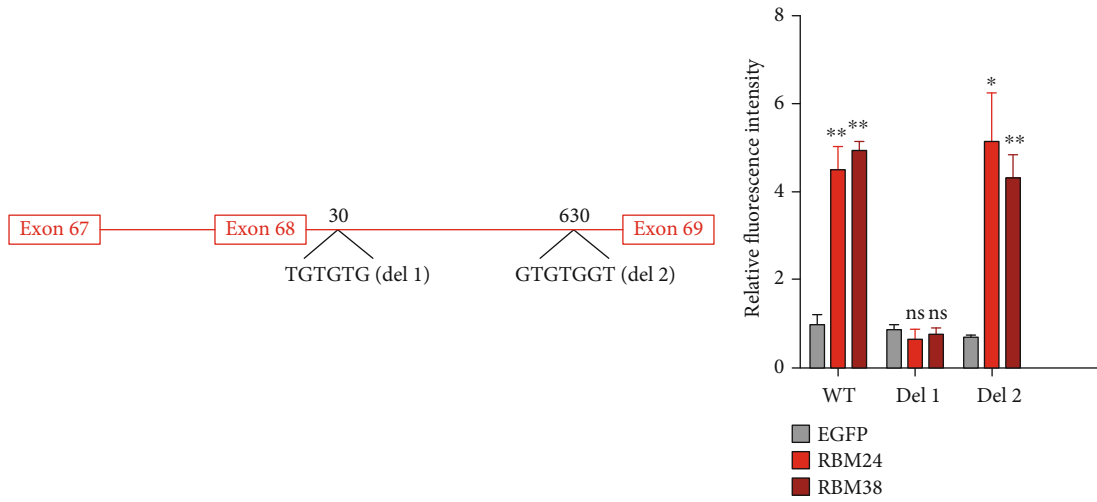


FIGURE 3: Continued.

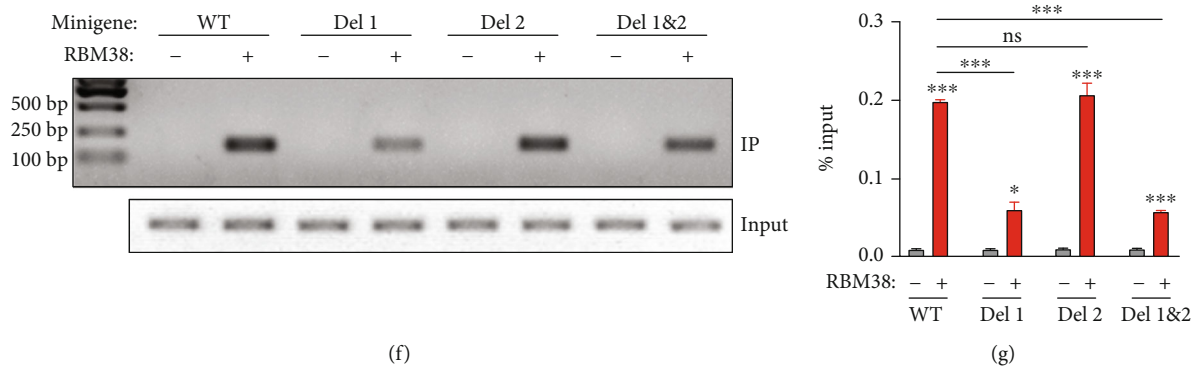


FIGURE 3: An ISE is required for RBM24-/RBM38-mediated *Cdh23* exon 68 inclusion. (a) Schematic drawing of the locations of the two potential RBM24/RBM38-binding ISEs. (b) Wild-type *Cdh23* minigene or mutants with deletion of the potential RBM24/RBM38-binding ISE were expressed together with RBM24 or RBM38 in COS7 cells. The mCherry fluorescence was examined using a confocal microscope and analyzed using ImageJ software. (c) Wild-type *Cdh23* minigene or mutants with deletion of the potential RBM24/RBM38-binding ISE were expressed together with RBM24 or RBM38 in COS7 cells, and the inclusion of exon 68 in the mature *Cdh23* mRNA was examined by performing RT-PCR. (d–g) Wild-type *Cdh23* minigene or mutants with deletion of the potential RBM24/RBM38-binding ISE were expressed together with RBM24 or RBM38 in COS7 cells. Binding of RBM24/RBM38 with *Cdh23* pre-mRNA was examined by performing native RIP followed by RT-PCR (d, f) or qPCR (e, g). Error bars represent mean \pm SEM from triplicate experiments. * $p < 0.05$, ** $p < 0.01$, and *** $p < 0.001$.

[26], and RT-PCR results reveal that both *Ptbp1* and *Ptbp2* transcripts are expressed in the inner ear (Figure 1(b)). However, our present data suggest that PTBP2 inhibits *Cdh23* exon 68 inclusion to a much lesser extent if any compared with PTBP1 (Figure 4(c)).

To mimic the various PTBP1 expression levels in different tissues, we overexpressed PTBP1 in COS7 cells in an increasing gradient. The results show that RBM24-mediated exon 68 inclusion is inhibited by PTBP1 in a dosage-dependent manner (Figure 4(d)). Lastly, we mutated the potential PTBP1-binding site TCTT in exon 68 to GCGC in the presence of the donor site mutation. The results show that the TCTT to GCGC mutation abolishes the inhibitory effect of PTBP1 on exon 68 inclusion (Figure 4(e)). Consistently, the TCTT to GCGC mutation also significantly reduces the binding of *Cdh23* pre-mRNA to PTBP1 revealed by RIP experiment (Figures 4(f) and 4(g)). Taken together, our present data suggest that PTBP1 inhibits *Cdh23* exon 68 inclusion through binding to an ESS motif (UCUU).

3.4. RBM24 Regulates the Alternative Splicing of Endogenous *Cdh23* Exon 68. The results discussed above are all obtained using the artificially constructed *Cdh23* minigene. We then used the inner ear cell line HEI-OC-1 to investigate the alternative splicing of endogenous *Cdh23* mRNA. RT-PCR results show that *Cdh23*(-68) is the main splicing isoform expressed in HEI-OC-1 (Figure 5(a)). When RBM24 or RBM38 is overexpressed, *Cdh23*(+68) expression level is significantly increased, suggesting that RBM24 and RBM38 could enhance endogenous *Cdh23* exon68 inclusion (Figure 5(a)).

Lastly, RBM24-mediated alternative splicing of *Cdh23* exon 68 in the inner ear was examined using *Rbm24* knockout mice. *Rbm24* conventional knockout mice die between embryonic day 12.5 (E12.5) and E14.5 because of cardiac problems [24]. In the present work, we used *Rbm24* conditional knockout (cko) mice that disrupt *Rbm24* gene expres-

sion in the hair cells. To do so, *Rbm24*^{loxP/loxP} mice are crossed with *Atoh1-cre* mice that express Cre recombinase in the developing cochlear hair cells from E14.5 [27]. RT-PCR results show that *Cdh23* exon 68 inclusion is significantly decreased in the inner ear of *Rbm24* cko mice compared with that of control mice (Figure 5(b)), suggesting that RBM24 is required for *Cdh23* exon 68 inclusion *in vivo*.

4. Discussion

Cdh23 exon 68 is subjected to alternative splicing, and *Cdh23*(+68) is preferentially expressed in the inner ear [8, 11–13]. The underlying mechanism for this inner ear-specific alternative splicing of *Cdh23* exon 68 remained unknown. In the present work, we show that the alternative splicing of *Cdh23* exon 68 is regulated by RBM24, RBM38, and PTBP1. RBM24 and RBM38 promote the inclusion of *Cdh23* exon 68, whereas PTBP1 inhibits it.

Several lines of evidences support our conclusion. First, overexpression of RBM24 or RBM38 enhances exon 68 inclusion of the *Cdh23* minigene, while overexpression of PTBP1 inhibits it. Second, mutations of the potential binding sites of RBM24, RBM38, or PTBP1 in the *Cdh23* minigene affect exon 68 inclusion. Third, RIP experiments show that RBM24, RBM38, and PTBP1 bind *Cdh23* pre-mRNA, which is affected by mutations of their potential binding sites. Fourth, knockdown of *Rbm24* expression with siRNAs decreases exon 68 inclusion of the *Cdh23* minigene. Fifth, overexpression of RBM24 or RBM38 promotes exon 68 inclusion of endogenous *Cdh23* in HEI-OC-1 cells. Last, inclusion of *Cdh23* exon 68 is reduced in the inner ear of *Rbm24* cko mice.

There are two potential RBM24/RBM38-binding ISEs downstream of exon 68, and our data suggest that mutation of site 1 but not site 2 affects the alternative splicing of *Cdh23* exon 68. Alignments of genomic sequences flanking

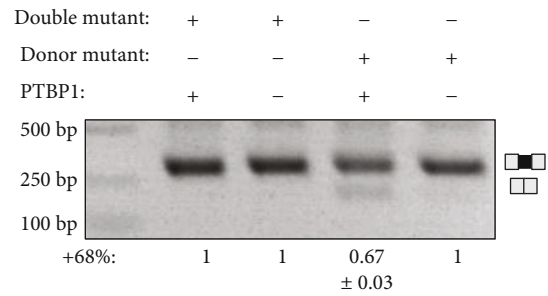
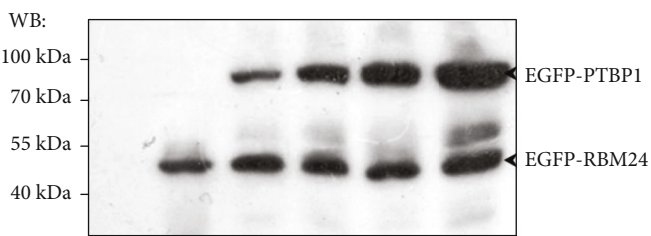
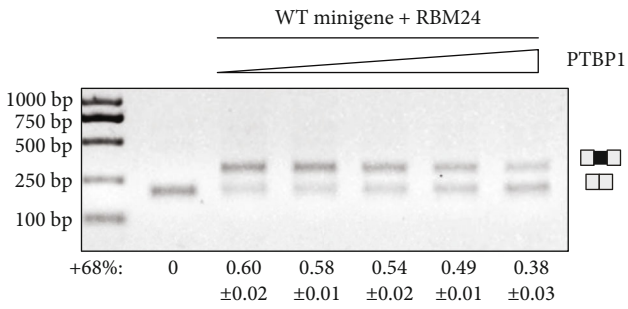
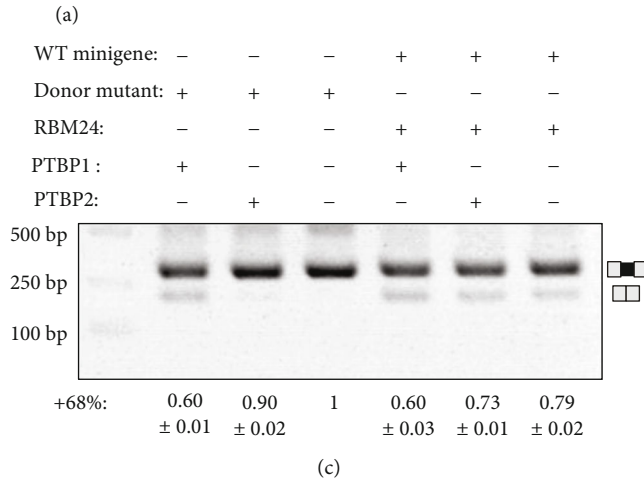
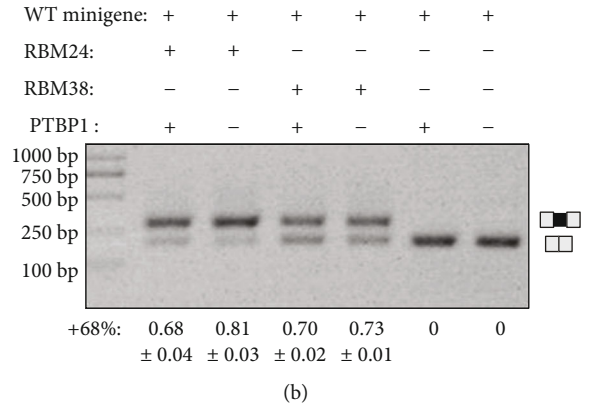
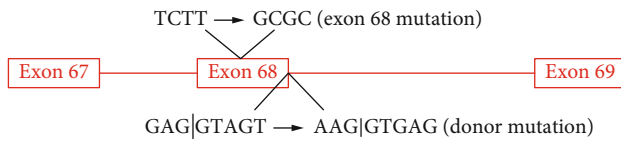


FIGURE 4: Continued.

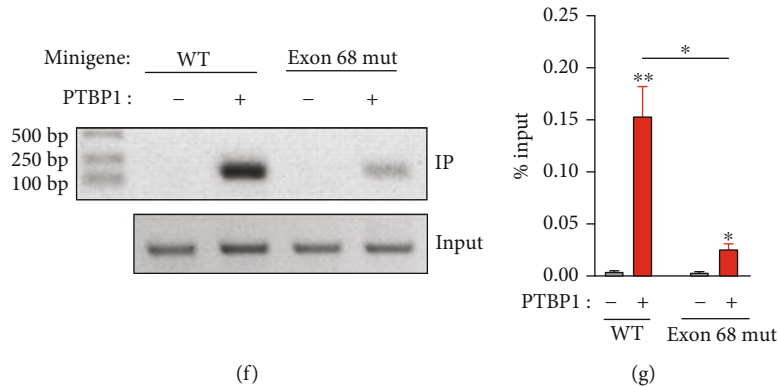


FIGURE 4: An ESS is required for PTBP1-mediated inhibition of *Cdh23* exon 68 inclusion. (a) Schematic drawing of the location of the potential PTBP1-binding ESS and the donor splicing site of intron 68. (b) *Cdh23* minigene was expressed in COS7 cells together with the splicing regulators as indicated, and the inclusion of *Cdh23* exon 68 was examined by performing RT-PCR. (c) Wild-type *Cdh23* minigene or minigene with donor site mutation was expressed in COS7 cells together with the splicing regulators as indicated, and the inclusion of *Cdh23* exon 68 was examined by performing RT-PCR. (d) *Cdh23* minigene was expressed in COS7 cells together with constant amount of RBM24 and various amount of PTBP1, and the inclusion of *Cdh23* exon 68 was examined by performing RT-PCR. The expression level of RBM24 and PTBP1 was confirmed by performing western blot. (e) *Cdh23* minigene with donor site mutation or donor site/ESS double mutations was expressed in COS7 cells together with PTBP1, and the inclusion of *Cdh23* exon 68 was examined by performing RT-PCR. (f, g) Wild-type *Cdh23* minigene or mutant with deletion of the potential PTBP1-binding ESS was expressed in COS7 cells with or without PTBP1. Binding of PTBP1 with *Cdh23* pre-mRNA was examined by performing native RIP followed by RT-PCR (f) or qPCR (g). Error bars represent mean \pm SEM from triplicate experiments. * $p < 0.05$; ** $p < 0.01$.

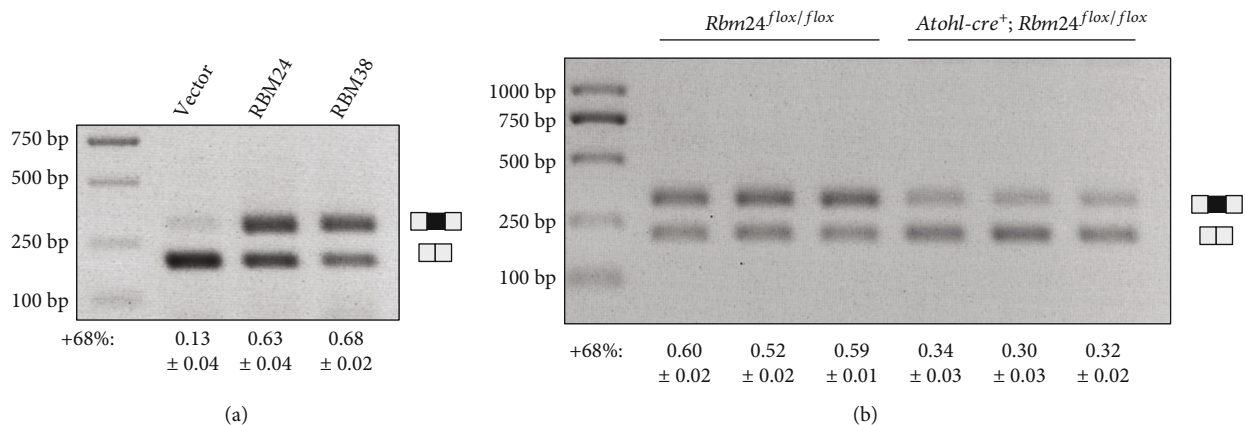


FIGURE 5: RBM24 regulates the alternative splicing of endogenous *Cdh23* pre-mRNA. (a) RBM24 or RBM38 was overexpressed in HEI-OC-1 cells, and exon 68 inclusion of endogenous *Cdh23* mRNA was examined by performing RT-PCR. (b) RT-PCR was performed to examine *Cdh23* exon 68 inclusion in the inner ear of P2 *Atoh1-cre⁺; Rbm24^{flox/flox}* ($n = 3$) or *Rbm24^{flox/flox}* mice ($n = 3$).

Cdh23 exon 68 among different mammals show that site 1 is evolutionally conserved while site 2 is not (data not shown), consistent with an important role of site 1 in mediating *Cdh23* exon 68 inclusion. There is also a potential PTBP1-binding ESS located in *Cdh23* exon 68, and mutation of this site affects the inhibition of *Cdh23* exon 68 inclusion by PTBP1. Interestingly, the PTBP1 homolog PTBP2 shows a much weaker inhibitory effect on *Cdh23* exon 68 inclusion, albeit it is expressed in the inner ear and recognizes similar binding motifs.

A question that remained is how relatively ubiquitously expressed RBM24, RBM38, and PTBP1 regulate inner ear-specific alternative splicing of *Cdh23* exon 68. Alternative splicing has been proposed to be regulated by the combinato-

rial action of splicing enhancers and repressors [25]. Transcriptome RNAseq reveals high expression level of *Rbm24* and low expression level of *Rbm38* and *Ptbp1* in the auditory and vestibular hair cells, which is consistent with the inner ear-specific *Cdh23* exon 68 splicing [28]. Additionally, there might be other splicing factors that regulate the alternative splicing of *Cdh23* exon 68 but are not included in our screening in the present work. In line with this, *Cdh23* exon 68 inclusion is decreased but still present in the inner ear of *Rbm24* cko mice. qPCR reveals that *Rbm38* expression remains on the similar low level in the inner ear of *Rbm24* cko mice (data not shown), suggesting that splicing enhancer other than RBM24 and RBM38 might be responsible for the remnant inclusion of *Cdh23* exon 68 in the *Rbm24* cko mice.

At present, only a few splicing factors have been identified to play important roles in the inner ear, including SRRM4, SFSWAP, and ESRP1 [18–20]. Our present work adds RBM24 to this growing list. RBM24 is an RNA-binding protein that contains an RNA-recognition motif (RRM) and an alanine-rich low-complexity region. It has been shown that RBM24 regulates pre-mRNA alternative splicing as well as mRNA stability and translation [24, 29–38]. RBM24 is a major regulator of muscle-specific alternative splicing, and global *Rbm24* inactivation affects cardiac development that eventually leads to embryonic death [24]. In the mouse inner ear, RBM24 expression is specifically detected in the hair cells, but its physiological role in the inner ear remains unknown [22, 39]. Here, we show that RBM24 regulates the alternative splicing of *Cdh23*; hence, it might play an important role in the development and/or function of hair cells. Meanwhile, immunostaining shows that RBM24 is also localized in the hair cell stereocilia, suggesting that it might also play some roles in the organization and/or function of this F-actin-based cell protrusion [22]. Super-resolution microscopy [40–42] and conditional knockout mice will certainly help to learn more about the role of RBM24 in the inner ear.

Data Availability

The data supporting the findings of this study are available within the article.

Conflicts of Interest

The authors declare that there are no competing interests regarding the publication of this paper.

Acknowledgments

This work was supported by grants from the National Key Basic Research Program of China (2018YFC1003600), the National Natural Science Foundation of China (81771001), Shandong Provincial Key Laboratory of Animal Cell and Developmental Biology (SPKLACDB-2019000), and the Fundamental Research Funds of Shandong University (2018JJC025).

References

- [1] M. C. Wahl, C. L. Will, and R. Luhrmann, “The spliceosome: design principles of a dynamic RNP machine,” *Cell*, vol. 136, no. 4, pp. 701–718, 2009.
- [2] M. Chen and J. L. Manley, “Mechanisms of alternative splicing regulation: insights from molecular and genomics approaches,” *Nature Reviews. Molecular Cell Biology*, vol. 10, no. 11, pp. 741–754, 2009.
- [3] T. W. Nilsen and B. R. Graveley, “Expansion of the eukaryotic proteome by alternative splicing,” *Nature*, vol. 463, no. 7280, pp. 457–463, 2010.
- [4] P. J. Grabowski and D. L. Black, “Alternative RNA splicing in the nervous system,” *Progress in Neurobiology*, vol. 65, no. 3, pp. 289–308, 2001.
- [5] D. L. Black, “Mechanisms of alternative pre-messenger RNA splicing,” *Annual Review of Biochemistry*, vol. 72, no. 1, pp. 291–336, 2003.
- [6] Y. Wang, Y. Liu, H. Nie, X. Ma, and Z. Xu, “Alternative splicing of inner-ear-expressed genes,” *Frontiers in Medicine*, vol. 10, no. 3, pp. 250–257, 2016.
- [7] J. A. Assad, G. M. G. Shepherd, and D. P. Corey, “Tip-link integrity and mechanical transduction in vertebrate hair cells,” *Neuron*, vol. 7, no. 6, pp. 985–994, 1991.
- [8] J. Siemens, C. Lillo, R. A. Dumont et al., “Cadherin 23 is a component of the tip link in hair-cell stereocilia,” *Nature*, vol. 428, no. 6986, pp. 950–955, 2004.
- [9] C. Söllner, the Tübingen 2000 Screen Consortium, G.-J. Rauch et al., “Mutations in *cadherin 23* affect tip links in zebrafish sensory hair cells,” *Nature*, vol. 428, no. 6986, pp. 955–959, 2004.
- [10] P. Kazmierczak, H. Sakaguchi, J. Tokita et al., “Cadherin 23 and protocadherin 15 interact to form tip-link filaments in sensory hair cells,” *Nature*, vol. 449, no. 7158, pp. 87–91, 2007.
- [11] F. Di Palma, R. Pellegrino, and K. Noben-Trauth, “Genomic structure, alternative splice forms and normal and mutant alleles of cadherin 23 (*Cdh23*),” *Gene*, vol. 281, no. 1–2, pp. 31–41, 2001.
- [12] J. Siemens, P. Kazmierczak, A. Reynolds, M. Sticker, A. Littlewood-Evans, and U. Muller, “The Usher syndrome proteins cadherin 23 and harmonin form a complex by means of PDZ-domain interactions,” *Proceedings of the National Academy of Sciences of the United States of America*, vol. 99, no. 23, pp. 14946–14951, 2002.
- [13] Z. Xu, A. W. Peng, K. Oshima, and S. Heller, “MAGI-1, a candidate stereociliary scaffolding protein, associates with the tip-link component cadherin 23,” *The Journal of Neuroscience*, vol. 28, no. 44, pp. 11269–11276, 2008.
- [14] S. Yonezawa, A. Hanai, N. Mutoh, A. Moriyama, and T. Kageyama, “Redox-dependent structural ambivalence of the cytoplasmic domain in the inner ear-specific cadherin 23 isoform,” *Biochemical and Biophysical Research Communications*, vol. 366, no. 1, pp. 92–97, 2008.
- [15] Z. Xu, K. Oshima, and S. Heller, “PIST regulates the intracellular trafficking and plasma membrane expression of cadherin 23,” *BMC Cell Biology*, vol. 11, no. 1, p. 80, 2010.
- [16] L. Wu, L. Pan, C. Zhang, and M. Zhang, “Large protein assemblies formed by multivalent interactions between cadherin23 and harmonin suggest a stable anchorage structure at the tip link of stereocilia,” *The Journal of Biological Chemistry*, vol. 287, no. 40, pp. 33460–33471, 2012.
- [17] M. Gagliardi and M. R. Matarazzo, “RIP: RNA immunoprecipitation,” *Methods in Molecular Biology*, vol. 1480, pp. 73–86, 2016.
- [18] Y. Nakano, I. Jahan, G. Bonde et al., “A mutation in the *Srrm4* gene causes alternative splicing defects and deafness in the Bronx waltzer mouse,” *PLoS Genetics*, vol. 8, no. 10, article e1002966, 2012.
- [19] Y. Moayed, M. L. Basch, N. L. Pacheco et al., “The candidate splicing factor *Sfswap* regulates growth and patterning of inner ear sensory organs,” *PLoS Genetics*, vol. 10, no. 1, article e1004055, 2014.
- [20] A. M. Rohacek, T. W. Bebee, R. K. Tilton et al., “ESRP1 mutations cause hearing loss due to defects in alternative splicing that disrupt cochlear development,” *Developmental Cell*, vol. 43, no. 3, pp. 318–331.e5, 2017.

- [21] Y. Liu, H. Nie, C. Liu et al., “Angulin proteins ILDR1 and ILDR2 regulate alternative pre-mRNA splicing through binding to splicing factors TRA2A, TRA2B, or SRSF1,” *Scientific Reports*, vol. 7, no. 1, p. 7466, 2017.
- [22] R. Grifone, A. Saquet, Z. Xu, and D. L. Shi, “Expression patterns of Rbm24 in lens, nasal epithelium, and inner ear during mouse embryonic development,” *Developmental Dynamics*, vol. 247, no. 10, pp. 1160–1169, 2018.
- [23] D. Ray, H. Kazan, K. B. Cook et al., “A compendium of RNA-binding motifs for decoding gene regulation,” *Nature*, vol. 499, no. 7457, pp. 172–177, 2013.
- [24] J. Yang, L. H. Hung, T. Licht et al., “RBM24 is a major regulator of muscle-specific alternative splicing,” *Developmental Cell*, vol. 31, no. 1, pp. 87–99, 2014.
- [25] C. W. J. Smith and J. Valcárcel, “Alternative pre-mRNA splicing: the logic of combinatorial control,” *Trends in Biochemical Sciences*, vol. 25, no. 8, pp. 381–388, 2000.
- [26] P. L. Boutz, P. Stoilov, Q. Li et al., “A post-transcriptional regulatory switch in polypyrimidine tract-binding proteins reprograms alternative splicing in developing neurons,” *Genes & Development*, vol. 21, no. 13, pp. 1636–1652, 2007.
- [27] H. Yang, X. Xie, M. Deng, X. Chen, and L. Gan, “Generation and characterization of Atoh1-Cre knock-in mouse line,” *Genesis*, vol. 48, no. 6, pp. 407–413, 2010.
- [28] D. I. Scheffer, J. Shen, D. P. Corey, and Z. Y. Chen, “Gene expression by mouse inner ear hair cells during development,” *The Journal of Neuroscience*, vol. 35, no. 16, pp. 6366–6380, 2015.
- [29] Y. Jiang, M. Zhang, Y. Qian, E. Xu, J. Zhang, and X. Chen, “Rbm24, an RNA-binding protein and a target of p53, regulates p21 expression via mRNA stability,” *The Journal of Biological Chemistry*, vol. 289, no. 6, pp. 3164–3175, 2014.
- [30] E. Xu, J. Zhang, M. Zhang, Y. Jiang, S. J. Cho, and X. Chen, “RNA-binding protein RBM24 regulates p63 expression via mRNA stability,” *Molecular Cancer Research*, vol. 12, no. 3, pp. 359–369, 2014.
- [31] J. Ito, M. Iijima, N. Yoshimoto, T. Niimi, S. Kuroda, and A. D. Maturana, “RBM20 and RBM24 cooperatively promote the expression of short enh splice variants,” *FEBS Letters*, vol. 590, no. 14, pp. 2262–2274, 2016.
- [32] T. Zhang, Y. Lin, J. Liu et al., “Rbm24 regulates alternative splicing switch in embryonic stem cell cardiac lineage differentiation,” *Stem Cells*, vol. 34, no. 7, pp. 1776–1789, 2016.
- [33] Y. Lin, K. T. Tan, J. Liu, X. Kong, Z. Huang, and X. Q. Xu, “Global profiling of Rbm24 bound RNAs uncovers a multitasking RNA binding protein,” *The International Journal of Biochemistry & Cell Biology*, vol. 94, pp. 10–21, 2018.
- [34] J. Liu, X. Kong, M. Zhang, X. Yang, and X. Xu, “RNA binding protein 24 deletion disrupts global alternative splicing and causes dilated cardiomyopathy,” *Protein & Cell*, vol. 10, no. 6, pp. 405–416, 2019.
- [35] M. M. G. van den Hoogenhof, I. van der Made, N. E. de Groot et al., “AAV9-mediated Rbm24 overexpression induces fibrosis in the mouse heart,” *Scientific Reports*, vol. 8, no. 1, p. 11696, 2018.
- [36] M. Zhang, Y. Zhang, E. Xu et al., “Rbm24, a target of p53, is necessary for proper expression of p53 and heart development,” *Cell Death and Differentiation*, vol. 25, no. 6, pp. 1118–1130, 2018.
- [37] M. Shao, T. Lu, C. Zhang, Y. Z. Zhang, S. H. Kong, and D. L. Shi, “Rbm24 controls poly(A) tail length and translation efficiency of crystallin mRNAs in the lens via cytoplasmic polyadenylation,” *Proceedings of the National Academy of Sciences of the United States of America*, vol. 117, no. 13, pp. 7245–7254, 2020.
- [38] S. Dash, L. K. Brastrom, S. D. Patel, C. A. Scott, D. C. Slusarski, and S. A. Lachke, “The master transcription factor SOX2, mutated in anophthalmia/microphthalmia, is post-transcriptionally regulated by the conserved RNA-binding protein RBM24 in vertebrate eye development,” *Human Molecular Genetics*, vol. 29, no. 4, pp. 591–604, 2020.
- [39] T. Cai, H. I. Jen, H. Kang, T. J. Klisch, H. Y. Zoghbi, and A. K. Groves, “Characterization of the transcriptome of nascent hair cells and identification of direct targets of the Atoh1 transcription factor,” *The Journal of Neuroscience*, vol. 35, no. 14, pp. 5870–5883, 2015.
- [40] Y. Liu, J. Qi, X. Chen et al., “Critical role of spectrin in hearing development and deafness,” *Science Advances*, vol. 5, no. 4, article eaav7803, 2019.
- [41] J. Qi, Y. Liu, C. Chu et al., “A cytoskeleton structure revealed by super-resolution fluorescence imaging in inner ear hair cells,” *Cell Discovery*, vol. 5, no. 1, p. 12, 2019.
- [42] J. Qi, L. Zhang, F. Tan et al., “Espn distribution as revealed by super-resolution microscopy of stereocilia,” *American Journal of Translational Research*, vol. 12, no. 1, pp. 130–141, 2020.

Research Article

A Neurophysiological Study of Musical Pitch Identification in Mandarin-Speaking Cochlear Implant Users

Jieqing Cai, Yimeng Liu, Minyun Yao, Muqing Xu, and Hongzheng Zhang 

Department of Otolaryngology Head & Neck Surgery, Zhujiang Hospital, Southern Medical University, Guangzhou, China 510282

Correspondence should be addressed to Hongzheng Zhang; zhanghz@outlook.com

Received 2 March 2020; Revised 26 May 2020; Accepted 24 June 2020; Published 22 July 2020

Academic Editor: Hai Huang

Copyright © 2020 Jieqing Cai et al. This is an open access article distributed under the Creative Commons Attribution License, which permits unrestricted use, distribution, and reproduction in any medium, provided the original work is properly cited.

Music perception in cochlear implant (CI) users is far from satisfactory, not only because of the technological limitations of current CI devices but also due to the neurophysiological alterations that generally accompany deafness. Early behavioral studies revealed that similar mechanisms underlie musical and lexical pitch perception in CI-based electric hearing. Although neurophysiological studies of the musical pitch perception of English-speaking CI users are actively ongoing, little such research has been conducted with Mandarin-speaking CI users; as Mandarin is a tonal language, these individuals require pitch information to understand speech. The aim of this work was to study the neurophysiological mechanisms accounting for the musical pitch identification abilities of Mandarin-speaking CI users and normal-hearing (NH) listeners. Behavioral and mismatch negativity (MMN) data were analyzed to examine musical pitch processing performance. Moreover, neurophysiological results from CI users with good and bad pitch discrimination performance (according to the just-noticeable differences (JND) and pitch-direction discrimination (PDD) tasks) were compared to identify cortical responses associated with musical pitch perception differences. The MMN experiment was conducted using a passive oddball paradigm, with musical tone C4 (262 Hz) presented as the standard and tones D4 (294 Hz), E4 (330 Hz), G#4 (415 Hz), and C5 (523 Hz) presented as deviants. CI users demonstrated worse musical pitch discrimination ability than did NH listeners, as reflected by larger JND and PDD thresholds for pitch identification, and significantly increased latencies and reduced amplitudes in MMN responses. Good CI performers had better MMN results than did bad performers. Consistent with findings for English-speaking CI users, the results of this work suggest that MMN is a viable marker of cortical pitch perception in Mandarin-speaking CI users.

1. Introduction

Hair cells (HCs) in the cochlea play a critical role in converting mechanical sound waves into electric signals for hearing [1]. HCs are vulnerable for multiple damages, including noise, different ototoxic drugs, inflammation, and aging [2–8]. In mammals, damaged HCs cannot be spontaneously regenerated [9–13]; thus, sensorineural deafness is permanent once HCs are damaged. Cochlear implants (CIs) can partially replace the function of HCs and are the primary clinical therapeutic devices for patients with severe and profound sensorineural deafness by far. According to incomplete statistics, more than 500,000 deaf patients worldwide have recovered hearing through cochlear implantation [14]. The basic working principle of a CI is as follows: the microphone picks up sound signals and converts them to digital sound waves, then

transmits the electrical signals to the speech processor, which encodes signals and generates electrical pulses corresponding to different electrodes to directly stimulate the auditory nerve fibers in different regions of the cochlea [15]. Although electrical hearing is extremely degraded and unnatural, most CI users can achieve good speech recognition in quiet conditions and meet the fundamental requirements of everyday verbal communication [16]. Nevertheless, many CI users show far from satisfactory performance in challenging listening tasks, such as tone recognition in Mandarin Chinese, speech recognition in noisy conditions or with competing sound sources, and music perception [17–19]. Music has more complex, abstract, and varied acoustic characteristics than does speech; its four primary elements are rhythm, pitch, volume, and timbre. The musical perception ability of CI users has been assessed according to rhythm, pitch, melody, and timbre

using various test platforms (e.g., the clinical assessment of music perception test (CAMP) and the musical sounds in cochlear implants perception test (MuSIC)) [20–22]. Many early behavioral studies revealed equivalent musical rhythm recognition in CI users and normal-hearing (NH) listeners, but poorer pitch, melody, and timbre recognition in CI users [20, 22–27]. Behavioral data obtained with the just-noticeable differences (JND) and pitch-direction discrimination (PDD) tasks are regarded as suitable for the measurement of pitch discrimination (i.e., definition of pitch perception thresholds) during peripheral auditory processing [18, 22, 28, 29].

Behavioral tests were used to evaluate the music perception of CI users in almost all early studies. However, with the development of electrophysiological technology, cortical auditory processing in music discrimination can be further understood by mismatch negativity (MMN) assessment. MMN is a component of the endogenous event-related potential, an electroencephalographic (EEG) response evoked by the insertion of any discernible deviation in a series of standard stimuli [30]. MMN is an electrophysiological index of the brain's automatic processing of sensory information, independent of listening tasks and selective attention. It can be elicited by a stimulus with deviation of any distinguishable acoustic characteristic, such as frequency, intensity, duration, or timbre, in pure tones, speech, and music [31–33]. Previous studies revealed that MMN is a viable, objective, and noninvasive measure of auditory discrimination [34].

Recently, MMN has also been used to evaluate speech recognition and rehabilitation in CI users. Turgeon et al. [35] measured MMN using a two-deviant oddball paradigm based on speech syllables (/da/, /ba/, and /ga/), revealing a significant positive correlation between the amplitude of MMN and the speech recognition score. These findings suggest that MMN is an objective measure of speech recognition ability in CI users. Another study showed that the MMN amplitude in a vowel-duration identification task was similar in children who had worn CIs for 4 months and in their NH counterparts, suggesting the existence of auditory cortex plasticity [36]. In addition to its extensive application in speech recognition studies, researchers have extended MMN to the measurement of music (e.g., rhythm, pitch, timbre, melody, and chord) perception [33]. The relationship between pre-attention and rhythm processing was studied by changing the rhythm structure [37]. In early studies, multifeature paradigms were used with MMN to examine CI users' perception of music timbre, intensity, and rhythm. The results showed that the latency of MMN was prolonged and its amplitude was reduced, reflecting impaired music perception ability, in CI users compared with NH listeners [38–41].

Several studies have used MMN to explore neurophysiological responses related to musical pitch discrimination in CI users. [42] used a multifeature MMN paradigm with deviant stimuli in different acoustic dimensions (i.e., frequency, intensity, and duration) to assess music perception in CI users. They found that the latency of MMN decreased and its amplitude increased with the increased frequency of deviant stimuli for NH subjects, but those changes were irregular, reflecting impaired pitch perception, for CI users. Another

study showed that MMN could be evoked by as few as two and four semitones of pitch deviation, with significantly prolonged MMN latency and reduced amplitude in CI users compared with NH subjects [39]. In previous research, behavioral tests have been used to obtain a perceptual threshold for timbre, with stimuli for MMN recording (including supra-threshold and subthreshold stimuli) set according to individual behavioral thresholds [43]. However, few studies have investigated MMN responses and their correlations with musical pitch discrimination thresholds using behavioral tests with Mandarin-speaking CI users and NH listeners.

Most active, ongoing neurophysiological studies of music perception do not involve CI users who speak tonal languages. Mandarin is the most widely spoken tonal language; lexical meanings are conveyed through four tone patterns with different pitch-change contours. The tones of Mandarin are classified according to the pattern of fundamental frequency (F0) variation and the absolute frequency of pitch and are distinguished predominantly by changes in the F0 contour and duration [44]. Musical pitch, a perceptual sound property, depends mainly on F0 and harmonic components. Several behavioral studies have demonstrated that pitch and lexical tone perception are correlated and have similar underlying mechanisms in CI-based electric hearing [19, 45, 46]. Therefore, accurate pitch discrimination is crucial for the understanding of tonal languages, such as Mandarin Chinese.

Mandarin-speaking CI users must process tonal information in everyday communication, but whether this processing has any impact on the auditory processing of musical pitch is unclear. In addition, clinical data regarding the characteristics of MMN in pitch perception in Mandarin-speaking CI users are insufficient. Therefore, the present study is aimed at providing evidence for the neurophysiological mechanisms underlying musical pitch discrimination in Mandarin-speaking CI users. Specifically, MMN characteristics (e.g., amplitudes and latencies) and their relationships to the minimal identification thresholds of pitch differences in JND and PDD tasks were examined. We hypothesized that automatic cortical processing related to musical pitch perception would be reflected in the MMN responses of CI users. Compared with NH listeners, CI users with higher behavioral thresholds had worse elicited performance according to EEG measures. In addition, MMN responses marked differences in cortical responses between CI users with good and poor musical pitch identification performance.

2. Methods

2.1. Subjects. Eleven CI users (seven females and four males) aged 10–40 years participated in this study. These subjects were recruited from Zhujiang Hospital, Southern Medical University. One participant had bilateral CIs (only one side was used during the test), and the others had unilateral CIs. The CI users' demographic information is shown in Table 1. All CI-using participants were right-handed, with normal verbal communication ability, normal mental and intellectual development, and no formal musical training; patients with auditory neuropathy and neurological diseases

TABLE 1: Clinical information of CI users. LVAS: large vestibular aqueduct syndrome.

Subject	Age	Deafness duration (years)	CI experience (years)	Etiology	Implant ear	Type of CI	Classification of deafness
CI01	19	16	1	LVAS	Left	Nucleus RE24	Postlingual
CI02	11	2	8.6	Congenital	Right	Nucleus RE24	Prelingual
CI03	14	10	0.3	LVAS	Left	AB HiRes 90K	Postlingual
CI04	14	12	0.3	LVAS	Right	Nucleus CI512	Postlingual
CI05	21	5	16	Congenital	Right	Nucleus R24	Prelingual
CI06	20	3	17	Congenital	Right	Nucleus R24	Prelingual
CI07	24	8	16	Congenital	Left	Nucleus RE24	Prelingual
CI08	40	20	Right: 11; left: 1	Progressive	Both	Nucleus R24	Postlingual
CI09	10	3	7	Congenital	Right	Nucleus RE24	Prelingual
CI10	25	7	5.8	Unknown	Right	Nucleus RE24	Postlingual
CI11	23	2	1.5	Unknown	Right	Nucleus RE24	Postlingual

were excluded. All subjects were required to complete behavioral and EEG testing. The CI users were divided into good and poor performance groups according to musical tone discrimination test results. The control group consisted of 12 NH subjects (6 females and 6 males) aged 19–25 years with pure tone audiometry thresholds < 25 dB HL at octave frequencies of 0.25–8 kHz. NH subjects had no history of otitis media or psychiatric or neurological disease. The Ethics Committee of Zhujiang Hospital, Southern Medical University, approved this study; the ethical approval number was 2017-EBYHZX-001. All subjects participated in the study voluntarily. Each participant provided written informed consent, and participants under the age of 16 gave written informed consent from their parents.

2.2. Stimuli. The test stimuli were synthetic complex tones. Each tone consisted of F0 and two harmonics with amplitudes attenuated by 20% per octave (first harmonic, 80% amplitude; second harmonic, 60% amplitude). The duration of each stimulus was 500 ms, including 25 ms each for onset and offset ramping to reduce sudden spectral shift. The intensity of the sound stimuli was normalized using the root-mean-square method. For the MMN test, the stimuli were the musical tones C4 (262 Hz), D4 (294 Hz, 2-semitone pitch interval from C4), E4 (330 Hz, 4-semitone interval), G#4 (415 Hz, 8-semitone interval), and C5 (523 Hz, 12-semitone interval).

The MMN experiment was conducted using a passive oddball paradigm, with tone C4 presented as the standard (~87% probability of occurrence) and tones D4, E4, G#4, and C5 presented as deviants (~13% probability of occurrence). The interstimulus interval (ISI) was 600 ms, and the stimuli were played in a pseudorandom sequence; at least three standard stimuli were presented between two deviant stimuli. The test comprised four blocks of stimuli (total, 2848 standard stimuli (4 × 712) and 420 deviant stimuli (105 each of D4, E4, G#4, and C5)).

The tests were carried out in a sound-insulated, electrically shielded room, with <30 dBA background noise. Experimental auditory stimuli were presented through a loudspeaker (model S1000MA; Edifier) placed 1.2 m in front of the subjects at a seated ear level. The sound intensity was

approximately 65 dBA. During the MMN experiment, the subjects were instructed to sit comfortably and to optionally watch the silent films presented, to pay no attention to the stimuli, to keep quiet and awake, and to reduce limb movements and blinking. The four test blocks were delivered to each subject in a counterbalanced sequence, with approximately 3 min rest between blocks.

2.3. Psychoacoustic Testing. Before testing, all participants filled out a questionnaire on their music experience, which was designed for this study. We selected three questionnaire items (on the frequencies with which respondents listened to music and sang and on their degree of enjoyment of music; see the appendix for details) for the evaluation of music experience. Scores ranged from 1 (“not at all”) to 10 (“very often”). CI users responded according to their postimplantation situations, and NH listeners responded according to their usual situations.

All participants performed the JND and PDD tasks using music perception evaluation software [47]. Before testing, they conducted preliminary runs to become familiarized with the test materials and procedures. Three alternative-forced choices with a three-down, one-up adaptive tracking procedure were used for the JND task, with an initial pitch interval of 12 semitones. The base frequency of the reference tone was C4. Three tones (one target and two references) were played randomly in each trial, with an ISI of 1 s. Participants were asked to identify the pitch that sounded “different.” The test was ended when the participant attained 12 reversals or 3 consecutive correct discriminations at a 1-semitone pitch interval. The mean of the last six reversals was calculated as the final threshold of pitch difference discrimination. The PDD task was implemented using a two-alternative-forced choice approach, a target tone and a reference tone. Subjects were asked to choose the tone with the higher pitch. The PDD test procedure and threshold calculation were the same as for the JND test.

2.4. EEG Recording. EEG data were obtained with a SynAmps amplifier (NeuroScan, Charlotte, NC, USA) using a 64-electrode cap placed according to the international 10-20 system. The reference electrodes were placed on the contralateral

mastoids (M1, M2) and the nasal tip of each subject. The vertical electrooculogram was monitored by an external electrode placed below the left eye. The EEG data were recorded with a band-pass filter setting of 0.1–100 Hz and a sampling rate of 500 Hz. Impedance in each electrode was kept below 5 k Ω before data acquisition. The electrodes located near the CI transmission coil were not used for CI-using participants.

2.5. EEG Data Analysis. EEG data were analyzed with EEGLAB 14.1.1 [48] in Matlab 2015b (MathWorks, Natick, MA, USA). First, the data were rereferenced using the contralateral mastoid signals. Then, continuous EEG data were filtered using a 50 Hz notch and a band-pass filter (1–30 Hz). EEG signals exceeding $\pm 50 \mu\text{V}$ and with nonstereotyped artifacts (<10% of individual subjects’ datasets) were regarded as bad blocks and were removed before further analysis. Data for electrodes located near CI transmission coils were interpolated using data from four adjacent electrodes. Next, infomax independent component analysis was performed for artifact (e.g., eye blinks, horizontal eye movement, electrocardiographic activity, and CI electrical stimulation) correction. After artifact removal, each epoch was selected between 100 ms prestimulus and 500 ms poststimulus and corrected with the baseline of the prestimulus time window, and event-related potentials were calculated by temporal averaging of epochs with the same type of stimulus.

MMN waveforms were obtained by subtracting the response to the standard (C4) from the response to each of the four deviants (E4, G#4, C5, and D4). Grand-average difference waveforms were, respectively, computed for the four deviants in the CI and NH groups. The Fz electrode in the frontocentral region was used for MMN analysis, the largest negative MMN peak is typically obtained at Fz [31, 49], and the neural response was consistent in different subjects. The peak amplitude and latency of MMN responses were calculated within the 156–236 ms window for the CI group and the 130–210 ms window for the NH group. Window selection was based on previous MMN studies [49, 50] and average MMN results for deviants in this experiment.

2.6. Statistical Analysis. Statistical analyses were implemented with SPSS 20.0. (PSS Inc., Chicago, IL, USA). Two independent-sample nonparametric tests and analysis of variance (ANOVA) were used to examine differences in JND and PDD task performance, age, and music experience between CI users and NH listeners. Repeated-measures ANOVA was conducted with the grand-average MMN amplitudes and latencies, with two main factors: listening status (CI and NH) and deviant type (E4, G#4, C5, and D4).

3. Results

3.1. Musical Pitch Recognition. The two groups were matched in terms of age and music experience ($p > 0.05$; Table 2). The two groups of CI users with good and poor performance were also matched in terms of music experience ($p > 0.05$). The mean thresholds for CI users in the JND and PDD tasks were 3.1 ± 1.4 (range, 1.0–5.0) semitones and 4.2 ± 4.2 (range, 1.0–15.8) semitones, respectively. For NH listeners, these

TABLE 2: Statistical results for age, music experience, and pitch discrimination scores for the two study groups.

Group	JND (semitone) (SD)	PDD (semitone) (SD)	Age (year) (SD)	Music experience (SD)
CI users	3.1 (1.4)	4.2 (4.2)	20.1 (8.4)	6.73 (2.33)
NH controls	1.2 (0.8)	1.9 (1.4)	21.3 (1.7)	7.54 (1.71)
<i>Z/F</i>	-3.698	-2.167	0.223	0.965
<i>p</i>	<0.001	0.030	0.646	0.337

JND: just-noticeable difference task; PDD: pitch-direction discrimination task; SD: standard deviation.

thresholds were 1.2 ± 0.8 (range, 1.0–3.8) and 1.9 ± 1.4 (range, 1.0–6.8) semitones, respectively. The thresholds were significantly higher for CI users than NH controls (JND task: $Z = -3.698$, $p < 0.001$; PDD task: $Z = -2.167$, $p = 0.030$; Table 2). According to the JND and PDD task results, CI users with minimum pitch discrimination ability ≤ 4 semitones were allocated to the good performance group ($n = 5$), and those with >4 -semitone discrimination ability were allocated to the poor performance group ($n = 6$).

3.2. MMN

3.2.1. NH Listeners vs. CI Users. Two-way repeated-measures ANOVA was conducted with two main factors: (1) pitch differences between the standard and deviants (12, 8, 4, and 2 semitones) and (2) listener group (NH listeners and CI users). The two-way repeated-measures ANOVA was conducted with data from seven CI users and seven NH listeners, as only seven CI users finished the experiments under four conditions with distinct pitch changes. The main effect of pitch difference on the MMN amplitude was observed in NH listeners and CI users ($F(3, 7) = 7.055$, $p < 0.05$), but no main effect was found for the listener group or interaction between these two factors. One-way ANOVA was performed to assess the effects of pitch difference in NH listeners and CI users. The MMN amplitude increased significantly with the pitch difference in NH listeners ($F(3, 12) = 6.978$, $p < 0.01$). Such increases were observed for large pitch changes (12, 8, and 4 semitones) in the 11 CI users ($F(2, 11) = 5.854$, $p < 0.05$).

Two (NH listeners and CI users) by four (pitch differences) repeated-measures ANOVA was used to further assess the effect of pitch difference on MMN latency. The analysis revealed an interaction between the subject group and pitch differences ($F(3, 7) = 7.542$, $p < 0.05$). The two-way interaction was characterized by significant differences between NH listeners and CI users in MMN latencies ($F(1, 7) = 7.945$, $p < 0.05$), which were shorter for a given pitch difference among NH listeners than among CI users. Figure 1 shows the MMN responses to 12-, 8-, 4-, and 2-semitone pitch differences in NH listeners and CI users. The peak amplitudes and latencies of MMN waveforms under different conditions are summarized in Table 3. Figure 2 shows the topological distribution of latencies at peak amplitudes in NH listeners and CI users.

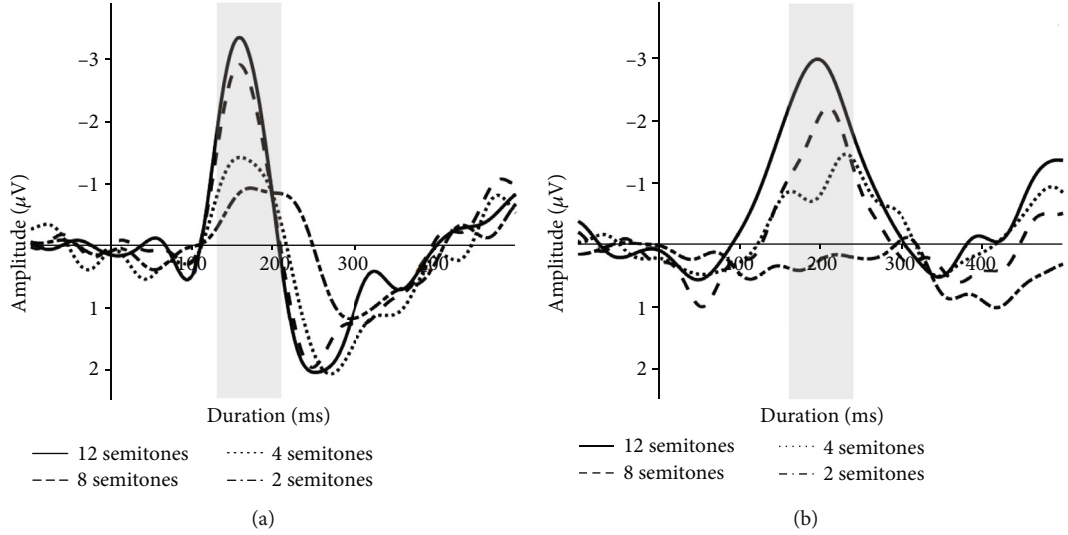


FIGURE 1: Grand-average MMN waveforms for distinct pitch differences for NH listeners (a) and CI users (b) at electrode Fz. Gray shading indicates time windows used to calculate amplitudes and latencies ((a) 130–210 ms; (b) 156–236 ms).

TABLE 3: Statistical results of the MMN amplitude and latency (average \pm standard deviant) for 12-semitone, 8-semitone, 4-semitone, and 2-semitone pitch changes in NH listeners and CI users.

	Pitch changes	Amplitude (μ V)	Latency (ms)
Normal hearing	12 semitones	-3.77 ± 0.55	153.83 ± 4.52
	8 semitones	-3.11 ± 0.41	159.67 ± 3.19
	4 semitones	-2.14 ± 0.41	165.50 ± 6.34
	2 semitones	-1.51 ± 0.24	184.67 ± 5.75
Cochlear implants	12 semitones	-3.83 ± 0.54	187.09 ± 7.92
	8 semitones	-2.78 ± 0.54	197.27 ± 8.74
	4 semitones	-2.42 ± 0.34	204.18 ± 10.04
	2 semitones	-0.69 ± 0.43	178.00 ± 10.34

3.2.2. CI Users with Good vs. Poor Performance. Figure 3 illustrates MMN waveforms according to pitch changes in CI users with good and poor performance, and Table 4 provides detailed MMN amplitude and latency results. Separate plots for CI users with good and poor performance are presented in Figures 2(c) and 2(d). Two-way ANOVA was conducted to assess whether MMN waveforms elicited by pitch differences were affected by CI users' pitch discrimination performance. The statistical analysis excluded data from 2-semitone pitch changes because only two CI users with poor performance participated in the test under this condition. Pitch changes had a main effect on the MMN amplitude in CI users with good and poor performance ($F(3, 5) = 10.904, p < 0.05$); the amplitude increased significantly with the difference between standard and deviant tones. Pitch changes had no significant effect on MMN latency in the two CI groups.

3.3. Correlations in CI Users. Bivariate correlation analysis revealed positive correlations between the JND task thresh-

old in well-performing CI users and MMN latency for E4 ($r = 0.873, p = 0.043$), G#4 ($r = 0.950, p = 0.013$), and C5 ($r = 0.870, p = 0.045$), but no correlation with MMN amplitude. For poorly performing CI users, the JND task threshold was correlated positively with the MMN latency for C5 ($r = 0.801, p = 0.046$). No correlation was observed between MMN latency or amplitude and the PDD task threshold, music experience, duration of deafness, CI experience, or age of cochlear implantation (Figure 4, Table 5).

4. Discussion and Conclusions

HCs in the inner ear cochlea play an important role for hearing [1, 51]. In mammal's inner ear cochlea, HCs are sensitive for multiple stresses and easy to be damaged. Thus, most of the sensorineural deafness induced by gene mutation, noise, different ototoxic drugs, inflammation, or aging are caused by the HC loss [52–57]. However, the mammals only have very limited HC regeneration ability; most of the damaged HCs cannot be spontaneously regenerated, which make the HC loss and hearing loss to be irreversible [58–62]. CIs are the most efficient clinical therapeutic devices for sensorineural deafness patients, and recent studies have shown that application of CI-based electric acoustic stimulation together with multiple biomaterials also can promote the differentiation of neural stem cell [63–66] and promote maturation of spiral ganglion neuron [67–70]. However, the neurophysiological study of musical pitch identification in CI users is still lacking in the hearing research field. The aim of the present study was to investigate neurophysiological responses relevant to musical pitch discrimination in CI users and NH listeners using an oddball paradigm with four deviant stimuli. Relationships between MMN response features and behavioral results in CI individuals with distinct musical pitch discrimination ability were also investigated.

CI users generally had difficulty discriminating musical pitch changes compared with NH controls. The neurophysiological

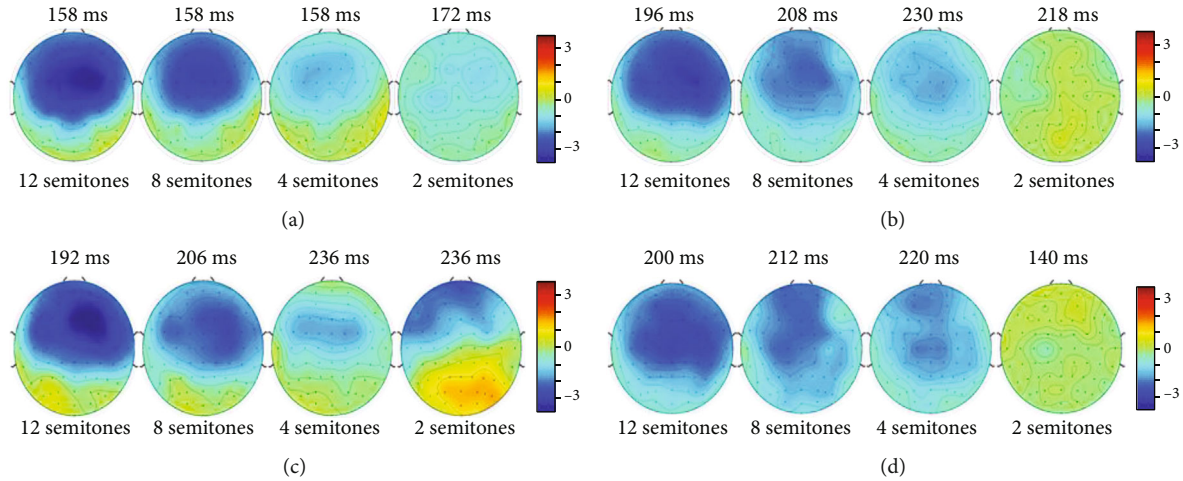


FIGURE 2: Contour maps of MMN amplitude for grand-average differences in waveforms for NH listeners (a) and CI users (b) and CI users with good (c) and poor (d) performance. Topological distributions are displayed at latencies with peak MMN amplitudes in each plane.

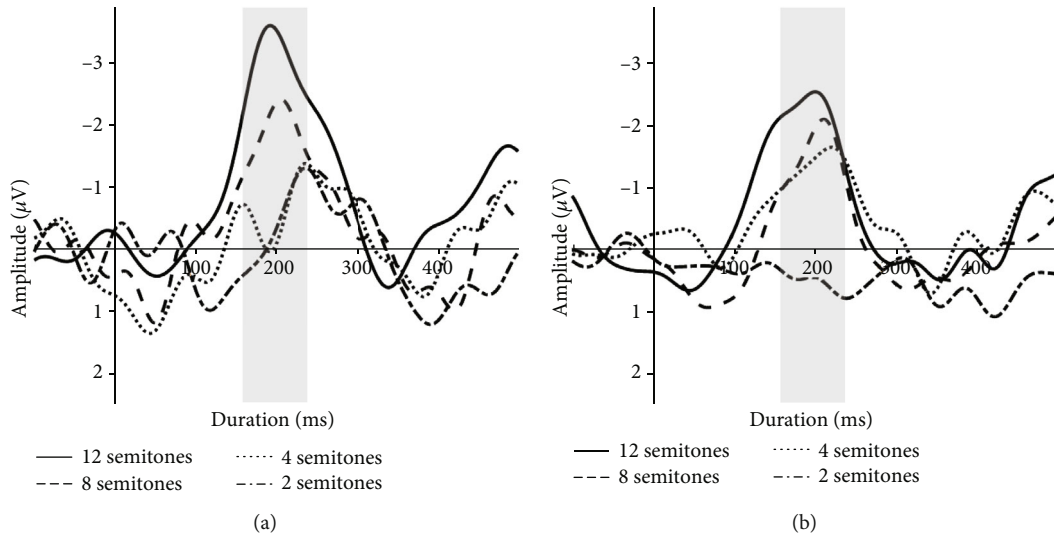


FIGURE 3: Grand-average MMN waveforms for distinct pitch differences for CI users with good (a) and poor (b) performance at electrode Fz. Gray shading indicates the time window used to calculate amplitudes and latencies (156–236 ms).

TABLE 4: MMN amplitude and latency (mean \pm standard deviation) according to pitch change in CI users with good and poor performance.

	Pitch changes	Amplitude (μV)	Latency (ms)
Cochlear implants (good performers)	12 semitones	-4.23 ± 0.94	196.00 ± 9.81
	8 semitones	-2.95 ± 0.82	190.80 ± 10.11
	4 semitones	-2.30 ± 0.06	202.00 ± 15.94
	2 semitones	-1.74 ± 0.87	209.00 ± 16.26
Cochlear implants (poor performers)	12 semitones	-3.50 ± 0.56	179.67 ± 11.13
	8 semitones	-2.64 ± 0.71	202.67 ± 13.23
	4 semitones	-2.51 ± 0.63	206.00 ± 12.68
	2 semitones	-0.27 ± 0.35	165.60 ± 7.72

data also demonstrated that CI users had more difficulty with preattentive discrimination of musical pitch than did NH listeners, reflected in significantly prolonged MMN latencies.

Researchers have suggested that poorer musical pitch perception in CI users compared with NH listeners is due to the lack of adequate temporal and spectral cues transmitted by the CI

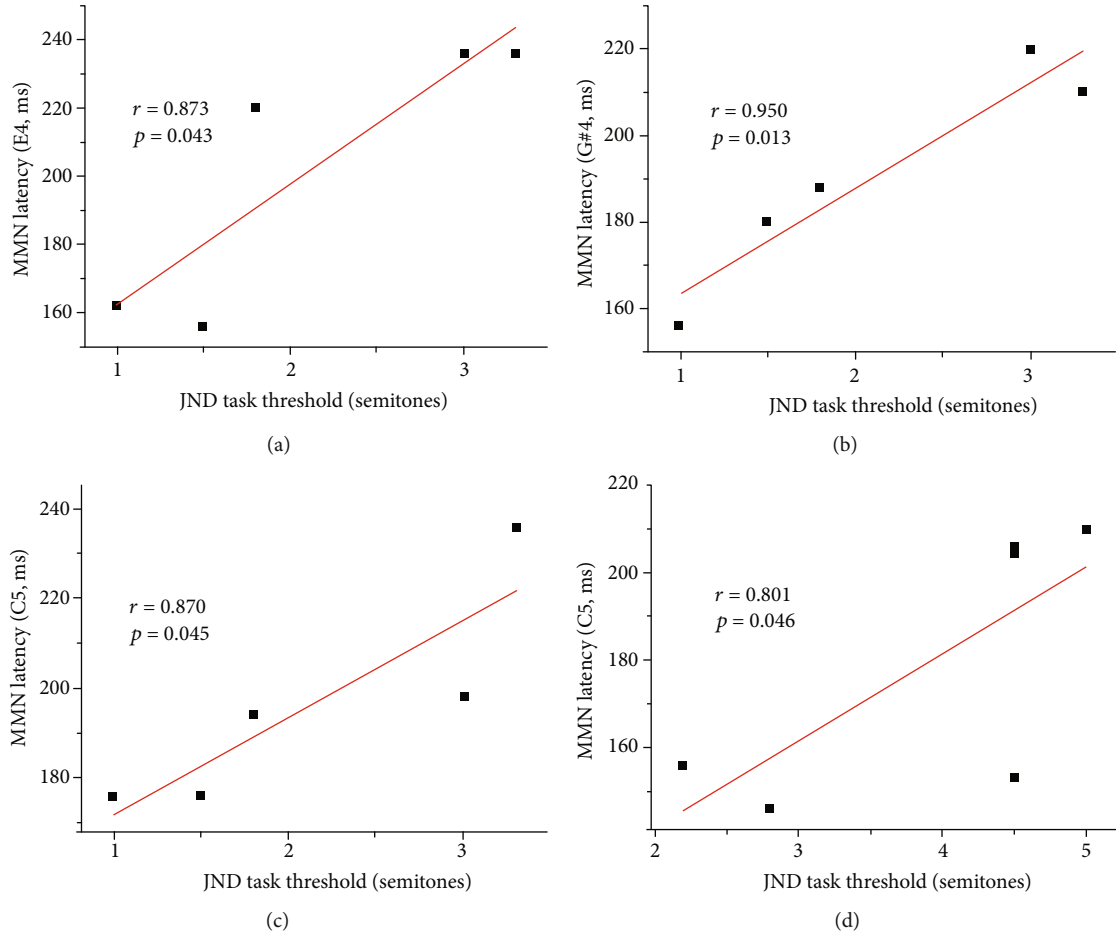


FIGURE 4: Correlations between JND task thresholds and MMN latency by pitch deviation in CI users with good (a–c) and poor (d) performance.

TABLE 5: Correlations between pitch discrimination thresholds and MMN amplitude and latency by pitch change in CI users with good and poor performance. Significant correlations ($p < 0.05$) are presented in bold.

MMN	Pitch changes	JND		PDD		
		r	p	r	p	
Cochlear implants (good performers)	Amplitude (μV)	12 semitones	-0.132	0.832	0.541	0.347
		8 semitones	-0.151	0.808	0.351	0.562
		4 semitones	-0.806	0.100	-0.100	0.873
	Latency (ms)	12 semitones	0.870	0.045	0.153	0.806
		8 semitones	0.950	0.013	-0.202	0.774
		4 semitones	0.873	0.043	-0.443	0.455
Cochlear implants (bad performers)	Amplitude (μV)	12 semitones	0.577	0.231	-0.386	0.450
		8 semitones	0.213	0.686	0.159	0.764
		4 semitones	0.152	0.774	0.005	0.992
	Latency (ms)	12 semitones	0.801	0.046	-0.631	0.179
		8 semitones	0.277	0.595	-0.556	0.242
		4 semitones	0.462	0.356	-0.679	0.138

device [46, 71]. The limited number of channels and crude spectral-temporal cues lead to poor spectral resolution, rendering the accurate comprehension of musical tones difficult [27]. In addition, the frequency information carried by the

electrodes likely does not match the actual frequency produced in the cochlea, which degrades pitch perception ability [72]. Moreover, the neurophysiological alterations and crossmodal plasticity of the auditory center that generally

accompany long-term deafness may interfere with auditory processing [73]. As in early studies [31], MMN responses were evoked mainly in the frontal area in this study. The topological distribution of MMN responses implies weaker preattentive auditory perception in CI users compared with NH listeners.

Early studies showed that CI users' pitch thresholds ranged from 1 to 24 semitones [24, 28]; we obtained similar behavioral results, with a range of 1.0–15.8 semitones and a high degree of variability among individuals. To better evaluate CI users' performance, we divided into good and poor performance groups according to JND and PDD task results. MMN responses have been proven to be objective predictors of musical pitch perception ability, with amplitudes and latencies sensitive to differences between deviant and standard stimuli [34]. Thus, we used MMN responses to compare preattentive cortical activation between well-performing and poorly performing CI users. The marginally significant increase in MMN amplitude for good performers relative to poor performers reflects consistency between the auditory cortical responses and behavioral results. In addition, well-performing, but not poorly performing, CI users showed MMN responses to 2-semitone pitch differences, reflecting the human brain's auditory plasticity after cochlear implantation and hearing rehabilitation. The behavioral results for all CI users did not reflect such sensitivity to 2-semitone differences; they reflect integrated auditory perception with peripheral and central stages, whereas MMN responses reflect only automatic preattentive pitch discrimination ability at the central level [74]. The MMN responses to 2-semitone pitch differences also support MMN as an effective cortical response predictor in the development of auditory training strategies and parameter settings for CI devices [75, 76].

This study revealed a positive correlation between the latency of MMN waveforms in CI users and the JND, but not PPD, task threshold. Some previous studies also demonstrated positive correlations between MMN responses and speech recognition scores [35, 39]. These results show that MMN responses are better for the identification of pitch difference discrimination ability in CI users. The lack of correlation with PDD results may arise from differences in behavioral test characteristics. The JND task requires subjects to detect differences in musical pitch, whereas the PDD task requires them to distinguish the highest of two pitches and to identify the contour of pitch changes in a successive pitch sequence. MMN responses are elicited when subjects preattentively detect differences between standard and deviant stimuli, which does not involve complex pitch recognition or advanced brain function. These properties may explain the correlation of these responses only with JND task performance. To further explore correlations between cortical responses and more complex cognitive behavioral results (i.e., of the PDD task), we will use an active experimental paradigm to examine EEG components in late latencies (e.g., P300 and N400) [77] in future studies.

Importantly, this work examined the musical pitch discrimination abilities of native Mandarin speakers using both behavioral and neurophysiological tests. Mandarin-speaking CI users may have advantages in pitch information identification due to their long-term exposure to the tonal

language environment. Early studies supported the similarity of the perceptual mechanism underlying the perception of Mandarin tones and musical pitches with electric stimulation [19, 78]. Consistent with previous findings [39, 42, 79, 80], we found that these CI users were able to distinguish musical pitches under a preattentive auditory condition. Furthermore, even slight (e.g., 2-semitone) pitch differences evoked MMN responses in Mandarin-speaking CI users with good behavioral performance. These findings suggest that the abilities to identify musical pitches and Mandarin tones are correlated. Better ability to discriminate Mandarin tones appears to facilitate the identification of musical pitch differences and vice versa.

In conclusion, this study evaluated the music pitch discrimination performance of Mandarin-speaking CI users and NH listeners using behavioral and MMN measures. MMN response latency was correlated strongly with the JND task pitch discrimination threshold in CI users. The CI users with good JND task performance had enhanced MMN amplitudes and shorter latencies compared with CI users with poor JND task performance. Consistent with findings from studies of English-speaking CI users, the findings from this work support the feasibility of MMN use for the evaluation of musical pitch identification performance and its potential to aid outcome evaluation following cochlear implantation and hearing rehabilitation among CI users.

Data Availability

The data used to support the findings of this study are available from the corresponding author upon request.

Conflicts of Interest

The authors declare that there is no conflict of interest regarding the publication of this paper.

Acknowledgments

The authors thank Dr. Ping LC and Professor Feng H who provided music assessment software for this study. We thank Lei Wang, Hua Li, and Fang Yu for assisting the EEG experiments. This work was supported by the National Natural Science Foundation of China (grant number 81670922), Science and Technology Planning Project of Guangdong Province (grant number 2017A020215144), and Natural Science Foundation of Guangdong Province (grant number 2020A151501253).

References

- [1] Y. Liu, J. Qi, X. Chen et al., "Critical role of spectrin in hearing development and deafness," *Science Advances*, vol. 5, no. 4, 2019.
- [2] S. Gao, C. Cheng, M. Wang et al., "Blebbistatin inhibits neomycin-induced apoptosis in hair cell-like HEI-OC-1 cells and in cochlear hair cells," *Frontiers in Cellular Neuroscience*, vol. 13, p. 590, 2019.

- [3] Z. He, L. Guo, Y. Shu et al., "Autophagy protects auditory hair cells against neomycin-induced damage," *Autophagy*, vol. 13, no. 11, pp. 1884–1904, 2017.
- [4] Z. H. He, S. Y. Zou, M. Li et al., "The nuclear transcription factor FoxG1 affects the sensitivity of mimetic aging hair cells to inflammation by regulating autophagy pathways," *Redox Biology*, vol. 28, p. 101364, 2020.
- [5] A. Li, D. You, W. Li et al., "Novel compounds protect auditory hair cells against gentamycin-induced apoptosis by maintaining the expression level of H3K4me2," *Drug Delivery*, vol. 25, no. 1, pp. 1033–1043, 2018.
- [6] H. Li, Y. Song, Z. He et al., "Meclofenamic acid reduces reactive oxygen species accumulation and apoptosis, inhibits excessive autophagy, and protects hair cell-like HEI-OC1 cells from cisplatin-induced damage," *Frontiers in Cellular Neuroscience*, vol. 12, p. 139, 2018.
- [7] W. Liu, X. Xu, Z. Fan et al., "Wnt signaling activates TP53-induced glycolysis and apoptosis regulator and protects against cisplatin-induced spiral ganglion neuron damage in the mouse cochlea," *Antioxidants & Redox Signaling*, vol. 30, no. 11, pp. 1389–1410, 2019.
- [8] Y. Zhang, W. Li, Z. He et al., "Pre-treatment with Fasudil prevents neomycin-induced hair cell damage by reducing the accumulation of reactive oxygen species," *Frontiers in Molecular Neuroscience*, vol. 12, p. 264, 2019.
- [9] C. Cheng, Y. Wang, L. Guo et al., "Age-related transcriptome changes in Sox2+ supporting cells in the mouse cochlea," *Stem Cell Research & Therapy*, vol. 10, no. 1, p. 365, 2019.
- [10] B. C. Cox, R. Chai, A. Lenoir et al., "Spontaneous hair cell regeneration in the neonatal mouse cochlea in vivo," *Development*, vol. 141, no. 4, pp. 816–829, 2014.
- [11] X. Lu, S. Sun, J. Qi et al., "Bmi1 regulates the proliferation of cochlear supporting cells via the canonical Wnt signaling pathway," *Molecular Neurobiology*, vol. 54, no. 2, pp. 1326–1339, 2017.
- [12] T. Wang, R. Chai, G. S. Kim et al., "Lgr5+ cells regenerate hair cells via proliferation and direct transdifferentiation in damaged neonatal mouse utricle," *Nature Communications*, vol. 6, no. 1, 2015.
- [13] S. Zhang, Y. Zhang, Y. Dong et al., "Knockdown of Foxg1 in supporting cells increases the trans-differentiation of supporting cells into hair cells in the neonatal mouse cochlea," *Cellular and Molecular Life Sciences*, vol. 77, no. 7, pp. 1401–1419, 2020.
- [14] G. M. Clark, "The multi-channel cochlear implant: multi-disciplinary development of electrical stimulation of the cochlea and the resulting clinical benefit," *Hearing Research*, vol. 322, pp. 4–13, 2015.
- [15] B. S. Wilson and M. F. Dorman, "Cochlear implants: a remarkable past and a brilliant future," *Hearing Research*, vol. 242, no. 1–2, pp. 3–21, 2008.
- [16] B. S. Wilson and M. F. Dorman, "Cochlear implants: current designs and future possibilities," *Journal of Rehabilitation Research and Development*, vol. 45, no. 5, pp. 695–730, 2008.
- [17] C. Garnham, M. O'Driscoll, R. Ramsden, and S. Saeed, "Speech understanding in noise with a Med-El COMBI 40+ cochlear implant using reduced channel sets," *Ear and Hearing*, vol. 23, no. 6, pp. 540–552, 2002.
- [18] C. J. Limb and A. T. Roy, "Technological, biological, and acoustical constraints to music perception in cochlear implant users," *Hearing Research*, vol. 308, pp. 13–26, 2014.
- [19] W. Wang, N. Zhou, and L. Xu, "Musical pitch and lexical tone perception with cochlear implants," *International Journal of Audiology*, vol. 50, no. 4, pp. 270–278, 2011.
- [20] S. J. Brockmeier, D. Fitzgerald, O. Searle et al., "The MuSIC perception test: a novel battery for testing music perception of cochlear implant users," *Cochlear Implants International*, vol. 12, no. 1, pp. 10–20, 2013.
- [21] R. Kang, G. L. Nimmons, W. Drennan et al., "Development and validation of the University of Washington Clinical Assessment of Music Perception test," *Ear and Hearing*, vol. 30, no. 4, pp. 411–418, 2009.
- [22] G. L. Nimmons, R. S. Kang, W. R. Drennan et al., "Clinical assessment of music perception in cochlear implant listeners," *Otology & Neurotology*, vol. 29, no. 2, pp. 149–155, 2008.
- [23] J. J. Galvin, Q.-J. Fu, and G. Nogaki, "Melodic contour identification by cochlear implant listeners," *Ear and Hearing*, vol. 28, no. 3, pp. 302–319, 2007.
- [24] K. Gfeller, C. Turner, J. Oleson et al., "Accuracy of cochlear implant recipients on pitch perception, melody recognition, and speech reception in noise," *Ear and Hearing*, vol. 28, no. 3, pp. 412–423, 2007.
- [25] K. Gfeller, S. Witt, M. Adamek et al., "Effects of training on timbre recognition and appraisal by postlingually deafened cochlear implant recipients," *Journal of the American Academy of Audiology*, vol. 13, no. 3, pp. 132–145, 2002.
- [26] K. Gfeller, S. Witt, G. Woodworth, M. A. Mehr, and J. Knutson, "Effects of frequency, instrumental family, and cochlear implant type on timbre recognition and appraisal," *The Annals of Otology, Rhinology, and Laryngology*, vol. 111, no. 4, pp. 349–356, 2002.
- [27] Y. Y. Kong, R. Cruz, J. A. Jones, and F. G. Zeng, "Music perception with temporal cues in acoustic and electric hearing," *Ear and Hearing*, vol. 25, no. 2, pp. 173–185, 2004.
- [28] K. Gfeller, C. Turner, M. Mehr et al., "Recognition of familiar melodies by adult cochlear implant recipients and normal-hearing adults," *Cochlear Implants International*, vol. 3, no. 1, pp. 29–53, 2002.
- [29] K. Gfeller, G. Woodworth, D. A. Robin, S. Witt, and J. F. Knutson, "Perception of rhythmic and sequential pitch patterns by normally hearing adults and adult cochlear implant users," *Ear and Hearing*, vol. 18, no. 3, pp. 252–260, 1997.
- [30] R. Näätänen, A. W. K. Gaillard, and S. Mäntysalo, "Early selective-attention effect on evoked potential reinterpreted," *Acta Psychologica*, vol. 42, no. 4, pp. 313–329, 1978.
- [31] R. Näätänen, P. Paavilainen, T. Rinne, and K. Alho, "The mismatch negativity (MMN) in basic research of central auditory processing: a review," *Clinical Neurophysiology*, vol. 118, no. 12, pp. 2544–2590, 2007.
- [32] R. Näätänen, M. Tervaniemi, E. Sussman, P. Paavilainen, and I. Winkler, "'Primitive intelligence' in the auditory cortex," *Trends in Neurosciences*, vol. 24, no. 5, pp. 283–288, 2001.
- [33] A. Sharp, A. Delcenserie, and F. Champoux, "Auditory event-related potentials associated with music perception in cochlear implant users," *Frontiers in Neuroscience*, vol. 12, p. 538, 2018.
- [34] R. Näätänen, B. Petersen, R. Torppa, E. Lonka, and P. Vuust, "The MMN as a viable and objective marker of auditory development in CI users," *Hearing Research*, vol. 353, pp. 57–75, 2017.
- [35] C. Turgeon, L. Lazzouni, F. Lepore, and D. Elleberg, "An objective auditory measure to assess speech recognition in

- adult cochlear implant users,” *Clinical Neurophysiology*, vol. 125, no. 4, pp. 827–835, 2014.
- [36] N. K. Vavatzanidis, D. Mürbe, A. Friederici, and A. Hahne, “The basis for language acquisition: congenitally deaf infants discriminate vowel length in the first months after cochlear implantation,” *Journal of Cognitive Neuroscience*, vol. 27, no. 12, pp. 2427–2441, 2015.
- [37] F. L. Bouwer, T. L. Van Zuijlen, and H. Honing, “Beat processing is pre-attentive for metrically simple rhythms with clear accents: an ERP study,” *PLoS One*, vol. 9, no. 5, 2014.
- [38] B. Petersen, E. Weed, P. Sandmann et al., “Brain responses to musical feature changes in adolescent cochlear implant users,” *Frontiers in Human Neuroscience*, vol. 9, 2015.
- [39] L. Timm, P. Vuust, E. Brattico et al., “Residual neural processing of musical sound features in adult cochlear implant users,” *Frontiers in Human Neuroscience*, vol. 8, 2014.
- [40] R. Torppa, M. Huotilainen, M. Leminen, J. Lipsanen, and M. Tervaniemi, “Interplay between singing and cortical processing of music: a longitudinal study in children with cochlear implants,” *Frontiers in Psychology*, vol. 5, 2014.
- [41] R. Torppa, E. Salo, T. Makkonen et al., “Cortical processing of musical sounds in children with cochlear implants,” *Clinical Neurophysiology*, vol. 123, no. 10, pp. 1966–1979, 2012.
- [42] P. Sandmann, A. Kegel, T. Eichele et al., “Neurophysiological evidence of impaired musical sound perception in cochlear-implant users,” *Clinical Neurophysiology*, vol. 121, no. 12, pp. 2070–2082, 2010.
- [43] T. Rahne, S. K. Plontke, and L. Wagner, “Mismatch negativity (MMN) objectively reflects timbre discrimination thresholds in normal-hearing listeners and cochlear implant users,” *Brain Research*, vol. 1586, pp. 143–151, 2014.
- [44] S. C. Peng, J. B. Tomblin, H. Cheung, Y. S. Lin, and L. S. Wang, “Perception and production of mandarin tones in prelingually deaf children with cochlear implants,” *Ear and Hearing*, vol. 25, no. 3, pp. 251–264, 2004.
- [45] V. Looi, E. R. Teo, and J. Loo, “Pitch and lexical tone perception of bilingual English-Mandarin-speaking cochlear implant recipients, hearing aid users, and normally hearing listeners,” *Cochlear Implants International*, vol. 16, supplement 3, pp. S91–S104, 2015.
- [46] D. Tao, R. Deng, Y. Jiang, J. J. Galvin III, Q. J. Fu, and B. Chen, “Melodic pitch perception and lexical tone perception in Mandarin-speaking cochlear implant users,” *Ear and Hearing*, vol. 36, no. 1, pp. 102–110, 2015.
- [47] L. Ping, M. Yuan, and H. Feng, “Musical pitch discrimination by cochlear implant users,” *The Annals of Otology, Rhinology, and Laryngology*, vol. 121, no. 5, pp. 328–336, 2012.
- [48] A. Delorme and S. Makeig, “EEGLAB: an open source toolbox for analysis of single-trial EEG dynamics including independent component analysis,” *Journal of Neuroscience Methods*, vol. 134, no. 1, pp. 9–21, 2004.
- [49] R. Näätänen, O. Syssoeva, and R. Takegata, “Automatic time perception in the human brain for intervals ranging from milliseconds to seconds,” *Psychophysiology*, vol. 41, no. 4, pp. 660–663, 2004.
- [50] S. Ylinen, A. Shestakova, M. Huotilainen, P. Alku, and R. Näätänen, “Mismatch negativity (MMN) elicited by changes in phoneme length: a cross-linguistic study,” *Brain Research*, vol. 1072, no. 1, pp. 175–185, 2006.
- [51] J. Qi, Y. Liu, C. Chu et al., “A cytoskeleton structure revealed by super-resolution fluorescence imaging in inner ear hair cells,” *Cell Discovery*, vol. 5, no. 1, 2019.
- [52] Y. He, X. Lu, F. Qian, D. Liu, R. Chai, and H. Li, “Insm1a is required for zebrafish posterior lateral line development,” *Frontiers in Molecular Neuroscience*, vol. 10, p. 241, 2017.
- [53] Z. He, Q. Fang, H. Li et al., “The role of FOXG1 in the postnatal development and survival of mouse cochlear hair cells,” *Neuropharmacology*, vol. 144, pp. 43–57, 2019.
- [54] L. Liu, Y. Chen, J. Qi et al., “Wnt activation protects against neomycin-induced hair cell damage in the mouse cochlea,” *Cell Death & Disease*, vol. 7, no. 3, p. e2136, 2016.
- [55] Y. Wang, J. Li, X. Yao et al., “Loss of CIB2 causes profound hearing loss and abolishes mechanoelectrical transduction in mice,” *Frontiers in Molecular Neuroscience*, vol. 10, p. 401, 2017.
- [56] X. Yu, W. Liu, Z. Fan et al., “c-Myb knockdown increases the neomycin-induced damage to hair-cell-like HEI- OC1 cells in vitro,” *Scientific Reports*, vol. 7, no. 1, 2017.
- [57] C. Zhu, C. Cheng, Y. Wang et al., “Loss of ARHGEF6 causes hair cell stereocilia deficits and hearing loss in mice,” *Frontiers in Molecular Neuroscience*, vol. 11, p. 362, 2018.
- [58] Y. Chen, X. Lu, L. Guo et al., “Hedgehog signaling promotes the proliferation and subsequent hair cell formation of progenitor cells in the neonatal mouse cochlea,” *Frontiers in Molecular Neuroscience*, vol. 10, p. 426, 2017.
- [59] C. Cheng, L. Guo, L. Lu et al., “Characterization of the transcriptomes of Lgr5+ hair cell progenitors and Lgr5- supporting cells in the mouse cochlea,” *Frontiers in Molecular Neuroscience*, vol. 10, p. 122, 2017.
- [60] F. Tan, C. Chu, J. Qi et al., “AAV-ie enables safe and efficient gene transfer to inner ear cells,” *Nature Communications*, vol. 10, no. 1, p. 3733, 2019.
- [61] J. Wu, W. Li, C. Lin et al., “Co-regulation of the Notch and Wnt signaling pathways promotes supporting cell proliferation and hair cell regeneration in mouse utricles,” *Scientific Reports*, vol. 6, no. 1, 2016.
- [62] D. You, L. Guo, W. Li et al., “Characterization of Wnt and Notch-responsive Lgr5+ hair cell progenitors in the striolar region of the neonatal mouse utricle,” *Frontiers in Molecular Neuroscience*, vol. 11, p. 137, 2018.
- [63] R. Guo, S. Zhang, M. Xiao et al., “Accelerating bioelectric functional development of neural stem cells by graphene coupling: implications for neural interfacing with conductive materials,” *Biomaterials*, vol. 106, pp. 193–204, 2016.
- [64] G. Li, K. Chen, D. You et al., “Laminin-coated electrospun regenerated silk fibroin mats promote neural progenitor cell proliferation, differentiation, and survival in vitro,” *Frontiers in Bioengineering and Biotechnology*, vol. 7, p. 190, 2019.
- [65] M. Tang, J. Li, L. He et al., “Transcriptomic profiling of neural stem cell differentiation on graphene substrates,” *Colloids and Surfaces. B, Biointerfaces*, vol. 182, p. 110324, 2019.
- [66] Y. Yang, Y. Zhang, R. Chai, and Z. Gu, “Designs of biomaterials and microenvironments for neuroengineering,” *Neural Plasticity*, vol. 2018, Article ID 1021969, 10 pages, 2018.
- [67] Z. He, S. Zhang, Q. Song et al., “The structural development of primary cultured hippocampal neurons on a graphene substrate,” *Colloids and Surfaces. B, Biointerfaces*, vol. 146, pp. 442–451, 2016.
- [68] G. Sun, W. Liu, Z. Fan et al., “The three-dimensional culture system with matrigel and neurotrophic factors preserves the structure and function of spiral ganglion neuron in vitro,” *Neural Plasticity*, vol. 2016, Article ID 4280407, 15 pages, 2016.

- [69] M. Waqas, S. Sun, C. Xuan et al., “Bone morphogenetic protein 4 promotes the survival and preserves the structure of flow-sorted Bhlhb5+ cochlear spiral ganglion neurons _in vitro_,” *Scientific Reports*, vol. 7, no. 1, p. 3506, 2017.
- [70] W. Yan, W. Liu, J. Qi et al., “A three-dimensional culture system with matrigel promotes purified spiral ganglion neuron survival and function in vitro,” *Molecular Neurobiology*, vol. 55, no. 3, pp. 2070–2084, 2018.
- [71] R. P. Carlyon, J. M. Deeks, and C. M. McKay, “The upper limit of temporal pitch for cochlear-implant listeners: stimulus duration, conditioner pulses, and the number of electrodes stimulated,” *The Journal of the Acoustical Society of America*, vol. 127, no. 3, pp. 1469–1478, 2010.
- [72] M. W. Skinner, D. R. Ketten, L. K. Holden et al., “CT-derived estimation of cochlear morphology and electrode array position in relation to word recognition in Nucleus-22 recipients,” *Journal of the Association for Research in Otolaryngology*, vol. 3, no. 3, pp. 332–350, 2002.
- [73] J. Rouger, S. Lagleyre, J. F. Démonet, B. Fraysse, O. Deguine, and P. Barone, “Evolution of crossmodal reorganization of the voice area in cochlear-implanted deaf patients,” *Human Brain Mapping*, vol. 33, no. 8, pp. 1929–1940, 2012.
- [74] P. Ungan, H. Karsilar, and S. Yagcioglu, “Pre-attentive mismatch response and involuntary attention switching to a deviance in an earlier-than-usual auditory stimulus: an ERP study,” *Frontiers in Human Neuroscience*, vol. 13, p. 58, 2019.
- [75] Q. J. Fu, G. Nogaki, and J. J. Galvin III, “Auditory training with spectrally shifted speech: implications for cochlear implant patient auditory rehabilitation,” *Journal of the Association for Research in Otolaryngology*, vol. 6, no. 2, pp. 180–189, 2005.
- [76] D. A. Nikjeh, J. J. Lister, and S. A. Frisch, “Preattentive cortical-evoked responses to pure tones, harmonic tones, and speech: influence of music training,” *Ear and Hearing*, vol. 30, no. 4, pp. 432–446, 2009.
- [77] A. G. Maglione, A. Scorpecci, P. Malerba et al., “Alpha EEG frontal asymmetries during audiovisual perception in cochlear implant users: a study with bilateral and unilateral young users,” *Methods of Information in Medicine*, vol. 54, no. 6, pp. 500–504, 2018.
- [78] X. Gu, B. Liu, Z. Liu et al., “A follow-up study on music and lexical tone perception in adult Mandarin-speaking cochlear implant users,” *Otology & Neurotology*, vol. 38, no. 10, pp. e421–e428, 2017.
- [79] P. Sandmann, T. Eichele, M. Buechler et al., “Evaluation of evoked potentials to dyadic tones after cochlear implantation,” *Brain*, vol. 132, no. 7, pp. 1967–1979, 2009.
- [80] F. Zhang, C. Benson, and Q. J. Fu, “Cortical encoding of pitch contour changes in cochlear implant users: a mismatch negativity study,” *Audiology & Neuro-Otology*, vol. 18, no. 5, pp. 275–288, 2013.

Research Article

Toxic Effects of 3,3'-Iminodipropionitrile on Vestibular System in Adult C57BL/6J Mice *In Vivo*

Shan Zeng,^{1,2} Wenli Ni,^{1,2} Hui Jiang,¹ Dan You,^{1,2} Jinghan Wang,^{1,2} Xiaoling Lu,^{1,2} Liman Liu,^{2,3} Huiqian Yu,^{1,2} Jingfang Wu,^{1,2} Fangyi Chen,⁴ Huawei Li,^{1,2} Yunfeng Wang ^{1,2}, Yan Chen ^{1,2} and Wenyan Li ^{1,2}

¹ENT Institute and Otorhinolaryngology Department of Affiliated Eye and ENT Hospital, State Key Laboratory of Medical Neurobiology, Fudan University, Shanghai 200031, China

²Institutes of Biomedical Sciences, Fudan University, Shanghai 200032, China

³The First Affiliated Hospital of Sun Yat-sen University, Guangzhou 510080, China

⁴Department of Biomedical Engineering, Southern University of Science and Technology, Shenzhen, Guangdong 518055, China

Correspondence should be addressed to Yunfeng Wang; yunfengwang@fudan.edu.cn, Yan Chen; mchenyan0528@163.com, and Wenyan Li; wenyan_li2000@126.com

Received 22 March 2020; Revised 1 June 2020; Accepted 11 June 2020; Published 3 July 2020

Academic Editor: Hai Huang

Copyright © 2020 Shan Zeng et al. This is an open access article distributed under the Creative Commons Attribution License, which permits unrestricted use, distribution, and reproduction in any medium, provided the original work is properly cited.

The utricle is one of the five sensory organs in the mammalian vestibular system, and while the utricle has a limited ability to repair itself, this is not sufficient for the recovery of vestibular function after hair cell (HC) loss induced by ototoxic drugs. In order to further explore the possible self-recovery mechanism of the adult mouse vestibular system, we established a reliable utricle epithelium injury model for studying the regeneration of HCs and examined the toxic effects of 3,3'-iminodipropionitrile (IDPN) on the utricle *in vivo* in C57BL/6J mice, which is one of the most commonly used strains in inner ear research. This work focused on the epithelial cell loss, vestibular dysfunction, and spontaneous cell regeneration after IDPN administration. HC loss and supporting cell (SC) loss after IDPN treatment was dose-dependent and resulted in dysfunction of the vestibular system, as indicated by the swim test and the rotating vestibular ocular reflex (VOR) test. EdU-positive SCs were observed only in severely injured utricles wherein above 47% SCs were dead. No EdU-positive HCs were observed in either control or injured utricles. RT-qPCR showed transient upregulation of *Hes5* and *Hey1* and fluctuating upregulation of *Axin2* and β -*catenin* after IDPN administration. We conclude that a single intraperitoneal injection of IDPN is a practical way to establish an injured utricle model in adult C57BL/6J mice *in vivo*. We observed activation of Notch and Wnt signaling during the limited spontaneous HC regeneration after vestibular sensory epithelium damage, and such signaling might act as the promoting factors for tissue self-repair in the inner ear.

1. Introduction

The sensory organs of the mammalian inner ear include the organ of Corti in the cochlea, which senses sound, and the macula sacculi, macula utriculi, and crista ampullaris from the vestibular system that sense acceleration and postural signals. HCs are the mechanoreceptors in all inner ear sensory organs and are thus responsible for normal auditory and balance functions. HCs are vulnerable to multiple injury factors, including genetic abnormalities, aging, noise, infection, oto-

toxic drugs, traumas, and tumors [1, 2]. Unlike nonmammalian vertebrates, the sensory organs of the mammalian inner ear have only very limited self-renewal capacity in the vestibular system and no self-renewal in the cochlea, and this means that dysfunction of vestibular sensation and hearing is permanent [1–3]. Thus, it is a very important task to promote HC regeneration and rebuild the function of the inner ear. However, unlike a cochlear injury model, there are few practical vestibular injury models reported with data of objective tests for evaluating the function of the vestibular

system in mice similar to the ABR test for hearing or the changes of gene expression. The present work focused on the development of the IDPN-induced adult mouse vestibular injury model.

The compound 3,3'-iminodipropionitrile (IDPN) has been reported to be neurotoxic and vestibulotoxic [4, 5] resulting in loss of vestibular sensory epithelial cells in rats and mice and leading to irreversible loss of peripheral vestibular function [6–10], and thus, IDPN can be used for an *in vivo* model of adult mammalian vestibular dysfunction. In the present study, we further evaluated the dose-dependent toxic effects of IDPN on the vestibular epithelium in adult C57BL/6J mice, and the rotating vestibular ocular reflex (VOR) was measured as an objective reflection of the function of the vestibular system, which was crossvalidated with the traditionally used swim test [10–12]. Furthermore, we investigated the limited self-renewal process in the mouse utricle after the injury induced by a single injection of IDPN, as well as the gene expression profile related to multiple signaling pathways during the HC regeneration process, which might provide the potential signaling targets for promoting the HC regeneration.

2. Materials and Methods

2.1. Animals. Adult C57BL/6J wild-type mice 30 days old (P30) and weighing about 20 g were provided by the Department of Laboratory Animal Science of Fudan University. Each animal in the acute injury group received a single intraperitoneal injection of IDPN (TCI Shanghai, No. I0010, 2, 3, 4, 5, or 6 mg IDPN/g body weight, $d = 1.02 \text{ g/mL}$, $1 \mu\text{L} \approx 1 \text{ mg}$) or saline (0.9% *w/v* NaCl) regardless of their gender or estrous cycle stages ($n = 3$ animals for each group). Each animal in the subacute injury group received a daily intraperitoneal injection of IDPN (0.5, 0.75, or 1 mg IDPN/g body weight) or saline (0.9% *w/v* NaCl) for 7 consecutive days ($n = 3$ animals for each group). To explore if there was spontaneous cell regeneration, EdU was intraperitoneally injected daily at 5 mg/mL starting at D6 after IDPN injection ($n = 3$ animals for each group). All animal experiments were approved by the Institutional Animal Care and Use Committee of Fudan University.

2.2. Vestibular Function Tests. The swim test was evaluated on day 7 (D7) after IDPN injection (0, 2, 4, and 6 mg IDPN/g body weight, $n = 3$ animals for each group). The mouse was placed in a standard cage with about 30 cm of warm water (about 37°C) in it. Swimming was recorded by camera and scored 0–3 according to their swim behavior [11]. Vestibular function was also evaluated by a binocular VOG-based VFT system provided by Prof. Fangyi Chen's team from Southern University of Science and Technology at 7 days (7d), 1 month (1m), and 3 months (3m) after IDPN injection (0, 2, 4, and 6 mg IDPN/g body weight, $n = 3$ animals for each group). IDPN-administrated mouse was placed in a custom-built box adapted to its weight and then fixed on the rotating platform. Mirror images of eye movement were synchronously recorded by the side cameras as the platform rotated at 0.25, 0.5, and 1 Hz under infrared illumination.

The recording frame rate was 30 fps, and each record contained at least 1000 frames. Videos of the mouse's pupil movements were then analyzed by customized software to acquire pupil position data. Exported eye-location data underwent Fourier transformation using the MATLAB 2016b software to obtain amplitude data for eye movement, then calculated to gain values, which are defined as the ratio of amplitude between response and stimulus [12].

2.3. Histological Labeling. Temporal bones were dissected after the animals were sacrificed by cervical dislocation. The utricles were harvested under a stereomicroscope then fixed in 4% paraformaldehyde (Sigma) for 20 min at 4°C, rinsed in PBS, and decalcified in 10% EDTA for 5–10 min at 37°C to remove the otolith. All utricles were blocked with 10% goat serum and 1% Triton X-100 in PBS overnight at 4°C. All antibodies were diluted in 1% Triton X-100 in PBS. Primary antibodies included rabbit anti-MyosinVIIa (anti-MyoVIIa, 1:800 dilutions, Proteus BioSciences, No.20-6790) to mark HCs and goat anti-Sox2 (1:300 dilutions, Santa Cruz, No.sc-17320) to mark Sox2+ cells. Alexa Fluor 647 Donkey anti-Rabbit (1:500 dilutions, Invitrogen, No. A-31573) and Alexa Fluor cy3 Donkey anti-Goat (1:500, dilutions, Jackson, No.705-165-003) were used for detection of primary antibodies. The Click-iT EdU Imaging Kit (Life Technologies, No. E10415) was used to identify proliferative cells. Nuclei were labeled with DAPI (1:1,000 dilutions, Invitrogen, No. D3571).

2.4. Cell Counts in the Utricle. Stained utricles were scanned with a confocal microscope (Leica TCS SP8, 40x oil objective, resolution 1024×1024 , slice thickness 1–1.5 μm). The numbers of MyoVIIa+ cells (HCs), Sox2+-supporting cells (SCs), and Sox2+/MyoVIIa+ cells (Sox2+ HCs) in the striolar and extrastriolar regions were counted with ImageJ software per $100 \mu\text{m} \times 100 \mu\text{m}$ area; two different areas were counted in the striolar and extrastriolar regions, for every utricle.

2.5. RNA Extraction and Real-Time PCR. TRIzol (Life Technologies, No.15596-026) was used to isolate total RNA, and mRNA was reverse transcribed with the GoScript Reverse Transcription System (GoTaq 2-Step RT qPCR System, Promega, No. A6010) according to the manufacturer's protocol. Utricle samples were dissected in cold PBS at 4°C and put into the TRIzol solution immediately and the RNA isolation was processed. Isolated RNA samples were preserved at -20°C. Quantitative real-time PCR was performed using the GoTaq qPCR Master Mix (GoTaq 2-Step RT qPCR System, Promega, No. A6010) and analyzed on an Applied Biosystems 7500. Samples were placed on ice throughout the experiment. The required cDNAs for each experiment were reversed from 1 μg RNA. All primers were provided by the Invitrogen company (see Table 1) and *Gapdh* was used as the internal reference. Three repetitions were performed in each experiment, and two batches of samples were repeated for each group. The $2^{-\Delta\Delta\text{CT}}$ method was used to analyze gene expression relative to *Gapdh* expression. Two-tailed Student's *t*-test was used to determine differences between groups.

TABLE 1: RT-PCR primer sequence.

Gene	Forward primer (5'-3')	Reverse primer (5'-3')
p27kip1	CGGTGCCTTTAATTGGGTCT	AGCAGGTCGCTTCC TCATC
β -Catenin	ATGCGCTCCCCTCAGATGGTGTC	TCGCGGTGGTGAGA AAGGTTGTGC
Axin2	TGACTCTCCTTCCAGATCCCA	TGCCACACTAGG CTGACA
Hes5	TGCTCAGTCCCAAGGAGAAA	AGCTTGGAGTTGG GCTGGT
Hey1	CACTGCAGGAGGAAAGGTTAT	CCCCAACTCC GATAGTCCAT
Notch1	GGAGGACCTCATCAACTCACA	CGTTCTTCAGGAG CACAACA
GAPDH	TGCGACTTCAACAGCAACTC	ATGAGGTCCACCACCTGT

2.6. Data Analysis. One-way or two-way ANOVA test and Tukey's multiple comparison test were employed for statistical analysis by GraphPad Prism 6.0. The detected difference was defined to be significant when $p < 0.05$. According to the acquired p values, three levels of significance ($p < 0.05$, $p < 0.01$, and $p < 0.001$) were rated and indicated in the results.

3. Results

3.1. A Single Injection of IDPN Caused Dose-Dependent Acute Utricular Sensory Epithelium Injury. In order to obtain a reliable adult mouse utricular injury model *in vivo*, we gave adult mice (P30) a single intraperitoneal injection of IDPN at different doses (2, 3, 4, 5, and 6 mg/g body weight). Compared with controls, the mice started to show minor abnormal behavior like head tossing/bobbing at D4 after IDPN injection, while no obvious sensory cell loss was observed in the utricle by immunostaining at this stage (data not shown). Vestibular dysfunction increased gradually until reaching a stable state at D6, and the utricles were harvested at D7. In the saline controls, HCs and SCs were arranged in an orderly fashion with no defects (Figures 1(a1)–1(c1)). The density of HCs decreased dose-dependently as the IDPN concentration increased from 2 to 6 mg/g body weight, especially in the striolar area (Figures 1(a1)–1(c6)). At 2, 3, 4, 5, and 6 mg IDPN/g body weight, the HCs were about $66.82 \pm 11.03\%$ and $87.01 \pm 9.69\%$, $42.26 \pm 10.69\%$ and $52.84 \pm 7.06\%$, $24.52 \pm 16.51\%$ and $35.45 \pm 13.83\%$, $3.41 \pm 3.11\%$ and $12.56 \pm 8.30\%$, and $0.12 \pm 0.31\%$ and $1.03 \pm 1.21\%$ that of controls in the striolar and extrastriolar areas, respectively. Total HC loss at each IDPN concentration in both the striolar and extrastriolar areas was significant compared with control group, respectively (Figure 1(d), $p < 0.01$). There was no SC loss until the IDPN concentration reached 5 mg/g body weight (Figure 1(e), $p < 0.001$). In contrast, no significant loss of Sox2+ HCs, which are assumed to be Type II HCs [13], was observed in both the extrastriolar and striolar regions of the 2 and 3 mg IDPN/g body weight mice (Figure 1(f), $p > 0.05$). The proportion of Sox2+ HCs among the HCs was $46.58 \pm 6.71\%$ in the extrastriolar area and $47.23 \pm 15.57\%$

in the striolar area when the IDPN dosage was 2 mg/g body weight, and this was similar to that of the control group (Figure 1(g), $p > 0.05$). As the IDPN dosage increased from 3 to 6 mg/g body weight, the proportion of Sox2+ HCs among the HCs also increased from $83.26 \pm 11.04\%$ in the extrastriolar area and $89.67 \pm 3.70\%$ in the striolar area to 100% in both areas (Figure 1(g), $p < 0.001$).

3.2. Consecutive Injection of IDPN Caused Dose-Dependent Subacute Utricular Sensory Epithelium Injury. P30 mice received daily intraperitoneal injections of IDPN (0.5, 0.75, or 1 mg/g body weight) or saline (0.9% w/v NaCl) for 7 consecutive days. The mice showed head tossing/bobbing starting at D7, and utricles were harvested at D14 (7 days after the last injection). In the control group, HCs and SCs were arranged in an orderly fashion and showed no obvious defects (Figures 2(a1)–2(c1)). The density of HCs decreased dose-dependently as the IDPN concentration increased from 0.5 to 1 mg/g body weight, especially in the striolar area (Figures 2(a2)–2(a4), 2(b2)–2(b4), 2(c2)–2(c4), and 2(d)). Obvious SC loss was observed in the utricles when 1 mg/g body weight IDPN was consecutively administered, and very few HCs survived in these samples (Figures 2(b2)–2(b4), 2(c2)–2(c4), and 2(e)). More than 90% of the surviving utricular HCs were Sox2+ HCs (Type II HCs) after consecutive injections of IDPN (Figure 2(g)).

There was no significant difference between the injury induced by either the single 4 mg/g body weight IDPN injection or the consecutive 0.5 mg/g body weight IDPN injections except SCs in the striolar area (the cumulative IDPN concentration was 3.5 mg/g body weight) (HCs in the extrastriolar area: 83.25 ± 32.48 vs. 85.50 ± 7.61 , $p = 0.87$; HCs in the striolar area: 49.75 ± 33.49 vs. 59.67 ± 5.09 , $p = 0.49$; SCs in the extrastriolar area: 278.42 ± 16.45 vs. 281.17 ± 15.16 , $p = 0.74$; SCs in the striolar area: 269.33 ± 13.57 vs. 252.17 ± 16.31 , $p = 0.03$). There was greater HC loss and Sox2+ SC loss caused by the single IDPN injection when we compared the samples between the cumulative 0.75 mg IDPN/g body weight injections and the single injection of 5 mg IDPN/g body weight (HCs in the extrastriolar area: 60.5 ± 14.8 vs. 29.50 ± 19.50 , $p = 0.004$; HCs in the striolar area: $31.67 \pm$

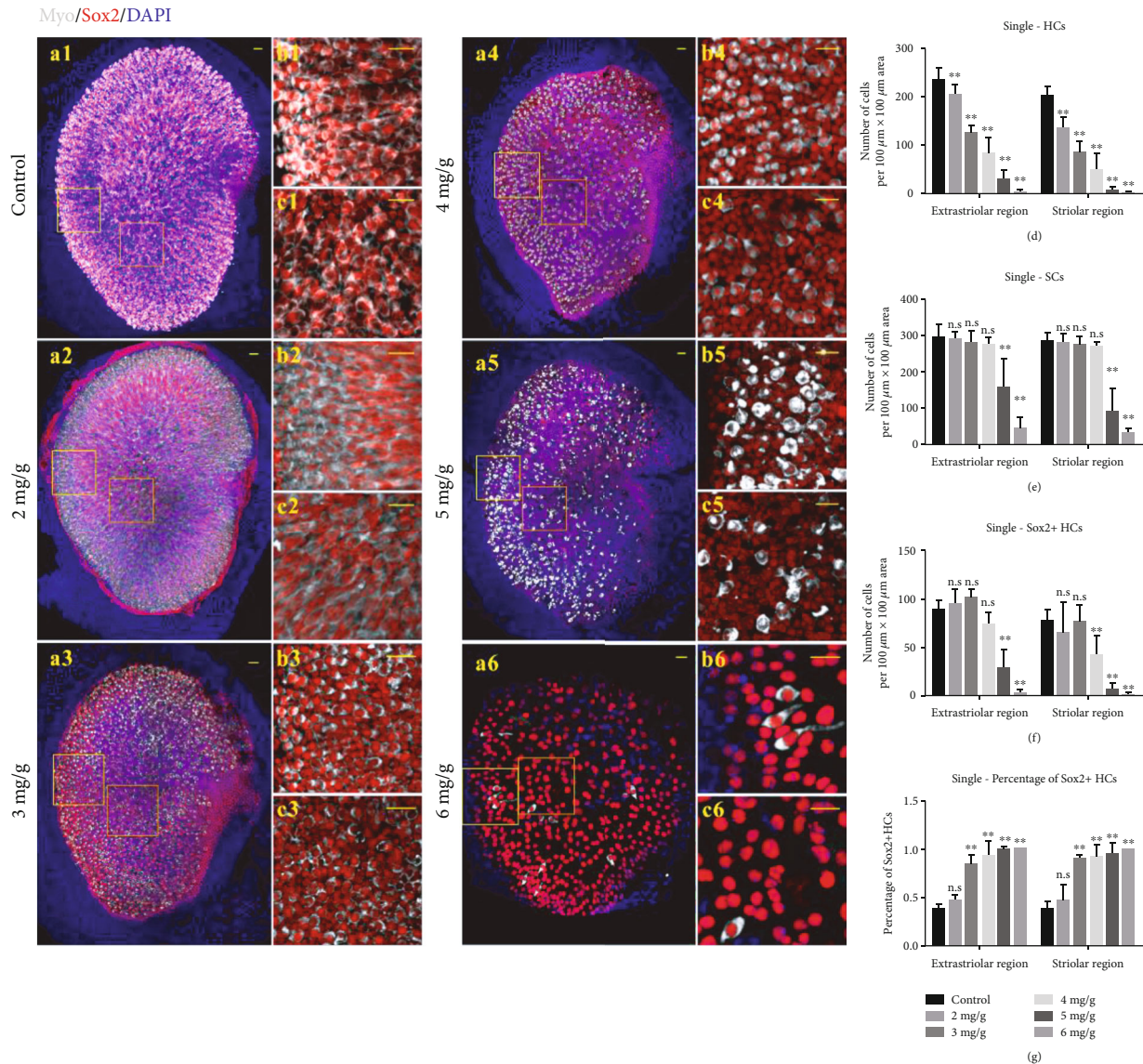


FIGURE 1: A single injection of IDPN induced dose-dependent acute utricular sensory epithelium injury. The numbers of HCs, SCs, and Sox2 + HCs were counted with ImageJ software per $100 \mu\text{m} \times 100 \mu\text{m}$ area, two different areas in the extrastriar region (yellow square frame) and striolar region (orange square frame) for every utricle (a1–a6). (b1–c6) showed zoomed pictures within the yellow (b1–b6) and orange (c1–c6) square rectangle tool. In controls (a1), MyoVIIa+ HCs, and Sox2+ SCs were arranged in an orderly fashion and showed no defects. MyoVIIa+ HCs became sparser dose-dependently, especially in the striolar area (b2–b6, c2–c6). No significant loss of Sox2+ SCs was observed until 5 or 6 mg IDPN/g body weight was injected (b2–b6, c2–c6). Graphs (d, e, f) show the average numbers of HCs, SCs, and Sox2+ HCs, in the extrastriar and striolar regions per $100 \mu\text{m} \times 100 \mu\text{m}$ area after a single IDPN injection. Graph (g) shows the percentage of Sox2+ HCs after a single IDPN injection. The scale bars indicate $20 \mu\text{m}$. $**p < 0.01$.

10.09 vs. 6.92 ± 6.32 , $p \leq 0.0001$; SCs in the extrastriar area: 259.83 ± 25.83 vs. 157.58 ± 79.68 , $p = 0.008$; SCs in the striolar area: 254.33 ± 17.24 vs. 94.42 ± 58.75 , $p < 0.0001$). Based on these results, a single IDPN injection may cause more severe vestibular damage as the IDPN concentration increases.

3.3. Rotating VOR Test Served as a More Sensitive Objective Measurement for the Function of the Vestibular System. Behavioral tests and electrophysiological examination are commonly used methods for vestibular assessment for mice [11, 14, 15]. However, it is very difficult to test the function

of the utricle exactly and directly without surgery. Behavior observation, swim test, and rotating VOR test were employed to evaluate the overall vestibular function after IDPN administration.

Because dysfunction of the vestibular system generally manifests as disequilibrium or disorientation, we observed the mice's behavior daily after IDPN injection to evaluate the function of the vestibular system [11]. The mice showed spontaneous head shaking at D4 after a single IDPN injection, and the severity of head shaking was positively correlated with the dose of IDPN. Furthermore, the mice showed trunk curling (Figures 3(a) and 3(b)) and circling

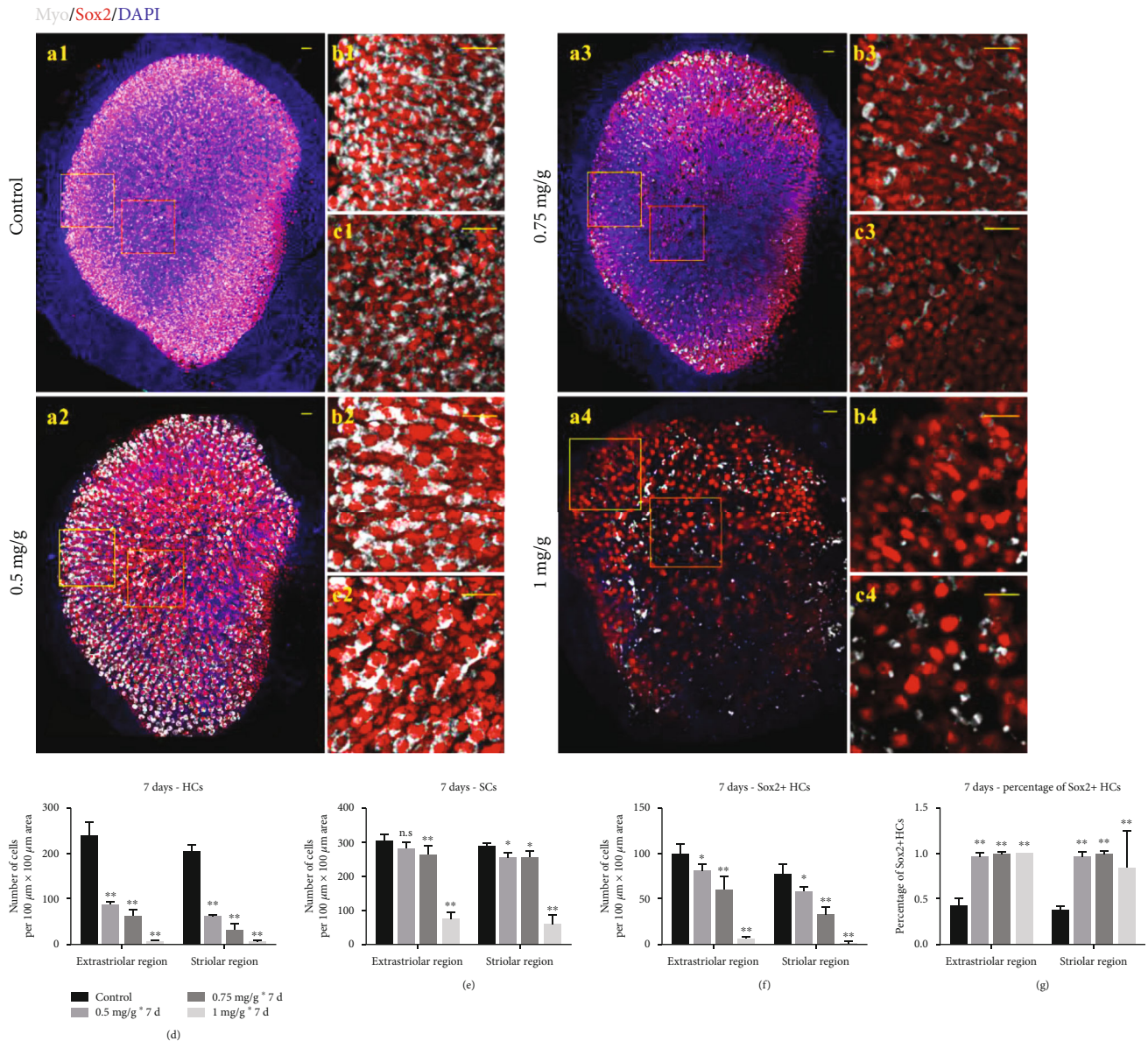


FIGURE 2: Consecutive injection of IDPN induced dose-dependent subacute utricular sensory epithelium injury. In controls (a1), MyoVIIa+ HCs and Sox2+ SCs were arranged in an orderly fashion and had no defects. MyoVIIa+ HCs also became sparser dose-dependently especially in the striolar area (b2–b4, c2–c4). A slight decrease in Sox2+ SCs can be seen in the utricle after 7 consecutive days of 0.5 and 0.75 mg IDPN/g body weight injection (c2–c3). Obvious loss of HCs and SCs was observed in the utricles when 1 mg/g body weight IDPN was consecutively administered, and only a few HCs survived (a4–c4). Graphs (d, e, f) showed the average numbers of HCs, Sox2+ SCs, and Sox2+ HCs, in the extrastriolar and striolar regions per 100 $\mu\text{m} \times 100 \mu\text{m}$ area after 7 consecutive days of IDPN injection. Graph (g) shows the percentage of Sox2+ HCs after 7 consecutive days of IDPN injection. The scale bars indicate 20 μm . * $p < 0.05$ and ** $p < 0.01$.

(Figures 3(c) and 3(d)) at D6 after a single injection of 4 mg IDPN/g body weight.

The swim test was performed at D7 to quantitatively evaluate the effect of IDPN on vestibular function [11]. Mice from the control group performed normal swimming behavior in which the tail propelled their movement through the water, and they balanced their heads and backs on the water with all four limbs in motion (Figure 3(e), score 0). Mice from the IDPN injection group displayed vestibular anomalies in the water. Mouse displayed normal swimming (score 0) or slightly unbalanced swimming behavior (score 1) after

2 mg/g body weight IDPN administration. When the dose of IDPN reached 4 mg/g body weight or more, the swim scores were all 2 or 3 (Figures 3(f) and 3(g)). Scores showed no difference after 2 mg/g body weight IDPN injection (Figure 3(h), average score 0.67 ± 0.47 , $p > 0.05$ compared with control mice) and were significantly raised when the IDPN dose increased from 4 to 6 mg/g body weight (Figure 3(h), average score 2.33 ± 0.47 and 2.67 ± 0.47 , respectively, all $p < 0.01$ compared with the control mice). There were no significant differences between the 4 and 6 mg IDPN/g body weight groups (Figure 3(h), $p > 0.05$).

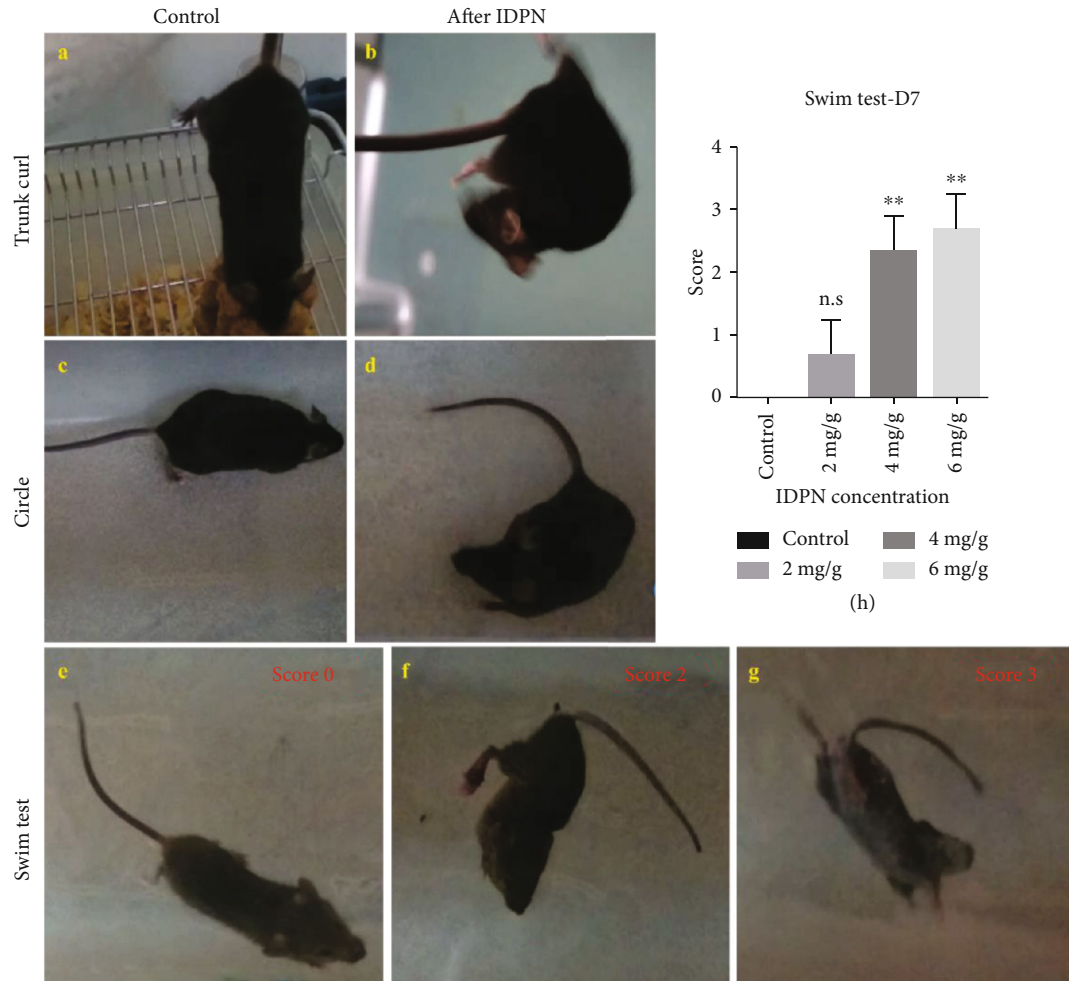


FIGURE 3: The behavioral tests showed the dysfunction of the vestibular system after IDPN injection. A simple trunk curl test showed that control mice would reach towards the horizontal surface when their tails were held (a), while the mice with vestibular injury would curl towards their abdomen (b). When placed on a table, control mice would walk straight and balanced (c), while animals with vestibular impairment would walk in circles chasing their tails (d). The swim test can yield a score for general vestibular function. Mice in water will swim (e) (score 0), swim irregularly (not shown in figure, score 1), float immobile (f) (score 2), or tumble underwater (g) (score 3). Graph (h) showed the swim test scores on D7 after different concentrations of single IDPN injections which get higher with the increase in IDPN dose. However, scores showed no significant difference in the 2 mg IDPN/g body weight injected mice compared to controls. Ordinary one-way ANOVA of swim test ($p = 0.0005$) with Tukey's multiple comparisons test were performed with GraphPad Prism 6.01. ** $p < 0.01$.

Dysfunction of the vestibular system also manifests as the interruption of rotating VOR, which is generally important for dynamic visual acuity, which is one essential vestibular function. Thus, we used a binocular VOG-based VFT system and customized software to quantitatively evaluate the vestibular function which served as an objective index for vestibular function. The rotating VOR test was performed at D7 after a single dose of IDPN or saline injection. The mouse was placed in a custom-built box adapted to its weight and then fixed on the rotating device (Figure 4(a)). Eye movements in the front mirror were recorded in real time by the side cameras as the platform rotated at 0.25, 0.5, and 1 Hz (Figure 4(b)).

Our results showed that the pixels of eye movement amplitude of control mice were 31.75 ± 4.65 , 46.00 ± 8.41 , and 48.57 ± 2.42 at 0.25, 0.5, and 1 Hz, respectively ($n = 3$). When we evaluated the VOR test 7 days after 2 mg/g body

weight IDPN injection, eye movement amplitude dropped to 14.33 ± 11.01 , 11.94 ± 5.46 , and 7.54 ± 4.67 at 0.25, and 0.5 Hz, respectively ($n = 3$). VOR gain showed significant decrease (Figure 4(c), $p < 0.01$ all three frequencies, compared with the control mice), which was more sensitive with vestibular dysfunction compared to the results of the swim test. There are no significant differences between 4 and 6 mg/g body weight IDPN injection groups (Figure 4(c), $p > 0.05$) since the eye movement amplitude dropped to 3.19 ± 2.50 , 9.24 ± 5.52 , and 4.71 ± 1.64 and 1.60 ± 0.98 , 3.02 ± 0.63 , and 5.12 ± 0.89 at 0.25, 0.5, and 1 Hz, respectively. To observe the vestibular function recovery or compensation, we performed rotating VOR test at 1 month and 3 months. Only two of three mice in the 6 mg/g body weight IDPN-injected group survived both 1 month and 3 months after IDPN injection (Figures 4(d) and 4(e)). VOR gain data stayed significantly decreased compared to that

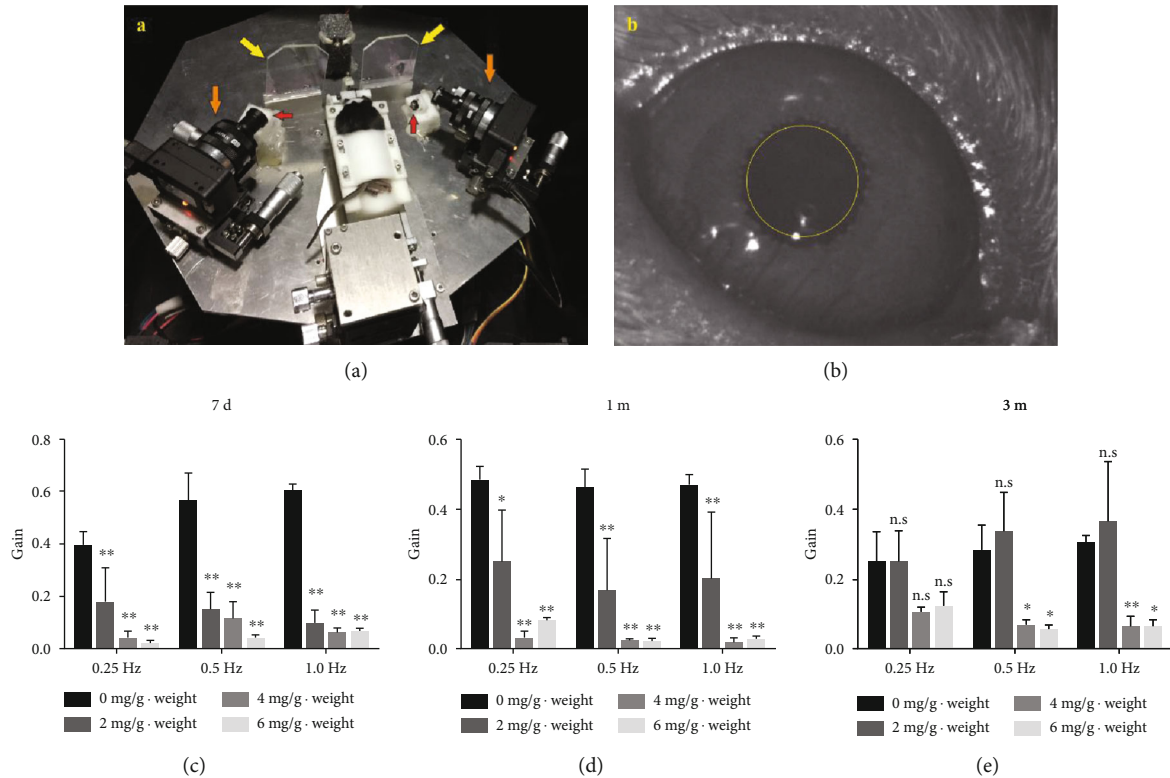


FIGURE 4: Rotating VOR test served as a sensitive measurement for evaluating the function of the vestibular system. Vestibular function was evaluated on a binocular VOG-based VFT system at 7 days (7 d), 1 month (1 m), and 3 months (3 m) after IDPN injection. A mouse was placed in the custom-built box adapted to its weight and then fixed on the rotating device (a). Yellow arrows, orange arrows, and red arrows point out the mirrors, cameras, and infrared lamps on the platform, respectively (a). Eye movements in the front mirror were recorded in real time by the side cameras as the platform rotated at 0.25, 0.5, and 1 Hz (b). Graphs (c, d, e) show the rotating VOR gain at 7 d, 1 m, and 3 m. VOR gain showed significant decrease at all three frequencies compared with control mice dose-dependently in day 7 (c) and 1 month (d). VOR gains of the 2 mg IDPN/g body weight injected mice showed no difference compared with those of the control mice after 3 months (e). Two-way ANOVA of VOR gains (all $p < 0.0001$) with Tukey's multiple comparison test was performed with GraphPad Prism 6.01. * $p < 0.05$ and ** $p < 0.01$.

of the control group at 1 month (Figure 4(d)). Results showed that eye movement amplitude data almost recovered to normal (20.48 ± 7.08 , 27.21 ± 9.32 , and 29.41 ± 14.10 at 0.25, 0.5, and 1 Hz, respectively, in 2 mg/g body weight group, all $p > 0.05$) compared with those of the control mice after 3 months. No VOR gain recovery appeared in the 4 mg/g body weight group (Figure 4(e), all $p > 0.05$, compared with control mice after 3 months). These data may conclude that vestibular function recovery or compensation depends on the remaining hair cells and supporting cells.

3.4. Transient Upregulation of Notch and Fluctuating Upregulation of Wnt Signaling-Related Genes after IDPN Administration. It has been reported that the utricle has a limited ability to repair itself after HC loss [16]. We observed a slight recovery of vestibular function according to the rotating VOR test results at 3 months after 2 mg IDPN/g body weight injection. To further evaluate the spontaneous regeneration of HCs and SCs in the utricle after HC loss induced by IDPN injection, we harvested the utricles at D12 after IDPN injection. In order to label the new HCs that were gen-

erated through proliferation, EdU was intraperitoneally injected daily at 5 mg/mL starting at D6 after IDPN injection (Figure 5(a)). There were no EdU+ HCs in the utricles from either control (data not shown) or IDPN-injected mice (Figures 5(b1)–5(e3)). We only observed EdU+ SCs at the striolar region of the utricles from the mice injected with higher doses of IDPN (Figures 5(e2), 5(e3), and 5(f), 5 mg/g body weight IDPN: 8.67 ± 8.24 , $p > 0.05$; 6 mg/g body weight IDPN: 31.67 ± 22.34 , $p < 0.01$), while no EdU+ SCs were seen in the controls or at lower doses of the IDPN injection (4 mg IDPN/g body weight), which suggested that utricles do indeed have limited proliferative regeneration potential in response to severe injury and subsequent loss of epithelial integrity.

Based on the results above, we chose 6 mg IDPN/g body weight-treated utricles to explore the potential mechanism of spontaneous HC regeneration in the utricle. Utricles were harvested for RT-qPCR at D1, D5, D6, D8, and D10 after 6 mg IDPN/g body weight injection or normal saline injection. Total RNA was extracted for RT-qPCR to identify the genes involved in the Notch and Wnt signaling pathway in addition to the genes related to the processes of HC differentiation and maturation. Compared with controls,

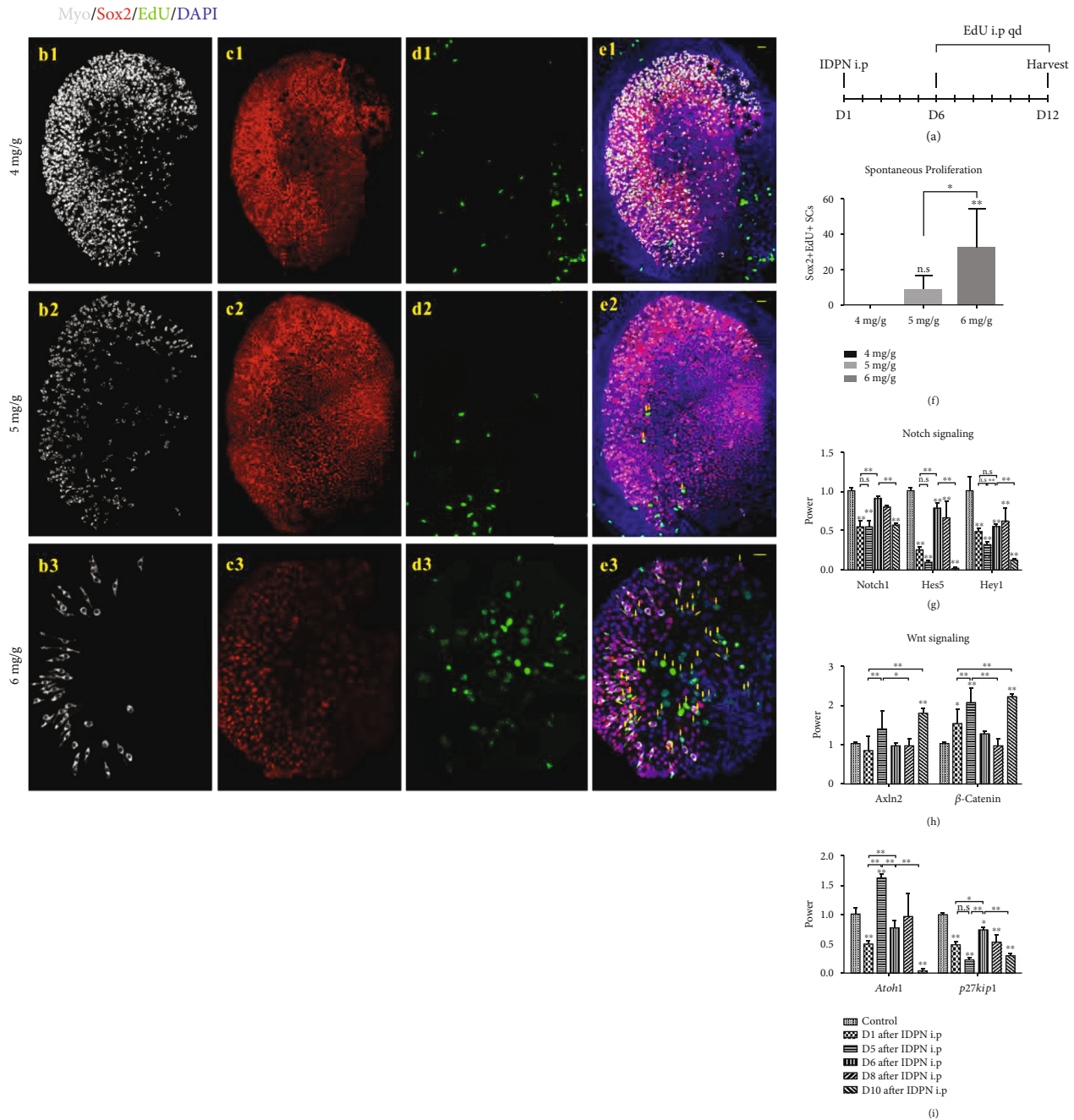


FIGURE 5: The limited proliferation in utricle sensory epithelium induced by IDPN injection. No MyoVIIa+/EdU+ cells were seen in any of the IDPN-treated utricles (c1–c3). EdU+/Sox2+ cells were not observed in the 4 mg IDPN/g body weight-treated utricles (e1). EdU+/Sox2+ cells appeared on the edge of the striolar area and the striolar area in the 5 and 6 mg IDPN/g body weight-treated utricles (yellow arrows) (e2, e3). Graph (f) shows the average number of EdU+/Sox2+ cells in the 4, 5, and 6 mg IDPN/g body weight-treated utricles. Graph (g) shows changes in Notch signaling genes at D1, D5, D6, D8, and D10 after 6 mg IDPN/g body weight injection. Graph (h) shows changes in Wnt signaling genes after IDPN injection. Graph (i) shows changes in *Atoh1* and *p27kip1* expression after IDPN injection. All hair cell development-related vital genes showed a fluctuating change. The scale bars indicate 20 μ m; * p < 0.05 and ** p < 0.01.

during the injury induced by IDPN injection and during the subsequent recovery process in the sensory epithelium of the utricle, *Notch1*, *Hey1*, and *Hes5* were downregulated during the whole process although with small fluctuations (Figure 5(g)). *Axin2*, β -catenin, and genes involved in the Wnt signaling pathway were upregulated (Figure 5(h)).

The expression of *Atoh1*, a crucial gene for HC differentiation, was also upregulated in a similar manner to the genes involved in Wnt signaling. Meanwhile, *p27kip1* was downregulated, which was coincident with the increased proliferation of SCs during the recovery process of the damaged utricle (Figure 5(i)).

4. Discussion

Khan et al. reported that the brain and vestibule appear to be major target sites of IDPN, and the behavioral deficits that IDPN induced were reported to be identical to those of a bilateral labyrinthectomy [5]. Seoane et al. showed that extrusion is a major mechanism of HC death in mammals; that necrosis, apoptosis, and extrusion form a continuum of modes of HC loss; and that the intensity of the damaging stimulus determines the prevalence of each mode [17]. The association of HC degeneration with behavioral syndrome was also found in dose-response studies in acute, repeated, and chronic dosing in rats [6, 18, 19]. In the current study, IDPN was used to establish an utricle injury model in adult mice in an acute (one high dose) or a subacute (multiple small doses) manner. We found that similar dose-dependent utricle injury patterns were induced by IDPN in both the acute (single injection) and subacute (7 days of injection at lower concentrations) treatments in mice. Sensory cells in the striolar area are more vulnerable to IDPN than those in the extrastriolar area, and Type I HCs (MyoVIIa+/Sox2- cells) are more vulnerable to IDPN than Type II HCs (MyoVIIa+/Sox2+ cells), while both types of HCs are more vulnerable than SCs [8, 20]. The range of sensitivity to IDPN might be due to differences in cell structure as well as differences in the expression of Sox2. It has been reported that Type I HCs have significantly more stereocilia than Type II HCs, which might imply that Type I HCs have more mechanoelectric transduction channels for the entrance of IDPN [21, 22]. Oesterle et al. reported that Sox2 is absent from auditory HCs and Type I HCs in the utricle and that Sox2- HCs are more vulnerable to the aminoglycoside kanamycin, while Sox2+ HCs and SCs might not be affected by the same dose of the ototoxic drug. The resistance against IDPN seen in the Sox2+ cells might be related to the function of Sox2 for the maintenance of sensory cells in the adult mouse inner ear [13] or might be similar to the protective effect of the “nNOS-Sox2-Shh” pathway against ischemic neuronal damage and ischemia reperfusion injury [23, 24].

As is well known, HC loss in the utricle results in dysfunction of the vestibular system in mice, manifesting as spontaneous head shaking, trunk curling, walking in circles, and abnormal swimming behavior [11]. When the concentration of IDPN was 2 mg/g body weight, it could already cause about $12.99 \pm 9.69\%$ HC loss in the extrastriolar area and $33.18 \pm 11.03\%$ loss in the striolar area. At this dose of IDPN, the swim test was scored 0 to 1, which implied no significant dysfunction of the vestibular system. On the contrary, when we tested the mice with the rotating VOR, the eye movement amplitude and VOR gain dropped considerably at all three frequencies, which suggested that the rotating VOR test is more sensitive than the swim test for evaluating the function of the vestibular system. However, when HC loss reached above 35%, no differences were seen between the swim test and rotating VOR test.

At 3 months after injury, eye movement amplitude only recovered in the 2 mg IDPN/g body weight group where HC losses were not severe. In the 4 and 6 mg IDPN/g body weight groups, there could be seen only partial recovery at

0.25 Hz, which suggested that the recovery of vestibular function after long-term repair depended on the HCs and SCs that remained. There were no EdU+ HCs seen in either the control or IDPN-treated utricles, which means that the limited regeneration capacity in the utricles might only be the result of direct nonmitotic regeneration of HCs through SC transdifferentiation [3, 16, 25].

Wnt and Notch signaling have been reported to be vital for the fate determination of SCs and HCs during mammalian inner ear development [26–29]. The expression of CDK inhibitors like *p27kip1* can trigger the differentiation of precursor cells during auditory development [30, 31]. Wang et al. reported that a posttrauma decrease of *Hes5* expression and an increase in *Atoh1* expression might lead to the limited capacity for spontaneous HC regeneration [25]. To explore the potential mechanism of utricular self-regeneration, we investigated the expression of the Notch and Wnt signaling pathway genes *Atoh1* and *p27kip1* at D1, D5, D6, D8, and D10 after 6 mg IDPN/g body weight injection in which the greatest number of spontaneously self-regenerated SCs was seen. We observed decreased mRNA expression of *Notch1*, *Hey1*, and *Hes5* after the sensory epithelium injury induced by IDPN. The expression of these genes was partially upregulated at D6–D8 but then decreased again and was sustained at a relatively low level from D10. The expression of *Axin2* and β -*catenin*, important genes of the Wnt signaling pathway, showed an inverse expression pattern compared to that of the genes related to Notch signaling. The expression of *Atoh1* was consistent with the change in Wnt signaling pathway genes, while *p27kip1* expression changed in a similar manner as the Notch signaling genes. Slowik and Bermingham-McDonogh reported that *Hes5* expression is maintained in some adult vestibular supporting cells [32, 33]. In this experiment, after IDPN administration, Notch signaling related genes and *p27kip1* experienced a transient decrease (D1–D5) which might be due to the cells undergoing IDPN striking. The subsequent transient activation of the Notch signal might be due to the activation of the Notch signal in the remaining cells after cell death. *Atoh1* experienced a very short downregulation (D1) then upregulated at D5. These fluctuating profiles of gene expression mimicked what is seen during inner ear development [26–29], which suggests that the limited proliferation of utricular SCs might be induced by the upregulation of Notch signaling and the *Atoh1* gene. The reported regeneration of HCs from SCs might be induced by the subsequent downregulation of Notch signaling and the *p27kip1* gene. Wnt/ β -catenin signaling has an important role in protecting HCs against drug-induced HC loss [34] which might induced the transient upregulation after IDPN administration. Wnt signaling related genes then showed completely opposite changes with Notch signaling which might be because inhibition of Notch signaling could activate Wnt signaling [35]. It can thus be assumed that coregulating the genes involved in the HC regeneration process might enhance the recovery of the sensory epithelium and subsequent functional recovery.

In summary, we conclude that a single injection of IDPN is a convenient and reliable way to cause HC loss in adult mouse utricles and corresponding vestibular dysfunction

in vivo. We also show that the rotating VOR test appears to be a more sensitive approach to evaluate the function of the vestibular system in a quantitative way. Finally, we conclude that it is likely that the limited HC self-regeneration ability in the adult mouse utricle includes the transient upregulation of Notch signaling and fluctuating upregulation of Wnt signaling.

Data Availability

The data statement has already been checked and are available from the corresponding author upon request.

Conflicts of Interest

The authors declare no competing financial interests.

Authors' Contributions

Shan Zeng and Wenli Ni contributed equally to this work.

Acknowledgments

We thank Prof. Fangyi Chen and his team at Southern University of Science and Technology for the VOR test device and assistance with data analysis. This work was supported by the National Science Foundation for Outstanding Young People (81922018), the National Natural Science Foundation of China (Nos. 81771011, 81700910, and 81700914), the Development Fund for Shanghai Talents (grant number 2017046), and the Excellent Personnel Training Plan for the Shanghai Health System (grant number 2017Q003).

References

- [1] E. Rubel, L. Dew, and D. Roberson, "Mammalian vestibular hair cell regeneration," *Science*, vol. 267, no. 5198, pp. 701–707, 1995.
- [2] J. Buelke-Sam, S. F. Ali, G. L. Kimmel, W. Slikker Jr., G. D. Newport, and J. R. Harmon, "Postnatal function following prenatal reserpine exposure in rats: neurobehavioral toxicity," *Neurotoxicology and Teratology*, vol. 11, no. 5, pp. 515–522, 1989.
- [3] J. S. Golub, L. Tong, T. B. Ngyuen et al., "Hair cell replacement in adult mouse utricles after targeted ablation of hair cells with diphtheria toxin," *The Journal of Neuroscience*, vol. 32, no. 43, pp. 15093–15105, 2012.
- [4] A. Seoane, D. Demmes, and J. Llorens, "Distal effects in a model of proximal axonopathy: 3,3'-iminodipropionitrile causes specific loss of neurofilaments in rat vestibular afferent endings," *Acta Neuropathologica*, vol. 106, no. 5, pp. 458–470, 2003.
- [5] H. A. Khan, A. S. Alhomida, and I. A. Arif, "Neurovestibular toxicities of acrylonitrile and iminodipropionitrile in rats: a comparative evaluation of putative mechanisms and target sites," *Toxicological Sciences*, vol. 109, no. 1, pp. 124–131, 2009.
- [6] J. Llorens, D. Dememes, and A. Sans, "The Behavioral Syndrome Caused by 3,3'-Iminodipropionitrile and Related Nitriles in the Rat Is Associated with Degeneration of the Vestibular Sensory Hair Cells," *Toxicology and Applied Pharmacology*, vol. 123, no. 2, pp. 199–210, 1993.
- [7] H. A. Khan, S. al Deeb, K. al Moutaery, and M. Tariq, "Influence of age on iminodipropionitrile-induced vestibular and neurobehavioral toxicities in rats," *Experimental and Toxicological Pathology*, vol. 55, no. 2-3, pp. 181–186, 2003.
- [8] J. Llorens, D. Dememes, and A. Sans, "The toxicity of IDPN on the vestibular system of the rat: new insights on its effects on behavior and neurofilament transport," *Neurotoxicology*, vol. 15, no. 3, pp. 643–647, 1994.
- [9] C. Soler-Martin, N. Diez-Padrisa, P. Boadas-Vaello, and J. Llorens, "Behavioral disturbances and hair cell loss in the inner ear following nitrile exposure in mice, guinea pigs, and frogs," *Toxicological Sciences*, vol. 96, no. 1, pp. 123–132, 2006.
- [10] B. A. Wilkerson, F. Artoni, C. Lea, K. Ritchie, C. A. Ray, and O. Bermingham-McDonogh, "Effects of 3,3'-iminodipropionitrile on hair cell numbers in cristae of CBA/CaJ and C57BL/6J mice," *Journal of the Association for Research in Otolaryngology*, vol. 19, no. 5, pp. 483–491, 2018.
- [11] R. E. Hardisty-Hughes, A. Parker, and S. D. M. Brown, "A hearing and vestibular phenotyping pipeline to identify mouse mutants with hearing impairment," *Nature Protocols*, vol. 5, no. 1, pp. 177–190, 2010.
- [12] X. Yang, S. Zhou, J. Wu et al., "Surgery-free video-oculography in mouse models: enabling quantitative and short-interval longitudinal assessment of vestibular function," *Neuroscience Letters*, vol. 696, pp. 212–218, 2019.
- [13] E. C. Oesterle, S. Campbell, R. R. Taylor, A. Forge, and C. R. Hume, "Sox2 and JAGGED1 expression in normal and drug-damaged adult mouse inner ear," *Journal of the Association for Research in Otolaryngology*, vol. 9, no. 1, pp. 65–89, 2008.
- [14] K. E. M. Klimpel, M. Y. Lee, W. M. King, Y. Raphael, J. Schacht, and R. L. Neitzel, "Vestibular dysfunction in the adult CBA/CaJ mouse after lead and cadmium treatment," *Environmental Toxicology*, vol. 32, no. 3, pp. 869–876, 2017.
- [15] A. E. Luebke, J. C. Holt, P. M. Jordan, Y. S. Wong, J. S. Caldwell, and K. E. Cullen, "Loss of Calcitonin Gene-Related Peptide (CGRP) Reduces the efficacy of the vestibulo-ocular reflex (VOR)," *The Journal of Neuroscience*, vol. 34, no. 31, pp. 10453–10458, 2014.
- [16] K. Kawamoto, M. Izumikawa, L. A. Beyer, G. M. Atkin, and Y. Raphael, "Spontaneous hair cell regeneration in the mouse utricle following gentamicin ototoxicity," *Hearing Research*, vol. 247, no. 1, pp. 17–26, 2009.
- [17] A. Seoane, D. Dememes, and J. Llorens, "Relationship between insult intensity and mode of hair cell loss in the vestibular system of rats exposed to 3,3'-iminodipropionitrile," *The Journal of Comparative Neurology*, vol. 439, no. 4, pp. 385–399, 2001.
- [18] J. Llorens and E. Rodriguez-Farre, "Comparison of behavioral, vestibular, and axonal effects of subchronic IDPN in the rat," *Neurotoxicology and Teratology*, vol. 19, no. 2, pp. 117–127, 1997.
- [19] J. Llorens, C. Soler-Martín, B. Cutillas, and S. Saldaña-Ruiz, "Nervous and vestibular toxicities of acrylonitrile and iminodipropionitrile," *Toxicological Sciences*, vol. 110, no. 1, pp. 244–245, 2009, author reply 246–8.
- [20] J. Llorens and D. Dememes, "Hair cell degeneration resulting from 3,3'-iminodipropionitrile toxicity in the rat vestibular epithelia," *Hearing Research*, vol. 76, no. 1-2, pp. 78–86, 1994.
- [21] R. Pujol, S. B. Pickett, T. B. Nguyen, and J. S. Stone, "Large basolateral processes on type II hair cells are novel processing units in mammalian vestibular organs," *The Journal of Comparative Neurology*, vol. 522, no. 14, pp. 3141–3159, 2014.

- [22] W. J. Moravec and E. H. Peterson, "Differences between stereocilia numbers on type I and type II vestibular hair cells," *Journal of Neurophysiology*, vol. 92, no. 5, pp. 3153–3160, 2004.
- [23] D. Zhang, H. Wang, H. Liu, T. Tao, N. Wang, and A. Shen, "nNOS translocates into the nucleus and interacts with Sox2 to protect neurons against early excitotoxicity via promotion of Shh transcription," *Molecular Neurobiology*, vol. 53, no. 9, pp. 6444–6458, 2016.
- [24] C. K. How, S. K. Hou, L. K. Chen et al., "Induced pluripotent stem cells alleviate lung injury from mesenteric ischemia-reperfusion," *Journal of Trauma and Acute Care Surgery*, vol. 79, no. 4, pp. 592–601, 2015.
- [25] G. P. Wang, I. Chatterjee, S. A. Batts et al., "Notch signaling and Atoh1 expression during hair cell regeneration in the mouse utricle," *Hearing Research*, vol. 267, no. 1-2, pp. 61–70, 2010.
- [26] R. Chai, B. Kuo, T. Wang et al., "Wnt signaling induces proliferation of sensory precursors in the postnatal mouse cochlea," *Proceedings of the National Academy of Sciences of the United States of America*, vol. 109, no. 21, pp. 8167–8172, 2012.
- [27] B. E. Jacques, C. Puligilla, R. M. Weichert et al., "A dual function for canonical Wnt/ -catenin signaling in the developing mammalian cochlea," *Development*, vol. 139, no. 23, pp. 4395–4404, 2012.
- [28] S. J. Bray, "Notch signalling: a simple pathway becomes complex," *Nature Reviews. Molecular Cell Biology*, vol. 7, no. 9, pp. 678–689, 2006.
- [29] S. J. Jeon, M. Fujioka, S. C. Kim, and A. S. B. Edge, "Notch signaling alters sensory or neuronal cell fate specification of inner ear stem cells," *The Journal of Neuroscience*, vol. 31, no. 23, pp. 8351–8358, 2011.
- [30] B. Malgrange, M. Knockaert, S. Belachew et al., "The inhibition of cyclin-dependent kinases induces differentiation of supernumerary hair cells and Deiters' cells in the developing organ of Corti," *The FASEB Journal*, vol. 17, no. 14, pp. 2136–2138, 2003.
- [31] P. Chen and N. Segil, "p27(Kip1) links cell proliferation to morphogenesis in the developing organ of Corti," *Development*, vol. 126, no. 8, pp. 1581–1590, 1999.
- [32] A. D. Slowik and O. Bermingham-McDonogh, "Hair cell generation by notch inhibition in the adult mammalian cristae," *Journal of the Association for Research in Otolaryngology*, vol. 14, no. 6, pp. 813–828, 2013.
- [33] B. H. Hartman, O. Basak, B. R. Nelson, V. Taylor, O. Bermingham-McDonogh, and T. A. Reh, "Hes5 expression in the postnatal and adult mouse inner ear and the drug-damaged cochlea," *Journal of the Association for Research in Otolaryngology*, vol. 10, no. 3, pp. 321–340, 2009.
- [34] L. Liu, Y. Chen, J. Qi et al., "Wnt activation protects against neomycin-induced hair cell damage in the mouse cochlea," *Cell Death & Disease*, vol. 7, no. 3, pp. e2136–e2136, 2016.
- [35] E. Kaemmerer, M. K. Jeon, A. Berndt, C. Liedtke, and N. Gassler, "Targeting Wnt signaling via Notch in intestinal carcinogenesis," *Cancers*, vol. 11, no. 4, p. 555, 2019.

Research Article

An In Vitro Study on Prestin Analog Gene in the Bullfrog Hearing Organs

Zhongying Wang,^{1,2,3} Minfei Qian,^{1,2,3} Qixuan Wang,^{1,2,3} Huihui Liu,^{1,2,3} Hao Wu^{ID},^{1,2,3} and Zhiwu Huang^{ID}^{1,2,3}

¹Department of Otolaryngology-Head and Neck Surgery, Shanghai Ninth People's Hospital, Shanghai Jiao Tong University School of Medicine, Shanghai, China

²Ear Institute, Shanghai Jiao Tong University School of Medicine, Shanghai, China

³Shanghai Key Laboratory of Translational Medicine on Ear and Nose Diseases, Shanghai, China

Correspondence should be addressed to Hao Wu; haowu@sh-jei.org and Zhiwu Huang; huangzw86@126.com

Received 7 February 2020; Revised 22 April 2020; Accepted 20 May 2020; Published 2 July 2020

Academic Editor: Renjie Chai

Copyright © 2020 Zhongying Wang et al. This is an open access article distributed under the Creative Commons Attribution License, which permits unrestricted use, distribution, and reproduction in any medium, provided the original work is properly cited.

The prestin-based active process in the mammalian outer hair cells (OHCs) is believed to play a crucial role in auditory signal amplification in the cochlea. Prestin belongs to an anion transporter family (SLC26A). It is densely expressed in the OHC lateral plasma membrane and functions as a voltage-dependent motor protein. Analog genes can be found in the genome of nonmammalian species, but their functions in hearing are poorly understood. In the present study, we used the gerbil prestin sequence as a template and identified an analog gene in the bullfrog genome. We expressed the gene in a stable cell line (HEK293T) and performed patch-clamp recording. We found that these cells exhibited prominent nonlinear capacitance (NLC), a widely accepted assay for prestin functioning as a motor protein. Upon close examination, the key parameters of this NLC are comparable to that conferred by the gerbil prestin, and nontransfected cells failed to display NLC. Lastly, we performed patch-clamp recording in HCs of all three hearing organs in bullfrog. HCs in both the sacculus and the amphibian papilla exhibited a capacitance profile that is similar to NLC while HCs in the basilar papilla showed no sign of NLC. Whether or not this NLC-like capacitance change is involved in auditory signal amplification certainly requires further examination; our results represent the first and necessary step in revealing possible roles of prestin in the active hearing processes found in many nonmammalian species.

1. Introduction

Hair cells (HCs) in the cochlea play a critical role in converting mechanical sound waves into neural signals for hearing [1–3]. The mammalian cochlea contains one row of inner hair cells (IHCs) that feed auditory signals to auditory afferent fibers, and three rows of outer hair cells (OHCs) that are able to contract upon depolarization and elongate when hyperpolarized [4–6]. This change of length (electromotility) happens at a microsecond time scale. This form of electromotility surprisingly does not require any force generator like ATP or calcium [4, 7, 8]. It is generally accepted that electromotility provides the physiological basis of a precise frequency selectivity and sensitivity of mammalian hearing [5, 9, 10].

Electromotility is the result of conformational changes of a transmembrane protein named prestin. Prestin belongs to a highly versatile solute carrier 26 (SLC26A) in the anion transporter family [11–13]. Almost all the SLC26A members transport different anion substrates across epithelia, and the mammalian prestin is unique owing to its functions as a voltage-dependent motor protein [13, 14]. The voltage-dependent charge movement conferred by prestin's voltage sensor can be measured as a nonlinear capacitance (NLC) of the cell membrane. The NLC is often used as a substitute for direct measurements of the somatic motility in outer HCs and prestin-transfected cells because it is linked to cell motility and can be easily assayed experimentally [5, 13, 15, 16].

Comparable to that in mammals, the inner ear of non-mammalian vertebrates varies significantly in anatomy across classes. Despite the fact that amphibian hair cells are not as highly differentiated as mammalian OHCs, their ears are also sensitive, sharply tuned, and can spontaneously emit sounds. Both spontaneous and evoked otoacoustic emissions from the American bullfrogs have been reported [17, 18]. The overall emission levels of amphibian ears are larger than those of avian and human ears [19, 20]. The hair bundle and prestin motors in the avian auditory HCs together generate a force underlying amplification and frequency tuning [21, 22]. It remains unclear whether frog HCs have prestin and if frog prestin participates in the active process with the hair bundle.

The American bullfrog has been widely used as an animal model for the study of auditory physiology because of its well-developed middle and inner ear anatomy. The inner ear of the American bullfrog contains three auditory organs: the amphibian papilla (AP), the basilar papilla (BP), and the sacculus (S). The AP receives acoustic stimuli within a frequency range of 100 Hz–1250 Hz, while the BP covers the higher portion of the auditory frequency range from about 1.2 kHz to 4 kHz [23]. The sacculus is a mixed-function organ which is most sensitive to low-frequency sounds (120 Hz \pm 24 Hz) and seismic sensation [24, 25]; however, none of these investigations have focused on prestin and electromotility. We generated stable cell lines transfected with the frog prestin by an AAVS1 site-specific integration. The NLC of the frog prestin, both in transfected cells and in primary HCs isolated from frog auditory organs, were measured using a patch-clamp technology. The goal of our work was to investigate whether frog HCs had prestin and if it functioned as an intrinsic motor for amplification and frequency selectivity with the hair bundle.

2. Methods

2.1. Cloning and Analyses of Prestin Orthologs. We obtained the prestin coding region of gerbil (*Meriones unguiculatus*), tropical clawed frog (*Xenopus tropicalis*), and the American bullfrog (*Rana catesbeiana*) using a BLAST analysis of the Ensembl and NCBI genomic databases. Genomic sequence data from gerbil and bullfrog were used to deduce the full coding cDNAs, which were then synthesized (HuaGene, China). The correct orientation and reading frame were verified by sequence analysis, and ortholog and paralog comparisons were conducted using UniProt, CLUSTALW, and Esript 3. All constructs were verified by gene sequencing.

2.2. Generation of Stable Cell Lines That Express *fPres* and *gPres*

2.2.1. Construction of Vectors for AAVS1 Site-Specific Integration. The AAVS1 safe harbor locus site-specific integration used CRISPR/Cas9-mediated gene editing. The sgRNA (GGGCCACTAGGGACAGGAT) targeting the AAVS1 site was cloned into a lentiviral vector (pLenti-CRISPR), which contained a SpCas9 expression cassette. A donor vector was generated by assembling PCR-amplified fragments by restriction digestion and ligation. The resulting vector contained two homology arms from HEK293T geno-

mic DNA that flanked an overexpression cassette with a puromycin selection marker on the plasmid backbone (pTOPO-AAVS1-EF1). This donor vector was designed for the expression of *fPres*- and *gPres*-enhanced GFP (EGFP) fusion proteins driven by the CMV promoter.

2.2.2. Cell Culture. HEK293T cells were cultured in the Dulbecco's Modified Eagle's Medium (DMEM) (Invitrogen, Carlsbad, CA, USA) supplemented with 10% fetal bovine serum (FBS) (Invitrogen) at 37°C in 5% CO₂. Mycoplasma testing was performed regularly using PCR detection. Cells were transfected at 60%–80% confluence using the Lipofectamine 2000 DNA transfection reagent (Thermo Fisher Scientific), typically with 2 μ g plasmid(s) and 5 μ L of the transfection reagent in a 6-well culture dish.

2.2.3. Expression of *fPres* and *gPres* in HEK293T Cells. Cells were cotransfected with a mixture of plasmids for sgRNA/Cas9 and the donor (donor : sgRNA/Cas9 = 1.5 μ g : 0.5 μ g). Then, 2 μ g/mL puromycin was added into the culture medium 24 h after transfection and cell pools expressing prestin and EGFP were identified after puromycin screening for 7 d–10 d.

2.3. Confocal Imaging. The cells from the stable cell line at passage six were cultured for 12 h before immunodetection. Cells were rinsed with phosphate-buffered saline (PBS) one time and fixed with 4% paraformaldehyde for 30 min. Then, the cells were washed twice for 15 min each before they were permeabilized with PBT (PBS, 1% Triton X-100) and blocked with 1% bovine serum albumin (BSA) in PBS for 1 h at room temperature (RT). Confocal imaging was conducted with a laser scanning microscope (Leica Microsystems, Germany) using a 63x oil immersion objective.

2.4. Animals. Adult American bullfrogs (*Rana catesbeiana*) were purchased from a local vendor. Two-week-old C57 mice were purchased from the SIPPR-BK Laboratory Animal Ltd. (Shanghai, China). The care and use of animals were conducted in accordance with the Guide for the Care and Use of Laboratory Animals (National Institutes of Health, USA) and approved by the University Committee of Laboratory Animals of Shanghai Jiao Tong University.

Bullfrogs were sedated in an ice bath for 20 min and then double-pithed and decapitated. Amphibian papillae, basilar papillae, and sacculi were dissected and recorded in an extracellular solution containing (in mM) 95 NaCl, 1 KCl, 1 MgCl₂, 20 TEA-Cl, 0.5 CaCl₂, 2 CoCl₂, and 10 HEPES at pH 7.30 (240 mosmol/L). NaOH was used for pH adjustment.

Cochleae and the apical coil of the organ of Corti were acutely dissected from C57 mice and fixed to a recording chamber. The external solution contained (mM) 120 NaCl, 20 TEA-Cl, 2 CoCl₂, 2 MgCl₂, 10 HEPES, and 5 glucose at pH 7.3. NaOH was used for pH adjustment.

2.5. Electrophysiology. Recordings of bullfrog HCs were performed at 20°C within 3 h of dissection. Patch pipettes were pulled from thick-walled borosilicate glass (World Precision Instruments) using a Narishige puller (model PP-830) to resistances of 5 M Ω –8 M Ω and coated with dental wax.

Internal solutions for the bullfrog HCs were composed of (in mM) 100 CsCl, 10 EGTA, 10 HEPES, and 1 MgCl₂ at pH 7.30 (240 mosmol/L). CsOH was used for pH adjustment. Whole-cell voltage-clamp recordings were performed with an EPC-10/2 (HEKA Electronics) patch-clamp amplifier and Pulse software (HEKA). The HCs were held at -80 mV. Offline analysis was performed mainly with the Igor Pro 5.0 software (WaveMetrics).

We recorded mouse OHCs at 20°C within 1.5 h of dissection. Patch pipettes were pulled from thick-walled borosilicate glass (World Precision Instruments) using a Narishige puller (model PP-830) to resistances of about 6 MΩ and then coated with dental wax. The internal solution consisted of (mM) 140 CsCl, 2 MgCl₂, 10 EGTA, and 10 HEPES at pH 7.3. CsOH was used for pH adjustment. The osmolarity was adjusted to 300 mosmol/L.

HEK cells were detached with trypsin (Invitrogen) treatment before recordings were collected. The detached cells were then bathed in an extracellular solution containing (in mM) 120 NaCl, 20 TEA-Cl, 2 CoCl₂, 2 MgCl₂, 10 HEPES, and 5 glucose at pH 7.2. Osmolarity was adjusted to 300 mosmol/L with glucose. Recording pipettes were pulled with resistances of 2.5 MΩ–5.0 MΩ and filled with internal solution (in mM): 140 CsCl, 2 MgCl₂, 10 EGTA, and 10 HEPES. NLC measurements were performed on cultured cells with a robust membrane-associated EGFP expression. After rupture, we selected the cells whose membrane resistance was over 300 MΩ and showed normal *C_m* and *R_m* values.

The sine +DC software lock-in function of Patchmaster was used to obtain the voltage-sensor displacement currents and capacitance; a voltage protocol was designed that included both ramp and sine stimulation (800 Hz with a 10 mV amplitude). Sine waves were superimposed onto ramps from -150 mV to 100 mV for a duration of 300 ms. The NLC was fitted with the derivative of a Boltzmann function:

$$C_m = \frac{Q_{\max} \alpha}{\exp[\alpha(V_m - V_{1/2})](1 + \exp[-\alpha(V_m - V_{1/2})])^2} + C_{\text{lin}}, \quad (1)$$

where Q_{\max} is the maximum charge transfer, $V_{1/2}$ is the voltage at half-maximum charge transfer, C_{lin} is the residual linear membrane capacitance, and α is the slope factor describing the voltage dependence. $\alpha = ze/kT$, where k is Boltzmann's constant, T is the absolute temperature, z is the valence of charge movement, and e is the electron charge.

3. Results

3.1. fPres Confers NLC to HEK293T Cells. In order to obtain the prestin coding region of the American bullfrog, we used a BLAST analysis of the Ensembl and NCBI genomic databases. Using the CLUSTAL method, alignment of the mouse, gerbil, *Xenopus*, and *Rana* prestin protein sequences was conducted (Figure 1). This alignment revealed nearly 97% identity among mouse and gerbil, 35% among gerbil and *Rana*, and 57% among gerbil and *Xenopus*. Our alignment results were consistent with former comparative peptide

sequence analyses of mammalian prestins that were much more conserved with only minor changes, while prestins were quite variable among vertebrate species like the bony fish, amphibians, and birds [26].

We examined the electrophysiological properties from HEK cells transfected with the fPres-EGFP protein fusions by a site-specific gene transfer at the human AAV site 1 (AAVS1) [27–30]. Transgene expression is influenced by the integration site and some random insertions or transient transfections which can interfere with genes or disturb their transcription, while site-specific integration can minimize variations between different cells and constructs [31, 32]. We chose the gerbil prestin as a positive control, while cells transfected only with the EGFP-vector were a negative control. Membrane expression of fPres and gPres was examined using confocal microscopy. Both the fPres- and gPres-transfected cells showed similar patterns of membrane expression (Figure 2(a)).

Voltage stimulus used for capacitance recordings consisted of a sine wave superimposed onto a voltage ramp. We measured the NLC from the OHCs (Figure 2(b)) and transfected cells. Figure 2(c) shows the currents of the fPres- and gPres-transfected cells and the OHCs. The fPres-transfected cells had an NLC (the red curve) similar to the bell-shaped curve conferred by the gerbil and mouse prestin (Figure 2(d); black and blue curves). We could not detect NLC in cells transfected only with the EGFP-vector ($n = 12$). An example of a flat response has been presented in Figure 2(e).

Using the first derivative of the Boltzmann function, four parameters (Q_{\max} , C_{lin} , $V_{1/2}$, and z) from nonlinear curve fitting of the NLC were calculated. Since the HEK cells varied in size, which is correlated with the C_{lin} value, we normalized the Q_{\max} to the C_{lin} to compare the magnitude of the charge movement measured from cells of different sizes. We measured the mouse OHCs as a control.

The NLC measurements were analyzed from 15 gPres- and 16 fPres-transfected cells. The means and SEMs of the gPres were $Q_{\max} = 0.27 \pm 0.04$ (fC), $Q_{\max}/C_{\text{lin}} = 16.9 \pm 2$ (fC/pF), $V_{1/2} = -68.3 \pm 4.4$ (mV), and $z = 0.74 \pm 0.04$. The means and SEMs of the fPres were $Q_{\max} = 0.18 \pm 0.02$ (fC), $Q_{\max}/C_{\text{lin}} = 14.9 \pm 2.02$ (fC/pF), $V_{1/2} = -58.1 \pm 3.5$ (mV), and $z = 0.72 \pm 0.03$. The means and SEMs of the OHCs were $Q_{\max}/C_{\text{lin}} = 136.4 \pm 5.98$ (fC/pF), $V_{1/2} = -71.5 \pm 3.6$ (mV), and $z = 0.77 \pm 0.03$. The magnitude of gPres and fPres NLC was considerably less than that of the OHC (Figures 3(a) and 3(b); $P < 0.005$, Student's *t*-test). The charge density represented by the Q_{\max}/C_{lin} was not significantly different between fPres- and gPres-expressing cells; however, the charge density of both transfected cell lines was significantly lower than that measured in OHCs. Another functional parameter of $V_{1/2}$ is worth noting (Figure 3(c)). We observed no significant differences in $V_{1/2}$ between the gPres- and fPres-transfected cells, or between transfected cells and OHCs. Moreover, there were also no significant difference in the z value between gPres, fPres, and the OHC (Figure 3(d)). All the data are shown in Table 1.

3.2. NLC Measurements of Frog HCs. The frog inner ear contains three auditory organs: the amphibian papilla (AP), the

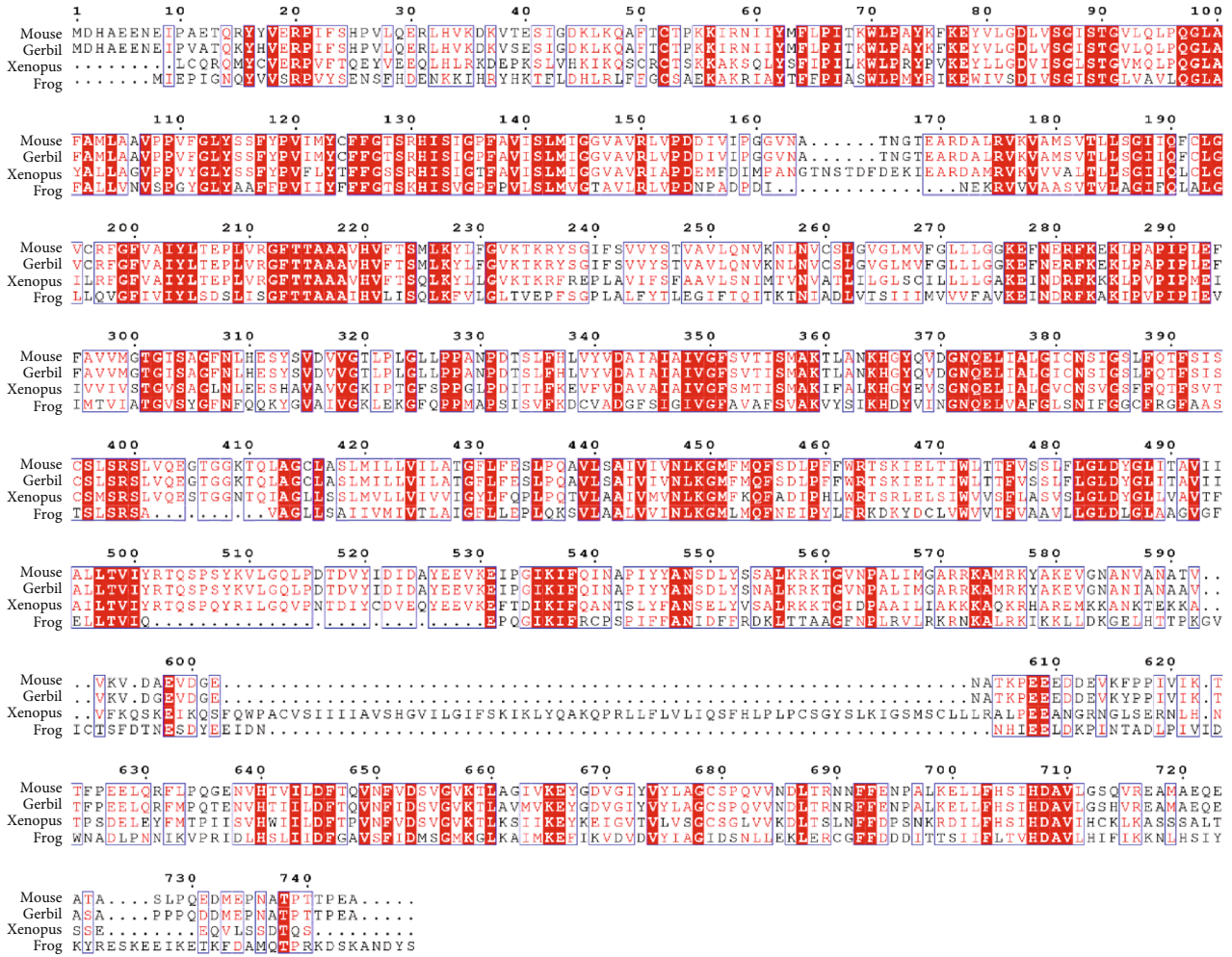


FIGURE 1: Alignment of amino acid sequences of SLC26A5 of mouse, gerbil, Xenopus, and bullfrog. Different colors had been used to represent identity of each residue among four species. Red block: full identity at a residue; red letter: partial identity at a residue; black: complete disparity at a residue. Gaps in the aligned sequences were indicated by the dashed line.

basilar papilla (BP), and the sacculus (S). The AP is composed of a patch of epithelium covered by HCs. The basilar papilla has a recess opening to the saccular space of the ear. The sacculus is a mixed-function organ which is sensitive to both hearing and vibration. The images of these three auditory organs are shown in Figures 4(a)–4(g). Mammalian, avian, and lizard HCs are located on a basilar membrane. However, the frog inner ear lacks such a sensitive substrate for its sensory cells. Without the basilar membrane, the frog inner ear relies on the tectorial membrane and HCs for frequency selectivity [33].

We used the same voltage stimulus protocol to record the NLC of the HCs from the AP, BP, and S organs. All AP and S HCs displayed a bell-shaped voltage-dependent NLC (Figure 5(a)). Measurements were analyzed from 10 AP HCs and 8 S HCs (Figure 5(b)). The means and SEMs of the AP HCs were $Q_{\max} = 10.4 \pm 1.4$ (fC), $Q_{\max}/C_{\text{lin}} = 14.9 \pm 1.01$ (fC/pF), $V_{1/2} = -33.8 \pm 3.3$ (mV), and $z = 1.8 \pm 0.16$. The means and SEMs of the S HCs were $Q_{\max} = 19.9 \pm 2.4$ (fC), $Q_{\max}/C_{\text{lin}} = 16.4 \pm 0.68$ (fC/pF), $V_{1/2} = -20.7 \pm 3.3$ (mV), and $z = 2.4 \pm 0.08$. The S HCs had a significant

gain of NLC when compared to those from AP ($P < 0.01$). The NLC magnitude of AP and S HCs was significantly less than that of the OHCs ($P < 0.005$, Student's t -test), and the charge density of S HCs was significantly higher than that of the AP HCs ($P < 0.005$, Student's t -test).

Compared with the mouse OHCs, the charge density of both the AP and S cells was significantly low. The $V_{1/2}$ of the AP HCs were more depolarized than that of the S cells ($P < 0.05$), with a difference of approximately 10 mV. The $V_{1/2}$ of the OHCs shifted in an even more depolarized direction than that measured in frog cells ($P < 0.005$), with a difference in the $V_{1/2}$ between frog HCs and OHCs of about 45 mV. The z value of the S HCs was significantly higher than that measured in AP cells ($P < 0.01$), while the z values of both AP and S HCs were significantly higher than that of the OHCs ($P < 0.005$).

Notably, we did not observe bell-shaped curves in the BP HCs. As shown in Figure 5(a), the blue curve represents the BP NLC and no evident peak was observed with the voltage applied to AP and S cells; therefore, no fitting results were obtained from the BP cells.

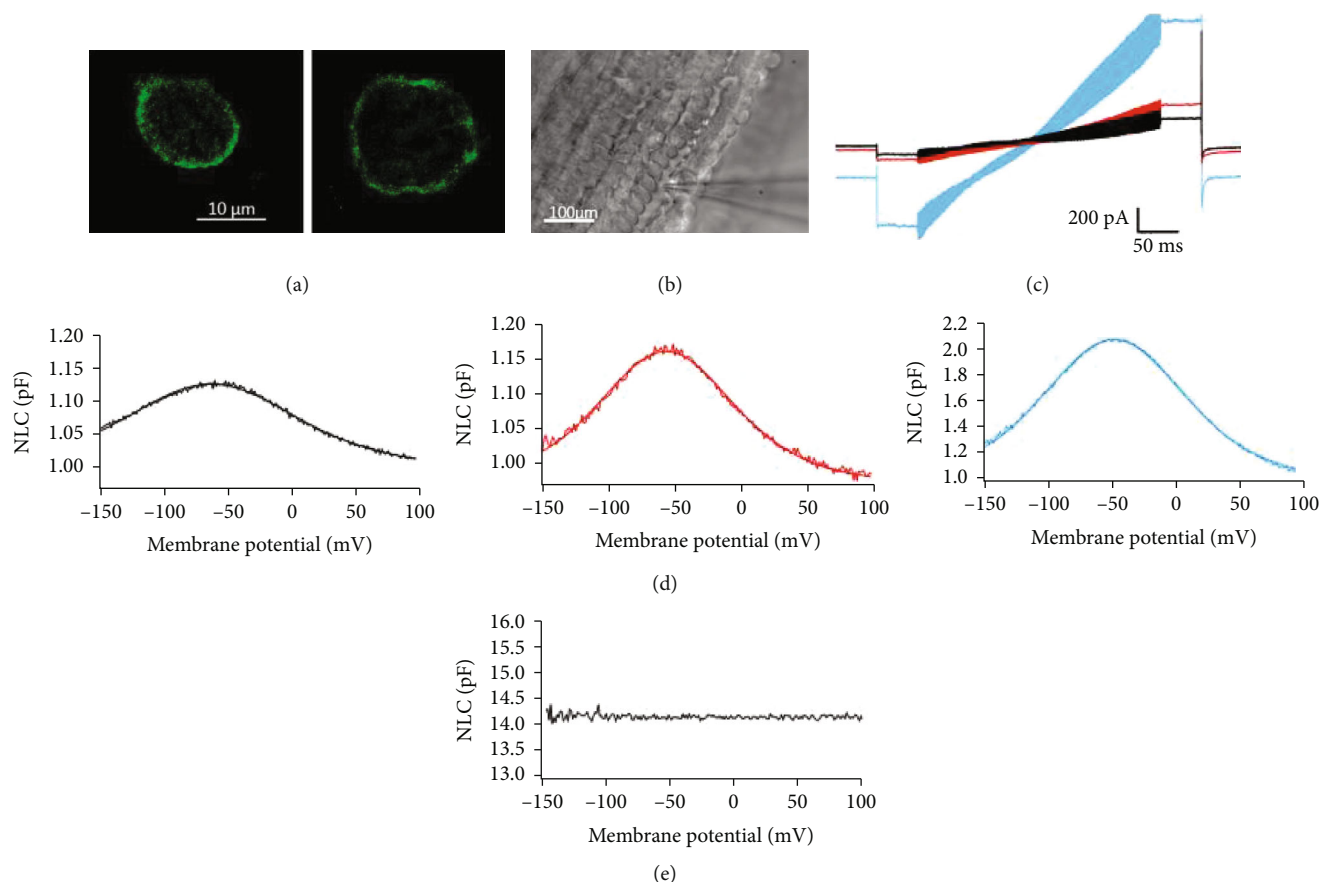


FIGURE 2: Nonlinear capacitance obtained from gPres- and fPres-transfected cells and a mouse OHC. (a) Confocal microscopy images of HEK cells transfected by gPres and fPres. (b) OHC patch. (c) Whole-cell currents of gPres- and fPres-transfected cells and OHC. Cells were held at -80 mV for current recordings. Voltage steps (300 ms in duration) varied from -150 to 100 mV in 10 mV steps. Black-gPres, red-fPres, blue-OHC. (d) NLC obtained from gPres- and fPres-transfected cells. Black-gPres, red-fPres. NLC obtained from the mouse OHC, blue curve. (e) This one showed the lack of detectable NLC in a representative control cell.

4. Discussion

Compared to mammals, many frog species do not have external ears or ear canals. In the frog family, a middle ear cavity is on the medial side of the tympanic membrane, which is coupled to the otic capsule via the stapes. The middle ear transmits acoustic information from the surrounding air to the inner ear, which contains fluid just like those of other vertebrates. Three distinct auditory organs are enveloped in this fluid-filled space: the amphibian papilla, the basilar papilla, and the sacculus. Low-frequency neurons that sense frequencies below 100 Hz innervate the sacculus, mid-frequency neurons that sense frequencies from 100 to 1000 Hz innervate the amphibian papilla, and high-frequency neurons that sense frequencies over 1000 Hz are connected to the basilar papilla [34].

The mammalian ear has frequency selectivity properties due to the propagation of an active traveling wave on the basilar membrane. In the mammalian inner ear, HCs are vulnerable to several forms of damage, including ototoxic drugs, inflammation, and aging [35–40]. The HCs play a critical role in converting mechanical sound waves into electrical signals along the pathway through the spiral gan-

glion neurons to the cochlear nucleus [41]. The inner HCs serve as sensory receptors, and the outer HCs have the ability to improve cochlear sensitivity and frequency selectivity [10]. Together, they form the basilar membrane–OHC–tectorial membrane complex. What is unique to frogs is that no basilar membrane is attached to their auditory organs. There are no differentiated populations of HCs as there are in mammals. Although there are dramatic anatomical variations between mammals and amphibians, they continue to have many functional similarities. Like mammals, the frog inner ear has a sharp frequency selectivity and can generate both evoked and spontaneous otoacoustic emissions [17]. Since the mechanism found in mammalian ears does not develop in frog ears, additional mechanisms must contribute to the active process of nonmammalian auditory organs.

In order to investigate whether frog prestin was functional, we expressed fPres in HEK293T cells by site-specific gene transferring at the human AAV site 1. Our data showed that fPres produced robust NLC and responded to changes in the membrane potential just like its mammalian ortholog. We used cells transfected with gPres and EGFP alone as positive and negative controls, respectively, to test

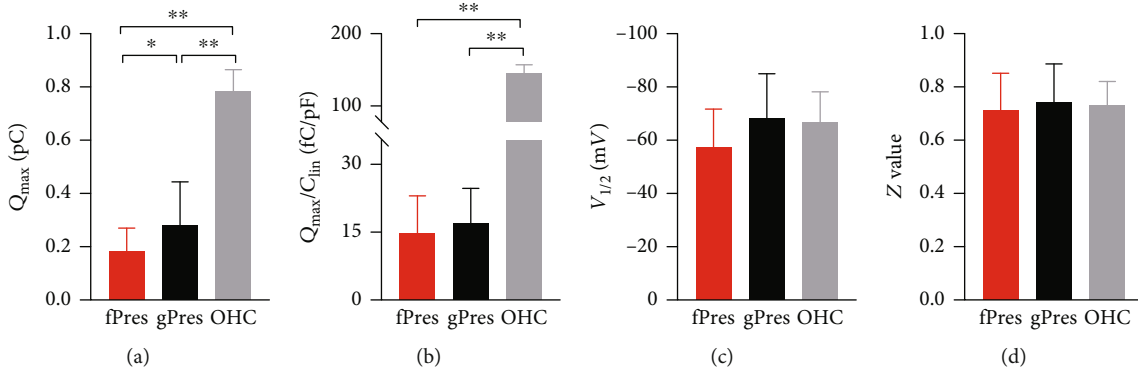


FIGURE 3: NLC functions of fPres, gPres, and mouse OHC. (a–d) Showed four parameters derived from curve fittings with Boltzmann’s function for fPres ($n = 16$), gPres ($n = 15$), and OHC ($n = 6$). Data were expressed as mean \pm s.d. * $P < 0.05$, ** $P < 0.01$.

TABLE 1: All the measurements performed in the present study are expressed as mean \pm sem.

	C_{lin} (pF)	Q_{\max} (fC)	$V_{1/2}$ (mV)	z	Q_{\max}/C_{lin} (fC/pF)
AP ($n = 10$)	14.9 ± 1.01	10.4 ± 1.4	-33.8 ± 3.3	1.8 ± 0.16	0.69 ± 0.07
S ($n = 8$)	16.4 ± 0.68	19.9 ± 2.4	-20.7 ± 3.3	2.4 ± 0.08	1.25 ± 0.19
fPres ($n = 16$)	12.7 ± 0.91	181.5 ± 22.5	-58.1 ± 3.5	0.07 ± 0.03	14.9 ± 2.02
gPres ($n = 15$)	15.9 ± 1.03	279.4 ± 41.7	-68.3 ± 4.4	0.07 ± 0.04	16.9 ± 2
Mouse OHC ($n = 9$)	5.74 ± 0.14	778.6 ± 26.2	-71.5 ± 3.6	0.77 ± 0.03	136.4 ± 5.98

the functional activity and found that the charge density, z value, and $V_{1/2}$ of fPres were very similar to that of gPres.

The otoacoustic emissions (OAEs) revealed much about the physiology of the ear. In mammals, OAEs were considered to be the active process generated by the electromotility of the outer HC. The nonmammalian vertebrate inner ear also exhibits an active process, and it is very interesting that the overall emission levels of amphibian ears is the largest, followed by the mammals, and then birds, which have the smallest emission level [19]. In addition to the role of the HC bundle in the active process, we cannot rule out the effect of prestin in amphibian HCs. Since no previous studies have measured amphibian HCs in auditory organs, we did not know if they generated NLC. We used the same voltage stimulus protocol to record HCs isolated from the AP, BP, and S from *Rana catesbeiana*. HCs of the AP and S displayed bell-shaped voltage-dependent NLC, while the cells from BP did not. Notably, our results explained the SOAE test reported by van Dijk et al., who measured SOAE in five frog species, including *Rana catesbeiana*. The highest emission frequency they tested was 1735 Hz, which was within the AP frequency range, and no emissions were recorded in the BP range [17]. It is likely that the prestin expression in the BP HCs was too low to be detected. Another explanation is that the inner ear of frog functions well at a very low frequency. The BP did not act like the AP and S, or even lost its active process ability for its relatively higher frequency sensing range. The Q_{\max} and charge density of S were higher than that measured in the AP cells. These results may be due to the larger cell size in the S organ, or there might be more prestin expressed in

the cell membrane of its tissue. Since charge density directly correlates with the level of prestin expression at the membrane, it is reasonable that S has a larger magnitude of NLC than AP [42].

When we compared the results of frog HCs and mouse OHCs, the charge density was dramatically different between these two taxa. The mouse OHC prestin had a greater charge density than the frog prestin, along with a significant shift of $V_{1/2}$ from positive to negative potentials. It is suggested that the functional evolution of prestin lies in the acquisition of NLC and the potential for $V_{1/2}$ to shift from positive to negative [26, 43]. Our study supports the hypothesis that the amphibian prestin is evolutionarily less advanced than mammalian prestin.

As we know, there is a charged voltage sensor within prestin that moves through the electrical field and gives rise to an electric current. This electric current, similar to a gating current, generates NLC. The z value was quite different between the mammalian and amphibian prestin proteins; however, we did not measure the motility or transport function of the frog prestin in this report. In previous studies, there is a reciprocal trend between NLC magnitude and anion transport properties during the functional evolution of prestin [44]. According to our results that the OHC has more prominent NLC than its nonmammalian orthologs, the transport capability of frog prestin might be stronger and its anion transport capability could be the dominant function of frog prestin. Nevertheless, without direct measurement of motility, the contribution of frog prestin to electromotility cannot be completely ruled out.

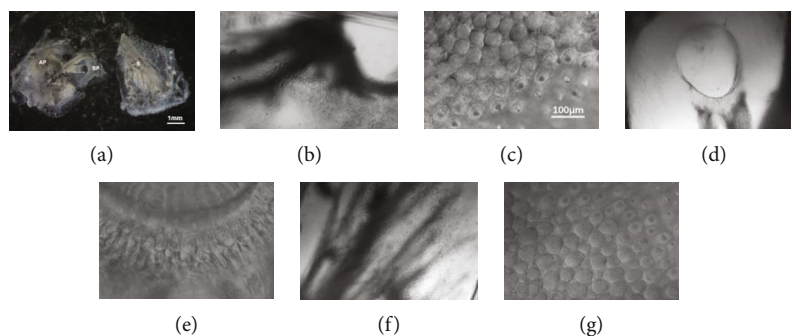


FIGURE 4: Images of frog's hearing organ. (a) Dissection of the frog's inner ear which contained three auditory organs (AP, BP, and S) under a 10x microscope. (b, c) Displayed was a higher magnification image of the AP under a 100x and 600x microscope. (d, e) Displayed was a higher magnification image of the BP under a 100x and 600x microscope. (f, g) Displayed was a higher magnification image of the S under a 100x and 600x microscope.

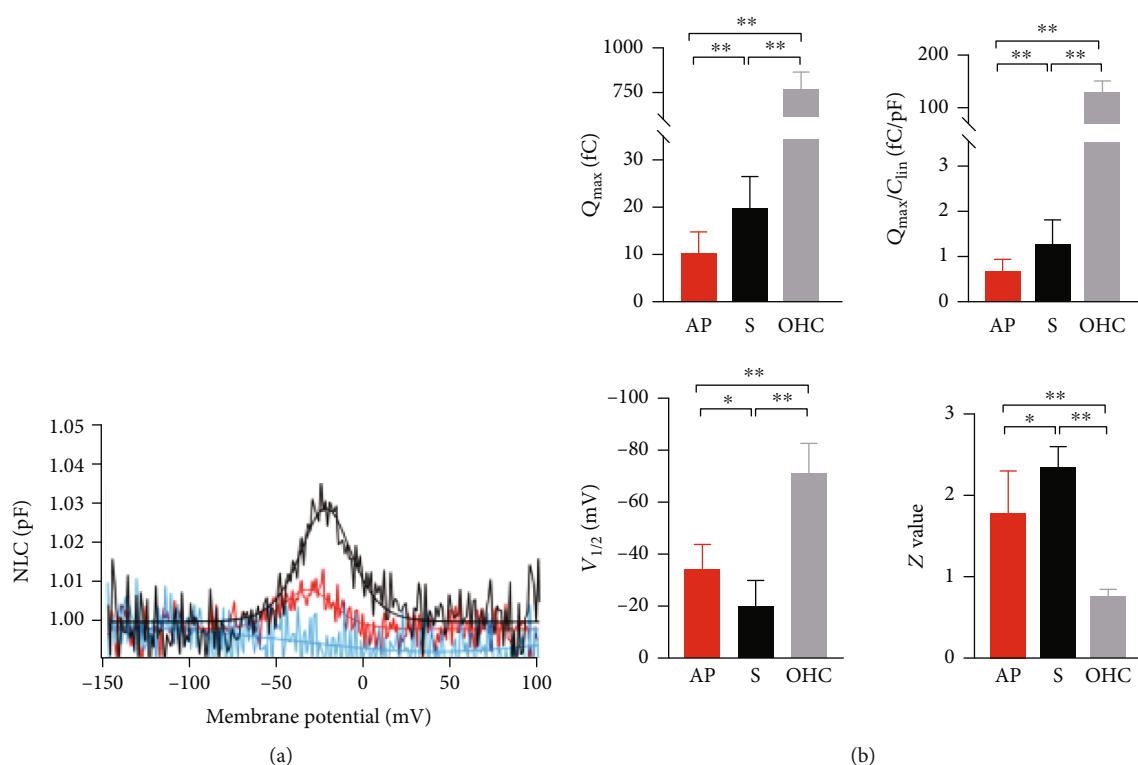


FIGURE 5: NLC functions of frog's three auditory organs (AP, BP, and S). (a) NLC obtained from the hair cells of three auditory organs. Red: the amphibian papilla (AP); black: the sacculus (S); blue: the basilar papilla (BP). No NLC was detected in the hair cells of the basilar papilla (BP). (b) Four parameters derived from curve fittings with Boltzmann's function for AP ($n = 10$) and S ($n = 8$). Mouse OHC was used as a control. Data are expressed as mean \pm s.d. $**P < 0.01$, $*P < 0.05$ (Student's t -test).

5. Conclusions

We observed acquisition of NLC both in fPres-transfected cells and in HCs isolated from frog auditory organs. Our results represent the first and necessary step in revealing possible roles of prestin in the active hearing processes found in many nonmammalian species. This might lead to the alternative hypothesis that both prestin and HC bundles might function together as the intrinsic kinetics for amplification and frequency selectivity in amphibian inner ears.

Data Availability

The data (data for prestin of bullfrog) used to support the findings of this study are included within the supplementary information file(s).

Conflicts of Interest

The authors declare that they have no conflicts of interest.

Acknowledgments

We thank Professor Geng-lin Li and professor Lei Song for technical support in electrophysiology. We also thank Geng-lin Li for the comments on our manuscript draft. This work was funded by the National Natural Science Foundation of China (NSFC) to H.W. (81730028) and the Shanghai Key Laboratory of Translational Medicine on Ear and Nose Diseases (14DZ2260300). The authors declare no competing financial interests.

Supplementary Materials

In our supplementary material, you may obtain all the NLC measurements of the mouse OHCs, HEK293T cells transfected with gPres and fPres, AP HCs, and S HCs from the frog auditory organ. (*Supplementary Materials*)

References

- [1] Y. Liu, J. Qi, X. Chen et al., "Critical role of spectrin in hearing development and deafness," *Science Advances*, vol. 5, no. 4, p. eaav7803, 2019.
- [2] J. Qi, Y. Liu, C. Chu et al., "A cytoskeleton structure revealed by super-resolution fluorescence imaging in inner ear hair cells," *Cell Discovery*, vol. 5, no. 1, p. 12, 2019.
- [3] X. Lu, S. Sun, J. Qi et al., "Bmi1 regulates the proliferation of cochlear supporting cells via the canonical Wnt signaling pathway," *Molecular Neurobiology*, vol. 54, no. 2, pp. 1326–1339, 2017.
- [4] B. Kachar, W. E. Brownell, R. Altschuler, and J. Fex, "Electrokinetic shape changes of cochlear outer hair cells," *Nature*, vol. 322, no. 6077, pp. 365–368, 1986.
- [5] J. Santos-Sacchi and W. Tan, "The frequency response of outer hair cell voltage-dependent motility is limited by kinetics of prestin," *The Journal of Neuroscience*, vol. 38, no. 24, pp. 5495–5506, 2018.
- [6] J. Santos-Sacchi and L. Song, "Chloride anions regulate kinetics but not voltage-sensor Qmax of the solute carrier SLC26a5," *Biophysical Journal*, vol. 110, no. 11, pp. 2551–2561, 2016.
- [7] T. Wang, R. Chai, G. S. Kim et al., "Lgr5+ cells regenerate hair cells via proliferation and direct transdifferentiation in damaged neonatal mouse utricle," *Nature Communications*, vol. 6, no. 1, p. 6613, 2015.
- [8] B. C. Cox, R. Chai, A. Lenoir et al., "Spontaneous hair cell regeneration in the neonatal mouse cochlea in vivo," *Development*, vol. 141, no. 4, pp. 816–829, 2014.
- [9] R. G. Kavlie, J. L. Fritz, F. Nies et al., "Prestin is an anion transporter dispensable for mechanical feedback amplification in Drosophila hearing," *Journal of Comparative Physiology. A, Neuroethology, Sensory, Neural, and Behavioral Physiology*, vol. 201, no. 1, pp. 51–60, 2015.
- [10] J. Santos-Sacchi and W. Tan, "Voltage does not drive prestin (SLC26a5) electro-mechanical activity at high frequencies where cochlear amplification is best," *iScience*, vol. 22, pp. 392–399, 2019.
- [11] Y. N. Chang, E. A. Jaumann, K. Reichel et al., "Structural basis for functional interactions in dimers of SLC26 transporters," *Nature Communications*, vol. 10, no. 1, p. 2032, 2019.
- [12] S. Takahashi, T. Yamashita, K. Homma et al., "Deletion of exons 17 and 18 in prestin's STAS domain results in loss of function," *Scientific Reports*, vol. 9, no. 1, p. 6874, 2019.
- [13] M. F. Kuwabara, K. Wasano, S. Takahashi et al., "The extracellular loop of pendrin and prestin modulates their voltage-sensing property," *The Journal of Biological Chemistry*, vol. 293, no. 26, pp. 9970–9980, 2018.
- [14] S. Lovas, D. Z. Z. He, H. Liu et al., "Glutamate transporter homolog-based model predicts that anion- π interaction is the mechanism for the voltage-dependent response of prestin," *The Journal of Biological Chemistry*, vol. 290, no. 40, pp. 24326–24339, 2015.
- [15] R. Guo, S. Zhang, M. Xiao et al., "Accelerating bioelectric functional development of neural stem cells by graphene coupling: implications for neural interfacing with conductive materials," *Biomaterials*, vol. 106, pp. 193–204, 2016.
- [16] A. Chang, C. Li, J. Huang, W. Pan, Y. Tian, and J. Tang, "Auditory brainstem response and outer hair cell whole-cell patch clamp recording in postnatal rats," *Journal of Visualized Experiments*, vol. 135, no. 135, 2018.
- [17] P. van Dijk, P. M. Narins, and J. Wang, "Spontaneous otoacoustic emissions in seven frog species," *Hearing Research*, vol. 101, no. 1-2, pp. 102–112, 1996.
- [18] R. Chai, B. Kuo, T. Wang et al., "Wnt signaling induces proliferation of sensory precursors in the postnatal mouse cochlea," *Proceedings of the National Academy of Sciences of the United States of America*, vol. 109, no. 21, pp. 8167–8172, 2012.
- [19] C. Bergevin, D. M. Freeman, J. C. Saunders, and C. A. SHERA, "Otoacoustic emissions in humans, birds, lizards, and frogs: evidence for multiple generation mechanisms," *Journal of Comparative Physiology. A, Neuroethology, Sensory, Neural, and Behavioral Physiology*, vol. 194, no. 7, pp. 665–683, 2008.
- [20] L. Chen, W. Sun, and R. J. Salvi, "Electrically evoked otoacoustic emissions from the chicken ear," *Hearing Research*, vol. 161, no. 1-2, pp. 54–64, 2001.
- [21] M. Beur, X. Tan, and R. Fettiplace, "A prestin motor in chicken auditory hair cells: active force generation in a non-mammalian species," *Neuron*, vol. 79, no. 1, pp. 69–81, 2013.
- [22] T. A. Jan, R. Chai, Z. N. Sayyid et al., "Tympanic border cells are Wnt-responsive and can act as progenitors for postnatal mouse cochlear cells," *Development*, vol. 140, no. 6, pp. 1196–1206, 2013.
- [23] R. L. M. Schoffelen, J. M. Segenhout, and P. van Dijk, "Mechanics of the exceptional anuran ear," *Journal of Comparative Physiology. A, Neuroethology, Sensory, Neural, and Behavioral Physiology*, vol. 194, no. 5, pp. 417–428, 2008.
- [24] S. Ji, D. Bozovic, and R. Bruinsma, "Amphibian sacculus and the forced Kuramoto model with intrinsic noise and frequency dispersion," *Physical Review E*, vol. 97, no. 4, article 042411, 2018.
- [25] J. B. Azimzadeh and J. D. Salvi, "Physiological preparation of hair cells from the sacculus of the American bullfrog (*Rana catesbeiana*)," *Journal of Visualized Experiments*, vol. 121, no. 121, 2017.
- [26] X. Tan, J. L. Pecka, J. Tang, S. Lovas, K. W. Beisel, and D. Z. Z. He, "A motif of eleven amino acids is a structural adaptation that facilitates motor capability of eutherian prestin," *Journal of Cell Science*, vol. 125, no. 4, pp. 1039–1047, 2012.

- [27] W. Chen, L. Tan, Q. Zhou et al., "AAVS1 site-specific integration of the CAR gene into human primary T cells using a linear closed-ended AAV-based DNA vector," *The Journal of Gene Medicine*, vol. 22, no. 4, p. e3157, 2020.
- [28] H. Yang, J. Wang, M. Zhao et al., "Feasible development of stable HEK293 clones by CRISPR/Cas9-mediated site-specific integration for biopharmaceuticals production," *Biotechnology Letters*, vol. 41, no. 8-9, pp. 941-950, 2019.
- [29] J. Zhang, X. Liu, Y. Zhang et al., "Human neural stem cells with GDNF site-specific integration at AAVS1 by using AAV vectors retained their stemness," *Neurochemical Research*, vol. 43, no. 4, pp. 930-937, 2018.
- [30] F. Tan, C. Chu, J. Qi et al., "AAV-ie enables safe and efficient gene transfer to inner ear cells," *Nature Communications*, vol. 10, no. 1, p. 3733, 2019.
- [31] Y. Luo, A. Frederick, J. M. Martin et al., "AAVS1-targeted plasmid integration in AAV producer cell lines," *Human Gene Therapy Methods*, vol. 28, no. 3, pp. 124-138, 2017.
- [32] C. Li, A. S. Mishra, S. Gil et al., "Targeted integration and high-level transgene expression in AAVS1 transgenic mice after in vivo HSC transduction with HDAd5/35++ vectors," *Molecular Therapy*, vol. 27, no. 12, pp. 2195-2212, 2019.
- [33] R. Fettiplace, "Diverse mechanisms of sound frequency discrimination in the vertebrate cochlea," *Trends in Neurosciences*, vol. 43, no. 2, pp. 88-102, 2020.
- [34] E. Lewis, R. Baird, E. Leverenz, and H. Koyama, "Inner ear: dye injection reveals peripheral origins of specific sensitivities," *Science*, vol. 215, no. 4540, pp. 1641-1643, 1982.
- [35] Z. H. He, S. Y. Zou, M. Li et al., "The nuclear transcription factor FoxG1 affects the sensitivity of mimetic aging hair cells to inflammation by regulating autophagy pathways," *Redox Biology*, vol. 28, p. 101364, 2020.
- [36] W. Liu, X. Xu, Z. Fan et al., "Wnt signaling activates TP53-induced glycolysis and apoptosis regulator and protects against cisplatin-induced spiral ganglion neuron damage in the mouse cochlea," *Antioxidants & Redox Signaling*, vol. 30, no. 11, pp. 1389-1410, 2019.
- [37] Z. He, L. Guo, Y. Shu et al., "Autophagy protects auditory hair cells against neomycin-induced damage," *Autophagy*, vol. 13, no. 11, pp. 1884-1904, 2017.
- [38] L. Liu, Y. Chen, J. Qi et al., "Wnt activation protects against neomycin-induced hair cell damage in the mouse cochlea," *Cell Death & Disease*, vol. 7, no. 3, p. e2136, 2016.
- [39] Z. He, Q. Fang, H. Li et al., "The role of FOXG1 in the postnatal development and survival of mouse cochlear hair cells," *Neuropharmacology*, vol. 144, pp. 43-57, 2019.
- [40] S. Zhang, Y. Zhang, Y. Dong et al., "Knockdown of Foxg1 in supporting cells increases the trans-differentiation of supporting cells into hair cells in the neonatal mouse cochlea," *Cellular and Molecular Life Sciences*, vol. 77, no. 7, pp. 1401-1419, 2020.
- [41] W. Yan, W. Liu, J. Qi et al., "A three-dimensional culture system with Matrigel promotes purified spiral ganglion neuron survival and function in vitro," *Molecular Neurobiology*, vol. 55, no. 3, pp. 2070-2084, 2018.
- [42] M. L. Seymour, L. Rajagopalan, G. Duret et al., "Membrane prestin expression correlates with the magnitude of prestin-associated charge movement," *Hearing Research*, vol. 339, pp. 50-59, 2016.
- [43] J. Tang, J. L. Pecka, B. Fritzsche, K. W. Beisel, and D. Z. Z. He, "Lizard and frog prestin: evolutionary insight into functional changes," *PLoS One*, vol. 8, no. 1, article e54388, 2013.
- [44] X. Tan, J. L. Pecka, J. Tang et al., "From zebrafish to mammal: functional evolution of prestin, the motor protein of cochlear outer hair cells," *Journal of Neurophysiology*, vol. 105, no. 1, pp. 36-44, 2011.

Research Article

High Frequency of *AIFM1* Variants and Phenotype Progression of Auditory Neuropathy in a Chinese Population

Hongyang Wang,^{1,2} Dan Bing,³ Jin Li,^{1,2} Linyi Xie,^{1,2} Fen Xiong,^{1,2} Lan Lan,^{1,2}
Dayong Wang,^{1,2} Jing Guan,^{1,2} and Qiuju Wang^{1,2} 

¹College of Otolaryngology, Head and Neck Surgery, Chinese PLA Institute of Otolaryngology, Chinese PLA General Hospital, Beijing 100853, China

²National Clinical Research Center for Otolaryngologic Diseases, Beijing 100853, China

³Department of Otolaryngology-Head and Neck Surgery, Tongji Hospital, Tongji Medical College, Huazhong University of Science and Technology, Wuhan 430030, China

Correspondence should be addressed to Qiuju Wang; wqcr301@vip.sina.com

Received 6 March 2020; Revised 14 May 2020; Accepted 2 June 2020; Published 1 July 2020

Academic Editor: Renjie Chai

Copyright © 2020 Hongyang Wang et al. This is an open access article distributed under the Creative Commons Attribution License, which permits unrestricted use, distribution, and reproduction in any medium, provided the original work is properly cited.

To decipher the genotype-phenotype correlation of auditory neuropathy (AN) caused by *AIFM1* variations, as well as the phenotype progression of these patients, exploring the potential molecular pathogenic mechanism of AN. A total of 36 families of individuals with AN (50 cases) with *AIFM1* variations were recruited and identified by Sanger sequencing or next-generation sequencing; the participants included 30 patients from 16 reported families and 20 new cases. We found that *AIFM1*-positive cases accounted for 18.6% of late-onset AN cases. Of the 50 AN patients with *AIFM1* variants, 45 were male and 5 were female. The hotspot variation of this gene was p.Leu344Phe, accounting for 36.1%. A total of 19 *AIFM1* variants were reported in this study, including 7 novel ones. A follow-up study was performed on 30 previously reported *AIFM1*-positive subjects, 16 follow-up cases (53.3%) were included in this study, and follow-up periods were recorded from 1 to 23 years with average 9.75 ± 9.89 years. There was no hearing threshold increase during the short-term follow-up period (1-10 years), but the low-frequency and high-frequency hearing thresholds showed a significant increase with the prolongation of follow-up time. The speech discrimination score progressed gradually and significantly along with the course of the disease and showed a more serious decline, which was disproportionately worse than the pure tone threshold. In addition to the X-linked recessive inheritance pattern, the X-linked dominant inheritance pattern is also observed in *AIFM1*-related AN and affects females. In conclusion, we confirmed that *AIFM1* is the primary related gene among late-onset AN cases, and the most common recurrent variant is p.Leu344Phe. Except for the X-linked recessive inheritance pattern, the X-linked dominant inheritance pattern is another probability of *AIFM1*-related AN, with females affected. Phenotypical features of *AIFM1*-related AN suggested that auditory dyssynchrony progressively worsened over time.

1. Introduction

Auditory neuropathy (AN) is a special type of sensorineural hearing loss with a main manifestation of impaired speech comprehension, accounting for 1.2-10% of cases of hearing loss, depending on the population [1, 2]. The affected hearing in AN is mainly low frequency, and the speech recognition rate is obviously disproportionately lower than the pure tone threshold (PTA). This type of disease may arise from the

inner hair cells (IHCs) of the cochlea, the synapses between the IHCs and the auditory nerve, the spiral ganglion neuron (SGN), the cochlear nerve fibers, and one or more of the auditory nerves [3].

The pathogenic mechanism of AN is currently unclear, and genetic factors may account for up to 40% of the pathogenesis of AN [4]. The inheritance pattern of AN includes autosomal recessive, autosomal dominant, and X-linked recessive inheritance. In 2006, our group located the gene

locus AUNX1 of X-linked recessive hereditary neuropathy in the Xq23-q27.3 region for the first time [5] and then further identified *AIFM1* as the gene responsible for this kind of AN using whole exome sequencing technology in 2015 [6]. Apoptosis-inducing factor (AIF) is a flavin protein that is located in the mitochondrial membrane space. It was originally discovered as the first apoptotic factor that causes caspase-independent apoptosis [7]. This protein plays a critical role in maintaining the normal morphology and physiological functions of mitochondria and causing apoptosis that is not dependent on caspase.

Since AN was first identified more than 20 years ago, diagnosis, particularly precision diagnosis with lesion site identification, remains a challenge. Cases with genetic basis and the identification of the genes may be helpful for the lesion site identification, deciphering the underlying mechanism of AN [8–9]. Except for diagnosis, intervention is another challenge for clinical management for AN. Hearing aids and cochlear implantations, which are typical intervention strategies for cochlear sensory hearing loss, have variable outcomes for AN cases depending on the affected lesion sites [3–10]. Gene therapy may provide possibility for the treatment of AN [11]. Since virally mediated gene expressions in almost 100% HCs are possible, the treatment of presynaptic AN is possible [12]. And the virally expressing genes in SGNs are also feasible, supporting the possibility of treating post-synaptic AN [13].

Up to date, there is no frequency data of *AIFM1*-positive cases in AN cases. In this study, we further identified another 20 AN cases with *AIFM1* variants, including 7 novel variants and one hotspot variant, showing that the proportion of AN caused by *AIFM1* in Chinese patients with delayed-onset AN was as high as 18.6% (36/194), higher than the 15.53% (16/103) observed in the previous study [6]. Genotype-phenotype correlation analyses of AN cases with *AIFM1* gene pathogenic mutations were carried out, including the clinical hearing vestibular test, comprehensive clinical follow-up study data, and an in-depth exploration of the clinical characteristics of the disease and the related pathogenesis, to explore the characteristics of *AIFM1* gene-positive AN, laying the theoretical basis of AN classification diagnosis. The X-linked dominant inheritance pattern is also firstly observed in *AIFM1*-related AN and affects females in the study as well.

2. Materials and Methods

2.1. Ethics Statement. The study was approved by the Committee of Medical Ethics of Chinese PLA General Hospital. Written informed consent was obtained from all participants.

2.2. Subject Recruitment and Clinical Evaluation. A total of 50 patients with *AIFM1* mutations who were diagnosed with AN in the Chinese PLA Institute of Otolaryngology, Chinese PLA General Hospital, from April 1997 to June 2019 were recruited for this study. The diagnostic criteria were as follows: The typical audiological characteristics were that the auditory brainstem response (ABR) had no obvious differen-

tiation waveform or severe abnormality and that the otoacoustic emission (OAE) and/or the cochlear microphonic (CM) potential could be normally extracted. Personal or family medical evidence of hearing loss, tinnitus, vestibular symptoms, and other clinical abnormalities of both the affected members and the unaffected members of these families was identified. Pure tone threshold (PTA), speech discrimination score (SDS), ABR, OAE, CM, and electrocochleography (ECoChG) were carried out as otological examination batteries to evaluate auditory status. In general, the low frequencies were primarily affected; thus, we focused on the low-frequency data and calculated PTA as the average of the thresholds of 250-1000 Hz to avoid bias in the assessment of the degree of AN hearing loss. Vestibular function evaluation included vestibular evoked myogenic potentials, oculomotor function tests, positional nystagmus tests, positioning nystagmus tests, and bithermal caloric tests. High-resolution computed tomography (CT) scans of the temporal bone and cerebral magnetic resonance imaging (MRI) were performed to exclude other possible neuropathic or anatomical disorders.

2.3. Genetic Techniques. Next-generation sequencing and Sanger sequencing were performed on the patients as previously described. Variation interpretation (evaluation of the pathogenicity) was based on the standards and guidelines of the American College of Medical Genetics and Genomics and the Association for Molecular Pathology (ACMG and AMP) [14].

2.4. Statistical Analysis. Statistical analysis was performed using SPSS 19.0 statistical software, Empower software (<http://www.empowerstats.com>, X&Y Solutions, Inc., Boston, MA) and R software (<https://www.R-project.org>), as well as G. Comparisons of the two sets of data were performed using an independent sample *t*-test. The comparisons of multiple sets of data were performed using one-way ANOVA. $p < 0.05$ represented a significant difference. Spline smoothing was performed using GMM (generalized additive mixed model) to explore the change in pure tone threshold with the length of follow-up time.

3. Results

3.1. General Clinical Information. Fifty patients with *AIFM1* mutations were recruited for this study, including 30 patients who have been previously studied and 20 novel patients who were identified recently (Table 1). All patients had no history of high-risk factors such as hyperbilirubinemia and hypoxia and denied a history of metabolic diseases such as diabetes. Nine (18%) patients had a history of ototoxic drug use, and one patient had a history of exposure to noise. Clinically, 37 patients (74%) complained of tinnitus at the first visit, and numbness of the extremities was the second most common symptom (12 patients), while few patients experienced visual impairment (10 patients) and vertigo (8 patients). Fifteen patients (30 ears) received cVEMP examination, among which 19 (63.3%) ears showed ipsilateral sacculus dysfunction, and 11 (36.7%) ears showed normal function. Nineteen

TABLE 1: Clinical phenotype of the 20 *AIFMI*-positive auditory neuropathy cases.

Number	Case ID	Gender ^a	Age of test (years)	Age of onset (years)	Hearing impairment phenotype			PB max (%) ^c	Tinnitus	Vertigo	Gait instability	Numbness of extremities	Visual impairment	Muscle deformity	Intellectual abilities	MRI of brain ^d
					Hearing loss degree (PTA) (L/R) ^b	Type of audiometry	Type of audiometry									
1	300005	F	17	15	Both mild	Upsloping	NA	+	-	NA	NA	Myopia	NA	-	NA	
2	300145	F	21	18	Both moderate	Upsloping	NA	+	-	NA	NA	-	NA	-	-	
3	300158	M	14	10	Moderate/moderately severe	Upsloping	NA	-	-	-	-	-	-	-	NA	
4	400352	M	20	16	Moderate/moderately severe	Upsloping	NA	NA	NA	NA	NA	Myopia	NA	-	NA	
5	400469	M	21	14	Severe/moderate	Other	NA	-	-	NA	NA	-	NA	-	CNH	
6	400738	M	28	20	Both moderate	Upsloping	28/24	+	NA	+	+	NA	NA	-	-	
7	501418	M	21	12	Both mild	Upsloping	50/84	+	-	-	-	-	-	-	NA	
8	602409	F	17	13	Both mild	Flat/upsloping	NA	-	-	-	-	-	-	-	NA	
9	602416	F	6	6	Normal/severe	Flat/downsloping	96/NA	+	-	+	+	-	NA	-	NA	
10	703306	M	27	12	Severe/moderately severe	Upsloping	NA	+	+	+	+	-	NA	-	NA	
11	804755	F	28	21	Mild/moderate	Upsloping	24/32	+	-	NA	NA	Myopia	NA	-	CNH	
12	1007198	M	20	10	Both moderately severe	Upsloping	0/0	+	+	-	-	-	-	-	NA	
13	1507328	M	28	15	Moderately severe/moderate	Upsloping	0/0	+	-	NA	NA	-	NA	-	NA	
14	1507329	M	24	10	Both moderately severe	Upsloping	36/40	-	-	NA	NA	-	NA	-	-	
15	1507366	M	20	8	Normal/mild	Upsloping/flat	NA	-	-	-	-	NA	-	-	NA	
16	1507405	M	34	17	Both moderate	Upsloping	56/52	+	-	NA	NA	-	NA	-	NA	
17	1507426	M	25	20	Moderate/normal	Upsloping/flat	0/68	+	-	NA	NA	NA	NA	-	-	
18	1707671	M	18	14	Both mild	Upsloping	8/60	-	-	NA	NA	Myopia	NA	-	NA	
19	1707676	M	21	14	Both mild	Upsloping	88/96	+	+	NA	NA	Myopia	NA	-	NA	
20	1707834	M	16	11	Both mild	Upsloping	56/28	+	-	NA	-	Myopia	NA	-	CNH	

Note: ^aF: female; M: male. ^bPTA: pure tone average; L: left; R: right. ^cCNH: cochlear nerve hypoplasia. NA: not available; +/ -: positive or negative finding.

patients underwent vestibular function tests; 15 sides (15/38, 39.5%) showed abnormalities, while the other 23 sides were normal. No abnormalities in temporal CT were found, and 3 patients (42.9%, 3/7) showed bilateral cochlear nerve hypoplasia in the MRI test.

The pure tone thresholds of each frequency were not significantly different between the left and right ears in all 50 patients (Figure 1(a)). The disease durations at the first visit ranged from 0 to 33 years (9.7 ± 7.7 years), and the PTAs among the 5-, 5- to 15-, and >15-year disease duration groups were not significantly different ($p > 0.05$) (Figure 1(b)). The onset ages of *AIFM1*-positive patients ranged from 5 to 20 years (13.4 ± 3.9). In addition, the earlier the onset, the more severe the hearing impairment. The pure tone averages (PTAs, 250-1000 Hz) of the <12-year-old group, 12- to 16-year-old group, and >16-year-old group were 55.7, 51.2, and 47.7 dB HL, respectively. The most severe hearing loss was observed in the youngest age group. However, the differences in hearing loss between the three onset age groups were not statistically significant (Figure 1(c)).

3.2. Mutation Spectrum of *AIFM1* (Table 2). Among the 20 novel cases found with *AIFM1* variations, seven novel and three reported variations were found, located in the FAD, NADH, and C-terminus. Pathogenicity was assessed using SIFT (<http://sift.jcvi.org/>), PolyPhen-2 (Polymorphism Phenotyping V.2, <http://genetics.bwh.harvard.edu/pph2>), LRT (http://www.genetics.wustl.edu/jflab/lrt_query.html), and MutationTaster (<http://www.mutationtaster.org>).

The seven novel variations were all pathogenic with the evidences of “PS×1 + PM×2 + PP×2” according to the ACMG and AMP guidelines [14]. Firstly, 18.6% of late-onset AN cases had variants in *AIFM1*, while the variations were absent in our sensorineural hearing loss group (PS4). Secondly, these variations were absent or at extremely low frequency in ESP, ExAC, gnomAD-EAS, or 1000genomes (PM2). Thirdly, in these families, the variations were cosegregated with AN phenotype, with proband’s mother carrying variation but having no AN performance (PM). Fourthly, these variants were predicted to be deleterious with SIFT, PolyPhen-2, LRT, MutationTaster, and so on (PP3). In addition, in terms of phenotype, these patients were all reported as AN(PP4). Furthermore, cells with the *AIFM1* mutation led to decreased dimerization and impaired mitochondrial functions (unpublished data), which may indicate that the mutations in *AIFM1* gene may affect auditory function, providing PS3 evidence.

The recurrent variants were p.Ile304Met, p.Leu344Phe, p.Arg422Trp, and p.Tyr560His, among which the most common variant in the AN population was p.Leu344Phe, which was present in 36.1% (13/36) of the positive cases, followed by p.Arg422Trp (13.9%, 5/36).

In total, 18 variations in *AIFM1* variations were related to the AN phenotype, with 9 variations located in FAD, 6 variations in NADH, and 4 variations in the C-terminal region. There was no overlap with the other *AIFM1* variations that caused other syndromes [6, 15–28] (Figure 2).

3.3. Genotype and Phenotype Correlation Analysis of the 20 Newly Identified Cases

3.3.1. Clinical Features of the 20 Newly Identified Cases with *AIFM1* Variants (Table 1). Except for families 0804755 and 1507328, who had a family history, 18 other cases with *AIFM1* variants were sporadic cases. The age of onset ranged from 6 to 20 years, with only one case (1507426) not complaining of childhood-onset AN. Except for one female case with unilateral AN, all other patients showed bilateral AN. The audiograms varied, with 31 ears (83.8%, 31/37) showing upsloping types. Seven of 20 patients underwent inclined sagittal MRI of the internal auditory canals, with 3 patients showing bilateral cochlear nerve hypoplasia.

3.3.2. Female Patients with *AIFM1* Variants (Possible X-Linked Dominant Inheritance Pattern). All of the female cases had the same variant, c.1030C>T (p.Leu344Phe), which was also the most common variant among AN-related *AIFM1* variations. Except for 0804755 (Figure 3(a)), the other female patients had no family history. There was no hearing threshold difference between male and female AN patients with this variant (Figure 3(b)). However, the audiograms of the females affected varied from normal to profound, including flat, upflopping, and downflopping as time went on (Figure 3(c)).

3.3.3. Phenotype Follow-Up of the 30 AN Patients with *AIFM1* Mutations. Sixteen patients (53.33%) underwent follow-up pure tone audiometry tests, and the follow-up period was 1-23 years, with a mean time of 9.75 ± 9.89 years. The hearing threshold change varied between patients (Figure 4). The average thresholds of low and high frequencies in the different follow-up groups were significantly different in all of the patients who had been followed for more than one year (Figure 1(d)). For the patients with a short-term follow-up period (1-10 years), the hearing deterioration was not apparent at all frequencies (Figure 1(e)), but with the prolongation of follow-up time (more than 10 years), the low-frequency (0.25 and 0.5 kHz) and high-frequency (4 and 8 kHz) hearing thresholds showed a significant increase (Figure 1(f)).

In addition, we performed spline smoothing by using GAMM to explore the change in the pure tone threshold with the length of follow-up time. Figure 5 illustrates the shape of the relationship between the hearing outcome at a frequency of 0.5 kHz and the follow-up time (edf = 1.427, $p = 0.0096$). This result suggested that the hearing threshold of 0.5 kHz in both ears worsened gradually over time. The hearing thresholds of 0.25, 1, 2, 4, and 8 kHz changed in a similar pattern as that of 0.5 kHz, although statistical significance was not reached in either ear (Figure 6).

Twenty-three patients (46/60 ears, 76.67%) with *AIFM1* mutations underwent binaural speech testing, and 10 patients (20 ears, 43.5%) were followed up. A total of 10 patients (20 ears) were followed up for SDS (Table S1), with a follow-up period of 1-15 years (6.80 ± 4.47 years). Of the 46 ears, 50% of patients with mild hearing loss had zero SDS, which was a much higher figure than that in the moderate and severe groups. Overall, the SDS of the mild hearing loss group was significantly lower than that of the moderate and severe groups ($p < 0.05$). Therefore, the degree of SDS decline in these patients with AN was not

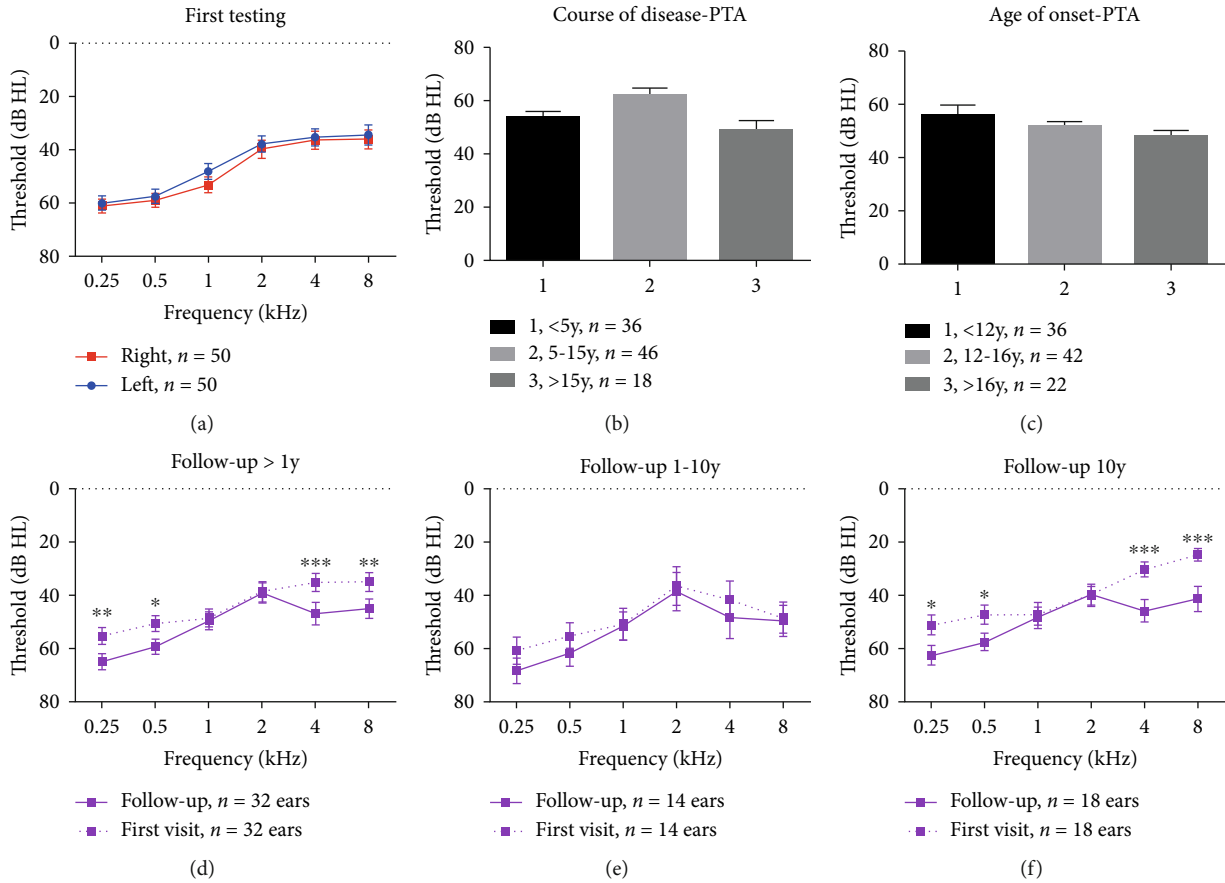


FIGURE 1: Pure tone test of the *AIFM1*-positive cases. (a) Average threshold of the 50 cases with *AIFM1* variations. (b) Mean PTA in the groups with different disease courses. (c) Mean PTA in the groups with different onset ages. (d-f) Mean threshold in each frequency with different follow-up periods. dB: decibels; Hz: Hertz; PTA: pure tone average.

proportional to the pure tone hearing threshold, and SDS was more severe in patients with mild hearing loss than in patients in the moderate and severe hearing loss groups (Table S2). Disease duration was another risk factor; of the 9 patients with a disease duration less than 5 years, none had an SDS score of zero. In patients with disease duration of more than 5 years, the proportion of patients with an SDS score of zero increased significantly, accounting for 50% of all ears (Table S3). This finding indicates that SDS decreased significantly with the prolongation of the disease course, and the difference was statistically significant ($p < 0.05$). The mean values of the left and right ears before and after follow-up were greater than zero, indicating that the SDS exhibited a downward trend before and after follow-up, but the difference between the two ears was not statistically significant ($p > 0.05$).

Among the 30 patients, 7 ears from 5 patients were able to elicit V-waves, but the waveform differentiation was poor, the amplitudes were reduced, and the latencies were prolonged. The PTAs of the 7 ears with the V-wave were relatively better, and the course of the disease was shorter than that of the unexposed ABR waveform, but the difference was not statistically significant ($p > 0.05$) (Table S4). Three of five patients had follow-up ABR data; their V-wave

latencies were gradually extended, and the V-wave of ABR was unextracted in the follow-up of one ear (left ear of 1007170-1) (Table S5).

All 30 patients underwent DPOAE; 29 patients passed with the elicitation of at least five frequencies, while one patient had no response at any of the frequencies. This individual was a member of family 1007170 and had a disease duration of 33 years. AN may progress to sensorineural hearing loss, with outer hair cell impairment as time goes on.

A total of 22 patients (44 ears) underwent electrocochleography examination, among whom, 6 patients underwent follow-up observation. The -SP waves were found in 21 patients, except for one person who had an unobvious wave. Nine patients (20.5%, 9/44) showed the -SP wave only, without an obvious CAP wave, while the remaining 35 ears showed both -SP and CAP waveforms, with absolute values of -SP/AP > 0.4 (Table S6). The degree of hearing loss in patients with AN who did not elicit CAP waveforms was significantly higher than that in patients with CAP, and the difference was statistically significant ($p < 0.001$). For the 6 cases (12 ears) with a follow-up ECoChG test (Figure S1), there were no differences between the absolute values of SP/AP.

TABLE 2: Variations identified in the 20 AIFMI-positive cases.

Nucleotide change	Amino acid change	Protein domain	Number of patients	Reported	SIFT ^a	PolyPhen-2-HVAR ^b	Prediction information		MutationTaster	ESP	Minor allele frequency ^c	
							LRT	MutationTaster			ExAC	gnomAD-EAS 1000genomes
c.547A>T	p.Thr183Ser	FAD	1	No	0.05	0.228	Deleterious	Disease-causing	-1	-1	NA	-1
c.881G>A	p.Arg294Gln	NADH	1	No	0.63	0.148	Deleterious	Disease-causing	-1	5.70399E-05	-1	-1
c.890A>T	p.Lys297Ile	NADH	1	No	0.01	0.788	Deleterious	Disease-causing	-1	-1	0.00291262	0.0005
c.912C>G	p.Ile304Met	NADH	2	No	0.11	0.846	Deleterious	Disease-causing	-1	-1	-1	NA
c.997C>T	p.Leu333Phe	NADH	1	No	0.11	0.846	Deleterious	Disease-causing	-1	NA	NA	NA
c.1030C>T	p.Leu344Phe	NADH	8	Yes	0.15	0.457	Deleterious	Disease-causing	-1	0.000205173	0.00291262	0.0005
c.1264C>T	p.Arg422Trp	FAD	2	Yes	0.09	0.999	Deleterious	Disease-causing	-1	-1	NA	-1
c.1394C>T	p.Ala465Val	FAD	1	No	0.002	1	Deleterious	Disease-causing	-1	NA	NA	NA
c.1492G>A	p.Val498Met	C-terminal	1	Yes	0.02	0.991	Deleterious	Disease-causing	1.13947E-05	-1	0.0000777001	-1
c.1678T>C	p.Tyr560His	C-terminal	2	No	0.01	0.9	Deleterious	Disease-causing	-1	NA	NA	NA

Note: ^adeleterious (≤ 0.05); tolerance > 0.05 . ^bProbably damaging (≥ 0.957), possibly damaging ($0.447 \leq \text{pp2_havr} \leq 0.909$), and benign (≤ 0.446). ^cAllele frequencies in each population database; it is marked as “-1” when the allele is not carried in the corresponding group. EAS: East Asians. NA: not available.

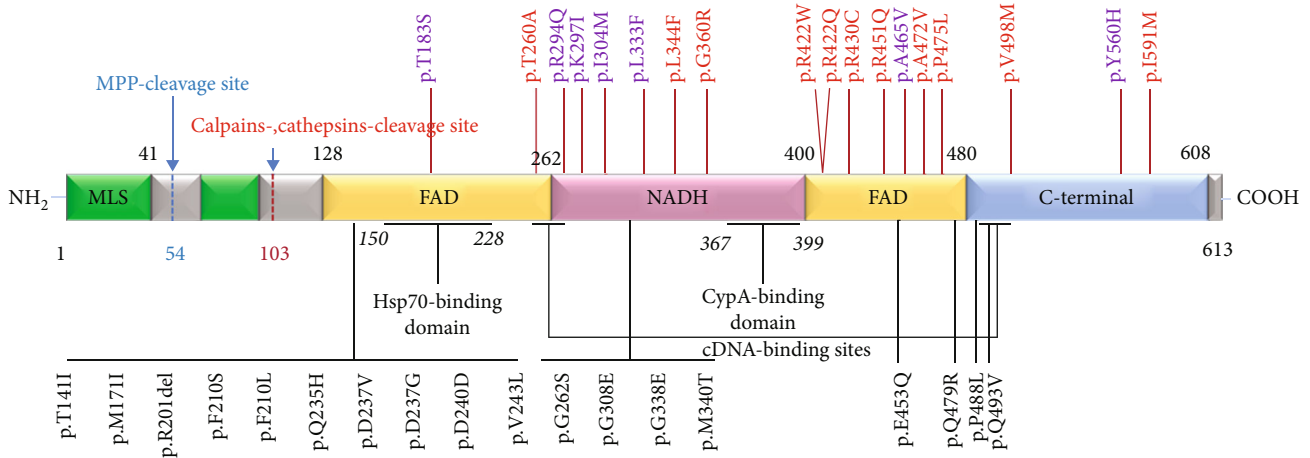


FIGURE 2: *AIFM1* variations in auditory neuropathy as well as other syndromes. The purple ones are the new variations identified in this study, the red ones are the previously reported AN-related variations, and the black ones are the variants that are related to syndromes such as cerebellar ataxia (modified from [6]).

4. Discussion

AN is a special type of hearing dysfunction disease, which is one of the critical diseases that cause speech communication disorders in infants and adolescents [3]. In the auditory system, HCs and SGNs are very important for hearing ability; HCs convert the sound waves into electrical signals, and SGNs transmit the electrical signals into the auditory cortex for hearing ability [29]. In a mammal's cochlea, HCs and SGNs are vulnerable for multiple damages, including noise, gene mutation, ototoxic drugs, inflammation, and aging [30–34]; while the mammal's cochlea only have very limited HC and SGN regeneration ability, majority of the damaged HC and SGN cannot be spontaneously regenerated [35–41]. Thus, hearing loss is usually irreversible, and AN may come from the damage of IHC and SGNs.

As a difficult and popular topic in international research, research on AN has been performed for 20 years, from preliminary reports to various explorations of its pathogenesis, and it is beginning to be gradually understood accurately. The etiology of AN varies with age, genetic factors, hyperbilirubinemia, low birth weight, premature birth, and hypoxia. More patients may be discovered as the use of genetic testing in the diagnosis of auditory neuropathy becomes more widespread [4–8]; however, no prevalence studies have been performed to date. In our previous study, we confirmed that *OTOF* is the most common gene-causing congenital auditory neuropathy [42]. In contrast, for patients with late-onset AN, the etiology varies and is associated with optic atrophy, sensorimotor neuropathy, and other peripheral neuropathies. Among the late-onset cases, *AIFM1* is reported to be the most common genetic cause [6]. In this study, we further confirmed that *AIFM1* is the most common genetic cause of all noninfant-onset AN cases. The identification of genes is helpful to identify related lesion sites of AN and contributes to a better understanding of the underlying pathogenic mechanisms [8, 9].

The *AIFM1* gene, also known as AIF, PDCD8, COXPD6, etc., is located in the human chromosome Xq25-q26 region,

with a full length of 36.471 kb and 16 exons encoding a full-length 613 amino acid protein. In the mitochondria, *AIFM1* acts as a FAD-dependent NADH oxidoreductase and plays a critical physiological role in the stable and mature mitochondrial oxidative respiratory chain complex I and the elimination of peroxide. In this study, we further expanded the mutation spectrum and long-term phenotypes of *AIFM1*-related cases. We found another 20 AN cases with *AIFM1* variants by whole genome sequencing and Sanger sequencing, including 7 novel variants. All 18 AN-related variations had no overlap with the other phenotype-related *AIFM1* variations (Table S7). In addition, we confirmed that the most common variation is *AIFM1* c.1030C>T (p.Leu344Phe). Due to its location in the loop region, this variation may have an influence on folding.

In this study, we found 5 female AN cases with *AIFM1* variants, the phenotype of whom was similar to those of the male cases with the same variant. *AIFM1* gene mutation AN may also be inherited in an X-linked dominant inheritance pattern. In our previous study, except for the patients undergoing whole exome sequencing, we did not pay attention to female AN cases; only male cases were tested for the *AIFM1* gene.

To decipher the phenotype progression of *AIFM1*-related AN, a follow-up study was performed. Further genotype-phenotype correlation analysis can effectively help physicians and patients understand the disease-causing mechanism, process, and outcome of disease by research methods. To further assist in the consultation and evaluation of prognosis in patients with clinical AN, the clinical phenotypes of *AIFM1*-related cases were as follows:

- (1) For the pure tone threshold, AN patients have large individual differences in audiologic phenotype. Although the ascending audiogram is the typical audiometric pattern of AN patients, audiograms with various configurations and varying severities may occur. The hearing of some patients may improve, while others' hearing loss may remain stable for a

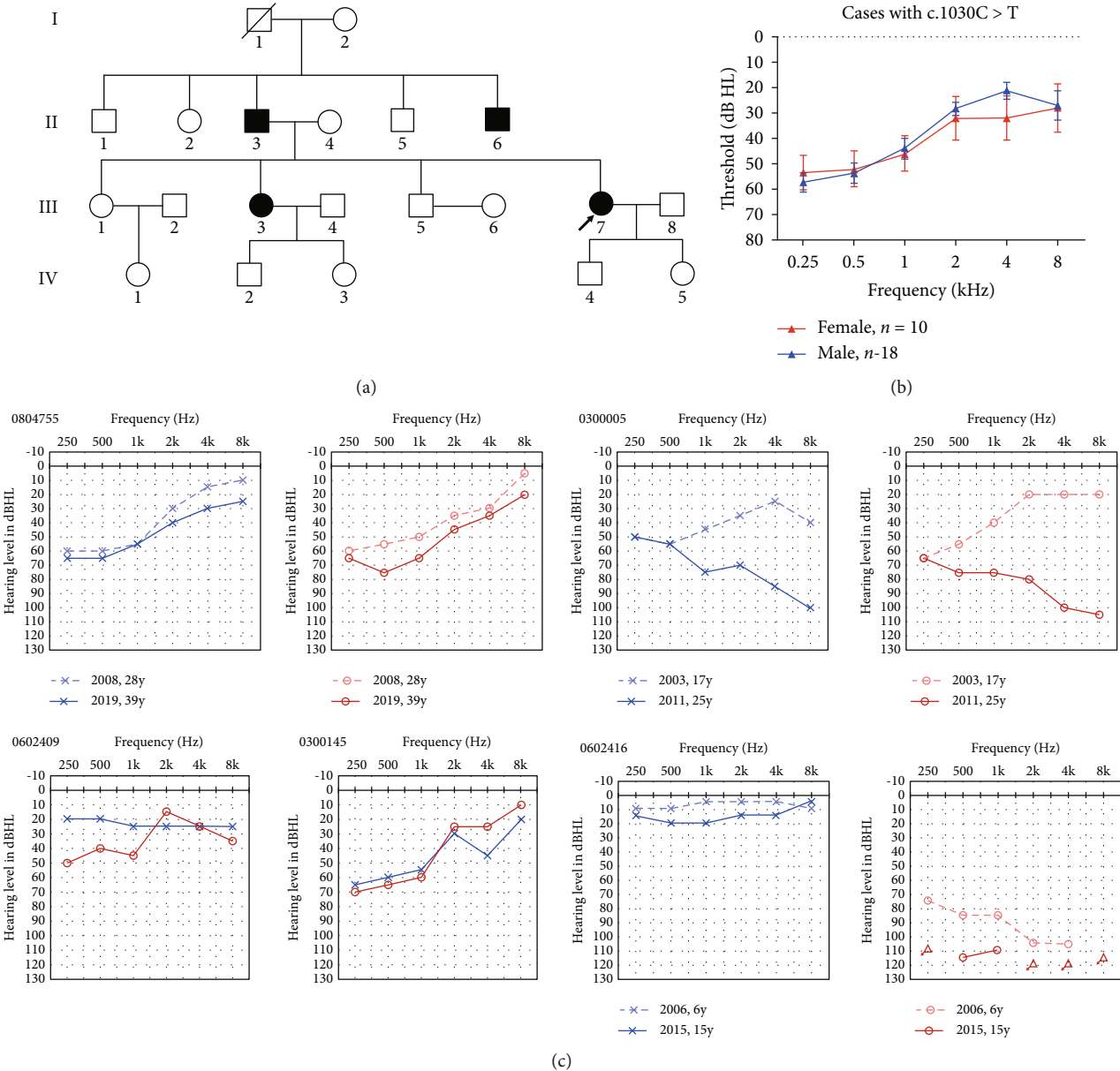


FIGURE 3: Family trees and audiological characteristics of the five female cases. (a) Family trees of the family 0804755. (b) Mean hearing threshold of the cases with the *AIFM1* c.1030C>T (p.Leu344Phe) variation. (c) Audiograms of the five female affected cases. Symbols “o” and “x” denote air conduction pure tone thresholds at different frequencies in the right and left ears. dB: decibels; Hz: Hertz. The dashed line represents the audiograms detected in the first time, while the solid lines were the latest audiological examinations. y: years old.

long time or even worsen. Among the very limited reports involving the follow-up characteristics of AN patients, the hearing outcomes in a long-term follow-up remain elusive [43]. Not surprisingly, we found, in the 50 *AIFM1*-positive cases, that the low frequency spectra were mostly affected, especially in the 0.25-1kHz range. Hearing impairment ranged from mild to moderate. No significant differences were detected in the hearing thresholds tested between the first and final visits within 1-10 years of follow-up. However, when the follow-up periods were prolonged to over ten years, hearing thresholds in both the low frequencies (0.25-0.5 kHz) and the

high frequencies (4-8 kHz) showed significant worsening. In addition, the pure tone threshold tended to deteriorate over time, especially at a frequency of 500 Hz

(2) For SDS, the AN patient’s prominent complaint is that he/she can hear voices without understanding the meaning. Our study found that patients with mild hearing loss had a high proportion of a score of zero when testing SDS, which was much more severe than the SDS in the moderate and severe hearing loss groups, and the degree of SDS was not consistent with the pure tone threshold. This fact suggests that

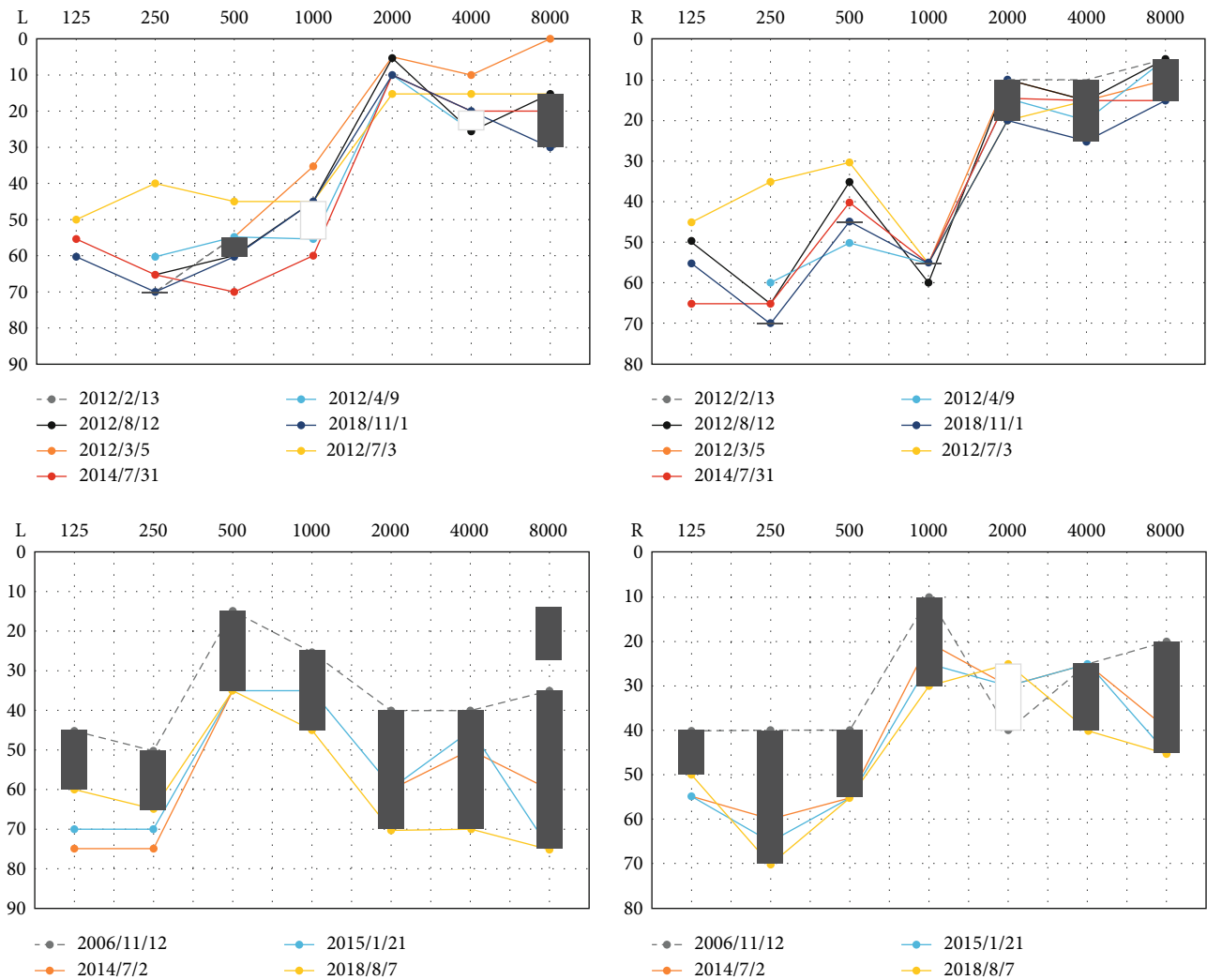


FIGURE 4: Typical cases with stable and progressive pure tone hearing thresholds.

in clinical audiology assessment, the SDS performance of AN patients is much more critical than that of PTA. The evaluation of the degree of hearing loss by PTA alone may underestimate the patient's condition. Furthermore, we followed up on the SDS of this type of AN patient and found that SDS decreased significantly with the prolongation of the disease course. This result indicates that the neurological synchronization of the *AIMF1* gene-related AN is gradually aggravated

- (3) ECochG revealed that -SP and CAP waves existed together in 80% of cases, but the SP/AP values were higher than normal. Patients showed worse hearing loss when their CAP waves disappeared. Compared with DPOAE, cochlear electrograms can help us locate the lesions of AN [44]. The -SP wave reflects the fractional depolarization process after the inner hair cells are subjected to the acoustic signal and is the maximum amplitude recorded by the needle electrode placed on the cochlear or round window

through the tympanic membrane [45]. The -SP waves are mainly derived from inner hair cells, and their amplitude and latency are objective indicators of the function of inner hair cells. Except for one patient without obvious one-time single-SP, the -SP wave of all of the other AN patients could be seen, suggesting that the AN lesion caused by *AIFM1* gene mutation may be located in the auditory conduction pathway outside the inner hair cells. CAP is produced in cochlear spiral ganglion cells and is an afferent nerve response. The decrease in CAP amplitude can prove the synchrony decline in auditory nerve activity. We observed that the -SP and CAP waveforms were present in 80% of patients at the same time, but the absolute value of -SP/AP was >0.4 , which was higher than normal, suggesting that there was a loss of synchronization of auditory nerve activity. This also explains why the SDS decline in this type of patient is more marked than the decrease in PTA from the perspective of physiology and pathology. Furthermore, we analyzed the patient's auditory condition based on

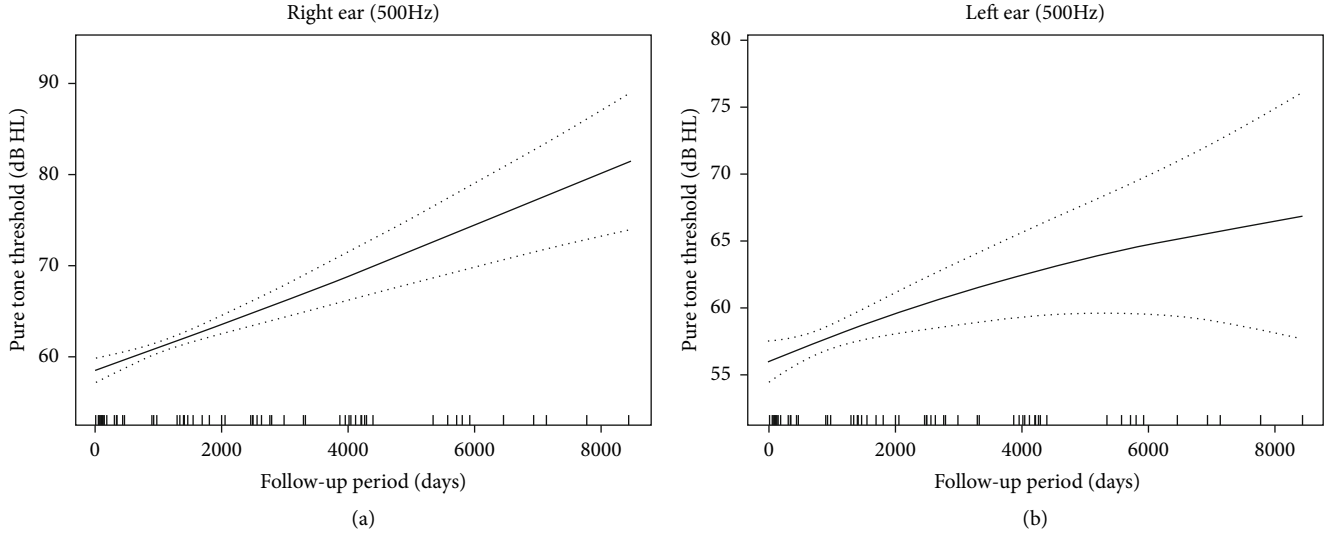


FIGURE 5: (a, b) The change of pure tone threshold of 0.5 kHz over time in both ears of *AIFM1*-positive AN patients. Spline smoothing was performed using GAMM (generalized additive mixed model) to explore the change of pure tone threshold with the length of follow-up time. The solid lines represent the fitting spline. The dashed lines represent the 95% confidence intervals. The vertical axis measures the change in pure tone hearing. The rug plot provides a visual representation of the frequency distribution for follow-up time. Each individual data point is represented by a single tick mark at the appropriate location on the chosen time scale (days).

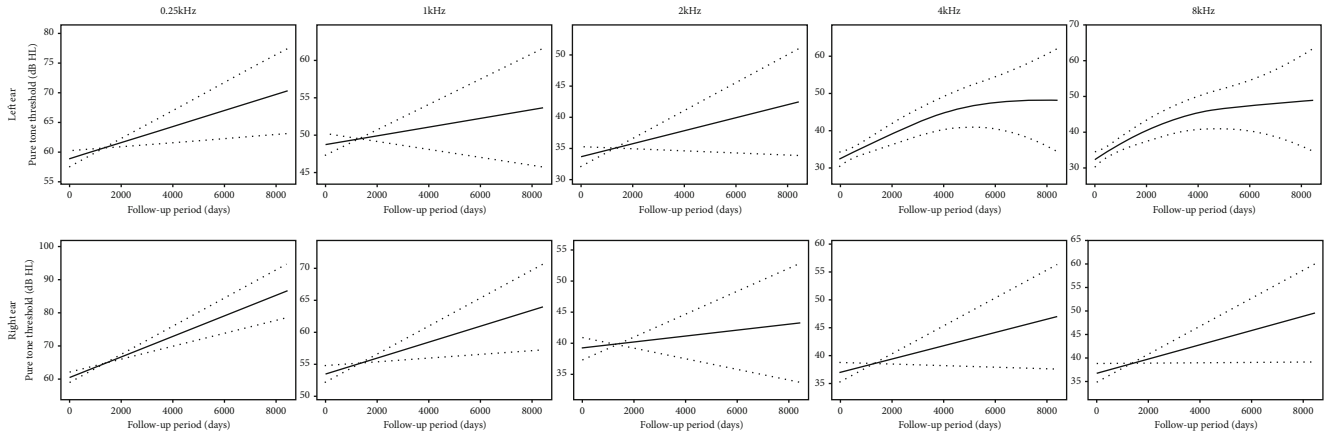


FIGURE 6: The change of pure tone threshold of 0.25, 1, 2, 4, and 8 kHz over time in both ears of *AIFM1*-positive AN patients. Spline smoothing was performed using GAMM (generalized additive mixed model) to explore the change of pure tone threshold with the length of follow-up time. The solid lines represent the fitting spline. The dashed lines represent the 95% confidence intervals.

the presence or absence of CAP waves, showing that the degree of hearing loss without CAP waveform was more serious. Clinically, the detection value should be increased, and the degree of hearing loss should be comprehensively judged

Individuals with lesions affecting the auditory nerve showed poor performance with cochlear implantation, since the neural transmission was affected [2]. The audiological phenotype features of *AIFM1*-related AN suggested that auditory dyssynchrony progressively worsened over time. Electrophysiological examinations of the cochlear nerve indicated that lesions would be located on the auditory pathway from postsynapses to acoustic fibers [3]. Further, the

diffusion-weighted MRI (dMRI) analysis techniques may contribute to the microstructure of the auditory tracts in vivo in individuals with AN [3, 46]; from the dMRI of some patients, we can see a reduction in apparent fiber density within the auditory brainstem tracts, which is consistent with the assumed pathophysiological mechanism of postsynapses to acoustic fibers (unpublished data). Thus, AN patients with *AIFM1* mutation may have poor efficiency from cochlear implantation.

The molecular disease-causing mechanism of *AIFM1* mutation-related hearing loss is still unclear; the mitochondrial function and the caspase-independent apoptosis to neuronal development and adult neurogenesis play a critical role in previous studies [47, 48]. In our recent study, we found

that the *AIFM1* mutation led to decreased dimerization and further impaired mitochondrial functions, such as increase of ROS production and impairment of mitochondrial membrane potential, thereby activating caspase-independent apoptosis (unpublished data). However, the complete and clear pathogenesis of AN and the genotype-phenotype correlation need to be further clarified.

In conclusion, (1) *AIFM1* is the most common genetic cause of late-onset AN, with the hotspot mutation of c.1030C>T (p.Leu344Phe). (2) In addition to the X-linked recessive inheritance pattern, the X-linked dominant inheritance pattern is another probability of *AIFM1*-related AN, which affects females. (3) The hearing threshold of AN patients with *AIFM1* mutation tends to worsen when the follow-up period is prolonged. Phenotype features of *AIFM1*-related AN suggested that auditory dyssynchrony progressively worsened over time. Electrophysiological examinations of the cochlear nerve indicated that lesions would be located on the auditory pathway from postsynapses to acoustic fibers.

Data Availability

The datasets used and/or analyzed during the current study are available from the corresponding author on reasonable request.

Disclosure

The funders had no role in study design, data collection and analysis, decision to publish, or preparation of the manuscript.

Conflicts of Interest

The authors have declared that no competing interests exist.

Authors' Contributions

Hongyang Wang, Dan Bing, and Jin Li contributed equally to this study.

Acknowledgments

This work was supported by the grants of the National Natural Science Foundation of China (Nos. 81830028, 81530032, 81900950, and 81900951) and the Military Medical Technology Incubation Project for Youth (19QNP058).

Supplementary Materials

Supplementary 1. Figure S1: follow-up ECochG test of 6 cases (12 ears); there was no difference between the absolute values of -SP/AP.F

Supplementary 2. Table S1: difference value of SDS in *AIFM1*-positive cases. Table S2: correlation of PTA and SDS. Table S3: SDS from cases with different disease courses. Table S4: the PTA and disease course of the cases with ABR V-wave. Table S5: follow-up of the cases with ABR V-wave. Table S6: CAP waves and PTA in *AIFM1*-positive AN cases. Table S7: the reported variations and diseases of *AIFM1*.

References

- [1] G. Rance, "Auditory neuropathy/dys-synchrony and its perceptual consequences," *Trends in Amplification*, vol. 9, no. 1, pp. 1–43, 2005.
- [2] A. E. Shearer and M. R. Hansen, "Auditory synaptopathy, auditory neuropathy, and cochlear implantation," *Laryngoscope Investigative Otolaryngology*, vol. 4, no. 4, pp. 429–440, 2019.
- [3] G. Rance and A. Starr, "Pathophysiological mechanisms and functional hearing consequences of auditory neuropathy," *Brain*, vol. 138, no. 11, pp. 3141–3158, 2015.
- [4] V. K. C. Manchaiah, F. Zhao, A. A. Danesh, and R. Duprey, "The genetic basis of auditory neuropathy spectrum disorder (ANS), *International Journal of Pediatric Otorhinolaryngology*, vol. 75, no. 2, pp. 151–158, 2011.
- [5] Q. J. Wang, Q. Z. Li, S. Q. Rao et al., "AUNX1, a novel locus responsible for X linked recessive auditory and peripheral neuropathy, maps to Xq23-27.3," *Journal of Medical Genetics*, vol. 43, no. 7, p. e33, 2005.
- [6] L. Zong, J. Guan, M. Ealy et al., "Mutations in apoptosis-inducing factor cause X-linked recessive auditory neuropathy spectrum disorder," *Journal of Medical Genetics*, vol. 52, no. 8, pp. 523–531, 2015.
- [7] S. A. Susin, H. K. Lorenzo, N. Zamzami et al., "Molecular characterization of mitochondrial apoptosis-inducing factor," *Nature*, vol. 397, no. 6718, pp. 441–446, 1999.
- [8] R. Santarelli, "Information from cochlear potentials and genetic mutations helps localize the lesion site in auditory neuropathy," *Genome Medicine*, vol. 2, no. 12, p. 91, 2010.
- [9] T. Moser and A. Starr, "Auditory neuropathy – neural and synaptic mechanisms," *Nature Reviews Neurology*, vol. 12, no. 3, pp. 135–149, 2016.
- [10] R. Santarelli, R. Rossi, P. Scimemi et al., "OPA1-related auditory neuropathy: site of lesion and outcome of cochlear implantation," *Brain*, vol. 138, no. 3, pp. 563–576, 2015.
- [11] W. Zhang, S. M. Kim, W. Wang et al., "Cochlear gene therapy for sensorineural hearing loss: current status and major remaining hurdles for translational success," *Frontiers in Molecular Neuroscience*, vol. 11, 2018.
- [12] B. Pan, C. Askew, A. Galvin et al., "Gene therapy restores auditory and vestibular function in a mouse model of Usher syndrome type 1c," *Nature Biotechnology*, vol. 35, no. 3, pp. 264–272, 2017.
- [13] R. Sacheli, L. Delacroix, P. Vandenaekerken, L. Nguyen, and B. Malgrange, "Gene transfer in inner ear cells: a challenging race," *Gene Therapy*, vol. 20, no. 3, pp. 237–247, 2013.
- [14] S. Richards, on behalf of the ACMG Laboratory Quality Assurance Committee, N. Aziz et al., "Standards and guidelines for the interpretation of sequence variants: a joint consensus recommendation of the American College of Medical Genetics and Genomics and the Association for Molecular Pathology," *Genetics in Medicine*, vol. 17, no. 5, pp. 405–423, 2015.
- [15] T. Kawarai, H. Yamazaki, K. Yamakami et al., "A novel *AIFM1* missense mutation in a Japanese patient with ataxic sensory neuronopathy and hearing impairment," *Journal of the Neurological Sciences*, vol. 409, p. 116584, 2020.
- [16] P. Bogdanova-Mihaylova, M. D. Alexander, R. P. Murphy et al., "Clinical spectrum of *AIFM1*-associated disease in an Irish family, from mild neuropathy to severe cerebellar ataxia with colour blindness," *Journal of the Peripheral Nervous System*, vol. 24, no. 4, pp. 348–353, 2019.

- [17] B. Wang, X. Li, J. Wang et al., "A novel *AIFM1* mutation in a Chinese family with X-linked Charcot-Marie-Tooth disease type 4," *Neuromuscular Disorders*, vol. 28, no. 8, pp. 652–659, 2018.
- [18] P. Sancho, A. Sánchez-Monteaudo, A. Collado et al., "A newly distal hereditary motor neuropathy caused by a rare *AIFM1* mutation," *Neurogenetics*, vol. 18, no. 4, pp. 245–250, 2017.
- [19] S. U. Morton, S. P. Prabhu, L. HGW et al., "*AIFM1* mutation presenting with fatal encephalomyopathy and mitochondrial disease in an infant," *Molecular Case Studies*, vol. 3, no. 2, p. a001560, 2017.
- [20] N. Miyake, N. I. Wolf, F. K. Cayami et al., "X-linked hypomyelination with spondylometaphyseal dysplasia (H-SMD) associated with mutations in *AIFM1*," *Neurogenetics*, vol. 18, no. 4, pp. 185–194, 2017.
- [21] H. Mierzevska, M. Rydzanicz, T. Biegański et al., "Spondyloepimetaphyseal dysplasia with neurodegeneration associated with *AIFM1* mutation - a novel phenotype of the mitochondrial disease," *Clinical Genetics*, vol. 91, no. 1, pp. 30–37, 2017.
- [22] B. Hu, M. Wang, R. Castoro et al., "A novel missense mutation in *AIFM1* results in axonal polyneuropathy and misassembly of OXPHOS complexes," *European Journal of Neurology*, vol. 24, no. 12, pp. 1499–1506, 2017.
- [23] D. Diodato, G. Tasca, D. Verrigni et al., "A novel *AIFM1* mutation expands the phenotype to an infantile motor neuron disease," *European Journal of Human Genetics*, vol. 24, no. 3, pp. 463–466, 2016.
- [24] M. Kettwig, M. Schubach, F. A. Zimmermann et al., "From ventriculomegaly to severe muscular atrophy: expansion of the clinical spectrum related to mutations in *AIFM1*," *Mitochondrion*, vol. 21, pp. 12–18, 2015.
- [25] A. Ardisson, G. Piscoquito, A. Legati et al., "A slowly progressive mitochondrial encephalomyopathy widens the spectrum of *AIFM1* disorders," *Neurology*, vol. 84, no. 21, pp. 2193–2195, 2015.
- [26] C. Rinaldi, C. Grunseich, I. F. Sevrioukova et al., "Cowchock syndrome is associated with a mutation in apoptosis-inducing factor," *The American Journal of Human Genetics*, vol. 91, no. 6, pp. 1095–1102, 2012.
- [27] I. Berger, Z. Ben-Neriah, T. Dor-Wolman et al., "Early prenatal ventriculomegaly due to an *AIFM1* mutation identified by linkage analysis and whole exome sequencing," *Molecular Genetics and Metabolism*, vol. 104, no. 4, pp. 517–520, 2011.
- [28] D. Ghezzi, I. Sevrioukova, F. Invernizzi et al., "Severe X-linked mitochondrial encephalomyopathy associated with a mutation in apoptosis-inducing factor," *The American Journal of Human Genetics*, vol. 86, no. 4, pp. 639–649, 2010.
- [29] Y. Liu, J. Qi, X. Chen et al., "Critical role of spectrin in hearing development and deafness," *Science Advances*, vol. 5, no. 4, p. eaav7803, 2019.
- [30] L. Liu, Y. Chen, J. Qi et al., "Wnt activation protects against neomycin-induced hair cell damage in the mouse cochlea," *Cell Death & Disease*, vol. 7, no. 3, p. e2136, 2016.
- [31] Z. He, L. Guo, Y. Shu et al., "Autophagy protects auditory hair cells against neomycin-induced damage," *Autophagy*, vol. 13, no. 11, pp. 1884–1904, 2017.
- [32] C. Zhu, C. Cheng, Y. Wang et al., "Loss of ARHGEF6 causes hair cell stereocilia deficits and hearing loss in mice," *Frontiers in Molecular Neuroscience*, vol. 11, 2018.
- [33] W. Liu, X. Xu, Z. Fan et al., "Wnt signaling activates TP53-induced glycolysis and apoptosis regulator and protects against cisplatin-induced spiral ganglion neuron damage in the mouse cochlea," *Antioxidants & Redox Signaling*, vol. 30, no. 11, pp. 1389–1410, 2019.
- [34] Z. H. He, S. Y. Zou, M. Li et al., "The nuclear transcription factor FoxG1 affects the sensitivity of mimetic aging hair cells to inflammation by regulating autophagy pathways," *Redox Biology*, vol. 28, p. 101364, 2020.
- [35] S. Zhang, Y. Zhang, Y. Dong et al., "Knockdown of Foxg1 in supporting cells increases the trans-differentiation of supporting cells into hair cells in the neonatal mouse cochlea," *Cellular and Molecular Life Sciences*, vol. 77, no. 7, pp. 1401–1419, 2020.
- [36] F. Tan, C. Chu, J. Qi et al., "AAV-ie enables safe and efficient gene transfer to inner ear cells," *Nature Communications*, vol. 10, no. 1, p. 3733, 2019.
- [37] C. Cheng, Y. Wang, L. Guo et al., "Age-related transcriptome changes in Sox2+ supporting cells in the mouse cochlea," *Stem Cell Research & Therapy*, vol. 10, no. 1, 2019.
- [38] W. Yan, W. Liu, J. Qi et al., "A three-dimensional culture system with Matrigel promotes purified spiral ganglion neuron survival and function in vitro," *Molecular Neurobiology*, vol. 55, no. 3, pp. 2070–2084, 2018.
- [39] X. Lu, S. Sun, J. Qi et al., "Bmi1 regulates the proliferation of cochlear supporting cells via the canonical Wnt signaling pathway," *Molecular Neurobiology*, vol. 54, no. 2, pp. 1326–1339, 2017.
- [40] T. Wang, R. Chai, G. S. Kim et al., "Lgr5+ cells regenerate hair cells via proliferation and direct transdifferentiation in damaged neonatal mouse utricle," *Nature Communications*, vol. 6, no. 1, 2015.
- [41] B. C. Cox, R. Chai, A. Lenoir et al., "Spontaneous hair cell regeneration in the neonatal mouse cochlea in vivo," *Development*, vol. 141, no. 4, pp. 816–829, 2014.
- [42] Q. J. Zhang, B. Han, L. Lan et al., "High frequency of OTOF mutations in Chinese infants with congenital auditory neuropathy spectrum disorder," *Clinical Genetics*, vol. 90, no. 3, pp. 238–246, 2016.
- [43] H. Wu, Y. Feng, L. Jiang et al., "Application of a new genetic deafness microarray for detecting mutations in the deaf in China," *PLoS One*, vol. 11, no. 3, article e0151909, 2016.
- [44] D. P. Wynne, F. G. Zeng, S. Bhatt, H. J. Michalewski, A. Dimitrijevic, and A. Starr, "Loudness adaptation accompanying ribbon synapse and auditory nerve disorders," *Brain*, vol. 136, no. 5, pp. 1626–1638, 2013.
- [45] W. P. Gibson, "The clinical uses of electrocochleography," *Frontiers in Neuroscience*, vol. 11, p. 274, 2017.
- [46] J. Zanin, T. Dhollander, S. Farquharson, G. Rance, A. Connelly, and B. A. Nayagam, "Review: using diffusion-weighted magnetic resonance imaging techniques to explore the microstructure and connectivity of subcortical white matter tracts in the human auditory system," *Hearing Research*, vol. 377, pp. 1–11, 2019.
- [47] C. Reinhardt, G. Arena, K. Nedara et al., "AIF meets the CHCHD4/Mia40-dependent mitochondrial import pathway," *Biochimica et Biophysica Acta (BBA) - Molecular Basis of Disease*, vol. 1866, no. 6, p. 165746, 2020.
- [48] E. Hangen, O. Féraud, S. Lachkar et al., "Interaction between AIF and CHCHD4 regulates respiratory chain biogenesis," *Molecular Cell*, vol. 58, no. 6, pp. 1001–1014, 2015.

Review Article

Auditory Neural Plasticity in Tinnitus Mechanisms and Management

Kunkun Wang,^{1,2} Dongmei Tang,^{1,2} Jiaoyao Ma,^{1,2} and Shan Sun^{1,2} 

¹ENT institute and Otorhinolaryngology Department of Eye & ENT Hospital, State Key Laboratory of Medical Neurobiology and MOE Frontiers Center for Brain Science, Fudan University, Shanghai 200031, China

²NHC Key Laboratory of Hearing Medicine, Fudan University, Shanghai 200031, China

Correspondence should be addressed to Shan Sun; shansun@fudan.edu.cn

Received 27 March 2020; Revised 15 June 2020; Accepted 20 June 2020; Published 1 July 2020

Academic Editor: Hai Huang

Copyright © 2020 Kunkun Wang et al. This is an open access article distributed under the Creative Commons Attribution License, which permits unrestricted use, distribution, and reproduction in any medium, provided the original work is properly cited.

Tinnitus, which is the perception of sound in the absence of a corresponding external acoustic stimulus, including change of hearing and neural plasticity, has become an increasingly important ailment affecting the daily life of a considerable proportion of the population and causing significant burdens for both the affected individuals and society as a whole. Here, we briefly review the epidemiology and classification of tinnitus, and the currently available treatments are discussed in terms of the available evidence for their mechanisms and efficacy. The conclusion drawn from the available evidence is that there is no specific medication for tinnitus treatment at present, and tinnitus management might provide better solutions. Therapeutic interventions for tinnitus should be based on a comprehensive understanding of the etiology and features of individual cases of tinnitus, and more high quality and large-scale research studies are urgently needed to develop more efficacious medications.

1. Introduction

Tinnitus refers to the perception of sound in the absence of a corresponding external stimulus, and tinnitus is one of the most common complaints of the auditory system globally. A study reviewed all available studies exploring adult populations over a 35-year period and reported a global prevalence of tinnitus ranging from 5.1% to 42.7% and showed that the prevalence increased with aging and noise exposure [1]. Similar epidemiological data regarding adults and younger populations have also been published [2–4]. The intensity of tinnitus varies from subtle noises just above the hearing threshold to high-intensity sounds that cannot be masked by any external sound. Additionally, tinnitus patients almost always suffer from comorbidities that can negatively influence normal life; thus, prevalence estimates for tinnitus provide only a snapshot of the potential population burden of this condition. The percentages of persons having tinnitus accompanied by anxiety and depression are 25.1% and 25.6%, respectively, and these rates greatly exceed those in populations without tinnitus [5, 6]. Concomitant issues with tinnitus can be mild, such as having difficulty concentrating,

or can have huge impacts such as recurrent insomnia and severe depression [7, 8]. Because tinnitus can only be heard by the patients in most cases, the adverse effects on daily life can be strong but easily misunderstood by other people, resulting in deterioration of the patient's mental state and even physical condition, and consequently both the quality of life and social function of patients are seriously affected. Because of its associated conditions, tinnitus causes a financial burden on society; for example, the National Health Service of the UK spends about £750 million annually on treating tinnitus patients, at an average cost of £717 per patient [9]. A thorough understanding of tinnitus is essential if its burden on society is to be reduced, and more effective clinical interventions are needed to reduce the adverse impacts on patients' daily life and eventually to eliminate tinnitus completely.

2. Tinnitus Classifications and Diagnosis

Tinnitus is divided into many different subtypes, and the most common classification categorizes tinnitus as objective or subjective according to whether or not the sound can be

heard by others or measured by instruments. The sounds perceived by tinnitus patients could be tonal ringing, buzzing, clicking, hissing, and other noises. The sounds generally appear in the ear, and sometimes specifically in the head, in which case the condition is referred to as tinnitus cerebri. Objective tinnitus, in which the sound often results from vascular abnormalities and myoclonus, is less common than subjective tinnitus [10, 11].

Accordingly, the diagnosis of tinnitus consists of a subjective evaluation and an objective examination. Questionnaires are generally used for subjective evaluations, and among them, the most frequently used are the Tinnitus Questionnaire, the Tinnitus Handicap Inventory (THI), and the Tinnitus Functional Index (TFI) [12]. In addition to these, there are also some scales used to evaluate the concomitant symptoms of tinnitus that can increase the comprehensive understanding of the patient's situation. There are also psychoacoustic measurements, i.e., tinnitus matching, mainly including tinnitus pitch, loudness, masking level, and residual inhibition, of which pitch matching is the primary sound therapy proven to be effective [13]. Traditional measurements are performed by an audiologist using pure tones, and new approaches involve computer-based or smartphone-based self-administered matching procedures [14].

In terms of objective measurements, palpation and auscultation of the head, neck, and ears are routine tests for objective tinnitus, while in subjective tinnitus electrophysiological measurements are most often used. As the name suggests, otoacoustic emissions refer to the phenomenon in which audio energy is generated within the cochlea and transmitted to the external auditory canal through the middle ear and then released in the form of air vibrations. Otoacoustic emissions represent the functional state of the cochlea and especially the functional state of the outer hair cells (OHCs) [15]. Spontaneous otoacoustic emissions and distortion-product otoacoustic emissions are most commonly used to diagnose tinnitus. Electric response audiometry includes other important electrophysiological measurements, including auditory brainstem response and auditory steady-state evoked response [16]. The function of each part of the auditory pathway can be measured by detecting various biological potentials generated along the auditory pathway [17]. In terms of radiological measurements, functional magnetic resonance imaging (fMRI) has expanded to a broader array of conditions, including tinnitus. Functional changes in the auditory center can be detected by measuring changes in hemodynamics caused by the activity of neurons in response to exogenous acoustic stimulation [18].

3. Tinnitus Etiology and Mechanisms

There are many causes of tinnitus, and the mechanisms are very complicated. Secondary tinnitus has obvious causes, such as auditory system diseases like hearing loss and Meniere's disease or systemic diseases such as cardiovascular diseases and diabetes [19, 20]. In contrast, primary tinnitus, or idiopathic tinnitus, is usually of unclear etiology and might not even be associated with sensorineural hearing loss until

the time of the clinical visit. In most cases, multiple factors lie behind the etiology of tinnitus.

The pathology leading to tinnitus can be located anywhere from the ear canal to the auditory cortex. Tinnitus often occurs along with hearing loss resulting from noise and aging, and thus, cochlear deafferentation is thought to be a trigger of tinnitus while subsequent changes in the central nervous system are thought to be responsible for the maintenance of tinnitus. This process is also known as neural plasticity [21, 22]. Different neural models within the structures of the central auditory system have been established to interpret the possible mechanisms of tinnitus according to neuroimaging techniques such as electroencephalography (EEG) and fMRI. Hearing impairment leads to deafferentation, which is thought to increase the output of pyramid cells in the dorsal cochlear nucleus according to the hyperactivity model [22]. The inferior colliculus then receives the projection fibers from the cochlear nucleus and shows an increased firing rate, and neurons in the upper structures such as the medial geniculate body of the thalamus and auditory cortex also engage in neuronal hypersynchrony [23–25]. In such cases, the tinnitus is most often related to noise trauma and hearing impairment induced by previous use of chemotherapy drugs [26–28].

Increases in oscillatory activity in the auditory cortex and thalamus have been observed [29, 30], especially in the gamma band oscillatory of the auditory cortex [31, 32], and highly active areas have also been found by fMRI [33, 34]. It has been suggested that tinnitus perception is based on low-frequency oscillations that cause a lateral inhibition imbalance between the normal auditory area and the area with pathological low-frequency activities, thus resulting in high-frequency gamma oscillations [35]. The increases in low-frequency delta band oscillations seen in tinnitus have been replicated in the laboratory along with the reduction in alpha band oscillations [36, 37].

In addition to the above connections within the auditory pathway, a network structure is formed between auditory and nonauditory structures, and this can account for the perception, emotional response, or other reactions to tinnitus. For example, the somatosensory pathway can activate the pyramid cells of the dorsal cochlear nucleus and increase their output [38, 39]. Also, the fibers projecting from the medial geniculate body to the amygdala might facilitate emotional responses to tinnitus. This is because the lateral amygdala receives inputs from neurons in the medial geniculate body and the auditory cortex, and the basal amygdala projects into the hypothalamus in return, thus forming the amygdala auditory feedback loop [40]. EEG measurements have demonstrated enhanced oscillatory electrical activity in the amygdala of tinnitus patients, and the amygdala has been shown by fMRI to respond more strongly to acoustic stimulation in blind individuals for whom the acoustic environment is more important [41, 42].

4. Tinnitus Management and Medications

A number of treatments for tinnitus have been developed, and these treatments have shown some efficacy against

tinnitus, but there are still a large number of patients around the world who do not have access to effective treatments and who can only try to cope with their symptoms and who must struggle to coexist with them. Therefore, tinnitus is still a clinically unsolved problem, and there is a long way to go to eliminate tinnitus. Treatments are divided into management and medications. Management includes physical therapy, acoustic therapy and psychotherapy, and it is different from the passive reception of medications by patients. In this situation, patients can choose their preferred treatments, and the initiative of involving the patient plays an important role in treating tinnitus. Tinnitus patients and medical professionals are eager to obtain effective drugs that can reduce clinical symptoms, and thus the clinical requirements for such drugs are quite extensive. The use of efficacious drugs to reduce tinnitus might prevent patients from suffering from comorbidities such as depression and anxiety, and thus, even a small effect on tinnitus might have a significant effect on the quality of life.

4.1. Tinnitus Management

4.1.1. Psychological Management. The common psychotherapies consist of counseling and cognitive behavioral therapy (CBT). In brief, counseling involves advice and relevant information to facilitate the habituation and comprehension of tinnitus and to help the patient cope with comorbidities brought on by tinnitus such as insomnia and anxiety. Furthermore, counseling is often given in conjunction with other procedures because it is important to help ensure good compliance with other treatments. CBT seeks to rectify and change the patient's maladaptation of cognitive patterns, thus replacing irrational beliefs with reasonable beliefs as a way to eliminate emotional and behavioral problems. CBT contains many elements such as relaxation training and psychological education. In the largest randomized clinical trial involving CBT in tinnitus patients, significant improvement was demonstrated in the quality of life compared with treatment as usual [43]. CBT has been combined with Internet applications in several recent studies, and it was found that both the short-term efficacy of 2 months of treatment and the long-term efficacy of 1 year of treatment were stable and that the quality of life of tinnitus patients was significantly improved [44, 45]. The latest European guidelines also recommend CBT for chronic tinnitus [12], and a Cochrane review also provides evidence that CBT can effectively reduce the impact of tinnitus on a patient's quality of life with few side effects [46]. Thus, it can be concluded that CBT is effective and safe in the treatment of tinnitus.

4.1.2. Physical Therapy. Physical therapy in the treatment of tinnitus involves electromagnetic stimulation, of which repetitive transcranial magnetic stimulation (rTMS) and transcranial direct current stimulation (tDCS) are the most frequently used. tDCS changes the excitability of cortical neurons through the current generated by the depolarization of two scalp electrodes with opposite polarity. rTMS was developed from tDCS and generates pulsed magnetic fields acting on the central nervous system, subsequently changing

the membrane potential of cortical neurons and producing induced currents and local electric fields and thus modulating the excitability of the neurons [47]. A Cochrane analysis concluded that the efficacy of short-term rTMS was detectable, but more evidence is needed before conclusions about the long-lasting effect can be drawn [48]. However, it has been shown that rTMS [49, 50] has no significant efficacy on tinnitus patients. Considering the dated references of the Cochrane review mentioned above, it might be more inclined to the invalidity of rTMS. tDCS has shown efficacy measured by TFI [51], THI, and VAS [52]. A review summarized the efficacy of tDCS treatment alleviating tinnitus-related symptoms and suggested further high-quality trials with large sample sizes to determine the efficacy of tDCS on tinnitus as well as any potential side effects [53].

4.1.3. Sound Therapy. Various methods of sound therapy have been developed and have been gaining popularity. The earliest proposed sound therapy was masking, which sought to suppress tinnitus or relieve tinnitus symptoms by listening to a specific external sound matching the loudness of the tinnitus tone under clinical guidance. Despite the wide application of masking therapy, evidence for its efficacy based on controlled studies is still insufficient [54]. Tinnitus retraining therapy (TRT), which aims for tinnitus habituation, was first proposed by Jastreboff and Hazell in 1993 [55]. Strictly speaking, this technique does not belong to pure sound therapy because it consists of a combination of sound therapy and counseling. The sound therapy used in TRT is distinct from that used in masking. In masking therapy, the tinnitus disappears when the masking sound is applied above the loudness of the tinnitus. In contrast, in TRT, the tinnitus and background sound can be perceived at the same time because the tinnitus can only be adapted under conditions in which it is still perceived. Different analogue sounds of natural sounds are applied in TRT: waves, creeks, wind, birdsongs, etc. A Cochrane review [56] reported that it could not reach a conclusion as to whether TRT was effective or not because the treatment principles and methods in most studies included did not strictly correspond to the initial method that Jastreboff and Hazell [55] proposed. Two randomized trials showed the contradictory results between TRT and standard nursing, but it must be noted that most of the subjects in the study showed efficacy of TRT were soldiers, so there was a lack of comparability between the two studies [57, 58]. Thus, further studies on TRT are required.

Music therapy has been incorporated into tinnitus treatment in recent years because individuals' tinnitus profiles often match the frequency spectrum of music. Among a variety of music models, including Heidelberg model music therapy [59] and Neuromonics [60], tailor-made notched music training (TMNMT) is the most prominent. TMNMT modifies enjoyable music by filtering out an octave range of the frequency band centered on the individual's tinnitus frequency, thus reinforcing lateral inhibition and suppressing the overactivity of the neurons in the auditory cortex [61–63]. However, a trial found no improvement after 3 months of training, but a significant reduction in tinnitus loudness was observed in a 1-month follow-up analysis,

indicating that the efficacy of TMNMT might need a long time to evolve and stabilize [64]. Two studies have treated tinnitus with TMNMT combined with other methods—tDCS [65] and Ginkgo biloba [66], respectively—and both studies indicated that the subjective perceptions of tinnitus were significantly improved. However, it is not clear where the specific action sites of the three treatment methods are or whether or not there are interactions between them. In addition, these studies lack appropriate designs that can distinguish the effects of two different treatment methods within the same study, and thus, more research is needed to confirm the efficacy of TMNMT alone. A systematic review focused on the research into different treatments online or through smartphones, including TMNMT, CBT, and other methods, and proposed that online treatments could have a positive effect in the daily life of tinnitus patients [67]. Therefore, it can be assumed that with the development of the Internet, treatments of tinnitus through smartphone applications or the Internet might form a new trend in treatment, and such methods might be more convenient and more accepted by patients compared to more traditional forms of treatment.

Hearing aids are also feasible for tinnitus accompanied by hearing loss, and there are several rationales for their use in treating tinnitus. An imbalance exists between excitation and inhibition within the auditory pathway after cochlear injury, and thus, tinnitus might be alleviated by providing extra acoustic input. Hearing aids amplify ambient sounds, which helps patients refocus on other sounds distinct from the tinnitus sound, and thus, hearing aids attenuate the perception of tinnitus [68]. According to the presumed neurological mechanisms of tinnitus, it can be hypothesized that hearing aids decrease afferent inhibition through sound enrichment in the central auditory system and thus achieve the goal of modulating neuroplastic changes. A study compared the effect on tinnitus between conventional hearing aids and frequency-lowering hearing aids in high-frequency hearing loss patients, and both groups found improvement in the quality of life [69]. Another study reported that spectrally notched hearing aids were more effective than unmodified hearing aids in treating tinnitus in hearing loss patients [70]. However, a Cochrane review concluded that there is no evidence to support or refute the application of hearing aids in tinnitus patients with coexisting hearing loss [71]. The hearing aids using notched environment sounds might be more convenient than conventional TMNMT because a specific acoustic environment is not required and patients can benefit from the treatment all the time. However, the studies on hearing aids have only included a small portion of tinnitus patients, and multicenter randomized trials might be helpful in reconfirming the efficacy of hearing aids.

4.2. Medications for Tinnitus. As traditional, simple, and acceptable therapeutics, tinnitus medications have huge potential to meet patients' demands, although there is still limited research progress in this area. Rapid improvement in symptoms and the maximization of normal living conditions are eagerly expected for future therapeutics; thus, research into drug treatment still has a long way to go.

Among the drugs discussed in this review, the most studied are antidepressants, which are mostly used to solve the problems like depression and anxiety caused by tinnitus. Accompanying the improvement of patients' depression, some patients' subjective perceptions of tinnitus are improved. However, due to the limited comprehension of tinnitus mechanisms, we could not accurately locate the specific targets of antidepressants in tinnitus, so it is hard to judge whether or not antidepressants have other therapeutic effects on tinnitus besides an antidepressant effect. We summarize the tinnitus-related compounds and drugs in Tables 1 and 2.

4.2.1. Psychotropic Drugs

(1) Benzodiazepines. Benzodiazepines are increasingly being used to treat nonepileptic diseases, including various mental disorders and pain syndromes, and their application in tinnitus is based on the presumption that tinnitus is affiliated with neuronal hyperactivity in the central auditory system. As positive allosteric modulators of the GABAA receptor [72], benzodiazepines may also reduce the comorbidities of tinnitus such as insomnia and anxiety due to their anxiolytic and hypnotic effects but not their anxiolytic and hypnotic effects. Studies on benzodiazepines in the treatment of tinnitus have included alprazolam and clonazepam. A trial involving 30 patients showed improvement in tinnitus loudness and annoyance as measured on a visual analogue scale (VAS) [73]. In another study, 3 weeks of clonazepam treatment showed obvious improvement in tinnitus loudness, VAS measurements of annoyance, and THI scores [74]. A retrospective study showed that clonazepam doses varying from 0.5 to 1 mg/day with 2–6-month treatment times alleviated tinnitus symptoms in 32% of over 3,000 subjects with vestibular or cochlear disorders [75]. As for alprazolam, two well-designed trials were performed, with the first reporting a reduction of tinnitus loudness in 76% of patients when measured by a tinnitus synthesizer compared to 5% of patients when measured by VAS [76]. Interestingly, the second trial showed improvement in VAS score but not in tinnitus loudness or THI score [77]. These studies suggested the potential of benzodiazepines in tinnitus treatment, but in consideration of the inconsistent performances in different scales and the adverse effect profiles, there is no mature evidence to recommend benzodiazepines as a pharmacologic approach to tinnitus. However, it is worth further exploring the refined mechanism of action in order to obtain better clinical results, at least improvement of the adverse symptoms brought about by tinnitus, and thus, more studies should be carried out to better understand the potential efficacy of benzodiazepines.

(2) Dopaminergic and Antidopaminergic Drugs. Dopaminergic pathways are speculated to be related to tinnitus in various areas of the brain, and it has been observed that dopamine is present in the first synaptic complex of the auditory pathway between IHCs and neurons, thus enabling the study of dopaminergic and antidopaminergic drugs on tinnitus [78, 79]. A study of the dopamine agonist pramipexole showed alleviation of presbycusis-related tinnitus [80]. The

TABLE 1: Clinical trials of psychotropic drugs for tinnitus.

Drugs	Authors & year	Effect targets	Conclusions
Gabapentin	[127]	Not clear, enhances the activity of GABA	Loudness reduced by 11–13.3 dB in the acoustic trauma subgroup
	[128]		Not effective
	[130]		Not effective
	[129]		Not effective
	[131]		Not effective
Clonazepam	[73]		VAS-A decreased by 2.9
	[74]	Antagonizes GABAR	Loudness reduced by 4 dB; VAS-L/A and THI decreased by 3/4 and 4, respectively
Alprazolam	[76]		Loudness reduced in 76% of the treatment group
	[77]	Not clear, interacts with GABAR	VAS decreased by 2.83
Sulpiride	[81, 82]	Antagonizes DR _{D2}	VAS-P decreased by 1.5 VAS-P decreased by 1.4
Piribedil	[83]	Agonizes DR _{D2/3}	Not effective
Pramipexole	[80]	Activates DR _{D3}	Percentage of loudness reduced by 15 dB with statistical significance
	[86]		Loudness reduced by 10 dB
Nortriptyline	[87]	SSRI; 5-HT _{2A} R blocker	HAMD and ITI decreased by 3.7 and 0.6, respectively; loudness reduced by 6.4 dB
	[88]		No more effective than biofeedback
Amitriptyline	[89]	SSRI; 5-HT _{2A} R blocker	ATAQ decreased by 2.95 and 2.55 in the right and left ear, respectively
	[90]	SSRI	TSQ decreased by 4.68; VAS-L decreased by 1.51
Paroxetine	[91]	SSRI	Not effective
Trazodone	[97]	SSRI; 5-HT _{2A/C} R blocker	Not effective
Tianeptine	[98]	SSRE	THI decreased by 8.6; BDI decreased by 9.18
Deanxit	[95]	5-HT _{2A} R/DR _{D1/2} blocker	VAS-A/S and TQ decreased by 9.5/1.2 and 11.0, respectively

GABAR: gamma aminobutyric acid receptor; VAS-L/A/P/S: visual analog scale of loudness/annoyance/tinnitus perception/somatization; THI: tinnitus handicap inventory; 3,4-dihydroxyphenethylamine receptor_{D1/2/3}; SSRI/E: selective serotonin reuptake inhibitor/enhancer; 5-HT_{2A/C}R: 5-hydroxytryptamine_{2A/C} receptor; HAMD: Hamilton Depression Scale; ITI: multidimensional pain inventory of tinnitus interference; ATAQ: 10-point scale from of the American Tinnitus Association questionnaire; TSQ: Tinnitus Severity Questionnaire; BDI: Beck Depression Inventory; NMDAR: N-methyl-D-aspartic acid receptor; TS: Tinnitus Scale; ETC: electron transport chain; TQ: Tinnitus Questionnaire; SOD: superoxide dismutase; 11-PBS-L/A: 11-point box scale-loudness/annoyance; TSS: Tinnitus Severity Score.

dopamine antagonist sulpiride was also found to be effective in reducing tinnitus perception both alone and in combination with either melatonin or hydroxyzine [81, 82]. Nevertheless, negative results for the dopamine agonist piribedil were also reported, and 19 out of 75 participants quit the study owing to side effects such as nausea and dizziness [83]. This demonstrates our insufficient understanding of the mechanisms involved in dopaminergic-related tinnitus, and thus, further studies are required to determine whether or not dopamine agonists or antagonists can benefit tinnitus sufferers despite their potential side effects.

(3) *Antidepressants*. Tinnitus is almost always accompanied by various psychological symptoms, of which depression and anxiety are the most commonly reported. In the auditory cortical neurons, it was found that the 5-hydroxytryptamine_{2A/C} (5-HT_{2A/C}) receptor agonist 2,5-dimethoxy-4-iodoamphetamine (DOI) could suppress the glycine receptor-mediated tonic current. DOI did not compete with glycine; instead, it initially activated the 5-HT_{2A/C}

receptor, which impaired microtubule-dependent glycine receptor transport resulting in a decrease in tonic current [84]. Seeing that tinnitus is associated with decreased lateral inhibition of the cortex, 5-HT receptor agonists might further reduce the glycine receptor-mediated tonic current through lateral inhibition of hearing; thus, there are reasons to believe that the 5-HT receptor participates in the pathogenesis of tinnitus. Interestingly, tricyclic antidepressants (TCAs) and selective serotonin reuptake inhibitors (SSRIs), which are the most commonly used antidepressants in the treatment of tinnitus, both inhibit serotonin reuptake, thus increasing the release of serotonin by elevating the endogenous serotonin concentration in the synaptic membrane followed by downregulation of 5-HT_{1A} receptors in the presynaptic membrane. This seems to be paradoxical, but the fact that TCAs also have a role in blocking 5-HT_{2A} shows that diverse pathways may contribute to the efficacy of antidepressants [85] (Figure 1). In fact, little is known of the pathogenesis of tinnitus, especially with regard to explaining the efficacy of antidepressant treatments. It should

TABLE 2: Clinical trials of other medications for tinnitus.

Drugs	Authors & year	Effect targets	Conclusions
Memantine	[111]	NMDAR antagonist	Not effective
Neramexane	[115]	NMDAR and 5-HT ₃ R	Not effective
Acamprosate	[116] [117]	Glu antagonist; GABA agonist	TS decreased by 3.87 Higher alleviating rate (92.5% vs. 12.5%)
AM-101	[118]	NMDAR antagonist	Not effective
AUT00063	[124]	Modulates Kv _{3.1/3.2} channels	Not effective
CoQ10	[148] [149]	Component of ETC Antioxidants	TQ scores decreased by 14 Lower tinnitus incidence rate (11.1% vs. 62.5%)
Zinc	[153] [152]	Component of SOD	Not effective THI reduced by 8.3
Pentoxifylline	[157]	Improves inner ear perfusion	VAS-P decreased by 5 and 3 compared to pretreatment and placebo, respectively
Sulodexide	[156]	Antithrombotic/anticoagulant	THI and Mini-TQ reduced by 10.3 and 3.9, respectively
Ginkgo biloba	[162] [163] [164]	Antioxidants	Mini-TQ and 11-PBS-L/A reduced by 2.19 and 0.74/1.06, respectively THI score reduced by >20 Not effective
Vitamin B12	[165] [167] [172]	Maintains the function of myelin, etc.	Not effective TSS reduced by 8.2 in patients with B12 deficiency No significance effect measured by THI
Melatonin	[171] [168] [173]	Scavenges free radicals, etc.	THI reduced by 10.4 compared with placebo THI scores decreased by 4.6 Higher alleviating rate (57% vs. 25%)

GABAR: gamma aminobutyric acid receptor; VAS-L/A/P/S: visual analog scale of loudness/annoyance/tinnitus perception/somatization; THI: tinnitus handicap inventory; 3,4-dihydroxyphenethylamine receptor_{D1/2/3}; SSRI/E: selective serotonin reuptake inhibitor/enhancer; 5-HT_{2A/C}R: 5-hydroxytryptamine_{2A/C} receptor; HAMD: Hamilton Depression Scale; ITI: multidimensional pain inventory of tinnitus interference; ATAQ: 10-point scale from of the American Tinnitus Association questionnaire; TSQ: Tinnitus Severity Questionnaire; BDI: Beck Depression Inventory; NMDAR: N-methyl-D-aspartic acid receptor; TS: Tinnitus Scale; ETC: electron transport chain; TQ: Tinnitus Questionnaire; SOD: superoxide dismutase; 11-PBS-L/A: 11-point box scale-loudness/annoyance; TSS: Tinnitus Severity Score.

be noted that the ideal drugs for treating tinnitus should both reduce the awareness of tinnitus and improve the patient's emotional status, thus increasing the quality of life of patients.

In two studies looking into the TCA nortriptyline [86, 87], patients with severe tinnitus showed improvement in depression and tinnitus loudness after treatment, and a greater reduction in symptoms was observed in subjects suffering from more severe depression; in other words, nortriptyline appears to be especially suitable for severely depressed tinnitus patients. Podoshin et al. [88] found no significant advantage of another TCA, amitriptyline, but a later study showed a distinct decrease in tinnitus severity in 95% of the experimental group [89]. SSRIs have also been applied in cases of tinnitus. Patients with depression and high risk of disabling tinnitus showed significant improvement after sertraline treatment, but it is important to note the relatively high dropout rate of 17% after sertraline administration [90]. Paroxetine treatment exhibited little difference in tinnitus loudness or other psychological measures except for tinnitus aggravation [91]. In addition, it is noteworthy that

there have been cases where tinnitus was induced or worsened during or after antidepressant treatment [92–94].

There is also a report of applying the compound Deanxit along with clonazepam in tinnitus patients, and the results indicated that Deanxit was more effective than placebo whether used alone or combined with clonazepam [95]. Trazodone is considered an atypical antidepressant and is classified as a serotonin antagonist and a reuptake inhibitor with complex pharmacological effects including both agonistic and antagonistic effects on the serotonin system [96]. Thus, dual mechanism might increase serotonin levels in the central auditory pathway, but a study found no difference between trazodone treatment and placebo [97]. Tianeptine belongs to the TCAs in terms of its structure, but its unique pharmacological effect of increasing 5-HT reuptake in the presynaptic membrane is different from the traditional TCAs. In a study of tianeptine treatment, the control group was made up of tinnitus patients without depressive mood, and tinnitus as measured by THI and depression as measured by the Beck Depression Inventory were significantly decreased after tianeptine treatment [98]. Therefore, whether the effect of antidepressants on 5-HT can restore tonic

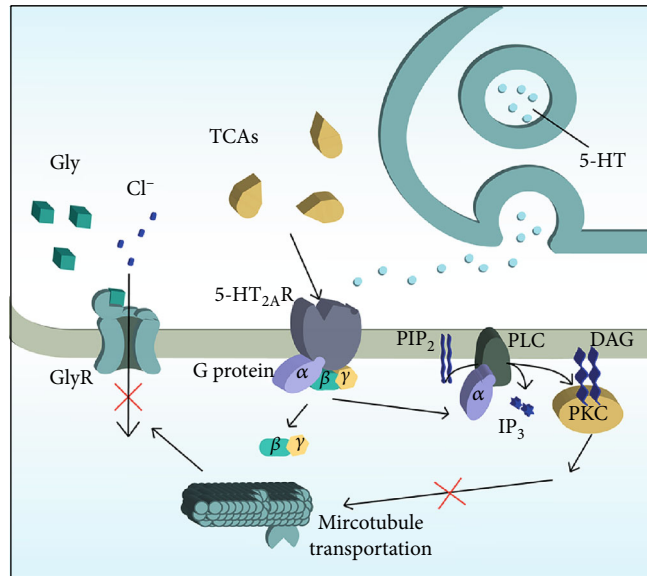


FIGURE 1: Possible therapeutic mechanism of TCAs on tinnitus. TCAs block the 5-HT_{2A} receptor, thus preventing 5-HT from binding to the 5-HT_{2A} receptor and activating the PLC-IP₃/DAG-PKC pathway and thus impairing downstream microtubule-dependent glycine receptor transport. This in turn acts as a barrier to glycine receptor binding on the surface of the cell membrane followed by a reduction of chloride influx and thus leading to a decrease in tonic current and an increase in intracellular potential and excitability. TCAs: tricyclic antidepressants; 5-HT_{2A}R: 5-hydroxytryptamine receptor _{2A} receptor; PIP₂: phosphatidylinositol 4,5-bisphosphate; PLC: phospholipase C; DAG: diacylglycerol; PKC: protein kinase C; IP₃: inositol 1,4,5-trisphosphate.

inhibition or reduce central excitability deserves further exploration. However, in view of the side effects of both SSRIs and TCAs, a more rigorous clinical scheme is needed to produce convincing results.

4.2.2. Ion Channel Drugs

(1) *Glutamate Receptor Antagonists.* Glutamate receptor antagonists reported in the treatment of tinnitus are all aimed at ion channel receptor subtypes. Previous studies have suggested that regulation of the endocochlear potential (EP) by OHCs contributes to increased spontaneous cochlear activity. A portion of the mechanoelectric transduction (MET) channels are open at rest in inner hair cells (IHCs), and alterations of the EP can lead to corresponding electrical activities in IHCs including depolarization and hyperpolarization [21]. By limiting or preventing the current through their MET channels, OHCs can reduce the opening probability of MET channels. Downregulating the influx of K⁺ through MET channels increases the EP, which leads directly to depolarization, the opening of voltage-gated Ca²⁺ channels, and fusion of the synaptic ribbon to the cytomembrane of IHCs. The release of glutamate at ribbon-type synapses is the result of IHC depolarization and causes cochlear fibers to depolarize [99, 100]. This might play a pivotal role by amplifying N-methyl-D-aspartic acid- (NMDA-) mediated neurotransmission in tinnitus, and the increased cochlear firing rate caused by glutamate has been found in salicylate-induced tinnitus through the activation of NMDA receptors [101, 102], which are expressed at all synapses of the lower auditory pathway in mammals [103]. Salicylate can inhibit the activity of cyclooxygenase and increase the concentration

of arachidonic acid in the cytomembrane of cochlear nerve fibers, thus increasing the possibility of NMDA receptor opening by altering the mechanical properties of the cytomembrane and thus bringing about both peripheral and central effects [104]. In addition to this, salicylate is also reported to reduce the electromotility of OHCs, which may have an effect on the mediation of stereocilium bundle deflection that influences the probability of MET channel opening [105, 106] (Figure 2).

Research using memantine has indicated a significant reduction of symptoms in tinnitus triggered by both salicylate [107, 108] and noise trauma in rats [109]. It was also seen that memantine attenuated the increased level of NMDA receptor subunit 2B protein, which was markedly induced by salicylate and might be associated with inhibition of NMDA receptors in the auditory cortex [108]. Washout of the memantine was performed after clear efficacy was observed, and tinnitus-related behavioral manifestations were partially reduced, which might be interpreted as either a prolonged effect of memantine or an insufficient washout period that failed to entirely eliminate the memantine [109]. A study observed a lack of suppression of tinnitus at lower memantine doses, which the investigators concluded to be the limitation of the conditioned suppression technique [110]. Another trial showed less satisfactory results due to poor improvement in the THI score and relatively serious side effects. In addition, the appearance of a significant interaction between efficacy and treatment order indicated the possibility that a delayed carryover effect exists for treatment with memantine along with a more pronounced placebo effect in the group previously treated with memantine

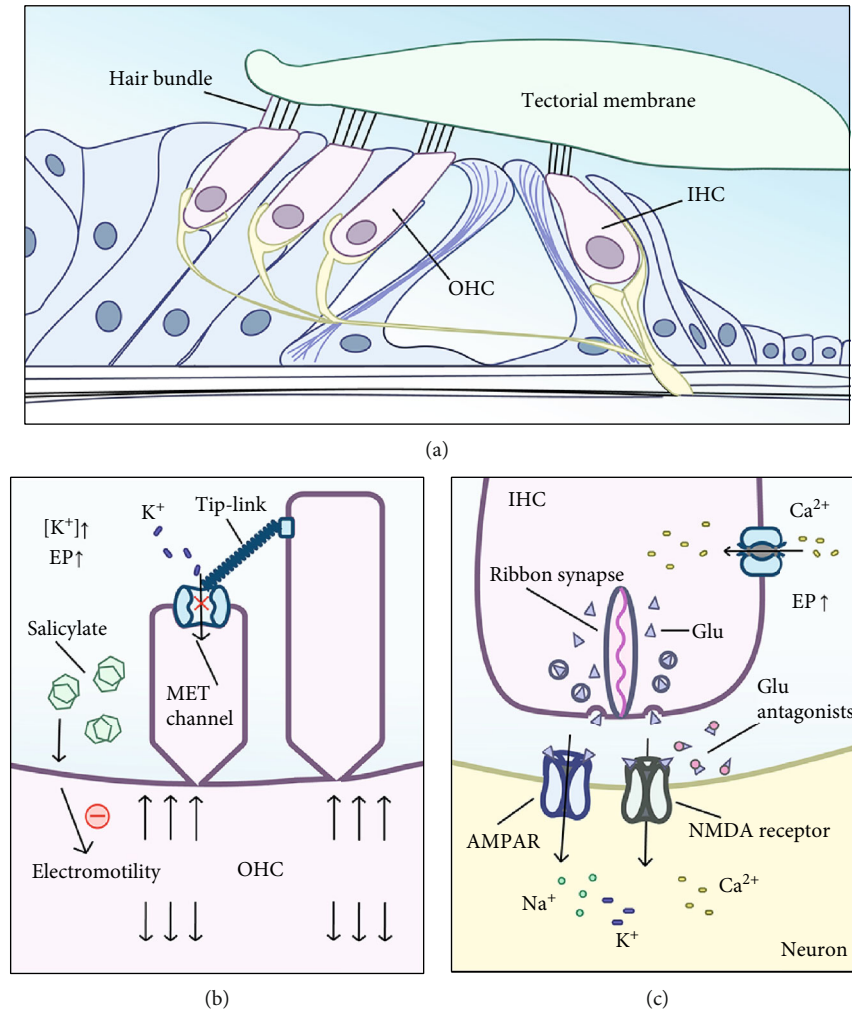


FIGURE 2: Possible therapeutic mechanism of glutamate antagonists on salicylate-induced tinnitus. (a) Schematic diagram of the organ of Corti. (b) Salicylate can inhibit the electromotility of OHCs, which reduces the opening probability of MET channels, downregulates the influx of K^+ through the MET channels, and increases the EP. The sets of three down and three up arrows represent the longitudinal extension of electromotility in OHCs. (c) The increased EP is followed by opening of the voltage-gated Ca^{2+} channels, fusion of the synaptic ribbon to the cytomembrane of the IHCs, and release of glutamate, and thus cochlear fibers depolarize abnormally and tinnitus occurs. Glutamate antagonists can inhibit the process by blocking AMPARs and NMDA receptors. IHC: inner hair cell; OHC: outer hair cell; EP: endocochlear potential; MET: mechano-electrical transduction; NMDA receptor: N-methyl-D-aspartic acid receptor; AMPAR: α -amino-3-hydroxy-5-methyl-4-isoxazole-propionic acid receptor.

[111]. The low affinity and rapid off-rate of memantine give it a more tolerable and lower adverse event profile despite having similar activity on the NMDA receptor as MK-801, another NMDA receptor antagonist [112].

A study reported that after salicylate injection, the levels of glutamate and ascorbate in the auditory cortex increased significantly and that MK-801 attenuated these reactions, suggesting that MK-801 might act as a neuroprotective agent against hyperactivity in salicylate-induced tinnitus [113]. In addition, systemic distribution of MK-801 might also decrease the hyperactivity of the lower auditory pathway, for instance, in the dorsal cochlear nucleus [114]. This indicates that MK-801 might play a role mainly in the central auditory structures. Tinnitus patients treated with neramexane had a consistent decrease in THI scores in the higher-dose groups after 8 weeks of initial treatment [115]. Investi-

gators also explored the efficacy of acamprosate, which showed a beneficial effect after at least 60 days of treatment, and approximately 87% of the patients taking acamprosate showed an improvement [116]. The efficacy of acamprosate was confirmed in another trial by showing a higher alleviation rate of 92.5% [117]. These studies suggest that NMDA receptor antagonists such as memantine, MK-801, and acamprosate may be worthy of further exploration for the treatment of tinnitus. However, Auris Medical announced that the phase III clinical trial of AM-101, an NMDA receptor antagonist, failed to achieve the primary endpoint in acute tinnitus, despite positive indications published during early phases of the trial [118]. In addition, another glutamate receptor, α -amino-3-hydroxy-5-methyl-4-isoxazole-propionic acid receptor (AMPA), might also be involved in the pathogenesis of salicylate-induced tinnitus through increased

expression on the excitatory neurons of the auditory cortex [119], for which BGG492 has been shown to reduce VAS values for chronic subjective tinnitus loudness and annoyance in a phase II study.

Numerous studies have looked at drugs targeting the ion channels of cells, but the results so far have been unsatisfactory. With progress in research on the mechanisms behind tinnitus in the central nervous system, our understanding of cell function such as neuron activity has gradually increased, but there have been no large leaps in our understanding of the molecular mechanisms behind tinnitus. Perhaps a better understanding of the mechanisms and heterogeneity of tinnitus will provide new sites for drug activity in the future.

(2) *Other Channel Modulators.* Generally, voltage-gated potassium channels are the predominating determinants of the intrinsic excitability of cells. Among them, Kv3.1 is a high-threshold potassium channel that is expressed in fast-spike neuron plasmalemma within the central auditory system [120]. The high voltage-activated potassium current, which might be the cause of the spontaneous hyperactivity of characteristic neurons in high-frequency burst firing, is downregulated by noise exposure in rats [121]. AUT00063 is a newly developed central neuron-targeted drug, and as a potent and selective regulator of Kv3.1 and Kv3.2 voltage-gated channels, AUT00063 can shift neurons' activated voltage dependence to a lower negative potential from which it is more difficult to obtain an elevation of intracellular potential. Indeed, AUT00063 has been shown to inhibit spontaneous hyperactivity induced by noise exposure in the fusiform cells of the dorsal cochlear nucleus, as well as multiunit activity recorded in the inferior colliculus in mice [122, 123]. However, a daily dose of 800 mg AUT00063 for 28 days showed safety and tolerance but resulted in no change in TFI scores [124]. Patients with intermittent typewriter-like tinnitus all responded positively to carbamazepine, and therefore, it is speculated that carbamazepine alleviates tinnitus by hindering the recovery from inactivation of the voltage-gated sodium channel and thus suppressing subsequent ephaptic axonal transmission in the cochlear nerve [125].

Gabapentin is a synthesized structural analog of GABA, and it has been found to bind to the α_2 - δ subunit of voltage-dependent calcium channels with high affinity [126]. There have been attempts at using gabapentin in the treatment of tinnitus, and a controlled trial in patients with tinnitus induced by acoustic trauma showed significant improvement in tinnitus annoyance and loudness [127]. Another pilot study with gabapentin found a significant improvement in tinnitus annoyance and a decrease in tinnitus handicap [128]. However, further trials did not detect any benefit on tinnitus by gabapentin [129, 130], and in another study, beneficial effects were only reported in the subgroup of tinnitus patients with hypertension, diabetes, or dyslipidemia, and there was no difference on the group level [131]. In addition, the use of anticonvulsants including gabapentin in treating tinnitus was analyzed in a Cochrane review, which

showed no evidence for a clinical effect and doubtful clinical significance as well as a high rate of side effects (18% of trial participants) in the treatment of tinnitus [132].

4.2.3. *Antioxidants.* Oxidative stress is involved in the pathogenesis of many diseases, including tinnitus. Several studies showed that oxidants were elevated accompanied by a reduction of antioxidants in tinnitus patients [133–136], and a study reported similar results in the internal jugular and brachial vein blood of acute idiopathic tinnitus patients. However, due to the exceedingly small portion that the inner ear occupies in the total brain effluent, we cannot jump to the conclusion that both endothelial dysfunction and oxidative stress originate from the inner ear microcirculation [137]. A study speculated that impairment of nitric oxide production could result in vascular dysregulation [138]. Oxidative stress damages the labyrinthine neurosensory epithelium and the vestibulocochlear nerve, as well as central auditory pathway, and the neurosensory epithelium is especially at risk of cochlear lesions induced by reactive oxygen species (ROS) [139–142]. One of the most important effects of ROS, lipid peroxidation, might mediate apoptosis of auditory neurons and ciliated cells [143]. In addition, ROS can cause endothelial dysfunction, which is more obvious in the terminal microcirculation. Thus, the established hypothesis is that ROS might cause damage to the stria vascularis and the capillary networks of the planum semilunatum [144–147].

Khan et al. reported that the application of coenzyme Q10 (CoQ10) alone only reduced Tinnitus Questionnaire scores in those who lacked CoQ10 [148]. However, in another CoQ10 study, patients undergoing cisplatin chemotherapy retained stable concentrations of ROS and fewer instances of hearing impairment and tinnitus, but because the efficacy was from a mixture of several different compounds, it is difficult to discriminate the efficacy of CoQ10 alone [149]. CoQ10 mainly acts on mitochondrial and cellular membranes, and it is involved in the electron transfer chain as part of the energy generation process. Therefore, the level of CoQ10 in plasma can only provide limited information about oxidative defense [150, 151]. Zinc is a structural component of superoxide dismutase which is the primary line of defense against oxidative stress. A significant improvement in the THI score was achieved in noise-induced hearing loss-associated tinnitus patients treated by zinc [152], while another study showed an adverse result in elderly tinnitus patients [153]. In any case, a Cochrane review concluded that there is no evidence of efficacy of oral zinc supplementation in adults with tinnitus [154]. The antioxidant N-acetyl-L-cysteine (NAC) was able to alleviate noise-induced hearing loss in soldiers, thus suggesting that NAC could attenuate the toxic effect of acoustic trauma and it might represent a new compound for treating inner ear injuries as well as tinnitus [155].

There are also reports of drugs that can improve the microcirculation of the cochlea by improving the blood flow and thus increasing the clearance of ROS through the bloodstream. Pentoxifylline has vasodilation activity and thereby increases blood flow, and sulodexide has antithrombotic and anticoagulant activities, both of which have been shown

to have positive effects in tinnitus patients, mainly by improving the subjective perception and emotional response to tinnitus [156, 157]. However, the changes of inner ear microcirculation in tinnitus are not completely clear yet, and various antioxidants still need to pass through the blood-labyrinth barrier; thus, the therapeutic effect is not very precise.

4.2.4. Herbal Medicines. A retrospective study reported that some medicinal plants, including Asteraceae, Lamiaceae, and Ginkgo biloba, had been used to treat tinnitus in Iran, but there was little concrete evidence for the efficacy and mechanism of these herbal medicines [158]. Ginkgo biloba contains various agents, including ginkgo-flavone glycosides, which can scavenge free radicals, and terpenoids, which act as antagonists of platelet-activating factor [159]. Looking through studies on Ginkgo biloba, we found contrary treatment effects on tinnitus, and a Cochrane review concluded that there was limited evidence to support the effectiveness for patients whose primary complaint was tinnitus [160]. This might be due to a lack of standard usage, a lack of optimal doses, and a lack of standard methodological measurements of efficacy [149, 161–164]. The efficacy of tinnitus is likely to be the mixture of multiple ingredients, which might not be conducive to guiding the treatment and avoiding adverse effects.

4.2.5. Dietary Supplements. In addition to their usage in treating neurological disorders and oxidative stress, dietary supplements have also been applied in the treatment of tinnitus. It is verified that mixed supplements of vitamins and phospholipids could reduce tinnitus intensity and subjective symptoms along with reduced ROS levels [143]. However, later, no benefit was found from the compounds (Ginkgo biloba, α -lipoic acid, vitamin C, papaverine hydrochloride, and vitamin E) in elderly patients with tinnitus [164]. Vitamin B12 deficiency is related to axonal degeneration and demyelination followed by the death of neurons. Efficacy was only shown in tinnitus patients who had vitamin B12 deficiency [165–167]. There have been studies investigating the efficacy of melatonin, either as monotherapy or in combination with sulodexide or vitamins. The plasma level of melatonin might be associated with tinnitus and might improve tinnitus-related sleep problems [168–171] and might only show obvious treatment effects in tinnitus patients with insomnia [172, 173]. Melatonin might not be able to directly improve the symptoms of tinnitus at all, but it might solve the sleep problems caused by tinnitus.

4.3. Discussion on Tinnitus Medications and Management. In terms of mechanisms, tinnitus management is mainly based on the neurophysiological changes of tinnitus that have been elaborated in different neurophysiological models [174–177], and such management takes a more holistic approach compared with the molecule-mechanism medications for tinnitus. Clinically, tinnitus management is more intuitive based on the current electrophysiological methods for diagnosing tinnitus. With the popularization of smartphone apps and the Internet, tinnitus self-management procedures based on

sound therapy or psychological consultation can be more readily put into use, and these are more likely to be promoted clinically due to their safety and ease of use. Currently, the European guidelines only strongly recommend CBT as a treatment for tinnitus. The safety of sound therapy has been verified, but there is no evidence of its efficacy. However, according to the lateral inhibition theory of tinnitus frequency-related cortical neurons, notched sounds can cause neural plasticity by constantly stimulating and changing the excitability of neurons, and thus, sound therapy is still a promising treatment for alleviating the subjective symptoms of tinnitus.

It is worth noting that the studies of the molecular mechanisms of tinnitus have also made some progress [178, 179]. Most of the medications treating tinnitus are off-label use, and drugs specifically developed for tinnitus have been proven ineffective [118, 122, 124]. The efficacy of the same drug observed in different studies might be inconsistent, and the incidence of side effects is higher than tinnitus management. Also, no medication is recommended to treat tinnitus in the guidelines, and in view of the side effects of different medications, they should be applied cautiously. The treatment of tinnitus presents a challenge, and there are several obstacles to the development of effective pharmaceutical treatments. For example, the heterogenetic nature of tinnitus makes it difficult to identify the corresponding characteristics of different tinnitus subtypes. Drugs applied in the treatment of tinnitus, regardless of their off-label usage, might reduce tinnitus-related complications and offer minor alleviation of tinnitus perception, but none are able to offer curative treatment. On the molecular level, neurotransmitters at all levels of the auditory pathway structures can be potential targets for drugs. For example, benzodiazepines are applied to treat tinnitus because of their positive allosteric regulatory effect on central GABA receptors, and it is very interesting that these drugs can both increase GABAergic inhibition and decrease GABAergic inhibition in the medial geniculate body [180]. Also, the nonauditory pathway structures, such as the areas associated with emotion, may be affected by antidepressants, and it is worth studying whether or not the therapeutic effect of TCAs is related to their antagonistic effect on 5-HT receptors in addition to the improvement of tinnitus-related depression.

On the whole, although it seems that there is no clear efficacy for medications targeting specific molecules due to the subjectivity and heterogeneity of tinnitus [181, 182], objective improvement is also difficult to observe in both the management and medical treatment of tinnitus patients. Thus, suggestions given by clinicians are primarily along the lines of “Don’t worry about it” or “Don’t pay attention to it”; that is to say, subjective adaptation is still the main method for patients in coping with tinnitus.

5. Conclusion

At present, standard therapeutics for tinnitus are absent. However, although there is no evidence to support the use of medications for tinnitus, they might still have a place in treatments as we gain a better understanding of the

pathogenesis of tinnitus. Our understanding of tinnitus is limited, and this might be overcome by more characteristic animal models and subsequently more high-quality clinical trials. Thus, in the absence of an effective therapeutic protocol for tinnitus, the treatment of tinnitus mainly focuses on eliminating disturbing symptoms in line with different situations. For example, patients suffering from tinnitus and depression can be treated with CBT and drugs, and hearing aids can be considered for hearing loss patients disturbed by tinnitus. In any case, clinicians should respect the individual's opinions and choose the most suitable treatment plan.

Conflicts of Interest

The authors claim that there are no conflicts of interest.

Authors' Contributions

Kunkun Wang and Dongmei Tang have contributed equally to this work.

Acknowledgments

This work is supported by the National Key R&D Program of China (No. 2017YFA0103900), the National Natural Science Foundation of China (Nos. 81970879, 81570913, 81620108005, 81830029, and 81800912), the Shanghai Science and Technology Committee (STCSM) Science and Technology Innovation Program (No. 19441900200), and the Shanghai Pujiang Talents Plan (No. 18PJ1401700).

References

- [1] A. McCormack, M. Edmondson-Jones, S. Somerset, and D. Hall, "A systematic review of the reporting of tinnitus prevalence and severity," *Hearing Research*, vol. 337, pp. 70–79, 2016.
- [2] B. Park, H. G. Choi, H. J. Lee et al., "Analysis of the prevalence of and risk factors for tinnitus in a young population," *Otology & Neurotology*, vol. 35, no. 7, pp. 1218–1222, 2014.
- [3] A. Gilles, G. van Hal, D. de Ridder, K. Wouters, and P. van de Heyning, "Epidemiology of noise-induced tinnitus and the attitudes and beliefs towards noise and hearing protection in adolescents," *PLoS One*, vol. 8, no. 7, article e70297, 2013.
- [4] H. Mahboubi, S. Olliaei, S. Kiumehr, S. Dwabe, and H. R. Djalilian, "The prevalence and characteristics of tinnitus in the youth population of the United States," *Laryngoscope*, vol. 123, no. 8, pp. 2001–2008, 2013.
- [5] J. Shargorodsky, G. C. Curhan, and W. R. Farwell, "Prevalence and characteristics of tinnitus among US adults," *The American Journal of Medicine*, vol. 123, no. 8, pp. 711–718, 2010.
- [6] N. H. Krog, B. Engdahl, and K. Tambs, "The association between tinnitus and mental health in a general population sample: results from the HUNT study," *Journal of Psychosomatic Research*, vol. 69, no. 3, pp. 289–298, 2010.
- [7] J. M. Bhatt, N. Bhattacharyya, and H. W. Lin, "Relationships between tinnitus and the prevalence of anxiety and depression," *Laryngoscope*, vol. 127, no. 2, pp. 466–469, 2017.
- [8] T. Crönlein, B. Langguth, M. Pregler, P. M. Kreuzer, T. C. Wetter, and M. Schecklmann, "Insomnia in patients with chronic tinnitus: cognitive and emotional distress as moderator variables," *Journal of Psychosomatic Research*, vol. 83, pp. 65–68, 2016.
- [9] D. Stockdale, D. McFerran, P. Brazier et al., "An economic evaluation of the healthcare cost of tinnitus management in the UK," *BMC Health Services Research*, vol. 17, no. 1, p. 577, 2017.
- [10] A. B. Elgoyhen, B. Langguth, D. de Ridder, and S. Vanneste, "Tinnitus: perspectives from human neuroimaging," *Nature Reviews. Neuroscience*, vol. 16, no. 10, pp. 632–642, 2015.
- [11] C. A. Bauer, "Tinnitus," *New England Journal of Medicine*, vol. 378, no. 13, pp. 1224–1231, 2018.
- [12] R. F. F. Cima, B. Mazurek, H. Haider et al., "A multidisciplinary European guideline for tinnitus: diagnostics, assessment, and treatment," *HNO*, vol. 67, no. S1, pp. 10–42, 2019.
- [13] C. Pantev, H. Okamoto, and H. Teismann, "Music-induced cortical plasticity and lateral inhibition in the human auditory cortex as foundations for tonal tinnitus treatment," *Frontiers in Systems Neuroscience*, vol. 6, p. 50, 2012.
- [14] T. S. Kim, N. Yakunina, Y. J. Ryu, I. J. Chung, and E. C. Nam, "Self-administered tinnitus pitch matching versus a conventional audiometric procedure," *Audiology & Neuro-Otology*, vol. 22, no. 1, pp. 1–8, 2017.
- [15] W. E. Brownell, "Outer hair cell electromotility and otoacoustic emissions," *Ear and Hearing*, vol. 11, no. 2, pp. 82–92, 1990.
- [16] S. Engel, R. D. H. Markewitz, B. Langguth, and M. Schecklmann, "Paired associative stimulation of the temporal cortex: effects on the auditory steady-state response," *Frontiers in Psychiatry*, vol. 8, p. 227, 2017.
- [17] R. Jackson, A. Vijendren, and J. Phillips, "Objective measures of tinnitus: a systematic review," *Otology & Neurotology*, vol. 40, no. 2, pp. 154–163, 2019.
- [18] A. M. Leaver, T. K. Turesky, A. Seydell-Greenwald, S. Morgan, H. J. Kim, and J. P. Rauschecker, "Intrinsic network activity in tinnitus investigated using functional MRI," *Human Brain Mapping*, vol. 37, no. 8, pp. 2717–2735, 2016.
- [19] A. Bener, A. O. A. A. al-Hamaq, K. Abdulhadi, A. H. Salahaldin, and L. Gansan, "Interaction between diabetes mellitus and hypertension on risk of hearing loss in highly endogenous population," *Diabetes and Metabolic Syndrome: Clinical Research and Reviews*, vol. 11, Supplement 1, pp. S45–s51, 2017.
- [20] P. C. D. Gibrin, J. J. Melo, and L. L. de Moraes Marchiori, "Prevalence of tinnitus complaints and probable association with hearing loss, diabetes mellitus and hypertension in elderly," *CoDAS*, vol. 25, no. 2, pp. 176–180, 2013.
- [21] A. J. Noreña, "Revisiting the cochlear and central mechanisms of tinnitus and therapeutic approaches," *Audiology and Neurotology*, vol. 20, no. 1, Supplement 1, pp. 53–59, 2015.
- [22] J. A. Henry, L. E. Roberts, D. M. Caspary, S. M. Theodoroff, and R. J. Salvi, "Underlying mechanisms of tinnitus: review and clinical implications," *Journal of the American Academy of Audiology*, vol. 25, no. 1, pp. 5–22, 2014.
- [23] A. J. Noreña and J. J. Eggermont, "Changes in spontaneous neural activity immediately after an acoustic trauma: implications for neural correlates of tinnitus," *Hearing Research*, vol. 183, no. 1-2, pp. 137–153, 2003.
- [24] B. I. Kalappa, T. J. Brozoski, J. G. Turner, and D. M. Caspary, "Single unit hyperactivity and bursting in the auditory

- thalamus of awake rats directly correlates with behavioural evidence of tinnitus,” *The Journal of Physiology*, vol. 592, no. 22, pp. 5065–5078, 2014.
- [25] D. P. Vogler, D. Robertson, and W. H. A. M. Mulders, “Hyperactivity following unilateral hearing loss in characterized cells in the inferior colliculus,” *Neuroscience*, vol. 265, pp. 28–36, 2014.
- [26] J. A. Kaltenbach, D. A. Godfrey, J. B. Neumann, D. L. McCaslin, C. E. Afman, and J. Zhang, “Changes in spontaneous neural activity in the dorsal cochlear nucleus following exposure to intense sound: relation to threshold shift,” *Hearing Research*, vol. 124, no. 1-2, pp. 78–84, 1998.
- [27] S. B. Melamed, J. A. Kaltenbach, M. W. Church, D. L. Burgio, and C. E. Afmar, “Cisplatin-induced increases in spontaneous neural activity in the dorsal cochlear nucleus and associated outer hair cell loss,” *Audiology*, vol. 39, no. 1, pp. 24–29, 2000.
- [28] J. A. Kaltenbach, J. D. Rachel, T. A. Mathog, J. Zhang, P. R. Falzarano, and M. Lewandowski, “Cisplatin-induced hyperactivity in the dorsal cochlear nucleus and its relation to outer hair cell loss: relevance to tinnitus,” *Journal of Neurophysiology*, vol. 88, no. 2, pp. 699–714, 2002.
- [29] R. Llinás, F. J. Urbano, E. Leznik, R. R. Ramírez, and H. J. F. van Marle, “Rhythmic and dysrhythmic thalamocortical dynamics: GABA systems and the edge effect,” *Trends in Neurosciences*, vol. 28, no. 6, pp. 325–333, 2005.
- [30] E. Houdayer, R. Teggi, S. Velikova et al., “Involvement of cortico-subcortical circuits in normoacoustic chronic tinnitus: a source localization EEG study,” *Clinical Neurophysiology*, vol. 126, no. 12, pp. 2356–2365, 2015.
- [31] N. Weisz, S. Muller, W. Schlee, K. Dohrmann, T. Hartmann, and T. Elbert, “The neural code of auditory phantom perception,” *The Journal of Neuroscience*, vol. 27, no. 6, pp. 1479–1484, 2007.
- [32] E. van der Loo, S. Gais, M. Congedo et al., “Tinnitus intensity dependent gamma oscillations of the contralateral auditory cortex,” *PLoS One*, vol. 4, no. 10, article e7396, 2009.
- [33] K. V. Gopal, B. P. Thomas, R. Nandy, D. Mao, and H. Lu, “Potential audiological and MRI markers of tinnitus,” *Journal of the American Academy of Audiology*, vol. 28, no. 8, pp. 742–757, 2017.
- [34] Y. C. Chen, J. Zhang, X. W. Li et al., “Aberrant spontaneous brain activity in chronic tinnitus patients revealed by resting-state functional MRI,” *NeuroImage: Clinical*, vol. 6, pp. 222–228, 2014.
- [35] R. R. Llinas, U. Ribary, D. Jeanmonod, E. Kronberg, and P. P. Mitra, “Thalamocortical dysrhythmia: a neurological and neuropsychiatric syndrome characterized by magnetoencephalography,” *Proceedings of the National Academy of Sciences of the United States of America*, vol. 96, no. 26, pp. 15222–15227, 1999.
- [36] N. Weisz, S. Moratti, M. Meinzer, K. Dohrmann, and T. Elbert, “Tinnitus perception and distress is related to abnormal spontaneous brain activity as measured by magnetoencephalography,” *PLoS Medicine*, vol. 2, no. 6, article e153, 2005.
- [37] P. Adjamian, M. Sereda, O. Zobay, D. A. Hall, and A. R. Palmer, “Neuromagnetic indicators of tinnitus and tinnitus masking in patients with and without hearing loss,” *Journal of the Association for Research in Otolaryngology*, vol. 13, no. 5, pp. 715–731, 2012.
- [38] R. Simmons, C. Dambra, E. Lobarinas, C. Stocking, and R. Salvi, “Head, neck, and eye movements that modulate tinnitus,” *Seminars in Hearing*, vol. 29, no. 4, pp. 361–370, 2008.
- [39] R. J. Pinchoff, R. F. Burkard, R. J. Salvi, M. L. Coad, and A. H. Lockwood, “Modulation of tinnitus by voluntary jaw movements,” *The American Journal of Otolaryngology*, vol. 19, no. 6, pp. 785–789, 1998.
- [40] K. S. Kraus and B. Canlon, “Neuronal connectivity and interactions between the auditory and limbic systems. Effects of noise and tinnitus,” *Hearing Research*, vol. 288, no. 1-2, pp. 34–46, 2012.
- [41] S. Vanneste, M. Plazier, E. van der Loo, P. van de Heyning, and D. de Ridder, “The differences in brain activity between narrow band noise and pure tone tinnitus,” *PLoS One*, vol. 5, no. 10, article e13618, 2010.
- [42] C. Klinge, B. Roder, and C. Buchel, “Increased amygdala activation to emotional auditory stimuli in the blind,” *Brain*, vol. 133, no. 6, pp. 1729–1736, 2010.
- [43] R. F. F. Cima, I. H. Maes, M. A. Joore et al., “Specialised treatment based on cognitive behaviour therapy versus usual care for tinnitus: a randomised controlled trial,” *The Lancet*, vol. 379, no. 9830, pp. 1951–1959, 2012.
- [44] E. W. Beukes, D. M. Baguley, P. M. Allen, V. Manchaiah, and G. Andersson, “Audiologist-guided internet-based cognitive behavior therapy for adults with tinnitus in the United Kingdom: a randomized controlled trial,” *Ear and Hearing*, vol. 39, no. 3, pp. 423–433, 2018.
- [45] E. W. Beukes, P. M. Allen, D. M. Baguley, V. Manchaiah, and G. Andersson, “Long-term efficacy of audiologist-guided internet-based cognitive behavior therapy for tinnitus,” *American Journal of Audiology*, vol. 27, no. 3S, pp. 431–447, 2018.
- [46] P. Martinez-Devesa, A. Waddell, R. Perera, and M. Theodoulou, “Cognitive behavioural therapy for tinnitus,” *Cochrane Database of Systematic Reviews*, vol. 1, article CD012614, 2020.
- [47] A. Londero, P. Bonfils, and J. P. Lefaucheur, “Transcranial magnetic stimulation and subjective tinnitus. A review of the literature, 2014–2016,” *European Annals of Otorhinolaryngology, Head and Neck Diseases*, vol. 135, no. 1, pp. 51–58, 2018.
- [48] Z. Meng, S. Liu, Y. Zheng, J. S. Phillips, and Cochrane ENT Group, “Repetitive transcranial magnetic stimulation for tinnitus,” *Cochrane Database of Systematic Reviews*, vol. 10, article CD007946, 2011.
- [49] J. Godbehere, J. Sandhu, A. Evans et al., “Treatment of tinnitus using theta burst based repetitive transcranial magnetic stimulation—a single blinded randomized control trial,” *Otology & Neurotology*, vol. 40, 5S Suppl 1, pp. S38–S42, 2019.
- [50] M. Formánek, P. Migařová, P. Krulová et al., “Combined transcranial magnetic stimulation in the treatment of chronic tinnitus,” *Annals of Clinical and Translational Neurology*, vol. 5, no. 7, pp. 857–864, 2018.
- [51] L. Jacquemin, G. Mertens, P. van de Heyning et al., “An exploratory study on the use of event-related potentials as an objective measure of auditory processing and therapy effect in patients with tinnitus: a transcranial direct current stimulation study,” *Otology & Neurotology*, vol. 40, no. 9, pp. E868–E875, 2019.
- [52] H. Y. Lee, “Adjunctive role of bifrontal transcranial direct current stimulation in distressed patients with severe

- tinnitus,” *Journal of Korean Medical Science*, vol. 34, no. 3, p. 8, 2019.
- [53] T. Yuan, A. Yadollahpour, J. Salgado-Ramírez, D. Robles-Camarillo, and R. Ortega-Palacios, “Transcranial direct current stimulation for the treatment of tinnitus: a review of clinical trials and mechanisms of action,” *BMC Neuroscience*, vol. 19, no. 1, 2018.
- [54] J. Hobson, E. Chisholm, and A. El Refaie, “Sound therapy (masking) in the management of tinnitus in adults,” *Cochrane Database of Systematic Reviews*, vol. 11, article Cd006371, 2012.
- [55] P. J. Jastreboff and J. W. P. Hazell, “A neurophysiological approach to tinnitus: clinical implications,” *British Journal of Audiology*, vol. 27, no. 1, pp. 7–17, 2009.
- [56] J. S. Phillips and D. McFerran, “Tinnitus Retraining Therapy (TRT) for tinnitus,” *Cochrane Database of Systematic Reviews*, vol. 3, article Cd007330, 2010.
- [57] C. A. Bauer, J. L. Berry, and T. J. Brozoski, “The effect of tinnitus retraining therapy on chronic tinnitus: a controlled trial,” *Laryngoscope Investigative Otolaryngology*, vol. 2, no. 4, pp. 166–177, 2017.
- [58] The Tinnitus Retraining Therapy Trial Research Group, “Effect of tinnitus retraining therapy vs standard of care on tinnitus-related quality of life a randomized clinical trial,” *JAMA Otolaryngology–Head & Neck Surgery*, vol. 145, no. 7, pp. 597–608, 2019.
- [59] A. K. NICKEL, T. Hillecke, H. Argstatter, and H. V. Bolay, “Outcome research in music therapy: a step on the long road to an evidence-based treatment,” *Annals of the New York Academy of Sciences*, vol. 1060, no. 1, pp. 283–293, 2005.
- [60] P. J. Hanley and P. B. Davis, “Treatment of tinnitus with a customized, dynamic acoustic neural stimulus: underlying principles and clinical efficacy,” *Trends in Amplification*, vol. 12, no. 3, pp. 210–222, 2008.
- [61] C. Pantev, C. Rudack, A. Stein et al., “Study protocol: münster tinnitus randomized controlled clinical trial-2013 based on tailor-made notched music training (TMNMT),” *BMC Neurology*, vol. 14, no. 1, p. 40, 2014.
- [62] H. Teismann, H. Okamoto, and C. Pantev, “Short and intense tailor-made notched music training against tinnitus: the tinnitus frequency matters,” *PLoS One*, vol. 6, no. 9, article e24685, 2011.
- [63] H. Okamoto, H. Stracke, W. Stoll, and C. Pantev, “Listening to tailor-made notched music reduces tinnitus loudness and tinnitus-related auditory cortex activity,” *Proceedings of the National Academy of Sciences of the United States of America*, vol. 107, no. 3, pp. 1207–1210, 2010.
- [64] A. Stein, R. Wunderlich, P. Lau et al., “Clinical trial on tonal tinnitus with tailor-made notched music training,” *BMC Neurology*, vol. 16, no. 1, p. 38, 2016.
- [65] H. Y. Lee, M. S. Choi, D. S. Chang, and C. S. Cho, “Combined bifrontal transcranial direct current stimulation and tailor-made notched music training in chronic tinnitus,” *Journal of Audiology and Otolology*, vol. 21, no. 1, pp. 22–27, 2017.
- [66] S. Y. Kim, M. Y. Chang, M. Hong, S. G. Yoo, D. Oh, and M. K. Park, “Tinnitus therapy using tailor-made notched music delivered via a smartphone application and Ginko combined treatment: a pilot study,” *Auris, Nasus, Larynx*, vol. 44, no. 5, pp. 528–533, 2017.
- [67] M. K. Nagaraj and P. Prabhu, “Internet/smartphone-based applications for the treatment of tinnitus: a systematic review,” *European Archives of Oto-Rhino-Laryngology*, vol. 277, no. 3, pp. 649–657, 2020.
- [68] C. McNeill, D. Távora-Vieira, F. Alnafjan, G. D. Searchfield, and D. Welch, “Tinnitus pitch, masking, and the effectiveness of hearing aids for tinnitus therapy,” *International Journal of Audiology*, vol. 51, no. 12, pp. 914–919, 2012.
- [69] N. Yakunina, W. H. Lee, Y. J. Ryu, and E. C. Nam, “Tinnitus suppression effect of hearing aids in patients with high-frequency hearing loss: a randomized double-blind controlled trial,” *Otology & Neurotology*, vol. 40, no. 7, pp. 865–871, 2019.
- [70] L. Haab, C. Lehser, F. I. Corona-Strauss et al., “Implementation and long-term evaluation of a hearing aid supported tinnitus treatment using notched environmental sounds,” *IEEE Journal of Translational Engineering in Health and Medicine*, vol. 7, pp. 1–9, 2019.
- [71] D. J. Hoare, M. Edmondson-Jones, M. Sereida, M. A. Akeroyd, and D. Hall, “Amplification with hearing aids for patients with tinnitus and co-existing hearing loss,” *Cochrane Database of Systematic Reviews*, vol. 1, article Cd010151, 2014.
- [72] T. Atkin, S. Comai, and G. Gobbi, “Drugs for insomnia beyond benzodiazepines: pharmacology, clinical applications, and discovery,” *Pharmacological Reviews*, vol. 70, no. 2, pp. 197–245, 2018.
- [73] F. M. Bahmad Jr., A. R. Venosa, and C. A. Oliveira, “Benzodiazepines and GABAergics in treating severe disabling tinnitus of predominantly cochlear origin,” *The International Tinnitus Journal*, vol. 12, no. 2, pp. 140–144, 2006.
- [74] S. S. Han, E. C. Nam, J. Y. Won et al., “Clonazepam quiets tinnitus: a randomised crossover study with Ginkgo biloba,” *Journal of Neurology, Neurosurgery, and Psychiatry*, vol. 83, no. 8, pp. 821–827, 2012.
- [75] M. Malavasi, H. H. Caovilla, F. Freitas et al., “Clonazepam in the pharmacological treatment of vertigo and tinnitus,” *The International Tinnitus Journal*, vol. 8, no. 1, pp. 50–53, 2002.
- [76] R. M. Johnson, R. Brummett, and A. Schleuning, “Use of alprazolam for relief of tinnitus. A double-blind study,” *Archives of Otolaryngology - Head & Neck Surgery*, vol. 119, no. 8, pp. 842–845, 1993.
- [77] M. M. Jalali, A. Kousha, S. E. Naghavi, R. Soleimani, and R. Banan, “The effects of alprazolam on tinnitus: a cross-over randomized clinical trial,” *Medical Science Monitor*, vol. 15, no. 11, pp. PI55–PI60, 2009.
- [78] J. L. Puel, “Chemical synaptic transmission in the cochlea,” *Progress in Neurobiology*, vol. 47, no. 6, pp. 449–476, 1995.
- [79] M. A. Lopez-Gonzalez and F. Esteban-Ortega, “Tinnitus dopaminergic pathway. Ear noises treatment by dopamine modulation,” *Medical Hypotheses*, vol. 65, no. 2, pp. 349–352, 2005.
- [80] I. Sziklai, J. Szilvassy, and Z. Szilvassy, “Tinnitus control by dopamine agonist pramipexole in presbycusis patients: a randomized, placebo-controlled, double-blind study,” *Laryngoscope*, vol. 121, no. 4, pp. 888–893, 2011.
- [81] M. A. Lopez-Gonzalez, F. Moliner-Peiro, J. Alfaro-Garcia, and F. Esteban-Ortega, “Sulpiride plus hydroxyzine decrease tinnitus perception,” *Auris Nasus Larynx*, vol. 34, no. 1, pp. 23–27, 2007.
- [82] M. A. Lopez-Gonzalez, A. M. Santiago, and F. Esteban-Ortega, “Sulpiride and melatonin decrease tinnitus

- perception modulating the auditolimbic dopaminergic pathway,” *The Journal of Otolaryngology*, vol. 36, no. 4, p. 213, 2007.
- [83] A. A. de Azevedo, B. Langguth, P. M. de Oliveira, and R. Rodrigues Figueiredo, “Tinnitus treatment with piribedil guided by electrocochleography and acoustic otoemissions,” *Otology & Neurotology*, vol. 30, no. 5, pp. 676–680, 2009.
- [84] B. Luo, L. Hu, C. Liu, Y. Guo, and H. Wang, “Activation of 5-HT_{2A/C} receptor reduces glycine receptor-mediated currents in cultured auditory cortical neurons,” *Amino Acids*, vol. 48, no. 2, pp. 349–356, 2016.
- [85] B. Cusack, A. Nelson, and E. Richelson, “Binding of antidepressants to human brain receptors: focus on newer generation compounds,” *Psychopharmacology*, vol. 114, no. 4, pp. 559–565, 1994.
- [86] M. D. Sullivan, C. S. Sakai, R. A. Dobie, and W. J. Katon, “Treatment of depressed tinnitus patients with nortriptyline,” *The Annals of Otology, Rhinology, and Laryngology*, vol. 98, no. 11, pp. 867–872, 2016.
- [87] M. Sullivan, W. Katon, J. Russo, R. Dobie, and C. Sakai, “A randomized trial of nortriptyline for severe chronic tinnitus: effects on depression, disability, and tinnitus symptoms,” *JAMA Internal Medicine*, vol. 153, no. 19, pp. 2251–2259, 1993.
- [88] L. Podoshin, Y. Ben-David, M. Fradis, S. Malatskey, and H. Hafner, “Idiopathic subjective tinnitus treated by amitriptyline hydrochloride/biofeedback,” *The International Tinnitus Journal*, vol. 1, no. 1, pp. 54–60, 1995.
- [89] N. Bayar, B. Böke, E. Turan, and E. Belgin, “Efficacy of amitriptyline in the treatment of subjective tinnitus,” *The Journal of Otolaryngology*, vol. 30, no. 5, p. 300, 2001.
- [90] S. Zoger, J. Svedlund, and K. M. Holgers, “The effects of sertraline on severe tinnitus suffering—a randomized, double-blind, placebo-controlled study,” *Journal of Clinical Psychopharmacology*, vol. 26, no. 1, pp. 32–39, 2006.
- [91] S. K. Robinson, E. S. Viirre, K. A. Bailey, M. A. Gerke, J. P. Harris, and M. B. Stein, “Randomized placebo-controlled trial of a selective serotonin reuptake inhibitor in the treatment of nondepressed tinnitus subjects,” *Psychosomatic Medicine*, vol. 67, no. 6, pp. 981–988, 2005.
- [92] D. Mendis and M. Johnston, “An unusual case of prolonged tinnitus following low-dose amitriptyline,” *Journal of Psychopharmacology*, vol. 22, no. 5, pp. 574–575, 2008.
- [93] B. Langguth, M. Landgrebe, M. Wittmann, T. Kleinjung, and G. Hajak, “Persistent tinnitus induced by tricyclic antidepressants,” *Journal of Psychopharmacology*, vol. 24, no. 8, pp. 1273–1275, 2010.
- [94] C. W. T. Miller, “Development of tinnitus at a low dose of sertraline: clinical course and proposed mechanisms,” *Case Reports in Psychiatry*, vol. 2016, 1790693 pages, 2016.
- [95] O. Meeus, D. De Ridder, and P. Van de Heyning, “Administration of the combination clonazepam-Deanxit as treatment for tinnitus,” *Otology & Neurotology*, vol. 32, no. 4, pp. 701–709, 2011.
- [96] R. N. Brogden, R. C. Heel, T. M. Speight, and G. S. Avery, “Trazodone: a review of its pharmacological properties and therapeutic use in depression and anxiety,” *Drugs*, vol. 21, no. 6, pp. 401–429, 1981.
- [97] G. C. Dib, C. A. Kasse, T. A. de Andrade, J. R. Gurgel Testa, and O. L. M. Cruz, “Tinnitus treatment with trazodone,” *Brazilian Journal of Otorhinolaryngology*, vol. 73, no. 3, pp. 390–397, 2007.
- [98] S. M. Hwang, S. H. Lim, D. J. Oh, S. K. Kim, H. H. Jung, and G. J. Im, “Effect of tianeptine on depressed tinnitus patients,” *Journal of Audiology and Otology*, vol. 20, no. 2, pp. 90–96, 2016.
- [99] A. Hudspeth, “The cellular basis of hearing: the biophysics of hair cells,” *Science*, vol. 230, no. 4727, pp. 745–752, 1985.
- [100] T. Moser, A. Brandt, and A. Lysakowski, “Hair cell ribbon synapses,” *Cell and Tissue Research*, vol. 326, no. 2, pp. 347–359, 2006.
- [101] M. J. Guitton, J. Caston, J. Ruel, R. M. Johnson, R. Pujol, and J. L. Puel, “Salicylate induces tinnitus through activation of cochlear NMDA receptors,” *The Journal of Neuroscience*, vol. 23, no. 9, pp. 3944–3952, 2003.
- [102] J. Ruel, C. Chabbert, R. Nouvian et al., “Salicylate enables cochlear arachidonic-acid-sensitive NMDA receptor responses,” *The Journal of Neuroscience*, vol. 28, no. 29, pp. 7313–7323, 2008.
- [103] J. T. Sanchez, S. Ghelani, and S. Otto-Meyer, “From development to disease: diverse functions of NMDA-type glutamate receptors in the lower auditory pathway,” *Neuroscience*, vol. 285, pp. 248–259, 2015.
- [104] J. L. Puel and M. J. Guitton, “Salicylate-induced tinnitus: molecular mechanisms and modulation by anxiety,” *Progress in Brain Research*, vol. 166, pp. 141–146, 2007.
- [105] P. Avan, B. Buki, and C. Petit, “Auditory distortions: origins and functions,” *Physiological Reviews*, vol. 93, no. 4, pp. 1563–1619, 2013.
- [106] H. J. Kennedy, M. G. Evans, A. C. Crawford, and R. Fettiplace, “Depolarization of cochlear outer hair cells evokes active hair bundle motion by two mechanisms,” *The Journal of Neuroscience*, vol. 26, no. 10, pp. 2757–2766, 2006.
- [107] M. Ralli, D. Troiani, M. V. Podda et al., “The effect of the NMDA channel blocker memantine on salicylate-induced tinnitus in rats,” *Acta Otorhinolaryngologica Italica*, vol. 34, no. 3, pp. 198–204, 2014.
- [108] C. H. Jang, S. Lee, I. Y. Park, A. Song, C. Moon, and G. W. Cho, “Memantine attenuates salicylate-induced tinnitus possibly by reducing NR2B expression in auditory cortex of rat,” *Experimental Neurobiology*, vol. 28, no. 4, pp. 495–503, 2019.
- [109] Y. Zheng, E. McNamara, L. Stiles, C. L. Darlington, and P. F. Smith, “Evidence that memantine reduces chronic tinnitus caused by acoustic trauma in rats,” *Frontiers in Neurology*, vol. 3, 2012.
- [110] E. Lobarinas, G. Yang, W. Sun et al., “Salicylate- and quinine-induced tinnitus and effects of memantine,” *Acta Oto-Laryngologica*, vol. 126, no. sup556, pp. 13–19, 2009.
- [111] R. R. Figueiredo, B. Langguth, P. M. de Oliveira, and A. A. de Azevedo, “Tinnitus treatment with memantine,” *Otolaryngology and Head and Neck Surgery*, vol. 138, no. 4, pp. 492–496, 2008.
- [112] D. Olivares, V. K. Deshpande, Y. Shi et al., “N-Methyl D-aspartate (NMDA) receptor antagonists and memantine treatment for Alzheimer’s disease, vascular dementia and Parkinson’s disease,” *Current Alzheimer Research*, vol. 9, no. 6, pp. 746–758, 2012.
- [113] S. Xiong, Y. Song, J. Liu et al., “Neuroprotective effects of MK-801 on auditory cortex in salicylate-induced tinnitus: involvement of neural activity, glutamate and ascorbate,” *Hearing Research*, vol. 375, pp. 44–52, 2019.

- [114] M. W. Criddle, D. A. Godfrey, and J. A. Kaltenbach, "Attenuation of noise-induced hyperactivity in the dorsal cochlear nucleus by pre-treatment with MK-801," *Brain Research*, vol. 1682, pp. 71–77, 2018.
- [115] M. Suckfüll, M. Althaus, B. Ellers-Lenz et al., "A randomized, double-blind, placebo-controlled clinical trial to evaluate the efficacy and safety of neramexane in patients with moderate to severe subjective tinnitus," *BMC Ear, Nose and Throat Disorders*, vol. 11, no. 1, 2011.
- [116] A. A. Azevedo and R. R. Figueiredo, "Tinnitus treatment with acamprosate: double-blind study," *Brazilian Journal of Otorhinolaryngology*, vol. 71, no. 5, pp. 618–623, 2005.
- [117] D. K. Sharma, S. Kaur, J. Singh, and I. Kaur, "Role of acamprosate in sensorineural tinnitus," *Indian Journal of Pharmacology*, vol. 44, no. 1, pp. 93–96, 2012.
- [118] P. van de Heyning, G. Muehlmeier, T. Cox et al., "Efficacy and safety of AM-101 in the treatment of acute inner ear tinnitus—a double-blind, randomized, placebo-controlled phase II study," *Otology & Neurotology*, vol. 35, no. 4, pp. 589–597, 2014.
- [119] C. Wu, X. Wu, B. Yi et al., "Changes in GABA and glutamate receptors on auditory cortical excitatory neurons in a rat model of salicylate-induced tinnitus," *American Journal of Translational Research*, vol. 10, no. 12, pp. 3941–3955, 2018.
- [120] A. R. Chambers, N. Pilati, P. Balaram, C. H. Large, L. K. Kaczmarek, and D. B. Polley, "Pharmacological modulation of Kv3.1 mitigates auditory midbrain temporal processing deficits following auditory nerve damage," *Scientific Reports*, vol. 7, no. 1, p. 17496, 2017.
- [121] N. Pilati, M. J. Ison, M. Barker et al., "Mechanisms contributing to central excitability changes during hearing loss," *Proceedings of the National Academy of Sciences*, vol. 109, no. 21, pp. 8292–8297, 2012.
- [122] L. Glait, W. Fan, G. Stillitano et al., "Effects of AUT00063, a Kv3.1 channel modulator, on noise-induced hyperactivity in the dorsal cochlear nucleus," *Hearing Research*, vol. 361, pp. 36–44, 2018.
- [123] L. A. Anderson, L. L. Hesse, N. Pilati et al., "Increased spontaneous firing rates in auditory midbrain following noise exposure are specifically abolished by a Kv3 channel modulator," *Hearing Research*, vol. 365, pp. 77–89, 2018.
- [124] D. A. Hall, J. Ray, J. Watson et al., "A balanced randomised placebo controlled blinded phase IIa multi-centre study to investigate the efficacy and safety of AUT00063 versus placebo in subjective tinnitus: the QUIET-1 trial," *Hearing Research*, vol. 377, pp. 153–166, 2019.
- [125] W. Sunwoo, Y. J. Jeon, Y. J. Bae, J. H. Jang, J. W. Koo, and J. J. Song, "Typewriter tinnitus revisited: the typical symptoms and the initial response to carbamazepine are the most reliable diagnostic clues," *Scientific Reports*, vol. 7, no. 1, p. 10615, 2017.
- [126] D. J. Dooley, C. P. Taylor, S. Donevan, and D. Feltner, "Ca²⁺ channel $\alpha_2\delta$ ligands: novel modulators of neurotransmission," *Trends in Pharmacological Sciences*, vol. 28, no. 2, pp. 75–82, 2007.
- [127] C. A. Bauer and T. J. Brozoski, "Effect of gabapentin on the sensation and impact of tinnitus," *Laryngoscope*, vol. 116, no. 5, pp. 675–681, 2006.
- [128] D. L. Witsell, M. T. Hannley, S. Stinnet, and D. L. Tucci, "Treatment of tinnitus with gabapentin: a pilot study," *Otology & Neurotology*, vol. 28, no. 1, pp. 11–15, 2007.
- [129] M. Bakhshae, M. Ghasemi, M. Azarpazhooh et al., "Gabapentin effectiveness on the sensation of subjective idiopathic tinnitus: a pilot study," *European Archives of Oto-Rhino-Laryngology*, vol. 265, no. 5, pp. 525–530, 2008.
- [130] J. F. Piccirillo, J. Finnell, A. Vlahiotis, R. A. Chole, and E. Spitznagel Jr., "Relief of idiopathic subjective tinnitus," *Archives of Otolaryngology – Head & Neck Surgery*, vol. 133, no. 4, pp. 390–397, 2007.
- [131] M. A. Dehkordi, S. Abolbashari, R. Taheri, and S. Einolghozati, "Efficacy of gabapentin on subjective idiopathic tinnitus: a randomized, double-blind, placebo-controlled trial," *Ear, Nose, & Throat Journal*, vol. 90, no. 4, pp. 150–158, 2019.
- [132] C. E. L. Hoekstra, S. P. Rynja, G. A. van Zanten, and M. M. Rovers, "Anticonvulsants for tinnitus," *Cochrane Database Syst Rev*, vol. 7, article Cd007960, 2011.
- [133] S. Koç, S. Akyüz, B. T. Somuk et al., "Paraoxonase activity and oxidative status in patients with tinnitus," *Journal of Audiology & Otology*, vol. 20, no. 1, pp. 17–21, 2016.
- [134] M. Celik and I. Koyuncu, "A comprehensive study of oxidative stress in tinnitus patients," *Indian Journal of Otolaryngology and Head & Neck Surgery*, vol. 70, no. 4, pp. 521–526, 2018.
- [135] K. Pawlak-Osińska, H. Kaźmierczak, M. Marzec et al., "Assessment of the state of the natural antioxidant barrier of a body in patients complaining about the presence of tinnitus," *Oxidative Medicine and Cellular Longevity*, vol. 2018, 1439578 pages, 2018.
- [136] A. Ekinci and K. Kamasak, "Avaliação da atividade da enzima serica prolidase e do estresse oxidativo em pacientes com zumbido," *Brazilian Journal of Otorhinolaryngology*, vol. 18, article id 30832-2, 2019.
- [137] S. Neri, S. Signorelli, D. Pulvirenti et al., "Oxidative stress, nitric oxide, endothelial dysfunction and tinnitus," *Free Radical Research*, vol. 40, no. 6, pp. 615–618, 2009.
- [138] A. R. Loiselle, A. Neustaeter, E. de Kleine, P. van Dijk, and N. M. Jansonius, "Associations between tinnitus and glaucoma suggest a common mechanism: a clinical and population-based study," *Hearing Research*, vol. 386, p. 107862, 2020.
- [139] A. Ciorba, C. Bianchini, A. Pastore, and M. Mazzoli, "Pathogenesis of tinnitus: any role for oxidative stress?," *The Journal of International Advanced Otology*, vol. 9, no. 2, pp. 249–254, 2013.
- [140] A. L. Poirrier, J. Pincemail, P. Van Den Ackerveken, P. P. Lefebvre, and B. Malgrange, "Oxidative stress in the cochlea: an update," *Current Medicinal Chemistry*, vol. 17, no. 30, pp. 3591–3604, 2010.
- [141] S. Y. Park, J. J. Han, J. H. Hwang, E. S. Whang, S. W. Yeo, and S. N. Park, "Comparison of tinnitus and psychological aspects between the younger and older adult patients with tinnitus," *Auris Nasus Larynx*, vol. 44, no. 2, pp. 147–151, 2017.
- [142] A. Gilles, B. Ihtijarevic, K. Wouters, and P. van de Heyning, "Using prophylactic antioxidants to prevent noise-induced hearing damage in young adults: a protocol for a double-blind, randomized controlled trial," *Trials*, vol. 15, no. 1, 2014.
- [143] M. Savastano, G. Brescia, and G. Marioni, "Antioxidant therapy in idiopathic tinnitus: preliminary outcomes," *Archives of Medical Research*, vol. 38, no. 4, pp. 456–459, 2007.
- [144] F. H. Epstein, J. R. Vane, E. E. Ånggård, and R. M. Botting, "Regulatory functions of the vascular endothelium," *The*

- New England Journal of Medicine*, vol. 323, no. 1, pp. 27–36, 1990.
- [145] G. W. De Keulenaer, L. J. Andries, S. U. Sys, and D. L. Brutsaert, “Endothelin-mediated positive inotropic effect induced by reactive oxygen species in isolated cardiac muscle,” *Circulation Research*, vol. 76, no. 5, pp. 878–884, 1995.
- [146] H. A. Lehr, B. Frei, A. M. Olofsson, T. E. Carew, and K. E. Arfors, “Protection from oxidized LDL-induced leukocyte adhesion to microvascular and macrovascular endothelium in vivo by vitamin C but not by vitamin E,” *Circulation*, vol. 91, no. 5, pp. 1525–1532, 1995.
- [147] K. J. Davies, S. W. Lin, and R. E. Pacifici, “Protein damage and degradation by oxygen radicals. IV. Degradation of denatured protein,” *The Journal of Biological Chemistry*, vol. 262, no. 20, pp. 9914–9920, 1987.
- [148] M. Khan, J. Gross, H. Haupt et al., “A pilot clinical trial of the effects of coenzyme Q10 on chronic tinnitus aurium,” *Otolaryngology—Head and Neck Surgery*, vol. 136, no. 1, pp. 72–77, 2016.
- [149] F. Scasso, A. E. Sprio, L. Canobbio et al., “Dietary supplementation of coenzyme Q10 plus multivitamins to hamper the ROS mediated cisplatin ototoxicity in humans: a pilot study,” *Heliyon*, vol. 3, no. 2, article e00251, 2017.
- [150] P. Niklowitz, T. Menke, W. Andler, and J. G. Okun, “Simultaneous analysis of coenzyme Q10 in plasma, erythrocytes and platelets: comparison of the antioxidant level in blood cells and their environment in healthy children and after oral supplementation in adults,” *Clinica Chimica Acta*, vol. 342, no. 1-2, pp. 219–226, 2004.
- [151] F. L. Crane, “Biochemical functions of coenzyme Q10,” *Journal of the American College of Nutrition*, vol. 20, no. 6, pp. 591–598, 2001.
- [152] C. W. Yeh, L. H. Tseng, C. H. Yang, and C. F. Hwang, “Effects of oral zinc supplementation on patients with noise-induced hearing loss associated tinnitus: a clinical trial,” *Biomedical Journal*, vol. 42, no. 1, pp. 46–52, 2019.
- [153] C. Coelho, S. A. Witt, H. Ji, M. R. Hansen, B. Gantz, and R. Tyler, “Zinc to treat tinnitus in the elderly,” *Otology & Neurotology*, vol. 34, no. 6, pp. 1146–1154, 2013.
- [154] O. C. Person, M. E. Puga, E. M. da Silva, and M. R. Torloni, “Zinc supplementation for tinnitus,” *Cochrane Database of Systematic Reviews*, vol. 11, article CD009832, 2016.
- [155] U. Rosenhall, B. Skoog, and P. Muhr, “Treatment of military acoustic accidents with N-acetyl-L-cysteine (NAC),” *International Journal of Audiology*, vol. 58, no. 3, pp. 151–157, 2019.
- [156] M. El Beaino, M. K. McCaskey, and E. Eter, “Sulodexide monotherapy in chronic idiopathic subjective tinnitus: a randomized controlled trial,” *Otolaryngology—Head and Neck Surgery*, vol. 158, no. 6, pp. 1107–1112, 2018.
- [157] L. Incandela, M. R. Cesarone, G. Belcaro, and M. T. De Sanctis, “Treatment of vascular inner ear disease with pentoxifylline: a 4-week, controlled, randomized trial,” *Angiology*, vol. 53, Suppl 1, pp. S19–S22, 2002.
- [158] M. R. Mahmoudian-Sani, M. Hashemzadeh-Chaleshtori, M. Asadi-Samani, and T. Luther, “A review of medicinal plants for the treatment of earache and tinnitus in Iran,” *The International Tinnitus Journal*, vol. 21, no. 1, pp. 44–49, 2017.
- [159] D. Schneider, L. Schneider, A. Shulman et al., “Ginkgo biloba (Rokan) therapy in tinnitus patients and measurable interactions between tinnitus and vestibular disturbances,” *The International Tinnitus Journal*, vol. 6, no. 1, pp. 56–62, 2000.
- [160] M. P. Hilton, E. F. Zimmermann, and W. T. Hunt, “Ginkgo biloba for tinnitus,” *Cochrane Database of Systematic Reviews*, vol. 3, article CD003852, 2013.
- [161] M. R. Mahmoudian-Sani, M. Hashemzadeh-Chaleshtori, M. Asadi-Samani, and Q. Yang, “Ginkgo biloba in the treatment of tinnitus: an updated literature review,” *International Tinnitus Journal*, vol. 21, no. 1, pp. 58–62, 2017.
- [162] K. Procházková, I. Šejna, J. Skutil, and A. Hahn, “Ginkgo biloba extract EGb 761 versus pentoxifylline in chronic tinnitus: a randomized, double-blind clinical trial,” *International Journal of Clinical Pharmacy*, vol. 40, no. 5, pp. 1335–1341, 2018.
- [163] C. L. Radunz, C. E. Okuyama, F. C. A. Branco-Barreiro, R. M. S. Pereira, and S. N. Diniz, “Clinical randomized trial study of hearing aids effectiveness in association with Ginkgo biloba extract (EGb 761) on tinnitus improvement,” *Brazilian Journal of Otorhinolaryngology*, vol. 19, article id 30055-2, 2019.
- [164] J. F. Polanski, A. D. Soares, and O. L. de Mendonca Cruz, “Efeito da terapia com antioxidantes sobre o zumbido em idosos,” *Brazilian Journal of Otorhinolaryngology*, vol. 82, no. 3, pp. 269–274, 2016.
- [165] G. Berkiten, G. Yildirim, I. Topaloglu, and H. Ugras, “Vitamin B12 levels in patients with tinnitus and effectiveness of vitamin B12 treatment on hearing threshold and tinnitus,” *B-ENT*, vol. 9, no. 2, pp. 111–116, 2013.
- [166] Z. Shemesh, J. Attias, M. Ornan, N. Shapira, and A. Shahar, “Vitamin B₁₂ deficiency in patients with chronic-tinnitus and noise-induced hearing loss,” *American Journal of Otolaryngology*, vol. 14, no. 2, pp. 94–99, 1993.
- [167] C. Singh, R. Kawatra, J. Gupta, V. Awasthi, and H. Dungana, “Therapeutic role of vitamin B12 in patients of chronic tinnitus: a pilot study,” *Noise & Health*, vol. 18, no. 81, pp. 93–97, 2016.
- [168] G. Neri, A. de Stefano, C. Baffa et al., “Treatment of central and sensorineural tinnitus with orally administered melatonin and sulodexide: personal experience from a randomized controlled study,” *Acta Otorhinolaryngologica Italica*, vol. 29, no. 2, pp. 86–91, 2009.
- [169] M. Miroddi, R. Bruno, F. Galletti et al., “Clinical pharmacology of melatonin in the treatment of tinnitus: a review,” *European Journal of Clinical Pharmacology*, vol. 71, no. 3, pp. 263–270, 2015.
- [170] A. Hosseinzadeh, S. K. Kamrava, B. C. J. Moore et al., “Molecular aspects of melatonin treatment in tinnitus: a review,” *Current Drug Targets*, vol. 20, no. 11, pp. 1112–1128, 2019.
- [171] U. C. Megwalu, J. E. Finnell, and J. F. Piccirillo, “The effects of melatonin on tinnitus and sleep,” *Otolaryngology—Head and Neck Surgery*, vol. 134, no. 2, pp. 210–213, 2016.
- [172] S. I. Rosenberg, H. Silverstein, P. T. Rowan, and M. J. Olds, “Effect of melatonin on tinnitus,” *Laryngoscope*, vol. 108, no. 3, pp. 305–310, 1998.
- [173] A. Hurtuk, C. Dome, C. H. Holloman et al., “Melatonin: can it stop the ringing?,” *Annals of Otology, Rhinology & Laryngology*, vol. 120, no. 7, pp. 433–440, 2011.
- [174] L. E. Roberts, “Neural plasticity and its initiating conditions in tinnitus,” *HNO*, vol. 66, no. 3, pp. 172–178, 2018.
- [175] S. E. Shore, L. E. Roberts, and B. Langguth, “Maladaptive plasticity in tinnitus – triggers, mechanisms and treatment,” *Nature Reviews. Neurology*, vol. 12, no. 3, pp. 150–160, 2016.

- [176] D. Ryan and C. A. Bauer, "Neuroscience of tinnitus," *Neuroimaging Clinics of North America*, vol. 26, no. 2, pp. 187–196, 2016.
- [177] S. E. Shore and C. Wu, "Mechanisms of noise-induced tinnitus: insights from cellular studies," *Neuron*, vol. 103, no. 1, pp. 8–20, 2019.
- [178] A. Miyakawa, W. Wang, S. J. Cho, D. Li, S. Yang, and S. Bao, "Tinnitus correlates with downregulation of cortical glutamate decarboxylase 65 expression but not auditory cortical map reorganization," *Journal of Neuroscience*, vol. 39, no. 50, pp. 9989–10001, 2019.
- [179] J. A. Lopez-Escamez, T. Bibas, R. F. F. Cima et al., "Genetics of tinnitus: an emerging area for molecular diagnosis and drug development," *Frontiers in Neuroscience*, vol. 10, 2016.
- [180] D. M. Caspary and D. A. Llano, "Auditory thalamic circuits and GABA_A receptor function: putative mechanisms in tinnitus pathology," *Hearing Research*, vol. 349, pp. 197–207, 2017.
- [181] A. J. Noreña and B. J. Farley, "Tinnitus-related neural activity: theories of generation, propagation, and centralization," *Hearing Research*, vol. 295, pp. 161–171, 2013.
- [182] A. J. Noreña, "Stimulating the auditory system to treat tinnitus: from alleviating the symptoms to addressing the causes," in *Tinnitus*, J. Eggermont, F. G. Zeng, A. Popper, and R. Fay, Eds., pp. 217–253, Springer New York, New York, NY, 2012.

Research Article

Four Novel Variants in *POU4F3* Cause Autosomal Dominant Nonsyndromic Hearing Loss

Tian-Yi Cui,^{1,2,3,4} Xue Gao,⁵ Sha-Sha Huang,^{1,2,3} Yan-Yan Sun,⁶ Si-Qi Zhang,⁶ Xin-Xia Jiang,⁶ Yan-Zhong Yang,⁶ Dong-Yang Kang,^{1,2,3} Qing-Wen Zhu ,⁶ and Yong-Yi Yuan ^{1,2,3}

¹College of Otolaryngology Head and Neck Surgery, Chinese PLA General Hospital, Chinese PLA Medical School, 28 Fuxing Road, Beijing 100853, China

²National Clinical Research Center for Otolaryngologic Diseases, State Key Lab of Hearing Science, Ministry of Education, China

³Beijing Key Lab of Hearing Impairment Prevention and Treatment, Beijing, China

⁴School of Basic Medical Sciences, Henan University, Kaifeng 475001, China

⁵Department of Otolaryngology, PLA Rocket Force Characteristic Medical Center, 16# XinWai Da Jie, Beijing 100088, China

⁶Department of Otolaryngology Head & Neck Surgery, The Second Hospital of Hebei Medical University, Heping West Road No. 215, Shijiazhuang, Hebei 050000, China

Correspondence should be addressed to Qing-Wen Zhu; zqw301@163.com and Yong-Yi Yuan; yyyymzh@163.com

Received 26 March 2020; Revised 16 May 2020; Accepted 9 June 2020; Published 1 July 2020

Academic Editor: Renjie Chai

Copyright © 2020 Tian-Yi Cui et al. This is an open access article distributed under the Creative Commons Attribution License, which permits unrestricted use, distribution, and reproduction in any medium, provided the original work is properly cited.

Hereditary hearing loss is one of the most common sensory disabilities worldwide. Mutation of POU domain class 4 transcription factor 3 (*POU4F3*) is considered the pathogenic cause of autosomal dominant nonsyndromic hearing loss (ADNSHL), designated as autosomal dominant nonsyndromic deafness 15. In this study, four novel variants in *POU4F3*, c.696G>T (p.Glu232Asp), c.325C>T (p.His109Tyr), c.635T>C (p.Leu212Pro), and c.183delG (p.Ala62Argfs*22), were identified in four different Chinese families with ADNSHL by targeted next-generation sequencing and Sanger sequencing. Based on the American College of Medical Genetics and Genomics guidelines, c.183delG (p.Ala62Argfs*22) is classified as a pathogenic variant, c.696G>T (p.Glu232Asp) and c.635T>C (p.Leu212Pro) are classified as likely pathogenic variants, and c.325C>T (p.His109Tyr) is classified as a variant of uncertain significance. Based on previous reports and the results of this study, we speculated that *POU4F3* pathogenic variants are significant contributors to ADNSHL in the East Asian population. Therefore, screening of *POU4F3* should be a routine examination for the diagnosis of hereditary hearing loss.

1. Introduction

Hearing loss is one of the most common hereditary sensory disabilities worldwide [1]. Hair cells (HCs) in the inner ear are critical for hearing ability. HCs transfer the mechanical vibration into an acoustic electrical signal, which can then be transmitted to the auditory cortex via spiral ganglion neurons (SGNs) [2]. The causes of deafness are complex, and most of the hearing loss is due to irreversible HCs loss. HCs are very sensitive and vulnerable to many stresses and damage, which can be divided mainly into genetic factors, environmental factors, ototoxic drugs, aging, inflammation, and other unknown etiologies [3–5]. Among all these factors, it

is estimated that genetic factors account for more than 50% of the causes of deafness [6]. Hereditary hearing loss can be classified as syndromic hearing loss or nonsyndromic hearing loss (NSHL) according to whether the patient has other symptoms or signs, and these account for 30% and 70% of cases of hearing loss, respectively [7]. NSHL can be further divided into three categories according to the mode of inheritance: autosomal dominant nonsyndromic hearing loss (ADNSHL), autosomal recessive nonsyndromic hearing loss, and X-linked nonsyndromic hearing loss. ADNSHL accounts for 15% of cases of NSHL [8]. One of the most significant characteristics of hereditary hearing loss is a high degree of heterogeneity. To date, 49 genes related to ADNSHL,

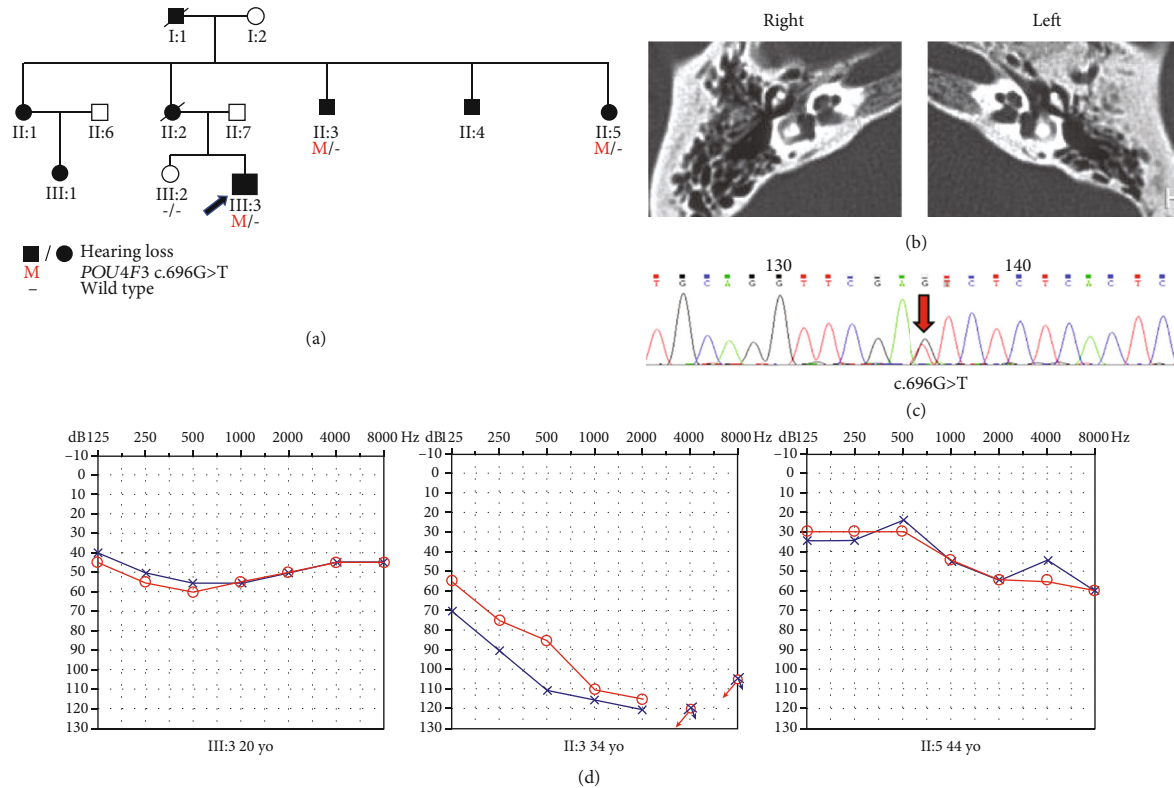


FIGURE 1: Pedigree, temporal bone CT, variant analysis, and audiogram of family A. (a) Affected subjects are denoted in black. Arrow shows the proband. (b) Temporal bone CT of the III:3 shows no structural change. (c) Chromatogram shows *POU4F3* heterozygous c.696G>T detected in patients. (d) Audiograms of the affected subjects. Hearing loss appears to be highly heterogeneous (red: right ear; blue: left ear).

including POU domain class 4 transcription factor 3 (*POU4F3*) and approximately 70 other loci, have been reported (<http://hereditaryhearingloss.org/>).

The *POU4F3* gene encodes POU4F3, a POU-domain class IV protein, has two exons, and encodes a protein of 338 amino acids that belongs to the POU-domain family of transcription factors, which are expressed specifically in inner ear hair cells and play a critical role in the maturation, differentiation, and maintenance of inner ear hair cells [9, 10]. POU4F3 contains two conserved DNA-binding domains (a POU-specific domain and a POU homeodomain), which are the main functional parts [10].

In 1998, *POU4F3* was first described as a disease-causing gene within the DFNA15 locus in an Israeli Jewish family [11]. To date, 32 variants (including those in this study) and whole-gene deletion of *POU4F3* have been reported to cause ADNSHL with variable ages of onset and degrees of severity in various ethnic groups, including Chinese, Japanese, Dutch, Korean, and Brazilian populations [12–24]. In 2017, Kitano et al. reported that *POU4F3* variants represent the third largest cause of ADNSHL (2.5%, 15/602) in Japan and the most prevalent configuration as midfrequency hearing loss type followed by high-frequency hearing loss [14]. He et al. reported that the *POU4F3* pathogenic variant is a relatively common (3/18) cause of ADNSHL among Chinese Hans [15]. Therefore, impairment of hair cells in the cochlea caused by pathogenic variants of *POU4F3* has been considered as one of the major causes of sensorineural hearing loss [14].

In this study, we identified four novel variants using targeted next-generation sequencing (NGS) of a panel of 168 deafness genes from four different Chinese families suffering from ADNSHL. Among the four novel variants, three are missense variants, c.696G>T (p.Glu232Asp) detected in family A, c.325C>T (p.His109Tyr) in family B, and c.635T>C (p.Leu212Pro) in family C, and the fourth is a frameshift variant, c.183delG (p.Ala62Argfs*22), which was identified in family D. Hearing loss in the four families analyzed in this study showed a high degree of variability, even in patients carrying the same variant within one family.

2. Materials and Methods

2.1. Subjects. Probands suffering from ADNSHL in the four families were recruited from the Chinese PLA General Hospital. The pedigrees of these four families are shown in Figures 1–4(a). In addition to the probands, three additional members of family A (II:3, II:5, and III:2), six additional members of family B (I:1, I:2, II:1, II:2, II:3, and II:4), five additional members of family C (II:1, II:2, II:5, III:6, and III:9), and four additional members of family D (II:1, II:3, II:6, and III:1) were recruited from our hospital. All of the subjects or their guardians provided written informed consent to participate in the study. This study was approved by the Ethics Research Committee of the Chinese PLA General Hospital.

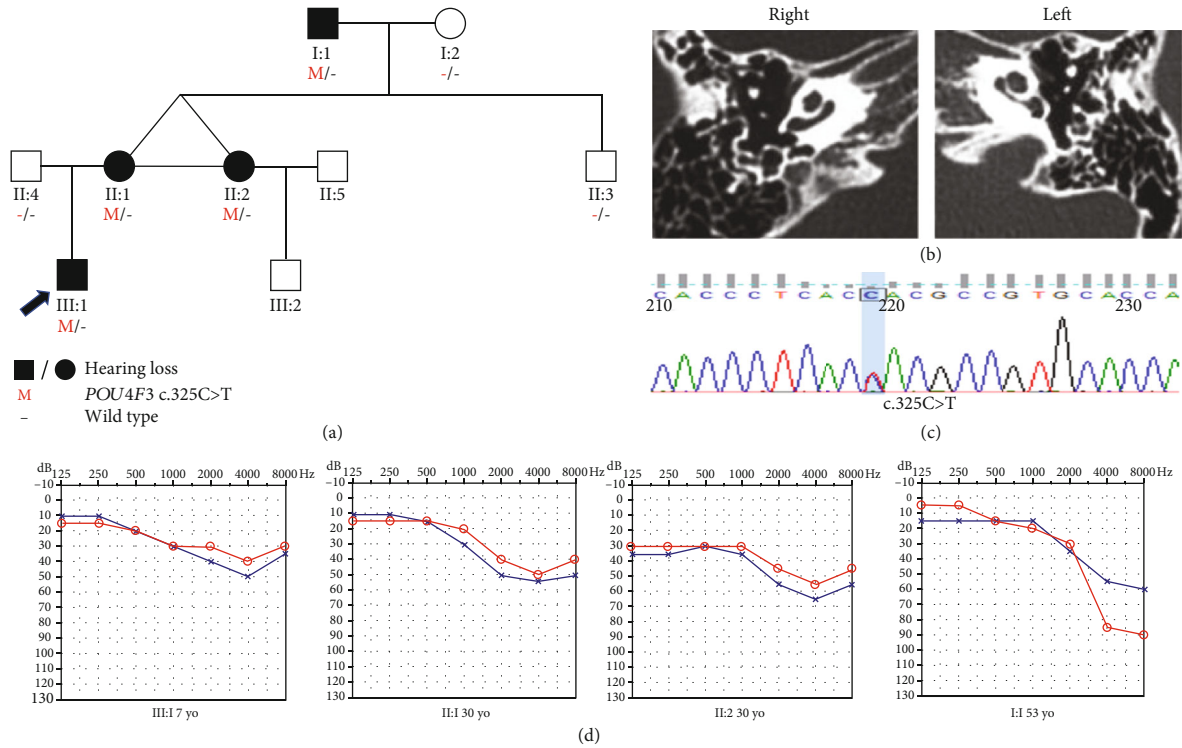


FIGURE 2: Pedigree, temporal bone CT, variant analysis, and audiogram of family B. (a) Affected subjects are denoted in black. Arrow shows the proband. (b) Temporal bone CT of the III:1 shows no structural change. (c) Chromatogram shows *POU4F3* heterozygous c.325C>T detected in patients. (d) Audiograms of the affected subjects. Hearing loss appears to involve high frequency (red: right ear; blue: left ear).

2.2. Clinical Information and Examination. Clinical information was obtained via multiple interviews with the subjects. Medical history was obtained using a questionnaire that elicited responses regarding the symmetry of hearing loss, subjective degree of hearing loss, use of hearing aids, age at onset, evolution, presence of tinnitus, noise exposure, medications, trauma history, and other relevant clinical manifestations. The subjects all received clinical examinations at the Department of Otorhinolaryngology, which included otoscopy, physical examination, pure tone audiometric examination (at frequencies from 125 to 8000 Hz), computed tomography scans of the temporal bone, and acoustic immittance testing. The tandem gait test was performed to evaluate the balance. The diagnosis of sensorineural hearing loss was made according to the WHO criteria based on audiometric examination performed as described previously (the methods description partly reproduces our wording) [12]. Tandem gait and Romberg tests were performed to evaluate balance.

2.3. Variant Analysis. DNA was extracted from peripheral blood samples from all subjects using a blood DNA extraction kit (TIANGEN, Beijing, China), according to the manufacturer’s instructions.

The most prevalent genes related to hearing loss, including *GJB2*, *SLC26A4*, and *mtDNA12SrRNA*, were screened in all of the probands and Chinese controls. The probands and some of the additional family members were examined using a gene panel containing 168 genes related to deafness (Supplementary Table 1). Capture sequencing and NGS of the coding exons of the 168 deafness-related genes and

their flanking 100 bp were performed on the Illumina HiSeq 2000 (Illumina, San Diego, CA, USA) using the MyGenostics gene enrichment system (MyGenostics, Boston, MA, USA).

The methods for DNA library preparation, amplification, capture, detection, sequencing, and bioinformatics analyses were described previously [12]. Nonsynonymous variants were further evaluated for candidate pathogenic variants. Variants were annotated by ANNOVAR; compared with multiple databases including gnomAD, dbSNP, and ExAC; and were predicted by the computational programs SIFT, PolyPhen-2, and MutationTaster. Potential pathogenic variants were filtered using a minimum allele frequency threshold ≤ 0.001 for dominant inheritance [25]. As *POU4F3* has an autosomal dominant inheritance pattern, only heterozygous subjects were selected.

Manual classification of those variants was conducted based on American College of Medical Genetics and Genomics (ACMG)/Association for Molecular Pathology (AMP) guidelines for genetic hearing loss [26]. Sanger sequencing was performed in members of the four families, and the candidate variant of each family was cosegregated with the hearing loss phenotype.

3. Results

3.1. Families and Clinical Characteristics. The pedigrees of the four families showed autosomal dominant inheritance patterns (Figures 1–4(a)). High-resolution CTs of the temporal bone in probands of four families were normal, excluding middle- and inner-ear malformations (Figures 1–4(b)). The

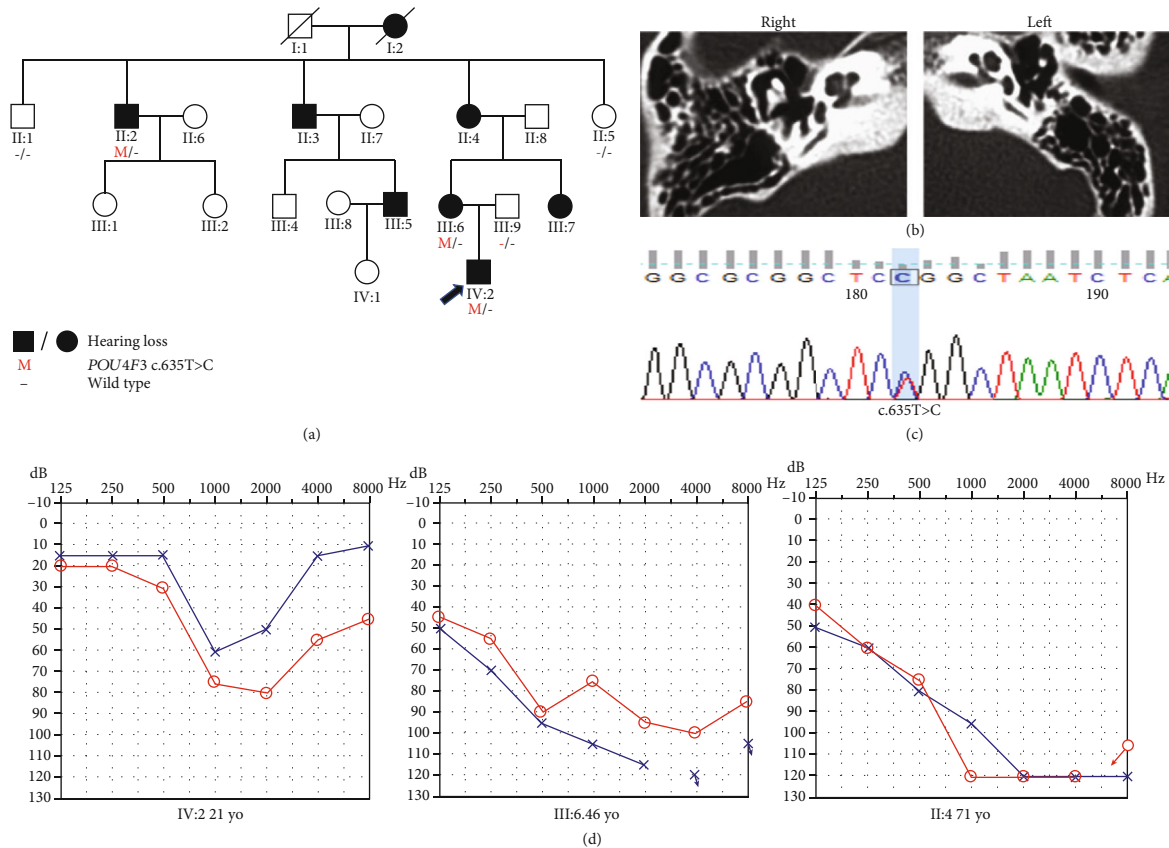


FIGURE 3: Pedigree, temporal bone CT, variant analysis, and audiogram of family C. (a) Affected subjects are denoted in black. Arrow shows the proband. (b) Temporal bone CT of the IV:2 shows no structural change. (c) Chromatogram shows *POU4F3* heterozygous c.635T>C detected in patients. (d) Audiograms of the affected subjects. Audiogram configuration of IV:2 was U-shaped. Downsloping audiogram configurations were observed in III:6 and II:4 (red: right ear; blue: left ear).

hearing impairments in these four families were sensorineural, postlingual, late onset, and progressive. Audiograms of some affected members of these four families are shown in Figures 1–4(d).

Family A was a three-generation Chinese family with ADNSHL and included eight affected patients (Figure 1). The ages at onset of the subjects ranged from 7 to 22 years old. The audiogram of the 20-year-old proband (III:3) with an onset age of 13 years showed all-frequency moderate hearing loss. The audiogram of II:3 showed profound hearing loss; interestingly, this subject had an onset age of 7 years old, which was the earliest in this family. The audiogram of II:5 showed a moderate level of hearing loss.

Family B was a three-generation Chinese family with ADNSHL and included four affected patients (Figure 2). The audiograms had a downsloping shape. The hearing loss in family B involved mostly high frequencies. The proband (III:1) was 7 years old with symmetric hearing loss, and the audiogram showed mild hearing impairment; thus, the proband could communicate with others normally. This family included one set of affected identical twin sisters (II:1 and II:2) who had similar audiograms but different hearing thresholds. Comparison of the audiograms of the proband and 53-year-old I:1 showed that although the hearing impair-

ment had progressed over time, the progression was slight in the affected individual I:1 and involved mainly high frequencies.

Family C was a four-generation Chinese family with ADNSHL and included eight affected patients (Figure 3). The audiogram of proband (IV:2) was asymmetric, and hearing loss involved mainly middle frequencies. Hearing impairment in family C was postlingual, with onset in the first or second decade of life and progression to profound deafness with advancing age. The onset age of the proband was 15 years, and hearing loss was progressive. There was no history of hearing aid use or artificial cochlear implants in the proband. With regard to other auditory symptoms, the proband had complained of tinnitus. Audiograms showed that although low-frequency and high-frequency hearing were normal in the beginning, hearing ultimately deteriorated at all frequencies in the order of middle, high, and low frequencies. Downsloping audiogram configurations were observed in two subjects, who were 46 (III:6) and 69 (II:4) years old, whereas the audiogram of IV:2 was U-shaped (Figure 3(d)). Audiograms were unavailable for the other affected subjects.

Family D was a four-generation Chinese family with ADNSHL and included five affected patients (Figure 4). The audiogram of the proband (III:2) had a downsloping

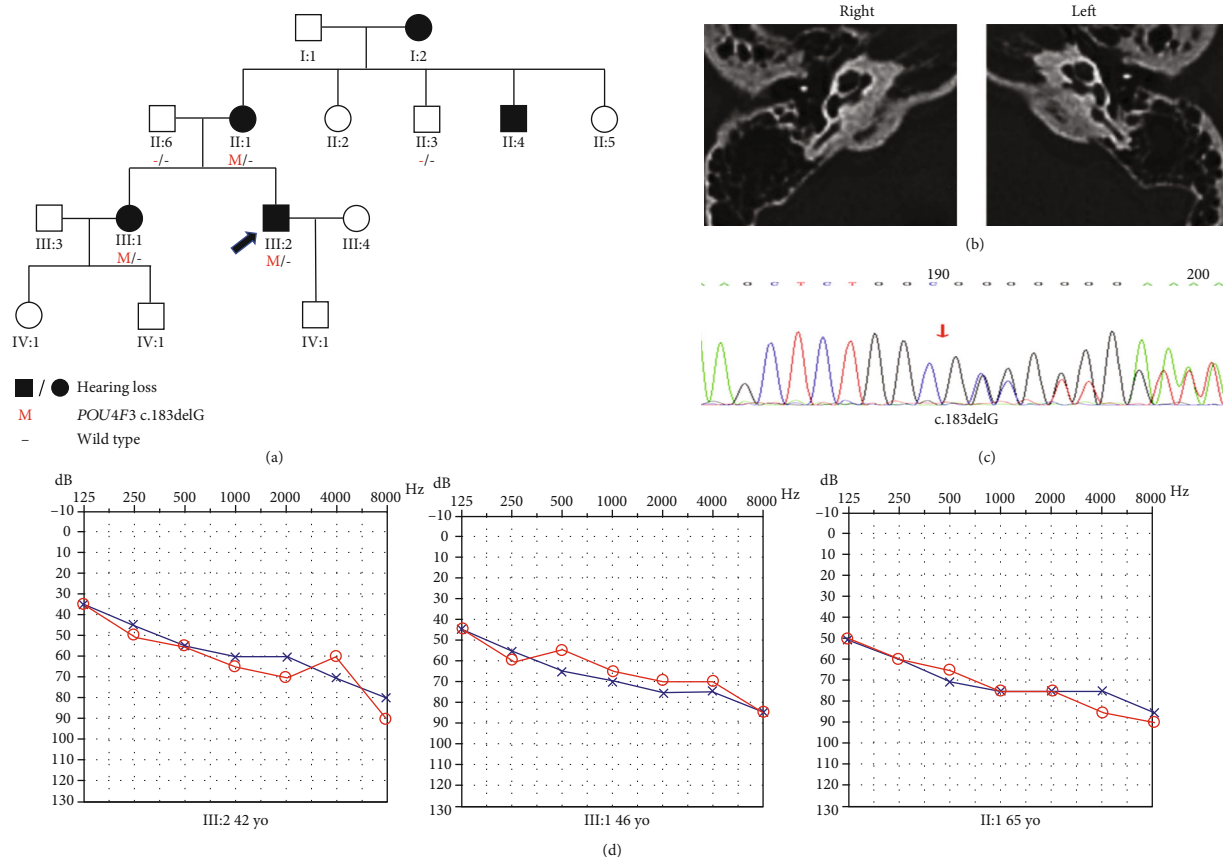


FIGURE 4: Pedigree, temporal bone CT, variant analysis, and audiogram of family D. (a) Affected subjects are denoted in black. Arrow shows the proband. (b) Temporal bone CT of the III:2 shows no structural change. (c) Chromatogram shows *POU4F3* heterozygous c.183delG detected in patients. (d) Audiograms of the affected subjects (red: right ear; blue: left ear).

shape. The hearing impairment of the proband was moderate. The proband had a history of using hearing aids, but the effect was unsatisfactory. With regard to other auditory-related symptoms, individual II:1 and the proband complained of tinnitus.

3.2. Variant Identification. According to the autosomal dominant pattern of inheritance, only variants that were heterozygous in the affected siblings were selected as candidates. Four novel variants were identified using targeted NGS of 168 known deafness-related genes in the four different ADNSHL Chinese families. Among the four novel variants, three were missense variants: c.696G>T (p.Glu232Asp) detected in family A, c.325C>T (p.His109Tyr) in family B, and c.635T>C (p.Leu212Pro) in family C. The fourth variant was a frameshift variant, c.183delG (p.Ala62Argfs*22), which was identified in family D. Sanger sequencing was performed in the other participating family members from these four families, which confirmed that these variants cosegregated with the hearing phenotypes (Figures 1–4(c)). The four variants have not been reported in previous studies and were not detected in 481 Chinese controls with normal hearing. The variants c.696G>T (p.Glu232Asp), c.635T>C (p.Leu212Pro), and c.183delG (p.Ala62Argfs*22) are not present in the gnomAD or ExAC database, and c.325C>T (p.His109Tyr) has an allele frequency of 0.0001 in both gnomAD (Asian)

and ExAC (Asian). The localizations of the four novel variants are shown in Figure 5(a). Conservation analysis was performed in the three families with missense variants (Figure 5(b)) and showed that the three variants are conserved among 11 species. Finally, the four novel variants were predicted to be deleterious by SIFT, Polyphen2, and CADD software. According to the American College of Medical Genetics and Genomics/Association for Molecular Pathology guidelines for genetic hearing loss [26, 27], c.696G>T (p.Glu232Asp) is classified as a likely pathogenic variant (PM1+PM2+PM5+PP1+PP3), c.325C>T (p.His109Tyr) is classified as a variant of uncertain significance (PP1), c.635T>C (p.Leu212Pro) is classified as a likely pathogenic variant (PM1+PM2+PP1+PP3), whereas c.183delG (p.Ala62Argfs*22) is classified as a pathogenic variant (PVS1+PM2+PP1) (Table 1).

4. Discussion

In mammals' cochlea, HCs are the key cell type for hearing function, which convert the mechanical vibrations into electronic neural signals [9]. HCs are sensitive to multiple stresses and injuries and are easy to damage. While a mammal's cochlea only has very limited HC regeneration ability, most of the HC damage is permanent and irreversible [28–34]. Genetic factor accounts for 50% of sensorineural hearing

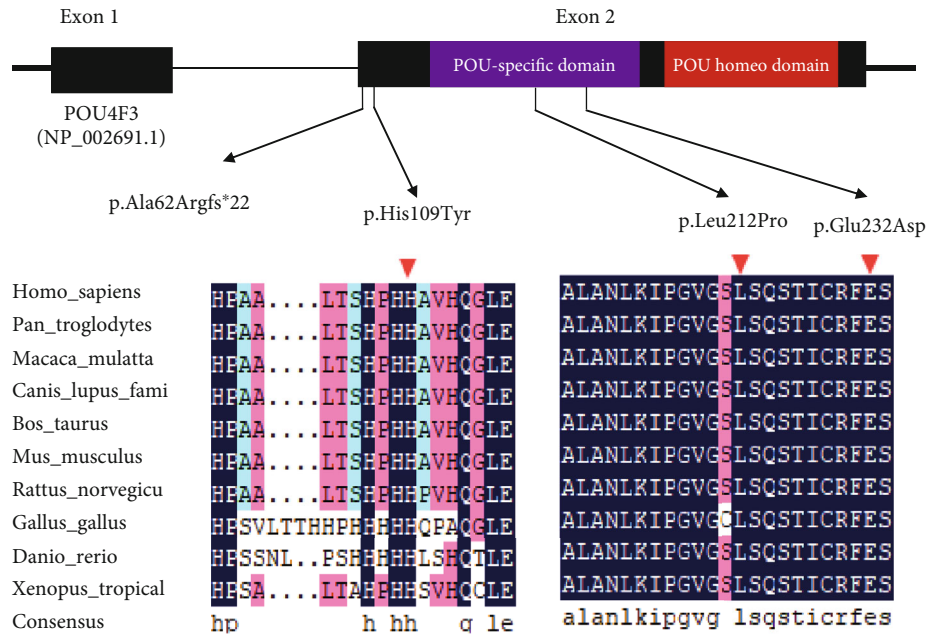


FIGURE 5: Protein structure of POU4F3 and conservation analysis. (a) Domain structure of POU4F3 showing the localization of four variants identified in this study. (b) Protein alignment showing that POU4F3 p.His109Tyr, p.Leu212Pro, and p.Glu232Asp all occur at evolutionarily conserved amino acids (shown by the red triangle) across 10 species.

loss. A genetic diagnosis is valuable for providing essential prognostic information needed for deciding optimal treatment/rehabilitation options and for genetic counseling [35]. Molecular epidemiological studies have found several common deafness genes in Chinese deafness population, such as *GJB2*, *SLC26A4*, and *mtDNA12SrRNA* [36]. However, genetic variants responsible for a large number of cases of hereditary hearing loss remain unknown. Next-generation sequencing has greatly increased the efficiency in screening known deafness genes for diagnostic purposes and in identifying new deafness genes [37–40].

In this study, we identified four novel variants in the *POU4F3* gene, three missense variants, and one frameshift variant, which led to sensorineural hearing loss in four different Chinese families. The variabilities in onset age and severity of hearing loss in these four families demonstrated the heterogeneity of these variants both interfamilial and intrafamilial.

In 1998, *POU4F3* was first discovered in an Israeli Jewish family. The results of a linkage analysis identified it as a novel independent locus for hearing loss, and the gene was designated as autosomal dominant nonsyndromic deafness 15 (DFNA15) [11]. The clinical presentation of DFNA15 is a form of progressive nonsyndromic sensorineural hearing loss with postlingual onset [13, 41]. In the present study, the earliest recorded age of hearing loss onset in affected individuals was 7 years old (III:1, family B). Among the 32 variants, 28 were reported in East Asian populations (13 in Japan, 12 in China, and 3 in Korea), and only 4 variants (2 in Netherlands, 1 in Israel, and 1 in Brazil) were reported from other areas, indicating that the *POU4F3* pathogenic variant is an important contributor to ADNSHL, especially in East Asian populations (Table 2). In summary, the variant of *POU4F3* is relatively common, especially in East Asian populations.

Therefore, screening of *POU4F3* should be a routine examination for the diagnosis of hereditary hearing loss. *POU4F3* contains only two exons, making it convenient for screening.

Hearing impairment involves mainly the middle frequency range (1000–2000 Hz) in a low percentage of cases of hereditary hearing loss. Kitano et al. reported that *POU4F3*-associated hearing loss usually presents with middle- or high-frequency hearing loss [14]. In 2018, we reported a family with middle-frequency hearing loss associated with *POU4F3* c.602T>C (p.Leu201Pro) [12]. In this study, the proband in family C presented with typical middle-frequency hearing loss, and the older patients showed downsloping audiograms and mainly middle- and high-frequency hearing loss. In accordance with our previous report, we proposed that the affected frequencies of certain types of *POU4F3*-associated hearing loss were in the order of middle (U-shaped audiogram), high (downsloping audiogram), and low frequencies (flatter audiogram). Accordingly, the different forms of auditory configuration represented different disease phases.

POU4F3 belongs to a family of proteins characterized by a well-conserved bipartite domain [42]. The bipartite domain is comprised of a POU-specific domain (amino acids 179–256) and a POU homeodomain (amino acids 274–333) separated by a linker [43]. These two domains are responsible for the main functions of *POU4F3*.

However, the specific mechanisms underlying sensorineural hearing loss caused by the *POU4F3* variant have remained unclear to date. Several previous studies have shown that although the wild-type *POU4F3* is localized almost exclusively in the nucleus, the mutant protein is also present in both the cytoplasm and the nucleus. Cytoplasmic localization of transcription factors obviously affects their

TABLE 1: Summary of the four *POU4F3* variants identified in this study.

Family	Nucleotide change	Amino acid change	hom/het	Allele frequency*	Pathogenicity	ACMG code	Computational evidence			Origin of variant	Cosegregation
							SIFT	PolyPhen	Mutation assessor		
A	c.696G>T	p.(Glu232Asp)	het	0.0001	Likely pathogenic	PM1+PM2+PM5+PP1+PP3	Deleterious	Probably damaging	High	De novo	Yes
B	c.325C>T	p.(His109Tyr)	het	—	Uncertain significance	PP1	Tolerated	Benign	Medium	De novo	Yes
C	c.635T>C	p.(Leu212Pro)	het	—	Likely pathogenic	PM1+PM2+PP1+PP3	Deleterious	Probably damaging	High	De novo	Yes
D	c.183delG	p.(Ala62Argfs*22)	het	—	Pathogenic	PVS1+PM2+PP1				De novo	Yes

*Allele frequency in East Asia reported by ExAC. hom: homozygous; het: heterozygous; —: no data. Notes: PVS1: null variant (nonsense, frameshift, canonical ± 1 or 2 splice sites, initiation codon, single, or multiexon deletion) in a gene where loss of function (LOF) is a known mechanism of disease; PM1: located in a mutational hot spot and/or critical and well-established functional domain (e.g., active site of an enzyme) without benign variation; PM2: a variant is absent from a large general population or a control cohort; PM5: novel missense change at an amino acid residue where a different missense change determined to be pathogenic has been seen before; PP1: segregation of a variant in a family; PP3: multiple lines of computational evidence support a deleterious effect on the gene or gene product.

TABLE 2: Summary of all reported pathogenic variants in *POU4F3*.

Number	Nucleotide change	Protein change	Exon	Domain	Onset age of hearing loss	Progression	Prevalence	Origin	Audiometric configuration	Reference
1	Whole deletion of <i>POU4F3</i>									
2	c.74dupA	p.His25fs*18	1		11~13 yo	Yes	N/A	Brazil	Flat and HF	Freitas et al. [13]
3	c.120+1G>C		1		~20 yo	Yes	15/602	Japan	HF	Kitano et al. [14]
4	c.183delG	p.A62Rfs*22	2		0~40 yo	Yes	3/16	China	Flat	He et al. [15]
5	c.191A>T	p.Asp64Val	2		25~44 yo	Yes	N/A	China	HF	This study
6	c.325C>T	p.His109Tyr	2		~30 yo	Yes	15/602	Japan	HF	Kitano et al. [14]
7	c.337C>T	p.Gln113Ter	2		7~30 yo	Yes	N/A	China	HF	This study
8	c.367delA	p.Ile123fs*3	2		14~40 yo	Yes	N/A	China		Zhang et al. [16]
9	c.427C>T	p.Gln143Ter	2		~40 yo	Yes	15/602	Japan	MF	Kitano et al. [14]
10	c.491C>G	p.Pro164Arg	2		3 yo	N/A	15/602	Japan	MF	Kitano et al. [14]
11	c.574G>T	p.Glu192Ter	2	POU	N/A	N/A	1/6	China	Flat and HF	Wei et al. [17]
12	c.581T>A	p.Phe194Tyr	2	POU	17~30 yo	Yes	15/602	Japan	HF	Kitano et al. [14]
13	c.602T>C	p.Leu201Pro	2	POU	20 yo	Yes	15/602	Japan	HF	Kitano et al. [14]
14	c.602delT	p.Leu201fs*3	2	POU	>10 yo	Yes	N/A	China	MF	Gao et al. [12]
15	c.603_604delGG	p.Val203Aspfs*11	2	POU	16~30 yo	Yes	N/A	China	HF	Cai et al. [18]
16	c.635T>C	p.Leu212Pro	2	POU	N/A	N/A	N/A	China	N/A	Yang et al. [19]
17	c.662_675del14	p.Gly221Gluufs*14	2	POU	10~20 yo	Yes	N/A	China	MF	This study
18	c.665C>T	p.Ser222Leu	2	POU	20 yo	N/A	1/42	Korea	HF	Lee et al. [20]
19	c.668T>C	p.Leu223Pro	2	POU	6 yo	Yes	15/602	Japan	HF	Kitano et al. [14]
20	c.680delC	p.Thr227fs*13	2	POU	13~20 yo	Yes	N/A	Netherlands	Flat, MF, and HF	Collin et al. [21]
21	c.694G>A	p.Glu232Lys	2	POU	0 yo	Yes	15/602	Japan	MF	Kitano et al. [14]
22	c.696G>T	p.Glu232Asp	2	POU	~20 yo	N/A	1/8	Korea	HF	Baek et al. [22]
23	c.718A>T	p.Asn240Tyr	2	POU	7~22 yo	Yes	N/A	China	HF	This study
24	c.841A>G	p.Ile281Val	2	POU homeobox	6 yo	Yes	15/602	Japan	MF	Kitano et al. [14]
25	c.865C>T	p.Leu289Phe	2	POU homeobox	50~54 yo	Yes	15/602	Japan	HF	Kitano et al. [14]
26	c.884_891del18	Ile295Thrfs*5	2	POU homeobox	13~20 yo	Yes	N/A	Netherlands	Flat, MF, and HF	Collin et al. [21]
27	c.896C>T	p.Pro299Leu	2	POU homeobox	18~30 yo	Yes	N/A	Israel	HF	Vahava et al. [11]
28	c.932T>C	p.Leu311Pro	2	POU homeobox	26~41 yo	Yes	15/602	Japan	MF	Kitano et al. [14]
29	c.976A>T	p.Arg326Ter	2	POU homeobox	10~20 yo	Yes	3/16	China	HF	He et al. [2]
30	c.977G>A	p.Arg326Lys	2	POU homeobox	Childhood	Yes	15/602	Japan	HF	Kitano et al. [14]
31	c.982A>G	p.Lys328Glu	2	POU homeobox	10~50 yo	N/A	N/A	Korea	HF	Kim et al. [41]
32	c.1007delC	p-Ala336fs*	2	POU homeobox	N/A	Yes	N/A	Taiwan	HF	Lin et al. [23]
					0 yo	Yes	1/3	Japan	N/A	Murai et al. [24]

yo: years old; HF: high frequency; MF: middle frequency; N/A: not available.

ability to activate downstream targets. Mutant proteins showed greatly reduced capability for binding to DNA as well as transcriptionally activating reporter gene expression [10, 16, 20, 21, 23]. One possible mechanism is that the variant in the POU homeodomain of *POU4F3* leads to a prematurely truncated protein with loss of the second and third helices, and the third helix is crucial for high-affinity binding to DNA; thus, the target gene cannot be induced, leading to impairment of inner ear hair cells [11].

Further studies showed that *POU4F3* contains two nuclear localization signals (NLSs): a monopartite NLS (amino acids 274–278) and bipartite NLS (amino acids 314–331) [10]. NLS is crucial for the trafficking of cytoplasmic proteins into the nucleus. Variant of *POU4F3* results in the absence of these two NLSs, which leads to subcellular protein mislocalization. The normal wild-type protein is localized mainly in the nucleus [44]. However, transient transfection studies revealed that NLS-mutated *POU4F3* proteins are localized mainly in the cytoplasm, most likely due to the absence of the NLSs. As *POU4F3* proteins are transcription factors, their function requires their entry into the nucleus and binding to DNA. In addition, the mutated *POU4F3* proteins have longer half-lives and much lower levels of transcriptional activity than those of the wild-type protein [11].

Although mice require only one copy of the functional *POU4F3* to retain hearing [45, 46], several previous studies supported that haploinsufficiency is the most likely molecular mechanism underlying the hearing loss caused by the *POU4F3* variant [13, 23, 24]. Heterozygous deletion of the entire *POU4F3* has been reported in a Brazilian family with ADNSHL [13]. Another study identified an ADNSHL-associated *POU4F3* heterozygous frameshift variant c.1007delC (p.Ala336fs*), which would produce a transcript without an in-frame stop codon, and presumably, the non-stop mRNA might be degraded through nonstop decay [24]. Both variants cause the loss of one copy of *POU4F3*, indicating the mechanism of haploinsufficiency [47]. Also, the subcellular protein mislocalization of mutant *POU4F3* shown in Lin et al. and other studies support the mechanism of haploinsufficiency [10, 16, 20]. ExAC pLI score of *POU4F3* is 0.721 which is not an indication for extreme loss of function intolerance. In addition, studies showed that the pathways downstream of *POU4F3* play crucial roles in the maintenance of inner ear hair cells, which also provides insight into the mechanisms underlying *POU4F3* mutation-induced hearing loss. A study performed in 2004 showed that the degeneration of outer hair cells caused by the *POU4F3* variant was mainly or entirely the result of inhibited expression of growth factor independence 1 (Gfi1), which is one of the target genes of *POU4F3* [46]. Gfi1 not only plays a late role in the differentiation and maintenance of hair cells but also promotes the formation of hair cells in cooperation with atonal BHLH transcription factor 1 (Atoh1) [48]. In addition, another study showed that Atoh1 is upstream of *POU4F3* and Gfi1 [49]. Thus, regulation of Atoh1 will affect the expression of Gfi1, and both Atoh1 and *POU4F3* are required for maintenance of Gfi1 expression [50]. Another possible mechanism is that the variant of *POU4F3* inhibits the expression of myosin VI, which plays a large role in the

maintenance of stereocilia of hair cells that are responsible for auditory transduction [51]. Tornari et al. reported that the orphan thyroid nuclear receptor Nr2f2, which is related to the development and survival of hair cells, is a target of *POU4F3* [52]. Although several downstream pathways and probable mechanisms have been reported, further studies are required to explore the mechanisms related to *POU4F3*.

In this study, we identified four novel variants in *POU4F3* (three missense variants and one frameshift variant) involved in hearing loss. The missense variant c.696G>T (p.Glu232Asp), detected in family A, is located in the POU-specific domain, and a different missense variant at the same locus, c.694G>A (p.Glu232Lys), has been reported previously [22]. The missense variant c.696G>T (p.Glu232Asp) in *POU4F3* leads to substitution of the glutamate at position 232 with an aspartic acid, which probably alters the structure of the α -helix of the POU-specific domain. The structural changes in the helix might affect the DNA-binding ability, what was probably responsible for the hearing loss in this family. The missense variant found in family C, c.635C>T (p.Leu212Pro), is also localized in the POU-specific domain, and it is possible that the mechanism of action is likely the same as described above. The missense variant observed in family B, c.325C>T (p.His109Tyr), is located in the transcriptional activation domain, which is not a functional domain, and this is likely why the hearing impairment in this family was mild. This variant is heterozygous in 0.016% (3/18,385 alleles) of East Asians, according to the gnomAD database. We speculate that its detection in the public database is due to the mild hearing loss associated with this variant. The frameshift variant, c.183delG (p.Ala62Argfs*22), identified in family D results in a truncated protein with loss of both functional domains crucial for high-affinity binding to DNA.

5. Conclusions

In summary, four novel variants in *POU4F3* were identified in four different families. These consisted of three missense variants, c.696G>T (p.Glu232Asp), c.325C>T (p.His109Tyr), and c.635C>T (p.Leu212Pro), and one frameshift variant, c.183delG (p.Ala62Argfs*22). These variants of *POU4F3* are considered to be responsible for ADNSHL, designated as DFNA15. *POU4F3* variants are not rare, and therefore, screening of *POU4F3* should be included in routine examinations for diagnosis of ADNSHL. Further studies are required to determine the specific mechanisms underlying hearing loss.

Data Availability

The patient's phenotype and the detected variants have been submitted to ClinVar (<https://www.ncbi.nlm.nih.gov/clinvar/>), and the Submission ID is SUB7170390.

Ethical Approval

This study was approved by the Ethics Committee of the Chinese People's Liberation Army General Hospital (reference number S2016-120-02).

Disclosure

The funders had no role in the study design, data collection and analysis, decision to publish, or preparation of the manuscript.

Conflicts of Interest

There are no financial relationships with any organizations that might have an interest in the submitted work, and there are no other relationships or activities that could appear to have influenced the submitted work.

Authors' Contributions

Tianyi Cui and Xue Gao contributed equally to this paper.

Acknowledgments

We sincerely thank all the family members for their participation and cooperation in this study. The English in this document has been checked by at least two professional editors, both native speakers of English. For a certificate, please see <http://www.textcheck.com/certificate/MccWLW>. This study was supported by grants from the National Key Research and Development Project of China (2016YFC1000706), National Natural Science Foundation of China (81873704), and Fostering Funds of Chinese PLA General Hospital for National Distinguished Young Scholar Science Fund (2017-JQPY-001) to Yong-Yi Yuan; a grant from the Foundation of the Second Hospital of Hebei Medical University (2h201816) to Qing-Wen Zhu; grants from the Beijing Natural Science Foundation (7192234) and National Natural Science Foundation of China (81570929) to Xue Gao; and a grant from the National Natural Science Foundation of China (81870731) to Sha-Sha Huang.

Supplementary Materials

In this study, we identified four novel variants using NGS of a panel of 168 deafness genes from four different Chinese families suffering from ADNSHL. The 168 deafness genes of the panel are listed concretely in Supplementary Table 1. (*Supplementary Materials*)

References

- [1] L. Liu, Y. Chen, J. Qi et al., "Wnt activation protects against neomycin-induced hair cell damage in the mouse cochlea," *Cell Death & Disease*, vol. 7, no. 3, p. e2136, 2016.
- [2] Z. He, L. Guo, Y. Shu et al., "Autophagy protects auditory hair cells against neomycin-induced damage," *Autophagy*, vol. 13, no. 11, pp. 1884–1904, 2017.
- [3] C. Zhu, C. Cheng, Y. Wang et al., "Loss of ARHGEF6 Causes Hair Cell Stereocilia Deficits and Hearing Loss in Mice," *Frontiers in Molecular Neuroscience*, vol. 11, p. 362, 2018.
- [4] W. Liu, X. Xu, Z. Fan et al., "Wnt Signaling Activates TP53-Induced Glycolysis and Apoptosis Regulator and Protects Against Cisplatin-Induced Spiral Ganglion Neuron Damage in the Mouse Cochlea," *Antioxidants & Redox Signaling*, vol. 30, no. 11, pp. 1389–1410, 2019.
- [5] Z. H. He, S. Y. Zou, M. Li et al., "The nuclear transcription factor FoxG1 affects the sensitivity of mimetic aging hair cells to inflammation by regulating autophagy pathways," *Redox Biology*, vol. 28, p. 101364, 2020.
- [6] R. J. H. Smith, J. F. Bale Jr., and K. R. White, "Sensorineural hearing loss in children," *Lancet*, vol. 365, no. 9462, pp. 879–890, 2005.
- [7] H. Kremer, "Hereditary hearing loss; about the known and the unknown," *Hearing Research*, vol. 376, pp. 58–68, 2019.
- [8] A. E. Shearer, M. S. Hildebrand, and R. J. H. Smith, "Hereditary hearing loss and deafness overview," in *GeneReviews*[®][Internet], University of Washington, Seattle, 2017.
- [9] B. C. Cox, R. Chai, A. Lenoir et al., "Spontaneous hair cell regeneration in the neonatal mouse cochlea in vivo," *Development*, vol. 141, no. 4, pp. 816–829, 2014.
- [10] S. Weiss, I. Gottfried, I. Mayrose et al., "The DFNA15 deafness mutation affects POU4F3 protein stability, localization, and transcriptional activity," *Molecular and Cellular Biology*, vol. 23, no. 22, pp. 7957–7964, 2003.
- [11] O. Vahava, R. Morell, E. D. Lynch et al., "Mutation in transcription factor POU4F3 associated with inherited progressive hearing loss in humans," *Science*, vol. 279, no. 5358, pp. 1950–1954, 1998.
- [12] X. Gao, J. C. Xu, W. Q. Wang et al., "A Missense Mutation in POU4F3 Causes Midfrequency Hearing Loss in a Chinese ADNSHL Family," *BioMed Research International*, vol. 2018, 7 pages, 2018.
- [13] É. L. Freitas, J. Oiticica, A. G. Silva, R. S. M. Bittar, C. Rosenberg, and R. C. Mingroni-Netto, "Deletion of the entire POU4F3 gene in a familial case of autosomal dominant non-syndromic hearing loss," *European Journal of Medical Genetics*, vol. 57, no. 4, pp. 125–128, 2014.
- [14] T. Kitano, M. Miyagawa, S.-y. Nishio et al., "POU4F3 mutation screening in Japanese hearing loss patients: Massively parallel DNA sequencing-based analysis identified novel variants associated with autosomal dominant hearing loss," *PLOS ONE*, vol. 12, no. 5, p. e0177636, 2017.
- [15] L. He, X. Pang, P. Chen, H. Wu, and T. Yang, "Mutation in the hair cell specific gene POU4F3 is a common cause for autosomal dominant nonsyndromic hearing loss in Chinese Hans," *Neural Plasticity*, vol. 2016, 6 pages, 2016.
- [16] C. Zhang, M. Wang, Y. Xiao et al., "A novel nonsense mutation of POU4F3 gene causes autosomal dominant hearing loss," *Neural Plasticity*, vol. 2016, 10 pages, 2016.
- [17] Q. Wei, H. Zhu, X. Qian et al., "Targeted genomic capture and massively parallel sequencing to identify novel variants causing Chinese hereditary hearing loss," *Journal of Translational Medicine*, vol. 12, no. 1, p. 311, 2014.
- [18] X. Z. Cai, Y. Li, L. Xia et al., "Exome sequencing identifies POU4F3 as the causative gene for a large Chinese family with non-syndromic hearing loss," *Journal of Human Genetics*, vol. 62, no. 2, pp. 317–320, 2017.
- [19] T. Yang, X. Wei, Y. Chai, L. Li, and H. Wu, "Genetic etiology study of the non-syndromic deafness in Chinese Hans by targeted next-generation sequencing," *Orphanet Journal of Rare Diseases*, vol. 8, no. 1, p. 85, 2013.
- [20] H. K. Lee, H. J. Park, K. Y. Lee, R. Park, and U. K. Kim, "A novel frameshift mutation of POU4F3 gene associated with autosomal dominant non-syndromic hearing loss," *Biochemical and Biophysical Research Communications*, vol. 396, no. 3, pp. 626–630, 2010.

- [21] R. W. J. Collin, R. Chellappa, R. J. Pauw et al., “Missense mutations in POU4F3 cause autosomal dominant hearing impairment DFNA15 and affect subcellular localization and DNA binding,” *Human Mutation*, vol. 29, no. 4, pp. 545–554, 2008.
- [22] J. I. Baek, S. K. Oh, D. B. Kim et al., “Targeted massive parallel sequencing: the effective detection of novel causative mutations associated with hearing loss in small families,” *Orphanet Journal of Rare Diseases*, vol. 7, no. 1, p. 60, 2012.
- [23] Y. H. Lin, Y. H. Lin, Y. C. Lu et al., “A novel missense variant in the nuclear localization signal of POU4F3 causes autosomal dominant non-syndromic hearing loss,” *Scientific Reports*, vol. 7, no. 1, p. 7551, 2017.
- [24] H. Mutai, N. Suzuki, A. Shimizu et al., “Diverse spectrum of rare deafness genes underlies early-childhood hearing loss in Japanese patients: a cross-sectional, multi-center next-generation sequencing study,” *Orphanet Journal of Rare Diseases*, vol. 8, no. 1, p. 172, 2013.
- [25] X. Gao, Y. Y. Yuan, Q. F. Lin et al., “Mutation of IFNLR1, an interferon lambda receptor 1, is associated with autosomal-dominant non-syndromic hearing loss,” *Journal of Medical Genetics*, vol. 55, no. 5, pp. 298–306, 2018.
- [26] S. Richards, on behalf of the ACMG Laboratory Quality Assurance Committee, N. Aziz et al., “Standards and guidelines for the interpretation of sequence variants: a joint consensus recommendation of the American College of Medical Genetics and Genomics and the Association for Molecular Pathology,” *Genetics in Medicine*, vol. 17, no. 5, pp. 405–423, 2015.
- [27] A. M. Oza, M. T. DiStefano, S. E. Hemphill et al., “Expert specification of the ACMG/AMP variant interpretation guidelines for genetic hearing loss,” *Human Mutation*, vol. 39, no. 11, pp. 1593–1613, 2018.
- [28] T. Wang, R. Chai, G. S. Kim et al., “Lgr5+ cells regenerate hair cells via proliferation and direct transdifferentiation in damaged neonatal mouse utricle,” *Nature Communications*, vol. 6, no. 1, 2015.
- [29] S. Zhang, Y. Zhang, Y. Dong et al., “Knockdown of Foxg1 in supporting cells increases the trans-differentiation of supporting cells into hair cells in the neonatal mouse cochlea,” *Cellular and Molecular Life Sciences*, vol. 77, no. 7, pp. 1401–1419, 2020.
- [30] X. Lu, S. Sun, J. Qi et al., “Bmi 1 regulates the proliferation of cochlear supporting cells via the canonical Wnt signaling pathway,” *Molecular Neurobiology*, vol. 54, no. 2, pp. 1326–1339, 2017.
- [31] F. Tan, C. Chu, J. Qi et al., “AAV-ie enables safe and efficient gene transfer to inner ear cells,” *Nature Communications*, vol. 10, no. 1, p. 3733, 2019.
- [32] C. Cheng, Y. Wang, L. Guo et al., “Age-related transcriptome changes in Sox2+ supporting cells in the mouse cochlea,” *Stem Cell Research & Therapy*, vol. 10, no. 1, p. 365, 2019.
- [33] S. Zhang, D. Liu, Y. Dong et al., “Frizzled-9+ supporting cells are progenitors for the generation of hair cells in the postnatal mouse cochlea,” *Frontiers in Molecular Neuroscience*, vol. 12, p. 184, 2019.
- [34] W. Yan, W. Liu, J. Qi et al., “A three-dimensional culture system with Matrigel promotes purified spiral ganglion neuron survival and function in vitro,” *Molecular Neurobiology*, vol. 55, no. 3, pp. 2070–2084, 2018.
- [35] ACMG Working Group on Update of Genetics Evaluation Guidelines for the Etiologic Diagnosis of Congenital Hearing Loss and for the Professional Practice and Guidelines Committee, “American College of Medical Genetics and Genomics guideline for the clinical evaluation and etiologic diagnosis of hearing loss,” *Genetics in Medicine*, vol. 16, no. 4, pp. 347–355, 2014.
- [36] Y. Yuan, Y. You, D. Huang et al., “Comprehensive molecular etiology analysis of nonsyndromic hearing impairment from typical areas in China,” *Journal of Translational Medicine*, vol. 7, no. 1, p. 79, 2009.
- [37] X. Lin, W. Tang, S. Ahmad et al., “Applications of targeted gene capture and next-generation sequencing technologies in studies of human deafness and other genetic disabilities,” *Hearing Research*, vol. 288, no. 1–2, pp. 67–76, 2012.
- [38] N. Idan, Z. Brownstein, S. Shivatzki, and K. B. Avraham, “Advances in genetic diagnostics for hereditary hearing loss,” *Journal of Basic and Clinical Physiology and Pharmacology*, vol. 24, no. 3, pp. 165–170, 2013.
- [39] C. M. Sloan-Heggen, A. O. Bierer, A. E. Shearer et al., “Comprehensive genetic testing in the clinical evaluation of 1119 patients with hearing loss,” *Human Genetics*, vol. 135, no. 4, pp. 441–450, 2016.
- [40] Y. Yuan, Q. Li, Y. Su et al., “Comprehensive genetic testing of Chinese SNHL patients and variants interpretation using ACMG guidelines and ethnically matched normal controls,” *European Journal of Human Genetics*, vol. 28, no. 2, pp. 231–243, 2020.
- [41] H. J. Kim, H. H. Won, K. J. Park et al., “SNP linkage analysis and whole exome sequencing identify a novel POU4F3 mutation in autosomal dominant late-onset nonsyndromic hearing loss (DFNA15),” *PLoS One*, vol. 8, no. 11, article e79063, 2013.
- [42] M. Wegner, D. W. Drolet, and M. G. Rosenfeld, “POU-domain proteins: structure and function of developmental regulators,” *Current Opinion in Cell Biology*, vol. 5, no. 3, pp. 488–498, 1993.
- [43] W. Herr and M. A. Cleary, “The POU domain: versatility in transcriptional regulation by a flexible two-in-one DNA-binding domain,” *Genes & Development*, vol. 9, no. 14, pp. 1679–1693, 1995.
- [44] M. Xiang, L. Gan, D. Li et al., “Essential role of POU-domain factor Brn-3c in auditory and vestibular hair cell development,” *Proceedings of the National Academy of Sciences of the United States of America*, vol. 94, no. 17, pp. 9445–9450, 1997.
- [45] E. M. Keithley, L. Erkman, T. Bennett, L. Lou, and A. F. Ryan, “Effects of a hair cell transcription factor, Brn-3.1, gene deletion on homozygous and heterozygous mouse cochleas in adulthood and aging,” *Hearing Research*, vol. 134, no. 1–2, pp. 71–76, 1999.
- [46] R. Hertzano, M. Montcouquiol, S. Rashi-Elkeles et al., “Transcription profiling of inner ears from Pou4f3ddl/ddl identifies Gfi1 as a target of the Pou4f3 deafness gene,” *Human Molecular Genetics*, vol. 13, no. 18, pp. 2143–2153, 2004.
- [47] A. A. Klauer and A. van Hoof, “Degradation of mRNAs that lack a stop codon: a decade of nonstop progress,” *Wiley Interdisciplinary Reviews: RNA*, vol. 3, no. 5, pp. 649–660, 2012.
- [48] A. Costa, L. M. Powell, S. Lowell, and A. P. Jarman, “Atoh1 in sensory hair cell development: constraints and cofactors,” *Seminars in Cell & Developmental Biology*, vol. 65, pp. 60–68, 2017.
- [49] D. Wallis, M. Hamblen, Y. Zhou et al., “The zinc finger transcription factor Gfi1, implicated in lymphomagenesis, is

required for inner ear hair cell differentiation and survival,” *Development*, vol. 130, no. 1, pp. 221–232, 2003.

- [50] K. T. Chonko, I. Jahan, J. Stone et al., “*Atoh1* directs hair cell differentiation and survival in the late embryonic mouse inner ear,” *Developmental Biology*, vol. 381, no. 2, pp. 401–410, 2013.
- [51] D. B. Ma, J. Chen, Y. Xia et al., “Inhibition of *Myo6* gene expression by co-expression of a mutant of transcription factor POU4F3 (BRN-3C) in hair cells,” *Molecular Medicine Reports*, vol. 9, no. 4, pp. 1185–1190, 2014.
- [52] C. Tornari, E. R. Towers, J. E. Gale, and S. J. Dawson, “Regulation of the orphan nuclear receptor *Nr2f2* by the DFNA15 deafness gene *Pou4f3*,” *PLoS One*, vol. 9, no. 11, article e112247, 2014.

Research Article

Targeted Next-Generation Sequencing Identified Compound Heterozygous Mutations in *MYO15A* as the Probable Cause of Nonsyndromic Deafness in a Chinese Han Family

Longhao Wang,^{1,2,3} Lin Zhao,⁴ Hu Peng,^{2,3,5} Jun Xu,^{2,3,6} Yun Lin,^{2,3,6} Tao Yang^{1,2,3,6} and Hao Wu^{1,2,3,6}

¹Department of Otorhinolaryngology-Head and Neck Surgery, Xinhua Hospital, Shanghai Jiao Tong University School of Medicine, Shanghai 200092, China

²Ear Institute, Shanghai Jiao Tong University School of Medicine, Shanghai 200125, China

³Shanghai Key Laboratory of Translational Medicine on Ear and Nose Diseases, Shanghai 200125, China

⁴Department of Health Management Center, Shanghai Eastern Hepatobiliary Surgery Hospital, Shanghai 200438, China

⁵Department of Otorhinolaryngology-Head and Neck Surgery, Changzheng Hospital, Second Military Medical University, Shanghai 200003, China

⁶Department of Otorhinolaryngology-Head and Neck Surgery, Ninth People's Hospital, Shanghai Jiao Tong University School of Medicine, Shanghai 200011, China

Correspondence should be addressed to Tao Yang; yangtfxl@sina.com and Hao Wu; haowu@sh-jei.org

Received 20 February 2020; Revised 10 May 2020; Accepted 29 May 2020; Published 15 June 2020

Academic Editor: Renjie Chai

Copyright © 2020 Longhao Wang et al. This is an open access article distributed under the Creative Commons Attribution License, which permits unrestricted use, distribution, and reproduction in any medium, provided the original work is properly cited.

Hearing loss is a highly heterogeneous disorder, with more than 60% of congenital cases caused by genetic factors. This study is aimed at identifying the genetic cause of congenital hearing loss in a Chinese Han family. Auditory evaluation before and after cochlear implantation and targeted next-generation sequencing of 140 deafness-related genes were performed for the deaf proband. Compound heterozygous mutations c.3658_3662del (p. E1221Wfs*23) and c.6177+1G>T were identified in *MYO15A* as the only candidate pathogenic mutations cosegregated with the hearing loss in this family. These two variants were absent in 200 normal-hearing Chinese Hans and were classified as likely pathogenic and pathogenic, respectively, based on the ACMG guideline. Our study further expanded the mutation spectrum of *MYO15A* as the c.3658_3662del mutation is novel and confirmed that deaf patients with recessive *MYO15A* mutations have a good outcome for cochlear implantation.

1. Introduction

Approximately one in every 1000 newborns is affected by congenital hearing loss, and genetic factors account for more than 60% of them [1]. To date, more than 100 deafness-causative genes have been found. Among them, autosomal recessive nonsyndromic hearing loss (ARNSHL) accounts for up to 80% of nonsyndromic hearing loss [2], with more than 70 causative genes being identified (<http://hereditaryhearingloss.org/>).

Stereocilia is critical for the development and function of cochlear hair cells (HCs) [3–5]. The *MYO15A* gene contains 66 coding exons [6], which encode an unconventional myo-

sin (myosin XVA) expressed at the tips of stereocilia in the cochlear HCs. Myosin XVA is essential for the mechano-transduction function of cochlear HCs. Myosin XVA interacts with the PDZ domain of whirlin and then delivers whirlin to the tips of stereocilia [7]. Myosin XVA-deficient mouse (shaker-2) shows abnormally short stereocilia bundles and diminished staircase [8–10]. In humans, mutations in *MYO15A* have been found to lead to recessive nonsyndromic deafness DFNB3 [11]. The prevalence of *MYO15A* mutations varies among different ethnic populations (3%–6.7%) and appears to be the third or fourth most frequent causes of ARNSHL [12–15].

Here, we report a nonconsanguineous Chinese Han family with profound ARNSHL, in which compound heterozygous mutations in *MYO15A* were identified as the probable cause of the deafness.

2. Materials and Methods

2.1. Subjects. A Chinese Han recessive deafness family (Figure 1) was enrolled in this study. All family members underwent clinical evaluation in the Department of Otolaryngology-Head and Neck Surgery, Xinhua Hospital, Shanghai Jiao Tong University School of Medicine. The evaluation included a detailed clinical interview and physical examination. As shown in Figure 2(a), the proband had bilateral profound deafness. This study was approved by the ethnic committee of Xinhua Hospital. Written informed consent was obtained for each participant.

2.2. Audiometric Evaluation. Audiometric assessments included otoscopic examination, pure tone audiometry (PTA), auditory brainstem response (ABR), and multiple steady-state responses (ASSR). Hearing level was assessed at 250, 500, 1000, 2000, 4000, and 8000 Hz. The hearing threshold was defined as the average of both sides. Inner-ear malformation and dysplasia of the auditory nerve related to the hearing loss were excluded by temporal bone Computerized Tomography (CT) scan and cranial Magnetic Resonance Imaging (MRI).

2.3. Mutation Identification. Blood samples were collected into an EDTA anticoagulant tube by venipuncture of the cubital vein. Extraction of genomic DNA was performed using a blood DNA extraction kit (QIAamp DNA Blood Mini Kit, Qiagen, Shanghai). As the first step, mutations in common deafness genes *GJB2*, *SLC26A4*, and *MT-RNR1* were excluded by Sanger sequencing. Targeted next-generation sequencing was then performed in the proband as previously reported [16]. A total of 140 known deafness-related genes were captured by a customized capture assay (MyGenostics, Beijing, China) (Supplementary Table 1). The targeted region included exon, splicing sites, and flanking intron region. Then, potentially candidate variants such as missense, nonsense, and indel variants and the splice site were screened for quality, and variants with minor allele frequencies (MAFs) below 0.005 were further studied using public databases including dbSNP, 1000 Genomes Project, and Exome Aggregation Consortium (EXAC) and in-house data from 200 ethnically matched normal-hearing controls. Intrafamilial segregation of the candidate mutations was examined by Sanger sequencing. The potential pathogenic effects of the candidate mutations were predicted by computational tools including PolyPhen-2, SIFT, and PROVEAN and classified following the American College of Medical Genetics and Genomics (ACMG) guidelines for the interpretation of sequence variants in 2015 [17]. Human Splicing Finder (HSF) (<http://www.umd.be/HSF3/>) was used to calculate the consensus values of potential splice sites.

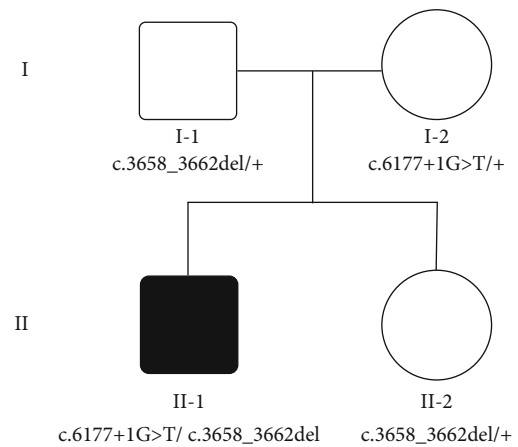
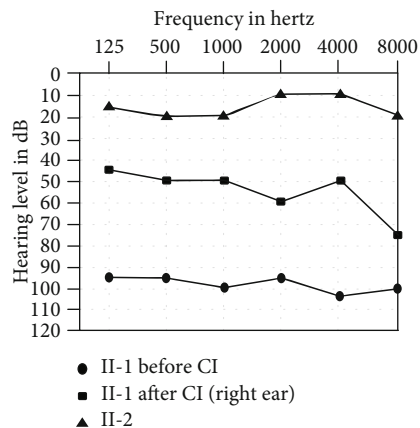


FIGURE 1: Pedigree and genotype of the Chinese Han family with *MYO15A* mutations.

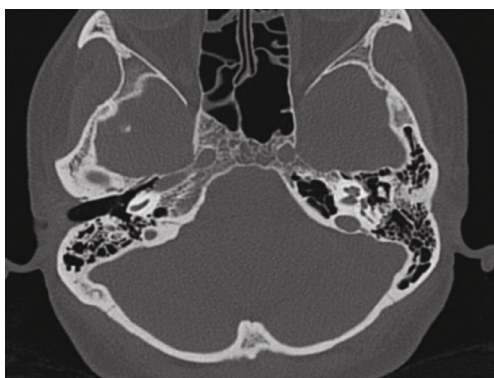
3. Results

3.1. Clinical Characterization. The proband was a 14-year-old male from Zhejiang Province, China. He had congenital, bilateral, profound hearing impairment with a threshold above 95 dBHL as revealed by the PTA (Figure 2(a)) and ABR tests. Hearing levels of this patient and his sister were normal. Otoacoustic emissions were absent for both ears. Temporal CT and cranial MRI showed no abnormalities (Figures 2(b) and 2(c)). No vestibular dysfunction was complained. No apparent syndromic features were found in the physical examination. The proband received unilateral cochlear implantation (Nucleus 5, Cochlear Corporation, Australia) through a typical round window route uneventfully at 12 years old. Hearing was markedly improved after cochlear implantation (Figure 2(a)).

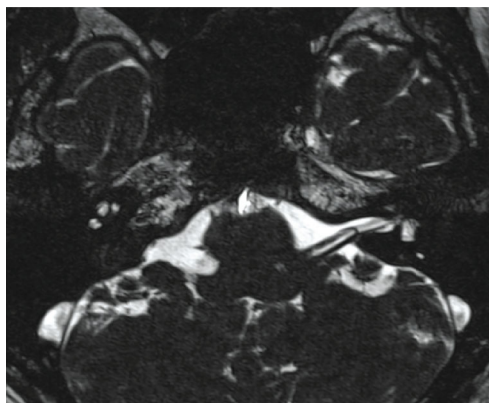
3.2. Mutation Analysis. By targeted next-generation sequencing of 140 deafness-causative genes in the proband, compound heterozygous mutations c.3658_3662del and c.6177+1>T in *MYO15A* (NM_016239) were identified as the only candidate pathogenic mutations consistent with a presumably autosomal recessive inheritance. The mean depth of sequencing was 364.43X, and 98% of the targeted region was covered with at least 20X. Cosegregation of these two mutations with the hearing phenotype was confirmed within the family members (Figure 3). These two variants were not seen in public databases dbSNP, 1000 Genomes Project, and EXAC and the in-house databases of 200 Chinese Han normal-hearing controls. The frameshifting c.3658_3662del (p.E1221Wfs*23) mutation is located in exon 3, and it is novel and is predicted to result in a truncated protein after the motor domain (Figure 3). The c.6177+1G>T splice site mutation was previously reported in another Chinese Han family [18] and is predicted to result in an in-frame skipping of exon 26 and a protein product with 17-residue deletion in the first MyTH4 domain. Following the ACMG guideline in 2015 [17], the c.3658_3662del and c.6177+1>T mutations were classified as likely pathogenic (PVS2+PM2) and pathogenic (PVS1+PS1+PM2), respectively.



(a)



(b)



(c)

FIGURE 2: (a) Audiogram of the proband (II-1) before and after cochlear implantation and that of his unaffected sister (II-2). (b) Temporal bone Computerized Tomography (CT) scan of the proband (II-1). (c) Cranial Magnetic Resonance Imaging (MRI) of the proband (II-1).

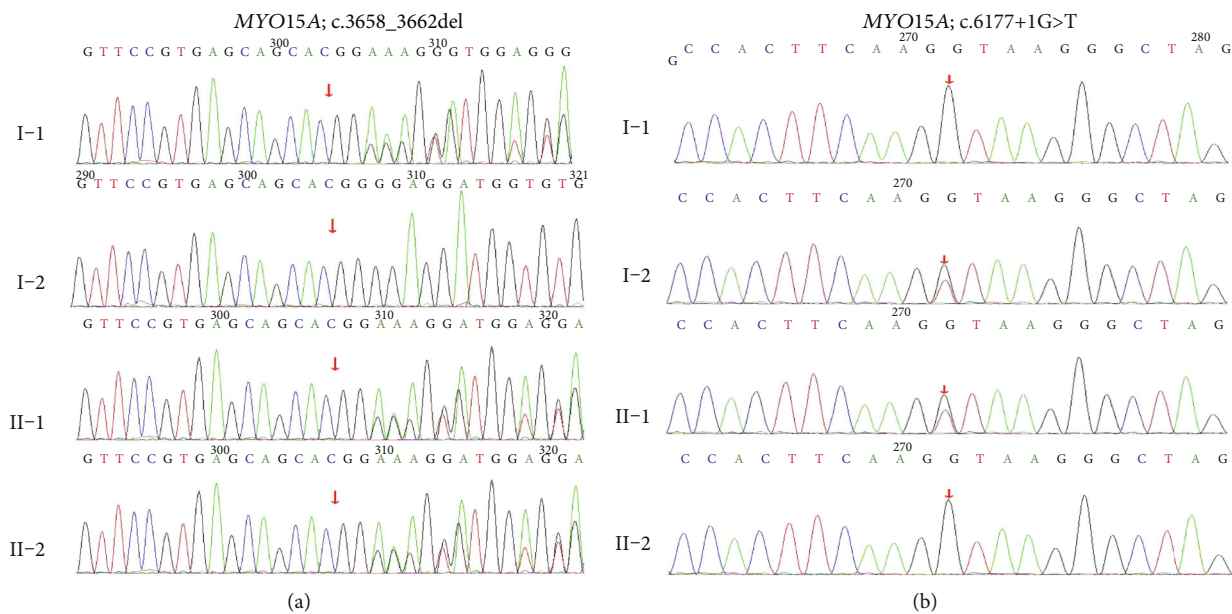


FIGURE 3: Sanger sequencing results of the c.3658_3662del and c.6177+1G>T mutations in the family members.

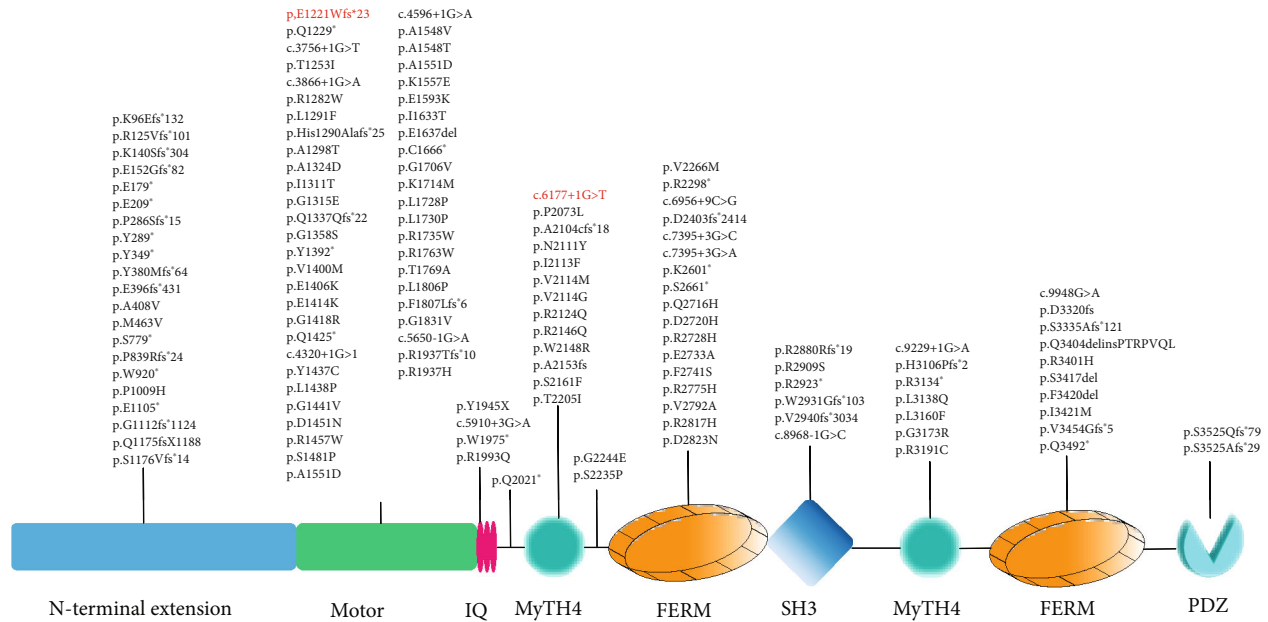


FIGURE 4: Schematic representation of the reported mutations in *MYO15A* and the corresponding protein structure. Mutations identified in this study were marked in red.

4. Discussion

HCs in the cochlea play a critical role in converting mechanical sound waves into neural signals for hearing, and most of the hearing loss induced by gene mutation, noise, different ototoxic drugs, inflammation, or aging is caused by the HC malfunction [19–27]. The association between *MYO15A* mutations and recessive deafness DFNB3 was first discovered by Friedman et al. in Bali, Indonesia [28], in which two missense mutations and one nonsense mutation in *MYO15A*, all in a homozygous state, result in congenital, severe-to-profound hearing loss [11]. To date, more than 100 mutations in *MYO15A* have been reported, mostly reported in consanguineous families from the Middle East [27, 29–35]. In this study, two variants p.E1221Wfs*23 and c.6177+1G>T in *MYO15A* were identified. Like many previously reported truncating mutations in *MYO15A*, the p.E1221Wfs*23 variant is predicted to result in a truncated protein product without Motor, IQ, MyTH4, FERM, SH3, and PDZ domains (Figure 4). The c.6177+1G>T variant was previously reported in another Chinese Han family by Chen et al. [18], suggesting that this mutation may be either a founder mutation or a reoccurrent hot spot. This mutation resides in the consensus splice acceptor site adjacent to exon 26 and is predicted to lead to an in-frame exon 26 skipping and a 17-amino acid residue deletion in the first myosin tail homology 4 (MyTH4) domain of myosin XVA. The MyTH4 domain provides a link between actin-based kinesin and the microtubule cytoskeleton. Mutation in this domain can disrupt the protein-protein interaction that is important for mechanotransduction of hearing [7].

Most recessive mutations in *MYO15A* are associated with congenital, severe-to-profound deafness [31, 33, 36], except for mutations affecting the N-terminal domain of MYOXVA

which may result in milder hearing loss with residual hearing of low frequency [37]. Both variants identified in our study are located outside of the N-terminal domain, and the associated profound hearing loss is consistent with the genotype-phenotype correlation for DFNB3 deafness. Consistent with the specific role of *MYO15A* in the sensory HCs, the proband in our study had a marked improvement for hearing after cochlear implantation, showing a good prospective outcome for a similar procedure in other DFNB3 patients.

5. Conclusion

The p.E1221Wfs*23 and c.6177+1G>T compound heterozygous mutations in *MYO15A* are the probable cause of congenital, profound deafness in the Chinese Han family. Patients with recessive mutations in *MYO15A* may markedly benefit from cochlear implantation.

Data Availability

The data underlying the findings of this study is available upon request.

Conflicts of Interest

The authors declare no conflicts of interests.

Authors' Contributions

Longhao Wang, Lin Zhao, and Hu Peng contributed equally to this work.

Acknowledgments

This research was supported by grants from the National Key R&D Program of China (2017YFC1001804 to HW), National Science Foundation of China (81730028 to HW, 81702643 to HP), Shanghai Municipal Science and Technology Commission (14DZ2260300 to HW) and Shanghai Municipal Education Commission—Gaofeng Clinical Medicine Grant (20152519 to TY), and Science Project of Shanghai Municipal Commission of Health and Family Planning (201540173 to HP).

Supplementary Materials

Supplementary Table 1: the 140 deafness-causative genes for targeted next-generation sequencing. (*Supplementary Materials*)

References

- [1] C. C. Morton and W. E. Nance, “Newborn hearing screening—a silent revolution,” vol. 354, pp. 2151–2164, 2006.
- [2] G. Van Camp, P. J. Willems, and R. J. Smith, “Nonsyndromic hearing impairment: unparalleled heterogeneity,” *American Journal of Human Genetics*, vol. 60, no. 4, pp. 758–764, 1997.
- [3] J. Qi, Y. Liu, C. Chu et al., “A cytoskeleton structure revealed by super-resolution fluorescence imaging in inner ear hair cells,” *Cell Discovery*, vol. 5, no. 1, 2019.
- [4] Y. Liu, J. Qi, X. Chen et al., “Critical role of spectrin in hearing development and deafness,” *Science Advances*, vol. 5, no. 4, p. eaav7803, 2019.
- [5] J. Qi, L. Zhang, F. Tan et al., “Espin distribution as revealed by super-resolution microscopy of stereocilia,” *American Journal of Translational Research*, vol. 12, pp. 130–141, 2020.
- [6] Y. Liang, A. Wang, I. A. Belyantseva et al., “Characterization of the Human and Mouse Unconventional Myosin XV Genes Responsible for Hereditary Deafness *DFNB3* and *Shaker 2*,” *Genomics*, vol. 61, no. 3, pp. 243–258, 1999.
- [7] I. A. Belyantseva, E. T. Boger, S. Naz et al., “Myosin-XVa is required for tip localization of whirlin and differential elongation of hair-cell stereocilia,” *Nature Cell Biology*, vol. 7, no. 2, pp. 148–156, 2005.
- [8] D. W. Anderson, F. J. Probst, I. A. Belyantseva et al., “The motor and tail regions of myosin XV are critical for normal structure and function of auditory and vestibular hair cells,” *Human Molecular Genetics*, vol. 9, no. 12, pp. 1729–1738, 2000.
- [9] I. J. Karolyi, F. J. Probst, L. Beyer et al., “*Myo15* function is distinct from *Myo6*, *Myo7a* and *pirouette* genes in development of cochlear stereocilia,” *Human Molecular Genetics*, vol. 12, no. 21, pp. 2797–2805, 2003.
- [10] F. J. Probst, R. A. Fridell, Y. Raphael et al., “Correction of deafness in *shaker-2* mice by an unconventional myosin in a BAC transgene,” *Science*, vol. 280, no. 5368, pp. 1444–1447, 1998.
- [11] A. Wang, Y. Liang, R. A. Fridell et al., “Association of unconventional myosin *MYO15* mutations with human nonsyndromic deafness *DFNB3*,” *Science*, vol. 280, no. 5368, pp. 1447–1451, 1998.
- [12] M. Miyagawa, S.-y. Nishio, M. Hattori et al., “Mutations in the *MYO15A* Gene are a significant cause of nonsyndromic hearing loss,” *Annals of Otolaryngology & Laryngology*, vol. 124, 1_suppl, pp. 158S–168S, 2015.
- [13] Y. Li, A. W. Lin, X. Zhang, Y. Wang, X. Wang, and D. W. Goodrich, “Cancer cells and normal cells differ in their requirements for *Thoc1*,” *Cancer Research*, vol. 67, no. 14, pp. 6657–6664, 2007.
- [14] T. Yang, X. Wei, Y. Chai, L. Li, and H. Wu, “Genetic etiology study of the non-syndromic deafness in Chinese Hans by targeted next-generation sequencing,” *Orphanet Journal of Rare Diseases*, vol. 8, no. 1, p. 85, 2013.
- [15] Z. Fattahi, A. E. Shearer, M. Babanejad et al., “Screening for *MYO15A* gene mutations in autosomal recessive nonsyndromic, *GJB2* negative Iranian deaf population,” *American Journal of Medical Genetics Part A*, vol. 158A, no. 8, pp. 1857–1864, 2012.
- [16] X. Wang, L. Wang, H. Peng, T. Yang, and H. Wu, “A Novel p.G141R Mutation in *ILDRI* Leads to Recessive Nonsyndromic Deafness *DFNB42* in Two Chinese Han Families,” *Neural Plasticity*, vol. 2018, Article ID 7272308, 6 pages, 2018.
- [17] ACMG Working Group on Update of Genetics Evaluation Guidelines for the Etiologic Diagnosis of Congenital Hearing Loss; for the Professional Practice and Guidelines Committee, “American College of Medical Genetics and Genomics guideline for the clinical evaluation and etiologic diagnosis of hearing loss,” *Genetics in Medicine*, vol. 16, no. 4, pp. 347–355, 2014.
- [18] S. Chen, C. Dong, Q. Wang et al., “Targeted next-generation sequencing successfully detects causative genes in Chinese patients with hereditary hearing loss,” *Genetic Testing and Molecular Biomarkers*, vol. 20, no. 11, pp. 660–665, 2016.
- [19] H. Li, Y. Song, Z. He et al., “Meclofenamic acid reduces reactive oxygen species accumulation and apoptosis, inhibits excessive autophagy, and protects hair cell-like HEI-OC1 cells from cisplatin-induced damage,” *Frontiers in Cellular Neuroscience*, vol. 12, 2018.
- [20] L. Liu, Y. Chen, J. Qi et al., “Wnt activation protects against neomycin-induced hair cell damage in the mouse cochlea,” *Cell Death & Disease*, vol. 7, no. 3, article e2136, 2016.
- [21] S. Gao, C. Cheng, M. Wang et al., “Blebbistatin inhibits neomycin-induced apoptosis in hair cell-like HEI-OC-1 cells and in cochlear hair cells,” *Frontiers in Cellular Neuroscience*, vol. 13, p. 590, 2020.
- [22] S. Zhang, Y. Zhang, Y. Dong et al., “Knockdown of *Foxg1* in supporting cells increases the trans-differentiation of supporting cells into hair cells in the neonatal mouse cochlea,” *Cellular and Molecular Life Sciences*, vol. 77, no. 7, pp. 1401–1419, 2020.
- [23] Y. Zhang, W. Li, Z. He et al., “Pre-treatment with fasudil prevents neomycin-induced hair cell damage by reducing the accumulation of reactive oxygen species,” *Frontiers in Molecular Neuroscience*, vol. 12, p. 264, 2019.
- [24] Z. He, L. Guo, Y. Shu et al., “Autophagy protects auditory hair cells against neomycin-induced damage,” *Autophagy*, vol. 13, no. 11, pp. 1884–1904, 2017.
- [25] Z. He, Q. Fang, H. Li et al., “The role of *FOXG1* in the postnatal development and survival of mouse cochlear hair cells,” *Neuropharmacology*, vol. 144, pp. 43–57, 2019.
- [26] Z.-h. He, S.-y. Zou, M. Li et al., “The nuclear transcription factor *FoxG1* affects the sensitivity of mimetic aging hair cells to inflammation by regulating autophagy pathways,” *Redox Biology*, vol. 28, article 101364, 2020.

- [27] X. Yu, Y. Lin, J. Xu et al., “Molecular epidemiology of Chinese Han deaf patients with bi-allelic and mono-allelic GJB2 mutations,” *Orphanet Journal of Rare Diseases*, vol. 15, no. 1, p. 29, 2020.
- [28] T. B. Friedman, Y. Liang, J. L. Weber et al., “A gene for congenital, recessive deafness *DFNB3* maps to the pericentromeric region of chromosome 17,” *Nature Genetics*, vol. 9, no. 1, pp. 86–91, 1995.
- [29] C.-C. Wu, C.-Y. Tsai, Y.-H. Lin et al., “Genetic epidemiology and clinical features of hereditary hearing impairment in the Taiwanese population,” *Genes*, vol. 10, no. 10, p. 772, 2019.
- [30] S. S. Di Ma, H. Gao, H. Guo et al., “A novel nonsense mutation in *MYO15A* is associated with non-syndromic hearing loss: a case report,” *BMC Medical Genetics*, vol. 19, no. 1, p. 133, 2018.
- [31] H. Zhou, A. Kuermanhan, Z. Zhang et al., “Identification of a novel homozygous mutation in the *MYO15A* gene in a Kazakh family with non-syndromic hearing loss,” *International Journal of Pediatric Otorhinolaryngology*, vol. 125, pp. 128–132, 2019.
- [32] N. Danial-Farran, Z. Brownstein, S. Gulsuner et al., “Genetics of hearing loss in the Arab population of Northern Israel,” *European Journal of Human Genetics*, vol. 26, no. 12, pp. 1840–1847, 2018.
- [33] N. Zarepour, M. Koohiyan, A. Taghipour-Sheshdeh et al., “Identification and clinical implications of a novel *MYO15A* variant in a consanguineous Iranian family by targeted exome sequencing,” *Audiology & Neurotology*, vol. 24, no. 1, pp. 25–31, 2019.
- [34] R. Cabanillas, M. Diñeiro, G. A. Cifuentes et al., “Comprehensive genomic diagnosis of non-syndromic and syndromic hereditary hearing loss in Spanish patients,” *BMC Medical Genomics*, vol. 11, no. 1, p. 58, 2018.
- [35] Z. Brownstein, L. M. Friedman, H. Shahin et al., “Targeted genomic capture and massively parallel sequencing to identify genes for hereditary hearing loss in Middle Eastern families,” *Genome Biology*, vol. 12, no. 9, p. R89, 2011.
- [36] J. Zhang, J. Guan, H. Wang et al., “Genotype-phenotype correlation analysis of *MYO15A* variants in autosomal recessive non-syndromic hearing loss,” *BMC Medical Genetics*, vol. 20, no. 1, p. 60, 2019.
- [37] N. Nal, Z. M. Ahmed, E. Erkal et al., “Mutational spectrum of *MYO15A*: the large N-terminal extension of myosin XVA is required for hearing,” *Human Mutation*, vol. 28, no. 10, pp. 1014–1019, 2007.

Research Article

Involvement of Cholesterol Metabolic Pathways in Recovery from Noise-Induced Hearing Loss

Na Sai ^{1,2,3,4}, Xi Shi,⁵ Yan Zhang,⁶ Qing-qing Jiang,^{1,2,3,4} Fei Ji,^{1,2,3,4} Shuo-long Yuan,^{1,2,3,4} Wei Sun,⁷ Wei-Wei Guo ^{1,2,3,4}, Shi-Ming Yang ^{1,2,3,4} and Wei-Ju Han ^{1,2,3,4}

¹College of Otolaryngology Head and Neck Surgery, Chinese PLA General Hospital, Beijing 100853, China

²National Clinical Research Center for Otolaryngologic Diseases, Beijing, China

³Key Lab of Hearing Science, Ministry of Education, China

⁴Beijing Key Lab of Hearing Impairment for Prevention and Treatment, Beijing, China

⁵Clinical Hearing Center of Affiliated Hospital of Xuzhou Medical College, Xuzhou, China

⁶Department of Otorhinolaryngology Head and Neck Surgery, The First Hospital of Jilin University, Changchun, Jilin 130021, China

⁷Department of Communicative Disorders and Sciences, Center for Hearing and Deafness, The State University of New York at Buffalo, Buffalo, New York, USA

Correspondence should be addressed to Wei-Wei Guo; gwent001@163.com, Shi-Ming Yang; yangsm301@263.net, and Wei-Ju Han; hanweiju@aliyun.com

Received 21 February 2020; Revised 8 May 2020; Accepted 15 May 2020; Published 12 June 2020

Academic Editor: Renjie Chai

Copyright © 2020 Na Sai et al. This is an open access article distributed under the Creative Commons Attribution License, which permits unrestricted use, distribution, and reproduction in any medium, provided the original work is properly cited.

The objective of this study was to explore the molecular mechanisms of acute noise-induced hearing loss and recovery of steady-state noise-induced hearing loss using miniature pigs. We used miniature pigs exposed to white noise at 120 dB (A) as a model. Auditory brainstem response (ABR) measurements were made before noise exposure, 1 day and 7 days after noise exposure. Proteomic Isobaric Tags for Relative and Absolute Quantification (iTRAQ) was used to observe changes in proteins of the miniature pig inner ear following noise exposure. Western blot and immunofluorescence were performed for further quantitative and qualitative analysis of proteomic changes. The average ABR-click threshold of miniature pigs before noise exposure, 1 day and 7 days after noise exposure, were 39.4 dB SPL, 67.1 dB SPL, and 50.8 dB SPL, respectively. In total, 2,158 proteins were identified using iTRAQ. Both gene ontology and Kyoto Encyclopedia of Genes and Genomes (KEGG) database analyses showed that immune and metabolic pathways were prominently involved during the impairment stage of acute hearing loss. During the recovery stage of acute hearing loss, most differentially expressed proteins were related to cholesterol metabolism. Western blot and immunofluorescence showed accumulation of reactive oxygen species and nuclear translocation of NF- κ B (p65) in the hair cells of miniature pig inner ears during the acute hearing loss stage after noise exposure. Nuclear translocation of NF- κ B (p65) may be associated with overexpression of downstream inflammatory factors. Apolipoprotein (Apo) A1 and Apo E were significantly upregulated during the recovery stage of hearing loss and may be related to activation of cholesterol metabolic pathways. This is the first study to use proteomics analysis to analyze the molecular mechanisms of acute noise-induced hearing loss and its recovery in a large animal model (miniature pigs). Our results showed that activation of metabolic, inflammatory, and innate immunity pathways may be involved in acute noise-induced hearing loss, while cholesterol metabolic pathways may play an important role in recovery of hearing ability following noise-induced hearing loss.

1. Introduction

Noise-induced hearing loss (NIHL) is the most common form of nonhereditary sensorineural hearing loss, the incidence which is increasing annually. An epidemiological

survey from 2005 showed that, worldwide, roughly 16% of cases of adult hearing loss were caused primarily by noise overexposure at work [1]. A recent investigation of American adults under 70 years old was performed by the Centers for Disease Control. The results showed that there are roughly

26 million people with NIHL, with prevalence rate of 15%. Furthermore, over 16% of American teenagers (12–19 years old) were shown to have hearing loss caused by excessive noise exposure [2]. NIHL has emerged as a heavy burden to daily communication for patients and for their physical and mental health.

Hair cells in the cochlea play a critical role in converting mechanical sound waves into neural signals for hearing [3–5]. Previous studies using mouse models showed that acoustic injury of the auditory system is caused by multiple factors, and most of the hearing loss induced by noise, different ototoxic drugs, infection, or aging are caused by the hair cells damage [6–13]. Impulse noise (>140 dB SPL) causes hearing loss primarily through mechanical damage of hair cells [14], while steady noise causes metabolic damage of hair cells [15]. However, the complex molecular pathways involved in NIHL remain incompletely understood.

Miniature pigs, which share numerous similarities with humans in terms of inner ear morphology and hearing function, represent a novel large animal model for studying NIHL. Except for primates, pigs and humans have the closest evolutionary relationship, sharing similarities in genetic, anatomical, and physiological factors. The structure of the pig inner ear is very similar to that of humans, and the size of the pig cochlear scala tympani is mostly the same as in humans [16, 17]. These observations suggest that the nerve nuclei of the entire auditory pathway of pigs are highly similar to those of humans. Therefore, the pig model is more suitable than rodents for studying NIHL.

Proteomic Isobaric Tags for Relative and Absolute Quantification (iTRAQ) has been used to identify abnormal protein expression in different diseases [18–20]. In the present study, we aimed to perform proteomic analysis of miniature pig cochleae as pertaining to acoustic trauma. Continuous stimulation with 120 dB (A) white noise was adopted to establish a stable model of NIHL [21]. iTRAQ was used to assay the comparative proteomics of miniature pig inner ears under conditions of noise exposure vs. no noise exposure. Gene ontology (GO) and Kyoto Encyclopedia of Genes and Genomes (KEGG) database analyses of differentially expressed proteins showed that immune pathways may play a key role in the development of NIHL. Major inflammatory factors enriched in KEGG analysis were validated by Western blot and immunofluorescence in noise-exposed pigs. Our results showed that within 24 h of noise exposure, there was significant upregulation and nuclear translocation of NF- κ B (p65) in hair cells. NF- κ B is a key transcription factor involved in inflammatory signaling pathways, responsible for initiation of transcription of downstream inflammatory factors.

2. Materials and Methods

2.1. Animals. Healthy miniature pigs (2–3 months, male and female, ~5 kg) were from Zhuozhou Kangning Miniature Pig Cultivation Company (Zhuozhou, China). All animals underwent baseline hearing evaluation. Procedures involving the use and care of animals were supported and controlled by

the local ethics committee in compliance with institutional animal protection regulations.

2.2. Experimental Procedures. After baseline hearing evaluation, pigs were randomly assigned to a noise exposure group or the control group (no noise exposure). Animals in the noise groups were subjected to noise exposure and scheduled hearing evaluations. Their cochleae were collected for proteomics analyses and pathological analysis at defined time points. Animals in the control group were subjected to the same protocol as in the noise groups except for noise exposure.

Data were objectively measured and analyzed independently by two individual researchers. All animals in the noise exposure groups were compared with corresponding controls, and pigs were randomly assigned to either the noise groups or control group. There were no animal deaths because of attrition, and no data were excluded from analysis.

2.3. Noise Exposure. Animals in the noise groups were placed in a wire mesh cage and exposed to white noise at 120 dB (A) for 3 h on 2 consecutive days. The white noise signal was routed through an attenuator (PA5 TDT, Alachua, FL, USA) and a power amplifier (MF-1201 MOSTET, ATech) to a loudspeaker (Aijie Audio Equipment Factory) which was positioned at 20 cm above the animal's head. The noise level at the position of the animal's head in the sound field was calibrated using a sound level meter (Brüel & Kjær, 2250L, Denmark), a preamplifier (RA4PA, 4-channel, TDT), and a condenser microphone (RA4LI, TDT). This noise exposure regime can cause permanent loss in cochlear sensitivity.

2.4. Auditory Brainstem Responses. Auditory brainstem response (ABR) measurements were conducted prenoise exposure, 1 day and 7 days postnoise exposure to assess hearing sensitivity of the animals (Figure 1(a)). Each animal was anesthetized with intramuscular injection of Sumianxin (0.1 ml/kg) and 3% pentobarbital sodium (1 ml/kg). Body temperature was maintained at 38°C with a warming blanket. Stainless steel needle electrodes were placed subdermally at the vertex (noninverting input) and behind the stimulated and nonstimulated ears (inverting input and ground, respectively). Each ear was stimulated separately with an open-field sound delivery system positioned at 1 cm from the animal's tested ear. ABRs were induced with clicks and tone bursts at 2, 4, 8, 16, and 24 kHz, generated digitally (SigGen, TDT) using a multifunction processor (RX6, TDT). This was then fed to a programmable attenuator (PA5, TDT), an amplifier (SA1, TDT), and an open-field loudspeaker (MF1-1250, TDT) at 90 dB SPL. The stimulus level was decreased by 10 dB steps until no response was identifiable. The signal was bandpass filtered (100–3000 Hz), amplified ($\times 50,000$), and averaged using Tucker Davis Technologies (TDT) System III hardware and SigGen/BioSig version 4.4.1 (TDT, RX6, Alachua, FL, USA) software. Responses were stored and displayed on a computer. The ABR threshold was defined as the lowest stimulus intensity that reliably induced a detectable response.

2.5. Cochlear Tissue Collection. Animals were decapitated under deep anesthesia with Sumianxin (0.1 ml/kg) and 3%

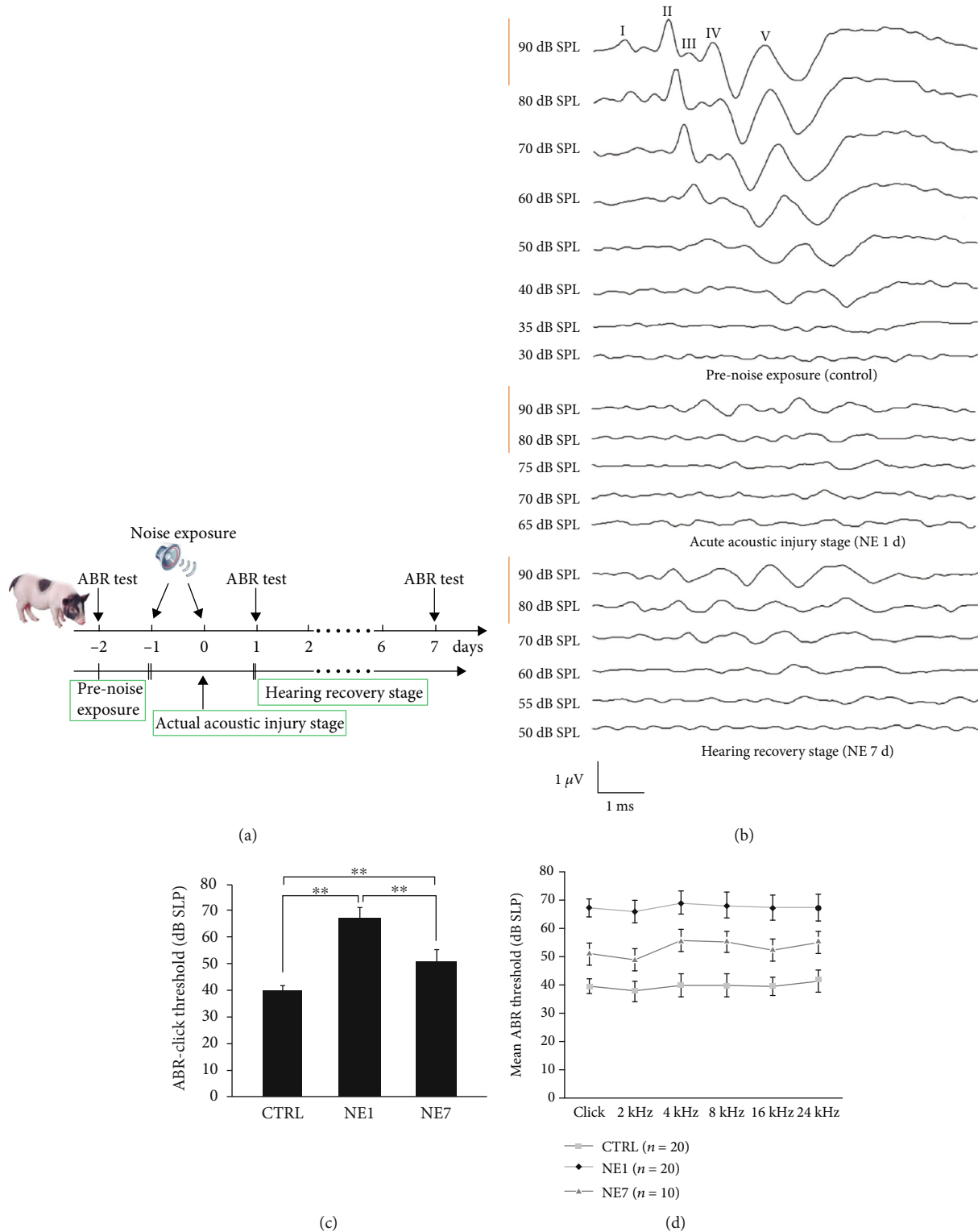


FIGURE 1: ABR results from three groups of animals. (a) Pattern of hearing changes during different stages of acoustic injury. (b) ABR-click waveforms for the three groups of animals: Top: Normal control individual (CTRL) ABR waveforms, I-V waves are well-differentiated, II- and V-waves are most stable, and this individual ABR threshold is 35 dB SPL. Middle: 1 day after of noise exposure (NE1) testing ABR, the amplitude at 90 dB SPL decreased, and the potential of I-V waves was prolonged. This individual ABR threshold was 70 dB SPL. Bottom: ABR waveforms were tested at 7 days after noise exposure (NE7), and the individual ABR threshold was 55 dB SPL. (c) There was a statistically significant difference in ABR-click thresholds between the three groups of animals. ** indicates $p < 0.01$, a significant difference (one-way ANOVA, Tukey test). (d) Comparison of ABR-click and tone-burst thresholds in the three groups of animals. n : the number of cochleae in each group.

pentobarbital sodium (1 ml/kg). Cochleae were quickly removed from the skull as previously described [22]. For proteomic and Western blot analyses, cochleae were rinsed with 0.01 M phosphate-buffered saline (PBS), frozen immediately in liquid nitrogen for 10 min, and stored at -80°C . For immunohistological and pathological examinations, cochleae were fixed with 4% paraformaldehyde at 4°C overnight. Cochleae were then dissected in PBS, and the organ of Corti and stria vascularis were collected.

2.6. Tissue Protein Extraction and Digestion. Briefly, tissues were harvested and resuspended in $400\ \mu\text{l}$ lysis buffer (8 M urea 50 mM NH_4HCO_3 , protease inhibitors) and sonicated on ice to extract total protein. The resulting extracts were centrifuged at 10,000 rpm for 30 min at 4°C . Supernatants were collected, and protein concentration was measured using a Bradford assay kit according to the manufacturer's instructions. Protein digestion was performed with the following steps. $200\ \mu\text{g}$ proteins were transferred into ultracentrifugation tube and reduced by adding a final concentration of 10.0 mM dithiothreitol for 60 min at 37°C and then were immediately alkylated by incubating with a final concentration of 20 mM iodoacetamide for 60 min at room temperature in the dark. $100\ \mu\text{L}$ 8 M urea, 50 mM NH_4HCO_3 were added into tube to clean the proteins in twice. $100\ \mu\text{L}$ 0.5 M triethylammonium bicarbonate (TEAB) were added into tube to exchange the buffer in triple times. Finally, the proteins were digested into the peptides using a trypsin-to-protein ratio of 1:50 overnight. The resulting peptides were collected by centrifugation and stored at -80°C .

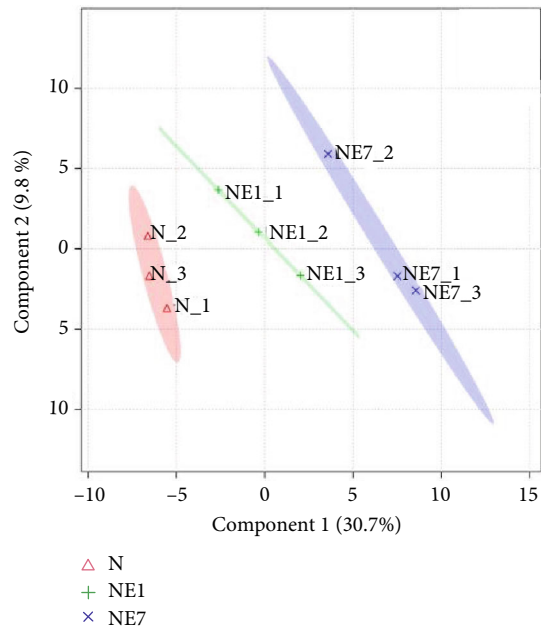
2.7. iTRAQ Labeling and Peptides Prefractionation by High pH Reverse Phase Chromatography. Peptides ($100\ \mu\text{g}$) in 100 mM TEAB from each group were labeled using an 8plex iTRAQ reagents multiplex kit (ABI, Foster City, CA, USA), of which isobaric tags 113 and 114 were for the control group; 115, 116, and 117 were for 1 day postnoise exposure; and 118, 119, and 121 were for 7 days postnoise exposure. In brief, the 8plex iTRAQ reagents were first centrifuged at room temperature and reconstituted with $50\ \mu\text{l}$ isopropyl alcohol to dissolve the iTRAQ labeling reagent. iTRAQ labeling reagents were added to the corresponding peptide samples and were allowed to react at room temperature for 1 h. A total of $100\ \mu\text{l}$ of water was added to prevent the labeling reaction. One aliquot of each sample was analyzed by MS for the test of labeling efficiency. A total of eight sample groups were pooled and vacuum-dried. Each pool of mixed peptides was lyophilized and dissolved in solution A (2% acetonitrile, pH 10, pH adjusted with ammonium hydroxide). Samples were then loaded onto a reverse-phase column (C18 $5\ \mu\text{m}$ $4.6 \times 250\ \text{mm}$, waters) and eluted using a step linear elution program: 5%–35% buffer B at flow rate of 0.7 ml/min (98% acetonitrile, without pH adjustment, solution B) for 30 min, 35%–95% buffer B for 2 min, 95% buffer B for 5 min, and 95%–5% buffer B for 2 min. Samples were collected every 1.5 min. The collected fractions (about 40) were finally combined into 10 pools and desalted on C18 Cartridges (Empore™ standard density SPE C18 Cartridges, bed I.D. 7 mm, 3 ml volume; Sigma, St. Louis, MO, USA).

2.8. LC-Electrospray Ionization-MS/MS Analysis. We referred to the method of Wang et al. [23]. NanoLC-MS/MS experiments were performed with a Q-Exactive HF mass spectrometer (Thermo Fisher Scientific, Waltham, MA, USA) coupled with a nano-high-performance liquid chromatography (Ulti-Mate 3000 LC Dionex; Thermo Fisher Scientific) system. iTRAQ-labeling peptides were loaded onto a C18-reversed phase column ($3\ \mu\text{m}$ C18 resin, $0.1 \times 20\ \text{mm}$) and separated on an analytical column ($1.9\ \mu\text{m}$ C18 resin, $0.15 \times 120\ \text{mm}$; Dr. Maisch GmbH, Ammerbuch, Germany) using mobile phase A: 0.5% formic acid (FA)/ H_2O and B: 0.5% FA/ACN at a flow rate of 600 nl/min, using a 90 min gradient. Spectra were acquired in data-dependent mode. The 20 most intensive ions were selected for MS scanning (300–1400 m/z , 120,000 resolution at m/z 400, accumulation of 3.0×10^6 ions for a maximum of 80 ms, one microscan). The isolation window was 1.6 m/z , and MS/MS spectra were measured at resolution of 15,000 at m/z 400. Dynamic precursor exclusion was allowed for 60 s after each MS/MS spectrum measurement. Normalized collision energy was 30%.

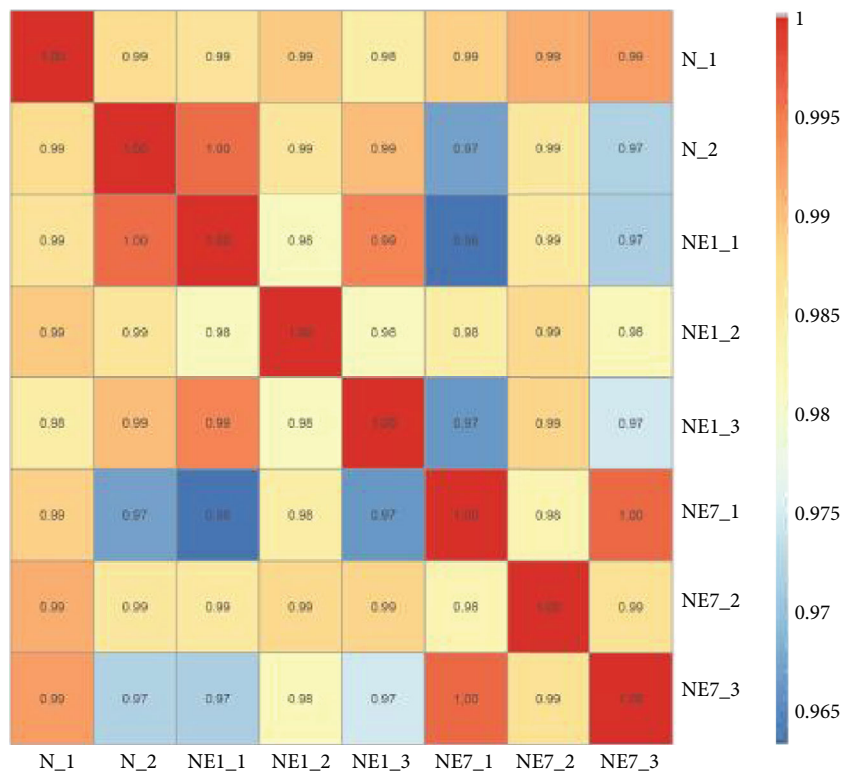
2.9. MS Data Analysis. Raw MS data were processed using Proteome Discoverer 1.4 (ver. 1.4.0.288; Thermo Fisher Scientific). Briefly, peptide identification was performed with Sequest HT search engine against a Uniprot Human Complete Proteome database supplemented with all frequently observed MS contaminants. The following options were used to identify the proteins: Peptide mass tolerance = ± 15 ppm, MS/MS tolerance = 0.2 Da, enzyme = trypsin, missed cleavage = 2; fixed modification: iTRAQ 8-plex (K) and iTRAQ 8-plex (N-term), variable modification: oxidation (M), database pattern = decoy. The peptide confidence was set to a high level (q -value < 0.01) for peptide filtering. Quantification experimental bias was set as normalize on total peptide amount. Up- or downregulated proteins with 1.2-fold changes were selected as being differentially expressed.

2.10. Bioinformatics Analysis. Gene ontology (GO) enrichment analysis (<http://www.geneontology.org>) of differentially expressed proteins with 1.2-fold changes was performed to classify molecular functions, cellular components, and biological processes. Interactions among these proteins pertaining to biological pathways were determined using Pathway Studio software and the ResNet database (KEGG) to better understand them in relation to the published literature. The Pathway Maps tool was used to enrich the pathways, and P values were calculated based on a hypergeometric distribution, with the default database used as the background. Significant pathway enrichment was defined as corrected FDR of $P \leq 0.05$, and proteins with ≥ 1.2 -fold changes were considered differentially abundant proteins.

2.11. Immunohistochemistry. Immunohistochemistry was used to examine changes in expression of NF- κ B (p65) and Apolipoprotein (Apo) A1 in cochleae. Animals were sacrificed on days 1 or 7 postnoise exposure. Cochleae were fixed with 4% paraformaldehyde at 4°C overnight. After dissection in 0.01 M PBS, the organ of Corti and stria vascularis were collected. Tissues were then permeabilized with 0.25%



(a)



(b)

FIGURE 2: Continued.

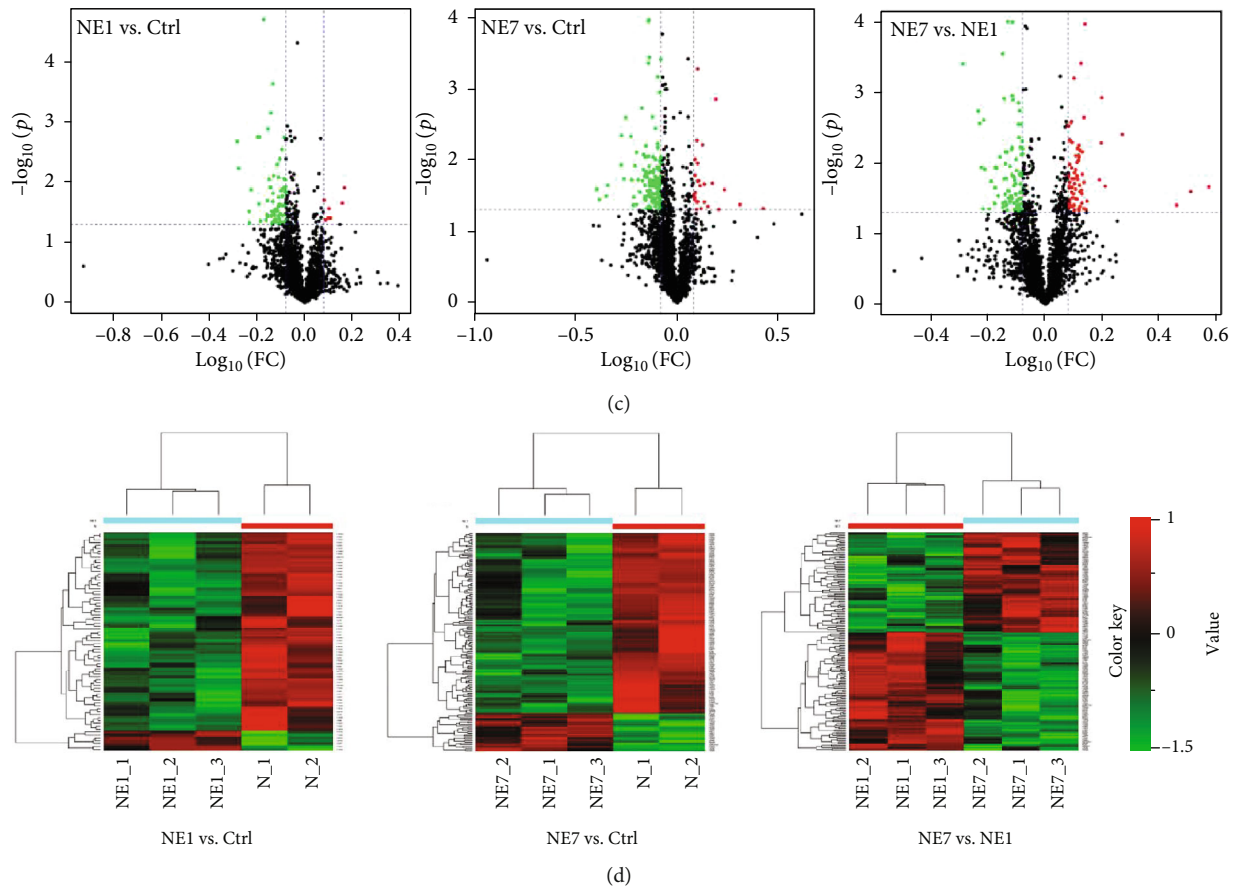


FIGURE 2: Proteomic clustering reveals three distinct groups. (a) Principal component analysis (PCA) of the three groups: normal control group (N), 1 day postnoise exposure group (NE1), and 7 days postnoise exposure group (NE7). (b) Correlation analysis between control and noise exposure pig cochleae. (c) Volcano analysis showing upregulated (red) and downregulated (green) proteins from NE1 vs. Ctrl (left), NE7 vs. Ctrl (middle), and NE1 vs. NE7 (right). (d) Heat map analysis showing upregulated (red) and downregulated (green) proteins from NE1 vs. Ctrl (left), NE7 vs. Ctrl (middle), and NE1 vs. NE7 (right).

Triton X-100 in PBS for 30 min, blocked with 5% goat serum in PBS for 30 min, and incubated overnight at 4°C with primary antibody at concentrations recommended by the manufacturer. Tissues were then rinsed with PBS (three times), incubated with secondary antibody at room temperature for 1 h, and counterstained with DAPI for 10 min.

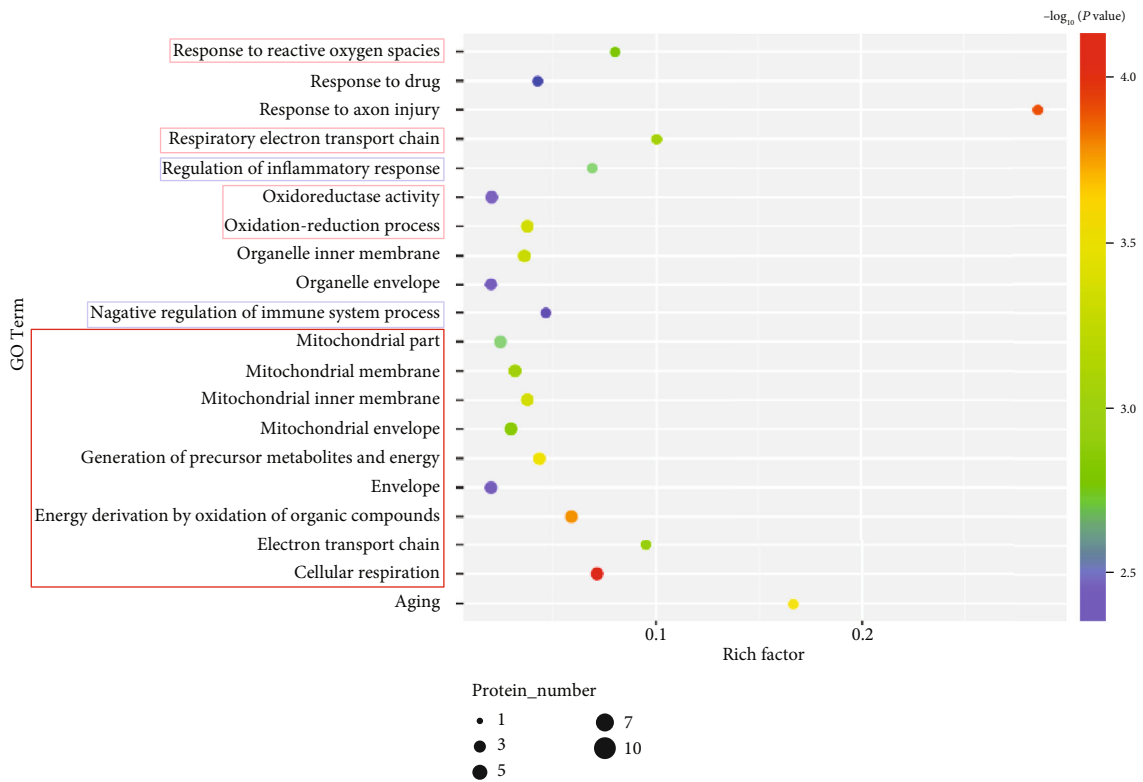
For the noise exposure groups, six cochleae each were used for NF- κ B (p65) (6956, Cell Signaling Technology, Inc) and Apo A1 (Abcam, ab64308) staining. Cochleae from six additional animals that were not subjected to noise exposure were used as controls. Several sections of tissue from cochleae were stained only with secondary antibodies to assess nonspecific staining.

Fluorescence was visualized under a confocal microscope (Zeiss LSM780 laser scanning confocal image system) as previously described [24]. The numbers of different stained hair cells were counted for further quantitative analysis as previously described [25].

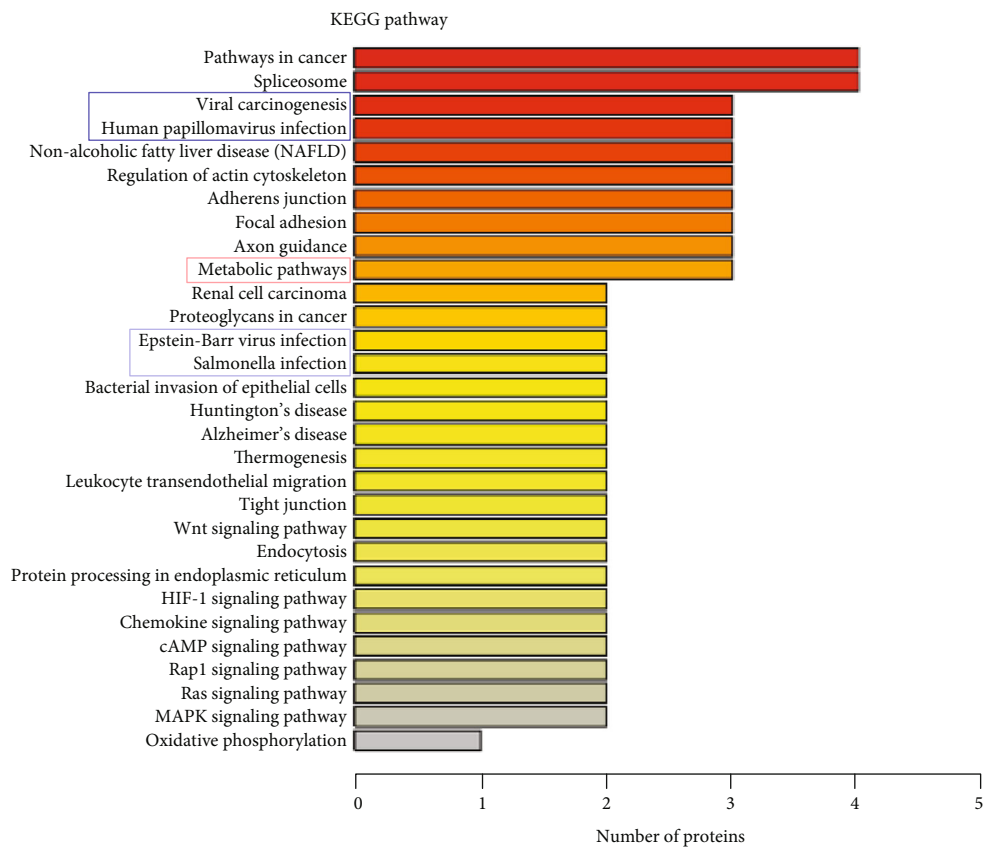
2.12. Detection of Intracellular Reactive Oxygen Species. The increasing fluorescence intensity of 2',7'-dichlorofluorescein (DCF) was used to measure the generation of intracellular reactive oxygen species (ROS). The reagent 2',7'

-dichlorodihydrofluorescein diacetate (DCFH-DA; Sigma-Aldrich, USA) can enter the cell, where the diacetate group is cleaved off by intracellular esterase. The resulting DCFH is retained in the cytoplasm and oxidized to DCF by ROS. The organ of Corti was dissected from the inner ears of normal control animals and from animals on day 1 after noise exposure and incubated in 200 μ l DCFH-DA working solution (20 mM) at 37°C for 30 min. Hair cells were observed under a confocal microscope (Zeiss LSM780 laser scanning confocal image system). The fluorescence of DCF was monitored at excitation and emission wavelengths of 485 nm and 530 nm, respectively.

2.13. Western Blot. Tissues from pig cochleae were lysed with RIPA. Western blotting was performed similarly to previous studies [26]. Briefly, proteins separated by SDS-PAGE were transferred to polyvinylidene fluoride membranes (Millipore, Bedford, MA). Membranes were treated with anti-NF- κ B p65 (6956, Cell Signaling Technology, Inc) and Apo A1 (Abcam, ab64308) antibodies. Each antibody preparation was diluted in 5% skim milk, and protein bands were visualized using an ECL plus chemiluminescence detection system (WBKLS0500, Millipore, USA) and photographed.



(a)



(b)

FIGURE 3: Continued.

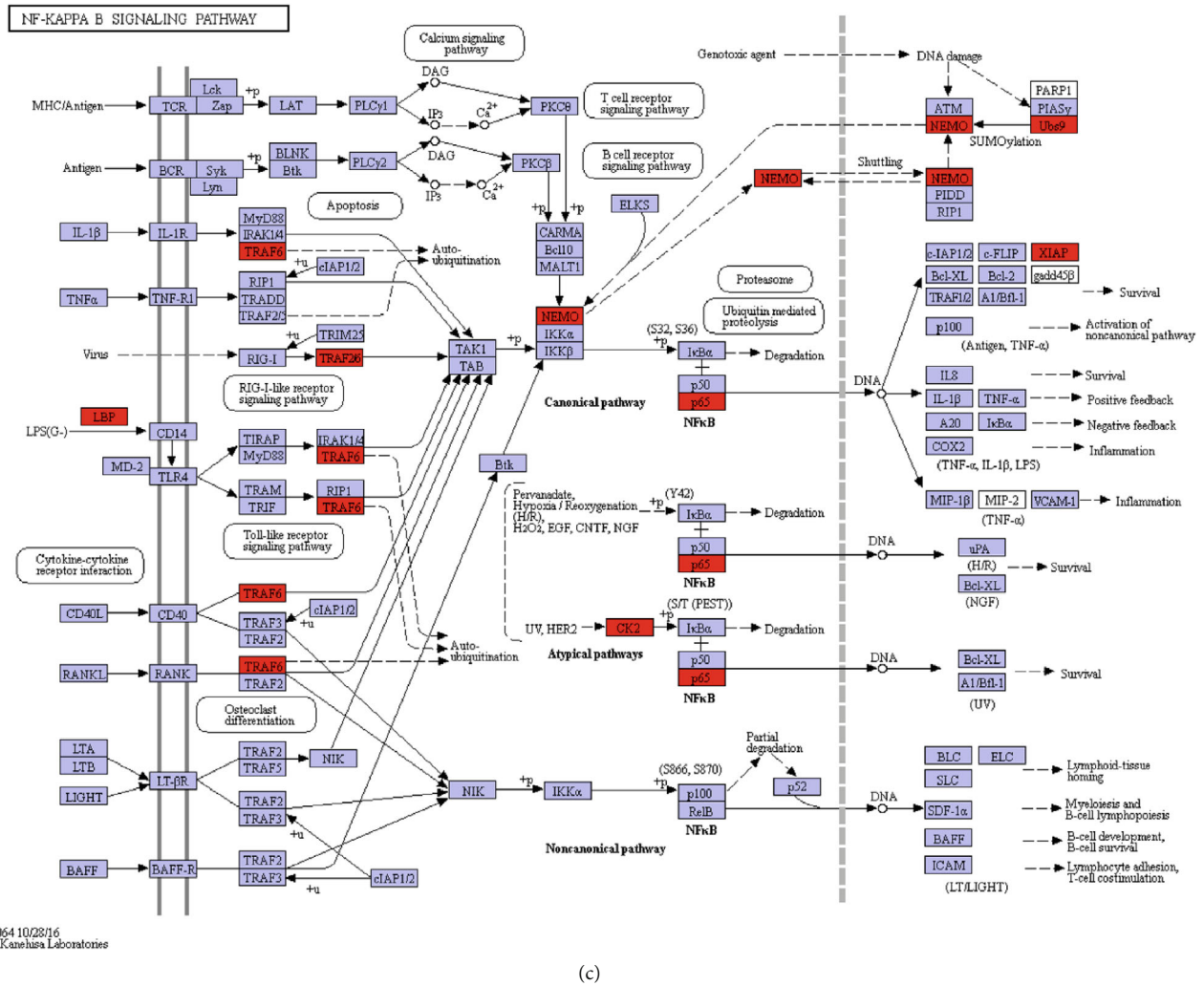


FIGURE 3: Activation of metabolic (red frame) and immune (blue frame) pathways in pig cochleae were prominent during the acute response to noise exposure. GO (a) and KEGG (b) analyses show that metabolic (red frame) and immune (blue frame) function were prominently enriched among proteins that changed in levels between control (Ctrl) and day 1 after noise exposure (NE1) pig inner ears. (c) The NF- κ B (p65) signaling pathway was primarily activated at day 1 after noise exposure (NE1) in pig inner ears.

2.14. Statistical Analysis. Data are presented as mean \pm standard deviation. Average ABR thresholds and immunoreactivity and protein expression obtained before and 1 and 7 days after noise exposure were compared using one-way ANOVA. If significant differences were observed from one-way ANOVA, the Tukey test or Kruskal-Wallis test was performed to delineate the nature of the differences using SPSS version 19.0 (SPSS, Inc., Chicago, IL, USA). $P \leq 0.05$ was considered statistically significant. The ratio of number of cells with nuclear malformations (fragmented or condensed) to total number of cells was calculated.

3. Results

3.1. Noise Exposure Causes Loss in Cochlear Sensitivity. We established a swine model of permanent hearing loss induced by noise exposure. One-month-old pigs (5 kg) with normal hearing ability (Figure 1(b) top panel) were exposed to 120 dB (A) white noise for 3 h on 2 consecutive days. ABR

measurements to monitor acute hearing loss and hearing recovery were performed on days 1 and 7 after noise exposure (Figure 1(a)). Noise exposure caused loss in cochlear sensitivity. All experimental animals underwent ABR-click to test baseline hearing level before noise treatment. ABR-click and tone burst were performed in three groups of animals (prenoise exposure and days 1 and 7 after noise exposure). The different ABR-click waveforms in the three groups are shown in Figure 1(b). There were 10 pigs ($n = 20$ ears) in the control group, 10 pigs ($n = 20$ ears) in the 1 day postnoise exposure group, and 5 pigs ($n = 10$ ears) in the 7 days postnoise exposure group. The average ABR-click threshold was 39.4 ± 2.6 dB SPL in prenoise exposure animals, 67.1 ± 4.1 dB SPL in 1 day postnoise exposure animals, and 50.8 ± 4.7 dB SPL in the 7 days postnoise exposure group (Figure 1(c)). Hearing loss was most severe at 4 kHz, and hearing loss at high frequency was more severe than at low frequency, which was consistent with human hearing performance in acute NIHL [15]. Average hearing threshold

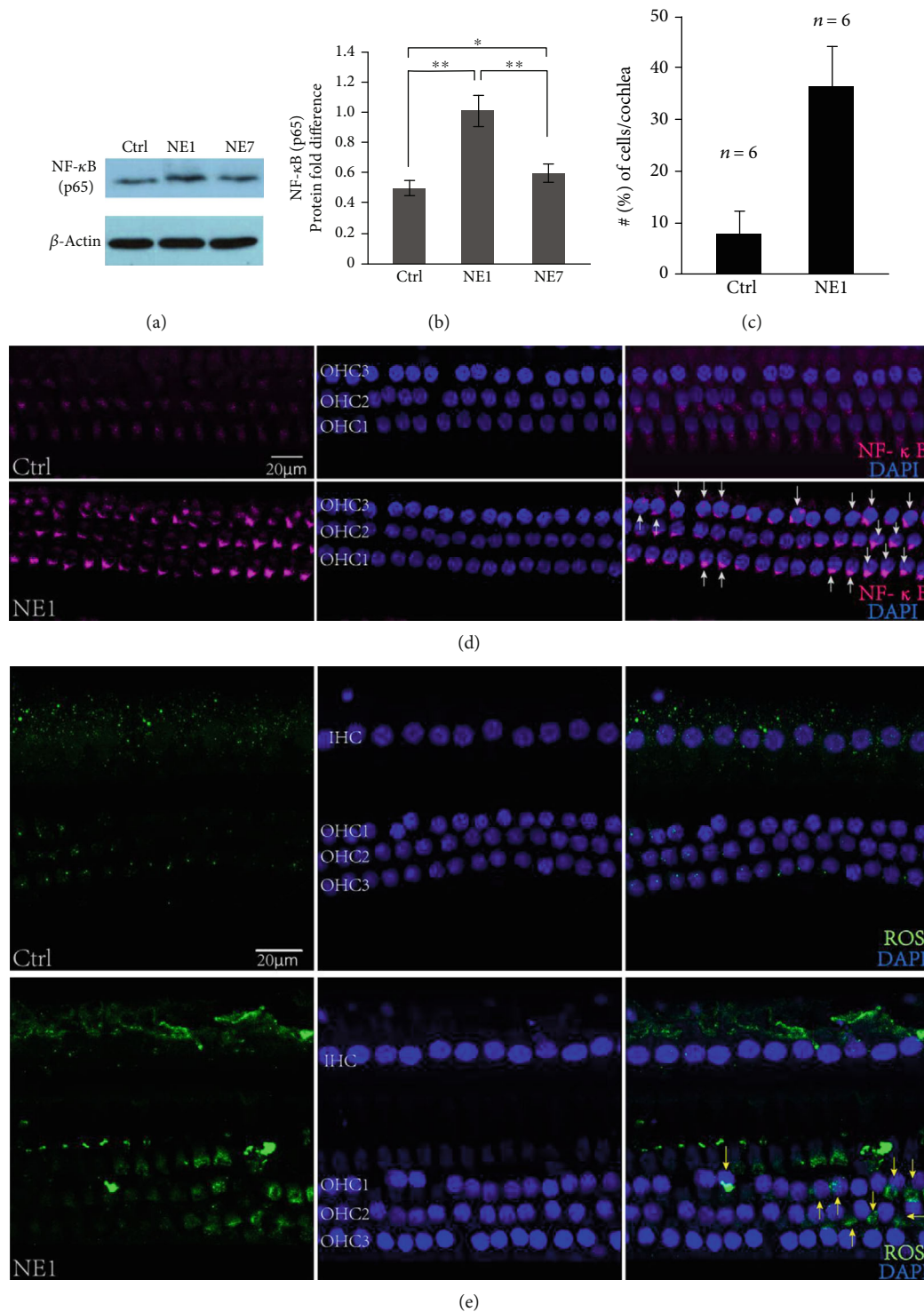


FIGURE 4: Accumulation of ROS and activation of NF-κB signaling were validated in NE1 pig inner ears. Upregulated NF-κB (p65) protein level were detected by Western blot (a) and analyzed statistically using Image Gallery software (b) based on (a). Asterisk indicates a significant difference ($*p < 0.05$, $**p < 0.01$, one-way ANOVA, Tukey test). (c) Average percentage of outer hair cells per cochlea that exhibited NF-κB (p65) translocation into the nucleus. (d) Immunofluorescence image showing nuclear translocation of NF-κB (p65) in outer hair cells (white arrow) 1 day after noise exposure. (e) Immunofluorescence image showing accumulation of ROS in hair cells (yellow arrow) 1 day after noise exposure. *n*: number of cochleae.

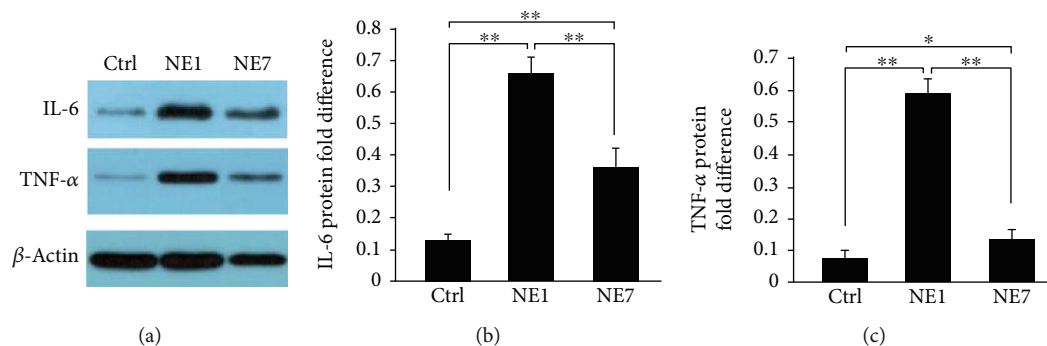


FIGURE 5: IL-6 and TNF- α were upregulated in the NE1 compared with the control group, and downregulated in the NE7, as determined by Western blot (a). Statistical analysis using Image Gallery software (b, c) based on (a). Asterisk indicates a significant difference ($*p < 0.05$, $**p < 0.01$, one-way ANOVA, Tukey test).

could be recovered to 14 ± 4.9 dB SPL higher than the normal level after 7 days from noise exposure, and hearing loss recovery from 4 kHz and higher frequencies was worse compared with the low frequency (Figure 1(d)).

3.2. Comparative Proteomic Analysis of Cochleae Prenoise Exposure and during the Acute and Recovery Stages Postnoise Exposure. Proteomic data were collected from miniature pigs of the control ($n = 2$), 1 day postnoise exposure ($n = 3$), and 7 days postnoise exposure groups ($n = 3$). Principal component analysis showed good distribution between the three groups (Ctrl, NE1, and NE7) (Figure 2(a)). Correlation analyses of samples from the same groups were over 98% (Figure 2(b)), indicating samples from the same groups had high similarity. Changes in protein expression induced by noise exposure are shown in a volcano plot and heat map analysis in Figures 2(c) and 2(d). 68 proteins were downregulated (green) and 7 proteins were upregulated (red) between the 1 day postnoise exposure and control groups. Between the 7 days postnoise exposure and control groups, 125 proteins were downregulated (green) and 26 proteins were upregulated (red). Between the 1 day postnoise exposure and 7 days postnoise exposure groups, 73 proteins were upregulated (red) and 88 proteins were downregulated (green).

3.3. Immune and Oxidative Stress Are Triggered during the Acute Acoustic Injury Period. To identify physiological changes in pig cochleae during the acute period following noise exposure, we compared dysregulated proteins between the NE1 and Ctrl groups. GO analysis (Figure 3(a)) showed that oxidative stress (red frame) and immune response (blue frame) were the two groups primarily annotated in response to noise-induced cochlear damage. Consistent observations were made following analysis of enriched proteins in KEGG analysis (Figures 3(b) and 3(c)). Moreover, we found that p65, part of the NF- κ B transcription factor family, was increased following noise exposure and contributed to inducing the acute period of cochlear damage (Figure 3(c)).

3.4. Accumulation of ROS and Activation of NF- κ B Signaling in Pig Hair Cells during the Acute Acoustic Injury Period. Protein expression of NF- κ B (p65) was examined by Western

blot. Noise exposure significantly increased p65 on 1 day after noise exposure, which gradually recovered by 7 days after noise exposure (Figures 4(a)–4(c)). The subcellular location of p65 in cochleae was examined using immunofluorescence. Nuclear translocation of NF- κ B (p65) was detected in outer hair cells after noise exposure (Figure 4(d)). Moreover, IL-6 and TNF- α were detected by Western blot and showing they are upregulated in NE-1 and partly decreased in NE-7 (Figures 5(a)–5(c)). The initiation of downstream inflammatory factors may be because of a significant accumulation of ROS in the hair cells on the 1st day after the noise treated (Figure 4(e)).

3.5. Cholesterol Metabolism Pathways Are Involved in Recovery from NIHL. To evaluate protein expression during the recovery stage of NIHL, we analyzed dysregulated proteins between the NE7 and Ctrl groups. Both GO (Figure 6(a)) and KEGG (Figure 6(b)) analyses showed that the PPAR and insulin pathways (green frames), involved in cholesterol metabolism, were involved during this stage. We also found that Apo AI was increased in NE7 cochleae (Figures 6(c) and 7) and may contribute to hearing recovery. Additionally, other proteins involved in inflammation were increased (blue frames). Through comparing NE7 with NE1 group, we found that some of these differential proteins were enriched in the negative regulation of humoral immune response (blue frame) (Figure 8), which suggested negative immune regulation pathways were involved in the hearing recovery stage. These results demonstrate that gene expression differed between stages after noise exposure. During the acute stage, inflammatory and oxidative stress-related pathways were involved in mediating cochlear damage, while during the recovery stage, inner ear damage induced by inflammation was resolved gradually via cholesterol metabolic pathways.

To determine whether our results were similar to those from prior studies in rodent models, we analyzed these studies and appropriate databases and found that the Apo A and Apo E genes were previously shown to be expressed in adult mice by inner and outer hair cells (Table 1). However, no genes were commonly increased between mouse and rat transcriptomics (Figure 9(a)). Apo E was unique in that it was upregulated in both mouse cochlear sensory

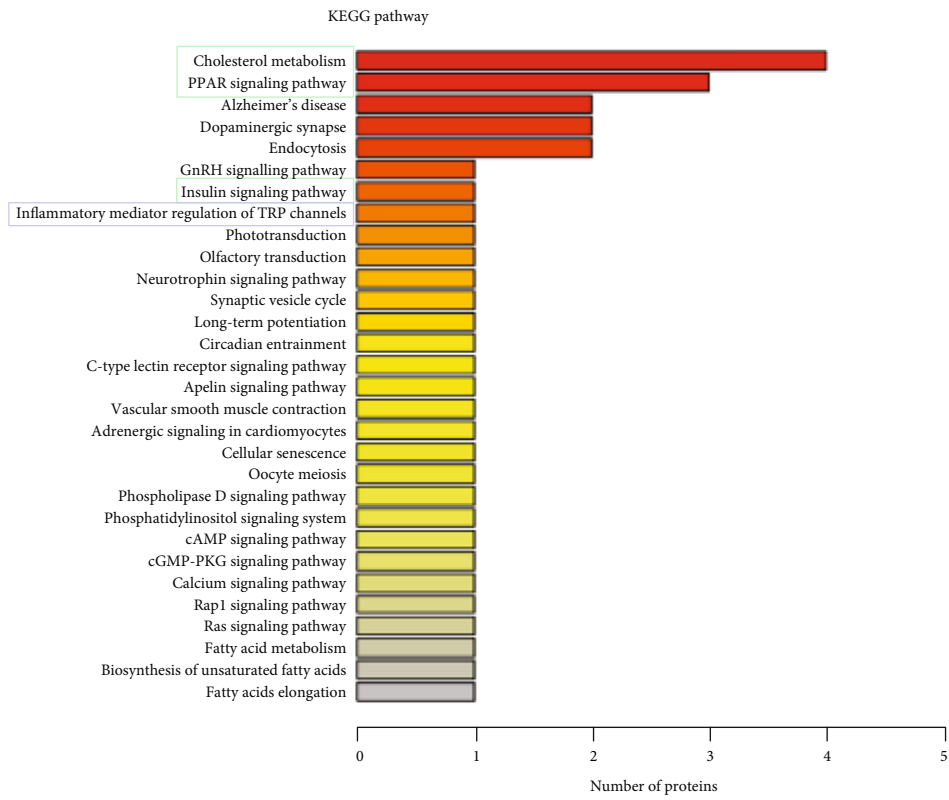
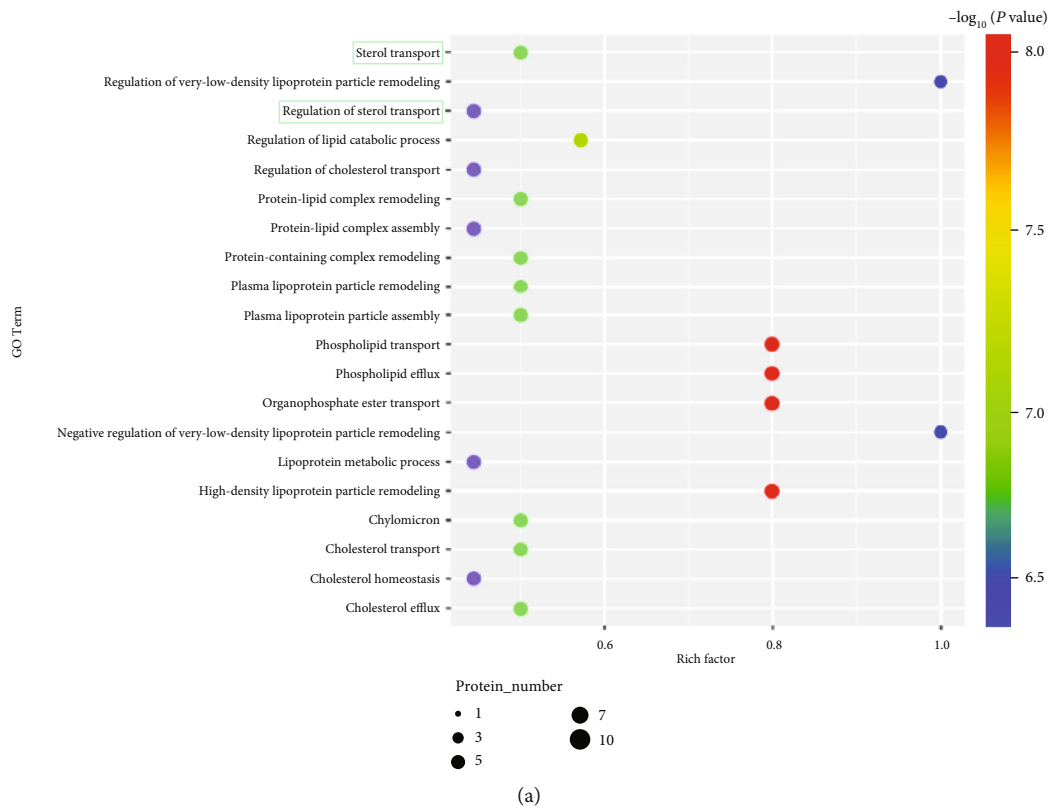


FIGURE 6: Continued.

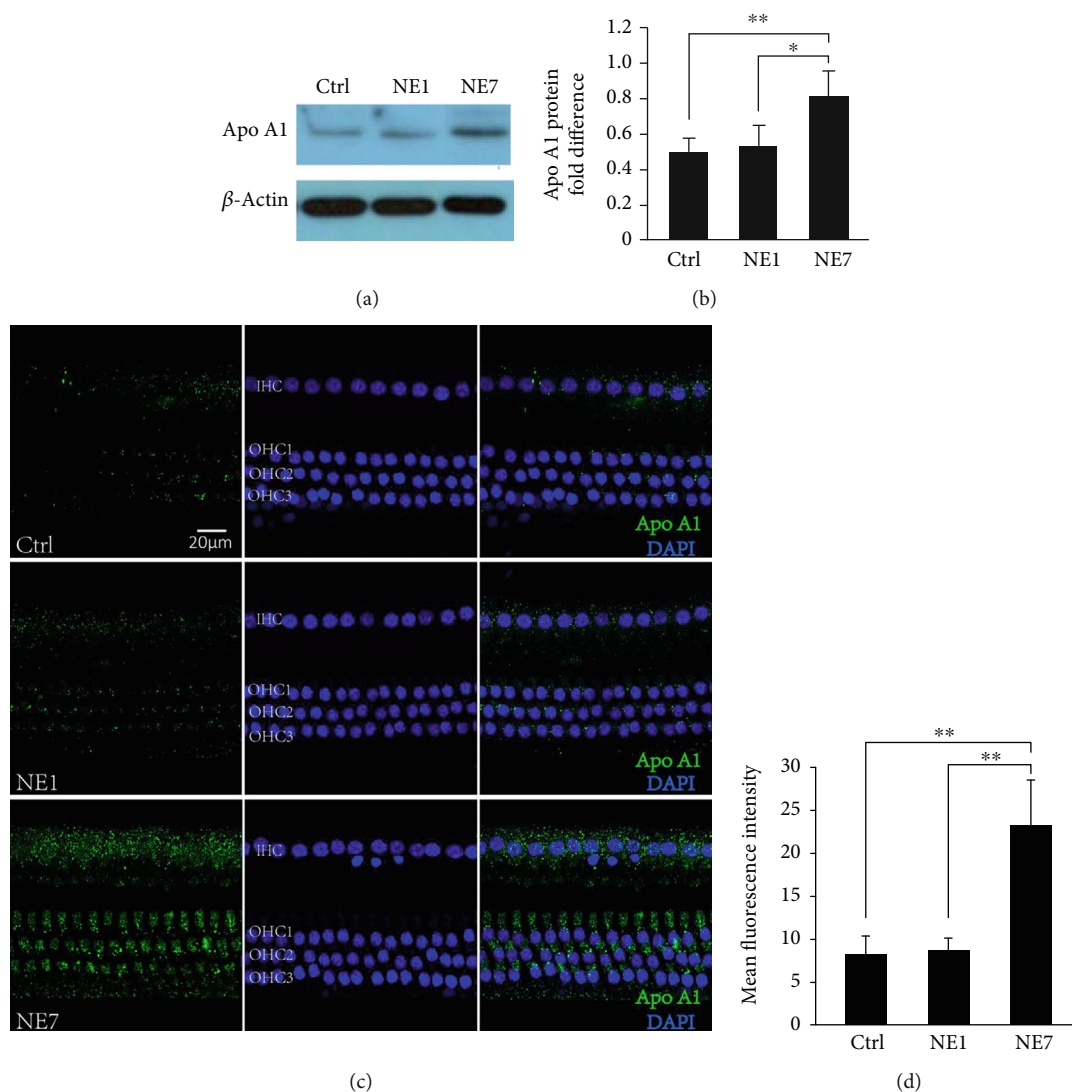


FIGURE 7: Apo A1 was upregulated in the NE7 group compared with the normal control and NE1 groups, as determined by Western blot (a). Statistical analysis using Image Gallery software (b) based on (a). Asterisk indicates a significant difference (** $p < 0.01$, * $p < 0.05$, one-way ANOVA, Tukey test). (c) Cholesterol metabolic pathways may play an important role in recovery from hearing loss after noise exposure. Immunofluorescence image shows that fluorescence intensity of Apo A1 in hair cells increased at 7 days after noise exposure. Statistical analysis of fluorescence intensity using Image J software (d) based on (c). Asterisk indicates a significant difference (** $p < 0.01$, one-way ANOVA, Tukey test).

the NF- κ B (p65) (Figures 4(a) and 4(b)). A report analyzing cochlear sensory epithelium using RNA sequencing showed that most upregulated genes were related to immunity, inflammation, and defense response after noise exposure [32], indicating that the immune/inflammatory response is an important mechanism in NIHL and the primary reaction of the cochlea to noise stimulation.

We also found that proteins involved in cholesterol metabolism, Apo E and Apo AI, were increased 7 days after noise exposure. Epidemiological evidence indicated that high levels of apoA-1/apoA-2 and Apo-E are associated with protection against atherosclerotic disease and negative regulation of cytokine secretion involved in immune responses. However, the mechanisms involved in these beneficial effects are not well established [33]. A recent study showed that Apo

E gene variants may have been associated with sudden sensorineural hearing loss in an Iranian population [34]. These studies indicate that cholesterol metabolism may be important in hearing loss recovery after noise exposure. Moreover, as shown in Table 1, the Apo-E, Apo-AI, and Apo-AII genes were expressed in adult mouse cochlear inner and outer hair cells, indicating that these genes have related biological functions in the inner ear. Notably, the involvement of Apo AI and Apo A II in NIHL has seldom been reported.

RNA transcriptomic analysis has been widely used in the hearing research fields to identify the differentially expressed genes [35–41]. Compared with previous studies that analyzed RNA transcriptomics, differential genes related to NIHL involve inflammation mediated by chemokines, cytokine pathways of the stress response, and immune pathways

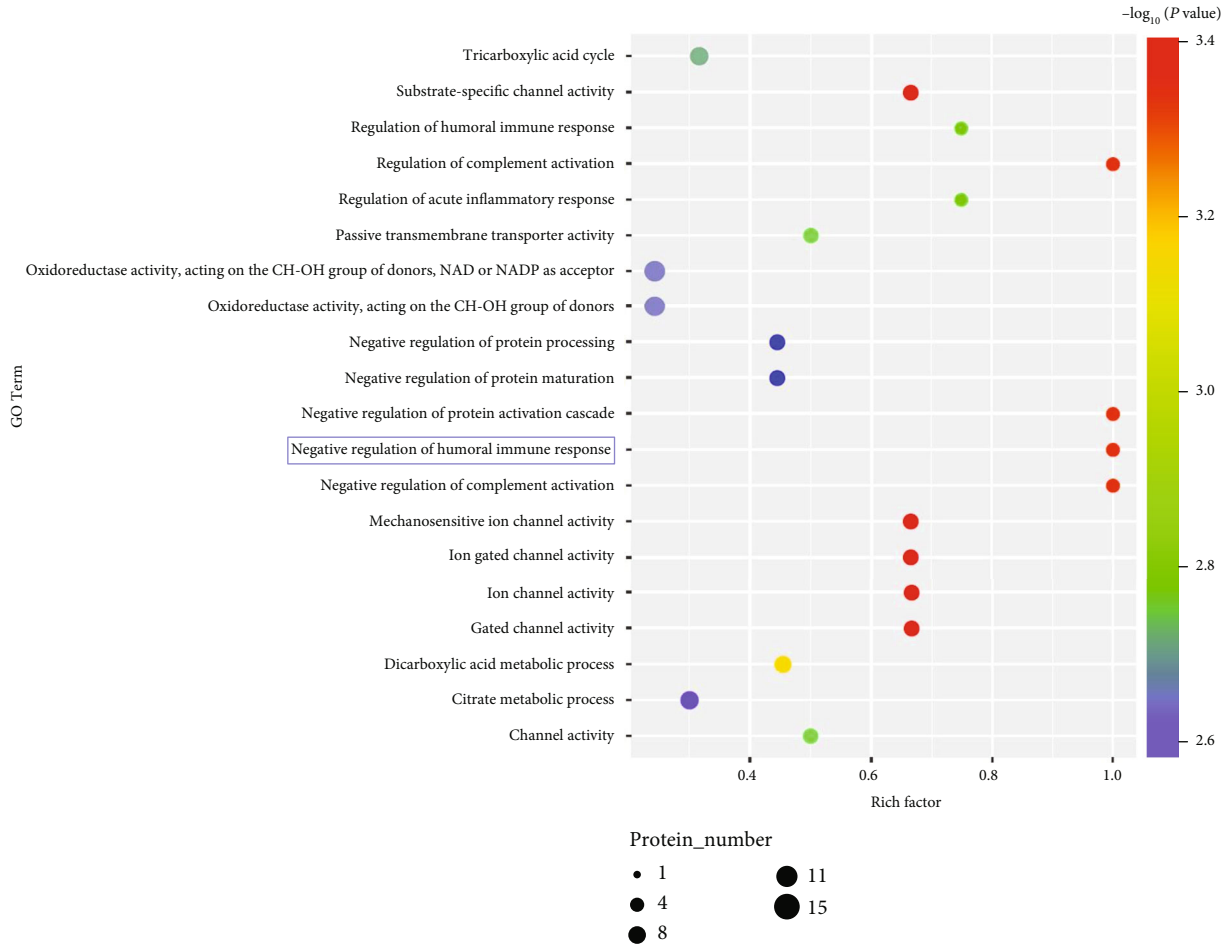


FIGURE 8: GO analysis shows that immune (blue frame) function were prominently enriched among proteins that changed in levels between day 7 after noise exposure (NE7) and day 1 after noise exposure (NE1) pig cochlea.

TABLE 1: Expression of ApoA and ApoE genes in adult mice assessed by inner (IHC) and outer Hair cells (OHC).

Probeset ID	IHC (mean \pm sd)	OHC (mean \pm sd) [OHC replicate]	Fold change (OHC/IHC)	False discovery rate (FDR)
ApoE 17487381	54.65 \pm 1.55	43.14 \pm 11.82 [65.40]	0.79	0.504
ApoA1 17516901	13.98 \pm 0.00	16.00 \pm 2.11 [12.85]	1.14	0.536
ApoA2 17219242	10.89 \pm 0.00	11.15 \pm 0.19 [10.89]	1.02	0.501

enriched by KEGG [32, 42]. These observations are consistent with this study. However, compared with the present study, only a small number of common differentially expressed genes were found in previous molecular profile studies of acoustic trauma in rodent cochlea. Apo-E was a common gene included in both subsets in this study (NE7 vs. Ctrl and NE7 vs. NE1) and in mouse normal cochlear sensory epithelium. However, no genes were found to be commonly expressed in all three species (rats, mice, and pigs) (Figure 9(a)) [33]. Possible explanations are as follows: (1) the noise processing conditions used in this study were different from previous studies; (2) pigs are large animals and may differ significantly from rodents in gene expression patterns; and (3) previous studies used RNA-seq transcripto-

omics, while proteomic analysis (iTRAQ) was used here. Previous studies showed that the consensus between differential gene expression analyzed by transcriptomics and proteomics under the same experimental conditions was less than 30% [43]. Therefore, it is possible that the results of proteomics analysis obtained herein will not overlap with differential genes from transcriptomics screenings of previous related studies of noise exposure in rodents. This indirectly reflected the necessity and advantages of using large animals and proteomics technology to study the mechanisms of auditory diseases. Large animals are more closely related to humans in terms of gene homology and regulation. In addition, proteins are the ultimate effector molecules for mediating biological processes. Therefore, analysis of disease

- [2] J. Shargorodsky, S. G. Curhan, G. C. Curhan, and R. Eavey, "Change in prevalence of hearing loss in US adolescents," *JAMA*, vol. 304, no. 7, pp. 772–778, 2010.
- [3] Y. Liu, J. Qi, X. Chen et al., "Critical role of spectrin in hearing development and deafness," *Science Advances*, vol. 5, no. 4, p. eaav7803, 2019.
- [4] J. Qi, Y. Liu, C. Chu et al., "A cytoskeleton structure revealed by super-resolution fluorescence imaging in inner ear hair cells," *Cell Discovery*, vol. 5, no. 1, 2019.
- [5] J. Qi, L. Zhang, F. Tan et al., "Espn distribution as revealed by super-resolution microscopy of stereocilia," *American Journal of Translational Research*, vol. 12, no. 1, pp. 130–141, 2020.
- [6] Z. H. He, S. Y. Zou, M. Li et al., "The nuclear transcription factor FoxG1 affects the sensitivity of mimetic aging hair cells to inflammation by regulating autophagy pathways," *Redox Biology*, vol. 28, p. 101364, 2020.
- [7] S. Gao, C. Cheng, M. Wang et al., "Blebbistatin inhibits neomycin-induced apoptosis in hair cell-like HEI-OC-1 cells and in cochlear hair cells," *Frontiers in Cellular Neuroscience*, vol. 13, 2020.
- [8] Y. Zhang, W. Li, Z. He et al., "Pre-treatment with Fasudil prevents neomycin-induced hair cell damage by reducing the accumulation of reactive oxygen species," *Frontiers in Molecular Neuroscience*, vol. 12, 2019.
- [9] W. Liu, X. Xu, Z. Fan et al., "Wnt signaling activates TP53-induced glycolysis and apoptosis regulator and protects against cisplatin-induced spiral ganglion neuron damage in the mouse cochlea," *Antioxidants & Redox Signaling*, vol. 30, no. 11, pp. 1389–1410, 2019.
- [10] S. Zhang, Y. Zhang, Y. Dong et al., "Knock-down of Foxg1 in supporting cells increases the transdifferentiation of supporting cells into hair cells in the neonatal mouse cochlea," *Cellular and Molecular Life Sciences*, vol. 77, no. 7, pp. 1401–1419, 2020.
- [11] F. Tan, C. Chu, J. Qi et al., "AAV-ie enables safe and efficient gene transfer to inner ear cells," *Nature Communications*, vol. 10, no. 1, p. 3733, 2019.
- [12] Z. He, L. Guo, Y. Shu et al., "Autophagy protects auditory hair cells against neomycin-induced damage," *Autophagy*, vol. 13, no. 11, pp. 1884–1904, 2017.
- [13] Z. He, Q. Fang, H. Li et al., "The role of FOXG1 in the postnatal development and survival of mouse cochlear hair cells," *Neuropharmacology*, vol. 144, pp. 43–57, 2019.
- [14] G. Ayna, D. V. Krysko, A. Kaczmarek, G. Petrovski, P. Vandenabeele, and L. Fesus, "ATP release from dying autophagic cells and their phagocytosis are crucial for inflammasome activation in macrophages," *PLoS One*, vol. 7, no. 6, article e40069, 2012.
- [15] X. Li, *Pathophysiology of the Cochlea*, People's Military Medical Press, 2011.
- [16] L. L. Zhong, Y. Zhang, X. J. Liang et al., "Inner ear structure of miniature pigs measured by multi-planar reconstruction techniques," *American Journal of Translational Research*, vol. 10, no. 3, pp. 709–717, 2018.
- [17] S. M. Yang, "The miniature pig as an animal model in otological research," *Chinese Journal of Otology*, vol. 14, no. 1, pp. 1–5, 2016.
- [18] P. Marianowski, I. Szymusik, J. Malejczyk, M. Hibner, and M. Wielgos, "Proteomic analysis of eutopic and ectopic endometriotic tissues based on isobaric peptide tags for relative and absolute quantification (iTRAQ) method," *Neuro Endocrinol Letters*, vol. 34, no. 7, pp. 717–721, 2013.
- [19] Q. Fang, Y. Zhang, X. Chen et al., "Three-dimensional graphene enhances neural stem cell proliferation through metabolic regulation," *Frontiers in Bioengineering and Biotechnology*, vol. 7, 2020.
- [20] S. Han, Y. Xu, J. Sun et al., "Isolation and analysis of extracellular vesicles in a Morpho butterfly wing-integrated microvortex biochip," *Biosensors & Bioelectronics*, vol. 154, p. 112073, 2020.
- [21] J. Wu, W. Han, X. Chen et al., "Matrix metalloproteinase-2 and -9 contribute to functional integrity and noise-induced damage to the blood-labyrinth-barrier," *Molecular Medicine Reports*, vol. 16, no. 2, pp. 1731–1738, 2017.
- [22] L. Chen, W. Guo, L. Ren et al., "A de novo silencer causes elimination of MITF-M expression and profound hearing loss in pigs," *BMC Biology*, vol. 14, no. 1, 2016.
- [23] C. Wang, D. Zhao, S. Z. A. Shah, W. Yang, C. Li, and L. Yang, "Proteome analysis of potential synaptic vesicle cycle biomarkers in the cerebrospinal fluid of patients with sporadic Creutzfeldt–Jakob disease," *Molecular Neurobiology*, vol. 54, no. 7, pp. 5177–5191, 2017.
- [24] X. Shi, N. Wu, Y. Zhang, W. Guo, C. Lin, and S. Yang, "Adeno-associated virus transformation into the normal miniature pig and the normal guinea pigs cochlea via scala tympani," *Acta Oto-Laryngologica*, vol. 137, no. 9, pp. 910–916, 2017.
- [25] B. H. Hu, Q. Cai, Z. Hu et al., "Metalloproteinases and their associated genes contribute to the functional integrity and noise-induced damage in the cochlear sensory epithelium," *The Journal of Neuroscience*, vol. 32, no. 43, pp. 14927–14941, 2012.
- [26] X. Shi, Y. Dong, Y. Li et al., "Inflammasome activation in mouse inner ear in response to MCMV induced hearing loss," *Journal of Otology*, vol. 10, no. 4, pp. 143–149, 2015.
- [27] R. D. Kopke, P. A. Weisskopf, J. L. Boone et al., "Reduction of noise-induced hearing loss using L-NAC and salicylate in the chinchilla," *Hearing Research*, vol. 149, no. 1-2, pp. 138–146, 2000.
- [28] L. P. Rybak, R. Ravi, and S. M. Somani, "Mechanism of protection by diethylthiocarbamate against cisplatin ototoxicity: antioxidant system," *Fundamental and Applied Toxicology*, vol. 26, no. 2, pp. 293–300, 1995.
- [29] L. E. Van Campen, W. J. Murphy, J. R. Franks, P. I. Mathias, and M. A. Toraason, "Oxidative DNA damage is associated with intense noise exposure in the rat," *Hearing Research*, vol. 164, no. 1-2, pp. 29–38, 2002.
- [30] A. R. Fetoni, F. Paciello, R. Rolesi, G. Paludetti, and D. Troiani, "Targeting dysregulation of redox homeostasis in noise-induced hearing loss: oxidative stress and ROS signaling," *Free Radical Biology and Medicine*, vol. 135, pp. 46–59, 2019.
- [31] J. Zhang, X. Wang, V. Vikash et al., "ROS and ROS-mediated cellular signaling," *Oxid Med Cell Longev*, vol. 2016, article 4350965, 18 pages, 2016.
- [32] S. Yang, Q. Cai, R. R. Vethanayagam, J. Wang, W. Yang, and B. H. Hu, "Immune defense is the primary function associated with the differentially expressed genes in the cochlea following acoustic trauma," *Hearing Research*, vol. 333, pp. 283–294, 2016.
- [33] G. Cimmino, B. Ibanez, G. Vilahur et al., "Up-regulation of reverse cholesterol transport key players and rescue from global inflammation by ApoA-IMilano," *Journal of Cellular and Molecular Medicine*, vol. 13, no. 9b, pp. 3226–3235, 2009.

- [34] A. K. Hamidi, N. Yazdani, K. H. Seyedjavadi et al., "MTHFR AND ApoE genetic variants association with sudden sensorineural hearing loss," *American Journal of Otolaryngology*, vol. 40, no. 2, pp. 260–264, 2019.
- [35] S. Zhang, Y. Zhang, P. Yu et al., "Characterization of Lgr5+ progenitor cell transcriptomes after neomycin injury in the neonatal mouse cochleae," *Frontiers in Molecular Neuroscience*, vol. 10, p. 213, 2017.
- [36] R. Guo, X. Ma, M. Liao et al., "Development and application of cochlear implant-based electric-acoustic stimulation of spiral ganglion neurons," *ACS Biomaterials Science & Engineering*, vol. 5, no. 12, pp. 6735–6741, 2019.
- [37] Y. Zhang, L. Guo, X. Lu et al., "Characterization of Lgr6+ cells as an enriched population of hair cell progenitors compared to Lgr5+ cells for hair cell generation in the neonatal mouse cochlea," *Frontiers in Molecular Neuroscience*, vol. 11, p. 147, 2018.
- [38] C. Cheng, L. Guo, L. Lu et al., "Characterization of the transcriptomes of Lgr5+ hair cell progenitors and Lgr5- supporting cells in the mouse cochlea," *Frontiers in Molecular Neuroscience*, vol. 10, p. 122, 2017.
- [39] C. Cheng, Y. Wang, L. Guo et al., "Age-related transcriptome changes in Sox2+ supporting cells in the mouse cochlea," *Stem Cell Research & Therapy*, vol. 10, no. 1, p. 365, 2019.
- [40] M. Tang, J. Li, L. He et al., "Transcriptomic profiling of neural stem cell differentiation on graphene substrates," *Colloids and Surfaces. B, Biointerfaces*, vol. 182, p. 110324, 2019.
- [41] D. You, L. Guo, W. Li et al., "Characterization of Wnt and notch-responsive Lgr5+ hair cell progenitors in the striolar region of the neonatal mouse utricle," *Frontiers in Molecular Neuroscience*, vol. 11, 2018.
- [42] Q. Cai, R. R. Vethanayagam, S. Yang et al., "Molecular profile of cochlear immunity in the resident cells of the organ of Corti," *Journal of Neuroinflammation*, vol. 11, no. 1, p. 173, 2014.
- [43] P. Mertins, NCI CPTAC, D. R. Mani et al., "Proteogenomics connects somatic mutations to signalling in breast cancer," *Nature*, vol. 534, no. 7605, pp. 55–62, 2016.
- [44] K. Li, D. Ching, F. S. Luk, and R. L. Raffai, "Apolipoprotein E enhances microRNA-146a in monocytes and macrophages to suppress nuclear factor- κ B-driven inflammation and atherosclerosis," *Circulation Research*, vol. 117, no. 1, pp. e1–e11, 2015.
- [45] V. S. Shavva, D. A. Mogilenko, E. V. Nekrasova et al., "Tumor necrosis factor α stimulates endogenous apolipoprotein A-I expression and secretion by human monocytes and macrophages: role of MAP-kinases, NF- κ B, and nuclear receptors PPAR α and LXRs," *Molecular and Cellular Biochemistry*, vol. 448, no. 1-2, pp. 211–223, 2018.
- [46] M. Zhang, G.-J. Zhao, K. Yin et al., "Apolipoprotein A-1 binding protein inhibits inflammatory signaling pathways by binding to apolipoprotein A-1 in THP-1 macrophages," *Circulation Journal*, vol. 82, no. 5, pp. 1396–1404, 2018.
- [47] X. Yang, S. Chen, Z. Shao et al., "Apolipoprotein E deficiency exacerbates spinal cord injury in mice: inflammatory response and oxidative stress mediated by NF- κ B signaling pathway," *Frontiers in Cellular Neuroscience*, vol. 12, 2018.
- [48] D. Liu, J. Liang, M. Zhao et al., "Lysine glycation of apolipoprotein A-I impairs its anti-inflammatory function in type 2 diabetes mellitus," *Journal of Molecular and Cellular Cardiology*, vol. 122, pp. 47–57, 2018.

Research Article

An Age-Related Hearing Protection Locus on Chromosome 16 of BXD Strain Mice

Qing Yin Zheng ¹, Lihong Kui,^{1,2} Fuyi Xu ³, Tihua Zheng,² Bo Li,² Melinda McCarty,³ Zehua Sun,^{1,2} Aizheng Zhang,¹ Luying Liu,^{1,2} Athena Starlard-Davenport,³ Ruben Stepanyan,^{1,4} Bo Hua Hu,⁵ and Lu Lu ³

¹Department of Otolaryngology-Head and Neck Surgery, Case Western Reserve University, Cleveland, Ohio, USA

²Hearing and Speech Rehabilitation Institute, College of Special Education, Binzhou Medical University, Yantai, China

³Department of Genetics, Genomics and Informatics, University of Tennessee Health Science Center, Memphis, TN 38106, USA

⁴Department of Neurosciences, Case Western Reserve University, Cleveland, Ohio, USA

⁵Center for Hearing and Deafness, University at Buffalo, NY 14214, USA

Correspondence should be addressed to Qing Yin Zheng; qing.zheng@case.edu and Lu Lu; llu@uthsc.edu

Received 23 April 2020; Revised 15 May 2020; Accepted 21 May 2020; Published 8 June 2020

Academic Editor: Renjie Chai

Copyright © 2020 Qing Yin Zheng et al. This is an open access article distributed under the Creative Commons Attribution License, which permits unrestricted use, distribution, and reproduction in any medium, provided the original work is properly cited.

Inbred mouse models are widely used to study age-related hearing loss (AHL). Many genes associated with AHL have been mapped in a variety of strains. However, little is known about gene variants that have the converse function—protective genes that confer strong resistance to hearing loss. Previously, we reported that C57BL/6J (B6) and DBA/2J (D2) strains share a common hearing loss allele in *Cdh23*. The cadherin 23 (*Cdh23*) gene is a key contributor to early-onset hearing loss in humans. In this study, we tested hearing across a large family of 54 BXD strains generated from B6 to D2 crosses. Five of 54 strains maintain the normal threshold (20 dB SPL) even at 2 years old—an age at which both parental strains are essentially deaf. Further analyses revealed an age-related hearing protection (*ahp*) locus on chromosome 16 (Chr 16) at 57–76 Mb with a maximum LOD of 5.7. A small number of BXD strains at 2 years with good hearing correspond roughly to the percentage of humans who have good hearing at 90 years old. Further studies to define candidate genes in the *ahp* locus and related molecular mechanisms involved in age-related resilience or resistance to AHL are warranted.

1. Introduction

Age-related hearing loss (AHL), or presbycusis, is a major sensory impairment [1] generally caused by the degeneration of hair cells within the organ of Corti [2]. AHL is characterized by a slow progressive decline in hearing sensitivity and balance [3]. AHL can contribute to social isolation, depression, and even cognitive decline [4, 5]. Approximately 35% of adults between 65 and 75 years old have some degree of hearing loss; and by 75 years, 40–50% have AHL. Like most age-related neurodegenerative diseases, AHL is genetically complex due to interaction with many environmental risk factors (e.g., noise, smoking, ototoxic drugs, and disease). Due to its late onset, genetic analysis is difficult [6, 7]. The

use of inbred mouse models can provide an ideal translational bridge to study AHL and to enable mechanistic and preclinical therapeutic studies aimed at devising new treatments.

Inbred strains of mice have been effectively used to investigate AHL [8, 9]. We and others have mapped several quantitative trait loci (QTLs) in a variety of inbred mice, including *ahl* [10, 11], *ahl2* [12], *ahl3* [13, 14], *ahl4* [15], *ahl5*, and *ahl6* [16], that greatly increase the risk of AHL. The *ahl* locus is now known to be a mutation in *Cdh23* [17, 18]. Both C57BL/6J (B6) and DBA/2J (D2) strains of mice are homozygous for the *Cdh23*^{c.753A} allele and have progressive hearing loss [10]. However, the D2 strain exhibits a much early-onset of hearing loss, starting from 3 weeks old, and most

animals are deaf by 3 months [8, 19, 20]. In contrast, B6 mice only develop high-frequency hearing loss starting at 3 months old, and the loss progresses to low-frequencies and worsen to a profound level only by 12 months [8, 10, 11, 21].

Recombinant inbred (RI) strains have been widely used in genetic mapping and studies of gene-gene, gene-environment, or gene-drug interactions, as well as gene expression-molecular pathways for Mendelian and quantitative traits [22, 23]. Conventional mouse RI strains are developed by crossing two inbred parental strains and repeatedly mating the resulting siblings for 20 generations or more to ensure that they are at least 99% inbred [24].

We conducted this study using BXD RI strains derived from crosses between B6 and D2 parents that are commonly used as models of AHL. BXDs are a very large mouse family ($N = 152$), which is optimal to replicate experiments across different laboratories or at different years as long as they have the same substrain name. At the same time, the diversity among the 152 strains offers a very powerful tool for mapping and analyzing the genetic origin of complex traits, such as hearing loss [25, 26]. The BXDs are an unrivaled resource for auditory system genetics because the parental strains are suitable hearing loss models with a significant difference in age-related progressions. Additionally, both parental strains and all of their highly diverse BXD RI progeny have been well-sequenced, and more than 6 million sequence variants have been identified and segregated among the BXD strains [27]. Data for investigating the BXD family is available on our open-source database (<http://www.genenetwork.org>), which is now widely used as an experimental platform for personalized and probabilistic medicine.

2. Materials and Methods

2.1. Mice. We completed a hearing screen of 2–5 cases for each of 54 BXD strains plus B6 and D2 parental strains in total 170 mice. All were between 12 and 32 months old when tested. Animals were housed and maintained on a 12:12 light/dark cycle, with *ad libitum* access to food and water. All experimental procedures were in accordance with the *Guidelines for the Care and Use of Laboratory Animals* published by the National Institutes of Health and were approved by the Animal Care and Use Committee at the University of Tennessee Health Science Center (UTHSC; Memphis, TN, USA).

2.2. Hearing Screening. Hearing acuity was assessed using an auditory-evoked brainstem response (ABR) test [8]. All the hearing evaluation was performed at UTHSC (University of Tennessee Health Science Center) by Dr. Zheng, who has experience in testing the ABR in over ten thousand mice. In brief, the mice were anesthetized with an intraperitoneal injection (IP) of ketamine, xylazine, and acepromazine at doses of 40, 5, and 1 mg/kg, respectively. The body temperature was maintained at 37–38°C. ABR testing was carried out using a SmartEP system from Intelligent Hearing Systems (Miami, FL). The ABRs were recorded using platinum subdermal needle electrodes inserted at the vertex (active electrode), ventrolateral to the right (reference electrode) and

left (ground electrode) ears. The acoustic stimuli were tone-bursts (3 ms duration with a 1.5 ms cosine-gated rise/fall time) that were delivered through a high-frequency transducer (closed system). The tone-bursts were delivered to both ears simultaneously, and the recorded responses represented the threshold of the better hearing ear. The stimuli were presented in a 5 or 10 dB step decrement from 70 dB SPL until the lowest intensity that could still evoke a reproducible ABR pattern was detected. Average ABR thresholds for mice with normal hearing were about 30, 20, and 45 dB SPL for 8, 16, and 32 kHz tone bursts, respectively. In the current study, we defined the threshold shift of 20–40 dB SPL as mild impairment, 41–60 dB as intermediate impairment, and greater than 60 dB as profound impairment [12].

2.3. Examination of Morphological Phenotype. Cross-sections for hematoxylin-eosin (H&E) staining and whole-mount basilar membrane surface preparations were performed to define the site and the level of cell damage. The inner ears from mice were collected, perfused with Bouin’s fixative, then left immersed in fixative for 48 h, decalcified with Cal-EX solution for 6 h, and embedded in paraffin. Tissue sections of 5 μm were cut, mounted on glass slides, and stained in H&E. The stained tissues were observed under a light microscope. We performed morphological analyses of six BXD strains with either extremely good or poor hearing.

2.4. Heritability Estimation of Hearing Phenotypes. We estimated the narrow heritability of three hearing phenotypes (8, 16, and 32 kHz stimuli) with the following equation [28], in which variances among strain means were compared to the total variance.

$$h^2 = \frac{0.5VA}{0.5VA + VE} \quad (1)$$

VA is the variance among strain means, and VE is the variance within strains.

2.5. Mapping of Auditory Acuity Loci. One of the primary uses of the BXD family is to map QTLs that modulate hearing phenotypes of the auditory system [29]. All ~7200 BXD informative genetic markers (http://www.genenetwork.org/webqtl/main.py?FormID=sharinginfo&GN_AccessionId=600) were checked for association with each hearing phenotype at 8, 16, and 32 kHz. This analysis was done using the WebQTL tool on our GeneNetwork website (<http://www.genenetwork.org>) [30, 31]. The likelihood ratio statistics (LRS) score computed with the Haley-Knott equations [32] was used to evaluate linkages between differences in traits and differences in particular genotype markers. Genome-wide significance (p value < 0.05) was calculated based on 1000 permutation tests. The phenotype-associated QTLs using the Haley and Knott method were further confirmed with GEMMA, a linear mixed model mapping algorithm that accounts for kinship among the BXD strains. For GEMMA mapping results, 4 LOD score (equal to $-\log(p)$ of 4) was set to the genome-wide significant threshold. The confidence interval was estimated by a 2 LOD drop-off method [33].

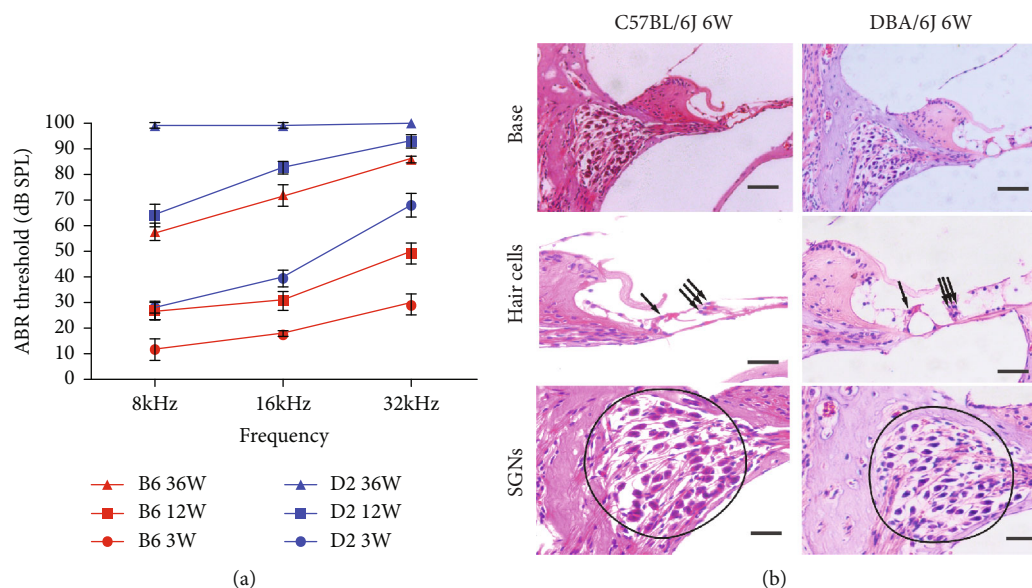


FIGURE 1: (a) ABR thresholds of three age groups in parental D2 and B6 strains ($n = 5$ for each group). ABR thresholds of D2 and B6 mice were determined at three frequencies shown on the x -axis. Error bars indicate the standard error of the mean (SEM). (b) Cross-sections ($5 \mu\text{m}$) through the modiolus of the cochleae from a D2 and a B6 mouse at the age of 6 weeks. Overall morphological characteristics of the basal turn (scale bars = $200 \mu\text{m}$) and degeneration of spiral ganglion cells and hair cells (scale bars = $50 \mu\text{m}$) were observed.

2.6. *Variant Identification.* Sequence differences segregating the BXDs have been described in a previous work [34]. In this study, we have focused on variants that change protein sequence, such as nonsense, missense, and frameshift mutations.

2.7. *Gene Expression Resource.* Gene expression levels of the inner ear for the genes within the QTL interval were explored at the gEAR portal online resource (<https://umgear.org/>). The gEAR portal is a website for visualization and analysis of multiomic data both in public and private domains. In addition, the gEAR portal enables upload, visualization, and analysis of single-cell RNA sequencing data (scRNA-seq data).

2.8. *Data Analysis.* Data Desk 8.1 software was used to calculate means, SD, and variance. Differences between two groups (such as two groups of strains with extremely good and poor hearing) were analyzed using a two-tailed Student's t -test.

3. Result

3.1. *D2 Mice Exhibit an Early-Onset Hearing Deficit and Associated Loss of Spiral Ganglion Neurons and Hair Cells.* We assessed the hearing sensitivity of B6 and D2 parental strains by ABR threshold measurements. Both B6 and D2 mice displayed progressive hearing loss. Loss of hearing in D2 mice occurred much earlier and was more profound than that in B6 mice. The D2 strain began to exhibit hearing loss as early as 3 weeks old, and the loss progressed to a severe level within 2–3 months. The B6 mouse strain showed hearing loss starting at 3 months old, and the loss progressed to a wider

frequency range and a profound level after 9 months (Figure 1(a)). Sections of the cochleae from B6 and D2 mice were examined microscopically for an initial gross assessment of cochlear pathology. Hearing loss in both B6 and D2 mice was accompanied by progressive degeneration of the organ of Corti and spiral ganglia. The SGNs began to lose at the age of 6 weeks in D2 when hearing loss developed (Figure 1(b)).

3.2. *The Hearing Threshold Is a Gradient Distribution in BXD Strains.* We screened 54 BXD strains (aged 12–32 months) for hearing loss at 8, 16, and 32 kHz. The heritability was around 50–70% for the 3 frequencies, suggesting that genetic factors significantly affected hearing loss with aging. The threshold level was found to be a gradient distribution in BXD strains (Figure 2(a)). The results showed that the thresholds of the three tested frequencies varied significantly among BXD strains. The 16 kHz measurement showed that some BXD strains (including BXD79, 155, and 74) had a favorable hearing threshold measured at 21 months, while others (including BXD198, 101, and 45) had severe hearing loss (100 dB SPL) at 1 year old (Figure 2(b)). We hypothesize that this gradient distribution of hearing in BXD strains is due to the segregation of genes carried by D2 and B6 inbred strains.

3.3. *Several BXD Strains Retain Excellent Hearing at the Age of Two Years.* Our ABR assessments revealed that several BXD strains retained excellent hearing at the age of two years (Figure 2(a)). For example, the 16 kHz threshold in BXD79 remained at the level of 20 dB SPL at the age of 21 months (Figure 3(a)). We observed that the D2 strain began to exhibit hearing loss at 3 weeks old which progressed to severe

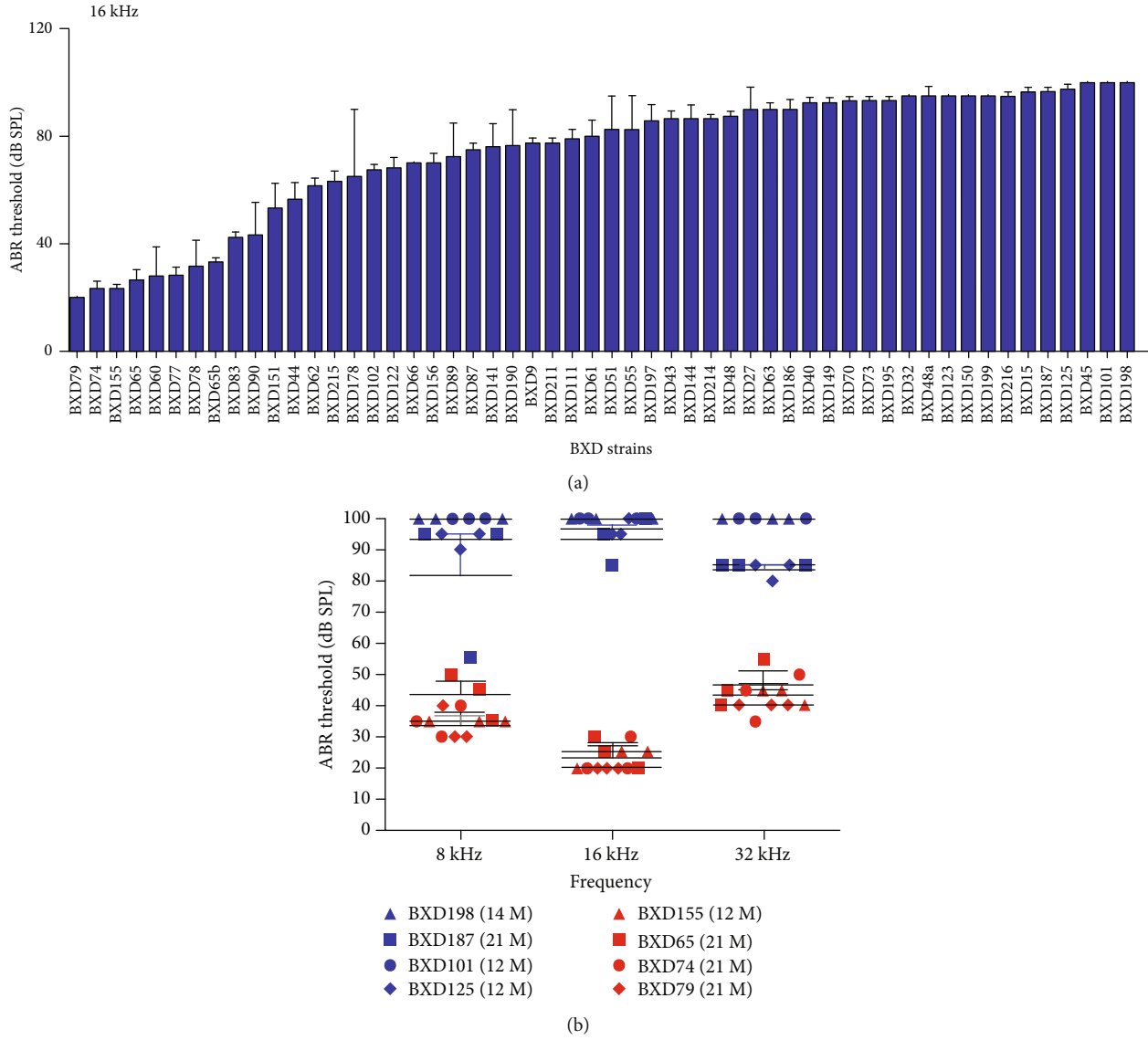


FIGURE 2: (a) The ABR thresholds of 54 BXD mouse strains at 2 years old display a gradient distribution at 16 kHz. Other frequencies have also been tested (data not shown). (b) ABR thresholds of good-hearing (BXD79, BXD74, BXD65, and BXD155) and poor-hearing (BXD198, BXD187, BXD101, and BXD125) mice are exemplified, respectively. Each data point represents an average threshold value (calculated as the arithmetic mean) for each age group ($n = 3$) described in the adjacent data point legend. Error bars indicate the standard deviation from the SEM. The ABR thresholds were also statistically analyzed, showing significant differences between the four good-hearing and four poor-hearing strains ($p < 0.05$ by ANOVA test).

hearing loss within 2–3 months. B6 mice had a normal hearing before 3 months old, and then their hearing began to decline starting from high frequencies (32 kHz) as we measured. The level of hearing loss among three-month-old D2 and 12-month-old B6 mice was more severe compared to the 2-year-old BXD79 strain (Figure 3(b)). We performed H&E staining of cross-sections of the inner ear for 3 strains with partial hearing loss and 3 strains with deafness at 1 year old. We observed a loss of the inner hair cells (IHCs) and outer hair cells (OHCs) and a decrease in the density of SGNs in the strains with deafness (Figures 3(c) and 3(d)).

3.4. A Novel Age-Related Hearing Protection (*ahp*) Locus Maps to Chr 16. One novel QTL for all three frequencies was identified on Chr 16 at 69.6 Mb, with a peak LOD score of 5.7, 5.2, and 4.6 for 8, 16, and 32 kHz, respectively (Figure 4). This QTL encompasses 19 Mb from 57 to 76 Mb. However, this novel QTL was unable to be detected when we performed QTL mapping by excluding several strains with relatively good hearing (ABR < 35 dB SPL), which suggests that including mice with a good hearing in the study is obligatory in discovering novel QTL associated with hearing protection. In addition, we identified a QTL on Chr 11

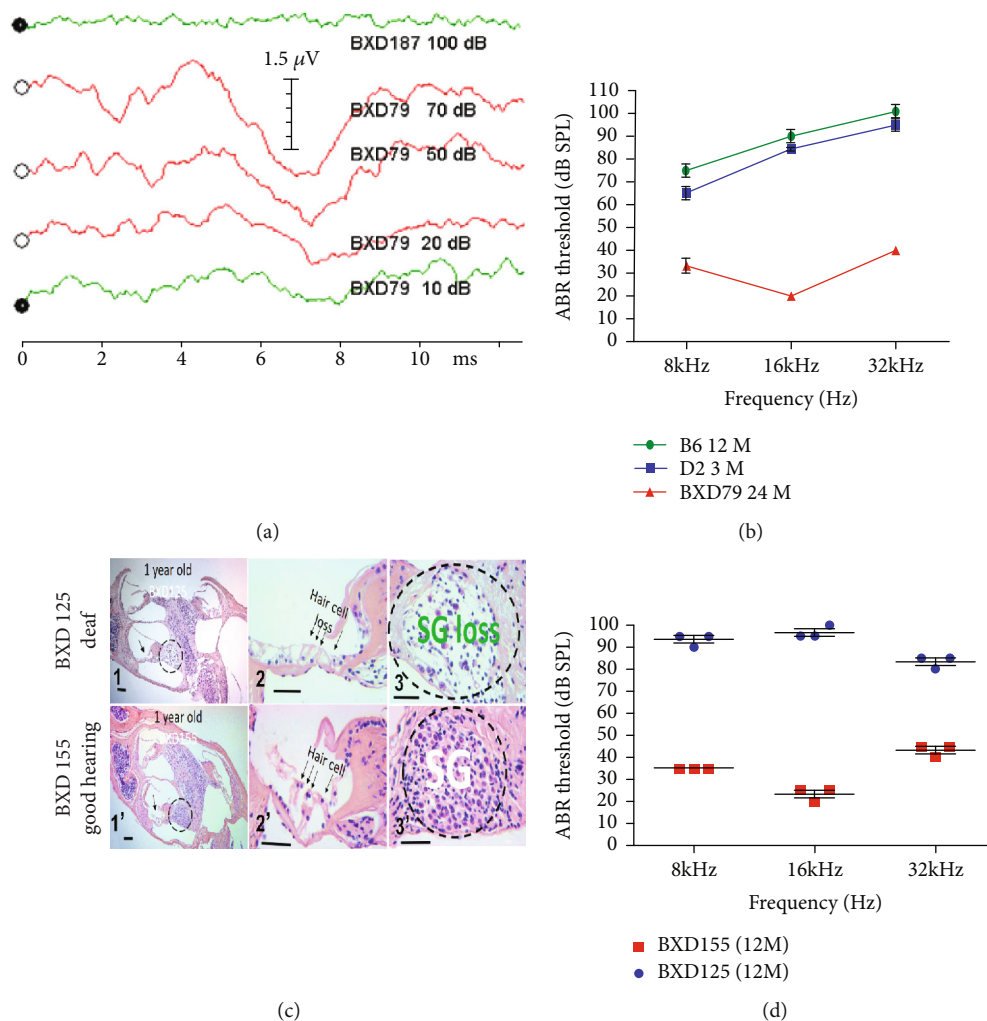


FIGURE 3: (a) 16 kHz ABR testing of a good-hearing BXD79 mouse revealed measurable responses to sound as low as 10 dB (bottomed greenline) and a deaf BXD187 mouse had no response to 100 dB (the top green line); both mice are at the age of 21 months. (b) ABR thresholds of parental 3-month-old D2 mice, 12-month-old B6 mice, and 24-month-old BXD79 mice that have the best hearing among the 54 examined BXD strains. (c) H&E stained cross-sections of the inner ears from a deaf mouse (BXD125) (C1-3) and a good hearing mouse (BXD155) (C1'-3'). Morphological contrast of the whole cochleae from the deaf BXD125 (C1) and the good hearing BXD155 (C1') strain. OHCs and IHCs are lost in the deaf ear (C2) but are present in the good ear (C2'). Spiral ganglion (SG) cells are lost in the deaf ear (C3) but are present in the good ear (C3'). Scale bars = 50 μm. The corrected densities of the SGNs (420 ± 28) in the basal cochlear turn in deaf BXD mice ($n = 3$) are significantly less than those of good hearing BXD mice (1411 ± 39) ($n = 3$; $p = 0 : 0001$ by t -test). No significant differences in the mean density of the SGNs in the apical cochlear turns were observed (data not shown). (d) ABR thresholds of deaf BXD125 and good-hearing BXD155 mice are exemplified at 1 year old ($n = 3$). Error bars indicate the standard deviation from the SEM. The ABR thresholds are significantly different between the two strains ($p < 0 : 05$ by ANOVA test).

significantly associated with all three frequencies, with peak LOD score of 4.9, 4.9, and 5.5 for 8, 16, and 32 kHz, respectively (Figure 4). This QTL overlapped with the previously identified AHL locus *ahl8* [20]. The *ahl8* was proven to be a nonsynonymous variant (rs26996001) of *Fscn2* gene in D2 mice, which causes an amino acid change from arginine to histidine at position 109 (R109H) [35]. The wild-type allele of this mutation prevents hearing loss. Loss of function of this gene has been shown to cause a variety of morphological and functional changes, including malformation of stereociliary bundles of cochlear hair cells, abnormal outer hair cell

physiology, abnormal ABR, abnormal distortion product otoacoustic emission, a decrease in the numbers of stereocilia in both inner and outer hair cells, an increase in the susceptibility to AHL, short cochlear hair cell stereocilia, and outer hair cell degeneration [35, 36].

3.5. Exploration of Candidate Genes in QTL Region of Chr 16. The QTL region at Chr 16 harbors 145 genes, including 67 protein-coding genes, among which 25 are olfactory receptor genes (Table 1). The remaining genes are predicted genes or pseudogenes.

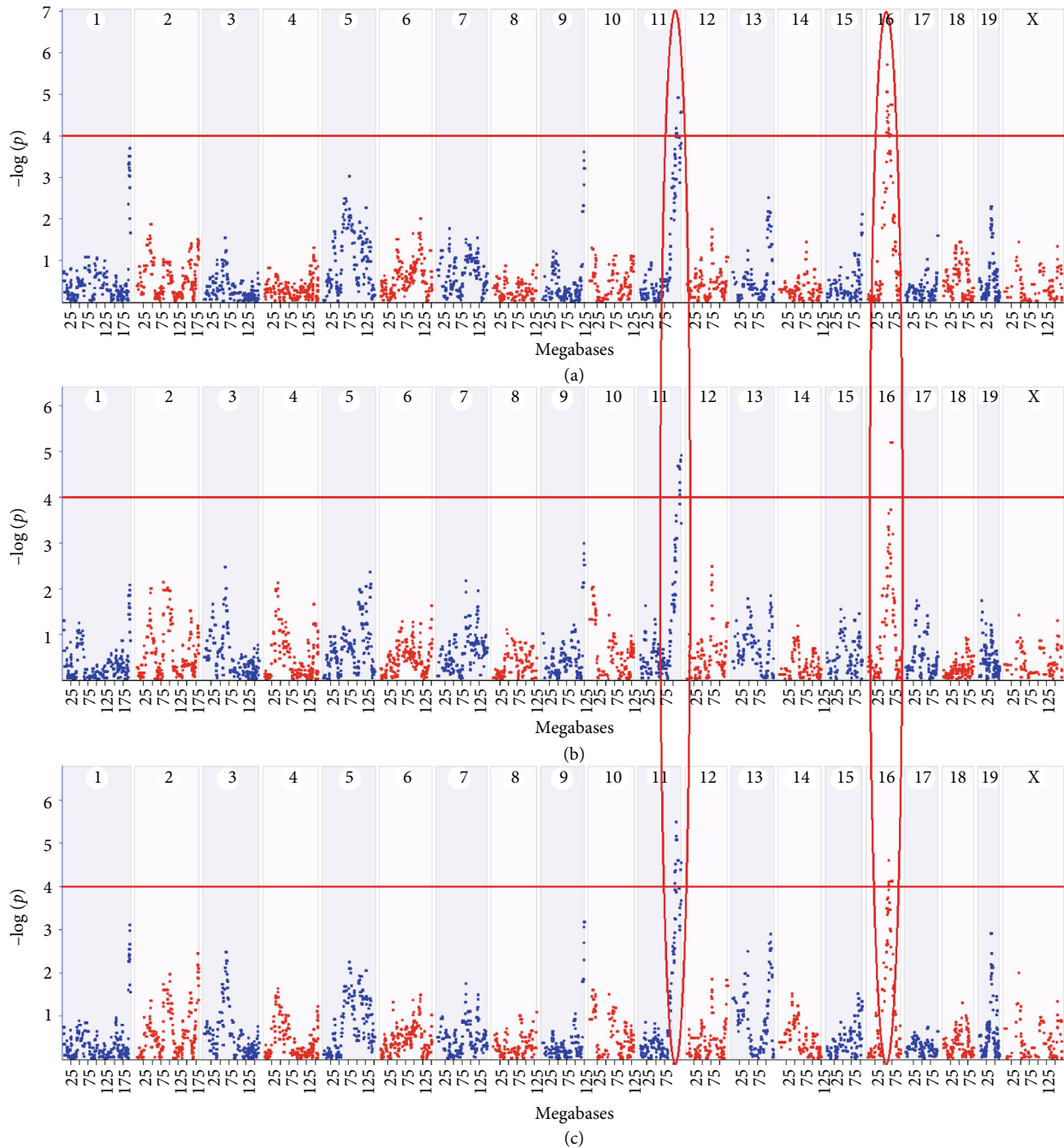


FIGURE 4: Manhattan plot of linkage to hearing phenotypes. QTL mapping identified one novel QTL on Chr 16 and one known QTL on Chr 11 for all three hearing phenotypes at 8, 16, and 32 kHz (a–c). The x -axis denotes a position on the mouse genome, in megabases (Mb), while the y -axis gives the $-\log(p)$ of linkage. The red line indicates a significant threshold for a genome-wide scan at a LOD score of 4 (equal to $-\log(p)$ of 4). Maps were computed with GEMMA using LOCO option. All analyses were performed on GeneNetwork.

We explored whether genes in the QTL region harbored protein-altering variants, which could be responsible for the generation of observed hearing phenotype. With our previously sequenced whole genome sequences of D2 and B6, we identified 10 genes that harbor nonsynonymous variants, including *Arl6*, *Crybg3*, *Epha3*, *Epha6*, *Filip1l*, *Gabrr3*, *Gbe1*, *Gpr15*, *Hspa13*, and *Samsn1* (Table 1). In addition, *Htr1f*

contains a frameshift variant. No protein-altering variants were found within the other genes in the QTL interval.

Next, we explored whether the genes in the QTL region, especially for those protein-coding genes, were expressed in the hearing relevant tissue or cell types. By searching the gEAR portal (<https://umgear.org/>), a database for gene expression analysis resource, we found 19 genes that are

TABLE 1: List of the protein-coding genes within the QTL region of Chr 16.

Entrez ID	Symbol	Location (Chr and Mb)	Distance to QTL peak (Mb)	Variant	Expression*	Candidates rank
224273	Crybg3	16:59.490775	-10.11	Nonsynonymous SNP	High	Top
56297	Arl6	16:59.613321	-9.99	Nonsynonymous SNP	High	Top
13837	Epha3	16:63.545218	-6.05	Nonsynonymous SNP	High	Top
110920	Hspa13	16:75.75519	6.16	Nonsynonymous SNP	High	Top
78749	Filip11	16:57.353277	-12.25	Nonsynonymous SNP	Low	Median
71223	Gpr15	16:58.717435	-10.88	Nonsynonymous SNP	Low	Median
328699	Gabrr3	16:59.407382	-10.19	Nonsynonymous SNP	Low	Median
13840	Epha6	16:59.641433	-9.96	Nonsynonymous SNP	Low	Median
15557	Htr1f	16:64.924729	-4.68	Frameshift	Low	Median
74185	Gbe1	16:70.313949	0.71	Nonsynonymous SNP	Low	Median
67742	Samsn1	16:75.858794	6.26	Nonsynonymous SNP	Low	Median
28185	Tomm70a	16:57.121714	-12.48	NA	High	Median
52633	Nit2	16:57.156665	-12.44	NA	High	Median
67581	Tbc1d23	16:57.168858	-12.43	NA	High	Median
71027	Tmem30c	16:57.266139	-12.33	NA	High	Median
12837	Col8a1	16:57.624256	-11.98	NA	High	Median
73379	Dcbld2	16:58.408426	-11.19	NA	High	Median
12892	Cpox	16:58.670208	-10.93	NA	High	Median
68146	Arl13b	16:62.793308	-6.81	NA	High	Median
19128	Pros1	16:62.854307	-6.75	NA	High	Median
72020	Zfp654	16:64.780347	-4.82	NA	High	Median
106143	Cggbp1	16:64.852001	-4.75	NA	High	Median
68942	Chmp2b	16:65.539133	-4.06	NA	High	Median
73569	Vgll3	16:65.815015	-3.78	NA	High	Median
19876	Robo1	16:72.027551	2.43	NA	High	Median
268902	Robo2	16:73.891976	4.29	NA	High	Median
54613	St3gal6	16:58.469742	-11.13	NA	Low	Low
106338	Nsun3	16:62.732444	-6.87	NA	Low	Low
68159	Stx19	16:62.814676	-6.79	NA	Low	Low
239857	Cadm2	16:66.655416	-2.94	NA	Low	Low
224344	Rbm11	16:75.592844	5.99	NA	Low	Low
69457	Tmem45a2	16:57.036967	-12.56	NA	NA	Low
66497	Cmss1	16:57.302	-12.30	NA	NA	Low
224250	Cldnd1	16:58.72791	-10.87	NA	NA	Low
67014	Riox2	16:59.47177	-10.13	NA	NA	Low
224291	Csnka2ip	16:64.47781	-5.12	NA	NA	Low
18736	Pou1f1	16:65.520629	-4.08	NA	NA	Low
224318	Speer2	16:69.856874	0.26	NA	NA	Low
52645	D16Erttd519e	16:70.616425	1.02	NA	NA	Low
751561	Mir691	16:74.34199	4.74	NA	NA	Low
102467647	n-TIaat1	16:75.434179	5.83	NA	NA	Low
320355	Lipi	16:75.540514	5.94	NA	NA	Low

Note: This list excluded the 25 olfactory receptor genes. * indicates that the genes are expressed in hair cells, epithelial nonhair cells, or the cochlear duct. Expression data were extracted from the gEAR portal (<https://umgear.org/>). Expression value greater than 1000 is defined as high expression. NA: data not available.

highly expressed in hair cells, epithelial nonhair cells, or the cochlear duct, including *Tomm70a*, *Nit2*, *Tbc1d23*, *Tmem30c*, *Col8a1*, *Dcbld2*, *Cpox*, *Crybg3*, *Arl6*, *Arl13b*, *Pros1*, *Epha3*, *Zfp654*, *Cggbp1*, *Chmp2b*, *Vgll3*, *Robo1*, *Robo2*, and *Hspa13* (Table 1). In addition, 11 genes have a relatively low level of

expression, including *Filip11*, *St3gal6*, *Gpr15*, *Gabrr3*, *Epha6*, *Nsun3*, *Stx19*, *Htr1f*, *Cadm2*, *Gbe1*, and *Rbm11*.

Based upon information, including gene mutation and expression, we categorized QTL candidates into three layers (Table 1): top priority, median priority, and low priority.

Top priority candidates included genes with functional mutation and highly expressed in cochlear hair cells, epithelial nonhair cells, or the cochlear duct. Median priority candidates included the followings: (1) genes with functional mutation and expressed in the hearing relevant tissue; and (2) genes with high expression in the hearing relevant tissue, but no functional variants. The rest of the candidates were defined as Low priority candidates.

It is worth noting that two genes within this locus have been implicated in the hearing function: *Arl6* (ADP-ribosylation factor-like 6) and *Pou1f1* (POU domain, class 1, transcription factor). *Arl6* has been linked to both sensorineural and conductive hearing impairment, while *Pou1f1* is associated with the abnormal orientation of outer hair cell stereociliary bundles, and abnormal morphology in outer hair cells, stria vascularis, and the tectorial membrane in the cochlea. *Pou1f1* is functionally associated with a decreased endocochlear potential, the absence of cochlear microphonics and distortion product otoacoustic emissions, and deafness [37].

4. Discussion

We have previously mapped several hearing loss QTLs, such as *ahl1* [10], *ahl2* [12], and *ahl4* [15]. We also located *ahl8* [20] within 32 BXD strains from the Jackson Laboratory. A QTL locus underlying the early-onset, low-frequency hearing loss in BXD strains has been mapped at chromosome 18, *ahl9* [38]. All of these previous data were collected from mice younger than one-year-old. The primary objective of previous studies was to identify variants that increase the risk of hearing loss. At present, only a limited number of deafness-resistant QTLs have been mapped. Thus, studies designed to identify genetic variants that protect from hearing loss are critical.

The BXD strains are currently the largest and best phenotyped genetic reference population. The genomes of both parental strains have been extraordinarily well-sequenced, giving us the information on essentially all sequence variants that segregate [26] among BXD strains. Most importantly, D2 and B6 are commonly used mouse models of AHL loss. We observed that hearing loss in D2 mice occurs much earlier than does the B6 as illustrated by our functional analysis with ABR. By 12 months, both B6 and D2 mice displayed massive hearing loss with D2 mice having even greater pathogenesis (see Figure 1 and our previous reports [8, 39, 40, 41, 42]). These features are quite similar to those of human presbycusis in which hearing loss starts from higher frequencies, followed by middle- and lower frequencies. The functional loss is associated with degenerative changes in highly energetic cells of the *stria vascularis*, spiral ganglion neurons, and cochlear hair cells, especially outer hair cells. Cells of the *stria vascularis* generate the endocochlear potential (EP; also called endolymphatic potential), a positive voltage of 80-100 mV in the cochlear endolymphatic space [43, 44]. Notably, although D2 mice functionally have much early and severe hearing loss, histologically, the loss of spiral ganglion cells and hair cells at 6 weeks old did not differ much from B6 mice, suggesting that the unique genetic background

in the D2 strain offers protection of spiral ganglion and hair cell bodies but not stereocilium tips where mutant fascin-2 disturbs crosslink function and slows actin depolymerization at stereocilium tips that are important for maintaining the stereocilium length as previously proposed [36].

The BXDs are a logical and powerful first resource for the systems genetics analysis of hearing loss. We have screened 2-5 mice per strain across 54 BXD strains and confirmed QTL on Chr 11 where *Fscn2* is identified as a causal gene of hearing loss [35] and found 1 novel QTL on Chr 16 in aged BXD mice that is most likely an *ahp* locus in BXD strains.

The hearing threshold has a gradient distribution in BXD strains (see Figure 2). Several BXD strains have remarkably intact hearing even at 2 years old—an age at which both parental strains are essentially deaf (Figure 3(b)). ABR thresholds of good-hearing BXD79 mice at 21 months old are much better than those of BXD187 mice at 12 months old ($p < 0.05$, see Figure 2(b)). This is mainly because the traits and genes of the parental strains begin to segregate. In previous studies, D2 mice have the early onset of progressive hearing loss with mutations in several genes known to cause hearing loss, including *Cdh23*^{c.753A} and *Fscn2*^{R109H} [10, 35]. The features of deafness in D2 mice segregate among BXD family members. The B6 mice share the *Cdh23*^{c.753A} mutation with D2 [11, 19], having mid-aged hearing loss. The features of hearing protection also segregate among BXD family members. Both D2 and B6 mice carry *Cdh23*^{c.753A}, and both are nearly deaf over a year old. All BXD strains should carry the *Cdh23*^{c.753A}. Why do a few BXD strains maintain good hearing even around 1-2 years old? We hypothesize that BXD strains harboring the protective locus preserve better hearing at older ages.

As demonstrated in previous studies and our current investigation, hearing loss in B6 and D2 mice are accompanied by degeneration of the organ of Corti and spiral ganglia (see Figure 1(b)) [19, 45]. This degeneration is caused mainly by *Cdh23* [17, 18, 46]. Our histological examination of the one-year-old BXD strains revealed a highly correlated change in hearing dysfunction and cochlear pathogenesis. Hair cell loss and spiral ganglia loss happened earlier and more severely in the basal turn of the cochlea, which corresponds to high-frequency hearing loss exhibited in both parental strains and the vast majority of BXD strains. Taken an example from the 5 best hearing BXD strains out of the 54 total strain so far we have tested, the good hearing strain (responded well to as low as 10-dB tone bursts, see the bottom green sweep in Figure 3(a)) corresponded to the nearly intact histological structures (1', 2', and 3' in Figure 3(c)). In contrast, the deaf strain (the top sweeps in Figure 3(a)) corresponded with the severe loss in hair cells and spiral ganglion cells (1, 2, and 3 in Figure 3(c)). The hearing threshold between the two strains showed a statistically significant difference (Figure 3(d)). These dramatic contrasts, both in hearing function and pathology, have not been reported in any BXD strains at such old age. This suggests that the protective loci in BXD strains interact with *Cdh23* to reduce the damage to the auditory system.

QTL analysis was used in our current research. We screened 54 aged BXD strains and performed a QTL analysis

for hearing phenotypes at 8, 16, and 32 kHz. This analysis unveiled one novel QTL on chromosome 16 (Chr 16) and one known QTL on chromosome 11 (Chr 11) for all 3 measurements (Figure 4). Nevertheless, the novel QTL on Chr16 is completely undetectable when we remove the mice with the ABR threshold <35 db SPL (6 strains with the best hearing, 11%), while Chr 11 QTL (*alh8*) shows enhanced signals at all 8, 16, and 32 kHz. We and others have reported that the locus on Chr11 (*ahl8*) contributing to progressive hearing loss in D2 mice is a missense variant of the *Fscn2* gene [20, 35]. The *Cdh23^{c.753A}* mutation is shared by both D2 and B6 [10], and it is consistent with our QTL analysis of 3 measurements. A total of 155 genes are mapped to the 73.6Mb interval of Chr 16; however, only 67 are protein-coding genes that include 25 olfactory receptor genes (Table 1). The rest of them are either predicted genes or pseudogenes. After filtering based on the protein-altering variants, the best candidate genes for Chr 16 are *Arl6*, *Crybg3*, *Epha3*, *Epha6*, *Filip1l*, *Gabrr3*, *Gbe1*, *Gpr15*, *Hspa13*, and *Samsn1*. *Htr1f* is identified as a frameshift variant.

MSM derived *Ahl3* in B6-Chr17 (MSM) consomic mice showed a prominent hearing loss resistance and was mapped on chromosome 17 in 2004 [13]. Apparently, identifying candidate genes in this locus will significantly help us understand age-related hearing protection at the molecular level and potentially help to define therapeutic drug target for preventing human presbycusis. But so far, the *Ahl3* has not been defined at the gene level because the disadvantage of the whole chromosome 17 substitution makes the genetic mapping impossible for narrowing down. Thus, we should take the advantages of many strains of BXD with each small segment of every chromosome that has reshuffled for over 20 generations. Nevertheless, RNA-seq data from the inner ear of BXD strains are needed for further investigation of the *ahp* at the gene and molecular levels.

Many of our commonly used hearing loss inbred mouse models carry the *Cdh23^{c.753A}* allele [10, 47], which are relatively numerous in our studies in mouse models. Mutations of the *Cdh23* gene are involved in a spectrum of hearing impairments, including hearing loss with vision loss, Usher syndrome 1D, early-onset progressive hearing loss, and AHL in humans or mouse models. Two recent studies have shown that *Cdh23* mutations significantly contribute to AHL in humans [47, 48]. As a result, *Cdh23* is an important gene linked to hearing loss. Thus, the protective locus may prevent hearing loss in humans.

In summary, using QTL mapping, we have identified a novel locus on Chr 16 that is a significant contributor to the protection of hearing. It lessens the decline of the auditory function and pathology related to AHL, a disease affects the quality of lives in more half of the elderly over 75 years old. The discovery of this locus will help to better understand the molecular mechanism of AHL and provide clues for identifying new candidate genes responsible for human senile deafness and other hearing impairment.

Data Availability

No additional data were used to support this study.

Conflicts of Interest

The authors declare no conflicts of interest.

Authors' Contributions

Qing Yin Zheng, Lihong Kui and Fuyi Xu contributed equally to this work.

Acknowledgments

This work was supported by the Pilot Program of Center for Integrative and Translational Genomics (CITG) at UTHSC. This work was supported by grants from the National Institutes of Health of the United States (R01DC015111 and R21DC005846) and grants from the National Natural Science Foundation of China (81530030, 81500797, and 81873697). We also thank Dr. Williams for his financial support and editing of the manuscript.

References

- [1] A. R. Kidd Iii and J. Bao, "Recent advances in the study of age-related hearing loss: a mini-review," *Gerontology*, vol. 58, no. 6, pp. 490–496, 2012.
- [2] L. E. Golovanova, M. Y. Boboshko, E. A. Kvasov, and E. S. Lapteva, "Hearing loss in adults in older age groups," *Advances in Gerontology*, vol. 32, no. 1-2, pp. 166–173, 2019.
- [3] J. Mazelova, J. Popelar, and J. Syka, "Auditory function in presbycusis: peripheral vs. central changes," *Experimental Gerontology*, vol. 38, no. 1-2, pp. 87–94, 2003.
- [4] M. R. Bowl and S. J. Dawson, "The mouse as a model for age-related hearing loss - a mini-review," *Gerontology*, vol. 61, no. 2, 2015.
- [5] N. M. Armstrong, J. A. Deal, J. Betz et al., "Associations of hearing loss and depressive symptoms with incident disability in older adults: health, aging, and body composition study," *The journals of gerontology. Series A, Biological sciences and medical sciences*, vol. 75, no. 3, pp. 531–536, 2018.
- [6] R. Bovo, A. Ciorba, and A. Martini, "Environmental and genetic factors in age-related hearing impairment," *Aging Clinical and Experimental Research*, vol. 23, no. 1, pp. 3–10, 2011.
- [7] N. Ohgami, M. Iida, I. Yajima, H. Tamura, K. Ohgami, and M. Kato, "Hearing impairments caused by genetic and environmental factors," *Environmental Health and Preventive Medicine*, vol. 18, no. 1, pp. 10–15, 2013.
- [8] Q. Y. Zheng, K. R. Johnson, and L. C. Erway, "Assessment of hearing in 80 inbred strains of mice by ABR threshold analyses," *Hearing Research*, vol. 130, no. 1-2, pp. 94–107, 1999.
- [9] J. F. Willott, L. C. Erway, J. R. Archer, and D. E. Harrison, "Genetics of age-related hearing loss in mice. II. Strain differences and effects of caloric restriction on cochlear pathology and evoked response thresholds," *Hearing Research*, vol. 88, no. 1-2, pp. 143–155, 1995.
- [10] K. R. Johnson, Q. Y. Zheng, and L. C. Erway, "A major gene affecting age-related hearing loss is common to at least ten inbred strains of mice," *Genomics*, vol. 70, no. 2, pp. 171–180, 2000.
- [11] K. R. Johnson, L. C. Erway, S. A. Cook, J. F. Willott, and Q. Y. Zheng, "A major gene affecting age-related hearing loss in

- C57BL/6J mice,” *Hearing Research*, vol. 114, no. 1-2, pp. 83–92, 1997.
- [12] K. R. Johnson and Q. Y. Zheng, “Ahl2 a second locus affecting age-related hearing loss in mice,” *Genomics*, vol. 80, no. 5, pp. 461–464, 2002.
- [13] M. Nemoto, Y. Morita, Y. Mishima et al., “Ahl3, a third locus on mouse chromosome 17 affecting age-related hearing loss,” *Biochemical and Biophysical Research Communications*, vol. 324, no. 4, pp. 1283–1288, 2004.
- [14] Y. Morita, S. Hirokawa, Y. Kikkawa et al., “Fine mapping of Ahl3 affecting both age-related and noise-induced hearing loss,” *Biochemical and Biophysical Research Communications*, vol. 355, no. 1, pp. 117–121, 2007.
- [15] Q. Y. Zheng, D. Ding, H. Yu, R. J. Salvi, and K. R. Johnson, “A locus on distal chromosome 10 (ahl4) affecting age-related hearing loss in A/J mice,” *Neurobiology of Aging*, vol. 30, no. 10, pp. 1693–1705, 2009.
- [16] M. Drayton and K. Noben-Trauth, “Mapping quantitative trait loci for hearing loss in Black Swiss mice,” *Hearing Research*, vol. 212, no. 1-2, pp. 128–139, 2006.
- [17] K. Noben-Trauth, Q. Y. Zheng, and K. R. Johnson, “Association of cadherin 23 with polygenic inheritance and genetic modification of sensorineural hearing loss,” *Nature Genetics*, vol. 35, no. 1, pp. 21–23, 2003.
- [18] P. Kazmierczak, H. Sakaguchi, J. Tokita et al., “Cadherin 23 and protocadherin 15 interact to form tip-link filaments in sensory hair cells,” *Nature*, vol. 449, no. 7158, pp. 87–91, 2007.
- [19] Q. Wang, H. Zhao, T. Zheng et al., “Otoprotective effects of mouse nerve growth factor in DBA/2J mice with early-onset progressive hearing loss,” *Journal of Neuroscience Research*, vol. 95, no. 10, pp. 1937–1950, 2017.
- [20] K. R. Johnson, C. Longo-Guess, L. H. Gagnon, H. Yu, and Q. Y. Zheng, “A locus on distal chromosome 11 (ahl8) and its interaction with Cdh23 ahl underlie the early onset, age-related hearing loss of DBA/2J mice,” *Genomics*, vol. 92, no. 4, pp. 219–225, 2008.
- [21] H. S. Li and E. Borg, “Age-related loss of auditory sensitivity in two mouse genotypes,” *Acta Oto-Laryngologica*, vol. 111, no. 5, pp. 827–834, 1991.
- [22] M. J. Justice, N. A. Jenkins, and N. G. Copeland, “Recombinant inbred mouse strains: models for disease study,” *Trends in Biotechnology*, vol. 10, no. 4, pp. 120–126, 1992.
- [23] D. A. Blizard, “Recombinant-inbred strains: general methodological considerations relevant to the study of complex characters,” *Behavior Genetics*, vol. 22, no. 6, pp. 621–633, 1992.
- [24] L. M. Silver, *Mouse Genetics*, Oxford University Press, New York, 1995.
- [25] J. L. Peirce, L. Lu, J. Gu, L. M. Silver, and R. W. Williams, “A new set of BXD recombinant inbred lines from advanced intercross populations in mice,” *BMC Genetics*, vol. 5, no. 1, p. 7, 2004.
- [26] B. A. Taylor, C. Wnek, B. S. Kotlus, N. Roemer, T. MacTaggart, and S. J. Phillips, “Genotyping new BXD recombinant inbred mouse strains and comparison of BXD and consensus maps,” *Mammalian Genome*, vol. 10, no. 4, pp. 335–348, 1999.
- [27] E. E. Geisert and R. W. Williams, “Using BXD mouse strains in vision research: a systems genetics approach,” *Molecular Vision*, vol. 26, pp. 173–187, 2020.
- [28] J. P. Hegmann and B. Possidente, “Estimating genetic correlations from inbred strains,” *Behavior Genetics*, vol. 11, no. 2, pp. 103–114, 1981.
- [29] K. F. Manly, R. H. Cudmore, and J. M. Meer, “Map Manager QTX, cross-platform software for genetic mapping,” *Mammalian Genome*, vol. 12, no. 12, pp. 930–932, 2001.
- [30] E. P. Mulligan, A. Anderson, S. Watson, and R. J. Dimeff, “The diagnostic accuracy of the lever sign for detecting anterior cruciate ligament injury,” *International Journal of Sports Physical Therapy*, vol. 12, no. 7, pp. 1057–1067, 2017.
- [31] E. J. Chesler, L. Lu, S. Shou et al., “Complex trait analysis of gene expression uncovers polygenic and pleiotropic networks that modulate nervous system function,” *Nature Genetics*, vol. 37, no. 3, pp. 233–242, 2005.
- [32] B. Feenstra, I. M. Skovgaard, and K. W. Broman, “Mapping quantitative trait loci by an extension of the Haley-Knott regression method using estimating equations,” *Genetics*, vol. 173, no. 4, pp. 2269–2282, 2006.
- [33] A. Manichaikul, J. Dupuis, S. Sen, and K. W. Broman, “Poor performance of bootstrap confidence intervals for the location of a quantitative trait locus,” *Genetics*, vol. 174, no. 1, pp. 481–489, 2006.
- [34] X. Wang, A. K. Pandey, M. K. Mulligan et al., “Joint mouse-human phenome-wide association to test gene function and disease risk,” *Nature Communications*, vol. 7, no. 1, 2016.
- [35] J. B. Shin, C. M. Longo-Guess, L. H. Gagnon et al., “The R109H variant of fascin-2, a developmentally regulated actin crosslinker in hair-cell stereocilia, underlies early-onset hearing loss of DBA/2J mice,” *The Journal of Neuroscience*, vol. 30, no. 29, pp. 9683–9694, 2010.
- [36] B. J. Perrin, D. M. Strandjord, P. Narayanan, D. M. Henderson, K. R. Johnson, and J. M. Ervasti, “Beta-Actin and fascin-2 cooperate to maintain stereocilia length,” *The Journal of Neuroscience*, vol. 33, no. 19, pp. 8114–8121, 2013.
- [37] M. Mustapha, Q. Fang, T. W. Gong et al., “Deafness and permanently reduced potassium channel gene expression and function in hypothyroid Pit1dw mutants,” *The Journal of Neuroscience*, vol. 29, no. 4, pp. 1212–1223, 2009.
- [38] A. P. Nagtegaal, S. Spijker, T. T. H. Crins, J. G. G. Borst, and N.-B. M. P. Consortium, “A novel QTL underlying early-onset, low-frequency hearing loss in BXD recombinant inbred strains,” *Genes, Brain, and Behavior*, vol. 11, pp. 911–920, 2012.
- [39] Q. Y. Zheng, Z. Sun, and A. Zhang, “Protective genetic variants forusher I syndrome and hearing loss,” *ARO Abstracts*, vol. 43, no. PD 124, p. 673, 2020.
- [40] J. Ohmen, E. Y. Kang, X. Li et al., “Genome-wide association study for age-related hearing loss (AHL) in the mouse: a meta-analysis,” *Journal of the Association for Research in Otolaryngology*, vol. 15, no. 3, pp. 335–352, 2014.
- [41] T. Zhao, X. Liu, Z. Sun et al., “RNA-seq analysis of potential lncRNAs for age-related hearing loss in a mouse model,” *Aging*, vol. 12, no. 8, pp. 7491–7510, 2020.
- [42] S. M. Jones, T. A. Jones, K. R. Johnson, H. Yu, L. C. Erway, and Q. Y. Zheng, “A comparison of vestibular and auditory phenotypes in inbred mouse strains,” *Brain Research*, vol. 1091, no. 1, pp. 40–46, 2006.
- [43] H. Lang, V. Jyothi, N. M. Smythe, J. R. Dubno, B. A. Schulte, and R. A. Schmiedt, “Chronic reduction of endocochlear potential reduces auditory nerve activity: further confirmation of an animal model of metabolic presbycusis,” *Journal of the Association for Research in Otolaryngology*, vol. 11, no. 3, pp. 419–434, 2010.
- [44] J. R. Dubno, M. A. Eckert, F. S. Lee, L. J. Matthews, and R. A. Schmiedt, “Classifying human audiometric phenotypes of

- age-related hearing loss from animal models,” *Journal of the Association for Research in Otolaryngology*, vol. 14, no. 5, pp. 687–701, 2013.
- [45] Q. Y. Zheng and K. R. Johnson, “Hearing loss associated with the modifier of deaf waddler (mdfw) locus corresponds with age-related hearing loss in 12 inbred strains of mice,” *Hearing Research*, vol. 154, no. 1-2, pp. 45–53, 2001.
- [46] B. Li, T. Zheng, C. Yan et al., “Chemical chaperone 4-phenylbutyrate prevents hearing loss and cochlear hair cell death in *Cdh23*^{erl/erl} mutant mice,” *Neuroreport*, vol. 30, no. 3, pp. 145–150, 2019.
- [47] A. Bouzid, I. Smeti, A. Chakroun et al., “CDH23 methylation status and presbycusis risk in elderly women,” *Frontiers in Aging Neuroscience*, vol. 10, p. 241, 2018.
- [48] B. J. Kim, A. R. Kim, C. Lee et al., “Discovery of CDH23 as a significant contributor to progressive postlingual sensorineural hearing loss in Koreans,” *PLoS One*, vol. 11, no. 10, article e0165680, 2016.

Research Article

Jervell and Lange-Nielsen Syndrome due to a Novel Compound Heterozygous *KCNQ1* Mutation in a Chinese Family

Yue Qiu,¹ Sen Chen,¹ Xia Wu,¹ Wen-Juan Zhang,² Wen Xie,¹ Yuan Jin,¹ Le Xie,¹ Kai Xu,¹ Xue Bai,¹ Hui-Min Zhang,¹ Xiao-Zhou Liu,¹ Xiao-Hui Wang,¹ Yu Sun ¹,
and Wei-Jia Kong ^{1,3}

¹Department of Otorhinolaryngology, Union Hospital, Tongji Medical College, Huazhong University of Science and Technology, Wuhan 430022, China

²Department of Otorhinolaryngology, Distinct HealthCare, Wuhan, China

³Institute of Otorhinolaryngology, Tongji Medical College, Huazhong University of Science and Technology, 430022 Wuhan, China

Correspondence should be addressed to Yu Sun; sunyu@hust.edu.cn and Wei-Jia Kong; entwjkong@hust.edu.cn

Received 16 February 2020; Accepted 2 May 2020; Published 16 May 2020

Academic Editor: Hai Huang

Copyright © 2020 Yue Qiu et al. This is an open access article distributed under the Creative Commons Attribution License, which permits unrestricted use, distribution, and reproduction in any medium, provided the original work is properly cited.

Jervell and Lange-Nielsen syndrome (JLNS) is a rare but severe autosomal recessive disease characterized by profound congenital deafness and a prolonged QTc interval (greater than 500 milliseconds) in the ECG waveforms. The prevalence of JLNS is about 1/1000000 to 1/200000 around the world. However, exceed 25% of JLNS patients suffered sudden cardiac death with kinds of triggers containing anesthesia. Approximately 90% of JLNS cases are caused by *KCNQ1* gene mutations. Here, using next-generation sequencing (NGS), we identified a compound heterozygosity for two mutations c.1741A>T (novel) and c.477+5G>A (known) in *KCNQ1* gene as the possible pathogenic cause of JLNS, which suggested a high risk of cardiac events in a deaf child. The hearing of this patient improved significantly with the help of cochlear implantation (CI). But life-threatening arrhythmias occurred with a trigger of anesthesia after the end of the CI surgery. Our findings extend the *KCNQ1* gene mutation spectrum and contribute to the management of deaf children diagnosed with JLNS for otolaryngologists (especially cochlear implant teams).

1. Introduction

Jervell and Lange-Nielsen syndrome (JLNS) is a rare autosomal recessive hereditary disorder characterized by profound congenital deafness and a prolonged QTc interval (greater than 500 milliseconds (msec)) in the ECG waveforms [1]. The prevalence of JLNS is about 1/1000000 to 1/200000 around the world [2]. Mutations of two genes, *KCNQ1* and *KCNE1* gene, are the causes of the disease. And approximately 90% of cases are due to *KCNQ1* gene mutations [1, 2]. Up to now, more than 550 mutations in the *KCNQ1* gene have been reported according to Human Gene Mutation Database (HGMD) (<http://www.hgmd.cf.ac.uk/ac/index.php>).

The *KCNQ1* gene, located on chromosome 11p15.5-p15.4, consists of 16 exons [3]. It encodes the α -subunit of a voltage-gated potassium ion channel (Kv7.1) [4]. The subunit contains six transmembrane segments (S1–S6), a pore-

loop between S5 and S6 and two intracellular domains (N-terminus and C-terminus) [5]. The C-terminus contains a region (~100 amino acids) called A-domain. The A-domain consists of three subdomains (head, linker, and tail) and directs Kv7.1 to specifically assemble with KCNE β -subunits but not with other KCNQ α -subunits [6, 7]. The A-domain Tail is involved in proper channel trafficking and normal cell surface expression [6, 8]. The Kv7.1 has to co-assemble with a β -subunit of the potassium channel (IsK, encoded by *KCNE1* gene) to produce a slow delayed rectifier K^+ current known as IKS, which is associated with regulation of potassium flow [4]. The *KCNQ1* and *KCNE1* gene are both expressed on the apical membranes of marginal cells of stria vascularis to form IKS, which contributes to the generation of endocochlear potential (EP) to maintain the inner ear potassium homeostasis [9, 10]. In addition, IKS is one of the repolarizing potassium currents in cardiovascular muscle cells that

contribute to the cessation of the cardiac action potential and regulates cardiac action potential duration [9, 11]. Animal experiments showed that *kcnq1*^{-/-} mice exhibited deafness, vestibular dysfunction, and altered cardiac repolarization resembling patients with JLNS. Histological analysis showed collapsed Reissner's membrane, massive loss of hair cells as well as abnormal morphology of saccule, utricle, and semicircular ducts in *kcnq1*^{-/-} mice [12]. *kcnq1*^{-/-} mice with *kcnq1* gene replacement therapy in immature scala media by Lin et al. showed significantly improved hearing ability, normal cochlear morphology, and almost normal vestibular function which is optimistic for treatment of JLNS patients [11].

JLNS patients have a high incidence of sudden cardiac death (exceed 25%) [13]. However, this disease can occur among deaf children without obvious symptoms of cardiac events [13, 14]. Exercise, emotion, swimming, auditory stimuli, anesthesia, and fever have been reported as triggers of cardiac arrhythmias in children with JLNS [14, 15]. Even though the clinical diagnosis of this disease is straightforward, genetic evaluation using next-generation sequencing (NGS) is essential, because it has been reported that the patients with *KCNE1* gene mutations have a relatively lower risk of arrhythmic events than that with mutations of *KCNQ1* gene [16]. This influences the management of patients. Here, we report a deaf case diagnosed with JLNS in a Chinese family and a novel compound heterozygous mutation in *KCNQ1* gene associated with the disease.

2. Materials and Methods

2.1. Family Information. This Chinese family, named family 1, is associated with JLNS and contains three family members (son, mother, and father) (Figure 1). The proband 1-II-1 is three years and four months old. He passed the neonatal hearing screen (NHS). However, his parents gradually found he had hearing loss and cannot speak words. The child began wearing hearing aids at the age of one year and 8 months. However, it has no effect. Then, he underwent cochlear implantation (CI) surgery in the right ear when he was 2 years and 8 months old. The proband had the history of convulsion. His parents' hearing is normal.

2.2. Clinical Assessment. A series of audiological assessment was performed for the proband 1-II-1, which included otoscopic examination, conditioned play audiometry (CPA), auditory brainstem response (ABR), auditory steady-state evoked response (ASSR), auditory immittance, and distortion product otoacoustic emission (DPOAE). The child also underwent electrocardiography (ECG) and imaging tests (computed tomography, CT and magnetic resonance imaging, MRI). According to Jervell and Lange-Nielsen syndrome updated in 2017 GeneReviews, the diagnosis of JLNS is established with the profound congenital sensorineural deafness and long QTc interval (>500 msec). Identification of biallelic pathogenic variants in either *KCNQ1* or *KCNE1* confirms the diagnosis [1]. The World Health Organization (WHO, 1991) hearing impairment (HI) grade system includes five grades: no impairment, ≤25 dB nHL; mild, 26-40 dB nHL; moderate, 41-60 dB nHL; severe, 61-80 dB nHL; profound,

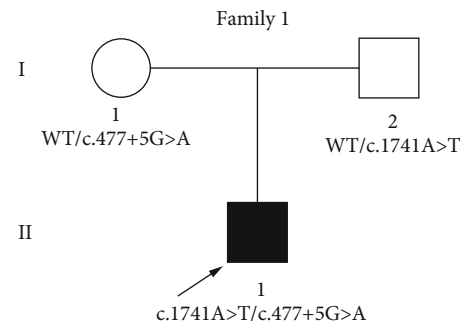


FIGURE 1: Pedigree of Family 1 associated with JLNS. A novel compound heterozygous mutation, c.1741A>T/c.477+5G>A was found in Family member 1-II-1. Family member 1-I-1 and Family member 1-I-2 were heterozygous carriers. The proband is shown in black and indicated by a black arrow. WT: wild type.

≥81 dB nHL; the audiometric dB nHL (International Standards Organization, ISO) values are averages of values at 500, 1000, 2000, and 4000 Hz for the better ear [17].

2.3. Genetic Tests. Written informed consent was obtained from the whole family. About 5 mL peripheral venous blood was collected from three family members for Deafness panel sequencing/NGS and Sanger sequencing which were performed by BGI Genomics (Wuhan, China). For the following experiments, the genomic DNA of blood samples was extracted according to the manufacturer's standard procedure of QIAamp DNA Blood Midi Kit (51185, Qiagen Inc., Valencia, CA, USA), then fragment the DNA by Covaris LE220 (Massachusetts, USA). The fragmented DNA (200-250 bp) was used to generate repair-end library according to Illumina protocols. Targeted DNA fragments were captured by SeqCap EZ Choice (NimbleGen, Madison, USA), followed by postcapture amplification. The products were sequenced on the BGISEQ-500 platform using BGISEQ-500RS High-throughput sequencing kit (PN: 85-05238-01, BGI). The SeqCap EZ Choice was designed to cover all exons together with the flanking exon and intron boundaries (±15 bp) of 127 known deafness-related nuclear genes and deafness-related mitochondrial regions. Postsequencing, a few unqualified sequences were removed from the primary data using a local dynamic programming algorithm. Then, the filtered clean reads were aligned to the Genome Reference Consortium Human genome build 37 (GRCh37)/Human genome build 19 (hg19) by the BWA (Burrows Wheeler Aligner) Multi-Vision software package. After alignment, the single-nucleotide variants (SNVs) and inserts and deletions (InDels) were called by SOAPsnp software and Samtools. All variants were further filtered and estimated via multiple databases including National Center for Biotechnology Information (NCBI) (<https://www.ncbi.nlm.nih.gov>), 1000 Genomes (<http://phase3browser.1000genomes.org/index.html>), Nucleotide Polymorphisms (dbSNP) (<http://www.ncbi.nlm.nih.gov/projects/SNP/>), HGMD (<http://www.hgmd.cf.ac.uk/ac/index.php>). Pathogenic variants are assessed under the American College of Medical Genetics and Genomics-Association for Molecular Pathology (ACMG-AMP) guideline. Filtered candidate variants were

confirmed by conventional Sanger sequencing methods. The methods we used have previously been published [18]. The complete nucleotide and amino acid sequence of the *KCNQ1* gene is shown in the NCBI (<https://www.ncbi.nlm.nih.gov/gene/>).

3. Results

3.1. Clinical Data. The testing results for proband 1-II-1 were as follows. CPA showed a response of 90 dB nHL at 250 Hz (left ear) and no response of both ears in the remaining frequencies (Figure 2(a)). Bilateral tympanograms were type A. No wave of ABR can be elicited at 105 dB nHL bilaterally (data not shown). DPOAEs were absent in both ears (data not shown). The thresholds of ASSR were 100 dB nHL at 500 Hz, 100 dB nHL at 1 KHz (left ear), and 90 dB nHL at 500 Hz, 95 dB nHL at 1KHz (right ear). After hearing aids were fitted, CPA revealed response of 80 dB nHL at 250 Hz of both ears (Figure 2(b)). The CI was implanted into the right temporal bone. Three months after CI surgery, average of audiometric values of all frequencies was 45.8 dB nHL (Figure 2(c)). ECG detected a prolonged QT interval (QT/QTc: 480/523 msec), dome and dart T waves in V3 before CI surgery (Figure 3(a)). After end of the surgery, ECG exhibited T wave change and T wave alternans (TWA), and the QT/QTc interval is 628/661 msec (Figure 3(b)). Imaging tests (CT and MRI) showed no abnormalities.

3.2. Variants Identification and Analysis. Using deafness panel sequencing, we excluded *KCNE1* gene mutation which was identified as the cause of JLNS and found a novel compound heterozygous mutation c.1741A>T/c.477+5G>A in *KCNQ1* gene of proband 1-II-1 (Figure 4). The c.1741A>T (p.K581X) was a novel mutation, and the c.477+5G>A (IVS2+5G>A) has been reported [15, 19]. The mutation c.1741A>T was a nonsense mutation with substitution of no. 1741 nucleotide from adenine to thymine (Figure 4). It occurred in exon 15 (Figure 5). The c.477+5G>A occurred in intron 2 with a mutation of no. 477+5 nucleotide from guanine to adenine (Figures 4 and 5). It was a splice mutation. Both mutations were not polymorphic sites, and the prevalence of them was 0 in 1000 Genomes. The mutation p.K581X was not listed in dbSNP and has not been reported before. The IVS2+5G>A has been recorded in HGMD [15], and its RS number in dbSNP was rs397508111. The parents of the child were both heterozygous carriers (Figure 1). According to the 2015 American College of Medical Genetics and Genomics–Association for Molecular Pathology (ACMG–AMP) guidelines [20] and its refinement in 2017 [21], the variant c.1741A>T (p.K581X) was likely pathogenic, and the variant c.477+5G>A (IVS2+5G>A) was pathogenic.

4. Discussion

A novel compound heterozygous mutation c.1741A>T/c.477+5G>A in *KCNQ1* gene was found in the proband 1-II-1 with JLNS. Combining the medical history and results of audio-

logical examinations, family member 1-II-1 was diagnosed with profound congenital sensorineural deafness according to the 2018 international consensus (ICON) on audiological assessment of hearing loss in children [22] and the WHO-HI grade system. The child passed the NHS which was an OAE-based test; we speculated that it was because the function of hair cells was not affected at birth. It was reported by Casimiro et al. that *kcnq1*^{-/-} mice exhibited the normal hair cell morphology at birth and delayed hair cell loss [12]. Normal QTc interval in males is <440 msec [1]. ECG detected a prolonged QTc interval (523 msec) in the patient before cochlear implantation (Figure 3). Therefore, the proband 1-II-1 was diagnosed with JLNS according to the diagnostic criteria above. It has been reported that mutations of *KCNQ1* and *KCNE1* gene were the causes of JLNS [1, 2]. We used NGS+Sanger sequencing to identify the genotype of the patient. Genetic testing results showed the *KCNE1* gene mutation was excluded. And two mutations in *KCNQ1* gene, c.1741A>T (p.K581X) and c.477+5G>A (IVS2+5G>A) were identified in the family (Figure 1). The variant p.K581X was novel, while the other one IVS2+5G>A was known previously. The IVS2+5G>A had been reported in individuals affected with LQTS or prolonged QT intervals [15, 23, 24]. And this variant had also been identified to be compound heterozygous with p.Y171X in a patient with JLNS [19]. Research on assessment of variant of unknown significance in LQTS revealed that IVS2+5G>A carrier had a prolonged end-recovery QTc interval underwent an exercise stress [25]. Millat et al. have raised a “double-dose” effect that multiple or compound gene mutations occurring in LQTS families may result in a more severe clinical phenotype [23]. This can explain that individuals shared the same single mutation IVS2+5G>A but with varying degree symptoms (no symptoms, only with a prolonged QT intervals, with cardiac events, with profound deafness [15, 19, 23, 25]). According to the ACMG–AMP criteria and its refinement, the variant IVS2+5G>A was pathogenic. Here, we found IVS2+5G>A was compound heterozygous with p.K581X in proband 1-II-1 (Figure 1). The amino acid residues at the novel mutation site (p.K581X) were highly conserved across different species (Figure 5(c)). Through filtration and estimation via multiple databases, the mutation p.K581X was not a polymorphic site and not listed in 1000 Genomes. The p.K581X was judged as a likely pathogenic variant by ACMG criteria. And the parents of Proband 1-II-1 were both heterozygous carriers without deafness (Figure 1). These all suggested that the compound heterozygous mutation p.K581X/IVS2+5G>A may have a “double-dose” effect contribute to pathogenesis of JLNS.

KCNQ1 gene mutations may impair the structural and/or functional ion channel (Kv7.1) resulting in dysfunction of IKS, abnormal regulation of potassium flow, and the onset of JLNS. IVS2+5G>A occurred in consensus splice site of intron 2 with the nucleotide substitution from guanine to adenine (Figures 4 and 5(a)). Nucleotide substitutions within the consensus splice site are relatively common causes of aberrant splicing [26]. And a study on the mutation pattern of aberrant 5' splice sites revealed that the point mutations at the position +5 were particularly prone to aberrant splicing

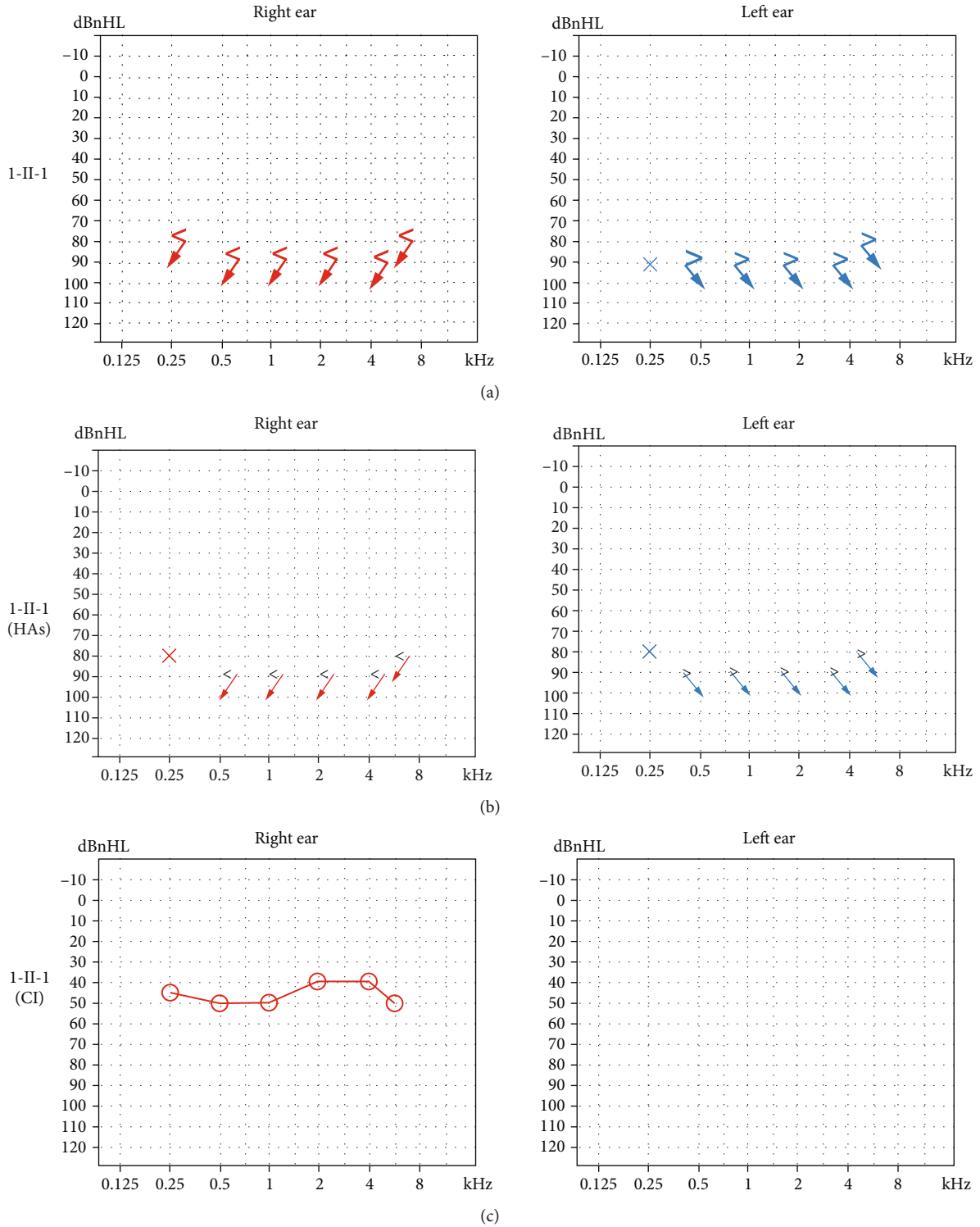


FIGURE 2: CPA results for proband 1-II-1 before and after wearing hearing aids (HAs) and with cochlear implant (CI). (a) Testing results before wearing hearing aids. (b) Testing results after fitting of hearing aids. (c) Sound field thresholds of the right ear 3 months after CI surgery. Arrows: no response at the specific frequency. Cross and circle: threshold at the specific frequency.

[27]. Experiments to evaluate the significance of consensus splice sequence in splicing have shown that mutation at the +5 position of the exon 2 of the rabbit β -globin gene disturbed correct splicing and resulted in joining of exon 1 to exon 3 [28]. The variant p.K581X occurred in exon 15 lead-

ing to premature termination of peptide synthesis. This nonsense mutation may result in no protein synthesis or synthesizing truncation proteins. Researches have revealed that mutations in A-domain impaired the ability of the channel to reach the plasma membrane. And the integrity of the

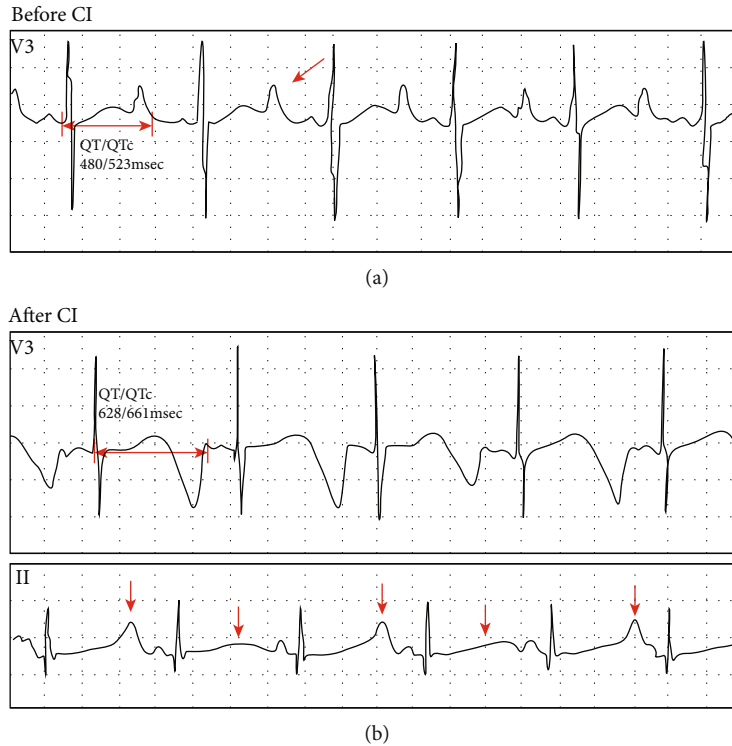


FIGURE 3: ECG detected in Proband 1-II-1. (a) The ECG waveforms before cochlear implantation (CI). Two-way arrow: QT/QTc interval. One-way arrow: dome and dart T wave. (b) The ECG waveforms after cochlear implantation (CI). Two-way arrow: QT/QTc interval. One-way arrows and arrowheads indicate T wave alternans (TWA).

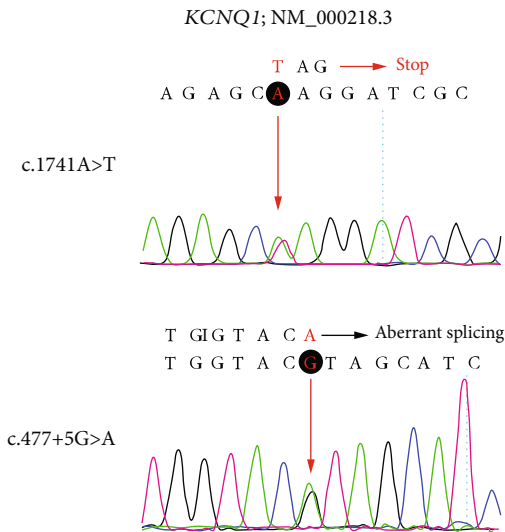


FIGURE 4: Mutated *KCNQ1* sequences of the identified c.1741A>T (above) and c.477+5G>A (below) variant. The mutated nucleotide is shown in red. Red “stop” indicates termination of synthesis. I: boundary of corresponding exon and intron. Red arrows and black rounds: sites of nucleotide changes.

A-domain Tail is critical for normal cell surface expression of Kv7.1 [6, 8]. The variant p.K581X occurred in A-domain Linker which may synthesize a truncation protein without A-domain Tail (Figure 5). Amino acid sequence analysis showed the residues of the region containing the novel muta-

tion site were highly conserved in *Homo sapiens*, *Mus musculus*, *Rattus norvegicus*, *Equus caballus*, and *Macaca mulatta* (Figure 5(c)). Therefore, we speculated that p.K581X resulted in affecting normal cell surface expression of Kv7.1 leading to dysfunction of IKS and impaired regulation of potassium flow in the heart and inner ear. Profound hearing loss is one of the clinical phenotypes in all JLNS patients. It was confused that *KCNQ1* gene mutation resulted in such a severe phenotype. Besides affected EP, *kcnq1*^{-/-} mice showed massive loss of hair cells [12]. As EP reduction not always lead to profound deafness [29], hair cell loss in *kcnq1*^{-/-} mice should be noticed. Degeneration of hair cells was observed in most deafness mice models induced by gene mutations, ototoxic drugs, and noise [30–33]. And lots of experiments on regeneration hair cells have been carried out [34, 35], which may be a new strategy to improve the hearing ability of JLNS patients. It is not clear why the knockout *kcnq1* gene resulted in hair cell loss. Apoptosis or autophagy of hair cells has been observed in kinds of deafness mice models [36–38], which may be involved in the degeneration of hair cells in *kcnq1*^{-/-} mice. Next, we need to conduct experiments to verify the dysfunction of Kv7.1 induced by *KCNQ1* gene mutations and explore the mechanism of deafness.

Cochlear implant (CI) is beneficial to improving the hearing ability of JLNS patients. A review of literature about the outcome of CI in these patients confirms good auditory outcome with their devices [13]. Because of no effect of wearing hearing aids and good auditory outcome with CI, proband 1-II-1 successfully underwent a CI surgery in the

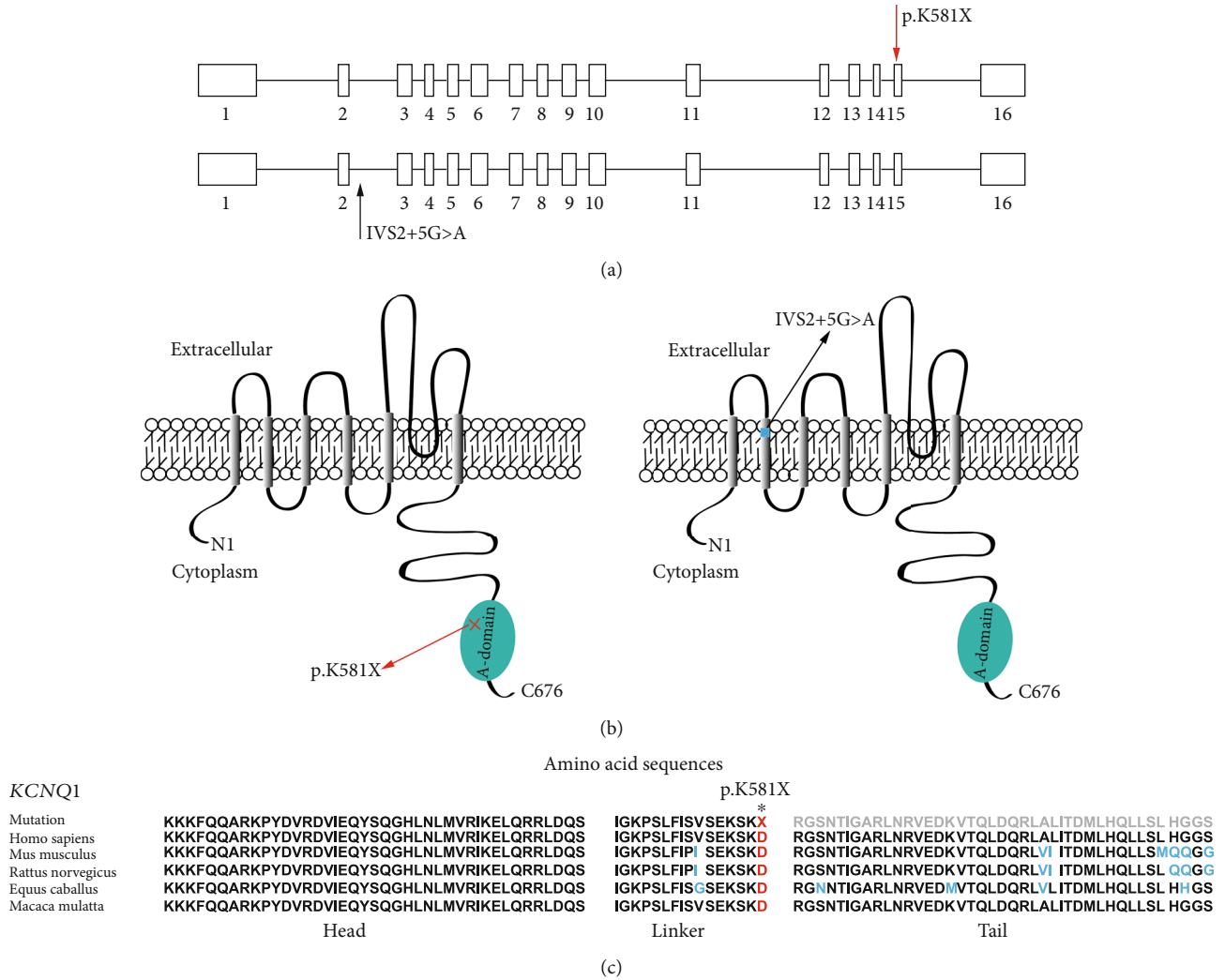


FIGURE 5: Molecular basis for the case of JLNS is detailed at gene and protein levels and evolutionary conservation of amino acids in A-domain affected by the nonsense mutation. (a) Schematic diagram of 16 exons and 15 introns encoded by biallelic *KCNQ1* genes (*KCNQ1*; NM 000218.3). Two variants were indicated by arrows. Novel mutation is shown in red and known mutation is shown in black. Rectangle: exon. Line: intron. (b) Schematic diagram of α -subunit of IKS encoded by biallelic *KCNQ1* genes (*KCNQ1*; NM_000218.3) with pathogenic mutations of p.K581X (red cross) or IVS2+5G>A (blue rectangle). Six transmembrane segments (S1-S6) are indicated by gray columns and the pore-loop is located between S5 and S6. Green oval: A-domain. Red arrow: novel mutation. Black arrow: previously-reported mutation. (c) Evolutionary conservation of A-domain (head, linker, and tail). Mutated site is indicated by asterisk. Gray residues cannot be translated. Different residues were indicated in blue.

right ear and acquired good ability of hearing (Figure 2). With the mapping of CI, the child exhibited satisfactory auditory outcome in daily life. However, after the end of the surgery, the child had a convulsion and life-threatening cardiac arrhythmias (Figure 3). With propranolol treatment and accurate management in pediatric intensive care unit (PICU), no cardiac events occurred. As anesthesia has been identified as a trigger of cardiac arrhythmias in JLNS patients [13], careful attentions should be given at the induction of anesthesia, during wake up and after the surgery. It suggested that JLNS patients should be equipped with paddles for defibrillation during surgery for being exposed to ventricular arrhythmias [14]. The genotype of the proband 1-II-1 showed a compound heterozygous mutation in *KCNQ1* gene. According to Schwartz et al., JLNS patients with *KCNQ1*

gene mutations had six-fold greater risk of arrhythmic events than that with mutations in *KCNE1* gene [16]. These all warned that otolaryngologists (especially cochlear implant teams) should be aware of the risk of the disease and take precautions dealing with the deaf children diagnosed with JLNS.

5. Conclusions

As mentioned above, we found a novel compound heterozygous *KCNQ1* gene mutation (c.1741A>T/c.477+5G>A) associated with JLNS, which suggested a high risk of cardiac events in our patient. In the process of management, the child had a good outcome with CI. However, life-threatening arrhythmias occurred with a trigger of anesthesia after the end of surgery. This warned that otolaryngologists (especially

cochlear implant teams) should be aware of the hazards and take precautions dealing with the deaf children diagnosed with JLNS. Our findings extend the *KCNQ1* mutation spectrum and contribute to the management of deaf patients who are diagnosed with JLNS.

Data Availability

The data which support the conclusions of our study is included within the article.

Ethical Approval

The study compliances with the ethical standards of the responsible committee on human experimentation (Tongji Medical College, Huazhong University of Science and Technology) and with the Declaration of Helsinki (1964).

Conflicts of Interest

The authors declare that they have no competing interests regarding the publication of this paper.

Authors' Contributions

Yue Qiu and Sen Chen contributed equally to this work.

Acknowledgments

We thank all family members who participate in this study. This research was supported by the National Nature Science Foundation of China (grant numbers 81771003, 81470696, 81500793, 81570923, and 81600800).

References

- [1] L. Tranebjærg, "Jervell and Lange-Nielsen Syndrome," in *Genetic Hearing Loss*, Seattle (WA), 2003.
- [2] K. Pabba and R. K. Chakraborty, "Jervell and Lange Nielsen Syndrome," in *Stat Pearls*, Treasure Island (FL), 2020.
- [3] M. Nishimura, M. Ueda, R. Ebata et al., "A novel *KCNQ1* nonsense variant in the isoform-specific first exon causes both jervell and Lange-Nielsen syndrome 1 and long QT syndrome 1: a case report," *BMC Medical Genetics*, vol. 18, no. 1, p. 66, 2017.
- [4] S. Vojdani, S. Amirsalari, S. Milanizadeh et al., "Mutation screening of *KCNQ1* and *KCNE1* genes in Iranian patients with Jervell and Lange-Nielsen syndrome," *Fetal and Pediatric Pathology*, vol. 38, no. 4, pp. 273–281, 2019.
- [5] S. Bendahhou, C. Marionneau, K. Haurogne et al., "In vitro molecular interactions and distribution of *KCNE* family with *KCNQ1* in the human heart," *Cardiovascular Research*, vol. 67, no. 3, pp. 529–538, 2005.
- [6] R. J. Howard, K. A. Clark, J. M. Holton, and D. L. Minor Jr., "Structural insight into *KCNQ* (*Kv7*) channel assembly and channelopathy," *Neuron*, vol. 53, no. 5, pp. 663–675, 2007.
- [7] M. Schwake, T. J. Jentsch, and T. Friedrich, "A carboxy-terminal domain determines the subunit specificity of *KCNQ* K^+ channel assembly," *EMBO Reports*, vol. 4, no. 1, pp. 76–81, 2003.
- [8] H. Kanki, S. Kupersmidt, T. Yang, S. Wells, and D. M. Roden, "A structural requirement for processing the cardiac K^+ channel *KCNQ1*," *The Journal of Biological Chemistry*, vol. 279, no. 32, pp. 33976–33983, 2004.
- [9] G. Dixit, C. Dabney-Smith, and G. A. Lorigan, "The membrane protein *KCNQ1* potassium ion channel: functional diversity and current structural insights," *Biochimica et Biophysica Acta (BBA) - Biomembranes*, vol. 1862, no. 5, p. 183148, 2020.
- [10] H. Hibino, F. Nin, C. Tsuzuki, and Y. Kurachi, "How is the highly positive endocochlear potential formed? The specific architecture of the stria vascularis and the roles of the ion-transport apparatus," *Pflügers Archiv - European Journal of Physiology*, vol. 459, no. 4, pp. 521–533, 2010.
- [11] Q. Chang, J. Wang, Q. Li et al., "Virally mediated *Kcnq1* gene replacement therapy in the immature scala media restores hearing in a mouse model of human Jervell and Lange-Nielsen deafness syndrome," *EMBO Molecular Medicine*, vol. 7, no. 8, pp. 1077–1086, 2015.
- [12] M. C. Casimiro, B. C. Knollmann, S. N. Ebert et al., "Targeted disruption of the *Kcnq1* gene produces a mouse model of Jervell and Lange-Nielsen syndrome," *Proceedings of the National Academy of Sciences of the United States of America*, vol. 98, no. 5, pp. 2526–2531, 2001.
- [13] A. Eftekharian and M. H. Mahani, "Jervell and Lange-Nielsen syndrome in cochlear implanted patients: our experience and a review of literature," *International Journal of Pediatric Otorhinolaryngology*, vol. 79, no. 9, pp. 1544–1547, 2015.
- [14] G. Siem, A. Fruh, T. P. Leren, K. Heimdal, E. Teig, and S. Harris, "Jervell and Lange-Nielsen syndrome in Norwegian children: aspects around cochlear implantation, hearing, and balance," *Ear and Hearing*, vol. 29, no. 2, pp. 261–269, 2008.
- [15] M. J. Ackerman, D. J. Tester, and C.-B. J. Porter, "Swimming, a gene-specific arrhythmogenic trigger for inherited long QT syndrome," *Mayo Clinic Proceedings*, vol. 74, no. 11, pp. 1088–1094, 1999.
- [16] P. J. Schwartz, C. Spazzolini, L. Crotti et al., "The Jervell and Lange-Nielsen syndrome: natural history, molecular basis, and clinical outcome," *Circulation*, vol. 113, no. 6, pp. 783–790, 2006.
- [17] L. E. Humes, "Examining the validity of the World Health Organization's long-standing hearing impairment grading system for unaided communication in age-related hearing loss," *American Journal of Audiology*, vol. 28, no. 3S, pp. 810–818, 2019.
- [18] Y. Qiu, S. Chen, L. Xie et al., "Auditory neuropathy spectrum disorder due to two novel compound heterozygous OTOF mutations in two Chinese families," *Neural Plasticity*, vol. 2019, 7 pages, 2019.
- [19] J. R. Giudicessi and M. J. Ackerman, "Prevalence and Potential Genetic Determinants of Sensorineural Deafness in *KCNQ1* Homozygosity and Compound Heterozygosity," *Circulation: Cardiovascular Genetics*, vol. 6, no. 2, pp. 193–200, 2013.
- [20] S. Richards, N. Aziz, S. Bale et al., "Standards and guidelines for the interpretation of sequence variants: a joint consensus recommendation of the American College of Medical Genetics and Genomics and the Association for Molecular Pathology," *Genetics in Medicine*, vol. 17, no. 5, pp. 405–423, 2015.
- [21] The Invitae Clinical Genomics Group, K. Nykamp, M. Anderson et al., "Sherloc: a comprehensive refinement of the ACMG–AMP variant classification criteria," *Genetics in Medicine*, vol. 19, no. 10, pp. 1105–1117, 2017.

- [22] A. Farinetti, A. Raji, H. Wu, B. Wanna, and C. Vincent, "International consensus (ICON) on audiological assessment of hearing loss in children," *European Annals of Otorhinolaryngology, Head and Neck Diseases*, vol. 135, no. 1, pp. S41–S48, 2018.
- [23] G. Millat, P. Chevalier, L. Restier-Miron et al., "Spectrum of pathogenic mutations and associated polymorphisms in a cohort of 44 unrelated patients with long QT syndrome," *Clinical Genetics*, vol. 70, no. 3, pp. 214–227, 2006.
- [24] I. Splawski, J. Shen, K. W. Timothy et al., "Spectrum of mutations in long-QT syndrome genes. KVLQT1, HERG, SCN5A, KCNE1, and KCNE2," *Circulation*, vol. 102, no. 10, pp. 1178–1185, 2000.
- [25] M. N. Obeyesekere, R. W. Sy, G. J. Klein et al., "End-recovery QTc: a useful metric for assessing genetic variants of unknown significance in long-QT syndrome," *Journal of Cardiovascular Electrophysiology*, vol. 23, no. 6, pp. 637–642, 2012.
- [26] M. Q. Zhang, "Statistical features of human exons and their flanking regions," *Human Molecular Genetics*, vol. 7, no. 5, pp. 919–932, 1998.
- [27] E. Buratti, M. Chivers, J. Královičová et al., "Aberrant 5' splice sites in human disease genes: mutation pattern, nucleotide structure and comparison of computational tools that predict their utilization," *Nucleic Acids Research*, vol. 35, no. 13, pp. 4250–4263, 2007.
- [28] M. Aebi, H. Hornig, R. A. Padgett, J. Reiser, and C. Weissmann, "Sequence requirements for splicing of higher eukaryotic nuclear pre-mRNA," *Cell*, vol. 47, no. 4, pp. 555–565, 1986.
- [29] J. Chen, Y. Zhu, C. Liang, J. Chen, and H. B. Zhao, "Pannexin1 channels dominate ATP release in the cochlea ensuring endocochlear potential and auditory receptor potential generation and hearing," *Scientific Reports*, vol. 5, no. 1, 2015.
- [30] L. Liu, Y. Chen, J. Qi et al., "Wnt activation protects against neomycin-induced hair cell damage in the mouse cochlea," *Cell Death & Disease*, vol. 7, no. 3, p. e2136, 2016.
- [31] W. W. Liu, X. C. Xu, Z. M. Fan et al., "Wnt signaling activates TP53-induced glycolysis and apoptosis regulator and protects against cisplatin-induced spiral ganglion neuron damage in the mouse cochlea," *Antioxidants & Redox Signaling*, vol. 30, no. 11, pp. 1389–1410, 2019.
- [32] Y. Liu, J. Qi, X. Chen et al., "Critical role of spectrin in hearing development and deafness," *Science Advances*, vol. 5, no. 4, p. eaav7803, 2019.
- [33] Y. F. Wang, Q. Chang, W. X. Tang et al., "Targeted connexin26 ablation arrests postnatal development of the organ of Corti," *Biochemical and Biophysical Research Communications*, vol. 385, no. 1, pp. 33–37, 2009.
- [34] F. Tan, C. Chu, J. Qi et al., "AAV-*ie* enables safe and efficient gene transfer to inner ear cells," *Nature Communications*, vol. 10, no. 1, p. 3733, 2019.
- [35] L. L. Jiang, J. C. Xu, R. Jin et al., "Transcriptomic analysis of chicken cochleae after gentamicin damage and the involvement of four signaling pathways (Notch, FGF, Wnt and BMP) in hair cell regeneration," *Hearing Research*, vol. 361, pp. 66–79, 2018.
- [36] Z. H. He, L. N. Guo, Y. L. Shu et al., "Autophagy protects auditory hair cells against neomycin-induced damage," *Autophagy*, vol. 13, no. 11, pp. 1884–1904, 2017.
- [37] A. Li, D. You, W. Y. Li et al., "Novel compounds protect auditory hair cells against gentamycin-induced apoptosis by maintaining the expression level of H3K4me2," *Drug Delivery*, vol. 25, no. 1, pp. 1033–1043, 2018.
- [38] H. Yuan, X. R. Wang, K. Hill et al., "Autophagy attenuates noise-induced hearing loss by reducing oxidative stress," *Antioxidants & Redox Signaling*, vol. 22, no. 15, pp. 1308–1324, 2015.